Cover Picture

Rolf Gausepohl, Pascal Buskens, Jochen Kleinen, Angelika Bruckmann, Christian W. Lehmann, Jürgen Klankermayer, and Walter Leitner*

Chiral solvents are capable of inducing high enantioselectivities in asymmetric reactions after all. Functionalized chiral ionic liquids are particularly suitable for this purpose as they can interact strongly (e.g., through electrostatic interactions and hydrogen bonding) with substrates and/or intermediates. W. Leitner and co-workers show in their Communication on page 3689 ff. that this concept can be used for the aza-Baylis–Hillman reaction to achieve products with up to 84% *ee*.

Energetic Salts
In their Review on page 3584 ff., J. M. Shreeve et al. present recent developments in the field of nitrogen-rich energetic salts and ionic liquids. The properties of the corresponding molecular compounds are a benchmark for this emerging substance class.

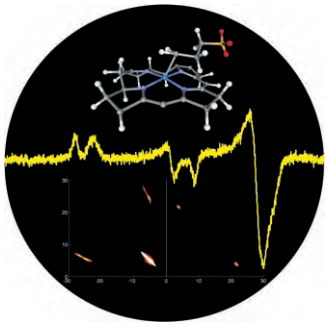

Bioinorganic Chemistry
Evidence for the formation of a nickel–carbon bond at the active site of the enzyme involved in the key step of methanogenesis is described by J. Harmer, B. Jaun, and co-workers in their Communication on page 3602 ff.

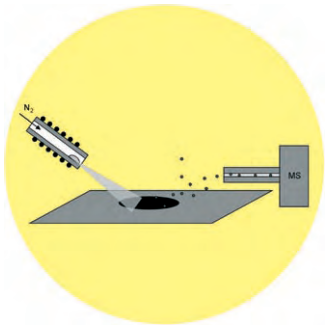

Gas-phase Reactions
In their Communication on page 3656 ff., R. G. Cooks et al. describe a method to generate gas-phase ions from a variety of organic salts, including ionic liquids and transition-metal salts, and perform ion–molecule reactions at atmospheric pressure.

Contents

The following Communications have been judged by at least two referees to be "very important papers" and will be published online at www.angewandte.org soon:

*C. Burke, Y. Shi**
Regio- and Enantioselective Epoxidation of Dienes by a Chiral Dioxirane: Synthesis of Optically Active Vinyl *cis*-Epoxides

C.-W. So, H. Roesky, J. Magull, R. Oswald*
Synthesis and Characterization of [{PhC(NtBu)$_2$}SiCl]: A Stable Monomeric Chlorosilylene

*H. Yu, S. Huang, H. Chokhawala, M. Sun, H. Zheng, X. Chen**
Highly Efficient Chemoenzymatic Synthesis of Naturally Occurring and Non-Natural α2,6-Linked Sialosides: A *P. damsela* α2,6-Sialyltransferase with Extremely Flexible Donor Substrate Specificity

*D. Rohde, C.-J. Yan, H.-J. Yan, L.-J. Wan**
From Lamellar to Hexagonal Self-Assembly of Bis(dioxaborin) Molecules

Meeting Reviews

The Many Facets of Photochemistry — *J. Mattay* — **3570**

Books

Bioorganometallics — Gérard Jaouen — *reviewed by B. Lippert* — **3572**

Artificial Photosynthesis — Anthony F. Collings, Christa Critchley — *reviewed by L. Hammarström, O. Johansson, A. Magnuson* — **3573**

Highlights

Molecular Capsules

L. Cronin* — **3576 – 3578**

Inorganic Molecular Capsules: From Structure to Function

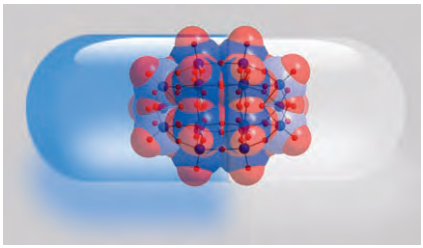

Capsule "hotels" for molecular guests: The binding, release, and even reaction of guests within the cavities of inorganic cages or capsules (see picture) can be performed with an unprecedented level of control. In view of this host–guest chemistry, such functional frameworks are promising in catalysis and for model studies of ion channels in biological membranes.

Aryne Insertions

D. Peña,* D. Pérez, E. Guitián* — **3579 – 3581**

Insertion of Arynes into σ Bonds

Enjoying a revival: Following a quiet period, numerous reports have recently appeared regarding the insertion of arynes into σ bonds (see scheme) as a result of milder, high-yielding methods for generating arynes and the introduction of palladium catalysis into aryne chemistry. The methodology shows promise as a means of preparing complex *ortho*-disubstituted arenes.

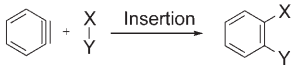

InterScience

© 2006 Wiley-VCH Verlag GmbH & Co. KGaA, Weinheim

Reviews

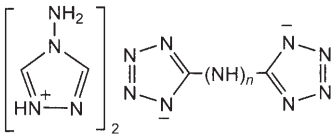

Full of energy: Energetic ionic salts offer many advantages over traditional molecular energetic compounds. Nitrogen-containing cations and anions contribute to higher heats of formation and higher densities, and the low amounts of carbon and hydrogen also allows for a good oxygen balance. Because a higher percentage of the decomposition products will be dinitrogen, these nitrogen-rich compounds are promising high-energetic materials.

Explosives

R. P. Singh, R. D. Verma, D. T. Meshri, J. M. Shreeve* ——— **3584 – 3601**

Energetic Nitrogen-Rich Salts and Ionic Liquids

Communications

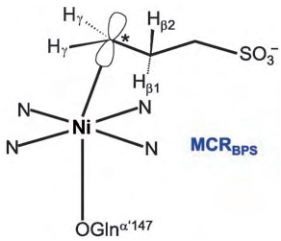

The spin reveals all: Electron paramagnetic resonance spectroscopy reveals the formation of a nickel–alkyl bond in the active site of methyl-coenzyme M reductase (MCR), the key enzyme of methanogenesis, when active MCR_{red1} reacts with the irreversible inhibitor 3-bromopropane sulfonate to form the MCR_{BPS} species.

Bioinorganic Chemistry

D. Hinderberger, R. P. Piskorski, M. Goenrich, R. K. Thauer, A. Schweiger, J. Harmer,* B. Jaun* ——— **3602 – 3607**

A Nickel–Alkyl Bond in an Inactivated State of the Enzyme Catalyzing Methane Formation

Hip hip array: Lectins are involved in a wide range of biological processes and are used frequently as tools for basic and applied research. Through the use of a carbohydrate microarray, high-throughput analysis of lectin specificity was carried out on 24 different lectins. Many of the carbohydrate ligands identified for the lectins were unexpected based on previous information.

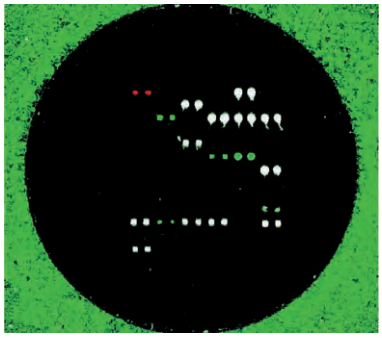

Carbohydrate Microarrays

J. C. Manimala, T. A. Roach, Z. Li, J. C. Gildersleeve* ——— **3607 – 3610**

High-Throughput Carbohydrate Microarray Analysis of 24 Lectins

For the USA and Canada:
ANGEWANDTE CHEMIE International Edition (ISSN 1433-7851) is published weekly by Wiley-VCH PO Box 191161, D 69451 Weinheim, Germany. Air freight and mailing in the USA by Publications Expediting Inc. 200 Meacham Ave., Elmont, NY 11003. Periodicals postage paid at Jamaica NY 11431. US POSTMASTER: send address changes to *Angewandte Chemie*, Wiley-VCH, 111 River Street, Hoboken, NJ 07030. Annual subscription price for institutions: US$ 5685/5168 (valid for print and electronic / print or electronic delivery); for individuals who are personal members of a national chemical society prices are available on request. Postage and handling charges included. All prices are subject to local VAT/sales tax.

© 2006 Wiley-VCH Verlag GmbH & Co. KGaA, Weinheim

The best in chemistry – for more than hundred years

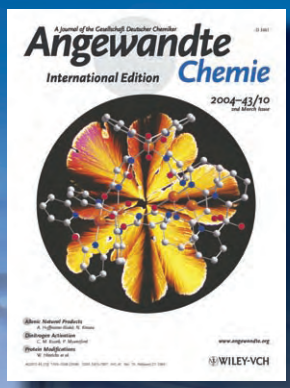

A Journal of the Gesellschaft Deutscher Chemiker

Angewandte
International Edition **Chemie**

www.angewandte.org

1888: ***The beginning of a success story***

Constant Innovations

1962: *First issue of the International Edition*
1976: *Graphical abstracts*
1979: *Cover pictures*
1988: *Centenary of Angewandte*
1989: *Routine use of color*
1991: *New section: Highlights*
1992: *Computerized editorial tracking system*
1995: *Internet service for readers*
1998: *Regular press service; full-text online*
2000: *New section: Essays; EarlyView: Communications available online ahead of the printed version*
2001: *New section: Microreviews*
2002: *Online submission of manuscripts*
2003: *Weekly publication; new section: News; new layout*
2004: *Backfiles (1962-1997); ManuscriptXpress: Online system for authors and referees*

Angewandte's advisors...

K.C. Nicolaou
The Scripps Research Institute and University of California San Diego (La Jolla, USA)

» ***Angewandte Chemie*** *has been highly influential in shaping the art of publishing chemical innovations and I feel privileged to be part of its Advisory Board. Eliciting admiration and respect from both readers and authors alike, its editorial staff should be commended for creating a new and exciting image of this most admired journal.* «

Angewandte Chemie International Edition *is a journal of the German Chemical Society (GDCh)*

GDCh

WILEY InterScience® DISCOVER SOMETHING GREAT

WILEY-VCH

95203123_gu

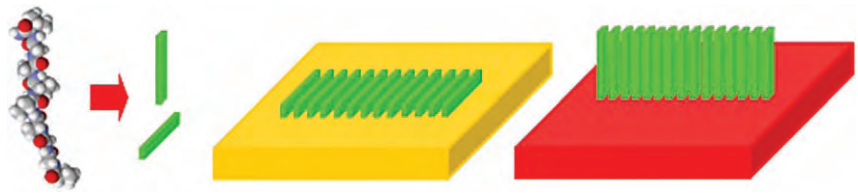

Taking a stand: Self-assembled peptide aggregates adopt interfacial orientations in which they either lie horizontally (on highly ordered pyrolytic graphite, hydrophobic) or are oriented upright (on mica, hydrophilic) to form nanofilaments with different heights. This process is controlled by the interfacial hydrophobic or electrostatic interactions.

Peptide Nanofilaments

F. Zhang, H.-N. Du, Z.-X. Zhang, L.-N. Ji, H.-T. Li, L. Tang, H.-B. Wang, C.-H. Fan, H.-J. Xu, Y. Zhang,* J. Hu, H.-Y. Hu, J.-H. He* ——— **3611 – 3613**

Epitaxial Growth of Peptide Nanofilaments on Inorganic Surfaces: Effects of Interfacial Hydrophobicity/Hydrophilicity

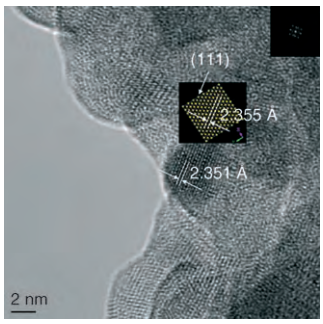

Support system: The stability of a $LaPO_4$-supported Au nanocatalyst for CO oxidation exceeds that of Au nanocatalysts with oxide supports. Activation is achieved by high-temperature calcination under an oxidative atmosphere (see transmission electron microscopy image of crystalline Au nanoparticles on hexagonal $LaPO_4$). The use of phosphates as supports for highly active gold catalysts opens up new routes in the search for ultrastable and sinter-resistant catalysts.

Nanoparticle Catalyst

W. F. Yan, S. Brown, Z. W. Pan, S. M. Mahurin, S. H. Overbury, S. Dai* ——— **3614 – 3618**

Ultrastable Gold Nanocatalyst Supported by Nanosized Non-Oxide Substrate

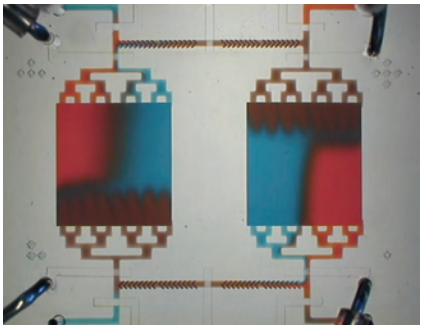

Order from chaos: Microfluidic chaotic mixing shows a significant improvement in the equilibration time of hybridization in DNA microarrays over conventional techniques. These results illustrate a new concept for performing kinetics studies in microfluidic devices.

DNA Microarrays

J. Liu, B. A. Williams, R. M. Gwirtz, B. J. Wold, S. Quake* ——— **3618 – 3623**

Enhanced Signals and Fast Nucleic Acid Hybridization By Microfluidic Chaotic Mixing

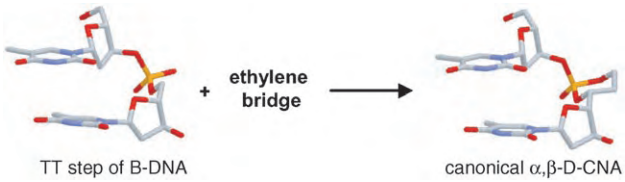

Constrained nucleic acids (α,β-D-CNAs) have an ethylene bridge that locks the α and β backbone torsion angles of DNA in the canonical (*gauche*(−),*trans*) conformation, as in B-form DNA (see picture), or in the noncanonical (*gauche*(+),*trans*) conformation. Canonical α,β-D-CNAs enhance the duplex-forming ability of oligonucleotides with complementary DNA, while noncanonical α,β-D-CNAs stabilize distorted B-DNA structures.

Nucleic Acids

C. Dupouy, N. Iché-Tarrat, M.-P. Durrieu, F. Rodriguez, J.-M. Escudier,* A. Vigroux* ——— **3623 – 3627**

Watson–Crick Base-Pairing Properties of Nucleic Acid Analogues with Stereocontrolled α and β Torsion Angles (α,β-D-CNAs)

© 2006 Wiley-VCH Verlag GmbH & Co. KGaA, Weinheim

Contents

Mechanistic Studies

C. Fish, M. Green,* R. J. Kilby, J. M. Lynam,* J. E. McGrady,* D. A. Pantazis, C. A. Russell,* A. C. Whitwood, C. E. Willans ——— **3628 – 3631**

A New Reaction Pathway in Organophosphorus Chemistry: Competing S_N2 and AE′ Pathways for Nucleophilic Attack at a Phosphorus–Carbon Cage Compound

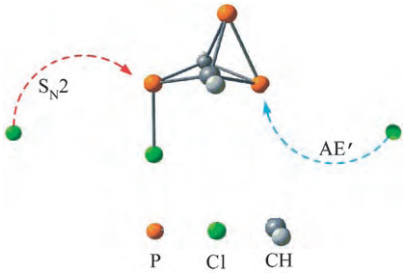

Competition: A combination of ^{31}P NMR spectroscopic and calculational studies have shown that nucleophilic substitution in the phosphorus–carbon cage compound $ClP_3(CtBu)_2$ occurs through competing S_N2- and AE′-type reaction pathways (see scheme for model compound $ClP_3(CH)_2$). The AE′ mechanism results in the formation of a C_{2v}-symmetric intermediate prior to release of the chloride ion.

Nanotechnology

Q. Xu, J. Bao, F. Capasso, G. M. Whitesides* ——— **3631 – 3635**

Surface Plasmon Resonances of Free-Standing Gold Nanowires Fabricated by Nanoskiving

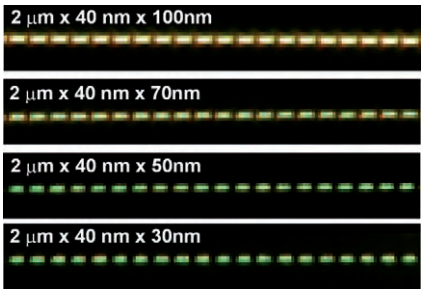

Down to the wire: A top-down technique that combines photolithography, thin-film metal deposition, and thin-film sectioning has been developed to fabricate patterned arrays of gold nanowires of uniform, controllable length, width, and height. A systematic study of the dependence of the surface plasmon resonance (see picture) on the geometry of these wires is presented.

Multicomponent Reactions

N. Kumagai, G. Muncipinto, S. L. Schreiber* ——— **3635 – 3638**

Short Synthesis of Skeletally and Stereochemically Diverse Small Molecules by Coupling Petasis Condensation Reactions to Cyclization Reactions

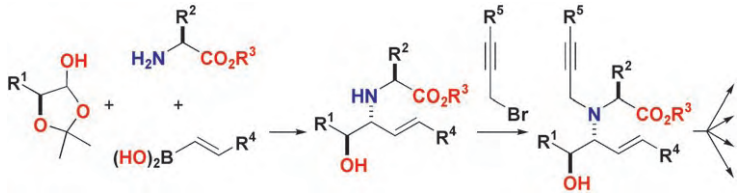

An efficient synthetic pathway to skeletally and stereochemically diverse molecules is described. Densely functionalized amino alcohols were readily synthesized through a Petasis three-component, boronic acid Mannich reaction. Their intramolecular cyclization provided a collection of diverse single-isomer compounds with 15 different types of skeletons in three to five steps.

Porphyrins

Y. J. Li, X. F. Li, Y. L. Li,* H. B. Liu, S. Wang, H. Y. Gan, J. Li, N. Wang, X. R. He, D. B. Zhu* ——— **3639 – 3643**

Controlled Self-Assembly Behavior of an Amphiphilic Bisporphyrin–Bipyridinium–Palladium Complex: From Multibilayer Vesicles to Hollow Capsules

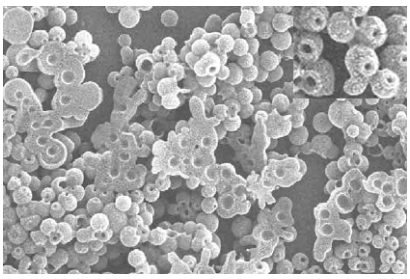

Gas-filled: Porphyrin-based amphiphiles can self-assemble into multibilayer vesicles. These vesicles can be converted into hollow capsules and wormlike structures (see picture) by controlling the release rate of methanol encapsulated through changing the heating temperature and pattern.

© 2006 Wiley-VCH Verlag GmbH & Co. KGaA, Weinheim

Food for tubes: Cyclophane-type macrocycles are used as building blocks for the formation of tubular structures. The inclusion properties of these molecules are studied, and the "cyclophane in cyclophane" **1** was characterized by X-ray crystallography.

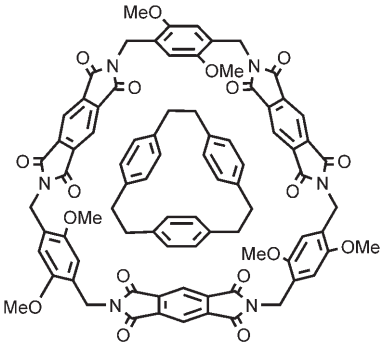

1

Molecular Tubes

T. Iwanaga, R. Nakamoto, M. Yasutake, H. Takemura, K. Sako, T. Shinmyozu* _____ **3643 – 3647**

Cyclophanes within Cyclophanes: The Synthesis of a Pyromellitic Diimide-Based Macrocycle as a Structural Unit in a Molecular Tube and Its Inclusion Phenomena

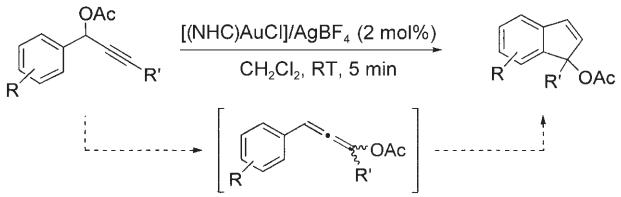

Dignified auration: The rearrangement of phenylpropargyl acetates to substituted indenes is catalyzed by [Au^{I}(NHC)] complexes (see scheme, NHC = N-heterocyclic carbene) under extremely mild reaction conditions. This chemoselective transformation involves 1,3-migration of the acetate group and is proposed to proceed through an allene intermediate. TMS = trimethylsilyl, TBS = *tert*-butyldimethylsilyl.

Synthetic Methods

N. Marion, S. Díez-González, P. de Frémont, A. R. Noble, S. P. Nolan* _____ **3647 – 3650**

Au^{I}-Catalyzed Tandem [3,3] Rearrangement–Intramolecular Hydroarylation: Mild and Efficient Formation of Substituted Indenes

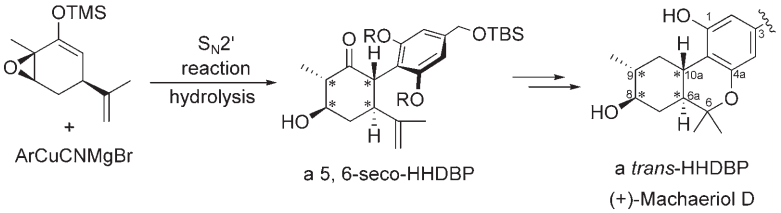

A general strategy for the synthesis of hexahydrodibenzopyrans (HHDBPs) is illustrated in the enantioselective total synthesis of (+)-machaeriol D. In the key step, an S_N2' reaction of an aryl cyanocuprate with a silyl enol ether of an optically active α,β-epoxycyclohexanone enabled the construction of the four stereocenters of the natural product with high regio- and stereoselectivity (see scheme; R = methoxymethyl). TMS = trimethylsilyl, TBS = *tert*-butyldimethylsilyl.

Natural Product Synthesis

Q. Wang, Q. Huang, B. Chen, J. Lu, H. Wang, X. She,* X. Pan* _____ **3651 – 3653**

Total Synthesis of (+)-Machaeriol D with a Key Regio- and Stereoselective S_N2' Reaction

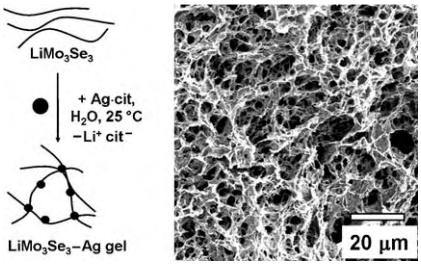

Giant holes: Macroporous solids with high electrical conductivity and adjustable pore sizes can be synthesized by the covalent cross-linking of $LiMo_3Se_3$ nanowires with citrate-stabilized Ag nanoparticles (see picture, cit = citrate). The ease of synthesis and the possibilities for functionalization with redox-active groups make these xerogels potentially useful in applications such as batteries, capacitors, and electrochemical catalysts.

Porous Solids

N. N. Akl, O. Trofymluk, X. Qi, J. Y. Kim, F. E. Osterloh,* A. Navrotsky* _____ **3653 – 3656**

A Nanowire–Nanoparticle Cross-Linking Approach to Highly Porous Electrically Conducting Solids

© 2006 Wiley-VCH Verlag GmbH & Co. KGaA, Weinheim

Contents

Analytical Methods

H. Chen, Z. Ouyang, R. G. Cooks* ——— 3656 – 3660

Thermal Production and Reactions of Organic Ions at Atmospheric Pressure

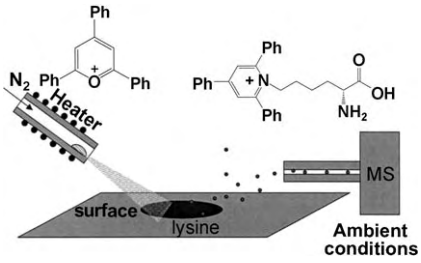

The heat is on: Thermal ionization of a variety of organic salts including ionic liquids and transition-metal salts occurs at atmospheric pressure. This thermal method allows for the study of ion–molecule reactions; for example, the fast selective desorption and derivatization of D-lysine occurs when thermally generated pyrylium ions react with solid lysine under ambient conditions (see picture).

C–N-Coupled Azolyl Nucleosides

P. Lagisetty, L. M. Russon, M. K. Lakshman* ——— 3660 – 3663

A General Synthesis of C6-Azolyl Purine Nucleosides

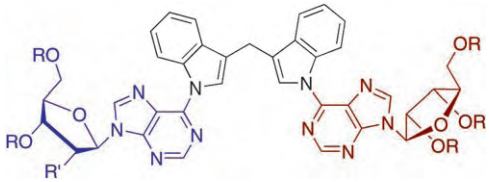

Catalysis by a Pd–Xantphos complex allows the synthesis of unusual symmetrical and unsymmetrical nucleoside dimers (see structure; R′ = OR, H). Various azolyl units can be introduced at the C6 position of purine nucleosides, including systems such as melatonin and an amino acid. Bromo- and chloropurine ribo- and 2′-deoxyribonucleosides are effective substrates for this C–N(sp^2) bond-forming reaction.

Hydrogen-Storage Materials

J. M. Bellosta von Colbe, W. Schmidt, M. Felderhoff, B. Bogdanović, F. Schüth* ——— 3663 – 3665

Hydrogen-Isotope Scrambling on Doped Sodium Alanate

Titanium facilitates hydrogen dissociation at the surface of sodium alanate, an extensively studied hydrogen-storage material, and diffusion of hydrogen into the bulk, according to hydrogen-isotope scrambling experiments on Ti-doped $NaAlH_4$ (see picture). Kinetics studies indicate that the rate-limiting step of the charging/discharging process appears to be mass transfer into the solid.

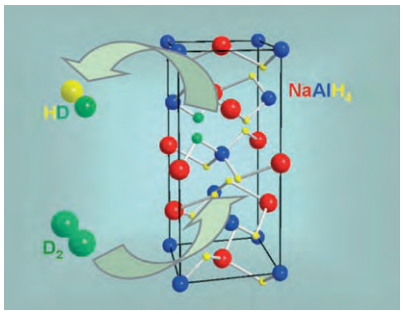

Selective DNA Cleavage

B. Breiner, J. C. Schlatterer, S. V. Kovalenko, N. L. Greenbaum, I. V. Alabugin* ——— 3666 – 3670

Protected ^{32}P-Labels in Deoxyribonucleotides: Investigation of Sequence Selectivity of DNA Photocleavage by Enediyne–, Fulvene–, and Acetylene–Lysine Conjugates

Finding a compromise: The sequence selectivity of DNA photocleavage by enediyne–, acetylene–, and fulvene–lysine conjugates was investigated by using labeled DNA oligomers. Since the external ^{32}P label was removed by these photocleavers, the label was protected by translocation inside the oligomer (see figure). The selectivity of cleavage is controlled by a compromise between AT selectivity for binding and G selectivity for electron transfer.

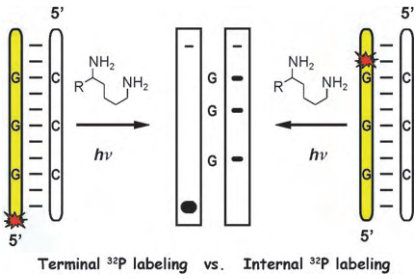

© 2006 Wiley-VCH Verlag GmbH & Co. KGaA, Weinheim

Short and to the point: A three-centered hydrogen bond is present in 6,16-dimesityl-11-phenylsubpyriporphyrin, a non-aromatic free-base triphyrin(1.1.1)-related molecule. X-ray crystal structural analysis shows this compound contains the shortest known N···N distance (2.370 Å) for two N atoms involved in hydrogen bonding. The molecule also acts as a ligand, as shown by the formation of a boron complex.

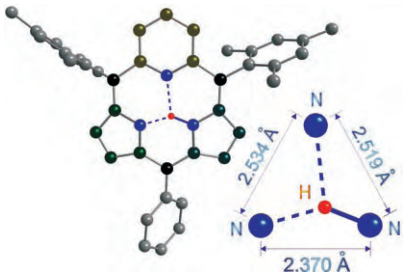

Porphyrinoids

R. Myśliborski, L. Latos-Grażyński,*
L. Szterenberg, T. Lis ——— **3670 – 3674**

Subpyriporphyrin—A [14]Triphyrin(1.1.1) Homologue with an Embedded Pyridine Moiety

Wrapping up water: Two non-fluorinated CO_2-philic surfactants are used to generate water in carbon dioxide microemulsion dispersions. Detailed analyses of high-pressure small-angle neutron scattering data provide evidence for formation of spherical D_2O nanodroplets (red), stabilized by surfactant interfacial monolayers (lines), and dispersed in CO_2 (yellow in the schematic scattering length density (sld) profile).

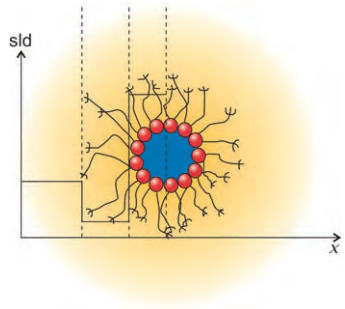

Green Solvents

J. Eastoe,* S. Gold, S. Rogers, P. Wyatt, D. C. Steytler, A. Gurgel, R. K. Heenan, X. Fan, E. J. Beckman, R. M. Enick ——— **3675 – 3677**

Designed CO_2-Philes Stabilize Water-in-Carbon Dioxide Microemulsions

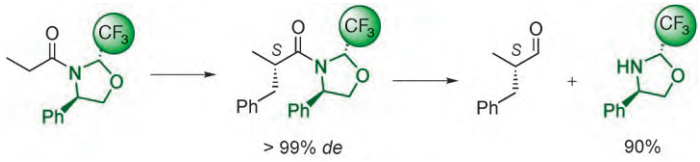

A bit on the side: Extremely high diastereoselectivities (>99% *de*) were attained in the α-alkylation and -allylation of amides by using a trifluoromethylated (sphere) oxazolidine as a chiral auxiliary. Reductive cleavage of the amide bond led to the recovery of this fluorinated chiral auxiliary in high yield.

Asymmetric Synthesis

A. Tessier, J. Pytkowicz, T. Brigaud* ——— **3677 – 3681**

Chiral 4-Phenyl-2-trifluoromethyloxazolidine: A High-Performance Chiral Auxiliary for the Alkylation of Amides

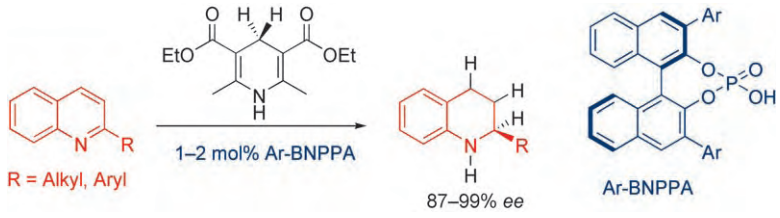

A categorical success: A Brønsted acid catalyzed cascade transfer hydrogenation provides direct access to 2-aryl- and 2-alkyl-substituted tetrahydroquinolines with excellent enantioselectivities under mild conditions and using very low amounts of catalyst (see scheme). The best results were achieved with the binol phosphate catalyst, where Ar = 9-phenanthryl, used successfully in the Strecker reaction.

Brønsted Acid Catalysis

M. Rueping,* A. P. Antonchick, T. Theissmann ——— **3683 – 3686**

A Highly Enantioselective Brønsted Acid Catalyzed Cascade Reaction: Organocatalytic Transfer Hydrogenation of Quinolines and their Application in the Synthesis of Alkaloids

© 2006 Wiley-VCH Verlag GmbH & Co. KGaA, Weinheim

Contents

Asymmetric Synthesis

D. Soorukram, P. Knochel* **3686 – 3689**

Copper-Catalyzed Preparation of Ketones Bearing a Stereogenic Center in α Position

A highly enantioselective synthesis of α-alkylated and -arylated ketones can be achieved by using a reaction sequence consisting of a stereoselective *anti*-S_N2' allylic substitution in the presence of CuCN·2 LiCl following by the oxidation of an intermediate cycloalkenyl lithium species using $(Me_3SiO)_2$ or $(MeO)_3B$/$NaBO_3 \cdot 4\,H_2O$.

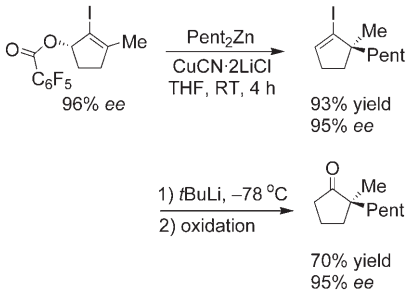

Chiral Solvents

R. Gausepohl, P. Buskens, J. Kleinen, A. Bruckmann, C. W. Lehmann, J. Klankermayer, W. Leitner* **3689 – 3692**

Highly Enantioselective Aza-Baylis–Hillman Reaction in a Chiral Reaction Medium

Let's twist again! The first highly enantioselective asymmetric reaction in which a chiral reaction medium is the sole source of chirality is presented. The aza-Baylis–Hillman reaction in an ionic liquid with a chiral anion, whose design is based on mechanistic insights, gave products with up to 84% *ee*.

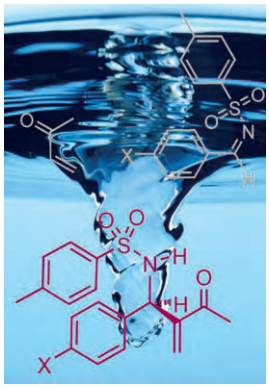

Heterogeneous Catalysis

T. Schalow, B. Brandt, D. E. Starr, M. Laurin, S. K. Shaikhutdinov, S. Schauermann, J. Libuda,* H.-J. Freund **3693 – 3697**

Size-Dependent Oxidation Mechanism of Supported Pd Nanoparticles

The oxidation and reduction of Fe_3O_4-supported Pd nanoparticles is strongly size-dependent and implies that the oxidation mechanism is controlled by the metal oxide interface. Molecular beam experiments and scanning tunneling microscopy indicate that this size dependence gives rise to a pronounced maximum of the oxygen-storage capacity as a function of metal loading.

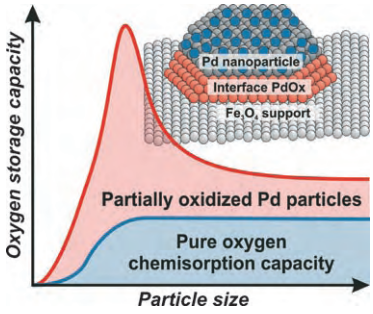

Ionic Liquids

T. Köddermann, C. Wertz, A. Heintz, R. Ludwig* **3697 – 3702**

The Association of Water in Ionic Liquids: A Reliable Measure of Polarity

Water molecules can be used as a sensitive probe for measuring the polarity of ionic liquids (ILs). A combination of FTIR spectroscopy and DFT calculations was used to determine the molecular state of water in ILs. The picture shows a possible configuration of H_2O in 1-ethyl-3-methylimidazolium bis(trifluoromethylsulfonyl)-imide (red O, white H, blue N, black C, yellow S, shaded yellow F).

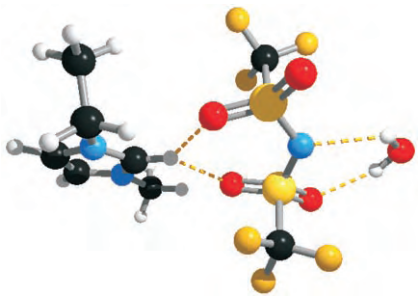

© 2006 Wiley-VCH Verlag GmbH & Co. KGaA, Weinheim

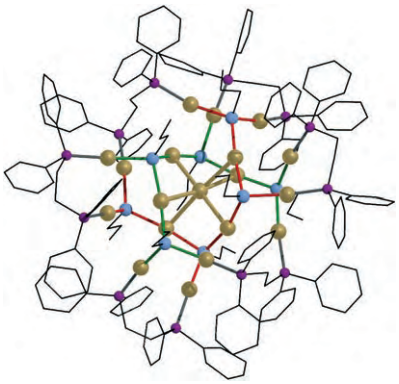

A heart of gold: The reaction of silylated arsenic derivatives with gold(I) phosphine complexes produces gold–arsenic clusters, such as $[Au_{19}(AsnPr)_8(dppe)_6]^{3+}$ ($dppe = Ph_2P(CH_2)_2PPh_2$). This complex cation (see picture; Au gold, As blue, P violet) can be described as two crossing Au_9As_4 chains (red and green), and contains a gold octahedron centered by a gold atom.

Cluster Compounds

P. Sevillano, O. Fuhr, M. Kattannek, P. Nava, O. Hampe, S. Lebedkin, R. Ahlrichs, D. Fenske,* M. M. Kappes ——— **3702 – 3708**

The Phosphine-Stabilized Gold–Arsenic Clusters $[Au_{19}(AsnPr)_8(dppe)_6]Cl_3$, $[Au_{10}(AsnPr)_4(dppe)_4]Cl_2$, $[Au_{17}(AsnPr)_6(As_2nPr_2)(dppm)_6]Cl_3$, and $[Au_{10}(AsPh)_4(dppe)_4]Cl_2$: Synthesis, Characterization, and DFT Calculations

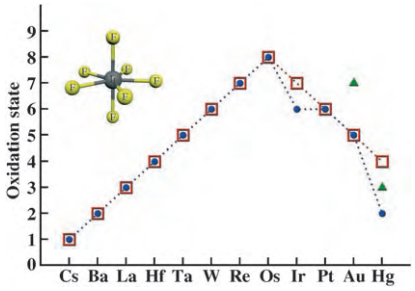

The magnificent VII? High-level quantum chemical calculations show iridium in oxidation state +VII to be a viable synthetic target, whereas higher oxidation states of this element appear unlikely. With the theoretically predicted Ir^{VII} and Hg^{IV} included, a linear descent of maximum oxidation states from Os to Hg is found in the 5d series (see Figure: ● highest experimentally known values, ▲ probably incorrect experimental assignments, and □ most likely predicted values).

High Oxidation States

S. Riedel, M. Kaupp* ——— **3708 – 3711**

Revising the Highest Oxidation States of the 5d Elements: The Case of Iridium(+VII)

Sources

Product and Company Directory

You can start the entry for your company in "Sources" in any issue of *Angewandte Chemie*.

If you would like more information, please do not hesitate to contact us.

Wiley-VCH Verlag – Advertising Department
Tel.: 0 62 01 - 60 65 65
Fax: 0 62 01 - 60 65 50
E-Mail: MSchulz@wiley-vch.de

Service

Keywords ——— *3712*

Authors ——— *3713*

Vacancies ——— *3574, A31*

Preview ——— *3715*

For more information on ChemMedChem see www.chemmedchem.org

© 2006 Wiley-VCH Verlag GmbH & Co. KGaA, Weinheim

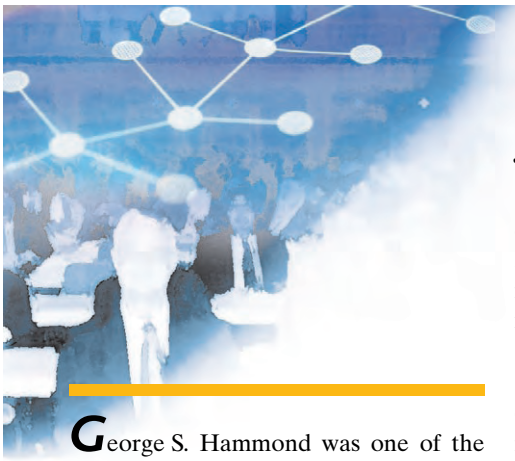

The Many Facets of Photochemistry**

Jochen Mattay

George S. Hammond was one of the initiators of the IUPAC Symposium on Photochemistry, which first took place in 1964 in Strasbourg, France. Since then, this conference has been held biannually in Europe. This year marked the first time the conference was held outside of Europe—in Kyoto, Japan, with Masahiro Irie (Kyushu University) and Atsuhiro Otsuka (Kyoto University) acting as chairmen. The opening presentation of the conference was devoted to George S. Hammond. In an obituary, David Whitten (University of New Mexico, Albuquerque) paid tribute to the personality and scientific work of this pioneer of photochemistry and physical organic chemistry, who passed away in 2005 at the age of 84 (see *Angew. Chem.* **2006**, *118*, 1034; *Angew. Chem. Int. Ed.* **2006**, *45*, 1018).

As in previous years, the numerous presentations this year reflected the interdisciplinary character of photochemistry. The spectrum of topics ranged from the classical fields of chemistry—inorganic, organic, physical, and theoretical chemistry—to physics, biological chemistry, and materials science.

Spectroscopy was one of the central themes. Accordingly, W. E. Moerner (Stanford University, USA) reported on "*Single Molecules as Nanoscale Reporters in Biophysics, Chemistry, and Materials Science*". Frans De Schryver (University of Leuven, Belgium) addressed the same topic with the objective of "*Probing Molecular Properties and the Role of the Environment at Simple Molecule Level*". Niek F. van Hulst (University of Twente, The Netherlands) reported on how "*Ultrafast Femtosecond Single Molecule Spectroscopy Reveals the Effect of Disorder on Exciton Dynamics*". Spectroscopic time resolution plays, of course, a crucial role in this context. Paul Corkum (National Research Council of Canada, Ottawa) discussed in impressive fashion the concept of "*Attosecond Imaging*", a technique that differs fundamentally from femtosecond spectroscopy and will offer completely new insights into reaction dynamics.

Another topic that was covered was photoinduced electron transfer (PET). This process possesses such fundamental significance that it was discussed in many of the presentations from chemistry, materials science, and biologically oriented disciplines. For instance, electron transfer played an important role in Klaus Müllen's (Max Planck Institute, Mainz, Germany) talk on "*Nanoemitters by Design*". Yet this lecture also addressed further important aspects of modern dye chemistry, for example the control of absorption in fluorescence and energy transfer through, among other means, supramolecular assembly. Frank Würthner (University of Würzburg, Germany) also addressed this aspect in his presentation on "*Photoluminescent Arrays and Aggregates Based on Perylene Bisimide Dyes*". Aggregates composed of linear arenes and the role of energy transfer within self-assemblies were discussed by Jean-Pierre Desvergne (Université Bordeaux I, France).

PET as a tool of modern synthetic chemistry remains a topic of current interest. Norbert Hoffmann (Université de Reims, France) reported on the "*Efficient Radical Addition of Tertiary Amines to Alkenes Using Photochemical Electron Transfer*". By providing excellent examples, he demonstrated the wide applicability of the technique he developed.

The basics of PET, as well as its role in biological systems, simple model systems, and materials, were discussed in a workshop. Dirk M. Guldi (University of Erlangen, Germany) outlined "*Novel Opportunities for Electron Transfer—Versatile Carbon Nanostructures*". David I. Schuster (New York University, NY, USA) reported on "*Topological Effects on Electron Transfer in Porphyrin–Fullerene Hybrids*". "*PET to Triplet Flavins*" was presented by Silvia E. Braslavsky (Max Planck Institute, Mülheim, Germany). Michael R. Wasielewski (Northwestern University, USA) discussed "*Photoinduced Charge Separation and Transport in Self-Assembled Biomimetic Systems*". Two engaging and quite controversial presentations on "*Design of Long-Lived Charge-Separated States and Applications*" and "*Long-Lived Charge Transfer States in Compact Dyads; Pitfalls and Opportunities*" were given by Shunichi Fukuzumi (Osaka University, Japan) and Jan W. Verhoeven (University of Amsterdam, The Netherlands), respectively. The latter speaker seriously questioned the unusually long-lived charge-transfer states by presenting his own extensive experiments.

Biological and other aspects of electron transfer and energy transfer were treated in the following presentations. Frederick D. Lewis (Northwestern University, USA) spoke about "*DNA Photonics*", Gary B. Schuster (Georgia Institute of Technology, Atlanta, USA) about "*Long Distance Radical Cation Migration in Duplex DNA*", Monique M. Martin (Ecole Normale Supérieure, Paris, France) about "*Charge Transfer as the Driving Force for the Photoactivity of the Chromophore of Photoactive Yellow Protein in Solution*", and Jaques-E. Moser (EPFL, Lausanne, Switzerland) about "*Dynamics of Light-Induced Interfacial Electron Transfer in the Dye-Sensitization of Nanocrystalline Oxide Semiconductors*".

At a conference organized by Masahiro Irie, it came as no surprise that the subject of photoswitches took on a wide scope. Though the groundwork is already established for this field, photoswitches are currently garnering much interest in chemistry, physics, and the

WILEY InterScience DISCOVER SOMETHING GREAT
© 2006 Wiley-VCH Verlag GmbH & Co. KGaA, Weinheim

life sciences. This trend has come thanks to Masahiro Irie, as the diaryl ethylene chromophore that was developed by him certainly represents one of the most stable and widely applicable photoswitches known. In the numerous poster and oral presentations on the subject, the focus was not just about switching between molecular properties, rather also applications of a quite different sort: switching of spin states, of chirality, of optoelectronic features, of reactivity, of energy and electron transfer, and so on. Jochen Mattay (University of Bielefeld, Germany), in his lecture titled "*On the Way to Supramolecular Photochemistry at the Single Molecule Level*", reported on calixarene–anthracene photoswitches, which were investigated at the single-molecule level by atomic force microscopy. The first application of dynamic force spectroscopy enabled not only the determination of the off rates, but also a "glimpse of the binding pocket" of the host–guest complex. Neil Branda (Simon Fraser University, Canada) reported on "*Relating Photochromism and Reactivity in Molecular Switching*". This lecture as well dealt with the topic of "Irie diaryl switches", which had however been modified in various ways and "trimmed" to meet specific reactions.

Of course, attention was also given in this context to other photochromic systems: as always the classical azobenzene, but also fulgides und especially the spiropyranes, which drastically change polarity upon switching from the "closed" to "open" state.

Light as a "traceless reagent" and control element in biological systems also received much attention. The topics spanned a wide range—from the development of new technologies for imaging, for example the "*Molecular Engineering of Two-Photon Absorbing Molecules for Bioimaging*" as described by Mireille Blanchard-Desce (Université de Rennes, France), to "*Drug-Biomolecule Interactions in the Excited State*", to which the lecture by Miguel A. Miranda (Universidad Politécnica de Valencia, Spain) was devoted.

Heiko Ihmels (University of Siegen, Germany) presented his latest results in his lecture on the "*Detection of Biomolecules with Fluorescent Light-Up Probes*", and Isao Saito (Nihon University, Japan) reported on "*Highly Selective Fluorescent Nucleobases for Designing Base-Discriminating Fluorescence Probes*".

The extent to which photochemistry can play a deciding role in addressing future issues such as solving energy shortages was elucidated in the lecture by Kazunari Domen (The University of Tokyo, Japan), who spoke on an "*Overall Water Splitting Reaction on Non-Oxide Based Photocatalysts*".

The use of fundamental photophysical processes and light-induced charge separation as potential means of energy storage, as they are used in photosynthesis, were also comprehensively investigated in model systems. Franco Scandola (University of Ferrara, Italy) reported on "*Photophysics of Metal-mediated Assemblies of Porphyrins and Perylene Bisimides*", Dongho Kim (Yonsei University, Seoul, Korea) on "*Ultrafast Excitation Energy Migration Processes in Various Multiporphyrin Arrays*", Villy Sundström (Lund University, Sweden) on "*Light-induced Processes in Organic Semiconductors*", David Whitten (University of New Mexico, Albuquerque, USA) on "*Cooperative Self-Assembly of Cyanines and Carboxy-methylamylose*", and Andrew Beeby (University of Durham, UK) on "*An Interesting Twist of Molecular Wires*".

An interesting and technologically meaningful application of photochemical methods was discussed by Lei Jiang (Center of Molecular Sciences, CAS Beijing, P. R. China), who reported on a "*UV-Manipulated Switch between Superhydrophobicity and Superhydrophilicity*".

There were also two workshops devoted to the application of OLEDs and photocatalysis. Peter I. Djurovich (University of Southern California, Los Angeles, USA) reported on "*Blue Phosphorescent Materials for OLEDs*", and Chihaya Adachi (Kyushu University, Japan) on "*Prospects for Organic Semiconductor Lasers from an Organic Solid-State Film*". In the workshop on photocatalysis, Jean-Marie Hermann (Université Lyon, France) gave a talk on "*Photocatalysis in Environmental Green Chemistry*", Akihiko Kudo (Tokyo University of Science, Japan) on "*Development of Powdered Photocatalysts for Water Splitting*", and Jae Sung Lee (Pohang University, Korea) on "*Engineered Nanocomposite Photocatalysts for Visible Light Harvest*".

Out of a total of 462 posters, 131 were selected to be short presentations, and three authors were additionally recognized with prizes: Hisao Shimizu (Toyama University, Japan), A. O. Chapman (University of Nottingham, UK), and Jong Won Chung (Seoul National University, Korea).

The 21st IUPAC Symposium ended with one additional highlight, the awarding of the Porter Medal to Howard E. Zimmerman (University of Wisconsin, Madison, USA) and Hiroshi Masuhara (Osaka University, Japan). Howard Zimmerman, also one of the cofounders of this conference and a pioneer of organic photochemistry, is also known to organic chemists from the Zimmerman–Traxler model, which plays a significant role in stereochemistry. Hiroshi Masuhara has made important contributions in laser physics and laser chemistry which have had an impact in many areas of materials and biological sciences.

This IUPAC Symposium has once again shown just how diverse the many facets of photochemistry are, and it has aroused interest in the next conference in this series, which is anticipated to take place in July 2008 in Göteborg (Sweden).

DOI: 10.1002/anie.200601561

 © 2006 Wiley-VCH Verlag GmbH & Co. KGaA, Weinheim

Molecular Capsules

DOI: 10.1002/anie.200600090

Inorganic Molecular Capsules: From Structure to Function

*Leroy Cronin**

Keywords:
cluster compounds · molecular capsules · polyoxometalates · self-assembly

The assembly of nanoscale capsules or cages using metal coordination represents one of the most interesting and challenging areas of chemical nanoscience. These high-symmetry capsules are invariably comprised of many metal–ligand components, which often self-assemble rapidly and in high yield into a single gigantic species—sometimes even protein-sized.[1] However, the interest in these systems goes far beyond aesthetics. An understanding of the mechanisms of the assembly process that leads to their formation will allow systems with unmatched physical properties and functionalities to be designed from first principles. As the emphasis changes from *structure* to *function*, cages have been constructed that can serve as supramolecular containers, reaction vessels, and ion channel models for biological cells. In this Highlight, the very recent advances in the formation of cages and capsules through metal ion coordination is explored.

The self-assembly process of coordination cages mediated by metal–ligand coordination depends critically upon the building blocks chosen and their respective reactivities. One very important route to the formation of metallosupramolecular architectures involves the selection of building blocks that are preorganized, kinetically stable, that incorporate labile coordination sites, and are complementary. For instance, the $[Pd(en)]^{2+}$ unit (en = ethylenediamine) has emerged as a versatile building block in molecular self-assembly.[2] Importantly, the 90° coordination angle present between one of the blocking groups and one of the labile ligands at the Pd^{II} metal ion has been judiciously used in the design of new discrete two- and three-dimensional structures ranging from cages, bowls, boxes, tubes, catenanes, and spheres. An example of an octahedral cage is $[\{Pd(en)\}_6L_4]^{12+}$ (**1**; Figure 1), which is based on the coordination of six Pd^{II} centers with $[Pd(en)]^{2+}$ corners and four 2,4,6-tris(4-pyridyl)-1,3,5-triazine units. The cage has a large hydrophobic cavity, yet the outer part is hydrophilic. The tricoordinated ligand in **1** is relatively electron-deficient, therefore the cavity binds preferentially electron-rich aromatic guests.

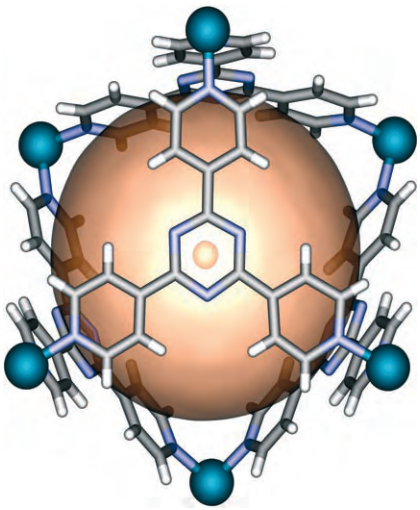

Figure 1. Molecular structure of $[\{Pd(en)\}_6L_4]^{12+}$ (**1**; L = 2,4,6-tris(4-pyridyl)-1,3,5-triazine), in which the Pd^{II} ions occupy the corners of an octahedron (the en ligands and guest molecule are omitted for clarity). The cavity is illustrated by the large orange–brown sphere; Pd^{II} ions blue spheres; stick representation: C gray, N blue, H white.

The cavity of **1** is well-defined stereochemically and is able to control chemical reactions. For example, Diels–Alder reactions are dramatically accelerated by a factor of over 100, and [2+2] photodimerizations of olefins proceed faster and with high regio- and stereoselectivity.[3] The formation of "molecular ice" within variants of **1**, whereby ten water molecules are complexed within the cavity,[4] may help further the understanding of the reactivity and host–guest binding properties of such capsules. Indeed, the sequence-specific binding of tripeptides was observed with capsule **1**,[5] wherein the encapsulation of Trp-Trp-Ala was favored over other sequences and singly mutated tripeptides. The encapsulation of paramagnetic moieties has also revealed interesting results, and the pH-responsive switching of spin–spin interactions of stable organic radicals has been possible in **1**.

The design of a similar cage, **2**, comprising two 2,4,6-tris(4-pyridyl)-1,3,5-triazine units and three 4,4′-bipyridine ligands with six $[Pd(en)]^{2+}$ corner units yielded a pillared cylinder. The organic-pillared nature of the cylinder resulted in interesting guest-binding properties through a combination of interactions. The complexation of tetrathiafulvalene (TTF) allowed the generation of a mixed-valence radical dimer cation within the self-assembled cage **2**.[6] This result is significant because this noncovalently bound species can only be generated in such a cage or by covalent linking. A similar effect is observed in the complexation of **2** with large planar aromatic organic mole-

[*] Prof. L. Cronin
WestCHEM, Department of Chemistry
The University of Glasgow
Glasgow, G12 8QQ (UK)
Fax: (+44) 141-330-4888
E-mail: l.cronin@chem.gla.ac.uk

InterScience
© 2006 Wiley-VCH Verlag GmbH & Co. KGaA, Weinheim

cules[7] and causes the stacking of $[M^{II}(acac)_2]$ moieties (M = Pt, Pd, Cu; acac = acetylacetonate), which exhibit M–M interactions.[8]

Another way to construct spherical capsules with well-defined pores was demonstrated using polyoxometalate-based building blocks. Polyoxometalates are clusters based on MO_x units (typically M = Mo, W, V; $4 \le x \le 7$), which form structures that contain between 6 and 368 metal atoms.[9] Interestingly, even comparably small clusters can display remarkable physical properties as a result of encapsulating electronically or chemically active moieties.[10] However, by far the most interesting cluster types for nanoscience are those with ring and spherical shapes, comprising pentagonal $\{(Mo)Mo_5\}$ (pent) building blocks.[9]

All the spherical and approximately icosahedral clusters have the general formula $[\{(pent)_{12}(link)_{30}\}]$ (link = binuclear linker). One example is the capsule $[\{(Mo)Mo_5O_{21}(H_2O)_6\}_{12}\{Mo_2O_4(L)\}_{30}]^{n-}$ ($n = 72$; L = sulfate), in which 12 central pentagonal units span an icosahedron and the linkers form a distorted truncated icosahedron. The highly charged nanoscale capsule, with an inner cavity diameter of approximately 2.5 nm, allows different types of encapsulations. For example, well-structured large water assemblies (up to 100 molecules) were observed with an onionlike layer structure enforced by the outer shell.[9,11] Most importantly, the capsule contains 20 well-defined pores and the functionalities of the internal shell can be tuned precisely through the nature of the bidentate ligands. With binuclear $\{Mo^{V}_2O_4\}^{2+}$ linkers, the pores are $\{Mo_9O_9\}$ rings with diameters of 0.6–0.8 nm that function as crown ethers. The pores can be reversibly closed, for example, through hydrogen-bonding interactions between guanidinium cations and the rings.[11] In a related smaller capsule with mononuclear linkers, the $\{Mo_6O_6\}$ pores are closed upon complexation with smaller potassium ions.[12]

Perhaps the most intriguing and exciting property of such highly negatively charged capsules is that they can mediate cation transfer from the solution to the inner nanocavity. Indeed, reaction of the above-mentioned 72-fold negatively charged capsule with different cations such as Na^+, Cs^+, Ce^{3+}, $C(NH_2)_3^+$, and $OC(NH_2)NH_3^+$ in aqueous solution leads to assemblies that exhibit well-defined cation separations within the channels of the capsules ("nano-ion-chromatograph" behavior).[13] A temperature-dependent equilibrium process that involves the uptake and release of Li^+ ions through the capsule pores was also observed. In this process, the porous capsule behaves as a semipermeable inorganic membrane, allowing only H_2O and small cations through.[14] Furthermore, the 20 pores of the same capsule that are blocked by protonated urea as "stoppers" could be opened in solution, thus allowing uptake of calcium(II) ions, before closing occured again (see Figure 2).[15] Thus, pore-gating (a model of biological ion transport) can be demonstrated: After initial cation uptake, the negative charge (or more precisely the electrochemical gradient) of the capsule decreases and subsequent cations are resultantly found hydrated outside the pores.[16]

In summary, recent work has shown that the designed assembly of nanoscale capsules by using coordinative interactions can open doors to new areas of chemistry. In particular, parallels can be drawn between such systems under confined conditions and processes in biological cells, such as cell response and ion transport. Generally speaking, matter can be studied under confined conditions; however, new systems resulting from encapsulation often reveal new phenomena that are not observable by bulk-phase investigations. Examples include the study of "confined water" with or without electrolytes, as well as chemical reactions. Programming of the architectures of the inner cluster walls to give well-defined cavities and gated pores results in the specific interaction of capsules with their environments and the selective uptake and binding of guests. The future of capsule systems is exciting, and a better understanding of the principles that underpin the assembly mechanisms of such capsules should allow the designed construction of extremely complex and specifically interacting systems, thus, in the broadest sense, bringing inorganic chemistry to life.

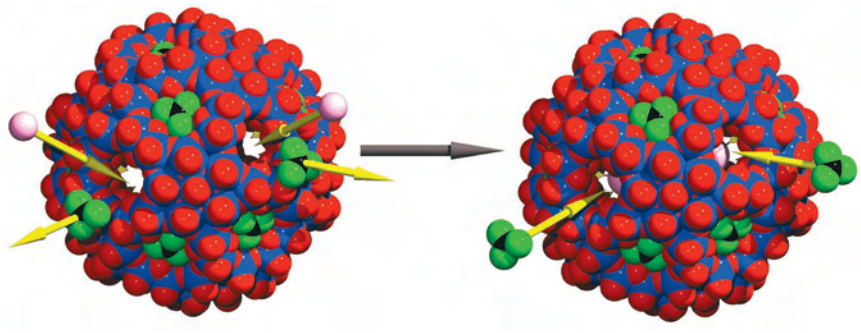

Figure 2. Space-filling representation of $[\{(Mo)(Mo_5O_{21}(H_2O)_6\}_{12}\{Mo_2O_4(SO_4)\}_{30}]^{72-}$ and a simplified view of the uptake of Ca^{2+} ions by the capsule. The pores are initially closed, but treatment of a solution of the capsule with Ca^{2+} ions (pink spheres) leads to cation uptake (left); following their uptake, the pores close again (right). Mo blue, O red, C black, N/O(urea) green; yellow arrows indicate the direction of motion.

[1] A. Müller, E. Krickemeyer, H. Bögge, M. Schmidtmann, B. Botar, M. O. Talismanova, *Angew. Chem.* **2003**, *115*, 2131; *Angew. Chem. Int. Ed.* **2003**, *42*, 2085.

[2] a) M. Fujita, M. Tominaga, A. Hori, B. Therrien, *Acc. Chem. Res.* **2005**, *38*, 371; b) S. R. Seidel, P. J. Stang, *Acc. Chem. Res.* **2002**, *35*, 972.

[3] M. Yoshizawa, Y. Takeyama, T. Kusukawa, M. Fujita, *Angew. Chem.* **2002**, *114*, 1403; *Angew. Chem. Int. Ed.* **2002**, *41*, 1347.

[4] M. Yoshizawa, T. Kusukawa, M. Kawano, T. Ohhara, I. Tanaka, K. Kurihara, N. Niimura, M. Fujita, *J. Am. Chem. Soc.* **2005**, *127*, 2798.

[5] S. Tashiro, M. Tominaga, M. Kawano, B. Therrien, T. Ozeki, M. Fujita, *J. Am. Chem. Soc.* **2005**, *127*, 4546.

[6] M. Yoshizawa, K. Kumazawa, M. Fujita, *J. Am. Chem. Soc.* **2005**, *127*, 13456.

[7] M. Yoshizawa, J. Nakagawa, K. Kurnazawa, M. Nagao, M. Kawano, T. Ozeki, M. Fujita, *Angew. Chem.* **2005**, *117*, 1844; *Angew. Chem. Int. Ed.* **2005**, *44*, 1810.

 © 2006 Wiley-VCH Verlag GmbH & Co. KGaA, Weinheim

[8] M. Yoshizawa, K. Ono, K. Kumazawa, T. Kato, M. Fujita, *J. Am. Chem. Soc.* **2005**, *127*, 10800.
[9] L. Cronin in *Comprehensive Coordination Chemistry II*, *Vol. 7* (Eds.: J. A. McCleverty, T. J. Meyer), Elsevier, Amsterdam, **2004**, pp. 1–56.
[10] a) D. L. Long, P. Kögerler, L. Cronin, *Angew. Chem.* **2004**, *116*, 1853; *Angew. Chem. Int. Ed.* **2004**, *43*, 1817; b) D. L. Long, H. Abbas, P. Kögerler, L. Cronin, *Angew. Chem.* **2005**, *117*, 3481; *Angew. Chem. Int. Ed.* **2005**, *44*, 3415.
[11] A. Müller, E. Krickemeyer, H. Bögge, M. Schmidtmann, S. Roy, A. Berkle, *Angew. Chem.* **2002**, *114*, 3756; *Angew. Chem. Int. Ed.* **2002**, *41*, 3604.
[12] A. Müller, B. Botar, H. Bögge, P. Kögerler, A. Berkle, *Chem. Commun.* **2002**, 2944.
[13] A. Müller, S. K. Das, S. Talismanov, S. Roy, E. Beckmann, H. Bögge, M. Schmidtmann, A. Merca, A. Berkle, L. Allouche, Y. S. Zhou, L. J. Zhang, *Angew. Chem.* **2003** *115*, 5193; *Angew. Chem. Int. Ed.* **2003**, *42*, 5039.
[14] a) A. Müller, D. Rehder, E. T. K. Haupt, A. Merca, H. Bögge, M. Schmidtmann, G. Heinze-Brückner, *Angew. Chem.* **2004**, *116*, 4566; *Angew. Chem. Int. Ed.* **2004**, *43*, 4466; Corrigendum: A. Müller, D. Rehder, E. T. K. Haupt, A. Merca, H. Bögge, M. Schmidtmann, G. Heinze-Brückner, *Angew. Chem.* **2004**, *116*, 5225; *Angew. Chem. Int. Ed.* **2004**, *43*, 5115; b) E. T. K. Haupt, C. Wontorra, D. Rehder, A. Müller, *Chem. Commun.* **2005**, 3912.
[15] A. Müller, L. Toma, H. Bögge, C. Schäffer, A. Stammler, *Angew. Chem.* **2005**, *117*, 7935; *Angew. Chem. Int. Ed.* **2005**, *44*, 7757.
[16] A. Müller, Y. Zhou, H. Bögge, M. Schmidtmann, T. Mitra, E. T. K. Haupt, A. Berkle, *Angew. Chem.* **2006**, *118*, 474; *Angew. Chem. Int. Ed.* **2006**, *45*, 460.

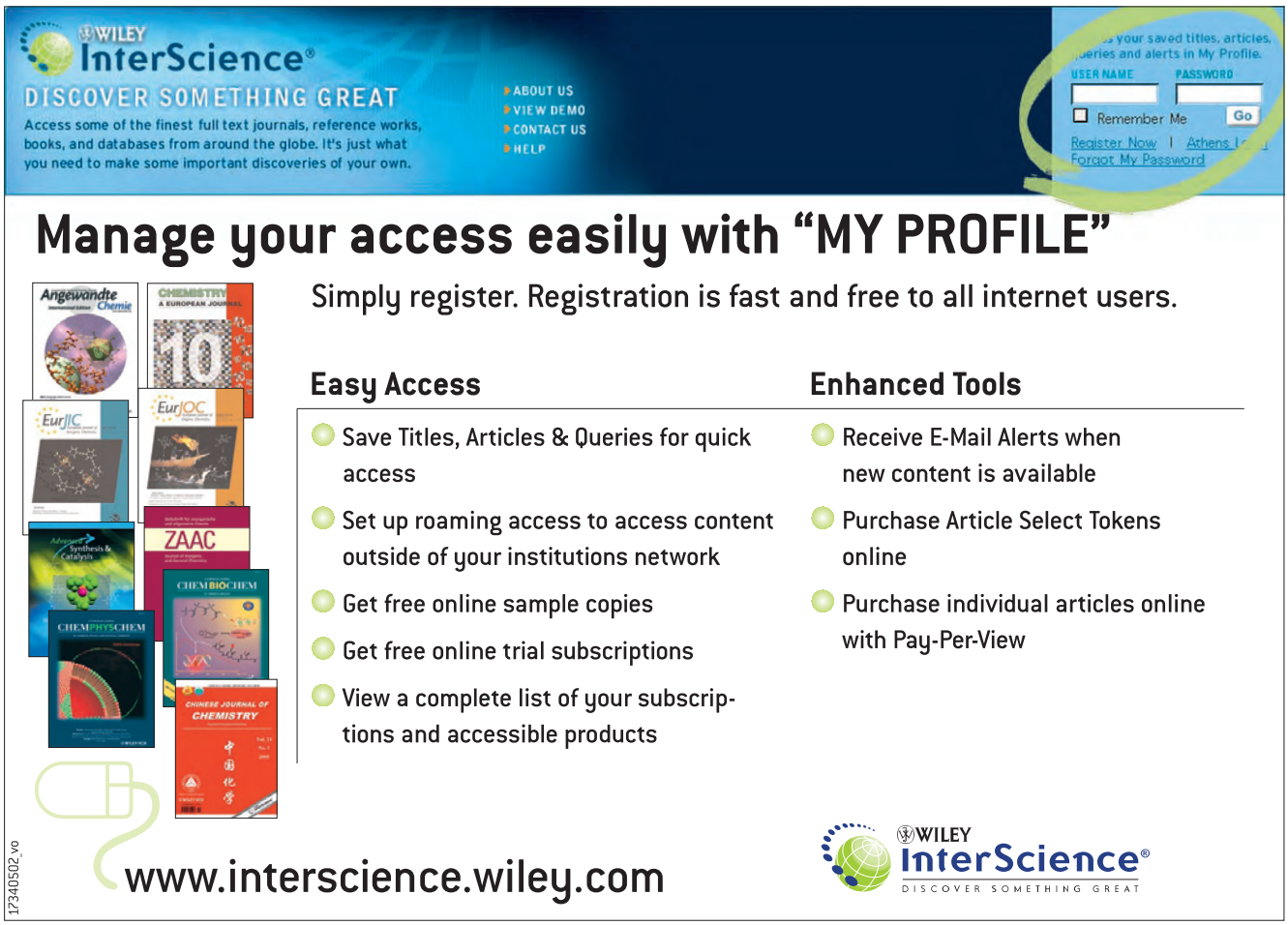

 © 2006 Wiley-VCH Verlag GmbH & Co. KGaA, Weinheim

DOI: 10.1002/anie.200600291

Aryne Insertions

Insertion of Arynes into σ Bonds**

Diego Peña, Dolores Pérez, and Enrique Guitián**

Dedicated to Professor Rafael Suau on the occasion of his 60th birthday

Keywords:
arenes · arynes · insertion · palladium · stannanes

It is well known that the high strain created by the formal triple bond of arynes makes these compounds powerful electrophiles.[1] The addition of a nucleophile X to benzyne leads to the formation of an aryl carbanion that can be trapped with an electrophile Y. If X and Y belong to the same molecule, with a σ bond between them, the overall process is usually the formal insertion of the aryne into the X–Y bond (Scheme 1). If X and Y are linked by

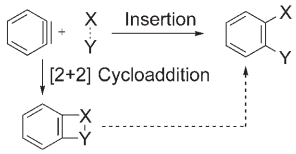

Scheme 1. Insertion of benzyne into an X–Y bond (X is a nucleophile, while Y is an electrophile).

multiple bonds, a formal [2+2] cycloaddition can result in the formation of a four-membered ring, which in some cases can be opened to obtain the insertion product.

Some insertions of this type have been extensively discussed with respect to arynes. Typical examples are the additions of alcohols and amines (XY = OH or NH) to arynes which can be considered formally as the insertion of the aryne into a heteroatom–hydrogen bond.[2] Another frequently studied insertion is the addition of organometallic reagents with strongly polarized carbon–metal bonds (e.g. XY = CLi or CMg) or heteroatom–metal bonds (e.g. XY = NLi, OLi, NMg, or SMg) which leads to aryl carbanions that can subsequently be trapped with external electrophiles.[3]

Apart from the examples described above, the insertion of arynes into σ bonds was only reported sporadically during the second half of the 20th century. Although it was shown that benzyne can insert into P–P,[4a] O–C,[4b] O–B,[4c] Cl–Sn,[4d] I–I,[4e] Se–Se,[4f] C–C,[4g,h] C–Si,[4i] and S–S[4j] bonds, interest in these reactions decreased as a result of low insertion yields, the formation of complex mixtures, harsh reaction conditions, difficulties in the preparation of aryne precursors, and limited scope regarding substitution on the aromatic ring.

As for the related insertion of alkynes into σ bonds, the story was completely different. The introduction of transition-metal catalysis led to growing activity in this field during the 1990s, resulting in the development of efficient protocols for the insertion of alkynes into Si–Si, C–Si, B–Si, B–Sn, and C–Sn bonds, among others.[5] The finding that arynes can undergo transition metal-catalyzed reactions[6] opened new perspectives for aryne insertions. In 2001, Shirakawa, Hiyama, and co-workers showed that a palladium catalyst that promotes the insertion of alkynes into C–Sn bonds[7] could also induce the carbostannylation of arynes to afford *ortho*-substituted arylstannanes (Table 1, entry 1).[8] The reaction is probably initiated by oxidative addition of organostannane **2** to the Pd^0 complex, after which insertion of benzyne into the Sn–Pd or C–Pd bond, followed by reductive elimination, would afford *ortho*-substituted arylstannane **3** (Scheme 2). An alternative mechanism initiated by the coordination of benzyne to palladium and reaction of the resulting complex with the organostannane was also proposed.[8]

A key to the success of the above reaction is the generation of benzyne by treatment of commercially available *ortho*-(trimethylsilyl)phenyl triflate (**1**) with fluoride.[9] Whereas previous aryne insertions had generated benzyne by using strong bases, stoichiometric amounts of alkaline earth metals, or thermal decomposition of precursors,[4] treatment of **1** with fluoride can be carried out under neutral conditions and at moderate temperatures. Thus, it is compatible with transition-metal catalysts, with a broad range of substituents on the aromatic ring, and with most reaction partners.

Shirakawa, Hiyama, and co-workers then reported the first insertion of benzyne into the N–CO bond of ureas, obtaining 1-amino-2-(aminocarbonyl)-arenes (Table 1, entry 2).[10] The nucleophilicity of nitrogen is presumably sufficient to bring about addition of the urea moiety to benzyne and thereby activate the σ bond, without any need for a transition-metal catalyst (Scheme 3). The corresponding zwitterion, **5**, would then evolve through intramolecular nucleophilic substitution at the carbonyl carbon atom to give the amides **7**.

Recently, Yoshida, Kunai, and co-workers reported the insertion of arynes into several other σ bonds. The insertions into Si–Si[11] and Sn–Sn[12] bonds involved homogeneous catalysis based

[*] Dr. D. Peña, Prof. Dr. D. Pérez, Prof. Dr. E. Guitián
Departamento de Química Orgánica
Facultad de Química
Universidad de Santiago de Compostela
15782 Santiago de Compostela (Spain)
Fax: (+34) 981-59-1014
E-mail: qodpena@usc.es
qoenrgui@usc.es

[**] Financial support from the Spanish Ministry of Education and Science (MEC, CTQ2004-05752), FEDER, and Xunta de Galicia (DXID, 05PXIC20904PN) is gratefully acknowledged. D. Peña thanks the MEC for the award of a Ramón y Cajal research contract.

© 2006 Wiley-VCH Verlag GmbH & Co. KGaA, Weinheim

Table 1: Recent examples of the insertion of benzyne into σ bonds.

Entry	Substrate	X–Y	Cat.	Product	Ref.
1	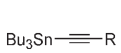	Sn–C	Pd	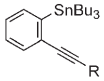	[8]
2	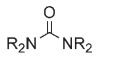	N–C	–	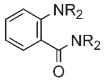	[10]
3	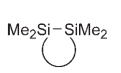	Si–Si	Pd	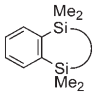	[11]
4[a]	$R_3Sn–SnR_3$	Sn–Sn	Pd	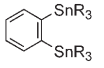	[12a]
5[b]	$R_3Sn–SnR_3$	Sn–Sn	Pd	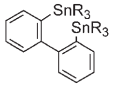	[12b]
6	$ArS–SnR_3$	S–Sn	–	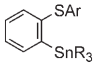	[13a]
7	$R_2N–SiMe_2Ph$	N–Si	–	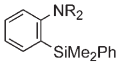	[13b]
8	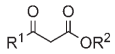	C–C	–	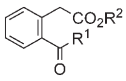	[14, 15a]
9	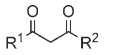	C–C	–	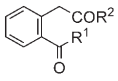	[15a]
10	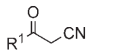	C–C	–	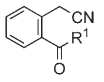	[15b]
11	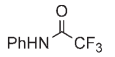	N–C	–	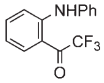	[16]
12	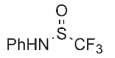	N–S	–	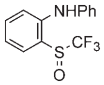	[16]
13	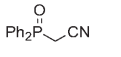	C–P	–	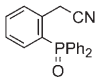	[17]

[a] An isocyanide was used as ligand. [b] A bicyclic phosphite was used as ligand.

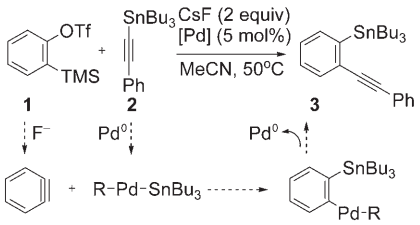

Scheme 2. Palladium-catalyzed carbostannylation of benzyne. TMS = trimethylsilyl; Tf = trifluoromethanesulfonyl.

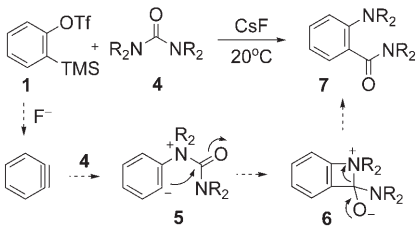

Scheme 3. Addition of ureas to benzyne.

on palladium complexes (Table 1, entries 3 and 4), but the insertions into S–Sn[13a] and N–Si[13b] bonds proceeded in the absence of catalyst (Table 1, entries 6 and 7). Curiously, by appropriate choice of the palladium catalyst the reaction with distannanes could be selectively directed either toward the insertion of one or two arynes into the Sn–Sn σ bond (Table 1, entries 4 and 5). Notably, in all these reactions benzyne was generated by the same method, namely fluoride-induced decomposition of *ortho*-(trimethylsilyl)phenyl triflate (**1**).

Tambar and Stoltz recently reported an efficient process for the acyl-alkylation of arynes by insertion of these intermediates into the α,β C–C bond of β-ketoesters (Table 1, entry 8).[14] Although there were precedents for this type of insertion,[4g,h] the mildness of this reaction and its efficiency in the formation of two new C–C bonds make it especially useful for the synthesis of *ortho*-disubstituted arenes. Other recent reports include the insertion of benzyne into C–C bonds of β-dicarbonyl[15a] and α-cyanocarbonyl[15b] compounds (Table 1, entries 8–10), the insertion of arynes into the N–C bonds of amides and the N–S bonds of sulfinamides (Table 1, entries 11 and 12),[16] and the carbophosphinylation of arynes with cyanomethyldiphenylphosphine oxide (Table 1, entry 13).[17]

Reports of the insertion of arynes into multiple bonds are rarer. Among the few examples reported so far are the insertions of benzyne into C=P[18a] and C=C[18b] double bonds, which probably involve [2+2] cycloaddition followed by the opening of the resulting four-membered ring (Scheme 1). Recently, Yoshida et al. reported the insertion of benzyne into the C=O double bond of aldehydes (Scheme 4), which produces

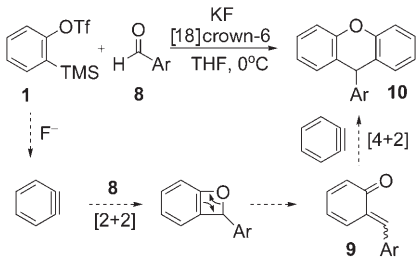

Scheme 4. Insertion of benzyne into C=O bonds.

o-quinoid intermediates **9** that afford xanthenes **10** when subsequently trapped by [4+2] cycloaddition of another molecule of benzyne.[19]

In conclusion, the insertion of arynes into σ bonds has undergone a remarkable revival over the past few years. The key to this surprising resurgence seems to be the use of a high-yielding method for the generation of benzyne and its derivatives under mild reaction conditions from commercially available or easily prepared aryne precursors. The

 © 2006 Wiley-VCH Verlag GmbH & Co. KGaA, Weinheim

instances reported so far suggest that aryne insertion has a promising future as a means of preparing complex *ortho*-disubstituted arenes, as it is compatible with a broad range of substituents on the aryne. We predict the rapid expansion of this methodology in the near future, with respect not only to insertions into σ bonds between other pairs of elements and into a variety of multiple bonds (probably with the help of metal complexes as bond-activating catalysts) but also in the development of enantioselective versions.

Published online: May 3, 2006

[1] a) R. W. Hoffmann, *Dehydrobenzene and Cycloalkynes*, Academic Press, New York, **1967**; b) H. Pellissier, M. Santelli, *Tetrahedron* **2003**, *59*, 701 – 730.

[2] For recent examples of these reactions resulting in the N- or O-arylation of amines or phenols, see: a) Z. Liu, R. C. Larock, *Org. Lett.* **2003**, *5*, 4673 – 4675; b) Z. Liu, R. C. Larock, *Org. Lett.* **2004**, *6*, 99 – 102.

[3] For a recent example of the insertion of arynes into SMg and NMg bonds, see: W. Lin, I. Sapountzis, P. Knochel, *Angew. Chem.* **2005**, *117*, 4330 – 4333; *Angew. Chem. Int. Ed.* **2005**, *44*, 4258 – 4261.

[4] a) J. Chatt, F. A. Hart, H. C. Fielding (Imperial Chemical Industries Ltd.), US 2922819, **1960** [*Chem. Abstr.* **1960**, 54, 9847b]; b) M. Stiles, U. Burckhardt, A. Haag, *J. Org. Chem.* **1962**, *27*, 4715 – 4716; c) C.-L. Tseng, K.-M. Chang, S.-H. Tung, *Hua Hsueh Hsueh Pao* **1964**, *30*, 415 – 417 [*Chem. Abstr.* **1964**, 61, 16084h]; d) C.-L. Tseng, S.-H. Tung, K.-M. Chang, *Ko Hsueh Tung Pao* **1964**, *2*, 165 – 166 [*Chem. Abstr.* **1964**, 61, 7035h]; e) L. Friedman, F. M. Logullo, *Angew. Chem.* **1965**, *77*, 217 – 218; *Angew. Chem. Int. Ed. Engl.* **1965**, *4*, 239 – 240; f) N. Petragnani, V. G. Toscano, *Chem. Ber.* **1970**, *103*, 1652 – 1653; g) P. Caubere, *Acc. Chem. Res.* **1974**, *7*, 301 – 308; h) E. R. Biehl, S. P. Khanapure, *Acc. Chem. Res.* **1989**, *22*, 275 – 281; i) Y. Sato, Y. Kobayashi, M. Sugiura, H. Shirai, *J. Org. Chem.* **1978**, *43*, 199 – 202; j) J. Nakayama, T. Tajiri, M. Hoshino, *Bull. Chem. Soc. Jpn.* **1986**, *59*, 2907 – 2908.

[5] K. Oshima in *Handbook of Organopalladium Chemistry for Organic Synthesis* (Ed.: E. Negishi), Wiley, New York, **2002**, pp. 2825 – 2839.

[6] a) D. Peña, S. Escudero, D. Pérez, E. Guitián, L. Castedo, *Angew. Chem.* **1998**, *110*, 2804 – 2806; *Angew. Chem. Int. Ed.* **1998**, *37*, 2659 – 2661; b) D. Peña, D. Pérez, E. Guitián, L. Castedo, *J. Am. Chem. Soc.* **1999**, *121*, 5827 – 5828.

[7] E. Shirakawa, H. Yoshida, T. Kurahashi, Y. Nakao, T. Hiyama, *J. Am. Chem. Soc.* **1998**, *120*, 2975 – 2976.

[8] H. Yoshida, Y. Honda, E. Shirakawa, T. Hiyama, *Chem. Commun.* **2001**, 1880 – 1881.

[9] a) Y. Himeshima, T. Sonoda, H. Kobayashi, *Chem. Lett.* **1983**, 1211 – 1214; b) D. Peña, A. Cobas, D. Pérez, E. Guitián, *Synthesis* **2002**, 1454 – 1458.

[10] H. Yoshida, E. Shirakawa, Y. Honda, T. Hiyama, *Angew. Chem.* **2002**, *114*, 3381 – 3383; *Angew. Chem. Int. Ed.* **2002**, *41*, 3247 – 3249.

[11] a) H. Yoshida, J. Ikadai, M. Shudo, J. Ohshita, A. Kunai, *J. Am. Chem. Soc.* **2003**, *125*, 6638 – 6639; b) H. Yoshida, J. Ikadai, M. Shudo, J. Ohshita, A. Kunai, *Organometallics* **2005**, *24*, 156 – 162.

[12] a) H. Yoshida, K. Tanino, J. Ohshita, A. Kunai, *Angew. Chem.* **2004**, *116*, 5162 – 5165; *Angew. Chem. Int. Ed.* **2004**, *43*, 5052 – 5055; for an example of a modification of this reaction to obtain 2,2′-distannylbiaryls, see: b) H. Yoshida, K. Tanino, J. Ohshita, A. Kunai, *Chem. Commun.* **2005**, 5678 – 5680.

[13] a) H. Yoshida, T. Terayama, J. Ohshita, A. Kunai, *Chem. Commun.* **2004**, 1980 – 1981; b) H. Yoshida, T. Minabe, J. Ohshita, A. Kunai, *Chem. Commun.* **2005**, 3454 – 3456.

[14] U. K. Tambar, B. M. Stoltz, *J. Am. Chem. Soc.* **2005**, *127*, 5340 – 5341.

[15] a) H. Yoshida, M. Watanabe, J. Ohshita, A. Kunai, *Chem. Commun.* **2005**, 3292 – 3294; b) H. Yoshida, M. Watanabe, J. Ohshita, A. Kunai, *Tetrahedron Lett.* **2005**, *46*, 6729 – 6731.

[16] Z. Liu, R. C. Larock, *J. Am. Chem. Soc.* **2005**, *127*, 13112 – 13113.

[17] H. Yoshida, M. Watanabe, J. Ohshita, A. Kunai, *Chem. Lett.* **2005**, *34*, 1538 – 1539.

[18] a) E. Zbiral, *Tetrahedron Lett.* **1964**, *5*, 3963 – 3967; b) S. Miki, T. Ema, R. Shimizu, H. Nakatsuji, Z. Yoshida, *Tetrahedron Lett.* **1992**, *33*, 1619 – 1620.

[19] H. Yoshida, M. Watanabe, H. Fukushima, J. Ohshita, A. Kunai, *Org. Lett.* **2004**, *6*, 4049 – 4051.

 © 2006 Wiley-VCH Verlag GmbH & Co. KGaA, Weinheim

Explosives

DOI: 10.1002/anie.200504236

Energetic Nitrogen-Rich Salts and Ionic Liquids**

*Rajendra P. Singh, Rajendar D. Verma, Dayal T. Meshri, and Jean'ne M. Shreeve**

Keywords:
density · energetic salts · heat of formation · ionic liquids · thermochemistry

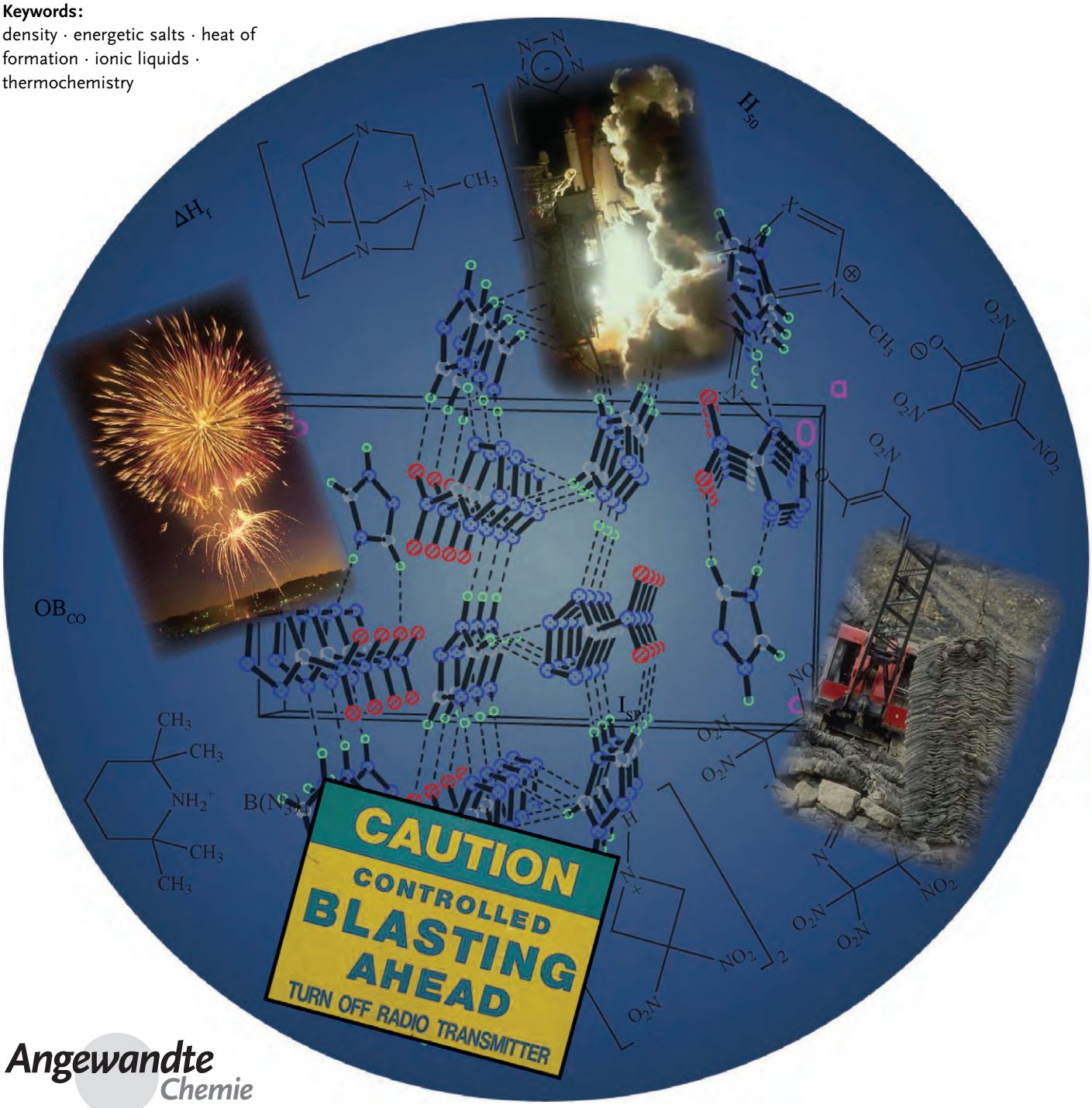

© 2006 Wiley-VCH Verlag GmbH & Co. KGaA, Weinheim

Energetic salts offer many advantages over conventional energetic molecular compounds. The use of nitrogen containing anions and cations contributes to high heats of formations and high densities. Their low carbon and hydrogen content gives rise to a good oxygen balance. The decomposition of these compounds is predominantly through the generation of dinitrogen which makes them very promising candidates for highly energetic materials for industrial or military applications.

From the Contents

1. Introduction	3585
2. Triazolium-Based Ionic Salts	3586
3. Tetrazole-Based Salts	3591
4. Urotropinium-Based Salts	3595
5. Tetrazine-Based Salts	3596
6. Azetidinium-Based Salts	3597
7. Picrate-Based Salts	3597
8. Polynitrogen-Containing Salts	3598
9. Imidazolium-Based Salts	3599
10. Miscellaneous	3599
11. Conclusion	3600

1. Introduction

More energetic materials are consumed in peaceful applications than in armed conflict; modern advances and modern life would be impossible without such energetic species. Energetic materials store relatively large amounts of energy in a compact and readily deliverable form. The power output is a function of the rate at which energy is liberated. Wherever a readily controllable source of energy is required for periods of time ranging from milliseconds (in guns) to many seconds (in rockets), propellants which evolve gases are employed. They are used for propelling projectiles and rockets, shearing bolts and wires, driving turbines, operating pumps, moving pistons, and starting engines. When very rapid rates of energy application and high pressures are essential, explosives are employed. They are used to produce high-intensity shock waves in air, water, and rock; for blasting, mining, cratering, and other civil engineering purposes; for cutting, metal welding and forming, and fragmentation; in shaped charges and many specialty devices requiring high rates of energy transmission; and for initiation of detonation phenomena. More than 90% of the energetic materials used for industrial purposes are ammonium nitrate based.[1] The single-component explosives most commonly used for military compositions are HMX (1,3,5,7-tetranitro-1,3,5,7-tetraazacyclooctane), RDX (1,3,5-trinitro-1,3,5-triazacyclohexane), or TNT (2,4,6-trinitrotoluene), nitroglycerin, and nitrocellulose.[1–12]

There are research programs worldwide to develop high-energy density materials (HEDM) with higher performance and/or enhanced insensitivity with respect to thermal shock, friction, and electrostatic discharge. These modern HEDMs derive most of their energy either from: 1) oxidation of the carbon backbone, as with traditional energetic materials[13,14] or 2) their very high positive heats of formation. Examples of the first class are: TNT, RDX, and HMX.[15] Examples of the second class of energetic materials include modern nitrocompounds, such as: CL-20 (2,4,6,8,10,12-(hexanitrohexaaza)cyclododecane),[16,17] TNAZ (1,3,3-trinitroazetidine), FOX-7 (1,1-diamino-2,2-dinitroethene),[18] hepta- and octanitrocubanes (which have high densities and energies arising from their substantial cage strain), 3,3′-azobis(6-amino-1,2,4,5-tetrazine), and tetrazole azide.

Recently, a new group of energetic ionic salts containing a large number of nitrogen atoms has been studied. These so-called "high-nitrogen" compounds form a unique class of energetic materials whose energy is derived from their very high heats of formation rather than from the overall heat of combustion. The high heat of formation is directly attributable to the large number of energetic N–N and C–N bonds.[19] Generally, heterocyclic molecular compounds have been utilized in energetic roles owing to their higher heats of formation, density, and oxygen balance compared to those of their carbocyclic analogues. Heterocyclic rings (containing amino, nitro, or azide substituents) paired with nitrate, perchlorate, dinitramide, or picrate anions form highly energetic salts. These energetic ionic salts are more environmentally acceptable (with the exception of perchlorate), since a higher percentage of their decomposition products is dinitrogen. Another area of increasing interest is based on high-energy ionic salts in which both the cation and the anion are high-nitrogen species. These energetic ionic salts possess advantages over non-ionic molecules owing to their lower vapor pressures and higher densities. While the use of high-nitrogen compounds is likely to be limited because of cost, the

[*] Prof. R. D. Verma, Prof. J. M. Shreeve
Department of Chemistry
University of Idaho
Moscow, ID 83844-2343 (USA)
Fax: (+1) 208-885-9146
E-mail: jshreeve@uidaho.edu
Dr. R. P. Singh, Dr. D. T. Meshri
Advance Research Chemicals, Inc.
1110 W. Keystone Avenue, Catoosa, OK 74015 (USA)

[**] J.M.S. acknowledges the AFOSR (F49620-03-1-0209), NSF (CHE0315275), and ONR (N00014-02-1-0600) for support of work accomplished at the University of Idaho.

Supporting information for this article is available on the WWW under http://www.angewandte.org or from the author.

 © 2006 Wiley-VCH Verlag GmbH & Co. KGaA, Weinheim

main advantages of such compounds would be for tactical missiles (low signature) and for applications where low flame temperature (low gun-barrel corrosion) or low smoke production are advantageous.

Although ionic liquids have been known for nearly a century, interest in exploring ionic liquids as high-energy materials, explosives, and propellants has grown markedly in recent years. The tunable properties associated with ionic liquids, such as melting point $<100\,^{\circ}C$, low vapor pressure, long liquid range, high thermal and hydrolytic stabilities, and high density make them likely candidates for energetic applications. Most hydrolytically stable ionic liquids have organic cations and inorganic polyatomic anions. Ionic liquids have been used as solvents and catalysts in green chemistry, and their chemistry has been summarized in several reviews.[20–25]

Over the past few years a large number of publications describing energetic ionic salts and energetic ionic liquids have appeared but no comprehensive Review of these materials is currently available. Our continuing interest in this subject prompts us to review this burgeoning field. This Review covers the chemistry of energetic ionic salts, including energetic ionic liquids, from 1999 to the end of 2005.

2. Triazolium-Based Ionic Salts

Triazoles are five-membered aromatic heterocycles that contain three nitrogen atoms located at the 1,2,4- or 1,2,3-positions in the ring. A large number of ionic salts that contain a triazole derivative have been reported to be energetic materials.

2.1. 1,2,4- and 1,2,3-Triazolium Salts

1,2,4-Triazole and 1,2,3-triazole have positive heats of formation of 109 kJ mol^{-1} and 272 kJ mol^{-1}, respectively.[26,27] The ionic salts consisting of either of the protonated heterocyclic cations paired with nitrate, perchlorate, and dinitramide anions were the first to be synthesized.[28] Reactions of 1,2,4-triazole or its 1,2,3-isomer with concentrated nitric acid, perchloric acid, and dinitramidic acid gave excellent yields of 1,2,4- or 1,2,3-triazolium nitrate (**1a**) or (**2a**), perchlorate (**1b**) or (**2b**), and dinitramide (**1c**) or (**2c**), respectively (Scheme 1). All the salts were characterized by IR, Raman,

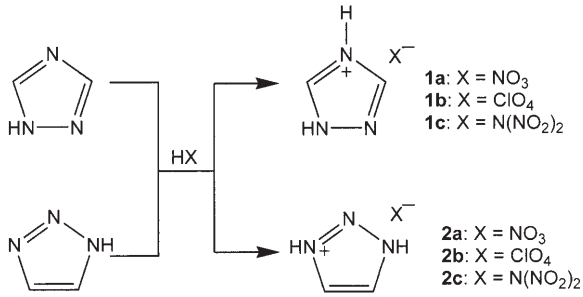

Scheme 1.

Rajendra P. Singh was born in India and obtained his Ph.D. in 1985 from Banaras Hindu University. After several teaching and research projects in Japan and India, he worked for two years as an ERATO researcher with Prof. Ryoji Noyori. In 1995, he became a post-doctoral fellow with Professor D. S. Matteson at Washington State University before he joined the University of Idaho's fluorine research group in 1998. Since March 2003, he has been associate research director at Advance Research Chemicals, Inc. His research interests center around the development of new synthetic methodologies in organofluorine chemistry.

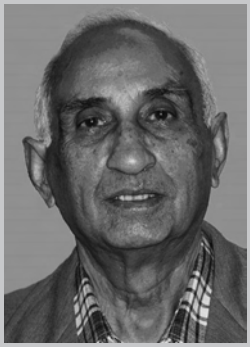

Rajendar D. Verma was born in Amritsar (India). He received his M.Sc. from Birla Institute of Technology and Science, Pilani in 1955. He taught in a degree college for 8 years before joining Panjab University, Chandigarh as a research student in 1963. He was appointed a Lecturer in Chemistry in 1966 and received his Ph.D. in 1968. He established a fluorine research group at Panjab University Department of Chemistry. Professor Verma retired in 1996. He had the privilege of collaborating with Professors George H. Cady, Charles B. Colburn, and Jean'ne M. Shreeve.

Dayal Meshri was born in British India. He received his B.Sc. from Gujarat University, M.Sc. from the MR Institute of Science, his Ph.D. from the University of Idaho, and did postdoctoral work at Cornell University. He then joined Ozark-Mahoning Co.-Pennwalt Corp. as Head of Research and Research Director. In 1987, he founded Advance Research Chemicals, Inc. (ARC) where he is President and CEO. ARC has become one of the largest inorganic fluoride specialty chemical producers in the world and delivers to automobile, electronic, semiconductor, plastic, and pharmaceutical industries.

Jean'ne M. Shreeve is a Montana native. She received a B.A. in chemistry from the University of Montana, an M.S. in analytical chemistry from the University of Minnesota, and a Ph.D. in inorganic chemistry from the University of Washington, Seattle. She joined the University of Idaho faculty in 1961, became department head in 1973, and in 1987, assumed the role of Vice-President for Research and Graduate Studies. Since July 2004, she has been the Jean'ne M. Shreeve Professor of Chemistry. Her research interests include the syntheses, characterization, and reactions of new fluorine-containing compounds as well as energetic compounds.

 © 2006 Wiley-VCH Verlag GmbH & Co. KGaA, Weinheim

and NMR spectroscopy, material balance, density determination, elemental analysis, DSC (differential scanning calorimetry), TGA (thermogravimetric analysis), and initial safety testing. 1,2,3-Triazolium salts melt at lower temperatures than their 1,2,4-triazolium analogues (Table S1 in the Supporting Information). Some of these salts (**1b**,**c**, **2a–c**) have melting points $<100\,^{\circ}C$, categorizing them as ionic liquids. These salts are energetic and are stable at moderate temperatures, with the two perchlorate salts the most thermally stable and the dinitramides the least. A single-crystal X-ray diffraction study of **1b** showed significant hydrogen bonding between the perchlorate anion and the protonated 1,2,4-triazolium ring, which contributes to its relatively high density of 1.96 $g\,cm^{-3}$. Interestingly, the 1,2,3-triazolium perchlorate is nearly 0.2 $g\,cm^{-3}$ less dense, which is attributable to less efficient packing in the crystal.

2.2. Triazolium Salts Containing Amino Substituents

From the analysis of the structures of thermally stable explosives, it has been found that the incorporation of amino groups into a heterocyclic triazole ring is one of the simplest routes to enhance thermal stability.[6] The N-amino group behaves as an electron withdrawing group in these high-nitrogen heterocycles that, when paired with nitrate, perchlorate or dinitramide anions, form energetic salts. 4-Amino-1,2,4-triazolium salts (**3a–c**; Scheme 2), are formed by the reaction of 4-amino-1,2,4-triazole with concentrated HNO_3, $HClO_4$, and $HN(NO_2)_2$, respectively, under reaction conditions as utilized for **1a–c** and **2a–c**.[28]

1-Amino-1,2,4-triazole with concentrated HNO_3 or $HClO_4$ led to the formation of the corresponding salts (**4a**) and (**4b**) in excellent yields (Scheme 2).[29] When 1-amino-1,2,4-triazole was treated with iodomethane, a quaternary salt (**5**) was produced that underwent metathesis with $AgNO_3$ or $AgClO_4$ to give high yields of the corresponding nitrate (**6a**) and perchlorate (**6b**) salts, respectively. Similarly when 1-methyl-4-amino-1,2,4-triazolium iodide (**7**) under went metathesis with $AgNO_3$ or $AgClO_4$, the nitrate (**8a**) and perchlorate (**8b**) were formed.[30] The syntheses of 1,5-diamino-1,2,4-triazolium nitrate (**9a**) and perchlorate (**9b**) were also reported (Scheme 2).[29] Characterization by elemental analysis, and vibrational, and multinuclear NMR spectroscopy, and mass spectrometry confirmed these structures. Single-crystal X-ray analysis of **8b** showed the existence of significant hydrogen bonding between the perchlorate anion and the amino group and that methylation had occurred at N1. (Physical and thermal characteristics of these salts are tabulated in Table S2 of the Supporting Information.)[30]

Inspection of these data reveals certain interesting facts regarding thermal characteristics of the compounds. For example, the position of the methyl group on the ring does not influence the melting points (glass transition temperatures) of 1-amino-4-methyl-1,2,4-triazolium nitrate (**6a**) ($T_g=-62\,^{\circ}C$) and the 1-methyl-4-amino derivative **8a** ($T_g=-60\,^{\circ}C$). The corresponding perchlorate salts **6b** and **8b** melt at 91 °C and 86 °C, respectively. However, the nitrate salts of the 1-amino derivative **3a** ($T_m=69\,^{\circ}C$) and the 4-amino

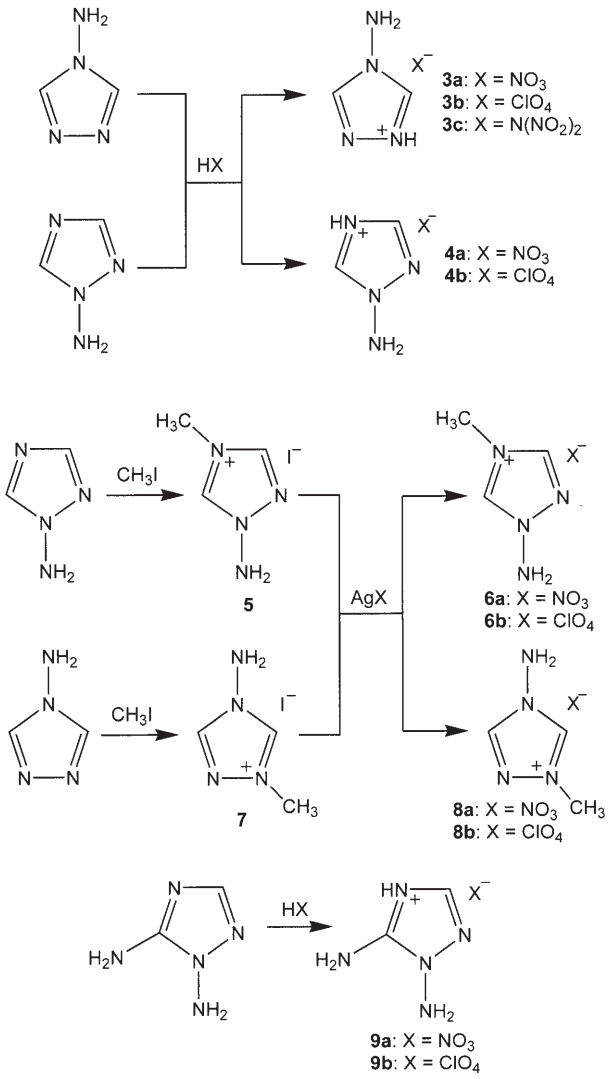

Scheme 2.

derivative **4a** ($T_m=121\,^{\circ}C$), are considerably higher melting than their methyl-substituted analogues. Clearly, the opportunity for hydrogen bonding, as well as modified packing effects and reduced lattice energies, is markedly reduced in the methylated salts. Thermal degradation temperatures for both nitrate and perchlorate salts are increased when a methyl group is present in the ring. Introduction of a second amino functionality causes the melting point (**4b** versus **9b**) to increase and the enthalpy of formation to become less positive, but appears to have essentially no impact on other properties. The combustion energies and standard molar enthalpies of formation for perchlorate salts are higher than those of nitrates.

The synthesis and characterization of a series of nitrate salts, based on the 1-alkyl-4-amino-1,2,4-triazolium cations **10a–d**, have been reported.[31] Single-crystal X-ray diffraction studies of 1-isopropyl-4-amino-1,2,4-triazolium (**10b**; tri-

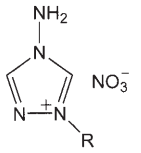

10a: R = methyldecyl
10b: R = isopropyl
10c: R = allyl
10d: R = methylcyclohexyl

 © 2006 Wiley-VCH Verlag GmbH & Co. KGaA, Weinheim

clinic, $P\bar{1}$ symmetry) and methylcyclohexyl-4-amino-1,2,4-triazolium (**10d**; monoclinic, $P2_1/n$ symmetry) suggested that in both cations, the amino group is twisted and does not straddle the triazole ring in a symmetric fashion. This arrangement is most likely due to extensive hydrogen bonding within the crystal structure which, however, does not affect the bond lengths in the structures in a significant manner.[31]

2.3. Triazolium Salts Containing Azido Substituents

Hydrogen atoms of azoles can be substituted readily by various energetic functional groups. When endothermic moieties, such as the azido group, are incorporated into azoles, the enthalpies of formation of the azoles are increased.[30,32,33] For example, the standard heat of formation for 3-azido-1,2,4-triazole ($\Delta H_f^o = +458$ kJ mol^{-1})[33] is approximately four-times larger than that of 1-*H*-1,2,4-triazole.[28] These azido-substituted azoles, when paired with nitrate, perchlorate, or azolate (e.g., 4,5-dinitroimidazolate or 5-nitrotetrazolate anions), formed energetic salts.[30,34]

Various energetic salts based on azido-1,2,4-triazoles (**11a–d**; Scheme 3)[30] were readily quaternized in good

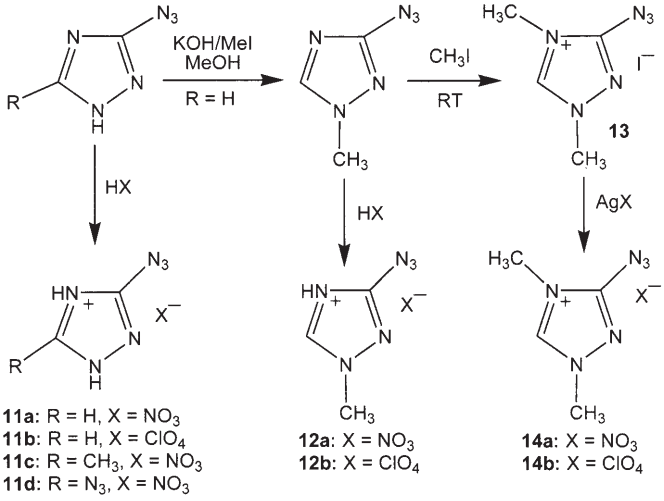

Scheme 3.

yields with concentrated nitric or perchloric acid in methanol. Under similar reaction conditions, 1-methyl-3-azido-1,2,4-triazole reacted with concentrated nitric or perchloric acids to give 1-methyl-3-azido-1,2,4-triazolium nitrate (**12a**), and perchlorate (**12b**), respectively. When 1-methyl-3-azido-1,2,4-triazole was quaternized with iodomethane the salt **13** formed. Subsequent metathesis with $AgNO_3$ or $AgClO_4$ led to the 1,4-dimethyl-3-azido-1,2, 4-triazolium nitrate (**14a**) and perchlorate (**14b**), salts respectively (Scheme 3).

These azido triazolium salts were characterized by elemental analysis, IR, ^{1}H and ^{13}C NMR spectroscopy, mass spectrometry, and DSC studies. Examination of the crystal structures of **11a** and **14a** illustrated the influence of significant hydrogen bonding between the nitrate anion and the protonated 1,2,4-triazole ring for **11a**. This hydrogen bonding accounts for the higher density, (1.76 g cm^{-3}) and melting point ($T_m = 147$ °C) of **11a**, compared with that of **14a** ($\rho = 1.58$ g cm^{-3}, $T_m = 98$ °C), in which the presence of the methyl group on the triazole ring reduces the opportunity for hydrogen bonding (Table S3 of the Supporting Information).

The chemistry of energetic ionic salts and ionic liquids containing azidoethyl substituents on the triazolium rings was examined.[34] Reaction of 1-(2-azidoethyl)-1,2,4-triazole with nitric acid, perchloric acid, 4,5-dinitroimidazole, or 5-nitrotetrazole gave the corresponding1-(2-azidoethyl)-1,2,4-triazolium salts **15a–d**, in over 97% yield (Scheme 4). 1-(2-Azidoethyl)-1,2,4-triazole was also treated with iodomethane

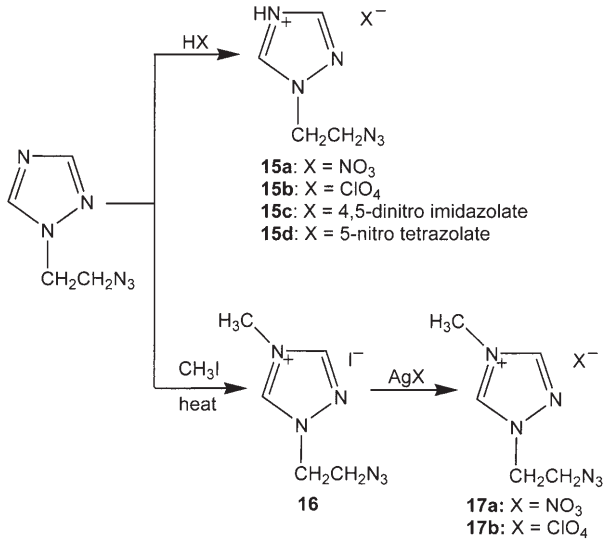

Scheme 4.

to form 1-(2-azidoethyl)-4-methyl-1,2,4-triazolium iodide (**16**), which upon metathesis with the silver salts of nitric or perchloric acids formed the nitrate **17a**, and perchlorate **17b**, respectively, in very good yields (Scheme 4). The melting points of all these salts were found to be lower than 100 °C, and most of them are liquids at room temperature. The standard heats of formation for the salts with perchlorate anion are more positive than those of the nitrate analogues. Most of these salts showed good thermal stability and high density (Table S3 of the Supporting Information).

The reaction of 1-(2-azidoethyl)-3-azido-1,2,4-triazole with concentrated nitric acid or 5-nitrotetrazole gave 1-(2-azidoethyl)-3-azido-1,2,4-triazolium nitrate (**18a**) and the 5-nitro tetrazolate **18b**, respectively (Scheme 5). Metathesis of 1-(2-azidoethyl)-4-amino-1,2,4-triazolium bromide or 1-methyl-4-(2-azidoethyl)-1,2,4-triazolium bromide with $AgNO_3$ or $AgClO_4$ gave good yields of the nitrates **19a** and **20a** and the perchlorates **19b** and **20b**, respectively (Scheme 5).[34]

Density and thermal characteristics of azido- and azidoethyl-containing triazolium derivatives are summarized in Table S3 of the Supporting Information. The data show that the influence of the position of a substituent group on the triazolium ring plays an important role, for example the

 © 2006 Wiley-VCH Verlag GmbH & Co. KGaA, Weinheim

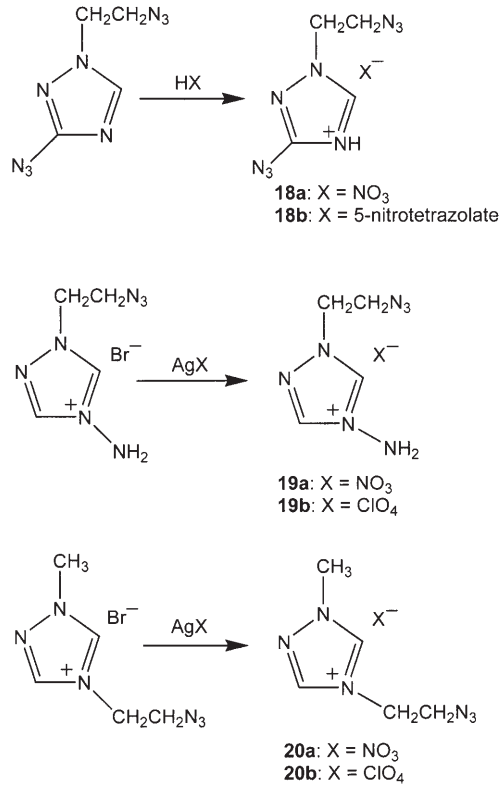

Scheme 5.

substituted triazoles **21a–c** with iodomethane to form quaternary salts **22a–c**, metathesis of which with various metal salts resulted in the ionic liquids and energetic salts **23a–c** (Scheme 6). The yields of products are usually excellent.

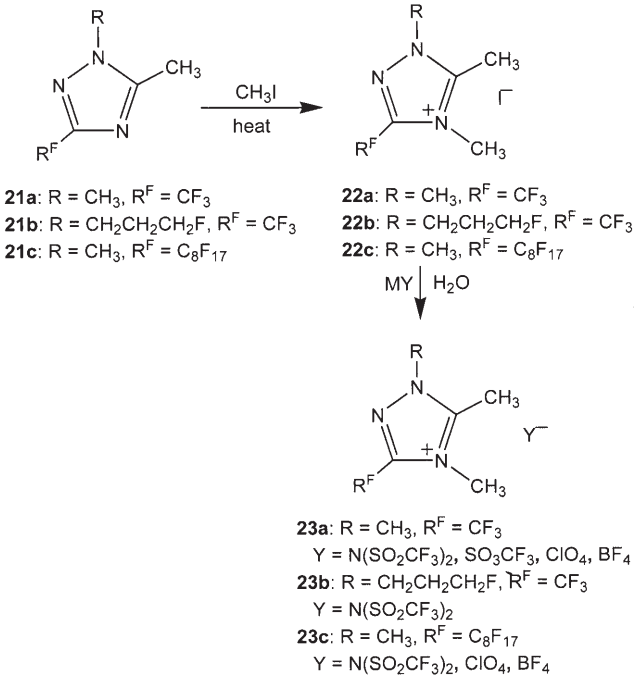

Scheme 6.

T_g values for 1-(2-azidoethyl)-4-methyl-1,2,4-triazolium nitrate (**17a**; −57 °C)) and 1-methyl-4-(2-azidoethyl)-1,2,4-triazolium nitrate (**20a**; −56 °C) are essentially the same, but their decomposition temperatures (**17a**, $T_d = 119$ °C; **20a**, $T_d = 143$ °C) differ markedly.[34] For the analogous perchlorate salts, the melting points and thermal degradation temperatures are $T_g = -52$ °C and $T_d = 192$ °C for **17b**, and $T_m = 63$ °C and $T_d = 152$ °C for **20b**, respectively.

Density and enthalpy of formation are important characteristics of energetic salts and are governed by their molecular structures. In general, the densities for the salts having perchlorate as anions are higher than those of the analogous nitrates (see the data in Table S3 of the Supporting Information). Comparing the standard molar enthalpy (ΔH_f^o) of the salts, when perchlorate is used as an anion, the positive heats of formation as well as heats of combustion are higher than those of the corresponding nitrates. Considering **15a–d**, the impact of the anions on heats of formation of 1-(2-azidoethyl) 1,2,4-triazolium salts decreases in the order: 5-nitro-tetrazolate > perchlorate > 4,5-dinitro-imidazolate > nitrate.

2.4. Triazolium Salts Containing Fluoroalkyl Substituents

Incorporation of substituents at carbon atoms of 1,2,4-triazoles was efficiently accomplished by construction of triazoles with the required substituents in place.[35] By utilizing this process various fluoroalkyl-substituted 1,2,4-triazolium salts were obtained,[36] first by reaction of 1,3,5-

These ionic salts were characterized by elemental analyses, IR and multinuclear NMR spectroscopy, and GC mass spectrometry. The bis(trifluoromethanesulfonyl)amide salts **23** ($Y = N(SO_2CF_3)_2$) are insoluble in water, which helps in purification. The solubilities of these salts in organic solvents increase with increasing dielectric constant of the solvent. Their melting points decrease in the order $SO_3CF_3^- > BF_4^- > ClO_4^- > N(SO_2CF_3)_2^-$,[36] which could be attributed to the diffuse charge on the latter anion. Ionic salts with larger cations have a lower melting point owing to less-efficient packing in the solid phase.

Reactions of 1-alkyl-1,2,4-triazoles with polyfluoroalkyl halides resulted in quaternization at N4 of the triazole ring to yield **24a–n**. Metathesis of **24a–n** with various metal salts gave excellent yields of ionic salts **25a–n** (Table 1).[37] Ionic salts containing longer alkyl and polyfluoroalkyl substituents have lower melting points because of less-efficient packing in the solid. The densities were found to be higher with elongation of the fluoroalkyl substituent and with higher fluorine concentration. Cations with bulkier alkyl groups resulted in salts of lower density.

In another study,[38] a high-yield, efficient procedure to make functionalized alkyl-/fluoroalkyl-containing triazolium salts and triazolium ionic liquids led to triazolium cations that contained covalently bound anionic groups, such as sulfonate, fluorocarboxy, fluorohomoallylic, and fluoroalkanol. These were converted by metathesis with fluorine-containing anions into low-melting ionic salts (**26a**,**b**, **27**, **28a**,**b**, **29c**,**d**, **30**;

 © 2006 Wiley-VCH Verlag GmbH & Co. KGaA, Weinheim

Table 1: Synthesis of triazolium salts **25** containing fluorinated side chains.

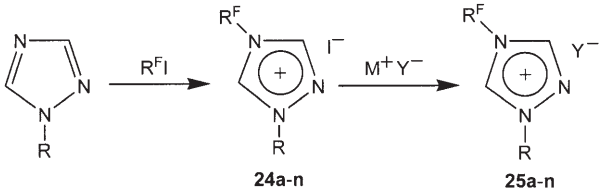

	R	R^F	Y	T_g [°C]	T_d [°C]
25a	CH_3	$(CH_2)_2CF_3$	$N(SO_2CF_3)_2$	−58	376
25b	$(CH_2)_3CH_3$	$(CH_2)_2CF_3$	$N(SO_2CF_3)_2$	−67	395
25c	$(CH_2)_6CH_3$	$(CH_2)_2CF_3$	$N(SO_2CF_3)_2$	−67	402
25d	$(CH_2)_9CH_3$	$(CH_2)_2CF_3$	$N(SO_2CF_3)_2$	−68	400
	R	R^F	Y	T_m [°C]	T_d [°C]
25e	$(CH_2)_3CH_3$	$(CH_2)_2(CF_2)_3CF_3$	$N(SO_2CF_3)_2$	69	394
25f	$(CH_2)_6CH_3$	$(CH_2)_2(CF_2)_3CF_3$	$N(SO_2CF_3)_2$	55	396
25g	$(CH_2)_9CH_3$	$(CH_2)_2(CF_2)_3CF_3$	$N(SO_2CF_3)_2$	53	396
25h	CH_3	$(CH_2)_2(CF_2)_5CF_3$	$N(SO_2CF_3)_2$	62	381
25i	$(CH_2)_3CH_3$	$(CH_2)_2(CF_2)_5CF_3$	$N(SO_2CF_3)2$	53	396
25j	$(CH_2)_6CH_3$	$(CH_2)_2(CF_2)_5CF_3$	$N(SO_2CF_3)_2$	22	405
25k	$(CH_2)_3CH_3$	$(CH_2)_2(CF_2)_3CF_3$	PF_6	296	357
25l	$(CH_2)_6CH_3$	$(CH_2)_2(CF_2)_3CF_3$	PF_6	298	354
25m	$(CH_2)_3CH_3$	$(CH_2)_2(CF_2)_5CF_3$	PF_6	289	361
25n	$(CH_2)_3CH_3$	$(CH_2)_2(CF_2)_3CF_3$	SO_3CF_3	173	391

Scheme 7).[38a] These functionalized triazolium salts have many characteristics of excellent ionic liquids with respect to air, water, and thermal stability, and all are liquids at 25 °C.

A method for the syntheses of 1-alkyl-1,2,4-triazolium 4-nitroimides was developed based on alkylation of the metal salts of 4-nitramino-1,2,4-triazole with halo-and dihaloalkanes (Scheme 8).[38b] The salts **31**–**37** are solid and characterized by IR and NMR spectroscopy and elemental analysis. In the IR spectra the characteristic absorption bands arising from an *N*-nitroimido group bound to a heterocycle are observed at 1280–1300 and 1390–1415 cm^{-1}. The nitramino group that would have given absorption bands at 1550–1620 cm^{-1} is absent. In the ^1H NMR spectra, the signals for the protons of the triazole ring are nonequivalent and shifted downfield relative to the signals for the protons in the starting salt, evidence that supports the imide structure. This conclusion is supported by the ^{13}C NMR spectroscopic data. No thermal or physical properties were reported.

2.5. 1,2,4-Triazolium Azolate Salts

The need for new, safe, high-performance propellants and other industrial applications, coupled with the desire to reduce environmental footprints and overall exposure to hazardous and potentially toxic materials, has led to renewed efforts to explore new, advanced, energetic salts. Lithium dicyanotriazolate was reported as a useful electrolyte (**38**).[39] 1-Butyl-3-methylimidazolium 3,5-dinitro-1,2,4-triazolate (**39**; $T_m = 32$ °C, $T_d = 239$ °C) resulted from the metathesis of 1-butyl-3-methylimidazolium halide with potassium 3,5-dinitro-1,2,4-triazolate.[40] However, no energetic characterization was carried out for this material. Some novel ionic liquids made up of azolium cations and azolate anions were also reported.[41] These salts are: 1-ethyl-3-methylimidazolium 1,2,4-triazolate (**40**) ($T_g = -76$ °C, $T_d = 207$ °C, $\eta = 60.2$ cP at 25 °C) and tetrazolate (**41**) ($T_g = -89$ °C, $\eta = 42.5$ cP at 25 °C). Compounds **40** and **41** were prepared by coupling of 1-ethyl-3-methylimidazolium hydroxide with triazole or tetrazole, respectively.[41]

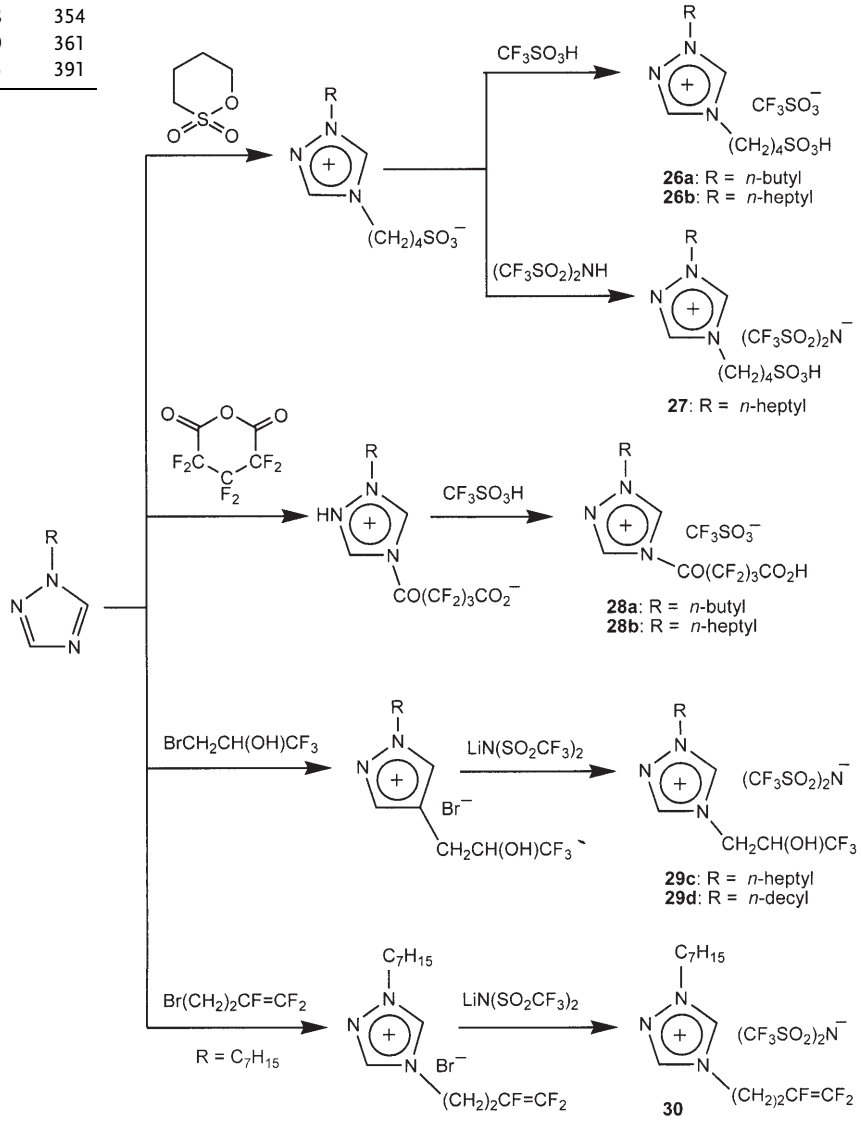

Scheme 7.

 © 2006 Wiley-VCH Verlag GmbH & Co. KGaA, Weinheim

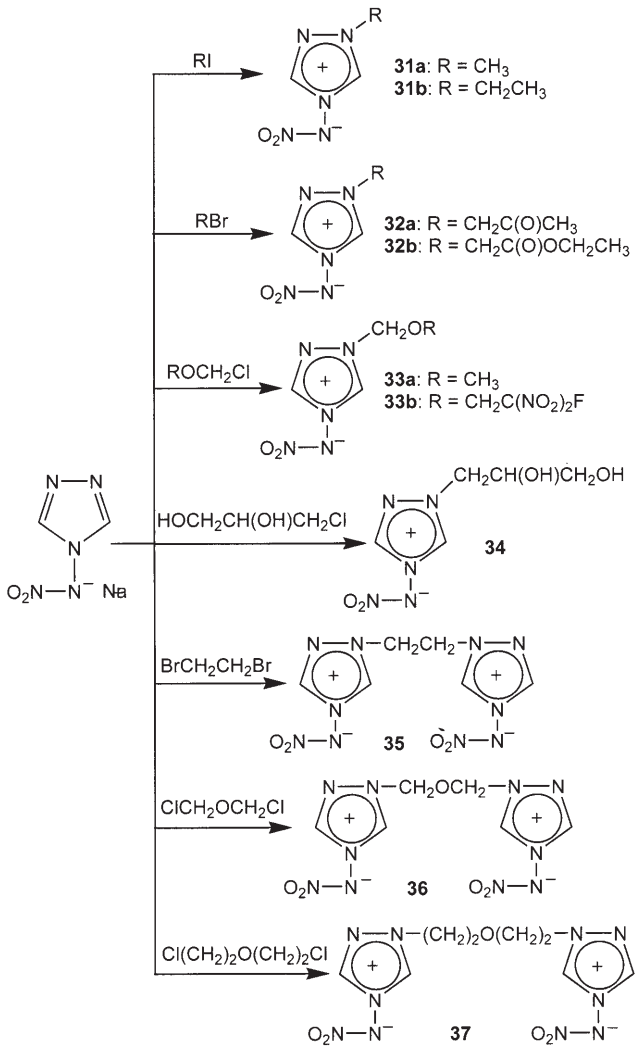

Scheme 8.

By taking advantage of the fact that both 4,5-dinitroimidazole and 5-nitrotetrazole are strong NH acids ($pK_a = 0.8$ for 5-nitrotetrazole),[42] energetic salts with various 1,2,4-triazolium derivatives as cations and 4,5-dinitroimidazolate and 5-nitrotetrazolate as anions (Scheme 9) were obtained.[43] 4,5-Dinitroimidazole and 5-nitrotetrazole were treated with variously 4-substituted derivatives of 1,2,4-triazoles to produce energetic ionic salts **42a–d** and **43a–d** (Scheme 9).

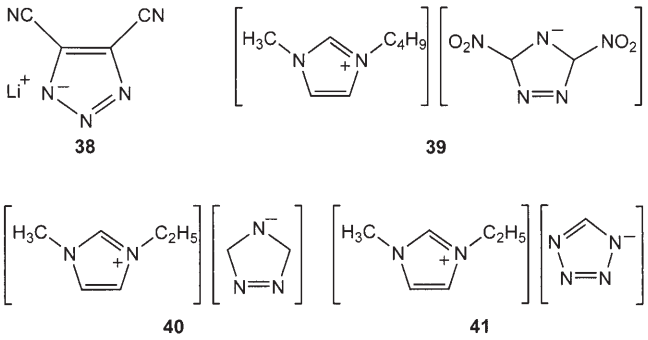

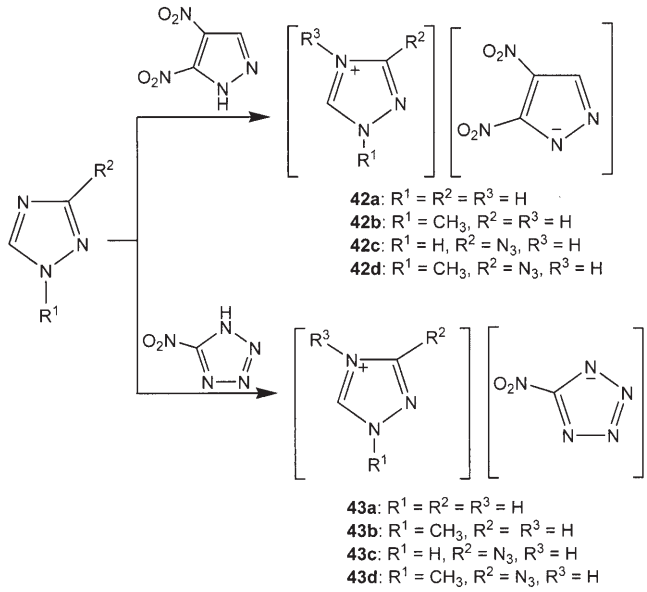

Scheme 9.

When 5-nitrotetrazolate was used as the anion, the melting points of the compounds were lower than those of the corresponding 4,5-dinitroimidazolates, while the thermal decomposition temperatures were higher (Table S4 of the Supporting Information). In addition to modified packing effects and reduced lattice energies, the opportunity for hydrogen bonding with the anion is reduced in methyl-substituted compounds, which results in lower melting points. The densities exceed 1.45 $g\,cm^{-3}$ for all the compounds. Energetic salts that incorporate a nitro group have a substantially improved oxygen balance which results in higher heats of combustion and possible detonation processes. The oxygen coefficients (α)[44] for the salts are between 0.18 and 0.33 and are within the range reported for energetic compounds.[45] Of all the azolium azolate compounds, 1-methyl-3-azido-1,2,4-triazolium 5-nitrotetrazolate (**43d**) has the highest heat of formation.

3. Tetrazole-Based Salts

Tetrazoles are unsaturated five-membered heterocycles with four nitrogen atoms in the ring. The enthalpies of energetic chemical systems are governed by their molecular structure. From imidazole ($\Delta H_f^o = +58.5\ kJ\,mol^{-1}$) to 1,2,4-triazole ($\Delta H_f^o = +109.0\ kJ\,mol^{-1}$) to tetrazole ($\Delta H_f^o = +237.2\ kJ\,mol^{-1}$),[32] the heats of formation get increasingly positive. Since the generation of molecular nitrogen as an end-product of propulsion or explosion is highly desired to avoid environmental pollution and health risks, as well as to reduce detectible plume signatures, compounds containing a backbone of directly linked nitrogen atoms (catenated nitrogen) are of great interest. The high nitrogen content of tetrazole and its derivatives has led to investigations for their use as potential energetic materials.

 © 2006 Wiley-VCH Verlag GmbH & Co. KGaA, Weinheim

3.1. Tetrazolium Salts Containing Amino Substituents

Aminotetrazoles have a high nitrogen content and, despite their large positive enthalpies of formation,[46] are thermally stable.[47] Aminotetrazoles are, therefore, prospective high-energy materials. The synthesis of various tetrazolium salts containing amino substituents on the ring through the reactions of 1-amino-5-methyltetrazole or 2-amino-5-methyltetrazole with iodomethane resulted in quaternary salts **44** and **46**. Metathesis with $AgNO_3$ or $AgClO_4$ formed 1-amino-4,5-dimethyltetrazolium nitrate (**45a**) or perchlorate (**45b**), and 2-amino-4,5-dimethyltetrazolium nitrate (**47a**) or perchlorate (**47b**), respectively, in high yield (Scheme 10).[29,30] Proof of synthesis was supported by elemental analyses, IR and multinuclear NMR spectroscopy and mass spectrometry.

A high-yield synthesis of 5-aminotetrazolium nitrate (**48**) is reported from the reaction of 5-aminotetrazole with nitric acid (Scheme 11).[48] Its characterization was by IR, Raman, and multinuclear (^1H, ^{13}C, ^{15}N) NMR spectroscopy, and DSC. Bomb calorimetry, sensitivity measurements, and ab initio calculations were also performed. From the combined experimental and theoretical calculations, **48** is predicted to be a powerful and promising explosive with a good oxygen balance and low sensitivity.

Recently the syntheses of 1,5-diamino-4-methyltetrazolium salts were realized by quaternization, for example, treatment of 1,5-diamino-1*H*-tetrazole with iodomethane to form 1,5-diamino-4-methyltetrazolium iodide (**49**) in 86% yield.[49] Subsequent metathesis of **49** with silver nitrate, silver dinitramide, or silver azide led to the 1,5-diamino-4-methyltetrazolium nitrate (**50a**), dinitramide (**50b**), or azide (**50c**) in good yields. Most of these salts were thermally stable. The salt **50b** melts at $<100\,^{\circ}C$ which places it in the category of an energetic ionic liquid. The enthalpies of combustion (ΔH_c°) of **50a–c** were determined experimentally using oxygen bomb calorimetry, and the values are $-2456\,cal\,g^{-1}$ for **50a**, $-2135\,cal\,g^{-1}$ for **50b**, and $-3594\,cal\,g^{-1}$ for **50c**. The detonation velocities (D) and detonation pressure (P) for **50a–c** were calculated using empirical equations of Kamlet and Jacob; the values are $D=7682\,m\,s^{-1}$, $P=23.4$ GPa for **50a**, $D=8827\,m\,s^{-1}$, $P=33.66$ GPa for **50b**, $D=7405\,m\,s^{-1}$, $P=20.8$ GPa for **50c** (Table S5 of the Supporting Information).

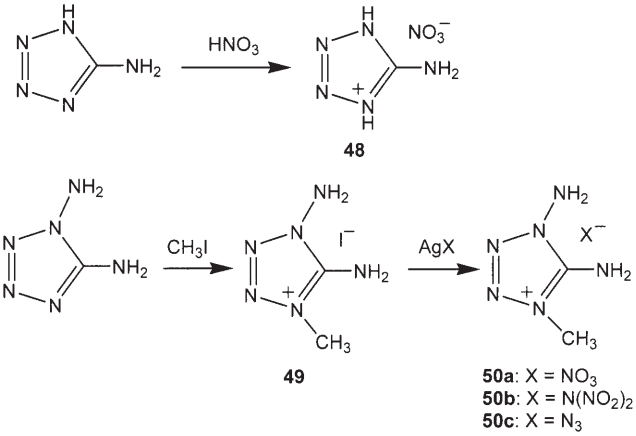

Scheme 11.

These salts were characterized by IR, Raman, and NMR spectroscopy, mass spectrometry, elemental analysis, X-ray diffraction. In initial safety testing low impact sensitivities were demonstrated. Compounds **45a**,**b**, and **47a** also fall into the ionic-liquid class. Densities and thermochemical characteristics of substituted amino-, aminomethyl-, and polymethyltetrazolium salts are summarized in Table S5 of the Supporting Information. While all of these new salts exhibit thermal stabilities $>170\,^{\circ}C$ based on DSC/TGA studies (except the azide) and positive heats of formation, the perchlorates **45b**, **47b**, as well as the dinitramide **50b** and the azido **50c** are highest. The densities of 1-amino-4,5-dimethyltetrazolium perchlorate (**45b**) and 1-methyl-4,5-diaminotetrazolium dinitramide (**50b**) are markedly higher than the others.

3.2. Energetic Salts Containing 5,5′-Azotetrazolate Anions

In the 1890s, Thiele first prepared sodium 5,5′-azotetrazolate (**51**) from the oxidation of 5-amino-tetrazole with potassium permanganate.[50] Reaction of strontium and barium chlorides with an aqueous solution of **51** gave strontium 5,5′-azotetrazolate (**52a**) and barium 5,5′-azotetrazolate (**52b**), respectively.[51] Both salts were insoluble in water. Salt **52b**, was used with various metal sulfates to

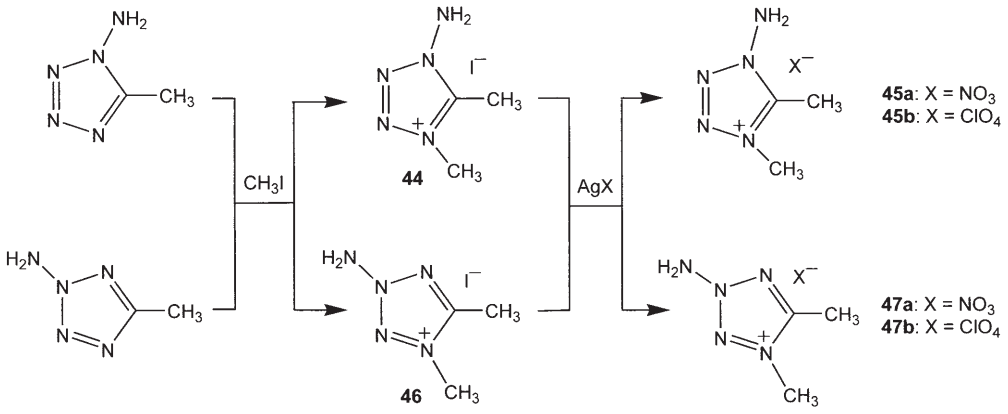

Scheme 10.

 © 2006 Wiley-VCH Verlag GmbH & Co. KGaA, Weinheim

produce the corresponding 5,5′-azotetrazolate salts **53a–d**, **54a**,**b**, and **55a–f** (Scheme 12). These metal salts often contain water of crystallization, and loss of water has been observed during storage.[51] Upon loss of water, the sensitivity of the

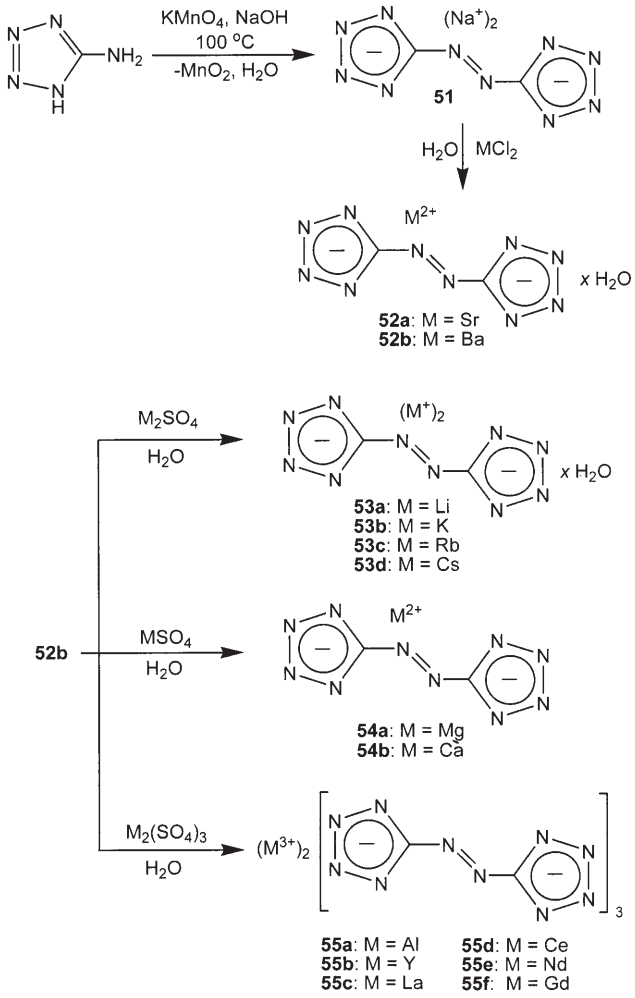

Scheme 12.

compounds to shock and friction increases drastically. The salts were characterized by IR, Raman, and NMR spectroscopy, and their thermal properties were studied by DSC and TGA. X-ray crystal studies on the pentahydrates **51** and **52b**, hexahydrate **53a**, dihydrate **53c**, octahydrate **54b**, docosahydrate **55b**, and gadolinium 5,5′-azo-tetrazolate hydrate (**55f**) show that the water molecules were either in the coordination sphere of the cation or bound by hydrogen bonds. The azotetrazolate ion is not connected to the harder cations, such as calcium or yttrium, and the salt decomposed in water to form tetrazolhydrazine with concomitant evolution of nitrogen. The free acid 5,5′-azotetrazolate, synthesized from the sodium salt with HBF_4, was decomposed within seconds at room temperature but could be retained at −30 °C.

Salts of 5,5′-azotetrazolate with protonated nitrogen bases (e.g., ammonium, guanidinium, and triaminoguanidinium) are unique gas-generating agents producing little smoke or residue, which may lead to a variety of applications, including gas generators and explosives.[52] Salts of the 5,5′-azotetrazolate dianion with various methylated ammonium (**56a–e**) and hydrazinium (**57a–d**,**f**) cations were obtained from the reactions of barium 5,5-azotetrazolate (**52b**) with appropriate ammonium and hydrazinium sulfates.[52,53] *N*,*N*,*N*-Trimethylhydrazinium 5,5′-azotetrazolate (**57e**) was obtained by the metathesis of trimethylhydrazinium iodide and silver 5,5-azotetrazolate (Scheme 13).

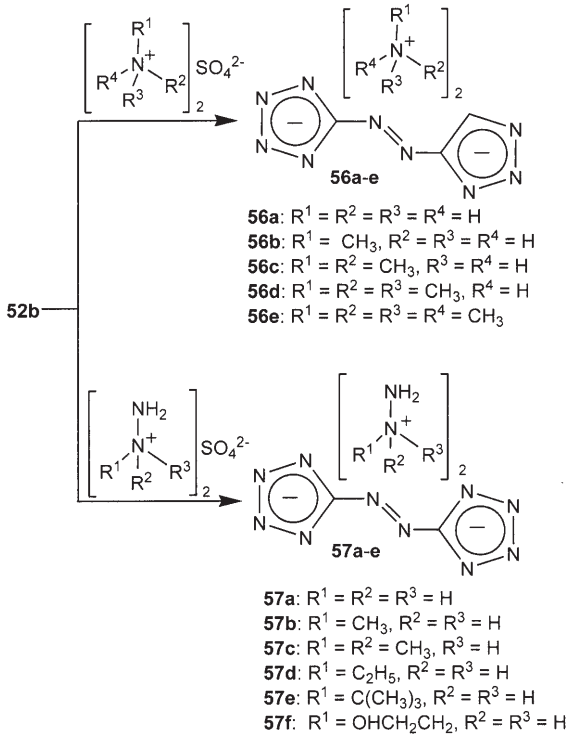

Scheme 13.

The 5,5′azotetrazolates **57g–n** are salts that contain organic nitrogen-base cations.[53b,54a] These salts were characterized by IR, Raman, NMR spectroscopy, and elemental analyses; X-ray crystal structures of **56a**, **56c**, **56e**, **57a**, **57e**, **57j**, and **57l** were determined.

The salts were insensitive to shock, friction, or electric discharge ($\approx$20 kV). Detonation was not observed in either the drop hammer test (5 kg, 50 cm) or when the salts were ground forcefully in a mortar. None of these salts melts, but rather they decompose at specific temperatures with rapid gas evolution. Above the decomposition point, explosion occurred upon rapid heating to give nitrogen gas as the main product, especially if the compound was compressed before heating. The decomposition temperature decreased for salts with NH^+ groups as the number of methyl groups increased. The hydrazine salts also produced large amounts of hydrogen, which decreased with the increasing number of methyl groups. The ammonium compounds (**56a–c**) produced only small amounts of hydrogen, whereas none was detected for **56d**,**e**.[53b] The formation of methane was observed for all salts.

Heats of formation of hydrazinium,[53a] guanidinium,[54b] and ammonium 5,5′-azotetrazolates[54a] were found to be

 © 2006 Wiley-VCH Verlag GmbH & Co. KGaA, Weinheim

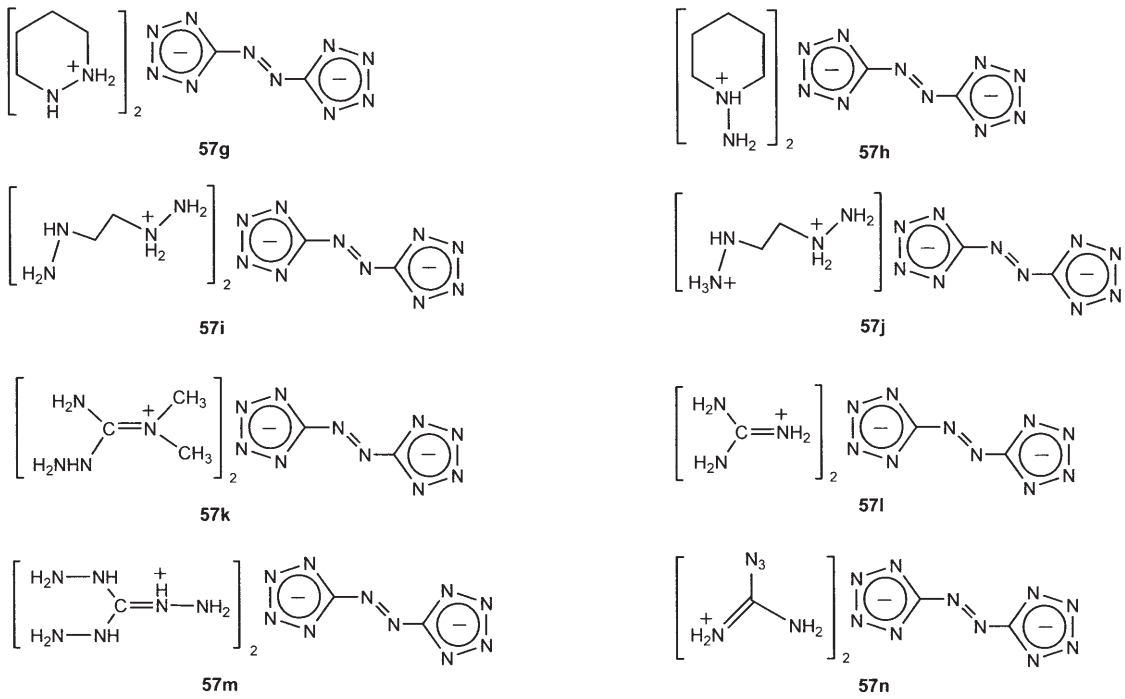

$\Delta H_f^\circ = +858$, $+410$, and $+443\ kJ\,mol^{-1}$, respectively. To compare these properties with azotetrazolates that contain heterocyclic cations, imidazolium, triazolium, and tetrazolium derivatives were synthesized and characterized (Scheme 14).[55] Surprisingly, while most azotetrazolates exhibit melting points in excess of 160 °C, [bis(1-butyl-3-methyl-imidazolium)] 5,5′-azotetrazolate (**58a**) was an ionic liquid at 25 °C with a melting point of 3 °C, similar to its 3,5-dinitrotetrazolate analogue.[40a] This compound is of little value with respect to energetic contributions, given its density of 1.26 $g\,cm^3$. This is different from [bis(1,3-dimethyl-4-nitroimidazolium)] 5,5′azotetrazolate (**58b**), which has a positive heat of formation, higher than that of bis(triaminoguanidinium) 5,5′azotetrazolate (**57m**).

Although the quaternized salts of 4-amino-1,2,4-triazole, that is, bis(1-methyl-4-amino-1,2,4-triazolium) (**59a**), and bis(1,4-diamino-1,2,4-triazolium) (**59b**) 5,5′-azotetrazolate have lower nitrogen content than the bis(triaminoguanidinium) derivative **57m**, their heats of formation are much higher at $+1580$ and $+1705\ kJ\,mol^{-1}$, respectively, with densities of approximately 1.57–1.59 $g\,cm^{-3}$. The structure of **59a**, determined by single-crystal X-ray analysis, shows that the unit cell was packed as a layered structure with hydrogen bonds and an interlayer distance of 3.04 Å. Perhaps somewhat surprisingly, bis(1,2,5-trimethyltetrazolium) 5,5′-azotetrazolate (**60**) has a lower density and much lower positive heat of formation. In contrast to the metal azotetrazolates,[51] none of these salts (except **60**) was solvated. Compounds **58b–60** decomposed violently upon melting. Microwaving **59a** at 200 °C caused violent decomposition leading to the formation of a carbon black powder. With the exception of **59b**, which spontaneously evolved nitrogen gas, most of the salts were stable at room temperature for at least two months.

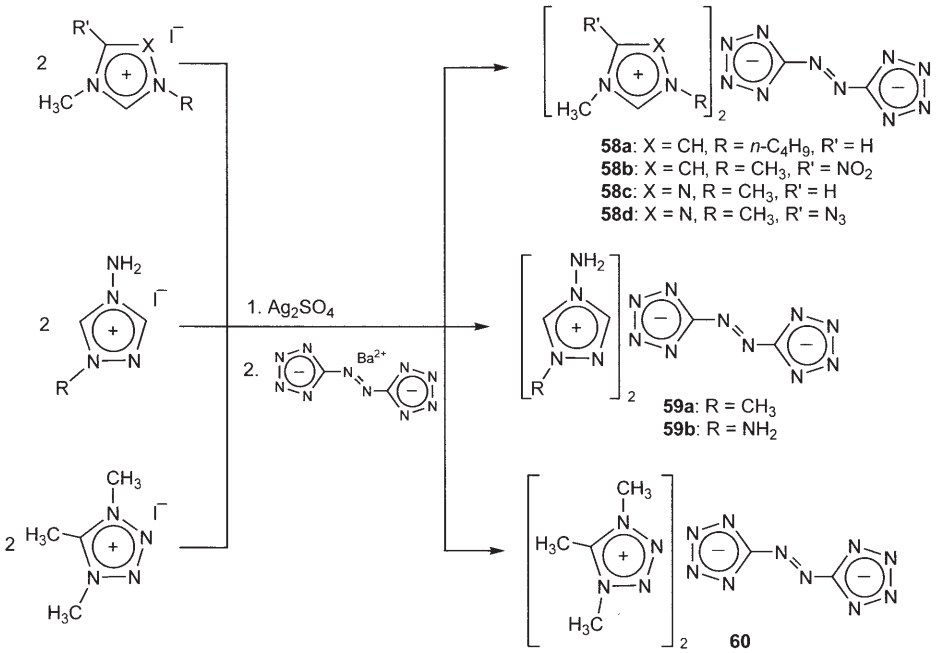

Scheme 14.

 © 2006 Wiley-VCH Verlag GmbH & Co. KGaA, Weinheim

3.3. Energetic Salts of Bistetrazolates

Although there are several reports of 5,5′-bistetrazolate[56] and iminobis(5-tetrazolate)[57] salts, most are described in the patent literature. Some processes have been developed for preparing various 5,5′-tetrazolate salts, which were very useful as low toxic and easy to handle gas-generating agents for air bags and as high-molecular-weight foaming agents. In methanol at reflux, bistriazole or iminobis(5-tetrazole) readily quaternized 4-amino-1,2,4-triazole to give [bis(4-amino-triazolium)] 5,5′-bistetrazolate (**61a**) or the iminobis(5-tetrazolate) **61b**, respectively (Scheme 15).[55] While the densities of these two salts are still in the same range as the azotetrazolates, and, although the heat of formation of **61a** decreased somewhat, the values for **60** and **61b** are dramatically lower.

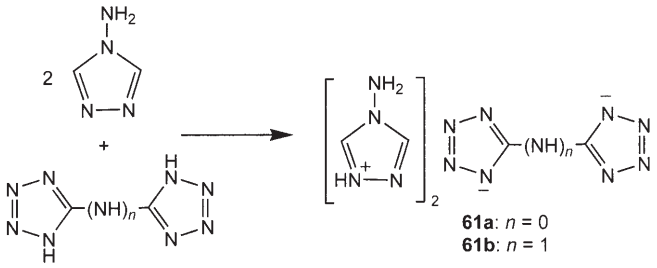

Scheme 15.

The diammonium (**62**), disodium (**63**), disilver (**64**), and manganese(II) (**65**) 5,5′ bistetrazolates are also known.[56] Chemistry of copper complexes with bis(tetrazolyl)amine has also been studied and some of them are of interest as additives in pyrotechnics and ammonium perchlorate-based propellants.[56e]

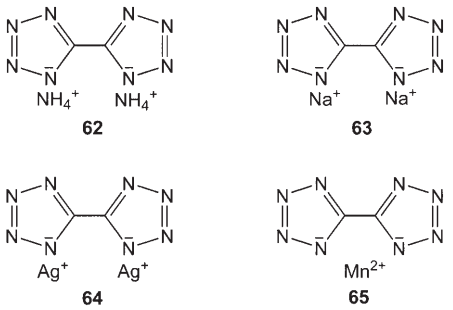

4. Urotropinium-Based Salts

The chemistry of high-energy density materials (HEDM) containing only C, H, N, and O atoms is of great interest. Urotropine is a nitrogen-rich cage molecule, which when paired with energetic anions forms energetic salts. The initial preparation of urotropinium salts was carried out in the 1950s,[58] and subsequently the syntheses of a variety of them were reported.[59] Urotropinium nitrate (**66**; colorless crystals, $T_m = 157–161\,°C$ (dec.), $\rho = 1.47\,g\,cm^{-3}$(from X-ray)) was prepared by the reaction of urotropine with nitric acid. *N*-methylurotropinium azide (**67a**; white solid, $T_m = 165–170\,°C$ (dec.), $\rho = 1.4\,g\,cm^{-3}$), *N*-methylurotropinium dinitramide (**67b**; white solid, $T_m = 121–124\,°C$ (dec.), $\rho = 1.46\,g\,cm^{-3}$), and *N*-methylurotropinium azotetrazolate (**67c**; yellow crystals, $T_m = 181–184\,°C$ (dec.), $\rho = 1.46\,g\,cm^{-3}$) were prepared from either the corresponding iodide or sulfate (Scheme 16).

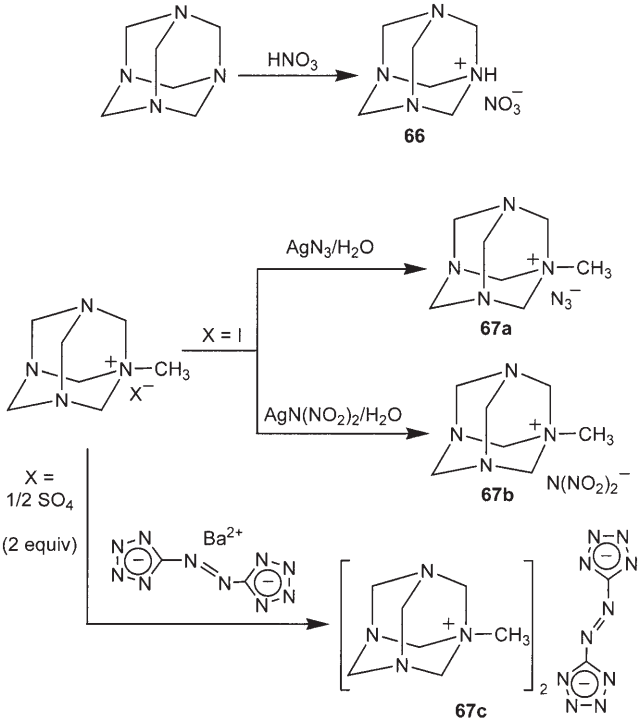

Scheme 16.

Owing to the high sensitivity and explosive nature of anhydrous silver azide, an alternative route for **67a** using sodium azide with *N*,*N*-dimethylurotropinium diiodide was utilized.[59] All the salts were handled easily, were insensitive to air or light, and were soluble in polar organic solvents. They were characterized by analytical and spectroscopic (IR, Raman, ^1H, ^{13}C, ^{14}N, NMR) methods and X-ray diffraction techniques. The crystal structure of **66** (monoclinic, space group $P2_1/C$) consisted of an urotropinium cation linked to a planar nitrate group by hydrogen bonds. The structures of **67a–c** revealed that there is no contact between the anions and cations. The azide ion in **67a** (monoclinic, space group $P2_1/m$) is linear; the dinitramide ion in **67b** (monoclinic, space group $P2_1$) is asymmetric; and the azotetrazolate anion in **67c** (monoclinic, space group $C2/m$) is planar.

Syntheses of urotropinium and *N*-methylurotropinium salts were broadened to include several other energetic organic and inorganic anions, such as 3,5-dinitropyrazolate, 4,5-dinitroimidazolate, 3,5-dinitro-1,2,4-triazolate, 5-nitrotetrazolate, perchlorate, nitrate, and azide.[60] In methanol solution, urotropine was found to react readily with 3,5-dinitropyrazole, 4,5-dinitroimidazole, 3,5-dinitro-1,2,4-triazole, and 5-nitrotetrazole to form urotropinium salts **68a–d**. Reaction of silver salts of 3,5-dinitro-1,2,4-triazole, nitric, perchloric, and hydrofluoric acid with *N*-methylurotropinium

 © 2006 Wiley-VCH Verlag GmbH & Co. KGaA, Weinheim

iodide led to *N*-methylurotropinium 3,5-dinitro-1,2,4-triazolate (**70a**), nitrate (**70b**), perchlorate (**70c**), and fluoride (**70d**) salts. *N*-Methylurotropinium azide (**67a**) is also accessible by the reaction of **69d** with $(CH_3)_3SiN_3$ (Scheme 17).[60]

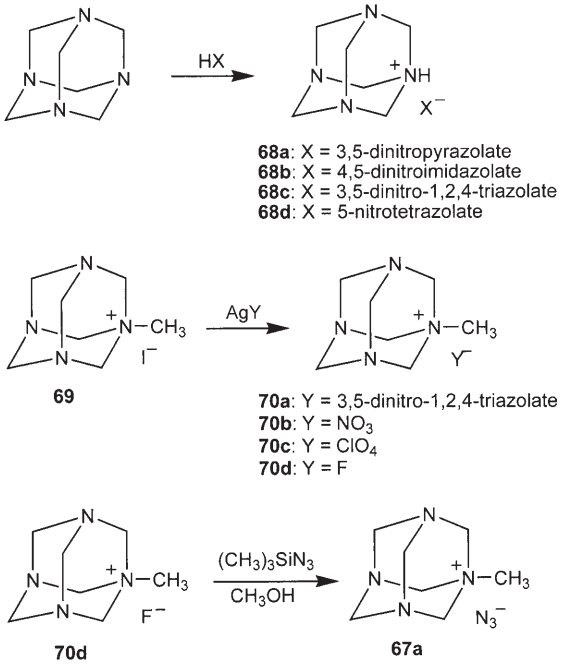

68a: X = 3,5-dinitropyrazolate
68b: X = 4,5-dinitroimidazolate
68c: X = 3,5-dinitro-1,2,4-triazolate
68d: X = 5-nitrotetrazolate

69

70a: Y = 3,5-dinitro-1,2,4-triazolate
70b: Y = NO_3
70c: Y = ClO_4
70d: Y = F

70d **67a**

Scheme 17.

Most of the new salts exhibit high positive heats of formation, which are higher for salts with organic anions (**68a–d**, **70a**) than those of their inorganic anion (**70b–d**, **67a**) analogues (Table S7 of the Supporting Information). The structure of **70b** was confirmed by single crystal X-ray analysis.

5. Tetrazine-Based Salts

There has been considerable interest in the study of the reactivity and properties of various tetrazine derivatives. The 1,2,4,5-tetrazine ring system is electroactive and has a high electron affinity. Tetrazines possess high positive heats of formation and large crystal densities—properties important in energetic materials applications. Additionally, they seem to be insensitive friction, impact, and electrostatic discharge.

The synthesis and properties of various ionic 1,2,4,5-tetrazine explosives and energetic materials such as **71–76** have been reported.[61] Energetic salts **71a**,**b**, **72a**,**b**, and **75a**,**b** were synthesized by the reaction of nitric acid and perchloric acid with 3,6-diguanidino-1,2,4,5-tetrazine, 3,6-diguanidino-1,2,4,5-tetrazine-1,4-di-*N*-oxide, and 3,6-dihydrazino-1,2,4,5-tetrazine, respectively, whereas **75c** was made by the reaction of $HN(NO_2)_2$ with 3,6-dihydrazino-1,2,4,5-tetrazine. Synthesis of **73** and **74** involved the reaction of the disodium salt of 3,6-bis(nitroguanyl)tetrazine with $AgNO_3$ and triaminoguanidinium hydrochloride, respectively.

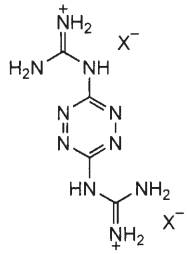

71a: X = ClO_4
71b: X = NO_3

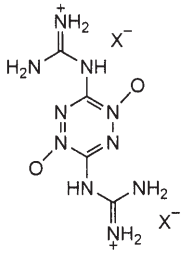

72a: X = ClO_4
72b: X = NO_3

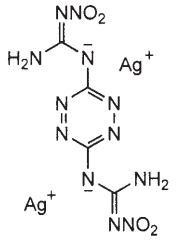

73

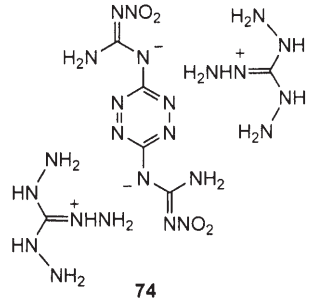

74

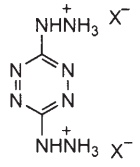

75a: X = ClO_4
75b: X = NO_3
75c: X = $N(NO_2)_2$

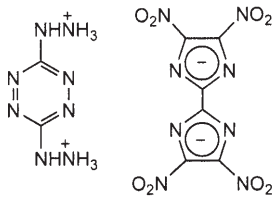

76

Poly-rho tests, which are single shot experiments to determine detonation velocity as a function of density, were performed on **71a**,**b**. When **71a** is formulated with 5 wt% of Kel-F 800 binder, a maximum pellet density of 1.79 $g\,cm^{-3}$ is obtained. At this density, the detonation velocity measured was 8.07 $km\,s^{-1}$. The dinitrate derivative (**71b**) was formulated with 3 wt% Estane binder and 3 wt% nitro-plasticizer. At a maximum pellet density of 1.60 $g\,cm^{-3}$, a detonation velocity of 7.31 $km\,s^{-1}$ was obtained. Salt **72b** was found to be unstable based on DSC analysis, whereas salt **72a** showed improved thermal stability but less than **71a**.[61a] The crystal density of **74** was reported to be 1.61 $g\,cm^{-3}$, and the heat of formation was 300 ± 2 $kcal\,mol^{-1}$.[61c] The densities of **75a–c**, **76** are reported to be in the range of 1.80 to 1.96 $g\,cm^{-3}$.[61b] When these salts were heated over the temperature range 40–500 °C at a scan rate of 20 °C min^{-1}, **75a–c** left no residue, whereas **76** left an orange powder. In DSC studies, **75a** and **75c** exhibited their major exotherm between 152 and 164 °C, respectively. Salt **75b** exhibited an exotherm at 190 °C and **76** showed the highest exotherm (220 °C).[61b] All tetrazine-based salts seem to have interesting explosive performance and extraordinary combustion properties.[61]

 © 2006 Wiley-VCH Verlag GmbH & Co. KGaA, Weinheim

6. Azetidinium-Based Salts

Azetidine-based explosives, such as 1,3,3-trinitroazetidine[62] demonstrate excellent performance partly because of the high strain associated with the four-membered ring. The basicity ($pK_b = 6.5$) of 3,3-dinitroazetidine[63] allowed the preparation of a variety of solid energetic 3,3-dinitroazetidinium salts **77**–**79** with high oxygen-balance.[64] These salts

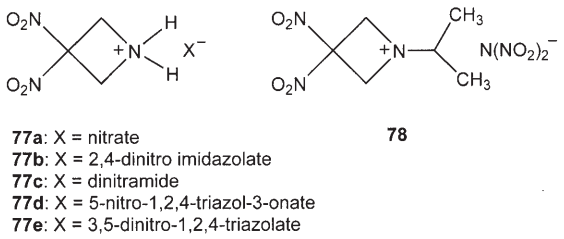

77a: X = nitrate
77b: X = 2,4-dinitro imidazolate
77c: X = dinitramide
77d: X = 5-nitro-1,2,4-triazol-3-onate
77e: X = 3,5-dinitro-1,2,4-triazolate

78

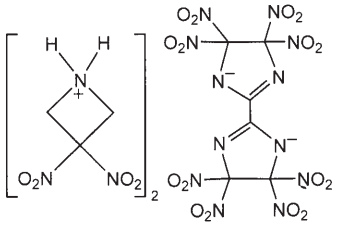

79

were synthesized in 82–95 % yields, either by mixing the free-base 3,3-dinitroazetidine with the appropriate acid or by metathesis of 3,3-dinitroazetidinium trifluoromethane sulfonate[63] with ammonium salts of the acid. They were characterized by elemental analyses, IR and ^{13}C NMR spectroscopy. Densities and thermal characteristics are tabulated in Table S8 of the Supporting Information. All the salts were subjected to small-scale thermal and sensitivity tests.[64]

The single-crystal X-ray structures of 3,3-dinitroazetidinium dinitramide (**77c**; orthorhombic, space group $C_{mc}2_1$) and 1-isopropyl-3,3-dinitroazetidinium dinitramide (**78**; orthorhombic, space group *Pbca*) were also reported.[65] The latter was formed during an attempt to crystallize 3,3-dinitroazetidinium nitrate (**77a**) from acetone. X-ray structures have confirmed that the dinitramide ions in **77c** and **78** have quite different conformations with different bend, twist, and torsion angles. The possible reason for these dramatic differences is claimed to be due to the different symmetries for this ion found in the two structures, as well as the absence of hydrogen-bonding interactions in **78**.[65] Dehydration of **77a** with acetic anhydride provided an alternate route for the synthesis of 1,3,3-trinitroazetidine.[64] The synthesis and characterization of ^{15}N-labeled isotopomers of **77a** was also reported.[66]

7. Picrate-Based Salts

Although anhydrous picric acid is unstable, and its impact and friction sensitivities are higher than those of trinitrotoluene, many organic and inorganic picrates have been reported.[7] The picrate anion, when combined with high-nitrogen azolium cations, forms energetic salts with high positive heats of formation. By taking advantage of the acidic properties of picric acid, energetic salts containing picrate and dipicrate anions have been prepared.[67] Scheme 18 depicts synthetic routes to salts **80**–**83** composed of azolium cations with picrate as the anion. Scheme 19 shows the synthetic routes to the energetic bisazolium dipicrate salts **84** and **85a**,**b**.[67]

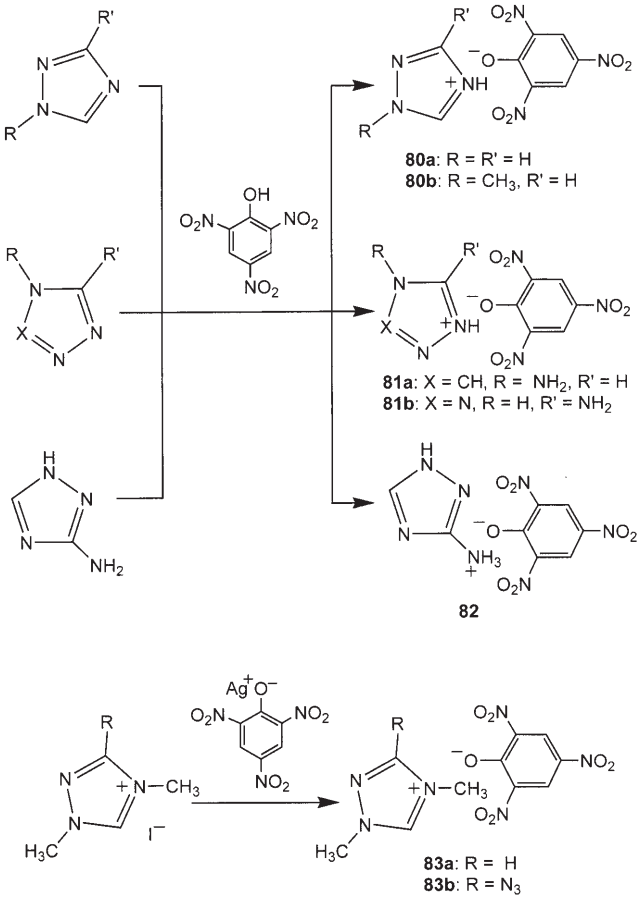

80a: R = R' = H
80b: R = CH_3, R' = H

81a: X = CH, R = NH_2, R' = H
81b: X = N, R = H, R' = NH_2

82

83a: R = H
83b: R = N_3

Scheme 18.

Triazolium or substituted triazolium picrates were first prepared by direct reaction of the triazole with picric acid in methanol or by quaternization with methyl iodide and treatment with silver picrate (Scheme 18). Bridged bis(imidazolyl)- or bis(tetrazolyl)methane compounds were treated with picric acid to form dipicrates, or they were quaternized and then metathesized to yield the desired salts (Scheme 19).

All of these salts were well-characterized, and X-ray crystal structures of **81a** and **81b** were also determined. Their physical characteristics and thermochemical properties, along with those of other energetic materials, are given in Table S9 of the Supporting Information. Most of the picrates have good thermal stabilities and relatively high densities and oxygen balance. The bridged azolium ion picrates are more stable thermally than their monocationic analogues. In general, the majority of these picrates were found to be more stable

 © 2006 Wiley-VCH Verlag GmbH & Co. KGaA, Weinheim

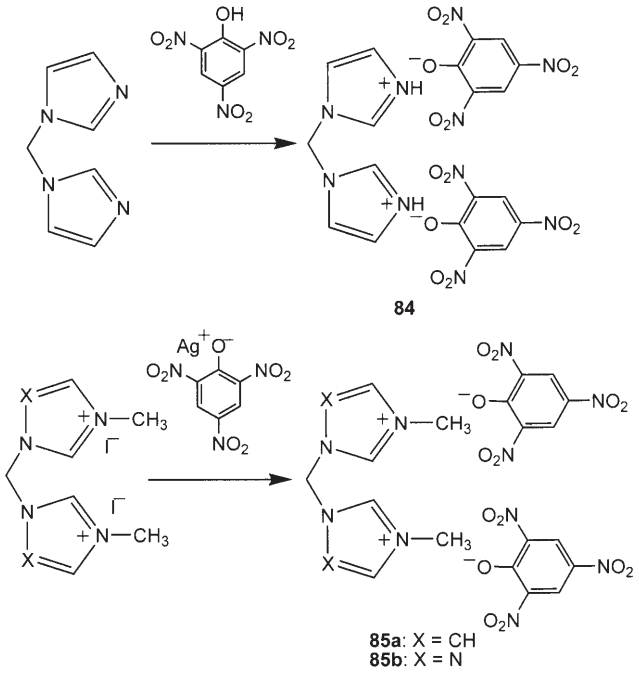

Scheme 19.

thermally than their nitrate analogues and less than the perchlorates. Not surprisingly, the azido derivative (**83b**) exhibited the highest enthalpy of formation but also one of the lowest thermal stabilities of this family of picrates, decomposing at 176 °C. 5-Aminotetrazolium picrate (**81b**) was the densest of the picrate salts at 1.85 g cm^{-3} (determined by X-ray), which places it between picric acid (1.77 cm g^{-3}) and HMX (1.90 g cm^{-3}). Protonation in **81a** occurred at one of the ring nitrogen atoms rather than on the N-bound amino group. However, in contrast, in the reaction of picric acid with the C-amino triazole, a high melting ammonium salt **82** was formed.

8. Polynitrogen-Containing Salts

Polynitrogen compounds are of significant interest as high-energy materials for propulsion or explosive applications.[68] In spite of numerous theoretical studies, in which certain all-nitrogen compounds have been predicted to be stable, only a few unsuccessful experimental studies aimed at their actual syntheses have been reported. Although the two simplest, N_2 and N_3^-, are well known, some other species such as N_4 ≪, N_3^+, N_4^+ have been observed only as free gaseous or matrix-isolated ions or radicals. Theoretically, some polynitrogen species, such as N_4, N_8, $[N(N_3)_2]^-$, $N(N_3)_3$, and $[N(N_4)_4]^+$ should be vibrationally stable. In the past few years, the single most important breakthrough has been the synthesis and study of the N_5^+ ion.[69]

The synthesis of $N_5^+[AsF_6]^-$ (**86**) was accomplished by the reaction of $[N_2F]^+[AsF_6]^-$ and HN_3 in the presence of HF (Scheme 20).[69] In this reaction a small excess of HN_3 is used to ensure the complete conversion of the $[N_2F]^+[AsF_6]^-$. The only by-product was protonated HN_3 (less than 20%).

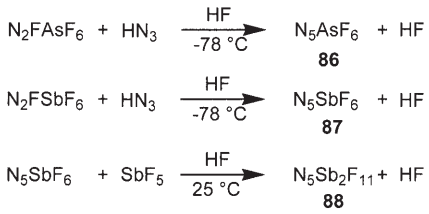

Scheme 20.

Compound **86** was a white solid that was sparingly soluble in anhydrous HF and marginally stable at 22 °C. However, it was storable for weeks at −78 °C without noticeable decomposition. With water, **86** was violently explosive. The high energy density of N_5^+ was confirmed by the G2 method of calculation, and the enthalpies of formation were $\Delta H_f^\circ = 1478$ and $\Delta H_f^{298} = 1469$ kJ mol^{-1} for free gaseous N_5^+.

The stable salt $N_5^+[SbF_6]^-$ (**87**) was also synthesized using a similar procedure and characterized.[70] When **87** was treated with an equimolar amount of SbF_5 in anhydrous HF at room temperature, the salt $N_5^+[Sb_2F_{11}]^-$ (**88**) was obtained (Scheme 20). Both **87** and **88** are colorless, hygroscopic solids that are soluble in anhydrous HF and stable at room temperature. Based on DSC measurements, thermal decomposition started at 70 °C. The structure for **88** has been obtained using single-crystal X-ray analyses.

A large number of compounds with the N_5^+ ion have subsequently been synthesized in anhydrous HF (Scheme 21).[71] Salts **89** and **90** are friction-sensitive white solids. Compounds **91** and **92** are extremely shock-sensitive and explode upon warming to room temperature. Compound **93** is a clear, colorless liquid and a very useful intermediate in the synthesis of other N_5^+ salts. Salts **94**, **95**, and **96** are marginally stable white solids that were characterized by vibrational (IR, Raman), and NMR spectroscopy.

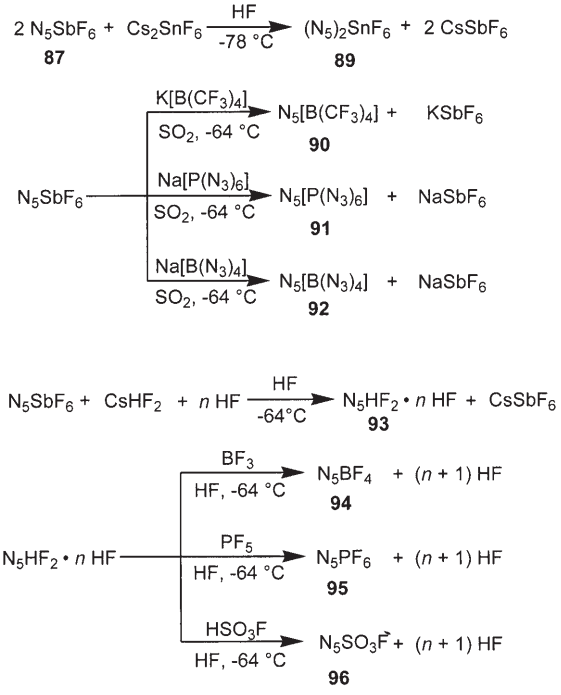

Scheme 21.

 © 2006 Wiley-VCH Verlag GmbH & Co. KGaA, Weinheim

Theoretical studies on the N_6^{2+} and N_4^{2+} ions and their N_{10} and N_{12} azido derivatives were carried out.[72] Enthalpies of formation of gas-phase N_3, N_3^-, N_5^+, and N_5^- have been calculated from ab initio molecular orbital theory. The salts $N_5^+N_3^-$ and $N_5^+N_5^-$ were shown to be unstable and should decompose spontaneously into $N_3^{\cdot}$ and N_2.[73]

9. Imidazolium-Based Salts

Imidazolium salts with fluorine-containing anions have dominated the field of ionic liquids.[74] However, nitro- and azido-substituted imidazoles, when paired with nitrate or perchlorates, form solid energetic salts **97a–h** in excellent yields.[30] Salts **97a–f** were made by the metathesis of the

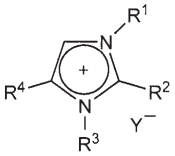

97a: $R^1 = CH_3$, $R^2 = H$, $R^3 = CH_3$, $R^4 = NO_2$, $Y = ClO_4$
97b: $R^1 = CH_3$, $R^2 = H$, $R^3 = CH_3$, $R^4 = NO_2$, $Y = NO_3$
97c: $R^1 = R^2 = R^3 = CH_3$, $R^4 = NO_2$, $Y = ClO_4$
97d: $R^1 = R^2 = R^3 = CH_3$, $R^4 = NO_2$, $Y = NO_3$
97e: $R^1 = R^2 = CH_3$, $R^3 = C_2H_5$, $R^4 = NO_2$, $Y = ClO_4$
97f: $R^1 = R^2 = CH_3$, $R^3 = C_2H_5$, $R^4 = NO_2$, $Y = NO_3$
97g: $R^1 = H$, $R^2 = N_3$, $R^3 = H$, $R^4 = H$, $Y = ClO_4$
97h: $R^1 = H$, $R^2 = N_3$, $R^3 = H$, $R^4 = H$, $Y = NO_3$

corresponding iodide salt with $AgClO_4$ and $AgNO_3$, whereas **97g,h** are formed by the reactions of 2-azidoimidazole with $HClO_4$ and HNO_3, respectively. All these compounds are well-characterized solids. In general, the nitrate salts have lower melting points and thermal stabilities than the corresponding perchlorates. Energetic ionic salts containing imidazolium triazolate or tetrazolate, and tetrazolium imidazolate are described in Section 2.5.

10. Miscellaneous

Crystal structures of hydrazinium dinitramide, $[NH_2NH_3]^+[N(NO_2)_2]^-$, (**98**) and hydroxylammonium dinitramide , $[NH_3OH]^+[N(NO_2)_2]^-$, (**99**) salts show the presence of protonated amine cations and dinitramide anions that are linked by hydrogen bonding.[75] In addition, in **99** there are both neutral and zwitterionic hydroxylamine moieties involved in the hydrogen-bonding scheme. The actual formula for **99** was claimed to be $[NH_3^+OH]_2[N_3O_4^-]_2 \cdot (NH_2OH) \cdot [NH_3^+O^-]$ in which, the hydroxylamine exists in its three possible forms: protonated, neutral, and zwitterionic.

Reaction of *tert*-butylhydrazine with HN_3 is reported to yield *tert*-butylhydrazinium azide, $[(CH_3)_3CNH_2NH_2]^+N_3^-$ (**100**), and *N,N,N*-trimethylhydrazinium azide, $[NH_2N(CH_3)_3]^+N_3^-$ (**101**) is obtained by the reaction of silver azide with *N,N,N*-trimethylhydrazinium iodide.[76] Both of these salts are characterized by X-ray structural analysis, IR, Raman, and multinuclear NMR spectroscopy. Compound **100**, unlike **101**, is very hygroscopic.

There is a report on high energetic tetraazidoborate salts (Scheme 22).[77,78] Tetraphenylphosphonium tetraazidoborate

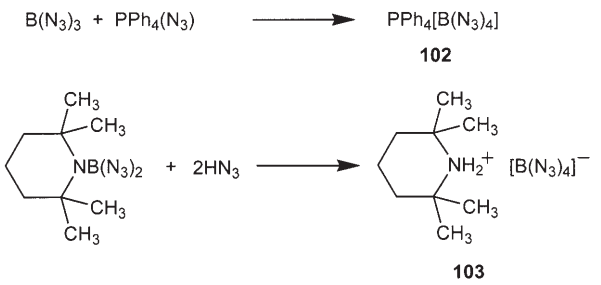

Scheme 22.

(**102**) is made from $B(N_3)_3$ and $PPh_4(N_3)$ and characterized by X-ray crystal structure.[77] When 2,2,6,6-tetramethylpiperidinoboron diazide was treated with HN_3, the salt 2,2,6,6-tetramethylpiperidinium tetraazidoborate (**103**) resulted.[78]

Various metal azides and their binary azide salts have been also reported.[79] Reaction of metal fluorides with trimethylsilylazide led to the formation of **104a,b** and **105**. When these metal azides were further treated with tetraphenylphosphonium azide or tetramethylamonium azide, **106a–d** and **107** are formed (Scheme 23).

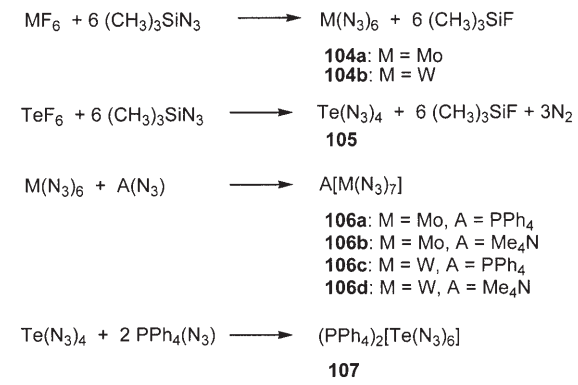

Scheme 23.

The salts **104a,b**, **106a–d** are obtained as dark red solids whereas **105** and **107** are bright yellow and orange solids, respectively. All these polyazide metal salts are very shock sensitive and can explode violently. Binary salts **106a–d**, **107** are claimed to be more shock-sensitive than their corresponding metal azide salts **104a,b** and **105**.

Very recently the synthesis of highly energetic, tetrazolium polynitratoaluminate **108** which has a good oxygen balance was reported.[80]

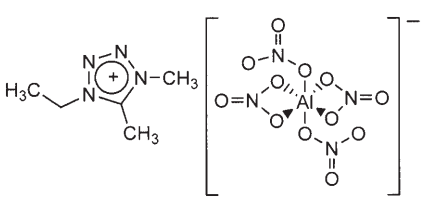

108

 © 2006 Wiley-VCH Verlag GmbH & Co. KGaA, Weinheim

11. Conclusion

Energetic ionic salts, whether solid or liquid, offer many advantages over traditional molecular energetic compounds. Salt-based energetic materials tend to exhibit lower vapor pressures and higher densities and, in many cases, an enhanced thermal stability compared to their atomically similar non-ionic analogues. The use of heterocyclic nitrogen-containing cations and anions contributes to higher heats of formation and higher densities, and the low amounts of carbon and hydrogen also allow for a good oxygen balance to be achieved more readily than with their carbocyclic analogues. Because a higher percentage of the decomposition products will be dinitrogen, these nitrogen-rich compounds are promising high-energetic materials that may be more acceptable than their alternatives for both industrial and military uses.

Received: November 29, 2005

[1] a) C. E. Gregory, *Explosives for North American Engineers*, *Vol. 5*, Trans Tech Publications, Clausthal-Zellerfeld, **1984**; b) T. L. Davis, *The Chemistry of Powder and Explosives*, *Vol. 2*, Wiley, New York, **1943**.

[2] a) M. A. Cook, *The Science of High Explosives*, Reinhold, New York, **1958**; b) *Encyclopedia of Chemical Technology*, *Vol. 10*, Wiley, New York, **1994**.

[3] T. Urbanski, *Chemistry and Technology of Explosives*, *Vol. 3*, Pergamon, Oxford, **1964**.

[4] A. Bailey, S. G. Murray, *Explosives, Propellents and Pyrotechnics*, Brassey's, Oxford, **1989**.

[5] T. Urbanski, *Chemistry and Technology of Explosives*, *Vol. 4*, Pergamon, Oxford, **1984**, p. 202.

[6] J. P. Agrawal, *Prog. Energy Combust. Sci.* **1998**, *24*, 1 – 30.

[7] G. Singh, I. P. S. Kapoor, S. M. Mannan, J. Kaur, *J. Hazard. Mater.* **2000**, *79*, 1 – 18.

[8] L. E. Fried, M. R. Manaa, P. F. Pagoria, R. L. Simpson, *Annu. Rev. Mater. Res.* **2001**, *31*, 291 – 321.

[9] V. A. Shlyapochnikov, M. A. Tafipolsky, I. V. Tokmakov, E. S. Baskir, O. V. Anikin, Y. A. Strelenko, O. A. Luk'yanov, V. A. Tartakovsky, *J. Mol. Struct.* **2001**, *559*, 147 – 166.

[10] P. F. Pagoria, G. S. Lee, A. R. Mitchell, R. D. Schmidt, *Thermochim. Acta* **2002**, *384*, 187 – 204.

[11] A. I. Lesnikovich, O. A. Ivashkevich, S. V. Levchik, A. I. Balabanovich, P. N. Gaponik, A. A. Kulak, *Thermochim. Acta* **2002** *388*, 233 – 2051.

[12] a) A. K. Sikder, N. J. Sikder, *J. Hazard. Mater.* **2004**, *112*, 1 – 15; b) "Ideas to Expand Thinking About New Energetic Materials": J. Bottaro, *Adv. Ser. Phys. Chem.* **2005**, *16*, 473 – 501.

[13] H. Feuer, A. T. Nielsen, *Nitro Compounds*, VCH, New York, **1990**.

[14] A. T. Nielsen, *Nitrocarbons*, VCH, New York, **1995**.

[15] J. Köhler, R. Meyer, *Explosivstoffe*, 7th ed., Wiley-VCH, Weinheim, **1991**; J. Köhler, R. Meyer, *Explosivstoffe*, 9th ed., Wiley-VCH, Weinheim, **1998**.

[16] T. M. Klapötke, B. Krumm, G. Holl, M. Kaiser, *Energetic Materials: Modeling of Phenomena, Experimental Characterization, Environmental Engineering*, Fraunhofer-Institut, Karlsruhe, **2000**.

[17] R. L. Simpson, P. A. Urtiew, D. L. Ornellas, G. L. Moody, K. S. Scribner, D. M. Hofman, *Propellants Explos. Pyrotech.* **1997**, *22*, 249 – 255, zit. Lit.

[18] "New Energetic Materials": H. H. Krause in *Energetic Materials* (Ed.: U. Teipal), Wiley-VCH, Weinheim, **2005**.

[19] M. A. Hiskey, D. E. Chavez, D. L. Naud, S. F. Son, H. L. Berghout, C. A. Bolme, *Proc. Int. Pyrotech. Semin.* **2000**, *27*, 3 – 14.

[20] T. Welton, *Chem. Rev.* **1999**, *99*, 2071 – 2083.

[21] P. Wasserscheid, W. Keim, *Angew. Chem.* **2000**, *112*, 3926 – 3945; *Angew. Chem. Int. Ed.* **2000**, *39*, 3772 – 3789.

[22] P. Wasserscheid, T. Welton, *Ionic Liquids in Synthesis*, Wiley-VCH, Weinheim, Germany, **2003**.

[23] R. D. Rogers, K. R. Seddon, *Ionic Liquids as Green Solvents: Progress and Prospects*, *ACS Symposium Series 856*, American Chemical Society, Washington, DC, **2003**.

[24] R. D. Rogers, K. R. Seddon, *Ionic Liquids: Industrial Applications to Green Chemistry*, *ACS Symposium Series 818*, American Chemical Society, Washington, DC, **2002**.

[25] a) N. Jain, A. Kumar, S. Chauhan, S. M. S. Chauhan, *Tetrahedron* **2005**, *61*, 1015 – 1060; b) H. Xue, R. D. Verma, J. M. Shreeve, *J. Fluorine Chem.* **2006**, *127*, 159 – 176.

[26] P. Jiminez, M. V. Roux, C. J. Turrion, *Chem. Thermodyn.* **1989**, *21*, 759 – 764.

[27] J. B. Pedley, *Thermochemical Data and Structure of Organic Compounds*, *Vol. I*, Thermodynamic Research Center, College Station, **1994**.

[28] a) G. W. Drake, T. Hawkins, A. Brand, L. Hall, M. McKay, A. Vij, I. Ismail, *Propellants Explos. Pyrotech.* **2003**, *28*, 174 – 180; b) G. W. Drake, US Patent 6,509,473 B1, **2003**; c) M. W. Schmidt, M. S. Gordon, J. A. Boatz, *J. Phys. Chem. A* **2005**, *109*, 7285 – 7295.

[29] H. Xue, S. W. Arritt, B. Twamley, J. M. Shreeve, *Inorg. Chem.* **2004**, *43*, 7972 – 7977.

[30] H. Xue, Y. Gao, B. Twamley, J. M. Shreeve, *Chem. Mater.* **2005**, *17*, 191 – 198.

[31] a) G. W. Drake, T. Hawkins, K. Tollison, L. Hall, A. Vij, S. Sobaski in *Ionic Liquids-III A: Fundamentals, Progress, Challenges, and Opportunities*, *ACS Symposium Series 902* (Eds.: R. D. Rogers, K. R. Seddon), American Chemical Society, Washington, DC, **2005**, pp. 259 – 302; b) S. Trohalaki, R. Pachter, G. W. Drake, T. Hawkins, *Energy Fuels* **2005**, *19*, 279 – 284.

[32] V. A. Ostrovskii, M. S. Pevzner, T. P. Kofman, I. V. Tselinskii, *Targets Heterocycl. Syst.* **1999**, *3*, 467 – 526.

[33] C. C. Denault, P. C. Marx, H. H. Takimoto, *J. Chem. Eng. Data* **1968**, *13*, 514 – 516.

[34] H. Xue, J. M. Shreeve, *Adv. Mater.* **2005**, *17*, 2142 – 2146.

[35] a) S. Buscemi, A. Pace, I. Pibiri, N. Vivona, D. Spinelli, *J. Org. Chem.* **2003**, *68*, 605 – 608; b) K. Funabiki, N. Noma, K. Shibata, *J. Chem. Res. Synop.* **1999**, 300 – 301, zit. Lit.

[36] H. Xue, B. Twamley, J. M. Shreeve, *J. Org. Chem.* **2004**, *69*, 1397 – 1400.

[37] a) Y. R. Mirzaei, J. M. Shreeve, *Synthesis* **2003**, 24 – 26; b) Y. R. Mirzaei, J. M. Shreeve, *J. Org. Chem.* **2002**, *67*, 9340 – 9345.

[38] a) Y. R. Mirzaei, H. Xue, J. M. Shreeve, *Inorg. Chem.* **2004**, *43*, 361 – 367; b) O. P. Shitov, V. L. Korolev, V. S. Bogdanov, V. A. Tartakovsky, *Russ. Chem. Bull.* **2003**, *52*, 695 – 699.

[39] M. Egashira, B. Scrosati, M. Armand, S. Beranger, C. Michot, *Electrochem. Solid-State Lett.* **2003**, *6*, A71 – A73.

[40] a) A. Katritzky, S. Singh, K. Kirichenko, J. D. Holbrey, M. Smiglak, M. W. Reichert, R. D. Rogers, *Chem. Commun.* **2005**, 868 – 870; b) M. I. Sitzmann, *J. Org. Chem.* **1978**, *43*, 3389 – 3391; c) T. P. Kofman, E. A. Paketina, *Russ. J. Org. Chem.* **1997**, *33*, 1125 – 1132; d) V. M. Chernyshev, N. D. Zemlyakov, V. B. Il'in, V. A. Taranushich, *Zh. Prikl. Khim.* **2000**, *73*, 791 – 793.

[41] W. Ogihara, M. Yoshizawa, H. Ohno, *Chem. Lett.* **2004** *33*, 1022 – 1023.

[42] H. Xue, Y. Gao, B. Twamley, J. M. Shreeve, *Inorg. Chem.* **2005**, *44*, 5068 – 5072.

 © 2006 Wiley-VCH Verlag GmbH & Co. KGaA, Weinheim

[43] A. R. Martin, H. J. Yallop, *Trans. Faraday Soc.* **1958**, *54*, 257 – 267.
[44] V. A. Ostrovskii, G. I. Koldobskii, N. P. Shirokova, V. S. Poplavskii, *Khim. Geterotsikl. Soedin.* **1981**, *4*, 559 – 562.
[45] I. M. Krakovskii, M. S. MolChanova, A. V. Evtushenko, V. A. Shlyapochnikova, *Russ. Chem. Bull.* **1998**, *47*, 1266 – 1273.
[46] A. A. Kozyro, V. V. Simirsky, A. P. Krasulin, V. M. Sevruk, G. J. Kabo, M. L. Gopanik, Y. V. Grigotiev, *Zh. Fiz. Khim.* **1990**, *64*, 656 – 661.
[47] A. Gao, Y. Oyumi, T. B. Brill, *Combust. Flame* **1991**, *83*, 345 – 352.
[48] M. von Denffer, T. M. Klapötke, G. Kramer, G. Spiess, J. M. Welch, G. Heeb, *Propellants Explos. Pyrotech.* **2005**, *30*, 191 – 195.
[49] a) T. M. Klapötke, P. Mayer, A. Schulz, J. J. Weigand, *J. Am. Chem. Soc.* **2005**, *127*, 2032 – 2033; b) J. C. Gálvez-Ruiz, G. Holl, K. Karaghiosoff, T. M. Klapötke, K. Löhnwitz, P. Mayer, H. Nöth, K. Polborn, C. J. Rohbogner, M. Suter, J. J. Weigand, *Inorg. Chem.* **2005**, *44*, 4237 – 4253; c) G. Fisher, G. Holl, T. M. Klapötke, J. J. Weigand, *Thermochim. Acta* **2005**, *437*, 168 – 178; d) J. Geith, T. M. Klapötke, J. Weigand, *Propellants Explos. Pyrotech.* **2004**, *29*, 3 – 8; e) A. Hammerl, T. M. Klapötke, H. Nöth, L. M. Warchhold, G. Holl, *Propellants Explos. Pyrotech.* **2003**, *28*, 165 – 173; f) A. Hammerl, T. M. Klapötke, P. Mayer, J. J. Weigand, G. Holl, *Propellants Explos. Pyrotech.* **2005**, *30*, 17 – 26.
[50] a) J. Thiele, *Justus Liebigs Ann. Chem.* **1892**, *270*, 54 – 63; b) J. Thiele, J. T. Marais, *Justus Liebigs Ann. Chem.* **1893**, *273*, 144 – 160; c) J. Thiele, *Ber. Dtsch. Chem. Ges.* **1893**, *26*, 2645 – 2646; d) J. Thiele, *Justus Liebigs Ann. Chem.* **1898**, *303*, 57 – 75.
[51] A. Hammerl, G. Holl, T. M. Klapötke, P. Mayer, H. Noth, H. Piotrowski, M. Warchhold, *Eur. J. Inorg. Chem.* **2002**, 834 – 845.
[52] a) M. A. Hiskey, N. Goldman, J. R. Stine, *J. Energ. Mater.* **1998**, *16*, 119 – 127; b) Y. Peng, C. Wong, US Pat. 5,877,300, **1999**.
[53] a) A. Hammerl, T. M. Klapötke, H. Nöth, M. Warchhod, G. Holl, M. Kaiser, U. Ticmanis, *Inorg. Chem.* **2001**, *40*, 3570 – 3575; b) A. Hammerl, G. Holl, M. Kaiser, T. M. Klapötke, P. Mayer, H. Piotrowski, M. Vogt, *Z. Naturforsch.* **2001**, 847 – 856; c) A. Hammerl, G. Holl, M. Kaiser, T. M. Klapötke, P. Mayer, H. Nöth, H. Piotrowski, M. Suter, *Z. Naturforsch.* **2001**, 857 – 870; d) T. M. Klapotke, G. Holl, *Green Chem.* **2001**, G75 – G76.
[54] a) A. Hammerl, A. M. A. Hiskey, G. Holl, T. M. Klapötke, K. Polborn, J. Stierstorfer, J. Weigand, *Chem. Mater.* **2005**, *17*, 3784 – 3793; b) M. A. Hiskey, D. E. Chavez, D. L. Naud, S. F. Son, H. L. Berghout, C. A. Bolme, *Proc. Int. Pyrotech. Semin.* **2000**, *27*, 3 – 14.
[55] C. Ye, J.-C. Xiao, B. Twamley, J. M. Shreeve, *Chem. Commun.* **2005**, 2750 – 2752.
[56] a) S. Hyoda, M. Kita, H. Sawada, S. Nemugaki, S. Otsuka, Y. Miyawaki, T. Ogawa, Y. Kubo, US Pat. 6,040,453, **2000**; b) S. Hyoda, M. Kita, A. Sugino, T. Ueta, K. Sato, Eur. Pat. 1162198, **2001**; c) S. Hyoda, M. Kita, H. Swada, S. Nemugaki, T. Ueta, K. Satoh, S. Otsuka, Y. Miyawaki, H. Taniguchi, Eur. Pat. Appl., Eur. Pat. 1016662, **2000**; d) S. Torii, M. Tsuyama, Y. Miyawaki, Y. Kubo, T. Ogawa, Jpn. Kokai Tokkyo Koho, JP 2000281662, **2000**; e) M. Friedrich, J. C. Gálvez-Ruiz, T. M. Klapötke, P. Mayer, B. Weber, J. J. Weigand, *Inorg. Chem.* **2005**, *44*, 8044 – 8052; f) A. Hammerl, G. Holl, M. Kaiser, T. M. Klapötke, H. Piotrowski, *Z. Anorg. Allg. Chem.* **2003**, *629*, 2117 – 2121.
[57] a) M. Kita, T. Ueda, Jpn. Kokai Tokkyo Koho, JP 2004067544, **2004**; b) D. L. Naud, M. A. Hiskey, US Pat. Appl. Publ., 2003060634, **2003**; c) T. K. Highsmith, R. M. Hajik, R. B. Wardle, G. K. Lund, R. J. Blau, US Pat. 5,468,866, **1995**.
[58] M. E. Foss, E. L. Hirst, J. K. N. Jones, H. D. Springall, A. T. Thomas, T. Urbanski, *J. Chem. Soc.* **1950**, 624 – 628.
[59] H.-G. Ang, W. Fraenk, K. Karaghiosoff, T. M. Klapötke, H. Nöth, J. Sprott, M. Sutter, M. Vogt, M. Z. Warchhold, *Z. Anorg. Allg. Chem.* **2002**, *628*, 2901 – 2906.
[60] H. Xue, B. Twamley, J. M. Shreeve, unpublished results.
[61] a) D. E. Chavez, M. A. Hiskey, D. I. Naud, *Propellants Explos. Pyrotech.* **2004**, *29*, 209 – 215; b) J. C. Oxley, J. L. Smith, H. Chen, *Thermochim. Acta* **2002**, *384*, 91 – 99; c) D. E. Chavez, M. A. Hiskey, R. D. Gilardi, *Org. Lett.* **2004**, *6*, 2889 – 2891.
[62] a) T. G. Archibald, R. Gilardi, K. Baum, C. George, *J. Org. Chem.* **1990**, *55*, 2920 – 2924; b) M. D. Coburn, M. A. Hiskey, T. G. Archibald, *Waste Manage.* **1997**, *17*, 143 – 146.
[63] M. A. Hiskey, M. D. Coburn, M. A. Mitchell, B. C. Benicewicz, *J. Heterocycl. Chem.* **1992**, *29*, 1855 – 1856.
[64] M. A. Hiskey, M. M. Stincipher, J. E. Brown, *J. Energ. Mater.* **1993**, *11*, 157 – 165.
[65] R. D. Gilardi, R. J. Butcher, *J. Chem. Crystallogr.* **1998**, *28*, 163 – 169.
[66] M. D. Coburn, M. A. Hiskey, J. C. Oxley, J. L. Smith, W. Zheng, E. Rogers, *J. Energ. Mater.* **1998**, *16*, 73 – 99.
[67] C. M. Jin, C. Ye, C. Piekarski, B. Twamley, J. M. Shreeve, *Eur. J. Inorg. Chem.* **2005**, 3760 – 3767.
[68] a) G. Chung, M. W. Schmidt, M. S. Gordon, *J. Phys. Chem. A* **2000**, *104*, 5647 – 5650; b) S. Fau, R. J. Bartlett, *J. Phys. Chem. A* **2001**, *105*, 4096 – 4106; c) N. T. Nguyen, *Coord. Chem. Rev.* **2003**, *244*, 93 – 113; d) K. O. Christe, D. A. Dixon, D. McLemore, W. W. Wilson, J. A. Sheehy, J. A. Boatz, *J. Fluorine Chem.* **2000**, *101*, 151 – 153.
[69] K. O. Christe, W. W. Wilson, J. A. Sheehy, J. A. Boatz, *Angew. Chem.* **1999**, *111*, 2112 – 2118; *Angew. Chem. Int. Ed.* **1999**, *38*, 2004 – 2009.
[70] a) A. Vij, W. W. Wilson, V. Vij, F. S. Tham, J. A. Sheehy, K. O. Christe, *J. Am. Chem. Soc.* **2001**, *123*, 6308 – 6313; b) S. D. Kunikeev, H. S. Taylor, T. Schroer, R. Haiges, C. J. B. Jones, K. O. Christe, *Inorg. Chem.* **2006**, *45*, 437 – 442.
[71] a) W. W. Wilson, A. Vij, V. Vij, E. Bernhardt, K. O. Christe, *Chem. Eur. J.* **2003**, *9*, 2840 – 2844; b) R. Haiges, S. Schneider, T. Schroer, K. O. Christe, *Angew. Chem.* **2004**, *116*, 5027 – 5032; *Angew. Chem. Int. Ed.* **2004**, *43*, 4919 – 4924.
[72] G. A. Olah, G. K. S. Prakash, G. Rasul, *J. Am. Chem. Soc.* **2001**, *123*, 3308 – 3310.
[73] D. A. Dixon, D. Feller, K. O. Christe, W. W. Wilson, A. Vij, V. Vij, D. B. Jenkins, R. M. Olson, M. S. Gordon, *J. Am. Chem. Soc.* **2004**, *126*, 834 – 843.
[74] H. Xue, J. M. Shreeve, *Eur. J. Inorg. Chem.* **2005**, 2573 – 2580.
[75] R. Gilardi, R. J. Butcher, *J. Chem. Crystallogr.* **2000**, *30*, 599 – 604.
[76] T. Habereder, A. Hammerl, G. Holl, T. M. Klapötke, J. Knizek, H. Nöth, *Eur. J. Inorg. Chem.* **1999**, 849 – 852.
[77] W. Fraenk, H. Nöth, T. M. Klapötke, M. Suter, *Z. Naturforsch. B* **2002**, *57*, 621 – 624.
[78] W. Fraenk, T. Habereder, A. Hammerl, T. M. Klapötke, B. Krumm, P. Mayer, H. Nöth, M. Warchhold, *Inorg. Chem.* **2001**, *40*, 1334 – 1340.
[79] a) R. Haiges, R. Bau, S. Schneider, T. Schroer, M. Yousufuddin, K. O. Christe, *Angew. Chem.* **2005**, *117*, 1894 – 1899; *Angew. Chem. Int. Ed.* **2005**, *44*, 1860 – 1865; b) C. Knapp, J. Passmore, *Angew. Chem.* **2004**, *116*, 4938 – 4941; *Angew. Chem. Int. Ed.* **2004**, *43*, 4834 – 4836; c) K. O. Christe, R. Haiges, M. Gerken, S. Schneider, T. Schroer, *Angew. Chem.* **2003**, *115*, 6027 – 6031; *Angew. Chem. Int. Ed.* **2003**, *42*, 5847 – 5851; d) R. Haiges, J. A. Boatz, A. Vij, V. Vij, M. Gerken, S. Schneider, T. Schroer, M. Yousufuddin, K. O. Christe, *Angew. Chem.* **2004**, *116*, 6844 – 6848; *Angew. Chem. Int. Ed.* **2004**, *43*, 6676 – 6680.
[80] K. O. Christe, A. Vij, V. Vij, W. W. Wilson, J. Boatz, C. B. Jones, T. Schroer, R. Haiges, H. Taylor, S. Kounikeev, M. Yousufuddin, Program No. 1536. International Chemical Congress of Pacific Basin Societies, Honolulu, HI, December **2005**.

 © 2006 Wiley-VCH Verlag GmbH & Co. KGaA, Weinheim

Communications

DOI: 10.1002/anie.200600366

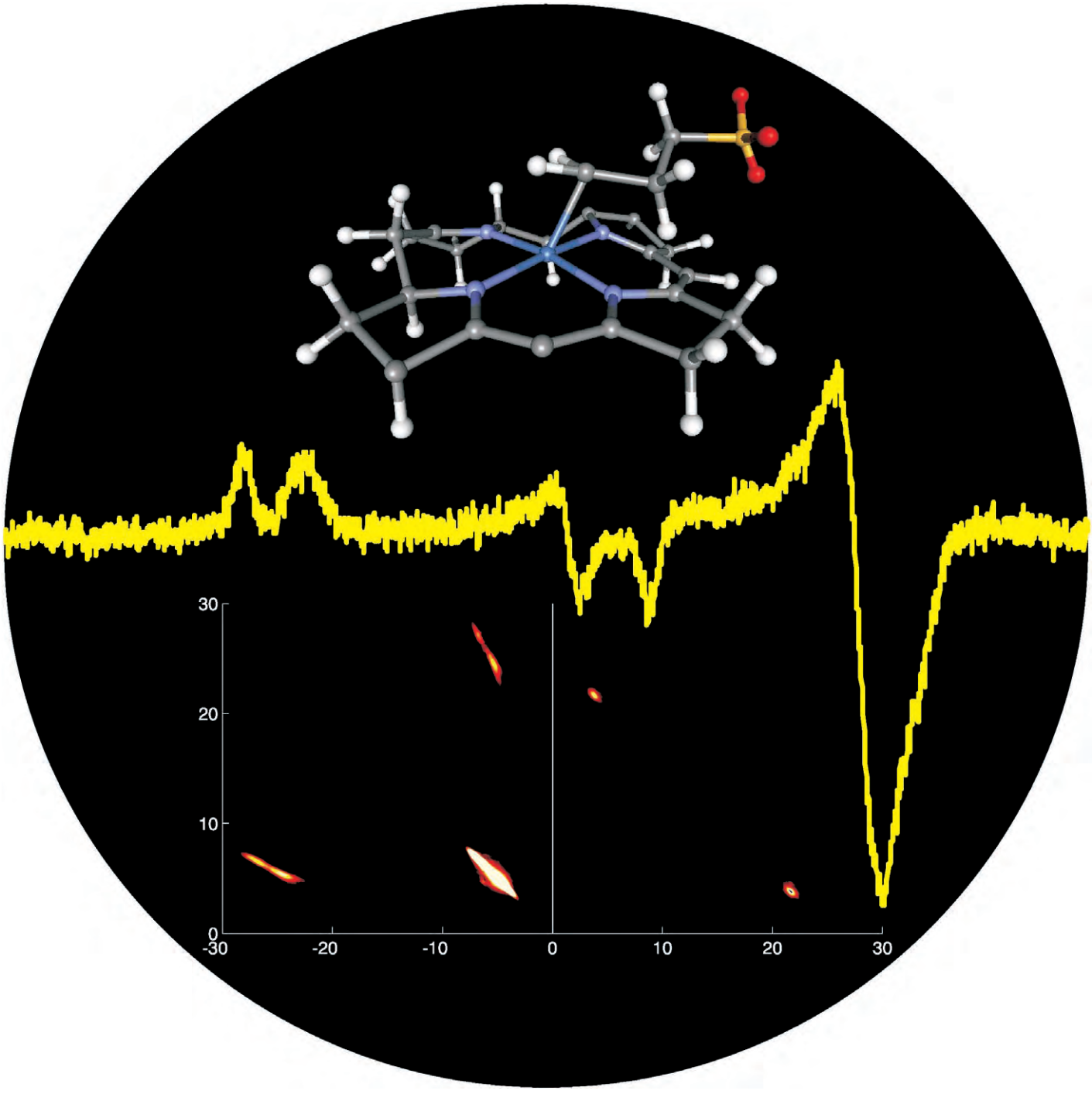

An EPR study has shown that a Ni–C bond is formed at the active site of methyl-coenzyme M reductase, the enzyme which catalyzes the key step of methanogenesis in *archaea*, upon reaction with the irreversible inhibitor 3-bromopropane sulfonate. For more details see the Communication by J. Harmer, B. Jaun et al. on the following pages.

WILEY InterScience DISCOVER SOMETHING GREAT
© 2006 Wiley-VCH Verlag GmbH & Co. KGaA, Weinheim

Bioinorganic Chemistry

DOI: 10.1002/anie.200600366

A Nickel–Alkyl Bond in an Inactivated State of the Enzyme Catalyzing Methane Formation**

Dariush Hinderberger, Rafal P. Piskorski, Meike Goenrich, Rudolf K. Thauer, Arthur Schweiger†, Jeffrey Harmer, and Bernhard Jaun**

The cobalt–carbon bonds of methyl cobalamin and adenosyl cobalamin are the only transition-metal–alkyl bonds verified to date in the active site of enzymes. Methyl–nickel bonds have been postulated to be formed during two enzyme-catalyzed steps, for which, however, experimental evidence has not been provided. These reactions are the synthesis of acetyl-coenzyme A from methyl tetrahydrofolate, carbon monoxide, and coenzyme A when catalyzed by acetyl-coenzyme A synthase (decarbonylase),[1] and methane formation from methyl-coenzyme M and coenzyme B when catalyzed by methyl-coenzyme M reductase (MCR).[2,3]

Herein we show, by using electron paramagnetic resonance (EPR) spectroscopy, that a Ni–C bond is formed at the active site of MCR upon reaction with the irreversible inhibitor 3-bromopropane sulfonate (BPS)[4] (Scheme 1). MCR catalyzes the key step of methanogenesis in *archaea*, namely the reduction of methyl-coenzyme M (CH_3S-CoM) with coenzyme B (HS-CoB) to methane and the heterodisulfide CoM-S-S-CoB [Equation (1) and Scheme 1].

$$CH_3S\text{-CoM} + \text{HS-CoB} \rightarrow CH_4 + \text{CoM-S-S-CoB} \qquad \Delta G^{0\prime} = -30\ \text{kJ mol}^{-1} \qquad (1)$$

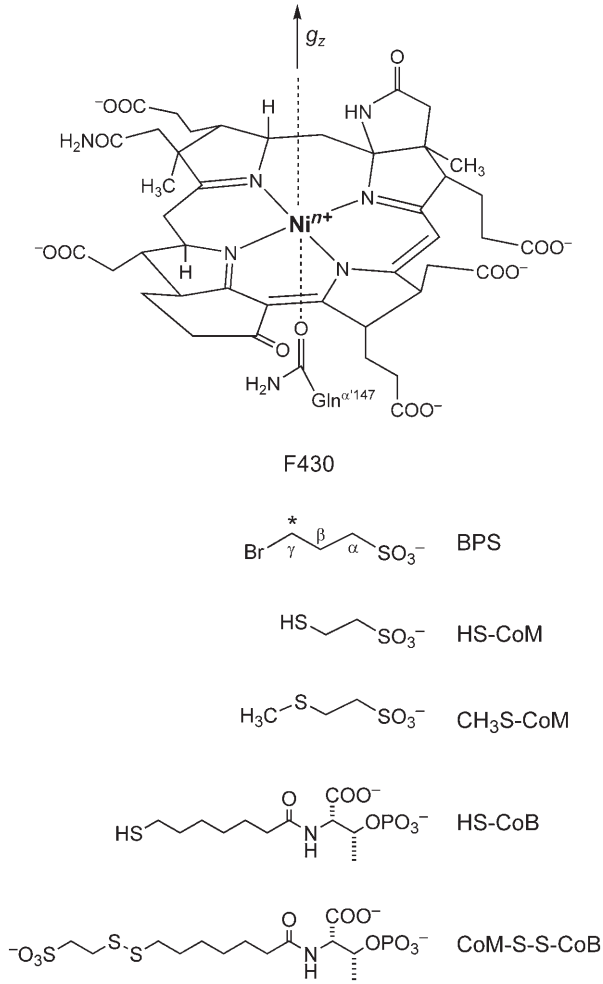

Scheme 1. Schematic representation of F_{430} (Ni^{III}: $n=2$) and the direction of the g_z axis. The substrates or substrate analogues are: BPS: 3-bromopropane sulfonate (the asterisk marks the position of the ^{13}C isotope labeling); HS-CoM: coenzyme M; CH_3S-CoM: methyl-coenzyme M; HS-CoB: coenzyme B; CoM-S-S-CoB: heterodisulfide formed from methyl-coenzyme M and coenzyme B.

Methanogenic archaea are found in strictly anoxic habitats, for example, wetlands, sewage sites, or the rumen and guts of animals, and they gain the energy necessary for ATP synthesis by producing methane from substrates such as H_2/CO_2, acetate, formate, or methanol.[3] This process is responsible for the largest part of the annual emission (estimated 5×10^8 tons per year) of this very effective greenhouse gas into the atmosphere. All methanogens contain MCR, and X-ray crystallographic analysis of inactive Ni^{II} forms shows that the enzyme has two identical active sites, each containing one molecule of factor F_{430} (Scheme 1).[2,3] In the active state, designated MCR_{red1}, the central metal ion is in the Ni^{I} valence state and its EPR spectrum is characteristic of a d^9 $S=1/2$ species with the unpaired electron in a molecular orbital of predominantly Ni $d_{x^2-y^2}$ character.[5]

The catalytic mechanism of the reduction [Eq. (1)] at the nickel center is widely disputed.[6–12] In essence, two mechanisms, which mainly differ in the nature of the initial cleavage of the sulfur–carbon bond of CH_3S-CoM are currently

[*] Dr. D. Hinderberger, Prof. Dr. A. Schweiger, Dr. J. Harmer
Laboratory of Physical Chemistry
Department of Chemistry and Applied Biosciences
ETH Zurich
8093 Zurich (Switzerland)
Fax: (+41) 44 6321021
E-mail: harmer@phys.chem.ethz.ch
Dr. R. P. Piskorski, Prof. Dr. B. Jaun
Laboratory of Organic Chemistry
Department of Chemistry and Applied Biosciences
ETH Zurich
8093 Zurich (Switzerland)
Fax: (+41) 446-321-475
E-mail: jaun@org.chem.ethz.ch
Dr. M. Goenrich, Prof. Dr. R. K. Thauer
Max Planck Institute for Terrestrial Microbiology
Department of Biochemistry, Karl-von-Frisch-Strasse
35043 Marburg (Germany)

[†] Deceased on 4 January 2006

[**] We thank the Swiss National Science Foundation (SNF) and the Fonds der Chemischen Industrie for financial support. D.H. gratefully acknowledges a research scholarship (HI 1094/1-1) from the Deutsche Forschungsgemeinschaft (DFG). We are grateful to Brian M. Hoffman (Northwestern Univ.) for helpful discussions.

Supporting information for this article is available on the WWW under http://www.angewandte.org or from the author.

 © 2006 Wiley-VCH Verlag GmbH & Co. KGaA, Weinheim

discussed. In mechanism "A", proposed by Pelmenschikov et al.[8,9] on the basis of DFT calculations, the Ni^{I} center is assumed to attack the thioether sulfur atom of methyl-CoM, thus generating a methyl radical and the thiolate complex [CoM-S-$Ni^{II}F_{430}$] as intermediates.

According to mechanism "B", the Ni^{I} center initially acts as a nucleophile attacking methyl-coenzyme M at the carbon atom of the CH_3S group, thus generating a CH_3-$Ni^{III}F_{430}$ intermediate and HS-CoM.[10–13] Whereas corresponding CH_3-$Ni^{II}F_{430}$ derivatives have been generated in situ and characterized spectroscopically,[14] no experimental evidence for the existence of a CH_3-$Ni^{III}F_{430}$ species, such as that postulated in mechanism "B", has been reported to date. However, the results of mechanistic studies on the reaction of free $Ni^{I}F_{430}$ derivatives with electrophilic methyl donors such as methyl dialkylsulfonium ions and methyl halides are consistent with mechanism "B", and [CH_3-Ni^{III}L] species have been postulated as intermediates in pulse radiolytic studies with simpler model nickel complexes.[15] Wondimagegn and Ghosh have investigated a model similar to the postulated [CH_3-$Ni^{III}F_{430}$] intermediate by hybrid DFT methods and concluded that this species is a minimum on the hypersurface with a $(d_{xy})^2(d_{xz})^2(d_{yz})^2(d_{x^2-y^2})^1$ ground-state configuration.[16]

The active enzyme MCR_{red1} reacts very rapidly and irreversibly with simple alkyl halides such as chloroform, which has been routinely used to quench the Ni^{I} state and generate Ni^{II} species. The two inhibitors 2-bromoethane sulfonate and 3-bromopropane sulfonate both react irreversibly with MCR_{red1}, but the resulting states are completely different: while 2-bromoethane sulfonate generates a Ni^{II} ion and a carbon-centered protein radical similar to a glycine radical, 3-bromopropane sulfonate reacts to give the MCR_{BPS} species which has a nickel-based, axial X-band continuous-wave EPR (CW-EPR) spectrum.[4]

In view of the known reactivity of free [$Ni^{I}F_{430}$] towards alkyl halides and the results of the DFT study,[16] we considered the possibility that the MCR_{BPS} species might correspond to an [alkyl-$Ni^{III}F_{430}$] derivative resulting from reaction of [$Ni^{I}F_{430}$] with 3-bromopropane sulfonate to give a bromide ion and [$^{-}O_3S(CH_2)_3$-$Ni^{III}F_{430}$] in the active site of MCR. To test this hypothesis we synthesized [3-^{13}C]-3-bromopropane sulfonate (see Scheme 1 and the Supporting Information), then treated active MCR_{red1} with it, and investigated the resulting ^{13}C-MCR_{BPS} samples by using high-frequency CW-EPR (W-band, microwave frequency ca. 94 GHz), high-resolution pulse electron nuclear double resonance (ENDOR), and hyperfine sublevel correlation (HYSCORE) spectroscopy.[17] As a control, MCR_{BPS} samples induced by reaction of MCR_{red1} with unlabeled 3-bromopropane sulfonate were also studied.

Figure 1a displays the echo-detected Q-band (35.3 GHz) EPR spectrum of ^{13}C-MCR_{BPS}. The arrows indicate the observer positions of the Q-band Davies ENDOR (Figure 1b, positions 1–3), and HYSCORE (Figure 1c, position 1) measurements. Figure 1d shows a simulation of the HYSCORE spectrum in Figure 1c.

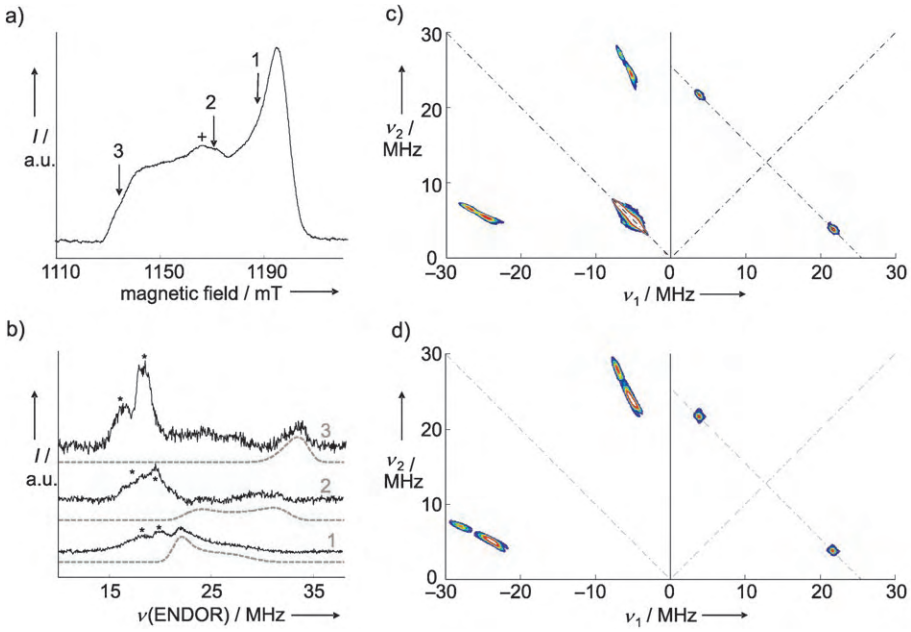

Figure 1. Representative Q-band (35.3 GHz) EPR experiments on ^{13}C-MCR_{BPS} (experiments at additional field positions are presented in the Supporting Information). a) Echo-detected field-swept EPR spectrum. The cross indicates a small MCR_{ox1} impurity.[18,19] b) Davies ENDOR spectra and simulations of the $^{13}C_\gamma$ signals measured at the field positions marked "1–3" in (a). Only the high-frequency peaks are shown. Features marked by asterisks represent peaks from the hydropyrrolic ^{14}N nuclei of F_{430} (see the Supporting Information for simulations). c) HYSCORE spectrum measured at position "1" showing $^{13}C_\gamma$ signals. d) Simulation of (c) by using the $^{13}C_\gamma$ hyperfine parameters given in Table 1.

The EPR spectrum in Figure 1a is consistent with previous reports and shows the typical *g*-value ordering and small orthorhombicity (Table 1) for a singly occupied molecular orbital (SOMO) comprised predominantly of a Ni $d_{x^2-y^2}$ orbital. The W-band (94.1 GHz) CW-EPR spectrum and a simulation performed with the *g* values listed in Table 1 can be found in the Supporting Information.[18] Similar EPR spectra are observed for MCR_{red1},[5] MCR_{ox1},[19] and the model complexes nickel(I)octaethylisobacteriochlorin ([Ni^{I}-(oeibc)])[20a] and [$(CN)_2Ni^{III}$tpp] (tpp = tetraphenylporphyrin),[20b] all of which have a $d_{x^2-y^2}$ SOMO. The ENDOR spectra in Figure 1b show signals from both ^{14}N and ^{13}C nuclei. The nitrogen features could be simulated with hyperfine couplings of approximately 30 MHz and are similar to those found in the MCR_{red1} state (see the Supporting Information). This result also supports our interpretation of the *g* values stem-

 © 2006 Wiley-VCH Verlag GmbH & Co. KGaA, Weinheim

Table 1: MCR_{BPS} *g* matrix and ^{13}C and ^{1}H hyperfine matrices as determined from simulations of the experimental spectra.[a]

	g_x	g_y	g_z		
BPS	2.1081 ± 0.0005	2.1116 ± 0.0005	2.2193 ± 0.0005		
	A_x [MHz]	A_y [MHz]	A_z [MHz]	A_{iso} [MHz]	α, β, γ [°]
$^{13}C_\gamma$	17.6 ± 0.5	18.3 ± 0.5	45.0 ± 1	27.0 ± 0.7	42, 19 ± 6, 28
$H_{\gamma 1}$	−8.0 ± 0.4	−1.5 ± 0.4	13.3 ± 0.4	1.3 ± 0.4	−84, 35, −76
$H_{\gamma 2}$	−10.0 ± 0.4	1.0 ± 0.4	13.8 ± 0.4	1.6 ± 0.4	−95, 30, 40
$H_{\beta 1}$	16.3 ± 0.2	8.0 ± 0.2	20.7 ± 0.2	15.0 ± 0.2	−73, 58, −3

[a] The *g*-matrix principal values were determined from the simulation of the W-band CW-EPR spectrum shown in the Supporting Information, while the hyperfine parameters were determined from simulations of pulse ENDOR and HYSCORE data (Figures 1 and 2, as well as the Supporting Information). For an assignment of the respective nuclei see Figure 3. The Euler angles α, β, γ define the passive rotation of the hyperfine principal axes system into the *g*-matrix principal axes system, $\mathbf{A} = \mathbf{R}(\alpha, \beta, \gamma)\,\mathbf{A}_{diagonal}\,\mathbf{R}^{+}(\alpha,\beta,\gamma)$. The error margins on the Euler angle β are ±12° if not stated otherwise. Signs of A_H are based on the point-dipole model.

ming from a nickel center in a $d_{x^2-y^2}$ ground state. As indicated in Scheme 1, the *g*-value ordering leads to the conclusion that the principal axis (g_z) of the *g* matrix is perpendicular to the plane of F_{430}, while g_x and g_y are assumed to bisect the nickel–nitrogen bonds.[19]

The spectra in Figure 1b and c clearly show that there is a large hyperfine interaction between the paramagnetic center and the $^{13}C_\gamma$ nucleus of the propane sulfonate moiety (corresponding peaks were not detected in spectra of the unlabeled MCR_{BPS} sample, see the Supporting Information).

Simulation of all the Davies ENDOR spectra at Q-band, as well as of the HYSCORE spectra at Q-band (see the Supporting Information) provided the full ^{13}C hyperfine matrix ($A_x = 17.6 \pm 0.5$, $A_y = 18.3 \pm 0.5$, $A_z = 45.0 \pm 1$) MHz with the Euler angles (42°, 19 ± 6°, 28°) in the *g*-matrix reference frame. From the isotropic part of the hyperfine coupling $A_{iso} = (A_x + A_y + A_z)/3 = 27.0 \pm 0.7$ MHz, one can calculate the electron spin population in the s-type ^{13}C orbitals to be $\rho_s \approx 0.7\,\%$.[21] The spin population in the ^{13}C p-type orbitals can be estimated from the dipolar part $\mathbf{A}_{dip}$ of the matrix, $\mathbf{A}_{dip} = \mathbf{A} - A_{iso} = (-9.4 \pm 0.7, -8.7 \pm 0.7, 18.0 \pm 0.7)$ MHz, which after correction for the contribution stemming from the dipolar interaction between the spin population on the nickel center and the ^{13}C nucleus yields $\rho_p \approx 6\,\%$.[21] Based on the orientation of the principal axis of A_z and the calculated spin populations we interpret the binding situation in MCR_{BPS} as follows: The Ni–C_γ bond is slightly tilted (ca. 20°) away from the g_z principal axis direction. Since the spin population is small in the s-type orbitals but amounts to 6% in the p-type orbitals the most likely atomic orbitals to contribute to the SOMO—beside the Ni $d_{x^2-y^2}$ orbital—are the Ni d_{z^2} orbital and a p orbital of the C_γ atom, thus suggesting a hybridization closer to sp^2 than sp^3. As a consequence of the tilt of about 20°, the overall symmetry of the complex is reduced, thus allowing for an admixture of the Ni d_{x^2} orbital with the Ni $d_{z^2-y^2}$ ground-state configuration and thereby for the transfer of spin population to the carbon atom.

The proton signals were investigated to further clarify the coordination geometry. Figure 2a depicts three representative Davies ENDOR spectra taken at the observer positions indicated in the echo-detected EPR spectrum (insert), and Figure 2b depicts an X-band HYSCORE spectrum (observer position shown in the inset). Hyperfine couplings from two sets of protons could be clearly resolved from the complete set of data (see the Supporting Information): one with a large isotropic and a relatively small anisotropic component (dashed arrows in Figure 2b), and a second set corresponding to two protons having a small isotropic and large anisotropic component (full arrows in Figure 2b, see Table 1). Signals from the latter couplings are especially well separated from the many weakly coupled protons (with $A < 4$ MHz) in the HYSCORE spectrum since a large anisotropy results in a large shift from the antidiagonal.

The two hyperfine interactions with the large anisotropic components are assigned to the two γ protons since they are closest to the centers carrying the spin population

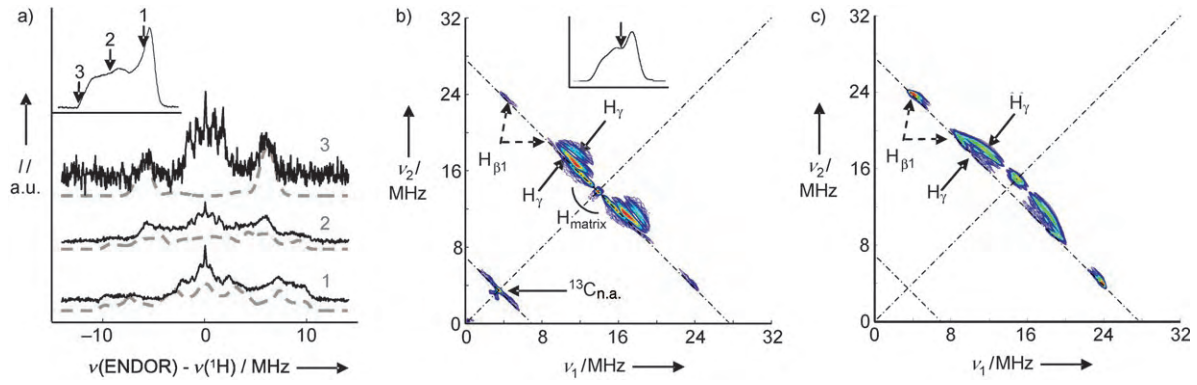

Figure 2. Representative Q-band (35.3 GHz) proton Davies ENDOR and X-band (9.74 GHz) HYSCORE spectra of MCR_{BPS}. The full set of spectra are shown in the Supporting Informtion. a) Q-band Davies ENDOR spectra and simulations of three ^{1}H nuclei at three different field positions marked "1–3" in the echo-detected EPR spectrum (see inset). b) X-band HYSCORE spectrum measured at the marked position in the echo-detected EPR spectrum (see inset). c) Simulation of (b) by using the hyperfine parameters given in Table 1. n.a. = natural abundance.

 © 2006 Wiley-VCH Verlag GmbH & Co. KGaA, Weinheim

($\rho(C\gamma) \cong 7\%$, $r \cong 0.1$ nm; $\rho(Ni) \cong 75\%$, $r \cong 0.21$ nm). A calculation using the point-dipolar model satisfactorily reproduces the magnitude of this experimental anisotropy ($T_{cal} \approx T_{exp} \approx 6$ MHz). We attribute the small isotropic hyperfine couplings of these two protons (< 1.6 MHz, see Table 1) to the flattened bonding geometry (closer to sp^2 hybridization) at C_γ: the two protons $H_{\gamma 1}$ and $H_{\gamma 2}$ are situated in (or close to) a nodal plane of the nonhybridized p_z orbital of the C_γ atom that hence has very little overlap with the hydrogen 1s orbitals.

The other hyperfine interaction, with the small anisotropic but large isotropic component, is assigned to the β proton closest to the nickel ion (Figure 3a). The anisotropy

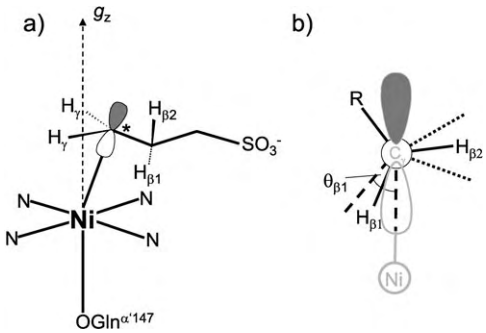

Figure 3. a) Schematic representation of the proposed coordination at the active site in MCR_{BPS}. The p_z orbital of the proposed near sp^2-hybrid carbon atom has been drawn to indicate the direction of the Ni–C_γ bond. The nickel d_{z^2} orbital overlapping with the C_γ p_z orbital has been omitted for clarity. The asterisk marks the position of ^{13}C labeling. b) Newman projection along the C_γ–C_β bond indicating the angular range of $0° < \theta_{\beta 1} < 50°$ (see the Supporting Information) as determined from the isotropic hyperfine couplings of $H_{\beta 1}$ and $H_{\beta 2}$. For clarity, the Ni–C_γ bond has been elongated, the p_z orbital of C_γ has been drawn in gray and the γ protons have been omitted. R = $-CH_2$-SO_3^-.

of this coupling can be satisfactorily calculated from the point-dipole model by assuming our spin population distribution and using the Ni–$H_{\beta 1}$ and C_γ–$H_{\beta 1}$ distances. We explain the large isotropic hyperfine coupling of $H_{\beta 1}$ in MCR_{BPS} by a very efficient transfer of spin population to $H_{\beta 1}$, presumably as a result of spin delocalization from the p_z orbital of C_γ ($2p_z$-σ spin delocalization or "hyperconjugation"),[22] but it could also arise as a result of spin polarization. A Newman projection of the deduced conformation at the C_β atom is shown in Figure 3b. The hyperfine coupling to $H_{\beta 2}$ is assumed to be too small (< 4 MHz) to be distinguished from the couplings to protons in the macrocycle and the surrounding protein ("matrix line"). A detailed analysis of the proton hyperfine couplings is presented in the Supporting Information.

The EPR results presented here leave little doubt that there is a bond between the nickel center of coenzyme F_{430} and the C_γ atom of the propane sulfonate residue in the MCR_{BPS} state of methyl-coenzyme M reductase. The deduced spin populations of approximately 7% on the C_γ atom and 75% in the Ni $d_{x^2-y^2}$ orbital are in close agreement with the results of DFT calculations on a [CH_3-$Ni^{III}F_{430}$] model structure.[16] It should be noted, however, that the EPR data does not allow the determination of the total number of electrons in the system and that our assignment of a formal alkyl-Ni^{III} state rests on the assumption that after the reaction of MCR and BPS a bromide ion is generated as a reaction by-product. The significant contribution of the C 2p orbital to the SOMO suggests a bonding geometry of the γ-methylene group closer to planar than to tetrahedral. Further experiments will be needed to fully understand the bonding situation. This is, however, the first account of a transition-metal–alkyl derivative found in an enzyme in which the alkyl group is not bound to a cobalt center. Our experimental detection of this alkyl–nickel species in the active site of MCR adds plausibility to proposed mechanisms proceeding via such intermediates, but of course does not constitute direct evidence with regard to the catalytic cycle involving the natural substrate. In view of the still indirect but growing body of evidence for "reverse methanogenesis", that is, anaerobic oxidation of methane catalyzed by Ni–hydrocorphinate-containing enzymes closely resembling MCR,[23,24] we consider that the new type of alkyl–nickel species reported here could play a crucial role in the C-H activation step.

Received: January 27, 2006
Published online: April 26, 2006

Keywords: bioinorganic chemistry · enzymes · EPR spectroscopy · methanogenesis · nickel

[1] T. G. Spiro, *Science* **1997**, *278*, 17, and references therein.
[2] U. Ermler, W. Grabarse, S. Shima, M. Goubeaud, R. K. Thauer, *Science* **1997**, *278*, 1457.
[3] R. K. Thauer, *Microbiology* **1998**, *144*, 2377.
[4] M. Goenrich, F. Mahlert, E. C. Duin, C. Bauer, B. Jaun, R. K. Thauer, *J. Biol. Inorg. Chem.* **2004**, *9*, 691.
[5] M. Goubeaud, G. Schreiner, R. K. Thauer, *Eur. J. Biochem.* **1997**, *243*, 110.
[6] Y.-C. Horng, D. F. Becker, S. W. Ragsdale, *Biochemistry* **2001**, *40*, 12875.
[7] A. Ghosh, T. Wondimagegn, H. Ryeng, *Curr. Opin. Chem. Biol.* **2001**, *5*, 744.
[8] a) V. Pelmenschikov, M. R. A. Blomberg, P. E. M. Siegbahn, R. H. Crabtree, *J. Am. Chem. Soc.* **2002**, *124*, 4039; b) V. Pelmenschikov, P. E. M. Siegbahn, *J. Biol. Inorg. Chem.* **2003**, *8*, 653.
[9] On the difficulties of calculating transition-metal–carbon bond energies using DFT see: K. P. Jensen, U. Ryde, *J. Phys. Chem. A* **2003**, *107*, 7539.
[10] B. Jaun, *Helv. Chim. Acta* **1990**, *73*, 2209.
[11] W. Grabarse, F. Mahlert, E. C. Duin, M. Goubeaud, S. Shima, R. K. Thauer, V. Lamzin, U. Ermler, *J. Mol. Biol.* **2001**, *309*, 315.
[12] M. Goenrich, E. C. Duin, F. Mahlert, R. K. Thauer, *J. Biol. Inorg. Chem.* **2005**, *10*, 333.
[13] E. C. Duin, L. Signor, R. Piskorski, F. Mahlert, M. D. Clay, M. Goenrich, R. K. Thauer, B. Jaun, M. K. Johnson, *J. Biol. Inorg. Chem.* **2004**, *9*, 563.
[14] S.-K. Lin, B. Jaun, *Helv. Chim. Acta* **1991**, *74*, 1725.
[15] A. Sauer, H. Cohen, D. Meyerstein, *Inorg. Chem.* **1988**, *27*, 4578.
[16] T. Wondimagegn, A. Ghosh, *J. Am. Chem. Soc.* **2001**, *123*, 1543.
[17] A. Schweiger, G. Jeschke, *Principles of Pulse Electron Paramagnetic Resonance*, Oxford Univ. Press, Oxford, **2001**.

 © 2006 Wiley-VCH Verlag GmbH & Co. KGaA, Weinheim

[18] In Figure 1a, the Supporting Information, and the insets of Figure 2, spectral features can be seen (marked with a cross), which stem from the MCR_{ox1} species (see Ref. 19). Impurities of MCR_{ox1} are present in some MCR preparations.
[19] J. Harmer, C. Finazzo, R. Piskorski, C. Bauer, B. Jaun, E. C. Duin, M. Goenrich, R. K. Thauer, S. Van Doorslaer, A. Schweiger, *J. Am. Chem. Soc.* **2005**, *127*, 17744.
[20] a) J. Telser, Y.-C. Fann, M. W. Renner, J. Fajer, S. Wang, H. Zhang, R. A. Scott, B. M. Hoffman, *J. Am. Chem. Soc.* **1997**, *119*, 733; b) J. Seth, V. Palaniappan, D. F. Bocian, *Inorg. Chem.* **1995**, *34*, 2201.
[21] $\rho_s \approx 27.0\ \text{MHz}/4050\ \text{MHz} \approx 0.007 = 0.7\,\%$ and $\rho_p \approx 7\ \text{MHz}/115\ \text{MHz} = 0.06 = 6\,\%$. The value used for the calculation of ρ_p has been corrected for the through-space dipolar interaction of spin population that is located on the nickel center, which reduces the dipolar contribution T from approximately 9 MHz to approximately 7 MHz. For details see the Supporting Information.
[22] In the MCR_{ox1} state (see Ref. 19) no large isotropic hyperfine coupling to protons can be observed despite the fact that there are two methylene protons at the same position in the bound molecule (HS-CoM for MCR_{ox1}, see Scheme 1). This is a clear indication that the spin population on the C_γ atom in MCR_{BPS} is efficiently transferred to one of the β protons, while this is not true in MCR_{ox1}. This is illustrated in Figure 3b.
[23] M. Krüger, A. Meyerdierks, F. O. Glöckner, R. Amann, F. Widdel, M. Kube, R. Reinhardt, J. Kahnt, R. Böcher, R. K. Thauer, S. Shima, *Nature* **2003**, *426*, 878.
[24] S. Shima, R. K. Thauer, *Curr. Opin. Microbiol.* **2005**, *8*, 643.

 © 2006 Wiley-VCH Verlag GmbH & Co. KGaA, Weinheim

Carbohydrate Microarrays

DOI: 10.1002/anie.200600591

High-Throughput Carbohydrate Microarray Analysis of 24 Lectins**

*Joseph C. Manimala, Timothy A. Roach, Zhitao Li, and Jeffrey C. Gildersleeve**

Lectins, non-immunoglobulin proteins that bind carbohydrates, play a central role in a wide range of biological processes such as cell–cell recognition, viral and bacterial pathogenesis, and inflammation.[1,2] Moreover, they are used extensively as research tools, diagnostics, and therapeutics. For example, mistletoe lectin is in clinical trials as an anticancer agent.[3] Therefore, a fundamental understanding of carbohydrate–protein interactions and comprehensive information on lectin specificity is critical. Unfortunately, evaluation of lectin specificity is not trivial. One common method involves measuring the binding of lectins to cells, tissues, and glycoproteins. This approach frequently uncovers interesting and useful binding properties, however, cells, tissues, and glycoproteins display complex mixtures of carbohydrate epitopes. Therefore, it is exceedingly difficult to determine the specific carbohydrate structures being recognized by the lectin. An alternative approach involves measuring binding to structurally defined carbohydrate epitopes through techniques such as isothermal calorimetry (ITC), mono- and oligosaccharide inhibition studies, enzyme-linked lectin assays (ELLA), and surface plasmon resonance assays (SPR). Unfortunately, these methods can be labor intensive, require large amounts of carbohydrates, and/or be difficult to perform in a high-throughput fashion. Moreover, these studies have typically been limited to the small number of carbohydrate epitopes that were readily accessible. Although lectin specificity has been studied often, much more comprehensive information is still needed.

Carbohydrate microarrays are an emerging technology for the high-throughput evaluation of carbohydrate-macromolecule interactions.[4–27] Analogous to DNA and protein arrays, carbohydrate microarrays contain numerous carbohydrate epitopes immobilized on a solid support in a miniaturized fashion. The microarray format allows one to rapidly evaluate many potential interactions with a minimal amount of sample. Our group has recently developed a carbohydrate microarray and a highly sensitive assay to detect binding.[21] To maximize throughput, each slide contained 16 wells with an entire array printed in each well (see Figure 1a). To illustrate the capabilities of our microarray and study lectin sepcificity, 24 lectins were evaluated at eight different concentrations by using the microarray. As one of the largest and most-comprehensive lectin studies ever reported, the results should be a useful resource for scientists conducting basic and applied research with lectins. Interestingly, microarray analysis revealed unexpected ligands for many of the lectins.

Our approach for fabricating arrays involves printing carbohydrate–bovine serum albumin (BSA)/human serum albumin (HSA) conjugates and glycoproteins on epoxide-functionalized glass microscope slides. This strategy permits immobilization of both structurally discrete synthetic carbohydrates as well as natural carbohydrates presented on glycoproteins. Our first array contained 29 components. To increase the diversity, 23 additional glycans were chemically synthesized and 21 were purchased (see the Supporting Information). The array then contained 73 different components: 4 controls, 54 BSA/HSA conjugates, and 15 glycoproteins (see Figure 1c).

Lectins were evaluated by using our previously reported assay. Briefly, slides were incubated with biotinylated lectins in serial dilutions, washed, and then incubated with streptavidin–horseradish peroxidase (HRP). Finally, wells were incubated with a Cy3-labeled tyramide substrate. The fluorescence intensities of each spot were then measured by using

[*] Dr. J. C. Manimala, Dr. T. A. Roach, Dr. Z. Li, Dr. J. C. Gildersleeve
Laboratory of Medicinal Chemistry
Center for Cancer Research, NCI-Frederick
376 Boyles St., 376/109, Frederick, MD 21702 (USA)
Fax: (+1) 301-846-6033
E-mail: gildersleevej@ncifcrf.gov

[**] We thank Jack Simpson (Protein Chemistry Laboratory, SAIC/NCI-Frederick) for MALDI-MS analysis of BSA conjugates. This research was supported by the Intramural Research Program of the NIH, NCI.

Supporting information for this article is available on the WWW under http://www.angewandte.org or from the author.

 © 2006 Wiley-VCH Verlag GmbH & Co. KGaA, Weinheim

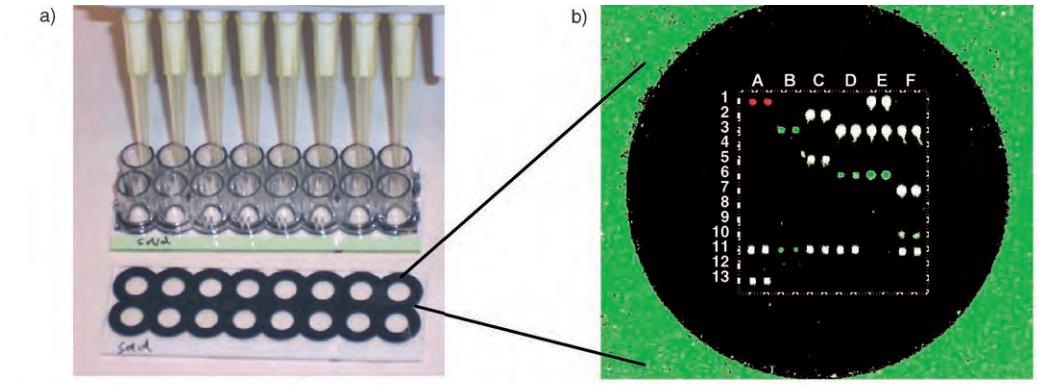

c)

1. Cy5-BSA (position A1)
2. BSA
3. HSA
4. Glc-β -BSA
5. GalNAc-α -BSA
6. Glc-α -BSA
7. Man-α -BSA
8. GlcNAc-β -BSA
9. GalNAc-β -BSA
10. Fuc-β -BSA
11. Fuc-α -BSA
12. Rha-α -BSA
13. Rha-β -BSA
14. Gal-α -BSA
15. Gal-β -BSA
16. GalNAcα1-Thr-Gly-BSA (Tn)
17. GalNAcα1-6Galβ -BSA
18. GalNAcα1-3Galβ -BSA (A_{di})
19. GlcNAcα1-4Galβ -BSA
20. Galα1-3Gal-BSA (Bdi)
21. Galβ1-4GlcNAc-BSA (LacNAc)
22. Galβ1-3GalNAc-HSA (TF_{di})
23. Galβ1-4Glcβ -BSA (Lac)
24. Galβ1-3GlcNAcβ -BSA (Le^c)
25. Galβ1-6Man-α -BSA
26. Manα1-6Man-α -BSA
27. GalNAcβ1-4Galβ -BSA ($GA2_{di}$)
28. Glcβ1-4Glcβ -BSA (Cellobiose)
29. Glcα1-4Glcβ -BSA (Maltose)
30. Glcα1-6Glcβ -BSA (Isomalt)
31. Manα1-6[Manα1-3]Manα - BSA (ManT)
32. Galα1-4Galβ -BSA
33. Sialyl2-3Galβ1-4GlcNAc - BSA (3'SLacNAc)
34. GalNAcα1-3(Fucα1-2)Galβ - BSA (BG-A)
35. Galα1-3(Fucα1-2)Galβ -BSA (BG- B)
36. Fucα1-2Galβ1-3GlcNAcβ1-3Galβ1-4Glcβ - HSA (BG-H1)
37. Galβ1-3[Fucα1-4)GlcNAcβ1-3Galβ1-4Glcβ - BSA (Le^a)
38. Fucα1-2Galβ1-3[Fucα1-4)GlcNAcβ1-3Galβ1-4Glcβ - BSA (Le^b)
39. Fucα1-2Galβ1-4[Fucα1-3)GlcNAc - HSA (Le^y)
40. Galβ1-4[Fucα1-3)GlcNAc -HSA (Le^x)
41. SLe^x - BSA
42. Galα1-4Galβ1-4Glc - HSA (Gb3)
43. Xylβ1-4Xylβ1-4Xylβ1-4Xylβ1 - BSA (Xylβ4)
44. Araα1-5Araα1-5Araα1-5Araα1-5Araα1 - BSA (Ara5)
45. Xylα1-6Glcβ1-4(Xylα1-6)Glcβ1-4(Xylα1-6)Glcβ1 - BSA (X3Glc3)
46. 3'Sialyllactose - HSA (GM3)
47. 6'Sialyllactose - HSA (6'SLac)
48. Sia-LeA - HSA (SLe^a)
49. Di-LeX – BSA
50. Manβ1-4Manβ1-4Manβ1-4Manβ1-BSA (Manβ4)
51. Manβ1-4(Galα1-6)Manβ1-4(Galα1-6)Manβ1-4Manβ-BSA (G2M4)
52. Glcα1-6Glcα1-4Glcα1-4Glcβ -BSA
53. Galβ1-3GlcNAcβ1-3Galβ -BSA (LNT)
54. Sia2-3Galβ1-3GlcNAcβ1-3Galβ1-BSA (LSTa)
55. Galβ1-3(Sia2-6)GlcNAcβ1-3Galβ-BSA (LSTb)
56. Sia2-6Galβ1-3GlcNAcβ1-3Galβ-BSA (LSTc)
57. Galβ1-3GalNAcβ1-4Galβ-BSA (GA1)
58. KLH
59. oxKLH
60. Bovine submaxillary mucin (BSM)
61. Asialo-BSM (aBSM)
62. Deacetylated-BSM (deAcBSM)
63. Ovine submaxillary mucin (OSM)
64. asialo-OSM (aOSM)
65. Glycophorin (Gn)
66. asialo-glycophorin (aGn)
67. Prostate Specific Antigen (PSA)
68. Heat Shock Protein 90 (hsp90)
69. Thyroglobulin (Tgl)
70. Alpha fetoprotein (AFP)
71. Carcinoembryonic antigen(CEA)
72. Fatty Acid Binding Prot. (FABP)
73. Cy3-BSA (position A13)

Figure 1. The carbohydrate microarray: a) the 16-well slide format; b) typical assay results for a single well; c) components of the array in the order that they were printed (black = controls, blue = BSA/HSA conjugates, green = glycoproteins).

a standard DNA microarray scanner (for an image of a typical well, see Figure 1b). At any single concentration of lectin, some spots may be saturated while others are barely distinguishable from the background signal. By evaluating binding over a broad range of lectin concentrations, one can determine the relative affinities for many ligands. Relative binding has been expressed in terms of the detection limit (DL), which is the lowest concentration of lectin that produced a signal five-times higher than the background for a given epitope. Better ligands have lower detection limits.

Results for each of the 24 lectins are summarized in Table 1.[28] Several findings are of special interest. First, many lectins that bound epitopes would not have been predicted based on their designated specificity.[29] For example, BPL is known as a GalNAc/Galβ1–3GalNAc-binding lectin and RCA120 is considered a Gal/GalNAc-binding lectin. Interestingly, both lectins bound tightly to rhamnose (DL = 80 pM for BPL and 21 pM for RCA120). Furthermore, soluble rhamnose competitively inhibited the binding of these lectins to lactose (see the Supporting Information). From a chemical perspective, recognition of both galactose and rhamnose is remarkable given the significant structural differences (i.e. stereochemistry of the hydroxyl groups at the 2- and 4-positions, oxygenation compared with deoxygenation at the 6-position, and overall D compared with L stereochemistry; see Scheme 1). Recognition of rhamnose may also be important biologically as rhamnose is found in a variety of plant and bacterial carbohydrates. ACL, a Galβ1-3GalNAc binding lectin, was found to bind Manβ1-4Manβ1-4Manβ1-4Man (DL = 29 nM), a plant oligosaccharide. Again, Galβ1-3GalNAc and Manβ1-4Man contained substantial structural differences (see Scheme 1). As a third example, a lectin that binds sialic acid, SNA, demonstrated good binding to some glycans that lack sialic acid such as blood group B (DL =

 © 2006 Wiley-VCH Verlag GmbH & Co. KGaA, Weinheim

Table 1: Lectin specificity profiles.

Lectin (specificity)[a]	Epitopes bound by the lectin (detection limits)[b]
ACL (Galβ1-3GalNAc)	a-Gn, Di-Le^x (1 nM); Le^x, SLe^x, Gn (4 nM); aOSM, PSA, HSP90, AFP (14 nM); Manβ4, aBSM (29 nM)
BPL (TF, GalNAc)	a-Gn, aOSM, aBSM, Le^X, Di-Le^X (40 pM); GalNAc-β, Rha-β, Tn, GalNAcα1-6Galβ, A_{di}, LNT (80 pM); TF_{di}, Lac, Le^c, LSTb, GA1 (164 pM); FABP (320 pM); Galα1-3Gal, $GA2_{di}$, KLH, OSM (1 nM); GalNAc-α (3 nM); BG-A, BG-B, Le^a, BSM, deAcBSM, Gn, PSA, HSP90, Tgl, AFP, CEA (10 nM)
Con A (Manα, Glcα)	ManT (51 pM), Tgl (102 pM), Man-α (200 pM); KLH, CEA (410 pM); Glc-α (820 pM); BSM, AFP, aBSM, deAcBSM, OSM (3 nM); Maltose, Glc4 (5 nM); oxKLH, aOSM, PSA (10 nM); GlcNAcα 1-4Galβ, Manα1-6Manα (12 nM)
DBL (GalNAcα)	BG-A (892 pM); Tn , GalNAcα1-6Galβ, A_{di} (4 pM); BG-B (7 nM)
ECL (LacNAc)	aGn (9 nM); Lac (11 nM); LacNAc (22 nM); aBSM, aOSM (44 nM); Gal-α, Tgl (88 nM)
GS-I (Gal/GalNAcα)	BG-B (55 pM); Gal-α (110 pM); Gb3 (440 pM); Galα1-3Gal (880 pM); aOSM (4 nM)
GS-II (GlcNAc)	GlcNAcα1-4Galβ (110 pM); a-Gn, aBSM (440 pM); aOSM (880 pM); GlcNAc-β (9 pM); Le^y, Le^X, Di-Le^X, BSM, DeAcBSM (18 nM)
HAA (GalNAcα)	Tn, GalNAcα1-6Galβ, A_{di}, BG-A (7.9 nM); BG-B, aGn, GlcNAcα1-4Galβ (16 nM); GalNAc-α, OSM, aOSM (32 nM)
HPL (GalNAcα)	aBSM, aOSM (13 pM); Tn, GalNAcα1-6Galβ, A_{di}, GlcNAcα1-4Gal, BG-A, OSM, aGn (26 pM); GalNAc-α (53 pM); BG-B (110 pM); BSM (210 pM); DeAcBSM (790 pM); Gn (2 nM); GalNAc-β (3 nM); GlcNAc-β (6 nM)
LBA (BG-A)	BG-B (25 nM); BG-A (100 nM)
LTL (Fuc, Le^x)	Fuc-α (170 pM); Le^y, Le^x (340 pM); Di-Le^x, CEA, Fuc-β (680 pM)
MPL (GalNAcα)	aBSM, aOSM, aGn (780 pM); Tn (6 nM); BG-B, GalNAc-α, Gal-α, GalNAcα1-6Galβ, OSM (25 nM)
PNA (Galβ1-3GalNAc)	a-Gn (11 pM); GA1 (1 nM); TF_{di} (2 nM); Lac (5 nM); BG-B (6 nM); aBSM (11 nM)
PTL (Gal/GalNAc)	BG-A, BG-B (1 nM); A_{di} (6 nM); Tn, GalNAcα1-6Galβ, aOSM (11 nM); aBSM (29 nM); GalNAc-α (57 nM)
RCA120 (Gal/GalNAc)	Rha-β, a-Gn (21 pM); Lac, Tgl (330 pM); LacNAc, BG-B, LSTc, aBSM, OSM, aOSM, Gn, FABP (1 nM); Gal-α, GalNAcα1-6Galβ, Galα1-3Gal, TF_{di}, Galβ1-3GlcNAcβ, Gb3, LNT, LSTb, BSM, CEA (2 nM); Galα1-4Galβ, BG-H1, KLH, deAcBSM, PSA, AFP (4 nM); HSA, (5 nM); GalNAc-β, GA1 (10 nM)
SBA (GalNAc)	aBSM, aOSM (33 pM); Tn, Gb3 (65 pM); GalNAcα1-6Galβ, A_{di} (130 pM); GalNAc-α (260 pM); OSM (520 pM); GalNAc-β (1 nM); aGn (4 nM); $GA2_{di}$ (5 nM); BG-A, BG-B, deAcBSM (10 nM); Gal-α, BSM (21 nM); Gn (42 nM)
SNA (Siaα2-6Gal)	AFP (420 pM); LSTc (830 pM); BG-B, aOSM, Tgl (3.3 nM); TF_{di}, GM3, 6′SLac, BSM, aBSM, deAcBSM, OSM, Gn, PSA, CEA, FBP (6.7 nM); HSA, GalNAc-α, Man3, aGn (13 nM)
SSA (Tn)	aBSM, aOSM (100 nM)
UEA-I (Fucα)	Le^y (6 pM); Fuc-α, Fuc-β (590 pM); BG-B, aGn (6 nM); BG-H1, BSM (12 nM)
VAA (Galβ)	aOSM, a-Gn (17 μM)
VFA (Manα, Glcα)	Tgl (200 nM)
VVL-B4 (Tn)	aOSM (8 pM); aBSM (15 pM); Tn (60 pM); GalNAcα1-6Galβ, A_{di}, OSM (240 pM); GalNAc-α, DeAcBSM, a-Gn (480 pM); GalNAc-β, $GA2_{di}$, BSM (719 pM)
WFA (GalNAcα/β)	aOSM (11 pM); aBSM (23 pM); Tn (46 pM); GalNAcα1-6Galβ, A_{di} (92 pM); GalNAc-β, aGn (180 pM); GalNAc-α, $GA2_{di}$ (730 pM); Lac, Le^c, LNT, LSTb (2 nM); OSM, Gn, Tgl (3 nM) BSM, deAcBSM (29 nM)
WGA (GlcNAc)	GalNAc-α, GalNAc-β, GlcNAc-β, A_{di}, GlcNAcα1-4Gal (36 pM); BG-A, aBSM (140 pM); 3′SLacNAc, aOSM, Gn, (290 pM); Tn, GalNAcα1-6Gal (580 pM); SLe^a,OSM, a-Gn (1 nM); SLe^x, GM3, 6′Slac, LSTa, oxKLH, BSM, deAcBSM (5 nM); PSA, Tgl, AFP, CEA (17 nM); LacNAc (35 nM)

[a] Nominal specificities listed by the commercial suppliers. [b] The detection limit (DL) is the lowest concentration of lectin that produced a signal 5-times higher than the background. Abbreviations (highest concentration tested): ACL = *Amaranthus caudatus* lectin (29 nM), BPL = *Bauhinia purpurea* lectin (10 nM), Con A = concanavalin A (12 nM), DBL = *Dolichos biflorus* agglutinin (7 nM), ECL = *Erythrina cristagalli* lectin (88 nM), GS-I = *Griffonia simplicifolia* I (4 nM), GS-II = *Griffonia simplicifolia* II (18 nM), HAA = *Helix aspersa* agglutinin (130 nM), HPL = *Helix pomatia* lectin (13 nM), LBA = Lima bean agglutinin or *Phaseolus lunatus* (100 nM), LTL = *Lotus tetragonolobus* lectin (7 nM), MPL = *Maclura pomifer* lectin (50 nM), PNA = peanut agglutinin (46 nM), PTL = *Psophocarpus tetragonolobus* lectin (57 nM), RCA120 = *Ricinus communis* agglutinin I (10 nM), SBA = soybean agglutinin (42 nM), SSA = *Salvia sclarea* agglutinin (400 nM), SNL = *Sambucus nigra* lectin or eldeberry lectin (13 nM), UEA-I = *Ulex europaeus* agglutinin I (12 nM), VAA = *Viscum album* agglutinin or mistletoe lectin (17 mM), VFA = *Vicia faba* agglutinin (29 nM), VVL-B4 = *Vicia villosa* lectin B4 (14 nM), WFL = *Wisteria floribunda* lectin (29 nM), WGA = wheat germ agglutinin (140 nM).

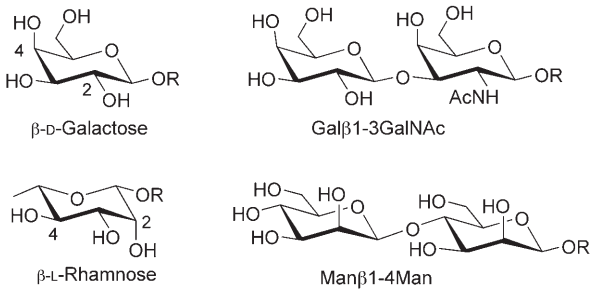

Scheme 1. Structures of selected carbohydrates.

3.3 nM) and the T disaccharide (Galβ1-3GalNAc, DL = 6.7 nM). Interestingly, binding to LSTc, a carbohydrate with a sialic acid at the nonreducing end, could be inhibited with the T disaccharide but not with blood group B. Perhaps one of the most unexpected results was that SNA and RCA120 bound to HSA (non-glycosylated protein used as a control in our array).[30] HSA competitively inhibited carbohydrate binding. These results highlight how easily proteins, cells, and tissues could be mischaracterized when using lectins.

Several other features of lectin binding should also be mentioned. First, lectins frequently exhibit binding requirements beyond simple mono/disaccharide specificity. For

 © 2006 Wiley-VCH Verlag GmbH & Co. KGaA, Weinheim

example, RCA120 showed little or no binding within the concentration range tested to a number of Gal and GalNAc terminal carbohydrates such as GalNAcα1-4Galβ, GalNAcα1-3Galβ, Galβ1-6Manα, GalNAcβ1-4Gal, BG-A, Le^a, and Le^x. Although this aspect of lectin recognition is known, detailed information on secondary binding requirements is not available for most lectins. Carbohydrate microarrays provide rapid access to comprehensive binding profiles. Second, lectin specificity can be difficult to predict based on binding (or lack of binding) to closely related structures. For example, the GalNAc binding lectin SBA showed little or no binding to the Galα monosaccharide and the Galα1-3Gal disaccharide. However, SBA bound very well to Gb3 (DL = 65 pM, Galα1-4Galβ1-4Glc). Therefore, it is critical to evaluate binding to a wide range of carbohydrates.

In summary, a carbohydrate microarray was used to evaluate over 1700 potential lectin–ligand interactions over a range of lectin concentrations. The format allowed for very rapid analysis with a minimal amount of expensive and difficult to obtain carbohydrates. For comparison, an ELLA assay carried out in 96-well plates would have required at least 150 plates and 100-fold larger quantities of each BSA conjugate and protein. The unexpected binding properties uncovered in this study and the extensive binding information obtained highlight the utility of carbohydrate microarrays for rapid evaluation of carbohydrate–protein interactions.

Received: February 14, 2006
Published online: April 26, 2006

Keywords: carbohydrates · glycoconjugates · glycosides · lectins · microarrays

[1] H. Lis, N. Sharon, *Chem. Rev.* **1998**, *98*, 637.
[2] N. Sharon, H. Lis, *Glycobiology* **2004**, *14*, 53R.
[3] P. Schoffski, S. Riggert, P. Fumoleau, M. Campone, O. Bolte, S. Marreaud, D. Lacombe, B. Baron, M. Herold, H. Zwierzina, K. Wilhelm-Ogunbiyi, H. Lentzen, C. Twelves, *Ann. Oncol.* **2004**, *15*, 1816.
[4] B. T. Houseman, M. Mrksich, *Chem. Biol.* **2002**, *9*, 443.
[5] E. W. Adams, J. Ueberfeld, D. M. Ratner, B. R. O'Keefe, D. R. Walt, P. H. Seeberger, *Angew. Chem.* **2003**, *115*, 5475; *Angew. Chem. Int. Ed.* **2003**, *42*, 5317.
[6] M. Schwarz, L. Spector, A. Gargir, A. Shtevi, M. Gortler, R. T. Altstock, A. A. Dukler, N. Dotan, *Glycobiology* **2003**, *13*, 749.
[7] D. N. Wang, *Proteomics* **2003**, *3*, 2167.
[8] O. Blixt, S. Head, T. Mondala, C. Scanlan, M. E. Huflejt, R. Alvarez, M. C. Bryan, F. Fazio, D. Calarese, J. Stevens, N. Razi, D. J. Stevens, J. J. Skehel, I. van Die, D. R. Burton, I. A. Wilson, R. Cummings, N. Bovin, C. H. Wong, J. C. Paulson, *Proc. Natl. Acad. Sci. USA* **2004**, *101*, 17033.
[9] M. C. Bryan, F. Fazio, H. K. Lee, C. Y. Huang, A. Chang, M. D. Best, D. A. Calarese, C. Blixt, J. C. Paulson, D. Burton, I. A. Wilson, C. H. Wong, *J. Am. Chem. Soc.* **2004**, *126*, 8640.
[10] M. D. Disney, P. H. Seeberger, *Chem. Biol.* **2004**, *11*, 1701.
[11] T. Feizi, W. G. Chai, *Nat. Rev. Mol. Cell Biol.* **2004**, *5*, 582.
[12] C. Galustian, C. G. Park, W. G. Chai, M. Kiso, S. A. Bruening, Y. S. Kang, R. M. Steinman, T. Feizi, *Int. Immunol.* **2004**, *16*, 853.
[13] L. Nimrichter, A. Gargir, M. Gortler, R. T. Altstock, A. Shtevi, O. Weisshaus, E. Fire, N. Dotan, R. L. Schnaar, *Glycobiology* **2004**, *14*, 197.
[14] D. M. Ratner, E. W. Adams, J. Su, B. R. O'Keefe, M. Mrksich, P. H. Seeberger, *ChemBioChem* **2004**, *5*, 379.
[15] S. Angeloni, J. L. Ridet, N. Kusy, H. Gao, F. Crevoisier, S. Guinchard, S. Kochhar, H. Sigrist, N. Sprenger, *Glycobiology* **2005**, *15*, 31.
[16] M. B. Biskup, J. U. Muller, R. Weingart, R. R. Schmidt, *ChemBioChem* **2005**, *6*, 1007.
[17] B. S. Bochner, R. A. Alvarez, P. Mehta, N. V. Bovin, O. Blixt, J. R. White, R. L. Schnaar, *J. Biol. Chem.* **2005**, *280*, 4307.
[18] D. A. Calarese, H. K. Lee, C. Y. Huang, M. D. Best, R. D. Astronomo, R. L. Stanfield, H. Katinger, D. R. Burton, C. H. Wong, I. A. Wilson, *Proc. Natl. Acad. Sci. USA* **2005**, *102*, 13372.
[19] V. I. Dyukova, E. I. Dementieva, D. A. Zubtsov, O. E. Galanina, N. V. Bovin, A. Y. Rubina, *Anal. Biochem.* **2005**, *347*, 94.
[20] K. S. Ko, F. A. Jaipuri, N. L. Pohl, *J. Am. Chem. Soc.* **2005**, *127*, 13162.
[21] J. Manimala, Z. Li, A. Jain, S. VedBrat, J. C. Gildersleeve, *ChemBioChem* **2005**, *6*, 2229.
[22] I. Shin, S. Park, M. R. Lee, *Chem. Eur. J.* **2005**, *11*, 2894.
[23] S. J. van Vliet, E. van Liempt, E. Saeland, C. A. Aarnoudse, B. Appelmelk, T. Irimura, T. B. H. Geijtenbeek, O. Blixt, R. Alvarez, I. van Die, Y. van Kooyk, *Int. Immunol.* **2005**, *17*, 661.
[24] M. Vila-Perello, R. G. Gallego, D. Andreu, *ChemBioChem* **2005**, *6*, 1831.
[25] C. Y. Huang, D. A. Thayer, A. Y. Chang, M. D. Best, J. Hoffmann, S. Head, C. H. Wong, *Proc. Natl. Acad. Sci. USA* **2006**, *103*, 15.
[26] J. C. Kehr, Y. Zilliges, A. Springer, M. D. Disney, D. D. Ratner, C. Bouchier, P. H. Seeberger, N. T. de Marsac, E. Dittmann, *Mol. Microbiol.* **2006**, *59*, 893.
[27] M. M. Ngundi, C. R. Taitt, S. A. McMurry, D. Kahne, F. S. Ligler, *Biosens. Bioelectron.* **2006**, *21*, 1195.
[28] Different lectins contain different levels of biotin incorporation. As the biotin/lectin ratio will affect the detection limit, the results for different lectins should be compared qualitatively rather than quantitatively.
[29] Some epitopes contain a thioglycoside linker at the reducing end of the sugar. Although the linker can potentially affect recognition, inhibition was also observed with sugar lactols (see the Supporting Information).
[30] Although possible, several lines of evidence suggest that the observed binding is not due to a minor glycoprotein impurity. First, the manufacturer states that the HSA is non-glycosylated, greater than 99% pure, and essentially free of globulins. Second, binding to HSA was not observed with other lectins with similar specificity. Recognition of proteins/peptides by carbohydrate-binding proteins has been reported previously; for examples, see A. Pashov, M. Perry, M. Dyar, M. Chow, T. Kieber-Emmons, *Curr. Top. Med. Chem.* **2005**, *5*, 1171 and K. R. Oldenburg, D. Loganathan, I. J. Goldstein, P. G. Schultz, M. A. Gallop, *Proc. Natl. Acad. Sci. USA* **1992**, *89*, 5393.

 © 2006 Wiley-VCH Verlag GmbH & Co. KGaA, Weinheim

Peptide Nanofilaments

DOI: 10.1002/anie.200503636

Epitaxial Growth of Peptide Nanofilaments on Inorganic Surfaces: Effects of Interfacial Hydrophobicity/Hydrophilicity**

Feng Zhang, Hai-Ning Du, Zhi-Xiang Zhang, Li-Na Ji, Hong-Tao Li, Lin Tang, Hua-Bin Wang, Chun-Hai Fan, Hong-Jie Xu, Yi Zhang, Jun Hu, Hong-Yu Hu, and Jian-Hua He**

The self-assembly of peptides and proteins has recently attracted much attention because of its scientific importance and widespread applications in the fields of nanomaterials,[1–5] crystallography,[6–8] and pathology.[9–13] Particularly, one-dimensional growth of peptides or proteins on inorganic substrates has been recognized as a potential approach to the fabrication of functional nanostructures.[14–16] In these cases the peptide (or protein) is precisely assembled with the assistance of inorganic templates.[7,8] This feature allows the arrangement of peptide molecules in a predesignated orientation on substrates by proper design of the peptide sequences.

Previous studies showed that different substrates have significant effects on the formation of nanofilaments.[17–20] As it is generally accepted that the hydrophobic interaction between the side chains is a driving force in the formation of peptide nanofilaments, it is very important to explore the effects of the substrate hydrophobicity/hydrophilicity on the relevant template-assisted epitaxial growth, which has not been systematically studied so far.

Herein, we compare the self-assembly behavior of the peptide GAV-9 on hydrophilic mica and hydrophobic HOPG (highly ordered pyrolytic graphite) surfaces by in situ atomic force microscopy (AFM) to investigate how interfacial hydrophobicity/hydrophilicity influences the epitaxial growth of peptide nanofilaments.

GAV-9, NH_2-VGGAVVAGV-$CONH_2$ (Figure 1a), consists of hydrophobic amino acid residues and is a conserved consensus of three neurodegenerative-disease-related proteins: α-synuclein, amyloid β protein, and prion protein, which are capable of forming amyloid fibrils in vivo and in vitro.[20–22] Unlike α-synuclein, GAV-9 with a concentration of 1.6 mM or less cannot form amyloid fibrils even when its solution is incubated under fibrillization-accelerating conditions[21] for a long time (≈6 days), as characterized by AFM and turbidity measurements (data not shown). Circular dichroism experiments show that GAV-9 in fresh solutions adopts a random-coil structure, but forms β-sheets when dried (Supporting Information).

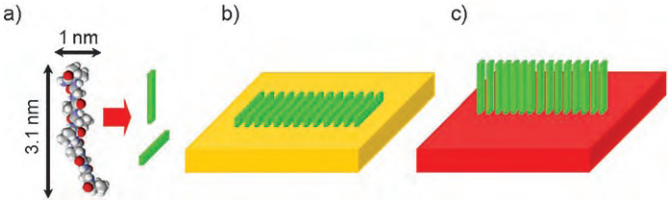

Figure 1. Schematic representation of self-assembled GAV-9 nanofilaments and their interfacial orientations at hydrophobic and hydrophilic surfaces. a) The "spacefill" model (left), which is represented by a green stick (right); b) GAV-9 tapes lying horizontally on HOPG (yellow slab); c) GAV-9 fibrils oriented upright on mica (red slab).

However, AFM studies indicate that GAV-9 forms uniform nanofilaments from random-coil monomeric solutions through template-assisted growth on surfaces, including tape-like objects[19] on HOPG and fibrillike aggregates[23] on mica (Figure 2). Both the tapes and fibrils grow epitaxially across the surface and show three preferred orientations at 120° to each other. The Fourier transform confirms its threefold symmetry (inset of Figure 2b and Figure 2e). It was also found that orientations of the tapes and the fibrils are consistent with the underlying atomic lattice of the substrates (Figure 2a and Figure 2b, Supporting Information). These results indicate that the self-assembly of GAV-9 is a one-dimensional epitaxial growth process, similar to those previously reported.[14–17]

Solid-state ATR (attenuated total reflectance) IR spectroscopy of the fibrils on a mica surface shows an absorption at $\tilde{\nu} = 1628\ cm^{-1}$ together with a weak band at $\tilde{\nu} = 1690\ cm^{-1}$, indicating an antiparallel β-sheet structure[2] (Supporting Information). Surprisingly, the fibrils are 3.0 ± 0.1 nm in height, which is almost equal to the length (3.1 nm) of the GAV-9 peptide in an extended antiparallel β-sheet conformation.[24] The high quality of the fibrils with very uniform height (Figure 2b–d) equal to the length of a single molecule

[*] F. Zhang, Z.-X. Zhang, L.-N. Ji, L. Tang, H.-B. Wang, C.-H. Fan, H.-J. Xu, Y. Zhang, J. Hu, J.-H. He
Shanghai Institute of Applied Physics
Chinese Academy of Sciences
Shanghai 201800 (P.R. China)
Fax: (+86) 21-5955-3021
Fax: (+86) 21-5955-2394
E-mail: yzhang@sinap.ac.cn
hejh@sinap.ac.cn

H.-N. Du, H.-T. Li, H.-Y. Hu
Institute of Biochemistry and Cell Biology
Shanghai Institutes for Biological Sciences
Chinese Academy of Sciences
Shanghai 200031 (P.R. China)

J. Hu
Bio-X Life Sciences Research Center
College of Life Science and Biotechnology
Shanghai JiaoTong University
Shanghai 200030 (P.R. China)

[**] We thank Dr. Bin Li, Xing-Fei Zhou, Yun-Chang Guo, and Hai Li for valuable discussions and Miss Stefanie Maerz for the helpful revisions. This work was supported by grants from the Shanghai Institute of Applied Physics, the National Natural Science Foundation of China (No. 10335070, 10404032, and 30400064), and the Science and Technology Commission of Shanghai Municipality (No. 04qmx1466 and 0552nm033).

Supporting information for this article is available on the WWW under http://www.angewandte.org or from the author.

© 2006 Wiley-VCH Verlag GmbH & Co. KGaA, Weinheim

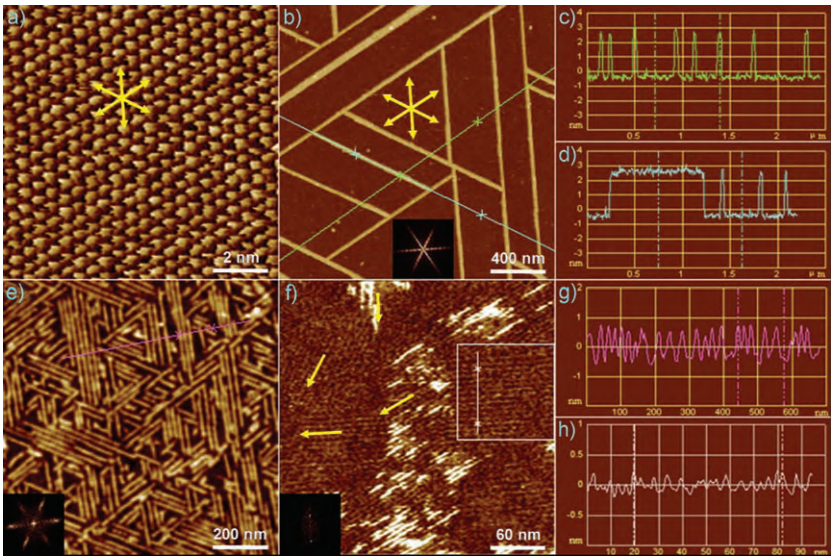

Figure 2. AFM images and analysis of nanofilaments. a) The atomic lattice of the mica surface; b) GAV-9 (1.6 mM) fibrils with apparent widths of 40–70 nm on the same mica surface as in a); inset: Fourier transform. the yellow arrows in a) and b) indicate the consistency of the orientations; c) section analysis of the green line marked in b); d) section analysis along a fibril marked by the blue line in b); e) GAV-9 (1.6 nM) tapes with an apparent width of 20 nm on HOPG; inset: Fourier transform; f) layers of GAV-9 (0.3 mM) tapes on HOPG; yellow arrows indicate their orientations; inset: Fourier transform of the region marked with a white box; g) section analysis of the pink line marked in e); h) section analysis of the white line marked in f).

suggests that GAV-9 is oriented upright on mica surfaces (Figure 1). Peptide fibrils growing in this "upright" style with the peptide backbone perpendicular to the substrate have not been reported previously. In this case, the electrostatic interaction between the negatively charged substrate and the positively charged peptide terminal is the driving force for the ordered assembly of GAV-9. Control experiments show that the growth of fibrils on two positively charged surfaces is significantly inhibited (Supporting Information). The combination of the above results strongly supports an upright orientation.

On the HOPG surface, the height and deconvoluted width[16,25] of GAV-9 tapes are 0.9 ± 0.1 nm and 3–4 nm, respectively. They are approximately equal to the dimensions of GAV-9 (1.0 nm in diameter, 3.1 nm in length). This indicates that the tapes lie with their hydrophobic side chains in contact with the hydrophobic surface of the HOPG substrate (Figure 1). Similar phenomena have been found in other systems.[14–20] When the concentration of GAV-9 increases, multiple layers of tapes are often observed (Figure 2 f), and the tapes sometimes adopt an orientation of 30° to each other (besides 60° or 120°). At concentrations higher than 1.6 mM, the growth of tapes on HOPG is too fast to be investigated by AFM. Furthermore, the peak-to-peak distance of 5.0 ± 0.2 nm between the adjacent tapes (Figure 2 f and Figure 2 h) indicates the presence of a gap (≈ 2 nm).

To investigate the dynamic details of the ordered assembly process, in situ AFM studies have also been carried out. When the concentration of GAV-9 reached 1.6 mM, nucleation seeds with heights of 5–15 nm appeared on the mica surface (see labels 1–26 in Figure 3). Fibrils then started to grow bidirectionally from these seeds at a growth rate of 1–20 nm s^{-1}. The rate varied at different locations and for different fibrils, which may reflect changes in the local environmental conditions. These fibrils can extend to lengths ranging from several microns to tens of microns, but they never overlap with one another. On the basis of AFM images of isolated fibrils, the width of fibrils were found to vary from tens to hundreds of nanometers (Figure 2 b and Supporting Information). However, in situ AFM observations showed that the width of any individual fibril remained constant (≈ 12 nm, after deconvolution) after the fibril had started to grow. As indicated by the arrows in Figure 3l, wider fibrils are most likely a result of the merger of adjacent ones, not of lateral growth of the original fibril. The scanning of the AFM tip sometimes disturbed the growth of fibrils thereby changing the direction of growth (Figure 3, labels 2, 3, 13, 17, and

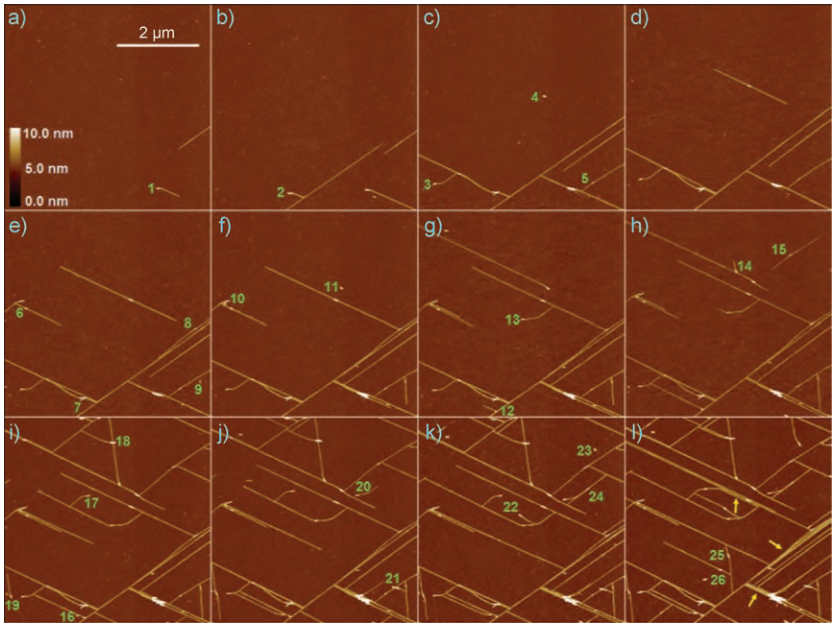

Figure 3. In situ AFM observation of GAV-9 fibrils (apparent width ≈ 40 nm) growing on mica. a–l) A series of snapshots of the growing process, which took about 100 min. The numerical labels indicate the formation of new nucleation seeds. The height and scale bars shown in a) apply to all images.

 © 2006 Wiley-VCH Verlag GmbH & Co. KGaA, Weinheim

22). On HOPG, however, the process is relatively fast (at a rate of 0.3 $\mu m\,s^{-1}$ at a concentration of 0.8 mM), and interactions of the AFM tip did not seem to affect the growth process (Supporting Information).

In summary, we have presented the in situ AFM investigation of the self-assembly of GAV-9 molecules into ordered nanofilaments on both hydrophilic and hydrophobic surfaces. The experimental results indicate that the growth of GAV-9 nanofilaments adopt a horizontal orientation on HOPG and an "upright" orientation on mica. The fibrils are highly uniform in height and may be hundreds of microns in length, which makes them an ideal biotemplate for generating functional nanomaterials. The substrate-directed assembly of peptides by employing surface hydrophobicity/hydrophilicity can be envisioned as a unique approach to fabricate specifically tailored nanostructures. Moreover, our results point to the significance of focusing physicochemical studies of the self-assembly of peptides on the hydrophilic/hydrophobic nature of surfaces, as the interfacial properties may dramatically affect the self-assembly process.

Experimental Section

GAV-9 was synthesized by using the Boc solid-phase method on an ABI 433 A peptide synthesizer (Appliedbiosystems) and cleaved from the MBHA resin (100–200 mesh, Fluka) with hydrogen fluoride. The peptide was purified through a TSK-40 (S) column (2.0 × 98 cm, Tosoh). Before used, GAV-9 was dissolved in 10 mM PBS buffer (phosphate 10 mM, NaCl 10 mM, pH 7.0).

A commercial AFM instrument (Nanoscope IIIa, Veeco) equipped with an E-scanner and a liquid cell was employed, and experiments were performed in the tapping mode. Silicon nitride cantilevers with a nominal spring constant of 0.58 $N\,m^{-1}$ (Veeco) were used. Atomic resolution images of the mica and HOPG surfaces were obtained by contact-mode AFM and scanning tunneling microscopy (STM), respectively, prior to the in situ experiments.

Received: October 14, 2005
Revised: February 17, 2006
Published online: April 26, 2006

Keywords: electrostatic interactions · hydrophobic effect · nanofilaments · peptides · self-assembly

[1] S. Vauthey, S. Santoso, H. Gong, N. Watson, S. Zhang, *Proc. Natl. Acad. Sci. USA* **2002**, *99*, 5355 – 5360.
[2] H. A. Lashuel, S. R. LaBrenz, L. Woo, L. C. Serpell, J. W. Kelly, *J. Am. Chem. Soc.* **2000**, *122*, 5262 – 5277.
[3] A. M. Bittner, *Naturwissenschaften* **2005**, *92*, 51 – 64.
[4] M. G. Ryadnov, B. Ceyhan, C. M. Niemeyer, D. N. Woolfson, *J. Am. Chem. Soc.* **2003**, *125*, 9388 – 9394.
[5] D. E. Wagner, C. L. Phillips, W. M. Ali, G. E. Nybakken, E. D. Crawford, A. D. Schwab, W. F. Smith, R. Fairman, *Proc. Natl. Acad. Sci. USA* **2005**, *102*,12656 – 12661.
[6] C. A. Orme, A. Noy, A. Wierzbicki, M. T. McBride, M. Grantham, H. H. Teng, P. M. Dove, J. J. DeYoreo, *Nature* **2001**, *411*, 775 – 779.
[7] L. Addadi, S. Weiner, *Angew. Chem.* **1992**, *104*, 159 – 176; *Angew. Chem. Int. Ed. Engl.* **1992**, *31*, 153 – 169.
[8] X. Liu, Y. Zhang, D. K. Goswami, J. S. Okasinski, K. Salaita, P. Sun, M. J. Bedzyk, C. A. Mirkin, *Science* **2005**, *307*, 1763 – 1766.
[9] M. J. Pandya, G. M. Spooner, M. Sunde, J. R. Thorpe, A. Rodger, D. N. Woolfson, *Biochemistry* **2000**, *39*, 8728 – 8734.
[10] K. Janek, J. Behlke, J. Zipper, H. Fabian, Y. Georgalis, M. Beyemmann, M. Bienert, E. Krause, *Biochemistry* **1999**, *38*, 8246 – 8252.
[11] C. Goldsbury, J. Kistler, U. Aebi, T. Arvinte, G. J. Cooper, *J. Mol. Biol.* **1999**, *285*, 33 – 39.
[12] H. K. Blackley, G. H. Sanders, M. C. Davies, C. J. Roberts, S. J. Tendler, M. J. Wilkinson, *J. Mol. Biol.* **2000**, *298*, 833 – 840.
[13] M. Zhu, P. O. Souillac, C. Ionescu-Zanetti, S. A. Carter, A. L. Fink, *J. Biol. Chem.* **2002**, *277*, 50914 – 50922.
[14] C. Ha, C. B. Park, *Biotechnol. Bioeng.* **2005**, *90*, 848 – 855.
[15] W. Hoyer, D. Cherny, V. Subramaniam, T. M. Jovin, *J. Mol. Biol.* **2004**, *340*, 127 – 139.
[16] C. L. Brown, I. A. Aksay, D. A. Saville, M. H. Hecht, *J. Am. Chem. Soc.* **2002**, *124*, 6846 – 6848.
[17] G. Yang, K. A. Woodhouse, C. M. Yip, *J. Am. Chem. Soc.* **2002**, *124*, 10648 – 10649.
[18] C. E. Giacomelli, W. Norde, *Macromol. Biosci.* **2005**, *5*, 401 – 407.
[19] C. Whitehouse, J. Fang, A. Aggeli, M. Bell, R. Brydson, C. W. Fishwick, J. R. Henderson, C. M. Knobler, R. W. Owens, N. H. Thomson, D. A. Smith, N. Boden, *Angew. Chem.* **2005**, *117*, 2001 – 2004; *Angew. Chem. Int. Ed.* **2005**, *44*, 1965 – 1968.
[20] T. Kowalewski, D. M. Holtzman, *Proc. Natl. Acad. Sci. USA* **1999**, *96*, 3688 – 3693.
[21] H. N. Du, L. Tang, X. Y. Luo, H. T. Li, J. Hu, J. W. Zhou, H. Y. Hu, *Biochemistry* **2003**, *42*, 8870 – 8878.
[22] D. A. Kocisko, J. H. Come, S. A. Priola, B. Chesebro, G. J. Raymond, P. T. Lansbury, B. Caughey, *Nature* **1994**, *370*, 471 – 474.
[23] A. Aggeli, I. A. Nyrkova, M. Bell, R. Harding, L. Carrick, T. C. B. McLeish, A. N. Semenov, N. Boden, *Proc. Natl. Acad. Sci. USA* **2001**, *98*, 11857 – 11862.
[24] T. E. Creighton, *Proteins: Structures and Molecular Properties*, 2nd ed., Freeman, New York, **1993**.
[25] a) S. Y. Fung, C. Keyes, J. Duhamel, P. Chen, *Biophys. J.* **2003**, *85*, 537 – 548; b) the AFM tips used in the in situ experiments have an estimated curvature radius of ≈ 35 nm, as calibrated with gold colloids (20 nm) under the same conditions.

 © 2006 Wiley-VCH Verlag GmbH & Co. KGaA, Weinheim

Nanoparticle Catalyst

DOI: 10.1002/anie.200503808

Ultrastable Gold Nanocatalyst Supported by Nanosized Non-Oxide Substrate**

*Wenfu Yan, Suree Brown, Zhengwei Pan, Shannon M. Mahurin, Steven H. Overbury, and Sheng Dai**

Since the discovery of the surprisingly high catalytic activity possessed by gold nanoparticles for the oxidation of CO at low temperature, investigations into the potential uses of gold for various industrially important catalytic processes have been actively pursued.[1,2] Notably, gold nanoparticles on oxide supports were regarded as highly active catalysts for the selective oxidation of hydrocarbons, methanol synthesis by hydrogenation of carbon dioxide, water–gas shift reaction, reduction of nitric oxide by hydrogen, propylene epoxidation, and preferential oxidation of CO (PROX reaction).[3–8] A number of oxides, such as TiO_2,[9–21] Fe_2O_3,[1,22–24] Co_3O_4,[1,25,26] NiO,[1,25,26] SiO_2,[27–29] Al_2O_3,[30,31] ZrO_2,[32] MgO,[33–35] CuO,[25,26,36] ZnO,[25,26,36–38] MnO_x,[25,39,40] Cr_2O_3,[25,26] CaO,[25] La_2O_3,[25,26,41] CeO_2,[41–43] Y_2O_3,[26,44] and U_3O_8,[26] have been investigated as supports for gold nanocatalysts. A strong dependence of Au catalytic activity on the type of oxide support was observed experimentally. Recent theoretical and experimental studies have also indicated that the interaction of Au nanoparticles with oxide surfaces could be essential in activating the catalytic properties through oxygen-vacancy F-center defects and charge transfer from the surface of metal oxides to gold nanoparticles.[45,46] A model based on the strong metal–support interaction (SMSI) investigated for Group VIII metals on oxide supports was proposed to rationalize such a dependence on the oxide support.[47,48]

On the contrary, few investigations of the catalytic properties of gold nanoparticles on non-oxide supports have appeared, with the exception of gold nanoparticles supported on carbon materials.[49,50] In the latter case, no appreciable catalytic activity for oxidation reactions was observed. Herein, we report the preparation of an ultrastable Au nanocatalyst supported on a non-oxide material based on $LaPO_4$ nanoparticles. The stability of this Au nanocatalyst under high-temperature treatment in O_2 is much better than that of the TiO_2-supported Au reference nanocatalyst supplied by the World Gold Council as part of an initiative to promote the use of gold in this type of industrial procedure. The application of the phosphate-based supports opens up a new avenue in the search for highly active, stable, and selective gold catalysts for a number of catalytic reactions. The unique structural features of this non-oxide support (such as difficulty in undergoing oxygen exchange and reduction) could shed new light on the mechanism associated with gold-based catalysis.

The $LaPO_4$ nanoparticles were synthesized by a sonication method.[51] transmission electron microscopy (TEM) analyses showed that the average particle size of the as-synthesized $LaPO_4$ nanoparticles is about 6–8 nm (see Supporting Information); their Brunauer–Emmett–Teller (BET) surface area is 111 $m^2 g^{-1}$. The X-ray diffraction (XRD) pattern of the as-synthesized $LaPO_4$ nanoparticle substrate (see the Supporting Information) does not show any resemblance to that of the monoclinic $LaPO_4$ phase ($LaPO_4$-M), but can be assigned to the pattern attributed to a hexagonal $LaPO_4$ phase ($LaPO_4$-H; see the XRD patterns and indexing (Figure 3a)). However, the two XRD peaks with $2\theta \approx 20.3$ and 26.1° are shifted slightly from the corresponding peaks in the simulated hexagonal $LaPO_4$ XRD pattern, which could be attributed to the potential lattice distortion induced by the nanoparticles. A search of the commercial XRD database JADE (Materials Data, Livermore,) excluded the possibility of the presence of any impurity phases that originate from lanthanum oxide, lanthanum chloride, or lanthanum hydroxide. Research is currently under way to investigate the indexing of these two peaks.

To further rule out the possibility of the presence of amorphous La_2O_3, the calcination of $LaPO_4$-H was conducted at high temperature (950 °C) to induce the crystallization of potential amorphous La_2O_3. No detectable La_2O_3 phase or any other impurity was observed (see the Supporting Information). A clean and complete transformation of $LaPO_4$-H to $LaPO_4$-M was indicated, which further supported the basic elemental composition of $LaPO_4$-H with negligible impurities. Additional spectroscopic characterization and elemental analysis as well as phase-transition behaviors are given in the Supporting Information. The average particle size calculated on the basis of the line widths of the XRD peaks for the as-synthesized $LaPO_4$ nanoparticles is approximately 7 nm, which is consistent with the TEM estimation (see the Supporting Information). For comparison, a high-surface-area $LaPO_4$ sample with a monoclinic structure (Sigma-Aldrich; see the XRD pattern in Figure 3b) was also used as a

[*] Dr. W. F. Yan,[+] Dr. S. Brown, Dr. Z. W. Pan, Dr. S. M. Mahurin, Dr. S. H. Overbury, Dr. S. Dai
Chemical Sciences Division
Oak Ridge National Laboratory
Oak Ridge, TN 37831-6201 (USA)
Fax: (+1) 865-576-5235
E-mail: dais@ornl.gov

[+] Present address: State Key Laboratory of Inorganic Synthesis and Preparative Chemistry
College of Chemistry
Jilin University
Changchun 130012
P.R. China

[**] This work was conducted at the Oak Ridge National Laboratory and supported by the Division of Chemical Sciences, Office of Basic Energy Sciences, US Department of Energy, under contract no. DE-AC05-00OR22725 with UT-Battelle, LLC. We thank the SHARE Facility at ORNL for the transmission electron microscopy. This research was supported in part by an appointment for W.F.Y. to the ORNL Postdoctoral Research Associates Program, administered jointly by the Oak Ridge Institute for Science and Education and ORNL.

Supporting information for this article is available on the WWW under http://www.angewandte.org or from the author.

InterScience
© 2006 Wiley-VCH Verlag GmbH & Co. KGaA, Weinheim

support in the preparation of Au nanocatalysts. The average particle size estimated from the line widths of the XRD peaks is approximately 10 nm, which accounts well for the relatively small surface area (55 $m^2 g^{-1}$) of this $LaPO_4$-M sample. The gold precursor species were introduced on the hexagonal $LaPO_4$ (termed Au/$LaPO_4$-H) and the monoclinic $LaPO_4$ (termed Au/$LaPO_4$-M) samples using a deposition–precipitation (DP) method originally developed by Haruta and coworkers.[52] The Au loadings of Au/$LaPO_4$-H and Au/$LaPO_4$-M are 8.3 and 4.2 wt%, respectively. However, both catalysts have almost the same Au areal density for gold through normalization with respect to their corresponding surface areas. A TiO_2-supported Au reference nanocatalyst (termed Au/TiO_2-R) supplied by the World Gold Council was also used in catalyst testing for comparative purposes.

The light-off curves for CO oxidation were measured from low conversion to 100% conversion for the above three gold catalysts with and without treatment at 500 °C in 8% O_2/He for 2 h. The high-temperature calcination treatment is a very stringent test for the stability of gold nanocatalysts against sintering.[47,53] Conventional TiO_2-supported gold nanocatalysts are known to be readily deactivated under such conditions.[47] The sample weights of the three Au catalysts used in our plug-flow reactor tests were adjusted to maintain a constant Au content of 0.75 mg.

Figure 1a shows a comparison of the light-off curves for the three catalysts without the high-temperature calcination treatment. Based on these curves, the temperatures at which the specific rate reaches 0.66 $mol_{CO}\,g_{Au}^{-1}\,h^{-1}$ (50% conversion) were obtained for Au/$LaPO_4$-H, Au/$LaPO_4$-M, and Au/TiO_2-R (Figure 2). All the catalysts are very active, with Au/$LaPO_4$-M having the highest activity. However, after calcination at 500 °C in 8% O_2/He for 2 h (heating rate: 10 °C min^{-1}),

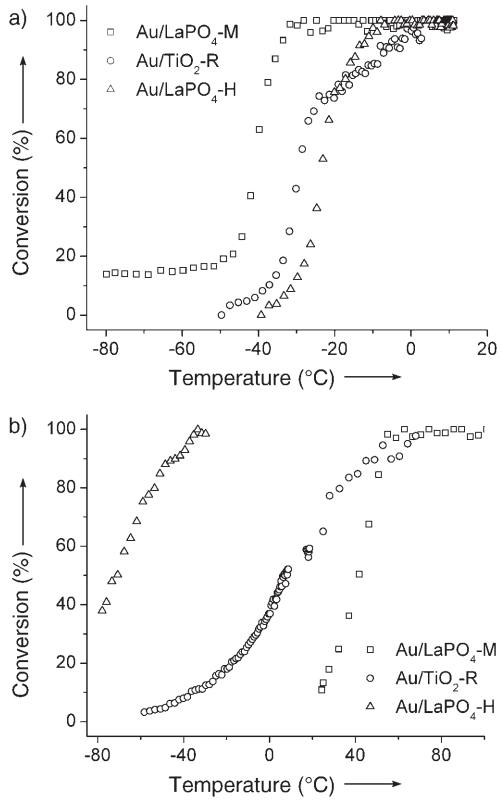

Figure 1. Light-off curves of a) as-synthesized and b) calcined Au/$LaPO_4$-H, Au/$LaPO_4$-M, and Au/TiO_2-R.

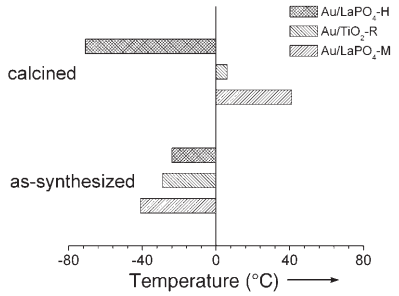

Figure 2. Temperature at which the specific rate reached 0.66 $mol_{CO}\,g_{Au}^{-1}\,h^{-1}$ (50% conversion) for Au/$LaPO_4$-H, Au/$LaPO_4$-M, and Au/TiO_2-R.

the activity sequence changed totally (see Figure 1b). Surprisingly, Au/$LaPO_4$-H was activated strongly, while both Au/$LaPO_4$-M and Au/TiO_2-R were deactivated. The latter observation is consistent with previous reports[14,15,54] showing that Au catalysts on oxide supports can be readily deactivated through sintering induced by calcination at high temperature (e.g., 500 °C). The calcined Au/$LaPO_4$-H unexpectedly reached the specific rate of 0.66 $mol_{CO}\,g_{Au}^{-1}\,h^{-1}$ (50% conversion) at a temperature as low as −71 °C, whereas 41 and 6 °C were required for Au/$LaPO_4$-M and Au/TiO_2-R to reach this specific rate, respectively (Figure 2). However, a slow conversion-increasing step in the light-off curve of Au/$LaPO_4$-H from −50 to −40 °C was observed, which might be indicative of carbonate formation at low temperature.[55]

To rule out the possibility that the observed activation at 500 °C was induced by potential amorphous La_2O_3 impurities, a gold catalyst supported on La_2O_3 (Au/La_2O_3) was prepared.[25] The catalysis test shows that Au/La_2O_3 can be readily deactivated by calcination at 500 °C in 8% O_2/He, which indicates that the structure of $LaPO_4$-H is the key to the observed activation process. Accordingly, the considerable activation of the Au/$LaPO_4$-H system by calcination at 500 °C in 8% O_2/He is very unusual.

Figure 3a shows the XRD pattern of the as-synthesized Au/$LaPO_4$-H; no metallic gold peaks are visible. The Au loading of Au/$LaPO_4$-H is as high as 8.3 wt% based on inductively couple plasma (ICP) analysis, and thus it is reasonably inferred that the absence of the Au peaks in the XRD pattern of the as-synthesized Au/$LaPO_4$-H sample can be related to the cationic nature of the Au precursors. Another interesting phenomenon which can be clearly seen from Figure 3a is that the XRD line widths of the $LaPO_4$-H sample remain broad after calcination at 500 °C. This observation further supports the fact that the $LaPO_4$-H nanoparticles are highly sinter-resistant. However, a very broad gold XRD peak at $2\theta \approx 38.2°$ and a weak peak at $2\theta \approx 44.5°$ appeared. This observation suggests that metallic Au nanoparticles with a very small particle size (≈2 nm,

 © 2006 Wiley-VCH Verlag GmbH & Co. KGaA, Weinheim

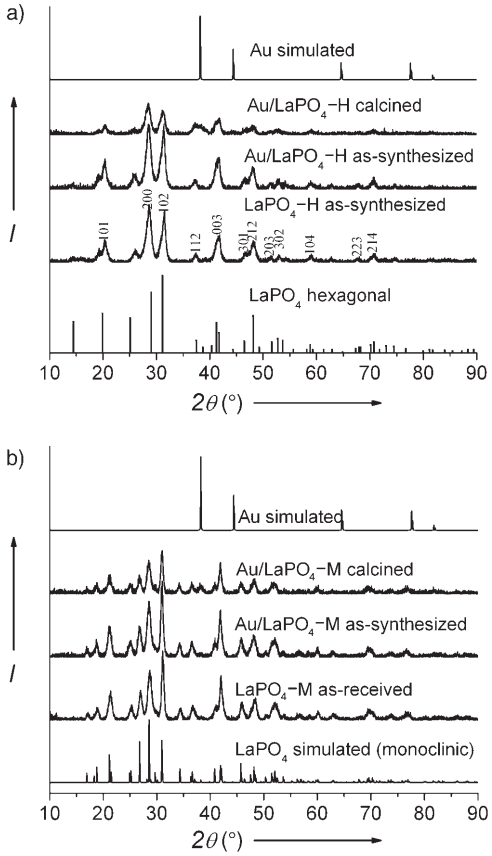

Figure 3. a) Comparison of the simulated XRD patterns of Au and hexagonal $LaPO_4$ with the experimental XRD patterns of the as-synthesized $LaPO_4$-H nanoparticles and both as-synthesized and calcined Au/$LaPO_4$-H. b) Comparison of the simulated XRD patterns of Au and monoclinic $LaPO_4$ with the experimental XRD patterns of as-received $LaPO_4$-M, and as-synthesized and calcined Au/$LaPO_4$-M.

Figure 4b) were formed during calcination through auto-reduction.

In contrast, the situation is very different with respect to the calcined Au/$LaPO_4$-M sample. Two sharp XRD peaks attributed to metallic gold particles appeared in its XRD pattern, which indicate the formation of much larger gold particles during calcination (Figure 3b). This observation is in agreement with the trend of the corresponding catalytic activities for CO oxidation and shows that the catalytic activity of Au/$LaPO_4$-H is much higher than that of Au/$LaPO_4$-M. Clearly, this observed difference can be correlated to the size of the gold nanoparticles. As discussed above, the areal density of Au for Au/$LaPO_4$-H and $LaPO_4$-M is very similar. Accordingly, the dispersion of gold nanoparticles on both substrates should be basically identical and have a similar stability against sintering if the surface properties of both $LaPO_4$-H and $LaPO_4$-M are similar. This is clearly in contradiction to our experimental observations. Thus, a stronger surface interaction of metallic gold species with $LaPO_4$-H than $LaPO_4$-M is indicated.

Our microscopy investigations provide further support for the strong interaction of metallic gold species with $LaPO_4$-H. As seen in Figure 4a, imaging with a high-angle annular dark-field (HAA-DF, also known as Z-contrast) scanning transmission electron microscope (STEM) shows tiny, highly uniform Au nanoparticles (0.8–2.0 nm diameter) distributed on $LaPO_4$-H for the as-synthesized Au/$LaPO_4$-H. Figure 5a shows a high-resolution TEM (HRTEM) image of the same material. The Au particles in the as-synthesized form are quite small and uniform with a mean size of about 1–2 nm, which is consistent with STEM analyses. The gold precursors exist in a

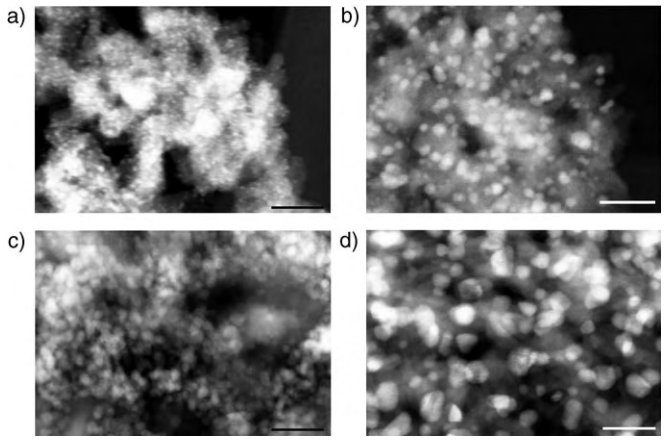

Figure 4. Z-contrast TEM image of a) as-synthesized Au/$LaPO_4$-H, b) calcined Au/$LaPO_4$-H, c) as-synthesized Au/$LaPO_4$-M, and d) calcined Au/$LaPO_4$-M. Scale bar = 20 nm.

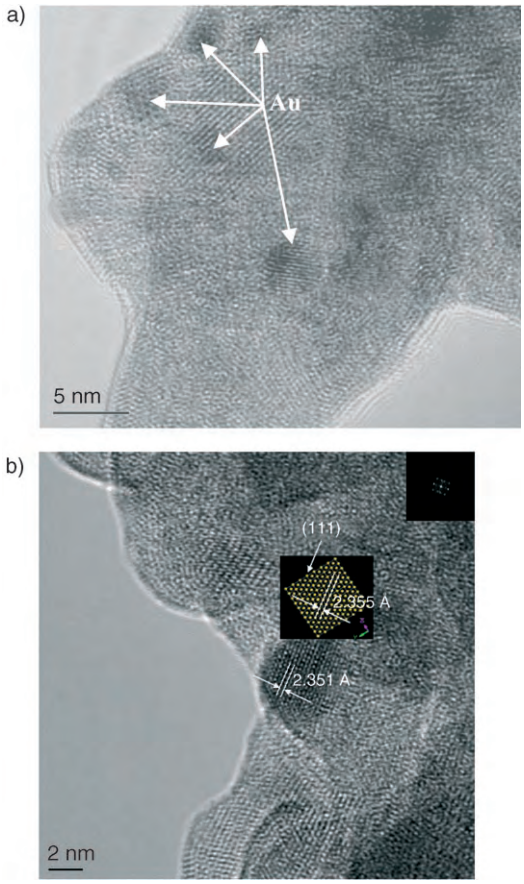

Figure 5. HRTEM images of a) as-synthesized and b) calcined Au/$LaPO_4$-H. For details, see text.

 © 2006 Wiley-VCH Verlag GmbH & Co. KGaA, Weinheim

cationic form on $LaPO_4$-H, and thus the lattice structure of the Au nanoparticles is not very clear in the HRTEM image. After high-temperature calcination, the Z-contrast image recorded on Au/$LaPO_4$-H at an identical magnification shows slight growth of the gold nanoparticles (Figure 4b) as a result of high-temperature sintering. The average size of the Au nanoparticles reaches 2–4 nm. The sintering of the gold nanoparticles of Au/$LaPO_4$-M (Figure 4c and d) is much more severe, which agrees with the above XRD observation and further indicates that the interaction of $LaPO_4$-H with gold nanoparticles is stronger than that of $LaPO_4$-M. The HRTEM image shown in Figure 5b clearly reveals the crystalline nature of the resulting Au metallic nanoparticles of calcined Au/$LaPO_4$-H. The distance between two (111) lattice planes measured from the HRTEM image is approximately 2.35 Å, which is consistent with the value of 2.36 Å measured from an Au model structure with the MS modeling program supplied by Accelrys (see the middle inset of Figure 5b). The top-right inset of Figure 5b is the electron-diffraction pattern of this Au nanoparticle, which demonstrates nicely the crystalline structure of the metallic particles.

The high dispersion and well-developed crystalline structure revealed by HRTEM for the Au nanoparticles supported on $LaPO_4$-H provide structural evidence for the unusual activation of the Au/$LaPO_4$-H system by calcination at 500 °C in 8% O_2/He. Our selected-area electron diffraction study indicates that the gold nanoparticles are mainly attached epitaxially on $LaPO_4$-H through the most densely packed (111) plane (Figure 5).[55] This activation process under the oxidative conditions is in sharp contrast to those required for the oxide-supported catalyst system.[47,48] Based on the SMSI model, the latter system requires the reduction of support oxides to invoke SMSI. The negligible reducibility of $LaPO_4$ implies that Au/$LaPO_4$-H needs to rely on other means of activation to enhance SMSI. One possible activation mechanism during the calcination of Au/$LaPO_4$-H could involve the surface restructuring of the gold/support interfaces. Deactivation of Au/$LaPO_4$-M was observed under the same calcination conditions, and hence the surface restructuring might be unique to the specific surface configuration of $LaPO_4$-H. Clearly, the smaller particle size of the $LaPO_4$-H support may play a key role in this surface-restructuring process through the supply of a high surface-defect concentration relative to that of the $LaPO_4$-M support. This observation is very similar to that of Corma and co-workers, which showed that gold nanoparticles deposited on CeO_2 nanocrystals by co-precipitation yielded an activity for CO oxidation that was two orders of magnitude higher than that for particles deposited on bulk CeO_2.[43] The unique restructuring properties of nanoparticles with ionic lattices have been recently revealed and utilized in the generation of new nanoparticle phases.[8,56]

In conclusion, a new non-oxide support system based on $LaPO_4$ nanoparticles has been developed for gold catalysts used in CO oxidation. The key feature of this catalytic system is that activation can be achieved through calcination under an oxidative atmosphere. This observation is in sharp contrast to conventional SMSI catalytic systems, which can only be activated under a reductive atmosphere. The high stability and activity of the gold nanoparticles deposited on the $LaPO_4$ nanoparticles suggest a unique interaction between the gold and the phosphate support, which highlights new opportunities in the development of ultrastable gold catalysts for reactions in oxidative and high-temperature environments.

Received: October 27, 2005
Revised: February 11, 2006
Published online: April 26, 2006

Keywords: gold · lanthanum · nanoparticles · oxidation · supported catalysts

[1] M. Haruta, N. Yamada, T. Kobayashi, S. Iijima, *J. Catal.* **1989**, *115*, 301.
[2] M. Haruta, S. Tsubota, T. Kobayashi, H. Kageyama, M. J. Genet, B. Delmon, *J. Catal.* **1993**, *144*, 175.
[3] G. C. Bond, D. T. Thompson, *Catal. Rev. Sci. Eng.* **1999**, *41*, 319.
[4] G. J. Hutchings, *Catal. Today* **2002**, *72*, 11.
[5] M. C. Daniel, D. Astruc, *Chem. Rev.* **2004**, *104*, 293.
[6] C. W. Corti, R. J. Holliday, D. T. Thompson, *Appl. Catal. A* **2005**, *291*, 253.
[7] G. J. Hutchings, *Catal. Today* **2005**, *100*, 55.
[8] D. H. Son, S. M. Hughes, Y. D. Yin, A. P. Alivisatos, *Science* **2004**, *306*, 1009.
[9] F. Moreau, G. C. Bond, A. O. Taylor, *Chem. Commun.* **2004**, 1642.
[10] M. Valden, X. Lai, D. W. Goodman, *Science* **1998**, *281*, 1647.
[11] W. F. Yan, B. Chen, S. M. Mahurin, S. Dai, S. H. Overbury, *Chem. Commun.* **2004**, 1918.
[12] M. S. Chen, D. W. Goodman, *Science* **2004**, *306*, 252.
[13] E. E. Stangland, K. B. Stavens, R. P. Andres, W. N. Delgass, *J. Catal.* **2000**, *191*, 332.
[14] S. D. Lin, M. Bollinger, M. A. Vannice, *Catal. Lett.* **1993**, *17*, 245.
[15] W. F. Yan, S. M. Mahurin, Z. W. Pan, S. H. Overbury, S. Dai, *J. Am. Chem. Soc.* **2005**, *127*, 10480.
[16] J. D. Grunwaldt, C. Kiener, C. Wogerbauer, A. Baiker, *J. Catal.* **1999**, *181*, 223.
[17] W. F. Yan, B. Chen, S. M. Mahurin, E. W. Hagaman, S. Dai, S. H. Overbury, *J. Phys. Chem. B* **2004**, *108*, 2793.
[18] J. D. Grunwaldt, A. Baiker, *J. Phys. Chem. B* **1999**, *103*, 1002.
[19] M. A. P. Dekkers, M. J. Lippits, B. E. Nieuwenhuys, *Catal. Lett.* **1998**, *56*, 195.
[20] W. F. Yan, S. M. Mahurin, B. Chen, S. H. Overbury, S. Dai, *J. Phys. Chem. B* **2005**, *109*, 15489.
[21] B. Schumacher, V. Plzak, J. Cai, R. J. Behm, *Catal. Lett.* **2005**, *101*, 215.
[22] M. J. Kahlich, H. A. Gasteiger, R. J. Behm, *J. Catal.* **1999**, *182*, 430.
[23] F. Boccuzzi, A. Chiorino, M. Manzoli, D. Andreeva, T. Tabakova, *J. Catal.* **1999**, *188*, 176.
[24] M. M. Schubert, S. Hackenberg, A. C. van Veen, M. Muhler, V. Plzak, R. J. Behm, *J. Catal.* **2001**, *197*, 113.
[25] G. Y. Wang, W. X. Zhang, Y. C. Cui, H. L. Lian, D. Z. Jiang, T. H. Wu, *Chin. J. Catal.* **2001**, *22*, 408.
[26] N. S. Patil, B. S. Uphade, D. G. McCulloh, S. K. Bhargava, V. R. Choudhary, *Catal. Commun.* **2004**, *5*, 681.
[27] M. Daté, M. Okumura, S. Tsubota, M. Haruta, *Angew. Chem.* **2004**, *116*, 2181; *Angew. Chem. Int. Ed.* **2004**, *43*, 2129.
[28] S. H. Overbury, L. Ortiz-Soto, H. G. Zhu, B. Lee, M. D. Amiridis, S. Dai, *Catal. Lett.* **2004**, *95*, 99.
[29] M. T. Bore, H. N. Pham, E. E. Switzer, T. L. Ward, A. Fukuoka, A. K. Datye, *J. Phys. Chem. B* **2005**, *109*, 2873.
[30] G. K. Bethke, H. H. Kung, *Appl. Catal. A* **2000**, *194*, 43.

 © 2006 Wiley-VCH Verlag GmbH & Co. KGaA, Weinheim

[31] C. K. Costello, M. C. Kung, H. S. Oh, Y. Wang, H. H. Kung, *Appl. Catal. A* **2002**, *232*, 159.
[32] A. Knell, P. Barnickel, A. Baiker, A. Wokaun, *J. Catal.* **1992**, *137*, 306.
[33] B. Yoon, H. Hakkinen, U. Landman, A. S. Worz, J. M. Antonietti, S. Abbet, K. Judai, U. Heiz, *Science* **2005**, *307*, 403.
[34] J. Guzman, B. C. Gates, *J. Am. Chem. Soc.* **2004**, *126*, 2672.
[35] L. M. Molina, B. Hammer, *Phys. Rev. Lett.* **2003**, *90*, 206102.
[36] G. J. Hutchings, M. R. H. Siddiqui, A. Burrows, C. J. Kiely, R. Whyman, *J. Chem. Soc. Faraday Trans.* **1997**, *93*, 187.
[37] G. Y. Wang, W. X. Zhang, H. L. Lian, D. Z. Jiang, T. H. Wu, *Appl. Catal. A* **2003**, *239*, 1.
[38] F. Boccuzzi, A. Chiorino, S. Tsubota, M. Haruta, *J. Phys. Chem.* **1996**, *100*, 3625.
[39] S. J. Lee, A. Gavriilidis, Q. A. Pankhurst, A. Kyek, F. E. Wagner, P. C. L. Wong, K. L. Yeung, *J. Catal.* **2001**, *200*, 298.
[40] G. B. Hoflund, S. D. Gardner, D. R. Schryer, B. T. Upchurch, E. J. Kielin, *Appl. Catal. B* **1995**, *6*, 117.
[41] F. Marino, C. Descorme, D. Duprez, *Appl. Catal. B* **2004**, *54*, 59.
[42] Q. Fu, A. Weber, M. Flytzani-Stephanopoulos, *Catal. Lett.* **2001**, *77*, 87.
[43] S. Carrettin, P. Concepcion, A. Corma, J. M. L. Nieto, V. F. Puntes, *Angew. Chem.* **2004**, *116*, 2592; *Angew. Chem. Int. Ed.* **2004**, *43*, 2538.
[44] J. Guzman, A. Corma, *Chem. Commun.* **2005**, 743.
[45] A. Sanchez, S. Abbet, U. Heiz, W. D. Schneider, H. Hakkinen, R. N. Barnett, U. Landman, *J. Phys. Chem. A* **1999**, *103*, 9573.
[46] U. Heiz, W. D. Schneider, *J. Phys. D* **2000**, *33*, R85.
[47] D. W. Goodman, *Catal. Lett.* **2005**, *99*, 1.
[48] S. J. Tauster, S. C. Fung, R. L. Garten, *J. Am. Chem. Soc.* **1978**, *100*, 170.
[49] L. Prati, G. Martra, *Gold Bull.* **1999**, *32*, 96.
[50] M. M. Maye, N. N. Kariuki, J. Luo, L. Han, P. Njoki, L. Y. Wang, Y. Lin, H. R. Naslund, C. J. Zhong, *Gold Bull.* **2004**, *37*, 217.
[51] S. S. Brown, H. J. Im, A. J. Rondinone, S. Dai, *J. Colloid Interface Sci.* **2005**, *292*, 127.
[52] S. Tsubota, M. Haruta, T. Kobayashi, A. Ueda, Y. Nakahara, *Stud. Surf. Sci. Catal.* **1991**, *63*, 695.
[53] B. K. Min, W. T. Wallace, D. W. Goodman, *J. Phys. Chem. B* **2004**, *108*, 14609.
[54] W. F. Yan, B. Chen, S. M. Mahurin, V. Schwartz, D. R. Mullins, A. R. Lupini, J. Pennycook, S. Dai, S. H. Overbury, *J. Phys. Chem. B* **2005**, *109*, 10676.
[55] M. Haruta, *CATTECH* **2002**, *6*, 102.
[56] H. Z. Zhang, B. Gilbert, F. Huang, J. F. Banfield, *Nature* **2003**, *424*, 1025.

 © 2006 Wiley-VCH Verlag GmbH & Co. KGaA, Weinheim

DNA Microarrays

DOI: 10.1002/anie.200503830

Enhanced Signals and Fast Nucleic Acid Hybridization By Microfluidic Chaotic Mixing**

*Jian Liu, Brian A. Williams, Richele M. Gwirtz, Barbara J. Wold, and Stephen Quake**

Nucleic acid hybridization techniques are widely used in both fundamental and clinical research to identify genes and mutants, to map their correlations, and to analyze their expression. DNA microarrays immobilize thousands of oligonucleotides, cDNA (c = complementary) clones, or polymerase-chain-reaction (PCR) products on the solid substrate, thus providing a powerful tool for the large-scale detection of target genes.[1,2] However, hybridization in conventional microarray experiments is performed in a diffusion-limited manner, which is quite inefficient. The hybridization process may take 8–24 h, during which period the characteristic distance (1–3 mm) that a target DNA molecule can diffuse is still one order of magnitude less than the typical size of most microarrays (> 10 mm).[3,4] Herein we describe an effective answer to that problem using microfluidic chaotic mixing. Our polydimethylsilicane (PDMS) devices use integrated peristaltic pumps to circulate the solution between two large chambers, while chaotically mixing the components of the solution in bridge channels at the same time. We demonstrate that this approach dramatically enhances hybridization signals and improves sensitivity by nearly one order of magnitude relative to the conventional static-hybridization method over the same length of time. Alternatively, for a desired sensitivity, dynamic mixing can be used to accelerate the hybridization process by a factor of three or more. This approach offers many benefits, including high sensitivity, rapid results, better reproducibility, low cost, compatibility with commercial microarray slides, and ease of large-scale integration.

[*] Prof. S. Quake
Department of Bioengineering and Howard Hughes Medical Institute
James Clark Center E300, Stanford University
Stanford, CA 94305 (USA)
Fax: (+1) 650-736-1961
E-mail: quake@stanford.edu

J. Liu, Dr. B. A. Williams, R. M. Gwirtz, Prof. B. J. Wold
California Institute of Technology
Pasadena, CA 94305 (USA)

[**] This research was supported by the NIH Director's Pioneer Award (7DP1 0D000251-02) and NIH 1R01 HG002644-01A1. We thank Yanxia Hao and Dr. Christopher S. Baker of the Genomics Core Laboratory, Gladstone Institutes for providing mouse-printed oligoarrays (17 K) and Frederick Balagadde of Caltech for technical assistance.

Supporting information for this article is available on the WWW under http://www.angewandte.org or from the author.

WILEY InterScience DISCOVER SOMETHING GREAT
© 2006 Wiley-VCH Verlag GmbH & Co. KGaA, Weinheim

The fundamental problem faced by DNA-microarray practitioners is how to continuously mix a sample solution at low Reynolds number and transport the DNA molecules to the proximity of the probes more rapidly than diffusion alone, thereby increasing valid molar-hybridization events. Many methods of active mixing have been developed, including surface acoustic-wave microagitation,[5] bubble-induced acoustic microstreaming,[3] alternative convection induced through several ports,[4] "drain-and-fill" or air-driven bladders,[6,7] magnetic stirring bars,[8] and shuttling sample plugs in a serpentine microtrench.[9] Some researchers developed electrokinetic methods to accelerate the transportation of DNA molecules.[10–12] Although these methods all allow shorter hybridization times and improved signals, they appear to suffer from one or several shortcomings: inhomogeneous mixing,[3–5] small arrays,[10–12] relatively low sensitivity,[3,4,6,8–12] or incompatibility with the widely used cyanine (Cy)-dye microarray format.[10–12] On the other hand, chaotic mixing has gained the interest of many researchers as a promising method of mixing solutions in microchannels.[13–15]

We constructed a two-layer PDMS microfluidic device[16] and sealed it to a spotted microarray slide to perform dynamic hybridization. As shown in Figure 1 a, the fluidic layer of the device contains two symmetric hybridization chambers (6 mm × 6.5 mm × 65 μm, 5 μL). They are connected to each other by bridge channels, the ceilings of which incorporate protrusions with a herring-bone pattern to produce chaotic mixing.[14] The bridge channels (400 μm wide, 40 μm high) are connected to the chambers by bifurcating channels that equalize the solution distributed into the chambers after mixing. Four input/output through-holes with corresponding micromechanical valves are used for loading samples or disposing waste solutions. These valves are actuated to form closed chambers during hybridization. Two sets of peristaltic pumps[17] are integrated to circulate the fluid between the hybridization chambers. The design allows different components in the solution to mix in a chaotic manner when they pass through the bridge channels, and then to be delivered through the hybridization chambers (Figure 1 b, c and Supporting Information). The peristaltic pumps create a fluid flux of $\approx 5.2\,\mathrm{nL\,s^{-1}}$. It takes about 16 min to complete one circulation of the two chambers. The flux can be further raised by increasing the cross-sectional area of the individual pumps.

We evaluated the efficiency of mixing by loading each chamber half with the blank solution and half with the solution containing fluorescent beads, then actuating the pumps, and performing fluorescence measurements. A fluorescence inverted microscope with a charge-coupled device (CCD) camera was set up to take images of the device. Chaotic mixing was confirmed by independent observations of the zigzag motion of the beads and their crossing each other through the bridge channels (images not shown). The fluorescence intensity was monitored in real time through 10 windows along the equator of one chamber. As shown in the Supporting Information, within minutes chaotic mixing dramatically decreased the fluorescence gradient along the equator. The control experiment followed all the above conditions except that a device without the herring-bone protrusions on the bridge channels was used. In this case, the fluorescence difference along the equator was still substantial even after the solutions have been circulated for 2 h, owing to the absence of effective lateral mixing (see Supporting Information). Therefore, the chaotic mixing introduced by

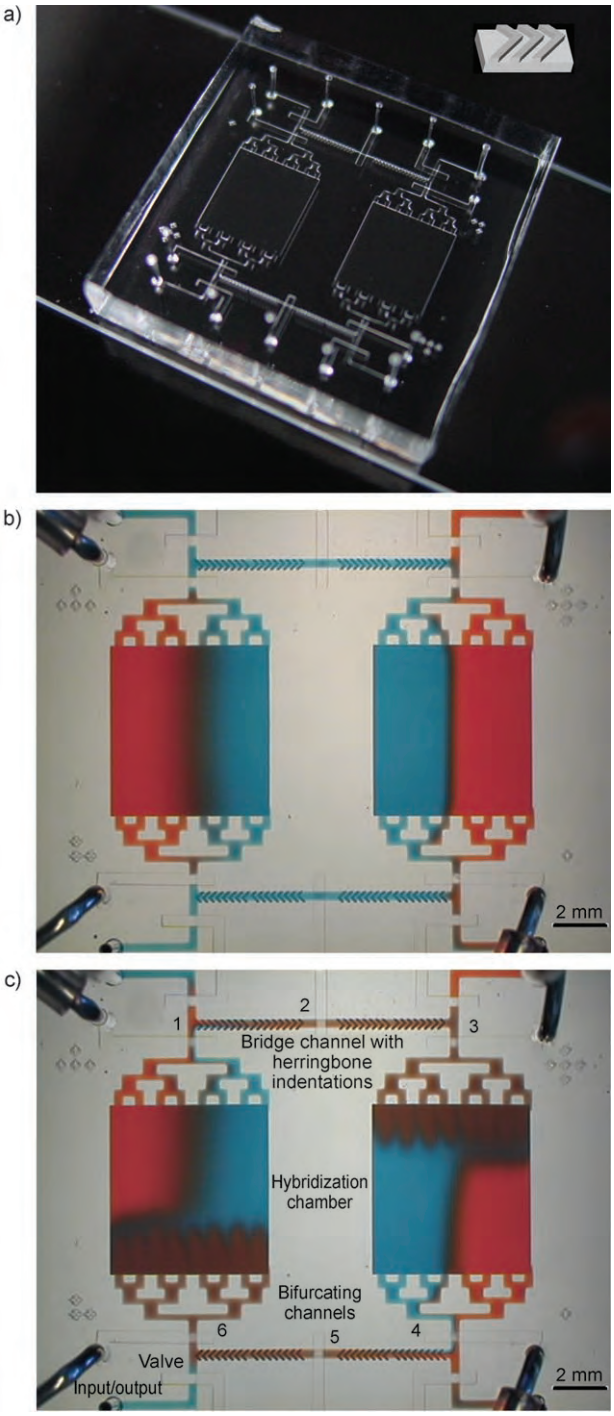

Figure 1. Optical micrographs of the PDMS device. a) The inset shows the 3D structure of the bridge channels with herringbone protrusions. b) The chambers were loaded half with the red and half with the blue solution. c) The peristaltic pumps (1–3 and 4–6) circulated the solutions clockwise in the device. The herringbone protrusions in the bridge channel produced chaotic mixing of the colors.

 © 2006 Wiley-VCH Verlag GmbH & Co. KGaA, Weinheim

the herring-bone protrusions is critical in homogenizing the solutions in the chambers. Ripples in fluorescence intensity were observed because the extra beadless solution initially loaded in the bridge channels also took part in the fluid circulation. Interestingly, they became a good indicator of the periodicity of the circulation (≈ 8 min/ripple).

We performed a series of dynamic and static (control) hybridizations for comparison. Two PDMS devices were sealed onto a single home-spotted microarray slide (VEPO-25C, CEL Associates, Inc.), thus covering areas of identical probe patterns (70-mer DNA oligonucleotides). Each area consisted of four identical blocks. As shown in Figures 2a and b, each block included 18 features (six spotting solutions repeated three times). Six of them were negative-control features. We prepared Cy3-labeled cDNA from the C2C12 mouse skeletal-muscle cell line, adding *Arabidopsis thaliana* CAB (chlorophyll a/b-binding protein) spikes (cat. #2552201, Stratagene) as a positive control. Details of total RNA isolation, mRNA (m = messenger) extraction, and the reverse-transcription protocols are described elsewhere.[18] The cDNA sample was diluted into a series of solutions and then separated into aliquots. They were spin-dried under vacuum and kept at 4 °C before use. Two identical aliquots were used to prepare the hybridization solutions with ArrayHyb buffer (A-7718, Sigma-Aldrich Co.). They were loaded into the PDMS devices sealed on the shared slide, which was mounted on the flat bed of a thermocycler (PTC-200, MJ Research) and prehybridized. We performed dynamic hybridization by actuating the peristaltic pumps in one of the devices, while static hybridization was performed in the other device as a control. After hybridization at 52 °C for 2 h (or other specified time), the PDMS devices were peeled away from the slide. The slide was immediately placed in a plastic tube for programmed posthybridization washing (AdvaWash 400, Advalytix). The slide was then spin-dried in a centrifuge (5804R, Eppendorf) and scanned (ArrayWorx, Applied Precision LLC) to obtain fluorescence images.

Hybridization with microfluidic chaotic mixing produced stronger signals and better sensitivity than the static control (Figure 2). When the amount of input molecules of CAB spikes was decreased to 5.5 amol, the signal-to-noise (S/N) ratio of the static method was slightly larger than 1, which indicates that the signals were nearly indistinguishable from the background at that point. However, the S/N ratio of dynamic hybridization did not collapse to 1 until the amount of input CAB molecules further decreased to 0.55 amol, which is an enhancement in sensitivity of one order of magnitude. To our knowledge, this sensitivity level is better than any other reported method designed for active mixing in hybridization. The above enhancement of signals was reproducible, as confirmed by independent hybridization experiments. Active mixing also reduced the spot-to-spot fluctua-

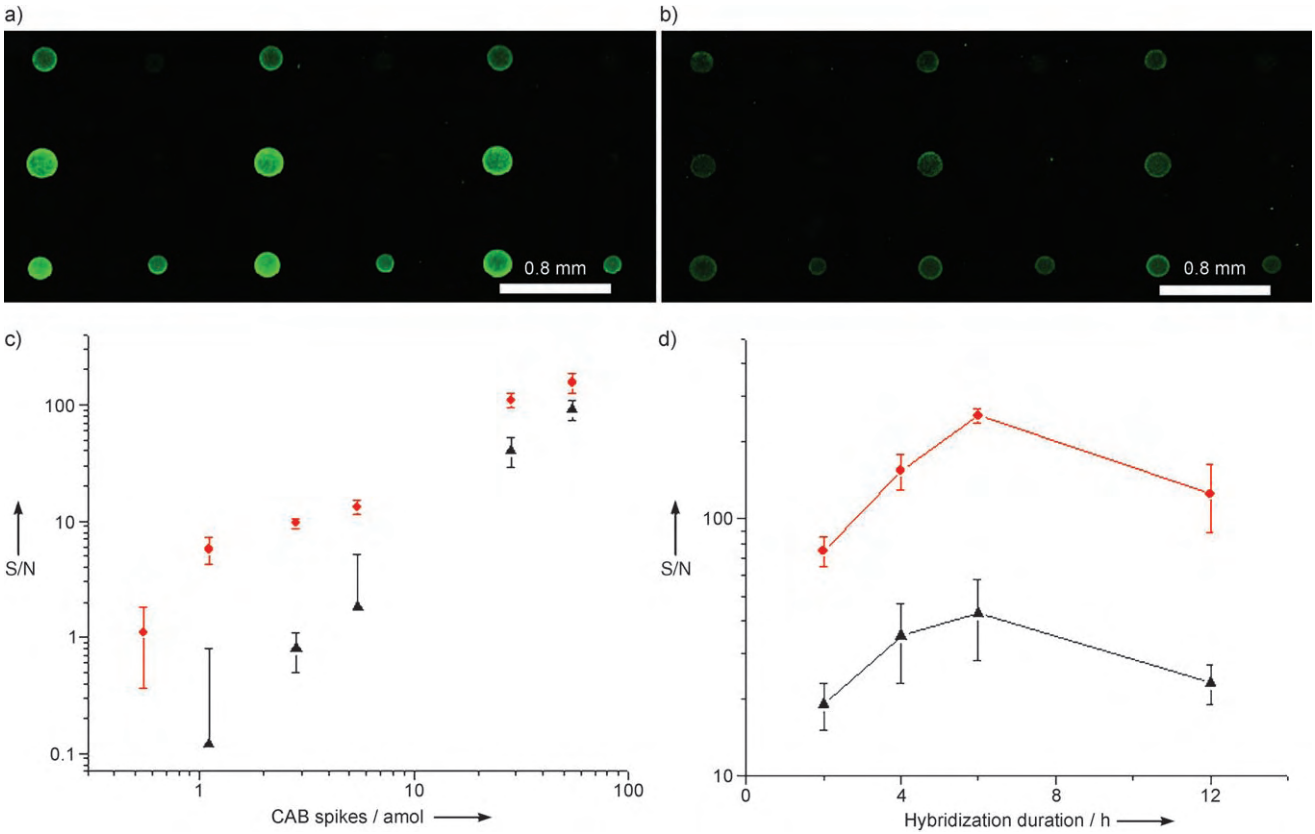

Figure 2. Signal improvement by microfluidic chaotic mixing. a) Dynamic- and b) static-hybridization blocks (each one of four identical) of the home-spotted microarray. The diameter of the features is about 200 μm. c) Titration curves and d) hybridization kinetics, with data analyzed from the features of myosin light-chain sense. Dynamic data are in red, static data are in black. The S/N ratio is calculated as the mean of the fluorescence signals subtracted by the mean of the background signal, then divided by the standard deviation of the background signal.

 © 2006 Wiley-VCH Verlag GmbH & Co. KGaA, Weinheim

tion of the signals. The coefficients of variation (CV) of the dynamic hybridization decreased to nearly half the values of the conventional static method (Table 1 and Figure 2c). The results of hybridization kinetics (Figure 2d) showed that

Table 1: The spot-to-spot coefficients of variation ($n = 12$) of dynamic versus static hybridization.[a]

	Dynamic	Static
myogenin sense	0.11	0.18
MCK sense	0.08	0.27
myosin light-chain sense	0.12	0.24
CAB (positive control)	0.10	0.23

[a] The negative-control solutions included a blank spotting buffer and a solution containing oligonucleotides for the *A. thaliana* RCA gene (not spiked in the sample). CAB = chlorophyll a/b-binding protein, MCK = muscle creatine kinase.

dynamic mixing consistently produced signals with higher S/N ratios than the static method. The signal from dynamic hybridization for 2 h was nearly twice that from the static control hybridized for 6 h. We noticed that the signals from both methods decreased after >6 h hybridization, which might be attributed to partial dehydration of the arrays, as PDMS is permeable to water vapor.

To evaluate the separate contributions of the circulatory motion of the fluid and chaotic mixing to the signal enhancement, we performed side-by-side comparison experiments that included an additional hybridization control with fluid circulation but without chaotic mixing. Identical aliquots of DNA target solutions were hybridized at 52 °C for 2 h under three distinct conditions: static (control 1), simple fluid circulation using the devices without the herring-bone protrusions (control 2), and fluid circulation with chaotic mixing. The experimental results (Table 2) clearly show that chaotic mixing played a significant part in the overall signal enhancement. Simple circulation of the fluid increased the signal intensity to 1.6–2.3-fold those obtained from the static control, whereas circulation with chaotic mixing improved the signals 3.4–6.9-fold. Therefore, microfluidic chaotic mixing has a major effect on the mass transfer of DNA targets to a solid reactive boundary by effectively homogenizing the solution.

We tested the compatibility of this approach with larger arrays, and found that microfluidic chaotic mixing can improve hybridization in high-density microarrays. We constructed a PDMS device with similar geometry but larger hybridization chambers (7.5 mm × 36 mm × 65 μm, 35 μL). It was sealed onto a commercial microarray (mouse-printed oligonucleotides array, 17 K, 70 mer, J. David Gladstone Institutes). Approximately 9500 spots on the slide were accessible within the hybridization chambers. All the experimental procedures followed that previously described, except that two identical microarray slides were used for comparison. The signals from hybridization with microfluidic chaotic mixing were dramatically enhanced (Figure 3). For individual features, we calculated the increase in the background-subtracted fluorescence by dynamic mixing over that of the static method and summarized the data in a histogram (Figure 4). The peak of the red columns (input-sample concentration 1.6 ng μL^{-1}) is located at a 3–4-fold increase. When the input Cy3-labeled cDNA was diluted to 0.8 ng μL^{-1} (blue columns), the peak shifted to a 7–8-fold increase. This result is consistent with our previous observation (Figure 2c) that the increase in the signals from dynamic over those from static hybridization became larger as the concentration of the input sample decreased. The signal enhancement of our approach was comparable to or slightly better than other reported values (mostly 2–5-fold) in the literature.[3,4,6–8]

Table 2: Increase (*x*-times) in the background-subtracted fluorescence of dynamic compared with static hybridization.

	Without chaotic mixing	With chaotic mixing
myogenin sense	2.1	4.2
MCK sense	1.6	6.9
myosin light-chain sense	2.2	3.4
CAB (positive control)	2.3	4.5

The specificity of the signals of the dynamic versus those of the static method was further examined (Figure 5) using receiver-operating-characteristics (ROC) analysis.[19] Dynamic hybridization reduced the overlap between the intensity distributions of the negative-control and the positive-probe features. The increase in the area under the ROC curves (Figure 5b and d)[19] also suggests that the dynamic approach allowed better signal specificity than the static method.

We attempted to determine how many cDNA molecules were actually hybridized onto the slide from the solution. The nucleotide concentration of the CAB-spiked cDNA solution was determined by UV/Vis spectroscopy. We manually deposited volume-defined droplets of Cy3-labeled cDNA molecules onto the slide by using microcapillary tubes (0.2 μL, Drummond) and obtained a standard curve of the fluorescence intensity versus the amount of deposited nucleotides. By estimating the CAB cDNA length, we calculated the number of hybridized CAB molecules on a given spot. The analysis was based on 2-h hybridization experiments. The data (Table 3) reveal that only a small percentage of target DNA molecules were actually hybridized with the static method, with a large portion of them remaining in the solution. Dynamic mixing can increase the percentage of molar-

Table 3: Percentages of hybridized CAB molecules out of the total number of initial spikes.[a],[b]

Input CAB [amol]	Dynamic hybridization [%]	Static hybridization [%]
55	9.4	1.3
28	4.1	0.66
5.5	1.2	0.20
2.8	1.6	0.20
1.1	1.9	0.54

[a] The yield of the labeling reaction was about 54% according to absorption measurements. [b] The full length of the CAB spikes (500 base pairs) was used in the above estimation. This represents a conservative lower limit as the hexamer-priming reaction may yield a distribution of cDNA lengths.

 © 2006 Wiley-VCH Verlag GmbH & Co. KGaA, Weinheim

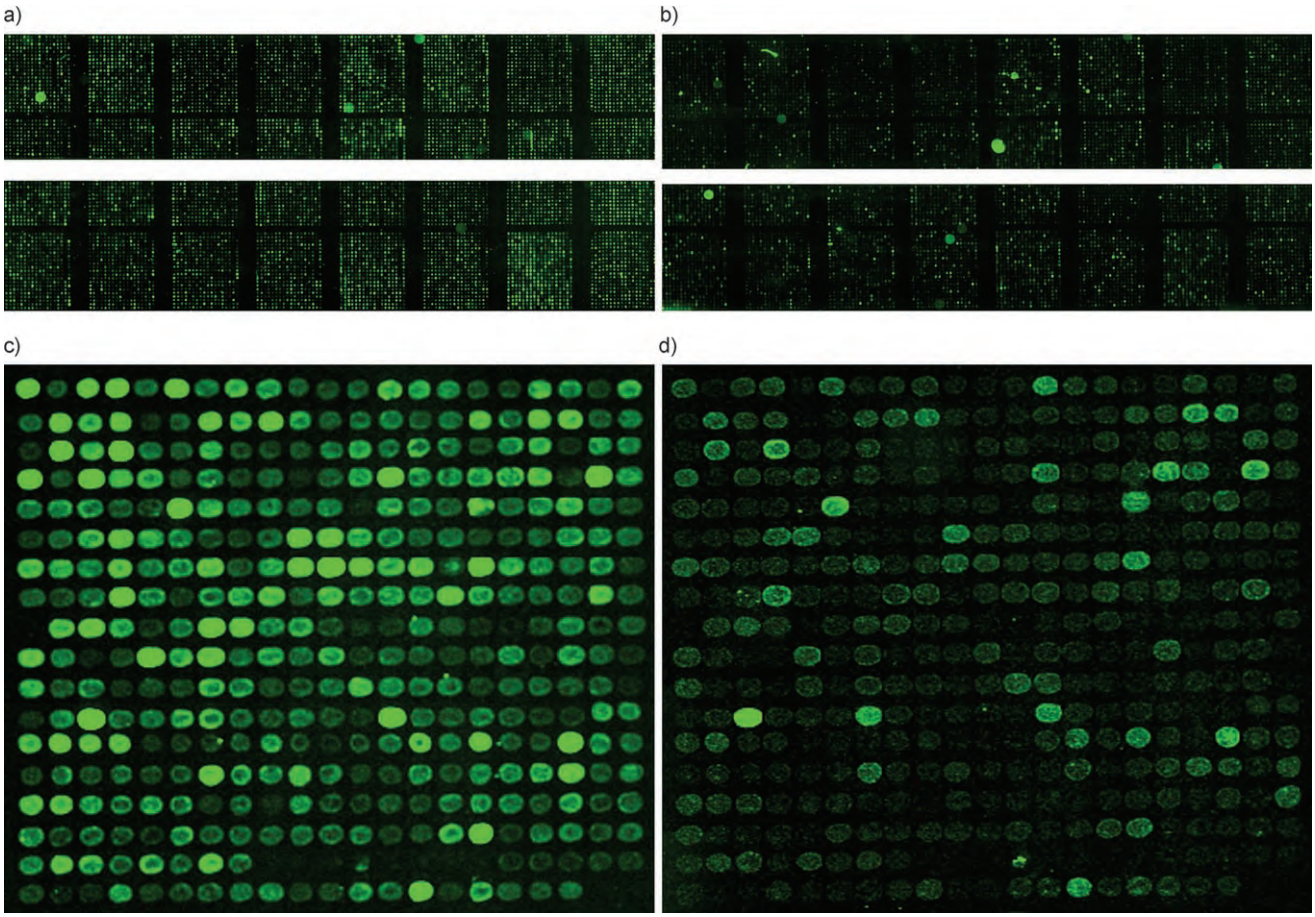

Figure 3. Fluorescence images of two side-by-side hybridization experiments (17-K microarray). a) Dynamic; b) static. c) and d) show magnified views of block #33 from a) and b), respectively. A PDMS device with larger chambers was used in each experiment. Notice the gap between the two chambers.

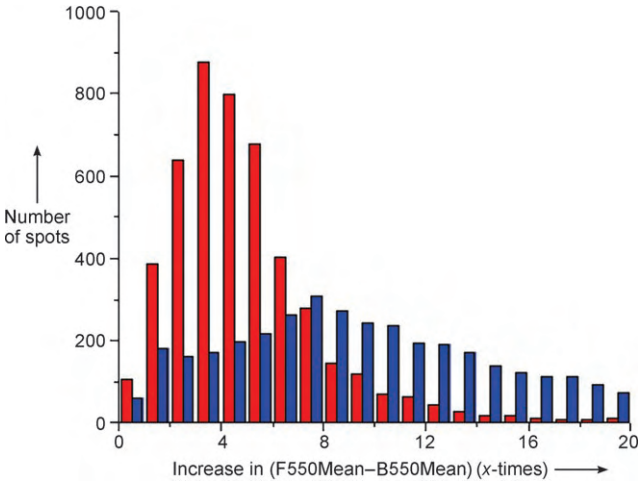

Figure 4. Histogram showing the increase in the background-subtracted fluorescence (F550 Mean−B550 Mean) of dynamic over static hybridization. The red and blue columns represent two sets of independent hybridization experiments that used different concentrations of the Cy3-labeled cDNA (red 1.6 ng μL^{-1}, blue 0.8 ng μL^{-1}). The wider spread in the distribution of the blue columns may result from a greater fluctuation of signal intensities when the static method was used with the more-dilute labeled target.

hybridization events several-fold. A new challenge may be to make better use of the unhybridized target DNA molecules in the solution.

We have demonstrated that microfluidic chaotic mixing enhances hybridization signals 3–8-fold through the introduction of lateral mixing, the facilitation of the delivery of target DNA molecules, and the increase in the number of molar-hybridization events. Our approach has improved the sensitivity of DNA-microarray experiments by nearly one order of magnitude and allowed better signal specificity than the static method. The time taken for the hybridization step of the conventional method has been shortened to 2 h with the new approach. Our PDMS device is disposable and compatible with high-density microarray slides. The device with larger chambers has the potential to hybridize about 135 000 array features in a single experiment, if new-generation array-printing tips[20] are used to spot ultrahigh-density microarrays (25 000 spots cm^{-2}).

Received: October 29, 2005
Revised: February 16, 2006
Published online: April 26, 2006

 © 2006 Wiley-VCH Verlag GmbH & Co. KGaA, Weinheim

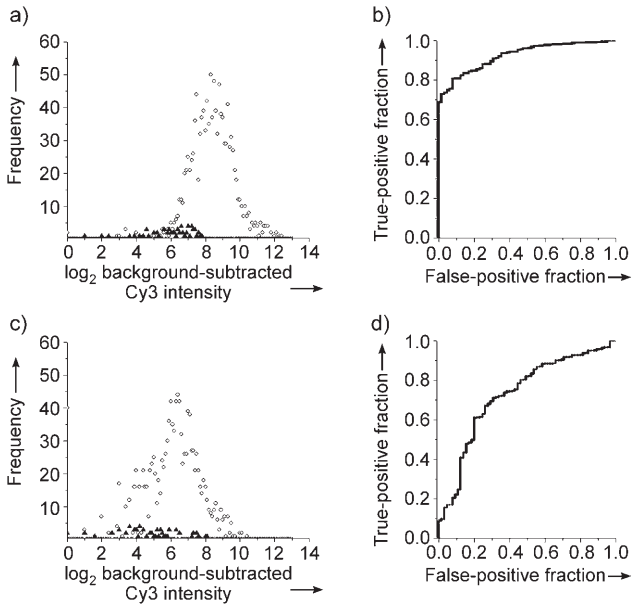

Figure 5. Distribution of positive/negative signals and ROC curves. a) Distribution of the positive-probe signals ○ and the negative-control signals ▲ for the dynamic experiment. b) ROC curve for the dynamic experiment, with an area under the curve of 0.92. c) Distribution of positive/negative signals for the static experiment. d) ROC curve for the static experiment, with an area under the curve of 0.73. Negative-control features (Operon) are sequences that were determined to be absent from the mouse genome. Positive features were identified from previous independent experiments (data not shown) as having signal intensities greater than three standard deviations above the median negative-control intensity in 72-h diffusion–hybridization experiments with labeled 36-h C2C12 cDNA. The true-positive and true-negative fractions are defined as the fraction of all positive-probe and negative-control features encountered at any given rank on the intensity scale, respectively.

Keywords: analytical methods · DNA microarrays · gene expression · hybridization · mixing devices

[1] M. Schena, D. Shalon, R. W. Davis, P. O. Brown, *Science* **1995**, *270*, 467.
[2] D. J. Duggan, M. Bittner, Y. D. Chen, P. Meltzer, J. M. Trent, *Nat. Genet.* **1999**, *21*, 10.
[3] R. H. Liu, R. Lenigk, R. L. Druyor-Sanchez, J. Yang, P. Grodzinski, *Anal. Chem.* **2003**, *75*, 1911.
[4] M. K. McQuain, K. Seale, J. Peek, T. S. Fisher, S. Levy, M. A. Stremler, F. R. Haselton, *Anal. Biochem.* **2004**, *325*, 215.
[5] Z. Guttenberg, A. Rathgeber, S. Keller, J. O. Radler, A. Wixforth, M. Kostur, M. Schindler, P. Talkner, *Phys. Rev. E* **2004**, *70*.
[6] N. B. Adey, M. Lei, M. T. Howard, J. D. Jensen, D. A. Mayo, D. L. Butel, S. C. Coffin, T. C. Moyer, D. E. Slade, M. K. Spute, A. M. Hancock, G. T. Eisenhoffer, B. K. Dalley, M. R. McNeely, *Anal. Chem.* **2002**, *74*, 6413.
[7] C. J. Schaupp, G. J. Jiang, T. G. Myers, M. A. Wilson, *Biotechniques* **2005**, *38*, 117.
[8] P. K. Yuen, G. S. Li, Y. J. Bao, U. R. Muller, *Lab-on-a-Chip* **2003**, *3*, 46.
[9] C. W. Wei, J. Y. Cheng, C. T. Huang, M. H. Yen, T. H. Young, *Nucleic Acids Res.* **2005**, *33*, e78.
[10] C. F. Edman, D. E. Raymond, D. J. Wu, E. Tu, R. G. Sosnowski, W. F. Butler, M. Nerenberg, M. J. Heller, *Nucleic Acids Res.* **1997**, *25*, 4907.
[11] D. Erickson, X. Liu, U. Krull, D. Li, *Anal. Chem.* **2004**, *76*, 7269.
[12] C. Gurtner, E. Tu, N. Jamshidi, R. W. Haigis, T. J. Onofrey, C. F. Edman, R. Sosnowski, B. Wallace, M. J. Heller, *Electrophoresis* **2002**, *23*, 1543.
[13] R. H. Liu, M. A. Stremler, K. V. Sharp, M. G. Olsen, J. G. Santiago, R. J. Adrian, H. Aref, D. J. Beebe, *J. Microelectromech. Syst.* **2000**, *9*, 190.
[14] A. D. Stroock, S. K. W. Dertinger, A. Ajdari, I. Mezic, H. A. Stone, G. M. Whitesides, *Science* **2002**, *295*, 647.
[15] C. Simonnet, A. Groisman, *Phys. Rev. Lett.* **2005**, *94*.
[16] M. A. Unger, H. P. Chou, T. Thorsen, A. Scherer, S. R. Quake, *Science* **2000**, *288*, 113.
[17] H. P. Chou, M. A. Unger, A. Scherer, S. R. Quake, *Biomed. Microdevices* **2001**, *3*, 323.
[18] B. A. Williams, R. M. Gwirtz, B. J. Wold, *Nucleic Acids Res.* **2004**, *32*, e81.
[19] N. N. Khodarev, J. Park, Y. Kataoka, E. Nodzenski, S. Hellman, B. Roizman, R. R. Weichselbaum, C. A. Pelizzari, *Genomics* **2003**, *81*, 202.
[20] M. O. Reese, R. M. van Dam, A. Scherer, S. R. Quake, *Genome Res.* **2003**, *13*, 2348.

 © 2006 Wiley-VCH Verlag GmbH & Co. KGaA, Weinheim

Nucleic Acids

DOI: 10.1002/anie.200504475

Watson–Crick Base-Pairing Properties of Nucleic Acid Analogues with Stereocontrolled α and β Torsion Angles (α,β-D-CNAs)**

Christelle Dupouy, Nathalie Iché-Tarrat, Marie-Pierre Durrieu, Frédéric Rodriguez, Jean-Marc Escudier, and Alain Vigroux**

It is well-established that conformational restriction may lead to favorable complex formation because of an entropic advantage.[1] The concept of structural preorganization of oligonucleotides using conformationally restricted bicyclic nucleoside monomers was introduced more than ten years ago by Leumann and co-workers as a means of increasing duplex stability.[2,3] Since then, mainly driven by the needs of

[*] C. Dupouy, Dr. N. Iché-Tarrat, M.-P. Durrieu, Dr. F. Rodriguez, Dr. J.-M. Escudier, Prof. A. Vigroux
Laboratoire de Synthèse et Physico-Chimie de Molécules d'Intérêt Biologique
UMR 5068 CNRS
Université Paul Sabatier
31062 Toulouse Cedex 9 (France)
Fax: (+33) 5-6155-6011
E-mail: escudier@chimie.ups-tlse.fr
vigroux@chimie.ups-tlse.fr

[**] We thank the Centre Informatique National de l'Enseignement Supérieur (CINES) and the Centre Interuniversitaire de Calcul de Toulouse (CALMIP) for the generous allocation of computer time and Dr. M. Erard for assistance with the CD experiments. D-CNAs = constrained nucleic acids with dioxaphosphorinane ring.

Supporting information for this article is available on the WWW under http://www.angewandte.org or from the author.

© 2006 Wiley-VCH Verlag GmbH & Co. KGaA, Weinheim

antisense technology,[4] this concept has been widely evaluated by a number of research groups and has led to conformationally restricted oligomers with increased thermal duplex stabilities and improved biostability.[5–9] Without doubt, the most prominent examples of this class of compounds are locked nucleic acids (LNAs), in which the ribofuranose subunit is strictly locked into the 3′-*endo* (N-type) conformation by a 2′-*O*,4′-*C*-methylene bridge.[10–13]

Although the concept of conformational restriction has proved successful when applied to the furanose framework, a few basic questions still have to be addressed. What binding properties can be expected by reducing the conformational flexibility of an oligonucleotide backbone without directly constraining its sugar unit? Could the conformational locking of the phosphate backbone contribute to preorganizing a single strand for duplex formation as efficiently as does the N-type conformational fixation of a ribose unit? To investigate the effects of the structural preorganization of the phosphodiester backbone on duplex formation, we recently developed a family of constrained nucleic acids (CNAs) in which the backbone torsion angles of the nucleic acids (Figure 1) are conformationally locked by a dioxaphosphorinane ring structure (D-CNA family).[14,15] The synthesis of α,β-D-CNA dimeric units featuring canonical (**1a**)[16] and noncanonical (**1b**)[14] α/β combinations (Table 1) has been realized recently. Herein, we report the synthesis and exceptional hybridizing properties of oligonucleotides containing these dimeric units.

The phosphoramidite building blocks of **1a** and **1b** were readily obtained by a conventional method, and the incorporation of these dinucleotide units into oligonucleotides was successfully undertaken by using standard protocols in automated DNA synthesis (see Supporting Information).[17] The duplex-forming ability of the modified oligonucleotides was investigated by determining the thermal stability of the duplexes formed with a DNA and RNA complement. Thermal stabilities (melting temperatures, T_m) were evaluated by UV melting-curve analysis; cooperative and monophasic transitions were observed in all cases (see Supporting Information).

At 100 mM NaCl (pH 7.0), the T_m values of the duplexes involving the parent DNA oligonucleotide 5′-d(GCGCTTGCCG)-3′ (**2**) and its DNA and RNA complements **5** and **5′** are 53 and 55.2 °C, respectively (Table 2, entry 1). From entry 1, it is clear that replacing the natural TT phosphate linker of **2** by the dioxaphosphorinane linker affects the thermal stability of the duplexes formed with **5** remarkably more than those formed with **5′**. Specifically, the neutral modification featuring the canonical ($\alpha = g^-$, $\beta = t$) conformation found in A- and B-type duplexes increases the thermal stability of the DNA duplex significantly more than the DNA:RNA heteroduplex. (Compare the T_m values of the modified duplexes **3**·**5** and **3**·**5′** with those of the control duplexes **2**·**5** and **2**·**5′**, respectively.) The remarkable stabilizing effect observed against DNA (+5 °C)

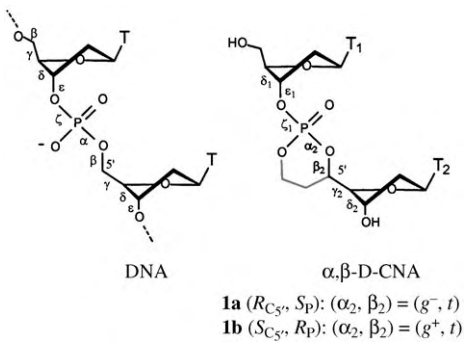

Figure 1. Left: the six backbone torsion angles (labeled α to ζ) of nucleic acids. Right: α,β-D-CNAs are nucleic acids in which α and β are stereocontrolled by a dioxaphosphorinane ring structure at 1) the canonical (*gauche*(−),*trans*) conformation, as in A- and B-form DNA duplexes (**1a**), or 2) the noncanonical (*gauche*(+),*trans*) conformation (**1b**).

Table 1: Backbone torsion angles [°] of α,β-D-CNA dimers **1a** and **1b** determined by DFT (B3LYP) calculations (see Supporting Information for details).[a]

	δ_1	ε_1	ζ_1	α_2	β_2	γ_2	δ_2
1a	140.6	−153.2	−164.9	−68.0 (g^-)	−173.2 (t)	51.0 (g^+)	129.9
1b	144.3	−86.9	156.7	69.5 (g^+)	173.1 (t)	52.8 (g^+)	141.8

[a] A very good agreement is obtained between the calculated and the experimentally determined crystal (**1a**)[16] and solution (**1a**/**1b**)[14,16] structures. The calculated values of the glycosyl (χ) and endocyclic (ν_0–ν_4) torsion angles along with the pseudorotation phase angles (*P*) of the sugar units are given in the Supporting Information. The torsion angle ranges are indicated in parentheses for α–γ: *gauche*(−) = 300 ± 30° (g^-), *gauche*(+) = 60 ± 30° (g^+), and *trans* = 180 ± 30° (t).

Table 2: Thermal melting temperatures [°C] of duplexes involving the parent DNA oligonucleotide **2** and the corresponding α,β-D-CNA-modified oligonucleotides **3** and **4** with matched and singly mismatched DNA and RNA sequences.[a]

	Target oligonucleotide	T_m (ΔT_m/mismatch) 5′-d(GCGCT**x**TGCCG)-3′ **2** (**x** = DE)[b]	**3** (**x** = **a**)[c]	**4** (**x** = **b**)[c]	Mismatch (**T**/**U**:Y)
1	3′-d(CGCGAACGGC)-5′ (**5**)	53.0	58.0	44.0	–
	3′-r(CGCGAACGGC)-5′ (**5′**)	55.2	56.1	49.1	–
2	3′-d(CGCGAA**T**GGC)-5′	38.2 (−14.8)	42.0 (−16.0)	26.3 (−17.7)	**T**G
	3′-r(CGCGAA**U**GGC)-5′	38.0 (−17.2)	38.0 (−18.1)	36.0 (−13.1)	**U**G
3	3′-d(CGCGA**T**CGGC)-5′	34.0 (−19.0)	45.5 (−12.5)	27.3 (−16.7)	**T**T
	3′-r(CGCGA**U**CGGC)-5′	48.5 (−6.7)	48.0 (−8.1)	49.0 (−0.1)	**U**T
4	3′-d(CGCG**T**ACGGC)-5′	37.2 (−15.8)	41.3 (−16.7)	23.3 (−20.7)	**T**T
	3′-r(CGCG**U**ACGGC)-5′	49.6 (−5.6)	49.0 (−7.1)	47.2 (−1.9)	**U**T
5	3′-d(CGC**T**AACGGC)-5′	20.3 (−32.7)	28.4 (−29.6)	< 10 (< −34.0)	**T**C
	3′-r(CGC**U**AACGGC)-5′	19.3 (−35.9)	24.0 (−32.1)	< 10 (< −39.1)	**U**C
		avg (−20.6)	avg (−18.7)	avg (< −26.7)	
		avg (−16.4)	avg (−16.4)	avg (< −13.6)	

[a] UV melting experiments were carried out in sodium phosphate buffer (10 mM, pH 7.0) containing NaCl (100 mM) and EDTA (1 mM). Total strand concentration = 10 μM. [b] DE = natural phosphodiester linkage. [c] **a** and **b** = dioxaphosphorinane linkages issuing from the dimeric units **1a** and **1b**, respectively.

 © 2006 Wiley-VCH Verlag GmbH & Co. KGaA, Weinheim

contrasts with the rather moderate effect observed against RNA (+0.9 °C). It is possible that this difference originates from the reluctance of the 5′-furanose unit of **1a** to undergo a significant conformational change from 2′-*endo* to 3′-*endo* in the hybrid duplex **3**·**5**′. Indeed, previous studies have shown that a neutral phosphotriester linkage can strongly push the 5′-uridine moiety of UU-modified dimers to adopt the unusual C2′-*endo* (S-type) conformation regardless of the presence of the 2′-*O*-methoxy group (which is known to stabilize the C3′-*endo* form).[18] It is therefore likely that the 5′-sugar units of **1a** and **1b** are somehow conformationally restricted in the C2′-*endo* conformation.

This extra property of α,β-D-CNAs would definitively imply that these oligonucleotide analogues are particularly well-suited to targeting single-stranded DNA sequences in preference to RNA sequences. Interestingly, the structural alteration of α, which deviates from its normal range of $-62 \pm 15°$ in B-DNA[19] to about $+70°$ in modification **1b** (Table 1), decreases the thermal stability of the heteroduplex appreciably less than the DNA duplex (−6.1 vs. −9 °C). Overall, these T_m data show that the modified oligonucleotides **3** and **4** possess clearly different hybridizing properties toward single-stranded DNA and RNA. Importantly, the differences in T_m values between the duplexes containing **1a** (**3**·**5** and **3**·**5**′) or **1b** (**4**·**5** and **4**·**5**′) and the natural control duplexes (**2**·**5** and **2**·**5**′) are largely insensitive to a 50-fold increase in the concentration of NaCl (in the 0.02–1.0 M range, see Supporting Information). This finding suggests that, at physiological ionic strength, the increased duplex stability observed with the "canonical" neutral dioxaphosphorinane linker reflects primarily conformational (rather than electrostatic) effects.

The stabilizing effect observed with **1a** contrasts strongly with previous results obtained with neutral linkers.[20,21] In most cases, it turned out that replacing a single phosphodiester linkage by a nonionic group, including R_P/S_P methylphosphonates and ethyl phosphotriesters,[22] bis(methylene) sulfones,[23] and many other flexible neutral linkers,[20] did not strengthen duplex stability, as often expected, but rather diminished it. These results underscored the important structural role played by the repeating negative charge of nucleic acids in preorganizing the single strands into extended conformations suitable for efficient and stable Watson–Crick base pairing.[24] Upon neutralization, the single strands are presumed to adopt "more folded" conformations which damage rule-based molecular recognition. This view suggests that rigidity must be built into nonionic backbone linkers to maintain stable and selective Watson–Crick base-pairing properties. The exceptional thermal stability induced by the dimeric unit **1a** demonstrates that the introduction of a conformationally restricted neutral linkage into an otherwise unmodified oligonucleotide is indeed a very promising way of improving its binding affinity (especially toward complementary DNA on account of the presumably more stable S-type conformation of the 5′-sugar units of phosphotriester linkages). Moreover, it can be concluded from the T_m values of Table 2 (entries 2–5) that base mismatches in the modified strand **3** contribute roughly equally to the DNA:DNA or DNA:RNA duplex destabilization as in the unmodified strand **2**. Thus, the "canonical" modification **1a** does not alter significantly the high sequence selectivity of natural DNA and RNA.

The modification **1b** was designed in such a way as to pose a particular conformational challenge, to which the double helix should respond by adopting the most energetically accessible *noncanonical* structure. A noncanonical *gauche*(+) conformation of α seems to play an important role in base-flipping processes,[25] and is typical of many bulge regions of nucleic acids.[26] Therefore, it is tempting to speculate that controlling this torsion at about $+70°$ in a duplex might result in the formation of localized non-base-paired conformations that closely resemble the conformations of single bulges and/or flipped-out bases. However, the possibility that this torsional stress can be tolerated structurally into a completely Watson–Crick helical structure, through specific adjustments in the phosphate backbone, cannot be excluded.

Thus, it was of interest to test whether the modified duplexes **4**·**5** and **4**·**5**′ could exhibit sequence discrimination as natural duplexes. This was done by UV-monitored thermal denaturation experiments aimed at evaluating the instability caused by a single mismatch **T**/**U**:Y in the four-nucleotide region of **5** or **5**′ facing the dioxaphosphorinane linkage of **4** (Table 2, entries 2–5). The same set of measurements were taken with the unmodified duplexes **2**·**5** and **2**·**5**′ as controls, so that a direct comparison of base-mismatch selectivities could be made in each case. The results show that with the singly mismatched DNA sequences, the average destabilization per mismatch is higher for the modified strand **4** (ΔT_m/mismatch < -26.7 °C) than for the unmodified DNA strand **2** (ΔT_m/mismatch $= -20.6$ °C). This finding implies that in the DNA duplex **4**·**5**, the eight complementary bases located around the dioxaphosphorinane linkage are held together by specific (presumably Watson–Crick) hydrogen bonds and base-stacking interactions. From these experiments we conclude that, in the DNA duplex, selective base pairing occurs at the site of modification despite the torsional stress $\alpha = g^+$. In the DNA:RNA duplex, however, the pairing selectivity is much less pronounced, especially when U is paired opposite T. Remarkably, the destabilizing effect induced by the UT mismatches in the natural heteroduplex (−6.7 and −5.6 °C; Table 2, entries 3 and 4) vanishes or becomes insignificant when the hybrid duplex is formed with the modified strand **4**. This suggests that the dimeric unit **1b** might favor the formation of two consecutive non-hydrogen-bonded A:T base pairs (an internal loop structure) in the middle of the fully complementary heteroduplex **4**·**5**′.

Preliminary information on the structure of the DNA duplexes **3**·**5** and **4**·**5** was obtained from CD spectroscopy. The CD spectra of the modified duplexes **3**·**5** and **4**·**5** were compared to that of the DNA control duplex **2**·**5** (Figure 2). In line with the thermal denaturation results, these CD spectra show all of the characteristics of a Watson–Crick base-paired B-type double helix. Specifically, the duplex with the dioxaphosphorinane backbone preorganized in a B-DNA conformation (**3**·**5**) appears to be an excellent mimic of a standard B-form duplex with a positive band at about 274 nm, comparable to that observed for the reference duplex **2**·**5**. The duplex structure **4**·**5** with one backbone torsion angle α constrained at the g^+ conformation deviates to some extent

 © 2006 Wiley-VCH Verlag GmbH & Co. KGaA, Weinheim

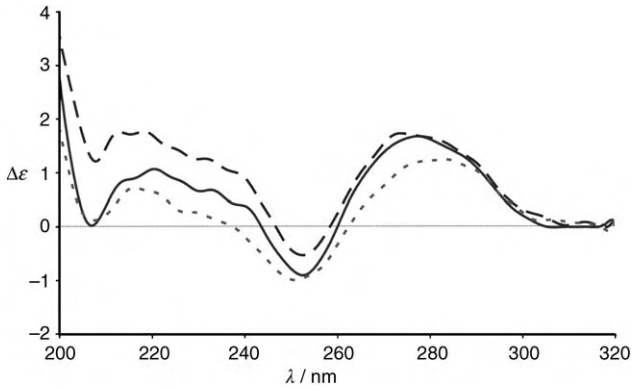

Figure 2. CD spectra of the duplexes a) **3·5** (– – –), b) **4·5** (-----), and c) **2·5** (——) in sodium phosphate (10 mM, pH 7.0), NaCl (100 mM), and EDTA (1 mM); $T = 20\,^{\circ}C$. Duplex concentration = 5 μM.

from the reference B-form duplex: the positive band is decreased in intensity by about 25% and its maximum is shifted to about 283 nm. Notably, these spectral variations are very similar to those usually observed in the response of B-DNA sequences to distortions induced by proteins,[27] which suggests that the dimeric unit **1b** deforms DNA, as do many proteins. This makes **1b** an interesting candidate to experimentally explore the possible role played by specific DNA distortions in protein–DNA interactions (indirect readout effects).

A 3D structural model of DNA clearly shows that the dimeric unit **1a** can fit into a B-form double helix without involving significant changes in the backbone torsion angles α–ζ, compared to a natural TT step in a B-form duplex (compare **A** and **B** in Figure 3 and Table 3). In contrast, the dioxaphosphorinane linkage of **1b** requires specific backbone distortions to accommodate the Watson–Crick helical structure. According to molecular dynamics simulations, to enable Watson–Crick B-type duplex formation with α_2 and β_2 constrained in the *gauche*(+) and *trans* conformations, respectively, it is necessary that the exocyclic torsion angles

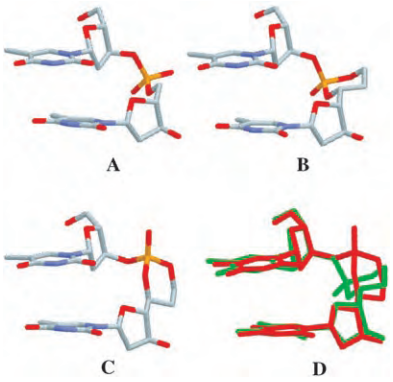

Figure 3. Comparison of the backbone structures of a natural TT step (**A**) extracted from the X-ray structure of a typical B-type DNA duplex (step $T_{19}T_{20}$, NDBID code: BD0007), and the two dioxaphosphorinane-modified TT steps (**B** and **C**) derived from molecular dynamics simulations of a B-DNA A_{10}·T_{10} duplex containing the dimeric unit **1a** (**B**) or **1b** (**C**) in its central region. Superimposition of the structures **B** and **C** is shown in **D**.

Table 3: Backbone torsion angles [°] (see Figures 1 and 3).[a]

	δ_1	ε_1	ζ_1	α_2	β_2	γ_2	δ_2
A	99.9	−178.1	−86.7	−60.4 (g^-)	174.3 (*t*)	48.7 (g^+)	117.7
B	124.4	−177.2	−103.4	−58.8 (g^-)	177.1 (*t*)	51.8(g^+)	123.6
C	116.6	**48.0**	**79.5**	**62.1 (g^+)**	177.7 (*t*)	**−179.5 (*t*)**	108.1

[a] Torsion angle ranges are given in parentheses, as indicated in Table 1. Noncanonical values of the backbone torsion angles are in boldface.

γ_2, ε_1, and ζ_1 of **1b** (Figure 1) deviate significantly from their normal range (compare **A** and **C** in Figure 3 and Table 3). The molecular dynamics results indicate that the overall B conformation of the double helix remains mostly intact, but at the price of a noticeable bending in the helical axis primarily caused by the propagation of this structural distortion along the phosphodiester backbone and base-sugar network. Importantly, in contrast to, for example, methylphosphonate linkages,[28] the disposition of the dioxaphosphorinane linker on the surface of the duplex is not expected to induce significant steric hindrance differences. Indeed, the two modified duplexes position the ethylene bridge of the linker away from the major and minor grooves and directly toward the solvent (**D**, Figure 3). Similar perturbational effects are therefore expected between the differently exposed ethylene groups and the surrounding solvent molecules. Thus, it is unlikely that the difference in stability observed between the duplexes **3·5** and **4·5** arises from significant differential steric and solvation effects. The most plausible explanation is that this difference reflects the intrinsic backbone deformation energy associated with the torsional stress $\alpha = g^+$. Interestingly, it has been shown recently that the most significant energetic contribution, in terms of backbone distortion induced by proteins, is made by the torsion angle α, most often in the form of noncanonical α/γ combinations in which $\alpha = g^+$.[29,30]

As already mentioned, LNAs stand out as the single nucleic acid modification that contributes to the highest duplex stability ever obtained by natural Watson–Crick hydrogen bonding. To compare the hybridizing properties of α,β-D-CNAs with LNAs, we incorporated one, two, and three dimeric units **1a** into a 12-mer DNA oligonucleotide sequence that has been extensively used by the Imanishi group to investigate the stabilizing effects induced by LNA substitutions.[31] Thus, quantitative comparisons can be made between the two types of modification. The differences in T_m values between the duplexes containing **1a** or LNA and the natural DNA:DNA and DNA:RNA duplexes are summarized in Table 4. Relative to the reference DNA:DNA duplex (Table 4, entries 1 and 2), the incorporation of one α,β-D-CNA induces the same duplex stabilization as the incorporation of one LNA monomer ($\Delta T_m = +6\,^{\circ}C$; entries 3 and 4).

To our knowledge, α,β-D-CNAs represent the first example of a modification that significantly increases the hybridizing properties of an oligonucleotide without forcing its sugar moieties to adopt the RNA-like C3′-*endo* conformation.[20] The ability of **1a** to fit seamlessly into a B-form double helix is reflected by the observed additivity of its stabilizing effect ($\Delta T_m = +5\,^{\circ}C$ per dimeric unit incorporated; Table 4,

 © 2006 Wiley-VCH Verlag GmbH & Co. KGaA, Weinheim

Table 4: Thermal melting data [°C] of α,β-D-CNA- and LNA-modified oligonucleotides with complementary DNA and RNA.[a]

	Oligonucleotide[b]	DNA			RNA		
		T_m	ΔT_m[c]	ΔT_m/mod	T_m	ΔT_m[c]	ΔT_m/mod
1	5′-d(GCGTTTTTTGCT)-3′	49	ref		47	ref	
2		47[d]	ref		45[d]	ref	
3	5′-d(GCGTTT**a**TTTGCT)-3′ (**6**)	55	+6	+6	50.2	+3.2	+3.2
4	5′-d(GCGTTT^{L}TTTGCT)-3′	53[d]	+6	+6	52[d]	+7	+7
5	5′-d(GCGTTT**a**TT**a**TGCT)-3′ (**7**)	59	+10	+5	52.2	+5.2	+2.6
6	5′-d(GCGTTT^{L}TT^{L}TGCT)-3′	54[d]	+7	+3.5	57[d]	+12	+6
7	5′-d(GCG**a**TT**a**TT**a**TGCT)-3′ (**8**)	64	+15	+5	55.3	+8.3	+2.8
8	5′-d(GCG^{L}TT^{L}TT^{L}TGCT)-3′	56[d]	+9	+3	62[d]	+17	+5.7

[a] The sequence of target DNA or RNA is 5′-(AGCAAAAAACGC)-3′. Data of entries 1, 3, 5, and 7 are from this work. See footnote [a] of Table 2 for the experimental conditions used. Data of entries 2, 4, 6, and 8 are taken from reference [31] (experimental conditions: sodium phosphate (10 mM, pH 7.2), NaCl (100 mM); total strand concentration 8 μM). [b] **a** = dioxaphosphorinane linkage issuing from the dimeric unit **1a**; T^{L} = LNA monomer with thymine. [c] ΔT_m values are calculated relative to entry 1 for the oligonucleotides **6**–**8** and relative to entry 2 for the remaining LNA-modified oligonucleotides. [d] Values taken from reference [31].

entries 5 and 7). In contrast, as a result of the cooperative effect exerted by the LNA units on the DNA strand conformation,[32] the corresponding duplexes with LNA monomers display ΔT_m/mod values which level off at +3 °C (Table 4, entries 6 and 8; mod = modified). Relative to the reference DNA:RNA duplex, the average stabilizing effect induced by α,β-D-CNA (ΔT_m/mod ≈ +2.9 °C) is approximately half the average stabilizing effect promoted by LNA (ΔT_m/mod ≈ +6.2 °C). As already mentioned, this difference might result from the incapacity of α,β-D-CNAs to adjust the puckering mode of their 5′-furanose units to properly fit into A-type duplexes.

In summary, this work highlights the importance of the canonical g^- conformation of the torsion angle α for nucleic acid duplex stability, as well as the relative ease with which the DNA backbone can compensate for the torsional stress $\alpha = g^+$. A key feature of our study is the demonstration that the conformational restriction of the phosphodiester linkage, by its transformation into a neutral stereocontrolled dioxaphosphorinane ring structure, is an effective means of stabilizing canonical and specifically distorted B-DNA double helices. With their exceptional Watson–Crick base-pairing properties, α,β-D-CNAs definitively represent interesting candidates worthy of further exploration.

Received: December 16, 2005
Revised: February 16, 2006
Published online: April 26, 2006

Keywords: conformation analysis · DNA structures · helical structures · nucleic acids · oligonucleotides

[1] D. J. Cram, *Angew. Chem.* **1988**, *100*, 1041 – 1052; *Angew. Chem. Int. Ed. Engl.* **1988**, *27*, 1009 – 1020.
[2] M. Tarköy, C. Leumann, *Angew. Chem.* **1993**, *105*, 1516 – 1518; *Angew. Chem. Int. Ed. Engl.* **1993**, *32*, 1432 – 1434.
[3] M. Tarköy, M. Bolli, B. Schweizer, C. Leumann, *Helv. Chim. Acta* **1993**, *76*, 481 – 510.
[4] J. Kurreck, *Eur. J. Biochem.* **2003**, *270*, 1628 – 1644.
[5] P. Herdewijn, *Liebigs Ann.* **1996**, 1337 – 1348.
[6] E. T. Kool, *Chem. Rev.* **1997**, *97*, 1473 – 1487.
[7] P. Herdewijn, *Biochim. Biophys. Acta* **1999**, *1489*, 167 – 179.
[8] M. Meldgaard, J. Wengel, *J. Chem. Soc. Perkin Trans. 1* **2000**, 3539 – 3554.
[9] C. J. Leumann, *Bioorg. Med. Chem.* **2002**, *10*, 841 – 854.
[10] T. Imanishi, S. Obika, *Chem. Commun.* **2002**, 1653 – 1659.
[11] S. Obika, *Chem. Pharm. Bull.* **2004**, *52*, 1399 – 1404.
[12] M. Petersen, J. Wengel, *Trends Biotechnol.* **2003**, *21*, 74 – 81.
[13] B. Vester, J. Wengel, *Biochemistry* **2004**, *43*, 13233 – 13241.
[14] I. Le Clezio, J.-M. Escudier, A. Vigroux, *Org. Lett.* **2003**, *5*, 161 – 164.
[15] I. Le Clezio, H. Gornitzka, J.-M. Escudier, A. Vigroux, *J. Org. Chem.* **2005**, *70*, 1620 – 1629.
[16] The synthesis as well as crystal and solution structures of **1a** will be detailed elsewhere: I. Le Clezio, C. Dupouy, P. Lavedan, H. Gornitzka, J.-M. Escudier, A. Vigroux, unpublished results.
[17] M. H. Caruthers, *Acc. Chem. Res.* **1991**, *24*, 278 – 284.
[18] M. Sekine, O. Kurasawa, K. Shohda, K. Seio, T. Wada, *J. Org. Chem.* **2000**, *65*, 6515 – 6524.
[19] B. Schneider, S. Neidle, H. M. Berman, *Biopolymers* **1997**, *42*, 113 – 124.
[20] S. M. Freier, K.-H. Altmann, *Nucleic Acids Res.* **1997**, *25*, 4429 – 4443.
[21] A. De Mesmaeker, R. Haener, P. Martin, H. E. Moser, *Acc. Chem. Res.* **1995**, *28*, 366 – 374.
[22] For self-complementary octamers containing a) one methylphosphonate or b) one ethyl phosphotriester linkage in the center of the oligonucleotide chain, see: a) M. Bower, M. F. Summers, C. Powel, K. Shinozuka, J. B. Regan, G. Zon, W. D. Wilson, *Nucleic Acids Res.* **1987**, *15*, 4915 – 4930; b) M. Bower, M. F. Summers, C. Powel, K. Shinozuka, J. B. Regan, G. Zon, W. D. Wilson, *Nucleic Acids Res.* **1986**, *14*, 7421 – 7436.
[23] D. Hutter, M. O. Blaettler, S. A. Benner, *Helv. Chim. Acta* **2002**, *85*, 2777 – 2806.
[24] S. A. Benner, D. Hutter, *Bioorg. Chem.* **2002**, *30*, 62 – 80.
[25] a) P. Várnai, R. Lavery, *J. Am. Chem. Soc.* **2002**, *124*, 7272 – 7273; b) N. K. Banavali, A. D. Mackerell, Jr., *J. Mol. Biol.* **2002**, *319*, 141 – 160.
[26] For example, see: a) E. Ennifar, M. Yusupov, P. Walter, R. Marquet, B. Ehresmann, C. Ehresmann, P. Dumas, *Structure* **1999**, *7*, 1439 – 1449; b) V. Tereshko, S. T. Wallace, N. Usman, F. E. Wincott, M. Egli, *RNA* **2001**, *7*, 405 – 420; c) L.-W. Hung, E. L. Holbrook, S. R. Holbrook, *Proc. Nat. Acad. Sci. USA* **2000**, *97*, 5107 – 5112.
[27] For example, see: A. Polyanichko, H. Wieser, *Biopolymers* **2005**, *78*, 329 – 339.
[28] V. Thiviyanathan, K. V. Vyazovkina, E. K. Gozansky, E. Bichenchova, T. V. Abramova, B. A. Luxon, A. V. Lebedev, D. G. Gorenstein, *Biochemistry* **2002**, *41*, 827 – 838.
[29] K. Zakrzewska, *Biopolymers* **2003**, *70*, 414 – 423.
[30] P. Várnai, D. Djuranovic, R. Lavery, B. Hartmann, *Nucleic Acids Res.* **2002**, *30*, 5398 – 5406.
[31] S. Obika, O. Nakagawa, A. Hiroto, Y. Hari, T. Imanishi, *Chem. Commun.* **2003**, 2202 – 2203.
[32] G. A. Jensen, S. K. Singh, R. Kumar, J. Wengel, J. P. Jacobsen, *J. Chem. Soc. Perkin Trans. 2* **2001**, 1224 – 1232.

 © 2006 Wiley-VCH Verlag GmbH & Co. KGaA, Weinheim

Mechanistic Studies

DOI: 10.1002/anie.200504546

A New Reaction Pathway in Organophosphorus Chemistry: Competing S_N2 and AE′ Pathways for Nucleophilic Attack at a Phosphorus–Carbon Cage Compound**

Cheryl Fish, Michael Green, Richard J. Kilby, Jason M. Lynam,* John E. McGrady,* Dimitrios A. Pantazis, Christopher A. Russell,* Adrian C. Whitwood, and Charlotte E. Willans*

The S_N2 character of nucleophilic-substitution reactions at carbon atoms and other first-row centers is well-established, both experimentally and theoretically.[1] For phosphorus[2] and second-row atoms in general,[3] where expansion of the octet is possible, there is evidence that, at least in the gas phase, nucleophilic substitution proceeds instead via an addition–elimination (AE) pathway featuring a hypervalent intermediate. Herein, we use a combination of temperature-dependent ^{31}P NMR spectroscopy and density functional theory to show that both S_N2- and AE-type pathways contribute simultaneously to chloride exchange in the tricyclic phosphorus–carbon cage **1a** (Scheme 1). In a series of recent papers, we have demonstrated the synthetic potential of **1a**, which reacts with the Lewis acid $AlCl_3$ (in CH_2Cl_2) to give the novel *nido* ionic species [3,5-tBu$_2$-1,2,4-C_2P_3][$AlCl_4$] (**2**).[4] In contrast, alkali metals and magnesium react with **1a** at room temperature in THF to form, selectively and in quantitative yield, M[3,5-tBu$_2$-1,2,4-C_2P_3] (**3**; M = Li, Na, K, or $Mg_2(\mu\text{-Cl})_3(thf)_6$), which contain the important aromatic C_2P_3 anion.[4,5]

In the course of monitoring the reduction of **1a** with lithium in [D_8]THF by in situ ^{31}P NMR spectroscopy, we were surprised to observe that, whilst the characteristic resonance of **1a** at $\delta = -302.2$ ppm remained relatively sharp throughout the course of the reaction, the resonances at $\delta = 234.7$ and -121.4 ppm were significantly broadened. Similar broadening of these two resonances was also observed when small amounts of either LiCl or nBu$_4$NCl were added to a solution of **1a** in [D_8]THF. Moreover, when the solution of **1a** in [D_8]THF containing 0.05 equivalents of nBu$_4$NCl was cooled from 325 K to 255 K, the two broad resonances at $\delta = 234.7$ and -121.4 ppm became sharpened, and the line shape of the resonance at $\delta = -302.2$ ppm also showed significant changes (Figure 1).

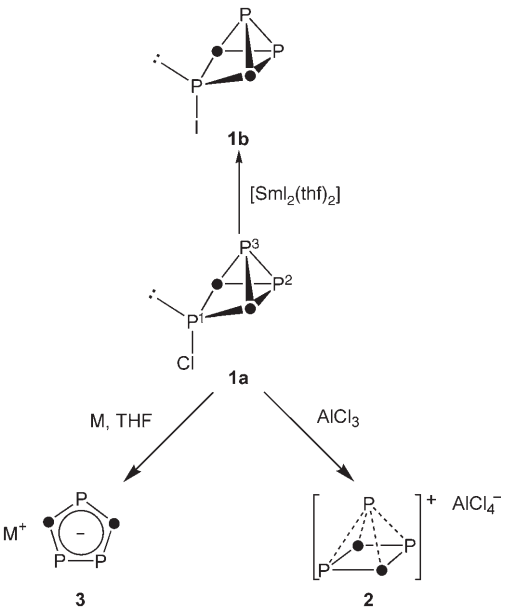

Scheme 1. ● = CtBu; M = Li, Na, K, or $Mg_2(\mu\text{-Cl})_3(thf)_6$.

To fully rationalize these observations, it was clear that knowledge of the precise topology of **1a** was required. Previously, Binger, Regitz, and co-workers had assigned the structure of **1a** simply on the basis of three ^{31}P NMR resonance signals at $\delta = 234.7$, -121.4, and -302.2 ppm, which relate to the three magnetically distinct environments of P^1, P^2, and P^3 (Scheme 1), respectively, in the tricyclic cage.[6] The computed ^{31}P NMR chemical shifts (at the B3LYP/6-311G** level of theory) of $\delta = 354$ (P^1), -93.4 (P^2), and -298.6 ppm (P^3) for the model compound $ClP_3(CH)_2$ (**1a′**) are fully consistent with this assignment. However, all attempts to confirm the structure of **1a** by single-crystal X-ray diffraction have been unsuccessful. Fortunately, we have been able to support this structural assignment by the serendipitous preparation and crystallographic characterization of **1b** (Figure 2), the iodo analogue of **1a**, formed by the reaction of **1a** with [$SmI_2(thf)_2$]. The very similar $^{31}P\{^1H\}$ NMR characteristics of **1b** ($\delta = 248.7$, -101.8 and -241.3 ppm in [D_8]toluene at 298 K) and **1a** provide convincing evidence that the two species are isostructural.

To probe the dynamic processes associated with chloride exchange, the $^{31}P\{^1H\}$ NMR spectra of **1a** were simulated using the gNMR suite of programs.[7] Critically, the accurate simulation of all three resonances in the ^{31}P NMR spectra over the range of temperatures and concentrations employed

[*] C. Fish, Prof. M. Green, Dr. R. J. Kilby, Dr. C. A. Russell
School of Chemistry
University of Bristol
Cantock's Close, Bristol BS81TS (UK)
E-mail: michael804902@aol.com
Chris.Russell@bris.ac.uk
Dr. J. M. Lynam, Dr. A. C. Whitwood, C. E. Willans
Department of Chemistry
University of York
Heslington, York YO105DD (UK)
E-mail: jml12@york.ac.uk
Prof. J. E. McGrady, Dr. D. A. Pantazis
WestCHEM
Department of Chemistry
Joseph Black Building
University of Glasgow
Glasgow, G128QQ (UK)
E-mail: j.mcgrady@chem.gla.ac.uk

[**] We acknowledge the EPSRC (R.J.K., D.A.P., C.E.W.), the Universities of Bristol (M.G., C.A.R., C.F.) and York (C.E.W., J.M.L.), and The Royal Society (University Research Fellowship for C.A.R.) for financial assistance. We thank Dr. Craig Butts (Bristol) for helpful comments in preparing this manuscript.

InterScience
© 2006 Wiley-VCH Verlag GmbH & Co. KGaA, Weinheim

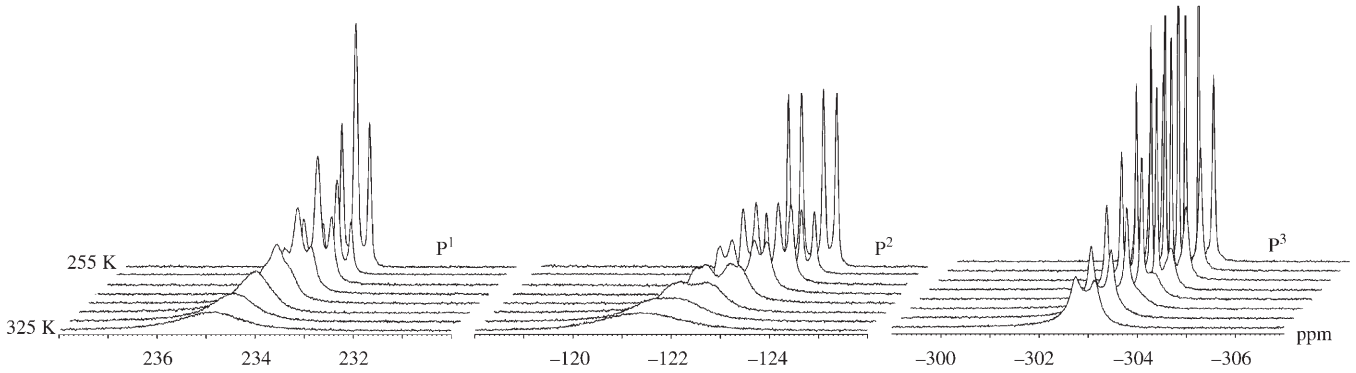

Figure 1. Variable-temperature $^{31}P\{^1H\}$ NMR spectra of **1a**/nBu$_4$NCl in [D$_8$]THF. Spectra are shown in 10 K increments.

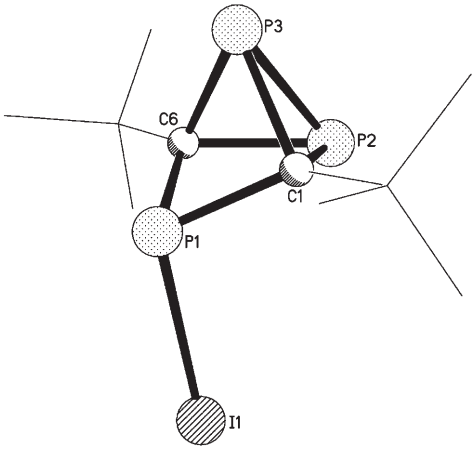

Figure 2. X-ray crystal structure of **1b**. Selected bond lengths [Å] and angles [°]: P(1)-I(1) 2.561(1), P(2)-P(3) 2.154(1), P(1)-C(1) 1.826(2), P(1)-C(6) 1.832(2), P(2)-C(1) 1.862(2), P(2)-C(6) 1.862(1), P(3)-C(1) 1.911(2), P(3)-C(6) 1.917(2); C(1)-P(2)-P(3) 56.27(7), C(1)-P(2)-C(6) 74.52(10), C(1)-P(3)-C(6) 72.24(1), C(1)-P(1)-I(1) 104.67(7), C(1)-P(1)-C(6) 76.17(10).

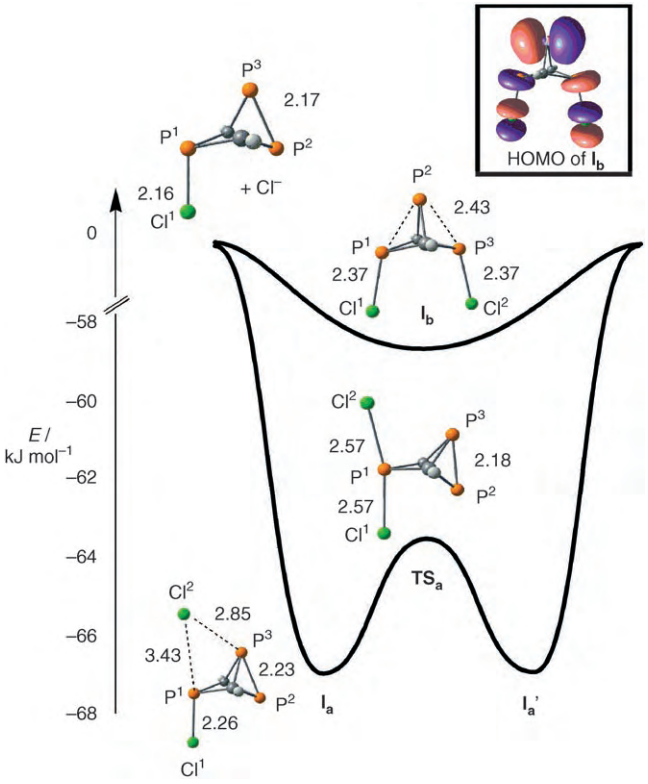

Figure 3. Potential-energy surface for nucleophilic attack on **1a**′ by a Cl$^-$ ion. Interatomic separations are given in Å.

could only be achieved when two distinct dynamic processes were invoked, one involving the exchange of P^1 and P^2 and the other involving the exchange of P^2 and P^3. The simulations yielded activation parameters of $\Delta H^{\neq} = 37.7 \pm 0.8\ kJ\,mol^{-1}$ and $\Delta S^{\neq} = -73.1 \pm 2.7\ J\,mol^{-1}\,K^{-1}$ for the $P^1 \leftrightarrow P^2$ exchange process and $\Delta H^{\neq} = 37.3 \pm 4.3\ kJ\,mol^{-1}$ and $\Delta S^{\neq} = -90.1 \pm 14.1\ J\,mol^{-1}\,K^{-1}$ for the $P^2 \leftrightarrow P^3$ exchange. The negative $\Delta S^{\neq}$ values imply that both processes are associative, a conclusion that is also consistent with the linear dependence of both rates of exchange on the concentrations of both chloride anion and **1a**. The activation parameters indicate that the two processes are competitive within the temperature regime employed and that the $P^1 \leftrightarrow P^2$ exchange becomes more favored at higher temperatures.

The origin of these experimental observations was revealed when density functional theory was employed to explore the potential-energy surface for the nucleophilic attack of a chloride ion on the model compound $ClP_3(CH)_2$ (**1a**′, Figure 3).[8] The topology of **1a**′ offers five distinct trajectories for nucleophilic attack by a chloride ion (Scheme 2), each of which was probed explicitly. For trajectory (a), the potential-energy surface shows a classic S_N2-type profile in which a C_{2v}-symmetric transition state **TS$_a$** connects two degenerate precursor intermediates **I$_a$**. The S_N2 character of this pathway contrasts markedly with chloride exchange at the related species $ClPH_2$, for which Radom and co-workers reported an AE mechanism with a C_{2v}-symmetric intermediate rather than a transition state.[2d] The significant difference between $ClPH_2$ and the tricyclic species **1a**′ can be traced to the different acceptor orbitals available in each case. In the case of $ClPH_2$, the only available acceptor orbital is σ*(P–Cl), and interaction of this orbital with a chloride lone pair of electrons leads directly to the hypervalent C_{2v}-symmetric intermediate. In tricyclic $ClP_3(CH)_2$, in contrast, a second

 © 2006 Wiley-VCH Verlag GmbH & Co. KGaA, Weinheim

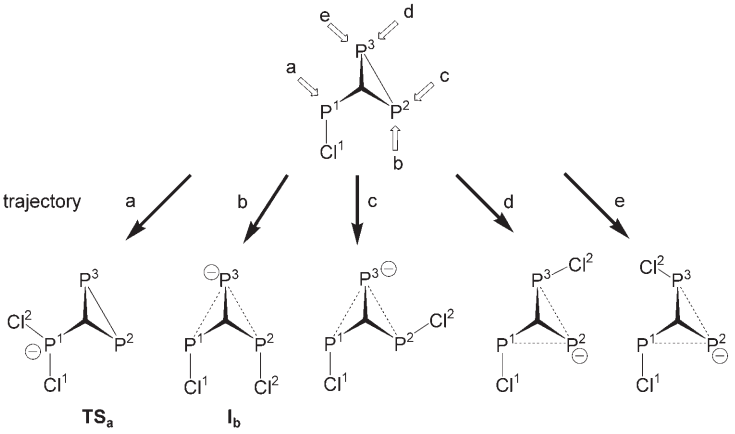

Scheme 2. Conceptual trajectories and resultant transition states/intermediates for nucleophilic attack of Cl^- on **1a**′.

acceptor orbital, σ*(P^2–P^3), is available to accommodate the chloride lone pair. In fact, the P^3–Cl^2 separation in $\mathbf{I_a}$ (2.85 Å) is actually shorter than the P^1–Cl^2 separation (3.43 Å), suggesting that the major interaction in $\mathbf{I_a}$ is between the chloride ion and the σ*(P^2–P^3) orbital rather than the σ*(P^1–Cl^1) orbital.

A further ramification of this interaction is that introduction of a Cl^- ion via trajectory (e) also results in the formation of $\mathbf{I_a}$. Indeed trajectories (a) and (e) proved to be indistinguishable as the calculated reaction coordinate is a hybrid of these two conceptual pathways. Progression along the reaction coordinate from $\mathbf{I_a}$ towards the transition state $\mathbf{TS_a}$ enhances overlap of the chloride lone pair of electrons with the σ*(P^1–Cl^1) orbital, but only at the cost of reduced overlap with the σ*(P^2–P^3) orbital, and the competition between the two acceptor orbitals leads to an S_N2-type, rather than an AE-type, profile. Trajectory (b), in contrast, gives a classic AE-type potential-energy surface which features only a C_{2v}-symmetric intermediate $\mathbf{I_b}$. In comparison to $\mathbf{TS_a}$, the P^2–P^3 bond in $\mathbf{I_b}$ is substantially elongated ($\mathbf{I_b}$ 2.43 Å, $\mathbf{TS_a}$ 2.18 Å) while both P–Cl bonds in $\mathbf{I_b}$ are shorter ($\mathbf{I_b}$ 2.37 Å, $\mathbf{TS_a}$ 2.57 Å), thus suggesting that the primary charge transfer interaction in this case is again between the chloride lone pair of electrons and the σ*(P^2–P^3) orbital. The attack of a chloride ion at the remote P^2 center, as opposed to the one bound to chloride (P^1), marks a subtle distinction from previous examples of the AE mechanism, in which the entering and leaving groups are bound to the same center. The distinction is, in fact, reminiscent of that between the well-known S_N2 and S_N2' pathways[9] in carbon-centered nucleophilic-substitution reactions. By analogy, we propose that trajectory (b) represents the first example of an AE′-type mechanism in a phosphorus compound.

The presence of two distinct pathways for nucleophilic attack corresponding to trajectories (a) and (b) is sufficient to explain fully the observed ^{31}P NMR spectra: trajectory (a) or (e) leads to exchange of P^2 and P^3, while trajectory (b) leads to exchange of P^1 and P^2. Scheme 2 suggests that there are two other possible trajectories, (c) and (d), but we have been unable to locate any stationary points for these cases: both result in the expulsion of chloride. The unique stability of $\mathbf{I_b}$, as distinct from the putative intermediates arising from trajectories (c) and (d), is a consequence of the stabilization of the negative charge on P^3 by delocalization into *both* σ*(P–Cl) orbitals (see HOMO of $\mathbf{I_b}$, inset in Figure 3). In contrast, attack along trajectories (c) or (d) would direct either one (trajectory (c)) or both (trajectory (d)) of the σ*(P–Cl) orbitals away from the negatively charged phosphorus center, thus preventing effective delocalization of the negative charge.

In summary, the ^{31}P NMR spectra of solutions containing **1a** and Cl^- ions, in conjunction with a detailed analysis of the potential-energy surface for nucleophilic attack on **1a**′ by a Cl^- ion, have revealed the presence of competing S_N2- and AE′-type mechanisms for chloride exchange. The much greater complexity of this transformation as compared to nucleophilic attack at monophosphorus systems can be traced to the presence of the low-lying σ*(P–P) orbital in the valence manifold which strongly perturbs the trajectories of the incoming nucleophile. Such an effect has not been previously observed, and we are presently exploring the implications of this interesting finding.

Experimental Section

All experimental procedures were performed under an atmosphere of nitrogen or argon by using standard Schlenk-line and glovebox techniques.

NMR studies were performed on either a Bruker AMX 300 spectrometer (operating frequencies 300.13 MHz (^1H), 121.49 MHz (^{31}P)) or a Bruker AV 500 spectrometer (operating frequencies 500.13 MHz (^1H), 202.47 MHz (^{31}P)). All NMR studies were performed in [D_8]THF (0.5 mL), and the required concentration of chloride anion was obtained by adding the appropriate amount of a 2.26×10^{-3} M stock solution of nBu$_4$NCl in THF. Spectra were simulated over a range of temperatures by using the gNMR suite of programs, and the resulting rate constants in the temperature range 325 K to 285 K were used to generate Eyring plots from which activation parameters were extrapolated.

Single-crystal X-ray diffraction data for **1b**: $C_{10}H_{18}IP_3$, $M_r = 358.05\ g\,mol^{-1}$, crystal dimensions $0.34\times0.05\times0.04\ mm^3$, orthorhombic, space group $P2_12_12_1$, $a = 6.2694(4)$, $b = 13.2771(9)$, $c = 17.2491(12)$ Å, $V = 1435.81(17)$ Å^3, $Z = 4$, $\rho_{calcd} = 1.656\ Mg\,m^{-3}$, $F(000) = 704$, $\mu Mo_{K\alpha} = 2.531\ mm^{-1}$, $\theta = 1.94$ to 29.05°, 15466 measured reflections, 3798 independent reflections, $R_{int} = 0.0295$, $-8 \leqq h \leqq 8$, $-18 \leqq k \leqq 18$, $-23 \leqq l \leqq 23$, $R_1(I>2\sigma) = 0.0203$, $wR_2(I>2\sigma) = 0.0399$, R_1(all data) = 0.0243, wR_2(all data) = 0.0408, GOF = 1.015. Diffraction data were collected at 115 K on a Bruker Smart Apex diffractometer with $Mo_{K\alpha}$ radiation ($\lambda = 0.71073$ Å) by using a SMART CCD camera. Diffractometer control, data collection, and initial unit-cell determination were performed with SMART (version 5.625, Bruker-AXS). Frame integration and unit-cell refinement were carried out with SAINT+ (version 6.22, Bruker AXS). Absorption corrections were applied by SADABS (version 2.03, Sheldrick). Structures were solved by direct methods with SHELXS-97 (Sheldrick, 1997) and refined by full-matrix least squares with SHELXL-97 (Sheldrick, 1997). All non-hydrogen atoms were refined anisotropically. Hydrogen atoms were placed by using a riding model and included in the refinement at calculated positions. CCDC-293160 contains the supplementary crystallographic data for this paper. These data can be obtained free of charge from The Cambridge Crystallographic Data Centre via www.ccdc.cam.ac.uk/data_request/cif.

All calculations were carried out with the Gaussian 03 series of programs.[10] Geometry optimizations were performed with the

 © 2006 Wiley-VCH Verlag GmbH & Co. KGaA, Weinheim

B3LYP functional[11] in conjunction with the 6-31 + G(d,p) basis set.[12] The optimized stationary points were characterized as minima by analytic vibrational-frequency calculations at the same level of theory. Shielding parameters (σ) were calculated by using the GIAO formalism[13] and converted to chemical shifts (δ) using the relation $\delta = 328.5 - \sigma$, where 328.5 is the absolute shielding parameter for the ^{31}P NMR reference standard 85% H_3PO_4.[14]

Received: December 21, 2005
Published online: April 26, 2006

Keywords: density functional calculations · NMR spectroscopy · nucleophilic substitution · phosphorus · structure elucidation

[1] a) S. Gronert, *J. Am. Chem. Soc.* **1991**, *113*, 6041; b) S. Shaik, H. B. Schlegel, S. Wolfe, *Theoretical Aspects of Physical Organic Chemistry, The S_N2 Mechanism*, Wiley, New York, **1992**; c) M. N. Glukhovtsev, A. Pross, L. Radom, *J. Am. Chem. Soc.* **1996**, *118*, 6273.

[2] a) J. Li, P. Beak, *J. Am. Chem. Soc.* **1992**, *114*, 9206; b) S. M. Bachrach, D. C. Mulhearn, *J. Phys. Chem.* **1993**, *97*, 12229; c) S. M. Bachrach, D. C. Mulhearn, *J. Phys. Chem.* **1996**, *100*, 3535; d) T. I. Sølling, A. Pross, L. Radom, *Int. J. Mass Spectrom.* **2001**, *210*, 1.

[3] a) A. P. Bento, M. Solà, F. Bickelhaupt, *J. Comput. Chem.* **2005**, *26*, 1497; b) T. L. Windus, M. S. Gordon, L. P. Davis, L. W. Burggraf, *J. Am. Chem. Soc.* **1994**, *116*, 3568; c) D. C. Mulhearn, S. M. Bachrach, *J. Am. Chem. Soc.* **1996**, *118*, 9415; d) S. M. Bachrach, B. D. Gailbreath, *J. Org. Chem.* **2001**, *66*, 2005.

[4] J. M. Lynam, M. C. Copsey, M. Green, J. C. Jeffery, J. E. McGrady, C. A. Russell, J. M. Slattery, A. C. Swain, *Angew. Chem.* **2003**, *115*, 2884; *Angew. Chem. Int. Ed.* **2003**, *42*, 2778.

[5] C. Fish, M. Green, J. C. Jeffery, R. J. Kilby, J. M. Lynam, C. A. Russell, C. E. Willans, *Organometallics* **2005**, *24*, 5789.

[6] P. Binger, T. Wettling, R. Schneider, F. Zurmühlen, U. Bergsträsser, J. Hoffmann, G. Maas, M. Regitz, *Angew. Chem.* **1991**, *103*, 208; *Angew. Chem. Int. Ed. Engl.* **1991**, *30*, 207.

[7] gNMR, version 5.0.5.0, Ivory Software, **2005**.

[8] The negative energy values for the intermediates and transition states are simply a consequence of the gas-phase nature of the calculations.

[9] J. P. Clayden, N. Greeves, S. Warren, P. D. Wothers, in *Organic Chemistry*, Oxford University Press, Oxford, **2001**, pp. 609.

[10] Gaussian 03, Revision B.03, M. J. Frisch, G. W. Trucks, H. B. Schlegel, G. E. Scuseria, M. A. Robb, J. R. Cheeseman, J. A. Montgomery, Jr., T. Vreven, K. N. Kudin, J. C. Burant, J. M. Millam, S. S. Iyengar, J. Tomasi, V. Barone, B. Mennucci, M. Cossi, G. Scalmani, N. Rega, G. A. Petersson, H. Nakatsuji, M. Hada, M. Ehara, K. Toyota, R. Fukuda, J. Hasegawa, M. Ishida, T. Nakajima, Y. Honda, O. Kitao, H. Nakai, M. Klene, X. Li, J. E. Knox, H. P. Hratchian, J. B. Cross, V. Bakken, C. Adamo, J. Jaramillo, R. Gomperts, R. E. Stratmann, O. Yazyev, A. J. Austin, R. Cammi, C. Pomelli, J. W. Ochterski, P. Y. Ayala, K. Morokuma, G. A. Voth, P. Salvador, J. J. Dannenberg, V. G. Zakrzewski, S. Dapprich, A. D. Daniels, M. C. Strain, O. Farkas, D. K. Malick, A. D. Rabuck, K. Raghavachari, J. B. Foresman, J. V. Ortiz, Q. Cui, A. G. Baboul, S. Clifford, J. Cioslowski, B. B. Stefanov, G. Liu, A. Liashenko, P. Piskorz, I. Komaromi, R. L. Martin, D. J. Fox, T. Keith, M. A. Al-Laham, C. Y. Peng, A. Nanayakkara, M. Challacombe, P. M. W. Gill, B. Johnson, W. Chen, M. W. Wong, C. Gonzalez, J. A. Pople, Gaussian, Inc., Wallingford, CT, **2004**.

[11] a) A. D. Becke, *J. Chem. Phys.* **1993**, *98*, 5648; b) C. Lee, W. Yang, R. G. Parr, *Phys. Rev. B* **1988**, *37*, 785.

[12] a) W. J. Hehre, R. Ditchfield, J. A. Pople, *J. Chem. Phys.* **1972**, *56*, 2257; b) P. C. Hariharan, J. A. Pople, *Chem. Phys. Lett.* **1972**, *16*, 217; c) M. M. Francl, W. J. Pietro, W. J. Hehre, J. S. Binkley, D. J. DeFrees, J. A. Pople, M. S. Gordon, *J. Chem. Phys.* **1982**, *77*, 3654.

[13] a) R. Ditchfield, *Mol. Phys.* **1974**, *27*, 789; b) K. Wolinski, J. F. Hinton, P. Pulay, *J. Am. Chem. Soc.* **1990**, *112*, 8251.

[14] C. J. Jameson, A. De Dios, A. K. Jameson, *Chem. Phys. Lett.* **1990**, *167*, 575.

 © 2006 Wiley-VCH Verlag GmbH & Co. KGaA, Weinheim

Nanotechnology

DOI: 10.1002/anie.200600394

Surface Plasmon Resonances of Free-Standing Gold Nanowires Fabricated by Nanoskiving**

*Qiaobing Xu, Jiming Bao, Federico Capasso, and George M. Whitesides**

Herein we present both a simple, experimentally convenient method for the fabrication of gold nanowires with uniform, controlled dimensions (Figure 1), and a systematic study of the dependence of the plasmon resonance of these gold nanowires on the geometry of these wires. The length of the wires is determined by photolithography; the width is determined by the thickness of a film fabricated by deposition from the vapor; the height is determined by sectioning ("nanoskiving") with the diamond knife of a microtome.[1,2] The cross sections of the wires can be as small as 10 nm × 30 nm. We measure the surface plasmon resonances of individual gold wires, and show these resonances to be determined by their cross-sectional dimensions.

Nanoparticles of noble metals (Ag or Au) show different colors as a result of their surface plasmon resonances.[3,4] These particles interact strongly with visible light through the resonant excitation of the collective oscillations of their conduction electrons.[3,4] As a result of these oscillations, local

[*] Q. Xu, Prof. G. M. Whitesides
Department of Chemistry and Chemical Biology
Harvard University
Cambridge, MA 02138 (USA)
Fax: (+1) 617-495-9857
E-mail: gwhitesides@gmwgroup.harvard.edu
Dr. J. Bao, Prof. F. Capasso
Division of Engineering and Applied Sciences
Harvard University
Cambridge, MA 02138 (USA)

[**] This research was supported by the NIH (GM065364), by DARPA (sub-award to G.M.W. from the Center for Optofluidic Integration at the California Institute of Technology), and by a MURI AFOSR sub-award to F.C. MRSEC and NSEC shared facilities supported by the NSF under awards DMR-0213805 (MRSEC) and PHY-0117795 (NSEC) were utilized. We thank Ertugrul Cubukcu, Dr. Marko Loncar, Dr. Brian Mayers, and Prof. Kenneth Crozier for helpful discussions.

Supporting information for this article is available on the WWW under http://www.angewandte.org or from the author.

© 2006 Wiley-VCH Verlag GmbH & Co. KGaA, Weinheim

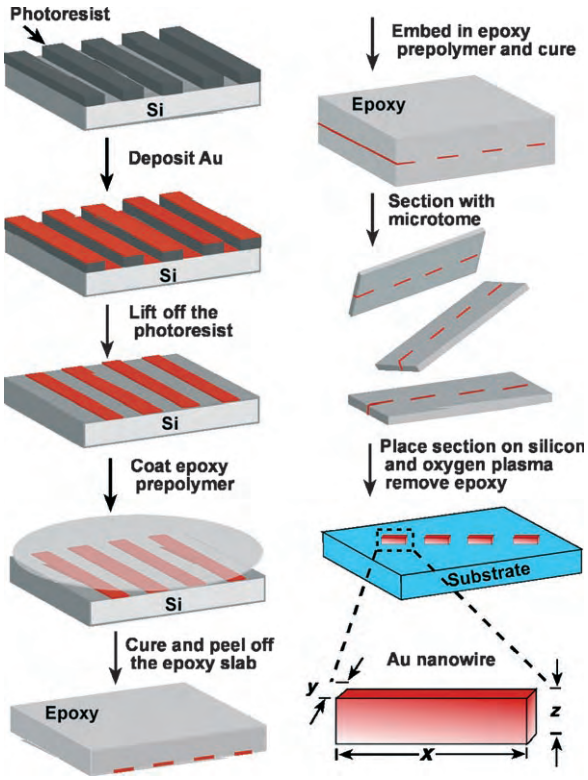

Figure 1. Schematic illustration of the procedure used to fabricate metal nanowires with a controllable size. The length of the metal structure (*x*) is determined by photolithography (ca. 2 μm), and the width of the structures (*y*) is determined by the thickness of the deposited metal film (10, 20, or 40 nm). The thickness of the sectioned polymer slab (*z*) is controlled by the microtome (30, 50, 70, or 100 nm).

electromagnetic fields near the particle can be many orders of magnitude higher than the incident fields; these strong, oscillating fields generate intense scattered light around the wavelength of the resonant peak. The magnitude, peak wavelength, and spectral bandwidth of the plasmon resonance of a nanoparticle depend on the size, shape, material of fabrication, and local environment of the particle.[3–6] The enhancement in local field and strong scattering is useful for a number of applications, including surface-enhanced Raman scattering,[7,8] subwavelength optical waveguides,[9–16] biolabels,[17–19] and biosensors.[20–25]

Nanostructures with different geometries in a range of materials have been synthesized by using chemical methods.[26–32] These nanostructures are usually not uniform in size nor geometry. The integration of these nanostructures into optical devices is also challenging because of the difficulty of selecting and manipulating specific nanoparticles. Nanoparticles fabricated by nanosphere lithography have been used for chemosensing and biosensing.[21–24] This technique, although very useful, can only produce nanostructures with limited flexibility in dimensions and geometries. Electron-beam lithography is widely used to fabricate metal nanostructures for studying surface plasmon coupling and subwavelength optical waveguides.[9,13–16,33–35] However, electron-beam lithography is still not conveniently available to general users, and it is also challenging to fabricate wires with widths below 30 nm and high aspect ratios. Exploration and development of new techniques for the fabrication of nanostructures relevant to plasmonics is desirable.[36,37] The technique described herein is not intended to replace these existing methods, but rather to provide a simple alternative for the fabrication of relevant nanostructures with well-controlled dimensions, and to aid the study of their optical properties.

Figure 1 shows the procedure used to fabricate free-standing gold nanowires. This procedure combines photolithography, vapor deposition, and microtome sectioning; we have used a related procedure previously to fabricate nanoelectrodes.[1] We first generated a pattern with rectangular lines (2-μm wide with 2-μm spacing in this case) on a silicon substrate (with 2-nm-thick native oxide) by using standard photolithography with a Shipley 1805 photoresist. We subsequently deposited 10–40 nm of gold film by using electron-beam evaporation on this patterned substrate. Removal of the photoresist with acetone generated gold wires (10–40-nm thick and 2-μm wide) on the silicon substrate. We then cast a layer of epoxy (araldite 502) prepolymer on this substrate. After curing the epoxy, we mechanically peeled it from the substrate; the gold film transferred to the epoxy film because of the weak adhesion between the gold and the silicon substrate. We embedded this epoxy substrate into more of the epoxy prepolymer; curing generated an epoxy slab containing a layer of embedded, patterned metal film.

We sectioned the epoxy block in a plane that intersected the wire perpendicularly by using a microtome (Leica MZ6) equipped with a diamond knife (Diatome ultra 35°) and with water filling the sample-collection boat.[2] Sectioning with a microtome generated polymer slabs with thickness ranging from 30 to 100 nm; these slabs floated at the air–water interface in the sample-collection boat. We transferred the epoxy sections to a bare silicon substrate by immersing it in the water, and withdrawing it in a way that the floating polymer films were captured by means of capillarity. Before optical characterization of the gold nanowires, we removed the polymer matrix by using an oxygen plasma; this process left the gold nanowires intact and supported on the silicon substrate, usually in the orientation in which they were embedded in the slab. The length (*x*) of the nanowires is defined by the width of the initial wires relative to the plane of the sections (2 μm for all the samples described herein, but this length can be longer or much shorter). Figure 2 shows the SEM image of gold nanowires with two different sizes. These free-standing wires usually do not fall over even when they have a large height-to-width ratio; we attribute this stability in orientation to the interfacial interaction between the gold and the silicon dioxide of the substrate.

Standard light microscopes equipped with dark-field illumination have been used extensively to study the surface plasmon behavior of nanostructures.[3,4,17] Figure 3a outlines the apparatus used to select individual nanowires and record their scattering spectrum. We illuminated the nanowires with unpolarized, focused, white light from a high-intensity fiber light source (Fiber Illuminator OSL1). The incident beam of light was perpendicular to the long axis of the nanowire at an angle of about 60° with respect to the normal of the silicon

 © 2006 Wiley-VCH Verlag GmbH & Co. KGaA, Weinheim

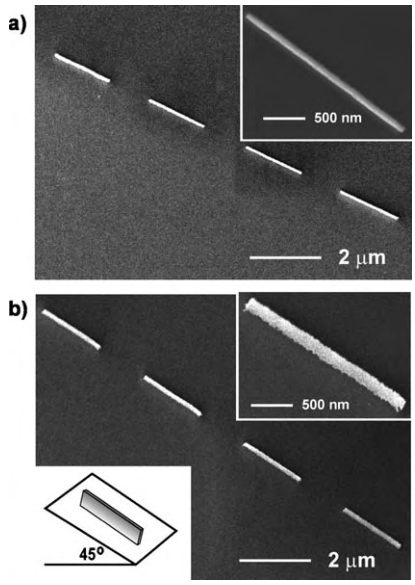

Figure 2. SEM images of typical free-standing gold nanowires viewed on an angle. a) Gold nanowires with dimensions (x, y, z) of approximately 2 μm × 40 nm × 50 nm. b) Gold nanowires with dimensions of approximately 2 μm × 10 nm × 100 nm. The insets show high-magnification images of the same samples. The orientations of (a) and (b) are at a 45° oblique angle.

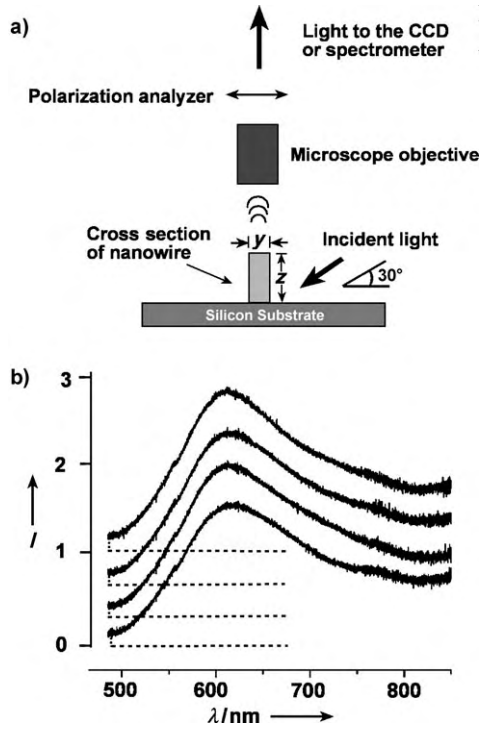

Figure 3. a) Experimental setup used for measurement of optical scattering of gold nanowires. b) The scattering spectra of four randomly selected individual nanowires (2 μm × 20 nm × 50 nm). The spectra are vertically displaced to show reproducibility.

substrate. Scattered light from the nanowire was collected selectively through a microscopic objective with a long working distance (Mitutoyo SL50, numerical aperture (NA) = 0.55). This dark-field illumination maximized the scattering from the nanoparticles, and minimized the background scattering from the substrate. The collected light then passed through a polarizer parallel to the short axis of the nanowire (y direction) and focused on the plane of the entrance slit of a single-grating monograph (Jobin Yvon Horiba Triax 550); this apparatus allowed us both to take a video image of the nanowires and to measure their spectrum. The polarizer allowed us to select surface plasmon resonances with polarization traverse to the long axis of the wire. An individual nanowire, or a small group of nanowires, could be selected for analysis by adjusting the width and height of the slit. The spectra obtained depended on the spectrum of the incident white light, the focusing and collecting optics, and the response of the spectrometer. To remove these effects and isolate the plasmon resonance spectrum of the nanowires, we replaced the nanowire sample with a broad-band white-light target (which has a constant scattering response over wide range of frequencies) and obtained its scattering spectrum by using the same procedure. We then normalized the obtained spectrum of the nanowires to the reference spectrum of the broad-band target.[17] Figure 3b shows the normalized scattering spectra of four nanowires randomly selected from a single sample. The variation in position of the resonance peak among the nanowires is negligible. We also found the spectral variation between nanowires from separate slabs of the same thickness to be negligible. These observations established the optical homogeneity of the nanowires generated by this sectioning technique, and implied their constancy in size.

We fabricated nanowires with different cross-sectional dimensions by changing the thicknesses of the metal film and the sections. Figure 4a–c shows color, dark-field, optical images of nanowires with different cross sections obtained by using a standard optical microscopic with dark-field illumination (Nikon 43300–522 with CCD camera). All optical images were obtained under the same conditions with polarization perpendicular to the long axis of the nanowires. For each set of wires with the same width (y), the color shows a red shift with increasing nanowire height (z). Figure 4d–f shows the scattering spectra of the gold nanowires shown in Figure 4a–c. We usually collected the emission from four nanowires simultaneously to increase the signal-to-noise ratio and to average the small spectral variations betweens the wires. The peak maximum shifts to longer wavelength with increase in the height of wires from the same set with fixed width. This observation agrees well with the optical color images.

To rationalize these spectra, we simulated them by using finite-difference time-domain (FDTD) techniques.[38] The frequency-dependent dielectric constant of gold was obtained from the literature.[39] The configuration of the simulation was the same as that in the experiment (Figure 3a) except that in the simulation the wire was suspended in air rather than supported on the Si/SiO_2 substrate. For each simulation, the plane of the incident excitation wave was at the same angle (60°). We calculated the scattering amplitude at individual wavelengths and obtained the far-field scattered field. The scattering spectrum was then calculated by integrating the scattered field over angles set by the numerical aperture of the collecting objective (NA = 0.55). Figure 5a–c shows the

 © 2006 Wiley-VCH Verlag GmbH & Co. KGaA, Weinheim

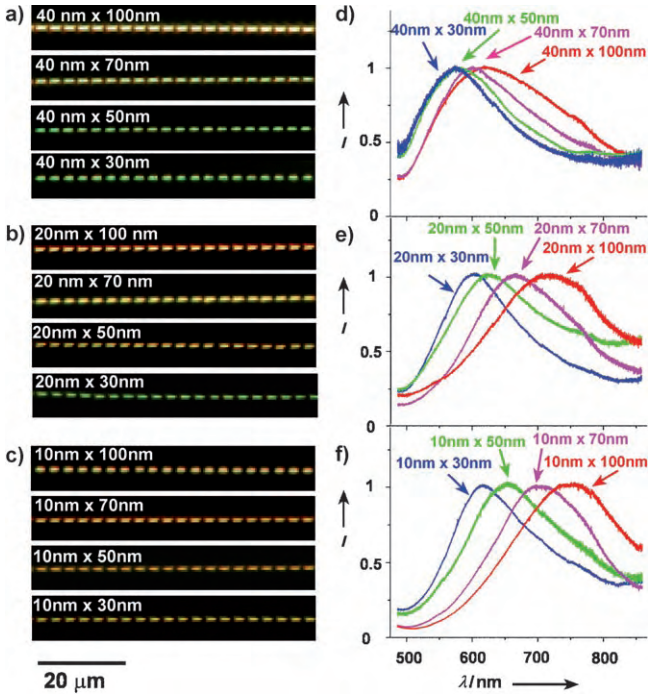

Figure 4. Surface plasmon resonances of gold nanowires with different cross-sectional dimensions. a–c) Dark-field optical images of gold nanowires having different dimensions (all 2-μm long (*x*); dimensions of the cross section marked in the figure as *y*×*z*). The nanowires appear larger than their actual dimensions owing to optical diffraction. d–f) Scattering spectra of gold nanowires with different dimensions, corresponding to the gold nanowires shown in (a–c).

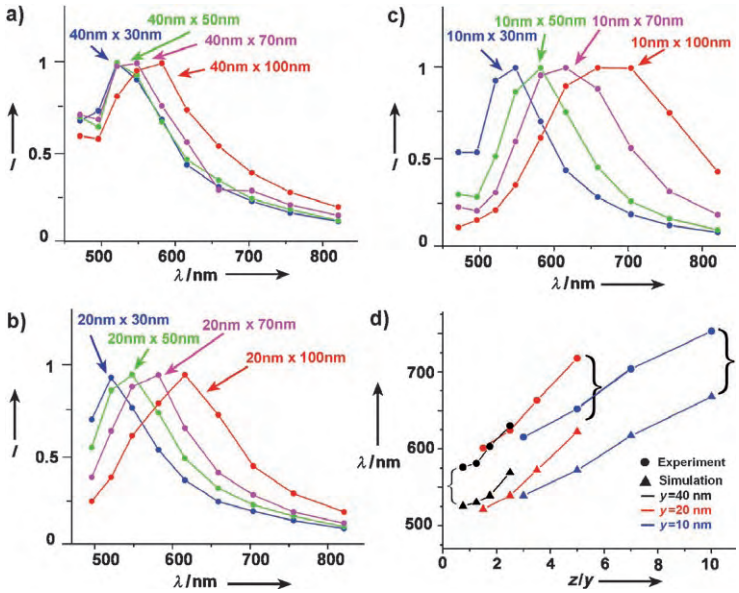

Figure 5. FDTD simulations and comparison with experimental results. a–c) Finite-difference time-domain simulations of scattering spectra. For each set of fixed widths (10, 20, or 40 nm), the resonance peak moves to longer wavelength as the height increases. The dimensions of the cross section are marked in each figure as *y*×*z*. d) Dependence of maximum wavelength of the scattering resonances as a function of aspect ratio *z*/*y* for data from experiment and FDTD simulation. The corresponding experimental and simulation data are paired by braces for clarity.

results of these FDTD simulations. The simulations and the experimental results showed the same trend in the red shift of the maxima as the *z*/*y* ratio increased. Since the polarization of the incident light was at 60° with respect to the *z* axis in the *z*–*y* plane, two modes of surface plasmons, polarized along the *z* and *y* directions, were excited. The total scattering spectrum arises from the plasmons excited by the *z* and *y* components of the incident electric field. Analysis of data from the simulations shows that the scattered field was almost the superposition of fields generated by two dipoles oscillating along the *z* and *y* directions. In our experimental configuration, the light-collection efficiency for *y*-polarized emission is 8 times larger than for *z*-polarized emission, and the contributions to the recorded intensity are about equal when the *z*/*y* aspect ratio is 1.5. For wires with aspect ratios larger than 1.5, the spectra are dominated by the scattering generated by *z*-polarized plasmons, especially near the resonance wavelength. Figure 5 d plots the dependence of the wavelength of maximum plasmon scattering on the *z*/*y* aspect ratio (from 0.75 to 10) for the experimental measurements and the simulation. Both the experimental data and the FDTD simulation showed a similar red shift when the aspect ratio of the nanowire cross section increased. The resonance peaks of the experimental data were, however, consistently at longer wavelengths than those of the simulations (Figure 5 d). We believe that this discrepancy reflects the fact that the simulations assumed that the nanowires were suspended in air rather than supported on silicon substrates with a thin layer of native SiO_2. Similar effects have been reported.[14,15]

The technique we describe herein offers a convenient way to make free-standing gold nanostructures with uniform and well-controlled size and shape. These structures are well-suited for fundamental studies of the relationships between the shape of nanostructures and their properties as plasmon resonators. This technique can be used to fabricate nanostructures that are impossible or very difficult to make with other techniques. It can be used with most metals that can be deposited from the vapor (we are still investigating the behavior of brittle materials upon sectioning). A major benefit of this technique is that the nanostructures can be easily positioned by manipulating the macroscopic epoxy slabs (the epoxy can be removed conveniently after positioning by oxygen plasma etching). The ability to tune the shape and composition of the nanostructures, and the ability to position the nanostructures, will, we believe, combine to make this technique useful in the fabrication of prototype optical devices such as subwavelength optical waveguides and biosensors.

Received: January 30, 2006
Published online: April 28, 2006

Keywords: gold · microtome · nanotechnology · sectioning · surface plasmon resonance

[1] Q. Xu, B. D. Gates, G. M. Whitesides, *J. Am. Chem. Soc.* **2004**, *126*, 1332.

 © 2006 Wiley-VCH Verlag GmbH & Co. KGaA, Weinheim

[2] A. M. Glauert, *Practical Methods in Electron Microscopy*, Elsevier, New York, **1974**.
[3] C. F. Bohren, D. R. Huffman, *Absorption and Scattering of Light by Small Particles*, Wiley, New York, **1983**.
[4] U. Kreibig, M. Vollmer, *Optical Properties of Metal Clusters*, *Vol. 25*, Springer, Berlin, **1995**.
[5] S. Link, M. A. El-Sayed, *J. Phys. Chem. B* **1999**, *103*, 8410.
[6] K. L. Kelly, E. Coronado, L. L. Zhao, G. C. Schatz, *J. Phys. Chem. B* **2003**, *107*, 668.
[7] X. S. Xie, *Acc. Chem. Res.* **1996**, *29*, 598.
[8] S. Nie, S. R. Emory, *Science* **1997**, *275*, 1102.
[9] J.-C. Weeber, A. Dereux, C. Girard, J. R. Krenn, J.-P. Goudonnet, *Phys. Rev. B* **1999**, *60*, 9061.
[10] W. L. Barnes, A. Dereux, T. W. Ebbesen, *Nature* **2003**, *424*, 824.
[11] K. B. Crozier, A. Sundaramurthy, G. S. Kino, C. F. Quate, *J. Appl. Phys.* **2003**, *94*, 4632.
[12] P. G. Kik, S. A. Maier, H. A. Atwater, *Mater. Res. Soc. Symp. Proc.* **2002**, *705*, 101.
[13] S. A. Maier, H. A. Atwater, *J. Appl. Phys.* **2005**, *98*, 011101.
[14] G. Schider, J. R. Krenn, W. Gotschy, B. Lamprecht, H. Ditlbacher, A. Leitner, F. R. Aussenegg, *J. Appl. Phys.* **2001**, *90*, 3825.
[15] J. R. Krenn, B. Lamprecht, H. Ditlbacher, G. Schider, M. Salerno, A. Leitner, F. R. Aussenegg, *Europhys. Lett.* **2002**, *60*, 663.
[16] D. A. Genov, V. M. Shalaev, A. K. Sarychev, *Phys. Rev. B* **2005**, *72*, 113102.
[17] S. Schultz, D. R. Smith, J. J. Mock, D. A. Schultz, *Proc. Natl. Acad. Sci. USA* **2000**, *97*, 996.
[18] D. A. Schultz, *Curr. Opin. Biotechnol.* **2003**, *14*, 13.
[19] C. Loo, L. Hirsch, M.-H. Lee, E. Chang, J. West, N. Halas, R. Drezek, *Opt. Lett.* **2005**, *30*, 1012.
[20] Y. C. Cao, R. Jin, C. A. Mirkin, *Science* **2002**, *297*, 1536.
[21] A. J. Haes, R. P. Van Duyne, *J. Am. Chem. Soc.* **2002**, *124*, 10596.
[22] A. J. Haes, L. Chang, W. L. Klein, R. P. Van Duyne, *J. Am. Chem. Soc.* **2005**, *127*, 2264.
[23] A. J. Haes, S. Zou, G. C. Schatz, R. P. Van Duyne, *J. Phys. Chem. B* **2004**, *108*, 109.
[24] C. R. Yonzon, E. Jeoung, S. Zou, G. C. Schatz, M. Mrksich, R. P. Van Duyne, *J. Am. Chem. Soc.* **2004**, *126*, 12669.
[25] L. R. Hirsch, J. B. Jackson, A. Lee, N. J. Halas, J. L. West, *Anal. Chem.* **2003**, *75*, 2377.
[26] Y. Xia, N. J. Halas, *MRS Bull.* **2005**, *30*, 338.
[27] M. A. El-Sayed, *Acc. Chem. Res.* **2001**, *34*, 257.
[28] R. Jin, Y. Cao, C. A. Mirkin, K. L. Kelly, G. C. Schatz, J. G. Zheng, *Science* **2001**, *294*, 1901.
[29] J. J. Mock, S. J. Oldenburg, D. R. Smith, D. A. Schultz, S. Schultz, *Nano Lett.* **2002**, *2*, 465.
[30] Y. Xiong, J. Chen, B. Wiley, Y. Xia, Y. Yin, Z.-Y. Li, *Nano Lett.* **2005**, *5*, 1237.
[31] C. L. Nehl, N. K. Grady, G. P. Goodrich, F. Tam, N. J. Halas, J. H. Hafner, *Nano Lett.* **2004**, *4*, 2355.
[32] B. Wiley, Y. Sun, J. Chen, H. Cang, Z.-Y. Li, X. Li, Y. Xia, *MRS Bull.* **2005**, *30*, 356.
[33] S. A. Maier, P. G. Kik, H. A. Atwater, S. Meltzer, E. Harel, B. E. Koel, A. A. G. Requicha, *Nat. Mater.* **2003**, *2*, 229.
[34] K. H. Su, Q. H. Wei, X. Zhang, J. J. Mock, D. R. Smith, S. Schultz, *Nano Lett.* **2003**, *3*, 1087.
[35] Q. H. Wei, K. H. Su, S. Durant, X. Zhang, *Nano Lett.* **2004**, *4*, 1067.
[36] Y. Xia, G. M. Whitesides, *Angew. Chem.* **1998**, *110*, 568; *Angew. Chem. Int. Ed.* **1998**, *37*, 550.
[37] B. D. Gates, Q. Xu, M. Stewart, D. Ryan, C. G. Willson, G. M. Whitesides, *Chem. Rev.* **2005**, *105*, 1171.
[38] XFDTD, a full-wave time-domain solver from REMCOM (http://www.remcom.com).
[39] P. B. Johnson, R. W. Christy, *Phys. Rev. B* **1972**, *6*, 4370.

 © 2006 Wiley-VCH Verlag GmbH & Co. KGaA, Weinheim

Multicomponent Reactions

DOI: 10.1002/anie.200600497

Short Synthesis of Skeletally and Stereochemically Diverse Small Molecules by Coupling Petasis Condensation Reactions to Cyclization Reactions**

*Naoya Kumagai, Giovanni Muncipinto, and Stuart L. Schreiber**

Herein, we report a short and efficient synthetic pathway that uses intramolecular cyclization reactions of readily synthesized and densely functionalized amino alcohols. The research illustrates the implementation of a strategy that enables the synthesis, in only three to five steps, of a diverse collection of single-isomer small molecules whose members have over 15 different types of skeleton. In the future, this research should also enable the consequences of the unique structural features of the compounds in small-molecule screens to be determined.[1,2]

We used the Petasis three-component, boronic acid Mannich reaction[3] followed by an amine propargylation to yield β-amino alcohols **1**. These compounds bear polar (amino, hydroxy, ester) and nonpolar (alkene, alkyne, cyclopropane) functionalities strategically placed as handles for subsequent skeletal diversification reactions (Scheme 1).

The Petasis reaction of (*S*)-lactol **2a** (from L-phenyllactic acid), L-phenylalanine methyl ester (**3a**), and (*E*)-2-cyclopropylvinylboronic acid (**4**) proceeded smoothly under ambient conditions in EtOH to afford the *anti* diastereomer **5aa** exclusively in 85% yield.[4] The same conditions but with (*R*)-lactol **2b** afforded the corresponding (2*R*,3*S*) isomer **5ba** exclusively (Scheme 2). These reactions indicate that the secondary hydroxy group adjacent to the intermediate imines directs the stereochemical outcome of the reaction, overriding any directing effects of the stereocenter in **3a**.[3b] These

[*] Prof. Dr. S. L. Schreiber
Broad Institute of Harvard and MIT
Howard Hughes Medical Institute
Department of Chemistry and Chemical Biology
Harvard University
12 Oxford Street, Cambridge, MA 02138 (USA)
Fax: (+1) 617-495-0751
E-mail: stuart_schreiber@harvard.edu
Dr. N. Kumagai, G. Muncipinto
Department of Chemistry and Chemical Biology
Harvard University
12 Oxford Street, Cambridge, MA 02138 (USA)

[**] The NIGMS-sponsored Center of Excellence in Chemical Methodology and Library Design (Broad Institute CMLD) enabled this research. We thank Nilesh Kumar and Drs. Paul Clemons, Ryan Looper, Xiang Wang, and Damian Young for helpful discussions. G.M. is a visiting PhD student from the Dipartimento Farmacochimico, University of Bari (Italy). S.L.S. is an Investigator with the Howard Hughes Medical Institute.

Supporting information for this article is available on the WWW under http://www.angewandte.org or from the author.

 © 2006 Wiley-VCH Verlag GmbH & Co. KGaA, Weinheim

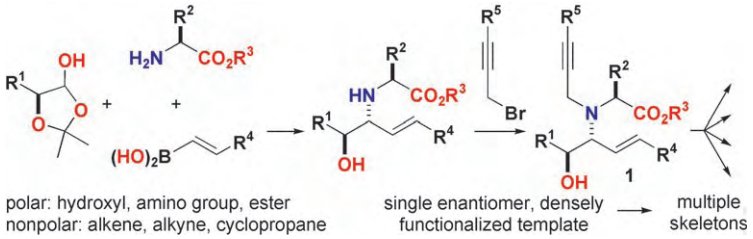

Scheme 1. The Petasis reaction followed by amine propargylation to yield β-amino alcohols **1**.

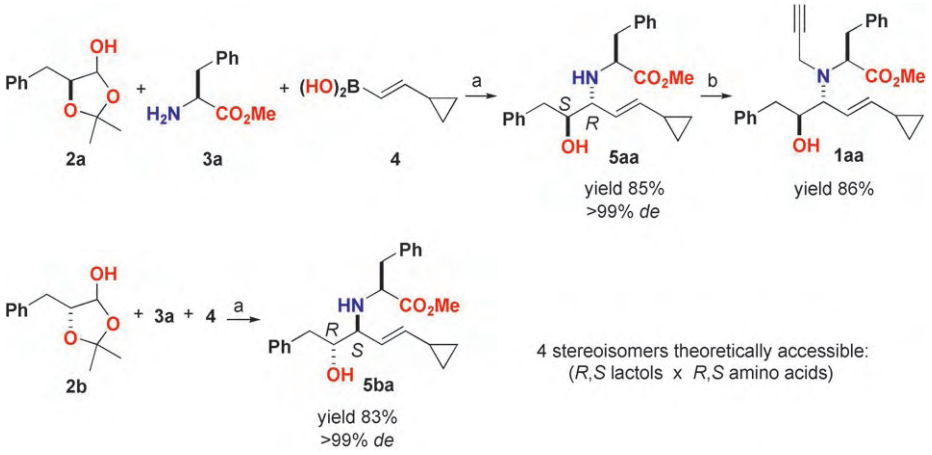

Scheme 2. a) EtOH, RT; b) propargyl bromide, $NaHCO_3$, *N*,*N*,-dimethylformamide (DMF), 70 °C.

results suggest that all four of the possible *anti* amino alcohol stereoisomers can be generated by appropriate combination of stereoisomeric lactols and amino acids, thus leading to stereochemical diversity in the final products of this pathway. Although not explored herein, there is a reasonable assumption that appendage diversification may also be achieved by variation of the lactol building block; appendage diversification by varying the amino component is described below. To prepare a test substrate for subsequent skeletal diversification, the *N*-selective alkylation of **5aa** with propargyl bromide afforded the template **1aa** in 86% yield.

We next explored a series of skeletal diversification reactions with **1aa** (Scheme 3).[4] Cycloisomerization catalyzed by $[Pd(PPh_3)_2(OAc)_2]$ resulted in opening of the cyclopropyl ring to afford triene **6aa** by a β-hydride elimination/reductive elimination sequence,[5] whereas cycloisomerization catalyzed by $[CpRu(CH_3CN)_3PF_6]$ (Cp = cyclopentadienyl) resulted in a [5+2] reaction to afford cyclic diene **7aa** by a cyclopropyl ring-opening/reductive elimination sequence.[6] Both reactions proceeded in a diastereoselective manner to afford single diastereomers. To the best of our knowledge, there have been no reports on palladium-catalyzed cycloisomerizations accompanied by opening of a cyclopropyl ring to furnish a triene. A Pauson–Khand reaction of **1aa** with $[Co_2(CO)_8]$ in the presence of trimethylamine *N*-oxide[7] proceeded efficiently to provide azabicyclo-[3.3.0] **8aa** diastereoselectively (>10:1 d.r.). Enyne metathesis of **1aa** using the Hoveyda–Grubbs catalyst[8] gave diene **9aa**, which, following Diels–Alder reaction with 4-methyl-1,2,4-triazolin-3,5-dione at room temperature, afforded tricyclic compound **10aa**. The stereochemistry of the only isolated isomer **10aa** results from the dienophile approaching the side opposite to the substituent on the pyrroline ring of **9aa**. Electrophilic activation of the alkyne functionality in **1aa** with $NaAuCl_4$ in MeOH led to the intramolecular cyclization of the hydroxy group followed by incorporation of MeOH to provide a morpholine skeleton **11aa** as a single diastereomer,[9] likely because of an anomeric effect. Treatment of **1aa** with NaH at room temperature gave lactone **12aa** in 88% yield without epimerization. Lactone **12aa** was subjected to the same reaction conditions as those for template **1aa** to furnish the corresponding bicyclic triene **13aa**, fused tricyclic [5+2] product **14aa**, fused tricyclic enone **15aa**, and bicyclic diene **16aa** in good yield. Diene **16aa** was further converted into fused tetracyclic compound **17aa** by a Diels–Alder reaction using the same conditions as before. Transformations of lactone **12aa** also proceeded with high diastereoselectivity to afford each product as a single detectable diastereomer.

We next demonstrated this diversity-oriented synthesis (DOS) pathway using different starting building blocks. A Petasis reaction with methyl 1-amino-1-cyclopentanecarboxylate (**3b**) afforded *anti* amino alcohol **5ab** exclusively in 84% yield under modified conditions (solvent system: CH_2Cl_2/1,1,1,3,3,3-hexafluoroisopropanol).[4,10] Subsequent propargylation furnished **1ab** in 81% yield (Scheme 4).

The cyclopentyl template **1ab** was next subjected to the same skeletal diversification reactions described above to provide the corresponding products with a spiro ring system (Scheme 5).[4] The reactions afforded skeletally distinct compounds **6ab**–**20ab** in good yield with high diastereoselectivity, whereas **8ab** cyclized under reaction conditions to form lactone **15ab**. The mild and chemoselective nature of these diversification reactions allows the use of chemically complex building blocks, such as 6-aminopenicillanic acid methyl ester (**3c**). The two-step preparation of the common template **1ac** with **3c** proceeded with excellent diastereoselectivity (Scheme 4).[4] The transition-metal-catalyzed diversification reactions worked well under the same conditions described for the L-Phe series despite the sulfur atom in the penam skeleton, whereas basic treatment resulted in ring opening of β-lactam to afford lactone **21ac** bearing a thiazolidine ring (Scheme 5).

We initiated this research with the hypothesis that densely substituted small molecules with diverse skeletons and stereochemistries will be especially effective in small-molecule screens. This new DOS pathway should enable the further testing of this hypothesis in an effective way owing to its ability to yield remarkably diverse, rigid, and complex small molecules with considerable efficiency. We are encouraged by preliminary results that have assigned, among others, high-feature signatures to a cluster of compounds that result from this pathway using multidimensional, cell-based screen-

 © 2006 Wiley-VCH Verlag GmbH & Co. KGaA, Weinheim

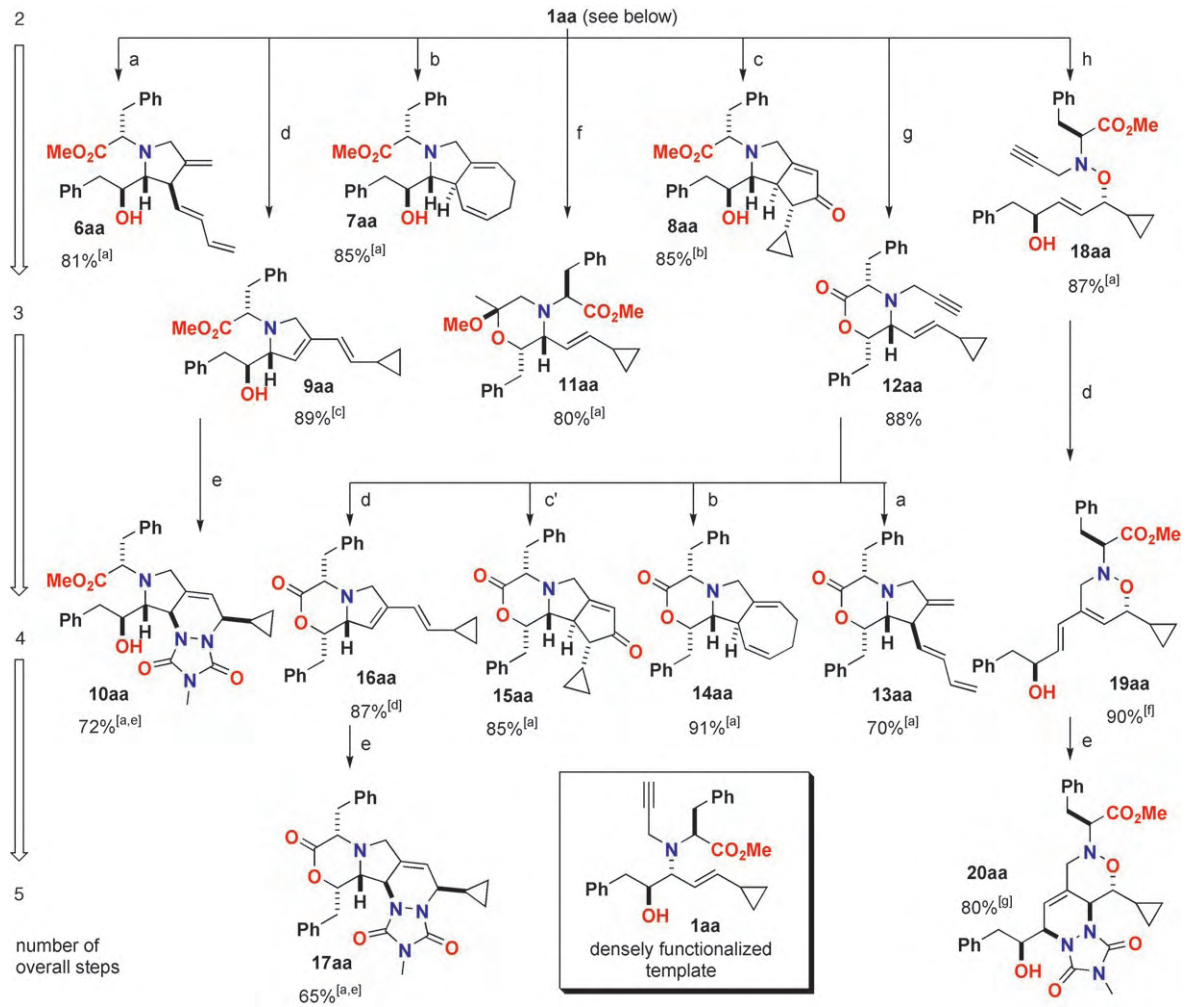

Scheme 3. a) $[Pd(PPh_3)_2(OAc)_2]$ (10 mol%), benzene, 80°C; b) $[CpRu(CH_3CN)_3PF_6]$ (10 mol%), acetone, RT; c') $[Co_2(CO)_8]$, trimethylamine *N*-oxide, NH_4Cl (for conditions c), benzene, RT; d) Hoveyda–Grubbs second-generation catalyst (10 mol%), CH_2Cl_2, reflux; e) 4-methyl-1,2,4-triazoline-3,5-dione, CH_2Cl_2, RT; f) $NaAuCl_4$ (10 mol%), MeOH, RT; g) NaH, toluene, RT; h) *m*CPBA, THF, −78→0°C. [a] Single diastereomer; [b] >10:1 d.r.; [c] *trans*/*cis* = 6.7:1; [d] *trans*/*cis* = 6.4:1; [e] from *trans* diene; [f] *trans*/*cis* = 3:1; [g] combined yield from the *trans* and *cis* dienes. *m*CPBA = *m*-chloroperbenzoic acid.

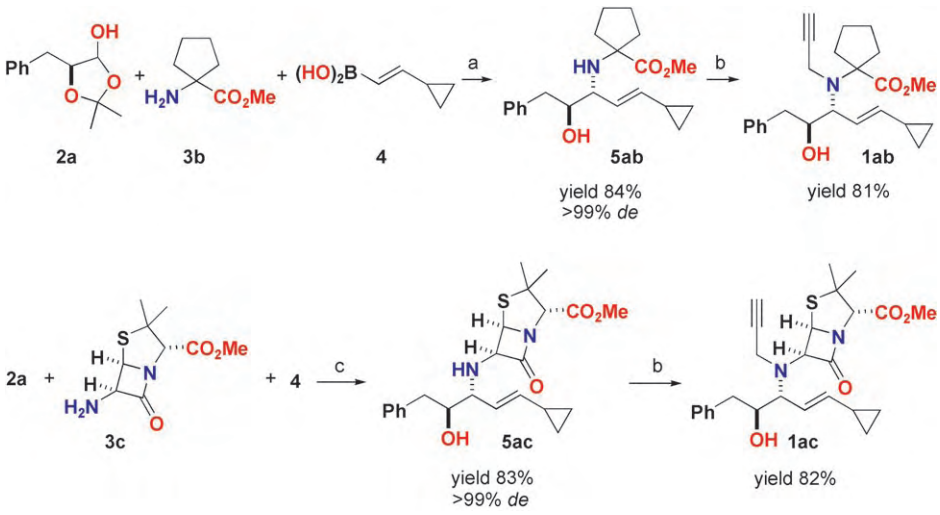

Scheme 4. a) CH_2Cl_2/1,1,1,3,3,3-hexafluoroisopropanol = 9:1, RT; b) propargyl bromide, $NaHCO_3$, DMF, 70°C; c) EtOH/1,1,1,3,3,3-hexafluoroisopropanol (9:1), RT.

ing.[11] Small molecules prepared by this pathway are being included in a public effort to assess comparatively the role of structural features in assay measurements.[12] Such studies are hoped to illuminate the variation of assay outcomes that result from small molecules distinct in both their origins (natural and non-natural) and structural features.

Received: February 7, 2006
Published online: April 28, 2006

Keywords: amino alcohols · diversity-oriented synthesis · multicomponent reactions · Petasis reaction · synthesis design

 © 2006 Wiley-VCH Verlag GmbH & Co. KGaA, Weinheim

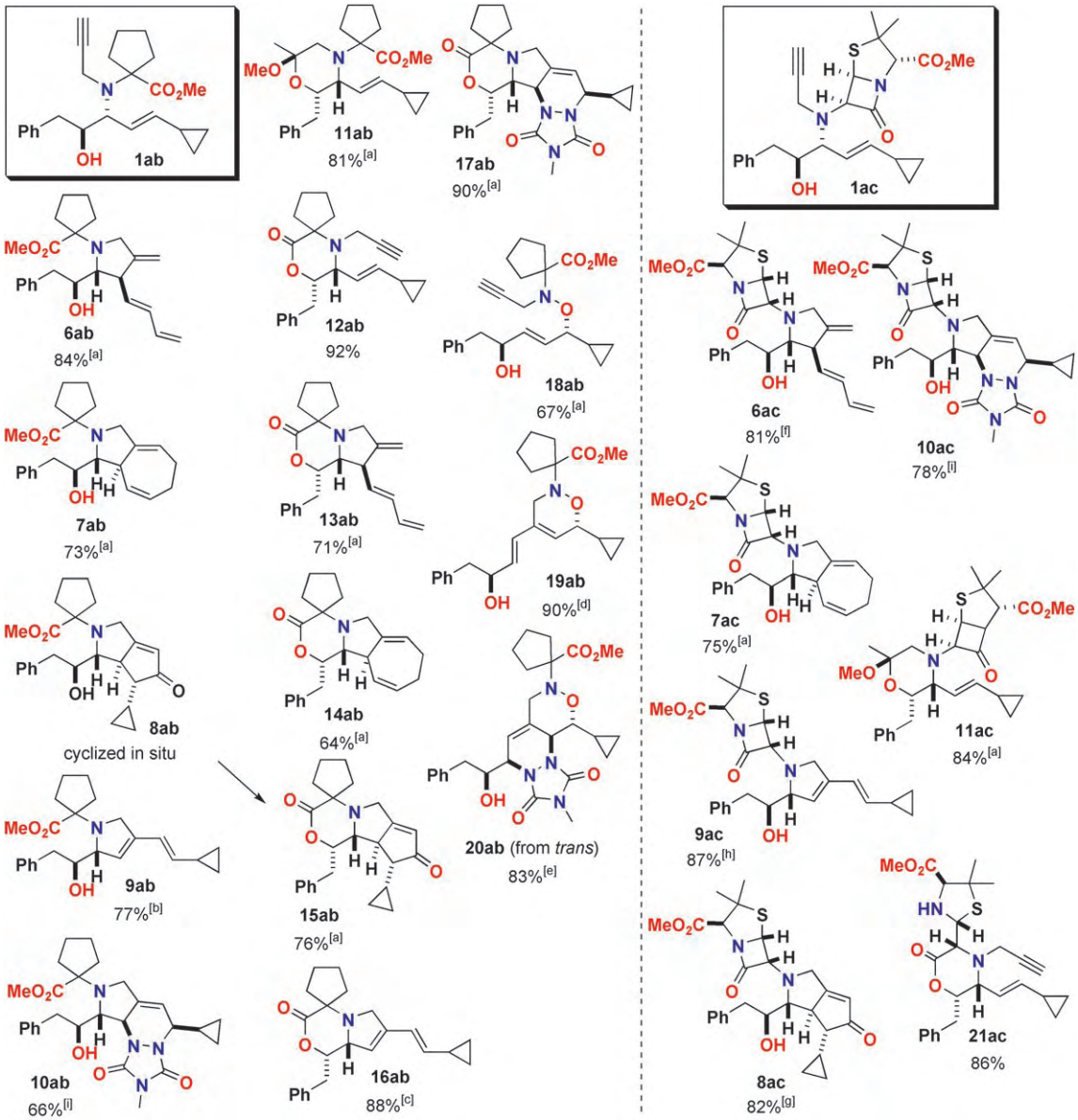

Scheme 5. [a] Obtained as a single diastereomer; [b] *trans*/*cis* = 3:1; [c] *trans*/*cis* > 13:1; [d] *trans*/*cis* = 5:1; [e] combined yield from the *cis* and *trans* dienes; [f] 3:1 d.r.; [g] > 12:1 d.r.; [h] *trans*/*cis* = 5.6:1; [i] from the *trans* diene.

[1] S. L. Schreiber, *Chem. Eng. News* **2003**, *81*, 51.

[2] R. L. Strausberg, S. L. Schreiber, *Science* **2003**, *300*, 294.

[3] a) N. A. Petasis, I. A. Zavialov, *J. Am. Chem. Soc.* **1997**, *119*, 445; b) N. A. Petasis, I. A. Zavialov, *J. Am. Chem. Soc.* **1998**, *120*, 11798.

[4] The structures and stereochemistry of all the reported compounds were determined by detailed spectroscopic analyses, including an X-ray structure of a diastereomer of **10aa** prepared from **5ba** (see the Supporting Information).

[5] For a review of cycloisomerization of 1,6-enynes, see: a) B. M. Trost, M. J. Krische, *Synlett* **1998**, 1; b) C. Aubert, O. Buisine, M. Malacria, *Chem. Rev.* **2002**, *102*, 813; c) G. C. Lloyd-Jones, *Org. Biomol. Chem.* **2003**, *1*, 215.

[6] a) B. M. Trost, F. D. Toste, H. Shen, *J. Am. Chem. Soc.* **2000**, *122*, 2379; for pioneering studies of [5+2] cycloadditions, see: b) P. A. Wender, H. Takahashi, B. Witulski, *J. Am. Chem. Soc.* **1995**, *117*, 4720.

[7] a) I. U. Khand, G. R. Knox, P. L. Pauson, *J. Chem. Soc. Perkin Trans. 1* **1977**, 977; b) P. L. Pauson, *Tetrahedron* **1985**, *41*, 5855; c) S. Shambayati, W. E. Crowe, S. L. Schreiber, *Tetrahedron Lett.* **1990**, *31*, 5289.

[8] S. B. Garber, J. S. Kingsbury, B. L. Gray, A. H. Hoveyda, *J. Am. Chem. Soc.* **2000**, *122*, 8168.

[9] Y. Fukuda, K. Utimoto, *J. Org. Chem.* **1991**, *56*, 3729.

[10] K. K. Nanda, B. W. Trotter, *Tetrahedron Lett.* **2005**, *46*, 2025.

[11] P. A. Clemons, unpublished results; such signatures reflect both the activity and selectivity of these compounds in a panel of 16 cell-based assays. These preliminaries studies follow the concepts reported in: Y.-K. Kim, M. A. Arai, T. Arai, J. O. Lamenzo, E. F. Dean III, N. Patterson, P. A. Clemons, S. L. Schreiber, *J. Am. Chem. Soc.* **2004**, *126*, 14740–14745.

[12] This public effort ("The Forma Project") is sponsored by the NCI Initiative for Chemical Genetics, see: http://www.broad.harvard.edu/chembio; all assay measurements will be made publicly available in ChemBank.[2]

 © 2006 Wiley-VCH Verlag GmbH & Co. KGaA, Weinheim

Porphyrins

DOI: 10.1002/anie.200600554

Controlled Self-Assembly Behavior of an Amphiphilic Bisporphyrin–Bipyridinium–Palladium Complex: From Multibilayer Vesicles to Hollow Capsules**

Yongjun Li, Xiaofang Li, Yuliang Li, Huibiao Liu, Shu Wang, Haiyang Gan, Junbo Li, Ning Wang, Xiaorong He, and Daoben Zhu**

The construction of supramolecular assemblies with well-defined nano-structures is of great interest owing to their potential applications in diverse fields such as molecular electronics, light-energy conversion, and catalysis.[1,2] The ability to control the specific shapes, dimensions, and pattern formation of supramolecular organization by nonconvalent interactions is still a challenging task in the materials field.[3] Nanoscale hollow capsules represent an important class of materials because their unique structural, optical, and surface properties may lead to a wide range of applications, such as capsule agents for drug delivery, filters, coatings, chemical catalysis, or templates for functional architectural composite materials.[4] Various efforts have been made to prepare inorganic[5] and organic[6] hollow capsules. Hollow polymer spheres were produced by McDonald et al. through the encapsulation of hydrocarbon solvents within polymer particles during an emulsion polymerization.[7] C_{60}-derived amphiphiles have a tendency to form closed submicrospheres with a bilayer shell below the critical aggregation concentration and multibilayer vesicles above the critical aggregation concentration.[8] Meanwhile, 1D nanotubes and nanowires have attracted much attention because of their unique optical, electronic, and mechanical properties, which result in promising applications in electrical and optoelectronic nanodevices.[9]

Porphyrins have remarkable photo-, catalytic-, electro-, and biochemical properties, and so the self-assembly of porphyrin derivatives has attracted considerable attention in recent years.[10,11] The introduction of molecular recognition motifs into the porphyrin building blocks, such as hydrogen bonding, π-π stacking, electrostatic interactions, and metal–ligand bonds offers an easy way to access well-defined arrays such as fibers, sheets, grids, cubes, wheels, and rings.[12–14] Amphiphilic porphyrins have been exploited in the preparation of simple micelles,[15] fibers,[16] and vesicles.[17] Their optoelectronic features are strictly related to their aggregation states and strongly depend on the microstructural environment.[18]

Herein, we describe the aggregation behavior of a new zinc porphyrin derivative **1** (Scheme 1) in which two zinc porphyrins were attached to the 4,4′-position of the 2,2′-bipyridyl group, and the 2,2′-bipyridine (bpy) was complexed with palladium (II) dichloride. The precursor of **1**, bpy–ZnP, has one structural feature: the two porphyrin units can rotate freely around the central bipyridine bond and as such, the relative position of two porphyrins can be controlled by the addition/elimination equilibrium of metal ions.[19] Bipyridyl groups are strong ligands for various transition metal ions, **1** is an amphiphile because the bipyridine–$PdCl_2$ units exhibit hydrophilic properties and the porphyrin units show hydrophobic interactions under specific solvent environments.[20,21]

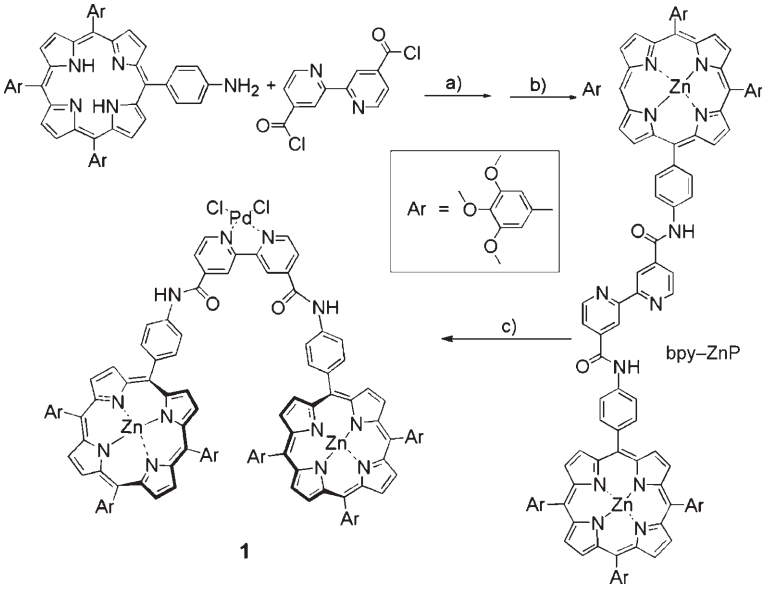

Scheme 1. Synthesis of bpy–ZnP and **1**. a) toluene/pyridine, RT, 60%; b) $Zn(OAc)_2$/CH_3OH, $CHCl_3$, 98%; c) $PdCl_2(CH_3CN)_2$, $CHCl_3/CH_3CN$.

Compound **1** was synthesized according to Scheme 1. Characterization was performed through NMR spectroscopy and MALDI-TOF MS. The MALDI-TOF mass spectra of **1** exhibited two signals that could be assigned as [M−2Cl] and [M−$PdCl_2$].

Although the growth of a single crystal from bpy–ZnP in different solvents was not successful, we succeeded in growing the single crystal of the bpy–ZnP–pyridine complex in *n*-hexane (the crystal data are shown in the Supporting Information). The single-crystal X-ray structure analysis showed that the porphyrin rings are distorted. Each zinc

[*] Y. J. Li, Dr. X. F. Li, Prof. Y. L. Li, Dr. H. B. Liu, Prof. S. Wang, H. Y. Gan, J. Li, N. Wang, X. R. He, Prof. D. B. Zhu
CAS Key Laboratory of Organic Solids
Institute of Chemistry
Chinese Academy of Sciences
Beijing 100080 (P.R. China)
Fax: (+86) 10-8261-6576
E-mail: ylli@iccas.ac.cn
zhudb@iccas.ac.cn

[**] This work was supported by the National Natural Science Foundation of China (20531060, 10474101, 20418001, 20571078, and 20421101), and the Major State Basic Research Development Program (2005CB623602). This project is partly supported by National Center for Nanoscience and Technology, China.

Supporting information for this article is available on the WWW under http://www.angewandte.org or from the author.

© 2006 Wiley-VCH Verlag GmbH & Co. KGaA, Weinheim

porphyrin coordinates with one pyridine molecule that alternates above and below the plane (Figure 1). The distance between the nitrogen atom with the coordinated pyridine and the zinc atom is 2.113 Å. The two nitrogen atoms of bipyridine

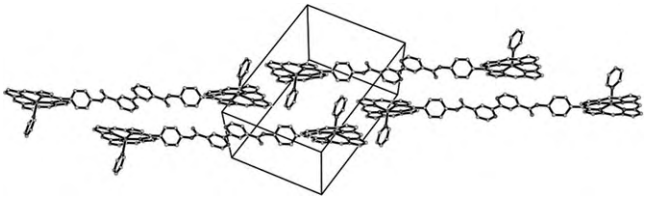

Figure 1. Crystal structure of the bpy–ZnP–pyridine complex. Hydrogen atoms, 3,4,5-trimethoxyphenyl, and solvent molecules are omitted for clarity.

face in the opposite direction, whereas the bipyridine and two amides are nearly planar (the mean deviation from the plane is 0.0321). The two benzene rings connecting the porphyrin and the amide are parallel (the dihedral angel is 0°). The dihedral angel between these benzene rings and the bipyridine plane is 30.1°. From the crystal-packing mode of the bpy–ZnP–pyridine complex, we can see that the bipyridine of one molecule overlaps with the porphyrin part of another molecule.

The growth of a single crystal of **1** in a variety of different solvents was not successful. Computer simulations were used to gain insight into the structure.[6a] The simulation results indicated that bpy–ZnP showed linear conformers similar to the X-ray crystal structure, which indicated that this simulation method was fit for our porphyrin dimer system. The simulation results showed that **1** was a V-shaped structure (Figure 2), which was confirmed by NMR spectroscopic-titration experiments. After the addition of 2.2 equivalents of $[PdCl_2(CH_3CN)_2]$, palladium complex **1** was completely formed along with the $[PdCl_2(pyridine)_2]$ complex.[19] The large downfield shift of 1-H (+1.5 ppm) reflected the development of a $\delta+$ charge upon complexation with $PdCl_2$. The most-sensitive shielding effect of the porphyrin-ring current appeared at the *meso* phenyl groups. According to symmetry, there were two sets of *meso* phenyl groups in bpy–ZnP, namely, four 3,4,5-trimethoxyphenyl groups adjacent to, and two opposite to the bipyridyl groups. Before complexation, these groups were not distinguishable from one another in the ^{1}H NMR spectrum because of free and rapid rotation around the bond connecting the two pyridyl units. Thus, the protons of the *meso* phenyl groups (*meso*-Ph-H) appeared as a single peak near $\delta = 7.4$ ppm; the *para*-methoxy and *meta*-methoxy groups in these *meso* phenyl groups appeared as a single peak near $\delta = 4.06$ and 3.89 ppm, respectively. When palladium complex **1** was formed, each of the single peaks split into a doublet. Peak separations between the *meso*-Ph-H as well as between the methoxy groups in the two sets of *meso* phenyl groups became detectable owing to differences in the distances from the facing porphyrin plane. These results showed that the addition of 2.2 equivalents of Pd^{II} completely converted the

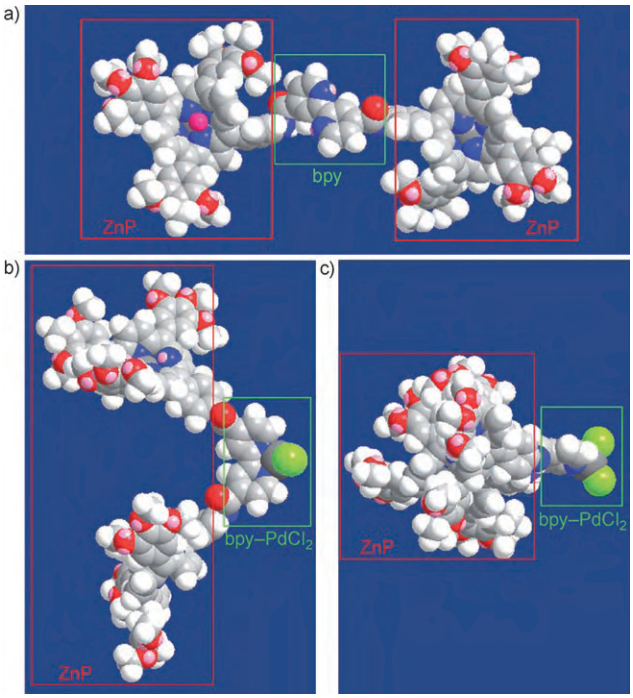

Figure 2. Space-filling models of bpy–ZnP from a top view (a), and a top view (b) and side view (c) of complex **1**. The MM2 force field was used to calculate the minimium-energy conformation.

bpy–ZnP from a freely rotating conformation to a cofacial V-shaped one.

The aggregation behavior of **1** was subsequently studied by injecting a solution of **1** in $CHCl_3$ (at a concentration of 1×10^{-4} M) into CH_3OH to give a final chloroform/methanol ratio of 1:1 (*v*/*v*). After the solution was allowed to equilibrate over one day, one drop of the solution was evaporated on silicon slides to observe the aggregate behavior in the solid state. The morphology of molecule **1** on the substrate was examined by scanning electron microscopy (SEM; Figure 3). In SEM images, spherical particles with a uniform diameter of about 200 nm were observed. Energy-dispersive X-ray spectroscopy (EDX) indicated the presence of C, N, O, Cl, Pd, and Zn, and the atom ratio of Cl/Pd/Zn was about 2:1:2. The majority of the spherical particles were larger than the typical micelle size of 20–30 nm in diameter as they were derived from small molecular amphiphiles.[22] A few of the particles started to form opening holes on their surfaces, which showed that they had a hollow interior. To confirm this possibility and substantiate whether these vesicles are hollow in nature, the perfect spherical vesicles (Figure 3a) prepared at a 5.0×10^{-5} M were subjected to heat treatment for one hour (heating pattern I). This then allowed us to see that the holes were formed on the particles surface (Figure 3b); one example of the typical open vesicles is shown in the inset of Figure 3b. TEM images also showed that some capsulelike structures with holes were formed (Figure 3c). According to the irregularity of the size and shape of the hole and the location of defective sites at the surface, we suggested that these holes are not a result of the density–gradient image of the spherical

 © 2006 Wiley-VCH Verlag GmbH & Co. KGaA, Weinheim

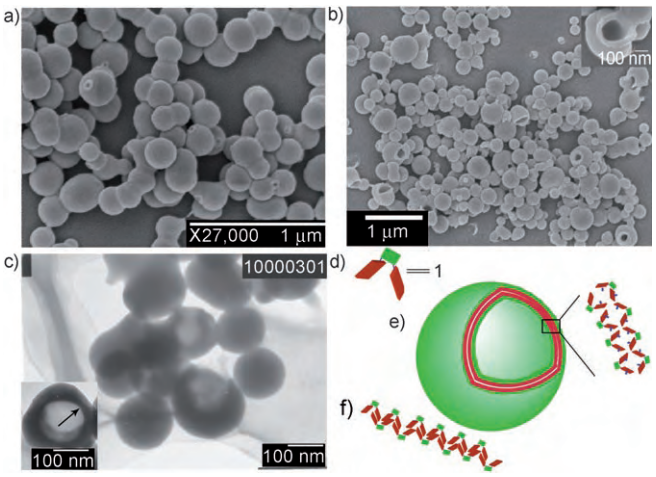

Figure 3. a) SEM of **1** derived vesicles prepared in $CHCl_3/CH_3OH$ (1:1) at room temperature. b) SEM and c) TEM of compound **1** vesicles derived from the heat treatment (pattern I at 70 °C) of the vesicles prepared as in a). The inset of b) shows a close up of a vesicle, and the inset of c) shows the membrane thickness, indicated by arrows. d) Schematic representation of compound **1**. e) Schematic representation of a compound **1** vesicle formed in methanol with a close up of the vesicle membrane showing the proposed multibilayer structure. The blue dots represent the ligated CH_3OH. f) Schematic representation of an interdigitated bilayer structure.

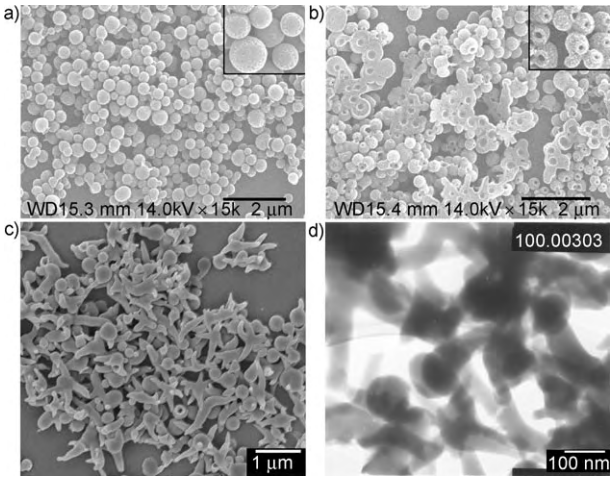

Figure 4. Morphology transition of the vesicle heated a) at 60 °C for 0.5 h (inset 2.6× enlargement), b) at 80 °C for 0.5 h (inset 2.6× enlargement), and wormlike aggregates of **1** derived from the heat treatment (heating pattern II) of the vesicles prepared as Figure 3 a, c) SEM and d) TEM.

vesicles.[22] The edge of these holes should be measurable to reveal the thickness of the vesicle shell. As shown in the inset of Figure 3 c, we found that the morphology of the slightly "tilted" shell membrane on the top was surrounded by a dark ring area with an irregular wall width and shape. Measuring the membrane-wall thickness at the tilted-membrane site (perpendicular to the view as marked by the arrow) gave an edge width of about 15–20 nm. These distances across the membrane wall fit approximately with 2–3 bilayers with a molecular dimension of 12–18 nm, estimated by the 3D molecular structural modeling of **1.** These results indicate that the most likely membrane structure of the hollow spherical vesicles in methanol was a shell-like complex multilayer structure resembling that of a liposome at the vesicle surface (Figure 3 c). Our vesicles were very stable on the solid surface, even when heated at 50–60 °C (Figure 4 a) or stored for 12 days (see the Supporting Information). Furthermore, they were unlike other vesicles that showed an immediate collapse on solid surfaces;[23] dried samples of egg-yolk lecithin vesicles showed only planar circles and bolaamphiphile vesicles crystallized quickly upon drying to form circular platelets of double-layer thickness.[24]

Figure 4 and the Supporting Information show SEM images of the vesicles on a silica slide after heating at different temperatures for 0.5 h and then cooling to room temperature. The volume of encapsulated methanol expanded when the vesicles were heated at 40 °C (lower than the boiling point of methanol) and as such, the methanol that flowed from the aperture of the membrane couldn't evaporate quickly. The nearby molecules then flowed with the methanol and formed the "tail" morphology. "Tails" located close to each other could fuse together during this process. When the vesicles were heated at 50–60 °C, the methanol escaped and evaporated quickly from the aperture of the membrane without resulting in obvious changes in morphology. However, when heated at 70–80 °C (higher than the boiling point of methanol), the evaporating methanol bumped and the gas broke quickly through the membrane. This resulted in deformation and the hollow spherical vesicles were formed. When heated at 90 °C for 0.5 h, in addition to the escape of methanol (some hollow capsules were visible), the molecular motion of **1** was excited and rearrangement was achieved during the cooling process. Some fused vesicles were found in which the hollow capsules were empty. Although heated with pattern II, a wormlike morphology was observed by using SEM as shown in Figure 4 c, and TEM images (Figure 4 d) also confirmed the wormlike structure. These results indicated that heating temperature and pattern are able to control the rate of methanol release and lead to a controllable process for producing hollow capsules and wormlike structures from these vesicles.

The UV/Vis spectra of the aggregated species were significantly different from that of the corresponding porphyrin solutions. The absorption spectra of the films resulting from a chloroform/methanol mixture (*v*/*v*, 1:1) are shown in Figure 5. Together with the expected bands at 440 nm and the Q bands in the range from 500–700 nm, there was one additional band at 680 nm. Both the Soret and Q absorption bands of the films were broadened and red shifted when compared with the organic solution phase. These vesicular supramolecular structures suggest "J-type" (edge-to-edge) interaction in the vesicles.[21,25]

In selective solvents, block copolymer systems or amphiphilic molecules like liposomes form micellar or vesicular supramolecular structures that would normally belong to the superstrong segregation limit (SSSL). This is mainly owing to

 © 2006 Wiley-VCH Verlag GmbH & Co. KGaA, Weinheim

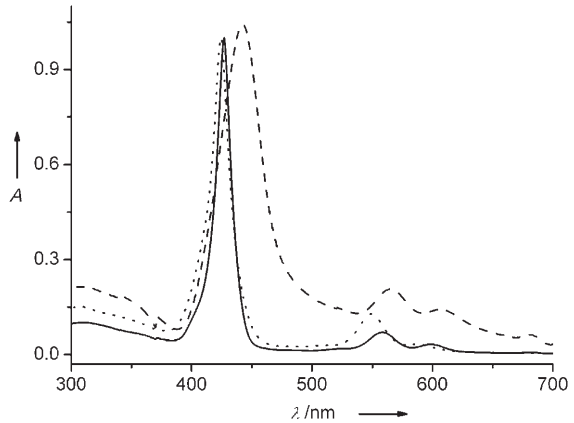

Figure 5. UV/Vis spectra of solutions of **1** in chloroform (dotted line), chloroform/methanol (1:1; solid line), and the film cast from the chloroform/methanol (1:1) solution (dashed line).

the different solubility of the blocks or the hydrophilic and hydrophobic units.[26] For **1**, methanol was a good solvent for the bipyridine–Pd complex unit, but was a poor solvent for the porphyrin moiety. On the contrary, chloroform was a good solvent for porphyrin but not for the bipyridine–Pd complex unit. In this solvent system, **1** became an amphiphilic molecule and could assemble into layered structures that could then close to form vesicles. These two parts should completely segregate in the membrane. Because methanol can coordinate with zinc porphyrin (see the Supporting Information), the amphiphiles self-organize into a bilayer structure (Figure 3e) and the resulting membrane has many little holes owing to the loose packing of porphyrin. With the removal of methanol by heating with pattern II, **1** rearranged into the dense packing and low interfacial free energy interdigitated layer (Figure 3f), which resulted in the worm-like aggregates shown in Figure 4c,d.

In summary, a novel amphiphilic porphyrin derivative composed of two porphyrins connected with 2,2′-bipyridyl group, in which 2,2′-bipyridine was complexed with palladium(II) dichloride, has been synthesized. The crystal structure of the Pd-free porphyrin–bipyridine derivative was obtained. Computer simulations and NMR spectroscopic-titration experiments indicated that the Pd complex showed a V-shaped conformer. A simple and controllable process for producing the hollow capsules from vesicles was described. SEM and TEM imagines confirmed that this molecule is able to self-assemble into vesicles with a diameter of 200 nm in $CHCl_3/CH_3OH$. These vesicles could assemble into hollow capsules and wormlike structure on demand.

Experimental Section

Heat treatment of the samples: Pattern I, the silicon slides containing the samples were placed in a petri dish and the petri dish was heated with water at 40, 50, 60, 70, 80, and 90 °C, for 0.5 h each. Pattern II, the silicon slides containing the samples were placed in a petri dish, which was then set on water at 90 °C and the water was then allowed to cool to room temperature.

SEM images were taken by using a field emission scanning electron microscope (JEOL JSM 6700F and Hitachi S4300) operated at an acceleration voltage of 5–15 kV. TEM images were taken by using a JEOL-100 microscope operated at 50 kV. The samples were prepared by transferring them from the silicon slides by carbon–copper grids dampened with methanol.

Received: February 10, 2006
Revised: March 15, 2006
Published online: April 27, 2006

Keywords: amphiphiles · porphyrinoids · self-assembly · vesicles

[1] a) G. W. Orr, L. J. Barbour, J. L. Atwood, *Science* **1999**, *285*, 1049; b) V. Percec, C.-H. Ahn, G. Ungar, D. J. P. Yeardley, M. Möller, S. S. Sheiko, *Nature* **1998**, *391*, 161; c) J.-M. Lehn, *Angew. Chem.* **1990**, *102*, 1347; *Angew. Chem. Int. Ed. Engl.* **1990**, *29*, 1304; d) A. C. Grimsdale, K. Müllen, *Angew. Chem.* **2005**, *117*, 5732; *Angew. Chem. Int. Ed.* **2005**, *44*, 5592.

[2] a) H. Y. Gan, H. B. Liu, Y. J. Li, et al., *J. Am. Chem. Soc.* **2005**, *127*, 12452; b) Y. Liu, J. P. Zhuang, H. B. Liu, Y. L. Li, F. S. Lu, H. Y. Gan, T. G. Jiu, N. Wang, X. R. He, D. B. Zhu, *ChemPhysChem* **2004**, *5*, 1210.

[3] a) R. Dagani, *Chem. Eng. News* **1998**, *76*(23), 35; b) F. J. M. Hoeben, P. Jonkheijm, E. W. Meijer, A. P. H. J. Schenning, *Chem. Rev.* **2005**, *105*, 1491; c) T. Shimizu, M. Masuda, H. Minamikawa, *Chem. Rev.* **2005**, *105*, 1401.

[4] a) Y. R. Ma, L. M. Qi, J. M. Ma, H. M. Cheng, *Langmuir* **2003**, *19*, 4040; b) C. E. Fowler, D. Khushalani, S. Mann, *Chem. Commun.* **2001**, 2028; c) F. Caruso, *Adv. Mater.* **2001**, *13*, 11.

[5] a) F. Caruso, *Chem. Eur. J.* **2000**, *6*, 413; b) S. Schacht, Q. Huo, I. G. Viogt-Martin, G. D. Stucky, F. Schüth, *Science* **1996**, *273*, 768; c) T. Liu, Y. Xie, B. Chu, *Langmuir* **2000**, *16*, 9015; d) S. H. Yu, H. Cölfen, M. Antonietti, *J. Phys. Chem. B* **2003**, *107*, 7396.

[6] a) M. Yang, W. Wang, F. Yuan, X. Zhang, J. Li, F. Liang, B. He, B. Minch, G. Wegner, *J. Am. Chem. Soc.* **2005**, *127*, 15107; b) S. A. Jenekhe, X. L. Chen, *Science* **1999**, *283*, 372; c) F. Caruso, R. A. Caruso, H. Mohwald, *Science* **1998**, *282*, 1111; d) X. Y. Liu, J.-S. Kim, J. Wu, A. Eisenberg, *Macromolecules* **2005**, *38*, 6749; e) H.-K. Lee, K. M. Park, Y. J. Jeon, D. Kim, D. H. Oh, H. S. Kim, C. K. Park, K. Kim, *J. Am. Chem. Soc.* **2005**, *127*, 5006; f) M. Lee, S.-J. Lee, L.-H. Jiang, *J. Am. Chem. Soc.* **2004**, *126*, 12724; g) D. M. Vriezema, J. Hoogboom, K. Velonia, K. Takazawa, P. C. M. Christianen, J. C. Maan, A. E. Rowan, R. J. M. Nolte, *Angew. Chem.* **2003**, *115*, 796; *Angew. Chem. Int. Ed.* **2003**, *42*, 772.

[7] C. J. McDonald, K. J. Bouck, A. B. Chaput, C. J. Stevens, *Macromolecules* **2000**, *33*, 1593.

[8] a) M. Sano, K. Oishi, T. Ishi-i, S. Shinkai, *Langmuir* **2000**, *16*, 3773; b) C. Burger, J. Hao, Q. Ying, H. Isobe, M. Sawamura, E. Nakamura, B. Chu, *J. Colloid Interface Sci.* **2004**, *275*, 632; c) S. Zhou, C. Burger, B. Chu, M. Sawamura, N. Nagahama, M. Toganoh, U. E. Hackler, H. Isobe, E. Nakamura, *Science* **2001**, *291*, 1944.

[9] a) S. Iijima, *Nature* **1991**, *354*, 56; b) C. R. Martin, *Science* **1994**, *266*, 1961; c) C. G. Wu, T. Bein, *Science* **1994**, *264*, 1757; d) A. M. Morales, C. M. Lieber, *Science* **1998**, *279*, 208.

[10] J.-C. Chambron, V. Heitz, J.-P. Sauvage in *The Porphyrin Handbook*, *Vol. 6* (Eds.: K. M. Kadish, K. M. Smith, R. Guilard), Academic Press, New York, **2000**, p. 1.

[11] a) T. S. Balaban, R. Goddard, M. Linke-Schaetzel, J.-M. Lehn, *J. Am. Chem. Soc.* **2003**, *125*, 4233; b) M. Grätzel, *Nature* **2001**, *414*, 338; c) J. Duschl, M. Michl, W. Kunz, *Angew. Chem.* **2004**, *116*, 644; *Angew. Chem. Int. Ed.* **2004**, *43*, 634.

 © 2006 Wiley-VCH Verlag GmbH & Co. KGaA, Weinheim

[12] a) S. Lehninger, B. Oleyunk, J. P. Stang, *Chem. Rev.* **2000**, *100*, 853; b) C. Mak, N. Bampos, S. L. Darling, M. Montali, L. Prodi, J. K. M. Sanders, *J. Org. Chem.* **2001**, *66*, 4476; c) A. Klyszez, M. Lauer, M. Kopaczynska, C. Bottcher, F. Gonzaga, J. H. Fuhrhop, *Chem. Commun.* **2004**, 2358.
[13] a) S.-I. Tamaru, M. Nakamura, M. Takeuchi, S. Shinkai, *Org. Lett.* **2001**, *3*, 3631; b) J. M. Ribo, J. Crusats, F. Sagues, J. Claret, R. Rubires, *Science* **2001**, *292*, 2063.
[14] P. H. J. Schenning, F. B. G. Benneker, H. P. M. Geurts, X. Y. Liu, R. J. M. Nolte, *J. Am. Chem. Soc.* **1996**, *118*, 8549.
[15] R. Guilard, N. Senglet, Y. H. Liu, D. Sazou, E. Findsen, D. Faure, T. Des Courieres, K. M. Kadish, *Inorg. Chem.* **1991**, *30*, 1898.
[16] a) S-i. Kawano, S-i. Tamaru, N. Fujita, S. Shinkai, *Chem. Eur. J.* **2004**, *10*, 343; b) S-i. Tamaru, M. Takeuchi, M. Sano, S. Shinkai, *Angew. Chem.* **2002**, *114*, 881; *Angew. Chem. Int. Ed.* **2002**, *41*, 853.
[17] a) T. Komatsu, E. Tsuchida, C. Bottcher, D. Donner, C. Messerschmidt, U. Siggel, W. Stocker, J. P. Rabe, J.-H. Fuhrhop, *J. Am. Chem. Soc.* **1997**, *119*, 11660; b) R. Charvet, D. L. Jiang, T. Aida, *Chem. Commun.* **2004**, 2664.
[18] W. I. White in *The Porphyrin*, *Vol. 5s* (Ed.: D. Dolphin), Academic Press, New York, **1978**, chap. 7.
[19] Y. Tomohiro, A. Satake, Y. Kobuke, *J. Org. Chem.* **2001**, *66*, 8442.
[20] N. C. Maiti, S. Mazumdar, N. Periasamy, *J. Phys. Chem. B* **1998**, *102*, 1528.
[21] X. Gong, T. Milic, C. Xu, J. D. Batteas, C. M. Drain, *J. Am. Chem. Soc.* **2002**, *124*, 14290.
[22] S. Verma, T. Hauck, M. E. El-Khouly, P. A. Padmawar, T. Canteenwala, K. Pritzker, O. Ito, L. Y. Chiang, *Langmuir* **2005**, *21*, 3267.
[23] J. Rädler, M. Radmacher, E. Gaub, *Langmuir* **1994**, *10*, 3111.
[24] J.-H. Fuhrhop, H.-H. David, J. Mathieu, U. Liman, H.-J. Winter, E. Boekema, *J. Am. Chem. Soc.* **1986**, *108*, 1785.
[25] R. Purrello, L. M. Scolaro, E. Bellacchio, S. Gurrieri, A. Romeo, *Inorg. Chem.* **1998**, *37*, 3647.
[26] M. Antonietti, S. Förster, *Adv. Mater.* **2003**, *15*, 1323.

 © 2006 Wiley-VCH Verlag GmbH & Co. KGaA, Weinheim

Molecular Tubes

DOI: 10.1002/anie.200504499

Cyclophanes within Cyclophanes: The Synthesis of a Pyromellitic Diimide-Based Macrocycle as a Structural Unit in a Molecular Tube and Its Inclusion Phenomena**

*Tetsuo Iwanaga, Ryoma Nakamoto, Mikio Yasutake, Hiroyuki Takemura, Katsuya Sako, and Teruo Shinmyozu**

Since the discovery of multi-walled[1] and single-walled[2] carbon nanotubes (SWNTs) by Iijima and Ichihashi, there has been growing interest in the properties of the empty cylindrical space of tubular molecules in which the encapsulation of atoms or molecules is expected.[3] In fact, this space in SWNTs not only allows for inclusion[4–7] but is also a suitable site for chemical reactions.[6a,7]

We are interested in the inclusion phenomena of tubes, as represented by SWNTs, and planned to synthesize artificial molecular tubes with definite molecular weights and a reasonable solubility in organic solvents. Various kinds of other artificial nanotubes are known, for example nanotubes that self-assemble via hydrogen bonds of cyclic peptides,[8] lipid nanotubes,[9] dendrimer-based tubes,[10] covalently linked polymeric α-cyclodextrin (CD) tubes,[11] and calixarene-based tubes,[12] as well as tubes formed by metal coordination.[13]

[*] T. Iwanaga, R. Nakamoto, Prof. Dr. T. Shinmyozu
Institute for Materials Chemistry and Engineering (IMCE) and
Department of Molecular Chemistry
Graduate School of Sciences
Kyushu University
Hakozaki 6-10-1, Higashi-ku, Fukuoka 812-8581 (Japan)
Fax: (+81) 92-642-2735
E-mail: shinmyo@ms.ifoc.kyushu-u.ac.jp
Dr. H. Takemura
Department of Chemistry
Faculty of Science
Kyushu University
Ropponmatsu 4-2-1, Chuo-ku, Fukuoka 810-8560 (Japan)
Dr. M. Yasutake
Department of Applied Chemistry
Faculty of Engineering
Saitama University
Shimo-okubo 255, Saitama 338-8570 (Japan)
Prof. Dr. K. Sako
Department of Systems Management and Engineering
Nagoya Institute of Technology
Gokiso, Showa-ku, Nagoya 406-8555 (Japan)

[**] Molecular Tubes and Capsules, Part 1. We gratefully acknowledge the financial support by a Theme Project of Molecular Architecture of Organic Compounds for Functional Design (Prof. Tahsin J. Chow) from the Institute of Chemistry, Academia Sinica, Taiwan R.O.C. We are also grateful for partial financial support by the Joint Project of Chemical Synthesis Core Research Institutions, Research and Education for Inter-University Research Project, MEXT, Japan.

Supporting Information for this article is available on the WWW under http://www.angewandte.org or from the author.

© 2006 Wiley-VCH Verlag GmbH & Co. KGaA, Weinheim

We designed the diameter of the tubes to be 1–5 nm, which is adequate for the inclusion of organic molecules. For the construction of the molecular tubes, we first synthesized a cyclophane that can form inclusion compounds with organic guests as a structural unit. We chose a pyromellitic diimide moiety for the skeleton of the structural units because it has four connecting sites: two nitrogen atoms for the construction of the cyclophanes, and two carbon atoms in *para* position at the benzene ring for the connection of the cyclophanes. Pyromellitic diimide is a π-electron acceptor; therefore the selective inclusion of an electron-rich guest due to a charge-transfer (CT) interaction[14] is expected for pyromellitic diimide-based cyclophanes.[14–16] Furthermore, the photophysical and redox properties of pyromellitic diimide are also interesting,[17] and the carbonyl oxygen atoms of the pyromellitic diimide moiety may serve as hydrogen acceptors in the formation of supramolecules. We planned to synthesize molecular tubes by connecting a cap molecule to a functionalized cyclophane, followed by stepwise connection of the resultant capsule to another cyclophane (Scheme 1). We describe here the successful synthesis of the novel pyromellitic diimide-based cyclophane **1** as a structural unit of the molecular tube, as well as its very interesting inclusion properties.

The pyromellitic diimide-based cyclophanes have a rigid structure and take advantage of the CT interaction as a driving force for the inclusion of the guests. We synthesized them by a dehydration reaction between an amine and an anhydride.[14,15] The coupling reaction was accomplished under pseudo-high-dilution conditions to obtain the macrocyclic 3:3 (amine/anhydride) oligomer **1** as the major product, along with the 4:4 (**2**) and 5:5 macrocycles (**3**; see the Experimental Section and Scheme 2). The ^{1}H NMR spectrum of **1** is very similar to those of the higher cyclic oligomers **2** and **3**, where the singlet for the aromatic protons indicates that each aromatic ring rotates freely at room temperature.

The cyclophane **1** was recrystallized from CH_2Cl_2/*p*-xylene to produce the inclusion complex (*p*-xylene)$_2$@**1** as yellow crystals; its structure in the solid state is shown in Figure 1.[18] The host **1** has a triangular shape with the angle N(imide)–C(CH_2)–C(Ar) being 112.5–115.3°. The ring size defined by the distance between the center of the mean plane

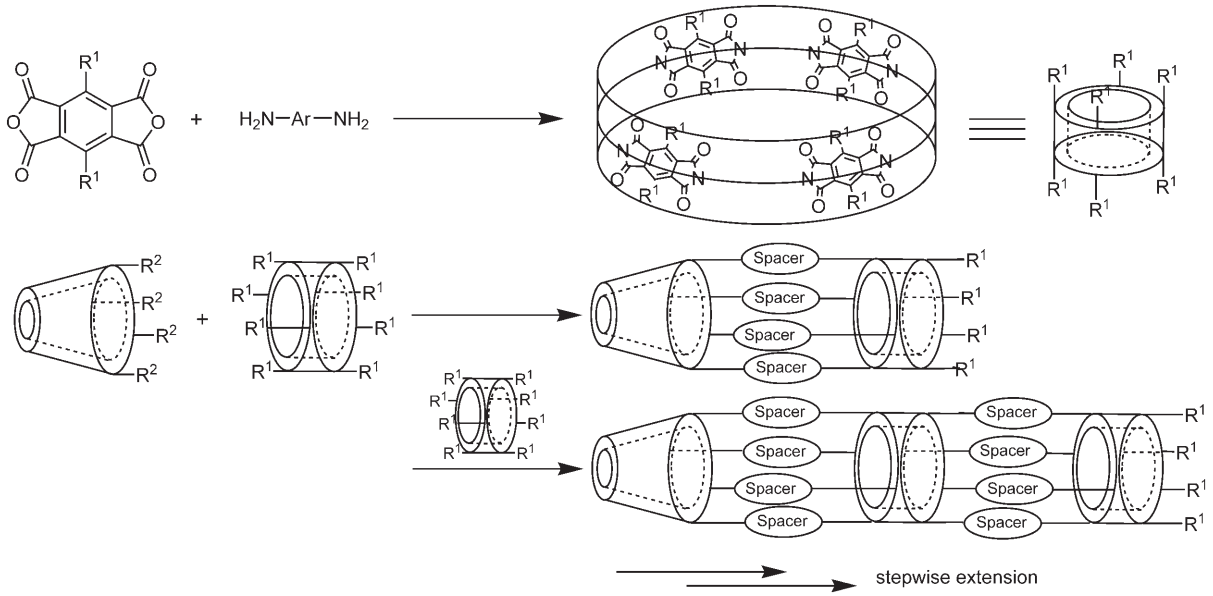

Scheme 1. A synthetic strategy towards a molecular tube.

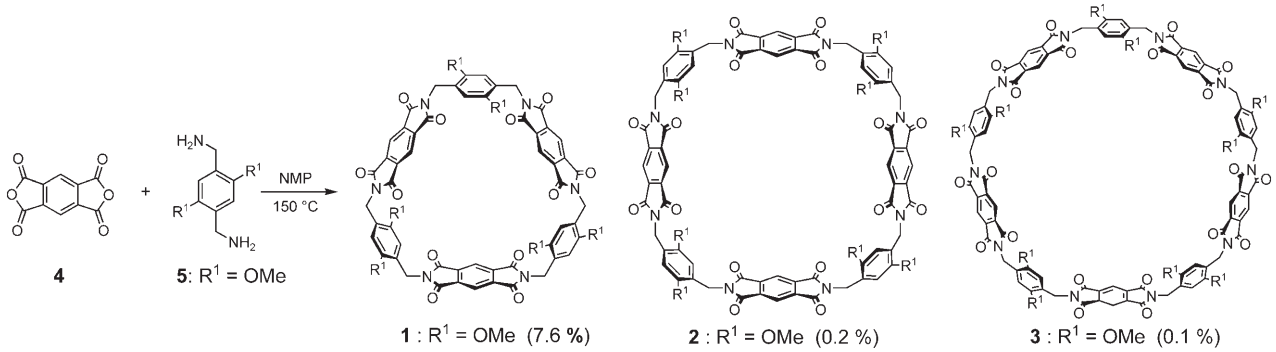

Scheme 2. Synthesis of the novel pyromellitic diimide-based host molecules **1**–**3** from pyromellitic dianhydride (**4**) and 1,4-bis(aminomethyl)-2,5-dimethoxybenzene (**5**, R^1 = OMe). NMP = *N*-methyl-2-pyrrolidone.

 © 2006 Wiley-VCH Verlag GmbH & Co. KGaA, Weinheim

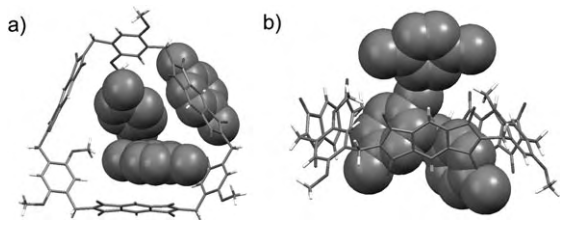

Figure 1. Structure of the complex (*p*-xylene)$_2$@**1** in the solid state at −150 °C: a) top view; b) side view. *p*-Xylene hydrogen atoms have been omitted for clarity.

of the imide benzene ring and the facing dimethoxybenzene ring is 1.2–1.3 nm. In the relatively large cavity, one of the two *p*-xylenes is almost parallel to the associated pyromellitic diimide moiety, at a distance of about 3.58 Å, which suggests the presence of a weak intermolecular CT interaction. In the crystal-packing diagram of (*p*-xylene)$_2$@**1** (Figure 2), the host

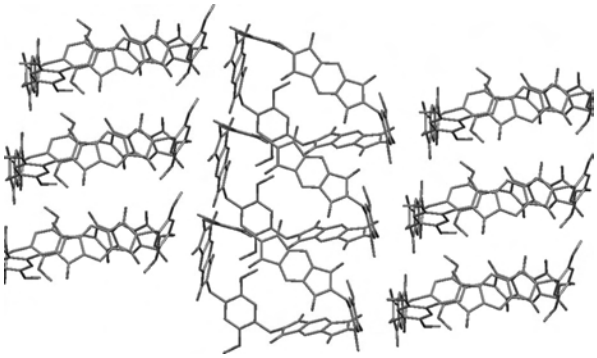

Figure 2. View of the nanotubular organization of (*p*-xylene)$_2$@**1** at −150 °C along the channel axis. The solvent molecules and hydrogen atoms have been omitted for clarity.

1 stacks regularly to form a tubular structure in which two types of *p*-xylene molecules are aligned. When toluene is used in place of *p*-xylene during the crystallization, the complex (toluene)$_3$@**1** is formed (Figure S10 in the Supporting Information). Formation of organic nanotubes in the solid state by hydrogen bonding[8,19] and chalcogen–chalcogen interactions[20] have been reported.

More importantly, a guest molecule is arranged in a parallel fashion with the benzene ring of the facing pyromellitic diimide moiety in the crystal structure of (*p*-xylene)$_2$@**1** and (toluene)$_3$@**1**, which suggests the importance of a CT-type π–π interaction for the inclusion of guest molecules. In sharp contrast, zigzag crystal packing is observed for (CHCl$_3$)$_4$@**1** (Figures S11 and S12). These results indicate that the crystal packing of **1** can be controlled by changing the guest molecules.

In order to maximize the interaction between the electron-deficient host **1** and electron-rich guests, we examined various π-donating cyclophanes[21] with triangular shapes as potential guests by the ^{1}H NMR titration technique; only [2^3]PCP (**6**) interacts to some extent with the host **1** (Scheme 3). In the ^{1}H NMR spectra of a 1:1 mixture of **1** and **6** in CDCl$_3$ (Figure S13), both the aromatic and benzylic

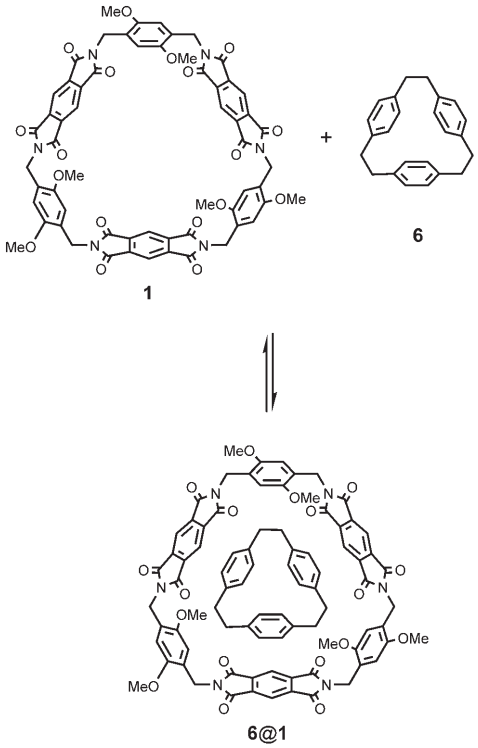

Scheme 3. Formation of **6@1** in CDCl$_3$ at 25 °C.

proton signals of **6** show slight upfield shifts of 0.14 and 0.16 ppm, respectively, relative to the corresponding protons of free **6** due to the diamagnetic ring-current effect of the benzene rings of the host **1**. The association constant estimated from the ^{1}H NMR titration experiment is quite small (30–40 M^{-1} in CDCl$_3$).[22] In the UV/Vis spectrum (THF), a new broad absorption band of low intensity in the region 450–560 nm clearly supports a CT interaction (see the Supporting Information).

The FAB mass spectrum of a 1:1 mixture of **1** and **6** in CHCl$_3$ (*m*-nitrobenzyl alcohol as matrix) supports the formation of **6@1**; the observed exact mass number (*m*/*z* 1446.4435) is in good agreement with the calculated value (1446.4434). Yellow single crystals were obtained by slow evaporation of a solution containing **1** and **6** in CH$_2$Cl$_2$/*p*-xylene, and the formation of **6@1** was eventually confirmed by an X-ray structural analysis (Figure 3).

In **6@1**, all benzene rings of **6** face the pyromellitic diimide moieties of **1** in a parallel fashion at a distance of 3.47–3.52 Å. These distances are slightly longer than the van

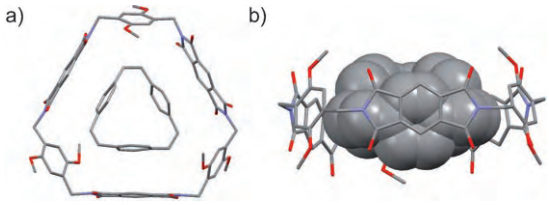

Figure 3. Structure of **6@1** in the solid state at −150 °C: a) top view; b) side view. Hydrogen atoms have been omitted for clarity.

© 2006 Wiley-VCH Verlag GmbH & Co. KGaA, Weinheim

der Waals diameter of two benzene rings (3.4 Å), but the maximum contacts of the benzene rings required for a CT-type electronic interaction are realized. This complex also stacks regularly to form a tubular structure along the (100) plane.

There have been several reports of macrocycles within macrocycles.[23–29] For example, Higuchi et al. have reported the lithium-coordinated complex [12]crown-4@γ-CD[23] and Kim et al. have discovered the formation of [2.2.2.2]cyclene@cucurbit[8]uril.[24] Recently, Kawase et al. have reported inclusion complexes of cyclic [*n*]paraphenyleneacetylene (CPPA)[28] by ^{1}H NMR spectroscopy and the formation of very interesting double-inclusion complexes (onion-type supramolecular complex) C_{60}@[6]CPPA@[9]CPPA, reminiscent of the Russian doll "Matrioshka".[28d] While no X-ray structural data are available yet for this first "cyclophane in cyclophane", complex **6@1** is probably the first "cyclophane within cyclophane" that has been confirmed by X-ray crystallography and whose driving force is a CT interaction.

The molecular motion of the guest **6** in the cavity in the solid state should be interesting, and shuttling between the cyclophane moieties can be expected in a host molecule containing two or more structural units. Further efforts toward the synthesis of molecular tubes are now in progress.

Experimental Section

1–3: A mixture of **5** (R^1 = OMe)[30] (681 mg, 3.47 mmol) in NMP (200 mL) was added dropwise over a period of 6 h to a solution of **4** (757 mg, 3.47 mmol) in NMP (200 mL) under argon at 150 °C. After the addition, the mixture was stirred for an additional 18 h. After cooling, the reaction mixture was concentrated under reduced pressure, water was poured into the concentrate, and the resultant yellow precipitate was collected by filtration. The filtrate was continuously extracted with $CHCl_3$ in a Soxhlet extractor. The combined extracts were washed with aqueous $NaHCO_3$, dried with Na_2SO_4, and filtered. The filtrate was passed through a short column of silica gel with CH_2Cl_2/AcOEt (4:1) as the eluent, followed by separation by preparative HPLC (GPC column, $CHCl_3$), to give the macrocycle **1** (100 mg, 7.6%) along with **2** (3.9 mg, 0.2%) and **3** (1.6 mg, 0.1%).

1: Yellow crystals ($CHCl_3$ after drying in vacuo), m.p. > 300 °C. ^{1}H NMR (300 MHz, $CDCl_3$): δ = 3.77 (s, 18H; OMe), 4.88 (s, 12H; CH_2), 6.95 (s, 6H; ArH), 8.14 ppm (s, 6H; imide); ^{13}C NMR (75 MHz, $CDCl_3$): δ = 37.51 (CH_2), 56.33 (OMe), 114.12 (Ar), 118.09 (imide Ar), 124.04 (CH_2-Ar), 137.00 (CO-*C*-Ar), 151.25 (Ar-*C*-OMe), 165.73 ppm (*C*=O). HR-MS (FAB) calcd for $C_{60}H_{42}O_{18}N_6$ [M^+]: 1134.2521, found 1134.2556. IR (KBr): $\tilde{\nu}$ = 1774, 1718 cm^{-1} (C=O); UV/Vis (THF): λ_{max} (ε) = 241 (95200), 298 (20800), 318 nm (sh, 8100). C,H,N analysis (%) calcd for $C_{60}H_{42}N_6O_{18}\cdot 0.25\,CHCl_3$: C 62.12, H 3.66, N 7.21; found: C 62.12, H 3.70, N 7.25.

2: Yellow powder, m.p. > 300 °C. ^{1}H NMR (300 MHz, $CDCl_3$): δ = 3.73 (s, 27H; OMe), 4.88 (s, 18H; CH_2), 6.84 (s, 9H; ArH), 8.20 ppm (s, 9H; imide); ^{13}C NMR (75 MHz, $CDCl_3$): δ = 37.66 (CH_2), 56.30 (OMe), 113.45 (Ar), 118.27 (imide Ar), 124.02 (CH_2-Ar), 137.12 (CO-*C*-Ar), 151.18 (Ar-*C*-OMe), 165.80 ppm (*C*=O). HR-MS (FAB) calcd for $C_{80}H_{56}N_8O_{24}$ [M^+]: 1512.3407, found 1512.3383.

3: Yellow powder, m.p. > 300 °C. ^{1}H NMR (300 MHz, $CDCl_3$): δ = 3.74 (s, 36H; OMe), 4.88 (s, 24H; CH_2), 6.86 (s, 12H, ArH), 8.20 ppm (s, 12H, imide); ^{13}C NMR (75 MHz, $CDCl_3$): δ = 37.65 (CH_2), 56.30 (OMe), 113.46 (Ar), 118.24 (imide Ar), 124.04 (CH_2-Ar), 137.16 (CO-*C*-Ar), 151.20 (Ar-*C*-OMe), 165.77 ppm (*C*=O). MALDI-TOF MS calcd for $C_{100}H_{70}N_{10}O_{30}$ [M + Na]$^+$: 1913.42, found 1913.48.

Received: December 19, 2005
Revised: March 6, 2006
Published online: April 28, 2006

Keywords: charge transfer · cyclophanes · inclusion compounds · materials science · pyromellitic diimide

[1] S. Iijima, *Nature* **1991**, *354*, 56–58.
[2] S. Iijima, T. Ichihashi, *Nature* **1993**, *363*, 603–605.
[3] *Carbon Nanotubes* (Eds.: M. Endo, S. Iijima, M. S. Dresselhaus), Pergamon, **1996**, Oxford.
[4] H. Shinohara, *Rep. Prog. Phys.* **2000**, *63*, 843–892.
[5] a) B. W. Smith, M. Monthioux, D. E. Luzzi, *Nature* **1998**, *396*, 323–324; b) T. Takahashi, A. Ito, M. Inakuma, H. Shinohara, *Phys. Rev. B* **1995**, *52*, 13812–13814; c) T. Pichler, M. S. Golden, M. Knupfer, J. Fink, U. Kirbach, P. Kuran, L. Dunsch, *Phys. Rev. Lett.* **1997**, *79*, 3026–3029; Y. Zhang, S. Iijima, Z. Shi, Z. Gu, *Philos. Mag. Lett.* **1999**, *79*, 473–479; d) J. Sloan, A. I. Kirkland, J. L. Hutchinson, M. L. H. Green, *Chem. Commun.* **2002**, 1319–1332.
[6] a) K. Suenaga, M. Tence, C. Mory, C. Colliex, H. Kato, T. Okazaki, H. Shinohara, K. Hirahara, S. Bandow, S. Iijima, *Science* **2000**, *290*, 2280–2282; b) K. Hirahara, K. Suenaga, S. Bandow, H. Kato, T. Okazaki, H. Shinohara, S. Iijima, *Phys. Rev. Lett.* **2000**, *85*, 5384–5387; c) K. Suenaga, S. Iijima, H. Kato, H. Shinohara, *Phys. Rev. B* **2000**, *62*, 1627–1630.
[7] T. Okazaki, K. Suenaga, K. Hirahara, S. Bandow, S. Iijima, H. Shinohara, *J. Am. Chem. Soc.* **2001**, *123*, 9673–9674.
[8] For self-assembling nanotubes, see: a) M. R. Ghadiri, J. R. Granja, R. A. Milligan, D. E. McRee, N. Khazanovich, *Nature* **1993**, *366*, 324–327; b) M. R. Gradiri, J. R. Granja, L. K. Buehler, *Nature* **1994**, *369*, 301–304; c) J. R. Granja, M. R. Ghadiri, *J. Am. Chem. Soc.* **1994**, *116*, 10785–10786; d) D. T. Bong, T. D. Clark, J. R. Granja, M. R. Ghadiri, *Angew. Chem.* **2001**, *113*, 1016–1041; *Angew. Chem. Int. Ed.* **2001**, *40*, 988–1011.
[9] T. Shimizu, M. Matsuda, H. Minamikawa, *Chem. Rev.* **2005**, *105*, 1401–1443.
[10] a) Y. Kim, M. F. Mayer, S. C. Zimmerman, *Angew. Chem.* **2003**, *115*, 1153–1158; *Angew. Chem. Int. Ed.* **2003**, *42*, 1121–1126; b) D. Yan, Y. Zhou, J. Hou, *Science* **2004**, *303*, 65–67.
[11] a) A. Harada, J. Li, M. Kamachi, *Nature* **1992**, *356*, 325–327; b) A. Harada, J. Li, M. Kamachi, *Nature* **1993**, *364*, 516–518.
[12] a) V. G. Organo, A. V. Leontiev, V. Sgarlata, H. V. R. Dias, D. M. Rudkevich, *Angew. Chem.* **2005**, *117*, 3103–3107; *Angew. Chem. Int. Ed.* **2005**, *44*, 3043–3047; b) S. Matile, A. Som, N. Sorde, *Tetrahedron* **2004**, *60*, 6450–6435; c) V. Sidorov, F. W. Kotch, G. Abdrakhmanova, R. Mizani, J. C. Fettinger, J. T. Davis, *J. Am. Chem. Soc.* **2002**, *124*, 2267–2278; d) L. Baldini, F. Sansone, A. Casnati, F. Ungaro, *J. Supramol. Chem.* **2002**, 219–226; e) A. Ikeda, S. Shinkai, *J. Chem. Soc. Chem. Commun.* **1994**, 2375–2376; f) A. Ikeda, M. Kawaguchi, S. Shinkai, *Quim. Anal.* **1997**, *93*, 408–414; g) J.-A. Perez-Adelmar, H. Abraham, C. Sanchez, K. Rissanen, P. Prados, J. de Mendoza, *Angew. Chem.* **1996**, *108*, 1088–1090; *Angew. Chem. Int. Ed. Engl.* **1996**, *35*, 1009–1011; h) S. K. Kim, W. Sim, J. Vincens, J. S. Kim, *Tetrahedron Lett.* **2003**, *44*, 805–809; i) S. K. Kim, J. Vincens, K.-M. Park, S. S. Lee, J. S. Kim, *Tetrahedron Lett.* **2003**, *44*, 993–997.
[13] a) M. Aoyagi, K. Biradha, M. Fujita, *J. Am. Chem. Soc.* **2001**, *123*, 7457–7458; b) T. Yamaguchi, S. Tashiro, M. Tominaga, M. Kawano, T. Ozeki, M. Fujita, *J. Am. Chem. Soc.* **2004**, *126*, 10818–10819; c) S. Tashiro, M. Tominaga, T. Kusukawa, M. Kawano, S. Sakamoto, K. Yamaguchi, M. Fujita, *Angew. Chem.*

 © 2006 Wiley-VCH Verlag GmbH & Co. KGaA, Weinheim

2003, *115*, 3389 – 3392; *Angew. Chem. Int. Ed.* **2003**, *42*, 3267 – 3270; d) M. Tomonaga, S. Tashiro, M. Aoyagi, M. Fujita, *Chem. Commun.* **2002**, 2038 – 2039.

[14] a) E. Buncel, N. L. Mailloux, R. S. Brown, B. P. Kazmaier, J. Dust, *Tetrahedron Lett.* **2001**, *42*, 3559 – 3562; b) J. G. Hansen, K. S. Bang, N. Thorup, J. Becker, *Eur. J. Org. Chem.* **2000**, 2135 – 2144; c) H. M. Colquhoun, D. J. Williams, Z. Zhu, *J. Am. Chem. Soc.* **2002**, *124*, 13346 – 13347.

[15] a) J. Jazwinski, A. J. Blacker, J.-M. Lehn, M. Cesario, J. Guilhem, C. Pascard, *Tetrahedron Lett.* **1987**, *28*, 6057 – 6060; b) H. Langhals, R. Ismael, *Eur. J. Org. Chem.* **1998**, 1915 – 1917; c) H. A. Staab, D. G. Zhang, C. Krieger, *Liebigs Ann./Recl.* **1997**, 1551 – 1556; d) H. A. Staab, S. Nikolic, *Eur. J. Org. Chem.* **1999**, 1459 – 1470; e) C. Chen, J. T. Lean, M. Alcak, T. E. Mallouk, *J. Org. Chem.* **2001**, *66*, 3021 – 3030; f) E. Buncel, N. L. Mailloux, R. S. Brown, P. M. Kazmaier, J. Dust, *Tetrahedron Lett.* **2001**, *42*, 3554 – 3562.

[16] a) D. G. Hamilton, L. Prodi, N. Feeder, J. K. M. Sanders, *J. Chem. Soc. Perkin Trans. 1* **1999**, 1057 – 1065; b) J. G. Hansen, N. Feeder, D. G. Hamilton, M. J. Gunter, J. Becher, J. K. M. Sanders, *Org. Lett.* **2000**, *2*, 449 – 452; c) M. J. Gunter, S. M. Farquhar, *Org. Biomol. Chem.* **2003**, *1*, 3450 – 3453.

[17] D. G. Hamilton, M. Montalti, L. Prodi, M. Fontani, P. Zanello, J. K. M. Sanders, *Chem. Eur. J.* **2000**, *6*, 608 – 612.

[18] All measurements were made with a Rigaku RAXIS-RAPID-S imaging plate area detector with graphite-monochromated $Cu_{K\alpha}$ ($\lambda = 1.54178$ Å) or $Mo_{K\alpha}$ ($\lambda = 0.71069$ Å) radiation and a rotating anode generator. The crystal structures were solved by direct methods with SHELX-97.[31] The non-hydrogen atoms were refined anisotropically with SHELX-97, while hydrogen atoms were refined isotropically. A summary of the crystallographic data is shown in Table S1. CCDC-2093024, -2093025, -2093026, and -2093027 contain the supplementary crystallographic data for this paper. These data can be obtained free of charge from The Cambridge Crystallographic Data Centre via www.ccdc.cam.ac.uk/data_request/cif.

[19] a) V. Semetey, C. Didierjean, J.-P. Briand, A. Aubry, G. Guichard, *Angew. Chem.* **2002**, *114*, 1975 – 1978; *Angew. Chem. Int. Ed.* **2002**, *41*, 1895 – 1978; b) C. H. Görbitz, *Chem. Eur. J.* **2001**, *7*, 5153 – 5159.

[20] a) R. Gleiter, D. B. Werz, B. J. Rausch, *Chem. Eur. J.* **2003**, *9*, 2676 – 2683; b) D. B. Werz, R. Gleiter, F. Rominger, *J. Org. Chem.* **2004**, *69*, 2945 – 2952; c) J.-H. Schulte, D. B. Werz, F. Rominger, R. Gleiter, *Org. Biomol. Chem.* **2003**, *1*, 2788 – 2794; d) D. B. Werz, R. Gleiter, F. Rominger, *J. Am. Chem. Soc.* **2002**, *124*, 10638 – 10639.

[21] The examined cyclophanes are [2²]- and [3²]PCP, [3³]PCP, as well as [2²]PCP-dione and [3³]PCP-trione.

[22] The binding constants were calculated by fitting for the titration data, using the *NMRTit* software (download available from http://seitai.chemistry.or.jp/).
$\Delta\delta_{obs} = \Delta\delta/2\, K[G]_0[1\, K[H]_0 + K[G]_0 - \{(1\, K[H]_0 + K[G]_0)^2 - 4\, K^2[H]_0[G]_0\}^{1/2}]$, where K is the association constant, and $[H]_0$ and $[G]_0$ are the initial concentrations of the host and guest, respectively. In the NMR titrations, the concentration of **1** was kept at 5.29×10^{-3} M and that of **6** was varied from 0.00 to 7.40×10^{-3} M ($CDCl_3$). The measurements were carried out at 23 °C.

[23] S. Kamitori, K. Hirotsu, T. Higuchi, *J. Am. Chem. Soc.* **1987**, *109*, 2409 – 2414.

[24] S.-Y. Kim, I.-S. Jung, E. Lee, J. Kim, S. Sakamoto, K. Yamaguchi, K. Kim, *Angew. Chem.* **2001**, *113*, 2177 – 2179; *Angew. Chem. Int. Ed.* **2001**, *40*, 2119 – 2121.

[25] S.-H. Chiu, A. R. Pease, J. F. Stoddart, A. J. P. White, D. J. Williams, *Angew. Chem.* **2002**, *114*, 280 – 284; *Angew. Chem. Int. Ed.* **2002**, *41*, 275 – 277.

[26] A. I. Day, R. J. Blanch, A. P. Arnold, S. Lorenzo, G. R. Lewis, I. Dance, *Angew. Chem.* **2002**, *114*, 285 – 287; *Angew. Chem. Int. Ed.* **2002**, *41*, 270 – 274.

[27] J. C. Loren, M. Yoshizawa, R. F. Haldimann, A. Linden, J. S. Siegel, *Angew. Chem.* **2003**, *115*, 5880 – 5883; *Angew. Chem. Int. Ed.* **2003**, *42*, 5702 – 5705.

[28] a) T. Kawase, N. Ueda, K. Tanaka, Y. Seirai, M. Oda, *Tetrahedron Lett.* **2001**, *42*, 5509 – 5511; b) T. Kawase, K. Tanaka, Y. Seirai, N. Shiono, M. Oda, *Angew. Chem.* **2003**, *115*, 5755 – 5758; *Angew. Chem. Int. Ed.* **2003**, *42*, 5597 – 5600; c) T. Kawase, Y. Seirai, H. R. Darabi, M. Oda, Y. Sarakai, K. Tashiro, *Angew. Chem.* **2003**, *115*, 1659 – 1662; *Angew. Chem. Int. Ed.* **2003**, *42*, 1621 – 1624; d) T. Kawase, K. Tanaka, N. Shiono, Y. Seirai, M. Oda, *Angew. Chem.* **2004**, *116*, 1754 – 1756; *Angew. Chem. Int. Ed.* **2004**, *43*, 1722 – 1724.

[29] L. T. Scott, *Angew. Chem.* **2003**, *115*, 4265 – 4267; *Angew. Chem. Int. Ed.* **2003**, *42*, 4133 – 4235.

[30] S. Sasaki, M. Mizuno, K. Naemura, Y. Tobe, *J. Org. Chem.* **2000**, *65*, 275 – 283.

[31] G. M. Sheldrick, SHELX-97, A Program for the Solution of Crystal Structures, University of Göttingen, Germany, **1997**.

 © 2006 Wiley-VCH Verlag GmbH & Co. KGaA, Weinheim

Synthetic Methods

DOI: 10.1002/anie.200600571

Au^{I}-Catalyzed Tandem [3,3] Rearrangement–Intramolecular Hydroarylation: Mild and Efficient Formation of Substituted Indenes**

*Nicolas Marion, Silvia Díez-González, Pierre de Frémont, April R. Noble, and Steven P. Nolan**

Recent reports have highlighted the use of gold(I) and gold(III) complexes as efficient homogeneous catalysts in several organic transformations.[1] Notably, gold catalysts, in both oxidation states, enable the cycloisomerization of enynes.[2] Based on these earlier studies, we reasoned that the electron-rich phenyl ring could replace an alkene moiety and lead to

[*] N. Marion, Dr. S. Díez-González, P. de Frémont, A. R. Noble, Prof. Dr. S. P. Nolan
Department of Chemistry
University of New Orleans
2000 Lakeshore Drive, New Orleans, LA 70148 (USA)
Fax: (+1) 504-280-6860
E-mail: snolan@uno.edu

[**] The National Science Foundation is gratefully acknowledged for financial support of this work. S.D.G. thanks the Education, Research, and Universities Department of the Basque Government (Spain) for a postdoctoral fellowship. We also thank the Department of Chemistry of the University of Ottawa, and more specifically Prof. Deryn Fogg, for hosting our group while the University of New Orleans was recovering from Hurricane Katrina. Degussa AG, Umicore AG, and Strem are also gratefully acknowledged.

Supporting information for this article is available on the WWW under http://www.angewandte.org or from the author.

© 2006 Wiley-VCH Verlag GmbH & Co. KGaA, Weinheim

valuable cyclized products. Surprisingly, the only related examples of intramolecular hydroarylation employ a heteroatom-containing tether to provide indoles, benzofurans, or coumarins.[3] Carbocycles, especially indenes, are compounds of great interest as synthetic targets and building blocks for pharmaceutical[4] and materials chemistry.[5] As the inter- or intramolecular formation of indenes usually requires high temperature and/or a prolonged reaction time,[6] a mild and efficient assembly protocol would be highly desirable.

Keeping in mind that propargylic acetates, in the presence of cationic gold complexes, undergo 1,2-migration of the acetate group and subsequent formation of carbenoid species,[7] we first examined the reactivity of **1a** with an equimolar amount of [(IPr)AuCl] (IPr = *N*,*N*′-bis(2,6-diisopropylphenyl)imidazol-2-ylidene) and $AgBF_4$. After five minutes at room temperature, the reaction with **1a** cleanly yielded indene **2a** (Table 1, entry 1). Interestingly, although

Table 1: Catalyst optimization.[a]

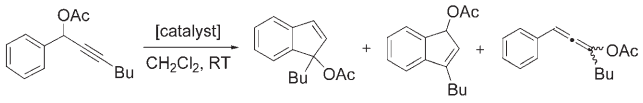

1a **2a** **3a** **4a**

Entry	Catalyst (2 mol%)	*t*	**2a** [%][b]	**3a** [%][b]	**4a** [%][b]
1	[(IPr)AuCl]/$AgBF_4$	5 min	92	–	–
2	[(IPr)AuCl]	overnight	no reaction		
3	$AgBF_4$	30 min	–	–	87
4	[(IPr)AuCl]/$AgPF_6$	5 min	90	–	–
5	[(IPr)AuCl]/$AgSbF_6$	5 min	73	–	–
6	[(SIPr)AuCl]/$AgBF_4$	5 min	88	5	–
7	[(IMes)AuCl]/$AgBF_4$	5 min	76	3	–
8	[(ITM)AuCl]/$AgBF_4$	5 min	54	23	11
9	[(IAd)AuCl]/$AgBF_4$	15 min	89	–	–
10	[(PPh_3)AuCl]/$AgBF_4$	5 min	51	32	8
11	AuCl	30 min	unidentified mixture		
12	AuCl/$AgBF_4$	5 min	unidentified mixture		
13	$PtCl_2$	overnight	–	–	53

[a] Reaction conditions: alkyne **1a** (0.5 mmol), catalyst (2 mol%), CH_2Cl_2 (20 mL). [b] NMR spectroscopic yields with respect to 1,2-dichloroethane.

the formation of indenes from aryl propargyl acetates such as **1a** has two precedents in the literature, both leading to products of type **5**,[8] the structure of **2a** is unexpected (see Scheme 3). Reaction of **1a** with $AgBF_4$ (Table 1, entry 3) resulted in the formation of allene **4a**, which showed only minor decomposition and no formation of cyclized product upon prolonged stirring.[9] [(IPr)AuCl] alone was found to be inactive toward alkyne **1a** (Table 1, entry 2).

To gauge the influence of the ligand in this transformation, we carried out reactions with various [(NHC)AuCl] complexes[10] (NHC = N-heterocyclic carbene, Scheme 1) and silver tetrafluoroborate. Sterically demanding NHCs led to sluggish reactions (Table 1, entry 9) while less encumbered NHCs,[11] as well as PPh_3, led to poor selectivity (Table 1, entries 8 and 10).[12] Further optimization revealed that tetrafluoroborate or hexafluorophosphate were both suitable counterions (Table 1, entries 1 and 4), whereas hexafluoroantimonate produced a significant amount of oligomerization (Table 1, entry 5). It is noteworthy that AuCl alone or in conjunction with $AgBF_4$ did not lead to **2a** (Table 1, entries 11 and 12). Furthermore, $PtCl_2$, which has been reported recently to catalyze a closely related reaction,[8b] did not lead to **2a** under our conditions (Table 1, entry 13).

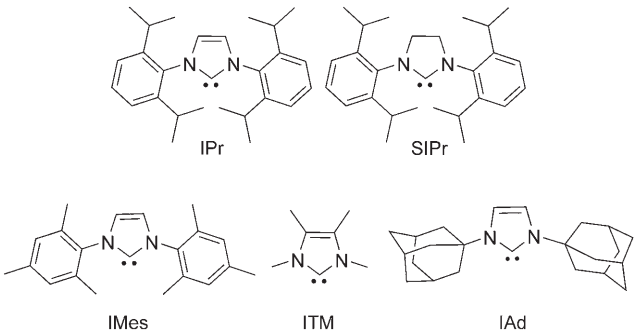

Scheme 1. Structures of NHC ligands.

The scope of the reaction was investigated with a variety of reactants **1**, and the results are presented in Table 2. The formation of indenes **2** was found to be compatible with electron-poor or electron-rich arenes **1b–d**. Benzodioxole **1e** reacted regioselectively to give **2e** in excellent yield. *Ortho*-substituted arenes **1f** and **1g** gave **2f** and **2g′** and led to the formation of indenes of type **3** as minor products. Interest-

Table 2: Gold(I)-catalyzed formation of indenes from propargylic acetates.

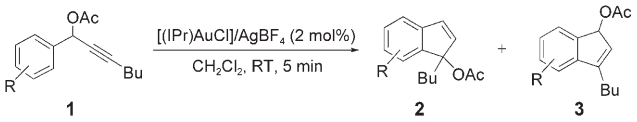

1 **2** **3**

1	Major product	Minor product
1a	**2a** (92%)	
1b	**2b** (81%)	
1c	**2c** (78%)	
1d	**2d** (63%)	**4d** (13%)
1e	**2e** (90%)	
1f	**2f** (88%)	**3f** (9%)
1g	**2g'** (78%)	**3g** (11%)
1h	**2h** (67%)	**3h** (18%)

 © 2006 Wiley-VCH Verlag GmbH & Co. KGaA, Weinheim

ingly, the naphthalene **1g** produced the phenalene **2g′** regioselectively.[13] To further explore the generality of this transformation, we carried out the reaction using **1h**, which cleanly produced indenes **2h** and **3h**.[14] Strikingly, no trace of bicyclo[3.1.0] compounds was observed,[2a,h] thus highlighting the chemoselectivity of the reaction. Furthermore, the latter reaction shows that tertiary acetates are also suitable substrates in this transformation. Finally, varying the substituent at the acetylenic position with a phenyl group in place of the butyl group resulted in oligomerization of the starting material. On the other hand, with a proton at the acetylenic position, the formation of **5i** was observed, resulting primarily from a 1,2-migration of the propargylic acetate group in **1i** (Scheme 2). In this latter case, the reactivity of the aryl

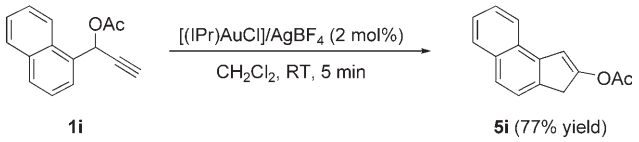

Scheme 2. An example of gold(I)-catalyzed formation of an indene from a terminal alkyne.

propargyl acetate is similar to that observed in transformations reported by the research groups of Uemura and Sarpong with ruthenium and platinum catalysts, respectively.[8] Therefore, it appears that the behavior of the $[(IPr)Au]^+$ catalyst and, subsequently, the outcome of the reaction are highly dependent on the substitution pattern at the acetylenic position. The apparent 1,3-migration of the acetate moiety in products of type **2** and the observation of allene **4d** led us to propose the mechanism depicted in Scheme 3. π Complexation of the in situ generated cationic gold complex to the C≡C bond and subsequent direct nucleophilic attack by the electron-rich phenyl ring would lead to products of type **3**.[15,16] On the other hand, electrophilic activation of the alkyne could trigger two successive 1,2-migrations (or a single 1,3-migration) of the acetate group[17] to produce allene **III**, which would be further activated by the $[Au^+]$ fragment for hydroarylation,[18,19] thus leading to products of type **2**.[20] To gain insight into the mechanism, we synthesized allenes **4a**,**c**,**d** by treating **1a**,**c**,**d** with $AgSbF_6$ and subjected the allenes to cyclization conditions. We observed the formation of the corresponding indenes **2a**,**c**,**d** after 15 minutes (Table 3).

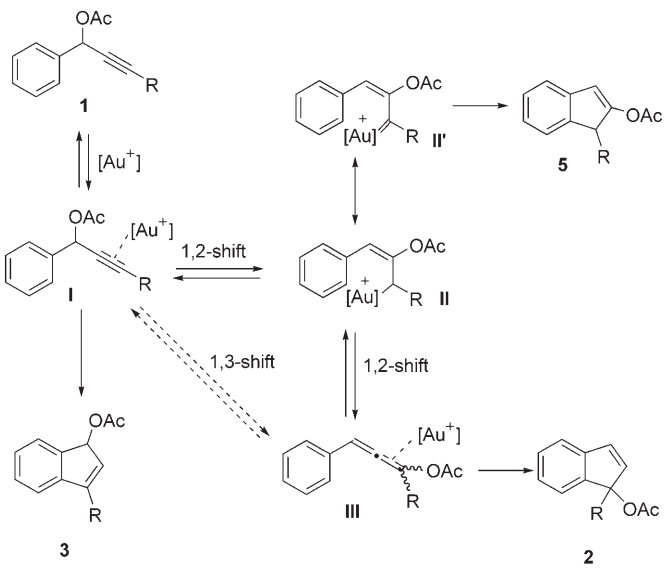

Scheme 3. Proposed mechanism.

Table 3: Gold(I)-catalyzed formation of indenes from aryl allenes.

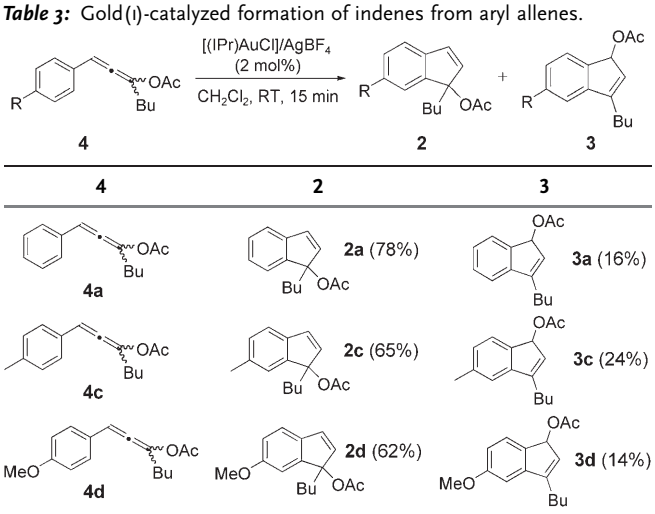

Unexpectedly, the reaction times were slightly longer than with the propargylic acetates. This could be a consequence of a higher "alkynophilicity" than "allenophilicity" of the $[(IPr)Au]^+$ fragment, a difference which is not observed starting from **1** as a result of the mandatory proximity of the gold center to the newly formed allene moiety.[21] Finally, the minor formation of **3a**,**c**,**d**, products of the direct hydroarylation of the alkyne, emphasizes the reversibility of the gold(I)-catalyzed [3,3] rearrangement and the advantage of using alkynes in this reaction for a higher selectivity.

In summary, we have described a novel type of metal-mediated formation of indenes from aryl propargyl acetates. This chemoselective transformation proceeds under extremely mild reaction conditions. Studies aimed at exploring mechanistic aspects of this transformation and developing further uses of $[(IPr)AuCl]$[22] are ongoing.

Experimental Section

General Procedure: $AgBF_4$ (2 mg, 0.02 mmol) was added in the absence of light to a solution of [(IPr)AuCl] (12.4 mg, 0.02 mmol) in anhydrous CH_2Cl_2 (35 mL) in a round-bottom flask equipped with a septum. The solution instantly became cloudy. A solution of propargylic acetate **1** (1 mmol) in anhydrous CH_2Cl_2 (5 mL) was then injected through the septum. When TLC analysis showed total consumption of the starting material, the solvent was removed under vacuum. The resulting mixture was dissolved in pentane, filtered through celite, and evaporated. The crude oil was purified by flash chromatography on silica gel.

2a: The above general procedure employing **1a** (230 mg) yielded **2a** after flash chromatography on silica gel (pentane/methyl *tert*-butyl ether, 95:5). Yield: 212 mg, 92%; ^1H NMR (300 MHz, $CDCl_3$): $\delta =$ 7.35 (d, $J = 7.2$ Hz, 1H, ArH), 7.24–7.14 (m, 2H, ArH), 7.21–7.18 (m, 1H, ArH), 6.70 (d, $J = 5.7$ Hz, 1H, $C_{Ar}CH{=}CH$), 6.56 (d, $J = 5.7$ Hz, 1H, $C_{Ar}CH{=}CH$), 2.22 (dt, $J = 12.6$, 4.5 Hz, 1H, CCH_2CH_2), 1.99 (s,

 © 2006 Wiley-VCH Verlag GmbH & Co. KGaA, Weinheim

3H, OAc), 1.93 (dt, $J = 12.6$, 4.5 Hz, 1H, CCH_2CH_2), 1.32–1.19 (m, 4H, $CH_2CH_2CH_3$), 0.83 ppm (t, $J = 7.5$ Hz, 3H, CH_2CH_3); ^{13}C NMR (75 MHz, $CDCl_3$): $\delta = 170.0$ (C=O), 145.8 (C_{Ar}), 142.4 (C_{Ar}), 137.9 ($C_{Ar}H$), 132.4 ($C_{Ar}CH{=}CH$), 128.7 ($C_{Ar}H$), 126.2 ($C_{Ar}CH{=}CH$), 122.2 ($C_{Ar}H$), 121.7 ($C_{Ar}H$), 91.0 (*C*OAc), 35.7 (CCH_2CH_2), 26.4 ($CH_2CH_2CH_3$), 23.1 (CH_2CH_3), 21.9 (CH_3, OAc), 14.0 ppm (CH_2CH_3). Elemental analysis (%) calcd for $C_{15}H_{18}O_2$ (M_r 230.30): C 78.23, H 7.88; found: C 78.15, H 7.94.

Received: February 12, 2006
Published online: April 26, 2006

Keywords: alkynes · allenes · gold · hydroarylation · indenes

[1] For recent reviews on gold-catalyzed reactions, see: a) A. Hoffmann-Röder, N. Krause, *Org. Biomol. Chem.* **2005**, *3*, 387–391; b) A. S. K. Hashmi, *Angew. Chem.* ***2005***, *117*, 7150–7154; *Angew. Chem. Int. Ed.* **2005**, *44*, 6990–6993.

[2] For recent contributions on gold-catalyzed enyne cycloisomerization, see: a) M. R. Luzung, J. P. Markham, F. D. Toste, *J. Am. Chem. Soc.* **2004**, *126*, 10858–10859; b) L. Zhang, S. A. Kozmin, *J. Am. Chem. Soc.* **2004**, *126*, 11806–11807; c) C. Nieto-Oberhuber, S. López, A. M. Echavarren, *J. Am. Chem. Soc.* **2005**, *127*, 6178–6179; d) N. Mézailles, L. Ricard, F. Gagosz, *Org. Lett.* **2005**, *7*, 4133–4136; e) C. Ferrer, A. M. Echavarren, *Angew. Chem.* **2006**, *118*, 1123–1127; *Angew. Chem. Int. Ed.* **2006**, *45*, 1105–1109; f) C. Nieto-Oberhuber, S. López, M. P. Muñoz, E. Jiménez-Núñez, E. Buñuel, D. J. Cárdenas, A. M. Echavarren, *Chem. Eur. J.* **2006**, *12*, 1694–1702; g) T. Shibata, Y. Ueno, K. Kanda, *Synlett* **2006**, 411–414; h) A. Fürstner, P. Hannen, *Chem. Eur. J.* **2006**, *12*, 3006–3019.

[3] a) For a review on hydroarylation of alkynes, see: C. Nevado, A. M. Echavarren, *Synthesis* **2005**, 167–182.

[4] A. Korte, J. Legros, C. Bolm, *Synlett* **2004**, *13*, 2397–2399.

[5] a) J. Barberá, O. A. Rakitin, M. B. Ros, T. Torroba, *Angew. Chem.* **1998**, *110*, 308–312; *Angew. Chem. Int. Ed.* **1998**, *37*, 296–299; b) J. Yang, M. V. Lakshmikantham, M. P. Cava, D. Lorcy, J. R. Bethelot, *J. Org. Chem.* **2000**, *65*, 6739–6742.

[6] For recent selected reports on indene formation, see: a) Z. Xi, R. Guo, S. Mito, H. Yan, K.-i. Kanno, K. Nakajima, T. Takahashi, *J. Org. Chem.* **2003**, *68*, 1252–1257; b) M. Lautens, T. Marquardt, *J. Org. Chem.* **2004**, *69*, 4607–4614; c) K.-J. Chang, D. K. Rayabarapu, C.-H. Cheng, *J. Org. Chem.* **2004**, *69*, 4781–4787; d) R. J. Madhushaw, C.-Y. Lo, C.-W. Hwang, M.-D. Su, H.-C. Shen, S. Pal, I. R. Shaikh, R.-S. Liu, *J. Am. Chem. Soc.* **2004**, *126*, 15560–15565; e) M. Shi, B. Xu, J.-W. Huang, *Org. Lett.* **2004**, *6*, 1175–1178; f) I. Nakamura, Y. Mizushima, I. D. Gridnev, Y. Yamamoto, *J. Am. Chem. Soc.* **2005**, *127*, 9844–9847; g) Y. Kuninobu, A. Kawata, K. Takai, *J. Am. Chem. Soc.* **2005**, *127*, 13498–13499; h) D. Zhang, E. K. Yum, Z. Liu, R. C. Larock, *Org. Lett.* **2005**, *7*, 4963–4966.

[7] a) M. J. Johansson, D. J. Gorin, S. T. Staben, F. D. Toste, *J. Am. Chem. Soc.* **2005**, *127*, 18002–18003; see also reference [2h]; b) V. Mamane, T. Gress, H. Krause, A. Fürstner, *J. Am. Chem. Soc.* **2004**, *126*, 8654–8655.

[8] Ruthenium-catalyzed: a) K. Miki, K. Ohe, S. Uemura, *J. Org. Chem.* **2003**, *68*, 8505–8513; platinum-catalyzed: b) B. A. Bhanu Prasad, F. K. Yoshimoto, R. Sarpong, *J. Am. Chem. Soc.* **2005**, *127*, 12468–12469.

[9] The silver-catalyzed formation of allene from propargylic acetate has been described: H. Schlossarczyk, W. Sieber, M. Hesse, H.-J. Hansen, H. Schmid, *Helv. Chim. Acta* **1973**, *56*, 875–944.

[10] For the synthesis of a series of [(NHC)AuCl] complexes, see: P. de Frémont, N. M. Scott, E. D. Stevens, S. P. Nolan, *Organometallics* **2005**, *24*, 2411–2418.

[11] For a study on the steric and electronic properties of NHCs, see: R. Dorta, E. D. Stevens, N. M. Scott, C. Costabile, L. Cavallo, C. D. Hoff, S. P. Nolan, *J. Am. Chem. Soc.* **2005**, *127*, 2485–2495.

[12] For details, see the Supporting Information.

[13] Characteristic signals for the expected indene could be observed in the ^1H NMR spectrum of the crude reaction mixture and accounted for < 5% of the signal intensity, but this product could not be cleanly isolated.

[14] Compounds **2h** and **3h** were easily separated by flash chromatography.

[15] For selected examples of intramolecular electrophilic activation of an alkyne toward aromatic substitution, see: a) B. M. Trost, F. D. Toste, *J. Am. Chem. Soc.* **1996**, *118*, 6305–6306; b) C. Jia, D. Piao, J. Oyamada, W. Lu, T. Kitamura, Y. Fujiwara, *Science* **2000**, *287*, 1992–1995; c) H. Inoue, N. Chatani, S. Murai, *J. Org. Chem.* **2002**, *67*, 1414–1417; d) A. Fürstner, V. Mamane, *J. Org. Chem.* **2002**, *67*, 6264–6267; e) C. Nevado, A. M. Echavarren *Chem. Eur. J.* **2005**, *11*, 3155–3164.

[16] For an extensive study of gold-catalyzed intermolecular hydroarylation, see: M. T. Reetz, K. Sommer, *Eur. J. Org. Chem.* **2003**, 3485–3496.

[17] For mechanistic considerations, see: O. N. Faza, C. S. Lopez, R. Alvarez, A. R. de Lera, *J. Am. Chem. Soc.* **2006**, *128*, 2434–2437.

[18] For examples of gold-catalyzed activation of allenes, see: a) A. S. K. Hashmi, L. Schwarz, J.-H. Choi, T. M. Frost, *Angew. Chem.* **2000**, *112*, 2382–2385; *Angew. Chem. Int. Ed.* **2000**, *39*, 2285–2288; b) A. Hoffmann-Röder, N. Krause, *Org. Lett.* **2001**, *3*, 2537–2538; c) N. Morita, N. Krause, *Org. Lett.* **2004**, *6*, 4121–4123; d) A. W. Sromek, M. Rubina, V. Gevorgyan, *J. Am. Chem. Soc.* **2005**, *127*, 10500–10501; e) L. Zhang, *J. Am. Chem. Soc.* **2005**, *127*, 16804–16805; f) L. Zhang, S. Wang, *J. Am. Chem. Soc.* **2006**, *128*, 1442–1443.

[19] Intramolecular hydroarylation of aryl allenes leading to indenes can be catalyzed by strongly acidic media, by metals (Al, Rh, Co), or photochemically and usually requires high temperature and/or a prolonged reaction time for a moderate chemical yield; for reviews, see: a) D. R. Taylor, *Chem. Rev.* **1967**, *67*, 317–359; b) *Allenes in Organic Synthesis* (Eds.: H. F. Schuster, G. M. Coppola), Wiley, New York, **1984**; c) *Modern Allene Chemistry* (Eds.: N. Krause, A. S. K. Hashmi), Wiley-VCH, Weinheim, **2004**.

[20] Cyclization occuring through C–H activation and arene auration cannot at this time be ruled out (see scheme below); for examples of arene gold(III) complexes involved in catalytic transformations, see: Z. Shi, C. He, *J. Am. Chem. Soc.* **2004**, *126*, 13596–13597.

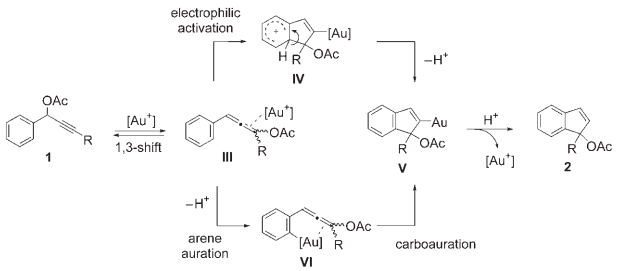

[21] An alternate explanation would imply that the reaction might not go through a discrete allene intermediate; hence, a concerted mechanism would be worth consideration.

[22] For an example of diazoacetate transfer catalyzed by [(IPr)AuCl], see: M. R. Fructos, T. R. Belderrain, P. de Frémont, N. M. Scott, S. P. Nolan, M. M. Díaz-Requejo, P. J. Pérez, *Angew. Chem.* **2005**, *117*, 5418–5422; *Angew. Chem. Int. Ed.* **2005**, *44*, 5284–5288.

 © 2006 Wiley-VCH Verlag GmbH & Co. KGaA, Weinheim

Natural Product Synthesis

DOI: 10.1002/anie.200600006

Total Synthesis of (+)-Machaeriol D with a Key Regio- and Stereoselective S_N2' Reaction**

Qiaoling Wang, Qinggang Huang, Bo Chen, Jiangping Lu, Hui Wang, Xuegong She, and Xinfu Pan**

Since its discovery in 1964, tetrahydrocannabinol (THC) and related derivatives (cannabidiol (CBD), non-natural hexahydrocannabinol (HHC)) have captured the imagination of research groups all over the world.[1] The structurally related 5,6-secohexahydrodibenzopyrans (5,6-seco-HHDBPs) machaeridiol A–C and *trans*-HHDBPs machaeriol A–D were recently isolated from the stem bark of *Machaerium multiflorum* spruce (Fabaceae) (Scheme 1).[2] Although much effort has been devoted to the synthesis of this class of natural products,[3] the stereocontrolled construction of the three or four stereocenters located on the cyclohexane ring still represents a significant synthetic challenge. Herein, a general strategy is described for the first enantioselective total synthesis of (+)-machaeriol D (**1**), one of the most complex HHDBPs, via a 5,6-seco-HHDBP and with an S_N2' reaction[4] as a key step.

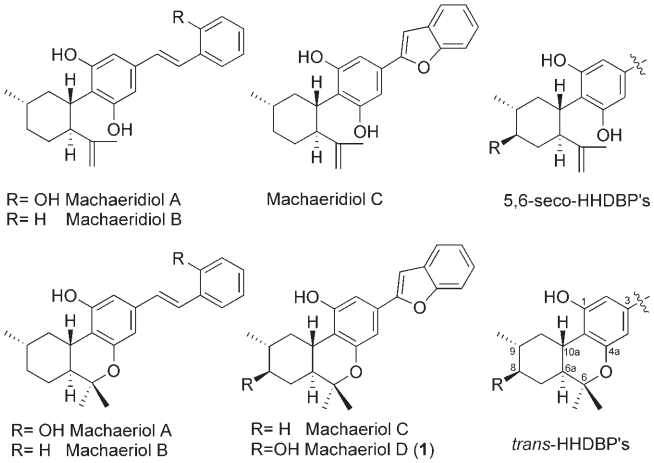

Scheme 1. Representative 5,6-seco-HHDBPs and *trans*-HHDBPs.

The highly regio- and stereoselective S_N2' reaction of aryl or alkyl cyanocuprates with silyl enol ether epoxides has become an important method for C–C bond formation (Scheme 2).[5] The *anti* adduct can be subjected to mild hydrolysis to afford a β-hydroxy ketone, which is a particularly versatile building block in organic synthesis.[5d,e] The distinct advantage of the S_N2' reaction prompted us to investigate its scope and its potential in the enantioselective synthesis of natural products. We present herein the total synthesis of (+)-machaeriol D as an example of our new synthetic strategy, in which a tandem S_N2'–hydrolysis reaction sequence is used to establish four stereocenters of the 5,6-seco-HHDBPs and HHDBPs enantioselectively.

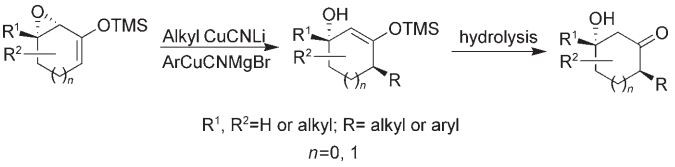

Scheme 2. Key S_N2' reaction. TMS = trimethylsilyl.

Our retrosynthetic analysis is depicted in Scheme 3. We envisaged that the target molecule **1** could be accessed from the 5,6-seco-HHDBP benzofuran **2** by an acid-catalyzed cyclization. In turn, **2** might be prepared from ketone **3** by several transformations, including Barton deoxygenation,[6] a Corey–Fuchs reaction,[7] Sonogashira coupling,[8] and cycliza-

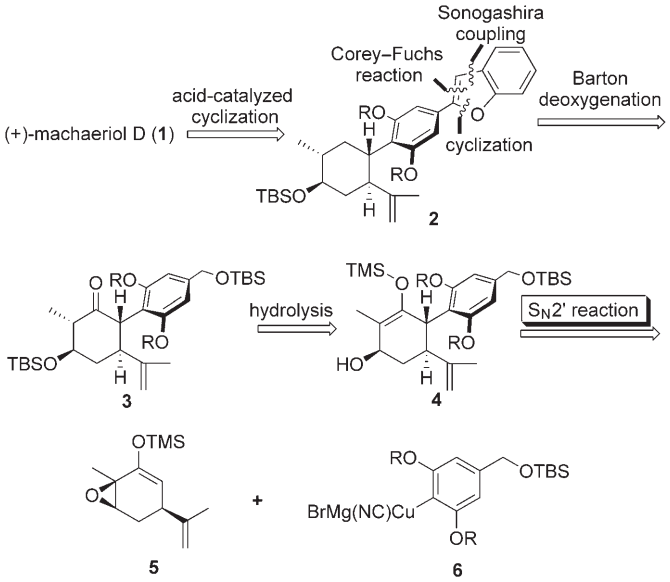

Scheme 3. Retrosynthetic analysis of (+)-machaeriol D. R = MOM = methoxymethyl, TBS = *tert*-butyldimethylsilyl.

[*] Q. Wang, Q. Huang, B. Chen, J. Lu, H. Wang, Prof. X. She, Prof. X. Pan
State Key Laboratory of Applied Organic Chemistry and Department of Chemistry
Lanzhou University
Fax: (+86) 931-891-2582
E-mail: shexg@lzu.edu.cn
panxf@lzu.edu.cn
Prof. X. She
State Key Laboratory for Oxo Synthesis and Selective Oxidation
Lanzhou Institute of Chemical Physics
Chinese Academy of Sciences
Lanzhou 730000 (P.R. China)

[**] We are grateful for the financial support of the NSFC (No. 20572036, QT program), the Special Doctorial Program Funds of the Ministry of Education of China (20040730008), GanSu Science Foundation (No. 3ZS051A25-004), and the Key Grant Project of the Ministry of Education of China (No.105169).

Supporting information for this article is available on the WWW under http://www.angewandte.org or from the author.

 © 2006 Wiley-VCH Verlag GmbH & Co. KGaA, Weinheim

tion. As the key strategy-level step, a highly regio- and stereoselective S_N2' reaction of the aryl cyanocuprate **6** with the optically active silyl enol ether **5** would provide the desired adduct **4**, which can be converted readily into **3** with the requisite stereoselectivity by mild hydrolysis.

Our synthetic journey began with the preparation of substrates **5** and **6.** As shown in Scheme 4, the (+)-*cis*-epoxy

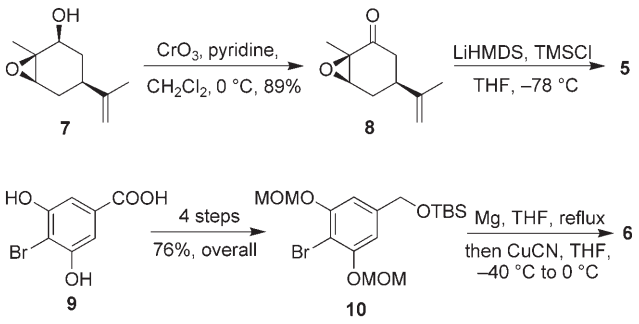

Scheme 4. Preparation of the silyl enol ether **5** and the aryl cyanocuprate reagent **6**. HDMS = hexamethyldisilazide.

alcohol **7**[9] was readily oxidized[10] to the corresponding epoxy ketone **8**, which was converted into its trimethylsilyl enol ether **5** in high overall yield. The reaction between the freshly prepared aryl magnesium bromide derived from compound **10** (see the Supporting Information) and copper cyanide led to the aryl cyanocuprate reagent **6**.[11]

With the necessary components in hand, we carried out the *anti* S_N2' reaction (Scheme 5). Following the slow addition of **5** (1 equiv) to freshly prepared **6** (2 equiv) at −78 °C, the

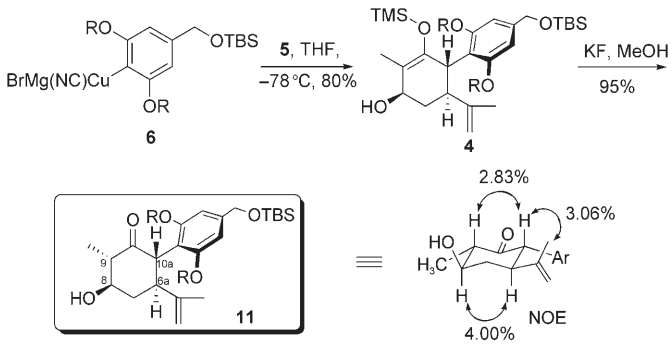

Scheme 5. S_N2' reaction of **6** with **5**. R = MOM.

reaction mixture was warmed to −10 °C over 45 min and stirred for an additional 3 h at −10 to 0 °C. The silyl enol ether **4** was formed in 80% yield as a single diastereoisomer, as determined by ^{1}H NMR spectroscopy. This unstable adduct **4** was immediately subjected to mild hydrolysis to afford the 5,6-seco-HHDBP **11**[5c] with the desired four stereocenters (C8, C9, C6a, C10a) present in the final target. The relative configuration of **11** was determined by 1D NOE spectroscopic analysis (see Scheme 5).

The secondary hydroxy group of **11** was readily protected as its TBS ether **3** (Scheme 6). Efforts to convert the superfluous carbonyl group (C10) into the corresponding

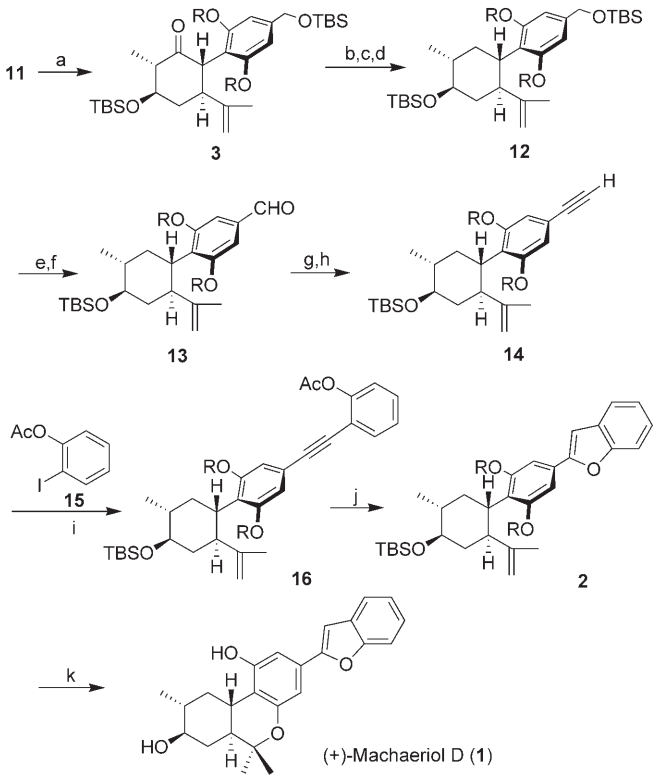

Scheme 6. Total synthesis of (+)-machaeriol D (**1**). a) TBSCl, imidazole, DMF, 89%; b) $LiAlH_4$, THF, −30 °C; c) NaH, CS_2, MeI, 50 °C; d) AIBN (cat.), nBu_3SnH, toluene, 90 °C, 56% (three steps); e) NH_4F, MeOH, reflux, 95%; f) PDC, CH_2Cl_2, 94%; g) CBr_4, PPh_3, Zn dust, CH_2Cl_2, 68%; h) *n*BuLi, THF, −78 °C, 95%; i) [$Pd(PPh_3)_4$], CuI, Et_3N, then **15**, reflux, 89%; j) K_2CO_3, MeOH, reflux, 92%; k) TsOH, MeOH, reflux, 90%. AIBN = azobisisobutyronitrile, DMF = *N*,*N*-dimethylformamide, PDC = pyridinium dichromate, Ts = *para*-toluenesulfonyl; R = MOM.

thioketal or tosylhydrazone for deoxygenation were unsuccessful.[12] Finally, compound **12** was accessed through the reduction of **3** and elaboration of the product[13] to give the methyl xanthate derivative in 85% yield, followed by reduction by Barton radical deoxygenation.[6]

To construct the benzofuran moiety, **12** was first desilylated regioselectively to afford the corresponding primary alcohol, which was oxidized to **13** with PDC. Installation of the requisite alkyne was initiated by the treatment of **13** with CBr_4/PPh_3/Zn according to the Corey–Fuchs protocol[7] to provide the homologated dibromoalkene in 68% yield. Treatment of this material with *n*BuLi then furnished alkyne **14** (95%). Sonogashira coupling[8] of **14** with the commercially available compound **15** (2-iodophenyl acetate) gave the intermediate **16**. Subsequent saponification of the phenolic acetate with concomitant cyclization afforded the desired benzofuran **2** in high yield.

To reach the HHDBP **1** from the 5,6-seco-HHDBP **2**, MOM deprotection and formation of the benzopyran moiety was required. Compound **2** was heated in MeOH at reflux in the presence of TsOH for 12 h to afford the desired product (+)-machaeriol D (**1**) in 90% yield. The spectral properties of the synthetic material were in agreement with those of the natural product.[2]

 © 2006 Wiley-VCH Verlag GmbH & Co. KGaA, Weinheim

In summary, we have developed a new and general strategy for the synthesis of HHDBPs via 5,6-seco-HHDBPs with a highly regio- and stereoselective S_N2' reaction of an aryl cyanocuprate with a silyl enol ether of an optically active α,β-epoxycyclohexanone as the key step. In this way, we have completed the first total synthesis of (+)-machaeriol D. The application of this method to more complex important molecules is currently under investigation by our research group.

Received: January 2, 2006
Published online: April 28, 2006

Keywords: allylic substitution · asymmetric synthesis · benzopyrans · cyanocuprate reagents · natural products

[1] For natural THC, see: a) Y. Gaoni, R. Mechoulam, *J. Am. Chem. Soc.* **1964**, *86*, 1646; b) Y. Gaoni, R. Mechoulam, *J. Am. Chem. Soc.* **1971**, *93*, 217; for natural CBD, see: c) R. Mechoulam, Y. Shvo, *Tetrahedron* **1963**, *19*, 2073; d) R. Mechoulam, Y. Gaoni, *Tetrahedron Lett.* **1967**, 1109; for non-natural HHC, see: e) H. Edery, Y. Grunfeld, Z. Ben-Zvi, R. Mechoulam, *Ann. N. Y. Acad. Sci.* **1971**, *191*, 40; f) R. Mechoulam, N. Lander, T. H. Varkony, I. Kimmel, O. Becker, Z. Ben-Zvi, *J. Med. Chem.* **1980**, *23*, 1068.

[2] I. Muhammad, X.-C. Li, M. R. Jacob, B. L. Tekwani, D. C. Dunbar, D. Ferreira, *J. Nat. Prod.* **2003**, *66*, 804.

[3] For total syntheses of THC and CBD, see: a) R. K. Razdan in *The Total Synthesis of Natural Products, Vol. 4* (Ed.: J. ApSimon), Wiley, New York, **1981**, pp. 185–262; b) R. Mechoulam, N. K. McCallum, S. Burstein, *Chem. Rev.* **1976**, *76*, 1; c) W. E. Childers, H. W. Pinnick, *J. Org. Chem.* **1984**, *49*, 5276; d) L. Crombie, W. M. L. Crombie, S. V. Jamieson, C. J. Palmer, *J. Chem. Soc. Perkin Trans. 2* **1988**, 1243; e) D. A. Evans, E. A. Shaughnessy, D. M. Barnes, *Tetrahedron Lett.* **1997**, *38*, 3193; f) L. Crombie, W. M. L. Crombie, C. J. Palmer, S. V. Jamieson, *Tetrahedron Lett.* **1983**, *24*, 3129; g) R. W. Rickards, H. Ronnenberg, *J. Org. Chem.* **1984**, *49*, 572; h) S.-H. Baek, M. Srebnik, R. Mechoulam, *Tetrahedron Lett.* **1985**, *26*, 1083; i) V. Vaillancourt, K. F. Albizati, *J. Org. Chem.* **1992**, *57*, 3627; for total syntheses of HHC, see: j) L.-F. Tietze, G. von Kiedrowski, B. Berger, *Angew. Chem.* **1982**, *94*, 222; *Angew. Chem. Int. Ed. Engl.* **1982**, *21*, 221; k) Z. Lu, N. Sato, S. Inoue, K. Sato, *Chem. Lett.* **1992**, 1237; l) G. Casiraghi, M. Cornia, G. Casnati, G. G. Fava, M. F. Belicchi, *J. Chem. Soc. Chem. Commun.* **1986**, 271; m) M. Cornia, G. Casiraghi, G. Casnati, L. Zetta, *Gazz. Chim. Ital.* **1989**, *119*, 329; n) J. P. Marino, S. L. Dax, *J. Org. Chem.* **1984**, *49*, 3671; o) J. J. Talley, *J. Org. Chem.* **1985**, *50*, 1695; p) T. Wang, J. P. Burgess, P. H. Reggio, H. H. Seltzman, *Synth. Commun.* **2000**, *30*, 1431.

[4] For a review of S_N2' reactions, see: a) J. A. Marshall, *Chem. Rev.* **1989**, *89*, 1503; for recent reports of S_N2' reactions, see: b) L. Li, D. K. Rayabarapu, M. Nandi, C. Cheng, *Org. Lett.* **2003**, *5*, 1621; c) A. B. Smith III, S. M. Pitram, M. J. Gaunt, S. A. Kozmin, *J. Am. Chem. Soc.* **2002**, *124*, 14516; d) C. Spino, C. Beaulieu, J. Lafrenière, *J. Org. Chem.* **2000**, *65*, 7091; e) X. Wang, Y. Wu, S. Jiang, G. Singh, *J. Org. Chem.* **2000**, *65*, 8146; f) C. Xie, P. Nowak, Y. Kishi, *Org. Lett.* **2002**, *4*, 4427; g) Y. Iura, T. Sugahara, K. Ogasawara, *Org. Lett.* **2001**, *3*, 291; h) N. Harrington-Frost, H. Leuser, M. I. Calaza, F. F. Kneisel, P. Knochel, *Org. Lett.* **2003**, *5*, 2111; i) D. Soorukram, P. Knochel, *Org. Lett.* **2004**, *6*, 2409; j) M. I. Calaza, X. Yang, D. Soorukram, P. Knochel, *Org. Lett.* **2004**, *6*, 529.

[5] a) J. P. Marino, N. Hatanaka, *J. Org. Chem.* **1979**, *44*, 4467; b) P. A. Wender, J. M. Erhardt, L. J. Letendre, *J. Am. Chem. Soc.* **1981**, *103*, 2114; c) J. P. Marino, J. C. Jaén, *J. Am. Chem. Soc.* **1982**, *104*, 3165; d) J. P. Marino, M. G. Kelly, *J. Org. Chem.* **1981**, *46*, 4389; e) J. P. Marino, F. Pradilla, E. Laborde, *J. Org. Chem.* **1987**, *52*, 4898; f) D. L. J. Clive, P. L. Wickens, G. V. J. Silva, *J. Org. Chem.* **1995**, *60*, 5532; g) P. S. Banran, J. M. Richter, *J. Am. Chem. Soc.* **2005**, *127*, 15394.

[6] a) D. H. R. Barton, S. W. McCombie, *J. Chem. Soc. Perkin Trans. 2* **1975**, *16*, 1574; b) D. H. R. Barton, D. C. A. Lobberding, S. Z. Zard, *Tetrahedron* **1986**, *42*, 2329; c) for a review, see: D. Crich, L. Quintero, *Chem. Rev.* **1989**, *89*, 1413.

[7] E. J. Corey, P. L. Fuchs, *Tetrahedron Lett.* **1972**, 3769.

[8] K. Sonogashira, Y. Tohda, N. Hagihara, *Tetrahedron Lett.* **1975**, 4467.

[9] a) L. Garver, P. Eikeren, *J. Org. Chem.* **1976**, *41*, 2773; b) A. Yasuda, H. Yamamoto, H. Nozaki, *Bull. Chem. Soc. Jpn.* **1979**, *52*, 1757.

[10] R. Ratcliffe, R. Rodehorst, *J. Org. Chem.* **1970**, *35*, 4000.

[11] The freshly prepared aryl magnesium bromide was added to an equivalent amount of reagent-grade cuprous cyanide (Aldrich) in anhydrous THF at −40 °C under a nitrogen atmosphere. The initially suspended cuprous cyanide went into solution within 1 h upon warming from −40 to 0 °C.

[12] Back-transformation of **3** to **11** in the presence of acid was the reason for the failure of these reactions.

[13] No evidence of a second diastereomer was seen by ^{1}H NMR spectroscopy (400 MHz).

 © 2006 Wiley-VCH Verlag GmbH & Co. KGaA, Weinheim

Porous Solids

DOI: 10.1002/anie.200503950

A Nanowire–Nanoparticle Cross-Linking Approach to Highly Porous Electrically Conducting Solids**

Nidhal N. Akl, Olga Trofymluk, Xiubin Qi, Jin Y. Kim, Frank E. Osterloh, and Alexandra Navrotsky**

As a result of their high surface-to-volume ratios, porous inorganic solids have found technological applications as

[*] N. N. Akl, X. Qi, J. Y. Kim, Prof. F. E. Osterloh
Department of Chemistry
University of California at Davis
One Shields Avenue, Davis, CA 95616 (USA)
Fax: (+1) 530-752-8995
E-mail: fosterloh@ucdavis.edu

O. Trofymluk, Prof. A. Navrotsky
Thermochemistry facility and NEAT ORU
University of California at Davis
One Shields Avenue, Davis, CA 95616 (USA)
Fax: (+1) 530-752-8995
E-mail: anavrotsky@ucdavis.edu

[**] This work was supported by a grant (CTS 04-27418) from the National Science Foundation. We thank Prof. Susan Kauzlarich for providing a furnace for the synthesis of starting materials.

Supporting information (full experimental details) for this article is available on the WWW under http://www.angewandte.org or from the author.

 © 2006 Wiley-VCH Verlag GmbH & Co. KGaA, Weinheim

molecular sieves, ion exchangers, and catalysts.[1] Recent research in the area of porous solids has also led to materials that combine high surface areas with electrical conductivity.[2] These porous conductors are desirable components in batteries, sensors, fuel cells, capacitors,[3] and electrocatalysts.[4] Porous conductors are typically synthesized by chemical linkage of electrically conductive colloidal building blocks (e.g. V_2O_5)[5,6] and their precursors (e.g. resorcine),[7] or by applying conductive coatings (e.g. RuO_2)[4] to existing porous solids. Another approach is to introduce mobile ions into porous structures.[8,9] We describe herein a novel approach to metallic porous solids that is based on cross-linking $LiMo_3Se_3$ nanowires with Ag nanoparticles. $LiMo_3Se_3$ nanowires (for structure see bottom of Figure 1) can be obtained easily by exfoliation of the corresponding Chevrel phase.[10,11] Owing to their metallic properties[12,13] the nanowires have been investigated as components in electrically conducting composites,[14–17] as electrode materials for Li-battery applications,[18] and as analyte-detection devices in nanowire-film chemiresistors.[19] When an aqueous dispersion of $LiMo_3Se_3$ nanowires is added to an aqueous dispersion of citrate-coated silver nanoparticles (15 ± 5 nm), a gel forms within minutes (Figure 1). Further analysis (see below) shows that the gel is

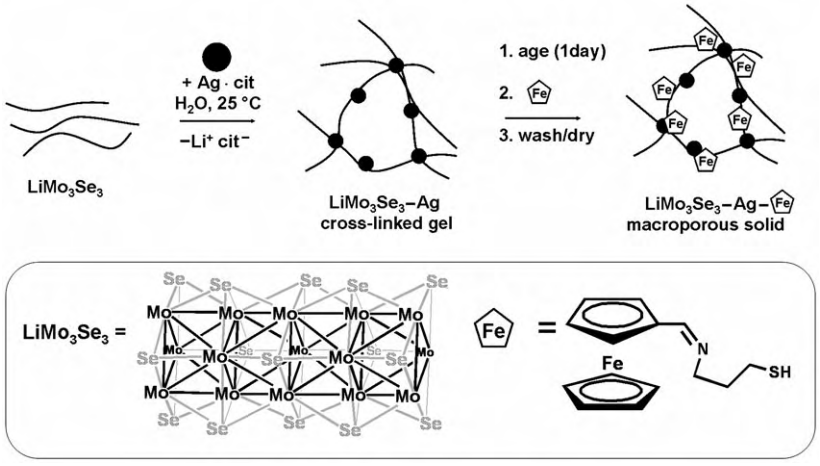

Figure 1. Synthesis and derivatization of the $LiMo_3Se_3$–Ag xerogel. cit = citrate; black circle = Ag nanoparticle. Li ions are omitted in the schematic structure of $LiMo_3Se_3$.

composed of silver nanoparticles that connect nanowire bundles through presumably covalent bonds between the silver and selenide ions. Similar covalent interactions occur in $LiMo_3Se_3$–Au and $LiMo_3Se_3$–CdSe composites.[17] These Ag–Se bonds form within seconds after mixing the reagents, as proven by the fact that centrifugation of a fresh reaction mixture leads to complete sedimentation of all inorganic materials whereas separate dispersions of silver nanoparticles and $LiMo_3Se_3$ nanowires are stable for weeks under similar conditions.

When left at 5 °C for 12 h, the gel shrinks to about 0.25 % of its original volume leaving behind a clear solution that is yellow owing to residual silver colloids (Figure 2 A). We postulate that the densification is driven by the tendency of the composite to maximize nanoparticle–nanowire interac-

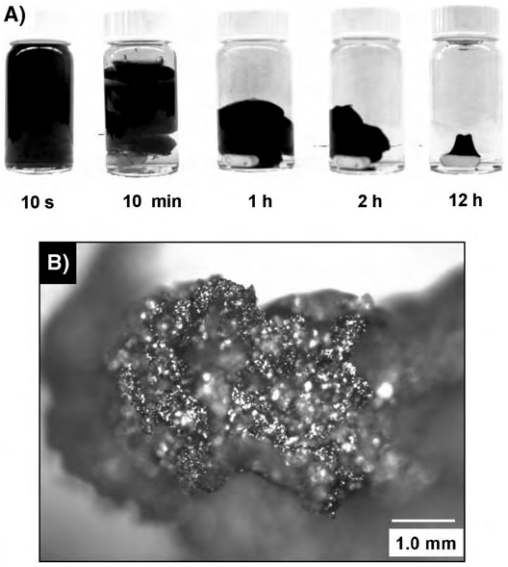

Figure 2. A) Evolution of the gel over time (note the stir bar at the bottom of the vial). B) Optical micrograph of the xerogel after drying in vacuum.

tions. The decrease of gel volume is accompanied by expulsion of pore fluid (syneresis) from the gel.[20] By decanting the clear mother liquor after 12 h and drying the deep-red solid in vacuo, one obtains a reflective solid with a volume of approximately 0.06 cm^3. The optical appearance of the xerogel (Figure 2 B) is indicative of metallic character.

Electron micrographs of a typical xerogel are shown in Figure 3 A–D. The images show that the solid contains a network of 2–6-μm large, irregularly shaped macropores. Furthermore, there are mesopores with sizes ranging from 15 to 130 nm (mean size 40 ± 21 nm, averaged over 45 mesopores) contained in the walls (Figure 3 D) of the xerogel. While these mesopores result from random packing of nanowires and nanoparticles, the macropores seem to form during expansion of the solvent (water) during vacuum drying. If the water is replaced by methanol prior to the drying step, the xerogels contain only mesopores with a mean size of 25 ± 10 nm (averaged over 35 mesopores). This observation demonstrates that water is essential for the formation of the macropores.

By altering the nanoparticle–nanowire stoichiometry in the synthesis, it is possible to tailor the size of the macropores of the xerogel. Figure 3 E shows pore-size distributions for gels assembled with the indicated stoichiometric ratios. The average pore size increases with increasing nanoparticle–nanowire ratio. This seems counterintuitive, as one might expect that increasing the number of cross-linkage points would produce a tighter-knit nanowire network. Instead, it seems that the pore sizes are determined by the kinetics of water evaporation. We hypothesize that the formation vapor bubbles is suppressed in the tightly knit and probably mechanically more robust mesh. Most of the water therefore evaporates from a small number of large water-vapor bubbles.

 © 2006 Wiley-VCH Verlag GmbH & Co. KGaA, Weinheim

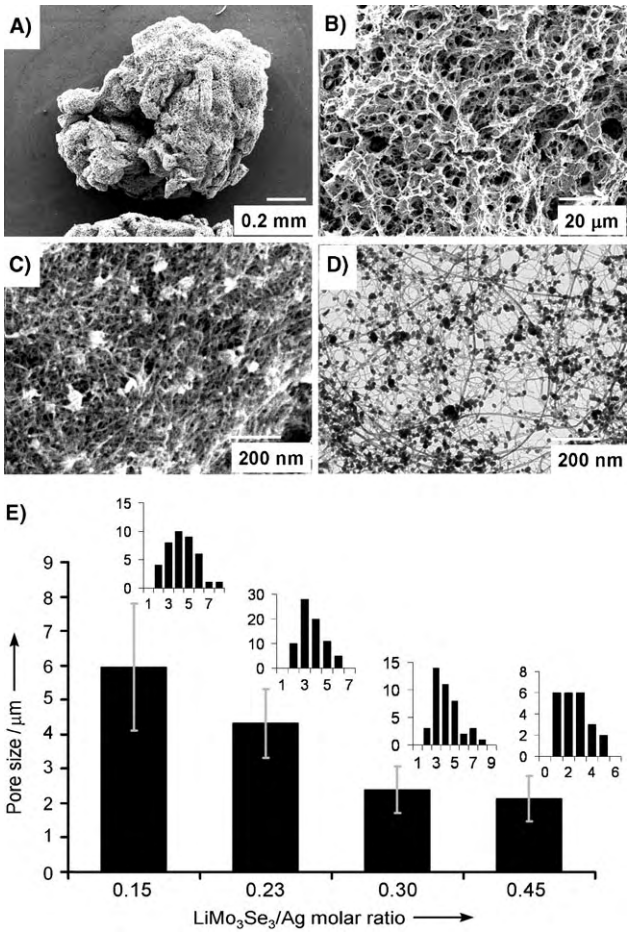

Figure 3. Variable magnification SEM (A–C) and TEM (D) images of the porous solid obtained with a $LiMo_3Se_3$/Ag ratio of 0.45. The thickness of the $LiMo_3Se_3$ nanowires (8.0 ± 1.7 nm) indicates the presence of bundles.[19] E) Effect of nanowire–nanoparticle stoichiometry on the mean mesopore sizes and the pore-size distributions (insets). Pore sizes were obtained from SEM images by measuring at least 80 pores in each sample. The error bars show standard deviations.

Smaller bubbles form (but in greater numbers) in the less tightly knit and mechanically less robust nanowire network, which eventually leads to a smaller mean pore size. This hypothesis is supported by the observation (from microscopy) that the number density of pores is smaller for xerogels with larger pores.

Nitrogen-adsorption porosimetry measurements were performed to complement the SEM/TEM analysis of the porous materials for pore sizes below 0.5 µm. For $LiMo_3Se_3$–Ag (0.23 mole ratio), the measurements reveal a rather wide pore-size distribution in the range 3–500 nm with an average pore size of 28 nm (see the Supporting Information). This value is in good agreement with the SEM data for the mesopores (40 ± 21 nm). The pore volume and the specific surface area (BET) were determined as $0.89\ cm^3\,g^{-1}$ and $760\ m^2\,g^{-1}$, respectively. These relatively large values indicate extensive porosity comparable with that in mesoporous silica.[21]

Resistance measurements reveal that the specific conductivity of the $LiMo_3Se_3$–Ag xerogel is $1.6\ S\,cm^{-1}$ (at 300 K). This value is significantly above that for conductive xerogels containing RuO_2 (10^{-3}–$10^{-7}\ S\,cm^{-1}$),[3,4] or MoO_3 ($10^{-5}\ S\,cm^{-1}$), and even exceeds the values for MoO_3–polypyrrol aerogel composites ($4 \times 10^{-3}\ S\,cm^{-1}$).[2] The low resistivity of the xerogel is attributable to the metallic character of its components and the connectivity of its framework.

A useful feature of the $LiMo_3Se_3$–Ag xerogels is their propensity for chemical derivatization with redox-active groups that become electrochemically accessible through the nanowire–nanoparticle network. Treatment of the gel with 3-{[(*E*)-ferrocenylmethylidene]amino}-1-propanethiol in methanol (as shown in Figure 2A) leads to a solid that contains approximately 1 mol% thiol (calculated on the basis of the Fe content observed with energy-dispersive spectroscopy). Control experiments show that the ferrocene thiol derivative also binds to pure $LiMo_3Se_3$ nanowires. We therefore conclude that thiol groups in the xerogel are bonded to both the silver and the nanowire portions.

Cyclic voltammograms (CVs) of $LiMo_3Se_3$–Ag and $LiMo_3Se_3$–Ag–Fc′ are shown in Figure 4 (Fc′ = thiol-functionalized ferrocene). The CV of $LiMo_3Se_3$–Ag reveals a broad

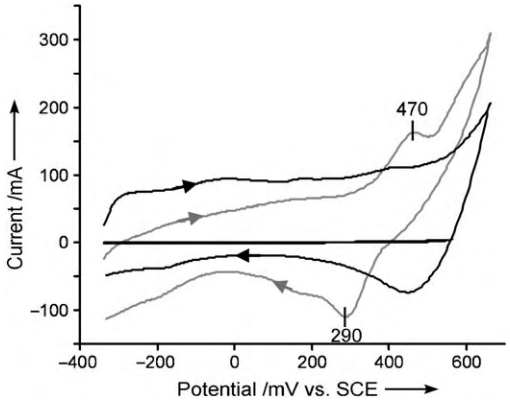

Figure 4. Cyclic voltammograms of porous monoliths (ca. 0.1 mg) in acetonitrile. $LiMo_3Se_3$–Ag (gray curve), $LiMo_3Se_3$–Ag–Fc′ (black curve). At around +0.50 V (vs. SCE) the nanowires of both composites are irreversibly oxidized.

feature that is consistent with capacitive charging under the applied potential. At potentials greater than +500 mV (vs. SCE), the nanowires in the xerogel are oxidized. The limited stability of $LiMo_3Se_3$ towards oxidation is a drawback of this material.

The CV of the thiol-functionalized solid is similar to that of the nonfunctionalized xerogel, except for the presence of additional redox features at +0.47 and +0.29 V, which correspond to the reversible oxidation process involving the ferrocene thiol derivative. The observed redox potential of +0.38 V (vs. SCE) is lower than that of the free thiol in CH_2Cl_2 (+0.49 V), which may be attributable to the different solvents (the potential for ferrocene moves from +0.46 V in CH_2Cl_2 to +0.40 V in the more polar MeCN).[22] The separation of the peaks by 0.18 V is likely caused by the finite mobility of the electrolyte NBu_4PF_6 in the porous network which limits the reversibility of the redox process. At

 © 2006 Wiley-VCH Verlag GmbH & Co. KGaA, Weinheim

higher scan rates (ca. 100 mV s^{-1}) this effect leads to the complete disappearance of the thiol redox peaks. The CV shows that the electroactive groups inside the pores of the xerogel are electrically accessible through the metallic network.

In conclusion, we have shown that electrically conducting porous materials with adjustable pore sizes can be synthesized by using a new and very simple nanowire–nanoparticle cross-linking approach. The combination of high surface area, good electrical conductivity, and the ease of chemical derivatization make the material interesting as a high-surface-area electrode material for use in batteries or in electrocatalytic applications. The use of $LiMo_3Se_3$–Ag as a precursor to aerogels is currently under investigation.

Experimental Section

$LiMo_3Se_3$–Ag: To prepare the gel, variable volumes (0.1–0.3 mL) of a $LiMo_3Se_3$ nanowire solution (1.88 mM) were added dropwise to silver nanoparticle (15 ± 5 nm) solution (5.0 mL, 0.25 mM) in a 20-mL vial with rapid stirring. The resulting mixture was capped and stored in a refrigerator at 5 °C. After 12 h, the reddish gel had shrunk to about 0.25 % of its original volume. The clear aqueous layer was decanted, and the gel was washed carefully by addition of water to remove excess electrolytes. Drying in vacuo produced the metallic xerogel in quantitative yield (based on $LiMo_3Se_3$).

Thiol-functionalized $LiMo_3Se_3$–Ag: The $LiMo_3Se_3$–Ag gel as synthesized above was washed with methanol to remove residual water, then immersed in a solution of 3-{[(*E*)-ferrocenylmethylidene]amino}-1-propanethiol (5 mL, 0.125 M) in methanol. After 12 h, the gel was removed from the solution and carefully washed with three 20-mL aliquots of methanol. After the gel was soaked in fresh methanol for 12 h, the supernatant was decanted, and the solid was dried in a vacuum to obtain the thiol-modified xerogel.

Received: November 8, 2005
Revised: March 9, 2006
Published online: April 26, 2006

Keywords: Chevrel phases · gels · mesoporous materials · nanostructures

[1] N. Husing, U. Schubert, *Angew. Chem.* **1998**, *110*, 22; *Angew. Chem. Int. Ed.* **1998**, *37*, 23.
[2] D. R. Rolison, B. Dunn, *J. Mater. Chem.* **2001**, *11*, 963.
[3] J. W. Long, K. E. Swider, C. I. Merzbacher, D. R. Rolison, *Langmuir* **1999**, *15*, 780.
[4] J. V. Ryan, A. D. Berry, M. L. Anderson, J. W. Long, R. M. Stroud, V. M. Cepak, V. M. Browning, D. R. Rolison, C. I. Merzbacher, *Nature* **2000**, *406*, 169.
[5] F. Carn, N. Steunou, J. Livage, A. Colin, R. Backov, *Chem. Mater.* **2005**, *17*, 644.
[6] W. Dong, J. S. Sakamoto, B. Dunn, *Sci. Technol. Adv. Mater.* **2003**, *4*, 3.
[7] J. W. Long, B. M. Dening, T. M. McEvoy, D. R. Rolison, *J. Non-Cryst. Solids* **2004**, *350*, 97.
[8] T. Kamiya, H. Hosono, *Semicond. Sci. Technol.* **2005**, *20*, S92.
[9] O. Trofymluk, Y. Toda, H. Hosono, A. Navrotsky, *Chem. Mater.* **2005**, *17*, 5574.
[10] M. Potel, R. Chevrel, M. Sergent, J. C. Armici, M. Decroux, O. Fischer, *J. Solid State Chem.* **1980**, *35*, 286.
[11] J. M. Tarascon, F. J. DiSalvo, C. H. Chen, P. J. Carroll, M. Walsh, L. Rupp, *J. Solid State Chem.* **1984**, *54*, 290.
[12] L. Venkataraman, C. M. Lieber, *Phys. Rev. Lett.* **1999**, *83*, 5334.
[13] J. H. Song, B. Messer, Y. Y. Wu, H. Kind, P. D. Yang, *J. Am. Chem. Soc.* **2001**, *123*, 9714.
[14] J. K. Vassiliou, R. P. Ziebarth, F. J. Disalvo, *Chem. Mater.* **1990**, *2*, 738.
[15] J. H. Golden, F. J. Disalvo, J. M. J. Frechet, *Chem. Mater.* **1995**, *7*, 232.
[16] J. H. Golden, F. J. Disalvo, J. M. J. Frechet, J. Silcox, M. Thomas, J. Elman, *Science* **1996**, *273*, 782.
[17] F. E. Osterloh, J. S. Martino, H. Hiramatsu, D. P. Hewitt, *Nano Lett.* **2003**, *3*, 125.
[18] J. M. Tarascon, *J. Electrochem. Soc.* **1985**, *132*, 2089.
[19] X. B. Qi, F. E. Osterloh, *J. Am. Chem. Soc.* **2005**, *127*, 7666.
[20] C. J. Brinker, G. W. Scherer, *Sol–Gel Science*, Academic Press, New York, **1990**.
[21] D. Y. Zhao, Q. S. Huo, J. L. Feng, B. F. Chmelka, G. D. Stucky, *J. Am. Chem. Soc.* **1998**, *120*, 6024.
[22] N. G. Connelly, W. E. Geiger, *Chem. Rev.* **1996**, *96*, 877.

 © 2006 Wiley-VCH Verlag GmbH & Co. KGaA, Weinheim

Analytical Methods

DOI: 10.1002/anie.200600660

Thermal Production and Reactions of Organic Ions at Atmospheric Pressure**

*Hao Chen, Zheng Ouyang, and R. Graham Cooks**

Ionization of nonvolatile compounds has been accomplished by a wide selection of desorption ionization (DI) methods in which the sample is converted from the condensed phase into vapor-phase ions by high-energy particles (neutral species or ions with energies of 5 keV–100 MeV), photon beams (UV or IR energy range), or high electric fields (ca. $10^{10}\,V\,m^{-1}$). Particular examples include secondary-ion mass spectrometry (SIMS),[1] fast atom bombardment (FAB),[2,3] plasma desorption (PD),[4] laser desorption (LD),[5,6] and field desorption (FD).[7] We now report a simple desorption method in which organic ions are generated efficiently by heating organic salts at atmospheric pressure; we also report reactions of these ions under ambient conditions. Although thermal ionization of low ionization energy elements is well-known,[8,9] atmospheric-pressure thermal desorption ionization (APTDI) of organic ions, as reported here, is unprecedented. Appropriate choices of the matrix and solvent strongly increase ion

[*] Dr. H. Chen, Dr. Z. Ouyang, Prof. R. G. Cooks
Department of Chemistry
Purdue University
560 Oval Drive, West Lafayette, IN 47907 (USA)
Fax: (+1) 765-494-9421
E-mail: cooks@purdue.edu

[**] This work was supported by the US National Science Foundation (CHE04-12782).

Supporting information for this article is available on the WWW under http://www.angewandte.org or from the author.

WILEY InterScience DISCOVER SOMETHING GREAT
© 2006 Wiley-VCH Verlag GmbH & Co. KGaA, Weinheim

intensities in APTDI. Significantly, atmospheric pressure ion–molecule reactions, which have relied on either radiolysis[10–12] or special high-pressure mass spectrometers,[13] now can be studied easily in the atmosphere by using thermally produced ions. Reactions in this pressure regime bridge condensed-phase and gas-phase ion chemistry.[10,14]

Figure 1 shows the positive-ion APTDI mass spectra of representative organic salts recorded after rapidly heating them in a nitrogen gas stream which carries the ions to a distant mass spectrometer (see apparatus description in the Supporting Information). The model compounds have either

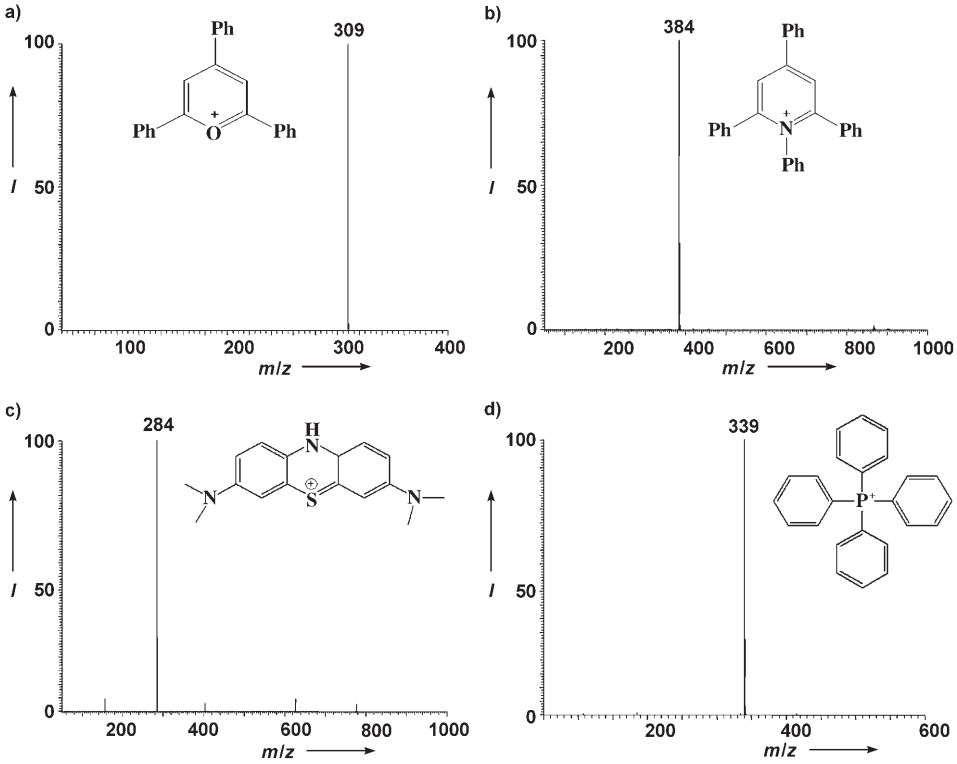

Figure 1. APTDI mass spectra of organic salts: a) $\mathbf{1}^+BF_4^-$, b) $\mathbf{2}^+ClO_4^-$, c) $\mathbf{3}^+Cl^-$, and d) $\mathbf{4}^+Br^-$.

O-, N-, S-, or P-centered positive charges, as represented by 2,4,6-triphenylpyrylium tetrafluoroborate ($\mathbf{1}^+BF_4^-$), 1,2,4,6-tetraphenylpyridinium perchlorate ($\mathbf{2}^+ClO_4^-$), methylene blue ($\mathbf{3}^+Cl^-$), and tetraphenylphosphonium bromide ($\mathbf{4}^+Br^-$). In these and related spectra, the cation typically appears as the base peak and fragmentation is insignificant. Collision-induced dissociation (CID) can be used to produce fragmentation; for example, the thermally generated cation $\mathbf{1}^+$ (*m*/*z* 309) gives rise to the benzoyl cation $PhCO^+$ at *m*/*z* 105 as well as fragment ions of *m*/*z* 203 and 231 arising from the loss of benzaldehyde and benzene, respectively. This result matches the dissociation behavior seen for the same ion generated by electrospray ionization (ESI; see the Supporting Information) or by electron ionization (EI),[15,16] thus confirming the structure of the cation generated by thermal desorption at atmospheric pressure.

The hypothesis that ions can be formed in a field-independent thermal desorption process was initially proposed by Holland et al.[17] in connection with a model for ionization by field desorption (FD) and it was later unambiguously observed in the thermal evaporation of quaternary ammonium and phosphonium salts in vacuo by Stoll and Röllgen[18] as well as by Cotter and Yergev.[19] The present work, however, appears to represent the first case of thermal desorption of organic salts at atmospheric pressure. Remarkably, we find that two popular ionic liquids,[20] 1-ethyl-3-methyl-1,3-imidazolium tetrafluoroborate ($\mathbf{5}^+BF_4^-$; see the Supporting Information) and 1,3-dimethylimidazolium methyl sulfate ($\mathbf{6}^+CH_3SO_4^-$), generate the corresponding imidazolium cations during heating, despite the fact that ionic liquids are known to have negligible vapor pressures.[20,21] The emission of ions from the viscous ionic liquids at moderately elevated temperature indicates that the strong ionic interactions in the liquid can be broken thermally. Collision-induced dissociation of $\mathbf{5}^+$ (*m*/*z* 111) yields a fragment ion of *m*/*z* 83 through loss of ethylene, the same process as observed for the ESI-generated imidazolium ion. The present observations on ion desorption from heated ionic liquids corroborate a very recent report[22] on the distillation and volatility of ionic liquids that we learned of after completing this study. Besides these nonmetallic organic salts, we also investigated the thermal ionization of organometallic salts and observed the formation of intact cations from organometallic salts by APTDI (see the Supporting Information for the example of bis(cyclopentadienyl)cobalt(III) hexafluorophosphate ($\mathbf{7}^+PF_6^-$)). Anions were also observed (for example, the production of a perchlorate ion (*m*/*z* 99 and 111) from APTDI of the salt $\mathbf{2}^+ClO_4^-$; see the Supporting Information). In other cases, adduct ions accompanied the observed intact cations, for example, from tertiary and quaternary ammonium salts (see the Supporting Information).

Favorable effects of matrix on ion yields were observed in APTDI, analogous to those seen in conventional desorption ionization, including MALDI. The intensity of the signal corresponding to the $\mathbf{2}^+$ ion (*m*/*z* 384) generated from $\mathbf{2}^+ClO_4^-$ was enhanced by more than 20 times in the presence of $\mathbf{1}^+BF_4^-$ (Figure 2). It is rationalized that the addition of the matrix decreases the thermal decomposition of $\mathbf{2}^+ClO_4^-$, probably by decreasing the sublimation temperature. A related observation is that doping of the nitrogen carrier gas with a polar solvent such as methanol also greatly increases the ion yield. For example, the signal for the $\mathbf{1}^+$ ion at *m*/*z* 309

 © 2006 Wiley-VCH Verlag GmbH & Co. KGaA, Weinheim

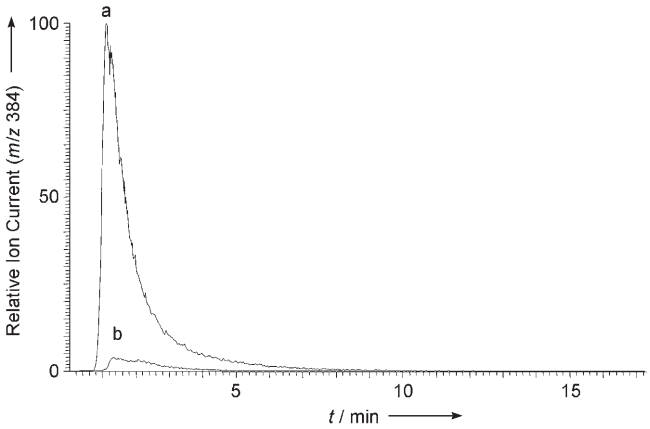

Figure 2. Relative ion currents of the $\mathbf{2}^+$ ion (m/z 384) recorded during APTDI of salt $\mathbf{2}^+ClO_4^-$ with (trace a) and without a matrix of salt $\mathbf{1}^+BF_4^-$ (trace b). During APTDI, the signal corresponding to the matrix ion $\mathbf{1}^+$ was also observed at m/z 309.

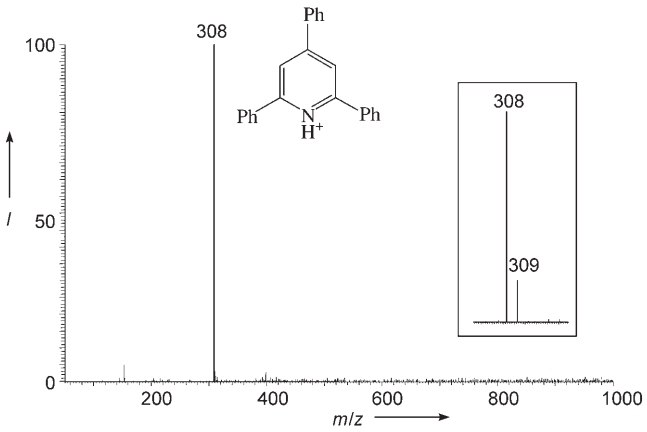

Figure 3. Mass spectrum recorded on heating neutral 2,4,6-triphenylpyridine with methanol/water-doped nitrogen carrier gas. The heater temperature was set at 100 °C. The inset shows the intact cation region.

from salt $\mathbf{1}^+BF_4^-$ was increased by about 30 times using methanol-doped N_2 carrier gas (see the Supporting Information). It is likely that methanol effectively solvates the generated cations/anions and prevents their recombination. The solvated ions subsequently undergo complete desolvation before mass analysis.

Strong ion signals are seen for organic salts such as $\mathbf{2}^+ClO_4^-$ and tetrapropylammonium bromide ($\mathbf{8}^+Br^-$) even using amounts as small as 200 pg (see the Supporting Information). The relatively low efficiency of ionization achieved in previous vacuum thermal evaporation experiments[23,24] (large quantities of sample were used, for example, 1 mg) limited their applicability as an analytical method. Counterintuitively, desorption is more efficient when heating is carried out at atmospheric pressure, probably because the numerous collisions at atmospheric pressure favor charge separation.

The most distinctive feature of the APTDI method is that ion desorption occurs at atmospheric pressure. Charge separation and ion formation in the gas phase occur outside the mass spectrometer, as demonstrated by the drop in ion intensity when a deflecting electrical field (which can be thought of as an ion switch, see the Supporting Information) is placed ahead of the ion-sampling atmospheric-pressure interface of the mass spectrometer. A demonstration of the complete removal of a strong stable signal by the simple "ion switch" is shown in the Supporting Information.

The dramatic solvent-doping effect encouraged us to perform an experiment in which thermal evaporation of a neutral base was followed by gas-phase protonation[25] using a protic-solvent-doped carrier gas. As shown in Figure 3, successful ionization of neutral 2,4,6-triphenylpyridine was observed.

The reactivity of thermally produced ions has also been examined. Since APTDI usually generates intact cations/anions from salts and gives very simple mass spectra, it is possible to perform atmospheric pressure ion–molecule reactions without mass-selection of the reactant ions—currently a formidable task outside the mass spectrometer. Gas-phase ion chemistry under conditions of very high pressure ($0.01 \approx 10$ atm)[12,13] gives kinetic, structural, and stereochemical information which allows meaningful correlations between gas-phase and condensed-phase ion chemistry.[10] To perform atmospheric pressure ion–molecule reactions we generated reactant ions by APTDI in the presence of a neutral reagent in a nitrogen gas stream which served to carry the ion–molecule reaction products into the mass spectrometer. The reaction of cation $\mathbf{1}^+$ with aniline to give $\mathbf{2}^+$ represents an example. In addition to such homogeneous ion/molecule reactions, heterogeneous reactions can also be studied (for example, the reaction of thermally generated gas-phase reactant ions in a gas stream with condensed-phase neutral reagents present on a surface). Such reactions[26] differ in several important characteristics from conventional ion–molecule reactions: 1) they take place at the heterogeneous gas–solid interface; 2) the neutral analyte molecule can be heavy, polar, and nonvolatile; 3) in situ derivatization of the analyte on the surface allows its fast selective detection. The inset of Figure 4 displays the ion–molecule reaction of $\mathbf{1}^+$ (m/z 309) generated by APTDI of $\mathbf{1}^+BF_4^-$ with solid D-lysine present on a metal surface to yield the norleucyl-substituted pyridinium product ion of m/z 437 (Figure 4a). The conversion of pyrylium into pyridinium ions[27–29] is an important route for the conversion of primary amino groups into a variety of other functionalities such as halide, ester, alcohol, nitrate, thiocyanate, and azide. The structure of the product ion (m/z 437) was confirmed by its CID spectrum, which showed the formation of a signal at m/z 308 arising from the loss of 2-amino-5-hexenoic acid.

An alternative general approach for carrying out heterogeneous or homogeneous ion–molecule reactions at atmospheric pressure is to label the reactant with a charge site which is responsible for thermal desorption but is remote from the active functional group at which ion–molecule reactions can occur. As a demonstration, 1-(4-aminophenyl)-2,4,6-triphenylpyridinium cation ($\mathbf{9}^+$, m/z 399) was chosen as the reactant ion (charge-labeled aniline, shown in Figure 5). The organic salt $\mathbf{9}^+BF_4^-$ used in this study was synthesized

 © 2006 Wiley-VCH Verlag GmbH & Co. KGaA, Weinheim

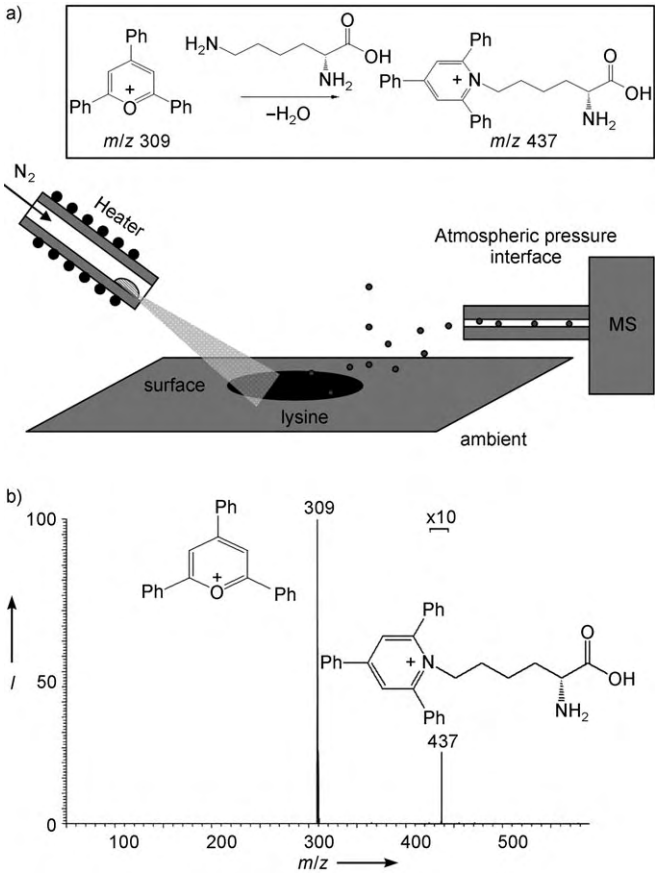

Figure 4. a) Schematic representation of the desorption ionization of D-lysine by the thermally produced $\mathbf{1}^+$ ion (*m*/*z* 309) at atmospheric pressure; b) mass spectrum showing the generation of norleucyl-substituted pyridinium ion (*m*/*z* 437) in a heterogeneous ion/molecule reaction.

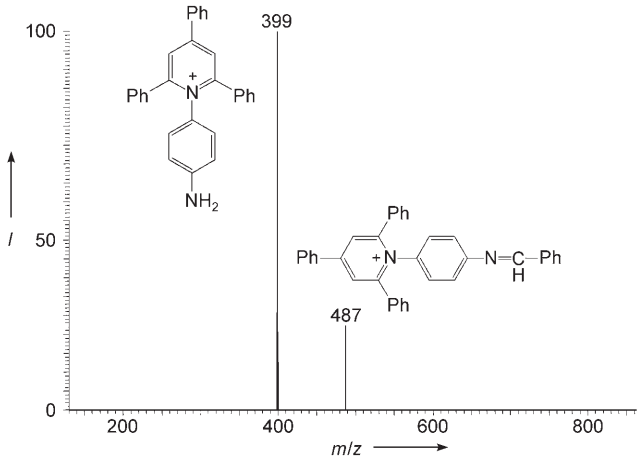

Figure 5. Mass spectrum showing the ion–molecule reaction of the thermally generated $\mathbf{9}^+$ ion and benzaldehyde in the homogeneous phase to form a Schiff base at atmospheric pressure.

from $\mathbf{1}^+BF_4^-$ and *para*-phenylenediamine following the standard procedure for the synthesis of pyrydinium salts[27] (characterization data are shown in the Supporting Information). In this case, thermally generated ions $\mathbf{9}^+$ were transported in a pure nitrogen gas stream into a reactor where they reacted with benzaldehyde vapor. The reactor volume is outside the mass spectrometer and the Schiff base product is carried into the instrument by the nitrogen stream and is observed at *m*/*z* 487 (Figure 5). When benzaldehyde was replaced by propionaldehyde or *para*-tolualdehyde, the corresponding product ions of *m*/*z* 439 or 501 were observed, respectively (see the Supporting information).

In conclusion, we have shown a new atmospheric pressure method (APTDI) to generate gas-phase ions as well as novel protocols for performing ion–molecule reactions at atmospheric pressure. Organic salts are readily available and the simplicity of direct thermal evaporation at atmospheric pressure together with the possibility of studying the reactivity of the thermally produced ions gives these findings potential to have a significant impact in gas-phase ion chemistry as well as to have promising applications for in situ chemical analysis. These results, including the general lack of fragmentation in the reported spectra, point to the unexpected possibility that many materials, when heated in an inert atmosphere at an appropriate rate, will sublime rather than decompose or polymerize.

Received: February 20, 2006
Published online: April 26, 2006

Keywords: analytical methods · ionic liquids · ion–molecule reactions · mass spectrometry · thermal desorption

[1] A. Benninghoven, H. W. Werner, F. G. Rudenauer, *Secondary Ion Mass Spectrometry: Basic Concepts, Instrumental Aspects, Applications*, Wiley-Interscience, New York, **1986**.
[2] M. Barber, R. S. Bordoli, R. D. Sedgwick, A. N. Tyler, *J. Chem. Soc. Chem. Commun.* **1981**, 325.
[3] C. Fenselau, R. J. Cotter, *Chem. Rev.* **1987**, *87*, 501.
[4] C. J. McNeal, R. D. Macfarlane, *J. Am. Chem. Soc.* **1981**, *103*, 1609.
[5] M. Karas, U. Bahr, U. Giessmann, *Mass Spectrom. Rev.* **1991**, *10*, 335.
[6] F. Hillenkamp, M. Karas, R. C. Beavis, B. T. Chait, *Anal. Chem.* **1991**, *63*, 1193A.
[7] H. D. Beckey, *Principles of Field Ionization and Field Desorption in Mass Spectrometry*, Pergamon, Oxford, **1977**.
[8] D. W. Koppenaal, *Anal. Chem.* **1988**, *60*, 113R.
[9] D. H. Smith, *Pract. Spectrosc.* **2000**, *25*, 1.
[10] F. Cacace, *Acc. Chem. Res.* **1988**, *21*, 215.
[11] M. Attina, F. Cacace, P. Giacomello, M. Speranza, *J. Am. Chem. Soc.* **1980**, *102*, 6896.
[12] M. Speranza, *Mass Spectrom. Rev.* **1992**, *11*, 73.
[13] W. B. Knighton, E. P. Grimsrud, *Adv. Gas Phase Ion Chem.* **1996**, *2*, 219.
[14] R. G. Cooks, H. Chen, M. N. Eberlin, X. Zheng, W. A. Tao, *Chem. Rev.* **2006**, *106*, 188.
[15] K. L. Busch, B.-H. Hsu, K. W. Wood, R. G. Cooks, *J. Org. Chem.* **1984**, *49*, 764.
[16] A. M. Deffield, C. Djerassi, A. T. Balaban, *Org. Mass Spectrom.* **1971**, *5*, 87.
[17] J. F. Holland, B. Soltmann, C. C. Sweeley, *Biomed. Mass Spectrom.* **1976**, *3*, 340.
[18] R. Stoll, F. W. Röllgen, *J. Chem. Soc. Chem. Commun.* **1980**, 789.
[19] R. J. Cotter, A. L. Yergey, *J. Am. Chem. Soc.* **1981**, *103*, 1596

 © 2006 Wiley-VCH Verlag GmbH & Co. KGaA, Weinheim

[20] J. Dupont, J. Spencer, *Angew. Chem.* **2004**, *116*, 5408; *Angew. Chem. Int. Ed.* **2004**, *43*, 5296.
[21] T. Welton, *Chem. Rev.* **1999**, *99*, 2071.
[22] M. J. Earle, J. M. S. S. Esperanc, M. A. Gilea, J. N. C. Lopes, L. P. N. Rebelo, J. W. Magee, K. R. Seddon, J. A. Widegren, *Nature* **2006**, *439*.
[23] B. L. Mil'man, *Zh. Anal. Khim.* **1986**, *41*, 1934.
[24] R. Stoll, F. W. Rollgen, *Org. Mass Spectrom.* **1981**, *16*, 72.
[25] For methods of studying atmospheric pressure proton transfer reactions, see Z. Takáts, J. M. Wiseman, B. Gologan, R. G. Cooks, *Anal. Chem.* **2004**, *76*, 4050.
[26] H. Chen, I. Cotte-Rodriguez, R. G. Cooks, *Chem. Commun.* **2006**, 597.
[27] A. R. Katritzky, D. E. Leahy, *J. Chem. Soc. Perkin Trans. 2* **1985**, 171.
[28] A. R. Katritzky, R. H. Manzo, J. M. Lloyd, R. C. Patel, *Angew. Chem.* **1980**, *92*, 315; *Angew. Chem. Int. Ed. Engl.* **1980**, *19*, 306.
[29] A. R. Katritzky, *Tetrahedron* **1980**, *36*, 679.

 © 2006 Wiley-VCH Verlag GmbH & Co. KGaA, Weinheim

C–N-Coupled Azolyl Nucleosides

DOI: 10.1002/anie.200504565

A General Synthesis of C6-Azolyl Purine Nucleosides**

*Pallavi Lagisetty, Larry M. Russon, and Mahesh K. Lakshman**

Palladium-catalyzed C–N bond forming reactions of nucleosides are becoming increasingly important in the synthesis of biologically relevant compounds.[1] Appending heterocyclic systems to nucleosides yields unusual compounds with unique properties and applications. For instance, pyrazole-linked adenosine nucleosides have recently been investigated for their interactions with the adenosine A_2 and A_3 receptors, which are associated with important biofunctions.[2] These studies showed that compounds containing C–N linkages between the heterocycle and the nucleobase display higher activity than those with C–C linkages.[2] C6-pyrrolyl compounds have been evaluated as antiarrhythmic agents,[3] and the pyrrolyl moiety has also been investigated as protecting group for the exocyclic amines of purine nucleosides.[4] C6-1,2,4-triazolyl[5] and C6-imidazolyl[6] derivatives are useful for displacement reactions and can be converted into other modified nucleosides. More recently, C6-imidazolyl, C6-benzimidazolyl, and C6-1,2,4-triazolyl nucleoside analogues have found utility in C–C bond formation catalyzed by Ni–N-heterocyclic carbene complexes.[7] Despite the assortment of applications for azolyl purines and nucleosides, there is no general method for the synthesis of such compounds. We were attracted to the notion that metal-mediated C–N bond formation could provide a single, unifying method for the synthesis of C6-azolyl nucleosides. Herein we report our results for the Pd-catalyzed C–N(sp^2) bond forming reactions of nucleosides.

For this study four nucleoside precursors were chosen for analysis (Scheme 1). These were TBDMS-protected 6-bromo- and 6-chloropurine ribonucleosides **1** and **2**, 6-bromopurine 2′-deoxyribonucleoside **3**, and an O^6-sulfonate derivative of 2′-deoxyguanosine, **4**.[8] This selection was made to gain an understanding of bromo- versus chloropurine nucleoside activation, to analyze the differences (if any) between ribo- and 2′-deoxyribonucleosides in this reaction, and to determine the reactivity of arylsulfonyl derivatives. The three ligands shown in Scheme 1 were chosen to constitute the catalytic system. Among these, Xantphos (**L1**) has not received much attention for nucleoside modification, but 2-(dicyclohexylphosphanyl)-2′-(*N*,*N*-dimethylamino)-1,1′-biphenyl (**L2**) and (±)-Binap (**L3**) have been successfully utilized for amination reactions of nucleosides.[1]

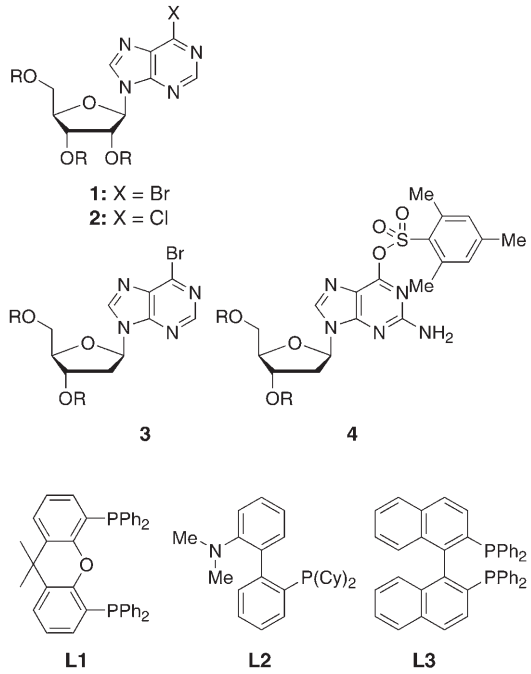

Scheme 1. Four nucleoside substrates and three ligands that were studied in the amination reactions. R = *tert*-butyldimethylsilyl (TBDMS), Cy = cyclohexyl.

[*] Dr. P. Lagisetty, Prof. M. K. Lakshman
Department of Chemistry
The City College and The City University of New York
138th Street at Convent Avenue, New York, NY 10031 (USA)
Fax: (+1) 212-650-6107
E-mail: lakshman@sci.ccny.cuny.edu
Dr. L. M. Russon
Analytica of Branford Inc.
29 Business Park Drive, Branford, CT 06405 (USA)

[**] This work was supported by a National Institutes of Health grant (no.: S06 GM008168-24S1), partially by a National Science Foundation (NSF) grant (no.: CHE-0314326), and by a PSC-CUNY 36 award. Acquisition of a 500 MHz NMR spectrometer and a mass spectrometer was funded by NSF grants (nos.: CHE-0210295 and CHE-0520963, respectively). Dr. P. Pradhan is thanked for his assistance.

Supporting information for this article is available on the WWW under http://www.angewandte.org or from the author.

InterScience
© 2006 Wiley-VCH Verlag GmbH & Co. KGaA, Weinheim

Initial experimentation commenced with an analysis of the reaction between bromopurine nucleoside **1** and 3-methylindole catalyzed by $Pd(OAc)_2$-based systems. The ligand, solvent, and catalyst loading were varied and the results from these experiments are summarized in Table 1.

Table 1: Analysis of C–N bond formation between **1**, **2**, **3**, or **4** and 3-methylindole.

Entry	Substrate	Conditions,[a] ligand, solvent	*t*, yield[b]
1	**1**	A, **L1**, toluene	2 h, 91%
2	**1**	A, **L2**, 1,4-dioxane	3 h, 58%
3	**1**	B, **L1**, toluene	8 h, 79%
4	**1**	B, **L3**, toluene	8 h, 34%[c]
5	**1**	B, **L2**, 1,4-dioxane	48 h, –[d]
6	**1**	B, **L1**, 1,4-dioxane	24 h, 69%
7	**2**	B, **L1**, toluene	4 h, 69%
8	**2**	A, **L3**, toluene	8 h, 37%
9	**3**	B, **L1**, toluene	4.5 h, 83%
10	**4**	A, **L1**, toluene	4.5 h, 39%
11	**4**	B, **L1**, toluene	8 h, 17%
12	**4**	A, **L2**, 1,4-dioxane	3 h, 40%
13	**4**	B, **L2**, 1,4-dioxane	48 h, –[d]

[a] Reactions were conducted at 0.1 M substrate concentration. Conditions: A = 10 mol% $Pd(OAc)_2$/15 mol% ligand/1.5 mol equiv Cs_2CO_3; B = 5 mol% $Pd(OAc)_2$/7.5 mol% ligand/1.5 mol equiv Cs_2CO_3. [b] Reactions were monitored by thin-layer chromatography; yields are given for isolated and purified products. [c] Product was impure. [d] Reaction was incomplete.

The $Pd(OAc)_2$/**L1**/Cs_2CO_3 system emerged as the most effective at both the higher (10 mol% $Pd(OAc)_2$/15 mol% ligand) and lower (5 mol% $Pd(OAc)_2$/7.5 mol% ligand) catalyst loadings, although a slower reaction and lowered yield was observed with the latter (Table 1, entry 1 versus 3). Solvent also seemed to play a role, as reflected in the reaction time and product yield, with better results in toluene than in 1,4-dioxane (Table 1, entry 3 versus 6). To ensure that the reaction was indeed metal catalyzed and that direct displacement was not the leading mechanism, a reaction was performed with all components except $Pd(OAc)_2$. Under these conditions no product formation was observed in 24 h, thereby excluding direct displacement.

Attention was then directed to the amination of chloropurine ribonucleoside **2**, and the lower $Pd(OAc)_2$/**L1** catalyst loading proved quite successful in this case (Table 1, entry 7). These results demonstrated that the **L1**-based catalytic system was effective for this C–N bond forming reaction. Notably, Pd insertion into the C–Cl bond of **2** occurred readily and amination of this substrate was feasible. Next, evaluation of the 6-bromopurine 2′-deoxynucleoside **3** was conducted, in order to analyze whether major differences existed in the reactions of the ribo- and 2′-deoxyribonucleoside analogues. Here again, the 5 mol% $Pd(OAc)_2$/7.5 mol% **L1** system produced very satisfactory results (Table 1, entry 9).

The reaction of 3-methylindole with nucleoside arylsulfonate **4** provided an interesting insight into reactivity differences between sp^3 and sp^2 nitrogen atoms in the Pd-catalyzed arylamination of nucleosides. Although reactions of **4** proceed smoothly with aniline derivatives even with 5 mol% of $Pd(OAc)_2$ with **L2** as the supporting ligand,[9] **4** reacted poorly under a variety of conditions in the present case (Table 1, entries 10–13).

With these preliminary reactivity data for the nucleosides and catalytic systems complete, the generality of the amination was evaluated on substrates **1**–**3**. The results of these experiments are summarized in Table 2

Table 2: Results of the reactions of nucleosides **1**–**3** with various azoles.[a]

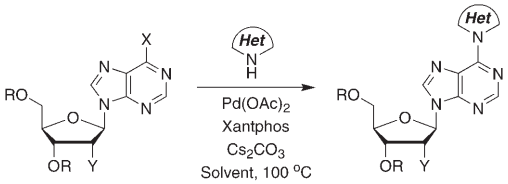

Entry	Amine	Sub strate	Solvent, conditions[b]	Product	*t*, yield[c]
1	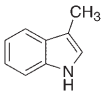	**1**	toluene, A	**5a**	2 h, 91%
2		**1**	toluene, B	**5a**	8 h, 79%
3		**1**	1,4-dioxane, B	**5a**	24 h, 69%
4		**2**	toluene, B	**5a**	4 h, 69%
5		**3**	toluene, B	**6a**	4.5 h, 83%
6	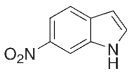	**1**	toluene, B	**5b**	4 h, 81%
7		**1**	1,4-dioxane, B	**5b**	8 h, 38%
8		**2**	toluene, B	**5b**	8 h, 89%
9		**3**	toluene, B	**6b**	4 h, 69%
10		**1**	toluene, A	**5c**	3 h, 72%
11		**1**	toluene, B	**5c**	4 h, 50%
12		**2**	toluene, A	**5c**	18 h, 73%
13		**2**	toluene, B	**5c**	22 h, 55%
14		**3**	toluene, B	**6c**	4 h, 94%
16	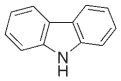	**1**	1,4-dioxane, B	**5d**	4 h, 78%
17		**2**	1,4-dioxane, B	**5d**	4 h, 85%
18		**3**	1,4-dioxane, B	**6d**	4 h, 61%
19		**1**	toluene, A	**5e**	30 h, 44%
20		**2**	toluene, A	**5e**	30 h, 45%
21		**3**	toluene, A	**6e**	30 h, 40%
22		**1**	toluene, B	**5f**	24 h, 88%
23		**2**	toluene, B	**5f**	32 h, 84%
24		**3**	toluene, B	**6f**	6 h, 83%
25		**1**	toluene, B	**5g**	24 h, 87%
26		**1**	1,4-dioxane, B	**5g**	24 h, 95%
27		**2**	1,4-dioxane, B	**5g**	24 h, 96%
28		**3**	toluene, B	**6g**	4 h, 75%
29		**3**	1,4-dioxane, B	**6g**	4 h, 87%
29		**1**	1,4-dioxane, A	**5h**	32, 74%
30		**1**	1,4-dioxane, B	**5h**	48, 65%
31		**2**	1,4-dioxane, A	**5h**	30, 85%
32		**3**	1,4-dioxane, A	**6h**	24, 68%

[a] Reactions were conducted at 0.1 M substrate concentration. [b] Conditions: A = 10 mol% $Pd(OAc)_2$/15 mol% **L1**/1.5 mol equiv Cs_2CO_3; B = 5 mol% $Pd(OAc)_2$/7.5 mol% **L1**/1.5 mol equiv Cs_2CO_3. [c] Reactions were monitored by thin-layer chromatography; yields are given for isolated and purified products.

 © 2006 Wiley-VCH Verlag GmbH & Co. KGaA, Weinheim

(a comprehensive table can be found in the Supporting Information).

The choice of solvent is important and toluene was generally better than 1,4-dioxane (Table 2, entries 2 versus 3 and 6 versus 7). With benzimidazole, 1,4-dioxane was marginally superior to toluene (Table 2, entries 25 versus 26 and 28 versus 29), but it was significantly superior with carbazole and 1,2,4-triazole. Whether these solvent effects are related to solubility of the amines is currently not clear, although this may be a contributing reason at least in some cases. In the case of 7-methylindole it is plausible that the generally lowered yields are due to steric impedance proximal to the reaction site (Table 2, entries 19–21). It should be noted that, with the more acidic 1,2,4-triazole, a control reaction was conducted without $Pd(OAc)_2$ and again no reaction was observed. In contrast to the generally good Pd-catalyzed reactions of 1,2,4-triazole, the isomeric 1,2,3-triazole produced low yields for reasons that are not clear presently (see the Supporting Information for compounds **5i** and **6i**).

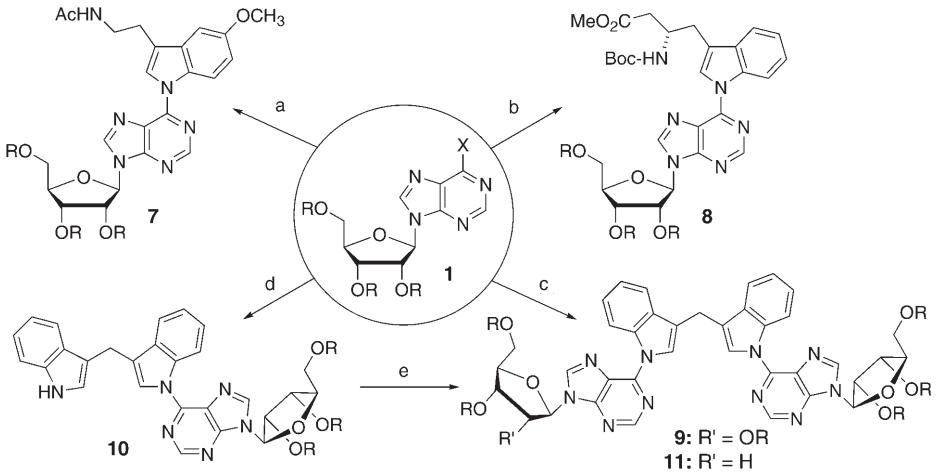

Scheme 2. Synthesis of nucleoside derivatives by C–N(sp^2) bond formation with a) melatonin, b) N_β-Boc-L-β-homotryptophan methyl ester, and c)–e) 3,3′-diindolylmethane. Boc = *tert*-butoxycarbonyl.

Xantphos (**L1**) is a wide-bite-angle ligand,[10] and Pd^{II} complexes of **L1** have been shown to adopt *trans* phosphane coordination.[11] It has been proposed, in the case of Ni^0 complexes, that wide-bite-angle phosphanes produce species more resistant to deactivation and also increase the rate of reductive elimination.[12] **L1** also possesses an apical oxygen atom. This has been postulated to stabilize cationic intermediates in the *cis–trans* isomerization of oxidative-addition complexes,[11b] although its importance is not completely clear. It is possible that a combination of these factors is responsible for the catalyst activity observed. Interestingly, **L2** and **L3**, which have proven effective for other Pd-catalyzed amination reactions of nucleosides with the sp^3 nitrogen atoms of aniline derivatives and hindered sp^3 nitrogen atoms, were less effective here than **L1**.[1,9]

Finally, to demonstrate the versatility of this method in providing access to unusual structural entities, amination reactions of **1** with a substituted indole (melatonin), a protected β-amino acid (N_β-*tert*-butoxycarbonyl-L-β-homotryptophan methyl ester), and a bis-indole (3,3′-diindolylmethane) were conducted (Scheme 2). By using the lower catalyst loading (5 mol% $Pd(OAc)_2$/7.5 mol% **L1**), compounds **7** and **8** were obtained in yields of 72 and 78% from melatonin and N_β-Boc-L-β-homotryptophan methyl ester, respectively. In each case, the reaction occurred at the indolyl nitrogen atom and not at the amide or carbamate. Symmetrical dimer **9** was also synthesized in 82% yield from 3,3′-diindolylmethane with the lower catalyst loading. Synthesis of unsymmetrical dimer **11** from 3,3′-diindolylmethane was then considered. First, monoaryl compound **10** was obtained by using the lower catalyst loading and 2 equivalents of 3,3′-diindolylmethane (**10**: 59% yield, **9**: 10% yield). Subsequently, the reaction of **10** with 2 equivalents of 6-bromopurine 2′-deoxynucleoside **3** by using the 10 mol% $Pd(OAc)_2$/15 mol% **L1** catalyst system yielded the unsymmetrical dimer **11** in 74% yield.

In summary, we have developed the first general route to C6-azolyl nucleosides with metal catalysis as the unifying basis. Bromo- and notably chloropurine nucleosides, both ribo- and 2′-deoxyribonucleoside analogues, undergo efficient conversion. The method appears amenable to the synthesis of relatively complex structures and will probably find broad applicability for the modification of other heteroaryl systems.

Received: December 22, 2005
Revised: February 10, 2006
Published online: April 26, 2006

Keywords: amination · C–N coupling · nucleosides · palladium · phosphane ligands

[1] For reviews, see: a) M. K. Lakshman, *J. Organomet. Chem.* **2002**, *653*, 234–251; b) M. K. Lakshman, *Curr. Org. Synth.* **2005**, *2*, 83–112.
[2] a) V. P. Palle, E. O. Elzein, S. A. Gothe, Z. Li, Z. Gao, S. Meyer, B. Blackburn, J. A. Zablocki, *Bioorg. Med. Chem. Lett.* **2002**, *12*, 2935–2939; b) E. Elzein, V. Palle, Y. Wu, T. Maa, D. Zeng, J. Zablocki, *J. Med. Chem.* **2004**, *47*, 4766–4773.
[3] K. G. Estep, K. A. Josef, E. R. Bacon, P. M. Carabateas, S. Rumney IV, G. M. Pilling, D. S. Krafte, W. A. Volberg, K. Dillon, N. Dugrenier, G. M. Briggs, P. C. Canniff, W. P. Gorczyca, G. P. Stankus, A. M. Ezrin, *J. Med. Chem.* **1995**, *38*, 2582–2595.
[4] I. Nowak, M. J. Robins, *Org. Lett.* **2003**, *5*, 3345–3348.
[5] V. Samano, R. W. Miles, M. J. Robins, *J. Am. Chem. Soc.* **1994**, *116*, 9331–9332.
[6] X. Lin, M. J. Robins, *Org. Lett.* **2000**, *2*, 3497–3499.
[7] J. Liu, M. J. Robins, *Org. Lett.* **2004**, *6*, 3421–3423.
[8] Compounds **1** and **3** were synthesized based upon a known procedure: M. K. Lakshman, J. C. Keeler, J. H. Hilmer, J. Q. Martin, *J. Am. Chem. Soc.* **1999**, *121*, 6090–6091; in the Supporting Information for that manuscript, the use of CBr_4

 © 2006 Wiley-VCH Verlag GmbH & Co. KGaA, Weinheim

for the synthesis of **3** is an error and should be $CHBr_3$. Compound **1** has been reported in E. A. Véliz, P. A. Beal, *J. Org. Chem.* **2001**, *66*, 8592 – 8598. The known compound **2** was prepared by silylation of the commercially available chloropurine nucleoside: D. E. Bergstrom, P. A. Reddy, *Tetrahedron Lett.* **1982**, *23*, 4191 – 4194. Compound **4** has been reported in Y. Hayakawa, M. Hirose, R. Noyori, *J. Org. Chem.* **1993**, *58*, 5551 – 5555.

[9] P. Gunda, L. M. Russon, M. K. Lakshman, *Angew. Chem.* **2004**, *116*, 6532 – 6537; *Angew. Chem. Int. Ed.* **2004**, *43*, 6372 – 6377; see also the corrigendum: P. Gunda, L. M. Russon, M. K. Lakshman, *Angew. Chem.* **2005**, *117*, 1178; *Angew. Chem. Int. Ed.* **2005**, *44*, 1154.

[10] M. Kranenburg, Y. E. M. van der Burgt, P. C. J. Kamer, P. W. N. M. van Leeuwen, *Organometallics* **1995**, *14*, 3081 – 3089.

[11] a) J. Yin, S. L. Buchwald, *J. Am. Chem. Soc.* **2002**, *124*, 6043 – 6048; b) M. A. Zuideveld, B. H. G. Swennenhuis, M. D. K. Boele, Y. Guari, G. P. F. van Strijdonck, J. N. H. Reek, P. C. J. Kamer, K. Goubitz, J. Fraanje, M. Lutz, A. L. Spek, P. W. N. M. van Leeuwen, *J. Chem. Soc. Dalton Trans.* **2002**, 2308 – 2317.

[12] Z. Freixa, P. W. N. M. van Leeuwen, *Dalton Trans.* **2003**, 1890 – 1901.

 © 2006 Wiley-VCH Verlag GmbH & Co. KGaA, Weinheim

Hydrogen-Storage Materials

DOI: 10.1002/anie.200504425

Hydrogen-Isotope Scrambling on Doped Sodium Alanate**

*José M. Bellosta von Colbe, Wolfgang Schmidt, Michael Felderhoff, Boris Bogdanović, and Ferdi Schüth**

Doped sodium alanate is one of the most advanced and best studied hydrogen-storage materials for mobile applications.[1,2] It decomposes according to Equation (1) in two steps, giving a total theoretical capacity of 5.6 wt % hydrogen.

$$\underset{\text{1st step}}{NaAlH_4 \overset{\text{cat.}}{\rightleftharpoons} {}^1/_3\, Na_3AlH_6 + {}^2/_3\, Al + H_2} \underset{\text{2nd step}}{\overset{\text{cat.}}{\rightleftharpoons} NaH + Al + {}^1/_2\, H_2} \quad (1)$$

The reaction was considered to be basically irreversible under reasonable conditions, until Bogdanović and Schwickardi discovered that sodium alanate can be rehydrogenated if it is doped with transition-metal compounds, most efficiently with titanium compounds.[3]

The disadvantages of doped $NaAlH_4$ lie mainly in its de- and rehydrogenation temperatures, which are somewhat high for the intended purpose as a hydrogen-storage material in transportation applications, but especially in its slow hydrogenation, which needs relatively high pressures of about 89–150 bar.[4] Although substantial progress has been made on an empirical basis over the last few years, and rehydrogenation times of less than ten minutes have been achieved,[5] the function of the catalysts remains elusive. The kinetics of the reaction in Equation (1) have been studied in both the hydrogenation[6,7] and the dehydrogenation directions[8,9] without conclusive results as to the mechanism. Moreover, proposed mechanisms could not be confirmed.[10] Until very recently, it was not even clear what the oxidation state of titanium during de- and rehydrogenation was, and it could only be shown recently, in three independent publications, that it is zero-valent during cycling and basically does not change over the complete cycle.[11–13]

To hydrogenate a decomposed $NaAlH_4$ sample, hydrogen must 1) diffuse to the surface of the material, 2) be adsorbed and 3) dissociated, and 4) be transported into the bulk of the material. During the last process, substantial mass transfer of the solid must also occur, since the decomposition reaction forms aluminum and NaH particles in the size range of several hundred nanometers. Each of the above steps could be rate-limiting for the overall reaction, and knowledge about the rate-limiting elementary step is crucial for rational improvement of the materials. To gain more insight into the role of the titanium catalyst and to study the path taken by the hydrogen on its way from the gaseous form in the reactor atmosphere to the bound form in the solid storage material, a series of isotope-exchange experiments with deuterium were undertaken. These experiments were carried out first at room temperature and near-ambient pressure, to investigate the activity of doped sodium alanate as a superficial catalyst in the splitting of the hydrogen molecule. In a second step, high-temperature experiments at higher pressures were carried out to evaluate the rate and extent of hydrogen exchange between the doped sodium alanate sample and the reactor atmosphere.

The low-pressure, room-temperature experiments were carried out in a steel pressure vessel on purified $NaAlH_4$ doped with 2 mol % of $Ti(OnBu)_4$. After evacuating the reactor, an atmosphere of 0.5 bar of H_2 was established. On adding 1 bar of D_2, the mass spectrometer detected an immediate increase in the signal corresponding to the HD molecule (Figure 1).

This isotopic scrambling of hydrogen and deuterium in the gas phase only takes place in the presence of doped $NaAlH_4$, since neither with an empty reactor nor with undoped alanate was an HD signal detected. This demonstrates that the titanium species formed in the doped material (probably in a similar state to that in $TiAl_3$)[11] is active for dissociating the hydrogen molecule and effecting the scrambling reaction [Eq. (2)], a prerequisite for the incorporation of hydrogen

$$H_2 + D_2 \overset{\text{cat.}}{\rightleftharpoons} 2\,HD \quad (2)$$

[*] J. M. Bellosta von Colbe, Dr. W. Schmidt, Dr. M. Felderhoff, Dr. B. Bogdanović, Prof. Dr. F. Schüth
Max-Planck-Institut für Kohlenforschung
45470 Mülheim an der Ruhr (Germany)
Fax: (+49) 208-306-2995
E-mail: schueth@mpi-muelheim.mpg.de

[**] This work was partially supported by General Motors Fuel Cell Activities, in addition to the basic funding by the Max-Planck-Gesellschaft.

Supporting information for this article is available on the WWW under http://www.angewandte.org or from the author.

 © 2006 Wiley-VCH Verlag GmbH & Co. KGaA, Weinheim

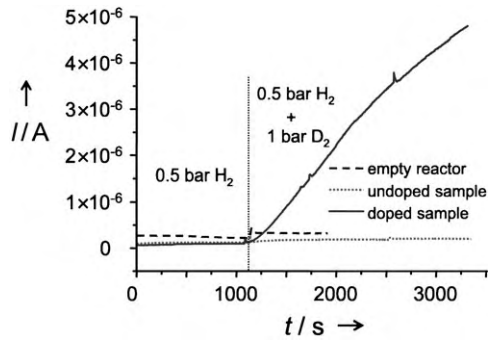

Figure 1. Mass-spectrometer ion current *I* for the gaseous HD species in an experiment in which a 1:2 H_2/D_2 mixture at 1.5 bar reacted at room temperature in the presence of a doped $NaAlH_4$ sample (2 mol% Ti(O*n*Bu)$_4$). Under these conditions the doped alanate acts as a scrambling catalyst for the gas phase, but no exchange with the solid takes place.

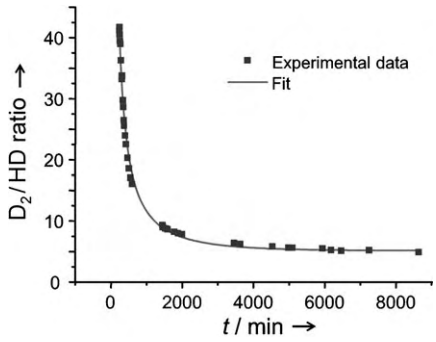

Figure 2. D_2/HD ratio versus reaction time for a sample of $NaAlH_4$ doped with 4 mol% of $TiCl_3$ by ball milling for 4 h. The sample reacted with an atmosphere of pure D_2 at 20 bar and 50 °C. At the end of the experiment, 1.3 of the four hydrogen atoms of the formula unit had been exchanged against deuterium.

into the storage material. The finding also suggests that the titanium resides at least partly on the surface of the material. The dissociation of hydrogen on an Al- and Ti-containing surface of decomposed Ti-doped $NaAlH_4$ was recently studied by density functional theory (DFT) calculations.[14]

However, over the duration of these experiments no exchange with the hydrogen of the bulk storage material was observed when only a deuterium gas phase was admitted to the sample. This result indicates that the activity of the titanium catalyst was not sufficient for this process.

Owing to the conditions of the process envisaged for the practical use of doped sodium alanate as a hydrogen-storage material, it is of even more interest to study the interaction of gas and solid at higher pressures and temperatures. To quantify the observed effects, errors brought about by different diffusion coefficients in the inlet system of the mass spectrometer had to be accounted for. To calibrate for this, a 1:1 mixture of D_2 and H_2 under 20 bar of pressure was admitted to the reactor in which a Pt and a Ru catalyst had been placed, and the system was heated to 50 °C. Scrambling of the isotopes proceeded until a constant ratio of concentrations had been reached after about 5 h. After waiting for five more days, the ion currents measured were used for calibration against the statistical ratio of $H_2/HD/D_2 = 1:2:1$ which is expected for an initial H_2/D_2 ratio of 1:1 after complete scrambling. The correction factors thus determined were in good agreement with response factors determined separately for H_2 and D_2 against N_2 as the internal standard.

For the high-pressure experiments somewhat different samples were used, since progress in doping methods had revealed superior properties of $TiCl_3$-doped samples synthesized by ball milling. The sample (1.211 g of $NaAlH_4$ doped with 4 mol% of $TiCl_3$) was subjected to 20 bar of pure D_2 at 50 °C. The resulting mass-spectrometric raw data were corrected by using the response factors determined by the method described above.

Figure 2 shows the corrected peak-area ratio D_2/HD against time in such an experiment. The exponentially decreasing D_2/HD ratio reveals that exchange with the hydrogen in the bulk occurred. Also, H_2 was detected in small amounts, as expected. The exchange can be described by model Equation (3).

$$MH_{(s)} + D_2 \underset{k_2}{\overset{k_1}{\rightleftharpoons}} HD + MD_{(s)} \tag{3}$$

In this model, the hydrogen-containing solid $MH_{(s)}$ incorporates deuterium atoms from the gas. To accomplish this, the gaseous D_2 molecules must split, and when reforming, incorporate an H atom to yield HD. Formation of a small amount of hydrogen (partial pressure only 1.5% of total pressure) was neglected for simplicity.

Assuming first-order kinetics, this model yields Equation (4) for the D_2/HD ratio α as a function of time.

$$\alpha = \frac{1 + k_2/k_1}{e^{(k_1+k_2)t} - 1} + \frac{k_2}{k_1} \tag{4}$$

Equation (4) was fitted to the data from the experiment with the doped $NaAlH_4$ sample. The fit was very satisfactory (solid line in Figure 2). The fitting parameters are $k_2/k_1 = 5.1 \pm 0.3$ and $1/(k_1+k_2) = 1504 \pm 87$ min. The parameter k_2/k_1 is the inverse of the equilibrium constant for the process described in Equation (3), which points to a small difference in free enthalpy between hydrogen and deuterium incorporated in the alanate, under the assumption that equilibrium is indeed reached (if the free enthalpy ΔG of the exchange reaction did not change, k_1 should be equal to k_2 to fulfill $\Delta G = -RT\ln(k_1/k_2) = 0$ kJ mol^{-1}).

From the ratio of D_2 and HD, the system volume, the pressure, and the sample weight, one can calculate the degree of exchange of the hydrogen atoms by deuterium in the sample. The result of this calculation is that on average 1.3 of the four hydrogen atoms of the formula unit are exchanged. In absolute numbers, 2.22×10^{-2} mol of D atoms are absorbed by the sample. To cross-check the result, the system was evacuated and the sample was heated first to 120 °C and then to 180 °C to dehydrogenate it completely. Afterwards, analysis of the gas phase revealed 2.13×10^{-2} mol of desorbed D atoms, in excellent agreement with the adsorbed amount of deuterium.

 © 2006 Wiley-VCH Verlag GmbH & Co. KGaA, Weinheim

This set of experiments clarifies one important effect of the titanium dopant during de- and rehydrogenation of $NaAlH_4$: The titanium dissociates hydrogen and activates it for exchange with the solid. However, the findings also illustrate an additional, highly significant point. The isotope exchange experiment is essentially done under steady-state conditions, that is, no decomposition of the alanate takes place. The H/D exchange is much faster than rehydrogenation of decomposed sodium alanate. This feature means that the titanium must have an additional effect in facilitating the rehydrogenation beyond increasing the rate of hydrogen exchange with the solid. This additional effect is most probably related to mass transfer, which must be very substantial, since separation of aluminum and sodium hydride as decomposition products proceeds on a scale of about 10 nm up to the micrometer range.[11]

The investigation reported herein clarifies part of the action of the titanium catalyst in doped sodium alanate during hydrogen storage. The catalyst facilitates dissociation of hydrogen at the surface of the material and diffusion of hydrogen in the bulk of the samples, as alluded to previously.[1] However, the rate-limiting step of the charging/discharging process seems to be mass transfer of the solid, because hydrogen diffusion under quasi-equilibrium conditions is appreciably faster than the actual hydrogenation reaction. This result is in accord with earlier suggestions.[11,15] If the mode of action of the titanium can be clarified also for these steps, this could provide insight which would allow rational improvement of the kinetics of hydrogen absorption and release. Since $NaAlH_4$ is prototypical for hydrogen-storage materials based on complex hydrides, at least for other alanates, this would be highly important for further development of such materials towards practical applications.

Experimental Section

The room-temperature isotope-exchange experiments were carried out on 3.1 g sodium alanate doped with 2 mol% of $Ti(OnBu)_4$. Blank experiments were carried out with the empty reactor (DIN 1.4571 steel, volume 36 mL) and 4.1 g of undoped sodium alanate. No isotope exchange was registered in these blank experiments, neither with D_2 nor with a 1:1 mixture of D_2 and H_2, at room temperature or at 50 °C and 20 bar gas pressure.

The high-pressure isotope-exchange experiments were carried out with 0.466, 1.312, and 1.211 g of sodium alanate doped with 4 mol% of $TiCl_3$ in a 203-mL reactor; measurements were made for up to 143.9 h. Mass-spectrometric analysis was performed with a Balzers Thermostar GSD 300T mass spectrometer (running Balzers Quadstar 422 software) attached directly to the reactor with a capillary. Hydrogen (99.999%) and deuterium (99.7%) were supplied by Messer. Commercial sodium alanate (Aldrich) was purified by dissolving it in THF and filtering through a 4-μm frit. Afterwards, it was precipitated in pentane and dried in vacuum to constant weight. $Ti(OnBu)_4$ was 97%, and $TiCl_3$ 99% pure, both commercial products (Aldrich). Doping of the room-temperature samples was carried out by suspending $NaAlH_4$ and $Ti(nOBu)_4$ in toluene, stirring at room temperature for 12 h, and drying under vacuum overnight. All manipulations were performed under Ar by using Schlenk techniques. The high-pressure samples were doped by ball milling of $NaAlH_4$ and $TiCl_3$ in a Retsch MM 200 mill for about 6 h. Loading of the 20-mL steel milling vials was performed under Ar in a glove box. Milling was performed with a 32-g steel ball with a ball-to-sample weight ratio of 15.

Received: December 13, 2005
Published online: April 27, 2006

Keywords: aluminum · deuterium · hydrogen storage · hydrogen · reaction kinetics

[1] F. Schüth, B. Bogdanović, M. Felderhoff, *Chem. Commun.* **2004**, 2249–2258.
[2] L. Schlapbach, A. Züttel, *Nature* **2001**, *414*, 353–358.
[3] B. Bogdanović, M. Schwickardi, *J. Alloys Compd.* **1997**, *253–254*, 1–9.
[4] B. Bogdanović, M. Schwickardi, *Appl. Phys. A* **2001**, *72*, 221–223.
[5] B. Bogdanović, M. Felderhoff, A. Pommerin, F. Schüth, N. Spielkamp, *Adv. Mater.*, DOI:10.1002/adma.200501367.
[6] D. Sun, S. S. Srinivasan, G. Chen, C. M. Jensen, *J. Alloys Compd.* **2004**, *373*, 265–269.
[7] W. Luo, K. J. Gross, *J. Alloys Compd.* **2004**, *385*, 224–231.
[8] T. Kiyobayashi, S. S. Srinivasan, D. L. Sun, C. M. Jensen, *J. Phys. Chem. A* **2003**, *107*, 7671–7674.
[9] D. L. Anton, *J. Alloys Compd.* **2003**, *356–357*, 400–404.
[10] R. T. Walters, J. H. Scogin, *J. Alloys Compd.* **2004**, *379*, 135–142.
[11] M. Felderhoff, K. Klementiev, W. Grünert, B. Spliethoff, B. Tesche, J. M. Bellosta von Colbe, B. Bogdanović, M. Härtel, A. Pommerin, F. Schüth, C. Weidenthaler, *Phys. Chem. Chem. Phys.* **2004**, *6*, 4369–4374.
[12] A. Léon, O. Kircher, J. Rothe, M. Fichtner, *J. Phys. Chem. B* **2004**, *108*, 16372–16376.
[13] J. Graetz, J. J. Reilly, J. Johnson, A. Y. Ignatov, T. A. Tyson, *Appl. Phys. Lett.* **2004**, *85*, 500–502.
[14] S. Chaudhury, J. Muckerman, *J. Phys. Chem. B* **2005**, *109*, 6952–6957.
[15] M. Fichtner, P. Canton, O. Kirchner, A. Léon, *J. Alloys Compd.* **2005**, *404–406*, 732–737.

 © 2006 Wiley-VCH Verlag GmbH & Co. KGaA, Weinheim

Selective DNA Cleavage

DOI: 10.1002/anie.200504479

Protected ^{32}P-Labels in Deoxyribonucleotides: Investigation of Sequence Selectivity of DNA Photocleavage by Enediyne–, Fulvene–, and Acetylene–Lysine Conjugates**

*Boris Breiner, Jörg C. Schlatterer, Serguei V. Kovalenko, Nancy L. Greenbaum, and Igor V. Alabugin**

Since natural and synthetic photosensitizers can generate reactive intermediates on demand with a high degree of temporal and spatial control, they attract considerable interest as molecular tools for the modification of DNA.[1] Bis-tetrafluoropyridinyl (bis-TFP) enediynes are attractive organic DNA photocleavers because they do not require metals or reducing agents and because they are thermally and photochemically stable unless excited in the vicinity of a suitable electron donor such as DNA. Thus, not only light but also binding to DNA are necessary for the activation. Photoinduced electron transfer (PET) triggers transformation of these molecules into indenes (the C1–C5 cyclization, Scheme 1) with four concomitant formal H-atom abstractions.[2] In addition, bis-TFP enediynes can be excited with low-energy visible light under two-photon conditions,[3] the cyclization can be effectively controlled by substituents,[4] and, unlike the Bergman cyclization,[5,6] individual steps in the C1–C5 cascade can lead to DNA photocleavage through either oxidative or hydrogen-abstraction mechanisms. Intriguingly, the nature of the reaction products suggests that reactivation of fulvene intermediates can lead to further DNA damage that develops after the cyclization step.

In our recent work, we applied a supercoiled DNA relaxation assay to demonstrate that the ratio of double-stranded (ds) to single-stranded (ss) DNA photocleavage caused by lysine–enediyne conjugates **1** and **2** (Scheme 2) is greater than that expected for a series of random breaks.[8] The efficiency of the ds photocleavage compares favorably with DNA cleavage mediated by the natural enediyne calicheamicin γ1[9] and by bleomycin.[10,11] However, although this assay is a sensitive and convenient method for studies of new DNA photocleavers, it does not provide insight into the cleavage mechanism and sequence specificity of the DNA damage. Moreover, such important information is missing even in the case of more traditional enediyne photocleavers.

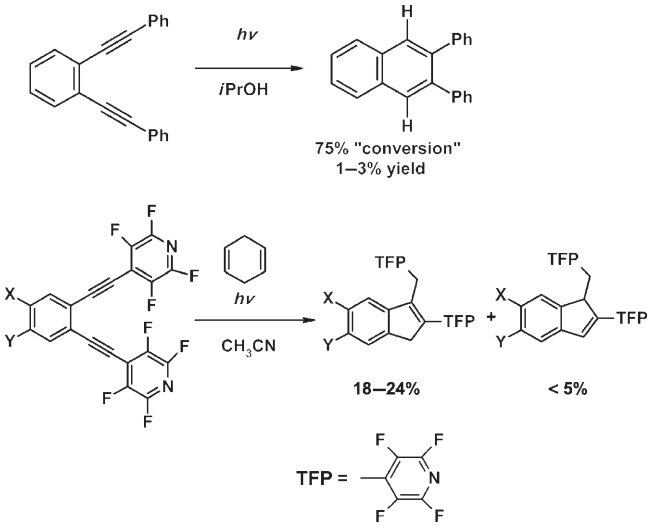

Scheme 1. Comparison of photochemical Bergman (top)[5c,7] and C1–C5 (bottom)[2] cyclizations of enediynes. X = Y = H; X = Y = Me; X = H, Y = Cl; X = H, Y = NHCOR.

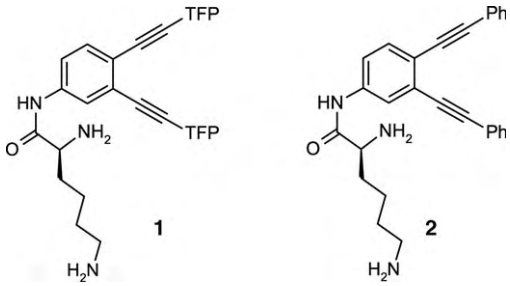

Scheme 2. Lysine–enediyne conjugates **1** and **2**.

In order to gain such an insight, we proceeded to investigate photoinduced damage of synthetic oligonucleotides by enediynes **1** and **2** equipped with a basic lysine moiety. These conjugates exhibit affinity towards DNA that is an order of magnitude greater[8] than that observed with spermine (29–36 μM),[12] a result suggesting that electrostatic binding of protonated amines to the negatively charged DNA backbone is complemented by noncovalent interactions with the enediyne moiety.

Structure of DNA: Initially, we investigated the behavior of enediynes towards a 5′-^{32}P-labeled ds-DNA oligomer (5′-*TAATACG^{7}ACTCACTATAG^{18}G^{19}CCCAG^{24}G^{25}G^{26}-AAAACTTG^{34}TAAAG^{39}G^{40}TCTACCTATCTATT, paired with a complementary counterstrand; ^{32}P-label indicated by asterisk) in aerated neutral phosphate buffer. This model 54-mer incorporates several isolated guanine (G) nucleotides as well as GG diads and GGG triads. Selective damage at these multiplet GGG or GG sites is a signature of PET from DNA,[13–17] which is the key step in the diversion of the reactivity of enediynes towards the C1–C5 pathway.

[*] B. Breiner, J. C. Schlatterer, S. V. Kovalenko, N. L. Greenbaum, Prof. Dr. I. V. Alabugin
Department of Chemistry and Biochemistry
Florida State University
Tallahassee, FL 32306-4390 (USA)
Fax: (+1) 850-644-5795
E-mail: alabugin@chem.fsu.edu

[**] I.A. is grateful to the National Science Foundation (grant no.: CHE-0316598) for partial support of this research and to the 3M Company for an Untenured Faculty Award. N.L.G. thanks the National Science Foundation (grant no.: MCB 0316494) and the National Institutes of Health (grant no.: RO1 GM54008) for their support. We are also grateful for technical support from Dr. L. Keller (Florida State University Biology Department).

Supporting information for this article is available on the WWW under http://www.angewandte.org or from the author.

InterScience
© 2006 Wiley-VCH Verlag GmbH & Co. KGaA, Weinheim

5′-^{32}P-labeled DNA oligomers are the most commonly used radiolabeled oligonucleotides in electrophoretic gel shift assays, where visualization is achieved by autoradiography. However, we found that the label itself appears to be the preferred site of photocleavage by lysine conjugate **1**. As a result, no discernable bands corresponding to labeled DNA fragments are present in Figure 1, with the exception of a low-

Figure 1. PAGE analysis of reactions on the 5′-labeled counterstrand (5′-*AATAGATAG GTA GAC CTT TAC AAG TTT TCC CTG GGC CTA TAG T-GA GTC GTA TTA-3′, label indicated by asterisk) of the DNA oligomer. Reactions were performed in 0.02 M phosphate buffer at pH 7, analyzed on a denaturing 12% polyacrylamide gel, and visualized by phosphorimaging. A + G and C + T refer to the corresponding Maxam–Gilbert sequencing reactions.

mass radioactive fragment with high mobility, which becomes dominant at higher concentrations of enediyne when the original 54-mer is completely consumed. These observations suggest that the 5′-radioactive label was removed from the oligomer upon photoexcitation,[18] thereby making it impossible to observe the cleavage bands. Interestingly, the failure of this common method is precedented,[19] but no solutions have been suggested.

In order to circumvent this problem, we moved the label to a different position, protected within the DNA backbone, near the 3′ end of the oligomer. The full-length 54-mer DNA (BW 54s) was synthesized through primer extension of a 51-mer oligonucleotide (BW 51s) by using a 39-mer template (BW 54as-15) with a TAA overhang in the presence of α-[^{32}P]-deoxyadenosine triphosphate (dATP), -deoxythymidine triphosphate (dTTP), and Taq polymerase (Figure 2). With the alternative labeling technique, the robustness of the label

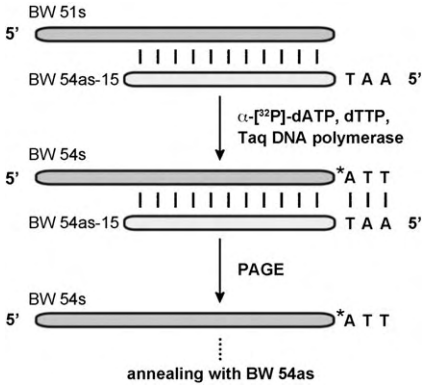

Figure 2. Synthesis of internally 3′-labeled DNA oligomer BW 54s by PCR with α-[^{32}P]-dATP, followed by isolation by use of denaturing PAGE and annealing with the corresponding counterstrand.

and sensitivity of analysis increased significantly, thus providing access to the otherwise unavailable mechanistic information reported below.

DNA cleavers: We capitalized on this finding by expanding our investigation towards a set of lysine conjugates with different photoactivatable moieties (Scheme 3). These sub-

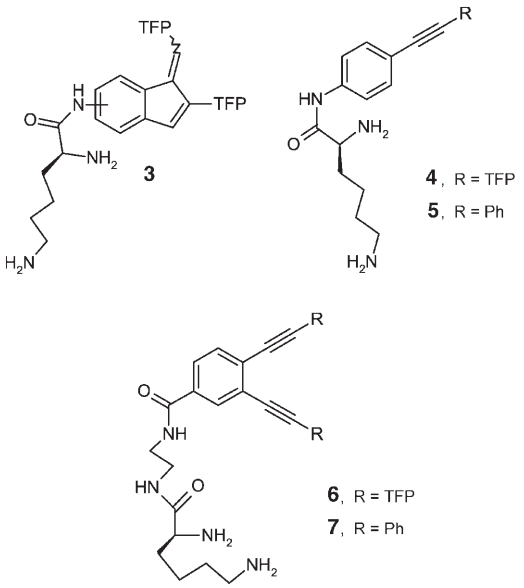

Scheme 3. Expanded list of substrates **3**–**7**.

strates simultaneously provide a reference point for the deeper understanding of the reactivity of bis-TFP enediynes and allow an insight into the nature of lysine–DNA interactions. From the list of new substrates, phenyl-substituted enediynes **2** and **7** were expected to undergo photochemical Bergman cyclization. Enediynes **6** and **7** were introduced to probe the role of a flexible linker.[20] Acetylenes **4** and **5** were used to investigate the intrinsic photoreactivity of the acetylene moiety when cyclizations are impossible. Finally, we set out to determine whether fulvenes, the proposed key intermediates in the C1–C5 cyclization of TFP-substituted

 © 2006 Wiley-VCH Verlag GmbH & Co. KGaA, Weinheim

enediynes, induce DNA cleavage. The requisite fulvene **3** was prepared by using tin-radical cyclization of enediyne **1**[21] and was used as a mixture of isomers.

Cleavage of the DNA 54-mer by all lysine conjugates at 10–20 μM concentrations is readily visualized with the internally labeled DNA (Figure 3). Although it is known that singlet excited states of diaryl acetylenes can oxidize adenine and guanine,[22] the DNA-cleaving ability per se appears to be unprecedented for fulvenes and alkynes. Thus, these results identify two new classes of DNA photocleavers.

In contrast with the earlier observation of efficient direct cleavage of plasmid DNA by both phenyl and TFP enediynes,[8] piperidine treatment is required to develop the cleavage of the 54-mer. Thus, the cleavage patterns observed here are unlikely to be the same as those responsible for the direct strand scission seen in the plasmid assay. While plasmids are much more sensitive to the damage than the shorter oligomers, such a significant difference is interesting and may indicate increased potency of this family of photocleavers towards certain plasmid sequences not present in the oligomer.

Preferential cleavage at guanosine residues[23] further supports the oxidative nucleobase damage suggested by the cleavage enhancement by piperidine. Unexpectedly, such a preference is observed not only for the TFP-containing substrates but also for the phenyl-substituted compounds, where cleavage is also mostly localized at the G sites, albeit concentrated to some extent at those G sites at the TAAA end of a 12-bp AT-rich $A^{27}AAACTTGTAAA^{38}$ sequence. Cleavage induced by the monoacetylenes **4** and **5** is the least selective but also mostly affects the above 12-bp oligomer section.

However, not all of the G bases are affected equally and the relative amount of damage at the different sites depends on the photocleaver. We show below that this selectivity stems from orthogonality between the intrinsic AT-binding preference and the G selectivity for PET and can be further modulated by the chemical properties of the photocleaver warheads.

It is well established that an electron hole, photochemically "injected" into the DNA through PET, is mobile and can travel along the DNA backbone between transient low-energy arrangements where it may be trapped.[13] As a result, the selectivity of PET-triggered DNA cleavage reaction may only reflect the location of the preferred binding sites when the hole-hopping process is slow relative to hole trapping. Intrinsic binding preferences become more obvious in those cases when they are not masked by the hole-hopping process and where the DNA damage originates from photochemically triggered H-atom abstraction (for example, the photochemical Bergman cyclization or hydrogen abstraction by a triplet excited state).

If the known tendency of protonated ammonium groups to bind to AT-rich regions of DNA (for example, AT tracts or A tracts[24]) is taken into account,[25,26] the preferred binding sites for the lysine conjugates are expected to be at parts of the $A^{27}AAACTTGTAAA^{38}$ sequence. In accordance with this notion, the unselective acetylenes **4** and **5** mostly target the base pairs within and in the vicinity of this region. Moreover, an independent estimate of binding of conjugate **1** to DNA 24-mers made of purely GC and AT sequences strongly suggests significant differences in binding with AT and GC sequences (Figure 4). The slopes of the plots are always greater for the AT DNA than for the GC DNA. Since

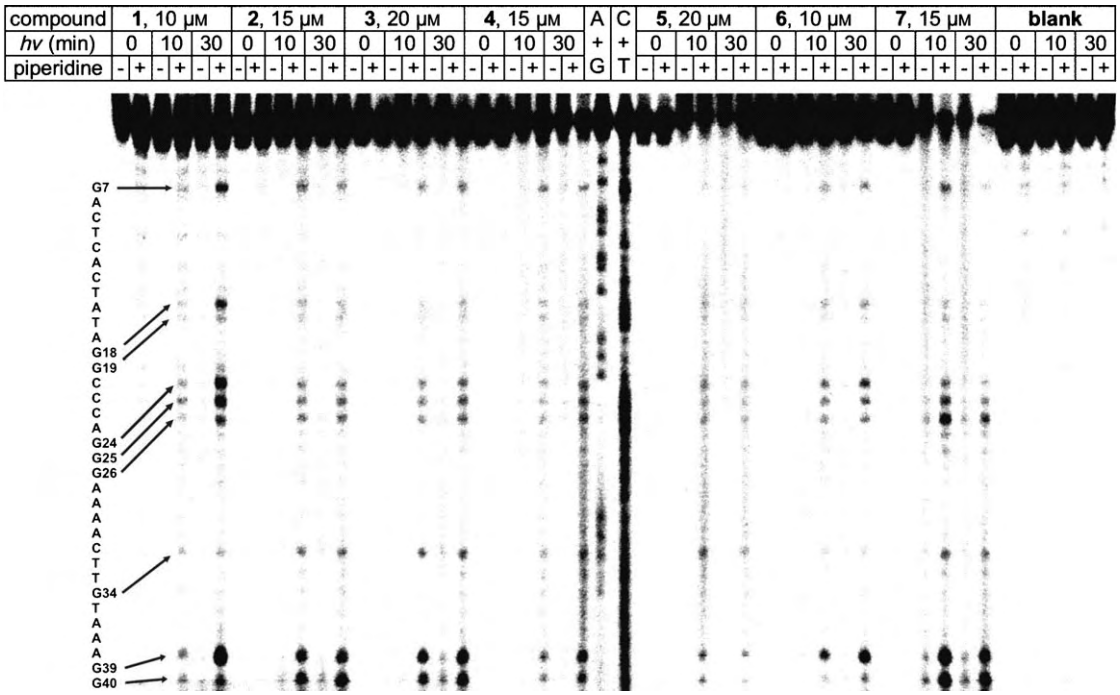

Figure 3. PAGE analysis of reactions with compounds **1**–**7**. Reactions were performed in 0.02 M phosphate buffer at pH 7 and analyzed on a denaturing 12% polyacrylamide gel before visualization by phosphorimaging.

 © 2006 Wiley-VCH Verlag GmbH & Co. KGaA, Weinheim

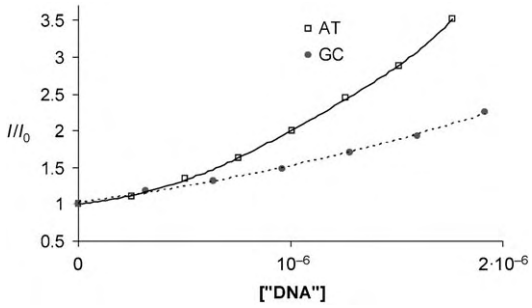

Figure 4. Stern–Volmer plots for the interaction of AT- and GC-type DNA oligomers with enediyne **1**.

PET from DNA (the main fluorescence quenching pathway) is expected to occur more efficiently in the vicinity of guanine residues which are the easiest to oxidize among the four DNA bases,[13–17] these results lend further support to the hypothesis that protonated lysine moieties direct the conjugates towards the AT-rich region of the 54-mer but also suggest that the sites are not optimal with respect to PET unless the DNA cleaver is positioned next to a GG or GGG moiety terminating an AT tract.

In accordance with these expectations, the guanosine sites flanking the above 12-bp A^{27}–A^{38} sequence are indeed the preferred cleavage sites for the TFP-substituted compounds **1**, **3**, **4**, and **6**. Phenyl-substituted substrates are less specific in their DNA damage but still show the greatest activity at the same sites, a result suggesting that the overall selectivity is a compromise between the AT selectivity of binding and the G selectivity of oxidative damage.

On the other hand, the selectivity between G sites reflects the dynamic competition between the hole-hopping and hole-trapping processes. In particular, all of the compounds except for the TFP enediynes[27] and acetylenes induce significant damage on the single G^{34} residue from the TGT moiety inside the above AT-rich sequence (Figure 3). The unusual observation of cleavage at a single G site in the presence of multiple GG and GGG sites suggests that hole trapping is much faster than hole hopping. Only for the stronger TFP acceptors, when the charge-separated $DNA^{\bullet+}/A^{\bullet-}$ pair is more stable, does the process of hole translocation to a more favorable thermodynamic sink lead to significant leakage to the remote $G^{18}G^{19}$ hole sink. This observation nicely complements the absence of G^{34} cleavage with these strong acceptor substrates.

In summary, incorporation of a radioactive ^{32}P label within the DNA backbone increases both the robustness of the label and the amount of mechanistic information available. This technique allowed us to establish that PET is involved in the mechanism of DNA photodamage by TFP-substituted enediyne–, fulvene–, and diarylacetylene–lysine conjugates. This result is consistent with the thermodynamics of PET,[2] isotope labeling experiments,[2] and computational analysis[4] reported in our earlier work. Moreover, the importance of PET is expanded towards the interaction of DNA with phenyl-substituted enediynes and aryl acetylenes.[28] The overall cleavage selectivity is a compromise between the AT selectivity for binding and the G selectivity for electron transfer. As a result, the cleavage is mostly localized at the GG and GGG hole traps flanking a 12-bp AT-rich A^{27}–A^{38} sequence. Depending on the oxidation potential of the photocleaver, additional damage is distributed to a variable extent between the remote $G^{18}G^{19}$ site and a single G moiety inside the A^{27}–A^{38} tract. Selective targeting of certain G sites is important due to the biological/genomic significance of damage at these positions in, for example, telomere shortening, mutagenesis, and the promotion of tumors.[29]

Received: December 16, 2005
Published online: April 27, 2006

Keywords: alkynes · DNA cleavage · electron transfer · fulvenes · photochemistry

[1] Selected reviews of DNA cleavage: a) G. Pratviel, J. Bernadou, B. Meunier, *Angew. Chem.* **1995**, *107*, 819; *Angew. Chem. Int. Ed. Engl.* **1995**, *34*, 746; b) D. S. Sigman, A. Mazumder, D. M. Perrin, *Chem. Rev.* **1993**, *93*, 2295; c) J. S. Stubbe, J. W. Kozarich, *Chem. Rev.* **1987**, *87*, 1107; d) B. Armitage, *Chem. Rev.* **1998**, *98*, 1171; e) H. T. Chifotides, K. R. Dunbar, *Acc. Chem. Res.* **2005**, *38*, 146; f) T. Da Ros, G. Spalluto, A. S. Boutorine, R. V. Bensasson, M. Prato, *Curr. Pharm. Des.* **2001**, *7*, 1781.

[2] I. V. Alabugin, S. V. Kovalenko, *J. Am. Chem. Soc.* **2002**, *124*, 9052.

[3] J. F. Kauffman, J. M. Turner, I. V. Alabugin, B. Breiner, S. V. Kovalenko, E. A. Badaeva, A. E. Masunov, S. Tretiak, *J. Phys. Chem. A* **2006**, *110*, 241.

[4] I. V. Alabugin, M. Manoharan, *J. Am. Chem. Soc.* **2003**, *125*, 4495.

[5] Direct photochemical activation of enediynes: a) J. Kagan, X. Wang, X. Chen, K. Y. Lau, I. V. Batac, R. W. Tuveson, J. B. Hudson, *J. Photochem. Photobiol. B* **1993**, *21*, 1352; b) R. L. Funk, E. R. R. Young, R. M. Williams, M. F. Flanagan, T. L. Cecil, *J. Am. Chem. Soc.* **1996**, *118*, 3291; c) A. Evenzahav, N. J. Turro, *J. Am. Chem. Soc.* **1998**, *120*, 1835; d) F. S. Fouad, J. M. Wright, G. Plourde II, A. D. Purohit, J. K. Wyatt, A. El-Shafey, G. Hynd, C. F. Crasto, Y. Lin, G. B. Jones, *J. Org. Chem.* **2005**, *70*, 9789; e) T. Kaneko, M. Takahashi, M. Hirama, *Angew. Chem.* **1999**, *111*, 1347; *Angew. Chem. Int. Ed.* **1999**, *38*, 1267; f) N. Choy, B. Blanco, J. Wen, A. Krishan, K. C. Russell, *Org. Lett.* **2000**, *2*, 3761.

[6] *Enediyne Antibiotics as Antitumor Agents* (Eds.: D. B. Borders, T. W. Doyle), Marcel Dekker, New York, **1995**.

[7] K. D. Lewis, A. Matzger, *J. Am. Chem. Soc.* **2005**, *127*, 9968.

[8] S. V Kovalenko, I. V. Alabugin, *Chem. Commun.* **2005**, 1444.

[9] The ds/ss ratio is 1:2 for plasmid DNA and 1:3 for cellular DNA: K. Elmroth, J. Nygren, S. Martensson, I. H. Ismail, O. Hammarsten, *DNA Repair* **2003**, *2*, 363.

[10] About 10 % of the DNA strand breaks induced by bleomycin are double-strand breaks: a) K. Charles, L. F. Povirk, *Chem. Res. Toxicol.* **1998**, *11*, 1580; b) L. F. Povirk, W. Wubker, W. Kohnlein, F. Hutchinson, *Nucleic Acids Res.* **1977**, *5*, 3573–3580.

[11] a) R. S. Lloyd, C. W. Haidle, R. R. Hewitt, *Cancer Res.* **1978**, *38*, 3191; b) A. Harsch, L. A. Marzilli, R. C. Bunt, J. Stubbe, P. Vouros, *Nucleic Acids Res.* **2000**, *28*, 1978; c) J. Stubbe, J. W. Kozarich, *Chem. Rev.* **1987**, *87*, 1107; d) R. M. Burger, *Chem. Rev.* **1998**, *98*, 1153; e) S. M. Hecht, *J. Nat. Prod.* **2000**, *63*, 158.

[12] K. D. Stewart, T. A. Gray, *J. Phys. Org. Chem.* **1992**, *5*, 461.

[13] a) For a review, see: G. B. Schuster, *Acc. Chem. Res.* **2000**, *33*, 253; b) C. Liu, Schuster, G. B. J. *Am. Chem. Soc.* **2003**, *125*, 6098; c) H. Cao, G. B. Schuster, *Bioconjugate Chem.* **2005**, *16*, 820; d) N. Dias, J. Goossens, B. Baldeyrou, A. Lansiaux, P.

 © 2006 Wiley-VCH Verlag GmbH & Co. KGaA, Weinheim

Colson, A. Di Salvo, J. Bernal, A. Turnbull, D. J. Mincher, C. Bailly, *Bioconjugate Chem.* **2005**, *16*, 949.
[14] K. Nakatani, C. Dohno, T. Nakamura, I. Saito, *Tetrahedron Lett.* **1998**, *39*, 2779.
[15] a) C. A. Hastings, J. K. Barton, *Biochemistry* **1999**, *38*, 10042; b) M. E. Nunez, D. B. Hall, J. K. Barton, *Chem. Biol.* **1999**, *6*, 85; c) T. T. Williams, C. Dohno, E. D. A. Stemp, J. K. Barton, *J. Am. Chem. Soc.* **2004**, *126*, 8148; d) A. K. Patra, M. Nethaji, A. R. Chakravarty, *Dalton Trans.* **2005**, *16*, 2798.
[16] a) I. Saito, M. Takayama, H. Sugiyama, K. Nakatani, A. Tsuchida, M. Yamamoto, *J. Am. Chem. Soc.* **1995**, *117*, 6406; b) A. K. Patra, M. Nethaji, A. R. Chakravarty, *Dalton Trans.* **2005**, *16*, 2798.
[17] a) A. Pothukuchy, S. Ellapan, K. Gopidas, M. Salazar, *Bioorg. Med. Chem. Lett.* **2003**, *13*, 1491; b) A. Pothukuchy, C. L. Mazzitelli, M. L. Rodriguez, B. Tuesuwan, M. Salazar, J. S. Brodbelt, S. M. Kerwin, *Biochemistry* **2005**, *44*, 2163.
[18] The origin of this phenomenon is under investigation.
[19] a) RNA: J.-M. A. Battigello, M. Cui, S. Roshong, B. J. Carter, *Bioorg. Med. Chem.* **1995**, *3*, 839; b) DNA: T. Da Ros, E. Vazquez, G. Spalluto, S. Moro, A. Boutorine, M. Prato, *J. Supramol. Chem.* **2002**, *2*, 327.
[20] M. F. Semmelhack, J. J. Gallagher, W. D. Ding, G. Krishnamurthy, R. Babine, G. A. Ellestad, *J. Org. Chem.* **1994**, *59*, 4357.
[21] a) S. V. Kovalenko, S. Peabody, M. Manoharan, R. J. Clark, I. V. Alabugin, *Org. Lett.* **2004**, *6*, 2457; b) S. Peabody, B. Breiner, S. V. Kovalenko, S. Patil, I. V. Alabugin, *Org. Biomol. Chem.* **2005**, *3*, 218.
[22] F. D. Lewis, X. Liu, S. E. Miller, R. T. Hayes, M. R. Wasielewski, *J. Am. Chem. Soc.* **2002**, *124*, 14020.
[23] The cleavage at the central 23 DNA bases was quantified by using SAFA software: R. Das, A. Laederach, S. Pearlman, D. Herschlag, R. Altman, *RNA* **2005**, *11*, 344. For quantified cleavage data, as well as other experimental details, please see the Supporting Information.
[24] F. Mocci, G. Saba, *Biopolymers* **2003**, *68*, 471.
[25] a) N. Korolev, A. P. Lyubartsev, A. Laaksonen, L. Nordenskioeld, *Biopolymers* **2004**, *73*, 542; b) H. Matsuno, K. Niikura, Y. Okahata, *Biochemistry* **2001**, *40*, 3615.
[26] a) L. McFail-Isom, C. C. Sines, L. D. Williams, *Curr. Opin. Struct. Biol.* **1999**, *9*, 298; b) F. D. Lewis, J. Liu, X. Zuo, R. T. Hayes, M. R. Wasielewski, *J. Am. Chem. Soc.* **2003**, *125*, 4850; c) Y. Yoshioka, H. Kawai, T. Sato, K. Yamaguchi, I. Saito, *J. Am. Chem. Soc.* **2003**, *125*, 1968.
[27] A comparison with the results for fulvene **3** suggests that a small amount of cleavage observed at this site for enediynes **1** and **6** may come from the fulvene intermediate.
[28] Exothermicity for electron transfer from DNA to compound **1** = $-17.8\ \text{kcal mol}^{-1}$ and to compound **2** > $-12.7\ \text{kcal mol}^{-1}$. (The estimates are based on the reduction potential of the unsubstituted chromophores because the reduction potential of the lysine conjugates could not be measured.)
[29] a) S. Oikawa, S. Tada-Oikawa, S. Kawanishi, *Biochemistry* **2001**, *40*, 4763; b) J. G. Levine, R. M. Schaaper, D. M. DeMarini, *Genomics* **1994**, *136*, 731; c) S. Kawanishi, S. Oikawa, M. Murata, H. Tsukitome, I. Saito, *Biochemistry* **1999**, *38*, 16733.

 © 2006 Wiley-VCH Verlag GmbH & Co. KGaA, Weinheim

Porphyrinoids

DOI: 10.1002/anie.200600589

Subpyriporphyrin—A [14]Triphyrin(1.1.1) Homologue with an Embedded Pyridine Moiety**

Radomir Myśliborski, Lechosław Latos-Grażyński, Ludmiła Szterenberg, and Tadeusz Lis*

Triphyrins are porphyrin analogues which contain only three pyrrole or pyrrole-related rings linked through meso-sp^2 carbon atoms, as found in [18]triphyrin(6.1.1) (vacataporphyrin), [15]triphyrin(1.1.3), dithiaethyneporphyrin, [18]triphyrin(2.2.2), and [18]heterotriphyrin(2.2.2).[1]

Subphthalocyanine,[2] subporphyrazine,[3] and tribenzosubporphine,[4] which have been isolated and characterized only as their boron complexes (**2**–**4**, respectively), can be directly related to the hypothetical [14]triphyrin(1.1.1) (**1**; Scheme 1). Extensive studies on the 14 π-electron system of

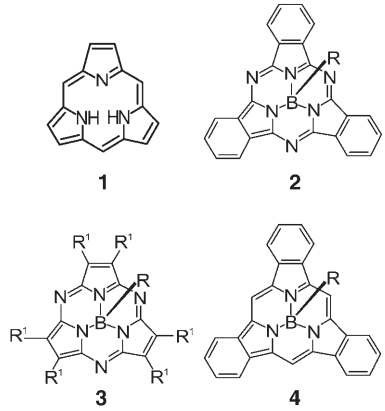

Scheme 1. [14]Triphyrin(1.1.1) (**1**) and the boron complexes of subphthalocyanine **2**, subporphyrazine **3**, and tribenzosubporphine **4**.

boron subphthalocyanines revealed interesting properties for application in the areas of dyes, nonlinear optics, and photonic devices.[2b] Thus, it remains a challenge to produce contracted porphyrins that display triphyrin(1.1.1)-like molecular frame-

[*] R. Myśliborski, Prof. Dr. L. Latos-Grażyński, Dr. L. Szterenberg, Prof. Dr. T. Lis
Department of Chemistry
University of Wrocław
14 F. Joliot-Curie St., 50-383 Wrocław (Poland)
Fax: (+48) 71-328-2348
E-mail: llg@wchuwr.chem.uni.wroc.pl

[**] Financial support from the Ministry of Scientific Research and Information Technology (Grant 3 T09A 162 28) is gratefully acknowledged. Quantum mechanical calculations were preformed at the Supercomputer Centers in Wrocław and Poznań.

Supporting information for this article is available on the WWW under http://www.angewandte.org or from the author.

InterScience
© 2006 Wiley-VCH Verlag GmbH & Co. KGaA, Weinheim

works that are potentially amenable to diverse structural modifications and applications.[5]

Here we report on the synthesis and characterization of subpyriporphyrin **5** (Scheme 2). Subpyriporphyrin ((SubPyP)H) is a novel type of contracted porphyrin—a homologue of [14]triphyrin(1.1.1) (**1**) with a pyridine moiety

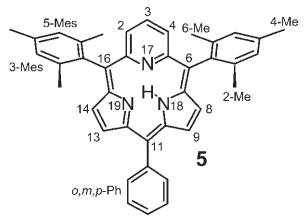

Scheme 2. Subpyriporphyrin **5** with the systematic numbering scheme.

embedded in the macrocyclic framework. It introduces the unique structural pattern of a free-base triphyrin, as distinguished by the location of three nitrogen atoms at the corners of an approximately equilateral triangle, and thus clearly approaches the limit of porphyrin contraction defined by **1**. The coordinating properties of **5** are exemplified by the formation of an organoboron complex.

The synthetic strategy (Scheme 3) incorporates some features used for the synthesis of 3-azabenziporphyrin.[6] In particular, the introduction of bulky substituents at the *ortho*

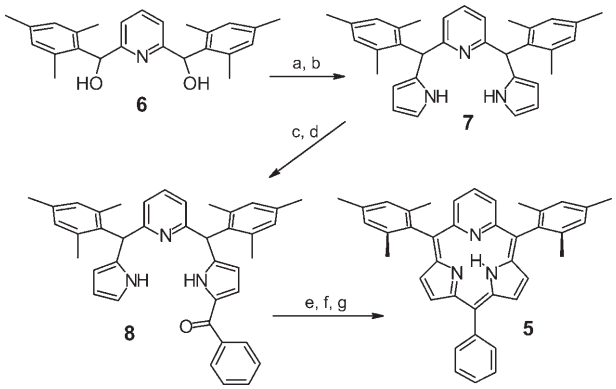

Scheme 3. Synthesis of subpyriporphyrin **5**: a) MsCl/TEA, b) pyrrole, c) EtMgBr, d) PhCOCl, e) $NaBH_4$, f) BF_3 or TFA/MeCN, g) TEA, DDQ (5 equiv). Ms = methanesulfonyl, TEA = triethylamine, TFA = trifluoroacetic acid, DDQ = 2,3-dichloro-5,6-dicyano-1,4-benzoquinone.

positions of the meso-aryl groups in **6**, adjacent to the incorporated pyridine ring, increased the stability of **7** toward acidolysis during the condensation, thus eliminating a scrambling effect. Monobenzoylation of **7** yielded **8**. Subsequent reduction of **8** gave the alcohol derivative which undergoes an intramolecular condensation to produce subpyriporphyrin **5**. Compound **5** was obtained as a green solid in 6% yield after oxidation and chromatographic workup.

X-ray crystal structure analysis showed that macrocycle **5** is slightly ruffled (Figure 1). The C–C bonds within the

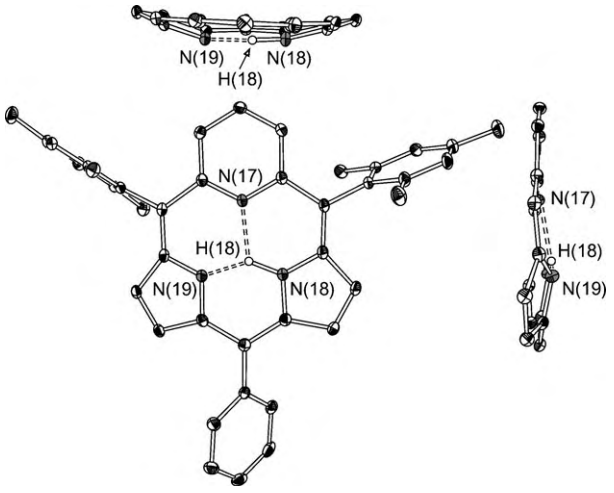

Figure 1. Molecular structure of **5** (30% thermal ellipsoids) at 80 K. The solvent molecule and hydrogen atoms (except for the directly detected NH group) are omitted for clarity (perspective view; top and right: side views, phenyl groups are omitted for clarity). The dihedral angles between the N_3 plane and the planes of the rings are: pyridine 12.5°; pyrrole-N(18) 20.7°; pyrrole-N(19) 25.5°. Selected distances: N(17)···N(18) 2.519(2) Å; N(17)···N(19) 2.534(2) Å; N(18)···N(19) 2.370(2) Å.[7]

dipyrrane subunit are conjugated and have similar length patterns in both pyrrolic subunits, while the bond lengths in the six-membered ring are pyridine-like. The determined N(18)···N(19) distance of 2.370(2) Å is the shortest N···HN hydrogen bond reported.[8] The N(17)···N(18) distance 2.534(2) Å also lies within the range for a very strong hydrogen-bonding interaction,[9] and thus the NH hydrogen atom of **5** is involved in three-centered (N(17), N(18), N(19)) hydrogen bonding.

Density functional theory (DFT) has been applied to model the molecular and electronic structure of two feasible tautomers **5** and **5′** of subpyriporphyrin (Scheme 4), and

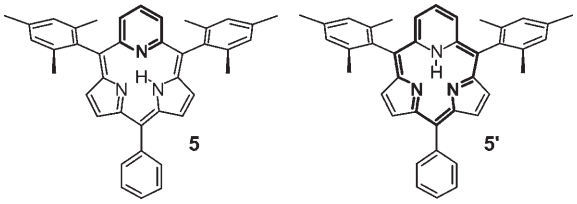

Scheme 4. Tautomers **5** and **5′** of subpyriporphyrin where π-delocalization pathways (6e and 14e, respectively) are marked with thick lines.

shows the preference for the protonation of a single pyrrole nitrogen atom over that of the pyridine ring (4.66 kcal mol^{-1}). Significantly, the calculated N···N distances (N(17)···N(18) 2.518 Å; N(17)···N(19) 2.585 Å, N(18)···N(19) 2.397 Å) closely resemble those determined by the X-ray data.

Application of the the theory of atoms in molecules (AIM)[10] allows chemically relevant information to be derived from the topology of the electron density in **5**. Figure 2 shows the bonding critical points (BCPs) and ring

 © 2006 Wiley-VCH Verlag GmbH & Co. KGaA, Weinheim

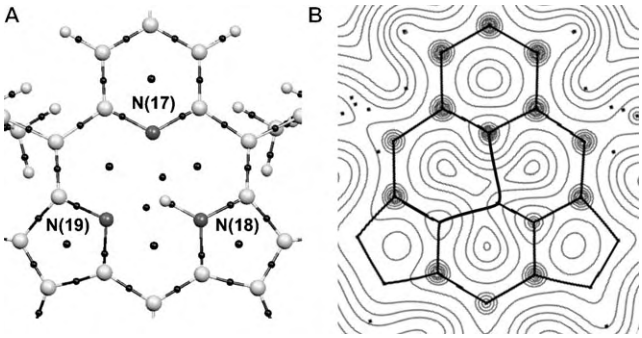

Figure 2. Molecular graph of the central part of **5** illustrating the existence of hydrogen bonding from AIM formalism. A) Position of bond critical points (BCPs) and ring critical points (RCPs). B) Electron-density distribution in **5**. The black solid curve shows bond paths of the hydrogen bond.

critical points (RCPs) in the central part of the structure of **5**. Most importantly, the bond critical points indicate a hydrogen-bonding pathway between H(18) and the N(17), N(18), and N(19) nitrogen atoms. The values of the parameters determined for the N(17)H, N(18)H, and N(19)H bond critical points (see the Supporting Information) agree with the presence of three-centred hydrogen bonds.[10b,c]

The electronic spectrum of **5** (Figure 3) shows two bands at 346 and 730 nm (very broad) that resemble the spectroscopic features of non-aromatic benziporphyrin[11] and 3-azabenziporphyrin.[6] The ^{1}H NMR spectrum of **5** shows

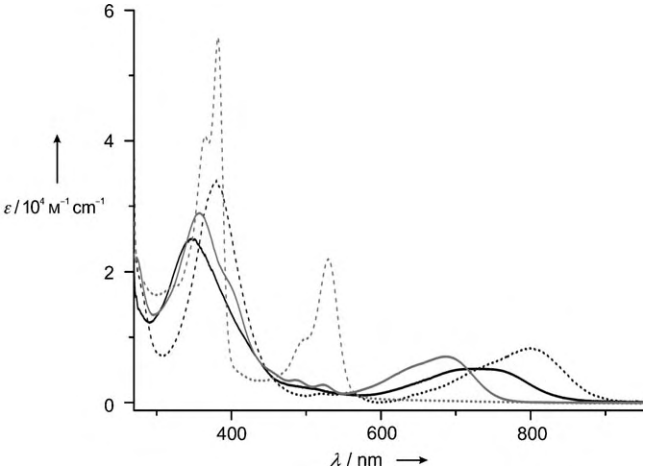

Figure 3. The electronic spectra of **5** (solid black line), **5**-H_2 (black dotted line), **9** (solid gray line), and **10** (dashed gray line).

resonances at chemical shifts that are consistent with a non-aromatic structure (Figure 4 A). The macrocyclic aromatic ring current is practically absent for **5**, as clearly illustrated by the positions of the pyrrole and pyridine resonances, assigned by 2D experiments (δ ppm: H(8/13) 7.07, H(9/12) 7.35, H(2/4) 7.70, H(3) 8.00; CD_2Cl_2, 203 K). A single NH resonance shows simultaneous scalar coupling to four pyrrolic hydrogen atoms. Thus, similar to porphycene[12] and tetraarylsap-

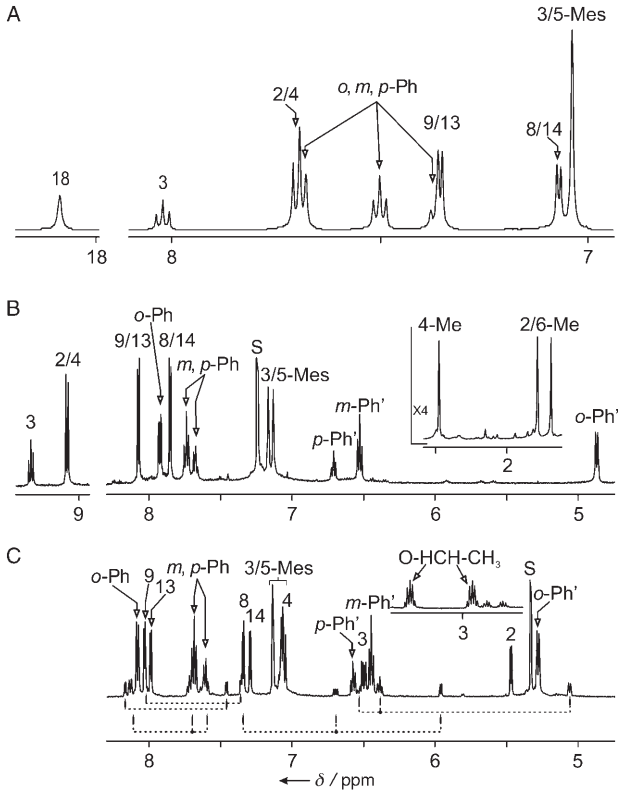

Figure 4. ^{1}H NMR spectra (downfield regions) of: A) **5** (203 K, CD_2Cl_2), B) **9** (298 K, $CDCl_3$), C) **10**-*s* and **10**-*a* (298 K, CD_2Cl_2). Resonance assignments (obtained from COSY and NOESY maps) follow the numbering given in Scheme 2. The resonances of **10**-*a* and their scalar connectivity marked by arrows are linked by dotted lines. *o*-Ph′, *m*-Ph′, and *p*-Ph′ denote resonances of the σ-phenyl ring. The domed structure of **9** is reflected by the substantial differentiation of the *m*-mesityl and *o*-CH_3 resonances (B, inset). The diasterotopic splitting of the CH_2 resonances of 2-ethoxide is shown (C, inset). S = solvent.

phyrin,[13] subpyriporphyrin **5** tautomerizes extremely fast between two equivalent tautomers even at 183 K: (N(17), N(18)H, N(1)) and (N(17), N(18), N(19)H). The rapid exchange of the inner proton involves two pyrrole nitrogen atoms but excludes the pyridine one. The extreme downfield shift of the N(18)H resonance (δ = 18.07 ppm; CD_2Cl_2, 203 K) results from the strong hydrogen-bonding interaction.

Two stages of protonation in [D_2]dichloromethane have been demonstrated. The addition of the first proton resulted solely in the formation of the symmetrical (N(17),N(18)H,N(19)H) tautomer **5**-H as confirmed by the (N)H–β-H scalar coupling. The significant upfield shift of the NH resonance (δ = 12 ppm) readily correlates with the profound structural changes accompanying the breaking of the internal hydrogen bond.[8d] The DFT calculations demonstrated the significant folding of **5**-H, as reflected by the significant increase in the optimized N(18)···N(19) distance (2.611 Å) by the tilting of the pyrrole rings in opposite directions (see the Supporting Information). Further titration results in protonation of the pyridine nitrogen atom to form **5**-H_2. The **5**-H_2 species remains in fast exchange both with **5**-H and the species formed by coordination of TFA by **5**-H_2 and

 © 2006 Wiley-VCH Verlag GmbH & Co. KGaA, Weinheim

accounts for the smooth changes in the chemical shifts during the course of the titration.

Compound **5** reacts with $PhBCl_2$ to yield green σ-phenyl boron(III) subpyriporphyrin $[(SubPyP)BPh]^+$ **9**, wherein the macrocycle acts as a monoanionic tridentate ligand. The electronic spectrum of **9** is not very different from that of **5**, except for the presence of two Q-like bands (ca. 500 nm).

The coordination of the boron(III) ion results in the pyrrole and pyridine ^1H NMR resonances of **9** being markedly downfield-shifted with respect to those of **5** ($\Delta\delta$ ppm: H(3) 1.55, H(2/4) 1.35, pyrr 0.72, pyrr, 0.70), thus revealing a significant contribution by the ring current effect. The most notable feature is the marked upfield shift of the axially coordinated σ-phenyl group (H^o 4.87, H^m 6.52, H^p 6.07), although less pronounced than that for typical diamagnetic metalloporphyrins with σ-phenyl groups,[14,15] but stronger than that for σ-phenylboron subphthalocyanine ((SubPh)BPh).[3,15] This observation confirms the aromatization arising from coordination and reflects the structural changes that allow delocalization of 14 π electrons as shown in **9′** (Scheme 5).

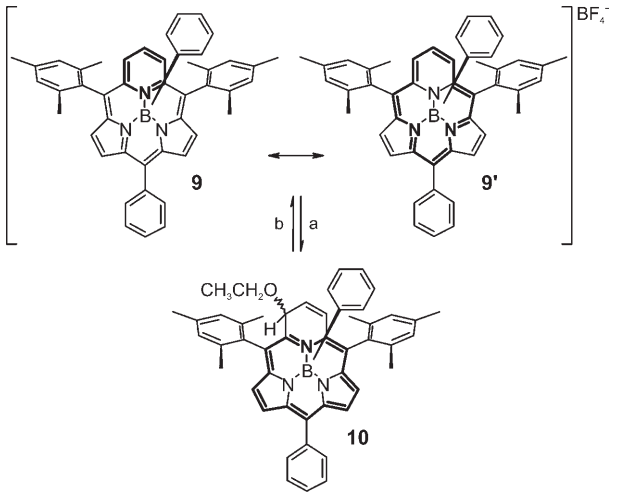

Scheme 5. Transformations of boron subpyriporphyrin: a) $CH_3CH_2O^-$/CH_3CH_2OH, b) H^+.

As demonstrated by DFT calculations, the coordination results in remarkable changes in the geometry that allows formation of a domed structure with the boron atom displaced from the N_3 plane by 0.581 Å (Figure 5).

The perimeter reactivity of **9** is essential when considering the perspective functionalization of subpyriporphyrins (Scheme 5). Thus addition of ethoxide to **9** afforded two aromatic steroisomers **10**-*a* and **10**-*s* as readily seen by two sets of resonances in the ^1H NMR spectrum.

As shown by a NOESY experiment and integration, a *syn* addition with respect to the σ-aryl group is unexpectedly preferred (1:4.5 molar ratio). The complex multiplets (**10**-*s*: $\delta = 3.31$ and 2.94 ppm; **10**-*a*: $\delta = 2.85$ and 2.76 ppm) of the ethoxymethylene group reflects the diastereotopic effect as the stereocenter is created at the tetrahedrally hybridized C(2) atom (^{13}C NMR shift of **10**-*s* C(2) $\delta = 67.6$ ppm).

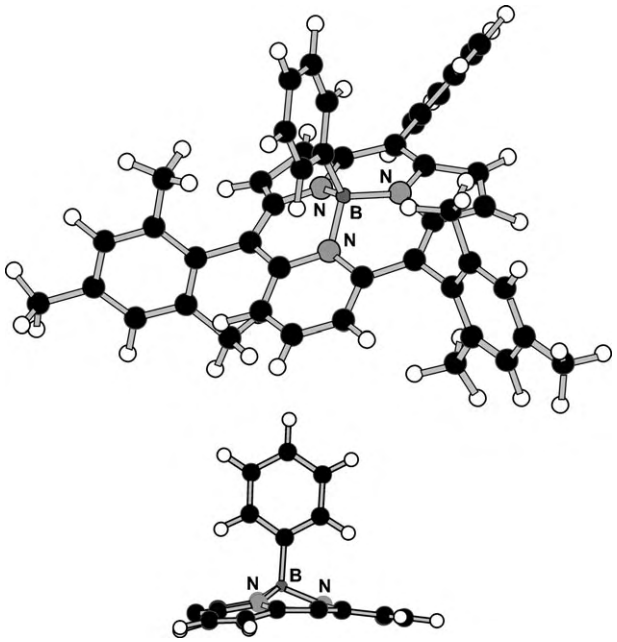

Figure 5. The DFT optimized structure of **9** (top: perspective view; bottom: side view).

Addition of acid to **10** recovers **9**. The UV/Vis spectrum confirms the aromaticity of **10**, as evident by the large extinction coefficients (Figure 3).

In conclusion we have presented a rational route for the synthesis of 6,16-dimesityl-11-phenylsubpyriporphyrin—the first free-base triphyrin(1.1.1)-related molecule—which revealed the shortest N···N distance between two nitrogen atoms involved in hydrogen bonding. The molecule acts as a ligand, as shown in its reaction with boron, thus opening up options to explore the coordination chemistry of subpyriporphyrin. The new system can potentially be linked into multielement porphyrin arrays by using the perimeter adjustments developed for tetraarylporphyrins, thus introducing a trigonal structural motif instead of a tetragonal one.

Experimental Section

5: $NaBH_4$ (155 mg, 40 equiv) was added in several portions to a solution of **8** (57.5 mg, 0.1 mmol) in THF/EtOH under N_2. The mixture was stirred for 3 h, and then CH_2Cl_2 (10 mL) was added. The organic layer was washed 3 times with dilute NaOH and water, dried with Na_2SO_4, evaporated, and dried in a vacuum for 1 h. The residue was dissolved in dry CH_3CN (200 mL) under N_2, and then TFA (200 μL, 2.6 mmol) or $Et_2O{\cdot}BF_3$ (25.5 μL, 0.2 mmol) added. The solution was then stirred for 4 h in the absence of light. The condensation was quenched by addition of excess TEA. DDQ (113.5 mg, 5 equiv) was then added and the reaction mixture was stirred for 1 h before the solvent was evaporated to dryness. The residue was dissolved in CH_2Cl_2 and purified by chromatography on grade II basic alumina. The first green fraction, containing **5**, was eluted with CH_2Cl_2. Recrystallization from CH_2Cl_2/CH_3OH produced 3.3 mg of **5** (yield 6%). ^1H NMR (500 MHz, $CDCl_3$, 213 K): $\delta = 17.82$ (s, 1H, H(18)), 8.00, 7.76 (AB_2, (1+2)H, $^3J_{H,H} = 7.95$ Hz, H(3), H(2/4)), 7.73, 7.53, 7.39 (A_2M_2X, (2+2+1)H, Ph), 7.41 (*A*B, 2H, $^3J_{H,H} = 4.62$ Hz, H(9/13)), 7.18 (A*B*, 2H, $^3J_{H,H} = 4.62$ Hz, H(8/14)), 7.05 (br s,

 © 2006 Wiley-VCH Verlag GmbH & Co. KGaA, Weinheim

4H, *m*-Mes), 2.41 (s, 6H, 4-Me), 1.99 ppm (s, 12H, 2/6-Me); ^{13}C NMR (125.7 MHz, $CDCl_3$, 213 K): $\delta = 157.9$, 149.8, 149.3, 139.3, 137.9, 137.7, 135.3, 133.7, 131.2, 130.7, 130.0, 128.7, 127.9, 126.1, 125.8, 123.2, 111.7, 108.2, 22.0, 21.5 ppm; UV/Vis (CH_2Cl_2) λ_{max} ($\log\varepsilon$) = 346 (4.40), 730 nm (very broad, 3.71). HRMS (ESI): *m*/*z*: 558.29054 (*m*/*z* calcd for $[C_{40}H_{35}N_3+H]^+$: 558.29038).

9: Phenylboron dichloride (8 μL, 10 equiv) was added to a solution of **5** (3.3 mg, 0.006 mmol) in dry toluene (under N_2). The mixture was stirred for 1.5 h. Excess $AgBF_4$ was added and the solvent was removed under vacuum. Green **9** was dissolved in CH_2Cl_2, filtrated, and purified by recrystallization from CH_2Cl_2/*n*-hexane. Yield 4.2 mg (95%). ^{1}H NMR (500 MHz, $CDCl_3$, 298 K): $\delta = 9.33$, 9.08 (AB_2, (2+1)H, $^3J_{H,H} = 8.08$ Hz, H(3) + H(2/4)), 8.07, 7.85 (AB, (2+2)H, $^3J_{H,H} = 5.01$ Hz, H(9/13), H(8/14)), 7.92, 7.74, 7.67 (A_2M_2X, (2+2+1)H, Ph), 7.16 (s, 2H, 5-Mes), 7.13 (s, 2H, 3-Mes), 6.07, 6.52, 4.87 (AM_2X_2, (1+2+2)H, Ph′), 2.47 (s, 6H, 4-Me), 1.79 (s, 6H, 2-Me), 1.69 ppm (s, 6H, 6-Me); ^{13}C NMR (125.7 MHz, $CDCl_3$, 298 K): $\delta =$ 150.4, 146.0, 140.6, 140.3, 139.6, 138.8, 133.4, 132.6, 132.0, 131.3, 129.9, 129.8, 129.6, 129.5, 129.4, 129.0, 128.7, 128.0, 127.4, 117.2, 21.7, 21.5, 21.0 ppm. UV/Vis λ_{max} ($\log\varepsilon$) = 358 (4.46), 485 (3.54), 523 (3.43), 687 nm (3.85). HRMS (ESI) *m*/*z*: 644.32356 (*m*/*z* calcd for $[C_{46}H_{39}N_3B]^+$: 644.32316).

Received: February 14, 2006
Published online: April 26, 2006

Keywords: hydrogen bonds · macrocycles · porphyrinoids · pyriporphyrins

[1] a) E. Pacholska, L. Latos-Grażyński, Z. Ciunik, *Chem. Eur. J.* **2002**, *8*, 5403; b) A. Krivokapic, A. R. Cowley, H. L. Anderson, *J. Org. Chem.* **2003**, *68*, 1089; c) A. Berlicka, L. Latos-Grażyński, T. Lis, *Angew. Chem.* **2005**, *117*, 5422; *Angew. Chem. Int. Ed.* **2005**, *44*, 5228; d) G. M. Badger, J. A. Elix, G. E. Lewis, *Proc. Chem. Soc.* **1964**, 82; e) G. M. Badger, J. A. Elix, G. E. Lewis, *Aust. J. Chem.* **1965**, *18*, 70; f) Z. Hu, J. L. Atwood, M. P. Cava, *J. Org. Chem.* **1994**, *59*, 8071.

[2] a) A. Meller, A. Ossko, *Monatsh. Chem.* **1972**, *103*, 150; b) C. G. Claessens, D. Gonzáles-Rodriguez, T. Torres, *Chem. Rev.* **2002**, *102*, 835.

[3] a) J. Rauschnabel, M. Hanack, *Tetrahedron Lett.* **1995**, *36*, 1629; b) M. S. Rodríguez-Morgade, S. Esperanza, T. Torres, J. Barberá, *Chem. Eur. J.* **2005**, *11*, 354.

[4] Y. Inokuma, J. H. Kwon, T. K. Ahn, M.-C. Yoo, D. Kim, A. Osuka, *Angew. Chem.* **2006**, *118*, 975; *Angew. Chem. Int. Ed.* **2006**, *45*, 961.

[5] T. Torres, *Angew. Chem.* **2006**, *118*, 2900; *Angew. Chem. Int. Ed.* **2006**, *45*, 2834.

[6] R. Myśliborski, L. Latos-Grażyński, *Eur. J. Org. Chem.* **2005**, 5039.

[7] Data collection: the measurement was performed on an Xcalibur PX κ-geometry diffractometer using $Mo_{K\alpha}$ radiation ($\lambda = 0.71073$ Å), $T = 100$ and 80 K for the same crystal. **5**·CH_2Cl_2: crystals were prepared by the slow diffusion of CH_3OH into a solution of **5** in CH_2Cl_2 to yield a dark-green crystal of $C_{40}H_{35}N_3{\cdot}CH_2Cl_2$, size $0.40 \times 0.12 \times 0.07$ mm^3, monoclinic, space group $P2_1/c$, $a = 12.737(3)$, $b = 11.687(3)$, $c = 22.894(4)$ Å, $\beta = 102.94(3)°$, $V = 3321.4(13)$ Å^3 for $T = 80$ K, $Z = 4$. total no. of reflections collected: 50231; no. of independent reflections: 9735 (of which $4774 > 2\sigma(I)$) were included in the refinement for 442 parameters; no absorption correction was applied. The structure was solved by using direct methods with SHELXS-97 and refined against $|F^2|$ using SHELXL-97 (G. M. Sheldrick, University of Göttingen, Germany, **1997**), final $R1/wR2$ indices (for $I > 2\sigma(I)$): 0.0459/0.1130; max./min. residual electron density: +0.25/−0.30 e Å^{-3}; H atoms except H(18) (NH) were fixed in idealized positions using the riding model constraints. The CH_2Cl_2 was disordered into two positions. CCDC-297978 and -297979 contain the supplementary crystallographic data for this paper. These data can be obtained free of charge from The Cambridge Crystallographic Data Centre via www.ccdc.cam.ac.uk/data_request/cif.

[8] a) E. Vogel, M. Kocher, H. Schmickler, J. Lex, *Angew. Chem.* **1986**, *98*, 262; *Angew. Chem. Int. Ed. Engl.* **1986**, *25*, 257; b) E. Vogel, B. Binsack, Y. Helllwig, C. Erben, A. Heger, J. Lex, Y. D. Wu, *Angew. Chem.* **1997**, *109*, 2725; *Angew. Chem. Int. Ed. Engl.* **1997**, *36*, 2612; c) H. Furuta, H. Maeda, A. Osuka, *J. Am. Chem. Soc.* **2001**, *123*, 6435; d) H. Furuta, T. Ishizuka, A. Osuka, T. Ogawa, *J. Am. Chem. Soc.* **2000**, *122*, 5748; e) I. Saltsman, I. Goldberg, Z. Gross, *Tetrahedron Lett.* **2003**, *44*, 5669; f) V. A. Ozeranskii, A. F. Pozharskii, A. Bieńko, W. Sawka-Dobrowolska, L. Sobczyk, *J. Phys. Chem. A* **2005**, *109*, 1637.

[9] The strong hydrogen bonding confined in a porphyrinoid core was previously detected in the case of oxoindole (2.448 Å),[8c] N-fused porphyrin (2.459 Å),[8d] isocorrole (2.544 Å),[8b] and porphycene (2.63 Å)[8a] as reflected by the N···N distances given in parentheses.

[10] a) R. F. W. Bader, *Atoms in Molecules—a Quantum Theory*, Oxford University Press, Oxford **1990**; b) P. Popelier, *Atoms In Molecules, An Introduction*, Pearson Education, Harlow, **2000**; c) I. Rozas, I. Alkorta, J. Elgureo, *J. Phys. Chem. A* **1998**, *102*, 9925.

[11] M. Stępień, L. Latos-Grażyński, *Chem. Eur. J.* **2001**, *7*, 5113.

[12] U. Langer, C. Hoelger, B. Wehrle, L. Latanowicz, E. Vogel, H.-H. Limbach, *J. Phys. Org. Chem.* **2000**, *13*, 23.

[13] P. J. Chmielewski, L. Latos-Grażyński, K. Rachlewicz, *Chem. Eur. J.* **1995**, *1*, 68.

[14] a) K. M. Kadish, J. M. Barbe, J. E. Anderson, R. Guilard, *J. Am. Chem. Soc.* **1987**, *109*, 7705; b) R. Guilard, A. Zrineh, A. Tabard, A. Endo, B. C. Han, C. Lecomte, M. Souhassou, A. Habbou, M. Ferhart, K. M. Kadish, *Inorg. Chem.* **1990**, *29*, 4476; c) M. Geyer, F. Plenzig, J. Rauschnabel, M. Hanack, B. Del Rey, A. Sastre, T. Torres, *Synthesis* **1996**, *9*, 1139.

[15] [(tpp)Ge(Ph)Et],[14a] H^o 0.42; H^m 4.85, H^p 5.34 ppm; [(tpp)AlPh],[14b] H^o 2.48; H^m 5.58, H^p 5.84 ppm), [(SubPh)BPh][3] (H^o 5.66; H^m 6.53, H^p 6.67).

 © 2006 Wiley-VCH Verlag GmbH & Co. KGaA, Weinheim

Green Solvents

DOI: 10.1002/anie.200600397

Designed CO_2-Philes Stabilize Water-in-Carbon Dioxide Microemulsions**

Julian Eastoe, Sarah Gold, Sarah Rogers, Paul Wyatt, David C. Steytler, Alexandre Gurgel, Richard K. Heenan, Xin Fan, Eric J. Beckman, and Robert M. Enick*

Herein is reported the first direct structural evidence for the formation of nanodomains in water-in-carbon dioxide (w/c) microemulsions by two non-fluorinated surfactants. Generation of O-surfactants, by incorporating oxygen into the surfactant tails, significantly improves CO_2-philicity, affording stabilization of w/c structures. Tests with standard hydrocarbon surfactants (H-surfactants) demonstrate that they are unable to support true w/c phases (see Supporting Information). This finding represents an important step forward in the design of commercially viable and environmentally responsible CO_2-philes, which has potential to expand research and commercial applications with supercritical or liquid CO_2 as a solvent.

It is widely recognized that waste petrochemical solvents pose a huge environmental threat; recently significant efforts have been made to develop dense CO_2 as an alternative "green" solvent.[1] CO_2 is well suited to applications in food or pharmaceutical industries since it is environmentally benign, biocompatible, nonflammable, nontoxic, cheap, abundant, and crucially, unregulated by the US Environmental Protection Agency. However, there are severe limitations because CO_2 is generally a poor solvent, especially for polar and/or high-molecular-weight solutes. Although water and carbon dioxide are weakly compatible (e.g. solubility of water in CO_2 at 15 °C, 450 bar is approximately 0.14 %), surfactants and polymers are needed to increase this low level, by stabilizing the CO_2–water interface. Hence, solubility levels in CO_2 could be significantly enhanced, and controlled by incorporation of pressure-sensitive reversed micelles or w/c microemulsion nanodroplets.

A recent review outlines the state-of-the-art in CO_2 surfactants;[1] the most efficient of these contain fluorine, making them environmentally and commercially unacceptable. It has been shown that high-pressure small-angle neutron scattering (HP-SANS) is one of the most reliable techniques for detecting aggregation in CO_2,[1] since it generates an unmistakable fingerprint SANS signal, which is characteristic of micelles or water nanodroplets (see Supporting Information). Reports have emerged, mainly based on spectral probe dye evidence, suggesting microemulsion formation in CO_2 with commercially available non-ionic hydrocarbon surfactants,[2,3] however, HP-SANS experiments do not support these claims (see Supporting Information). HP-SANS has provided direct proof of micelle formation with a custom-designed CO_2 surfactant (AOT4), an analogue of common Aerosol-OT (AOT), but bearing *tert*-butyl rather than methyl chain tips as for AOT.[4] Although AOT4 did not disperse water, another designer surfactant comprising twin vinyl acetate oligomeric chains AO-VAc (Figure 1) has shown promise as a stabilizer for w/c phases.[5] The design of AO-VAc was based on simulations demonstrating enhanced solubility of simple acylated sugars with CO_2,[6] hence the VAc chains are expected to promote CO_2-philicity compared to normal hydrocarbon tails. To confirm that oxygenated chains are essential for stabilization of w/c nanodroplets the surfactant AOK (Figure 1) was synthesized, bearing *tert*-butyl and carbonyl groups in the chain tips. Furthermore, two tails are often needed to induce reversed interfacial curvature.[1,4,5]

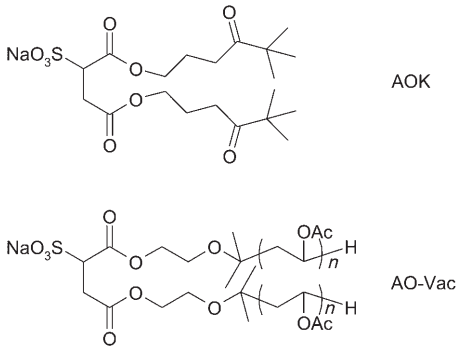

Figure 1. CO_2-philic surfactants used to stabilize water-in-carbon dioxide microemulsions: sodium bis(5,5-dimethyl-4-oxo-hexyloxycarbonyl) sulfosuccinate (Aerosol-octyl-ketone or AOK) and sodium bis(vinyl acetate)$_8$ sulfosuccinate (Aerosol-vinyl acetate or AO-VAc with $n = 8$).

HP-SANS experiments indicated that a range of standard commercially available hydrocarbon surfactants do not stabilize nanodroplet water pools in CO_2 (see Supporting Information). However, with the oxygenated AOK, SANS signals were detected: after successive additions of D_2O there

[*] Prof. J. Eastoe, S. Gold, S. Rogers, Dr. P. Wyatt
School of Chemistry, University of Bristol
Bristol, BS8 1TS (UK)
Fax: (+44) 117-928-9180
E-mail: julian.eastoe@bris.ac.uk
Dr. D. C. Steytler, Dr. A. Gurgel
School of Chemical Sciences and Pharmacy
University of East Anglia, Norwich NR4 7TJ (UK)
Dr. R. K. Heenan
ISIS-CCLRC Rutherford Appleton Laboratories
Chilton OX11 0QX (UK)
X. Fan, Prof. E. J. Beckman, Prof. R. M. Enick
Department of Chemical and Petroleum Engineering
University of Pittsburgh, Pittsburgh, PA 15261 (USA)

[**] S.G., A.G., and S.R. thank the University of Bristol DTA, CNPq Brazil, and EPSRC (EP/C523105/1) for studentships and a post-doctoral fellowship, respectively. CCLRC are thanked for beam time and consumables/travel grants. Alan Pitt (Kodak (UK)) is thanked for stimulating discussions. The University of Pittsburgh would like to express its appreciation to the US DOE NETL for supporting this research through contract DE-FG26-04NT-15533.

Supporting information for this article is available on the WWW under http://www.angewandte.org or from the author.

 © 2006 Wiley-VCH Verlag GmbH & Co. KGaA, Weinheim

was a progressive increase in intensity and a shift of the peak maximum to lower scattering vector Q, consistent with swelling of water nanodomains. With the oxygenated surfactant AO-VAc, SANS signals were not detected until the water loading reached $w_{corr} = 10.9$ (corresponding to an uncorrected $w = 50$),[5] and the inset to Figure 2 shows this curve. Figure 3

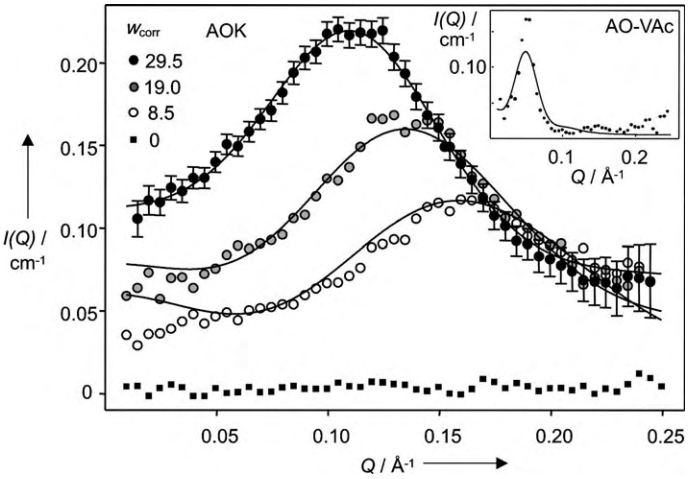

Figure 2. SANS data (symbols) and form factor fits (lines) for surfactant-stabilized D_2O-in-CO_2 microemulsions as a function of water loading $w_{corr} = \{[D_2O]_{added} - [D_2O]_{CO_2}\}/[surf]$. Fitted parameters are given in Table 1. Surfactant concentrations AOK = 50 mmol dm^{-3} ($\approx$2.4 wt%) and AO-Vac = 6.2 mmol dm^{-3} ($\approx$1 wt%). Experimental conditions 500 bar and 45 °C for AOK, but 25 °C for AO-VAc. Example error bars are shown for one AOK sample. Inset: SANS data for AO-Vac at $w_{corr} = 10.9$.

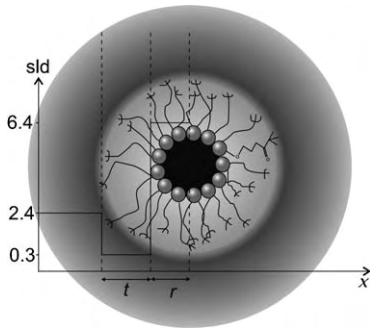

Figure 3. Schematic scattering length density (sld or $\rho \times 10^{10}$ cm^{-2}) profile fitted to SANS data from surfactant-stabilized D_2O-in-CO_2 microemulsion droplets. The values fixed in the form factor analyses were 2.4 for the external CO_2 phase (outer gray ring), 0.3 for the AOK surfactant shell (shown as lines), and 6.4×10^{10} cm^{-2} for the D_2O core (small gray spheres). See text for details. For the solvent, ρ_{CO_2} was calculated as in ref. [7].

shows the expected neutron scattering length density (ρ) profile for spherical D_2O nanodroplets coated by a surfactant monolayer, and dispersed in CO_2.[7] For this configuration the $I(Q)$ distribution should be described by a spherical core–shell form factor,[8] modified with a Schulz polydispersity function, as is routinely used in neutron contrast variation studies of water-in-oil microemulsions.[9] Owing to intra-particle interference effects this scattering law gives rise to a Q_{max} peak in the SANS profile, which is the signature of a core–shell structure (Figure 2, and Supporting Information). This form factor[8,9] was fitted to the $I(Q)$ curves in Figure 2, with the best fit parameters: core radius (r), shell thickness (t), and polydispersity (σ/r) given in Table 1. The fits

Table 1: Parameters obtained from polydisperse spherical core–shell form factor analyses of SANS data.[a]

Surfactant	w_{corr}	r [Å]	t [Å]	σ/r
AOK	8.5	15	8	0.15
	19.0	17	9	0.15
	29.5	21	10	0.15
AO-VAc	10.9	55	26	0.20

[a] Uncertainties on r and t are $\pm$1 Å.

shown in Figure 2 are reasonable given weak SANS intensities owing to poor contrast and low concentrations: for AO-VAc, the peak position is well reproduced, but not the intensity maximum. However, it is reassuring to see that the fitted shell thickness t increases from AOK to AO-Vac, both values being consistent with expected molecular lengths (Table 1). Therefore, these two new CO_2-philes show common macroscopic phase behavior and core–shell nanodroplet structures.

Compared to AOK and AO-VAc, common commercial surfactants display only weak aggregation (see Supporting Information) highlighting the need for specialized CO_2-philic groups to stabilize the water–CO_2 interface. Comparing the behaviors of AOK and CO_2-inactive Aerosol-OT,[4] shows that only minor chemical variations at the chain-tip extremities have significant effects on CO_2-philicity. This mirrors extensive studies of hydrocarbon and fluorocarbon AOT analogues at various model oil–water interfaces,[10] pointing to new design approaches for CO_2-philes, which could unlock the vast potential of CO_2 as a green processing, cleaning and separation medium.[11]

Experimental Section

The surfactants were synthesized and characterized as detailed elsewhere (Supporting Information and ref. [5]). The w/c samples were formulated using D_2O to provide contrast (Goss UK 99.9% D-atom) in a high-pressure cell on the LOQ SANS beam line at ISIS, UK, following experimental protocols described elsewhere.[4] The system variables were temperature T, pressure P, surfactant concentration, and water content, which was corrected for the partitioning of added D_2O into CO_2 so that $w_{corr} = \{[D_2O]_{added} - [D_2O]_{CO_2}\}/[surf]$. Both surfactants exhibited similar P-T phase behavior as seen with a certain fluorinated CO_2-philic surfactants. At low-P catastrophic separations were observed close to CO_2 vapor pressure, with apparently biphasic regions up to the maximum operating pressure of the HP-SANS cell (500 bar), comprising a majority transparent CO_2-rich phase in equilibrium with an approximately 2–5% by volume of a dense clear phase. The SANS data shown in Figure 2 were recorded after 5 min of vigorous stirring, so that the neutron beam illuminated CO_2-continuous phases. For AOK without added

 © 2006 Wiley-VCH Verlag GmbH & Co. KGaA, Weinheim

water ($w_{corr} = 0$), no SANS was detected, suggesting absence of micellization in CO_2.

Received: January 30, 2006
Published online: April 28, 2006

Keywords: green chemistry · microemulsions · small-angle neutron scattering · surfactants

[1] J. Eastoe, S. Gold, *Phys. Chem. Chem. Phys.* **2005**, *7*, 1353 – 1362.
[2] a) J. Liu, B. Han, J. Zhang, G. Li, X. Zhang, J. Wang, B. Dong, *Chem. Eur. J.* **2002**, *8*, 1356 – 1360; b) J. Liu, B. Han, G. Li, X. Zhang, J. He, Z. Liu, *Langmuir* **2001**, *17*, 8040 – 8043; c) J. Liu, J. Zhang, M. Tiancheng, B. Han, B. G. Li, J. Wang, B. J. Dong, *J. Supercrit. Fluids* **2003**, *26*, 275 – 280; d) J. Liu, B. Han, Z. Wang, J. Zhang, G. Li, G. Yang, *Langmuir* **2002**, *18*, 3086 – 3089.
[3] W. Ryoo, S. E. Webber, K. P. Johnston, *Ind. Eng. Chem. Res.* **2003**, *42*, 6348 – 6358.
[4] a) J. Eastoe, A. Paul, S. Nave, D. C. Steytler, E. Rumsey, M. Thorpe, B. H. Robinson, R. K. Heenan, *J. Am. Chem. Soc.* **2001**, *123*, 988 – 989; b) J. Eastoe, A. Dupont, D. C. Steytler, M. Thorpe, A. Gurgel, R. K. Heenan, *J. Colloid Interface Sci.* **2003**, *258*, 367 – 373.
[5] X. Fan, V. K. Potluri, M. C. McLeod, Y. Wang, J. Lui, R. M. Enick, A. D. Hamilton, C. B. Roberts, J. K. Johnston, E. J. Beckman, *J. Am. Chem. Soc.* **2005**, *127*, 11754 – 11762.
[6] P. Raveendran, S. L. Wallen, *J. Am. Chem. Soc.* **2002**, *124*, 7274 – 7275.
[7] J. B. McClain, D. Londono, J. R. Combes, T. J. Romack, D. A. Canelas, L. Betts, G. D. Wignall, E. T. Samulski, J. M. DeSimone, *J. Am. Chem. Soc.* **1996**, *118*, 917 – 918.
[8] I. Markovic, R. H. Ottewill, D. J. Cebula, I. Field, J. Marsh, *Colloid Polym. Sci.* **1984**, *262*, 648 – 656.
[9] J. Eastoe, S. Nave, A. Paul, A. R. Pitt, R. K. Heenan, *Langmuir* **2005**, *21*, 10021 – 10027.
[10] J. Eastoe, S. Gold, R. Tabor, *Langmuir* **2006**, *22*, 963 – 968.
[11] "ICI enters CO_2 dry cleaning": A. Tullo, *Chem. Eng. News* **2002**, *80*(35), 12.

 © 2006 Wiley-VCH Verlag GmbH & Co. KGaA, Weinheim

Asymmetric Synthesis

DOI: 10.1002/anie.200600738

Chiral 4-Phenyl-2-trifluoromethyloxazolidine: A High-Performance Chiral Auxiliary for the Alkylation of Amides**

*Arnaud Tessier, Julien Pytkowicz, and Thierry Brigaud**

Chiral-auxiliary-based alkylation at the α-position of amides remains the strategy of choice for the preparation of various building blocks useful for the synthesis of bioactive compounds. Oxazolidinones[1] and related heterocyclic structures,[2] sultames,[3] and amino alcohols, such as pseudoephedrine,[4] count among the most efficient chiral auxiliaries reported. The use of oxazolidines as chiral auxiliaries for the diastereoselective alkylation of amide enolates has rarely been reported.[5] This is probably due to the harsh reaction conditions required for the removal of the aminoacetal functional group and its low stability. Although the introduction of fluorine atoms into molecules dramatically perturbs their physical and chemical properties,[6] little is known about the use of fluorine-containing chiral auxiliaries in asymmetric synthesis.[7] Chiral 2-trifluoromethyloxazolidines were first reported by Mikami and co-workers[8] and have recently found several applications as synthons in the stereoselective synthesis of chiral trifluoromethylated amines and amino acids.[9] We now report their use as chiral auxiliaries for highly diastereoselective alkylation reactions of amide enolates. The introduction of the trifluoromethyl group in the 2-position of the oxazolidine ring is intended to increase its stability to hydrolysis and to enable the chiral auxiliary to be recovered. Unique effects of the fluorinated group on the diastereoselectivity are also expected.

The starting *N*-acyloxazolidines **2a–d** and **3a–d** were conveniently prepared by an acylation reaction of a diastereomeric mixture of the corresponding 2-trifluoromethyloxazolidines **1**[8a] (Scheme 1). The separation of (2*S*,4*R*)-**1** and (2*R*,4*R*)-**1** was quite difficult. However, after the acylation reaction, the separation of both the 2,4-*trans* and 2,4-*cis* diastereomers was achieved very efficiently by chromatography on silica gel (eluent: cyclohexane/ethyl acetate, 9:1). With this eluent system, the R_f value of each acylated diastereomer varied from 0.13 to 0.23. Each diastereomer

[*] A. Tessier, Dr. J. Pytkowicz, Prof. Dr. T. Brigaud
Laboratoire "Synthèse Organique Sélective et Chimie Organométallique" (SOSCO)
UMR CNRS 8123, Université de Cergy-Pontoise
5 Mail Gay-Lussac, Neuville sur Oise
95031 Cergy-Pontoise cedex (France)
Fax: (+33) 134-257-071
E-mail: thierry.brigaud@chim.u-cergy.fr

[**] We thank the French ministry of research for awarding a research fellowship to A.T. and the Central Glass Company for the generous gift of trifluoroacetaldehyde hemiacetal.

Supporting information for this article is available on the WWW under http://www.angewandte.org or from the author.

© 2006 Wiley-VCH Verlag GmbH & Co. KGaA, Weinheim

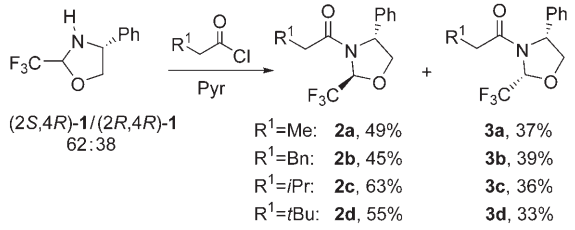

Scheme 1. Synthesis of *N*-acyl oxazolidines **2a–d** and **3a–d**. pyr = pyridine.

2a–d and **3a–d** was then obtained in good yield as the pure isolated product.

The benzylation of the *Z* enolate using the 2,4-*trans*-oxazolidine (2*S*,4*R*)-**1** as the chiral auxiliary, performed under standard conditions, occurred in good yield and with complete diastereoselectivity (Table 1). The *S* configuration of the new

Table 1: Highly diastereoselective benzylation of *N*-propanoyl oxazolidine **2a**.

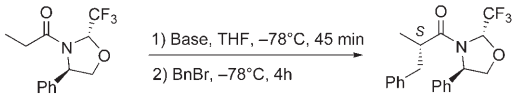

2a (*S*)-**4a**

Entry	Base[a]	Yield [%][b]	*de* [%][c]
1	LiHMDS	82	>99 (*S*)
2	NaHMDS	85	>99 (S)
3	KHMDS	63	>99 (S)

[a] 1.9 equivalents. [b] Yield of the isolated product. [c] One single diastereomer was detected by GC analysis of the crude reaction mixture.

stereogenic center was assigned after removal of the chiral auxiliary (see below). LiHMDS, NaHMDS, and KHMDS (HMDS = hexamethyldisilazane) proved to be the most suitable bases for this reaction. Difluoromethylene compounds that resulted from a base-mediated dehydrofluorination were detected as side products when lithium diisopropylamide (LDA) was used.

The NaHMDS-promoted alkylation of **2a** was then performed with various halogenated derivatives (Table 2). The alkylation was completely diastereoselective with ethyl iodide and allyl bromide (entries 1 and 2). The conversion and the stereoselectivity decreased when methoxymethyl (MOM) bromide was used (entry 3). However, the stereoselectivity could be raised up to 90% *de* by adding 1,3-dimethyltetrahydro-2-pyrimidinone (DMPU) as a cosolvent (entry 4). The reaction of **2a** with more hindered branched alkyl halides, such as isobutyl iodide (entry 5) and isopropyl iodide (entry 6), occurred in good yield and was also completely stereoselective. However, with these less reactive electrophiles, the reaction had to be performed at higher temperature (−55 °C) with longer reaction times and with 4–8 equivalents of alkyl halide. The influence of various substituents on the amide moiety was then investigated. The (*R*)-**4a** epimer was also obtained in good yield with complete diastereoselectivity by the complementary strategy which

Table 2: Diastereoselective alkylation reactions of *N*-acyl oxazolidines **2a–d**.

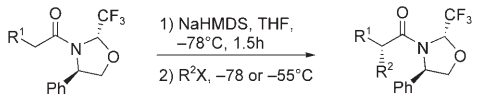

Entry	Substrate	R^2X	Product	Yield [%][a]	*de* [%]
1	**2a**, R^1 = Me	EtI[b]	(*S*)-**5a**	78	>99[c]
2	**2a**, R^1 = Me	allylBr[b]	(*S*)-**6a**	88	>98[d]
3	**2a**, R^1 = Me	MOMBr[b]	(*S*)-**7a**	60[e]	54[e]
4	**2a**, R^1 = Me	MOMBr[b,f]	(*S*)-**7a**	50[e]	90[g]
5	**2a**, R^1 = Me	*i*BuI[h]	(*S*)-**8a**	74	>99[c]
6	**2a**, R^1 = Me	*i*PrI[i]	(*S*)-**9a**	76[j]	>99[c]
7	**2b**, R^1 = Bn	MeI[b]	(*R*)-**4a**	78	>99[c]
8	**2c**, R^1 = *i*Pr	BnBr[b]	(*R*)-**4c**	71	>99[c]
9	**2d**, R^1 = *t*Bu	BnBr[k]	(*R*)-**4d**	56[l]	>99[c]

[a] Yield of isolated product. [b] Condiditions: 1.9 equivalents, −78 °C, 2–6 h. [c] One single diastereomer was detected by GC analysis of the crude reaction mixture. [d] One single diastereomer was detected by ^{19}F and ^{1}H NMR spectroscopic analysis of the crude reaction mixture. [e] Conversion of **2a** = 66%. [f] Reaction performed in the presence of DMPU as a cosolvent. [g] GC analysis of the crude reaction mixture. [h] Conditions: 4 equivalents, −55 °C, 24 h. [i] Conditions: 8 equivalents, −55 °C, 35 h. [j] Conversion = 95%. [k] Conditions: 4 equivalents, −55 °C, 35 h. [l] Conversion = 62%.

proceeded through the methylation reaction of 3-phenylpropanoylamide (**2b**; entry 7). This result highlights the great potential of this (*R*)-phenylglycinol-based fluorinated oxazolidine as a chiral auxiliary for asymmetric alkylation reactions. The benzylation of the isopropyl-substituted amide **2c** was performed under standard conditions to give (*R*)-**4c** in good yield with a total diastereoselectivity (entry 8). The benzylation of the more hindered *tert*-butyl-substituted amide **2d** occurred also with complete diastereoselectivity, but required a higher temperature (−55 °C), a longer reaction time, and 4 equivalents of alkyl halide (entry 9).

The complete diastereoselectivity of the alkylation reactions was confirmed by epimerization reactions of **4–6a**, **8**, and **9a** (Scheme 2).[10] These side-chain epimers were not detected by GC or NMR spectroscopic analysis of the crude mixture of the alkylation reaction.

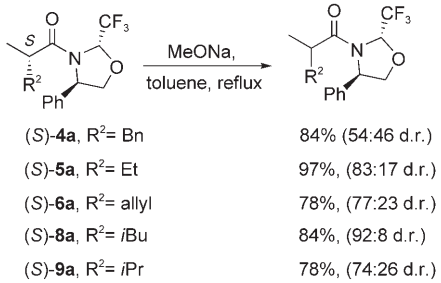

Scheme 2. Epimerization reactions of **4–6a**, **8**, and **9a**.

The results of the alkylation reactions using the 2,4-*cis*-oxazolidine (2*R*,4*R*)-**1** as the chiral auxiliary were somewhat disappointing (Scheme 3). The stereoselectivity of the benzylation of **3a** was very low and no stereoselectivity was induced

 © 2006 Wiley-VCH Verlag GmbH & Co. KGaA, Weinheim

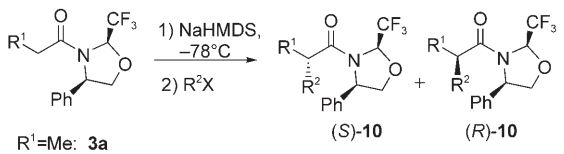

R¹=Me: **3a**
R¹=Bn: **3b**

R¹	R²X	Yield [%]	(*S*)-**10**/(*R*)-**10** (d.r.)
Me	BnBr	55	69:31
Bn	MeI	66	50:50

Scheme 3. Alkylation reactions of *N*-propanoyl oxazolidines **3a**, **b**.

during the methylation of **3b**. It is worthwhile noting that the same major *S* diastereomer was obtained from the benzylation of (2*S*,4*R*)-**2a** and (2*R*,4*R*)-**3a**. This underlines the preponderant influence of the configuration at C4 in the chiral auxiliary on the stereoselective induction. The pseudo-C_2 symmetry of the 2,4-*trans*-oxazolidine could be an explanation of its high performance as a chiral auxiliary. With this auxiliary, the same diastereotopic face of the enolate is shielded around the C1–N3 bond in both major conformations.

Key features of the use of this fluorinated oxazolidine as a chiral auxiliary that warrant future synthetic study are its removal and recovery. As all the standard methods known for the hydrolysis of amide bonds in acidic or basic media failed to give the corresponding carboxylic acid or caused epimerization, we examined reductive conditions. First lithium amidotrihydroborate (LiH_2NBH_3),[11] which transforms tertiary amides into the corresponding primary alcohols, was used (Scheme 4). With this reagent, the expected *S* alcohol **11**

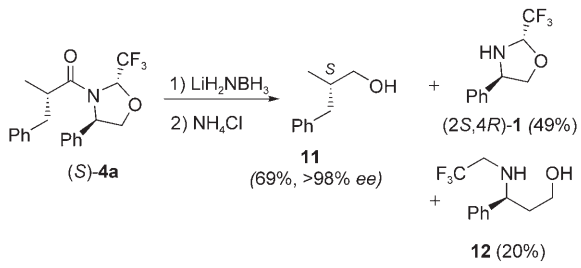

Scheme 4. Removal of the chiral auxiliary from (*S*)-**4a** with LiH_2NBH_3.

was obtained in enantiomerically pure form,[12] provided that the reaction was performed at 0 °C.[13] Unfortunately, the chiral auxiliary **1** was only recovered in 49% yield and the amino alcohol **12** that resulted from the reduction of the oxazolidine **1** was obtained in 20% yield.

This over-reduction of the chiral auxiliary could be easily avoided by using $LiAlH_4$ (Scheme 5). Under these conditions, aldehyde **13** was selectively obtained in good yield without any epimerization when the hydrolysis step was performed in a neutral medium. The *S* configuration of **13** was assigned by comparison with literature data[14] of the Mosher ester of the alcohol **11** obtained by quantitative reduction of **13** with $LiAlH_4$. The chiral auxiliary (2*S*,4*R*)-**1** was very efficiently recovered in 90% yield. It is important to note that neither the complete reduction of the amide group into an amine nor

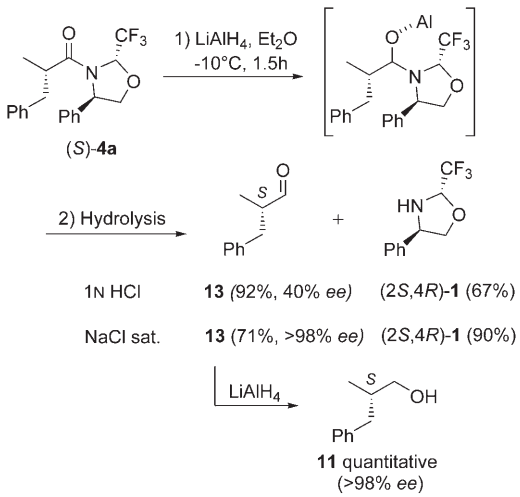

Scheme 5. Removal of the chiral auxiliary from (*S*)-**4a**, thus selectively giving aldehyde **13** in enantiomerically pure form.

the reduction of the oxazolidine ring occurred. The key intermediate of this reaction should be an aluminum hemiacetal, which is stable under the reaction conditions. The corresponding hemiacetal is then hydrolyzed[15] to give the expected aldehyde and the fluorinated oxazolidine in high yield. The hydrolysis should be performed under neutral rather than acidic conditions to avoid epimerization. As the aldehyde **13** could be quantitatively reduced into alcohol **11** and the chiral auxiliary was very efficiently recovered, this two-step procedure proved to be more efficient than the direct reduction of (*S*)-**4a** with LiH_2NBH_3.

The corresponding enantiopure carboxylic acid (*S*)-**14**[16] was also obtained in high yield and enantiomeric excess from (*S*)-**4a** in a two-step procedure, which involved the reduction of (*S*)-**4a** with $LiAlH_4$ followed by the oxidation of the aldehyde (Scheme 6). The chiral auxiliary was recovered in 97% yield.

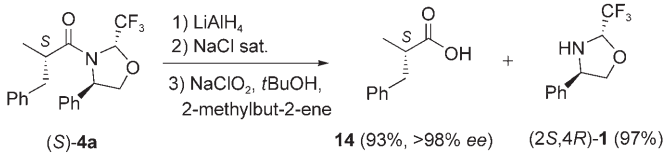

Scheme 6. Removal of the chiral auxiliary from (*S*)-**4a**, thus selectively giving carboxylic acid **14** in enantiomerically pure form.

In summary, we have reported the use of a 2-trifluoromethyloxazolidine as a chiral auxiliary for the first time. Alkylation reactions of the corresponding amides occurred with extremely high diastereoselectivity. As representative target molecules, (*S*)-α-methylbenzenepropanal, (*S*)-β-methylbenzenepropanol, and (*S*)-α-methylbenzenepropanoic acid were obtained in high yield in enantiopure form. Moreover, the highly stable fluorinated oxazolidine was conveniently recovered in high yield. Further investigations into understanding the extremely high diastereoselectivity and other

 © 2006 Wiley-VCH Verlag GmbH & Co. KGaA, Weinheim

synthetic applications are underway and will be reported in due course.

Experimental Section

General procedure for the alkylation reactions: The oxazolidine **2a–c** (1.19 mmol) was dissolved in THF (10 mL) under argon and cooled down to −78 °C. NaHMDS was added dropwise (1.1 mL, 2 M in THF, 2.24 mmol), the reaction mixture was stirred for 45 min–1.5 h at this temperature, and the electrophile (2.24 mmol) was added slowly. The reaction mixture was stirred for a further 2 h at −78 °C, quenched with a saturated solution of NH_4Cl (15 mL), and extracted with diethyl ether (2 × 30 mL) and dichloromethane (30 mL). The combined organic layers were dried over $MgSO_4$, evaporated under reduced pressure, and the resulting crude mixture was purified by filtration through a short pad of silica gel (20 g).

Reductive cleavage of (*S*)-**4a**: (*S*)-**4a** (400 mg, 1.1 mmol) was dissolved in anhydrous diethyl ether (10 mL) under argon and the solution was cooled down to −10 °C. $LiAlH_4$ (167 mg, 4.4 mmol) was added slowly and the reaction mixture was stirred for 1.5 h at −10 °C. A saturated solution of NH_4Cl (10 mL) was added dropwise at −10 °C, and the solution was vigorously stirred for 2.5 h at room temperature. At this stage, the intermediate hemiacetal could be detected. The aqueous layer was extracted with diethyl ether (2 × 20 mL) and dichloromethane (20 mL). The combined organic layers were dried over $MgSO_4$ and concentrated under reduced pressure. The resulting crude mixture was purified by column chromatography (cyclohexane/diethyl ether 98:2–95:5) to afford **13** as a colorless oil (116 mg, 71 %) and (2*S*,3*R*)-**1** (213 mg, 90 %).

Received: February 25, 2006
Published online: April 26, 2006

Keywords: alkylation · asymmetric synthesis · chiral auxiliaries · diastereoselectivity · fluorine

[1] a) D. A. Evans, M. D. Ennis, D. J. Mathre, *J. Am. Chem. Soc.* **1982**, *104*, 1737 – 1739; b) D. A. Evans, F. Urpi, T. C. Somers, J. S. Clark, M. T. Bilodeau, *J. Am. Chem. Soc.* **1990**, *112*, 8215 – 8216; c) S. D. Bull, S. G. Davies, R. L. Nicholson, H. J. Sanganee, A. D. Smith, *Tetrahedron: Asymmetry* **2000**, *11*, 3475 – 3479; d) S. G. Davies, H. J. Sanganee, *Tetrahedron: Asymmetry* **1995**, *6*, 671 – 674; e) T. Hintermann, D. Seebach, *Helv. Chim. Acta* **1998**, *81*, 2093 – 2126; f) C. L. Gibson, K. Gillon, S. Cook, *Tetrahedron Lett.* **1998**, *39*, 6733 – 6736; g) C. A. De Parrodi, A. Clara-Sosa, L. Pérez, L. Quintero, V. Maranon, R. A. Toscano, J. A. Avina, S. Rojas-Lima, E. Juaristi, *Tetrahedron: Asymmetry* **2001**, *12*, 69 – 79; h) C. A. De Parrodi, . E. Juaristi, L. Quintero, A. Clara-Sosa, *Tetrahedron: Asymmetry* **1997**, *8*, 1075 – 1082; i) A. K. Ghosh, H. Cho, M. Onishi, *Tetrahedron: Asymmetry* **1997**, *8*, 821 – 824; j) A. Sudo, K. Saigo, *Tetrahedron: Asymmetry* **1995**, *6*, 2153 – 2156; k) K. Kimura, K. Murata, K. Otsuka, T. Ishizuka, M. Haratake, T. Kunieda, *Tetrahedron Lett.* **1992**, *33*, 4461 – 4464; l) H. Matsunaga, K. Kimura, T. Ishizuka, M. Haratake, T. Kunieda, *Tetrahedron Lett.* **1991**, *32*, 7715 – 7718; m) T. Nakamura, N. Hashimoto, T. Ishizuka, T. Kunieda, *Tetrahedron Lett.* **1997**, *38*, 559 – 562; n) N. Hashimoto, T. Ishizuka, T. Kunieda, *Tetrahedron Lett.* **1994**, *35*, 721 – 724; o) M. R. Banks, A. J. Blake, J. I. G. Cadogan, I. M. Dawson, I. Gosney, K. J. Grant, G. Suneel, P. K. G. Hodgson, K. S. Knight, G. W. Smith, *Tetrahedron* **1992**, *48*, 7979 – 8006; p) T.-H. Yan, V.-V. Chu, T.-C. Lin, C.-H. Wu, L.-H. Liu, *Tetrahedron Lett.* **1991**, *32*, 4959 – 4962.

[2] For review and examples, see: a) D. J. Ager, I. Prakash, D. R. Schaad, *Chem. Rev.* **1996**, *96*, 835 – 875; b) G. Cardillo, A. D'Amico, M. Orena, S. Sandri, *J. Org. Chem.* **1988**, *53*, 2354 – 2356; c) K. Yokoyama, T. Ishizuka, N. Ohmachi, T. Kunieda, *Tetrahedron Lett.* **1998**, *39*, 4847 – 4850; d) A. Studer, T. Hintermann, D. Seebach, *Helv. Chim. Acta* **1995**, *78*, 1185 – 1206; e) K. S. Chu, G. R. Negrete, J. P. Konopelski, F. J. Lakner, N.-T. Woo, M. M. Olmstead, *J. Am. Chem. Soc.* **1992**, *114*, 1800 – 1812; f) S. G. Davies, D. J. Dixon, G. J.-M. Doisneau, J. C. Prodger, H. J. Sanganee, *Tetrahedron: Asymmetry* **2002**, *13*, 647 – 658; g) S. G. Davies, G. J.-M. Doisneau, J. C. Prodger, H. J. Sanganee, *Tetrahedron Lett.* **1994**, *35*, 2373 – 2376; h) S. G. Davies, D. J. Dixon, *Synlett* **1998**, 963 – 964; i) A. Abiko, O. Moriya, S. A. Filla, S. Masamune, *Angew. Chem.* **1995**, *107*, 869; *Angew. Chem. Int. Ed. Engl.* **1995**, *34*, 793 – 795; j) A. Abiko, J.-F. Liu, G. Wang, S. Masamune, *Tetrahedron Lett.* **1997**, *38*, 3261 – 3264; k) S. Najdi, D. Reichlin, M. J. Kurth, *J. Org. Chem.* **1990**, *55*, 6241 – 6244; l) M. Enomoto, Y. Ito, T. Katsuki, M. Yamaguchi, *Tetrahedron Lett.* **1984**, *25*, 1343 – 1344; m) Y. Kawanami, Y. Ito, T. Kitagawa, Y. Taniguchi, T. Katsuki, M. Yamaguchi, *Tetrahedron Lett.* **1985**, *26*, 857 – 860; n) D. Tanner, C. Birgersson, A. Gogoll, K. Luthman, *Tetrahedron* **1994**, *50*, 9797 – 9824; o) K.-S. Jeong, K. Parris, P. Ballester, J. Rebek, *Angew. Chem.* **1990**, *102*, 550 – 551; *Angew. Chem. Int. Ed. Engl.* **1990**, *29*, 555 – 556; p) G.-J. Lee, T. K. Kim, J. N. Kim, U. Lee, *Tetrahedron: Asymmetry* **2002**, *13*, 9 – 12; q) R. K. Boeckman, D. J. Boehmler, R. A. Musselman, *Org. Lett.* **2001**, *3*, 3777 – 3780.

[3] a) W. Oppolzer, R. Moretti, S. Thomi, *Tetrahedron Lett.* **1989**, *30*, 5603 – 5606; b) W. Oppolzer, I. Rodriguez, C. Starkemann, E. Walther, *Tetrahedron Lett.* **1990**, *31*, 5019 – 5022; c) J. Lin, W. H. Chan, A. W. M. Lee, W. Y. Wong, *Tetrahedron* **1999**, *55*, 13983 – 13998.

[4] a) A. G. Myers, B. H. Yang, H. Chen, J. L. Gleason, *J. Am. Chem. Soc.* **1994**, *116*, 9361 – 9362; b) A. G. Myers, B. H. Yang, H. Chen, L. McKinstry, D. J. Kopecky, J. L. Gleason, *J. Am. Chem. Soc.* **1997**, *119*, 6496 – 6511; c) A. G. Myers, J. L. Gleason, T. Yoon, D. W. Kung, *J. Am. Chem. Soc.* **1997**, *119*, 6496 – 6511.

[5] a) R. M. Kim, E. A. Rouse, K. T. Chapman, W. A. Schleif, D. B. Olsen, M. Stahlhut, C. A. Rutkowski, E. A. Emini, J. R. Tataa, *Bioorg. Med. Chem. Lett.* **2004**, *14*, 4651 – 4654; b) D. R. Gauthier, N. Ikemoto, F. J. Fleitz, R. H. Szumigala, D. Petrillo, J. Liu, R. A. Reamer, J. D. Armstrong, P. M. Yehl, N. Wu, R. P. Volante, *Tetrahedron: Asymmetry* **2003**, *14*, 3557 – 3567; c) A. G. Myers, J. K. Barbay, B. Zhong, *J. Am. Chem. Soc.* **2001**, *123*, 7207 – 7219; d) S. Kanemasa, K. Ueno, K. Onimura, T. Kikukawa, H. Yamamoto, *Tetrahedron* **1995**, *51*, 10453 – 10462.

[6] a) R. D. Chambers, *Fluorine in Organic Chemistry*, Oxford, Blackwell, Boca Raton, **2004**; b) T. Hiyama, *Organofluorine Compounds, Chemistry and Applications* (Ed: H. Yamamoto), Springer, Berlin, **2000**; c) *Organofluorine Chemistry: Principles and Commercial Applications* (Eds.: R. E. Banks, B. E. Smart, J. C. Tatlow), Plenum, New York, **1994**; d) B. E. Smart, *J. Fluorine Chem.* **2001**, *109*, 3 – 11; e) D. O'Hagan, H. S. Rzepa, *Chem. Commun.* **1997**, 645 – 652; f) M. Schlosser, *Angew. Chem.* **1998**, *110*, 1538 – 1556; *Angew. Chem. Int. Ed.* **1998**, *37*, 1496 – 1513.

[7] a) T. Kubota in *Enantiocontrolled Synthesis of Fluoro–Organic Compounds* (Ed. V. A. Soloshonok), Wiley, Chichester, UK, **1999**, pp. 469 – 495; b) J. E. Hein, P. G. Hultin, *Synlett* **2003**, 635 – 638; c) J. E. Hein, J. Zimmerman, M. P. Sibi, P. G. Hultin, *Org. Lett.* **2005**, *7*, 2755 – 2758; d) J. E. Hein, P. G. Hultin, *Tetrahedron: Asymmetry* **2005**, *16*, 2341 – 2347.

[8] a) A. Ishii, K. Higashiyama, K. Mikami, *Synlett* **1997**, 1381 – 1382; b) A. Ishii, F. Miyamoto, K. Higashiyama, K. Mikami, *Tetrahedron Lett.* **1998**, *39*, 1199 – 1202; c) A. Ishii, F. Miyamoto, K. Higashiyama, K. Mikami, *Chem. Lett.* **1998**, 119 – 120.

[9] a) N. Lebouvier, C. Laroche, F. Huguenot, T. Brigaud, *Tetrahedron Lett.* **2002**, *43*, 2827 – 2830; b) F. Gosselin, A. Roy, P. D. O'Shea, C. Cheng, R. P. Volante, *Org. Lett.* **2004**, *6*, 641 – 644; c) W. C. Black, C. I. Bayly, D. E. Davis, S. Desmarais, J.-P.

 © 2006 Wiley-VCH Verlag GmbH & Co. KGaA, Weinheim

Falgueyret, S. Leger, C. S. Li, F. Massé, D. J. McKay, J. T. Palmer, M. D. Percival, J. Robichaud, N. Tsou, R. Zamboni, *Bioorg. Med. Chem. Lett.* **2005**, *15*, 4741 – 4744; d) T. Billard, B. R. Langlois, *J. Org. Chem.* **2003**, *68*, 997 – 1000; e) J. Legros, F. Meyer, M. Coliboeuf, B. Crousse, D. Bonnet-Delpon, J.-P. Bégué, *J. Org. Chem.* **2003**, *68*, 6444 – 6446; f) J. Jiang, R. J. DeVita, G. A. Doss, M. T. Goulet, M. J. Wyvratt, *J. Am. Chem. Soc.* **1999**, *121*, 593 – 594; g) J. Jiang, R. J. DeVita, M. T. Goulet, M. J. Wyvratt, J.-L. Lo, N. Ren, J. B. Yudkovitz, J. Cui, Y. T. Yang, K. Cheng, S. P. Rohrer, *Bioorg. Med. Chem. Lett.* **2004**, *14*, 1795 – 1798; h) G. Kim, N. Kim, *Tetrahedron Lett.* **2005**, *46*, 423 – 425; i) F. Huguenot, T. Brigaud, *J. Org. Chem.* **2006**, *71*, 2159 – 2162.

[10] The removal of the chiral auxiliary proved that no epimerization had occurred at C2 of the oxazolidine.

[11] A. G. Myers, B. H. Yang, D. J. Kopecky, *Tetrahedron Lett.* **1996**, *37*,3623 – 3626.

[12] One single diastereomer of the corresponding Mosher ester was detected by ^{19}F and ^{1}H NMR spectroscopy; the corresponding aldehyde **13** was also obtained as a side product (15% yield of the isolated product).

[13] Compound **11** was obtained in 70% *ee* (^{19}F and ^{1}H NMR spectroscopic analysis of the corresponding Mosher ester) when the reaction was carried out at room temperature.

[14] A. G. Myers, B. H. Yang, H. Chen, *Org. Synth.* **2000**, *77*, 29 – 44.

[15] The hydrolysis of the hemiacetal could be monitored by NMR spectroscopy.

[16] One single diastereomer of the corresponding (*R*)-α-methylbenzylamide was detected by GC; see Ref. [14].

 © 2006 Wiley-VCH Verlag GmbH & Co. KGaA, Weinheim

Brønsted Acid Catalysis

DOI: 10.1002/anie.200600191

A Highly Enantioselective Brønsted Acid Catalyzed Cascade Reaction: Organocatalytic Transfer Hydrogenation of Quinolines and their Application in the Synthesis of Alkaloids**

Magnus Rueping, Andrey P. Antonchick, and Thomas Theissmann*

Dedicated to Professor David A. Evans on the occasion of his 65th birthday

The enantioselective hydrogenation of olefins, ketones, and imines still represents an important topic in organic synthesis and catalysis. Although many highly enantioselective processes based on chiral Rh, Ru, and Ir complexes have been reported,[1] most of these catalysts failed to give satisfactory results in the asymmetric hydrogenation of aromatic and heteroaromatic compounds. Examples of efficient catalysts for these conversions are rare.[2] This is also true for the partial reduction of readily available quinoline derivatives,[3] the most convenient route to 1,2,3,4-tetrahydroquinolines, which are of great synthetic importance in the preparation of pharmaceuticals and agrochemicals, as well as in material sciences.[4] Furthermore, many natural products, particularly alkaloids, consist of this structural key element. We wondered whether it would be possible to extend our recently developed biomimetic, enantioselective Brønsted acid catalyzed transfer hydrogenation of imines[5] [Eq. (1)] to the enantioselective

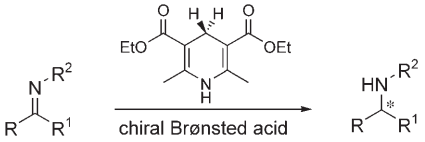

(1)

hydrogenation of quinolines. This would not only represent the first example of a metal-free reduction of heteroaromatic compounds but would additionally give straightforward access to optically pure tetrahydroquinoline derivatives.

We reasoned that activation of the quinoline by catalytic protonation would allow a cascade hydrogenation, which involves a 1,4-hydride addition, isomerization, and 1,2-hydride addition to generate the desired tetrahydroquinolines [Eq. (2)].[6]

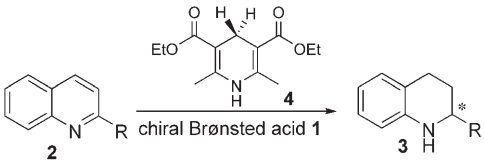

(2)

We initially focused on the exploration of appropriate Brønsted acid catalysts[7] and the examination of reaction parameters, such as catalyst loading, hydride source, temperature, and concentration. The best results, with respect to reactivity, yield, and selectivity, were obtained with catalytic amounts of Brønsted acid catalysts of type **1**,[5,8,9] 2-substituted quinoline derivatives **2**, and dihydropyridine **4** as the hydride source.[5,6,10]

Further examination of this new Brønsted acid catalyzed transfer hydrogenation concentrated on the catalyst structure (Table 1). From this survey sterically congested Brønsted acids emerged as the best catalysts for hydride transfer, and gave good to excellent levels of enantioselection. This finding is in agreement with our recently developed binol phosphate catalyzed Strecker reaction.[9] The highest selectivities were obtained with catalyst **1f**, which provided 2-phenyltetrahydroquinoline (**3**) in 97% *ee* (Table 1, entry 6).

Table 1: Survey of chiral Brønsted acid catalysts for the cascade transfer hydrogenation.

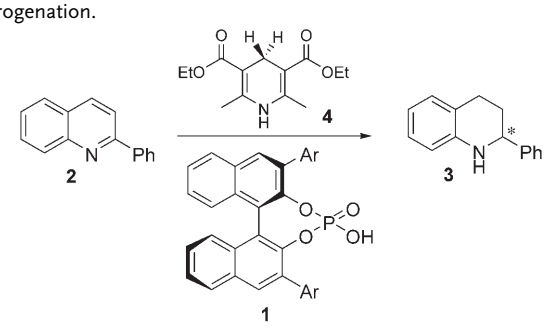

Entry[a]	Cat.	Ar	*ee* [%][b]
1	**1a**	phenyl	5
2	**1b**	4-biphenyl	35
3	**1c**	1-naphthyl	84
4	**1d**	2-naphthyl	26
5	**1e**	3,5-(CF_3)-C_6H_3	72
6	**1f**	9-phenanthryl	97

[a] Reaction conditions: **2**, **4** (2.4 equiv), 5 mol% **1** in benzene at 60°C. [b] Determined by HPLC analysis on a chiral phase (chiralcel OD-H).

Further investigations on the solvent employed (Table 2) showed that nonpolar solvents were essential for a high asymmetric induction. Excellent enantioselectivities of 2-phenyltetrahydroquinolines (95–97% *ee*) were observed in both chlorinated (CH_2Cl_2, $CHCl_3$, CCl_4) and aromatic solvents (benzene, toluene). The hydrogenation of 2-butylquinoline with a reduced amount of catalyst (2 mol%) could best

[*] Prof. M. Rueping, Dr. A. P. Antonchick, T. Theissmann
Degussa Endowed Professorship
Institute for Organic Chemistry and Chemical Biology
Johann Wolfgang Goethe-University Frankfurt am Main
Marie-Curie-Strasse 11, 60439 Frankfurt am Main (Germany)
Fax: (+49) 69-798-29248
E-mail: m.rueping@chemie.uni-frankfurt.de

[**] The authors acknowledge Degussa AG for generous funding.

Supporting information for this article is available on the WWW under http://www.angewandte.org or from the author.

 © 2006 Wiley-VCH Verlag GmbH & Co. KGaA, Weinheim

Table 2: Influence of the solvent on the Brønsted acid catalyzed transfer hydrogenation of quinolines.

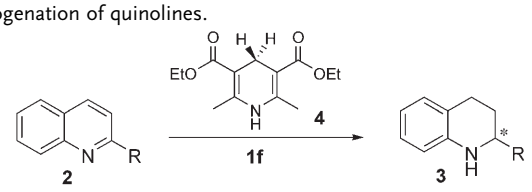

Entry[a]	Solvent	R = Ph *ee* [%][b,c]	R = *n*Bu *ee* [%][b,d]
1	CCl_4	96	84
2	$CHCl_3$[e]	95	82
3	CH_2Cl_2[e]	96	81
4	benzene	97	87
5	toluene	97	86

[a] Reaction conditions: **2**, **4** (2.4 equiv), and catalyst **1 f** at 60 °C. [b] Determined by HPLC analysis on a chiral phase (Chiralcel OD-H). [c] With 5 mol % **1 f**. [d] With 2 mol % **1 f**. [e] Reactions were performed at RT.

be performed in aromatic solvents (Table 2, entries 4 and 5), which is in accordance with our previously developed Brønsted acid catalyzed reactions.[5,9]

We explored the scope of the Brønsted acid catalyzed cascade transfer hydrogenation of 2-substituted quinolines under optimized conditions (Table 3). In general, high enantioselectivities and good yields of several tetrahydroquinolines with aromatic and heteroaromatic residues, as well as aliphatic substituents was observed. Interestingly, this metal-free hydrogenation procedure is even compatible with halogenated aromatic and aliphatic residues, such as 3-bromophenyl or chloromethyl substituents (Table 3, entry 11).

Table 3: Scope of the cascade hydrogenation reaction.

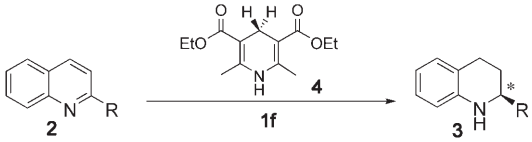

Entry[a]	R	*t* [h]	Yield [%][b]	*ee* [%][c]
1	phenyl	12	92	97
2	2-fluorophenyl	30	93	98
3	2-methylphenyl	48	54[d]	91
4	2,4-dimethylphenyl	60	65[e]	97
5	2-naphthyl	12	93	>99
6	3-bromophenyl	18	92	98
7	4-(CF_3)-C_6H_3	30	91	>99
8	1,1′-biphenyl-4-yl	12	91	>99
9	4-methoxyphenyl	12	90[f]	98
10	2-furyl	12	93	91
11	chloromethyl	12	91[f]	88
12	*n*-butyl	12	91	87
13	*n*-pentyl	12	88	90
14	2-phenylethyl	12	90	90
15	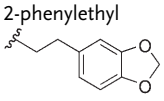	12	94[f]	91
16	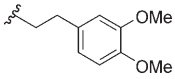	12	95[f]	90

[a] Reaction conditions **2**, **4** (2.4 equiv), 2 mol % catalyst **1 f** in benzene at 60 °C. [b] Yields after column chromatography. [c] Determined by HPLC analysis on a chiral phase (Chiralcel OD-H). [d] 45 % recovered starting material. [e] 5 mol % **1 f**. [f] 1 mol % **1 f**.

Having established a general and highly enantioselective cascade transfer hydrogenation of 2-substituted quinolines, we applied this new methodology to the synthesis of biologically active tetrahydroquinoline alkaloids: galipinine,[11] cuspareine,[11b,12] and angustureine.[11b,13] Brønsted acid catalyzed enantioselective hydrogenation of the corresponding 2-substituted quinolines,[14] which were prepared by simple alkylation of 2-methylquinoline, generated the tetrahydroquinoline derivatives with excellent enantioselectivity and subsequent N-methylation gave the desired natural products in good overall yields (Table 4).

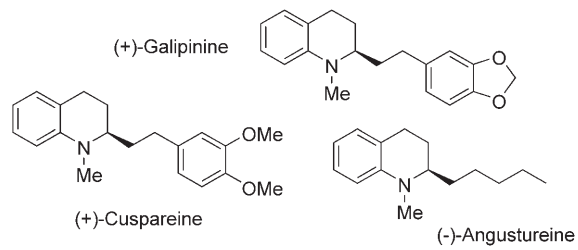

Table 4: Synthesis of alkaloids by Brønsted acid catalyzed transfer hydrogenation.

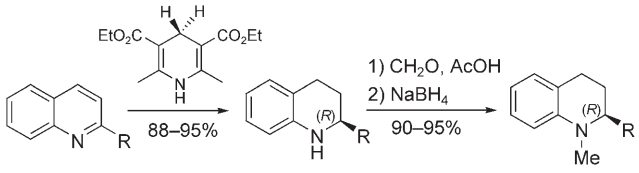

R	Compound[a]	Yield [%][b]	*ee* [%][c]
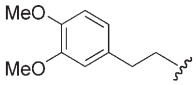	(+)-cuspareine	88	90
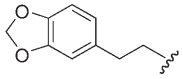	(+)-galipinine	89	91
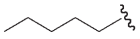	(−)-angustureine	79	90

[a] The absolute configuration was determined by comparison with literature data. [b] Yields over two steps after column chromatography. [c] Determined by HPLC analysis on a chiral phase (Chiralcel OD-H).

The absolute configuration[15] of the products can be explained by a stereochemical model derived from the X-ray crystal structure of the catalyst **1 f**. In the transition state the quinoline is activated by protonation of the chiral Brønsted acid **1 f**, thereby favoring approach of the hydride nucleophile from the less hindered *Si* face since the *Re* face is shielded by the large phenanthryl group of the catalyst (Figure 1).

Mechanistically we assume that the first step in the enantioselective cascade hydrogenation is the protonation of the quinoline **2** through the Brønsted acid catalyst **1** to generate the iminium ion **A** (Scheme 1). Subsequent transfer

 © 2006 Wiley-VCH Verlag GmbH & Co. KGaA, Weinheim

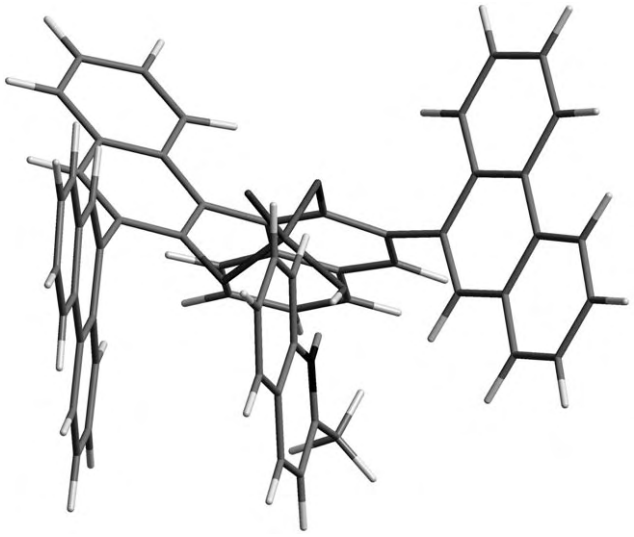

Figure 1. Proposed transition structure derived from an X-ray crystal structure of chiral Brønsted acid **1 f** and 2-methylquinoline.

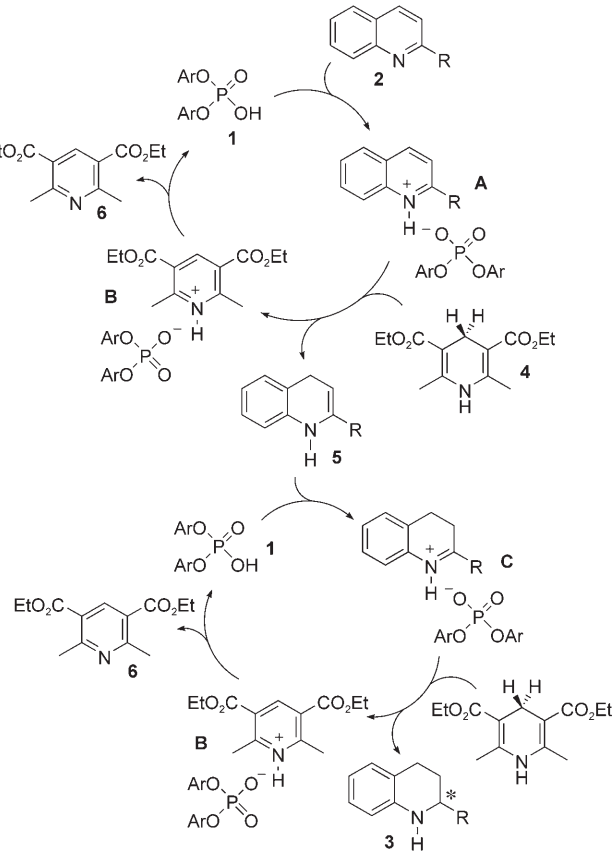

Scheme 1. Proposed mechanism for the Brønsted acid catalyzed cascade transfer hydrogenation.

of the first hydride from the dihydropyridine **4** generates the enamine **5** and pyridinium salt **B**, which undergoes proton transfer to regenerate the Brønsted acid **1** and Hantzsch pyridine **6**. The enamine **5** reacts in a second cycle with Brønsted acid **1** to produce iminium **C**, which will again be subjected to hydride transfer to give the desired tetrahydroquinoline **3**. Subsequent proton transfer will then recycle the Brønsted acid **1** and generate a second equivalent of the Hantzsch pyridine.

In summary, we have developed a Brønsted acid catalyzed cascade transfer hydrogenation, which provides direct access to a variety of 2-aryl- and 2-alkyl-substituted tetrahydroquinolines with excellent enantioselectivities and good yields. The mild reaction conditions of this metal-free reduction of heteroaromatic compounds, the operational simplicity and practicability, as well as the low catalyst loading render this transformation an attractive approach to optically active tetrahydroquinolines and their derivatives. Further work will be directed toward the application of this enantioselective Brønsted acid catalyzed transfer hydrogenation to multisubstituted quinolines and other heteroaromatic systems.

Received: January 17, 2006
Published online: April 26, 2006

Keywords: asymmetric hydrogenation · Brønsted acid · Hantzsch dihydropyridine · organocatalysis · tetrahydroquinoline

[1] For reviews, see: a) R. Noyori, *Angew. Chem.* **2002**, *114*, 2108; *Angew. Chem. Int. Ed.* **2002**, *41*, 2008; b) W. S. Knowles, *Angew. Chem.* **2002**, *114*, 2096; *Angew. Chem. Int. Ed.* **2002**, *41*,1998; c) H. U. Blaser, C. Malan, B. Pugin, F. Spindler, H. Steiner, M. Studer, *Adv. Synth. Catal.* **2003**, *345*, 103; d) W. Tang, X. Zhang, *Chem. Rev.* **2003**, *103*, 3029; e) T. Ohkuma, M. Kitamura, R. Noyori in *Catalytic Asymmetric Synthesis*, 2nd ed. (Ed.: I. Ojima), Wiley-VCH, New York, **2000**, chap. 1; f) T. Ohkuma, R. Noyori in *Comprehensive Asymmetric Catalysis*, Suppl. 1 (Eds.: E. N. Jacobsen, A. Pfaltz, H. Yamamoto), Springer, New York, **2004**, p. 43; g) H. Nishiyama, K. Itoh in *Catalytic Asymmetric Synthesis*, 2nd ed. (Ed.: I. Ojima), Wiley-VCH, New York, **2000**, chap. 2.; recent examples of highly enantioselective metal-catalyzed hydrogenations of imines: h) R. Kadyrov, T. H. Riermeier, *Angew. Chem.* **2003**, *115*, 5630; *Angew. Chem. Int. Ed.* **2003**, *42*, 5472; i) C. Moessner, C. Bolm, *Angew. Chem.* **2005**, *117*, 7736; *Angew. Chem. Int. Ed.* **2005**, *44*, 7564; organocatalytic, enantioselective hydrosilylations of imines: j) A. V. Malkov, A. Mariani, K. N. MacDougall, P. Kocovsky, *Org. Lett.* **2004**, *6*, 2253; k) F. Iwasaki, O. Omonura, K. Mishima, T. Kanematsu, T. Maki, Y. Matsumura, *Tetrahedron Lett.* **2001**, *42*, 2525.

[2] F. Glorius, *Org. Biomol. Chem.* **2005**, *3*, 4171.

[3] Asymmetric reductions of quinolines: a) W.-B. Wang, S.-M. Lu, P.-Y. Yang, X.-W. Han, Y.-G. Zhou, *J. Am. Chem. Soc.* **2003**, *125*, 10536; b) S.-M. Lu, X. W. Han, Y.-G. Zhou, *Adv. Synth. Catal.* **2004**, *346*, 909; c) P.-Y. Yang, Y.-G. Zhou, *Tetrahedron: Asymmetry* **2004**, *15*, 1145; d) L. Xu, K. H. Lam, J. Ji, J. Wu, Q.-H. Fan, W.-H. Lo, A. S. C. Chan, *Chem. Commun.* **2005**, 1390.

[4] For a comprehensive review on 1,2,3,4-tetrahydroquinolines, see: A. R. Katritzky, S. Rachwal, B. Rachwal *Tetrahedron* **1996**, *52*, 15031.

[5] a) M. Rueping, C. Azap, E. Sugiono, T. Theissmann, *Synlett* **2005**, 2367; b) M. Rueping, E. Sugiono, C. Azap, T. Theissmann, M. Bolte, *Org. Lett.* **2005**, *7*, 3781; for a subsequent optimization of this prodedure, see: c) S. Hofmann, A. M. Seayad, B. List, *Angew. Chem.* **2005**, *117*, 7590; *Angew. Chem. Int. Ed.* **2005**, *44*, 7424; d) R. I. Storer, D. E. Carrera, Y. Ni, D. W. C. MacMillan, *J. Am. Chem. Soc.* **2006**, *128*, 84.

 © 2006 Wiley-VCH Verlag GmbH & Co. KGaA, Weinheim

[6] For a report on the achiral transfer hydrogenation of differently substituted quinolines, see: M. Rueping, T. Theissmann, A. P. Antonchick, *Synlett*, in press.
[7] For reviews on chiral Brønsted acid catalysis, see: a) P. R. Schreiner, *Chem. Soc. Rev.* **2003**, *32*, 289; b) P. M. Pihko, *Angew. Chem.* **2004**, *116*, 2110; *Angew. Chem. Int. Ed.* **2004**, *43*, 2062; ; c) C. Bolm, T. Rantanen, I. Schiffers, L. Zani, *Angew. Chem.* **2005**, *117*, 1788; *Angew. Chem. Int. Ed.* **2005**, *44*, 1758; .
[8] a) T. Akiyama, J. Itoh, K. Yokota, K. Fuchibe, *Angew. Chem.* **2004**, *116*, 1592; *Angew. Chem. Int. Ed.* **2004**, *43*, 1566;; b) D. Uraguchi, M. Terada, *J. Am. Chem. Soc.* **2004**, *126*, 5356; c) D. Uraguchi, K. Sorimachi, M. Terada, *J. Am. Chem. Soc.* **2004**, *126*, 11804; d) T. Akiyama, H. Morita, J. Itoh, K. Fuchibe, *Org. Lett.* **2005**, *7*, 2583; e) M. Terada, K. Sorimachi, D. Uraguchi, *Synlett* **2006**, 13; f) T. Akiyama, Y. Tamura, J. Itoh, H. Morita, K. Fuchibe, *Synlett* **2006**, 141; g) J. Seayad, A. M. Seayad, B. List, *J. Am. Chem. Soc.* **2006**, *128*, 1087.
[9] M. Rueping, E. Sugiono, C. Azap, *Angew. Chem.* **2006**, *118*, 2679; *Angew. Chem. Int. Ed.* **2006**, *45*, 2617.
[10] a) J. W. Yang, M. T. Hechavarria Fonseca, N. Vignola, B. List, *Angew. Chem.* **2005**, *117*, 110; *Angew. Chem. Int. Ed.* **2005**, *44*, 108; b) S. G. Ouellet, J. B. Tuttle, D. W. C. MacMillan, *J. Am. Chem. Soc.* **2005**, *127*, 32.
[11] a) J. H. Rakotoson, N. Fabre, I. Jacquemond-Collet, S. Hannedouche, I. Fouraste, C. Moulis, *Planta Med.* **1998**, *64*, 762; b) I. Jacquemond-Collet, S. Hannedouche, N. Fabre, I. Fouraste, C. Moulis, *Phytochemistry* **1999**, *51*, 1167.
[12] P. J. Houghton, T. Z. Woldemariam, Y. Watanabe, M. Yates, *Planta Med.* **1999**, *65*, 250.
[13] I. Jacquemond-Collet, S. Hannedouche, N. Fabre, I. Fouraste, C. Moulis, *Phytochemistry* **1999**, *51*, 1167.
[14] For an interesting approach to 2-alkyl tetrahydroquinolines by an aza-xylene Diels–Alder reaction, see: a) H. Steinhagen, E. J. Corey, *Angew. Chem.* **1999**, *111*, 2054; *Angew. Chem. Int. Ed.* **1999**, *38*,1928; ; b) F. Avemaria, S. Vanderheiden, S. Bräse, *Tetrahedron* **2003**, *59*, 6785.
[15] The absolute *S* configuration in the case of the 2-aryl tetrahydroquinolines are based on a X-ray crystal structure of (3-bromophenyl)tetrahydroquinoline. Our corresponding optical rotation data are not in agreement with the previously reported data in Ref. [3a].

 © 2006 Wiley-VCH Verlag GmbH & Co. KGaA, Weinheim

Asymmetric Synthesis

DOI: 10.1002/anie.200600247

Copper-Catalyzed Preparation of Ketones Bearing a Stereogenic Center in α Position**

*Darunee Soorukram and Paul Knochel**

Dedicated to Professor K. Peter C. Vollhardt on the occasion of his 60th birthday

The enantioselective preparation of α-alkylated cyclic and acyclic ketones is important,[1] since chiral α-alkylated carbonyl moieties are present in numerous natural products.[2] Recently, we have described a highly selective *anti*-S_N2' substitution of allylic benzoates and phosphates which allows the preparation of chiral α-substituted alkenes[3,4] as well as 1,2-diols or 1,2-amino alcohols bearing a quaternary substituted carbon center.[5] Likewise, Breit et al. have reported efficient *syn*-selective S_N2' substitutions using a directing leaving group.[6]

Herein, we report the highly enantioselective preparation of chiral ketones of type **1** having a stereogenic center in the α position by two efficient oxidation procedures from the intermediate chiral cycloalkenyl lithium species **2**. These organometallic intermediates are readily obtained from the corresponding cycloalkenyl iodides **3** by I/Li exchange.[7] The enantiomerically enriched cycloalkenyl iodides **3** are prepared by a copper(I)-catalyzed *anti*-S_N2' allylic substitution with organozinc compounds starting either from allylic pentafluorobenzoates **4** or from the corresponding diethylphosphates **5** (Scheme 1 and Tables 1 and 2).

Thus, the reaction of $i\text{Pr}_2\text{Zn}$ (2.2 equiv) with (*R*)-2-iodo-2-cyclohexen-1-yl pentafluorobenzoate (98% *ee*)[3a,c] in the presence of CuCN·2 LiCl (2.2 equiv) in THF/*N*-methylpyrrolidinone (NMP) (3:1) between −30 °C and −10 °C for 20 h provided the expected iodide **3a** in 97% yield and 94% *ee*.[8] The reaction of **3a** with *t*BuLi (2 equiv) at −78 °C in THF provided the corresponding alkenyl lithium **2a**, which readily reacted with $Me_3SiOOSiMe_3$ [$(TMSO)_2$; 1.5 equiv] at −78 °C for 0.5 h. The resulting silyl enol ether was converted into the ketone **1a** using HF·pyridine in THF[9] (25 °C, 0.5 h, method A). This deprotection method provided the ketone **1a** in 93% yield and 94% *ee* (entry 1, Table 1).[10] Similarly, the

[*] Dipl.-Chem. D. Soorukram, Prof. Dr. P. Knochel
Department Chemie and Biochemistry
Ludwig-Maximilians-Universität München
Butenandtstrasse 5–13, Haus F, 81377 München (Germany)
Fax: (+49) 89-2180-77680
E-mail: paul.knochel@cup.uni-muenchen.de

[**] We thank the Fonds der Chemischen Industrie, the Deutsche Forschungsgemeinschaft (KN347/6-2), and Merck Research Laboratories for financial support. We also thank Chemetall GmbH (Frankfurt), BASF AG (Ludwigshafen) for the generous gift of chemicals.

Supporting information for this article is available on the WWW under http://www.angewandte.org or from the author.

WILEY InterScience DISCOVER SOMETHING GREAT
© 2006 Wiley-VCH Verlag GmbH & Co. KGaA, Weinheim

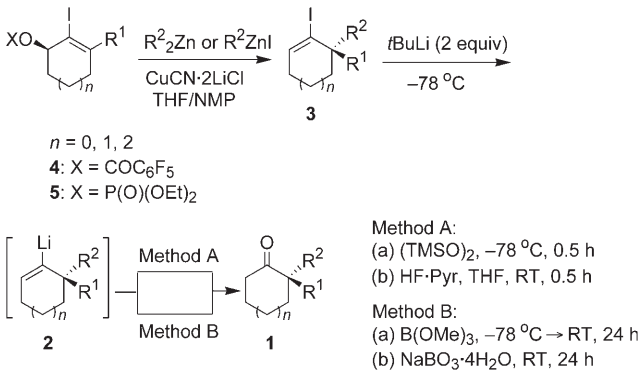

2 3 1

Scheme 1.

seven-membered cycloalkenyl iodide **3b** obtained in 96% *ee*[8] was converted into the chiral cycloheptanone **1b** in 76% yield and 96% *ee* (entry 2, Table 1). Five-membered cyclic ketones can also be prepared by this procedure. Thus, the cyclopentenyl iodide **3c** furnished, with the oxidation method A, (*S*)-2-pentylcyclopentanone (**1c**) in 70% yield and 93% *ee* (entry 3, Table 1). Various cyclohexanones with primary and secondary alkyl substituents were obtained in this way in 93–98% *ee* (entries 4–6, Table 1).

The preparation of 2-arylcyclohexanones is more difficult, since the protons in the position α to both the phenyl ring and the carbonyl group are much more acidic. Thus, the preparation of (*R*)-2-phenylcyclohexanone by method A and an S_N2 substitution mediated by the lithium cuprate $(PhMe_2CCH_2)(Ph)CuLi$ in THF[11] (−30 °C, 48 h) furnished the crude product **1g** with 90% *ee*. However, during the chromatographic purification some racemization occurred, and the ketone **1g** was obtained in pure form (70% yield) with 86% *ee* (entry 7, Table 1). Iodocyclohexene **3i** was prepared by an *anti*-S_N2' substitution using PhCu in CH_2Cl_2[12] and the corresponding phosphate as substrate (see the Experimental Section). The oxidation procedure A furnished ketone **1i** in 69% yield and 92% *ee* after chromatographic purification (entry 9, Table 1). Interestingly, the cyclohexanone bearing an α-para-methoxyphenyl substituent (**1h**) proved to be especially sensitive toward racemization, and attempts to purify the ketone **1h** by chromatography either on silica gel or alumina led to considerable racemization (5–24% *ee*). However, the recrystallization of this ketone from diethyl ether provided the pure product **1h** in 81% yield and 86% *ee*.

Although the oxidation of the alkenyl lithium derivatives of type **2** proceeded in good yields and excellent enantioselectivities, we were concerned with the scale-up and the safety of this oxidation procedure since it requires the use of the sensitive peroxide $(TMSO)_2$ (see the Experimental Section). Thus, we examined an alternative procedure in which the lithium intermediate of type **2** is transmetalated by reaction with $B(OMe)_3$ (2.5 equiv, −78 °C to 25 °C, 24 h) to give the cycloalkenyl(dimethoxy)borane, which is then oxidized with $NaBO_3·4H_2O$ (25 °C, 24 h).[13] Under these conditions, several cyclohexenyl iodides of type **3** were converted into the chiral ketones of type **1** in good yields and enantioselectivities (Scheme 1 and Table 2). A comparison of the two methods (entries 1–4 of Table 1 and Table 2) shows that similar high

Table 1: Preparation of α-chiral ketones of type **1** by the oxidation method A using $(TMSO)_2$.

Entry	Substrate of type **3**	Yield, *ee* [%, %][a]	Product of type **1**	Yield [%][b]	*ee* [%][c]
1	**3a**[d]	97, 94[g]	**1a**	93	94
2	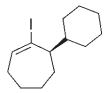 **3b**[d]	87, 96[g]	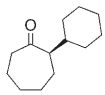 **1b**	76	96
3	**3c**[e]	96, 94	**1c**	70	93[h]
4	**3d**[e]	90, 99	**1d**	84	93
5	**3e**[d]	90, 99	**1e**	91	97
6	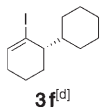 **3f**[d]	90, 98[g]	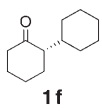 **1f**	88	98
7	**3g**[f]	60, 93	**1g**	70	86
8	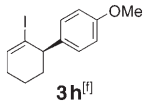 **3h**[f]	90, 98	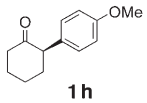 **1h**	81	86
9	**3j**[e]	53, 96	**1j**	69	92

[a] Yield of isolated produce. The enantiomeric excess was determined by either HPLC or GC analysis. In each case the racemic compound was also prepared for calibration. [b] Overall yield after oxidation and desilylation. [c] The enantiomeric excess was determined by either HPLC or GC analysis. In each case the racemic compound was also prepared for calibration. [d] Prepared from the corresponding pentafluorobenzoate (see the Supporting Information). [e] Prepared from the corresponding diethylphosphate (see the Supporting Information). [f] Prepared from the corresponding acetate (S_N2 substitution; see the Supporting Information). [g] Determined from the corresponding ketone. [h] Determined from the corresponding lactone (see the Supporting Information).

enantioselectivities were obtained for cyclohexanones and cycloheptanones, whereas for the cyclopentanone **1c** an enantioselectivity of only 81% *ee* was obtained with method B (entry 3, Table 2). Various chiral cyclohexanones bearing either a primary or a secondary alkyl substituent in α position were prepared in this way in 46–65% yield and 90–98% *ee* (entries 5–8, Table 2). Interestingly, ketones bearing a quaternary center in the position α to the carbonyl center were obtained by this method. Thus, the reaction of the pentafluorobenzoate **6** with $Pent_2Zn$ (2.4 equiv) and CuCN·2 LiCl (1.2 equiv) in THF for 4 h at 25 °C provided the S_N2'-substitution product **7** in 93% yield and 95% *ee*. Less than 5% of the S_N2-substitution product was found. Application of

 © 2006 Wiley-VCH Verlag GmbH & Co. KGaA, Weinheim

Table 2: Preparation of α-chiral ketones of type **1** by method B by transmetalation with $(MeO)_3B$ and further oxidation with $NaBO_3 \cdot 4H_2O$.

Entry	Substrate of type **3**	Yield, *ee* [%, %][a]	Product of type **1**	Yield [%][b]	*ee* [%][c]
1	**3a**[d]	97, 97[f]	**1a**	90	97
2	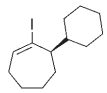 **3b**[d]	87, 98[f]	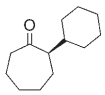 **1b**	86	98
3	**3c**[e]	96, 94	**1c**	90	81[g]
4	**3d**[e]	90, 99	**1d**	86	98
5	**3j**[e]	95, 98[f]	**1j**	56	98
6	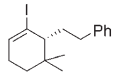 **3k**[e]	95, 98	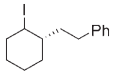 **1k**	65	97
7	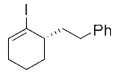 **3l**[d]	85, 99	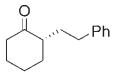 **1l**	61	95
8	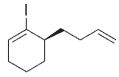 **3m**[d]	85, 98	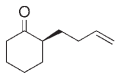 **1m**	46	90

[a] Yield of isolated product. The enantiomeric excess was determined by either HPLC or GC analysis. In each case the racemic compound was also prepared for calibration. [b] Overall yield of the two-step oxidation procedure. [c] The enantiomeric excess was determined by HPLC or GC analysis. In each case the racemic compound was also prepared for calibration. [d] Prepared from the corresponding pentafluorobenzoate (see the Supporting Information). [e] Prepared from the corresponding diethylphosphate (see the Supporting Information). [f] Determined from the corresponding ketone. [g] Determined from the corresponding lactone (see the Supporting Information).

method B provided the ketone **8** in 70% yield and 95% *ee* (Scheme 2).

As an application of this methodology, we prepared (*R*)-10-methyl-6-undecanolide (**9**), a caprolactone recently isolated from a marine streptomycete (isolate B6007)[14] (Scheme 3). Thus, the reaction of $(CH_3)_2CH(CH_2)_3ZnI$ (2 equiv) with compound **10** (98% *ee*)[3a,c] in the presence of CuCN·2 LiCl (2 equiv) in THF/NMP (3:1) between −30 °C and room temperature for 15 h provided the *anti*-S_N2'-substitution product **11** in 88% yield and 96% *ee*. The oxidation procedure A furnished the ketone **12** in 89% yield and 95% *ee*. Baeyer–Villiger oxidation of **12** with *m*-chloroperbenzoic acid in CH_2Cl_2 gave the caprolactone **9** in 91% yield and 95% *ee*.

In summary, we have developed a short synthetic sequence for the enantioselective preparation of various

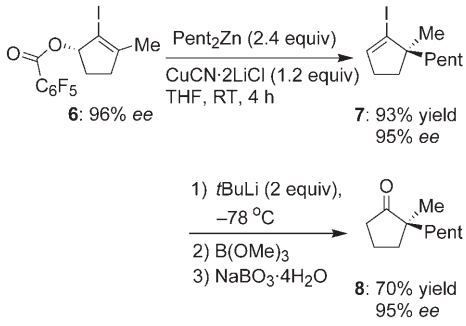

Scheme 2. Application of method B to provide **8**.

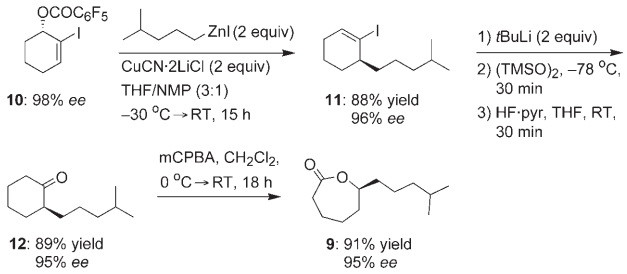

Scheme 3. Application to the preparation of **9**. *m*CPBA = *m*-chloroperbenzoic acid.

chiral ketones with an stereogenic center in α position. Extensions of this method to more complex substrates are underway in our laboratory.

Experimental Section

Typical procedure for the preparation **1a** (entry 1, Table 1) with $(TMSO)_2$ (method A): A flame-dried 25-mL flask equipped with a magnetic stirring bar, an argon inlet, and a septum was charged with **3a** (125 mg, 0.5 mmol, 1 equiv) and THF (4 mL). The mixture was cooled at −78 °C, then *t*BuLi (1.6 M in pentane, 0.63 mL, 1 mmol, 2 equiv) was added dropwise. The reaction mixture was stirred at −78 °C for 30 min, then $(TMSO)_2$ (neat, 0.16 mL, 0.75 mmol, 1.5 equiv) was added (**Caution: Explosive!**[15] The reagent must be transferred with a plastic syringe and teflon needle and added slowly). The reaction mixture was stirred continuously at −78 °C for 30 min, and then poured into water, extracted with pentane, and dried over $MgSO_4$. The solvents were removed, and the crude product was used in the next step without purification.

A flame-dried 25-mL flask equipped with a magnetic stirring bar, an argon inlet, and a septum was charged with dry pyridine (0.4 mL) and HF·pyridine complex (70%) (0.02 mL, 0.5 mmol, 1 equiv). A solution of the previously prepared silyl enol ether (see above) in THF (2 mL) was added dropwise at room temperature. The reaction mixture was stirred for 30 min, poured into water, extracted with Et_2O, washed with brine, and dried over $MgSO_4$. The solvents were removed, and the crude product was purified by column chromatography (silica gel, 10% Et_2O/pentane) to yield the chiral ketone **1a** (65 mg, 93% yield, 94% *ee*) as a colorless oil.

Typical procedure for the preparation of **1a** with $B(OMe)_3$ (method B): A flame-dried 25-mL flask equipped with a magnetic stirring bar, an argon inlet, and a septum was charged with **3a** (125 mg, 0.5 mmol, 1 equiv) and THF (4 mL). The mixture was cooled at −78 °C, then *t*BuLi (1.6 M in pentane, 0.63 mL, 1 mmol, 2 equiv) was added dropwise. The reaction mixture was stirred at −78 °C for 30 min, then $B(OMe)_3$ (neat, 0.14 mL, 1.25 mmol, 2.5 equiv) was added dropwise. The reaction mixture was slowly warmed up to RT

 © 2006 Wiley-VCH Verlag GmbH & Co. KGaA, Weinheim

and stirred for 24 h, then a suspension of $NaBO_3 \cdot 4H_2O$ (10 equiv, 769 mg, 5 mmol) in H_2O (6 mL) was added. After the mixture had been stirred at RT for 24 h, it was poured into water, extracted with Et_2O, washed with brine, and dried over $MgSO_4$. The solvents were removed, and the crude product was purified by column chromatography (silica gel, 10% Et_2O/pentane) to yield the chiral ketone **1a** (63 mg, 90% yield, 97% *ee*) as a colorless oil.

Received: January 20, 2006
Published online: April 28, 2006

Keywords: allylic substitution · asymmetric synthesis · carbonyl compounds · copper · zinc

[1] a) P. Fey, W. Hartwig in *Stereoselective Synthesis*, *Vol. 2* (Eds.: G. Helmchen, R. W. Hoffmann, J. Mulzer, E. Schaumann), Thieme, Stuttgart, **1996**, p. 969 and 994; b) E. J. Corey, D. Enders, *Tetrahedron Lett.* **1976**, *17*, 11; c) E. J. Corey, D. Enders, *Chem. Ber.* **1978**, *111*, 1337; d) E. J. Corey, D. Enders, *Chem. Ber.* **1978**, *111*, 1362;e) A. G. Doyle, E. N. Jacobsen, *J. Am. Chem. Soc.* **2005**, *127*, 62; f) C. A. Luchaco-Cullis, A. H. Hoveyda, *J. Am. Chem. Soc.* **2002**, *124*, 8192; g) S. Liao, D. B. Collum, *J. Am. Chem. Soc.* **2003**, *125*, 15114; h) A. Job, C. F. Janeck, W. Bettray, R. Peters, D. Enders, *Tetrahedron* **2002**, *58*, 2253; i) A. G. Myers, B. H. Yang, H. Chen, L. McKinstry, D. J. Kopecky, J. L. Gleason, *J. Am. Chem. Soc.* **1997**, *119*, 6496; j) M. Nakamura, T. Hatakeyama, K. Hara, E. Nakamura, *J. Am. Chem. Soc.* **2003**, *125*, 6362; k) T. Hirata, K. Shimoda, T. Kawano, *Tetrahedron: Asymmetry* **2000**, *11*, 1063; l) T. Ohta, T. Miyake, N. Seido, H. Kumobayashi, S. Takata, *J. Org. Chem.* **1995**, *60*, 357; m) J. Chae, J. Yun, S. L. Buchwald, *Org. Lett.* **2004**, *6*, 4809; n) T. Hamada, A. Chieffi, J. Åhman, S. L. Buchwald, *J. Am. Chem. Soc.* **2002**, *124*, 1261; o) J. M. Fox, X. Huang, A. Chieffi, S. L. Buchwald, *J. Am. Chem. Soc.* **2000**, *122*, 1360.

[2] a) D. Enders, H. Eichenauer, *Angew. Chem.* **1979**, *91*, 425; *Angew. Chem. Int. Ed. Engl.* **1979**, *18*, 397; b) D. Enders, H. Kipphardt, P. Fey, *Org. Synth.* **1987**, *65*, 183; c) Y. Zhou, Y. Kim, K. A. Mohammed, D. K. Jones, I. Muhammad, D. H. Dunbar, D. G. Nagle, *J. Nat. Prod.* **2005**, *68*, 947; d) S. Awale, S. P. Shrestha, Y. Tezuka, J. Ueda, K. Matsushige, S. Kadota, *J. Nat. Prod.* **2005**, *68*, 858.

[3] a) D. Soorukram, P. Knochel, *Org. Lett.* **2004**, *6*, 2409; b) N. Harrington-Frost, H. Leuser, M. I. Calaza, F. F. Kneisel, P. Knochel, *Org. Lett.* **2003**, *5*, 2111; c) M. I. Calaza, E. Hupe, P. Knochel, *Org. Lett.* **2003**, *5*, 1059.

[4] a) A. Alexakis, K. Croset, *Org. Lett.* **2002**, *4*, 4147; b) K. Tissot-Croset, D. Polet, A. Alexakis, *Angew. Chem.* **2004**, *116*, 2480; *Angew. Chem. Int. Ed.* **2004**, *43*, 2426; c) A. Alexakis, D. Polet, *Org. Lett.* **2004**, *6*, 3529; d) K. Tissot-Croset, A. Alexakis, *Tetrahedron Lett.* **2004**, *45*, 7375; e) A. Alexakis, A. Tomassini, O. Andrey, G. Bernardinelli, *Eur. J. Org. Chem.* **2005**, 1332; f) D. Polet, A. Alexakis, *Org. Lett.* **2005**, *7*, 1621.

[5] H. Leuser, S. Perrone, F. Liron, F. F. Kneisel, P. Knochel, *Angew. Chem.* **2005**, *117*, 4703; *Angew. Chem. Int. Ed.* **2005**, *44*, 4627.

[6] a) B. Breit, P. Demel, C. Studte, *Angew. Chem.* **2004**, *116*, 3874; *Angew. Chem. Int. Ed.* **2004**, *43*, 3785; see also: b) B. Breit, C. Herber, *Angew. Chem.* **2004**, *116*, 3878; *Angew. Chem. Int. Ed.* **2004**, *43*, 3790.

[7] a) E. Negishi, D. R. Swanson, C. J. Rousset, *J. Org. Chem.* **1990**, *55*, 5406; b) W. F. Bailey, T. T. Nurmi, J. J. Patricia, W. Wang, *J. Am. Chem. Soc.* **1987**, *109*, 2442; c) W. F. Bailey, J. J. Patricia, T. T. Nurmi, W. Wang, *Tetrahedron Lett.* **1986**, *27*, 1861; d) W. F. Bailey, J. J. Patricia, T. T. Nurmi, *Tetrahedron Lett.* **1986**, *27*, 1865; e) W. F. Bailey, K. Rossi, *J. Am. Chem. Soc.* **1989**, *111*, 765; f) W. F. Bailey, T. V. Ovaska, T. K. Leipert, *Tetrahedron Lett.* **1989**, *30*, 3901; g) W. F. Bailey, T. V. Ovaska, *Tetrahedron Lett.* **1990**, *31*, 627; h) G. Wu, F. E. Cederbaum, E. Negishi, *Tetrahedron Lett.* **1990**, *31*, 493.

[8] Determined from the corresponding ketone.

[9] D. A. Evans, S. W. Kaldor, T. K. Jones, J. Clardy, T. J. Stout, *J. Am. Chem. Soc.* **1990**, *112*, 7001.

[10] When tetrabutylammonium fluoride in THF was used (0 °C, 1 h), partial racemization of the ketone **1a** was observed (86% yield, 65% *ee*; see the Supporting Information.

[11] M. I. Calaza, X. Yang, D. Soorukram, P. Knochel, *Org. Lett.* **2004**, *6*, 529.

[12] For the use of $(Ph)_2CuLi$ in the presence of tetramethylsilyl chloride in CH_2Cl_2 for 1,4-addition reactions see: T. Hirata, K. Shimoda, T. Kawano, *Tetrahedron: Asymmetry* **2000**, *11*, 1063.

[13] A. Winqvist, R. Strömberg, *Eur. J. Org. Chem.* **2001**, 4305.

[14] K. Striyzke, S. Schulz, H. Laatsch, E. Helmke, W. Beil, *J. Nat. Prod.* **2004**, *67*, 395.

[15] a) A. Ricci, G. Seconi, R. Curci in *Advances in Silicon Chemistry*, *Vol. 3* (Ed.: G. L. Larson), JAI, Greenwich, CT, **1996**, p. 63; b) Bis(trimethylsilyl)peroxide $[(TMSO)_2]$ was purchased from ABCR Product List. Please refer to the warnings in the catalog.

 © 2006 Wiley-VCH Verlag GmbH & Co. KGaA, Weinheim

Chiral Solvents

DOI: 10.1002/anie.200600327

Highly Enantioselective Aza-Baylis–Hillman Reaction in a Chiral Reaction Medium**

*Rolf Gausepohl, Pascal Buskens, Jochen Kleinen, Angelika Bruckmann, Christian W. Lehmann, Jürgen Klankermayer, and Walter Leitner**

Dedicated to Professor Dieter Enders on the occasion of his 60th birthday

A chemical reaction that leads to enantiomerically enriched products can in principle be carried out with a source of chirality in any of the involved components—starting materi-

[*] R. Gausepohl, P. Buskens, J. Kleinen, A. Bruckmann, Dr. J. Klankermayer, Prof. Dr. W. Leitner
Institut für Technische und Makromolekulare Chemie
Rheinisch-Westfälische Technische Hochschule Aachen
Worringerweg 1, 52074 Aachen (Germany)
Fax: (+49) 241-80-22177
E-mail: leitner@itmc.rwth-aachen.de
Dr. C. W. Lehmann, Prof. Dr. W. Leitner
Max-Planck-Institut für Kohlenforschung
Kaiser-Wilhelm-Platz 1
45470 Mülheim an der Ruhr (Germany)

[**] This work was supported by the Deutsche Forschungsgemeinschaft (SPP 1179, SFB 380). R.G. and P.B. thank the Fonds der Chemischen Industrie and the Graduate School 440 "Methods in Asymmetric Synthesis", respectively, for PhD stipends. We thank Dr. K. Ditrich (BASF AG) for a generous gift of (*R*)-mandelic acid. Furthermore, we are very grateful to H. Eschmann and T. Steins for their technical support.

Supporting information for this article is available on the WWW under http://www.angewandte.org or from the author.

© 2006 Wiley-VCH Verlag GmbH & Co. KGaA, Weinheim

als,[1] catalysts,[2] or reaction media.[3] To date, all asymmetric transformations that yield appreciable enantioselectivities are based on the first two strategies. Herein we report the first example of a highly enantioselective asymmetric synthesis in which only the reaction medium contains chiral information.

We focused our investigations on the aza-Baylis–Hillman reaction, a C–C-bond forming reaction of activated alkenes (e.g., **2**) with imines (e.g., **1**).[4] This organocatalytic transformation is catalyzed by nucleophilic Lewis bases such as tertiary phosphines (**3**) and leads to highly functionalized chiral allylic amines (**4**) (Scheme 1). The previously developed methods for enantioselective synthesis of the allylic amine **4** provide the necessary chiral information within the substrate[5] or through catalysts.[6] We have prepared the ionic liquid (IL) **9**, which contains a chiral anion and induces high enantioselectivities (up to 84% *ee*) when used as reaction medium.

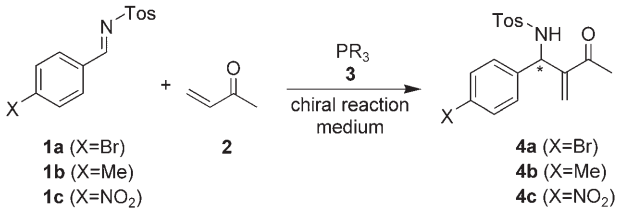

Scheme 1. The aza-Baylis–Hillman reaction. Tos = 4-toluenesulfonyl.

The strategy of applying chiral solvents in asymmetric synthesis was pioneered by Seebach and Oei.[7] They used a chiral amino ether as the solvent in the electrochemical reduction of ketones but observed only low enantioselectivities (up to 23.5% *ee*). Since then, all attempts to apply chiral solvents in asymmetric synthesis have resulted in similar or lower enantioselectivities. This led to the generally accepted conclusion that "asymmetric induction caused by chiral solvents is usually rather small".[3]

As ILs have attracted a lot of attention recently as a new class of solvents,[8] the incorporation of chiral information in these media has caught the interest of several groups.[9] Although details of the structure and dynamics of these solvents as well their interactions with dissolved substances remain largely elusive, chiral ILs have already started to emerge for various purposes[9] including asymmetric synthesis.[10] Very recently, Vo-Thanh and co-workers reported the largest presently known asymmetric induction caused by a chiral IL as the only source of chirality in an asymmetric reaction.[10a] In the DABCO-catalyzed Baylis–Hillman reaction (DABCO = 1,4-diazabicyclo[2.2.2]octane) of benzaldehyde and methylacrylate they obtained enantioselectivities up to 44% *ee* (e.r. = 2.6) by using an IL with chiral cations derived from (−)-*N*-methylephedrine. To the best of our knowledge, no significant asymmetric induction has been reported so far for ILs with chiral anions.

Previous investigations on the mechanism of the aza-Baylis–Hillman reaction by our group indicate that a bifunctional stabilization of the zwitterionic reaction intermediates is necessary to obtain high enantioselectivities and to prevent subsequent racemization of the reaction product **4**.[11] In conventional systems, this can be achieved by incorporating both a nucleophilic catalyst and a Brønsted acidic co-catalyst into one chiral molecule. ILs, however, offer the possibility of establishing a bifunctional interaction by incorporating the acidic center into the chiral anion of the solvent, thus allowing monofunctional achiral nucleophiles to be used as catalysts in the enantioselective aza-Baylis–Hillman reaction (Figure 1).

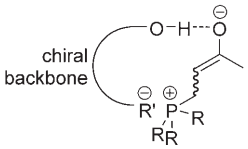

Figure 1. Possible bifunctional interaction of the zwitterionic intermediate of the aza-Baylis–Hillman reaction with the chiral anion of an IL containing a hydrogen-bond donor.

For ions containing hydrogen-bond donor functions, we targeted borate anions based on L-(−)-malic acid, which is available from the chiral pool (Scheme 2). The sodium dimalatoborate salt **8** was prepared by stirring an aqueous

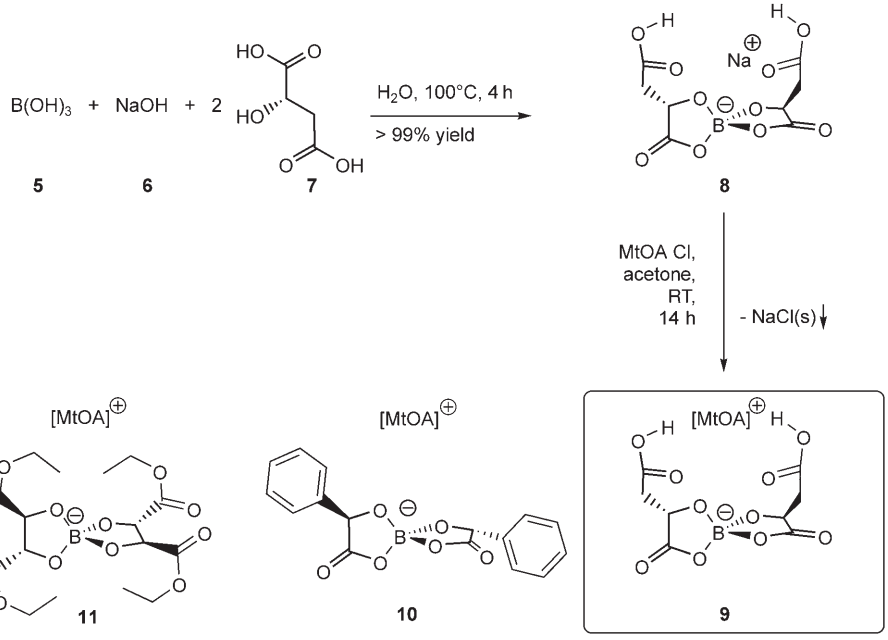

Scheme 2. Two-step synthesis of methyltrioctylammonium dimalatoborate (**9**). Only one of the two possible diastereoisomers is shown.

 © 2006 Wiley-VCH Verlag GmbH & Co. KGaA, Weinheim

solution of boric acid (**5**), sodium hydroxide (**6**), and L-(−)-malic acid (**7**) in an open flask at 100 °C.[12] Figure 2 depicts the molecular structure of the anion as revealed by X-ray crystal structure analysis,[13] which proves the connectivity and

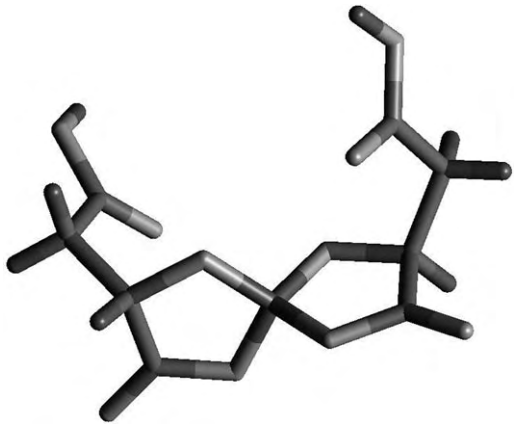

Figure 2. Molecular structure of the dimalatoborate anion in the solid state as revealed by X-ray single-crystal structure analysis of the corresponding sodium salt **8**. Only the *S,S,S* diastereoisomer is present in the crystal lattice. The O-B-O angles range from 103.9 to 105.1° within the five-membered ring and from 109.0 to 113.4° between the rings (see the Supporting Information for details).

configuration indicated in Scheme 2. Multinuclear NMR experiments confirmed the presence of the five-membered ring arrangement also in solution. Two sets of signals are observed in a 1:1 ratio in the ^{1}H and ^{13}C NMR spectra of samples of dissolved single crystals even at low temperature (233 K, $[D_4]$MeOH). This is due to the formation of a 1:1 mixture of the two possible diastereoisomers that result from the fixed chirality at the asymmetric carbon atoms and the labile chirality at the boron center of this spiro-type compound.[14]

The exchange of the sodium ions with methyltrioctylammonium (MtOA) was carried out with aliquat 336 (MtOACl) in acetone. Filtration of the precipitated NaCl and evaporation of the solvent yielded a colorless liquid with a melting point of −32 °C.[15] The related ILs **10** and **11**, which lack a potential hydrogen-bond donor, were prepared in a similar manner.

To assess the efficacy of the IL **9** for chiral induction, the aza-Baylis–Hillman reaction between methyl vinyl ketone (**2**) and *N*-(4-bromobenzylidene)-4-toluenesulfonamide (**1a**) was studied in the new reaction medium using PPh_3 (**3**, R = Ph) as the nucleophilic catalyst (see Experimental Section). The chiral allylic amine (*R*)-**4a** was obtained in this model reaction with reasonable conversion and high enantiomeric excess.[16] In a series of four independent experiments using various batches of **9**, conversion varied between 34% and 39% and the enantioselectivity ranged from 71–84% *ee*. The highest enantiomeric excess (84% *ee*) observed in these experiments corresponds to an enantiomeric ratio of 11.5 and hence a difference in activation energies $\Delta\Delta G^{\ddagger}$ of 6.05 kJ mol^{-1} for the formation of the two enantiomers. This is by far the highest asymmetric induction obtained with a chiral solvent as the sole source of chirality.

Several experiments were carried out to investigate the mechanism of the chirality transfer by the chiral reaction medium.[17] Notably, the structurally related ILs **10** and **11** resulted in lower conversions (15% and 14%, respectively) and the formation of racemic product, which indicates the necessity of a Brønsted acidic moiety within the chiral ion.[11] Dilution experiments with one equivalent of **9**, **8**, or **7** per molecule of **3** in THF or CH_2Cl_2 also resulted only in the formation of small amounts of racemic product. These results show that neither **9** nor any of its chiral precursors can be used as an additive for the asymmetric aza-Baylis–Hillman reaction in conventional solvents. Consequently, the use of **9** as a reaction medium is crucial for effective asymmetric transformation in this system.

Almost identical results were obtained with substrate **1a** using other aryl phosphines (**3**) as the achiral nucleophilic catalyst in **9** as the reaction medium ($P(o\text{-tolyl})_3$: 35% conversion, 74% *ee* (*R*); $(C_6F_5)PPh_2$: 9% conversion, 71% *ee* (*R*)). The catalyst PPh_3 also led to reasonable conversion (39%) and a high level of enantioselectivity (64% *ee*) for the *p*-methyl-substituted substrate **1b**. With the less electron-rich substrate **1c**, however, product **4c** was obtained in only 10% *ee*. A control experiment showed that this results from a lower level of intrinsic asymmetric induction, as no racemization of **4c** occurred under turnover conditions. A similar decrease in asymmetric induction was described by Vo-Thanh and co-workers for the mechanistically related Baylis–Hillman reaction of *p*-nitrobenzaldehyde and methylacrylate in ILs with chiral ephedrinium cations.[10a] They explained the drop in enantioselectivity by the formation of a hydrogen bond between the OH group of the chiral ion and the NO_2 function of the substrate.

In conclusion, we reported the first example of an asymmetric reaction in which a chiral reaction medium induces a high level of enantioselectivity. Using a specifically designed ionic liquid with a chiral anion as the only source of chirality, enantioselectivities of up to 84% *ee* ($\Delta\Delta G^{\ddagger} = 6.05$ kJ mol^{-1}) were obtained in the aza-Baylis–Hillman reaction. This is the highest enantioselectivity induced to date by a solvent as the sole source of chirality. These results are comparable with the values obtained with the best catalysts for the asymmetric aza-Baylis–Hillman reaction in conventional solvents (94% *ee*,[6e] 83% *ee*[6c,d]).

The results described herein demonstrate that, contrary to popular opinion, the strategy of applying chiral solvents in asymmetric synthesis can result in appreciable enantioselectivities. The key to effective chirality transfer lies in strong intermolecular interactions such as electrostatic attraction and hydrogen bonding between the solvent molecules and the intermediates or transition states of the enantioselective reaction step (see Figure 1). Functional ionic liquids offer unique possibilities to create such arrangements for a wide range of transformations.

Experimental Section

8: **7** (10.73 g, 80.0 mmol, 2.00 equiv) was dissolved in water (10 mL) and treated with boric acid (**5**, 2.47 g, 40.0 mmol, 1.00 equiv). A solution of sodium hydroxide (**6**, 1.60 g, 40.0 mmol, 1.00 equiv) in

 © 2006 Wiley-VCH Verlag GmbH & Co. KGaA, Weinheim

water (30 mL) was then added. The reaction mixture was stirred in an open flask at 100 °C. After evaporation of the water (ca. 4 h), **8** was isolated as a white powder (11.92 g; 40.0 mmol, > 99 % yield).

9: Methyltrioctylammonium chloride (3.54 g, 8.75 mmol, 1.00 equiv) was dissolved in acetone (20 mL) and treated with a solution of the sodium borate salt **8** (2.61 g, 8.75 mmol, 1.00 equiv) in acetone (20 mL). The reaction mixture was stirred at room temperature overnight. During this period, sodium chloride precipitated as a white solid. The reaction mixture was filtered and the solvent was removed in vacuo to yield **9** as a highly viscous, hygroscopic colorless liquid.

Typical procedure for the aza-Baylis–Hillman reaction: **4a**: Imine **1a** (0.125 mmol, 1.00 equiv) and catalyst **3** (12.5 μmol, 0.10 equiv) were dissolved in **9** (1.0 mL, 6.7 mL per mmol **1**). After addition of **2** (12.5 μL, 10.5 mg, 0.150 mmol, 1.20 equiv), the reaction was stirred at room temperature for 24 h. Excess **2** was removed in vacuo, a small sample of the reaction mixture was dissolved in [D_6]DMSO, and the conversion was determined by ^{1}H NMR spectroscopy. The rest of the reaction mixture was dissolved in water/methanol (1:1, 5 mL). Further methanol was added to obtain a clear solution of the reaction mixture. After (partly) exchanging the cation on an ion-exchange resin (contact time approximately 5 min), all volatile substances were removed in vacuo. The resulting solid was extracted with heptane/*i*PrOH (85:15, 1 mL), and the solution was directly analyzed by HPLC on a chiral phase to determine the enantiomeric excess of **4a**.

Received: January 25, 2006
Revised: March 10, 2006

Keywords: asymmetric synthesis · C–C coupling · chiral solvents · ionic liquids · organocatalysis

[1] G. H. Roos, *Compendium of Chiral Auxiliary Applications*, Academic Press, San Diego, **2001**.
[2] a) E. N. Jacobsen, A. Pfaltz, H. Yamamoto, *Comprehensive Asymmetric Catalysis*, Springer, Berlin, **1999**; b) A. Berkessel, H. Gröger, *Asymmetric Organocatalysis—From Biomimetic Concepts to Applications in Asymmetric Synthesis*, Wiley-VCH, Weinheim, **2005**.
[3] C. Reichardt, *Solvents and Solvent Effects in Organic Chemistry*, Wiley-VCH, Weinheim, **2003**.
[4] For a recent review on the Baylis–Hillman reaction, see: D. Basavaiah, A. J. Rao, T. Satayanarayana, *Chem. Rev.* **2003**, *103*, 811 – 891.
[5] X. Liu, J. Zhao, G. Jin, G. Zhao, S. Zhu, S. Wang, *Tetrahedron* **2005**, *61*, 3841 – 3851.
[6] a) M. Shi, Y.-M. Xu, *Angew. Chem.* **2002**, *114*, 4689 – 4692; *Angew. Chem. Int. Ed.* **2002**, *41*, 4507 – 4510; b) D. Balan, H. Adolfsson, *Tetrahedron Lett.* **2003**, *44*, 2521 – 2524; c) M. Shi, L.-H. Chen, *Chem. Commun.* **2003**, 1310 – 1311; d) M. Shi, L.-H. Chen, C.-Q. Li, *J. Am. Chem. Soc.* **2005**, *127*, 3790 – 3800; e) K. Matsui, S. Takizawa, H. Sasai, *J. Am. Chem. Soc.* **2005**, *127*, 3680 – 3681.
[7] D. Seebach, H. A. Oei, *Angew. Chem.* **1975**, *87*, 629 – 630; *Angew. Chem. Int. Ed. Engl.* **1975**, *14*, 634 – 635.
[8] a) P. Wasserscheid, W. Keim, *Angew. Chem.* **2000**, *112*, 3926 – 3945; *Angew. Chem. Int. Ed.* **2000**, *39*, 3772 – 3789; b) P. Wasserscheid, T. Welton, *Ionic Liquids in Synthesis*, Wiley-VCH, Weinheim, **2003**.
[9] For recent reviews on chiral ILs, see: a) C. Baudequin, D. Brégeon, J. Levillain, F. Guillen, J.-C. Plaquevent, A.-C. Gaumont, *Tetrahedron: Asymmetry* **2005**, *16*, 3921 – 3945; b) J. Ding, D. W. Armstrong, *Chirality* **2005**, *17*, 281 – 292.
[10] a) B. Pégot, G. Vo-Thanh, A. Loupy, *Tetrahedron Lett.* **2004**, *45*, 6425 – 6428; b) J. Ding, V. Desikan, X. Han, T. L. Xiao, R. Ding, W. S. Jenks, D. W. Armstrong, *Org. Lett.* **2005**, *7*, 335 – 337; c) Z. Wang, Q. Wang, Y. Zhang, W. Bao, *Tetrahedron Lett.* **2005**, *46*, 4657 – 4660.
[11] P. Buskens, J. Klankermayer, W. Leitner, *J. Am. Chem. Soc.* **2005**, *127*, 16762 – 16763.
[12] The corresponding Li salt: P. H. Cunningham, F. L. Warren, Jr., H. O. Marcy, M. J. Rosker (Rockwell International Corp., USA), EP-95-109113 693704, **1996**.
[13] Crystal data for **8**: $C_8H_8BNaO_{10}$, $M_r = 297.9$, crystal dimensions $0.36 \times 0.34 \times 0.25$ mm^3, monoclinic $P2_1$ (No. 4), $T = 100$ K $a = 5.40160(10)$, $b = 11.6781(2)$, $c = 9.4451(2)$ Å, $\beta = 105.0590(10)$, $V = 575.340(19)$ Å^3, $\rho_{calcd} = 1.720$ Mg m^{-3}, $Cu_{K\alpha}$ radiation, $\lambda = 1.54178$ Å. CCD scans yielded 10760 (1906 unique) reflections, $R_{int} = 0.038$. Multi-scan absorption correction, $\mu = 1.719$ mm^{-1}, $T_{min} = 0.85$, $T_{max} = 1.0$. Structure solution (direct methods) SHELXS-97, full-matrix least-squares refinement against F^2 SHELXL-97, 213 parameters, hydrogen atoms in idealized geometry (riding model) R = 0.025, wR = 0.077, highest residual electron density peak 0.2 Å^{-3}. Complete lists of atom coordinates and anisotropic displacement parameters as well as tables of bond lengths and bond angles are available as supplementary material. CCDC-297143 contains the supplementary crystallographic data for this paper. These data can be obtained free of charge from The Cambridge Crystallographic Data Centre via www.ccdc.cam.ac.uk/data_request/cif.
[14] a) J. Boeseken, J. A. Mijs, *Recl. Trav. Chim. Pays-Bas* **1925**, *44*, 758 – 762; b) S. Green, A. Nelson, S. Warriner, B. Whittaker, *J. Chem. Soc. Perkin Trans. 1* **2000**, 4403 – 4408; c) J. Lacour, V. Hebbe-Viton, *Chem. Soc. Rev.* **2003**, *32*, 373 – 382.
[15] The melting point was determined by differential scanning calorimetry; 72 ± 2 % conversion (determined from ^{1}H NMR spectroscopy); impurities: octanol (from aliquat 336, up to 6 %), water (200–2800 ppm, determined by Karl Fischer titration).
[16] The absolute configuration of **4a**–**c** was assigned as *R* by comparison with the work of Shi et al.[6d]
[17] The possibility of enrichment of one enantiomer during workup was excluded by subjecting a scalemic mixture of **4c** to the same experimental procedure. This control material had 74 % *ee* (*S*) before and 76 % *ee* (*S*) after the workup procedure.

 © 2006 Wiley-VCH Verlag GmbH & Co. KGaA, Weinheim

Heterogeneous Catalysis

DOI: 10.1002/anie.200504253

Size-Dependent Oxidation Mechanism of Supported Pd Nanoparticles**

Tobias Schalow, Björn Brandt, David E. Starr, Mathias Laurin, Shamil K. Shaikhutdinov, Swetlana Schauermann, Jörg Libuda, and Hans-Joachim Freund*

Nanometer-sized metal particles on oxide surfaces have numerous technological applications, particularly in the field of heterogeneous catalysis.[1,2] Many catalysts applied in the chemical industry for emission control or in energy technology are based on finely dispersed noble-metal aggregates on oxides. But is the surface of these metal aggregates truly metallic under reaction conditions? This seemingly elementary question turns out to be very difficult to answer. The reason is that the influence of the reactant atmosphere on the surface structure, morphology, and composition may be rather complex. Especially in the case of oxygen-containing environments, the situation turns out to be particularly intricate. Many different oxygen species may be present even on simple single-crystal surfaces, including various types of chemisorbed oxygen (i.e. oxygen adsorbed above the first atomic layer of the metal), subsurface oxygen (i.e. oxygen incorporated into the first layers of metal atoms), thin surface oxides (i.e. very thin structures consisting of oxygen and metal-ion layers), and bulk oxides.[3–16] The puzzling role of these multiple species in reaction kinetics is a major challenge for microscopic studies in catalysis, and the related questions are currently the subject of intensive discussion (see e.g.[17–19]).

For small particles on support materials, the situation is even more complex. These particles expose multiple sites, including different facets, edges, corners, and defects; they may show modified lattice constants and electronic structures; and they may show substantial interactions with the support. All of these effects may have an influence on the thermodynamic and kinetic aspects of the formation of the different oxide species and their reactivity.

[*] Prof. Dr. J. Libuda
Lehrstuhl für Physikalische Chemie II
Universität Erlangen-Nürnberg
Egerlandstrasse 3, 91058 Erlangen (Germany)
Fax: (+49) 9131-842-7308
E-mail: libuda@chemie.uni-erlangen.de
Dipl.-Ing. T. Schalow, Dipl.-Chem. B. Brandt, Dr. D. E. Starr, M. Laurin, Dr. S. K. Shaikhutdinov, Dr. S. Schauermann, Prof. Dr. H.-J. Freund
Fritz-Haber-Institut der Max-Planck-Gesellschaft
Faradayweg 4–6, 14195 Berlin (Germany)

[**] This work was funded by the Deutsche Forschungsgemeinschaft (SPP 1091) and the Fonds der Chemischen Industrie.

Supporting information for this article (experimental details) is available on the WWW under http://www.angewandte.org or from the author.

In a recent communication[20] we reported on a new oxidation and oxygen-storage mechanism for supported metal nanoparticle systems. For Pd crystallites on Fe_3O_4, initial oxidation of the metal was found to be largely dominated by the formation of a thin Pd oxide layer at the particle/support interface, which is substantially stabilized by the support. The formation and depletion of this interface oxide layer is reversible, providing the system with the ability to store and release large amounts of oxygen without major modifications of the remaining surface of the metal particle.

Here we show that this oxidation mechanism gives rise to pronounced particle-size effects: For small particles, full oxidation of the Pd particles occurs easily, but the total oxygen-storage capacity is limited by the small number of Pd atoms per unit of support surface area. For large particles, on the other hand, the Pd loading may be large, but strong kinetic hindrance inhibits Pd oxidation and, therefore, the oxygen-storage process. As a result, the supported Pd system shows a pronounced maximum of the oxygen-storage capacity at intermediate particles sizes. This size-dependent oxidation behavior and oxygen-storage functionality may be an important contribution to a microscopic-level understanding of the reaction kinetics on nanoparticle systems.

The experimental approach providing these insights is summarized in Figure 1. Briefly, we employed well-defined supported model catalysts, which were characterized in detail at the atomic level using surface-science techniques.[21–25] As a first step, particle size, morphology, and structure of these model surfaces were studied by scanning tunneling microscopy (STM). Subsequently, their reaction kinetics were probed quantitatively in a fully remote-controlled multimolecular beam (MB) experiment.[26–29] With this combination of STM and MB techniques we could obtain detailed information on the reaction kinetics as a function of the particle size and structure.

In the work presented here, we focused on Pd nanoparticles prepared in situ under ultrahigh-vacuum (UHV) conditions on an ordered Fe_3O_4 film.[30] Structure and adsorption properties of the support[30,31] and the Pd particles[20,32,33] were investigated previously. Size and density of the Pd particles can be varied within a wide range by choosing the appropriate preparation conditions. In this study, we varied the particle size between approximately 2 nm and 100 nm (corresponding to aggregates containing approximately 10^2 to 10^8 Pd atoms per particle) by changing the Pd loading (amount of Pd metal deposited per unit of support surface area). STM images of some representative samples are shown in Figure 2. Apart from the variations in particle size, it can be seen that in general the particles display a well-defined crystalline morphology. They grow in (111) orientation on the support and are terminated mainly by (111) facets as well as by a minor fraction (around 20%) of (100) side facets. Typically, the aspect ratio (height/diameter) is about 1:4 (for more details on the growth and particle morphology see Ref. [33]). The systems investigated were stabilized by thermal annealing followed by oxidation and reduction cycles prior to the experiments (see the Supporting Information). This procedure provided to a perfectly stable surface under the conditions of all kinetic experiments presented below.

 © 2006 Wiley-VCH Verlag GmbH & Co. KGaA, Weinheim

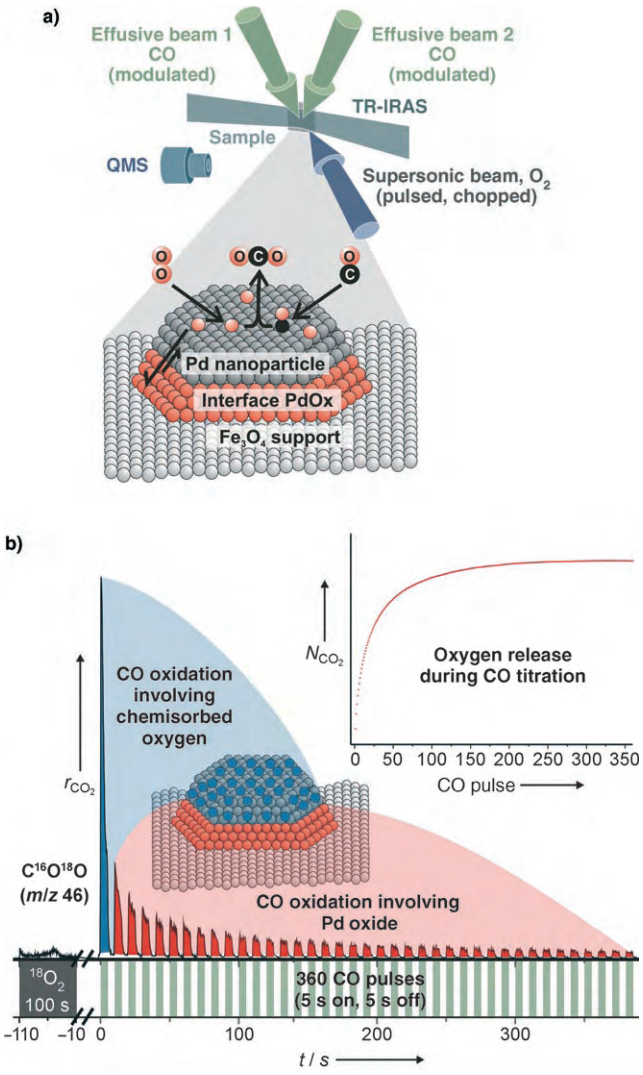

Figure 1. a) Schematic representation of the molecular beam experiment and the model catalyst surface used in this study; b) pulsed CO titration experiment on 7-nm Pd particles on Fe_3O_4 at 500 K. First, the sample was exposed to an oxygen pulse (100 s, ≈130 L). After a short delay time (10 s), 360 CO pulses (5 s on-time (≈3 L), 5 s off-time) were applied to withdraw the oxygen stored in the model catalyst in the form of CO_2. The CO_2 formation rate (r_{CO_2}) was recorded in the gas phase and integrated over the pulses (N_{CO_2}: integral CO_2 yield, inset) to determine the oxygen-storage capacity.

To probe the total oxygen-storage capacity of the Pd particles (oxygen chemisorption on metallic Pd and Pd oxide formation), a remote-controlled MB titration experiment was performed using modulated O_2 and CO beams (see Figure 1). Initially, the model surface was exposed to a pulse of oxygen. After a short delay time, the surface oxygen was titrated by pulses of CO. Reaction of CO, consuming oxygen from the chemisorption and oxide phases, led to formation of CO_2, which instantaneously desorbed from the surface and was detected in the gas phase via quadrupole mass spectrometry (QMS; see e.g. Refs. [34,35]).

The pulsed MB titration experiment was described previously.[20] It allows an exact quantification of the oxygen release and provides detailed insights into the related

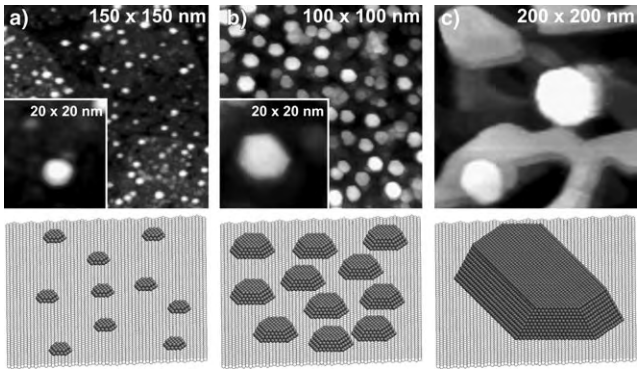

Figure 2. STM images and schematic representations of the model catalyst surface for different metal loadings after stabilization by oxidation and reduction cycles; nominal Pd thickness: a) 0.3 Å (average particle size 3 nm); b) 4.0 Å Pd (particle size 7 nm); c) 15 Å Pd (particle size ≈65 nm).

reduction kinetics. A typical example of a pulsed MB titration is shown in Figure 1b. The most important point to note is that the CO_2 signal reveals the presence of two reaction channels. During the first CO pulse, very fast CO_2 formation is observed. This fast reaction channel was previously attributed to the reaction of chemisorbed atomic oxygen on metallic Pd with CO. After a single CO pulse, however, the reservoir of chemisorbed O is depleted, and the following slower CO_2 formation involves oxygen that originates from Pd oxide. In a previous study[20] it was shown that this Pd oxide is formed preferentially at the Pd/Fe_3O_4 interface and not at the outer surface of the Pd particles. As a result, a large fraction of the outer particle surface remains metallic for particles of intermediate size (4–10 nm). Reduction of the Pd oxide phase proceeds by means of slow decomposition and release of oxygen onto the metallic part of the surface, followed by rapid reaction with adsorbed CO. Decomposition of the interface oxide is, in general, the rate-controlling step under the present experimental conditions. It limits the rate of oxygen release and CO_2 formation which is typically spread over up to 100 CO pulses. It should be pointed out that the oxidation and reduction process is fully reversible and can be repeated many times without significant decrease in the oxygen uptake.

The total amount of oxygen released from the system can be determined easily by integrating the CO_2 formation over all CO pulses. The corresponding result for 7-nm particles is shown in the inset in Figure 1. We found that the amount of oxygen stored in the Pd interface oxide layer by far exceeds the amount of oxygen that could be chemisorbed on a purely metallic Pd particle. For the 7-nm particles, for instance, the oxygen release is approximately four times greater than expected for pure chemisorption. These quantitative measurements of oxygen release by means of MB titration experiments were confirmed by measurements of the oxygen uptake by pulsed sticking coefficient measurements.[36] In the same study, it was shown by isotopic exchange experiments that oxidation and reduction of the Fe_3O_4 support does not contribute significantly to the oxygen uptake and release. Also, it was shown by photoelectron

 © 2006 Wiley-VCH Verlag GmbH & Co. KGaA, Weinheim

spectroscopy (PES) that the particles are fully reduced by extended CO exposure.

In the next step we considered the size dependence of the Pd particle oxidation. For an interface-controlled oxidation mechanism, we would expect a strong size dependence, because the accessibility of the particle/support interface is expected to decrease with increasing size. In order to experimentally verify this hypothesis, we systematically measured the oxygen release by means of pulsed MB titration experiments over a broad range of particle sizes from about 2 to 100 nm. The corresponding structural and morphological properties were extracted from STM (see Figure 2 and the Supporting Information).

To identify the role of particle-size-dependent Pd oxidation in the oxygen uptake and release process, we first estimated the amount of oxygen release that would be expected if there was no Pd oxide formation at all, but pure oxygen chemisorption on metallic Pd only. For this purpose, we determined the Pd surface area available for chemisorption per unit area of the Fe_3O_4 support by means of CO sticking coefficient measurements. The CO adsorption was converted into a hypothetical O uptake assuming O chemisorption only (for details see the Supporting Information). The result is shown in Figure 3a (blue curve): We found that initially the Pd surface area increases monotonically with increasing Pd loading or particle size, whereas for high Pd loadings or large particle sizes the Pd surface area is nearly constant. The reason is that for low loading (small particles) the island density changes only weakly, whereas the particle size increases with metal loading. At high loading (large particles), however, the particle density decreases rapidly due to coalescence. Increasing particle size and decreasing particle density nearly compensate, resulting in an almost constant Pd surface area. It should be noted that the measurements of the Pd surface area by means of the CO sticking coefficient are in full accordance with estimates derived from STM data.

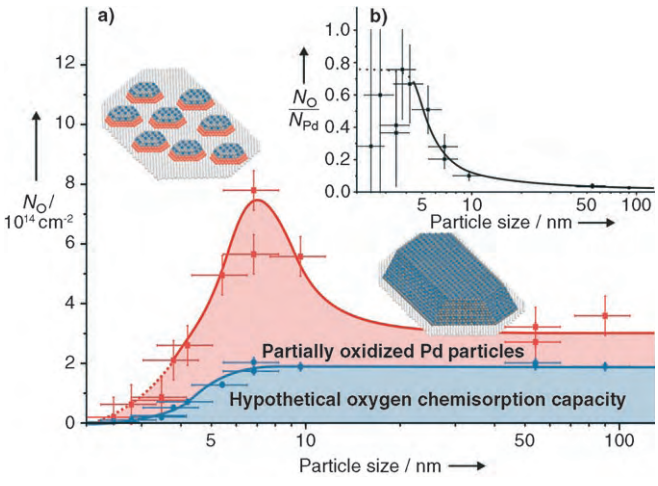

Figure 3. Oxygen storage on a Pd/Fe_3O_4 model catalyst after 100 s (≈130 L) oxygen exposure at 500 K as a function of Pd particle size: a) Hypothetical oxygen release assuming regular chemisorption on metallic Pd particles only and no oxidation (blue curve) and experimentally determined oxygen release on partially oxidized Pd particles (red curve); b) mean stoichiometry of the Pd particles after oxygen treatment.

In a second step, the actual oxygen-storage capacity was quantified by pulsed MB titration experiments (see Figure 3, red curve). We found that the experimentally determined oxygen release is completely different from that expected assuming chemisorption only: First, the release was significantly larger than expected for pure chemisorption. Secondly, a pronounced maximum of the total oxygen release was found for particle sizes around 7 nm.

The differences between the experimental oxygen release on the one hand and the hypothetical oxygen-chemisorption capacity on the other are attributed to the partial oxidation of the Pd particles. It is apparent that the contribution due to Pd oxide formation shows a pronounced size dependence. To obtain some additional information on the oxidation process, we calculated the total stoichiometry of the particles after oxygen treatment (see Figure 3b, calculated by dividing the total oxygen release by the total Pd loading). The result shows that the average Pd oxidation state monotonically decreases with increasing particle size: Whereas in the limit of small particles (< 3 nm) the stoichiometry corresponds to almost PdO, the oxygen/Pd ratio decreases to approximately $PdO_{0.25}$ at sizes around 7 nm and, finally, to $PdO_{<0.05}$ for the largest particles investigated. (Note that these values represent an average over metallic parts of the three-dimensional particles with chemisorbed oxygen and oxidized parts).

From this observation the following scenario can be derived: As shown in our previous work, oxidation of the Pd particles proceeds by initial chemisorption of oxygen on the metallic Pd particles and successive conversion of this chemisorbed oxygen to Pd oxide layers, preferentially at the particle/support interface.[20,36] For sufficiently small particles, no stable metal nucleus remains after formation of the interface oxide, resulting in complete oxidation of the nanoparticle (stoichiometry PdO). It is noteworthy that in a theoretical study Huber et al. recently showed that the interaction with the oxide support may lead to a significant stabilization of very small oxidized Pd clusters.[37] For larger particles (> 3 nm), however, oxidation is not complete and a metallic cap remains on top of the Pd interface oxide. It may be expected that for particles of this size interface, oxidation requires ion transport from the particle boundary along the metal/oxide interface. As shown experimentally, oxide formation and decomposition are rather slow processes, even for particles of intermediate size (around 7 nm). Thus, we may anticipate that with increasing particle size, interface transport finally becomes too slow to facilitate complete interface oxidation. As a result, oxygen storage by oxide formation at the Pd interface becomes kinetically hindered in the large particle limit (10–100 nm).

It is noteworthy that the hindrance of Pd oxide formed on large particles is directly reflected in the MB titration experiment. In Figure 4 a direct comparison of the CO_2 signal during the first few pulses of a MB titration experiment is shown for two samples corresponding to small (4 nm) and large (90 nm) particles. The CO_2 signal during the first CO pulse, which reflects the amount of chemisorbed oxygen on the metallic Pd surface, was significantly higher in case of the

 © 2006 Wiley-VCH Verlag GmbH & Co. KGaA, Weinheim

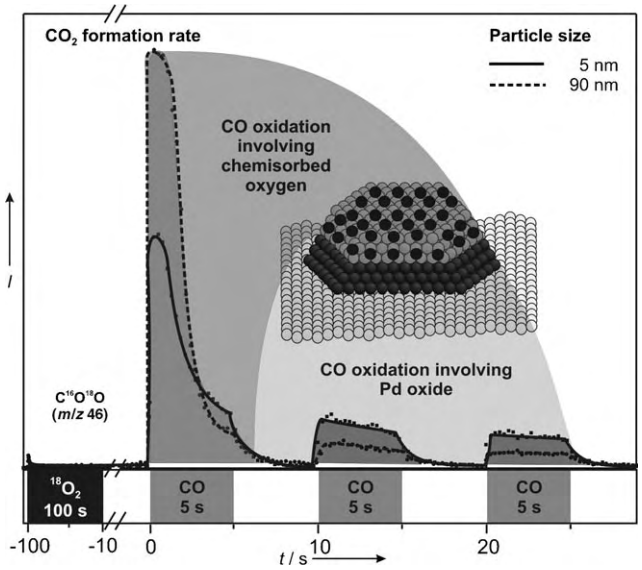

Figure 4. CO_2 formation rate during the first CO pulses of a CO titration experiment on preoxidized Pd/Fe_3O_4 model catalysts with different particles sizes.

large particles. In contrast, the CO_2 formation rate involving Pd oxide, which is represented by the following CO pulses, was less intense for the large particles further substantiating the strongly decreased oxide formation. (It should be noted that even on the largest particles a minor amount of oxide formation is detected. This remaining oxide formation may originate from particle sites that are more susceptible for oxidation such as (100) facets, steps, or defects and from remaining oxide formation at the particle boundaries; see Refs. [11–14] for a discussion of the interaction of Pd(111) and Pd(100) with oxygen.)

In summary we have shown that the interface-controlled oxidation mechanism for Pd nanoparticles supported on an Fe_3O_4 film gives rise to a pronounced particle-size dependence of the oxidation and reduction behavior: In the limit of small particles (<3 nm) complete oxidation to PdO occurs easily, whereas in the range of intermediate particle sizes (4–10 nm) only partial oxidation takes place, primarily at the metal/support interface. For larger particles (approximately 10–100 nm) the formation of the Pd interface oxide is kinetically hindered, presumably as a result of slow ion transport along the particle/support interface.

The formation of the interface oxide is fully reversible and allows uptake and release of much larger quantities of oxygen than would be expected for pure chemisorption on Pd metal. The size-dependent oxidation behavior has major implications for the oxygen-storage mechanism. In particular, it gives rise to a pronounced maximum of the oxygen-uptake capacity per unit of support surface area as a function of the metal loading. For low metal loading and small particles, oxidation is highly efficient, but the total oxygen-storage capacity is limited by the small amount of Pd available per catalyst surface area. (It should be noted that the oxygen-storage capacity cannot be increased by increasing the particle density because of oxygen-induced sintering effects at elevated temperatures, see Ref. [33]). For high metal loading and large particles, the amount of Pd available per support surface area is large, but the formation of Pd oxide becomes kinetically hindered. The maximum oxygen uptake is observed at intermediate Pd loading: Here, the particles are large enough to allow substantial amounts of interface oxide to be formed but are yet small enough to avoid strong kinetic hindrance to oxide formation.

The oxygen-storage mechanism and its size dependence are expected to play an important role in the kinetics of oxidation reactions on the present model system, especially under non-steady-state conditions. It might be anticipated that similar effects can be observed for other supported particle systems as well. Thus, it is likely that particle-size-dependent oxidation and reduction phenomena will have to be considered in the development of realistic microkinetic descriptions of catalytic reactions.

Received: November 30, 2005
Revised: February 23, 2006
Published online: April 26, 2006

Keywords: heterogeneous catalysis · nanoparticles · oxidation · palladium · surface chemistry

[1] *Handbook of Heterogeneous Catalysis* (Eds.: G. Ertl, H. Knoezinger, J. Weitkamp), VCH, Weinheim, **1997**.
[2] J. M. Thomas, W. J. Thomas, *Principle and Practice of Heterogeneous Catalysis*, VCH, Weinheim, **1997**.
[3] H. Conrad, G. Ertl, J. Küppers, E. E. Latta, *Surf. Sci.* **1977**, *65*, 235.
[4] R. Imbihl, J. E. Demuth, *Surf. Sci.* **1986**, *173*, 395.
[5] S.-L. Chang, P. A. Thiel, *J. Chem. Phys.* **1988**, *88*, 2071.
[6] X. Guo, A. Hoffman, J. T. Yates, Jr., *J. Chem. Phys.* **1989**, *90*, 5787.
[7] V. A. Bondzie, P. Kleban, D. J. Dwyer, *Surf. Sci.* **1996**, *347*, 319.
[8] E. H. Voogt, A. J. M. Mens, O. L. J. Gijzeman, J. W. Geus, *Surf. Sci.* **1997**, *373*, 210.
[9] F. P. Leisenberger, G. Koller, M. Sock, S. Surnev, M. G. Ramsey, F. P. Netzer, B. Klötzer, K. Hayek, *Surf. Sci.* **2000**, *445*, 380.
[10] V. A. Bondzie, P. H. Kleban, D. J. Dwyer, *Surf. Sci.* **2000**, *465*, 266.
[11] G. Zheng, E. I. Altman, *Surf. Sci.* **2000**, *462*, 151.
[12] G. Zheng, E. I. Altman, *Surf. Sci.* **2002**, *504*, 253.
[13] E. Lundgren, G. Kresse, C. Klein, M. Borg, J. N. Andersen, M. De Santis, Y. Gauthier, C. Konvicka, M. Schmid, P. Varga, *Phys. Rev. Lett.* **2002**, *88*, 246103.
[14] M. Todorova, E. Lundgren, V. Blum, A. Mikkelsen, S. Gray, J. Gustafson, M. Borg, J. Rogal, K. Reuter, J. N. Andersen, M. Scheffler, *Surf. Sci.* **2003**, *541*, 101.
[15] E. Lundgren, J. Gustafson, A. Mikkelsen, J. N. Andersen, A. Stierle, H. Dosch, M. Todorova, J. Rogal, K. Reuter, M. Scheffler, *Phys. Rev. Lett.* **2004**, *92*, 046101.
[16] M. Todorova, K. Reuter, M. Scheffler, *Phys. Rev. B* **2005**, *71*, 195403.
[17] H. Over, Y. D. Kim, A. P. Seitsonen, S. Wendt, E. Lundgren, M. Schmid, P. Varga, A. Morgante, G. Ertl, *Science* **2000**, *287*, 1474.
[18] G. Zheng, E. I. Altmann, *J. Phys. Chem. B* **2002**, *106*, 1048.
[19] B. L. M. Hendriksen, S. C. Bobaru, J. W. M. Frenken, *Surf. Sci.* **2004**, *552*, 229.
[20] T. Schalow, M. Laurin, B. Brandt, S. Schauermann, S. Guimond, H. Kuhlenbeck, D. E. Starr, S. K. Shaikhutdinov, J. Libuda, H.-J. Freund, *Angew. Chem.* **2005**, *117*, 7773; *Angew. Chem. Int. Ed.* **2005**, *44*, 7601.

 © 2006 Wiley-VCH Verlag GmbH & Co. KGaA, Weinheim

[21] C. R. Henry, *Surf. Sci. Rep.* **1998**, *31*, 231.
[22] V. P. Zhdanov, B. Kasemo, *Surf. Sci. Rep.* **2000**, *39*, 25.
[23] T. P. St. Clair, D. W. Goodman, *Top. Catal.* **2000**, *13*, 5.
[24] H.-J. Freund, M. Bäumer, J. Libuda, T. Risse, G. Rupprechter, S. Shaikhutdinov, *J. Catal.* **2003**, *216*, 223.
[25] J. Libuda, H.-J. Freund, *Surf. Sci. Rep.* **2005**, *57*, 157.
[26] G. Scoles, *Atomic and Molecular Beam Methods*, Oxford University Press, Oxford, **1988**.
[27] M. P. D'Evelyn, R. J. Madix, *Surf. Sci. Rep.* **1984**, *3*, 413.
[28] C. T. Rettner, D. J. Auerbach, J. C. Tully, A. W. Kleyn, *J. Phys. Chem.* **1996**, *100*, 13021.
[29] A. W. Kleyn, *Chem. Soc. Rev.* **2003**, *32*, 87.
[30] W. Weiss, W. Ranke, *Prog. Surf. Sci.* **2002**, *70*, 1.
[31] C. Lemire, R. Meyer, V. Henrich, S. K. Shaikhutdinov, H.-J. Freund, *Surf. Sci.* **2004**, *572*, 103.
[32] R. Meyer, S. K. Shaikhutdinov, H.-J. Freund, *Z. Phys. Chem.* **2004**, *218*, 905.
[33] T. Schalow, B. Brandt, D. E. Starr, M. Laurin, S. Schauermann, S. K. Shaikhutdinov, J. Libuda, H.-J. Freund, *Catal. Lett.* **2006**, *107*, 189.
[34] T. Engel, G. Ertl, *J. Chem. Phys.* **1978**, *69*, 1267.
[35] T. Engel, G. Ertl, in *The Chemical Physics of Solid Surfaces and Heterogeneous Catalysis*, *Vol. 4* (Eds.: D. A. King, D. P. Woodruff), Elsevier, Amsterdam, **1982**, p. 73.
[36] T. Schalow, B. Brandt, S. Schauermann, J. Libuda, H.-J. Freund, unpublished results.
[37] B. Huber, P. Koskinen, H. Häkkinen, M. Moseler, *Nat. Mater.* **2006**, *5*, 44.

 © 2006 Wiley-VCH Verlag GmbH & Co. KGaA, Weinheim

Ionic Liquids

DOI: 10.1002/anie.200504471

The Association of Water in Ionic Liquids: A Reliable Measure of Polarity**

*Thorsten Köddermann, Christiane Wertz, Andreas Heintz, and Ralf Ludwig**

Ionic liquids (ILs) are liquids formed solely of ions. Unlike inorganic molten salts such as NaCl, they are fluid at room temperature, or at least within the typical temperature range of most organic chemical reactions.[1,2] A number of properties make ionic liquids attractive in different areas of chemistry. They exhibit an almost vanishing vapor pressure, the characteristic electrical conductivity of an ionic conductor, and a considerable gap between the melting point and the temperature of decomposition.[1,3] The possibility of directing the course of chemical reactions along with the low vapor pressure make ILs an attractive alternative to traditional organic solvents for both laboratory and industrial purposes. Today ILs are regarded as "green solvents" and "designer media" for chemical reactions.[4–6] To expand the utility of ionic liquids, IL-based mixed solvents have come into focus.[7] In particular the addition of water can strongly affect the physical and chemical properties of ionic liquids such as viscosity,[8,9] electrical conductivity,[10] and reactivity,[11] as well as solvation and solubility properties.[12–16] Water is also an impurity commonly present in ILs since all known ILs are hygroscopic; traces of water are thought to be ubiquitous in these materials.

Interactions or molecular states of water dissolved in various solvents and absorbed in many materials, such as polymers, have been extensively studied using FTIR spectroscopy.[17] In particular, the vibrational modes of water that result in bands in the OH-stretching region (3000–3800 cm^{-1}) are sensitive to the environment and intermolecular interactions.[18,19] These modes have been used to understand the type of bonding between water molecules in the liquid, solid, and gas phases, as well as interactions between water and many chemical substances, including ILs. Cammarata et al.[20] studied interactions between ILs and water absorbed from the atmosphere by attenuated total reflectance (ATR) infrared spectroscopy. They concluded that anions are responsible for the interaction of ILs and water. No change in band positions and shapes was observed upon increasing water concentration. It was concluded that only one molecular state of water was present. In addition, they suggested that in ionic liquids containing $[BF_4]^-$ and $[PF_6]^-$ anions, water forms a symmetric complex in which the two water protons are bonded to two distinct anions. Tran et al.[21] reported differences in the near-infrared (NIR) spectrum of water dissolved in different ionic liquids, but their study focused on the quantitative determination of absorbed water in ionic liquids rather than on the investigation of its molecular state.

Herein we describe our investigation of the association of protonated and deuterated water molecules in two ILs presumed to have completely different polarities. A combination of FTIR spectroscopy and density functional calculations (DFT) clearly shows that water molecules are mainly H-bonded to the IL anions. The exact association of water molecules to the anions is a reliable indicator for the miscibility of water with ILs. Furthermore, we could demonstrate that the vibrational frequencies for single water molecules associated in ILs can be used as a good measure of the polarity of ILs. For this purpose we chose two fundamentally different ILs, 1-ethyl-3-methylimidazolium bis(trifluoromethylsulfonyl)imide ($[C_2MIM][NTf_2]$) and 1-ethyl-3-methylimidazolium ethylsulfate ($[C_2MIM][EtSO_4]$). Water is miscible with $[C_2MIM][EtSO_4]$ over the whole concentration range, whereas its solubility in $[C_2MIM][NTf_2]$

[*] T. Köddermann, R. Ludwig
Institut für Chemie
Abteilung Physikalische Chemie
Universität Rostock
Dr.-Lorenz-Weg 1, 18051 Rostock (Germany)
Fax: (+49) 381-498-6524
E-mail: ralf.ludwig@uni-rostock.de
C. Wertz, A. Heintz
Institut für Chemie
Abteilung Physikalische Chemie
Universität Rostock
Hermannstrasse 14, 18051 Rostock (Germany)

[**] This research was supported by the State of Mecklenburg-Western Pomerania (Hochschulwissenschaftsprogramm) and the German Science Foundation (DFG, FOR 436).

Supporting information for this article is available on the WWW under http://www.angewandte.org or from the author.

 © 2006 Wiley-VCH Verlag GmbH & Co. KGaA, Weinheim InterScience

is only 1.8 wt% (according to Ref. [22]) or 1.9 wt% (according to Ref. [14]). We recorded FTIR spectra for several water/IL mixtures by using pure ILs as background. At water concentrations of below 1 wt% the spectra did not show further changes with concentration and temperature. Thus we were confident that at these concentrations single water molecules are embedded in the IL environment and that no water clusters exist under these conditions. Water molecules are isolated from each other and interact with the ions of the ionic liquid by H-bonding.

Figure 1 a,b shows the FTIR spectra for H_2O and D_2O dissolved in ILs in the OH/OD-stretching region, respectively. The spectrum of water dissolved in $[C_2MIM][EtSO_4]$ appears

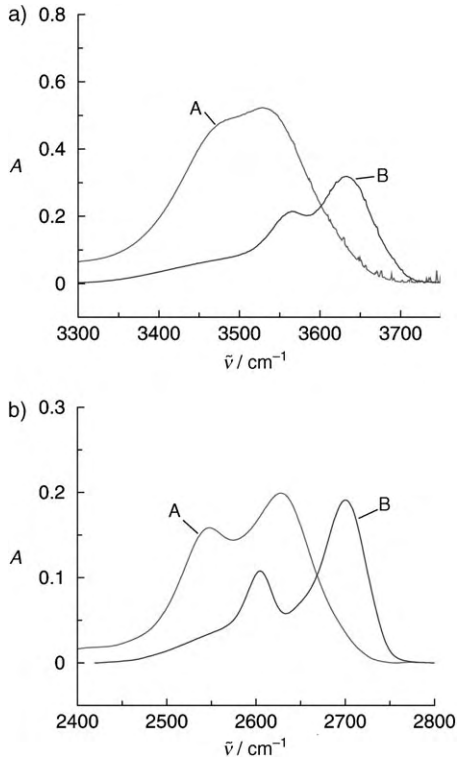

Figure 1. Infrared spectra of a) the OH-stretching region of 1 wt% H_2O solutions and b) the OD-stretching region of 1 wt% D_2O solutions in $[C_2MIM][NTf_2]$ (bands B) and $[C_2MIM][EtSO_4]$ (bands A). The vibrational bands are red-shifted for the solutions in $[C_2MIM][EtSO_4]$.

at lower wavenumbers than that of water in $[C_2MIM][NTf_2]$. Apparently water is more strongly bonded to $[C_2MIM][EtSO_4]$, indicating that this IL has a higher polarity. Because the two ILs include the same cation, this finding also suggests that the association of water is mostly determined by the anion. In the OH/OD-stretching region the two spectra have a similar shape and can be deconvoluted into four/five and five/six Voigt bands, respectively. As a result of the heavier isotope the D_2O spectra are better resolved. Thus the deconvoluted D_2O spectra are referred to in the following discussion (Figure 2). The bands for D_2O in $[C_2MIM][NTf_2]$ are found at 2573, 2605, 2663, 2701, and 2727 cm^{-1} (Figure 2 a). The D_2O bands in $[C_2MIM][EtSO_4]$ lie at 2374, 2508, 2545, 2590, 2630, and 2688 cm^{-1} (Figure 2 b).

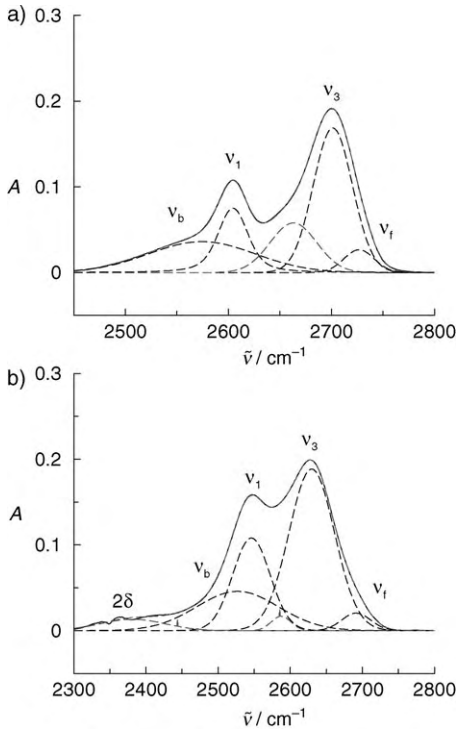

Figure 2. FTIR spectrum of 1 wt% D_2O in a) $[C_2MIM][NTf_2]$ and in b) $[C_2MIM][EtSO_4]$ showing the OD stretching vibrational region. The spectrum could be deconvoluted into five and six bands, respectively. See text for the assignment.

The two most intensive bands are assigned to the asymmetric and symmetric stretching vibrations, ν_3 and ν_1, respectively, of the D_2O molecules. The small central band comes from OD-stretching vibrations of HDO, which is formed by H/D isotope exchange with trace amounts of residual water H_2O. However, here we are interested in the molecular state of water present in ILs. Therefore, this band does not play a further role in our discussion. The two bands left and right of the symmetric and asymmetric stretches are labeled ν_b and ν_f. The band at higher wavenumbers indicates that not all OD groups of single water molecules are involved in D-bonding. We assign the bands at 2727 and 2688 cm^{-1} to OD groups that are "quasi free" (ν_f). The other OD groups of these water molecules are strongly D-bonded to an anion (ν_b). The additional band in the FTIR spectrum of D_2O in $[C_2MIM][EtSO_4]$ with the lowest wavenumber represents the overtone of the water bending modes, 2δ. This water overtone is typically missing in apolar solvents[23,24] and occurs only in strongly confined geometries. The fact that it occurs in $[C_2MIM][EtSO_4]$ and is missing in $[C_2MIM][NTf_2]$ is a first hint of the significantly different polarities of the two ILs.

We assigned our experimental data by comparing the observed with the calculated $\Delta\nu$ shifts, defined as the differences of the stretching vibrations ν_3 and ν_1, and ν_b and ν_f. The frequencies are presented in Table 1. In Figure 3 most representative associates of water molecules with ions of the two ILs are shown. In principle four structure types are possible: In a DD (double donor) structure the water molecule forms two H-bonds either to two anions ($EtSO_4^-$)

 © 2006 Wiley-VCH Verlag GmbH & Co. KGaA, Weinheim

Table 1: Measured and calculated vibrational modes for H_2O and D_2O associated in ionic liquids $[C_2MIM][NTf_2]$ and $[C_2MIM][EtSO_4]$.[a]

	DD			SD			AD		
	ν_3	ν_1	$\Delta\nu$	ν_b	ν_f	$\Delta\nu$	ν_b	ν_f	$\Delta\nu$
$[C_2MIM][NTf_2]$									
H_2O	3638	3561	77	3505	3689	184			
D_2O	2701	2605	96	2573	2727	154			
$[C_2MIM][EtSO_4]$									
H_2O	3540	3468	72	3419	3617	198			
D_2O	2629	2545	84	2696	2488	208			
$[C_2MIM][NTf_2]$									
H_2O	3663	3572	91	3470	3668	198	3657	3284	373
D_2O	2682	2577	105	2691	2522	169	2384	2664	280
$[C_2MIM][EtSO_4]$									
H_2O	3587	3498	89	3417	3633	216	3290	3668	378
D_2O	2612	2529	92	2649	2477	172	2387	2674	287

[a] Frequencies ν and frequency differences $\Delta\nu$ for water in structures DD, SD, and AD are given in wavenumbers [cm^{-1}]. Experimentally no large $\Delta\nu$ values assigned to AD structures could be found.

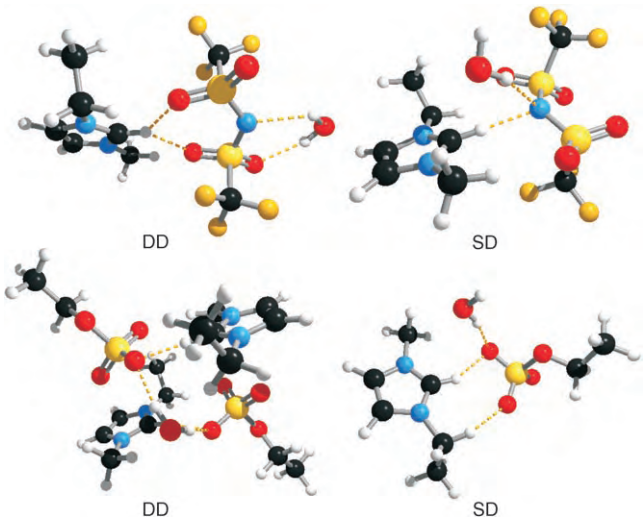

Figure 3. The experimentally possible molecular states of a water molecule in $[C_2MIM][NTf_2]$ (top) and in $[C_2MIM][EtSO_4]$ (bottom) obtained by DFT calculations. O red, H white, N blue, C black, S yellow, F shaded yellow. See text for the assignment.

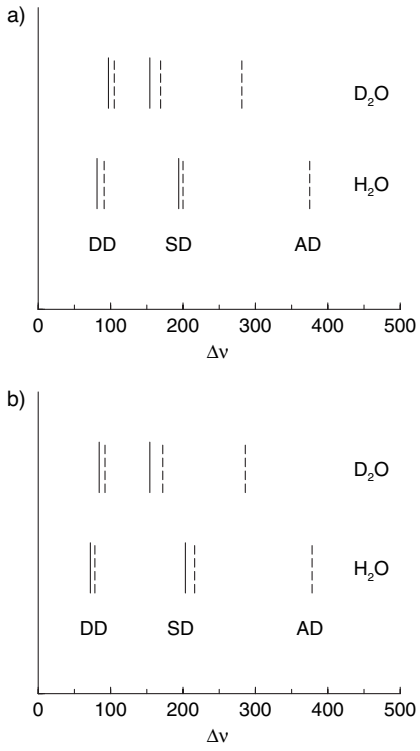

Figure 4. Calculated $\Delta\nu$ values (-----) for vibrational modes of H_2O and D_2O dissolved in a) $[C_2MIM][NTf_2]$ and in b) $[C_2MIM][EtSO_4]$. ——: measured $\Delta\nu$ values. The $\Delta\nu$ values are characteristic for water associated in the DD, SD, and AD structures. It can be clearly concluded that water is associated in the DD and SD structures only.

or to one anion ($EtSO_4^-$, NTf_2^-) only. In a SD (single donor) structure the water molecule forms one strong single H-bond to an anion. In an AD (acceptor and donor) structure water is H-bonded between the cation and the anion, and acts as both donor and acceptor simultaneously.

For these structure types, characteristic $\Delta\nu$ shifts for the stretching frequencies of the water molecule are expected as shown in Figure 4 for $[C_2MIM][NTf_2]$ and $[C_2MIM][EtSO_4]$. For the DD structure $\Delta\nu$ values between 70–80 cm^{-1} are calculated. For water molecules in the SD structure, in which one OH group is H-bonded to the anion and the other one is "quasi free", the value of $\Delta\nu$ increases up to 200 cm^{-1}. The largest gap of about 378 cm^{-1} is obtained for the AD structure, in which one OH group of the water molecule is a proton donor to the anion and a proton acceptor from the IL cation ("sandwich structure"). Because the $\Delta\nu$ values differ significantly for the given structure types, they can be used as a good indication of the molecular state of water in ILs. By comparing the calculated $\Delta\nu$ value with the measured frequency gap, we can conclude that AD structures do not exist and that DD and SD structures are present. Apparently the water molecules are either doubly H-bonded to the IL anion (dominant) or linked to the anion with one OH group and the other one "quasi free". The calculated and measured $\Delta\nu$ values for D_2O suggest the same structure types. It is interesting to note that the $\Delta\nu$ for the symmetric and asymmetric stretches for the DD structure is increased by isotopic substitution. The $\Delta\nu$ values for all other species

 © 2006 Wiley-VCH Verlag GmbH & Co. KGaA, Weinheim

become smaller on going from H_2O to D_2O because the two vibrational bands are no longer coupled. Another interesting finding is that $\Delta\nu$ values between 70 and 80 cm^{-1} do not necessarily suggest a symmetric 2:1 complex of water (2 ILs@1 H_2O) as usually assumed in literature.[20] Water doubly H-bonded to the anion yields comparable $\Delta\nu$ values.

We also show here that both the asymmetric stretch, ν_3, and the symmetric stretch, ν_1, of water are sensitive probes for the polarity of ionic liquids, as expressed by its dielectric constant (ε). Conventional methods for measuring static dielectric constants of ILs fail, because the samples are largely short-circuited as a result of the high electrical conductance. For this reason alternative polarity probes have been introduced based on solvatochromic shifts and fluorescence probe dyes,[22,25] partitioning of solutes in water/IL bilayers,[26] gas chromatography with ILs as stationary phases,[3] and solvent effects on chemical reactions.[27] However, the deduced polarities of ILs differ substantially. Recently, the first values for dielectric constants ε were published by Wakai et al.[28] They determined the static dielectric constants of five ILs by zero-frequency extrapolation of the complex dielectric functions measured by dielectric spectroscopy in the megahertz/gigahertz regime. However, we could not consider the ILs used by Wakai et al.[28] in our present study since four out of the five ILs are known to undergo substantial hydrolysis to form HF upon contact with water.[29]

The vibrational frequencies of single embedded water molecules prove to be a good measure of the polarity of ILs. For this purpose the stretching frequencies of H_2O and D_2O dissolved in trace amounts in simple organic solvents (Table 2) are plotted versus known dielectric constants, ε. Figure 5 shows a linear relationship between ε and the stretching frequencies. If we now plug in our measured frequencies of H_2O and D_2O dissolved in $[C_2MIM][NTf_2]$ and $[C_2MIM][EtSO_4]$), we can predict the dielectric constants of the two ILs. The ε values calculated as the arithmetic mean of the two single values for $\varepsilon(\nu_3)$ and $\varepsilon(\nu_1)$ are given in Table 2. The values are 15.0 and 14.7 for H_2O and D_2O in $[C_2MIM][NTf_2]$ and 37.3 and 38.6 for H_2O and D_2O in $[C_2MIM][EtSO_4]$, respectively. Whereas $[C_2MIM][EtSO_4]$ has a dielectric constant close to that of dimethyl sulfoxide and thus indicating strong polarity, $[C_2MIM][NTf_2]$ has a much lower ε value close to that of 1,2-dichloroethane. The predicted dielectric constants suggest that water is miscible with $[C_2MIM][EtSO_4]$ over the whole concentration range, whereas it shows a large miscibility gap in $[C_2MIM][NTf_2]$.[22]

We are confident that our method is a more reliable measure of the dielectric constant and polarity of an IL than the use of solvatochromatic shifts and fluorescence probe dyes.[25a] The unusually large negative solvatochromism of a standard betaine dye has been used to introduce an empirical scale of solvent polarity, referred to as the $E_T(30)$ or E^N_T scale. For $[C_2MIM][NTf_2]$, $E_T(30)$ values of about 52.6, 53.1, 47.6[25a] as well as estimated values of about 46.5, 47.7 and 48.5 have been reported.[25g] If one assumes a linear relationship between $E_T(30)$ and ε for simple organic solvents, dielectric constants between 27 and 44 are obtained for this IL (see Figure S1 in the Supporting Information). ILs having such high dielectric constants would be definitely miscible with water, in contradiction to experimental results. Additionally, the obtained ε values span a wide range which is in the order of the dielectric constant itself, indicating that predictions using this method are not really reliable.

Table 2: Wavenumbers [cm^{-1}] of the vibrational modes ν_3 and ν_1 of H_2O and D_2O in the gas phase, dissolved in organic solvents,[17c,f,19,20,24] and in the ionic liquids $[C_2MIM][NTf_2]$ and $[C_2MIM][EtSO_4]$.[a]

H_2O in solvent	ν_3	ν_1	ε	$\varepsilon(\nu_3)$[b]	$\varepsilon(\nu_1)$[b]
gas phase, no anion	3756	3657			
CCl_4	3708	3616	2.2		
benzene	3687	3598	2.3		
1,2-dichloroethane	3671	3592	10.65		
benzaldehyde	3639	3544	17.0		
acetophenone	3612	3535	18.3		
acetone	3605	3533	20.7		
DMSO	3504	3429	46.7		
γ_0	3707.97	3619.32			
m	−4.43865	−4.09055			
R	0.987174	0.988589			
$[C_2MIM][NTf_2]$	3635	3562		15.76	14.01
$[C_2MIM][EtSO_4]$	3540	3469		37.84	36.75
D_2O in solvent	ν_3	ν_1	ε	$\varepsilon(\nu_3)$[b]	$\varepsilon(\nu_1)$[b]
gas phase, no anion	2788	2671			
CCl_4	2752	2643	2.2		
benzene	2734	2630	2.3		
acetone	2681	2580	20.7		
DMSO	2608	2525	46.7		
γ_0	2749.19	2640.4			
m	−3.05007	−2.52958			
R	0.993054	0.992204			
$[C_2MIM][NTf_2]$	3635	3562		15.47	14.0
$[C_2MIM][EtSO_4]$	3540	3469		39.40	37.72

[a] In addition, the dielectric constants ε for organic solvents from experiments and the predicted $\varepsilon(\nu_3)$ and $\varepsilon(\nu_1)$ values for both ILs are given. [b] The predicted values are obtained by using the linear dependence of the vibrational modes of water and the dielectric constant of the organic solvents. Values of the intercepts γ_0, slopes m, and correlation coefficients R are given in the table.

If we apply our procedure to the IL $[C_4MIM][BF_4]$ for which ν_1 and ν_3 of dissolved water[20] are known, we predict a dielectric constant of 14.9, which is close the ε value of 11.7 ± 0.7 determined by microwave dielectric spectroscopy.[28] Again, $E_T(30)$ values[25a,g] for this IL give much too large dielectric constants ($\varepsilon = 28$–48). Moreover, depending on the method and the probe molecule used, a wide range of values results (see the Supporting Information).

Our proposed method may be limited by the assumption that ILs are homogeneous fluids. In fact there is evidence that imidazolium-based ILs have polar and non-polar regions, in particular upon addition of controlled amounts of water.[30] ILs may be regarded as nanostructured materials.[4,31] This must be checked by measuring more ionic liquids with different kinds of cations and anions.

With a combination of FTIR and ab initio calculations we have studied the structure of water molecules strongly confined by hydrogen bonding in two ILs. We find that two

 © 2006 Wiley-VCH Verlag GmbH & Co. KGaA, Weinheim

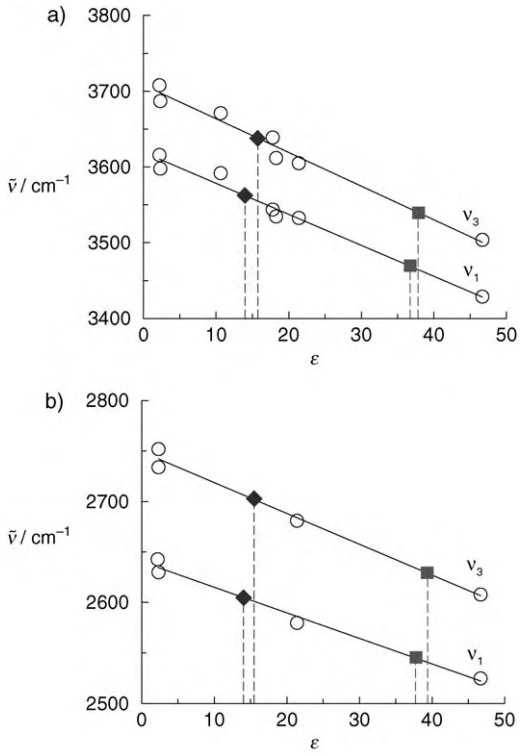

Figure 5. Predicted dielectric constants ε for $[C_2MIM][NTf_2]$ (◆) and $[C_2MIM][EtSO_4]$ (■). The symmetric and asymmetric stretch frequencies of a) H_2O and b) D_2O dissolved in simple organic liquids are plotted versus dielectric constants ε of the solvents.[17a,d,f,23,24] The linear relationships between both properties allows a prediction of ε by using the measured ν_3 and ν_1 values. The predicted ε value can be read off from the *x*-axis (-----).

water configurations exist. In the DD structure both OH/OD groups are bonded to the IL anion and in an SD structure only one OH/OD group is strongly H-bonded while the other one is "quasi free". We could show that the vibrational modes of single water molecules dissolved in ILs are sensitive probes for their polarity. This is particularly important because conventional methods to measure dielectric constants in ILs fail and alternative polarity probes based on solvatochromatic shifts and fluorescence probe dyes are not accurate. Our method based on standard FTIR spectroscopy is generally accessible and allows a straightforward determination of IL polarities.

Experimental Section

Mixtures of 0.4 wt% and 1.0 wt% of H_2O and D_2O (Sigma Aldrich, with a stated purity of 100 atom% D) and $[C_2MIM][NTf_2]$ and $[C_2MIM][EtSO_4]$) were prepared. $[C_2MIM][NTf_2]$ was synthesized by the group of P. Wasserscheid at the University of Erlangen. The halogen-free method of preparation for $[C_2MIM][NTf_2]$ has been described in detail.[32] $[C_2MIM][EtSO_4]$ (ECOENG™212), provided by Solvent Innovation, was used without further purification. The purity of the sample was specified as 98%. For all ionic liquids the H_2O content was determined by Karl Fischer titration.

Infrared measurements were performed with a Bruker Vector 22 FTIR spectrometer. An L.O.T.-Oriel variable-temperature cell equipped with CaF_2 windows having a path length of 0.025 mm was used for the variable-temperature experiments. For each spectrum 128 scans were recorded at a spectral resolution of 1 cm^{-1}. Solvent subtraction (ILs) was carried out by using reference spectra obtained at exactly the same temperatures as the sample spectra.

Density functional calculations were carried out using the Gaussian 98 program.[33] All clusters were calculated with the B3LYP nonlocal exchange correlation functional using a 6-31 + G* basis set. The calculated harmonic vibrational frequencies were scaled (0.96). Only the OH/OD-stretching vibrations were discussed.

Received: December 16, 2005
Revised: February 28, 2006
Published online: April 25, 2006

Keywords: density functional calculations · ionic liquids · IR spectroscopy · polarity · water

[1] D. Rogers, K. R. Seddon, S. Volkov, *Green Industrial Applications of ionic Liquids*, NATO Science Series, **2002**.
[2] P. Wasserscheid, T. Welton, *Ionic Liquids in Synthesis*, Wiley-VCH, Weinheim, **2003**, pp. 1–6.
[3] J. L. Anderson, J. Ding, T. Welton, D. W. Armstrong, *J. Am. Chem. Soc.* **2002**, *124*, 14247–14254.
[4] J. Dupont, R. F. de Souza, *Chem. Rev.* **2002**, *102*, 3667–3691.
[5] C. E. Song, *Chem. Commun.* **2004**, 1033–1043.
[6] C. Baudequin, J. Baudoux, J. Levillain, D. Cahard, A. C. Gaumont, J. C. Plaquevent, *Tetrahedron: Asymmetry* **2003**, *14*, 3081–3093.
[7] A. Heintz, *J. Chem. Thermodyn.* **2005**, *37*, 525–535.
[8] J. Wang, Y. Tian, Y. Zhao, K. Zhuo, *Green Chem.* **2003**, *5*, 618–622.
[9] J. A. Widegren, A. Laesecke, J. W. Magee, *Chem. Commun.* **2005**, 1610–1612.
[10] J. A. Widegren, E. M. Saurer, K. N. Marsh, J. W. Magee, *J. Chem. Thermodyn.* **2005**, *37*, 569–575.
[11] R. A. Brown, P. Mollet, E. McKoon, C. A. Eckert, C. L. Liotta, P. G. Jessop, *J. Am. Chem. Soc.* **2001**, *123*, 1254–1255.
[12] P. M. Mancini, G. G. Fortunate, L. R. Vottero, *Phys. Chem. Liq.* **2004**, *42*, 625–632.
[13] C. Debdeep, C. Anjan, S. Debabrata, S. Nilmoni, *J. Phys. Chem. A* **2005**, *109*, 1764–1769.
[14] A. Heintz, J. K. Lehmann, C. Wertz, J. Jacquemin, *J. Chem. Eng. Data* **2005**, *50*, 956–960.
[15] V. Najdanovic-Visak, L. P. N. Rebelo, M. N. da Ponte, *Green Chem.* **2005**, *7*, 443–450.
[16] V. Najdanovic-Visak, J. M. S. S. Esperança, L. P. N. Rebelo, M. N. da Ponte, H. J.R Guedas, K. R. Seddon, H. C. de Souza, J. Szydlowski J. *Phys. Chem. B* **2003**, *107*, 12797–12807.
[17] a) E. Zoidis, J. Yarwood, T. Tassaing, Y. Danten, M. Besnard, *J. Mol. Liq.* **1995**, *64*, 167–210; b) B. C. Bricknell, T. A. Ford, T. M. Letcher, *Spectrochim. Acta Part A* **1997**, *53*, 299–315; c) G. G. Devyatykh, P. G. Sennikov, *Usp. Khim.* **1995**, *64*, 817–830; d) P. Backx, S. Goldmann, *J. Phys. Chem.* **1981**, *85*, 2975–2979; e) S. G. Kazarian, N. M. B. Flichy, D. Coombs, G. Poulter, *Am. Lab.* **2001**, *33*, 44–49; f) J. R. Scherer in *Advances in Infrared Raman Spectroscopy*, *Vol. 5* (Eds.: R. J. H. Clark, R. E. Hester), Heyden, London, **1978**.
[18] R. Ludwig, *Angew. Chem.* **2001**,113, 1856–1876; *Angew. Chem. Int. Ed.* **2001**, *40*, 1808–1827.
[19] L. F. Scatena, M. G. Brown, G. L. Richmond, *Science* **2001**, *292*, 908–912.
[20] L. Cammarata, S. G. Kazarian, P. A. Salter, T. Welton, *Phys. Chem. Chem. Phys.* **2001**, *3*, 5192–5200.
[21] C. D. Tran, S. H. de Paoli Lacerda, D. Oliveira, *Appl. Spectrosc.* **2003**, *57*, 152–156.

 © 2006 Wiley-VCH Verlag GmbH & Co. KGaA, Weinheim

[22] P. Bonhôte, A.-P. Dias, N. Papageogiou, K. Kalyanasundaram, M. Grätzel, *Inorg. Chem.* **1996**, *35*, 1168 – 1178.
[23] Y. Danten, T. Tassaing, M. Besnard, *J. Phys. Chem. A* **2000**, *104*, 9415 – 9427.
[24] T. Köddermann, F. Schulte, M. Huelsekopf, R. Ludwig, *Angew. Chem.* **2003**, *115*, 5052 – 5056; *Angew. Chem. Int. Ed.* **2003**, *42*, 4904 – 4908.
[25] a) C. Reichardt, *Green Chem.* **2005**, *7*, 339 – 351; b) P. Wasserscheid, C. M. Gordon, C. Hilgers, M. J. Muldoon, I. R. Dunkin, *Chem. Commun.* **2001**, 1186 – 1187; c) S. N. V. K. Aki, J. F. Brennecke, A. Samanta, *Chem. Commun.* **2001**, 413 – 414; d) A. J. Carmichael, K. R. Seddon, *J. Phys. Org. Chem.* **2000**, *13*, 591 – 596; e) L. Crowhurst, P. R. Mawdseley, J. M. Perez-Arlandiz, P. A. Salter, T. Welton, *Phys. Chem. Chem. Phys.* **2003**, *5*, 2790 – 2795; f) R. Karmakar, A. Samanta, *J. Phys. Chem. A* **2003**, *107*, 7340 – 7346; g) R. Karmakar, A. Samanta, *J. Phys. Chem. A* **2002**, *106*, 6670 – 6675.
[26] J. G. Huddleston, H. D. Willauer, R. P. Swatloski, A. E. Visser, R. D. Rodgers, *Chem. Commun.* **1998**, 1765 – 1766.
[27] M. J. Earle, B. S. Engel, K. R. Seddon, *Aust. J. Chem.* **2004**, *57*, 149 – 150.
[28] C. Wakai, A. Oleinikova, M. Ott, H. Weingärtner, *J. Phys. Chem. B* **2005**, *109*, 17028 – 17030.
[29] P. Wasserscheid, R. v. Hal, A. Bösmann, *Electrochem. Soc. Proc.* **2002**, *19*, 146 – 154.
[30] U. Schröder, J. D. Wadhawan, R. G. Compton, F. Marken, P. A. Z. Suarez, C. S. Consorti, R. F. de Souza, J. Dupont, *New J. Chem.* **2000**, *24*, 1009 – 1015.
[31] M. Antonietti, D. Kuang, B. Smarsly, Y. Zhou, *Angew. Chem.* **2004**, *116*, 5096 – 5100; *Angew. Chem. Int. Ed.* **2004**, *43*, 4988 – 4992.
[32] A. Heintz, J. K. Lehmann, C. Wertz, *J. Chem. Eng. Data* **2003**, *48*, 472 – 474.
[33] Gaussian 98 (Revision A.1), M. J. Frisch, G. W. Trucks, H. B. Schlegel, G. E. Scuseria, M. A. Robb, J. R. Cheeseman, V. G. Zakrzewski, J. A. Montgomery, R. E. Stratmann, J. C. Burant, S. Dapprich, J. M. Millam, A. D. Daniels, K. N. Kudin, M. C. Strain, O. Farkas, J. Tomasi, V. Barone, M. Cossi, R. Cammi, B. Mennucci, C. Pomelli, C. Adamo, S. Clifford, J. Ochterski, G. A. Petersson, P. Y. Ayala, Q. Cui, K. Morokuma, D. K. Malick, A. D. Rabuck, K. Raghavachari, J. B. Foresman, J. Cioslowski, J. V. Ortiz, B. B. Stefanov, G. Liu, A. Liashenko, P. Piskorz, I. Komaromi, R. Gomperts, R. L. Martin, D. J. Fox, T. Keith, M. A. Al-Laham, C. Y. Peng, A. Nanayakkara, C. Gonzalez, M. Challacombe, P. M. W. Gill, B. G. Johnson, W. Chen, M. W. Wong, J. L. Andres, M. Head-Gordon, E. S. Replogle, J. A. Pople, Gaussian, Inc., Pittsburgh, PA, **1998**.

 © 2006 Wiley-VCH Verlag GmbH & Co. KGaA, Weinheim

Cluster Compounds

DOI: 10.1002/anie.200504566

The Phosphine-Stabilized Gold–Arsenic Clusters $[Au_{19}(AsnPr)_8(dppe)_6]Cl_3$, $[Au_{10}(AsnPr)_4(dppe)_4]Cl_2$, $[Au_{17}(AsnPr)_6(As_2nPr_2)(dppm)_6]Cl_3$, and $[Au_{10}(AsPh)_4(dppe)_4]Cl_2$: Synthesis, Characterization, and DFT Calculations**

Paloma Sevillano, Olaf Fuhr, Marco Kattannek, Paola Nava, Oliver Hampe, Sergej Lebedkin, Reinhart Ahlrichs, Dieter Fenske, and Manfred M. Kappes*

Dedicated to Professor Hans Georg von Schnering on the occasion of his 75th birthday

A limited number of gold–arsenic complexes have been described in the literature, including compounds containing arsenic bridges (for example, $[(Ph_3PAu)_4As]BF_4$,[1] $[Au_4(As_4Ph_4)_2(PnPr_3)_4]$,[2] and $[Au_{10}(AsPh)_4(PhAsSiMe_3)_2(PnPr_3)_6]$[2]) or terminal AsR_3 ligands (for example, $[(Ph_3As)_xAu]BF_4$ ($x=2$, 4),[3] $[(Ph_3AsAu)_3O]BF_4$,[3] $[Au(C_6F_5)\{(SPh_2)_2C(AuAsPh_3)_2\}]ClO_4$,[4] and $[Au_4Cl_2\{Ph_2PCH_2As(Ph)CH_2PPh_2\}_2]X_2$ ($X=PF_6$, NO_3)[5]), as well as $[Au_{16}(AsPh_3)_8Cl_6]$, which contains a centered icosahedron of 13 gold atoms.[6] In contrast, the rich chemistry of gold and gold–chalcogen clusters has been extensively studied.[7–10] At first, it seemed that gold clusters preferred icosahedral structures or fragments thereof,[7a,b,8d] but a variety of other structural motifs have since been encountered: tetrahedra ($[tBu_3PAu]_4(BF_4)_2$[9c] and $[(R_3PAu)_4O](BF_4)_2$ ($R=Ph$, o-C_6H_4Me)[9k]), square pyramids ($[(Ph_3PAu)_5P](BF_4)_2$,[9l]), trigonal bipyramids ($[\{(Ph_3P)_6Au_5\}P](BF_4)_3$[9j]), edge-sharing bi-tetrahedra ($[Au_6(PPh_3)_6](NO_3)_2$[8g]), noncentered and centered crowns (K[Au-

[*] Dr. P. Sevillano, Dr. O. Fuhr, Prof. Dr. D. Fenske
Institut für Anorganische Chemie
Universität Karlsruhe, 76128 Karlsruhe (Germany)
Fax: (+49) 721-608-8440
E-mail: dieter.fenske@aoc1.uni-karlsruhe.de
and
Institut für Nanotechnologie, Forschungszentrum Karlsruhe
Postfach 3640, 76021 Karlsruhe (Germany)
Dr. O. Hampe, Dr. S. Lebedkin, Prof. Dr. M. M. Kappes
Institut für Physikalische Chemie
Universität Karlsruhe, 76128 Karlsruhe (Germany)
and
Institut für Nanotechnologie, Forschungszentrum Karlsruhe
Postfach 3640, 76021 Karlsruhe (Germany)
M. Kattannek, Dr. P. Nava, Prof. Dr. R. Ahlrichs
Institut für Physikalische Chemie
Lehrstuhl für Theoretische Chemie
Universität Karlsruhe, 76128 Karlsruhe (Germany)

[**] This work was supported by the Deutsche Forschungsgemeinschaft (Center for Functional Nanostructures), the Deutsch-Israelisches Programm (DIP), and the Fonds der Chemischen Industrie. dppe = 1,2-bis(diphenylphosphanyl)ethane, dppm = bis(diphenylphosphanyl)methane.

© 2006 Wiley-VCH Verlag GmbH & Co. KGaA, Weinheim

$(AuCl)(AuPPh_3)_8](PF_6)_2$[9n] and $[Au_9\{P(p\text{-}C_6H_4OMe)_3\}_8](BF_4)_3$[8c]), and octahedra ($[Au_6\{P(p\text{-}C_6H_4Me)_3\}_6](BF_4)_2$[7c] and $[(Ph_3PAu)_6C](CH_3OBF_3)_2$[8i]).

Herein, we report the synthesis and properties of the new compounds **1**–**4** obtained from reactions of gold(I) phosphine complexes with $As(R)(SiMe_3)_2$ (R = *n*Pr, Ph; Scheme 1).

$$[(AuCl)_2dppe] + As(nPr)(SiMe_3)_2 \xrightarrow{CH_2Cl_2} [Au_{19}(AsnPr)_8(dppe)_6]Cl_3\ (\mathbf{1}) + [Au_{10}(AsnPr)_4(dppe)_4]Cl_2\ (\mathbf{2})$$

$$[(AuCl)_2dppm] + As(nPr)(SiMe_3)_2 \xrightarrow{CH_2Cl_2} [Au_{17}(AsnPr)_6(As_2nPr_2)(dppm)_6]Cl_3\ (\mathbf{3})$$

$$[(AuCl)_2dppe] + As(Ph)(SiMe_3)_2 \xrightarrow{CH_2Cl_2} [Au_{10}(AsPh)_4(dppe)_4]Cl_2\ (\mathbf{4})$$

Scheme 1. Synthesis of compounds **1**–**4**. dppm = $Ph_2PCH_2PPh_2$, dppe = $Ph_2P(CH_2)_2PPh_2$.

The structures of **1**–**4** were determined by single-crystal X-ray diffraction (Figures 1–3). However, the nature of the central atom in **1** and the charge of the cluster could not be unambiguously established on the basis of the diffraction analysis. Therefore, electrospray ionization mass spectrometry (ESI-MS) experiments[11–13] (for **1**–**3**) and density functional theory (DFT) calculations (for **1** and **3**) were performed. Furthermore, photoluminescence measurements were carried out to elucidate the origin of the unexpectedly dark color of **1**.

The positive-ion Fourier transform mass spectrum obtained upon electrospraying a CH_2Cl_2 solution of **1** and **2** is shown in Figure 4. The main peak V can be unambiguously assigned to the triply charged cluster ion $[Au_{19}(AsnPr)_8(dppe)_6]^{3+}$ in **1** on the basis of the *m*/*z* value (Table 1) and the highly resolved isotope splitting (Figure 4, inset). Peak VI

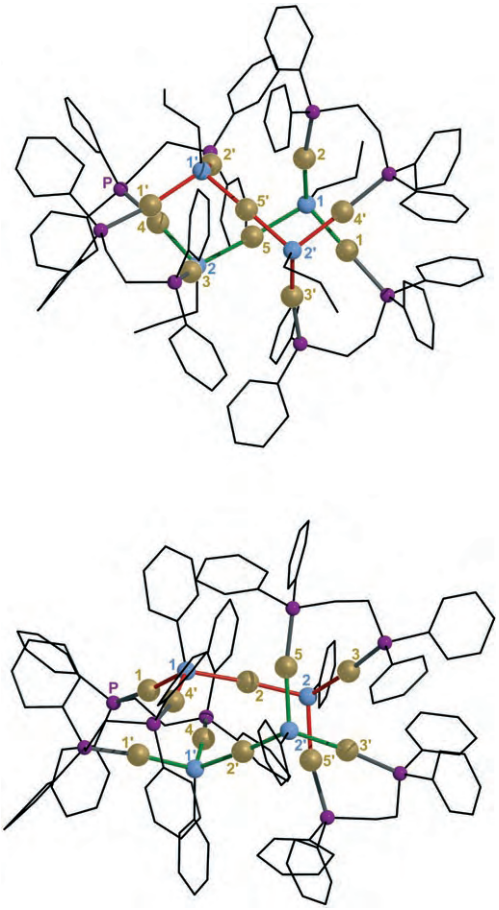

Figure 2. Molecular structures of the cations in **2** (top; one of two independent molecules) and **4** (bottom). For clarity atoms are only numbered; Au gold, As blue, P violet; organic groups represented with black sticks. Selected distances [pm] and angles [°]: **2**: Au–Au ≥ 298.0(2), Au–As 243.3(3)–245.8(3), Au–P 230.1(8)–233.2(9); As-Au-As 169.85(1)–172.62(1), As-Au-P 166.4(2)–169.6(2), Au-As-Au 99.1(1)–114.0(1). **4**: Au–Au ≥ 290.1(1), Au–As 242.9(2)–246.6(2), Au–P 230.1(5)–233.1(4); As1-Au2-As2 176.51(6), As-Au-P 165.3(1)–175.1(1), Au-As-Au 105.44(6)–111.99(7).

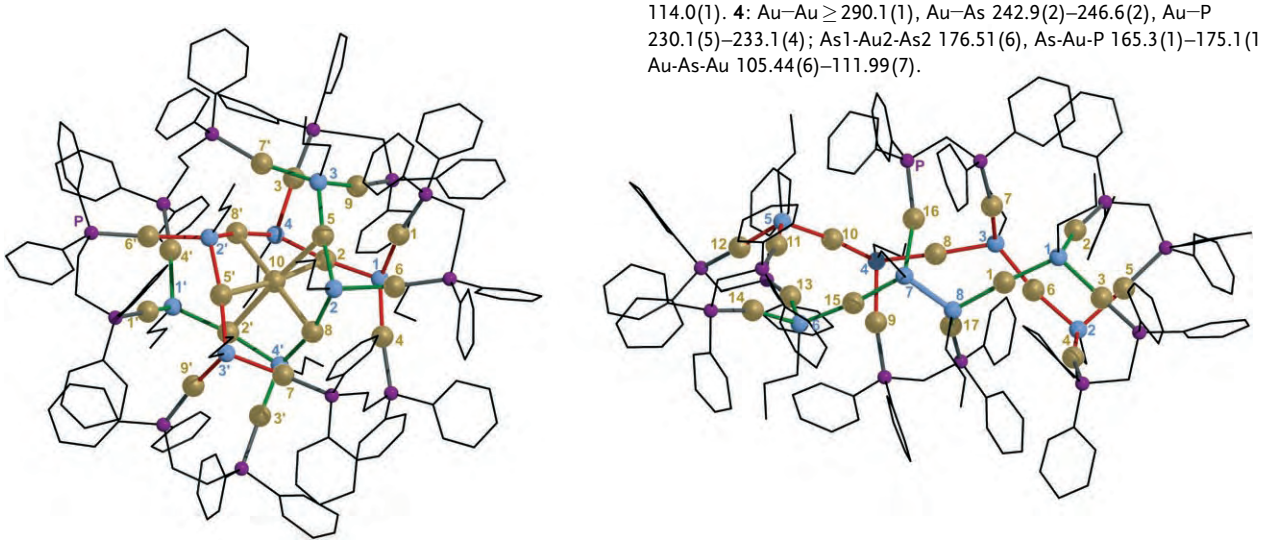

Figure 1. Molecular structures of the cations in **1** (left; molecule I) and **3** (right). For clarity atoms are only numbered; Au gold, As blue, P violet; organic groups represented with black sticks. Selected distances [pm] and angles [°]: **1**: Au10–Au8 263.0(1), Au10–Au5 286.4(1), Au10–Au2 287.7(1), other Au–Au ≥ 292.8(1), Au–As 239.6(3)–246.2(2), Au–P 228.9(7)–232.2(5); Au8-Au10-Au8′ 175.82(9), Au2-Au10-Au5′ 173.63(4), Au2-Au10-Au2′ 116.13(7), Au5-Au10-Au5′ 110.73(7), Au8-Au10-Au5 87.98(3), Au8-Au10-Au5′ 94.40(4), Au8-Au10-Au2 91.40(4), Au5-Au10-Au2 66.88(3), As-Au-As 163.9(1)–173.9(1), As-Au-P 162.4(2)–170.2(1), Au-As-Au 100.60(9)–117.23(8). **3**: As7–As8 239.7(3), Au–Au ≥ 290.7(2), Au–As 244.2(3)–241.0(3), Au–P 227.5(8)–232.0(7); As-Au-As 170.3(1)–173.7(1), As-Au-P 153.9(2)–173.7(2), Au-As-Au 96.53(9)–121.4(1), As-As-Au 108.9(1)–110.7(1).

 © 2006 Wiley-VCH Verlag GmbH & Co. KGaA, Weinheim

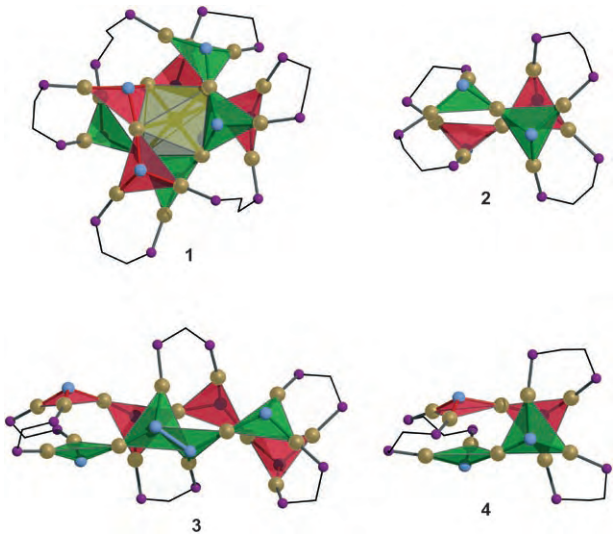

Figure 3. Polyhedral representations of the cations in **1**–**4** highlighting the chains of Au_3As (and Au_2As_2 in **3**) tetrahedra (red and green). Au gold, As blue, P violet; organic groups represented with black sticks; propyl and phenyl groups omitted for clarity.

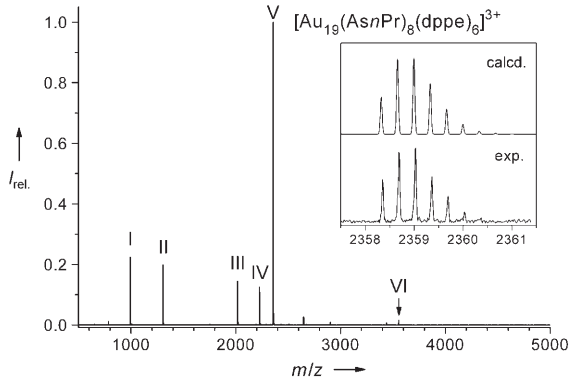

Figure 4. ESI mass spectrum (positive-ion mode) of **1** and **2** in CH_2Cl_2. Inset: comparison of the calculated isotope splitting of the $[Au_{19}(AsnPr)_8(dppe)_6]^{3+}$ ion and the observed isotope splitting of peak V. For a complete peak assignment, see Table 1.

Table 1: Assignment of monoisotopic *m*/*z* peaks observed in the ESI mass spectrum of **1** and **2** to cluster ions and comparison to the calculated *m*/*z* values (see Figure 4).

Peak	*m*/*z*		Ion
	exp.	calcd.	
I	993.235	993.236	$[Au(dppe)_2]^+$
II	1306.075	1306.077	$[Au_6(AsnPr)_2(dppe)_3]^{2+}$
III	2017.048	2017.053	$[Au_{10}(AsnPr)_4(dppe)_4]^{2+}$
IV	2227.006	2227.015	$[Au_{17}(AsnPr)_8(dppe)_6]^{3+}$
V	2358.301	2358.326	$[Au_{19}(AsnPr)_8(dppe)_6]^{3+}$
VI	3554.962	3554.974	$[Au_{19}(AsnPr)_8(dppe)_6Cl]^{2+}$

also stems from **1**: it results from the association of one Cl^- counterion to the trication (such ion-pair formation is common in ESI-MS). We assign peak III to the cluster cation of **2**, and peak IV to a cluster of composition $[Au_{17}(AsnPr)_8(dppe)_6]^{3+}$ with an unknown structure. In the ESI mass spectrum of a solution of **3**, we unequivocally identify the ion $[Au_{17}(AsnPr)_8(dppm)_6]^{3+}$, as well as the ion pair $[Au_{17}(AsnPr)_8(dppm)_6Cl]^{2+}$, which indicates the presence of Cl^- as a counterion in **3** (Figure 5).

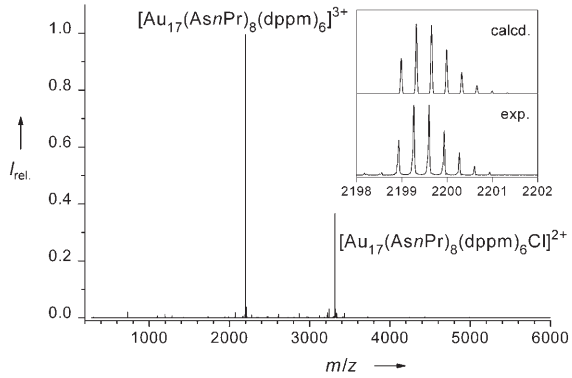

Figure 5. ESI mass spectrum (positive-ion mode) of **3** in CH_2Cl_2. Inset: comparison of the experimental and calculated isotope splitting of the $[Au_{17}(AsnPr)_8(dppm)_6]^{3+}$ ion peak.

Compounds **1**–**4** each contain two chains of corner-sharing Au_3As tetrahedra, which are compressed along their C_3 axes (Figure 3). The Au_3 faces of opposing tetrahedra in different chains form elongated trigonal antiprisms. The gold atoms within each chain are nearly linearly coordinated (153.9–176.5°) by either two arsenic atoms, or by one arsenic atom and one phosphorus atom. In most cases, the arsenic atoms are bonded to three gold atoms and an organic group, in a distorted tetrahedral arrangement. The bidentate phosphine ligands interconnect the chains of Au_3As tetrahedra. All Au–As and Au–P distances are within the expected ranges.

A new structural feature is found in **1**: a centered octahedron of seven gold atoms (Figure 1). Compound **1** crystallizes in the tetragonal space group $P4_2/nbc$ with twelve formula units per unit cell.[14] The asymmetric unit comprises one half and one quarter of two molecules (I and II), which occupy two different crystallographic positions (with site symmetries C_2 and D_2). The two molecules have identical compositions and slightly different structural parameters (Table 2). The trications of **1** consist of two helically arranged U-shaped Au_9As_4 chains, which are each built up from four corner-sharing Au_3As tetrahedra (Figures 1 and 3). The six gold atoms at the shared corners in the two chains form a distorted octahedron, which contains Au10 at its center. Interactions between the central atom and the vertex atoms lead to two very short distances (Au10–Au8) and four longer ones (Au10–Au5 and Au10–Au2; Table 2, entries 1–3). The angles between the gold atoms in the octahedron range from 66.88(3)–116.13(7)° (*cis*) and from 173.67(4)–175.82(9)° (*trans*). The resulting Au–Au edge distances, which are larger than 316.3 pm, indicate weak aureophilic interactions.[15]

Compound **2** crystallizes in the orthorhombic space group $C222_1$ with eight formula units per unit cell.[14] The asymmetric unit contains two half molecules, whose structural parameters are nearly identical within standard deviations.

 © 2006 Wiley-VCH Verlag GmbH & Co. KGaA, Weinheim

Table 2: Comparison of selected experimental and calculated interatomic distances [pm] in molecules I and II of **1** and in the model compounds **1a**, **1b**, and **1c**.[a]

Entry	Bond	Exp. I X = Au10 $q = +3$	Exp. II X = Au10 $q = +3$	**1a** X = Au $q = +3$	**1b** X = As $q = -1$	**1c** X = As $q = +1$
1	X–Au2	287.7(1)	281.8(1)	291.4	284.8	277.6
2	X–Au5	286.4(1)	281.8(1)	291.4	284.8	277.6
3	X–Au8	263.0(1)	265.9(1)	272.1	269.6	275.5
4	As1–Au2	243.4(2)	243.6(2)	247.8	249.0	246.8
5	As2–Au8	240.2(3)	240.0(2)	245.8	248.1	247.6
6	As3–Au5	242.8(2)	243.6(2)	247.8	249.0	246.8
7	As3′–Au7	243.8(2)	244.5(2)	246.9	246.5	246.8
8	As3–Au9	244.0(2)	246.2(2)	246.3	246.4	246.0
9	As4–Au2	242.7(2)	243.4(2)	246.5	249.8	250.2
10	As4′–Au8	239.6(3)	240.0(2)	245.8	248.1	247.6
11	As4–Au3	242.8(3)	241.2(2)	245.6	244.4	244.6
12	Au7–P	229.8(5)	230.5(6)	233.1	231.5	232.4
13	Au3–P	229.7(8)	228.9(7)	232.7	233.8	233.0
14	Au9–P	231.9(7)	231.5(6)	233.2	231.9	232.7

[a] The atomic numbering refers to Figure 1. Columns Exp. I and Exp. II contain the experimental data for molecules I (C_2 symmetry) and II (D_2 symmetry) of **1**, respectively. X specifies the central atom (Au10 in **1**; Figure 1) and q the charge (+3 in **1**) of the model compounds $[XAu_{18}(AsnPr)_8\{Me_2P(CH_2)_2PMe_2\}_6]^q$.

The cations consist of two opposing Au_5As_2 units that are composed of two corner-sharing Au_3As tetrahedra each (Figures 2 and 3). Analogous structures have been observed for gold selenide clusters, for example, $[Au_{10}Se_4(dppm)_4]^{2+}$, $[Au_{10}Se_4(dpppe)_4]^{2+}$ (dpppe = $Ph_2P(CH_2)_5PPh_2$), and $[Au_{10}Se_4(depe)_4]^{2+}$ (depe = $Et_2P(CH_2)_2PEt_2$).[10b,c]

Compound **3** crystallizes in the triclinic space group $P\bar{1}$ with two formula units per unit cell.[14] The molecular structure of the trication can be described as two opposing zigzag chains of gold–arsenic tetrahedra with the compositions Au_9As_4 and Au_8As_4 (Figures 1 and 3). The Au_9As_4 chain consists of four corner-sharing Au_3As tetrahedra, as observed in the chains **1** and **2**. The Au_8As_4 chain is built from two Au_3As tetrahedra and two interpenetrating Au_2As_2 tetrahedra, which share a common As1–As2 edge from an As_2nPr_2 group. The appearance of ligands containing As–As bonds, formed by redox side-reactions, has also been observed for arsenide clusters of other coinage metals.[2]

Compound **4** crystallizes in the orthorhombic space group *Pbcn* with four formula units per unit cell.[14] The dication in **4** has a structure very similar to that of **2** (Figures 2 and 3), containing two opposing Au_5As_2 units that are each composed of two Au_3As tetrahedra.

To clarify both the composition and the charge of the $[Au_{19}(AsnPr)_8(dppe)_6]^{3+}$ ion in **1**, DFT calculations were undertaken, prior to the ESI-MS characterization. The structure of the cation in **3** was also investigated to ascertain the performance of the computational method.

The calculated and experimental interatomic distances of the cation of **3** are compared in Figure 6. All of the calculated As–X (X = Au, As, P) and more than 90% of the calculated Au–X bond lengths are within 6 pm of the experimental lengths, the calculated values always being larger than the experimental ones. The largest deviations in the Au–Au

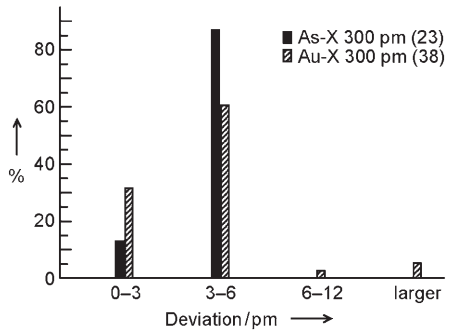

Figure 6. Histogram of deviations between experimental and calculated interatomic distances in the cation of **3**. Two types of distances are considered: As–X and Au–X (X = Au, As, P) up to 300 pm. The number of cases of each type is given in brackets.

distances occur for the nonbonded atom pairs Au3–Au4 (12 pm) and Au12–Au13 (17 pm; Figure 1). The proximity of these pairs of atoms is imposed by the bidentate phosphine ligands, which predictably leads to larger errors in the calculated distances. Thus, the accuracy of the calculated structure of **3** is similar to that attained for other cluster compounds;[11,16] with the exception of particularly long or weak bonds, the calculated and measured bond distances differ by less than 6 pm.

For the cluster of **1**, three model compounds **1a–c** of formula $[XAu_{18}(AsnPr)_8\{Me_2P(CH_2)_2PMe_2\}_6]^q$, where X is the atom in position Au10 (Figure 1), and q is the ion charge, were considered and structurally optimized.

$[AuAu_{18}(AsnPr)_8\{Me_2P(CH_2)_2PMe_2\}_6]^{3+}$ (X = Au, $q = +3$) **1a**

$[AsAu_{18}(AsnPr)_8\{Me_2P(CH_2)_2PMe_2\}_6]^{-}$ (X = As, $q = -1$) **1b**

$[AsAu_{18}(AsnPr)_8\{Me_2P(CH_2)_2PMe_2\}_6]^{+}$ (X = As, $q = +1$) **1c**

On the basis of the structural analysis, **1a** seemed to be the most likely variant. Model compounds **1b** and **1c** were chosen, because in these variants the gold atom at the center of the unusual Au_7 moiety in the cation of **1** is replaced by an anion. The $q = -1$ charge of **1b** corresponds to the most common oxidation states (Au^+, As^{3-}); the $q = +1$ charge of **1c** allows the accommodation of a chloride counterion. Structure optimizations were performed in D_2 symmetry, the point symmetry of molecule II of **1** (see above). In Table 2, the calculated and experimentally determined As–Au, Au–Au, and Au–P distances are compared.

The results are surprising, as the bond lengths for all three compounds match comparatively well with the experimental bond lengths, considering that structural differences also occur between the two crystallographically independent molecules I and II of **1** (Table 2, entries 1 and 2). A more detailed analysis is necessary to discriminate between the alternatives. If the shorter bonds are considered (Table 2, entries 4–14), it is apparent that the lengths calculated for **1a** are slightly greater than the experimental lengths, the deviations being in the usual range (less than 6 pm). The same holds for **1b** and **1c**, with the exception that the values in

 © 2006 Wiley-VCH Verlag GmbH & Co. KGaA, Weinheim

entries 5, 9, and 10 of Table 2 have deviations of up to 8 pm. As the calculated X–Au2 and X–Au5 distances for **1c** are too short and the calculated X–Au8 distance is clearly too long (Table 2, entries 1–3), this model can be discarded. On the basis of the calculated bond lengths, we prefer model **1a**, but cannot definitely exclude **1b**. Whether X = As or Au is present as the central atom in the cation of **1** can only be decided by ESI-MS.

Further support for the assignment of X = Au in the cation of **1** is provided by the comparison of the calculated electronic energies of **1a** with photoluminescence data for **1**. The photoluminescence excitation (PLE) and emission (PL) spectra of crystals of **1** and **3** dispersed in nujol are shown in Figure 7. Both clusters display weak near-infrared luminescence, the intensity of which strongly increases upon cooling below 50 K (Figure 7, insets). Similar, but very weak and broad PL peaks with maxima at $\lambda \approx 840$ and 890 nm were observed in CH_2Cl_2 solutions of **1** and **3** at ambient temperature (not shown).

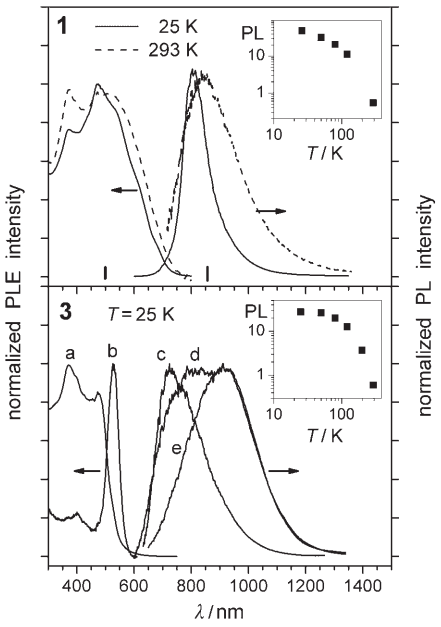

Figure 7. Normalized PLE and PL spectra of nujol mulls of crystals of **1** (top) and **3** (bottom). The emission and excitation wavelengths for the PLE and PL spectra, respectively, of **1** are indicated by short vertical lines. The emission wavelengths for the PLE spectra of **3** are a) 950 nm and b) 700 nm, and the excitation wavelengths for the PL spectra of **3** are c) 400 nm, d) 500 nm, and e) 550 nm. Insets: temperature dependence of the integrated PL intensities of **1** (excitation at 450 nm) and **3** (excitation at 400 nm).

The PLE spectrum of **1** consists of a poorly structured absorption band between $\lambda = 400$ and 700 nm, which is consistent with the black color of the crystals. The calculated vertical excitations of **1a** (point group D_2, excitation from the HOMO a to the LUMOs a, b_1, b_2, b_3) are: 1.38 (894) [^{3}A, dipole forbidden], 2.66 (465) [$^3B_1$], 2.62 (472) [$^3B_2$], and 2.59 eV (479 nm) [$^3B_3$].[17] These values are in good agreement with the PLE spectrum of **1**. Much smaller excitation energies, well under 1 eV, are calculated for the model compounds **1b** and **1c**, supporting the assignment of X = Au in the cation of **1**.

The emission of **1a** (vertical dipole-forbidden transition from the minimum of the lowest excited state ^{3}A to the ground state) is calculated at an energy of 1.18 eV (1048 nm), in reasonable agreement with the relatively weak PL peak observed at $\lambda = 810$ nm at $T = 25$ K. A possible reason for the difference between these values could be the replacement of the phenyl groups by methyl groups in the model compounds used for the calculations. We therefore replaced the eight methyl groups of the two bidentate phosphine ligands that connect Au4 to Au7 and Au4′ to Au7′ (Figure 1) in **1a** by phenyl groups. However, this model led to only slight changes in the calculated transition energies for absorption: 1.40 (886) [^{3}A], 2.58 (480) [$^3B_1$], 2.58 (480) [$^3B_2$], 2.46 eV (504 nm) [$^3B_3$]; and for luminescence: 1.21 eV (1025 nm) [^{3}A]. The difference between the observed and predicted PL energies may be due to a structural change in the excited state; that is, the luminescence may occur from an excited-state structure that is different from the one located.

At low temperatures, an unusual emission consisting of two components at $\lambda \approx 725$ and 910 nm is observed for **3** (Figure 7, curves c and e). The PLE spectrum corresponding to the first component (acquired at the emission wavelength of 700 nm) is dominated by a sharp peak at $\lambda \approx 525$ nm. Such a spectral shape cannot be explained by the presence of another isomer of **3** or another gold complex. Therefore, we suppose that the dual emission may be the result of different, weakly coupled radiative relaxation channels in **3**. This interesting issue is the subject of further investigation.

Experimental Section

All experiments were carried out under a purified nitrogen atmosphere. CH_2Cl_2 was dried over P_2O_5, THF over sodium/benzophenone, and *n*-pentane over $LiAlH_4$. As(*n*Pr)$(SiMe_3)_2$ was synthesized from $LiAs(SiMe_3)_2$ and *n*PrCl using a modified literature method.[18] As(Ph)$(SiMe_3)_2$,[19] [$(AuCl)_2$dppe],[10d] and [$(AuCl)_2$dppm][10d] were prepared according to standard procedures.

1, **2**: As(*n*Pr)$(SiMe_3)_2$ (0.03 mL, 0.116 mmol) was added to a suspension of [$(AuCl)_2$dppe] (0.1 g, 0.116 mmol) in CH_2Cl_2 (10 mL). The resulting deep yellow solution was layered with *n*-pentane, and black crystals of **1** and yellow crystals of **2** formed after a few days. The crystals were separated by hand for the spectroscopic measurements.

3: As(*n*Pr)$(SiMe_3)_2$ (0.033 mL, 0.124 mmol) was added to a solution of [$(AuCl)_2$dppm] (0.105 g, 0.124 mmol) in CH_2Cl_2 (10 mL). The resulting brown solution was layered with THF, and orange crystals of **3** formed after a few weeks.

4: As(Ph)$(SiMe_3)_2$ (0.04 mL, 0.116 mmol) was added to a suspension of [$(AuCl)_2$dppe] (0.1 g, 0.116 mmol) in CH_2Cl_2 (10 mL). By layering the resulting yellow solution with *n*-pentane, yellow crystals of **4** were obtained.

X-ray structure determination: Data were collected on a STOE IPDS II diffractometer using $Mo_{K\alpha}$ radiation ($\lambda = 0.71073$ Å). Structure solution and refinement against F^2 were carried out using the SHELXS and SHELXL programs.[20] CCDC-297861 (**1**), CCDC-297862 (**2**), CCDC-297863 (**3**), and CCDC-297864 (**4**) contain the supplementary crystallographic data for this paper. These data can be obtained free of charge from The Cambridge Crystallographic Data Centre via www.ccdc.cam.ac.uk/data_request/cif.

 © 2006 Wiley-VCH Verlag GmbH & Co. KGaA, Weinheim

Mass spectra were recorded on a Fourier transform ion cyclotron resonance (FT-ICR) mass spectrometer (Bruker Daltonics, APEX II) equipped with a 7T magnet and an electrospray ionization source (Analytica of Branford), as well as a noncommercial radio-frequency ion optics for improved sensitivity. Solutions of hand-picked crystals of **1** and **2**, and of **3** in CH_2Cl_2 were sprayed using nitrogen as nebulizing gas at a flow rate of 300 $\mu L\,h^{-1}$. The desolvation capillary was typically heated to 353 K.

For the collection of the PL and PLE spectra, crystals of **1** and **3** were dispersed in nujol, layered between two quartz plates, and placed in a closed-cycle optical cryostat (Leybold) operating at 20–293 K. The spectra of solutions of **1** and **3** in CH_2Cl_2 were measured in standard cuvettes at ambient temperature. Emission spectra were corrected for the wavelength-dependent response of the spectrometer.[10b]

DFT calculations were carried out with the TURBOMOLE program package.[21] The phenyl groups in the cations of **1** and **3** were replaced by methyl groups to reduce computational cost. The TPSS functional was chosen, because it describes the interactions of gold atoms particularly well and gives better structural parameters than other functionals (for example, BP86).[22] We used the newly developed triple zeta valence with polarization (TZVP) basis set (including an f set for P, As, and Au) with the corresponding auxiliary bases; for hydrogen atoms, the smaller split-valence (SV) basis was adopted.[23] A relativistic effective core potential (RECP) was used for gold.[24] All calculations were carried out using the multipole accelerated resolution of identity (MARI-J) technique.[25]

Received: December 22, 2005
Revised: March 3, 2006
Published online: May 8, 2006

Keywords: arsenic · cluster compounds · density functional calculations · gold · mass spectrometry

[1] E. Zeller, H. Beruda, A. Kolb, P. Bissinger, J. Riede, H. Schmidbaur, *Nature* **1991**, *352*, 141 – 143.
[2] D. Fenske, F. Simon, *Z. Anorg. Allg. Chem.* **1996**, *622*, 45 – 52.
[3] U. M. Tripathi, A. Schier, H. Schmidbaur, *Z. Naturforsch. B* **1998**, *53*, 171 – 174.
[4] B. Alvarez, E. J. Fernández, M. C. Gimeno, P. G. Jones, A. Laguna, J. M. López-de-Luzuriaga, *Polyhedron* **1998**, *17*, 2029 – 2035.
[5] A. L. Balch, E. Y. Fung, M. M. Olmstead, *J. Am. Chem. Soc.* **1990**, *112*, 5181 – 5186.
[6] M. Richter, J. Strähle, *Z. Anorg. Allg. Chem.* **2001**, *627*, 918 – 920.
[7] a) V. G. Albano, P. L. Bellon, M. Manassero, M. Sansoni, *Chem. Commun.* **1970**, 1210 – 1211; b) P. L. Bellon, M. Manassero, M. Sansoni, *J. Chem. Soc. Dalton Trans.* **1972**, 1481 – 1487; c) P. L. Bellon, M. Manassero, M. Sansoni, *J. Chem. Soc. Dalton Trans.* **1973**, 2423 – 2427; d) M. Manassero, L. Naldini, M. Sansoni, *J. Chem. Soc. Chem. Commun.* **1979**, 385 – 386; e) F. A. Vollenbroek, W. P. Bosman, J. J. Bour, J. H. Noordik, P. T. Berskeus, *J. Chem. Soc. Chem. Commun.* **1979**, 387 – 388.
[8] a) C. E. Briant, B. R. C. Theobald, J. W. White, L. K. Bell, D. M. P. Mingos, A. J. Welch, *J. Chem. Soc. Chem. Commun.* **1981**, 201 – 202; b) G. Schmidt, R. Pfeil, R. Boese, F. Bandermann, S. Meyer, G. H. M. Calis, J. W. A. van der Velden, *Chem. Ber.* **1981**, *114*, 3634 – 3642; c) K. P. Hall, B. R. C. Theobald, D. I. Gilmour, D. M. P. Mingos, A. J. Welch, *J. Chem. Soc. Chem. Commun.* **1982**, 528 – 530; d) J. J. Steggarda, J. J. Bour, J. W. A. van der Velden, *Recl. Trav. Chim. Pays-Bas.* **1982**, *101*, 164 – 170; e) C. E. Briant, K. P. Hall, A. C. Wheeler, D. M. P. Mingos, *J. Chem. Soc. Chem. Commun.* **1984**, 248 – 250; f) C. E. Briant, K. P. Hall, D. M. P. Mingos, *J. Chem. Soc. Chem. Commun.* **1984**, 290 – 291; g) C. E. Briant, K. P. Hall, D. M. P. Mingos, A. C. Wheeler, *J. Chem. Soc. Dalton Trans.* **1986**, 687 – 692; h) H. Schmidbaur, F. Scherbaum, B. Huber, G. Müller, *Angew. Chem.* **1988**, *100*, 441 – 443; *Angew. Chem. Int. Ed. Engl.* **1988**, *27*, 419 – 421; i) F. Scherbaum, A. Grohmann, B. Huber, C. Krüger, H. Schmidbaur, *Angew. Chem.* **1988**, *100*, 1602 – 1604; *Angew. Chem. Int. Ed. Engl.* **1988**, *27*, 1544 – 1546.
[9] a) H. Schmidbaur, G. Weidenhiller, O. Steigelmann, *Angew. Chem.* **1991**, *103*, 442 – 444; *Angew. Chem. Int. Ed. Engl.* **1991**, *30*, 433 – 435; b) H. Schmidbaur, O. Steigelmann, *Z. Naturforsch. B* **1992**, *47*, 1721 – 1724; c) E. Zeller, H. Beruda, H. Schmidbaur, *Inorg. Chem.* **1993**, *32*, 3203 – 3204; d) N. Dufour, A. Schier, H. Schmidbaur, *Organometallics* **1993**, *12*, 2408 – 2410; e) E. Zeller, H. Schmidbaur, *J. Chem. Soc. Chem. Commun.* **1993**, 69 – 70; f) A. Blumenthal, H. Beruda, H. Schmidbaur, *J. Chem. Soc. Chem. Commun.* **1993**, 1005 – 1006; g) O. Steigelmann, P. Bissinger, H. Schmidbaur, *Z. Naturforsch. B* **1993**, *48*, 72 – 78; h) G. M. T. Cheetham, M. M. Harding, J. L. Haggitt, D. M. P. Mingos, H. R. Powell, *J. Chem. Soc. Chem. Commun.* **1993**, 1000 – 1001; i) E. Zeller, H. Beruda, H. Schmidbaur, *Chem. Ber.* **1993**, *126*, 2033 – 2036; j) H. Beruda, E. Zeller, H. Schmidbaur, *Chem. Ber.* **1993**, *126*, 2037 – 2040; k) H. Schmidbaur, S. Hofreiter, M. Paul, *Nature* **1995**, *377*, 503 – 504; l) R. E. Bachman, H. Schmidbaur, *Inorg. Chem.* **1996**, *35*, 1399 – 1401; m) R. C. B. Copley, D. M. P. Mingos, *J. Chem. Soc. Dalton Trans.* **1996**, 479 – 489; n) J. Phete, C. Maichle-Mössmer, J. Strähle, *Z. Anorg. Allg. Chem.* **1998**, *624*, 1207 – 1210; o) J. Phete, J. Strähle, *Z. Naturforsch. B* **1999**, *54*, 381 – 384.
[10] a) D. Fenske, T. Langetepe, M. M. Kappes, O. Hampe, P. Weis, *Angew. Chem.* **2000**, *112*, 1925 – 1928; *Angew. Chem. Int. Ed.* **2000**, *39*, 1857 – 1860; b) S. Lebedkin, T. Langetepe, P. Sevillano, D. Fenske, M. M. Kappes, *J. Phys. Chem. B* **2002**, *106*, 9019 – 9026; c) P. Sevillano, T. Langetepe, D. Fenske, *Z. Anorg. Allg. Chem.* **2003**, *629*, 207 – 214; d) J. Olkowska-Oetzel, P. Sevillano, A. Eichhöfer, D. Fenske, *Eur. J. Inorg. Chem.* **2004**, 1100 – 1106; e) G. Pivoriunas, C. Maichle-Mössmer, S. Schwarz, J. Strähle, *Z. Anorg. Allg. Chem.* **2005**, *631*, 1743 – 1745.
[11] R. Ahlrichs, A. Eichhöfer, D. Fenske, O. Hampe, M. M. Kappes, P. Nava, J. Olkowska-Oetzel, *Angew. Chem.* **2004**, *116*, 3911 – 3915; *Angew. Chem. Int. Ed.* **2004**, *43*, 3823 – 3827.
[12] A. Eichhöfer, O. Hampe, *Chem. Phys. Lett.* **2005**, *407*, 186 – 191.
[13] C. von Hänisch, O. Hampe, *Angew. Chem.* **2002**, *114*, 2198 – 2200; *Angew. Chem. Int. Ed.* **2002**, *41*, 2095 – 2097.
[14] Crystallographic data: **1**·7 CH_2Cl_2: $C_{187}H_{214}As_8Au_{19}Cl_{17}P_{12}$, tetragonal, space group $P4_2/nbc$, $Z=12$, $a=4280.3(6)$, $c=3883.0(8)$ pm, $V=71\,140(20)\times10^6$ pm^3, $T=180(2)$ K, $\rho_{calcd}=2.179$ g cm^{-3}, 68 271 data measured, 26 514 unique data ($R_{int}=0.0531$), 1555 parameters, $wR_2=0.2026$ (all data), $R_1=0.0678$ ($I>2\sigma(I)$), max./min. electron density 2.946/−6.005 e A^{-3} (the remaining electron density is located near the lattice-bound solvent molecules, suggesting additional disorder). **2**: $C_{116}H_{124}As_4Au_{10}Cl_2P_8$, orthorhombic, space group $C222_1$, $Z=8$, $a=2237.6(5)$, $b=2339.5(5)$, $c=4667.6(9)$ pm, $V=24\,434(8)\times10^6$ pm^3, $T=200(2)$ K, $\rho_{calcd}=2.232$ g cm^{-3}, 67 071 data measured, 23 763 unique data ($R_{int}=0.0879$), 911 parameters, $wR_2=0.2259$ (all data), $R_1=0.0775$ ($I>2\sigma(I)$), max./min. electron density 4.676/−2.531 e A^{-3}, Flack parameter 0.05(2), e^2−1 = 0.779. **3**·2 CH_2Cl_2: $C_{176}H_{192}As_8Au_{17}Cl_7P_{12}$, triclinic, space group $P\bar{1}$, $Z=2$, $a=1776.4(4)$, $b=2151.2(4)$, $c=3221.4(6)$ pm, $\alpha=88.04(3)$, $\beta=77.25(3)$, $\gamma=73.93(3)°$, $V=11\,534(4)\times10^6$ pm^3, $T=200(2)$ K, $\rho_{calcd}=1.980$ g cm^{-3}, 108 569 data measured, 39 671 unique data ($R_{int}=0.1429$), 1114 parameters, $wR_2=0.2368$ (all data), $R_1=0.0824$ ($I>2\sigma(I)$), max./min. electron density 3.233/−1.484 e A^{-3}. **4**·2 CH_2Cl_2: $C_{130}H_{120}As_4Au_{10}Cl_6P_8$, orthorhombic, space group $Pbcn$, $Z=4$, $a=1938.7(4)$, $b=2865.0(6)$, $c=2810.9(6)$ pm, $V=15\,613(5)\times10^6$ pm^3, $T=200(2)$ K, $\rho_{calcd}=1.877$ g cm^{-3}, 64 894 data measured, 15 143 unique data ($R_{int}=0.1054$), 634 parameters, $wR_2=0.2184$ (all

 © 2006 Wiley-VCH Verlag GmbH & Co. KGaA, Weinheim

data), $R_1 = 0.0659$ ($I > 2\sigma(I)$), max./min. electron density 3.300/ −2.715 e A^{-3}.
[15] a) D. M. P. Mingos, *J. Chem. Soc. Dalton Trans.* **1996**, 561 – 566; b) H. Schmidbaur, *Chem. Soc. Rev.* **1995**, *24*, 391 – 400.
[16] R. Ahlrichs, D. Fenske, M. McPartlin, A. Rothenberger, C. Schrodt, S. Wieber, *Angew. Chem.* **2005**, *117*, 4002 – 4005; *Angew. Chem. Int. Ed.* **2005**, *44*, 3932 – 3936.
[17] The states ^3A, $^3B_1$, $^3B_2$, and $^3B_3$ can be calculated by standard DFT methods, as they are ground states of the corresponding symmetry.
[18] G. Becker, G. Gutekunst, H. J. Wessely, *Z. Anorg. Allg. Chem.* **1980**, *462*, 113 – 129.
[19] F. Simon, PhD Thesis, Universität Karlsruhe, **1995**.
[20] G. M. Sheldrick, SHELXTL-97, Program for the Refinement of Crystal Structures, Universität Göttingen, **1997**.
[21] a) R. Ahlrichs, M. Bär, M. Häser, H. Horn, C. Kölmel, *Chem. Phys. Lett.* **1989**, *162*, 165 – 169; b) O. Treutler, R. Ahlrichs, *J. Chem. Phys.* **1995**, *102*, 346 – 354.
[22] a) J. Tao, J. P. Perdew, V. N. Staroverov, G. E. Scuseria, *Phys. Rev. Lett.* **2003**, *91*, 146401; b) M. P. Johnsson, unpublished results; personal communication from F. Furche.
[23] a) F. Weigend, R. Ahlrichs, *Phys. Chem. Chem. Phys.* **2005**, *7*, 3297 – 3305; b) A. Schäfer, H. Horn, R. Ahlrichs, *J. Chem. Phys.* **1992**, *97*, 2571 – 2577; c) A. Schäfer, C. Huber, R. Ahlrichs, *J. Chem. Phys.* **1994**, *100*, 5829 – 5835; d) K. Eichkorn, F. Weigend, O. Treutler, R. Ahlrichs, *Theor. Chem. Acc.* **1997**, *97*, 119 – 124.
[24] D. Andrae, U. Häussermann, M. Dolg, H. Stoll, H. Preuss, *Theor. Chim. Acta* **1990**, *77*, 123 – 141.
[25] a) K. Eichkorn, O. Treutler, H. Öhm, M. Häser, R. Ahlrichs, *Chem. Phys. Lett.* **1995**, *242*, 652 – 660; b) M. Sierka, A. Hogekamp, R. Ahlrichs, *J. Chem. Phys.* **2003**, *118*, 9136 – 9148; c) R. Ahlrichs, *Phys. Chem. Chem. Phys.* **2004**, *6*, 5119 – 5121.

 © 2006 Wiley-VCH Verlag GmbH & Co. KGaA, Weinheim

High Oxidation States

DOI: 10.1002/anie.200600274

Revising the Highest Oxidation States of the 5d Elements: The Case of Iridium(+VII)**

*Sebastian Riedel and Martin Kaupp**

Dedicated to Professor Pekka Pyykkö on the occasion of his 65th birthday

The quest for the highest achievable oxidation states of the transition-metal elements is of fundamental interest, not least because complexes in very high oxidation states may serve as oxidation agents.[1–3] The maximum oxidation states for the early transition metals follow the group number up to Group 8 (that is, $[OsO_4]$ and $[RuO_4]$, the lack of evidence for an existence of $[FeO_4]$ marks the exception). The trends for the later transition metals tend to be less clear-cut (see Figure 1 in Ref. [4]). In the 5d series, the trend of the experimentally suggested maximum oxidation states appears to be irregular (see filled circles and dotted line in Figure 1).

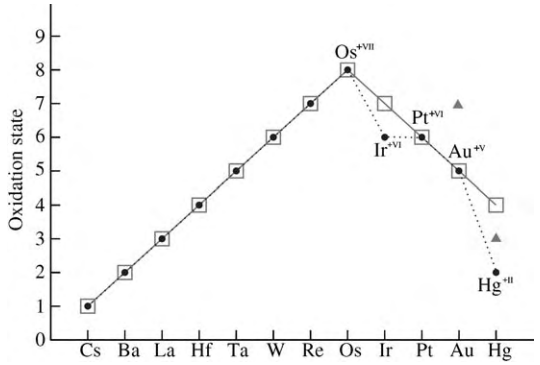

Figure 1. Maximum oxidation states of the 5d transition metals: (●) highest experimentally known values, (▲) probably incorrect experimental assignments, (□) suggested most likely values.

The highest experimentally known oxidation states after osmium are represented by the hexafluorides of iridium ($[IrF_6]$)[5] and platinum ($[PtF_6]$).[6] The isolation of $[AuF_7]$, claimed almost 20 years ago,[7] has recently been shown by high-level quantum chemical calculations to be highly improbable.[8] As the existence of $[AuF_6]$ is also unlikely,[8] oxidation state +V remains the highest oxidation state of gold that is known beyond doubt.[9] Quantum-chemical calculations have furthermore strongly supported the thermochemical stability of mercury(+IV) as gaseous $[HgF_4]$,[4,10–14] but no experimental confirmation has been obtained so far. The correctness of an early report of an electrochemically generated, spectroscopically characterized short-lived $[Hg^{III}(cyclam)][BF_4]_3$ species[15] appears unclear from today's perspective.

Combining the results of the most accurate quantum-chemical predictions and of reliable experimental studies, a revised trend of the highest oxidation states of the 5d transition-metal row is obtained. Apart from the lack of iridium(+VII), there is a linear descent after osmium (Figure 1).

To establish the highest achievable iridium oxidation states, we report herein structure optimizations by density functional theory (DFT) methods,[16] and of high-level coupled-cluster calculations[16] of the stabilities of iridium fluoride complexes up to $[IrF_9]$. Figure 2 shows the DFT-optimized[16] structures of $[IrF_9]$, $[IrF_7]$, and $[IrF_5]$. Whereas $[IrF_9]$ exhibits a minimum with D_{3h} symmetry on the potential-energy surface (singlet state), the gas-phase elimination of F_2 for this complex is computed to be highly exothermic (see Table 1). Calculations on oxo-fluoro complexes of Ir^{IX} (e.g. on $[IrO_3F_3]$) indicate also very exothermic

[*] S. Riedel, Prof. Dr. M. Kaupp
Institut für Anorganische Chemie der Universität Würzburg
Am Hubland, 97074 Würzburg (Germany)
Fax: (+49) 931-888-7135
E-mail: sebastian.riedel@mail.uni-wuerzburg.de
kaupp@mail.uni-wuerzburg.de

[**] We are grateful to M. Straka, R. Reviakine, and M. Patzschke for comments and technical assistance.

Supporting information for this article is available on the WWW under http://www.angewandte.org or from the author.

InterScience
© 2006 Wiley-VCH Verlag GmbH & Co. KGaA, Weinheim

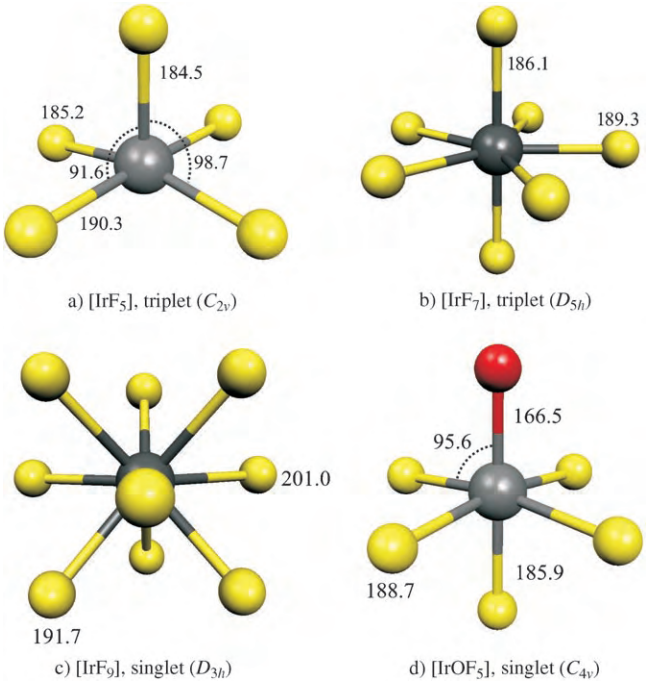

Figure 2. B3LYP-optimized minimum structures of $[IrF_5]$ (C_{2v}), $[IrF_7]$ (D_{5h}), $[IrF_9]$ (D_{3h}), and $[IrOF_5]$ (C_{4v}). Bond lengths [pm], angles [°].

Table 1: Computed reaction energies [kJ mol^{-1}] for iridium fluoride complexes.[a]

Reaction	CCSD	CCSD(T)	B3LYP[b]
a) $[IrF_9]\rightarrow[IrF_7]+F_2$	−401.9	−319.6	−375.5 (−385.9)
b) $[IrF_8]\rightarrow[IrF_6]+F_2$	−329.6	−249.6	−246.7 (−257.2)
c) $[IrF_7]\rightarrow[IrF_5]+F_2$	32.8	102.6	130.3 (119.6)
d) $[IrF_7]\rightarrow[IrF_6]+F$	−100.1	−44.3	−32.9 (−40.3)
e) $[IrF_6]\rightarrow[IrF_5]+F$	257.3	299.7	318.5 (308.2)
f) $[IrF_5]+[KrF_2]\rightarrow[IrF_7]+Kr$	−117.8	−163.5	−166.0
g) $[IrOF_5]\rightarrow[IrOF_3]+F_2$			261.6
h) $[IrOF_5]\rightarrow[IrF_4]+OF$			176.9
i) $[IrOF_5]\rightarrow[IrOF_4]+F$			172.8
j) $[IrOF_5]\rightarrow[IrF_5]+O$			256.1
k) $[IrF_6]^+\rightarrow[IrF_4]^++F_2$			216.7
l) $[IrF_6]^+\rightarrow[IrF_5]^++F$			154.5
m) $[KrF_2]\rightarrow Kr+F_2$[c]	−85.0	−60.9	−35.7
n) $F_2\rightarrow 2F$[d]	124.4	152.7	155.3

[a] Reaction energies given at scalar relativistic levels, for singlet $[IrF_9]$, doublet $[IrF_8]$, triplet $[IrF_7]$, quartet $[IrF_6]$, triplet $[IrF_5]$, quartet $[IrF_4]$, triplet $[IrOF_5]$, doublet $[IrOF_4]$, and singlet $[IrOF_3]$. Spin-orbit corrections at B3LYP level to reactions c, d, and e amount to −36.9 kJ mol^{-1}, −7.6 kJ mol^{-1}, and −29.3 kJ mol^{-1}, respectively. [b] Values in parentheses are counterpoise and zero-point vibration corrected. [c] The experimental value is −60.2 kJ mol^{-1}. [d] The experimental value is +159.7 kJ mol^{-1}.

decomposition pathways with low barriers (details of these studies will be provided elsewhere[17]). This situation makes the existence of the highest theoretically possible oxidation state of iridium highly unlikely.

What about Ir^{VIII}? Synthesis of the most likely Ir^{VIII} complex, $[IrO_4]$, has recently been attempted by matrix isolation but resulted in formation of the peroxide species $[(O_2)IrO_2]$.[19] This result reflects the energy gain from formation of an O–O bond. The homoleptic fluoride complex $[IrF_8]$ has a square antiprismatic (D_{4d}) minimum on the potential-energy surface (not shown). However, concerted F_2 elimination is computed to be highly exothermic (reaction (b) in Table 1). This elimination is so favorable because of the steric crowding in the Ir coordination sphere, which places this complex at very high energies (and probably leads to low barriers). Most mixed fluoro-oxo complexes of Ir^{VIII} are computed to be similarly unstable; only $[IrOF_6]$ exhibits somewhat less exothermic decomposition pathways.[17]

Things look rather different for Ir^{VII} (d^2 configuration): $[IrF_7]$ is computed to exhibit a pentagonal-bipyramidal triplet ground-state minimum (D_{5h} symmetry, see Figure 1).[18] In contrast to $[IrF_9]$, F_2 elimination from triplet $[IrF_7]$ is appreciably endothermic (reaction (c) in Table 1), in fact much more so than the best calculations suggest for the long-sought $[HgF_4]$.[4,10–14] Our coupled-cluster calculations predict an energy of +102.6 kJ mol^{-1} (Table 1). As for related cases triple excitations contribute substantially to this positive value,[4,8,12] and B3LYP DFT calculations compare reasonably well with the CCSD(T) results[8,12] (this makes B3LYP energies a good choice for larger systems where coupled-cluster calculations are not feasible).

A second potential channel for decomposition of $[IrF_7]$ involves the homolytic dissociation of an Ir–F bond to give $[IrF_6]$. Although this reaction is calculated to be slightly exothermic (reaction (d) in Table 1; larger basis sets are expected to render this value less negative[4,12]), the structural rearrangement required for this bond breaking is substantial and creates an appreciable barrier of +100.4 kJ mol^{-1} (scalar relativistic DFT results). The transition state is a singly capped octahedron with C_{3v} symmetry, where the cap represents the Ir–F bond to be broken.

We note in passing that nonrelativistic pseudopotential calculations provide approximately 100 kJ mol^{-1} less positive energies for F_2 elimination. Thus, as in all other cases studied to date,[4,8,20,21] the stability of the highest oxidation states of the 5d elements is largely due to relativistic effects.

Given the open-shell nature of several of the relevant species involved, we have also evaluated the influence of spin-orbit (SO) effects on stabilities, using single-point calculations with a recently implemented[22] two-component non-collinear spin-density functional approach.[16] Most of the relevant results are in footnote [a] of Table 1. While the SO stabilization increases from $[IrF_7]$ to $[IrF_6]$ to $[IrF_5]$, its influence on the decomposition reactions of $[IrF_7]$ is moderate and does not change the thermochemistry dramatically (the same holds for activation barriers; computed SO corrections to the barrier for homolytic Ir–F bond breakage amount to only −5.7 kJ mol^{-1}). Counterpoise corrections for basis-set superposition errors and zero-point vibrational energy corrections are also of no appreciable consequence for the relevant reaction energies (Table 1).

Thus it is likely that $[IrF_7]$ is a viable target for gas-phase synthesis (e.g. in molecular-beam experiments) or for matrix-isolation studies. Characterization of $[IrF_7]$ by vibrational spectroscopy may be aided by the harmonic vibrational frequency analysis provided in the Supporting Information. The electronic structure and oxidation state of Ir^{VII} species should be determinable by Mössbauer spectroscopy.

 © 2006 Wiley-VCH Verlag GmbH & Co. KGaA, Weinheim

Oxidation of $[IrF_5]$ by the endothermic fluorine compound KrF_2 is substantially exothermic (reaction (f) in Table 1). This situation is even more so with the strongest presently known oxidative fluorinating agent the $[KrF]^+$ ion.[23] Formation of the $[KrF][IrF_6]$ ion-pair complex from (gas-phase) $[KrF]^+$ and $[IrF_6]^-$ is highly exothermic (by $-491.6\ kJ\,mol^{-1}$ at B3LYP level) and provides a local minimum on the potential-energy surface (analogous to the known complex $[XeF][IrF_6]$[24]). However, the complex is calculated to decompose exothermically ($-118.5\ kJ\,mol^{-1}$) into $[IrF_7]$ and Kr. Figure 3 shows the reaction energies for $[NgF][MF_6]\rightarrow MF_7 + Ng$ for a range of complexes (Ng = Kr, Xe and M = Ir, Pt, Au) at the corresponding computational level.

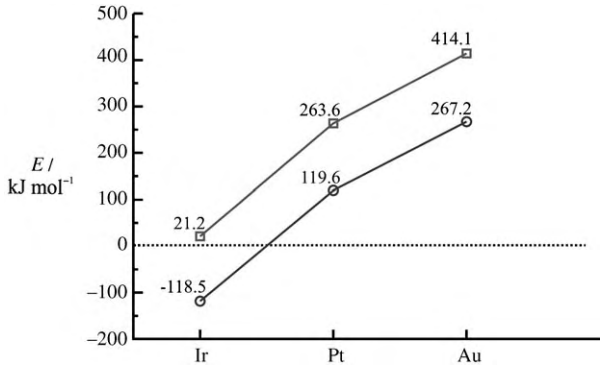

Figure 3. Computed energies (B3LYP) for the (gas-phase) reactions $[NgF][MF_6]\rightarrow[MF_7] + Ng$ (Ng = Kr, Xe; M = Ir, Pt, Au): □ $[XeF]^+$ complexes, ○ $[KrF]^+$ complexes.

While the formation of the ion-pair complexes from the separated ions is in all cases strongly exothermic (data not shown), only $[KrF][IrF_6]$ decomposes exothermically to give the heptafluoride (note that these energies will be generally somewhat more positive in the condensed phase owing to electrostatic stabilization of the ion-pair complexes). These computational results suggest a possible pathway to obtain Ir^{VII}. Interestingly, in contrast to several known $[KrF][MF_6]$ complexes of platinum and gold,[24–26] and in spite of the existence of $[XeF][IrF_6]$,[24] observation of $[KrF][IrF_6]$ has never been reported.

Initial data for an alternative Ir^{VII} target, the C_{4v}-symmetrical $[IrOF_5]$, have also been obtained (data for the triplet state are provided in Table 1 and Figure 1 d; the singlet is only $2.4\ kJ\,mol^{-1}$ higher at the scalar relativistic level, but this difference is enhanced by SO effects[17]). $[IrOF_5]$ has the advantage of a lower coordination number. Indeed, in this case elimination of F_2 is even more endothermic than for $[IrF_7]$, and elimination of OF is also still appreciably endothermic (reactions (g) and (h) in Table 1). Even the homolytic splitting of an Ir–F bond to give $[IrOF_4]$ is endothermic by $172.8\ kJ\,mol^{-1}$ (reaction (i) in Table 1). The harmonic vibrational frequencies of $[IrOF_5]$ are provided in the Supporting Information.

Another Ir^{VII} species that comes to mind is the $[IrF_6]^+$ ion. It is computed to prefer a triplet ground state with a slight Jahn–Teller distortion (D_{4h} symmetry, Ir–F_{ax} 179.3 pm, Ir–F_{eq} 184.7 pm). The adiabatic ionization potential $IrF_6\rightarrow[IrF_6]^+$ is calculated to be very large (13.5 eV at B3LYP level). The energies for concerted F_2 elimination and homolytic Ir–F dissociation are calculated to be both appreciably endothermic (reactions (k) and (l) in Table 1). As $[IrF_6]$ is a volatile complex, it is unclear at the moment why its molecular ion has apparently never been observed in a mass spectrometry experiment.

Our present state-of-the-art quantum chemical calculations suggest thus that the highest iridium oxidation state that has a realistic chance of experimental observation is Ir^{VII}. The experimentally known highest 5d oxidation states for Groups 8, 10, and 11 are Os^{VIII}, Pt^{VI}, and Au^{V}, respectively (see ref. [27] for the computationally verified instability of Pt^{VIII} and ref.[8] for exclusion of Au^{VII} and Au^{VI}). Adding the computationally predicted Hg^{IV} and Ir^{VII} states suggests that the trend for the later 5d metals should become a linear decrease once all computationally suggested possibilities have been verified experimentally (see solid line and open squares in Figure 1).

Received: January 22, 2006
Published online: April 26, 2006

Keywords: density functional theory calculations · fluorides · iridium · oxidation states · periodic table

[1] N. Bartlett, *Angew. Chem.* **1968**, *80*, 453; *Angew. Chem. Int. Ed. Engl.* **1968**, *7*, 433.
[2] B. C. Bales, P. Brown, A. Dehestani, J. M. Mayer, *J. Am. Chem. Soc.* **2005**, *127*, 2832.
[3] W. W. Dukat, J. H. Holloway, E. G. Hope, M. R. Rieland, P. J. Townson, R. L. Powell, *J. Chem. Soc. Chem. Commun.* **1993**, 1429.
[4] M. Kaupp, M. Dolg, H. Stoll, H. G. von Schnering, *Inorg. Chem.* **1994**, *33*, 2122.
[5] H. H. Claassen, B. Weinstock, *J. Chem. Phys.* **1960**, *33*, 436.
[6] B. Weinstock, H. H. Claassen, J. G. Malm, *J. Am. Chem. Soc.* **1957**, *79*, 5832.
[7] A. A. Timakov, V. N. Prusakov, Y. V. Drobyshevskii, *Dokl. Akad. Nauk SSSR* **1986**, *291*, 125.
[8] S. Riedel, M. Kaupp, *Inorg. Chem.* **2006**, *45*, 1228.
[9] I.-C. Hwang, K. Seppelt, *Angew. Chem.* **2001**, *113*, 3803; *Angew. Chem. Int. Ed.* **2001**, *40*, 3690.
[10] M. Kaupp, H. G. von Schnering, *Angew. Chem.* **1993**, *105*, 952; *Angew. Chem. Int. Ed. Engl.* **1993**, *32*, 861.
[11] W. Liu, R. Franke, M. Dolg, *Chem. Phys. Lett.* **1999**, *302*, 231.
[12] S. Riedel, M. Straka, M. Kaupp, *Phys. Chem. Chem. Phys.* **2004**, *6*, 1122.
[13] S. Riedel, M. Straka, M. Kaupp, *Chem. Eur. J.* **2005**, *11*, 2743.
[14] P. Pyykkö, M. Straka, M. Patzschke, *Chem. Commun.* **2002**, 1728.
[15] R. L. Deming, A. L. Allred, A. R. Dahl, A. W. Herlinger, M. O. Kestner, *J. Am. Chem. Soc.* **1976**, *98*, 4132.
[16] All molecular structures have been optimized at the B3LYP[16a–d] DFT level, using the Gaussian03[16a] program. Quasirelativistic energy-adjusted, small-core pseudopotentials (effective-core potentials, ECP) of the Stuttgart/Cologne group were used for the transition metals Au,[16e] Pt,[16f] and Ir[16f]. The def-TZVP (7s6p5d)[6s3p3d] valence basis set implemented in the Turbomole 5.6 package[16g] for Ir, Pt, and Au, augmented by one f-type polarization function[16h] ($\alpha = 0.967$, 0.993, 1.050 for Ir, Pt, and Au, respectively), were used together with a fluorine DZ + P[16i] basis set by Dunning. For the rare-gas atoms Kr and Xe we used

 © 2006 Wiley-VCH Verlag GmbH & Co. KGaA, Weinheim

energy-consistent, eight-valence-electron pseudopotentials and (6s6p3d1f)/[4s4p3d1f] valence basis sets.[16j] Stationary points on the potential-energy surface were characterized by harmonic vibrational frequency analyses at this level (providing also zero-point energy corrections to the thermochemistry). Subsequent single-point energy calculations at B3LYP DFT as well as coupled-cluster CCSD and CCSD(T) levels had the fluorine basis replaced by a larger aug-cc-pVTZ basis set.[16k] The coupled-cluster calculations were carried out with the MOLPRO 2002.6[16l] program package. Contributions of basis-set superposition errors (BSSE) to the energetics were estimated by the counterpoise (CP)[16m] procedure. Spin-orbit (SO) corrections to the energetics were computed at B3LYP level (with the same basis sets as used in the regular energy calculations above) using a relativistic two-component non-collinear-spin DFT method[16n] implemented recently into the in-house program ReSpect,[16o] together with a two-component ECP for Ir (made from a scalar relativistic part and an SO potential).[16f] a) Gaussian 03 (Revision B.04), M. J. Frisch,. G. W. Trucks, H. B. Schlegel, G. E. Scuseria, M. A. Robb, J. R. Cheeseman, J. A. Montgomery, Jr., T. Vreven, K. N. Kudin, J. C. Burant, J. M. Millam, S. S. Iyengar, J. Tomasi, V. Barone, B. Mennucci, M. Cossi, G. Scalmani, N. Rega, G. A. Petersson, H. Nakatsuji, M. Hada, M. Ehara, K. Toyota, R. Fukuda, J. Hasegawa, M. Ishida, T. Nakajima, Y. Honda, O. Kitao, H. Nakai, M. Klene, X. Li, J. E. Knox, H. P. Hratchian, J. B. Cross, C. Adamo, J. Jaramillo, R. Gomperts, R. E. Stratmann, O. Yazyev, A. J. Austin, R. Cammi, C. Pomelli, J. W. Ochterski, P. Y. Ayala, K. Morokuma, G. A. Voth, P. Salvador, J. J. Dannenberg, V. G. Zakrzewski, S. Dapprich, A. D. Daniels, M. C. Strain, O. Farkas, D. K. Malick, A. D. Rabuck, K. Raghavachari, J. B. Foresman, J. V. Ortiz, Q. Cui, A. G. Baboul, S. Clifford, J. Cioslowski, B. B. Stefanov, G. Liu, A. Liashenko, P. Piskorz, I. Komaromi, R. L. Martin, D. J. Fox, T. Keith, M. A. Al-Laham, C. Y. Peng, A. Nanayakkara, M. Challacombe, P. M. W. Gill, B. Johnson, W. Chen, M. W. Wong, C. Gonzalez, J. A. Pople, Gaussian, Inc., Pittsburgh, PA, **2003**; b) A. D. Becke, *J. Chem. Phys.* **1993**, *98*, 5648; c) C. Lee, W. Yang, R. G. Parr, *Phys. Rev. B* **1988**, *37*, 785; d) B. Miehlich, A. Savin, H. Stoll, H. Preuss, *Chem. Phys. Lett.* **1989**, *157*, 200; e) P. Schwerdtfeger, M. Dolg, W. H. E. Schwarz, G. A. Bowmaker, P. D. W. Boyd, *J. Chem. Phys.* **1989**, *91*, 1762; f) D. Andrae, U. Häussermann, M. Dolg, H. Stoll, H. Preuss, *Theor. Chim. Acta* **1990**, *77*, 123; g) R. Ahlrichs, M. Bär, M. Häser, H. Horn, C. Kölmel, *Chem. Phys. Lett.* **1989**, *162*, 165; h) A. W. Ehlers, M. Bohme, S. Dapprich, A. Gobbi, A. Hollwarth, V. Jonas, K. F. Kohler, R. Stegmann, A. Veldkamp, G. Frenking, *Chem. Phys. Lett.* **1993**, *208*, 111; i) T. H. Dunning, Jr., *J. Chem. Phys.* **1970**, *53*, 2823; j) A. Nicklass, M. Dolg, H. Stoll, H. Preuss, *J. Chem. Phys.* **1995**, *102*, 8942; k) T. H. Dunning, Jr., *J. Chem. Phys.* **1989**, *90*, 1007; l) H.-J. Werner, P. J. Knowles, R. Lindh, M. Schütz, P. Celani, T. Korona, F. R. Manby, G. Rauhut, R. D. Amos, A. Bernhardsson, A. Berning, D. L. Cooper, M. J. O. Deegan, A. J. Dobbyn, F. Eckert, C. Hampel, G. Hetzer, A. W. Lloyd, S. J. McNicholas, W. Meyer, M. E. Mura, A. Nicklass, P. Palmieri, R. Pitzer, U. Schumann, H. Stoll, A. J. Stone, R. Tarroni, T. Thorsteinsson, MOLPRO 2002.6 ed., Birmingham, UK, **2003**; m) S. F. Boys, F. Bernardi, *Mol. Phys.* **1970**, *19*, 553; n) I. Malkin, O. L. Malkina, V. G. Malkin, M. Kaupp, *J. Chem. Phys.* **2005**, *123*, 244103; o) V. G. Malkin, O. L. Malkina, R. Reviakine, A. V. Arbuznikov, M. Kaupp, B. Schimmelpfennig, I. Malkin, M. Repiský, S. Komorovský, P. Hrobárik, E. Malkin, T. Helgaker, K. Ruud, MAG-ReSpect 2.1 ed., **2005**.

[17] S. Riedel, M. Kaupp, unpublished results.

[18] A singlet minimum with C_s symmetry is calculated to be 82 kJ mol^{-1} above the triplet ground state of [IrF_7] at the scalar relativistic level. For the triplet ground state, the monocapped trigonal prism is a transition state at 27.1 kJ mol^{-1}, and the monocapped octahedron is a second-order saddle point at 29.7 kJ mol^{-1} above the D_{5h} minimum.

[19] A. Citra, L. Andrews, *J. Phys. Chem. A* **1999**, *103*, 4182.

[20] P. Schwerdtfeger, M. Dolg, W. H. E. Schwarz, G. A. Bowmaker, P. D. W. Boyd, *J. Chem. Phys.* **1989**, *91*, 1762.

[21] P. Pyykkö, *Chem. Rev.* **1988**, *88*, 563.

[22] I. Malkin, O. L. Malkina, V. G. Malkin, M. Kaupp, *J. Chem. Phys.* **2005**, *123*, 244103.

[23] K. O. Christe, D. A. Dixon, *J. Am. Chem. Soc.* **1992**, *114*, 2978.

[24] F. O. Sladky, P. A. Bulliner, N. Bartlett, *J. Chem. Soc. A* **1969**, *14*, 2179.

[25] J. F. Lehmann, G. J. Schrobilgen, *J. Fluorine Chem.* **2003**, *119*, 109.

[26] R. J. Gillespie, G. J. Schrobilgen, *Inorg. Chem.* **1976**, *15*, 22.

[27] R. Wesendrup, P. Schwerdtfeger, *Inorg. Chem.* **2001**, *40*, 3351.

 © 2006 Wiley-VCH Verlag GmbH & Co. KGaA, Weinheim

Cover Picture

Xiaoyi Hu, Anthony Addlagatta, Brian W. Matthews,* and Jun O. Liu*

The evolutionarily conserved enzymes, the methionine aminopeptidases (MetAPs), remove N-terminal methionine during protein synthesis. J. O. Liu et al. describe in their Communication on page 3772 ff. a new class of inhibitors for MetAPs and the crystal structure of the inhibitor complexed with MetAP1. These findings should facilitate the development of MetAP1-specific inhibitors that can serve as molecular probes for the function of MetAP1 and as potential leads for inhibitors of cancer cell growth.

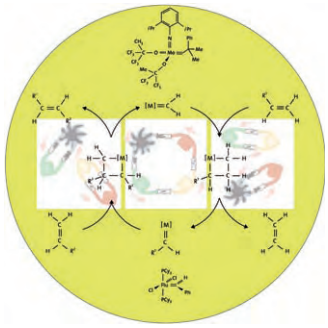

Nobel Lectures

Metathesis reactions take center stage in the Nobel Prize lectures from Yves Chauvin, Richard R. Schrock, and Robert H. Grubbs. The prizewinners present first-hand accounts of their discoveries in three Reviews beginning on page 3740 ff.

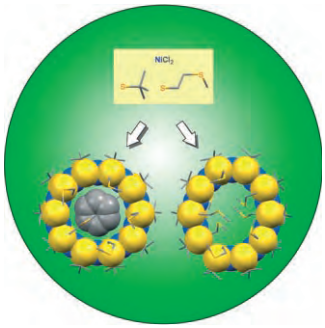

Supramolecular Chemistry

The *cyclo*-$Ni_{10}S_{20}$ toroid adopts a circular or ellipsoidal configuration depending on the presence or absence of an encapsulated guest molecule. In their Communication on page 3768 ff., K. Tatsumi and co-workers report their findings on the basis of X-ray crystallography.

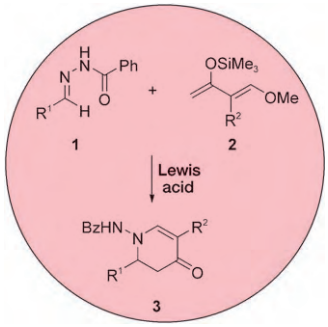

Organic Synthesis

S. Kobayashi and co-workers discuss two methods for the construction of carbon frameworks. They describe the addition of enecarbamates to aldehydes in the first of their Communications on page 3814 ff., while on page 3816 ff. the focus is aza-Diels–Alder reactions of acyl hydrazones.

Contents

VIP *The following Communications have been judged by at least two referees to be "very important papers" and will be published online at www.angewandte.org soon:*

*C. Burke, Y. Shi**
Regio- and Enantioselective Epoxidation of Dienes by a Chiral Dioxirane: Synthesis of Optically Active Vinyl *cis*-Epoxides

C.-W. So, H. Roesky, J. Magull, R. Oswald*
Synthesis and Characterization of [{PhC(N*t*Bu)$_2$}SiCl]: A Stable Monomeric Chlorosilylene

*H. Yu, S. Huang, H. Chokhawala, M. Sun, H. Zheng, X. Chen**
Highly Efficient Chemoenzymatic Synthesis of Naturally Occurring and Non-Natural α2,6-Linked Sialosides: A *P. damsela* α2,6-Sialyltransferase with Extremely Flexible Donor Substrate Specificity

*D. Rohde, C.-J. Yan, H.-J. Yan, L.-J. Wan**
From Lamellar to Hexagonal Self-Assembly of Bis(dioxaborin) Molecules

Meeting Reviews

A Closer Look at Nanoporous Materials — *J. Kärger, F. Grinberg* — **3732**

Books

Natural Products — Lixin Zhang, Arnold L. Demain — *reviewed by F. von Nussbaum* — **3735**

Reviews

Metathesis Reactions

Y. Chauvin* — **3740 – 3747**

Olefin Metathesis: The Early Days (Nobel Lecture)

R. R. Schrock* — **3748 – 3759**

Multiple Metal–Carbon Bonds for Catalytic Metathesis Reactions (Nobel Lecture)

R. H. Grubbs* — **3760 – 3765**

Olefin-Metathesis Catalysts for the Preparation of Molecules and Materials (Nobel Lecture)

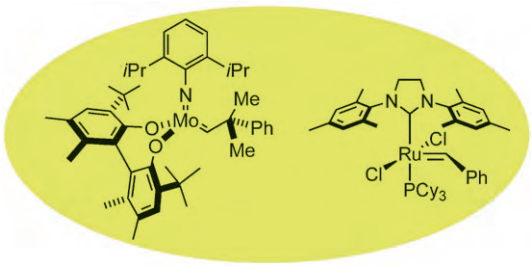

Metathesis reactions are among the most important processes in organic synthesis. The decisive breakthrough in making these reactions practical for industrial purposes, which range from the synthesis of polymers to pharmaceuticals, came with the discovery of the reaction mechanism by Yves Chauvin and the targeted development of transition-metal-based metathesis catalysts by Richard Schrock and Robert Grubbs. The winners of the Chemistry Nobel Prize in 2005 present first-hand accounts of these developments.

InterScience

© 2006 Wiley-VCH Verlag GmbH & Co. KGaA, Weinheim

Communications

A tale of two toroids: New cyclic nickel(II) thiolate complexes (see structures; Ni green, S red, C purple) were synthesized by stepwise introduction of two kinds of thiolates to a nickel(II) center. The flexible $\{Ni_{10}S_{20}\}$ core configuration crystallizes in different forms, either circular or ellipsoidal, depending on the presence or absence of an encapsulated guest molecule.

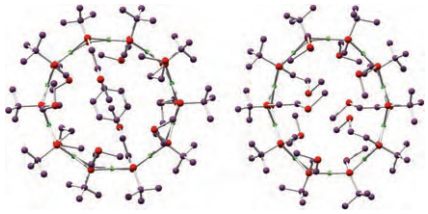

Nickel Thiolates

C. Zhang, S. Takada, M. Kölzer, T. Matsumoto, K. Tatsumi* **3768 – 3772**

Nickel(II) Thiolate Complexes with a Flexible *cyclo*-$\{Ni_{10}S_{20}\}$ Framework

High-throughput screening of a library of compounds has led to the identification of a new structural class of human methionine aminopeptidases inhibitors. They inhibited the processing of 14-3-3γ in cells and blocked proliferation of both endothelial cells and transformed cancer cell lines. The picture shows the crystal structure of the complex of one inhibitor (yellow) with the type 1 human methionine aminopeptidase (blue Co^{II}, red H_2O).

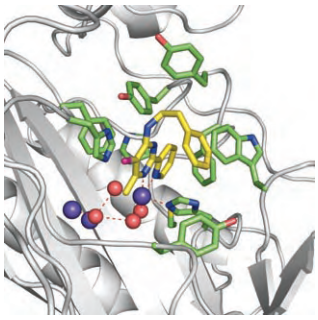

Drug Design

X. Hu, A. Addlagatta, B. W. Matthews,* J. O. Liu* **3772 – 3775**

Identification of Pyridinylpyrimidines as Inhibitors of Human Methionine Aminopeptidases

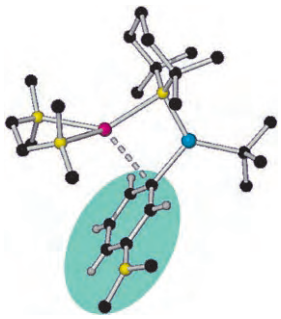

Move over directed *ortho*-metalation, here comes directed *meta*-metalation. The unprecedented *meta*-zincation of two anilides by a synergic mixed sodium/zinc dialkyl–amide base is presented. The orientation of the deprotonation of the anilides is remarkably switched to the *meta* site using this heterometallic mixed-metal system.

Aromatic Substitution

D. R. Armstrong, W. Clegg, S. H. Dale, E. Hevia, L. M. Hogg, G. W. Honeyman, R. E. Mulvey* **3775 – 3778**

Directed *meta*-Metalation Using Alkali-Metal-Mediated Zincation

Spinning around: By insertion of a bifunctional ligand that acts as an axle—one end tethered to a silver surface, the other bonded to the metal center of a metalloporphyrin—an entire population of porphyrin molecules can be induced to spin. Removal of the axle quenches the motion. The switching process may be repeated an indefinite number of times.

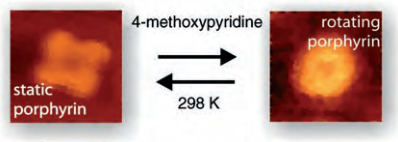

Molecular Devices

O. P. H. Vaughan, F. J. Williams, N. Bampos, R. M. Lambert* **3779 – 3781**

A Chemically Switchable Molecular Pinwheel

For the USA and Canada:
ANGEWANDTE CHEMIE International Edition (ISSN 1433-7851) is published weekly by Wiley-VCH PO Box 191161, D 69451 Weinheim, Germany. Air freight and mailing in the USA by Publications Expediting Inc. 200 Meacham Ave., Elmont, NY 11003. Periodicals postage paid at Jamaica NY 11431. US POSTMASTER: send address changes to *Angewandte Chemie*, Wiley-VCH, 111 River Street, Hoboken, NJ 07030. Annual subscription price for institutions: US$ 5685/5168 (valid for print and electronic / print or electronic delivery); for individuals who are personal members of a national chemical society prices are available on request. Postage and handling charges included. All prices are subject to local VAT/sales tax.

© 2006 Wiley-VCH Verlag GmbH & Co. KGaA, Weinheim

The best in chemistry –

for more than a hundred years

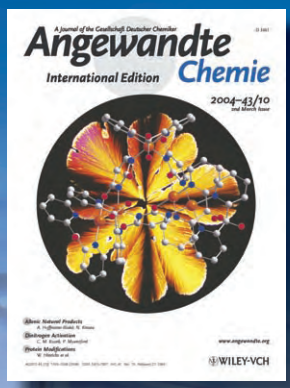

A Journal of the Gesellschaft Deutscher Chemiker

Angewandte
International Edition **Chemie**

www.angewandte.org

1888: ***The beginning of a success story***

Constant Innovations

1962: *First issue of the International Edition*
1976: *Graphical abstracts*
1979: *Cover pictures*
1988: *Centenary of Angewandte*
1989: *Routine use of color*
1991: *New section: Highlights*
1992: *Computerized editorial tracking system*
1995: *Internet service for readers*
1998: *Regular press service; full-text online*
2000: *New section: Essays; EarlyView: Communications available online ahead of the printed version*
2001: *New section: Minireviews*
2002: *Online submission of manuscripts*
2003: *Weekly publication; new section: News; new layout*
2004: *Backfiles (1962-1997); ManuscriptXpress: Online system for authors and referees*

Angewandte's advisors...

Ryoji Noyori
Nagoya University and RIKEN (Tokyo)

*»**Angewandte Chemie** is the best scientific arena for both players and audience. This international journal has taken a leading role in raising the potential of chemistry to the current high standard.«*

***Angewandte Chemie International Edition** is a journal of the German Chemical Society (GDCh)*

GDCh

WILEY InterScience® DISCOVER SOMETHING GREAT

WILEY-VCH

1871404_gu

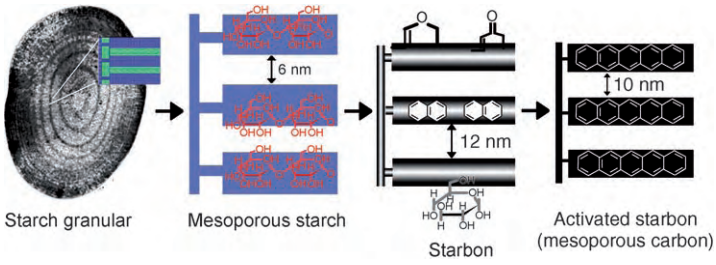

A star is born: The complex molecular architecture found in plants is used in the design of new nanostructured materials. Carbon-based mesoporous materials with tunable surfaces and bulk properties can be synthesized by the low-temperature carbonization of expanded natural starches that are in turn prepared by a simple gelatinization–retrogradation process.

Carbonaceous Materials

V. Budarin, J. H. Clark,* J. J. E. Hardy, R. Luque, K. Milkowski, S. J. Tavener, A. J. Wilson _____ **3782 – 3786**

Starbons: New Starch-Derived Mesoporous Carbonaceous Materials with Tunable Properties

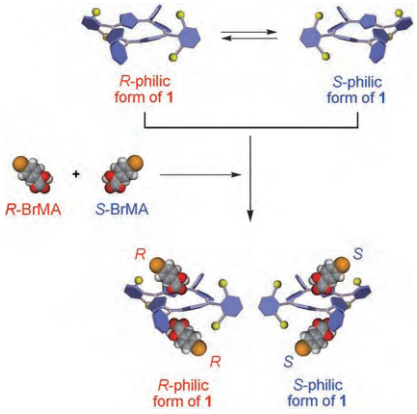

The dynamic dual chirality of D_2-symmetric saddle-shaped porphyrin **1** decreases the stereochemical complexity of cocrystallization with racemic mandelic acid derivatives, such as BrMA, and allows spontaneous optical resolution (see picture). Each resulting cocrystal is porous and consists of one-handed double-helical porphyrin arrays in which chiral guests are enantioselectively included.

Optical Resolution

Y. Mizuno, Md. A. Alam, A. Tsuda, K. Kinbara, K. Yamaguchi, T. Aida* _____ **3786 – 3790**

Hermaphroditic Chirality of a D_2-Symmetric Saddle-Shaped Porphyrin in Multicomponent Spontaneous Optical Resolution: Inclusion Cocrystals with Double-Helical Porphyrin Arrays

In the groove: The "drugability" of protein–protein interaction domains is still a matter of debate. The 3D structure of a complex of a small organic ligand and the AF6 PDZ domain revealed the creation of a binding pocket by the ligand (see picture). The derived compound is able to compete with a natural peptide ligand of the domain and represents a basic building block for the generation of selective PDZ inhibitors.

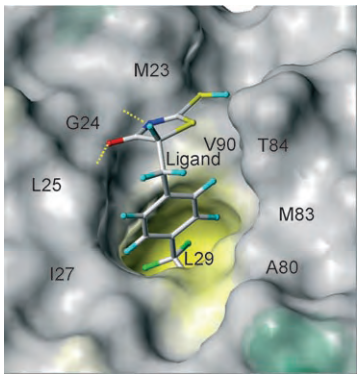

Protein–Protein Interactions

M. Joshi, C. Vargas, P. Boisguerin, A. Diehl, G. Krause, P. Schmieder, K. Moelling, V. Hagen, M. Schade,* H. Oschkinat* _____ **3790 – 3795**

Discovery of Low-Molecular-Weight Ligands for the AF6 PDZ Domain

© 2006 Wiley-VCH Verlag GmbH & Co. KGaA, Weinheim

Contents

Water Chemistry

N. J. Singh, M. Park, S. K. Min, S. B. Suh, K. S. Kim* ——— **3795 – 3800**

Magic and Antimagic Protonated Water Clusters: Exotic Structures with Unusual Dynamic Effects

It's a kinda magic! Contrary to conventional wisdom that O–H bonds associated with dangling hydrogen atoms and those in the H_3O^+ ion in molecular clusters display characteristic peaks in IR spectra, a dynamic effect makes such peaks disappear, even in the gas phase at low temperatures. This finding helps solve the long-standing problems of magic and antimagic protonated water clusters with 21 (top structures) and 22 (bottom structures) water molecules.

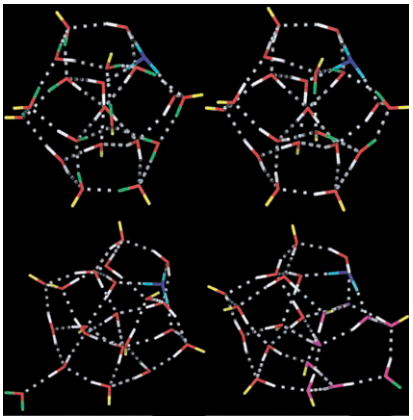

Chemosensors

D. Filippini, A. Alimelli, C. Di Natale, R. Paolesse, A. D'Amico, I. Lundström* ——— **3800 – 3803**

Chemical Sensing with Familiar Devices

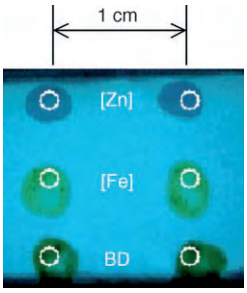

Seeing sense: The detection of detailed absorption and emission responses caused by amines, CO, and NO_x is possible using an inexpensive array of porphyrins as sensors combined with a computer screen and web camera. The computer-screen image shows the array in the presence of triethylamine. [Zn] = [Zn(tpp)], [Fe] = [Fe(tppCl)] (tpp = 5,10,15,20-tetraphenylporphyrin), BD = 2,3,17,18-tetraethyl-7,8,12,13-tetramethyl-*a*,*c*-biladiene dihydrobromide.

Multiple Bonds

M. Brynda,* L. Gagliardi,* P.-O. Widmark, P. P. Power, B. O. Roos ——— **3804 – 3807**

A Quantum Chemical Study of the Quintuple Bond between Two Chromium Centers in [PhCrCrPh]: *trans*-Bent versus Linear Geometry

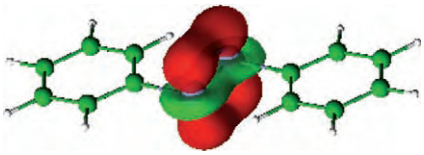

High five: Multiconfigurational quantum chemical methods show that a quintuple bond is present between the two Cr^I units in the model complex [PhCrCrPh]. The Cr–Cr (1.75 Å) and Cr–Ph (2.02 Å) bonds are shorter than those in the recently reported compound [Ar′CrCrAr′] (Ar′ = 2,6-(2,6-$iPr_2C_6H_3)_2C_6H_3$; 1.83 and 2.15 Å, respectively). This difference is attributed to the additional Cr–Ar′ interactions.

Water Clusters

P. S. Lakshminarayanan, E. Suresh, P. Ghosh* ——— **3807 – 3811**

A Hybrid Water–Chloride Structure with Discrete Undecameric Water Moieties Self-Assembled in a Heptaprotonated Octaamino Cryptand

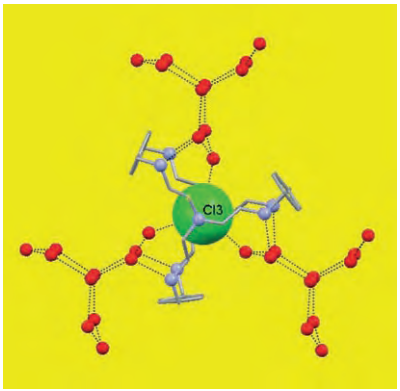

Odd water clusters: An unprecedented propeller-shaped undecameric water motif is stabilized within the lattice of the heptahydrochloride of a homoditopic octaamino cryptand with C_3 symmetry. The discrete water clusters are oriented symmetrically around the cryptand moiety and interact with encapsulated chloride inside the cavity (see structure; Cl green, O red, N blue).

© 2006 Wiley-VCH Verlag GmbH & Co. KGaA, Weinheim

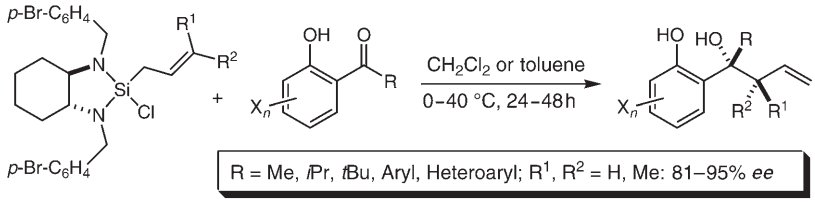

A strained allylsilane reagent is highly effective in the enantioselective allylation of hydroxyphenylketones. The method is uniquely tolerant both of sterically hindered aliphatic ketones and highly functionalized diaryl ketones and has been extended to include the first examples of highly diastereo- and enantioselective ketone crotylation, which provides access to both diastereomers.

Synthetic Methods

N. Z. Burns, B. M. Hackman, P. Y. Ng, I. A. Powelson, J. L. Leighton* ——— **3811 – 3813**

The Enantioselective Allylation and Crotylation of Sterically Hindered and Functionalized Aryl Ketones: Convenient Access to Unusual Tertiary Carbinol Structures

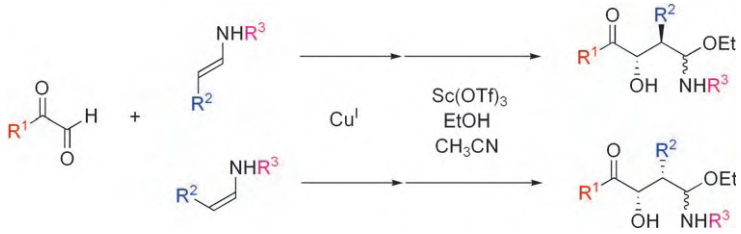

Added benefits: Catalytic enantio- and diastereoselective addition of aldehyde-derived enecarbamates to aldehydes is reported (see scheme). A copper(I)–diimine complex works well as the catalyst and the catalyst loading is not more than 1 mol% in most cases. By taking advantage of this reaction, the total synthesis of (2*S*,3*S*,4*S*)-3-hydroxy-4-methylproline has been accomplished.

Asymmetric Catalysis

R. Matsubara, N. Kawai, S. Kobayashi* ——— **3814 – 3816**

Catalytic Enantioselective and Diastereoselective Addition of Aldehyde-Derived Enecarbamates to α-Oxo Aldehydes

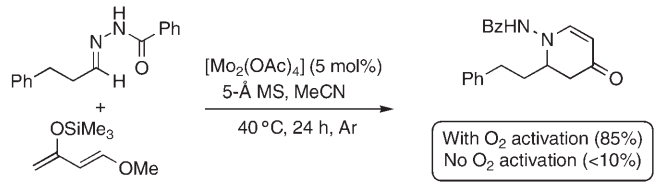

Easy activation: A Lewis acid catalyst based on molybdenum relies on activation by molecular oxygen for its high catalytic activity. The novel complex catalyzes the aza-Diels–Alder reaction of acyl hydrazones with Danishefsky dienes (see scheme) and other Lewis acid mediated reactions, such as the Mukaiyama aldol addition, Mannich-type reactions, and the addition of trimethylsilylcyanide to imines.

Transition-Metal Catalysis

Y. Yamashita, M. M. Salter, K. Aoyama, S. Kobayashi* ——— **3816 – 3819**

With Molecular-Oxygen-Activated Lewis Acids: Dinuclear Molybdenum Complexes for Aza-Diels–Alder Reactions of Acyl Hydrazones

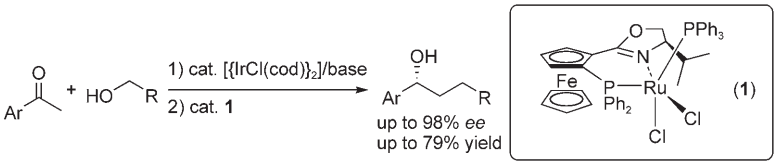

The compatibility between [{IrCl(cod)}$_2$] and ruthenium complex **1** to achieve asymmetric α-alkylative reduction of prochiral ketones with primary alcohols is an essential factor in obtaining optically active alcohols with elongation of the carbon skeleton in good yields with a high enantioselectivity.

Alkylation

G. Onodera, Y. Nishibayashi,* S. Uemura ——— **3819 – 3822**

Ir- and Ru-Catalyzed Sequential Reactions: Asymmetric α-Alkylative Reduction of Ketones with Alcohols

© 2006 Wiley-VCH Verlag GmbH & Co. KGaA, Weinheim

Contents

Tandem Annulation

R. Yanada, S. Obika, H. Kono, Y. Takemoto* ——— **3822 – 3825**

In(OTf)$_3$-Catalyzed Tandem Nucleophilic Addition and Cyclization of *ortho*-Alkynylarylaldimines to 1,2-Dihydroisoquinolines

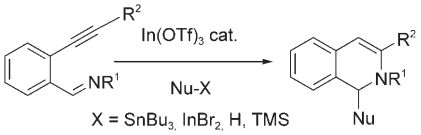

Multitasking catalyst: 1,2-Dihydroisoquinoline derivatives are prepared in good yields by an In(OTf)$_3$-catalyzed tandem annulation reaction. The catalyst activates both the imine and alkyne to the addition of various nucleophiles and the subsequent intramolecular cyclization (see picture; OTf = trifluoromethanesulfonate).

Nanostructures

X. W. Lou, C. Yuan, Q. Zhang, L. A. Archer* ——— **3825 – 3829**

Platinum-Functionalized Octahedral Silica Nanocages: Synthesis and Characterization

Hole in one! Octahedral silica nanocages are prepared by a facile one-step approach, which also enables controlled functionalization with Pt in the cavities. The strategy is based on mediated deposition of silica on simultaneously generated salt quasi-templates, which are simply removed by washing with water.

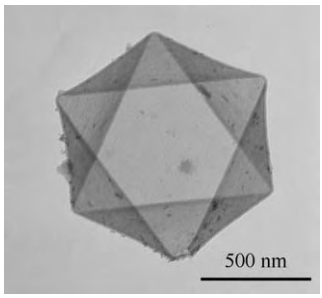

Nanotechnology

D. B. Cordes, S. Gamsey, B. Singaram* ——— **3829 – 3832**

Fluorescent Quantum Dots with Boronic Acid Substituted Viologens To Sense Glucose in Aqueous Solution

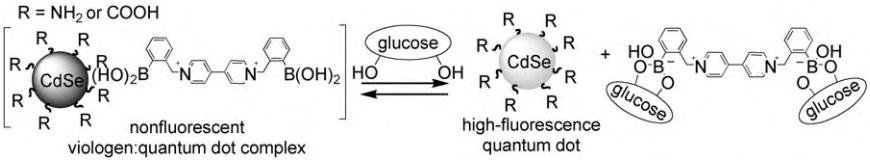

A quantum leap in glucose sensing: Commercially available fluorescent quantum dots are used in combination with boronic acid modified viologens to sense glucose in aqueous solution. The signal response is optimized by adjusting the ratio of quantum dots to viologen quencher.

Palladium-Catalyzed Hydrogenation

Q. Yang, G. Shang, W. Gao, J. Deng, X. Zhang* ——— **3832 – 3835**

A Highly Enantioselective, Pd–TangPhos-Catalyzed Hydrogenation of *N*-Tosylimines

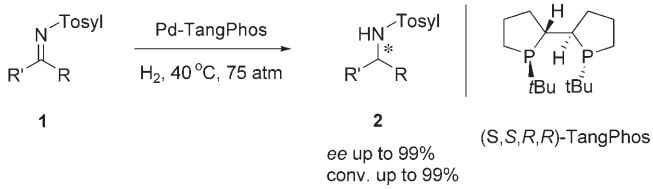

1

2

ee up to 99%
conv. up to 99%

(S,S,R,R)-TangPhos

A catalyst system composed of Pd(OCOCF$_3$)$_2$ complexed with the electron-donating, rigid chiral diphosphane TangPhos gives excellent enantioselectivities (up to 99% *ee*) and conversions (up to >99%) in the hydrogenation of *N*-tosylimines **1** (see scheme). A variety of aromatic, aliphatic, and cyclic chiral amines **2** can be prepared by this methodology.

© 2006 Wiley-VCH Verlag GmbH & Co. KGaA, Weinheim

Worthy of merit: The new class of nanostructured p-type thermoelectrics $Na_{1-x}Pb_mSb_yTe_{m+2}$ is reported. The exceptionally high thermoelectric figures of merit ZT of these materials (see graph), which exceed those of the state-of-the-art materials PbTe and $(GeTe)_{1-x}((Ag_2Te)_{1-y}(Sb_2Te_3)_y)_x$ (TAGS), derive from their very low lattice thermal conductivities.

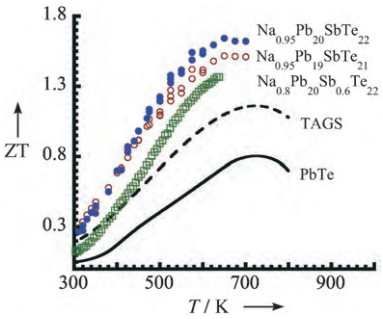

Thermoelectric Materials

P. F. P. Poudeu, J. D'Angelo, A. D. Downey, J. L. Short, T. P. Hogan, M. G. Kanatzidis* ——— **3835 – 3839**

High Thermoelectric Figure of Merit and Nanostructuring in Bulk p-type $Na_{1-x}Pb_mSb_yTe_{m+2}$

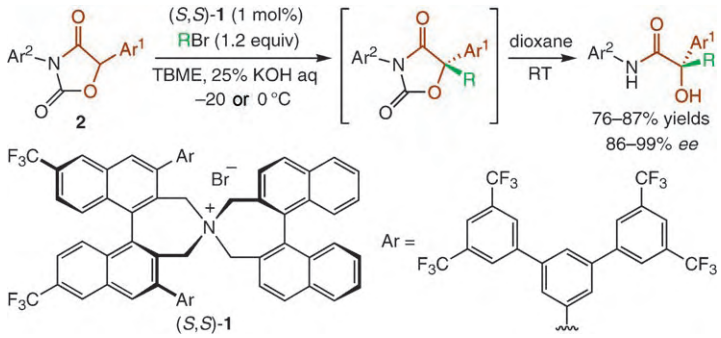

Center of attention: The chiral ammonium bromide **1** has been used as a catalyst for the highly enantioselective alkylation of diaryloxazolidindiones **2** under mild phase-transfer conditions (TBME = *tert*-butyl methyl ether). This method provides practical access to a variety of optically active tertiary α-hydroxycarboxylic acid derivatives.

Asymmetric Synthesis

T. Ooi, K. Fukumoto, K. Maruoka* ——— **3839 – 3842**

Construction of Enantiomerically Enriched Tertiary α-Hydroxycarboxylic Acid Derivatives by Phase-Transfer-Catalyzed Asymmetric Alkylation of Diaryloxazolidin-2,4-diones

Two merocyanine dyes are assembled by multiple hydrogen bonds with summation of their dipole moments (see formula; R = 2-ethylhexyl). It exhibits a strongly increased degree of dye alignment in an electric field according to electrooptical absorption spectroscopy.

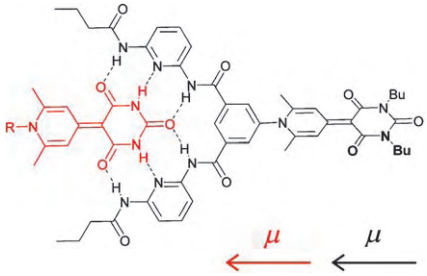

Nonlinear Optics

F. Würthner,* J. Schmidt, M. Stolte, R. Wortmann* ——— **3842 – 3846**

Hydrogen-Bond-Directed Head-to-Tail Orientation of Dipolar Merocyanine Dyes: A Strategy for the Design of Electrooptical Materials

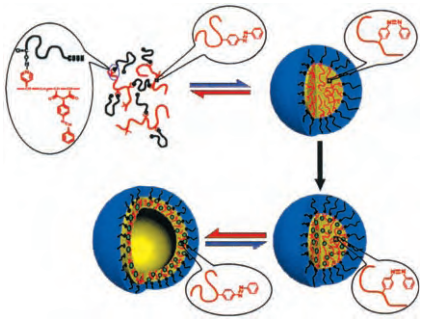

Light switch: Noncovalently connected micelles are formed by the photoisomerization of azobenzene groups in copolymer building blocks and the hydrogen-bonding interaction within the polymer pair. The UV-induced micellar structure can be fixed through core cross-linking, which allows the reversible optical switching of a micelle–hollow-sphere transition (see picture).

Photoisomerization

X. Liu, M. Jiang* ——— **3846 – 3850**

Optical Switching of Self-Assembly: Micellization and Micelle–Hollow-Sphere Transition of Hydrogen-Bonded Polymers

© 2006 Wiley-VCH Verlag GmbH & Co. KGaA, Weinheim

Contents

Oligosaccharide Synthesis

O. Kanie,* I. Ohtsuka, T. Ako, S. Daikoku, Y. Kanie, R. Kato ——— **3851 – 3854**

Orthogonal Glycosylation Reactions on Solid Phase and Synthesis of a Library Consisting of a Complete Set of Fucosyl Galactose Isomers

A dream team: Orthogonal glycosylation and solid-phase synthesis were shown to be an excellent combination for polysaccharide synthesis (see scheme). The method was applied to generate a complete library of structural isomers with an L-fucosyl-D-galactose sequence.

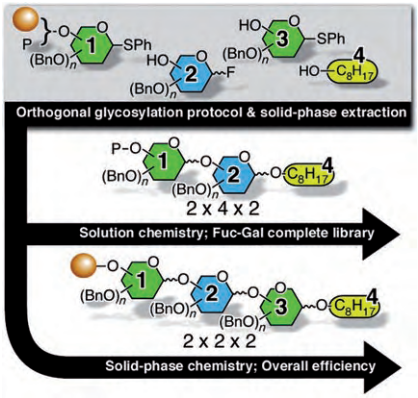

Quinone Complexes

J. Moussa, D. A. Lev, K. Boubekeur, M. N. Rager, H. Amouri* ——— **3854 – 3858**

A η^4-Dithio-*para*-benzoquinone Metal Complex

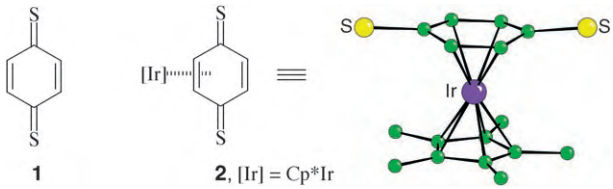

Overcoming a long-standing challenge: A rational synthetic procedure allows the isolation of the first stable η^4-dithio-*para*-benzoquinone complex (**2**; Cp* = C_5Me_5). The X-ray molecular structure of **2** confirms the coordination of the elusive intermediate **1** in an η^4 manner. Computational analyses of **2** support the role of the {Cp*Ir} fragment in stabilizing this reactive intermediate.

Carbocyclic Carbenes

W. A. Herrmann,* K. Öfele, S. K. Schneider, E. Herdtweck, S. D. Hoffmann ——— **3859 – 3862**

A Carbocyclic Carbene as an Efficient Catalyst Ligand for C–C Coupling Reactions

A new player on the field: Carbocyclic carbenes are potentially better control ligands than N-heterocyclic carbenes (NHCs) in catalyzed C–C coupling reactions. Pd^{II} complexes of cycloheptatrienylidene (see picture), which are readily prepared, thermally stable, and highly stable towards acid, are as effective as the familiar NHC complexes in Suzuki and Heck reactions or perform even better.

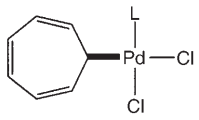

L = $P(C_6H_5)_3$, $P(c\text{-}C_6H_{11})_3$

Structure Elucidation

M. Nett, Ö. Erol, S. Kehraus, M. Köck, A. Krick, E. Eguereva, E. Neu, G. M. König* ——— **3863 – 3867**

Siphonazole, an Unusual Metabolite from *Herpetosiphon* sp.

Deep and complex: The first representative (see picture) of a new structural class has been isolated from a deep-rooted filamentous bacterium of the genus *Herpetosiphon*. Feeding with ^{13}C and ^{15}N-labeled precursors showed the complex biosynthesis to involve shikimate, the polyketide, and the amino acid metabolism.

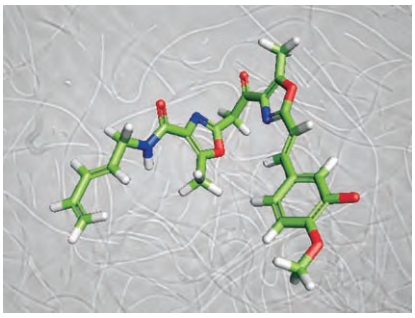

© 2006 Wiley-VCH Verlag GmbH & Co. KGaA, Weinheim

No doubt: The high-quality crystal structure of $[Cu(TMG_3tren)(O_2)]SbF_6$ (see picture) presents the first unambiguous characterization of a bioinorganic compound in which a dioxygen molecule coordinates end-on to a Cu^I ion. This species, which is best described as a superoxo copper(II) complex, serves as a model complex for initially formed $Cu–O_2$ adducts present in a variety of active sites of copper enzymes.

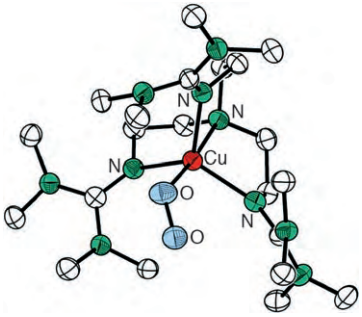

Copper Dioxygen Compounds

C. Würtele, E. Gaoutchenova, K. Harms, M. C. Holthausen,* J. Sundermeyer,* S. Schindler* ——— **3867 – 3869**

Crystallographic Characterization of a Synthetic 1:1 End-On Copper Dioxygen Adduct Complex

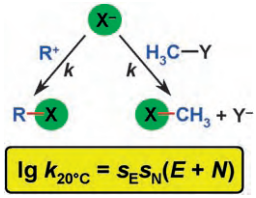

One for all? The nucleophilicity parameters *N*, which have been derived from the rate constants *k* of reactions of nucleophiles with carbocations, also hold for S_N2-type reactions (see scheme). A general equation is suggested which includes established correlations (Swain–Scott, Ritchie) as special cases.

Nucleophilicity Scales

T. B. Phan, M. Breugst, H. Mayr* ——— **3869 – 3874**

Towards a General Scale of Nucleophilicity?

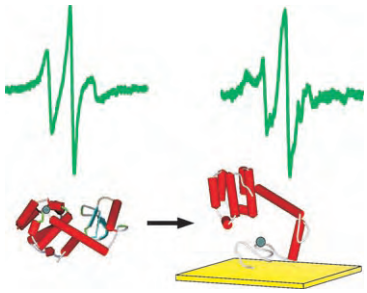

Spin doctoring: Site-directed spin labeling was used to determine the structure of T4 lysozyme adsorbed on quartz. At high ionic strength significant changes of the backbone fold are limited to the region around the enzymatic cleft. In contrast, at low ionic strength the previously unperturbed parts of the protein interact with the surface. Hydrophobic interactions are thought to play an important role in the partial unfolding at high ionic strength.

Protein Folding

K. Jacobsen, W. L. Hubbell, O. P. Ernst, T. Risse* ——— **3874 – 3877**

Details of the Partial Unfolding of T4 Lysozyme on Quartz Using Site-Directed Spin Labeling

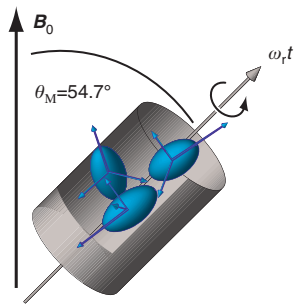

Slim peaks: Using a perdeuterated protein recrystallized from a 10:90 H_2O:D_2O mixture in magic-angle spinning (MAS) solid-state NMR spectroscopy experiments gives small ^1H line widths at moderate spinning frequencies without application of homonuclear decoupling. This labeling strategy opens new perspectives for assignment of large protein spin systems.

Protein NMR Spectroscopy

V. Chevelkov, K. Rehbein, A. Diehl, B. Reif* ——— **3878 – 3881**

Ultrahigh Resolution in Proton Solid-State NMR Spectroscopy at High Levels of Deuteration

© 2006 Wiley-VCH Verlag GmbH & Co. KGaA, Weinheim

Call for Papers

Print ISSN: 1861-4728
Online ISSN: 1861-471X
2006. Volume 1. 6 issues.

Rooted in Asia – Read all over the World

Readership:
Chemists of all disciplines

A sister journal of ***Angewandte Chemie*** and ***Chemistry – A European Journal***.

To submit your next excellent manuscript go to the journal's homepage:

www.ChemAsianJ.org

Chairman of the Editorial Board:

Ryoji Noyori

Nagoya University and
RIKEN, Saitama, Japan

WILEY-VCH

Chemistry – An Asian Journal is published with the Asian Chemical Editorial Society (ACES):

- Chinese Chemical Society
- Chemical Research Society of India
- Chemical Society of Japan
- Korean Chemical Society

Supported by the Gesellschaft Deutscher Chemiker

25410602_gu

Looking for outstanding employees?

Do you need another expert for your excellent team?
... Chemists, PhD Students, Managers, Professors, Sales Representatives...

Place an advert in the printed version and have it made available online for 1 month, free of charge!

Angewandte Chemie International Edition
Advertising Sales Department: Marion Schulz
Phone: 0 62 01 - 60 65 65
Fax: 0 62 01 - 60 65 50
E-Mail: MSchulz@wiley-vch.de

Service

Keywords ____ *3882*

Authors ____ *3883*

Vacancies ____ *A33*

Preview ____ *3885*

SCHERING
making medicine work

linking knowledge.

We at Schering know that a network of knowledge opens up fascinating possibilities, unlimited opportunities and intelligent answers. As an innovative pharmaceutical company, we work continuously for medical progress.
We cooperate with the best in clinical care, academic research and the pharmaceutical industry from around the world.
By bridging early diagnosis, prevention, treatment and therapy control we are able to provide new solutions to help resolve significant unmet medical needs.

Schering – making medicine work.

www.schering.de

A Closer Look at Nanoporous Materials**

Jörg Kärger and Farida Grinberg

The acronym INSIDE PORES stands for "In Situ Study and Development of Processes Involving Porous Solids" and indicates one of the Networks of Excellence (NoE) established within the 6th Frame Programme of the European Community. The initiative was launched to bring together researchers in the rapidly expanding field of nanoporous materials, with particular emphasis on the mechanisms of reactions and processes that occur in membranes, sorbents, and catalysts, including their in situ characterization. The scientific program included 16 invited lectures of tutorial character, with topics comprising the whole of the INSIDE PORES spectrum. Selected results of current research were highlighted in 20 oral contributions and 80 posters. Supported by a team of colleagues from the NoE core partners and her local associates, Deborah Jones, Montpellier, did an excellent job in organizing this workshop.

The first talk of the workshop, authored by Etienne Vansant and Peggy Cool, Antwerp, highlighted the fascinating novel synthetic routes for generating nanoporous materials with tailored mesostructures. Such methods open up completely new pathways towards transport-optimized adsorbents and catalysts. In his lecture "*How Nature Produces Porous Silica and What We Can Learn from It*" Peter Behrens, Hanover, illustrated the great potential for generating crystalline nanoporous substances still hidden in Mother Nature's laboratory.[1]

The presentations on sorption were commenced by Kenneth Sing, London, with an introduction to the challenges and pitfalls of employing adsorption measurements for characterizing nanoporous materials. In particular for the exploration of novel pore structures, he strongly recommended to apply a set of probe molecules with different size and molecular structure rather than using just one, and to combine the results with the information provided by other pore-sensitive measuring techniques, including mercury porosimetry. In his talk on "*The Role of Porosity and Functionality of Activated Carbon in Adsorption Processes*" Francisco Rodriguez-Reinoso, Alicante, provided an impressive overview of the manifold applications of activated carbon,[2] which uniquely combines the advantages of well-developed porosity, thermal and chemical stability, and low production costs.

In his talk on "*Molecular Simulation of Adsorption and Transport in Nanopores*" Nick Quirke, London, exemplified the considerable progress in our understanding of nanoscale phenomena, as based on detailed molecular models and the elaboration of idealized models of nanopores and nanoporous arrays, with particular emphasis on the remarkable properties associated with nanotubes. Francois Henn, Montpellier, combined the evidence accessible by dielectric relaxation spectroscopy with the results of modelling and computational simulation of surface thermodynamics of aluminosilicates.

The interrelation between molecular transport and the structural properties of the nanoporous host–guest systems under study was the focus of the presentations on molecular diffusion and permeation. Freek Kapteijn, Delft, highlighted the multitude of transport mechanisms, including viscous flow, Knudsen and molecular diffusion, adsorption, as well as surface and/or zeolitic diffusion, all of which occur during separation through membranes.[3] With examples[4,5] taken from the application of both pulsed field gradient (PFG) NMR and interference microscopy, Jörg Kärger, Leipzig, demonstrated that the rate of molecular propagation in zeolites may be far more complicated than can be adequately represented by just one (zeolitic) diffusion coefficient.

John D. F. Ramsay, Montpellier, emphasized the potential of small-angle radiation scattering using X-rays (SAXS) and neutrons (SANS) for the in situ characterization of nanomaterials over a range of 1 to >100 nm, including the observation of crystal formation during zeolite synthesis as a most spectacular application. Also the second talk within this section dealt with a technique which is bound to very special experimental specifications, in particular, magnetic resonance experiments with positive muons (elementary particles with spin $^1/_2$, a mass of close to one-ninth of the proton mass, and a lifetime of 2.20 μs), which can be generated only in powerful accelerators. Emil Roduner, Stuttgart, showed, however, that in some special cases, including the observation of free radicals in zeolites, the substantial expense of such experiments with muons may be justified.

In his talk on catalysis, Francois Fajula, Montpellier, ascribed the special position of nanoporous materials among other solid catalysts to the curvature of their internal surface on the atomic scale. Owing to this peculiarity as well as shape selectivity, zeolite-catalyzed reactions can be regarded as supermolecular transformations which resemble those occurring in enzymes. Following an analogous concept, Roger Gläser, Stuttgart, gave an overview of the potential of zeolite catalysts for producing organic intermediates and fine chemicals, and elaborated on their rele-

[*] Prof. J. Kärger, Dr. F. Grinberg
Fakultät für Physik und Geowissenschaften
Institut für Experimentelle Physik I
Abteilung Grenzflächenphysik
Universität Leipzig
Linnéstrasse 5
D-04103 Leipzig (Germany)
E-mail: kaerger@physik.uni-leipzig.de

[**] First INSIDE PORES Workshop, La Grande Motte (France), March 19–23, 2006

InterScience
© 2006 Wiley-VCH Verlag GmbH & Co. KGaA, Weinheim

vance as case studies within the INSIDE PORES project.

The application of nanoporous materials to novel processes was illustrated in two talks. Anthony Kucernak, London, introduced Pd-alloy catalysts with periodic mesoporous structures which were produced with the liquid-crystal templating technique[6] and which represent a new generation of more efficient electrocatalysts for fuel cells. Ahmed Khalil and Frank Marlow, Mülheim, reported their group's research on the variance in the structural hierarchy of mesoporous materials,[7] and the consequences of this variance on their optical functionality were discussed in detail.

At the center of the workshop, there was a panel discussion dedicated to the potential fields of cooperation between INSIDE PORES and the two projects "Integrated Design of Catalytic Nanomaterials for a Sustainable Production" (IDECAT) and "Nanoscale-based Membrane Technologies" (NANOMEMPRO). Both of these NoEs focus on special types of high-tech materials, while the main issue of INSIDE PORES is the in situ exploration of the processes that take place in these materials. Therefore, cooperation of these three closely related projects promises great potential for synergism. Correspondingly, the presentations of the network coordinators were particular highlights of the workshop. Gilbert Rios (Montpellier, coordinator of NANOMEMPRO) and Gabriele Centi (Messina, coordinator of IDECAT) presented a fascinating overview of the fabrication of high-performance membranes and catalysts based on specially designed nanoporous materials. The combined application of the various, often highly sophisticated methods of the in situ study of nanoporous materials was impressively illustrated by Nick Kanellopoulos (Athens, coordinator of INSIDE PORES). Owing to these powerful characterization techniques and the excellent options of swift communication within the network, the term "supertool" has been coined for such concerted investigations.

The prize for the best poster of the workshop was awarded to the Universities of St. Andrews and Leipzig, which collaborated on the fields of zeolite synthesis and diffusion measurements. Figure 1 illustrates the key technique applied in these studies, namely the application of interference microscopy to follow the evolution of intracrystalline concentration profiles during molecular uptake by zeolite crystallites. Pavel Kortunov, the lead author of this poster, received this award also in recognition of his other contributions to the workshop.

Dissemination of information is one of the key aims in the promotion of science by the European Community, in particular through the NoEs. The organizers of this workshop did their best to achieve this aim. Most of the plenary speakers followed the request of the organizers to make their presentations accessible to a wide audience. Interested readers are invited to experience the workshop atmosphere and to share in its scientific insights by visiting the website www.insidepores.fr/workshop/pages/index.htm.

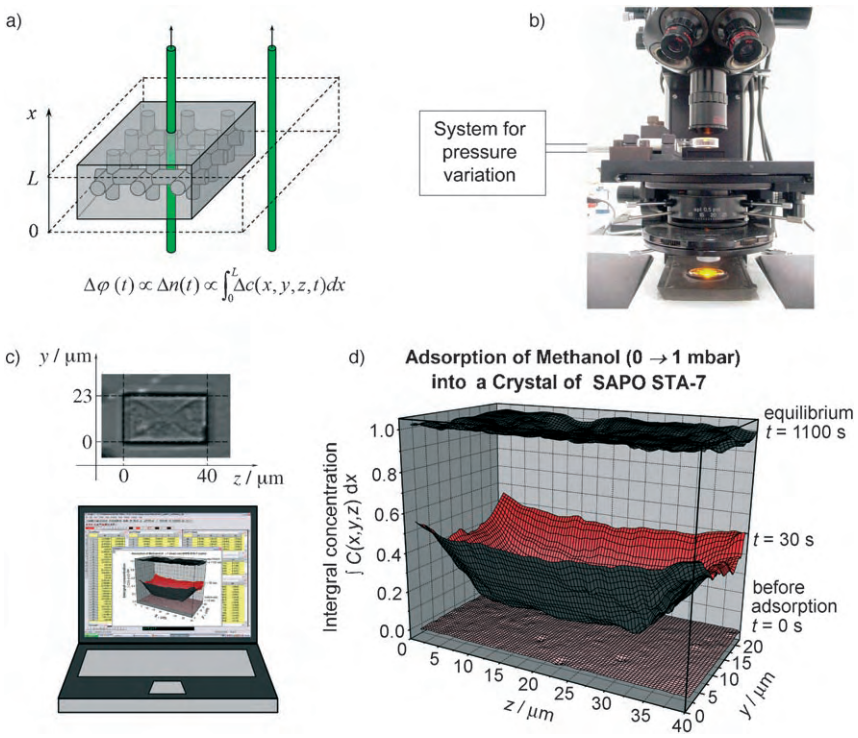

Figure 1. Application of interference microscopy to monitor intracrystalline concentration profiles. Interference microscopy is based on the comparison of the phases of two parallel light beams, one of which passes through the crystallite under study (a). Changes in the local concentration (Δc) lead to changes of the optical density of the crystal (Δn). The resulting phase shifts ($\Delta\varphi$) are observed in the interference patterns recorded by the microscope (b). Conversely, the concentration integrals in the observation direction may be calculated from the interference patterns (c), leading to two-dimensional profiles of integrated (and, hence, of mean) concentrations in the observation direction (d).

[1] M. Sumper, E. Brunner, *Adv. Funct. Mater.* **2006**, *16*, 17–26.

[2] H. Marsh, F. Rodriguez-Reinoso, *Activated Carbon*, Elsevier, Amsterdam, **2006**.

[3] F. Kapteijn, W. Zhu, J. A. Moulijn, T. Q. Gardner in *Structured Catalysts and Reactors* (Eds.: A. Cybulski, J. A. Moulijn), 2nd ed., Boca Raton, CRC Taylor & Francis, **2005**, 700–746.

[4] J. Kärger, F. Grinberg, P. Heitjans (Eds.), *Diffusion Fundamentals*, Leipziger Universitätsverlag, Leipzig, **2005**.

[5] J. Kärger, *Diffusion Fundamentals* **2005**, 1, 5.1–5.107.

[6] M. E. Raimondi, J. M. Seddon, *Liq. Cryst.* **1999**, *26*, 305–339.

[7] F. Marlow, W. Dong, *ChemPhysChem* **2003**, *4*, 549–554..

DOI: 10.1002/anie.200601629

© 2006 Wiley-VCH Verlag GmbH & Co. KGaA, Weinheim

THE NOBEL PRIZE IN CHEMISTRY 2005

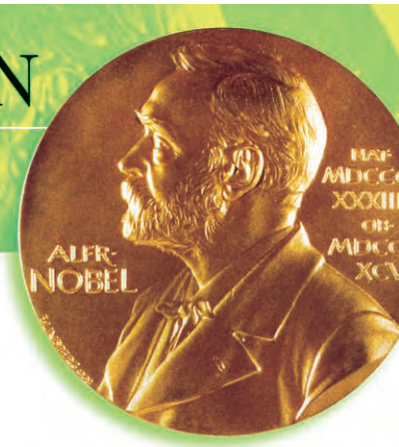

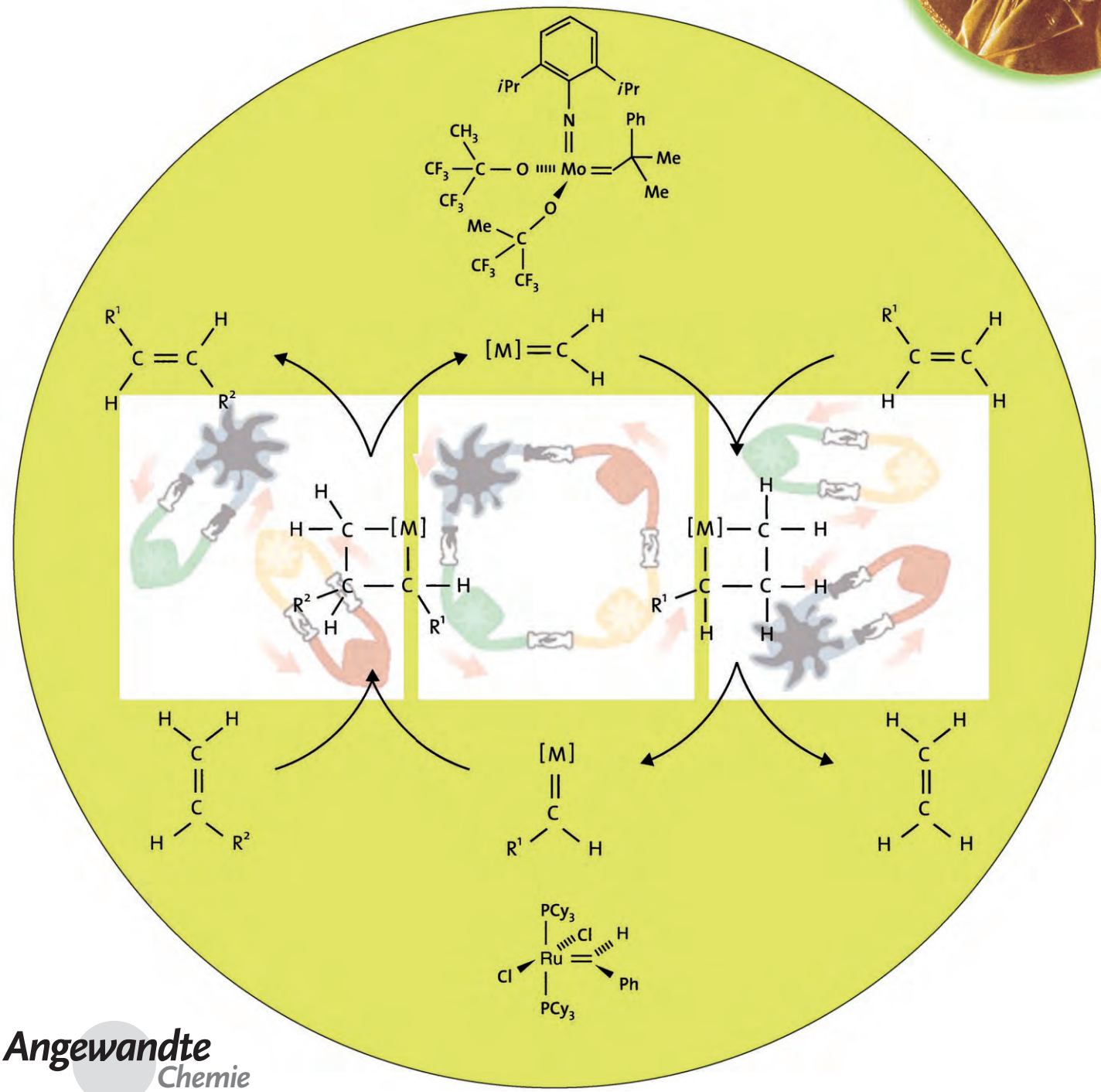

Angewandte Chemie

© 2006 Wiley-VCH Verlag GmbH & Co. KGaA, Weinheim

Metathesis Reactions

DOI: 10.1002/anie.200601234

Olefin Metathesis: The Early Days (Nobel Lecture)**

*Yves Chauvin**

Keywords:
homogeneous catalysis · metathesis · Nobel lecture · polymerization · ruthenium

Biographical Notes

I was born on October 10, 1930 in Menin (Menen in Flemish) in western Flanders, on the border between Belgium and France. My parents were French. To be more precise, they were not only both from the Tours region, but also descended from long-established families in the little village of Beaumont-la-Ronce. I used to spend my holidays there in my grandparents' large family house, with my numerous cousins. When I die, I am going to be buried in the village cemetery. My grandmother was fond of painting and playing the piano. She had been given lessons by Emmanuel Chabrier, who used to spend the summer months in nearby Membrolle. He said in his correspondence that he did not much care for his pupils on the whole and my grandmother found him very strict.

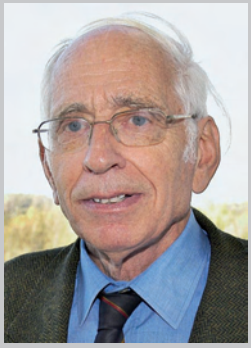

Most of my ancestors were small-scale farmers. My father was an electrical engineer. After three years of military service and quite a difficult time in the First World War, he was sent by the company that had taken him on after his demobilization to Ypres and then Menin, to work on rebuilding (building) the electricity network in this war-ravaged province. I remember him always being very motivated and working very long hours. He was sent to war again in 1939 and taken prisoner. There were five brothers and sisters in the family and we had quite a strict upbringing.

From my bedroom, I looked out over our large garden (roses and vegetables) and the Lys river, which at that particular point separates France from Belgium and was where the flax was retted in tanks then dried in little bundles in a field (what a foul smell!). I watched the barges go past, towed by horses or even by men. It was a fascinating sight: the man pulling the rope remained bent over and unmoving for several minutes before the barge started to move. I also remember Vauban's fortifications in this land of invasions, and the smell of roasted chicory. I still have many paintings of Flanders that my father bought from contemporary painters—somewhat classical, but not devoid of charm.

I went to pre-school in Flanders and then the French primary school, which meant that I crossed the border every day. I then continued my secondary and higher education in various towns. During the war, I managed to come through the bombings unscathed, though sometimes only just. The war taught me to eat what there was; I am still not a fussy eater, although I do enjoy good food.

To be perfectly truthful, I was not a very brilliant student, even at chemistry school. I chose chemistry rather by chance, because I firmly believed (and still do) that you can become passionately involved in your work whatever it is. Various circumstances, mainly to do with my military service, prevented me from doing a PhD and I have often regretted it, though you do need to choose the "right" supervisor in the "right" discipline—no easy task when you are totally inexperienced.

So I took a job in industry, but the fact that process development consisted primarily of copying what already existed, with no possibility of exploring other fields, prompted me to resign. Furthermore, I discovered that this was a very common attitude among managers. They are afraid of anything new: "Do what everyone else does and change as little as possible: at least we know it will work". It is the opposite of my way of thinking, which, I must admit, is a bit of an

[*] Y. Chauvin
Institut Français du Pétrole
Rueil-Malmaison
and
Centre National de la Recherche Scientifique
Lyon (France)

[**] Copyright© The Nobel Foundation 2005. We thank the Nobel Foundation, Stockholm, for permission to print this lecture. The title is taken from the excellent article by A. Maureen Rouhi, a scientific journalist, published in *Chemical & Engineering News* of 23 December 2002, a special issue on metathesis.

© 2006 Wiley-VCH Verlag GmbH & Co. KGaA, Weinheim

obsession! I have often got into arguments about it. My motto is more, "If you want to find something new, look for something new!" There is a certain amount of risk in this attitude, as even the slightest failure tends to be resounding, but you are so happy when you succeed that it is worth taking the risk.

The whole contradiction of research (whether applied or fundamental) generally lies in the fact that we have to start out with the knowledge handed down by our predecessors, but be able to depart from it "at the right time".

I joined Institut Français du Pétrole in 1960 and managed to focus my work on what I thought would be most interesting. I got married the same year and over the course of time we had two sons and five grandsons.

The oil industry essentially uses heterogeneous catalysis: cracking, reforming, hydrodesulfurization, hydrogenation, etc., but that was not what interested me. I have always tried to avoid areas that have been perfected with time. At the time, nothing much was being done in France on coordination chemistry, organometallics, or homogeneous catalysis by transition metals and I was fascinated by the achievements in Italy (G. Natta), Great Britain (J. Chatt), Germany (at the Max Planck Institute in Mülheim), and the United States. As a result, I unwittingly became the French specialist in these disciplines, which brought me into contact with both the positive and the unwieldy aspects of the various commissions at the CNRS. I spent the best part of my time on applied chemistry, which was what I had been employed for and which I was quite happy about. This was how I came to develop two homogeneous catalysis processes. The first one, which uses a nickel-based catalyst, was called "Dimersol" and exists in two basic versions: The "gasoline" version (Figure 1) consists of

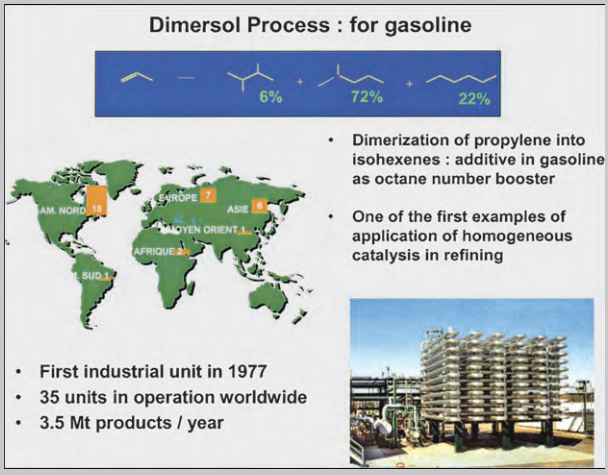

Figure 1.

dimerizing propene to high-octane isohexenes. There is, quite often, an excess of propene, especially in oil refineries that do not produce petrochemicals, as in the United States. There are currently 35 plants in operation (including 18 in the USA), with a combined annual output of 3.5 million tonnes. It was the first and only time that coordination catalysis had been used in refining.

The "chemical" version of the Dimersol process (Figure 2) consists of dimerizing *n*-butenes to isooctenes, basic inputs for plasticizers, using the "oxo" reaction. Current production levels stand at 400 000 tonnes a year.

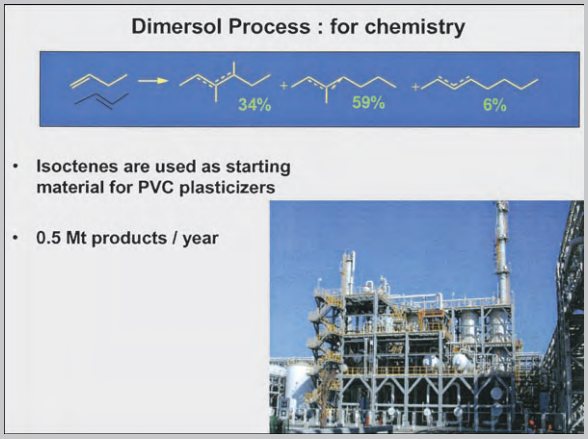

Figure 2.

The second process I developed, and which uses a titanium-based catalyst, was called "Alphabutol". It consists of dimerizing ethylene to 1-butene (Figure 3), the comono-

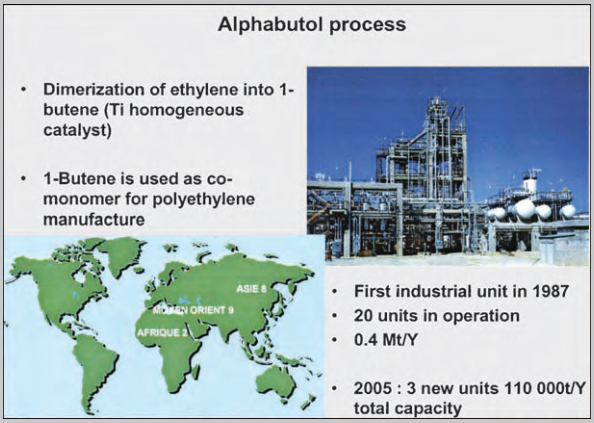

Figure 3.

mer of low-density linear polyethylene. The benefits of such a process were not evident to begin with and stem from a number of causes. There are currently 20 plants operating worldwide, with a combined output of 400 000 tonnes a year. However, others are under construction, which will take total output to over 0.5 million tonnes a year.

While there are obvious drawbacks to not having done a PhD (especially when you supervise those with them!), the advantage is that at least your mind is free to focus on whatever presents itself. At the time, I was working on

 © 2006 Wiley-VCH Verlag GmbH & Co. KGaA, Weinheim

batteries and, in particular, the non-aqueous electrolytes used to extend their electrochemical window. I thought it would be a good idea to try to use these electrolytes, which belong to the class of ionic liquids, as catalyst solvents. These liquids feature very low vapor pressure and virtual insolubility in hydrocarbons, paving the way for a biphasic catalysis. The mixture of alkylimidazolium chloride and aluminum chloride forms a liquid with a very low melting point (below ambient temperature; Figure 4). It proved to be a first-rate solvent for

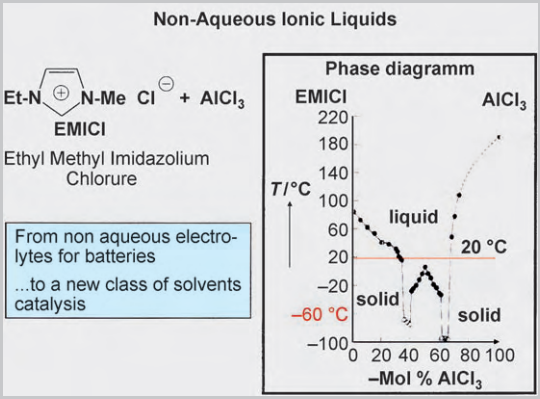

Figure 4.

nickel-based dimerization catalysts (Dimersol catalysts). The diagram for this process, called "Difasol", is shown in Figure 5. The reaction volume required for a biphasic system is 10-times smaller than for a homogeneous system (important for safety: refineries do not like to have large volumes in reaction because they are potential "bombs", especially at start-up); likewise for nickel consumption. This new process, dealt with in a PhD thesis in 1990, will see the light of day thanks to the inventiveness and determination of Hélène Olivier-Bourbigou, who took over from me in the laboratory.

What applied chemistry has taught me is the need for absolute solidarity between the research laboratory and the "downstream" side (pilot testing, marketing, setting up industrial plant): same enthusiasm, same determination, especially when everything goes wrong!

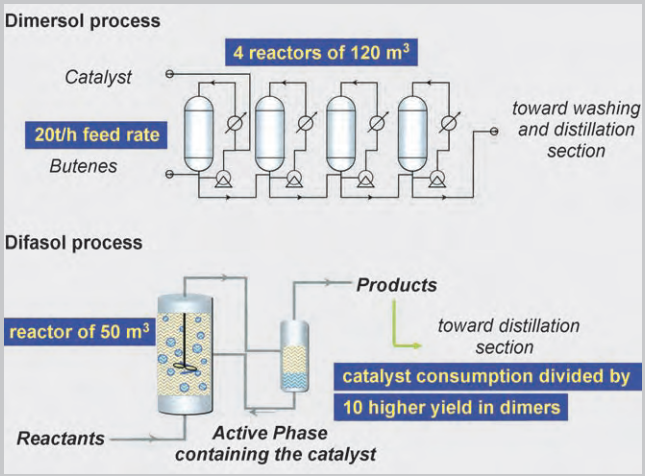

Figure 5.

There is no difference between fundamental research and applied research. Although this is my view, based on personal taste and the areas I have worked in, it is not necessarily true for others. The PhD work either led to, or was derived from processes. I have spoken so much about "processes" because they took up about three-quarters of my working time. However, I also took an interest in other aspects of coordination chemistry, such as palladium catalysis, rhodium catalysis, asymmetric amino acid synthesis, and so on. After retiring in 1995, I was invited to work in J.-M. Basset's laboratory in Lyon, which allows me to pursue a reasonable level of activity.

Olefin Metathesis: Discovery and First Achievements

At no time in my life did I dream of such a prize. Indeed, as I explained in my biography, I had no training in research as such and as a consequence I am in a sense self-taught. What I owe to the Institut Français du Pétrole is some freedom to choose my research area. I have always been an avid reader of chemical literature, eager for what is new. Like all sciences, chemistry is marked by magic moments. For someone fortunate enough to live such a moment, it is an instant of intense emotion: an immense field of investigation suddenly opens up before you. There were very many of these moments in the course of my career. For example, the discovery of ferrocene, the stereospecific polymerization of olefins by G. Natta (I never failed to read any of his articles!), the homogeneous catalysis of hydrogenation by rhodium complexes (G. Wilkinson), the homogeneous catalysis of dimerization of olefins by nickel complexes (G. Wilke and B. Bogdanovic) and the catalysis of asymmetric hydrogenation. I experienced the latter with an especially keen intensity because we were in very close touch with Henri Kagan, who came every month to tell us about his chemistry; it was outstanding! And 1964 was an especially magical year (Figure 6): a revelation for me, by R. L. Banks and G. C. Bailey of Phillips Petroleum, of the disproportionation of olefins catalyzed by a molybdenum- or tungsten-based heterogeneous catalyst deposited on alumina; the homogeneous catalysis of polymerization of cyclopentene by ring opening, published by G. Natta, and the existence of a new metal–carbon bond, the carbenes of E. O. Fischer. A priori these three had nothing in common.

The disproportionation of linear olefins (Banks and Bailey), since called metathesis, is an equilibrated reaction, governed basically by entropy. This is doubtless why, from the start, "pairwise mechanisms" were favored (Figure 7), which

 © 2006 Wiley-VCH Verlag GmbH & Co. KGaA, Weinheim

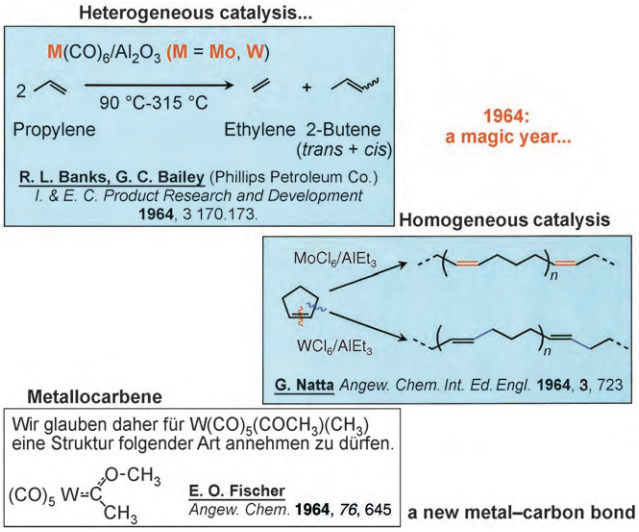

Figure 6.

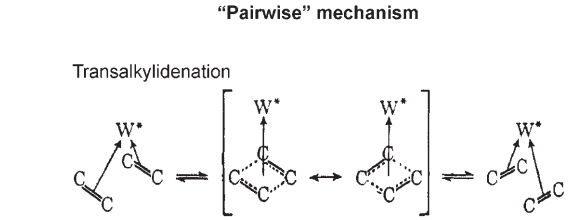

Figure 7.

assume a perfect symmetry of the reaction intermediates. In addition, these intermediates are based on the only bonds known at the time: π bonds and σ bonds between hydrocarbons and transition metals. Other mechanisms were proposed (Figure 8).

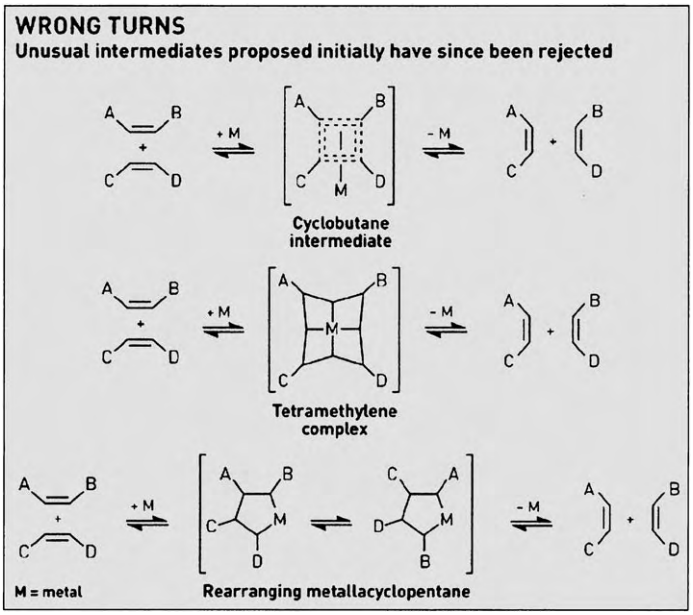

Figure 8.

The polymerization of cyclopentene into polypentenylene (Natta), for its part, is governed mainly by the enthalpy linked to the release of the ring strain when the ring is cleaved; but entropy also plays a part there owing to the multiple conformations of the chain and, like the metathesis of acyclic olefins, the reaction is equilibrated. These factors are no longer the same in the case of the higher cycles, as we shall see later. To explain the high molecular weights observed from the start of the reaction, Natta assumed the existence of a σ bond between the transition metal and the growing chain, the proposed mechanism being an α-cleavage of the ring such as is often invoked in classic organic chemistry.

My immediate reaction back in 1964 was the thought that disproportionation and ring opening were part of the same reaction. In addition to the fact that both reactions preserved the number and type of double bonds (only the molecular weight of the products was changed), they used the same transition metals, molybdenum and tungsten. In fact, at the time, in a way that may be surprising today, there was a gap—a total lack of understanding—between homogeneous catalysis and heterogeneous catalysis (some people even attributed the fundamental role in the transformation to the catalyst support!). Since I was familiar with both types of catalysis in our Institute, that was not a real problem for me. But how could the statistical aspect of the one be reconciled with the chain growth of the other? Meanwhile, N. Calderon had also started building a bridge between homogeneous catalysis and heterogeneous catalysis.[1] It then seemed obvious to associate the two reactions, where the enthalpy of ring opening would in a sense "freeze" the statistical reactivity of the acyclic olefin.[2] Accordingly we treated cyclopentene with 2-pentene in the molar ratio 1:1 with the homogeneous catalyst $WOCl_4$ and $SnBu_4$ or $AlEt_2Cl$. The result is shown in Figure 9 and Table 1: in addition to the C_{10}

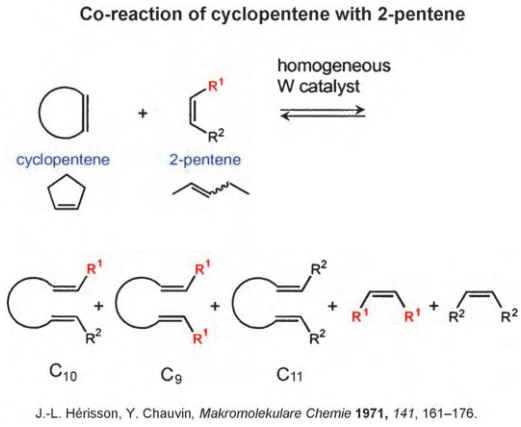

Figure 9.

di-unsaturated product of the expected coupling of cyclopentene with 2-pentene (5+5 carbon atoms), there were other products, also di-unsaturated (5+4) and (5+6), the ratio was 1:2:1 for the $C_9/C_{10}/C_{11}$ species, then higher tri-unsaturated products containing (5+5+5), (5+5+4), and (5+5+6) carbon atoms; and so on, in decreasing quantities, but in each case

 © 2006 Wiley-VCH Verlag GmbH & Co. KGaA, Weinheim

forming "triads". This was, then, a "telomerization" reaction in which the telogene is *n*-pentene and the taxogene is cyclopentene. Since the participation of the 2-pentene in the telomerization reaction is at each instant equal to its participation in the metathesis reaction, the telomerization products are as a consequence not derived from the metathesis products. The reaction, like the metathesis and polymerization of cyclopentene, is equilibrated. The general characters of the telomerization reaction have been verified for many pairs of olefins, such as 2-pentene/cyclooctene, 2-hexene/cyclopentene, and 3-heptene/cyclopentene. α-Olefins, such as propene and 1-pentene are, as in the case of metathesis, less reactive, but the telomers form in ratios from 1:10:1 to 1:20:1.

1,5-cyclooctadiene (cod) and 1,5,9-cyclododecatriene (cdt) lead to telomers of the same type, but in this case the successive "triads" are separated by four atoms of carbon and not by an integral multiple of the number of carbon atoms forming the ring.

This situation therefore means that alkylidene "residues" are left on the transition metal. The most obvious hypothesis is the formation of a metallocarbene sequestering an olefin to form a metallacyclobutane intermediate (Figure 10).

Table 1: Telomerization of cyclopentene with 2-pentene.

Catalyst and reaction time	$WOCl_4/Sn(C_4H_9)_4$				$WOCl_4/Al(C_2H_5)_2Cl$	
	7 min		14 min		24 h	
Relative molar quantity						
cyclopentene	32		35		148	
butenes	9.3		18.7			
pentenes	58		31.3			159
hexenes	8.8		17.7			
C_9H_{16}	4.5		8.1		16.8	
$C_{10}H_{18}$	9.5	18.3	18.1	34.4	36.8	70.4
$C_{11}H_{20}$	4.3		8.2		16.8	
$C_{14}H_{24}$	2.0		3.6		8.9	
$C_{15}H_{26}$	4.3	8.3	6.9	13.9	18.5	36.0
$C_{16}H_{28}$	2.0		3.4		8.6	
$C_{19}H_{32}$	1.0		1.5		5.0	
$C_{20}H_{34}$	2.8	4.8	3.0	6.0	8.7	18.6
$C_{21}H_{36}$	1		1.5		4.9	
$C_{24}H_{40}$			0.8		n.d.	
$C_{25}H_{42}$			1.6	3.1	n.d.	
$C_{26}H_{44}$			0.7		n.d.	
chlorobenzene	30		90		–	
D %	24		54		–	
C %	29		46		44	

The mechanism may be a little more complex in reality: the reactivity of cod and cdt as "butadienylidene" (=CH-CH_2-CH_2-CH=) even at the very start of the reaction, so that it

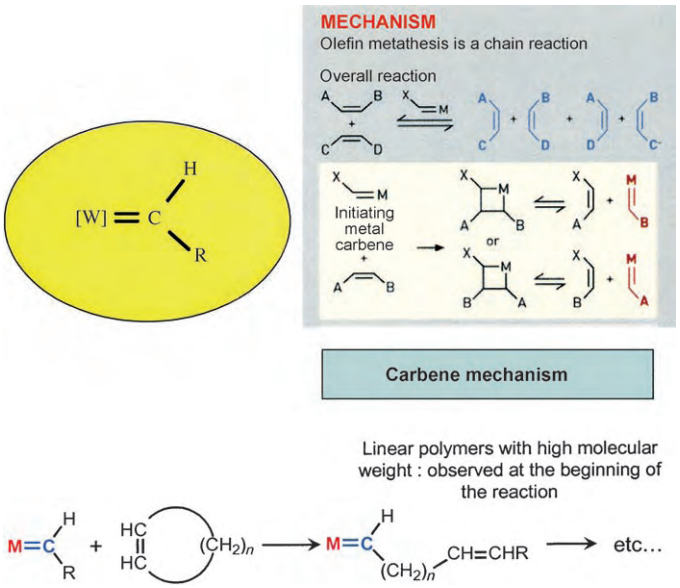

Figure 10.

cannot be explained as a "back-biting" reaction (reaction of the metallocarbene with one of the double bonds of the growing chain), remains to be explained.

While the cyclopentene is in equilibrium with its polymer (polypentenylene), this is not true of the higher cycles, such as cyclooctene and cyclooctadiene: their polymers are in equilibrium with the cyclooligomers.[3] This situation is due to the relative stability of the cycles, as P. J. Flory has shown in the case of the lactones (Figure 11).[4] These macrocycles are formed by back-biting.

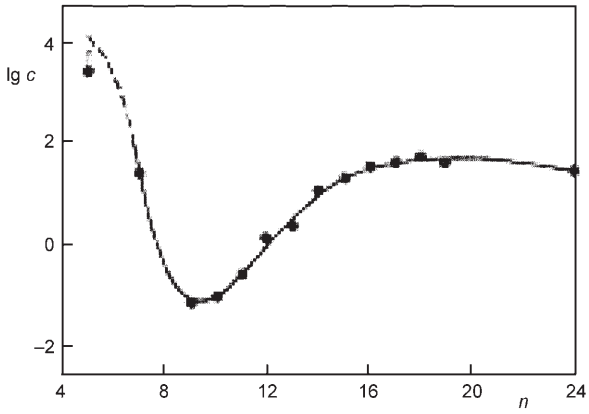

Figure 11. Logarithm of the cyclization constant *c* for the lactonization of ω-hydroxyacids versus ring size *n*.[4]

All three reactions (disproportionation, polymerization, telomerization) can be represented as shown in Figure 12. It remained to be shown how the initial metallocarbene forms when a tungsten halide and an organometallic species are mixed. For this investigation we chose methylated derivatives that cannot give rise to β-H elimination: methyllithium and tetramethyltin. All that could be hoped for was to favor α-H

 © 2006 Wiley-VCH Verlag GmbH & Co. KGaA, Weinheim

Reaction of disproportionation

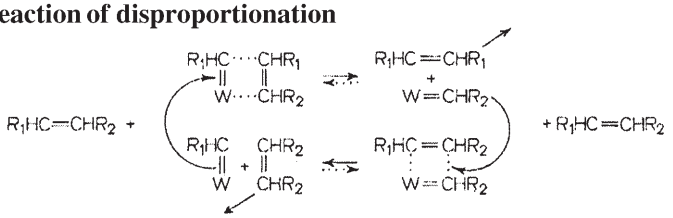

Reaction of polymerization

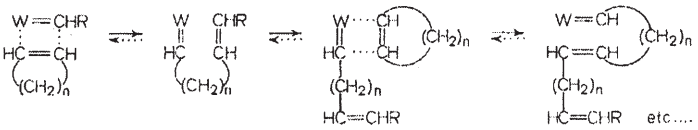

Reaction of telomerization

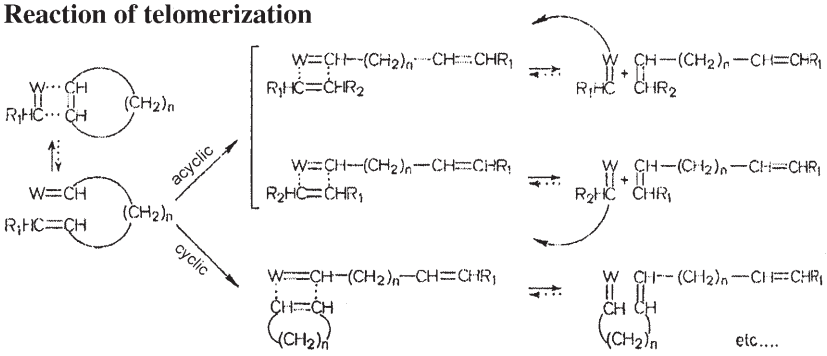

J.-L. Hérisson, Y. Chauvin, *Makromolekulare Chemie* **1971**, *141*, 161–176.

Figure 12.

elimination with the formation of a methylidene species that could simply be "trapped" by means of olefins with a di-substituted double bond: 2-butene, 2-pentene, 3-hexene. Figure 13 summarizes the results of these experiments.[5] The formation of propene and of 1-butene clearly demonstrates the existence on the tungsten of a methylidene group. The formation of methane is explained by an α-H elimination, doubtless followed by a reducing elimination resulting from a double alkylation of the tungsten.

E. O. Fischer's carbene is itself a very active catalyst for the polymerization of cyclopentene in the presence of $TiCl_4$ when activated, probably photochemically, by chlorination of the tungsten (it is well known that $TiCl_4$ is photochemically reduced by alkanes).[6]

It is also possible to characterize and count the metallocarbenes formed on rhenium peroxide impregnated on alumina, by means of reaction with a 1,2-disubstituted olefin. Subsequent reaction with ethylene leads to propene[7] by a sequence of reactions that might be as given in Equations (1) and (2) (where re is a symbol formerly used by K. Ziegler).

Formation of the metallocarbene: WCl_6 + $Sn(CH_3)_n$

TABLEAU

Produits de réaction entre W $(Cl)_6$, M $(CH_3)_n$ *et une oléfine*

Oléfine	W $(Cl)_6$ (g)	Coréactif (**)	Solvant	T (°C)	Oléfine / W $(Cl)_6$	% molaires par rapport au tungstène mis en œuvre: Méthane + éthane	Propylène	Butène-1
Butène-2.....	0,5	$LiCH_3$	Benzène (15 ml)	4	10	22	6,3	–
Butène-2.....	0,5	$Sn(CH_3)_4$	Benzène (15 ml)	4	10	3,5	3,6	–
Hexène-3.....	0,2	$Sn(CH_3)_4$	Benzène (30 ml)	4	10	n. d.	–	2,6
Pentène-2 (*)...	0,5	$LiCH_3$	Benzène (15 ml)	4	10	22	4,4	4,7
	0,2	$Sn(CH_3)_4$	Benzène (30 ml)	4	10	10	9,6	10,4
	0,2	$Sn(CH_3)_4$	Chlorobenzène (30 ml)	—20	10	n. d.	8,5	6,4
	0,4	$Sn(CH_3)_4$	Chlorobenzène (30 ml)	—20	2,5	n. d.	6,8	6,9

(*) On observe la formation de butène-2 et d'hexène-3 issus de la disproportion du pentène-2 en excès.

(**) Sn/W = 2; Li/W = 2.

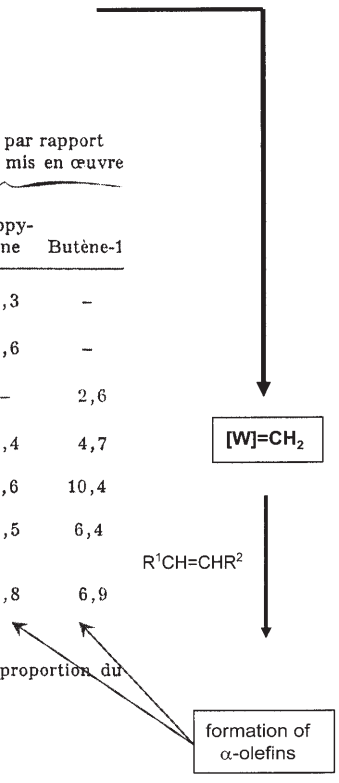

J.-P. Soufflet, D. Commereuc, Y. Chauvin, *C. R. Acad. Sci.* **1973**, *276*, 169–171

Figure 13.

 © 2006 Wiley-VCH Verlag GmbH & Co. KGaA, Weinheim

re=O + CH_3CH=$CHCH_3$ → re=$CHCH_3$ + CH_3CH=O (1)

re=$CHCH_3$ + CH_2=CH_2 → CH_3CH = H_2 + re=CH_2 (2)

Concluding Remarks

Obviously, not everyone has the opportunity to witness the birth of a new bond like the one discovered by E. O. Fischer, and the event is likely to become increasingly rare! Nor are they likely to be present at the birth of a unified concept encompassing two types of catalysis that until then had not been on speaking terms. It was an opportunity that had to be seized!

I owe a great deal to everyone who took part in what I can rightly call an "adventure", because at the start we could not be sure of reaching a significant result. And more particularly to the talented students directly involved—J.-L. Hérisson, J.-P. Soufflet, and G. Zaborowski—without whom this work (and therefore the prize!) would not have existed.

Received: March 29, 2006

[1] N. Calderon, H. Y. Chen, K. W. Scott, *Tetrahedron Lett.* **1967**, *8*, 3327 – 3329.
[2] J.-L. Hérisson, Y. Chauvin, *Makromol. Chem.* **1971**, *141*, 161 – 176; J. L.Hérisson, PhD Thesis, Paris, **1970**.
[3] Y. Chauvin, D. Commereuc, G. Zaborowsky, *Makromol. Chem.* **1978**, *179*, 1285 – 1290.
[4] P. J. Flory, *Principles of Polymer Chemistry*, Cornell University Press, New York, **1953**, p. 96, 497, 514.
[5] J.-P. Soufflet, D. Commereuc, Y. Chauvin, *C. R. Acad. Sci. Paris* **1973**, *276*, 169 – 171.
[6] Y. Chauvin, D. Commereuc, D. Cruypelinck, *Makromol. Chem.* **1976**, *177*, 2637 – 2646.
[7] Y. Chauvin, D. Commereuc, *J. Chem. Soc. Chem. Commun.* **1992**, 462 – 464.
[8] There have been many publications on metathesis; the last and without doubt the best documented of them is the *Handbook of Metathesis* by R. H. Grubbs (Wiley-VCH, Weinheim, **2003**).

 © 2006 Wiley-VCH Verlag GmbH & Co. KGaA, Weinheim

Metathesis Reactions

DOI: 10.1002/anie.200600085

Multiple Metal–Carbon Bonds for Catalytic Metathesis Reactions (Nobel Lecture)**

*Richard R. Schrock**

Keywords:
homogeneous catalysis · metathesis · molybdenum · Nobel lecture · tungsten

It's my great privilege to be here today, in a position I never thought possible. The story I will tell you I hope will give you some idea what I have contributed to the area for which the Nobel prize in chemistry was awarded this year.

The story begins 32 years ago in 1973, the year the Nobel prize was shared by G. Wilkinson and E. O. Fischer. Wilkinson's Nobel lecture[1] concerned the nature of a single bond between a transition metal and a carbon atom in an alkyl group, and emphasized the fact that the metal–carbon bond is not inherently weak. E. O. Fischer in his Nobel Lecture[2] summarized the extensive chemistry of transition-metal "carbene" complexes[3,4] that contain a metal–carbon double bond discovered by him and his group in 1964 (Scheme 1).[5] He also reported new "carbyne" complexes

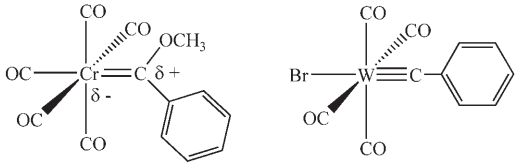

Scheme 1. "Low-oxidation-state" carbene (left) and carbyne complexes (right).

that contain a metal–carbon triple bond.[6] It was clear that metal–carbon single bonds were of great importance in the emerging area of homogeneous catalysis. However, no catalytic reactions involving species that contain metal–carbon double or triple bonds were known. When I went to the Central Research Department of E. I. DuPont de Nemours and Company in 1972, transition-metal organometallic chemistry and homogeneous catalysis were of great interest as a consequence of their huge potential in organic chemistry and therefore in industry.

In the early 1970s inorganic chemists knew that many transition metal species containing a metal–carbon bond are subject to various modes of decomposition that are much more rapid than in a non-transition-metal species such as $Zn(CH_2CH_3)_2$ or $Al(CH_2CH_3)_3$. The most common of these decomposition reactions involves transfer of a β hydrogen atom, from a metal-bound ethyl group ($M–CH_2CH_3$) for example, to the metal center (M) to yield a metal hydride and an alkene. The relative stabilities of high-oxidation-state "homoleptic" or "peralkyl" compounds such as $[M\{CH_2Si(CH_3)_3\}_4]$, $[M(CH_2C_6H_5)_4]$, and $[M\{CH_2C(CH_3)_3\}_4]$ (M = Ti, Zr, or Hf; Scheme 2), were rationalized on the basis of the

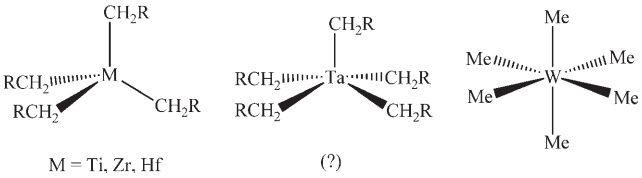

Scheme 2. "Peralkyl" complexes of Group 4, 5, and 6; metals are in their highest possible oxidation states.

fact that unlike a compound having an ethyl ligand, the alkyl ligands in these species lack β hydrogen atoms and so of course cannot undergo decomposition processes that involve β hydrogen atoms.[7] In 1973 Wilkinson published the synthesis of $[W(CH_3)_6]$.[8] Unlike $[M(CH_3)_4]$ species (where M = Ti, Zr, or Hf) $[W(CH_3)_6]$ is stable at 22 °C. The methyl carbon is α with respect to the metal center; there is no β carbon atom and so no β hydrogens. However, methyl species are not

[*] Prof. R. R. Schrock
Department of Chemistry 6-331
Massachusetts Institute of Technology
77 Massachusetts Avenue, Cambridge, MA 02139 (USA)
Fax: (+1) 617-253-7670
E-mail: rrs@mit.edu

[**] Copyright© The Nobel Foundation 2005. We thank the Nobel Foundation, Stockholm, for permission to print this lecture.

 © 2006 Wiley-VCH Verlag GmbH & Co. KGaA, Weinheim

sterically protected against bimolecular reactions that involve α hydrogens. As you can see from the note added in the proof of Wilkinson's Nobel address,[9] I was intrigued by high oxidation state peralkyl complexes and had chosen to explore the organometallic chemistry of tantalum soon after my arrival at DuPont. Little alkyl chemistry was known of the metals in Group 5 (V, Nb, Ta) at that time; I chose tantalum because it is next to tungsten in Group 6 (Cr, Mo, W), and like tungsten, tantalum is relatively stable in its highest possible oxidation state (+v). Peralkyl tantalum complexes therefore must be pentaalkyls.

My starting point for tantalum alkyl chemistry was a paper by Gordon Juvinall[10] in which he described the low-yield synthesis of niobium and tantalum trimethyl dichloride species through addition of dimethylzinc to the metal pentachlorides. I found that crystalline $[TaMe_3Cl_2]$ not only could be prepared quantitatively in pentane on a large scale [Eq. (1)], but it could be stored for long periods at −40 °C

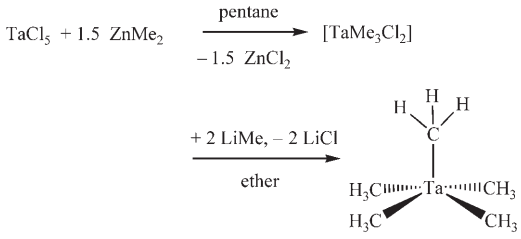

(1)

in the solid state. Moreover, it reacted with two equivalents of LiMe to generate volatile, yellow, crystalline $[Ta(CH_3)_5]$.[11] This species is much less stable than $[W(CH_3)_6]$, but much more stable than $[Hf(CH_3)_4]$. Pentamethyltantalum decomposes above 0 °C to yield approximately 3.7 equivalents of methane, and it does so in a bimolecular fashion. Pentamethyltantalum has 15 sterically unprotected α C–H bonds and the metal is highly electron-deficient (10 electrons, eight shy of the preferred 18 electron count). Interactions between one metal center and C–H bonds in another metal complex thereby are encouraged, and are easier in $[Ta(CH_3)_5]$ than in $[W(CH_3)_6]$ for simple steric reasons. Wilkinson had just published a reaction that yielded an unusual dimeric species containing what he called a "carbene bridge," μ-$CSiMe_3$ [actually a carbyne bridge; Eq. (2)]. With respect to $[Ta(CH_2SiMe_3)_5]$ he said "*It is assumed that a penta-alkyl complex cannot exist for steric reasons.*"[12] Therefore, I turned to experiments involving the neopentyl (CH_2CMe_3) ligand to probe the limit of steric crowding in homoleptic d^0 tantalum pentaalkyls and the nature of the decomposition pathways that might be observable in such circumstances. The crucial

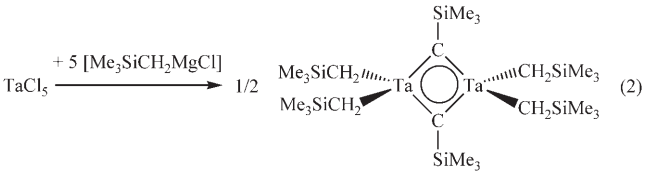

(2)

experiment consisted of an attempt to prepare $[Ta(CH_2CMe_3)_5]$ through addition of two equivalents of $[LiCH_2CMe_3]$ to $[Ta(CH_2CMe_3)_3Cl_2]$. Instead of $[Ta(CH_2CMe_3)_5]$, orange, crystalline, and thermally stable $[(Me_3CCH_2)_3Ta{=}CHCMe_3]$ was formed in quantitative yield [Eq. (3)].[13] The exact mechanism is still not known, but it is

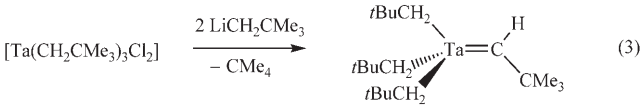

(3)

likely that an α hydrogen is activated by the metal and subsequently removed as a proton by a neopentyl group, possibly in an intramolecular manner in pentaneopentyltantalum itself [Eq. (4)]. $[(Me_3SiCH_2)_3Ta{=}CHSiMe_3]$ may be an

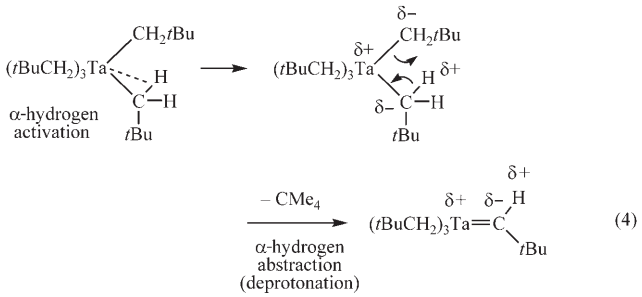

(4)

intermediate in the reaction shown in Equation (2), but it must decompose intermolecularly to give tetramethylsilane and the observed dimeric species; $[(Me_3CCH_2)_3Ta{=}CHCMe_3]$ does not.

The tantalum neopentylidene complex, $[(Me_3CCH_2)_3Ta{=}CHCMe_3]$, was new in several respects. It was the first example of a stable transition metal M=CHR species. Second, the terminal alkylidene was formed through a new type of reaction, an intramolecular α-hydrogen abstraction from an alkyl. Third, unlike "carbene" complexes discovered by Fischer and his group, $[(Me_3CCH_2)_3Ta{=}CHCMe_3]$ was highly electron-deficient (10 electrons in metal-based bonding orbitals). Fourth, $[(Me_3CCH_2)_3Ta{=}CHCMe_3]$ appeared to behave as if the metal were in its highest possible oxidation state with the Ta=C bond being polarized so that the metal is relatively positive and the carbon relatively negative, opposite to what is found in Fischer-type carbene complexes. Fifth, the high thermal stability and resistance of $[(Me_3CCH_2)_3Ta{=}CHCMe_3]$ toward intermolecular decomposition reactions, as well as toward further intramolecular reactions, suggested that other high-oxidation-state, four-coordinate species that contain four sterically demanding covalently bound ligands might be viable. This simple but important principle pervaded much of the high oxidation state chemistry that was developed over the next 30 years in my group.

"Deprotonation" of a neopentyl ligand to give a neopentylidene ligand suggested that a neopentylidene ligand might be deprotonated further by an external base. Indeed, addition of *n*-butyllithium to $[(Me_3CCH_2)_3Ta{=}CHCMe_3]$ led

© 2006 Wiley-VCH Verlag GmbH & Co. KGaA, Weinheim

to formation of the related high-oxidation-state, anionic, neopentylidyne species, [{$(Me_3CCH_2)_3Ta{\equiv}CCMe_3$}Li][14] [Eq. (5)].

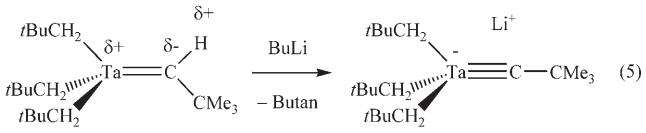

(5)

Finally, it was demonstrated that even a methylene ($Ta{=}CH_2$) species could be prepared through deprotonation of $[TaCp_2(CH_3)_2]^+$ ($Cp = C_5H_5$).[15,16] Even though $[TaCp_2(CH_3)(CH_2)]$ contains 18 electrons in metal-based orbitals, it is unstable toward bimolecular decomposition to yield an ethylene complex in 50% yield, plus related species that are formed in the presence of some ligand L [Eq. (6)]. Bimolecular decomposition of alkylidenes, especially methylenes, is a battle that continues to be fought today. The main point is that between 1973 and 1975 high-oxidation-state tantalum–carbon double and triple bonds had been prepared, and they appeared to be significantly different in several important respects from the low-oxidation-state species prepared by Fischer.

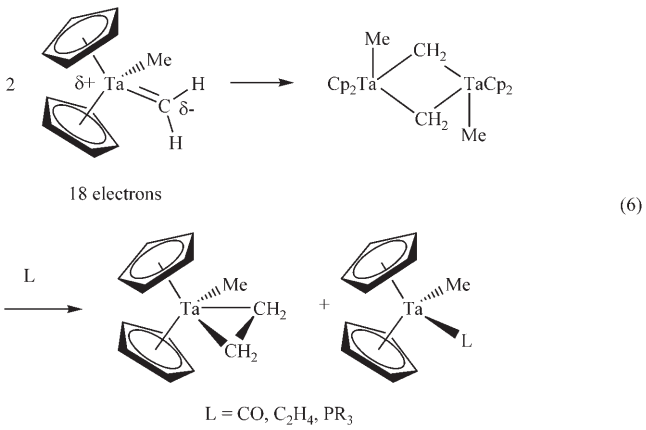

(6)

At some point in the early 1970s I became aware of the "olefin-metathesis" reaction [Eq. (7)], a startling and mysterious reaction catalyzed by homogeneous Mo and W catalysts (and heterogeneous Re catalysts), the identities of which were not known.[17–20] Physical organic experiments by Robert Grubbs,[21–23] Thomas Katz,[24,25] Charles Casey,[26] and Yves Chauvin[27] were designed to determine whether the reaction proceeded by a "pair-wise" or "non-pair-wise" mechanism.[20]

(7)

It was shown that the reaction proceeded in a "non-pair-wise" fashion, and Chauvin was the first to propose the correct "carbene/metalacyclobutane" mechanism [Eq. (8)] that would account for all observations.[27] However, at that time no "carbene" complexes were known that would react efficiently with ordinary olefins, as proposed by Chauvin.

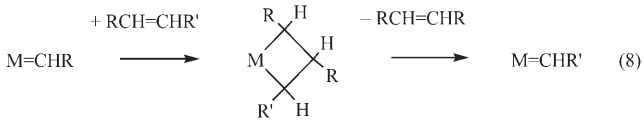

(8)

Alkyne metathesis [Eq. (9)], both heterogeneous[28,29] and homogeneous,[30] catalyzed by Mo and W compounds of unknown type, also had been discovered. Katz[24] proposed a mechanism of alkyne metathesis analogous to that for olefin metathesis [Eq. (10)], that is, one that involves formation of metalacyclobutadiene intermediates. Yet no "carbyne" complexes were known that would catalyze alkyne metathesis.

(9)

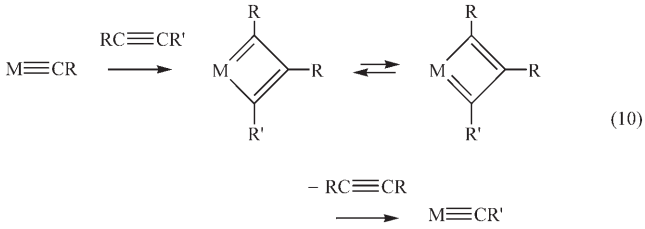

(10)

I asked myself whether the new types of tantalum "alkylidene" and "alkylidyne" complexes might not be at least the type of species that metathesize olefins and acetylenes, respectively, even though tantalum was not known to be a catalyst for either of these reactions at that time.

After my move to MIT in 1975, I began to explore reactions between various tantalum alkylidene complexes and olefins in some detail. It became clear that electron-deficient tantalum and niobium alkylidenes would react with olefins readily to give metalacyclobutane intermediates [Eq. (11)], but these species would rearrange via a β-hydride process to give as many as four of the possible rearrangement products instead of losing an olefin to reform a new alkylidene [Eq. (12) and (13)]; the alkylidene chain reaction never started and no metathesis products therefore were observed.[31] At an international symposium on olefin metathesis (ISOM III) in 1979 in Lyon, I reported that niobium and tantalum complexes that contain *tert*-butoxide ligands in

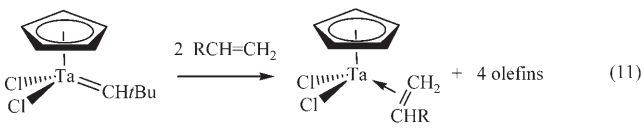

(11)

 © 2006 Wiley-VCH Verlag GmbH & Co. KGaA, Weinheim

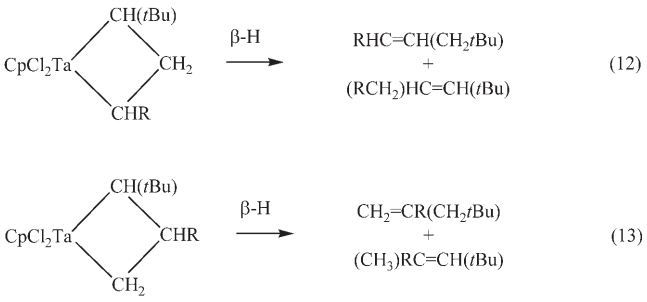

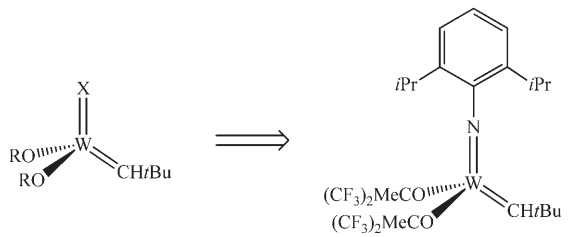

Scheme 3. Design of a stable tungsten imido alkylidene bisalkoxide complex.

place of chloride ligands, such as $[M(CH\textit{t}Bu)(O\textit{t}Bu)_2Cl(PMe_3)]$, could be coaxed into metathesizing olefins. Several dozen catalytic metathesis cycles could be observed for an olefin such as *cis*-2-pentene.[32] It was proposed that the *tert*-butoxide ligands "prevent reduction" of the metal and "promote metathesis." At that same conference I reported that an attempt to carry out a "Wittig-like" reaction between a tantalum alkylidene and a tungsten oxo complex to yield $[W(CH\textit{t}Bu)(O\textit{t}Bu)_4]$ and $[Ta(O)L_2Cl_3]$, instead produced an unanticipated 18-electron oxo neopentylidene complex of tungsten [Eq. (14)].[33] This oxo neopentylidene complex

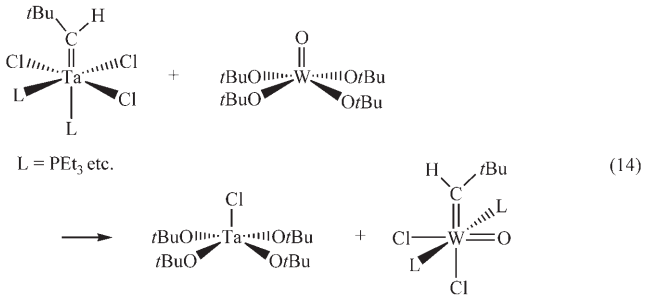

reacted with olefins to yield the metathesis products and new alkylidenes that would be expected from the metathesis reaction, including a methylene complex, and especially rapidly in the presence of a trace of $AlCl_3$. This was a convincing demonstration that the oxo alkylidene species react with olefins readily and reform an alkylidene complex of the same type from half an olefin that was present. The role of $AlCl_3$, it was proposed, was to remove either chloride or phosphine (reversibly) and thereby create an empty coordination site at the electronically saturated metal center.

A four-coordinate neopentylidene species containing large, covalently bound ligands was believed to be the most likely isolable, but reactive, electron-deficient species. A neopentylidene ligand clearly was required. We also knew that alkoxides were desirable, but what should the fourth, and necessarily dianionic, ligand X (Scheme 3) be? An oxo ligand was unsuitable because it almost certainly would encourage bimolecular decomposition reactions. We focused on an imido ($[NR]^{2-}$) ligand, an isoelectronic analogue of an oxo ligand, since the imido ligand could be sterically protected by a large R group. After considering the likely synthetic difficulties associated with R being a 2,6-di-*tert*-butylphenyl group, we settled on the 2,6-diisopropylphenyl group, a choice that in part was in response to a comment by Barry Sharpless concerning the value of isopropyl groups in general versus *tert*-butyl groups. (The 2,6-diisopropylphenyl group is found in many nitrogen-based ligands in a large variety of catalysts today.) Several large and sterically demanding tertiary alcohols and phenols were available, including fluorinated *tert*-butanols such as $(CF_3)_2MeCOH$ whose pK_a in water (≈ 9) is significantly less than that of *tert*-butanol itself (≈ 19). We felt that the electron withdrawing ability of the hexafluoro-*tert*-butoxide ligand should increase the electrophilicity of the metal dramatically and therefore also increase the rate of the reaction of an alkylidene complex with an olefin. Therefore, we aimed to prepare $[W(NAr)(CHCMe_3)\{OCMe(CF_3)_2\}_2]$ (Scheme 3) with the expectation that this 14-electron species not only could be isolated, but that it would metathesize olefins readily.

Being aware of the almost magical properties of the neopentyl ligand (as well as neopentylidene and neopentylidyne ligands), we also were curious about simple reactions between W^{VI} compounds (initially WCl_6) and neopentyllithium or neopentylmagnesium chloride, and had begun exploring such reactions in 1977. We discovered that a volatile, yellow, crystalline alkylidyne complex could be isolated from such reactions,[34] and that the reaction between $[W(OMe)_3Cl_3]$ and six equivalents of $[Me_3CCH_2MgCl]$ in diethyl ether produced that species in a yield of approximately 50% [Eq. (15)].[35] $[(Me_3CCH_2)_3W{\equiv}CCMe_3]$ is closely

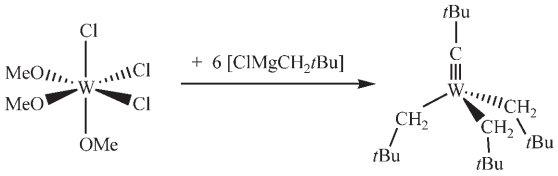

related to $[(Me_3CCH_2)_3Ta{=}CHCMe_3]$ in having four neopentyl or neopentyl-derived ligands around the metal. As we became aware of the benefits of alkoxides for efficient olefin metathesis, we became curious whether a trialkoxide species such as $[(Me_3CO)_3W{\equiv}CCMe_3]$ could be prepared and whether it would be an efficient alkyne metathesis initiator. We were pleased to find that $[(Me_3CO)_3W{\equiv}CCMe_3]$ in fact could be prepared readily [Eq. (16)], and especially pleased to find that alkynes are metathesized at room temperature with $[(Me_3CO)_3W{\equiv}CCMe_3]$ as the initiator[36] at rates thou-

 © 2006 Wiley-VCH Verlag GmbH & Co. KGaA, Weinheim

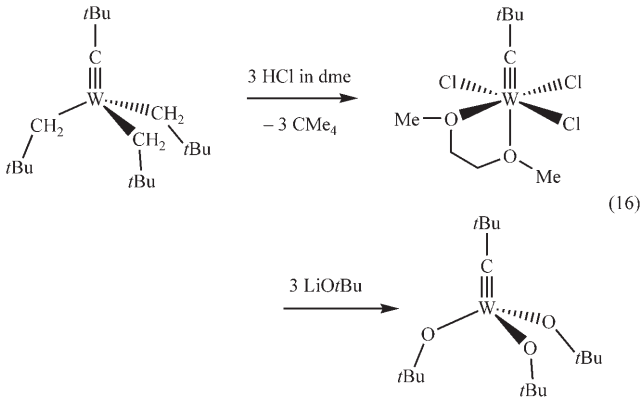

(16)

sands of times faster than "black box" catalysts known in the literature at that time. This finding proved to us that sterically bulky alkoxides were indeed highly beneficial for metathesis activity. In contrast to $[(Me_3CO)_3W{\equiv}CCMe_3]$, $[(dme)Cl_3W{\equiv}CCMe_3]$ does not metathesize alkynes, even though a tungstenacyclobutadiene intermediate necessary for that transformation, for example $[Cl_3W\{C(tBu)C(CH_3)C(CH_3)\}]$, could be isolated and crystallographically characterized.[37] Other reactions took precedence.[38–40] $[(Me_3CCH_2)_3W{\equiv}CCMe_3]$ also did not metathesize internal alkynes; it was simply too unreactive. When the OR group in $[(RO)_3W{\equiv}CCMe_3]$ was a more electron-withdrawing alkoxide or phenoxide, we could isolate and crystallographically characterize intermediate tungstenacyclobutadiene complexes in alkyne metathesis reactions and study them in detail.[41,42]

A large variety of species that contain tungsten–tungsten or molybdenum–molybdenum triple bonds, $X_3M{\equiv}MX_3$ species, were known at that time,[43,44] and in particular hexa(*tert*-butoxide) ditungsten, $[(Me_3CO)_3W{\equiv}W(OCMe_3)_3]$. An interesting question, therefore, was whether $[(Me_3CO)_3W{\equiv}W(OCMe_3)_3]$ would react with internal alkynes to yield $[(Me_3CO)_3W{\equiv}CR]$ complexes [Eq. (17)], which is effectively a metathesis-like reaction? The answer turned out to be yes,

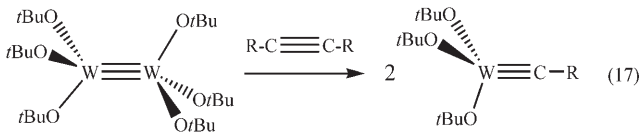

(17)

and it did so amazingly readily.[45] Although this is not a general reaction for all $X_3M{\equiv}MX_3$ species (M = Mo or W), the fact that it is facile only when X is a relatively sterically bulky alkoxide, had to be more than a coincidence. This discovery opened up a route to $[(Me_3CO)_3W{\equiv}CR]$ species that did not rely on α-hydrogen abstraction reactions,[46] and cemented the relationship between, and interconvertibility of, strong triple bonds between metal centers, between carbon atoms (in alkynes), and between a metal center and a carbon atom in an alkylidyne complex. It is interesting to note that the C≡N bond in nitriles is also cleaved readily, although the N≡N bond in dinitrogen is not. That spectacular reaction, which requires a (three-coordinate) triamido species, would not be reported until 1995.[47]

But tungsten alkylidynes were important for an additional reason. If a neopentylidyne species could be prepared by removing an α proton from a neopentylidene ligand, could not that reaction be run in the reverse direction, that is, could not a proton be added to a neopentylidyne species to yield a neopentylidene species? Moreover, could that not be accomplished in a manner that would produce the other desired metal–ligand multiple bond, namely the imido ligand, at the same time? An amido alkylidyne complex could in fact be prepared readily and the proton then moved from nitrogen to carbon by a base [Eq. (18)]. A large variety of $[W(NAr)(CHtBu)(OR)_2]$ complexes then could be prepared readily

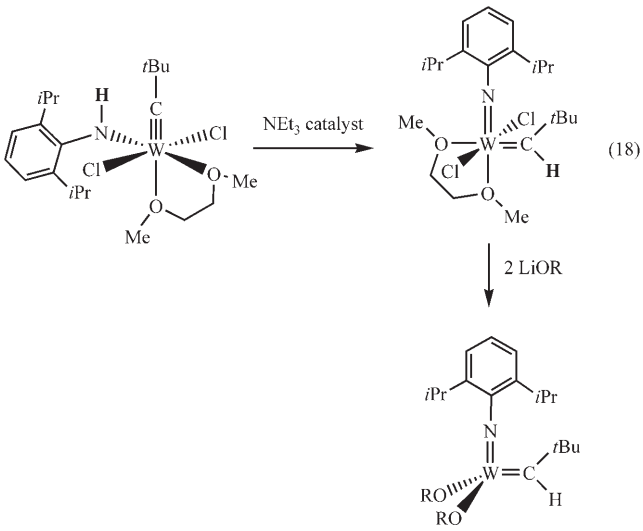

(18)

from the dichloride species, as long as the OR group was large enough to prevent complications that resulted from bimolecular reactions. X-ray structures, such as that in Figure 1,

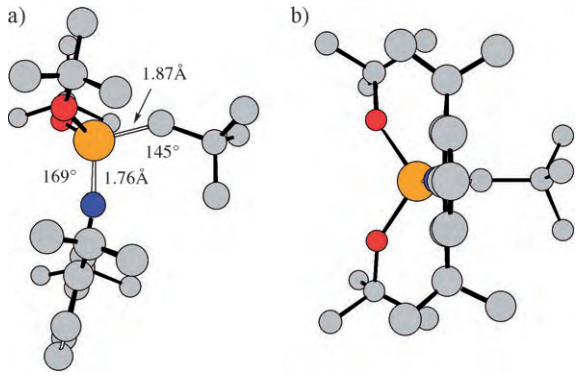

Figure 1. The structure of $[W(NAr)(CHtBu)(OtBu)_2]$; a) top view; b) side view.

showed how the *tert*-butyl group of the neopentylidene ligand points toward the imido ligand (a *syn* orientation), and how the diisopropylphenyl group on nitrogen protects the imido nitrogen and the alkylidene carbon atom against bimolecular reactions.

 © 2006 Wiley-VCH Verlag GmbH & Co. KGaA, Weinheim

It soon became clear that [W(NAr)(CH-*t*Bu)(OR)$_2$] species would metathesize olefins in the expected manner with an activity that correlated roughly with the electron-withdrawing power of the OR ligand. Catalysts that contain hexafluoro-*tert*-butoxide ligands appeared to have the highest activities. We found that tungstenacyclobutane intermediates, the very intermediates proposed by Chauvin in the metathesis reaction, actually could be isolated and crystallographically characterized.[48] However, tungstenacyclobutane stabilities proved to be a problem in some circumstances; loss of an olefin from an unsubstituted tungstenacyclobutane intermediate, in particular, could be relatively slow. The metal therefore would remain sequestered in the form of a tungstenacyclobutane. Since molybdenum–ligand bonds are generally weaker than tungsten–ligand bonds, we felt that a molybdacyclobutane complex might lose an olefin more readily. Therefore, we aimed to synthesize analogous [Mo(NAr)(CH*t*Bu)(OR)$_2$] catalysts. A synthesis of bisalkoxides was devised, the key feature of which is the use of an imido "protecting group" that is then removed upon addition of triflic acid [Eq. (19)], thereby forming in the process a

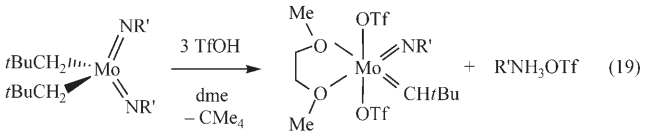

(19)

neopentylidene ligand from two neopentyl ligands through an α-hydrogen abstraction reaction in a hypothetical [Mo(NR′)(CH$_2$*t*Bu)$_2$(triflate)$_2$] intermediate.[49] The imido (NR′) and alkoxide groups could be varied widely and a large number of molybdenum catalysts therefore became accessible.

The molybdenum bisalkoxide catalysts are also remarkably active for a wide range of metathesis reactions, again especially when the alkoxide is the highly electron-withdrawing OCMe(CF$_3$)$_2$ group. In addition molybdacyclobutane intermediates are less stable than tungstacyclobutane intermediates toward loss of olefin. The steric bulk of the OCMe(CF$_3$)$_2$ and Ar (2,6-diisopropylphenyl) groups are also of considerable importance in preventing bimolecular reactions between the intermediate [Mo(NAr)(CHR′)(OR)$_2$] species in any given reaction. We slowly began to understand the extent to which the metathesis reaction could be controlled through systematic variation of the size and the electronic characteristics of the alkoxide and imido groups.

We also discovered that two isomers of any M=CHR catalyst are possible [Eq. (20)]. In the isomer that is usually observed, the alkylidene's substituent points toward the imido group (*syn*), while in the other isomer it points away from the imido group (*anti*). *Syn* and *anti* species can be formed during the course of a metathesis reaction, but *syn* and *anti* isomers of any given alkylidene also can interconvert simply through rotation about the Mo=C bond. The rate of rotation of a neopentylidene or neophylidene was found to vary by a factor of at least 10^6, and to depend (largely) on the nature of the alkoxide,[50,51] with rotation being relatively fast in the

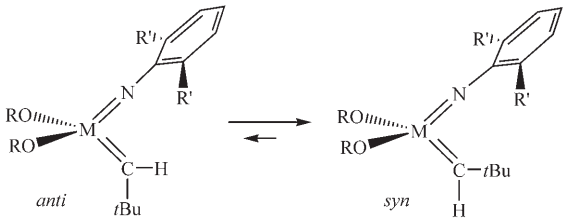

(20)

presence of alkoxide ligands such as *tert*-butoxide and relatively slow in the presence of hexafluoro-*tert*-butoxide ligands. In ring-opening metathesis polymerization (ROMP) studies, one of many variations of the basic olefin-metathesis reaction, we demonstrated (for one type of polymerizeable monomer) that the *anti* isomer was the more reactive by a factor of approximately 10^4. Therefore one, or the other, or both *syn* and *anti* intermediates in a catalytic reaction might be involved, with the outcome depending upon the nature of the imido and alkoxide groups, and the reactivity of the olefin involved in the reaction with *syn* and *anti* intermediates, and also the temperature and other variables. This circumstance complicates to a considerable degree a detailed understanding of the metathesis reaction by such catalysts, but at the same time dramatically increases the flexibility of the catalysts and offers the possibility that for a given metathesis reaction a catalyst can be found with which the reaction will proceed efficiently.

Ring-opening metathesis polymerization of cyclic olefins had been studied for many years before well-defined catalysts were developed.[17,18] We naturally asked whether well-defined catalysts behaved as polymerization catalysts for cyclic olefins, and if so, what advantages did they offer? In our only publication together, one that resulted from my sabbatical at Caltech as a Fairchild scholar in 1986, Robert Grubbs and I showed that these new well-defined catalysts did behave in the expected manner, and that the process could be "living" in the right circumstances, that is, intermediate alkylidenes that contain the growing polymer chain would not decompose.[52] In my laboratory we went on to show that the polymerization process could be controlled in a dramatic fashion to yield polymers with a highly regular repeating structure. Generally polymers with highly regular structures have the most interesting properties and therefore are the most desirable. In many cases we found that the entire polymer structure can be controlled through minute, but critical, changes in the catalyst structure. For example, a highly regular *cis,isotactic* polymer [Eq. (21)] is formed if the catalyst contains a specific binaphtholate ligand and a dimethylphenylimido group (R = CH$_3$ in the 2,6-disubstituted phenyl group).[53,54] In contrast, if the R group in the imido

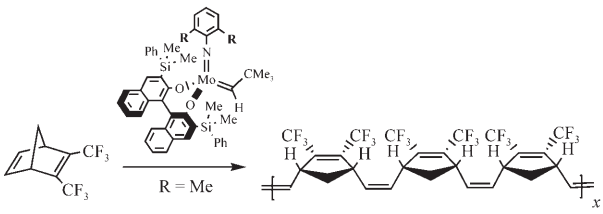

(21)

 © 2006 Wiley-VCH Verlag GmbH & Co. KGaA, Weinheim

ligand is isopropyl, then the polymer has a relatively random structure. The smaller dimethylphenylimido group is believed to allow polymerization to proceed solely via *syn* isomers to give *cis* linkages. Control of the "tacticity," that is, the way the five-membered rings point in this polymer, is greatest in the presence of a chiral (racemic) binaphtholate ligand. This control is a consequence of "enantiomorphic site control" over the polymerization process. In a series of experiments with related monomers that contain two esters made from enantiomerically pure alcohols, we could distinguish between *isotactic* and *syndiotactic* polymers, and therefore could demonstrate the *cis,isotactic* structure, which is formed through enantiomorphic site control, and the *trans,syndiotactic* structure, which is formed through chain-end control, for the first time in ROMP polymers.[55] The degree to which the polymer structure can be controlled through systematic, tiny variations of the catalyst is of great importance for many ROMP polymers that are made today with high-oxidation-state alkylidene catalyst initiators.

For some time it had been known that "classical" Mo and W catalysts that would metathesize olefins would also polymerize alkynes. This situation suggested that metal alkylidene species were responsible.[56–58] We showed that well-defined species do indeed polymerize alkynes[59] or cyclopolymerize 1,6-heptadiynes[60] [Eq. (22)] to yield polymers analogous to those described in the literature. In the case of a cyclopolymerization of 1,6-heptadiynes, such as diethyldipropargylmalonate, a six-membered or a five-membered ring can form, depending upon the regiochemistry of the addition of the first alkyne to the alkylidene. Since the optical properties of such polyenes vary with the polymer's structure and chain length,[61] it is highly desirable to make a polymer with a single structure and to control the molecular weight of that polymer through a polymerization with a well-defined catalyst. Although work is still ongoing in this area, it now appears possible to do so.[62,63]

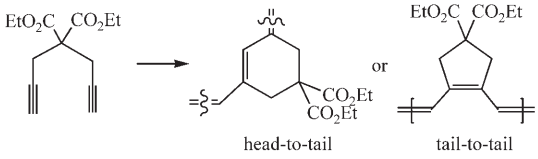

(22)

In 1992 Fu and Grubbs published two papers in which they demonstrated how [Mo(NAr)(CHCMe$_2$Ph){OCMe(CF$_3$)$_2$}$_2$] could be employed to make cyclic olefins quickly and efficiently that contain functionalities other than a C=C bond,[64,65] with the only other product being a volatile olefin such as ethylene, propylene, or butene (Scheme 4). Rings of many sizes, and even rings that contain tetrasubstituted olefinic bonds, could be prepared. These papers helped awaken organic chemists to the possibility that olefin metathesis by well-defined catalysts had significant potential in organic chemistry. The fact that the Mo and W catalysts in this general class are sensitive to air, moisture, and some functionalities did not prohibit their use in organic reactions. In 1995 Hoveyda and his group reported a synthesis of a cyclic

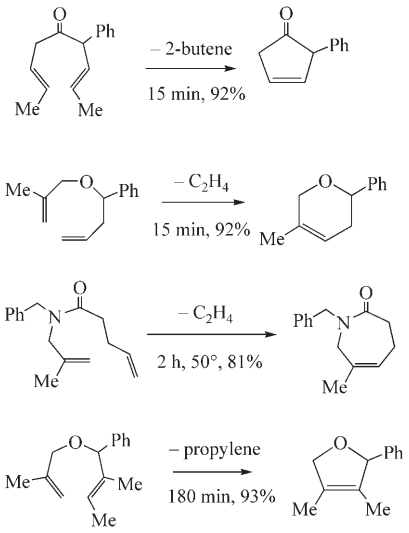

Scheme 4. Some ring-closing metatheses initiated by [Mo(NAr)(CHCMe$_2$Ph){OCMe(CF$_3$)$_2$}$_2$].

natural product, Fluvirucin-B$_1$, in which one of the steps consisted of a ring-closing metathesis (RCM) reaction [Eq. (23)].[66] This paper demonstrated that relatively complex molecules could be prepared by metathesis. These and other applications of metathesis technology, along with the commercial availability of [Mo(NAr)(CHCMe$_2$Ph){OCMe(CF$_3$)$_2$}$_2$], helped fuel applications of Mo metathesis technology to organic chemistry.[67] The possibility that metathesis could be employed routinely in organic chemistry I believe was a significant factor that drove Grubbs to develop ruthenium catalysts in the early 1990s.[20,68,69]

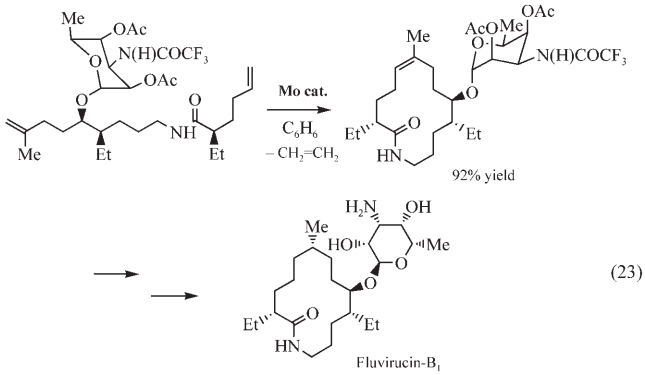

(23)

The use of alkyne metathesis catalysts for organic chemistry also was realized in the 1990s, primarily through work by Fürstner and co-workers, who showed that large rings could be prepared through alkyne metathesis with the [(Me$_3$CO)$_3$W≡CCMe$_3$] initiator.[70] A cyclic alkyne then could be hydrogenated selectively to yield a *cis* olefin (Lindlar reduction). This alternative to alkene metathesis circumvented a still unsolved problem, the formation of largely (≈75%) the thermodynamically more favored *trans* double bonds in alkene metathesis, instead of *cis* double bonds. An

 © 2006 Wiley-VCH Verlag GmbH & Co. KGaA, Weinheim

example of alkyne metathesis is the stereoselective synthesis of civetone [Eq. (24)].[71] Many other reactions that involve formation of a carbon–carbon triple bond through alkyne

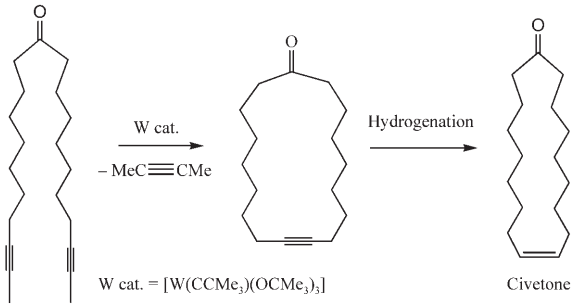

(24)

metathesis as part of a synthetic organic procedure began to appear, such as syntheses of the cytotoxic marine alkaloid motuporamine C,[72] prostaglandin E_2-1,15-lactone,[73] and epothilone A and C, all of which contain a *cis* olefin within a ring (Scheme 5).[74] Alkyne metathesis can be useful in other

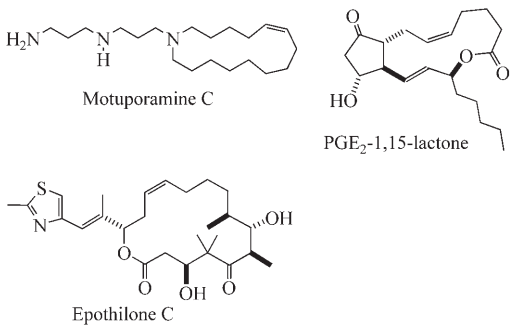

Scheme 5. Some molecules whose syntheses involve alkyne metathesis to create the *cis* double bond.

ways, as shown in the synthesis of *S*-(+)-Citreofuran [Eq. (25); BBN = 9-borabicyclo[3.3.1]nonane].[75] Although molybdenum-based alkyne metathesis catalysts were known,[76,77] work by Cummins,[78] Fürstner,[79] and Moore,[80] recently have demonstrated how these relatively inaccessible

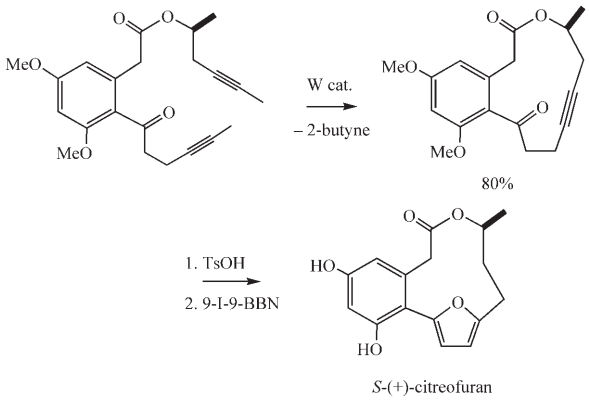

(25)

Mo catalysts can be prepared in situ from trisamidoalkylidyne precursors.

With the knowledge that certain sterically protected biphenolates and binaphtholates can be attached to Mo to yield stable neopentylidene or neophylidene ROMP initiators, we turned to the development of enantiomerically pure catalysts for asymmetric metathesis reactions in the mid 1990s. Some preliminary results were obtained with an enantiomerically pure biphenolate catalyst (Figure 2) in

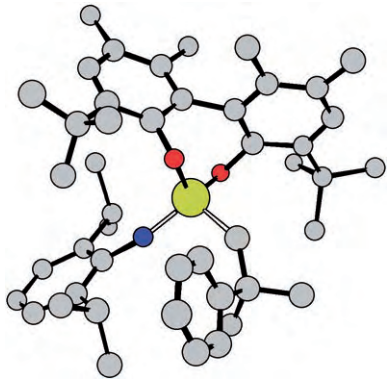

Figure 2. The structure of [Mo(NAr)(CHCMe$_2$Ph)(3,3′-di-*tert*-butyl-5,5′,6,6′-tetramethyl-1,1′-biphenyl-2,2′-diolate)].

1997. We then began a collaboration with Amir Hoveyda that was aimed at the application of asymmetric metathesis reactions to organic synthesis.[67,81,82] The modularity of the catalysts allowed us to prepare many enantiomerically pure variations that contain one of several different imido ligands and several different diolates (Scheme 6). It soon became apparent that with the right catalyst, asymmetric reactions could be efficient in terms of both yield and enantioselectivity,

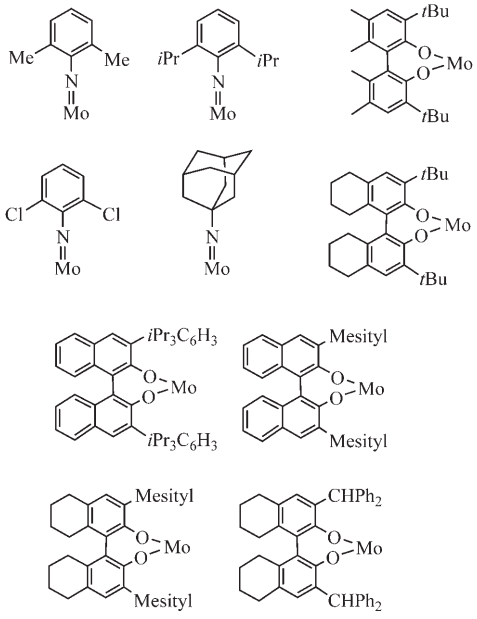

Scheme 6. Imido groups and enantiomerically pure diolates (shown in racemic form) that are employed to make asymmetric catalysts.

 © 2006 Wiley-VCH Verlag GmbH & Co. KGaA, Weinheim

in many cases producing a single enantiomerically pure product in virtually quantitative yield relatively quickly [Eq. (26) and (27)].[83] Again, byproducts usually consist of

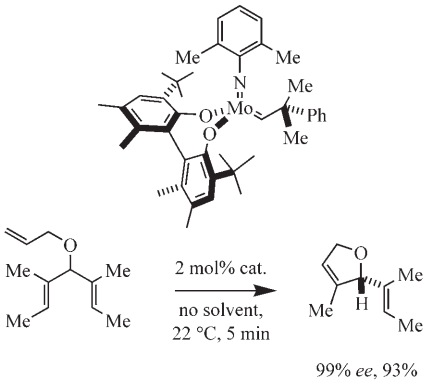

(26)

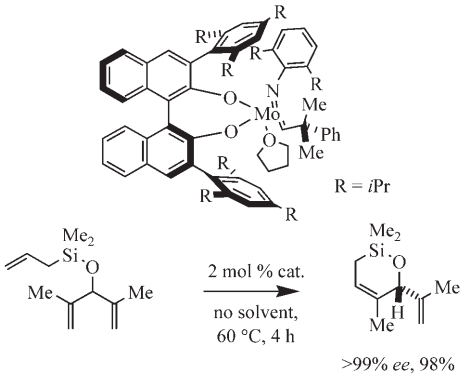

(27)

simple olefins, such as ethylene, propylene, or butene. A wide variety of other asymmetric reactions were developed, among them ring-opening/ring-closing metathesis [Eq. (28)],[84] ring-opening/cross metathesis [Eq. (29); MOM = methoxymethyl],[85] and the ring closing of tertiary amines to yield products resembling substructures of various drugs and other natural products [Eq. (30)].[86] It also was shown that the synthesis of drugs, such as tipranavir, an HIV protease inhibitor, could be shortened dramatically through the use of an asymmetric metathesis step to synthesize the problematic enantiomerically pure tertiary ether [Eq. (31)].[87,88] These are but a few examples of what has been accomplished in the last several years.

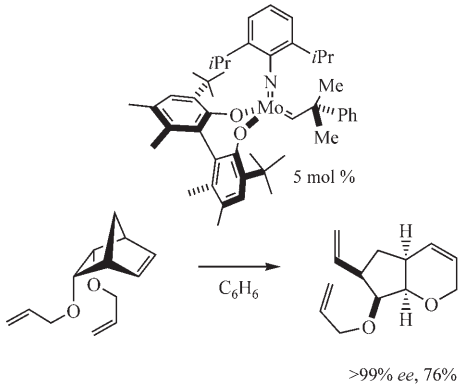

(28)

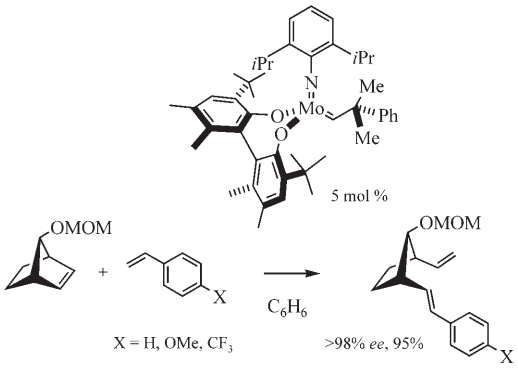

(29)

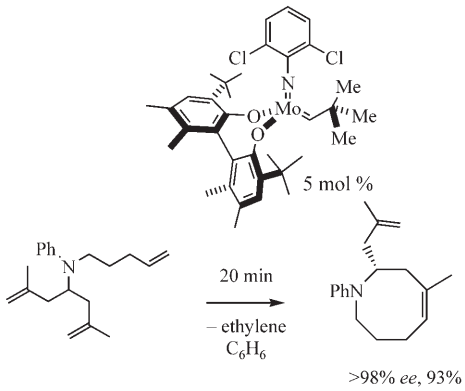

(30)

The isolation and testing of many catalyst variations side by side for one specific asymmetric reaction revealed that the efficiency of the asymmetric catalysts in terms of yield and

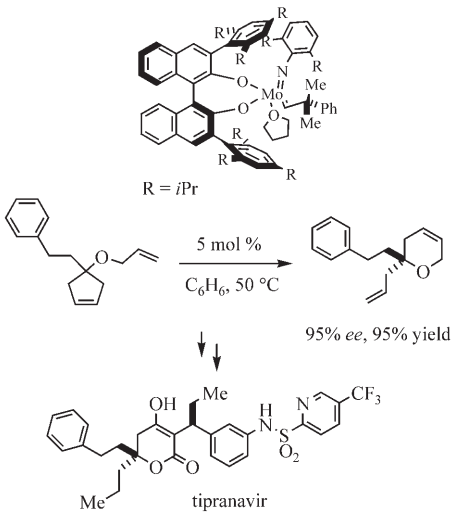

(31)

 © 2006 Wiley-VCH Verlag GmbH & Co. KGaA, Weinheim

enantioselectivity can vary dramatically, and that in the long run one could be relatively confident of finding an efficient catalyst. However, dozens of catalysts have to be prepared, isolated, and tested. Therefore, we have begun to explore the possibility of preparing catalysts in situ that we know exist as relatively stable species, either through addition of the biphenolate or binaphtholate to the bistriflate precursor [Eq. (19)], or through addition of the parent biphenol or binaphthol to a bisamido precursor [Eq. (32)]. We have

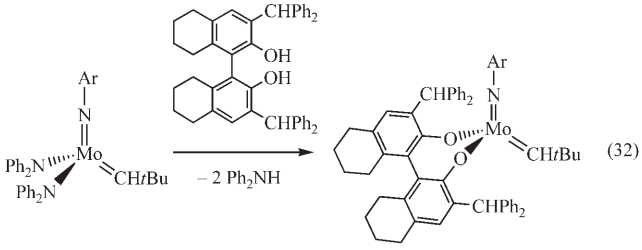

(32)

shown that catalysts prepared in situ for asymmetric metathesis reactions behave as well as catalysts that have been isolated and purified before use.[89] Surprisingly, similar approaches using dineopentyl species led to formation of monoalkoxide species [Eq. (33)].[90] Initially we thought these

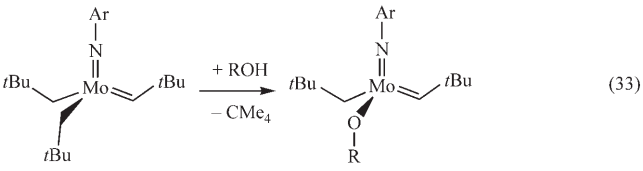

(33)

would be relatively poor metathesis catalysts, since dineopentyl species are essentially inactive for metathesis. The presence of one neopentyl and one alkoxide instead of two alkoxides therefore should be detrimental. However, preliminary results suggest that monoalkoxides are highly active catalysts. Recent theoretical calculations in related isoelectronic rhenium systems have suggested why this might be the case.[91]

Formation of only monoalkoxides from dineopentyl species recently has allowed the synthesis of "well-defined" and highly active molybdenum-based (and tungsten-based) metathesis catalysts on silica surfaces [Eq. (34)] that are relatively long-lived because the intermediate alkylidenes

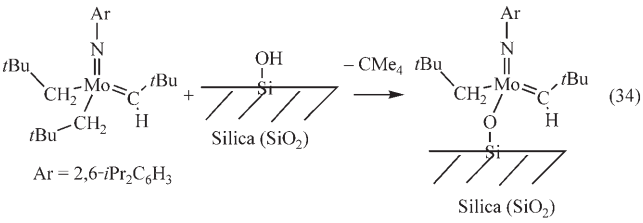

(34)

formed cannot decompose bimolecularly.[92] A variety of relatively well-defined catalysts now can be prepared on silica surfaces using other Ta^{V}, Mo^{VI}, W^{VI}, and Re^{VII} neopentyl precursors (Scheme 7).[93] In some cases entirely new reactions can be observed, such as tantalum-catalyzed "alkane metathesis".[94] This reaction has now been shown to involve alkene metathesis steps.[95]

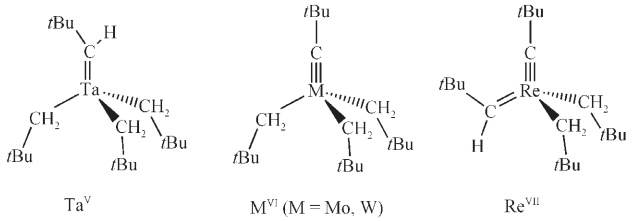

Scheme 7. "Clean" sources of catalysts formed upon addition of them to silica surfaces.

Rhenium forms metathesis catalysts of the "classical" type. Therefore we felt that we should be able to prepare well-defined catalysts. To maintain the four-coordinate geometry around a neutral Re center, a sterically demanding ligand that is triply bound to the metal is required. The only logical choice is a neopentylidyne ligand. In fact, well-defined Re^{VII} bisalkoxide catalysts for alkene metathesis can be prepared following the principles learned in W and Mo chemistry,[96,97] since the neopentylidyne ligand does not react with olefins readily (Scheme 8). Monoalkoxide mononeopentyl analogues

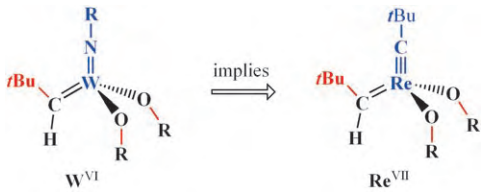

Scheme 8. Rhenium neopentylidyne bisalkoxide complexes are olefin-metathesis catalysts.

are believed to be even more reactive than bisalkoxides, especially on silica surfaces.[91]

Finally, we have found that M=M double bonds can form where M = Mo,[98] W,[99] or Re[100] as a consequence of decomposition of alkylidene species [Eq. (35)]. Metal–metal double bonds are unusual, especially when the double bond is not bridged by potentially bridging ligands, such as an alkoxide or an imido. The fact that these species themselves will metathesize certain olefins (slowly)[98] raises the possibility that alkylidenes are being reformed from M=M bonds. If this turns out to be the case, it would constitute strong evidence that interconversion of metal–metal, carbon–carbon, and metal–carbon bonds is possible for double bonds, as we know it to be for triple bonds [Eq. (17)].

We have come an enormous distance in the last 30 years, from "ill-defined" metathesis catalysts to those whose struc-

 © 2006 Wiley-VCH Verlag GmbH & Co. KGaA, Weinheim

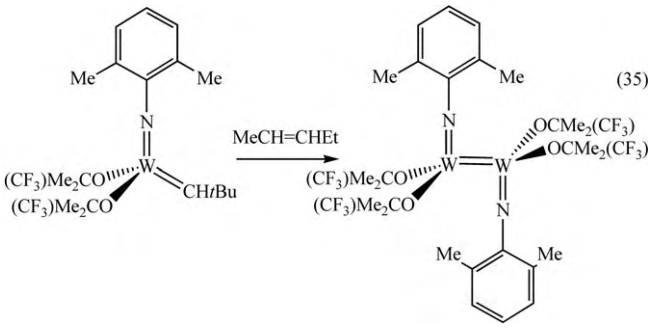

(35)

ture and reactivity in solution (and perhaps now on surfaces) we can control with pinpoint precision. Fundamental problems with known catalysts remain, the most important being how to prevent catalyst decomposition and/or how to regenerate catalysts from "clean" decomposition products. I expect these challenges to be met and hope that the consequences of the synthesis and fundamental study of new types of catalysts, and the application of them to a wide variety of problems, will continue to be felt in the coming years.

I am grateful for the freedom given to me in early years at the Central Research Department at duPont, for the opportunity to broaden my efforts and my interests at MIT, and for the support provided by various funding agencies (the National Science Foundation, the National Institutes of Health, the Office of Naval Research, the Army Research Office, and the Department of Energy) over the years for high-oxidation-state organometallic chemistry and other projects. I am forever indebted to my graduate and postdoctoral students, each of whom in his or her own way has contributed to the massive effort required to turn a few observations and new compounds into chemistry that has had a significant impact on fields outside of inorganic chemistry. Finally, I want to thank my wife and my family for their love and support.

Received: January 9, 2006
Published online: May 16, 2006

[1] G. Wilkinson, *Nobel Lecture*, December 11, **1973** (http://nobelprize.org/chemistry/laureates/1973/wilkinson-lecture.pdf); see also: *Angew. Chem.* **1974**, *86*, 664.
[2] E. O. Fischer, *Nobel Lecture*, December 11, **1973** (http://nobelprize.org/chemistry/laureates/1973/fischer-lecture.pdf); see also: *Angew. Chem.* **1974**, *86*, 651.
[3] E. O. Fischer, *Pure Appl. Chem.* **1970**, *24*, 407.
[4] E. O. Fischer, *Pure Appl. Chem.* **1972**, *30*, 353.
[5] E. O. Fischer, A. Maasbol, *Angew. Chem.* **1964**, *76*, 645; *Angew. Chem. Int. Ed. Engl.* **1964**, *3*, 580.
[6] E. O. Fischer, G. Kreis, C. G. Kreiter, J. Müller, G. Huttner, H. Lorenz, *Angew. Chem.* **1973**, *85*, 618; *Angew. Chem. Int. Ed. Engl.* **1973**, *12*, 564.
[7] R. R. Schrock, G. W. Parshall, *Chem. Rev.* **1976**, *76*, 243.
[8] A. J. Shortland, G. Wilkinson, *J. Chem. Soc. Dalton Trans.* **1973**, 872.
[9] "Note added in proof. *Hexamethylrhenium (K. Mertis and G. Wilkinson) and Pentamethyl[t]antalum (R. Schrock, DuPont, Wilmington, private communication) have recently been synthesized.*" G. Wilkinson, *Nobel Lecture*, December 11, 1973.
[10] G. L. Juvinall, *J. Am. Chem. Soc.* **1964**, *86*, 4202.
[11] R. R. Schrock, P. Meakin, *J. Am. Chem. Soc.* **1974**, *96*, 5288.
[12] W. Mowat, G. Wilkinson, *J. Chem. Soc. Dalton Trans.* **1973**, *10*, 1120.
[13] R. R. Schrock, *J. Am. Chem. Soc.* **1974**, *96*, 6796.
[14] L. J. Guggenberger, R. R. Schrock, *J. Am. Chem. Soc.* **1975**, *97*, 2935.
[15] R. R. Schrock, *J. Am. Chem. Soc.* **1975**, *97*, 6577.
[16] R. R. Schrock, L. J. Guggenberger, *J. Am. Chem. Soc.* **1975**, *97*, 6578.
[17] K. J. Ivin, *Olefin Metathesis*, Academic Press, New York, **1983**.
[18] K. J. Ivin, J. C. Mol, *Olefin Metathesis and Metathesis Polymerization*, Academic Press, San Diego, **1997**.
[19] R. H. Grubbs in *Comprehensive Organometallic Chemistry*, *Vol. 8* (Eds.: G. Wilkinson, F. G. A. Stone, E. W. Abel), Pergamon, New York, **1982**.
[20] *Handbook of Metathesis. Catalyst Development*, *Vol. 1* (Ed.: R. H. Grubbs), Wiley-VCH, Weinheim, **2003**.
[21] R. H. Grubbs, P. L. Burk, D. D. Carr, *J. Am. Chem. Soc.* **1975**, *97*, 3265.
[22] R. H. Grubbs, D. D. Carr, C. Hoppin, P. L. Burk, *J. Am. Chem. Soc.* **1976**, *98*, 3478.
[23] R. H. Grubbs, C. R Hoppin, *J. Chem. Soc. Chem. Commun.* **1977**, 634.
[24] T. J. Katz, J. McGinnis, *J. Am. Chem. Soc.* **1975**, *97*, 1592.
[25] J. McGinnis, T. J. Katz, S. Hurwitz, *J. Am. Chem. Soc.* **1976**, *98*, 605.
[26] C. P. Casey, T. J. Burkhardt, *J. Am. Chem. Soc.* **1974**, *96*, 7808.
[27] J. L. Hérrison, Y. Chauvin, *Makromol. Chem.* **1971**, *141*, 161.
[28] F. Pannella, R. L. Banks, G. C. Bailey, *J. Chem. Soc. D* **1968**, 1548.
[29] J. A. Moulijn, H. J. Reitsma, C. Boelhouwer, *J. Catal.* **1972**, *25*, 434.
[30] A. Mortreux, M. Blanchard, *J. Chem. Soc. Chem. Commun.* **1974**, 786.
[31] S. J. McLain, C. D. Wood, R. R. Schrock, *J. Am. Chem. Soc.* **1979**, *101*, 4558.
[32] R. R. Schrock, S. M. Rocklage, J. H. Wengrovius, G. Rupprecht, J. Fellmann, *J. Molec. Catal.* **1980**, *8*, 73.
[33] J. H. Wengrovius, R. R. Schrock, M. R. Churchill, J. R. Missert, W. J. Youngs, *J. Am. Chem. Soc.* **1980**, *102*, 4515.
[34] D. N. Clark, R. R. Schrock, *J. Am. Chem. Soc.* **1978**, *100*, 6774.
[35] R. R. Schrock, D. N. Clark, J. Sancho, J. H. Wengrovius, S. M. Rocklage, S. F. Pedersen, *Organometallics* **1982**, *1*, 1645.
[36] J. H. Wengrovius, J. Sancho, R. R. Schrock, *J. Am. Chem. Soc.* **1981**, *103*, 3932.
[37] M. R. Churchill, H. J. Wasserman, *J. Organomet. Chem.* **1984**, *270*, 201.
[38] M. R. Churchill, J. C. Fettinger, L. G. McCullough, R. R. Schrock, *J. Am. Chem. Soc.* **1984**, *106*, 3356.
[39] M. R. Churchill, J. W. Ziller, S. F. Pedersen, R. R. Schrock, *J. Chem. Soc. Chem. Commun.* **1984**, 485.
[40] R. R. Schrock, S. F. Pedersen, M. R. Churchill, J. W. Ziller, *Organometallics* **1984**, *3*, 1574.
[41] M. R. Churchill, J. W. Ziller, J. H. Freudenberger, R. R. Schrock, *Organometallics* **1984**, *3*, 1554.
[42] J. H. Freudenberger, R. R. Schrock, M. R. Churchill, A. L. Rheingold, J. W. Ziller, *Organometallics* **1984**, *3*, 1563.
[43] W. E. Buhro, M. H. Chisholm, *Adv. Organomet. Chem.* **1987**, *27*, 311.
[44] M. H. Chisholm, *Acc. Chem. Res.* **1990**, *23*, 419.
[45] R. R. Schrock, M. L. Listemann, L. G. Sturgeoff, *J. Am. Chem. Soc.* **1982**, *104*, 4291.
[46] M. L. Listemann, R. R. Schrock, *Organometallics* **1985**, *4*, 74.
[47] C. E. Laplaza, C. C. Cummins, *Science* **1995**, *268*, 861.

 © 2006 Wiley-VCH Verlag GmbH & Co. KGaA, Weinheim

[48] J. Feldman, R. R. Schrock, *Prog. Inorg. Chem.* **1991**, *39*, 1.
[49] R. R. Schrock, J. S. Murdzek, G. C. Bazan, J. Robbins, M. DiMare, M. O'Regan, *J. Am. Chem. Soc.* **1990**, *112*, 3875.
[50] J. H. Oskam, R. R. Schrock, *J. Am. Chem. Soc.* **1992**, *114*, 7588.
[51] J. H. Oskam, R. R. Schrock, *J. Am. Chem. Soc.* **1993**, *115*, 11831.
[52] R. R. Schrock, J. Feldman, L. Cannizzo, R. H. Grubbs, *Macromolecules* **1987**, *20*, 1169.
[53] K. M. Totland, T. J. Boyd, G. G. Lavoie, W. M. Davis, R. R. Schrock, *Macromolecules* **1996**, *29*, 6114.
[54] D. H. McConville, J. R. Wolf, R. R. Schrock, *J. Am. Chem. Soc.* **1993**, *115*, 4413.
[55] R. O'Dell, D. H. McConville, G. E. Hofmeister, R. R. Schrock, *J. Am. Chem. Soc.* **1994**, *116*, 3414.
[56] T. Masuda, T. Higashimura, *Adv. Polym. Sci.* **1987**, *81*, 122.
[57] T. Masuda, T. Higashimura, *Acc. Chem. Res.* **1984**, *17*, 51.
[58] S.-K. Choi, Y.-S. Gal, H.-H. Jin, H.-K. Kim, *Chem. Rev.* **2000**, *100*, 1645.
[59] R. R. Schrock, S. Luo, J. C. J. Lee, N. C. Zanetti, W. M. Davis, *J. Am. Chem. Soc.* **1996**, *118*, 3883.
[60] H. H. Fox, M. O. Wolf, R. O'Dell, B. L. Lin, R. R. Schrock, M. S. Wrighton, *J. Am. Chem. Soc.* **1994**, *116*, 2827.
[61] R. L. Christensen, A. Faksh, J. A. Meyers, I. D. W. Samuel, P. Wood, R. R. Schrock, K. C. Hultzsch, *J. Phys. Chem. A* **2004**, *108*, 8229.
[62] F. J. Schattenmann, R. R. Schrock, W. M. Davis, *J. Am. Chem. Soc.* **1996**, *118*, 3295.
[63] U. Anders, O. Nuyken, M. R. Buchmeiser, *J. Mol. Catal. A* **2004**, *213*, 89.
[64] G. C. Fu, R. H. Grubbs, *J. Am. Chem. Soc.* **1992**, *114*, 5426.
[65] G. C. Fu, R. H. Grubbs, *J. Am. Chem. Soc.* **1992**, *114*, 7324.
[66] A. F. Houri, Z. M. Xu, D. A. Cogan, A. H. Hoveyda, *J. Am. Chem. Soc.* **1995**, *117*, 2943.
[67] R. R. Schrock, A. H. Hoveyda, *Angew. Chem.* **2003**, *115*, 4740; *Angew. Chem. Int. Ed.* **2003**, *42*, 4592.
[68] *Handbook of Metathesis. Applications in Organic Synthesis*, *Vol. 2* (Ed.: R. H. Grubbs), Wiley-VCH, Weinheim, **2003**.
[69] *Handbook of Metathesis. Applications in Organic Synthesis*, *Vol. 3* (Ed.: R. H. Grubbs), Wiley-VCH, Weinheim, **2003**.
[70] A. Fürstner, G. Seidel, *Angew. Chem.* **1998**, *110*, 1758; *Angew. Chem. Int. Ed.* **1998**, *37*, 1734.
[71] A. Fürstner, G. Seidel, *J. Organomet. Chem.* **2000**, *606*, 75.
[72] A. Fürstner, A. Rumbo, *J. Org. Chem.* **2000**, *65*, 2608.
[73] A. Fürstner, K. Grela, *Angew. Chem.* **2000**, *112*, 1292; *Angew. Chem. Int. Ed.* **2000**, *39*, 1234.
[74] A. Fürstner, C. Mathes, C. W. Lehmann, *Chem. Eur. J.* **2001**, *7*, 5299.
[75] A. Fürstner, A.-S. Castanet, K. Radkowski, C. W. Lehmann, *J. Org. Chem.* **2003**, *68*, 1521.
[76] L. G. McCullough, R. R. Schrock, *J. Am. Chem. Soc.* **1984**, *106*, 4067.
[77] J. S. Murdzek, R. R. Schrock in *Carbyne Complexes*, VCH, New York, **1988**.
[78] Y. C. Tsai, P. L. Diaconescu, C. C. Cummins, *Organometallics* **2000**, *19*, 5260.
[79] A. Fürstner, C. Mathes, C. W. Lehmann, *J. Am. Chem. Soc.* **1999**, *121*, 9453.
[80] W. Zhang, S. Kraft, J. S. Moore, *Chem. Commun.* **2003**, 832.
[81] J. B. Alexander, D. S. La, D. R. Cefalo, A. Hoveyda, R. R. Schrock, *J. Am. Chem. Soc.* **1998**, *120*, 4041.
[82] J. B. Alexander, R. R. Schrock, W. M. Davis, K. C. Hultzsch, A. H. Hoveyda, J. H. Houser, *Organometallics* **2000**, *19*, 3700.
[83] D. S. La, J. B. Alexander, D. R. Cefalo, D. D. Graf, A. H. Hoveyda, R. R. Schrock, *J. Am. Chem. Soc.* **1998**, *120*, 9720.
[84] G. S. Weatherhead, J. G. Ford, E. J. Alexanian, R. R. Schrock, A. H. Hoveyda, *J. Am. Chem. Soc.* **2000**, *122*, 1828.
[85] D. S. La, J. G. Ford, E. S. Sattely, P. J. Bonitatebus, R. R. Schrock, A. H. Hoveyda, *J. Am. Chem. Soc.* **1999**, *121*, 11604.
[86] S. J. Dolman, E. S. Sattely, A. H. Hoveyda, R. R. Schrock, *J. Am. Chem. Soc.* **2002**, *124*, 6991.
[87] D. R. Cefalo, A. F. Kiely, M. Wuchrer, J. Y. Jamieson, R. R. Schrock, A. H. Hoveyda, *J. Am. Chem. Soc.* **2001**, *123*, 3139.
[88] A. F. Kiely, J. A. Jernelius, R. R. Schrock, A. H. Hoveyda, *J. Am. Chem. Soc.* **2002**, *124*, 2868.
[89] A. Sinha, unpublished results.
[90] A. Sinha, R. R. Schrock, *Organometallics* **2004**, *23*, 1643.
[91] X. Solans-Monfort, E. Clot, C. Copéret, O. Eisenstein, *J. Am. Chem. Soc.* **2005**, *127*, 14015.
[92] F. Blanc, C. Copéret, J. Thivolle-Cazat, J.-M. Basset, A. Sinha, R. R. Schrock, *Angew. Chem.* **2006**, *118*, 1238; *Angew. Chem. Int. Ed.* **2006**, *45*, 1216.
[93] C. Cóperet, M. Chabanas, R. P. Saint-Arroman, J.-M. Basset, *Angew. Chem.* **2003**, *115*, 164; *Angew. Chem. Int. Ed.* **2003**, *42*, 156.
[94] M. Taoufik, E. Schwab, M. Schultz, D. Vanoppen, M. Walter, J. Thivolle-Cazat, J.-M. Basset, *Chem. Commun.* **2004**, 1434.
[95] D. Soulivong, C. Copéret, J. Thivolle-Cazat, J.-M. Basset, B. M. Maunders, R. B. A. Pardy, G. J. Sunley, *Angew. Chem.* **2004**, *116*, 5480; *Angew. Chem. Int. Ed.* **2004**, *43*, 5366.
[96] R. Toreki, R. R. Schrock, *J. Am. Chem. Soc.* **1992**, *114*, 3367.
[97] R. R. Schrock, R. Toreki, G. A. Vaughan, A. Farooq in *Transition-Metal Carbyne Complexes* (Ed.: F. R. Kreissl), Kluwer, Dordrecht, **1992**.
[98] R. R. Schrock, L. P. H. Lopez, J. Hafer, R. Singh, A. Sinha, P. Müller, *Organometallics* **2005**, *24*, 5211.
[99] L. P. H. Lopez, R. R. Schrock, *J. Am. Chem. Soc.* **2004**, *126*, 9526.
[100] R. Toreki, R. R. Schrock, M. G. Vale, *J. Am. Chem. Soc.* **1991**, *113*, 3610.

 © 2006 Wiley-VCH Verlag GmbH & Co. KGaA, Weinheim

Metathesis Reactions

DOI: 10.1002/anie.200600680

Olefin-Metathesis Catalysts for the Preparation of Molecules and Materials (Nobel Lecture)**

*Robert H. Grubbs**

Keywords:
homogeneous catalysis · metathesis · Nobel lecture · polymerization · ruthenium

This is a story of our exploration of the olefin-metathesis reaction, a reaction that has been the major emphasis of my independent research. As with all stories of scientific discovery, there are three components: the discoveries, the resulting applications, and, perhaps the most important of all, the people involved. Starting from observations made from seemingly unrelated work, our investigations into the fundamental chemistry of this transformation have been an exciting journey, with major advances often resulting from complete surprises, mistakes, and simple intuition. Ultimately, these efforts have contributed to olefin metathesis becoming the indispensable synthetic tool that it is today.[1]

Much of modern organometallic and polymer chemistry, as we know it, started with a chance observation made in the early 1950s by the Ziegler group in Mülheim, Germany.[2] During this time, Ziegler was continuing work that had been initiated during World War II in exploring the use of alkyl aluminum complexes for the oligomerization of ethylene to produce lubricating oils. On one occasion, it was noted that this reaction produced 1-butene from ethylene instead of the C_{10}–C_{20} hydrocarbons normally observed. Subsequent analysis of the reaction autoclave found the presence of nickel. When nickel salts were deliberately added to this reaction, 1-butene was again observed. This discovery has since served as the foundation for an amazing array of nickel chemistry and catalysis. In addition, as nickel had been found to possess unexpected reactivity, other metal salts were also investigated. In particular, when titanium and zirconium halides were used in combination with alkyl aluminum compounds, a new form of polyethylene was obtained. Natta further demonstrated that similar catalysts could promote the formation of stereoregular polymers from propylene. The 1963 Nobel Prize in Chemistry was awarded to Ziegler and Natta for this work.

The application of Ziegler–Natta-type systems toward the polymerization of cyclic olefins afforded additional unexpected results. A group at DuPont observed that the polymerization of norbornene did not produce a saturated polymer as expected, but instead afforded an unsaturated polymer in which one of the rings had been opened. While surprising, the origin of this unexpected polymeric structure was not to be pursued until later. Natta subsequently observed a similar result when he attempted to polymerize cyclopentene using tungsten and molybdenum halides—he, too, obtained a ring-opened, unsaturated polymer. Finally, Banks and Bailey of Phillips Petroleum Co., while investigating the possible polymerization of propylene over cobalt molybdate, found instead the formation of ethylene and 2-butene. These three observations, seemingly unrelated, were beginning to indicate a fundamentally new olefin transformation.[3]

My involvement with this puzzle started in 1967 while I was a postdoctoral fellow at Stanford. Jim Collman, my postdoctoral mentor, had just returned from a trip to Phillips Petroleum, where he had learned of an amazing reaction that converted propylene into ethylene and 2-butene. During a group meeting (Barry Sharpless, Nobel Prize 2001 was also a member of the Collman group at that time), we began to discuss possible mechanisms for this transformation. With my earlier training in mechanistic organic chemistry as an undergraduate and master's student in the laboratories of

[*] Prof. R. H. Grubbs
Victor and Elizabeth Atkins Professor of Chemistry Arnold and Mabel Beckman Laboratories of Chemical Synthesis
California Institute of Technology
Pasadena, CA 91125 (USA)
Fax: (+1) 626–564–9297
E-mail: rhg@caltech.edu

[**] Copyright The Nobel Foundation 2005. We thank the Nobel Foundation, Stockholm, for permission to print this lecture

© 2006 Wiley-VCH Verlag GmbH & Co. KGaA, Weinheim

Merle Battiste, and as a doctoral student with Ron Breslow, I felt this unknown reaction mechanism would be an ideal problem to study.

Around this time, Calderon and his group at Goodyear had developed a soluble catalyst system that could not only induce polymerization via ring-opening, but also convert propylene into ethylene and 2-butene. Calderon's observations established that the polymerization of cyclic olefins observed by DuPont and Natta and the scrambling of acyclic olefins observed by Banks and Bailey were similar reactions. He also established that the mechanism of this reaction involved the cleavage of carbon–carbon double bonds rather than a transfer of alkyl groups between olefins through single-bond cleavage. This first critical mechanistic observation set the stage for subsequent studies. Banks and Bailey went on to propose a "quasicyclobutane" mechanism to account for their interchange reaction that was also consistent with Calderon's results. Other mechanisms were also proposed to account for this transformation, now termed olefin metathesis. What all these mechanisms had in common was the pair-wise involvement of carbon atoms in reaction intermediates. Theoretical studies of this reaction carried out by Frank Mango at Shell supported this pair-wise exchange of two-carbon fragments.[4]

My independent career started at Michigan State University in 1968, where I proposed an alternative pair-wise mechanism and initiated experimental work. Shortly thereafter, however, a growing body of evidence against such a mechanism began to appear. While investigating the effect of acyclic olefins in determining the molecular weight of polypentenamers, Chauvin and Hérrison observed products that were not consistent with the diolefin metal complexes proposed in the "quasicyclobutane"-type mechanisms. They instead proposed that the reaction did not go through a diolefin metal complex, but rather via a one-carbon metal carbene complex and metallocyclobutanes; intermediates that contain an odd number of carbon atoms. In a similar study, Katz proposed an analogous mechanism where he was able to rationalize the observations that Chauvin had found to be inconsistent with his non-pair-wise mechanism. Chuck Casey subsequently found a model for this transformation utilizing preformed metal carbene complexes, and Richard Schrock was able to determine that metal carbene complexes could, in fact, be generated under conditions similar to those used to prepare Ziegler–Natta-type catalysts.[5] Incorporating this new information into our mechanistic consideration, we designed an experiment that would allow most of the ambiguities of the Chauvin experiment to be addressed in detail. Rather than using a cross-metathesis reaction that would require us to analyze the role of alkyl groups on the intermediates, we instead selected to study the simplest system possible: isotopic substitution on a ring-closing metathesis (RCM) reaction.

The RCM of 1,7-octadiene generates cyclohexene and ethylene (Scheme 1). Cyclohexene is one of the few simple cyclic olefins that will not undergo subsequent metathesis reactions. Consequently, the fate of the two olefins in 1,7-octadiene can be determined by examination of the metathesis products. If the pair-wise mechanisms involving even numbers of carbon atoms were involved, the other two carbon

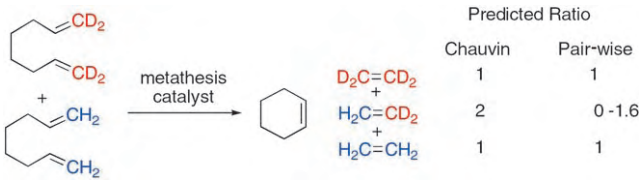

Scheme 1. Ring-closing metathesis of 1,7-octadiene.

atoms would be required to couple together. In contrast, the Chauvin mechanism would be expected to scramble the two terminal carbon atoms. A mixture of 1,1,8,8-tetradeutero-1,7-octadiene and 1,7-octadiene was used to investigate this. In the simplest case, the even-carbon mechanisms should produce only ethylene and tetradeuteroethylene, while the odd-carbon mechanisms should afford a statistical mixture of ethylene, dideuteroethylene, and tetradeuteroethylene in a 1:2:1 ratio. Careful analysis of all of our experiments found that a statistical mixture of ethylene compounds was kinetically formed in this reaction, a result consistent with the prediction made using the Chauvin (odd-carbon) mechanism. Subsequent studies by Katz on related systems provided additional support for this conclusion.[6]

By determining the key reaction intermediates in olefin metathesis, these combined mechanistic studies now enabled the use of rational design for further catalyst optimization. Prior to this time, metathesis catalysts were produced utilizing inconsistent, ill-defined systems. By confirming the non-pair-wise mechanism of Chauvin, the identification of new metal alkylidene (metal carbene) complexes capable of promoting olefin metathesis now became our target for further improving reaction efficiency.

Fred Tebbe, a co-worker of Schrock during his time at DuPont, developed one of the first well-defined metathesis systems. Now known as the Tebbe reagent, titanium complex **1**, a metal carbene precursor, was found to exhibit metathesis activity in addition to its ability to promote Wittig-type reactions on esters. As the Tebbe catalyst was well-defined, both the starting and propagating carbene species could now be observed during a metathesis reaction, making it an ideal system for mechanistic study. In particular, we became interested in investigating the stereochemistry of the intermediate metallacycle. Our initial efforts to isolate a metallacycle complex proved unsuccessful until Tom Howard was able to serendipitously isolate metallacycle **2** by employing dimethylamino pyridine (DMAP), which facilitated aluminum removal (Scheme 2). Tom was later able to demonstrate

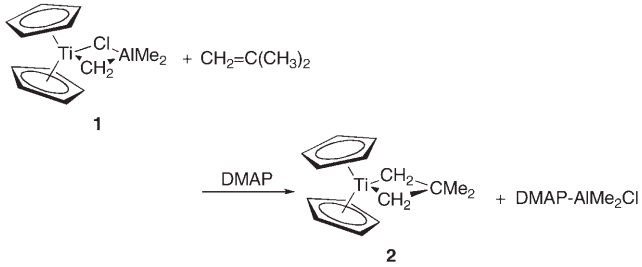

Scheme 2. Preparation of an isolable metallacycle.

© 2006 Wiley-VCH Verlag GmbH & Co. KGaA, Weinheim

this metallacycle to be the low-energy state for this catalyst system. In addition, **2** was found to be an active metathesis catalyst. This observation provided the first example of a metallacycle intermediate and demonstrated that metallacycles could function as kinetically competent catalysts for olefin metathesis.[7]

Utilizing the well-defined Tebbe system, additional mechanistic and synthetic studies were carried out. Laura Gilliam found that metathesis conducted using this system was inherently "living," allowing for the preparation of polymers with defined structures. Polymer preparation and analysis consequently became a major focus within my group to further explore these observations. It was during this period that Richard Schrock spent a four-month sabbatical at Caltech, where we co-authored a paper demonstrating that one of his tantalum catalysts could also serve as a living initiator. In fact, it is now well established that virtually all defined metathesis initiators can be used to generate polymer structures through living polymerization.[8]

Subsequent studies by the Schrock group resulted in the design and synthesis of a number of very efficient molybdenum and tungsten metathesis catalysts, the historical development of which are discussed in his lecture (see the preceding article in this issue). Despite the activity of Schrock systems, the use of these early-transition-metal catalysts had a major limitation: the oxophilicity of the metal center afforded poor functional-group tolerance and necessitated catalyst preparation and handling under an inert atmosphere. To fully exploit the potential of metathesis, we believed that the development of new, functional-group-tolerant catalysts would be crucial. Once again, serendipity would play a role in achieving this objective.

The development of ruthenium-based metathesis catalysts started with the goal of preparing interesting polymeric structures. Polymer chemistry provides an excellent means of studying metathesis catalysts: miniscule catalyst loadings have the capacity to generate large amounts of polymeric material, the structure of which can provide a historical record of catalyst activity. The polymer program within my group was focused on understanding the basic principles of living metathesis polymerization. From this knowledge, we hoped to develop novel polymers that possessed interesting structures and physical properties. During the course of this work, model building had suggested that the ring-opened polymer from 7-oxo-norbornenes could be used to produce ionophoric membranes for selective ion transport. Bruce Novak took on the challenge of making these desired polymers. Much to our dismay, however, none of the available catalysts was found to promote this reaction. Examining the literature, Bruce came upon reports by Michelotti[9] and later Natta, where late-transition-metal catalysts had been used to polymerize strained olefins in protic media. In the laboratory, Bruce was able to demonstrate that these systems could also effectively promote the formation poly-7-oxo-norbornenes. More importantly, he then discovered that ruthenium(II) complexes could serve as much more active polymerization catalysts. The outcome of Bruce's investigations resulted in the development of a robust catalyst system that tolerated most functional groups and aqueous media. Despite the activity of these ruthenium salt catalysts, however, only a small percentage of the ruthenium added to a reaction was found to produce an active catalytic center. In addition, as the structure of the active catalysts was totally undefined, it was impossible to make rational changes for further improvements.[10] However, this work defined the path forward; a ruthenium(II) complex and a strained olefin were found to be required to form an active catalyst system.

Assuming that olefin metathesis must occur via the formation of metal carbenes, we felt that the development of well-defined ruthenium carbene complexes was vital for further catalyst optimization. It took a few years, but eventually graduate student SonBinh Nguyen was able to prepare air-stable carbene complex **4** from the reaction of ruthenium(II) phosphine complex **3** with cyclopropene (Scheme 3). To our surprise, complex **4** was found to be an

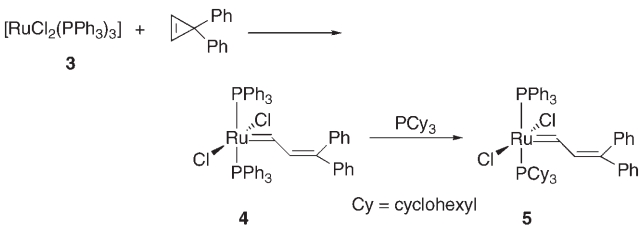

Scheme 3. Preparation of the first well-defined ruthenium carbene catalyst.

effective catalyst for the polymerization of norbornenes in protic media. Although **4** was not very active, its structure was well-defined, finally providing us with a scaffold by which to make structural changes for catalyst optimization. While many modifications have since been made (e.g. ligand exchange using tricyclohexylphosphine to generate the more active catalyst **5**), the basic structure of our catalyst systems still resembles that of our original "SonBinh Catalyst." This well-defined family of catalysts is distinguished by its amazing tolerance to oxygen and water, making it ideal for application to organic synthesis.[11]

In the early 1990s, Greg Fu joined our group as a postdoctoral scholar from Dave Evan's group at Harvard and began investigating the activity of various metathesis polymerization catalysts in organic synthesis. Relatively quickly, he was able to demonstrate that the Schrock molybdenum catalysts were effective for a number of important organic transformations, particularly those involving ring-closing reactions. Just prior to leaving the group to join the faculty at MIT, he was able to demonstrate that our newly prepared ruthenium systems could perform the same transformations on the benchtop without the use of a glovebox. In addition, many previously unreactive substrates were found to readily undergo ruthenium-catalyzed olefin metathesis in high yields.[12]

In our earlier work with the Tebbe reagent, we had found that its general use had been limited because of its air sensitivity and difficult preparation. In contrast, our user-friendly ruthenium catalysts were in high demand, and efforts now had to be made to make them readily available.

 © 2006 Wiley-VCH Verlag GmbH & Co. KGaA, Weinheim

Unfortunately, the SonBinh synthesis was difficult to run on large scale. Eventually, building off of work performed by Marcia France, Peter Schwab was able to develop a method based on the use of a diazo precursor. Although this reagent is potentially explosive, Mike Giardello developed a procedure to tame this reagent, allowing complex **6** to be commercially made on multikilogram scales (Figure 1).[13] With commercial sources, the organic synthetic community found a wide array of creative uses of olefin-metathesis catalysts in the synthesis of complex structures.

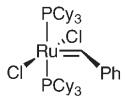

6

Figure 1. First-generation commercial catalyst.

Ruthenium's preference for soft Lewis bases and π-acids, such as olefins, over hard bases, such as oxygen-based ligands, is responsible for its high tolerance to air and water. It also makes ruthenium catalysts fundamentally different from titanium-, tungsten-, and molybdenum-based systems. Consequently, the rules learned in the development of early-transition-metal catalysts no longer applied: for example, as ruthenium possesses a metal center rich in d electrons, strongly electron-donating ligands, rather than electron-poor ones, are required for high catalyst activity. Detailed mechanistic studies to obtain an understanding of the catalyst's structure–activity profile were therefore required. During the course of such investigations, we found that five-coordinate complexes, such as **5** and **6**, are catalytic precursors. To generate the metathesis-active species, one of the neutral ligands must be lost. The remaining neutral ligand of the resulting 14-electron complex is responsible for catalyst turnover. This knowledge was used to rationalize why bulky, basic tricyclohexylphosphine ligands are more effective than triphenylphosphine ligands in the ruthenium-catalyzed metathesis of cyclooctene.[14]

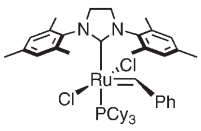

7

Figure 2. Second-generation commercial catalyst.

Further catalyst tuning through the substitution of one of the phosphine ligands on **6** with an N-heterocyclic carbene (NHC) ligand resulted in a series of highly active catalysts (e.g. catalyst **7**; Figure 2). This increase in metathesis activity was attributed to an increased rate of catalyst turnover owing to the favorable electron donation and steric bulk of the NHC ligand. Additional modification by replacing the phosphine in **7** with a weaker ligand, such as pyridine, resulted in an increase in activity up to a factor of 10^4 relative to catalyst **6**.[15] A number of other research groups have played a role in further optimizing these catalytic systems.

One of the most rewarding aspects of my research has been the opportunity to study the potential applications of a new catalyst. The facile preparation of the ruthenium catalysts, coupled with their functional-group tolerance and environmental stability, enabled olefin metathesis to finally realize its broad potential. Although olefin metathesis was already commercially utilized in the processing of hydrocarbons, the application of olefin metathesis in organic synthesis and in the preparation of highly functionalized polymers had yet to be fully developed.

Most commercial products that contain organic molecules possess at least one carbon–carbon double bond or, if one is not present, it is likely that an olefin was used in its preparation. This being the case, the potential applications of olefin metathesis are endless. To date, commercial products range from a wooden baseball bat, treated with metathesis-based polymers to improve durability, to the preparation of highly functionalized pharmaceutical agents, many of which are in the advanced stages of testing. For example, Boehringer Ingelheim recently reported the use of olefin metathesis for the commercial preparation of 400 kg of a compound under investigation to treat hepatitis C (Scheme 4).[16]

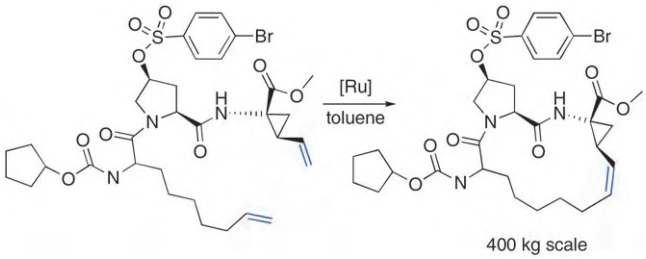

Scheme 4. Commercial application of ring-closing metathesis.

Some of the earliest commercial applications of olefin metathesis involved the ring-opening metathesis polymerization (ROMP) of monomers containing strained, unsaturated rings. The polymerization of dicyclopentadiene (DCPD) is one of the best-known examples of this (Scheme 5). DCPD is an attractive monomer for polymer

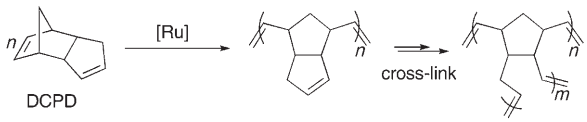

Scheme 5. Ring-opening metathesis polymerization for the preparation of dicyclopentadiene (DCPD) polymers.

production, as it is inexpensive, and the resulting polymer products are useful for a variety of applications. Hercules and Goodrich developed one of the first commercial processes for this reaction, where early-transition-metal complexes were combined with alkylaluminum to form catalysts to produce DCPD polymers by injection molding. Unfortunately, the extreme sensitivity of these catalysts toward air and water mandated the use of rigorous processing conditions and highly purified monomers. In contrast, the functional and environmental tolerance of the ruthenium catalysts enables DCPD polymerization to be carried out in open molds in the presence of numerous additives. In addition, DCPD monomers bearing functional groups for further synthetic elaboration can also be utilized. A wide variety of products, such as

 © 2006 Wiley-VCH Verlag GmbH & Co. KGaA, Weinheim

the baseball bats discussed previously, as well as bathroom fixtures, ballistic panels, and large equipment body parts, are currently in/or being developed for production utilizing ruthenium-catalyzed ROMP.[17]

The ruthenium systems can also be used to prepare polymers with well defined structures. Like the Tebbe complex, ruthenium olefin-metathesis catalysts can be used for the living polymerization of norbornene derivatives. In these cases, strained olefins are ring open polymerized by the metal center to produce a polymer that contains an active ruthenium alkylidene at the end of the polymer chain. After the first monomer added to the catalyst is consumed, a second monomer can be added and the polymers start to grow again. If the monomers contain different functional groups, the different segments of the polymer will have different properties and functions. Since the systems are living, if all the chains are initiated at the same time, the length of the chain and therefore the molecular weight is controlled by statistics and produces a very narrow distribution of chain lengths. Consequently, both the functionality and molecular weight of polymers produced using the ruthenium systems can be controlled. Since the ruthenium systems have been demonstrated to tolerate many functional groups on other applications, the polymers prepared using ruthenium initiators can contain many functionalities for use in a wide variety of applications. For example, if one of the blocks of the polymer is water soluble and the other is insoluble, the block copolymers form micelles (that are nanoparticles) that are being explored for applications in medical diagnostics. If the two blocks are incompatible, the solids formed from the block copolymers will have microphase separated structures that are important for a number of applications in materials science.

Ring-closing metathesis (RCM) and, to a lesser extent, cross metathesis (CM) have now become standard transformations in organic synthesis. As ruthenium catalysts will tolerate most functional groups, protection–deprotection strategies—which often hinder the application of other reaction methodologies—are seldom required. In addition, ruthenium-catalyzed olefin metathesis is ideal for use during the late stages of a total synthesis owing to the chemoselectivity exhibited by the catalyst and the mild reaction conditions required. Ruthenium metathesis catalysts are also ideally suited for use in tandem reactions involving acetylene derivatives and ring systems, as they are stable toward a variety of reaction conditions and reagents and, often, their presence will not impede subsequent reaction transformations. This favorable combination of reactivity and functional-group compatibility has resulted in the extensive use of olefin metathesis, which is reflected in large number of citations to the use of ruthenium-based metathesis catalysts.

A useful feature of olefin metathesis lies in the reaction's reversibility. Olefin metathesis is a thermodynamically controlled reaction; therefore, the self-assembly of the most stable product of a metathesis reaction can be attained by simply allowing the reaction to reach equilibrium. This feature has proven to be advantageous for a variety of

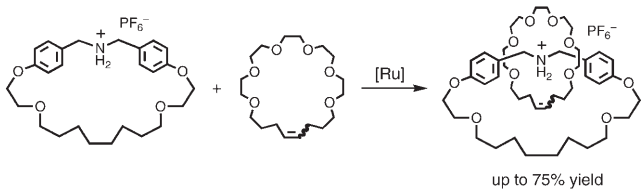

Scheme 6. Olefin metathesis for the preparation of "magic" rings.

applications, particularly in the use of RCM to produce interlocked, "magic" ring systems in high yield (Scheme 6).[18]

In a modern industrial setting, the use of efficient chemical processes, preferably those with minimal impact on the environment, is essential. The term "green chemistry" has evolved as an umbrella concept to represent this general approach of conducting reactions. Metathesis attains the goals of green chemistry in three ways: 1) by providing a more efficient route over traditional methods to carbon-carbon bond formation and avoiding by-product formation; 2) through enabling the use of renewable resources; and 3) by providing a means to attain environmentally friendly products. For instance, the processing of seed oils represents an excellent example of the first two goals. Using solvent-free conditions, olefin metathesis enables vegetable oils to be efficiently processed into compounds that can serve as renewable sources of petroleum product alternatives.[19]

The solvent-free CM of 1-hexene with hexenylacetate (Scheme 7) represents an example of the use of metathesis to generate environmentally friendly products. The product of this reaction can be readily converted into a pheromone of the peach twig borer moth, which can be used as an environmentally friendly means of insect control in lieu of the use of broad-spectrum pesticides. CM is currently under investigation for the commercial preparation of other pheromones, as this route represents an efficient means to generate these compounds starting from inexpensive starting materials.[20]

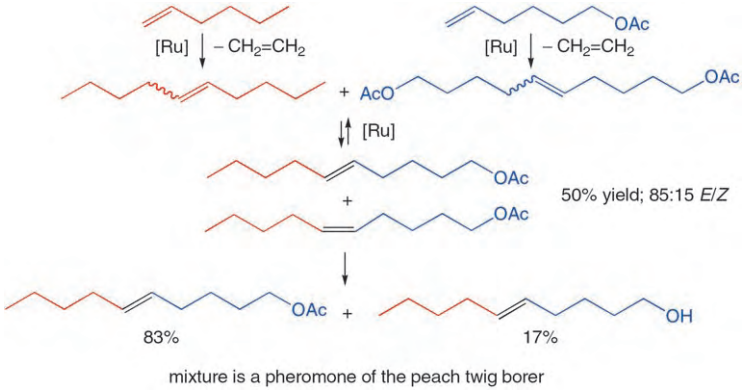

Scheme 7. Commercial application of cross-metathesis in the production of "green" compounds.

Beginning as merely an interesting anomaly over forty years ago, the olefin-metathesis reaction has transitioned into one of chemistry's most valuable reactions for carbon–carbon

 © 2006 Wiley-VCH Verlag GmbH & Co. KGaA, Weinheim

bond formation. In the early days of trying to understand this fundamental process, we never envisioned that this reaction would one day achieve the import that it has today. Our exploration of this reaction has been a fascinating journey, and it is one that is ongoing. As work on olefin metathesis continues in both industry and academia, we can look forward to exciting future developments.

I would like to thank the over 200 co-workers who have contributed to my work, as well as all the other interesting people I have interacted with during my career in chemistry. I would also like to thank the group at Materia Inc. who has played a significant role in making this technology available for many commercial applications. You have all made the journey very interesting. I especially want to thank my wife Helen and the kids (Barney, Brendan and Katy) who have provided the support that has made it all possible and worthwhile.

Received: February 21, 2006

[1] R. H. Grubbs, *Tetrahedron* **2004**, *60*, 7117; *Handbook of Metathesis*, *Vol. 3* (Ed.: R. H. Grubbs), Wiley-VCH, Weinheim, **2003**.
[2] *The Chain Straighteners: Fruitful Innovation: The Discovery of Linear and Steroregular Synthetic Polymers*, McMillan, London, **1979**.
[3] W. L. Truett, D. R. Johnson, I. M. Robinson, *J. Am. Chem. Soc* **1960**, 2337.
[4] N. Calderon, E. A. Ofstead, J. P. Ward, W. A. Judy, K. W. Scott, *J. Am. Chem. Soc.* **1968**, *90*, 4133; R. L. Banks, G. C. Bailey, *Ind. Eng. Chem. Prod. Res. Dev.* **1964**, 170.
[5] J. L. Hérisson, Y. Chauvin, *Makromol. Chem.* **1971**, *141*, 162; T. J. Katz, J. McGinnis, *J. Am. Chem. Soc.* **1975**, *97*, 1592; C. P. Casey, T. J. Burkhardt, *J. Am. Chem. Soc.* **1974**, *96*, 7808.
[6] R. H. Grubbs, D. D. Carr, C. Hoppin, P. L. Burk, *J. Am. Chem. Soc.* **1976**, *98*, 3478; R. H. Grubbs, P. L. Burk, D. D. Carr, *J. Am. Chem. Soc.* **1975**, *97*, 3265; T. J. Katz, R. Rothchild, *J. Am. Chem. Soc.* **1976**, *98*, 2519.
[7] T. R. Howard, J. B. Lee, R. H. Grubbs, *J. Am. Chem. Soc.* **1980**, *102*, 6876; S. H. Pine, R. Zahler, D. A. Evans, R. H. Grubbs, *J. Am. Chem. Soc.* **1980**, *102*, 3270; J. R. Stille, R. H. Grubbs, *J. Am. Chem. Soc.* **1986**, *108*, 855; F. N. Tebbe, G. W. Parshall, G. S. Reddy, *J. Am. Chem. Soc.* **1978**, *100*, 3611.
[8] L. R. Gilliom, R. H. Grubbs, *J. Am. Chem. Soc.* **1986**, *108*, 733; R. R. Schrock, J. Feldman, L. F. Cannizzo, R. H. Grubbs, *Macromolecules* **1987**, *20*, 1169.
[9] F. W. Michelotti, W. P. Keaveney, *J. Polym. Sci. Part A* **1965**, 895.
[10] B. M. Novak, R. H. Grubbs, *J. Am. Chem. Soc.* **1988**, *110*, 960.
[11] S. T. Nguyen, L. K. Johnson, R. H. Grubbs, J. W. Ziller, *J. Am. Chem. Soc.* **1992**, *114*, 3974; S. T. Nguyen, R. H. Grubbs, J. W. Ziller, *J. Am. Chem. Soc.* **1993**, *115*, 9858.
[12] G. C. Fu, S. T. Nguyen, R. H. Grubbs, *J. Am. Chem. Soc.* **1993**, *115*, 9856; G. C. Fu, R. H. Grubbs, *J. Am. Chem. Soc.* **1992**, *114*, 7324.
[13] P. Schwab, M. B. France, J. W. Ziller, R. H. Grubbs, *Angew. Chem.* **1995**, *107*, 2179; *Angew. Chem. Int. Ed. Engl.* **1995**, *34*, 2039; T. E. Welhelm, T. R. Belderrain, S. N. Brown, R. H. Grubbs, *Organometallics* **1997**, *16*, 3867.
[14] E. L. Dias, S. T. Nguyen, R. H. Grubbs, *J. Am. Chem. Soc.* **1997**, *119*, 3887; M. S. Sanford, M. Ulman, R. H. Grubbs, *J. Am. Chem. Soc.* **2001**, *123*, 749; M. S. Sanford, J. A. Love, R. H. Grubbs, *J. Am. Chem. Soc.* **2001**, *123*, 6543.
[15] M. Scholl, S. Ding. C. W. Lee, R. H. Grubbs, *Org. Lett.* **1999**, *1*, 953; C. W. Bielawski, R. H. Grubbs, *Angew. Chem.* **2000**, *112*, 3025; *Angew. Chem. Int. Ed.* **2000**, *39*, 2903; T. M. Trnka, J. P Morgan, M. S. Sanford, T. E. Wilhelm, M. Scholl, T.-L. Choi, S. Ding, M. W. Day, R. H. Grubbs, *J. Am. Chem. Soc.* **2003**, *125*, 2546; J. A. Love, M. S. Sanford, M. W. Day, R. H. Grubbs, *J. Am. Chem. Soc.* **2003**, *125*, 10103.
[16] T. Nicola, M. Brenner, K. Donsbach, P. Kreye, *Org. Process Res. Dev.* **2005**, 27; I. Kodota, H. Takamura, K. Sato, A. Ohno, K. Matusuda, Y. Yamamoto, *J. Am. Chem. Soc.* **2003**, *125*, 46.
[17] C. S. Woodson, Jr., R. H. Grubbs, Patent No. 6,310,121 B1, October 30, 2001; C. S. Woodson, Jr., R. H. Grubbs, U.S. Patent No. 5,939,504, August 17, 1999.
[18] J.-P. Sauvage, B. Mohr, R. H. Grubbs, M. Weck, *Angew. Chem.* **1997**, *109*, 1365; *Angew. Chem. Int. Ed. Engl.* **1997**, *36*, 1308; A. F. M. Kilbinger, S. J. Cantrill, A. W. Waltman, M. W. Day, R. H. Grubbs, *Angew. Chem.* **2003**, *115*, 3403; *Angew. Chem. Int. Ed.* **2003**, *42*, 3281; E. N. Guidry, S. J. Cantrill, J. F. Stoddart, R. H. Grubbs, *Org. Lett.* **2005**, *7*, 2129.
[19] Frost & Sullivan's Industrial Bioprocessing Alert, Sept. 9, 2005; http://www.epa.gov/greenchemistry/whats_gc.html.
[20] R. L. Pederson, R. H. Grubbs, U.S. Patent No. 6,696,597, February 24, 2004; R. L. Pederson, R. H. Grubbs, U.S. Patent No. 6,215,019 B1, April 3, 2001.

 © 2006 Wiley-VCH Verlag GmbH & Co. KGaA, Weinheim

Communications

DOI: 10.1002/anie.200600319

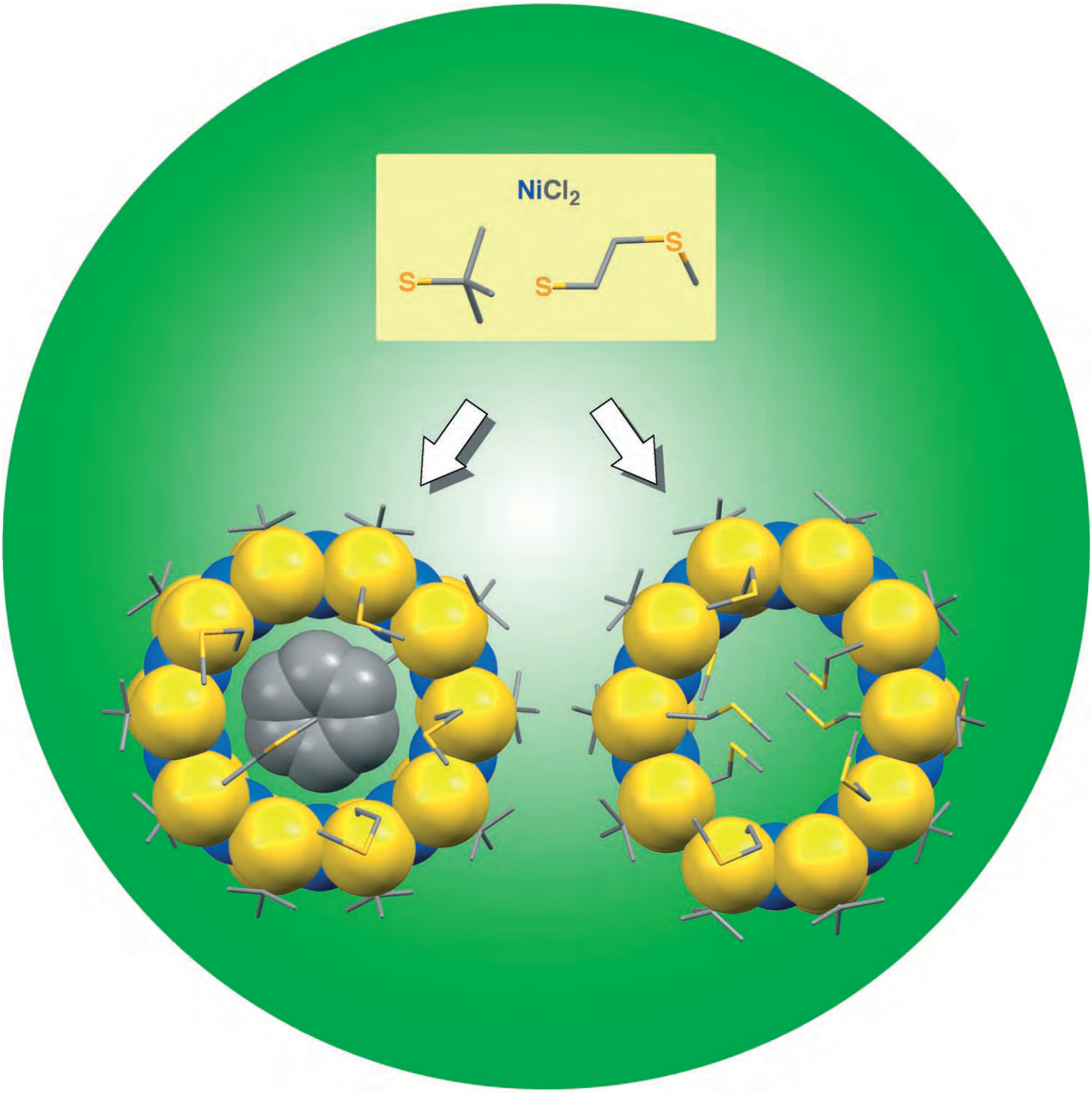

The flexible configuration of the new *cyclo*-$Ni_{10}S_{20}$ toroid was revealed by X-ray structural analysis to be circular or ellipsoidal, depending on the presence or absence of an encapsulated benzene molecule. For a more detailed discussion on the synthesis and structure, see the Communication by K. Tatsumi and co-workers on the following pages.

WILEY InterScience DISCOVER SOMETHING GREAT
© 2006 Wiley-VCH Verlag GmbH & Co. KGaA, Weinheim

Nickel Thiolates

DOI: 10.1002/anie.200600319

Nickel(II) Thiolate Complexes with a Flexible *cyclo*-{$Ni_{10}S_{20}$} Framework**

*Chi Zhang, Satoshi Takada, Michael Kölzer, Tsuyoshi Matsumoto, and Kazuyuki Tatsumi**

First-row transition-metal toroidal architectures are important motifs for potential applications in molecular recognition and magnetic materials.[1,2] In contrast to the ubiquitous O- or N-bridged metal rings, which exhibit fascinating cluster configurations,[3–9] the study of the S-bridged variants remains limited. Homoleptic nickel(II) thiolates [{Ni(μ-SR)$_2$}$_n$] occasionally generate cyclic structures by forming shared edges of the square NiS_4 coordination planes, and several hexanuclear ring clusters [{Ni(μ-SR)$_2$}$_6$] have been reported.[10] Tetranuclear[11] and pentanuclear cyclic complexes have also been isolated,[11c,12] but reports of the synthesis of larger cyclic complexes are still limited. The structure of [{Ni(μ-$SCH_2CO_2Et)_2$}$_8$] was reported by Dance et al. in which the substituent of one thiolate bridge is tilted inward to fill the cavity of the octanuclear ring.[13] Recently, the intriguing cyclic structures of nona- and undecanuclear complexes [{Ni(μ-SPh)$_2$}$_n$] ($n = 9$, 11) were determined by Dahl and co-workers, although in low yield.[14] Each of the cyclic nickel thiolates described above is composed of one kind of thiolate ligand. In contrast, Wolczanski and co-workers synthesized a dodecanuclear cyclic complex [{Ni(μ-SS*t*Bu$_3$)(μ-Br)}$_{12}$], in which the nickel atoms, in a tetrahedral geometry, are linked by a sterically demanding thiolate ligand and a bromine atom; however, the complex was obtained as a mixture with by-products.[15] As an extension of our study on transition-metal thiolates,[16] we became interested in thioether–thiolate hybrid ligands. Reported herein is a new synthetic route to cyclic nickel thiolate complexes with two different thiolate bridges, namely an alkylthiolate ligand (S*i*Pr or S*t*Bu) and 2-methylthioethanethiolate (mtet), and the use of these ligands resulted in the selective formation of *cyclo*-[{Ni(μ-S*i*Pr)(μ-mtet)}$_6$] and *cyclo*-[{Ni(μ-S*t*Bu)(μ-mtet)}$_{10}$]. We found that the ring configuration of the decanuclear nickel cluster is flexible and exhibits either a circular or ellipsoidal form which is dependent on the presence or absence of an encapsulated guest molecule.

The reaction of $NiCl_2 \cdot 6H_2O$ with one equivalent of [K(mtet)] at room temperature led to an immediate color change from light green to deep red, and the thiolate-bridged dinuclear nickel complex [{NiCl(μ-mtet)}$_2$] (**1**) was isolated in 70% yield as brown-red block-shaped crystals.[17,18] In the structure of **1**, the two mtet ligands link the Ni atoms through the thiolate sulfur atoms, and the thioether sulfur atoms and chloride atoms occupy the terminal positions. Thus, two square {$NiClS_3$} units are conjoined at an edge, and the Ni_2S_2 rhombus is puckered (dihedral angle: 117.8°). This complex was found to be a suitable precursor for the synthesis of a series of mixed-thiolato complexes of nickel. Thus, **1** was treated with two equivalents of K(S*i*Pr) in MeOH for six hours, and subsequent crystallization from a mixture of benzene/hexane generated deep-red hexagonal plates of [{Ni(μ-S*i*Pr)(μ-mtet)}$_6$]·C_6H_6 (**2**) in 35% yield (Scheme 1). The X-ray crystal analysis revealed a hexagonal {Ni_6S_{12}} framework (Figure 1), as was observed for the previously reported complexes [{Ni(μ-SR)$_2$}$_6$].[10,18] The cocrystallized benzene molecule is located outside the Ni_6 ring. The transannular Ni···Ni separations are in the range 5.757(2)–5.915(1) Å, and the dihedral angles between two adjacent NiS_2 planes (121.6–125.6°) are close in value to the interior angle of the ideal hexagon. The two kinds of thiolate ligands, mtet and S*i*Pr, are situated alternately above and below the Ni_6 plane. The *i*Pr groups are oriented away from the ring, and each thioether substituent of the mtet ligands extends above or below the Ni_6 plane.

When the reaction of **1** was carried out with K(S*t*Bu) instead of K(S*i*Pr), a decanuclear cluster [{Ni(μ-S*t*Bu)(μ-mtet)}$_{10}$] (**3**) was obtained in 62–66% yield as dark-red block-shaped crystals after recrystallization from benzene/HMDSO or toluene/HMDSO (HMDSO = hexamethyldisiloxane). The toroidal {$Ni_{10}S_{20}$} core geometry of **3** was determined by X-ray analysis, and analogously to the ligand conformation in **2**, the mtet and S*t*Bu ligands bridge the Ni atoms alternately above and below the Ni_{10} plane. Interestingly, **3** was found to crystallize in different forms depending on the solvent used for crystallization. In the X-ray structure of crystals obtained from a mixture of benzene/HMDSO, one of the three benzene molecules is encapsulated in the cavity formed by the {$Ni_{10}S_{20}$} toroid. Thus, the compound is formulated as [C_6H_6⊂{Ni(μ-S*t*Bu)(μ-mtet)}$_{10}$]·2 C_6H_6 (**3a**), and the toroidal {$Ni_{10}S_{20}$} core assumes a circular shape.[18] However, no solvent molecule was incorporated inside the ring when compound **3** was crystallized from a mixture of toluene/HMDSO. In this case, the {$Ni_{10}S_{20}$} core displays an ellipsoidal shape, and the compound is formulated as [{Ni(μ-S*t*Bu)(μ-mtet)}$_{10}$]·$CH_3C_6H_5$ (**3b**).[18]

In the crystal structure of **3a** (Figure 2), the benzene molecule inside the cavity lies approximately in the Ni_{10} plane but is tilted by 16.6°. As was the case for [{Ni(μ-S*i*Pr)(μ-mtet)}$_6$]·C_6H_6 (**2**), the *t*Bu groups are each oriented outward from the {$Ni_{10}S_{20}$} toroid. The mtet substituents are oriented above and below the Ni_{10} plane, except for two of the mtet

[*] Dr. C. Zhang, S. Takada, M. Kölzer, Dr. T. Matsumoto, Prof. Dr. K. Tatsumi
Research Center for Materials Science and Department of Chemistry
Graduate School of Science
Nagoya University
Furo-cho, Chikusa-ku, Nagoya 464-8602 (Japan)
Fax: (+81) 52-789-2943
E-mail: i45100a@nucc.cc.nagoya-u.ac.jp

[**] This research was financially supported by Grants-in-Aid for Scientific Research (Nos. 14078211, 16350031, and 17036020) from the Ministry of Education, Culture, Sports, Science, and Technology, Japan. C.Z. is grateful to the Japan Society for the Promotion of Science (JSPS) for a fellowship.

Supporting information for this article is available on the WWW under http://www.angewandte.org or from the author.

 © 2006 Wiley-VCH Verlag GmbH & Co. KGaA, Weinheim

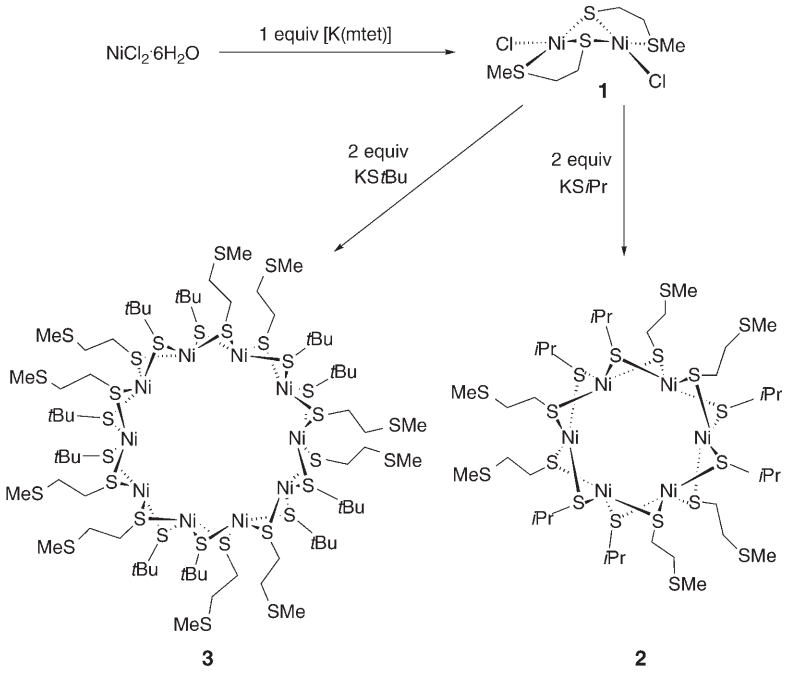

Scheme 1. The synthesis of **2** and **3**.

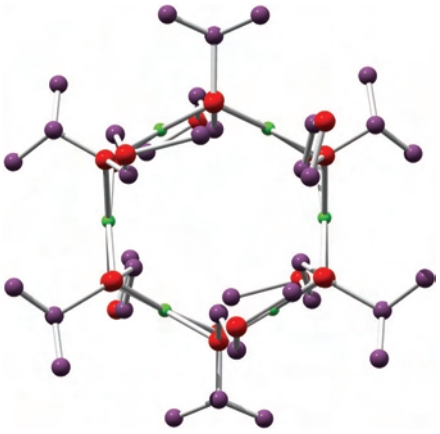

Figure 1. Molecular structure of **2** (Ni green, S red, C purple). All protons and the solvent molecule are omitted for clarity. Neighboring interatomic distances [Å]: Ni–S 2.188(2)–2.207(2) (av: 2.20), Ni–Ni 2.893(1)–2.951(1) (av: 2.92).

ligands which are extended toward the center of the toroid cavity such that the thioether groups clamp the encapsulated benzene molecule from above and below. The transannular Ni···Ni separations are nearly constant (10.075(2)–10.336(2) Å), thus consistent with the round shape of the $\{Ni_{10}S_{20}\}$ toroid. The dihedral angles between adjacent NiS_2 planes also do not vary significantly (144.1–147.8°) and are understandably larger than those of the hexanuclear core of **2**.

In the case of **3b** (Figure 3), the thioether substituents of four of the mtet ligands are extended toward the center of the $\{Ni_{10}S_{20}\}$ toroid, and two of these penetrate into the central cavity where the benzene molecule is incorporated for **3a**. In addition, the $\{Ni_{10}S_{20}\}$ toroid in **3b** possesses an ellipsoidal shape, and the consequences of this shape are the varied dihedral angles between two adjoining NiS_2 planes (138.4 to 152.4°) and the varied transannular Ni···Ni separations (9.496(2) to 11.113(3) Å, Figure 4). Thus, the geometry of the $\{Ni_{10}S_{20}\}$ toroid is flexible.

Expansion of the ring size from the hexanuclear cluster **2** to the decanuclear cluster **3a** or **3b** appears to be promoted by the change of bridging thiolate ligand, from S*i*Pr to S*t*Bu. A close inspection of the X-ray structures reveals that the averaged sum of the bond angles at the S atoms of the μ-S*t*Bu ligands is 310° (**3a**) or 311° (**3b**), while the corresponding sum for the μ-S*i*Pr ligands in hexanuclear **2** is distinctively smaller (294°). Although the difference is not large, we speculate that the bulkier *t*Bu group, relative to *i*Pr, would have caused the decrease in pyramidality at the thiolate sulfur atoms to minimize steric repulsion between the *t*Bu groups and the $\{Ni_2(\mu\text{-}S)_2\}$ core atoms. The steric hindrance is revealed in the short contacts between protons of the *t*Bu groups and both the S atoms of each μ-mtet ligand and Ni atoms within each $\{Ni_2S_2\}$ quadrangular unit;[19] these separations are close to the sums of the van der Waals radii of the individual atoms.[20] Dance et al.[13] pointed out that the Ni-S(R)-Ni bond angles of doubly bridged {Ni(μ-

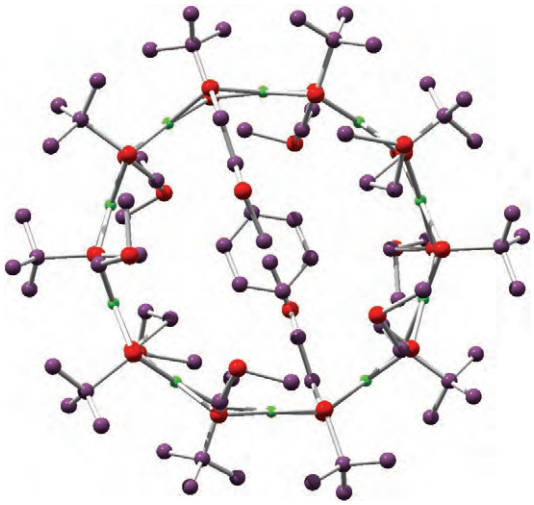

Figure 2. Molecular structure of **3a** (Ni green, S red, C purple). All protons and the solvent molecules are omitted for clarity. Neighboring interatomic distances [Å]: Ni–S 2.190(1)–2.214(1) (av: 2.20), Ni–Ni 3.1307(8)–3.172(1) (av: 3.16).

$SR)_2Ni\}$ units tend to increase as the pyramidality of the μ-S atoms decreases.[10–13,21] The averaged Ni-S(*t*Bu)-Ni bond angle of 92° for **3a** (and for **3b**) is evidently larger than that of **2** (83°) and those of the related complexes $[\{Ni(\mu\text{-}SR)_2\}_n]$ (n = 4, 5, 6, 8).[10–13] The larger Ni-S(*t*Bu)-Ni bond angles, in turn, bring about the larger dihedral angles between the adjacent NiS_2 planes of **3a** and **3b**, and the larger decanuclear ring is the consequence.

In conclusion, the decanuclear nickel(II) thiolato cluster $[\{Ni(\mu\text{-}StBu)(\mu\text{-mtet})\}_{10}]$ with a flexible core was synthesized by the reaction of the preformed complex $[\{NiCl(\mu\text{-mtet})\}_2]$ with KS*t*Bu. This approach using stepwise introduction of two

 © 2006 Wiley-VCH Verlag GmbH & Co. KGaA, Weinheim

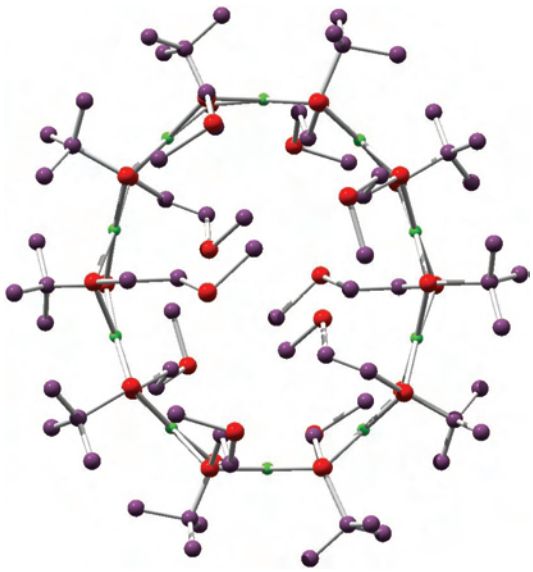

Figure 3. Molecular structure of **3b** (Ni green, S red, C purple). All protons and the solvent molecule are omitted for clarity. Neighboring interatomic distances (Å): Ni–S 2.196(1)–2.224(1) (av: 2.21), Ni–Ni 3.098(1)–3.224(1) (av: 3.17).

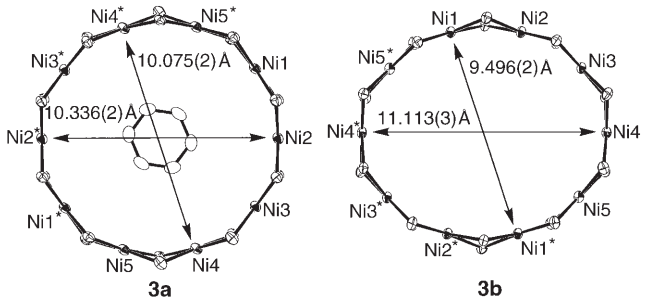

Figure 4. Top view of the $\{Ni_{10}S_{20}\}$ core configurations of **3a** and **3b**.

kinds of thiolate ligands to a nickel(II) center expands the scope of synthetic routes to cyclic polynuclear nickel(II) thiolates with various sizes and functions.

Experimental Section

1: The reported synthetic method was modified as follows.[17] [K(mtet)], prepared from H(mtet) (0.108 g, 1 mmol) and KO*t*Bu (0.112 g, 1 mmol), was slowly added to a solution of $NiCl_2 \cdot 6H_2O$ (0.237 g, 1 mmol) in MeOH (15 mL), and the mixture was stirred at room temperature for 4 h. The volatiles were removed, and the resulting brown residue was extracted with toluene and then dried in a vacuum. The dark red powder was dissolved in toluene and layered with hexane to afford brown-red block-shaped crystals of **1** (yield: 0.141 g, 70%).

2: KS*i*Pr, prepared from HS*i*Pr (0.076 g, 1 mmol) and KO*t*Bu (0.112 g, 1 mmol), was slowly added to a solution of $[NiCl(\mu\text{-mtet})]_2$ (**1**; 0.201 g, 0.5 mmol) in MeOH (20 mL) and stirred at room temperature for 6 h. A work up similar to that for **1** afforded a dark red powder, which was dissolved in benzene and layered with hexane to give **2** as deep-red hexagonal plates (yield: 0.089 g, 35%).

3: A similar synthetic procedure to that for **2**, except that KS*t*Bu was added instead of KS*i*Pr, gave a dark red powder, which was dissolved in benzene and layered with HMDSO to afford **3a** as black-red block-shaped crystals (yield: 0.173 g, 62%). Alternatively, analogous crystallization using toluene and HMDSO gave **3b** as black-red block-shaped crystals (yield: 0.174 g, 66%).

Received: January 25, 2006
Published online: April 19, 2006

Keywords: cluster compounds · nickel · S ligands · structure elucidation · supramolecular chemistry

[1] a) V. L. Pecoraro, A. J. Stemmler, B. R. Gibney, J. J. Bodwin, H. Wang, J. W. Kampf, A. Barwinski, *Prog. Inorg. Chem.* **1997**, *45*, 83–177; b) G. Mezei, P. Baran, R. G. Raptis, *Angew. Chem.* **2004**, *116*, 584–587; *Angew. Chem. Int. Ed.* **2004**, *43*, 574–577.

[2] a) D. Foguet-Albiol, T. A. O'Brien, W. Wernsdorfer, B. Moulton, M. J. Zaworotko, K. A. Abboud, G. Christou, *Angew. Chem.* **2005**, *117*, 919–923; *Angew. Chem. Int. Ed.* **2005**, *44*, 897–901; b) O. Cador, D. Gatteschi, R. Sessoli, F. K. Larsen, J. Overgaard, A. L. Barra, S. J. Teat, G. A. Timco, R. E. P. Winpenny, *Angew. Chem.* **2004**, *116*, 5308–5312; *Angew. Chem. Int. Ed.* **2004**, *43*, 5196–5200; c) C. Dendrinou-Samara, M. Alexiou, C. M. Zaleski, J. W. Kampf, M. L. Kirk, D. P. Kessissoglou, V. L. Pecoraro, *Angew. Chem.* **2003**, *115*, 3893–3896; *Angew. Chem. Int. Ed.* **2003**, *42*, 3763–3766.

[3] S. P. Watton, P. Fuhrmann, L. E. Pence, A. Caneschi, A. Cornia, G. L. Abbati, S. J. Lippard, *Angew. Chem.* **1997**, *109*, 2917–2919; *Angew. Chem. Int. Ed. Engl.* **1997**, *36*, 2774–2776.

[4] L. F. Jones, A. Batsanov, E. K. Brechin, D. Collison, M. Helliwell, T. Mallah, E. J. L. McInnes, S. Piligkos, *Angew. Chem.* **2002**, *114*, 4494–4497; *Angew. Chem. Int. Ed.* **2002**, *41*, 4318–4321.

[5] a) M. Murugesu, W. Wernsdorfer, K. A. Abboud, G. Christou, *Angew. Chem.* **2005**, *117*, 914–918; *Angew. Chem. Int. Ed.* **2005**, *44*, 892–896; b) A. J. Tasiopoulos, A. Vinslava, W. Wernsdorfer, K. A. Abboud, G. Christou, *Angew. Chem.* **2004**, *116*, 2169–2173; *Angew. Chem. Int. Ed.* **2004**, *43*, 2117–2121.

[6] C. M. Zaleski, E. C. Depperman, J. W. Kampf, M. L. Kirk, V. L. Pecoraro, *Angew. Chem.* **2004**, *116*, 4002–4004; *Angew. Chem. Int. Ed.* **2004**, *43*, 3912–3914.

[7] a) F. K. Larsen, J. Overgaard, S. Parsons, E. Rentschler, A. A. Smith, G. A. Timco, R. E. P. Winpenny, *Angew. Chem.* **2003**, *115*, 6160–6163; *Angew. Chem. Int. Ed.* **2003**, *42*, 5978–5981; b) A. L. Dearden, S. Parsons, R. E. P. Winpenny, *Angew. Chem.* **2001**, *113*, 155–158; *Angew. Chem. Int. Ed.* **2001**, *40*, 151–154.

[8] S. Piligkos, G. Rajaraman, M. Soler, N. Kirchner, J. van Slageren, R. Bircher, S. Parsons, H. U. Gudel, J. Kortus, W. Wernsdorfer, G. Christou, E. K. Brechin, *J. Am. Chem. Soc.* **2005**, *127*, 5572–5580.

[9] S. X. Liu, S. Lin, B. Z. Lin, C. C. Lin, J. Q. Huang, *Angew. Chem.* **2001**, *113*, 1118–1121; *Angew. Chem. Int. Ed.* **2001**, *40*, 1084–1087.

[10] a) P. Woodward, L. F. Dahl, E. W. Abel, B. C. Crosse, *J. Am. Chem. Soc.* **1965**, *87*, 5251–5253; b) E. W. Abel, B. C. Crosse, *J. Chem. Soc. A* **1966**, 1377–1378; c) T. A. Wark, D. W. Stephan, *Organometallics* **1989**, *8*, 2836–2843; d) K. Schulbert, R. Mattes, *Z. Naturforsch. B* **1994**, *49*, 770–772; e) H. Feld, A. Leute, D. Rading, A. Benninghoven, G. Henkel, T. Krüger, B. Krebs, *Z. Naturforsch. B* **1992**, *47*, 929–936; f) R. O. Gould, M. M. Harding, *J. Chem. Soc. A* **1970**, 875–881; g) A. H. Mahmoudkhani, V. Langer, *Polyhedron* **1989**, *8*, 3407–3410; h) M. Capdevila, P. Ginzales-Duarte, J. Soda, C. Focces-Foces, F. H. Cano, M. Martines-Ripoll, *Polyhedron* **1989**, *8*, 1253–1259; i) H. Berrera, J. C. Bayson, J. Suades, C, Germain, J. P. Declerq, *Polyhedron* **1984**, *3*, 969–975; j) J. Sletten, J. A. Kovacs, *Acta*

 © 2006 Wiley-VCH Verlag GmbH & Co. KGaA, Weinheim

Chem. Scand. **1994**, *48*, 929 – 932; k) F. F. Jian, K. Jiao, Y. Li, P. S. Zhao, L. D. Lu, *Angew. Chem.* **2003**, *115*, 5900 – 5902; *Angew. Chem. Int. Ed.* **2003**, *42*, 5722 – 5724.

[11] a) T. Krüger, B. Krebs, G. Henkel, *Angew. Chem.* **1989**, *101*, 54 – 55; *Angew. Chem. Int. Ed. Engl.* **1989**, *28*, 61 – 62; b) W. Gaete, J. Ros, X. Solans, M. Font-Altaba, J. L. Brianso, *Inorg. Chem.* **1984**, *23*, 39 – 43; c) M. Kriege, G. Henkel, *Z. Naturforsch. B* **1987**, *42*, 1121 – 1128.

[12] a) A. H. Mahmoudkhani, V. Langer, *Inorg. Chim. Acta* **1999**, *294*, 83 – 86; b) B. K. Koo, E. Block, H. Kang, S. Liu, J. Zubieta, *Polyhedron* **1988**, *7*, 1397 – 1399.

[13] I. G. Dance, M. I. Scudder, R. Secomb, *Inorg. Chem.* **1985**, *24*, 1201 – 1208.

[14] S. A. Ivanov, M. A. Kozee, W. A. Merrill, S. Agarwal, L. F. Dahl, *J. Chem. Soc. Dalton Trans.* **2002**, 4105 – 4115.

[15] a) O. L. Sydora, P. T. Wolczanski, E. B. Lobkovsky, E. Rumberger, D. N. Hendrickson, *Chem. Commun.* **2004**, 650 – 651; b) O. L. Sydora, P. T. Wolczanski, E. B. Lobkovsky, *Angew. Chem.* **2003**, *115*, 2789 – 2791; *Angew. Chem. Int. Ed.* **2003**, *42*, 2685 – 2687.

[16] a) Z. Li, Y. Ohki, K. Tatsumi, *J. Am. Chem. Soc.* **2005**, *127*, 8950 – 8951; b) Y. Ohki, H. Sadohara, Y. Takikawa, K. Tatsumi, *Angew. Chem.* **2004**, *116*, 2340 – 2343; *Angew. Chem. Int. Ed.* **2004**, *43*, 2290 – 2293; c) Y. Ohki, Y. Sunada, M. Honda, M. Katada, K. Tatsumi, *J. Am. Chem. Soc.* **2003**, *125*, 4052 – 4053; d) T. Komuro, T. Matsuo, H. Kawaguchi, K. Tatsumi, *Angew. Chem.* **2003**, *115*, 481 – 484; *Angew. Chem. Int. Ed.* **2003**, *42*, 465 – 468; e) T. Komuro, T. Matsuo, H. Kawaguchi, K. Tatsumi, *J. Am. Chem. Soc.* **2003**, *125*, 2070 – 2071; f) H. Kawaguchi, K. Yamada, S. Ohnishi, K. Tatsumi, *J. Am. Chem. Soc.* **1997**, *119*, 10871 – 10872; g) H. Kawaguchi, K. Yamada, J. Lang, K. Tatsumi, *J. Am. Chem. Soc.* **1997**, *119*, 10346 – 10358; h) H. Kawaguchi, K. Tatsumi, *J. Am. Chem. Soc.* **1995**, *117*, 3885 – 3886.

[17] B. C. Bloodworth, B. Demetriou, R. Grzeskowiak, *Transition Met. Chem.* **1979**, *4*, 187 – 190.

[18] Crystal data for **1**: $C_6H_{14}Ni_2S_4Cl_2$, monoclinic, space group $C2/c$ (No. 15), $a = 13.343(5)$, $b = 6.632(2)$, $c = 15.258(4)$ Å, $\beta = 91.00(2)°$, $V = 1350.0(7)$ Å^3, $Z = 4$, $T = 173$ K, $\lambda = 0.71073$ Å, $F(000) = 816$, $\mu = 37.63$ cm^{-1}, $\rho_{calcd} = 1.981$ g cm^{-3}, 7778 reflections ($2\theta < 55.20°$), 1824 independent ($R_{int} = 0.036$), $R1 = 0.029$ ($I > 2\sigma(I)$), $Rw = 0.073$ (all data). Crystal data for **2**: $C_{42}H_{90}Ni_6S_{18}$, triclinic, space group $P\bar{1}$ (No. 2), $a = 12.733(2)$, $b = 12.940(2)$, $c = 12.953(3)$ Å, $\alpha = 66.44(1)$, $\beta = 66.19(1)$, $\gamma = 60.92(1)°$, $V = 1650.2(5)$ Å^3, $Z = 1$, $T = 113$ K, $\lambda = 0.71073$ Å, $F(000) = 798$, $\mu = 22.75$ cm^{-1}, $\rho_{calcd} = 1.534$ g cm^{-3}, 12961 reflections ($2\theta < 54.96°$), 7211 independent ($R_{int} = 0.036$), $R1 = 0.080$ ($I > 2\sigma(I)$), $Rw = 0.216$ (all data). Crystal data for **3a**: $C_{88}H_{178}Ni_{10}S_{30}$, triclinic, space group $P\bar{1}$ (No. 2), $a = 15.337(4)$, $b = 15.542(4)$, $c = 16.396(4)$ Å, $\alpha = 104.5377(5)$, $\beta = 112.387(3)$, $\gamma = 107.078(2)°$, $V = 3149(1)$ Å^3, $Z = 1$, $T = 113$ K, $\lambda = 0.71073$ Å, $F(000) = 1466$, $\mu = 19.93$ cm^{-1}, $\rho_{calcd} = 1.468$ g cm^{-3}, 24747 reflections ($2\theta < 54.97°$), 13759 independent ($R_{int} = 0.017$), $R1 = 0.059$ ($I > 2\sigma(I)$), $Rw = 0.162$ (all data). Crystal data for **3b**: $C_{77}H_{168}Ni_{10}S_{30}$, triclinic, space group $P\bar{1}$ (No. 2), $a = 14.130(4)$, $b = 14.925(5)$, $c = 16.708(6)$ Å, $\alpha = 109.871(3)$, $\beta = 111.328(3)$, $\gamma = 98.234(2)°$, $V = 2940(1)$ Å^3, $Z = 1$, $T = 113$ K, $\lambda = 0.71073$ Å, $F(000) = 1390$, $\mu = 21.31$ cm^{-1}, $\rho_{calcd} = 1.493$ g cm^{-3}, 22982 reflections ($2\theta < 54.97°$), 12826 independent ($R_{int} = 0.020$), $R1 = 0.065$ ($I > 2\sigma(I)$), $Rw = 0.184$ (all data). All calculations were performed with the TEXSAN program package, and structures were solved by Patterson methods (DIRDIF94 PATTY) and refined by full-matrix least squares against F^2. The protons were placed at calculated positions (d(C–H): 0.97 Å). CCDC-295875 (**1**) and CCDC-294804–294806 (**2**, **3a**, **3b**) contain the supplementary crystallographic data for this paper. These data can be obtained free of charge from The Cambridge Crystallographic Data Centre via www.ccdc.cam.ac.uk/data_request/cif.

[19] The mean separations of the closest $C_{tBu}\cdots S_{mtet}$ and $C_{tBu}\cdots Ni$ contacts at the $\{Ni_2S_2\}$ quadrangle units of **3a** are 3.34 and 3.55 Å, respectively.

[20] A. Bondi, *J. Phys. Chem.* **1964**, *68*, 441 – 451.

[21] a) W. Tremel, B. Krebs, G. Henkel, *Angew. Chem.* **1984**, *96*, 604 – 605; *Angew. Chem. Int. Ed. Engl.* **1984**, *23*, 634 – 635; b) W. Tremel, B. Krebs, G. Henkel, *J. Chem. Soc. Chem. Commun.* **1986**, 1527 – 1529; c) A. D. Watson, C. P. Rao, J. R. Dorfman, R. H. Holm, *Inorg. Chem.* **1985**, *24*, 2820 – 2826; d) J. P. Fackler, Jr., W. J. Zegarski, *J. Am. Chem. Soc.* **1973**, *95*, 8566 – 8574; e) K. Schulbert, R. Mattes, *Z. Naturforsch. B* **1994**, *49*, 770 – 772.

 © 2006 Wiley-VCH Verlag GmbH & Co. KGaA, Weinheim

Drug Design

DOI: 10.1002/anie.200600757

Identification of Pyridinylpyrimidines as Inhibitors of Human Methionine Aminopeptidases**

Xiaoyi Hu, Anthony Addlagatta, Brian W. Matthews, and Jun O. Liu**

The proteolytic removal of N-terminal methionine is catalyzed by a family of enzymes known as methionine aminopeptidases (MetAPs). This is an evolutionarily conserved and essential process, as underscored by the lethal phenotype of *map* gene null-mutations in both bacteria and yeast.[1] Human type 2 MetAP (HsMetAP2) has been identified as the primary target of the fumagillin family of natural products that potently inhibit angiogenesis.[2,3] Recent efforts have culminated in the development of HsMetAP2-selective inhibitors for cancer[4] and autoimmune diseases.[5] In addition, small interfering RNA (siRNA) technology has also demonstrated the essential roles of both MetAP proteins in the control of cell proliferation.[6] In contrast to type 2 MetAP,

[*] X. Hu,[+] Prof. J. O. Liu
Department of Pharmacology and Molecular Sciences
Johns Hopkins University School of Medicine
725 N. Wolfe Street, Baltimore, MD 21205 (USA)
Fax: (+1) 410-955-4620
E-mail: joliu@jhu.edu
Dr. A. Addlagatta,[+] Prof. B. W. Matthews
Institute of Molecular Biology
Howard Hughes Medical Institute and Department of Physics
1229 University of Oregon, Eugene, OR 97403-1229 (USA)
Fax: (+1) 541-346-2572
E-mail: brian@uoxray.uoregon.edu
[+] These authors contributed equally to the work.

[**] We thank the National Cancer Institute, the Keck Center, and the Department of Pharmacology and Molecular Sciences for financial support, the Advanced Light Source for the use of beamline BL8.2.2 for X-ray data collection, and ASDI Inc. for the chemical library. X.H. is a DoD Predoctoral Fellow.

WILEY InterScience DISCOVER SOMETHING GREAT
© 2006 Wiley-VCH Verlag GmbH & Co. KGaA, Weinheim

little is known about the physiological function of type 1 human MetAP (HsMetAP1).

A number of different nonpeptidic inhibitors of bacterial MetAPs have been developed.[4,5,7–9] Some of these differ in potency toward the Mn^{II} and Co^{II} complexes of the enzyme.[10] We report here a novel class of MetAP inhibitors with a pyridinylpyrimidine core identified through high-throughput screening of a diverse chemical library. These compounds inhibit both human MetAP1 and MetAP2 in vitro and in vivo. In cultures, they also inhibit the proliferation of both endothelial and tumor cells. Analysis of the crystal structure of the inhibitor-bound HsMetAP1 complex suggests a metal-dependent mechanism of enzyme inhibition by this class of inhibitors.

Recombinant full-length HsMetAP1 produced in *Escherichia coli*[11] was screened against a library of approximately 175000 small organic compounds by using a proline aminopeptidase coupled assay.[12] The confirmed HsMetAP1 hits were also profiled for HsMetAP2 selectivity. A group of compounds with a pyridinylpyrimidine core structure were identified as inhibitors of both enzymes (Table 1). Compound **1** is the most potent with submicromolar IC_{50} values for both enzymes. Although some preferences for MetAP1 inhibition was observed for **2** and **4**, with MetAP1/MetAP2 IC_{50} ratios of 0.08:1 and 0.14:1, respectively, the other two compounds inhibit both enzymes with roughly equal potency. Truncated MetAP1 (01–89) has also shown to give similar results as the full-length protein (data not shown).

We determined the ability of **1**–**4** to inhibit cell proliferation in both bovine aortic endothelial cells (BAEC) and HeLa cells by using the established method of [^{3}H]thymidine incorporation[13] (Table 1). All four compounds were effective with IC_{50} values in the low micromolar range for both cell types. The inhibition of BAEC cell proliferation correlated well with the inhibition of the MetAP2 enzyme, as has been observed for fumagillin and its derivatives.[2,3] To test whether these compounds could target MetAPs inside the cells, we examined the processing of N-terminal methionine in 14-3-3γ protein, which has been shown to be a substrate for both MetAPs.[14] The presence of the initiating methionine is detectable by a monoclonal antibody (clone HS23) raised against the methionylated N-terminal fragment of the 14-3-3γ protein. When HeLa cells were treated with increasing doses of **2** for 24 h, we observed increased amounts of N-terminal methionine residues on the 14-3-3γ protein relative to controls (Figure 1), thus suggesting that **2** is capable of inhibiting the activities of both methionine aminopeptidases inside the cells.

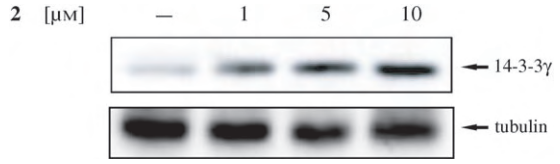

Figure 1. Inhibition of MetAPs by **2**. HeLa cells were treated for 24 h before harvesting for Western blot analysis against 14-3-3γ protein (upper panel) and tubulin (lower panel). Increased dosage of **2** resulted in the accumulation of N-terminal methionine on the 14-3-3γ proteins. The tubulin blot shows that the protein loading remains constant (see text)

The X-ray crystal structure of **2** bound to the Co^{II} form of truncated HsMetAP1 was determined at a resolution of 1.8 Å (Figure 2a).[15] The structure confirms the presence of the two cobalt ions found in the active site of all members of the MetAP family.[1] In addition, a third metal ion, presumably a Co^{II} ion, is observed coordinated to the N1 and N8 atoms of the inhibitor. This metal ion is also coordinated by the His212 residue that is highly conserved among all MetAPs. Three water molecules contribute to the overall hexacoordination around the Co3 ion (Figure 2a). Two of these water molecules are hydrogen bonded to the water/μ-hydroxo group that bridges between the two active-site cobalt ions, while one of these also forms a hydrogen bond with the $N^{\varepsilon 2}$ atom of His310. The A ring of the inhibitor is buried deeply in the hydrophobic pocket which is normally occupied by the methionine side chain of the substrate (Figure 2b). The pyridinylpyrimidine moiety of the inhibitor is accommodated well in the complementary hydrophobic pocket formed by several aromatic residues (Tyr195, Tyr196, Phe198, Tyr300, and Trp353). As expected, the A and B rings of the inhibitor are coplanar. The C ring stacks over the B ring with a centroid···centroid distance of 4.3 Å. His310, another highly conserved residue, forms a

Table 1: Structures of pyridinylpyrimidine inhibitors, and their inhibitions of human MetAP1, MetAP2, and cell proliferation.

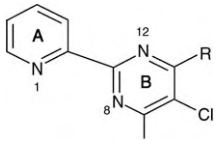

Cmpd	R	IC_{50} [μM] HsMetAP1	IC_{50} [μM] HsMetAP2	Ratio MetAP1/MetAP2	IC_{50} [μM] BAEC	IC_{50} [μM] HeLa
1		0.4 ± 0.14	0.8 ± 0.08	0.49:1	1.7 ± 0.1	0.9 ± 0.1
2	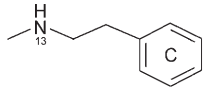	0.6 ± 0.06	7.6 ± 0.9	0.08:1	4.0 ± 0.6	9.6 ± 1.0
3	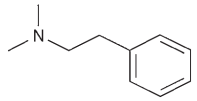	3.3 ± 0.2	3.3 ± 0.2	1:1	2.7 ± 0.4	0.6 ± 0.08
4	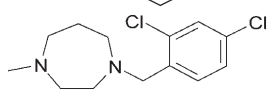	1.1 ± 0.1	8.1 ± 0.5	0.14:1	9.7 ± 1.0	5.9 ± 0.8

© 2006 Wiley-VCH Verlag GmbH & Co. KGaA, Weinheim

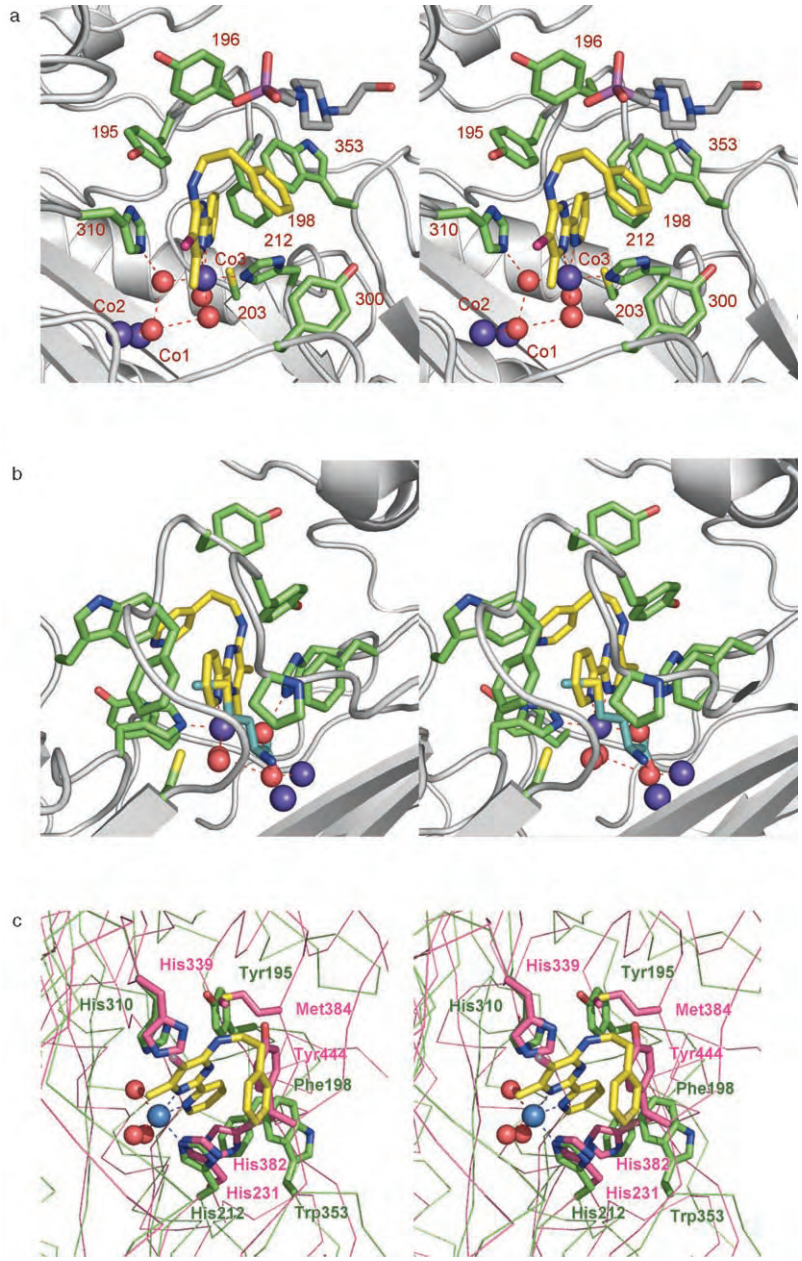

Figure 2. a) Stereoview showing the X-ray crystal structure of HsMetAP1 complexed with **2** (yellow). Co1 and Co2 form the dimetallic center in the active site (deep blue). Co3 is an additional metal ion that coordinates with the protein and the inhibitor. Except for Cys 203, all the residues that surround the inhibitor (green) are aromatic and provide a complementary hydrophobic binding pocket for the pyridinylpyrimidine moiety. A HEPES molecule (gray) also binds and contacts the exterior face of the inhibitor. Water molecules are shown in red. b) Stereoview showing a comparison of the mode of binding of **2** (in yellow) with that of the substrate, methionine (in cyan), based on the structural alignment of the HsMetAP1–**2** complex with methionine bound to *Mycobacterium tuberculosis* MetAP1c.[18] The direction of view is from the center of the protein looking outwards toward the active site. c) Stereoview showing the superposition of HsMetAP1 (green backbone) bound to **2** (yellow) on the structure of HsMetAP2 (magenta). The inhibitor has several steric clashes with side chains of HsMetAP2, thus explaining its weaker binding to this enzyme.

π–π stacking interaction with the B ring on the other side. Clear electron density for a 2-[4-(2-hydroxyethyl)-1-piperazinyl]ethanesulfonic acid (HEPES) molecule was identified on the exterior side of the C ring (Figure 2a). This molecule from the buffer shields the inhibitor from exposure to the solvent and probably provides extra stability. Although the enzyme assay solution also contains 25 mM HEPES, these compounds behaved similarly with 25 mM tris(hydroxymethyl)aminomethane (tris) buffer. Methyl and chloro substituents on the B ring stack perpendicularly to the main chain of the protein at Cys 301 (with the closest distance being 4.2 Å). The inhibitor has two free nitrogen atoms, one is exposed and the other is buried. Both can potentially act as hydrogen-bonding partners, but neither one appears to interact with the protein or with solvent molecules. Upon binding of the inhibitor, the side chain of Trp 353 retreats by about 0.6 Å and Tyr 195 retreats by about 0.5 Å to provide extra space for the inhibitor. Tyr 195 forms a short hydrogen bond (2.5 Å) with Glu 128, presumably as a consequence. Conformational changes also occur in the linker region (90–140), with movements as large as 0.5 Å in the backbone.

Figure 2c indicates the possible structural basis for the selectivity of **2** for MetAP1 over MetAP2. Ring C of the inhibitor in the present conformation would experience a severe steric clash with the Tyr 444 residue of MetAP2. Although this side chain could adopt an alternative conformation to avoid this clash, it would be forced into the solvent, presumably reducing the stability of the complex. His 339 and His 382 of MetAP2 would also have unfavorable interactions with **2**. These observations may facilitate the design of inhibitors that are more selective for MetAP1 over MetAP2.

In addition to the results described here, structural studies of other MetAP–inhibitor complexes have revealed a third Co^{II} or Mn^{II} ion in the active site. For example, the substrate-based keto-heterocyclic inhibitors of *Staphylococcus aureus* MetAP (SaMetAP) recruit a third cobalt ion that binds to His 178 (analogous to His 310 in HsMetAP1) rather than His 79 (His 212 of HsMetAP1).[16] The crystal structure of *E. coli* MetAP (EcMetAP) complexed with thiabendazole also revealed that it utilizes a third metal ion that is bound to His 79 (His 212 of HsMetAP1), similar to that observed for **2** in this study.[17] The possible physiological significance of the third metal ion remains unclear. Pyridine-2-carboxylic acid derivatives that utilize a third metal ion bind with high potency to EcMetAP in vitro but display only moderate antibacterial activity in vivo, thus raising the question as to whether MetAPs are targeted in the cells.[9] In the present study, the cell-based assay demonstrated that **2** inhibited the demethionylation of newly synthesized proteins, thus providing clear evidence for MetAP inhibition in the cells.

The essential roles of methionine aminopeptidases in cell proliferation have stimulated ongoing efforts to identify nonpeptidic inhibitors. We have reported here a group of compounds with a pyridinylpyrimidine core structure that strongly inhibit both human MetAPs, but discriminate only weakly between the type 1 and type 2

 © 2006 Wiley-VCH Verlag GmbH & Co. KGaA, Weinheim

enzymes. Their ability to inhibit MetAP in vivo and to block cell growth may provide new tools to study the functions of methionine aminopeptidases in cell proliferation.

Received: February 27, 2006

Keywords: cellular effects · drug design · enzymes · inhibitors · structure elucidation

[1] W. T. Lowther, B. W. Matthews, *Biochim. Biophys. Acta* **2000**, *1477*, 157 – 167.
[2] E. C. Griffith, Z. Su, B. E. Turk, S. Chen, Y. H. Chang, Z. Wu, K. Biemann, J. O. Liu, *Chem. Biol.* **1997**, *4*, 461 – 471.
[3] N. Sin, L. Meng, M. Q. Wang, J. J. Wen, W. G. Bornmann, C. M. Crews, *Proc. Natl. Acad. Sci. USA* **1997**, *94*, 6099 – 6103.
[4] J. Wang, G. S. Sheppard, P. Lou, M. Kawai, N. BaMaung, S. A. Erickson, L. Tucker-Garcia, C. Park, J. Bouska, Y. C. Wang, D. Frost, P. Tapang, D. H. Albert, S. J. Morgan, M. Morowitz, S. Shusterman, J. M. Maris, R. Lesniewski, J. Henkin, *Cancer Res.* **2003**, *63*, 7861 – 7869.
[5] S. G. Bernier, D. D. Lazarus, E. Clark, B. Doyle, M. T. Labenski, C. D. Thompson, W. F. Westlin, G. Hannig, *Proc. Natl. Acad. Sci. USA* **2004**, *101*, 10768 – 10773.
[6] S. G. Bernier, N. Taghizadeh, C. D. Thompson, W. F. Westlin, G. Hannig, *J. Cell. Biochem.* **2005**, *95*, 1191 – 1203.
[7] G. Zhou, C. W. Tsai, J. O. Liu, *J. Med. Chem.* **2003**, *46*, 3452 – 3454.
[8] X. Hu, J. Zhu, S. Srivathsan, D. Pei, *Bioorg. Med. Chem. Lett.* **2004**, *14*, 77 – 79.
[9] Q. L. Luo, J. Y. Li, Z. Y. Liu, L. L. Chen, J. Li, Z. Qian, Q. Shen, Y. Li, G. H. Lushington, Q. Z. Ye, F. J. Nan, *J. Med. Chem.* **2003**, *46*, 2631 – 2640.
[10] Q. Q. Huang, M. Huang, F. J. Nan, Q. Z. Ye, *Bioorg. Med. Chem. Lett.* **2005**, *15*, 5386 – 5391.
[11] A. Addlagatta, X. Hu, J. O. Liu, B. W. Matthews, *Biochemistry* **2005**, *44*, 14741 – 14749.
[12] Y. Zhou, X. C. Guo, T. Yi, T. Yoshimoto, D. Pei, *Anal. Biochem.* **2000**, *280*, 159 – 165.
[13] Y. Zhang, E. C. Griffith, J. Sage, T. Jacks, J. O. Liu, *Proc. Natl. Acad. Sci. USA* **2000**, *97*, 6427 – 6432.
[14] H. Towbin, K. W. Bair, J. A. DeCaprio, M. J. Eck, S. Kim, F. R. Kinder, A. Morollo, D. R. Mueller, P. Schindler, H. K. Song, O. J. van Oostrum, R. W. Versace, H. Voshol, J. Wood, S. Zabludoff, P. E. Phillips, *J. Biol. Chem.* **2003**, *278*, 52964 – 52971.
[15] MetAP enzyme assay: The methionine aminopeptidase assay was adapted from that developed by Zhou et al.[12] Briefly the assay was performed in 50 mM HEPES (pH 7.5), 150 mM NaCl, 100 μM $CoCl_2$, 700 μM Met-Pro-pNA, 0.5 unit mL^{-1} ProAP, and 5 μg mL^{-1} MetAP (reaction volume = 50 μL for high-throughput screening, and 100 μL for confirmation).[^{3}H]Thymidine incorporation for cell proliferation: The assay was adapted from that developed by Zhang et al.[13] Basically the cells were seeded in a 96-well plate before addition of compounds. [^{3}H]Thymidine was added during the last 6-h period of the 24-h incubation time before harvesting the cells for scintillation counting. Structure determination: The truncated version of HsMetAP1 (Δ1-89) was expressed and crystallized as reported earlier.[10] 2 mM $CoCl_2$ (fresh water) and 2 mM **2** (in DMSO) were added (final concentration) to the apo crystals in a 10 μL fresh drop of cryo solution (16% polyethylene glycol (PEG) monomethyl ether 2000, 25% glycerol, and 100 mM HEPES, pH 6.0). After incubating the drop for 12 h, the crystals were washed by transferring them into 10 μL of a fresh cryo solution and incubating them for 5 min before they were frozen directly in liquid nitrogen. X-ray diffraction data were collected at the Advanced Light Source, Berkeley, on beamline 8.2.2. Completeness 95%, R_{merge} 5.6% (41% last shell, 1.84–1.80 Å). R_{factor} 19.3%, R_{free} 24.1%. Coordinates were deposited into the protein data bank, ID 2G6P.
[16] A. Douangamath, G. E. Dale, A. D'Arcy, M. Almstetter, R. Eckl, A. Frutos-Hoener, B. Henkel, K. Illgen, S. Nerdinger, H. Schulz, S. A. Mac, M. Thormann, A. Treml, S. Pierau, S. Wadman, C. Oefner, *J. Med. Chem.* **2004**, *47*, 1325 – 1328.
[17] R. Schiffmann, A. Heine, G. Klebe, C. D. Klein, *Angew. Chem.* **2005**, *44*, 3620 – 3623; *Angew. Chem. Int. Ed.* **2005**, *44*, 3620 – 3623.
[18] A. Addlagatta, M. L. Quillin, O. Omotoso, J. O. Liu, B. W. Matthews, *Biochemistry* **2005**, *44*, 7166 – 7174.

 © 2006 Wiley-VCH Verlag GmbH & Co. KGaA, Weinheim

Aromatic Substitution

DOI: 10.1002/anie.200600720

Directed *meta*-Metalation Using Alkali-Metal-Mediated Zincation**

*David R. Armstrong, William Clegg, Sophie H. Dale, Eva Hevia, Lorna M. Hogg, Gordon W. Honeyman, and Robert E. Mulvey**

Transforming a carbon–hydrogen bond of an organic compound into a more useful, more reactive carbon–metal bond (so-called deprotonative metalation), which, in turn, can be treated with an electrophile to create a new carbon–carbon or carbon–heteroatom bond, is one of the most fundamental synthetic approaches that chemists employ to construct compounds.[1,2] Many of these reactions involve a special type of deprotonative metalation, in which an activating functional group is positioned adjacent to the hydrogen atom (strictly a proton) that is to be replaced by the metal cation.

[*] Dr. D. R. Armstrong, Dr. E. Hevia, L. M. Hogg, Dr. G. W. Honeyman, Prof. R. E. Mulvey
WestCHEM
Department of Pure and Applied Chemistry
University of Strathclyde
Glasgow, G1 1XL (UK)
Fax: (+44) 141-552-0876
E-mail: r.e.mulvey@strath.ac.uk
Prof. W. Clegg, Dr. S. H. Dale
School of Natural Sciences (Chemistry)
University of Newcastle
Newcastle upon Tyne, NE1 7RU (UK)

[**] This work was supported by the EPSRC (UK) through grant award no. GR/R81183/01 and GR/T27228/01, a Marie Curie Fellowship (EU) to E.H., and the Royal Society/Leverhulme Trust through a Fellowship to R.E.M.

Supporting information for this article is available on the WWW under http://www.angewandte.org or from the author.

© 2006 Wiley-VCH Verlag GmbH & Co. KGaA, Weinheim
InterScience

Directed *ortho*-metalation (DOM, in which the metal is usually lithium) represents the best-developed, most heavily utilized technique of this type.[3,4] Defined as a metalation (lithiation) of an aromatic ring directed towards a position adjacent (*ortho*) to an activating heteroatom-containing functional group, DOM now probably surpasses classical electrophilic aromatic substitution as the number one methodology for constructing regiospecifically substituted aromatic rings.[5] DOM is therefore practiced routinely in synthetic laboratories all across the world, both in academia, for general preparative purposes, and in industry, for the manufacture of fine chemicals, pharmaceuticals, and other biologically important aromatic compounds.

The tools most commonly employed for effecting DOM and the other types of metalation are single-metal (homometallic) reagents, typically alkyl lithium or lithium amide reagents. Recently, we and a few other research groups have begun to explore the behavior of related but mixed-metal (heterobimetallic) reagents with amide-based ligands in this important area of directed metalation.[6–10] These initial studies have established that in certain cases these mixed-metal alternatives can exhibit a remarkable chemical synergy that enables them to perform special metalation reactions that cannot be reproduced by either of the single-metal components that make up the mixed-metal reagent.[11] In these synergic metalation reactions, the departing hydrogen atom is replaced by magnesium or zinc, but the participation of an alkali metal is mandatory for the reaction to follow its special course. Metalation reactions of this type are therefore best regarded as an alkali-metal-mediated magnesiation (AMMM) or alkali-metal-mediated zincation (AMMZ).

In the context of the new work reported herein, the best example of synergic metalation to date has been achieved with the alkyl arene toluene. Conventional metalation reagents, such as the alkyl lithium BuLi·TMEDA (TMEDA = *N*,*N*,*N*′,*N*′-tetramethylethylenediamine), normally deprotonate toluene at the methyl (lateral) site to generate the resonance-stabilized benzyl "carbanion" ($PhCH_2^-$). In contrast, under AMMM conditions using the sodium–magnesium monoalkyl bisamido reagent [(tmeda)·Na(μ-Bu)(μ-tmp)Mg(tmp)] (TMP = 2,2,6,6-tetramethylpiperidide), the site of deprotonation is switched to the *meta* site on the ring and the methyl substituent remains intact.[12] Although the regiospecificity of this deprotonation is most unusual, it does not infringe any expected DOM effect, as toluene does not possess a heteroatom-containing functional group. To overcome any DOM effect and direct metalation to a normally inaccessible site would be exceptional news for chemists that could have major implications for synthetic chemistry. We report herein two case studies that prove that such a desirable situation can be engineered using the special chemistry inherent in AMMZ.

As *N*,*N*-dimethylaniline (**1**) possesses an activating dimethylamino substituent, it undergoes directed *ortho*-metalation with phenyllithium in poor yield or *n*-butyllithium in good yield.[13–15] Changing the metalation agent from these mainstream homometallic species to heterometallic [(tmeda)·Na(*t*Bu)(tmp)Zn(*t*Bu)] (**2**), a sodium TMP/zincate reagent recently introduced by our group, remarkably switches the orientation of the deprotonation to the *meta* site (Scheme 1).[16,17] The carbanion generated by this regiospecific *meta*-proton abstraction is stabilized through coordination to a bimetallic alkyl amido cation (the residue of the base following alkyl transfer), which advantageously permits the metalated product of the reaction [(tmeda)·Na(μ-Ar*)(μ-tmp)Zn(*t*Bu)] (**3**; Ar* = 3-$C_6H_4NMe_2$) to be obtained in a stable crystalline form, which is isolable at room temperature. Direct zincation of a tertiary anilide is not possible using mainstream alkyl zinc reagents, so the unprecedented carbon–hydrogen to carbon–zinc transformation accomplished can be attributed to the synergy inherent in AMMZ. Characterized in solution by ^{1}H and ^{13}C NMR spectroscopic studies, **3** was also subjected to an X-ray crystallographic study, which unambiguously established its molecular structure (Figure 1).[18] A four-element NaNZnC rhomboidal ring with a mixed TMP Ar* bridging ligand set forms the core, which is completed by terminal TMEDA (*N*,*N*-attached) and

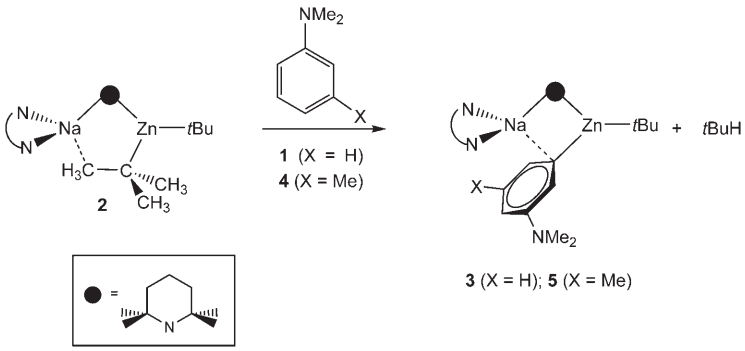

Scheme 1. Synergic metalation of *N*,*N*-dimethylaniline and its 3-methyl derivative using a sodium TMP/zincate base.

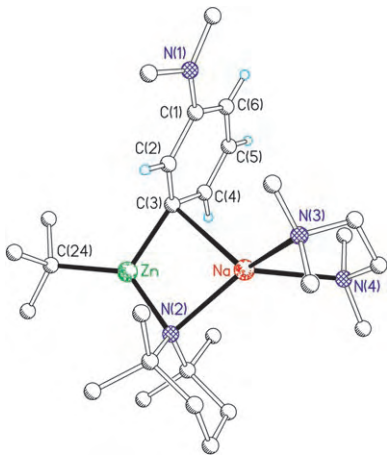

Figure 1. Molecular structure of **3** with selective atom labeling. Hydrogen atoms, apart from those of the anilide ring, and minor disorder components are omitted for clarity.

 © 2006 Wiley-VCH Verlag GmbH & Co. KGaA, Weinheim

*t*Bu (*C*-attached) ligands on the Na and Zn centers, respectively. In general terms, the structure can be categorized as an ion-contacted heterotrianionic zincate. Its key geometrical feature concerns how the deprotonated anilide engages differently with the two metal atoms: Zn forms a short bond to the *meta* C(3) atom (bond length: 2.035(4) Å), which is close to coplanarity with the aryl ring plane (the bond is inclined at 4.5° to the plane), whereas the Na–C(3) bond is significantly longer (2.691(4) Å) and inclined at an angle of 76.1° to the same plane. This parallel/perpendicular distinction to the deprotonated substrate–metal interactions, which implies more σ character for the former and more π character for the latter, has become a signature feature of these mixed-metal compounds,[10] which may provide a vital clue to the origin of the synergy (see below).

The second case study focused on 3-methyl-*N*,*N*-dimethylaniline (**4**), chosen as it has both a methyl (cf toluene) and a dimethylamino substituent on its aromatic ring. To our knowledge, **4** has never been previously metalated, though its 2- and 4-methyl isomers undergo preferential lithiation *ortho* to the activating dimethylamino substituent (methyl deprotonation in the case of the 2-methyl isomer).[19] However, applying AMMZ to **4** using the same reagent **2**, also achieves a *meta*-orientated deprotonation (Scheme 1), manifested in the crystalline product [(tmeda)·Na(μ-Ar**)(μ-tmp)Zn(*t*Bu)] (**5**; Ar** = 5-(3-Me)$C_6H_3NMe_2$). Characterized by NMR spectroscopic and X-ray crystallographic studies,[16] **5** adopts a molecular structure (Figure 2) remarkably similar to that of **3**, which includes the parallel (σ)/perpendicular (π) distinction in the aryl–metal bonding (corresponding angles: 4.5 and 67.8°, respectively).

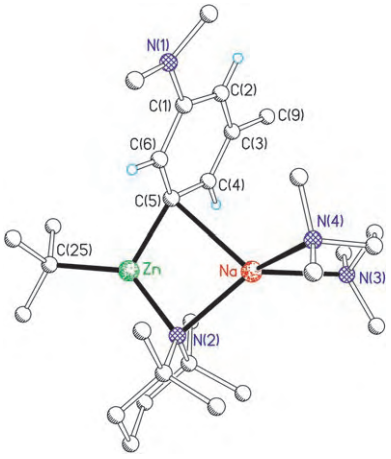

Figure 2. Molecular structure of **5** with selective atom labeling. Hydrogen atoms, apart from those of the anilide ring, and minor disorder components are omitted for clarity.

Theoretical calculations at the DFT level employing the B3LYP method and the 6-311G** basis set were used to compute the relative stabilities of the four regioisomers of **3**, in which the anilide ring is deprotonated at the *ortho* (**3A**), *meta* (**3B**), *para* (**3C**), or methyl (**3D**) positions (Figure 3).[17] In support of the experimental findings, the *meta* isomer **3B** is

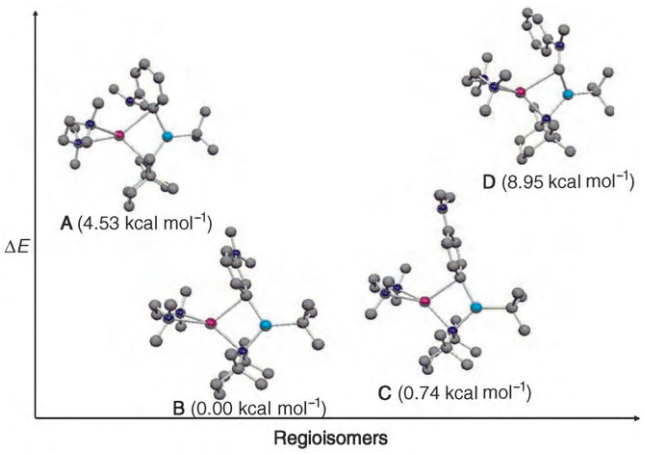

Figure 3. Relative energy sequence of the four theoretical regioisomers (**3A–D**) of the experimentally observed product **3**.

the energy minimum structure (relative energy: 0.00 kcal mol^{-1}); the *ortho* isomer is destabilized further (at 4.53 kcal mol^{-1}); and the least stable of all is the methyl isomer (at 8.95 kcal mol^{-1}). Through modeling studies, the overall reaction (**2**→**3B** + *t*BuH) is found to be exothermic by −22.21 kcal mol^{-1}. Comparison of the dimensions of **3B** and **3C** show that it is noticeable that the Na contacts to the aryl C atoms are invariably shorter in **3B** (bond lengths: 2.594, 3.070, 3.212, 3.959, 4.097, 4.403 Å) than in **3C** (bond lengths: 2.596, 3.178, 3.239, 4.135, 4.185, 4.596 Å). By contrast the Zn–C(aryl) bonds are within 0.001 Å of each other (2.084 and 2.083 Å, respectively). In the *ortho* isomer **3A**, the product expected from conventional metalation, the Na–C(*ortho*) bond is much longer (2.747 Å) and thus weaker than the Na–C(*meta*) bond in **3B** (2.594 Å) as a result of increased steric constraints. Therefore, the important distinction lies in maximizing the strength of the Na···Cπ contacts, and although they may be weak individually, collectively they must contribute significantly to the stability of **3B**. This favorable enthalpic effect, coupled with the minimal structural reorganization required by reagent **2** to form product **3** (in effect there is retention of structure except for the deprotonated anilide that refills the position vacated by the *t*Bu$^-$ base), appears to be a major factor in the unexpected *meta* selectivity observed.

To establish whether these *meta*-zincated dimethyl aniline complexes could be intercepted by electrophiles, we have carried out a preliminary iodolysis reaction of isolated crystals of **3** in a solution of THF with I_2. On the basis of ^{1}H NMR experiments with ferrocene as an internal standard, iodination at the *meta* position was quantitative within experimental error (±5%), thus producing *N*,*N*-dimethyl-3-iodoaniline.[20] This augurs well for opening up a gateway for *meta*-substituted derivatives previously closed to synthetic aromatic chemistry.

Experimental Section

Synthesis of **3** and **5**: A solution of tBu_2Zn (0.358 g, 2 mmol) in hexane (10 mL) was transferred by cannula to a suspension of NaTMP in

 © 2006 Wiley-VCH Verlag GmbH & Co. KGaA, Weinheim

hexane (prepared in situ by reaction of BuNa (0.16 g, 2 mmol) with TMP(H) (0.34 mL, 2 mmol)). This was followed by the addition of a molar equivalent of TMEDA (0.30 mL, 2 mmol). The resultant suspension was heated gently to form a yellow solution. At this stage, one molar equivalent (2 mmol) of the relevant dimethylaniline was introduced, and the reaction mixture was refluxed at 65 °C for 2 h. The resulting yellow solution was transferred to the freezer to aid crystallization. A crop of transparent crystals formed in solution which were suitable for X-ray crystallographic analysis in yields of 39 % for **3** (0.38 g) and 43 % for **5** (0.46 g) for the first batch of isolated crystals. See Supporting Information for the labeling scheme.

3: ^{1}H NMR (400 MHz, 25 °C, C_6D_6): $\delta = 7.34$ (d, 1H, H_{ortho} (Ar*)), 7.17 (t, 1H, $H_{meta'}$ (Ar*)), 7.10 (d, 1H, H_{ortho} (Ar*)), 6.54 (m, 1H, H_{para} (Ar*)), 2.63 (s, 6H, $N(CH_3)_2$ (Ar*)),1.65 (s, 9H, *t*Bu), 1.58 (s, broad, 14H, CH_3 (TMEDA) and H_γ (TMP)), 1.52 (s, broad, 14H, CH_3 (TMP), H_β (TMP), and CH_2 (TMEDA)), 1.16 ppm (s, broad, 6H, CH_3 (TMP)); ^{13}C{^{1}H} NMR (100.63 MHz, 25 °C, C_6D_6): $\delta = 170.79$ (Zn–C_{meta} (Ar*)), 150.87 (C_{ipso} (Ar*)), 128.87 ($C_{meta'}$ (Ar*)), 127.18 (C_{para} (Ar*)), 124.48 (C_{ortho} (Ar*)), 111.18 ($C_{ortho'}$ (Ar*)), 57.58 (CH_2 (TMEDA)), 53.22 (C_α (TMP)), 46.46 (CH_3 (TMEDA)), 40.41 (C_β (TMP)), 41.03 ($N(CH_3)_2$ (Ar*)), 36.75 (CH_3 (TMP)), 36.01 (CH_3 (*t*Bu)), 35.47 (CH_3 (TMP)), 21.10 (C_γ (TMP)), 21.01 ppm (C (*t*Bu)).

5: ^{1}H NMR (400 MHz, 25 °C, C_6D_6): $\delta = 7.08$ (d, 1H, H_{ortho} (Ar**)), 6.96 (s, broad, 1H, H_{para} (Ar**)), 6.37 (s, broad, 1H, $H_{ortho'}$ (Ar**)), 2.68 (s, 6H, $N(CH_3)_2$ (Ar**)), 2.25 (s, 3H, CH_3 (Ar**)), 1.68 (s, broad, 14H, CH_3 (TMEDA) and H_γ (TMP)), 1.66 (s, 9H, *t*Bu), 1.58 (s, 4H, CH_2 (TMEDA)), 1.53 (s, broad, 6H, CH_3 (TMP)), 1.31 (m, 4H, H_β (TMP)), 1.21 ppm (s, broad, 6H, CH_3 (TMP)); ^{13}C{^{1}H} NMR (100.63 MHz, 25 °C, C_6D_6): $\delta = 170.01$ (Zn–C_{meta} (Ar**)), 150.77 (C_{ipso} (Ar**)), 136.54 ($C_{meta'}$ (Ar**)), 128.52 (C_{para} (Ar**)), 121.55 (C_{ortho} (Ar**)), 111.86 ($C_{ortho'}$ (Ar**)), 57.37 (CH_2 (TMEDA)), 52.96 (C_α (TMP)), 46.23 (CH_3 (TMEDA)), 41.22 ($N(CH_3)_2$ (Ar**)), 40.76 (C_β (TMP)), 36.50 (CH_3 (TMP)), 35.77 (CH_3 (*t*Bu)), 35.32 (CH_3 (TMP)), 22.80 (CH_3 (Ar**)), 21.05 (C (*t*Bu)), 20.78 ppm (C_γ (TMP)).

Received: February 23, 2006
Published online: May 3, 2006

Keywords: anilides · deprotonation · metalation · sodium · zincation

[1] M. Schlosser, *Organometallics in Synthesis*, 2nd ed., Wiley, Chichester, **2002**, chap. 1.
[2] For an authoritative review on hydrogen–metal interconversion reactions in aromatic systems, see: M. Schlosser, *Angew. Chem.* **2005**, *117*, 380; *Angew. Chem. Int. Ed.* **2005**, *44*, 376.
[3] P. Beak, V. Snieckus, *Acc. Chem. Res.* **1982**, *15*, 306.
[4] "The Directed *ortho*-Metalation Reaction. A Point of Departure for New Synthetic Aromatic Chemistry": C. G. Hartung, V. Snieckus in *Modern Arene Chemistry* (Ed.: D. Astruc), Wiley-VCH, New York, **2002**, pp. 330–367.
[5] J. Clayden, *Organolithiums: Selectivity for Synthesis*, Pergamon, Elsevier Science, Oxford, **2002**.
[6] Y. Kondo, M. Shilai, M. Uchiyama, T. Sakamoto, *J. Am. Chem. Soc.* **1999**, *121*, 3539.
[7] P. C. Andrikopoulos, D. R. Armstrong, W. Clegg, C. J. Gilfillan, E. Hevia, A. R. Kennedy, R. E. Mulvey, C. T. O'Hara, J. A. Parkinson, D. M. Tooke, *J. Am. Chem. Soc.* **2004**, *126*, 11612.
[8] For the use in synthesis of lithium magnesiate reagents with only alkyl ligands, see: F. Mongin, A. Bucher, J. P. Bazureau, O. Bayh, H. Awad, F. Trécourt, *Tetrahedron Lett.* **2005**, *46*, 7989.
[9] The classical "LiCKOR" (Li–C + KOR) superbases are also heterobimetallic, see: a) M. Schlosser, *Mod. Synth. Methods* **1992**, *6*, 227; b) L. Lochmann, *Eur. J. Inorg. Chem.* **2000**, 115; c) see also reference [1].
[10] Mixed lithium–Grignard reagents are also making a considerable impact in metal–halogen exchange reactions, see: a) A. Krasovskiy, P. Knochel, *Angew. Chem.* **2004**, *116*, 3396; *Angew. Chem. Int. Ed.* **2004**, *43*, 3333; b) S. Kii, A. Akao, T. Iida, T. Mase, N. Yasuda, *Tetrahedron Lett.* **2006**, *47*, 1877.
[11] For a perspective article, see: R. E. Mulvey, *Organometallics* **2006**, *25*, 1060.
[12] P. C. Andrikopoulos, D. R. Armstrong, D. V. Graham, E. Hevia, A. R. Kennedy, R. E. Mulvey, C. T. O'Hara, C. Talmard, *Angew. Chem.* **2005**, *117*, 3525; *Angew. Chem. Int. Ed.* **2005**, *44*, 3459.
[13] Activation of *N,N*-dimethylaniline is primarily through an inductive, acidifying effect of the N atom; the coordination effect of the N atom is thought to be less important as a result of its conjugation with the π system of the ring; see reference [5], page 45.
[14] G. Wittig, H. Merkle, *Chem. Ber. Dtsch. Chem. Ges.* **1942**, *75*, 1491.
[15] A. R. Lepley, W. A. Khan, A. B. Giumanini, A. G. Giumanini, *J. Org. Chem.* **1966**, *31*, 2047.
[16] Complexation of *N,N*-dimethylaniline with $[Cr(CO)_3]$ leads to a mixture of *ortho*, *meta*, and *para* deprotonation upon lithiation; see: R. J. Card, W. S. Trahanovsky, *J. Org. Chem.* **1980**, *45*, 2560.
[17] Special cases of *meta* deprotonation can exist when a combination of substituents are present on an aromatic ring. Such cases, which because of the multiple substitution limit the number of sites available for deprotonation, are usually forced by steric constraints and therefore should be clearly distinguished from examples of monosubstituted aromatic rings in which *meta* deprotonation is orders of magnitude more difficult to realize. For a recent example involving trisubstituted (2,6-dihalophenyl) silanes, see: a) C. Hess, F. Cottet, M. Schlosser, *Eur. J. Org. Chem.* **2005**, 5236; for monosubstituted but *N,N*-crowded aniline examples, see: E. Baston, R. Maggi, K. Friedrich, M. Schlosser, *Eur. J. Org. Chem.* **2001**, 3985.
[18] Crystal data for **3**: $C_{27}H_{53}N_4NaZn$, $M_r = 522.1$, monoclinic, space group $P2_1/c$, $a = 16.170(3)$, $b = 11.0651(19)$, $c = 18.683(3)$ Å, $\beta = 112.614(3)°$, $V = 3085.8(9)$ Å^3, $Z = 4$, $T = 150$ K. 23451 measured reflections (CCD diffractometer, $Mo_{K\alpha}$ radiation, $\lambda = 0.71073$ Å), 6048 unique ($R_{int} = 0.042$), 362 refined parameters with constrained H atoms and disorder for TMEDA, $R = 0.061$ for F values of 4622 reflections with $F^2 > 2\sigma(F^2)$, $R_w = 0.152$ for all F^2 values, GOF = 1.14, final difference map extremes = +0.94 and −0.47 e Å^{-3}. Crystal data for **5**: $C_{28}H_{55}N_4NaZn$, $M_r = 536.1$, monoclinic, space group $P2_1/c$, $a = 15.291(7)$, $b = 11.391(5)$, $c = 18.729(8)$ Å, $\beta = 99.992(7)°$, $V = 3213(2)$ Å^3, $Z = 4$, $T = 150$ K. 24659 measured reflections, 6299 unique ($R_{int} = 0.032$), 475 refined parameters with constrained H atoms and disorder for all ligands except anilide, $R = 0.034$ for F values of 4948 reflections with $F^2 > 2\sigma(F^2)$, $R_w = 0.094$ for all F^2 values, t = 1.08, final difference map extremes = +0.43 and −0.32 e Å^{-3}. CCDC-297778 and -297779 contain the supplementary crystallographic data for this paper. These data can be obtained free of charge from The Cambridge Crystallographic Data Centre via www.ccdc.cam.ac.uk/data_request/cif. See http://www.ccdc.cam.ac.uk/products/csd/request/ for details.
[19] R. E. Ludt, G. P. Crowther, C. R. Hauser, *J. Org. Chem.* **1970**, *35*, 1288.
[20] The presence of *N,N*-dimethyl-3-iodoaniline was confirmed by comparing its ^{1}H NMR spectrum in $CDCl_3$ with that reported by S. Padmanabhan, N. L. Reddy, G. J. Durant, *Synth. Commun.* **1997**, *27*, 691; see the Supporting Information.

 © 2006 Wiley-VCH Verlag GmbH & Co. KGaA, Weinheim

Molecular Devices

DOI: 10.1002/anie.200600683

A Chemically Switchable Molecular Pinwheel**

*Owain P. H. Vaughan, Federico J. Williams, Nick Bampos, and Richard M. Lambert**

The bottom-up fabrication of nanoscopic devices such as gears,[1] ratchets,[2] turnstiles,[3] switches,[4] and elevators[5] continues to attract much attention. The interest in molecular rotors in solution,[6] inside crystals,[7–9] and in the gas phase[10] has recently been extended to surface-mounted rotors;[11–13] most recently, a light-driven molecular rotor anchored to a gold surface has been demonstrated,[13] and a recent comprehensive review of artificial molecular rotors is available.[14]

Derivatized porphyrins are versatile building blocks for the creation of many different types of assemblies, including supramolecular structures.[15] When adsorbed on surfaces, they can be imaged with scanning tunneling microscopy (STM). Copper tetra-(3,5-di-*tert*-butylphenyl)porphyrin (Cu–TBPP) adsorbed on Cu(100) was the first case in which single-molecule manipulation at room temperature[16] and conformational recognition were achieved by means of STM.[17] In subsequent work with Cu–TBPP, Moresco et al.[18] were able to observe tip-induced conformational changes in individual di-*tert*-butyl phenyl (tBP) groups through height changes in the STM images. More recently, a metal-free TBPP functionalized with cyanophenyl terminal groups and adsorbed on Au(111) was used to form molecular assemblies including tetramers and one-dimensional wires; the structures of these assemblies were controlled by purposeful synthetic design of the monomer molecule.[19] Photoexcited molecular rotors have been observed in solution,[20] and the rotation of individual adsorbed molecules has been induced by manipulation with an STM tip;[11] however, reports of surface-mounted rotors are extremely sparse.[14] We describe herein a self-assembly method for switching on the rotation of adsorbed porphyrin molecules by mounting them on an appropriately functionalized ligand, one end of which binds to the surface, the other to the "hub" of the porphyrin. This was achieved by using zinc tetra-(3,5-di-*tert*-butylphenyl)porphyrin[21] (Zn–TBPP; Scheme 1a), whose structure is such that interaction between the macrocycle component and the Ag(100) surface is minimized. As a result of steric repulsion,

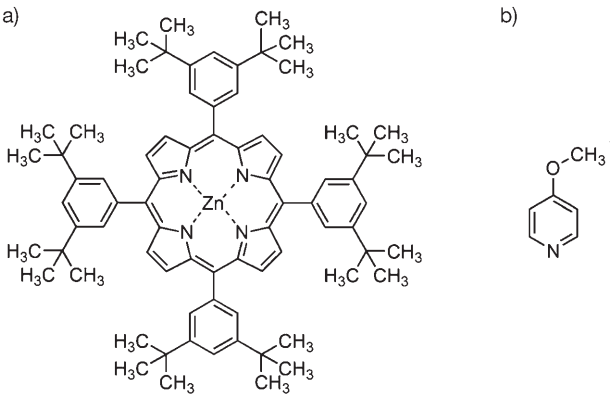

Scheme 1. a) Chemical structure of zinc tetra-(3,5-di-*tert*-butylphenyl)-porphyrin (Zn–TBPP). b) Chemical structure of 4-methoxypyridine, a ligand known to interact with Zn metalloporphyrins through the N atom.

the four tBP groups at the *meso* positions of this porphyrin lie essentially orthogonal to the plane of the macrocycle.[17] These tBP "legs" decouple the molecular π-electron system from the silver surface and provide the principal (relatively weak) interaction between the molecule and the metal surface. The result is an adsorbate that is sufficiently strongly bound so as to prevent unwanted diffusion, while at the same time is able to rotate in the plane should the molecule–surface interaction somehow be weakened sufficiently.

Zn–TBPP was deposited by evaporation under ultrahigh vacuum (source temperature 573 K) onto an atomically clean single-crystal Ag(100) surface held at 298 K. Individual Zn–TBPP molecules were distributed across the surface by annealing (523 K for 60 mins) and subsequently characterized by STM. Figure 1 shows images obtained for various degrees of coverage of the surface with Zn–TBPP. The individual molecules are imaged as four bright lobes,[21] each of which corresponds to one of the four tBP groups, and each molecule (circled in white) exhibits an apparent diameter of approximately 25 Å. Note that this adsorption geometry corresponds to the orientation of the porphyrin ring parallel to the Ag surface. At low surface coverages (Figure 1a and b), the molecules tend to form 2D islands on the terraces of the Ag surface but they exhibit no preferred orientation with respect to the underlying metal lattice, despite the fourfold rotational symmetry of both the porphyrin and the Ag(100) surface—this observation highlights the weak coupling between the molecule and the surface. At the highest coverage densities (approximately one monolayer = 1 ML), new features appeared (circled in black) that have approximately three times the apparent height of the flat-lying porphyrin molecules (Figure 1d). These features have an ellipsoidal aspect (ca. 17 Å × ca. 7 Å) with the major axis approximately equal to the width, and the minor axis approximately equal to the height of Zn–TBPP. This strongly suggests that these ellipsoidal objects are Zn–TBPP molecules tilted on edge and the flat→tilted transition is driven by interaction with neighboring molecules. Such coverage-dependent molecular reorientations are well known for simpler systems, for example, pyridine adsorbed on Ag(111).[22] In the present case, this

[*] O. P. H. Vaughan, Dr. F. J. Williams, Dr. N. Bampos, Professor R. M. Lambert
Department of Chemistry
University of Cambridge
Cambridge CB21EW (UK)
Fax: (+44) 1223-336-362
E-mail: rml1@cam.ac.uk

[**] O.P.H.V. acknowledges financial support from the UK Engineering and Physical Sciences Research Council. F.J.W. acknowledges the award of an Early Career Fellowship by the Leverhulme Trust.

Supporting information for this article is available on the WWW under http://www.angewandte.org or from the author.

© 2006 Wiley-VCH Verlag GmbH & Co. KGaA, Weinheim

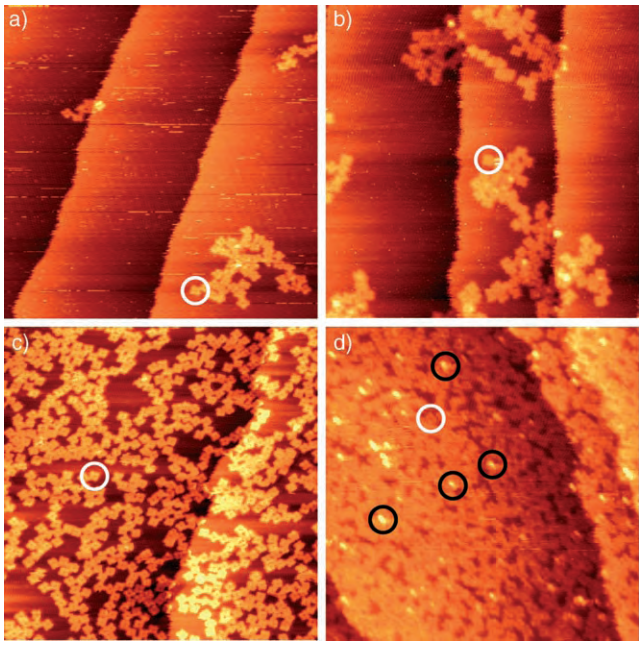

Figure 1. STM images taken at 298 K of Zn–TBPP molecules adsorbed on Ag(100) at surface coverages of a) ca. 0.1 ML, b) ca. 0.25 ML, c) ca. 0.75 ML, and d) ca. 1 ML. Conditions: $V_{tip} = 0.75$ V, $I = 0.1$ nA, 500 Å × 500 Å. As indicated by the white circles, at low coverage densities the porphyrin molecules lie with the ring parallel to the Ag(100) surface. As the coverage reaches one monolayer a new adsorption state is observed (circled in black), most likely one in which the macrocycle tilts so that the porphyrin ring is perpendicular to the metal surface.

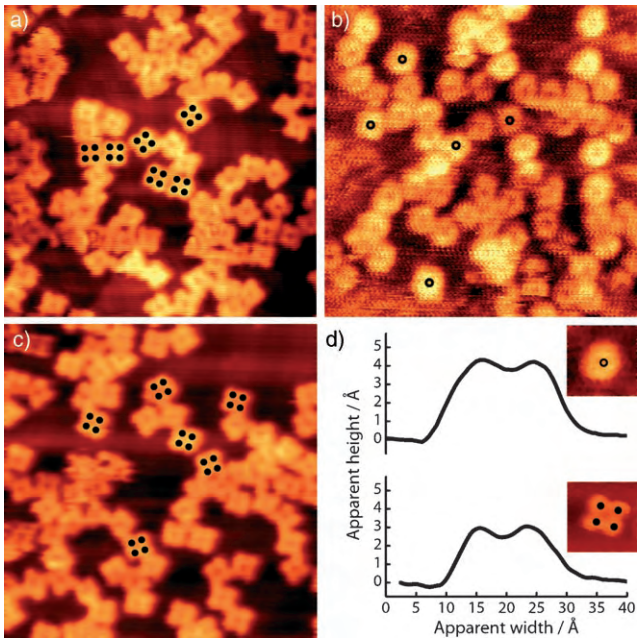

Figure 2. Sequence of STM images of Zn–TBPP molecules adsorbed on Ag(100) showing the effect of exposure to 4-methoxypyridine. Sub-monolayer coverage of Zn–TBPP: a) at 123 K; b) following a dosing of 100 Langmuirs of 4-methoxypyridine at 123 K; c) after warming to 298 K. Conditions: $V_{tip} = 1.0$ V, $I = 0.1$ nA, 200 Å × 200 Å. d) Typical line profiles of the two features shown: four-lobed (bottom) and toroidal species (top). The presence of the ligand converts Zn–TBPP from a structure imaged with four lobes into one that appears as a torus.

tilting transition provides further evidence that the silver–porphyrin interaction is relatively weak.

We have previously shown that the ligand 1,4-diazabicyclo[2.2.2]octane (DABCO), which does not adsorb on Ag(100) at 123 K, can reversibly cap the upper face of adsorbed Zn–TBPP through one of the N atoms.[21] That is, the ligand was bound on top of the adsorbed porphyrin because this provided the most favorable N→Zn^{2+} interaction. With this in mind, we chose a bifunctional ligand (4-methoxypyridine, Scheme 1b) that is known[23] to interact with Zn^{2+} through the N atom, while, at the other end, it is capable of O→Ag interaction with the silver surface.[24]

Figure 2a–c shows a sequence of images illustrating the effect of treating a sub-monolayer coverage of Zn–TBPP with the ligand 4-methoxypyridine. Figure 2a shows the initially adsorbed porphyrin molecules at 123 K, and Figure 2b shows the result of subsequent exposure of the sample to 100 Langmuirs of 4-methoxypyridine (1 Langmuir = 1.33×10^{-6} mbar s). A substantial change in the apparent molecular shape is observed: the originally fourfold-symmetric objects now appear toroidal. Figure 2c shows the effect of subsequently warming the system to 298 K, which resulted in desorption of 4-methoxypyridine to leave just the porphyrin on the Ag surface, thus restoring the initial condition. (4-methoxypyridine adsorbs on clean Ag at 123 K, desorbing at 298 K, see the Supporting Information). The sequence a–b–c was fully reversible and could be repeated an indefinite number of times on any given porphyrin covered surface.

Typical height profiles of these two types of objects, namely unmodified Zn–TBPP molecules (marked with four black circles, Figure 2a) and Zn–TBPP interacting with 4-methoxypyridine (marked with a single black circle, Figure 2b), are shown in Figure 2d. The Zn–TBPP molecules have an apparent height of around 3 Å and an apparent diameter of about 25 Å and are characterized by the lower line profile in Figure 2d—this profile consists of a line scan through a single molecule. The upper line profile (apparent height of ca. 4 Å) corresponds to Zn–TBPP modified by interaction with 4-methoxypyridine. Note that despite its greater apparent height, this object has essentially the same diameter and the same characteristic double-humped profile as a bare porphyrin molecule. Were the ligand to bind to the upper face of the porphyrin,[21] the appearance of the resulting object would be similar to that found previously for the Zn–TBPP–DABCO complex, the dark indentation at the center of the bare porphyrin being replaced by a bright protrusion. The present case stands in striking contrast: interaction with 4-methoxypyridine yields an elevated torus with a distinct central depression. This observation is consistent with the 4-methoxypyridine being located beneath the porphyrin, tethered to the Ag surface and to the porphyrin through its oxygen and nitrogen atoms, respectively. The resulting weakening of the porphyrin–surface interaction could then permit the macrocycle to rotate, thus yielding a time-averaged image in which the four lobes of the initially static porphyrin are reduced to a torus. Thus, we appear to have succeeded in assembling a molecular pinwheel. Crucially, if methoxybenzene is used in

 © 2006 Wiley-VCH Verlag GmbH & Co. KGaA, Weinheim

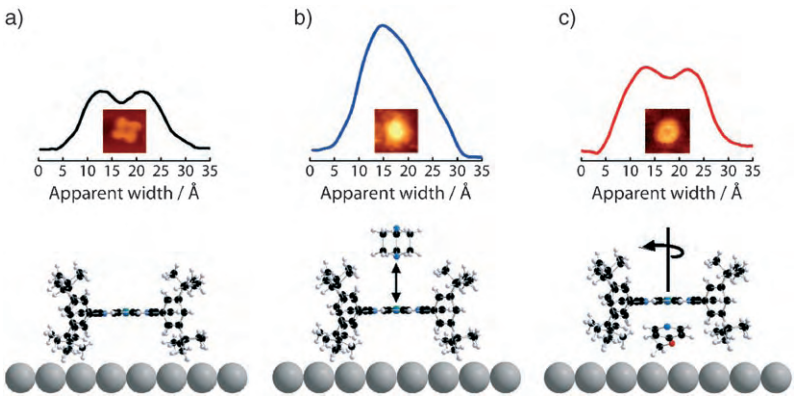

Figure 3. STM images, line profiles, and structural diagrams for Zn–TBPP on Ag(100): a) bare Zn–TBPP on Ag(100); b) the effect of capping the porphyrin with DABCO; c) the effect of inserting the 4-methoxypyridine "axle".

place of 4-methoxypyridine, the phenomenon is not observed: methoxybenzene resembles 4-methoxypyridine but lacks the N atom—it can bind to the surface but not to the porphyrin, therefore it cannot act as an axle. Figure 3 depicts the relationship between the various images, line profiles, and structural proposals discussed above.

Further evidence that the observed changes in our STM images are due to rotation of the porphyrin molecules is provided by the work of Gimzewski et al.,[11] who reported the creation and visualization by STM of individual molecular rotors made by depositing hexa-*tert*-butyl decacyclene molecules on Cu(100). Their images are comparable to those reported here: a lobed feature was reduced to a toroidal feature. In their case, transition from the static to the rotating state could be controlled locally by manipulating individual molecules with the STM tip: displacement of a molecule from within a two-dimensional lattice of immobilized molecules to a void within the lattice resulted in molecular rotation. Our system is very different—we have assembled a molecular pinwheel in which the transition to rotation is chemically driven by addition or removal of 4-methoxypyridine, which acts as an axle. Furthermore, rotation of all the molecules can be switched on or off simultaneously. This axle–wheel (ligand–porphyrin) structure is illustrated in Figure 3c.

Our results show that a well-chosen ligand can be used to convert a static array of metalloporphyrin molecules into an assembly of surface-mounted rotors. By judiciously altering the degree of coupling between the "wheel" and the surface and the "wheel" and the "axle", it should be possible to design systems that switch at different temperatures: with our approach, spinning is induced by lowering the barrier to in-plane rotation until it is of the order of kT. This could be achieved by varying the nature of the surface, the architecture of the porphyrin, and the structure and binding properties of the ligand, thus enabling a new means of bottom-up fabrication of nanoscopic devices.

Received: February 21, 2006
Published online: May 3, 2006

Keywords: molecular devices · nanotechnology · porphyrinoids · scanning probe microscopy · silver

[1] J. Clayden, J. H. Pink, *Angew. Chem.* **1998**, *110*, 2040; *Angew. Chem. Int. Ed.* **1998**, *37*, 1937.
[2] T. R. Kelly, I. Tellitu, J. P. Sestelo, *Angew. Chem.* **1997**, *109*, 1969; *Angew. Chem. Int. Ed. Engl.* **1997**, *36*, 1866.
[3] T. C. Bedard, J. S. Moore, *J. Am. Chem. Soc.* **1995**, *117*, 10662.
[4] B. L. Feringa, R. A. van Delden, N. Koumura, E. M. Geertsema, *Chem. Rev.* **2000**, *100*, 1789.
[5] J. D. Badjic, V. Balzani, A. Credi, S. Silvi, J. F. Stoddart, *Science* **2004**, *303*, 1845.
[6] V. Balzani, A. Credi, F. M. Raymo, J. F. Stoddart, *Angew. Chem.* **2000**, *112*, 3484; *Angew. Chem. Int. Ed.* **2000**, *39*, 3349.
[7] Z. Dominguez, H. Dang, M. J. Strouse, M. A. Garcia-Garibay, *J. Am. Chem. Soc.* **2002**, *124*, 2398.
[8] C. E. Godinez, G. Zepeda, M. A. Garcia-Garibay, *J. Am. Chem. Soc.* **2002**, *124*, 4701.
[9] Z. Dominguez, H. Dang, M. J. Strouse, M. A. Garcia-Garibay, *J. Am. Chem. Soc.* **2002**, *124*, 7719.
[10] K. Hoki, M. Yamaki, S. Koseki, Y. Fujimura, *J. Chem. Phys.* **2003**, *118*, 497.
[11] J. K. Gimzewski, C. Joachim, R. R. Schlitter, V. Langlais, H. Tang, I. Johannsen, *Science* **1998**, *281*, 531.
[12] X. Zheng, M. E. Mulcahy, D. Horinek, F. Galeotti, T. F. Magnera, J. Michl, *J. Am. Chem. Soc.* **2004**, *126*, 4540.
[13] R. A. van Delden, M. K. J. ter Wiel, M. M. Pollard, J. Vicario, N. Koumura, B. L. Feringa, *Nature* **2005**, *437*, 1337.
[14] G. S. Kottas, L. I. Clarke, D. Horinek, J. Michl, *Chem. Rev.* **2005**, *105*, 1281.
[15] I. Goldberg, *Chem. Commun.* **2005**, 1243.
[16] T. A. Jung, R. R. Schlittler, J. K. Gimzewski, H. Tang, C. Joachim, *Science* **1996**, *271*, 181.
[17] T. A. Jung, R. R. Schlittler, J. K. Gimzewski, *Nature* **1997**, *386*, 696.
[18] F. Moresco, G. Meyer, K.-H. Rieder, *Phys. Rev. Lett.* **2001**, *86*, 672.
[19] T. Yokoyama, S. Yokoyama, T. Kamikado, Y. Okuno, S. Mashiko, *Nature* **2001**, *413*, 619.
[20] M. F. Hawthorne, J. I. Zink, J. M. Skelton, M. J. Bayer, C. Liu, E. Livshits, R. Baer, D. Neuhauser, *Science* **2004**, *303*, 1849.
[21] F. J. Williams, O. P. H. Vaughan, K. J. Knox, N. Bampos, R. M. Lambert, *Chem. Commun.* **2004**, 1688.
[22] M. Bader, J. Haase, K. H. Frank, A. Puschmann, A. Otto, *Phys. Rev. Lett.* **1986**, *56*, 1921.
[23] N. Kanayama, T. Kanbara, H. Kitano, *J. Phys. Chem. B* **2000**, *104*, 271.
[24] B. Krüger, C. Benndorf, *Surf. Sci.* **1986**, *178*, 704.

 © 2006 Wiley-VCH Verlag GmbH & Co. KGaA, Weinheim

Carbonaceous Materials

DOI: 10.1002/anie.200600460

Starbons: New Starch-Derived Mesoporous Carbonaceous Materials with Tunable Properties**

Vitaly Budarin, James H. Clark, Jeffrey J. E. Hardy, Rafael Luque, Krzysztof Milkowski, Stewart J. Tavener, and Ashley J. Wilson*

The outstanding potential of mesoporous carbonaceous materials[1] requires a methodology that grants control over their surface chemistry and the distribution of pore sizes. The best current method that achieves control over pore-size distribution is the templating method. A typical procedure[1c] involves filling mesoporous silica with a carbon precursor (e.g. sucrose), which is subsequently carbonized through a series of high-temperature processes. The template is then removed by using hydrofluoric acid or caustic soda. The resultant activated carbons produced by this method possess well-ordered mesoporous structures with a large specific volume and physical properties amenable to a broad range of applications.[2] However, highly aggressive chemicals involved limit this approach to the production of stable graphitic carbons with inert hydrophobic surfaces.[3] To functionalize and open up new chemistry, further difficult chemical modifications are required. This is at the cost of reducing the availability of the mesopores.[4]

Herein we report a novel approach for the generation of a new family of mesoporous carbonaceous materials with surfaces ranging from hydrophilic to hydrophobic, which is controlled by the degree of carbonization. The method utilizes the natural ability of the amylose and amylopectin polymer chains within the starch granules to assemble into an organized nanoscale lamellar structure, which consists of crystalline and amorphous regions.[5] Our strategy was to synthesize mesoporous carbons (hereinafter referred to as "starbons") by using mesoporous expanded starch[6] as the precursor without the need for a templating agent. This process is gentle and provides the opportunity to produce a whole range of mesoporous carbon-based materials from starch to activated carbon, including amorphous oxygen-containing carbons that have many applications,[7] such as catalysis,[7a,b] adsorption,[7c] and medicine,[7d,e] owing to their varied surface functionalities.

The approach described is illustrated in Scheme 1. First, a simple process of gelatization in water opens up and disorders the dense biopolymer network,[8] after which it partially recrystallizes during a process of retrogradation.[9] Exchanging water with a lower-surface-tension solvent (usually ethanol) prevents collapse of the network structure during the drying process. After drying, the expanded mesoporous starch is obtained. In the final stage of the process, mesoporous starch is doped with a catalytic amount of organic acid (e.g. *para*-toluenesulfonic acid) and heated under vacuum. This enables fast carbonization and fixing of the mesoporous structure. Heating at different temperatures, ranging from 150 to 700 °C has produced a variety of mesoporous materials from amorphous carbons to graphite-like activated carbons. Native starch granules do not produce mesoporous materials when carbonized. This indicates that the formation of expanded starch as a precursor to starbon is crucial.

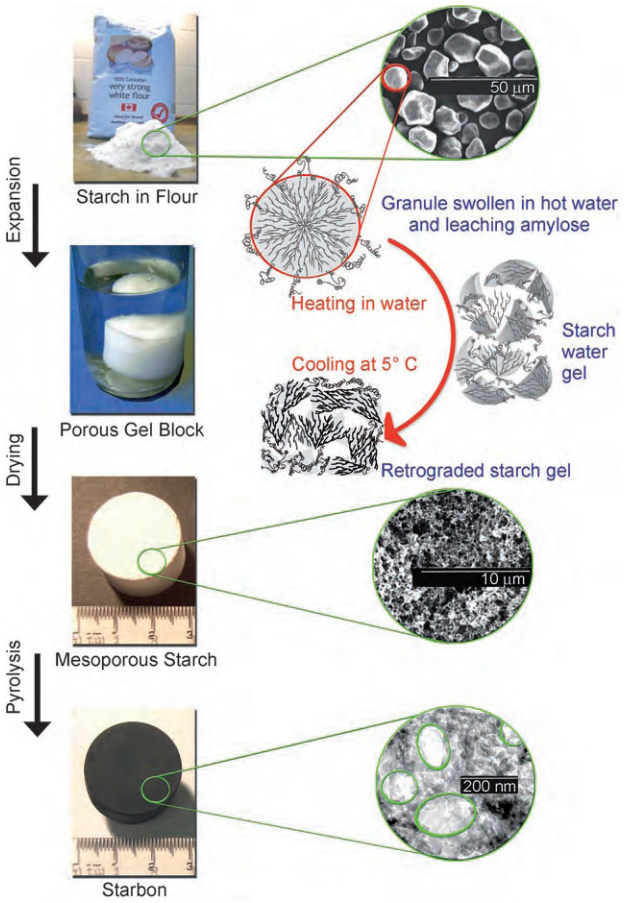

Scheme 1. Production of mesoporous carbon by controllable pyrolysis of expanded starch. (Magnified pictures of starch in flour and mesoporous starch obtained from scanning electron microscopy (SEM) and TEM for starbon).

[*] Dr. V. Budarin, Prof. J. H. Clark, Dr. R. Luque, Dr. K. Milkowski, Dr. S. J. Tavener, Dr. A. J. Wilson
Clean Technology Centre
Department of Chemistry
University of York
York YO105DD (UK)
Fax: (+44) 190-443-2705
E-mail: jhc1@york.ac.uk
Dr. J. J. E. Hardy
Royal Society of Chemistry
Burlington House, Piccadilly, London W1J0BA (UK)

[**] We thank the EPSRC for financial assistance and colleagues in the York Clean Technology Centre for their intellectual input. We thank P. Elliott, Dr. K. Wilson and M. Stark for their analytical support and advice, and Ms. S. Narayanaswamy for assistance in the manufacture of the starbons monolith.

Supporting information for this article is available on the WWW under http://www.angewandte.org or from the author.

InterScience
© 2006 Wiley-VCH Verlag GmbH & Co. KGaA, Weinheim

Expanded starch is obtained with a surface area of approximately 180 $m^2 g^{-1}$ and negligible microporosity. The average pore diameter in the mesoporous region for expanded starch is around 6 nm (see the Supporting Information), similar to the average distance between crystalline layers of native starch.[5e] The porous structure of starbon comes from the expanded starch (Scheme 1). This structure prevents the problem of micelle collapse that occurs in micelle templated polymer methods for the synthesis of mesoporous carbons[1d] and removes the need for synthesis of mesoporous templates such as silica to define the structure (Figure 1). The total pore volume remains essentially constant

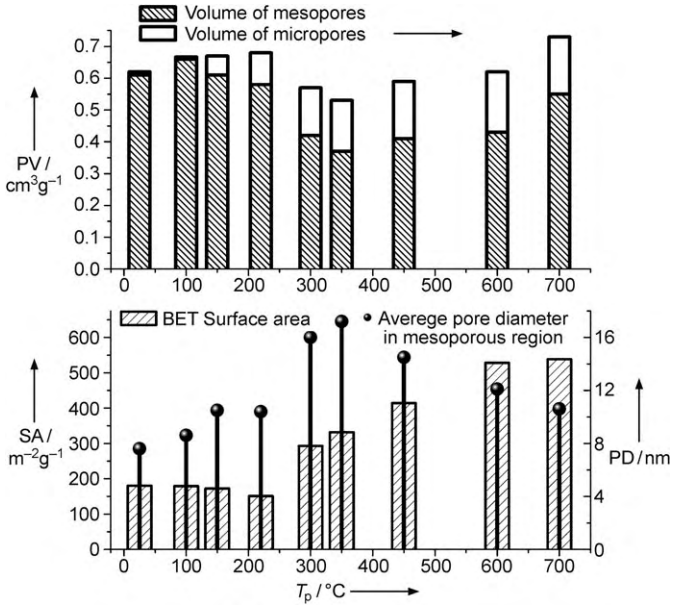

Figure 1. Pore characteristics and surface area of starbons. Expanded starch doped with acid and heated at the indicated temperature. PV = pore volume, SA = surface area, PD = pore diameter, T_p = temperature of starbon preparation.

throughout the carbonization process. The pore-size distribution indicates a predominance of mesopores with the volume and diameter of pores that lie in the range 0.4–0.6 $cm^3 g^{-1}$ and 8–16 nm, respectively. This diameter is greater than 5 nm, which is the typical pore size for carbons prepared by the templating method.[1e] Although at temperatures of approximately 300 °C there is a substantial increase in the contribution of the microporous region to the total surface area (this could be owing to noncatalytic starch decomposition at this temperature), the actual volume that this corresponds to is small in comparison to the total mesoporous volume (Figure 1). At temperatures higher than 600 °C, the materials develop remarkably well-defined micropores that are only 0.5 nm in diameter (measured by the micropore analysis (MP) method) and the porous distribution becomes bimodal with a predominanance of the mesopore region (see the Supporting Information).

TEM provides additional information about the mechanism of this process. In Figure 2, image A shows expanded starch with a homogeneous structure around the mesopore,

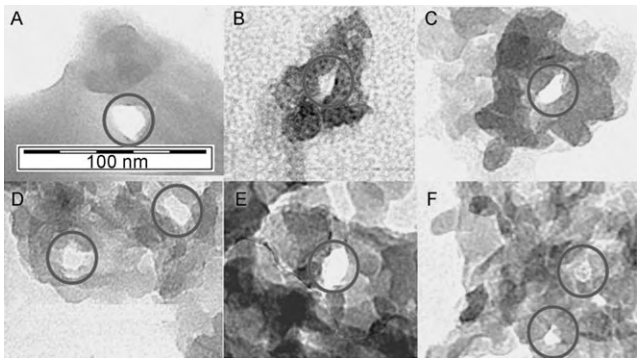

Figure 2. TEM of starbons produced at a range of temperatures: A) expanded starch; B) 100 °C; C–150 °C; D) 220 °C; E) 300 °C; F) 450 °C.

whereas images B–F show the structure of starbons prepared at increasingly higher temperatures. In images B and C, the small particles of carbon (dark areas around the mesopore) indicate that the process of carbonization initiates around the pores. This is because the added acid is absorbed on the surface of the expanded starch (on the outer surface and within the pores), and thus the carbonization reaction initiates from the outer layers and gradually moves to the bulk of the material. The images also indicate that starbon combines both carbon and starch-like properties at lower preparation temperatures (images B and C) and progressively gain more carbon-like characteristics with increasing temperatures (images D–F). X-ray photoelectron spectroscopy (XPS) further supports these observations, indicating a nearly linear increase in the carbon/oxygen ratio on the surface from 1.2 for expanded starch to 8 for starbon prepared at 700 °C (Figure 3). The carbonization trend is also reflected in the elemental analysis (EA), although the ratios are slightly lower for the bulk (EA) than for the surface (XPS) of the materials. This additionally confirms that the mechanism of the carbonization process initiates from the outer surface into the inner bulk of the material.

The changes in the chemical composition that occur during the preparation of starbons have also been inves-

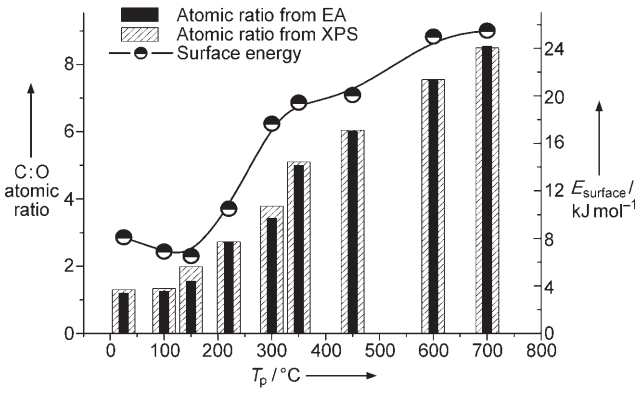

Figure 3. The influence of the temperature of preparation of starbons on the surface energy measured by the Dubinin–Radashkevich method ($E_{surface}$), and on the composition as measured by XPS and EA.

 © 2006 Wiley-VCH Verlag GmbH & Co. KGaA, Weinheim

tigated. In the temperature interval of up to 250 °C, loss of the starch hydroxy group functionality is evident from the diminishing peak intensity in FTIR spectra at 3300 and 1000 cm^{-1} (Figure 4). This could coincide with the diminishing

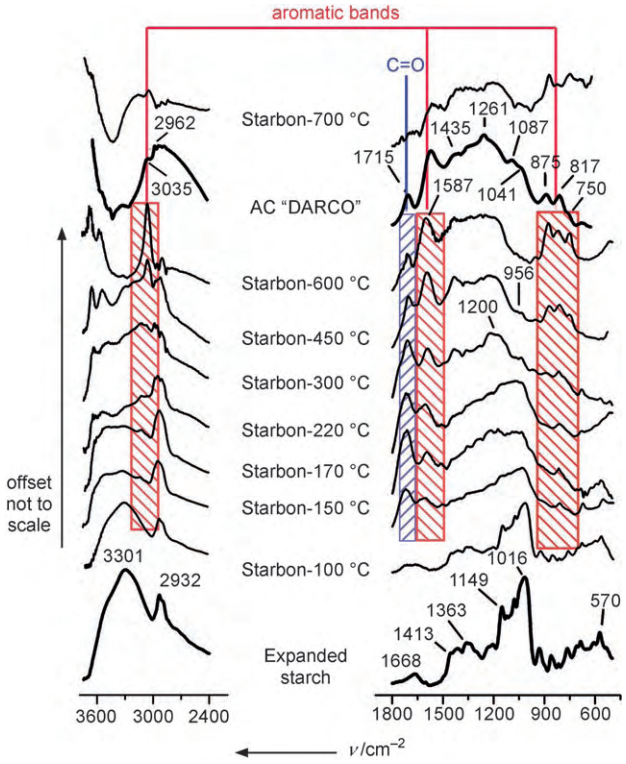

Figure 4. DRIFT spectra of starbons alongside that of expanded starch and commercial carbon Darco KB.

peak in the differential thermogravimetry (DTG) trace at approximately 310 °C (see the Supporting Information). For samples obtained between 100–250 °C, formation of carbonyl groups conjugated with olefinic (new bands at 956 and 1715 cm^{-1})[10,3a] and vinyl ethers groups (large, intense band ranging from 950–1200 cm^{-1} with a maximum at 1200 cm^{-1} and shoulder at about 1050 cm^{-1}) take place. The DTG trace of these samples show a peak at 740 °C that could correspond to the presence of these groups. Simultaneously, the growth of bands between 200 and 600 °C at 875, 817, and 750 cm^{-1} can be assigned to aromatic C–H out-of-plane bending vibrations.[11] This, accompanied with peaks at 1587 and 3035 cm^{-1}, indicate progressive development of aromatization in the starbons. Between 450 and 600 °C there is an additional peak in the DTG trace at around 620 °C that is characteristic of phenolic groups.[12] The intensity of all aromatic C–H bands decreases for starbons prepared at 700 °C, indicating formation of a graphite-like structure. Solid-state ^{13}C cross-polarization (CP) magic-angle-spinning (MAS) NMR spectra of the materials confirmed these main chemical changes in the transition from starch to starbon (see the Supporting Information). These changes are similar to those reported previously for ordinary starch,[13] but here, the corresponding steps occur at much lower temperatures.

Investigation of starbons prepared at high temperatures indicates that the properties of starbons are approaching those of conventional activated carbons. The FTIR spectra of starbons produced at the temperature range between 450 and 600 °C are very close to those of the commercial Darco KB (Figure 4) and other typical charcoals. Furthermore, thermogravimetric analysis (TGA) demonstrates that with increasing temperature of preparation, the thermal stability increases and the resultant materials become similar to activated carbons. For example starbons prepared at 700 °C decompose at 760 °C and lose only 6 % mass (for activated carbon Norit GAS 1240–780 °C and 2 %). The surface energy, $E_{surface}$ measured by the Dubinin–Radushkevich method, complements these data. Figure 3 illustrates an overall increase in the $E_{surface}$ as the preparation temperature rises. Starch-like properties of the surface are retained until about 200 °C, above which there are gradual changes towards a carbon-like value.[6e,14]

The properties of starbons obtained from TGA, ^{13}C MAS NMR spectroscopy, diffuse reflectance infrared fourier transform (DRIFT), and XPS spectroscopy are summarized in Figure 5. It can be seen that from a starch to graphite-like

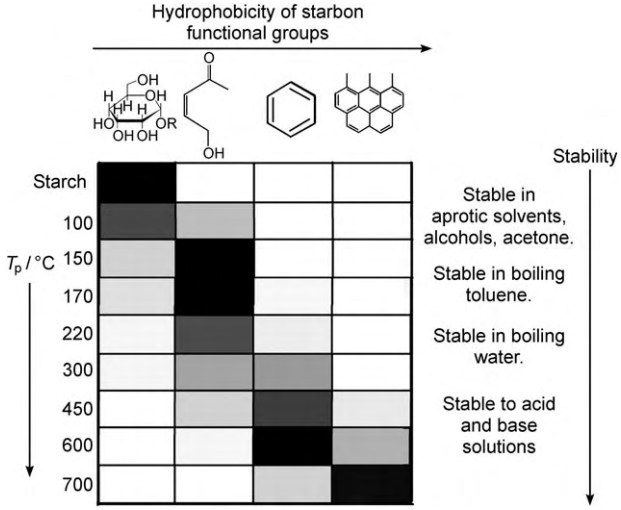

Figure 5. Distribution of functional groups on starbons prepared at different temperatures: color scale to indicate relative amounts of different groups (black represent highest). T_p = temperature of starbon preparation.

structure above 700 °C, there is a progressive increase in the hydrophobicity of the functional groups present. In the first step (100–200 °C), the CH_2OH groups in the starch condensed to carbonyl groups conjugated with olefinic groups. The second step (150–450 °C) involves the progressive degradation of these groups to the formation of aliphatic and alkene/aromatic functions. In the penultimate step (300–600 °C), these aliphatic groups are almost completely converted to aromatic π systems. Finally, as the temperature increases these aromatic compounds condense to graphite-type structures.

Information about the mechanism of starch decomposition gives us the opportunity to predict the temperature of

 © 2006 Wiley-VCH Verlag GmbH & Co. KGaA, Weinheim

starbon preparation for certain applications. The remaining starch functionality within starbons up to 250 °C enables the possible use of these materials in applications typical to starch such as chromatographic separation of enantiomers.[15] Preliminary studies have confirmed that they are effective as a stationary phase for liquid chromatography, allowing separation of a standard test mixture of substituted ferrocene compounds. Low-surface-area sulfonated aromatic carbonaceous materials have recently been shown to be effective solid-acid catalysts[7b] and, as starbons prepared between the temperatures of 300 and 600 °C have aromatic functionality, sulfonation of these materials should also result in useful solid-acid materials. Remarkably, in preliminary experiments, we have found that in the esterification of succinic acid with ethanol, the same level of conversion was achieved with sulfonated starbon (starbon material was prepared at 350 °C) in 1/10 of the time required with sulfonated commercial Darco. A further application for starbons is as a solid carrier for precious metal catalysts. We have found that palladium metal supported on starbons acts as an active catalyst for a model Heck reaction of iodobenzene with methyl acrylate. Again, the importance of the control over the surface chemistry of these materials is apparent: starbon prepared at 220 °C proved the most effective for this reaction.

The presence of functional groups typical to both starch and carbon indicates that the starbons prepared up to 300 °C may be modified chemically by using methodologies suitable for starch[16,6b,d] (e.g. silylation, alkylation, esterification, etherification, etc.) as well as those suitable for carbonaceous materials (e.g. bromination, amination, etc.),[17] which offers future opportunities for novel hybrids.

In summary, we have demonstrated that we can harness the natural ability of plant starch to form nanochannelled structures without the need for a templating agent. This provides an entirely new, simpler, and less wasteful route to mesoporous graphitizable carbons. It is well known that these materials are inert and have good heat and electro conductivities with potential applications in electrochemistry,[2a] catalysis,[2b] hydrogen storage,[2c] and adsorption[2d] and are used in certain types of supported catalysis. Unusually, we can synthesize mesoporous carbons with pores wider than 7 nm; at higher temperature the materials develop remarkably well-defined micropores which are only 0.5 nm wide, but materials prepared at all temperatures tested maintain a predominantly mesoporous structure. Furthermore, a new family of carbon-based mesoporous materials "starbons" with similar textural properties and progressively variable functionality can be synthesized by carbonization of expanded starches. Because of the diversity of surface functional groups, starbons can easily be modified. This, in conjuction with a high surface area in the mesoporous region and mechanical stability, makes starbons particularly suitable for applications such as catalysis and chromatography within the range of preparation. Of special interest for this application could be monolithic forms, in which starbons can be produced (Scheme 1).

Possible future applications of these materials could be chiral chromatography (low-temperature starbons, up to 300 °C), acid–base and fermentative catalysis, and specific adsorption of large organic molecules. The broad scope of applications, combined with structural differences in native starch gives almost unlimited possibilities for this new and exciting class of materials.

Experimental Section

Starbon synthesis: The method comprises three key stages. First, high-amylose cornstarch was gelatinized by heating in water and subsequently cooled to 5 °C for one to two days to yield a porous gel. The water was then exchanged with ethanol, acetone, and oven-dried to yield a predominantly mesoporous starch. In the final stage the mesoporous starch was doped with a catalytic amount of an organic acid (e.g. 0.1 mmol of *p*-toluenesulfonic acid per 1 g of starch) and heated under vacuum to various temperatures (up to 700 °C).

Measurements: Nitrogen-adsorption measurements were carried out at 77 K by using an ASAP 2010 volumetric adsorption analyzer from Micromeritics. Before measuring, the samples were under vacuum 3–4 h at the temperature equal to the temperature of sample preparation. Analysis of pore distribution has been done by standard procedures.[18] The MP method proposed by Mikhail et al.[18a] has been used for evaluation of microporous sample volumes. The Barret–Joyner–Halenda (BJH) equation[18b] was used to determine the volume of mesopores and pore-size distribution of the starbon materials. The characteristic energy of adsorption $E_{surface}$ was calculated from Dubinin–Radushkevich adsorption isotherm equation.[18c]

^{13}C MAS NMR and XPS spectra were recorded on Brüker DMX 400 and Kratos Analytical X-ray photoelectron spectrometers. To correct possible deviation caused by electric charge, the C1s line at 285.0 eV was used as the internal standard.

TGA was performed by using a Netzsch STA 409 at scan rates of 10 °C min^{-1}, with typically 20-mg sample under flowing N_2 at 100 mL min^{-1}.

TEM was carried out on a Technai 20 Transmission Electron microscope equipped with a Lanthanum hexaboride (LaB6) gun. Samples were viewed on scanning electron microscope Hitachi S-2400.

DRIFT spectra were recorded on a Brüker EQUINOX-55 instrument equipped with a liquid N_2 cooled MCT detector. The samples for DRIFT studies were prepared by mechanically grinding all reactants to a fine powder.

Received: February 3, 2006
Revised: March 22, 2006
Published online: May 3, 2006

Keywords: carbohydrates · carbon · mesoporous materials · surface chemistry · thermochemistry

[1] a) G. Che, B. B. Lakshmi, E. R. Fisher, C. R. Martin, *Nature* **1998**, *393*, 346–349; b) A. A. Zakhidov, R. H. Baughman, Z. Iqbal, C. Cui, I. Khayrullin, S. O. Dantas, J. Marti, V. G. Ralchenko, *Science* **1998**, *282*, 897–901; c) R. Ryoo, S. H. Joo, S. Jui, *J. Phys. Chem. B* **1999**, *103*, 7743–7746; d) Z. Li, W. Yan, S. Dai, *Carbon* **2004**, *42*, 767–770; e) A. Lu, W. Li, W. Schmidt, F. Schüth, *Microporous Mesoporous Mater.* **2005**, *80*, 117–128; f) A. Lu, W. Li, W. Schmidt, F. Schüth, *Microporous Mesoporous Mater.* **2005**, *80*, 117–128.

[2] a) J. Lee, S. Yoon, T. Hyeon, S. M. Oh, K. B. Kim, *Chem. Commun.* **1999**, 2177–2178; b) T. W. Kim, I. S. Park, R. Ryoo, *Angew. Chem.* **2003**, *115*, 4511–4515; *Angew. Chem. Int. Ed.* **2003**, *42*, 4375–4379; c) R. Gadoi, S. Saadallah, T. Piquero, P. David, J. Parmentier, C. Vix-Guterl, *Microporous Mesoporous Mater.* **2005**, *79*, 121–128; d) M. Hartmann, A. Vinu, G. Chandrasekar, *Chem. Mater.* **2005**, *17*, 829–833.

 © 2006 Wiley-VCH Verlag GmbH & Co. KGaA, Weinheim

[3] a) S. Jeong, C. Werth, *Environ. Sci. Technol.* **2005**, *39*, 3279–3288; b) K. Eusterhues, C. Rumpel, M. Kleber, I. Kogel-Knaber, *Org. Geochem.* **2003**, *34*, 1591–1600.
[4] a) Z. Li, S. Dai, *Chem. Mater.* **2005**, *17*, 1717–1721; b) Z. Li, W. Yan, S. Dai, *Langmuir* **2005**, *21*, 11999–12006.
[5] a) P. Calvert, *Nature* **1997**, *389*, 338–339; b) D. R. Daniels, A. M. Donald, *Biopolymers* **2003**, *69*, 165–175; c) H. Tang, B. Hills, *Biomacromolecules* **2003**, *4*, 1269–1276; d) D. R. Daniels, A. M. Donald, *Macromolecules* **2004**, *37*, 1312–1318; e) R. Vermeylen, B. Goderis, H. Reynaers, J. A. Delcour, *Biomacromolecules* **2004**, *5*, 1775–1786.
[6] a) M. Glen, D. J. Stern, US Pat. 5,958,589, **1999**; b) S. Doi, J. H. Clark, D. J. Macquarrie, K. Milkowski, *Chem. Commun.* **2002**, 2632–2633; c) J. H. Clark, F. E. I. Deswarte, J. J. E. Hardy, A. J. Hunt, F. M. Kerton, K. Milkowski, PCT Patent Application, PCT/GB2004/003276, **2004**; d) K. Milkowski, J. H. Clark, S. Doi, *Green Chem.* **2004**, *6*, 189–190; e) V. Budarin, J. H. Clark, F. E. I. Deswarte, J. J. E. Hunt, A. J. Hardy, F. M. Kerton, *Chem. Commun.* **2005**, 2903–2905.
[7] a) S. U. Son, S. I. Lee, Y. K. Chung, *Angew. Chem.* **2000**, *112*, 4318–4320; *Angew. Chem. Int. Ed.* **2000**, *39*, 4158–4160; b) M. Toda, A. Takagaki, M. Okamura, J. N. Kondo, S. Hayashi, K. Domen, M. Hara, *Nature* **2005**, *438*, 178; c) D. C. Ko, J. F. Porter, G. MaKay, *Chem. Eng. Sci.* **2000**, *55*, 5819–5829; d) O. E. Orisakwe, A. Oluboyo, S. Ofoefule, E. Obi, N. Ilondu, O. A. Afonne, A. Agbasi, D. H. Chiroma, *J. Health Sci.* **2001**, *47*, 491–494; e) M. Otero, C. A. Grande, A. E. Rodrigues, *React. Funct. Polym.* **2004**, *60*, 203–213.
[8] a) N. Atkin, R. Abeysekera, S. L. Cheng, A. W. Robards, *Carbohydr. Polym.* **1998**, *36*, 173–192; b) N. Atkin, R. Abeysekera, A. W. Robards, *Carbohydr. Polym.* **1998**, *36*, 193–204.
[9] K. Shamai, E. Shimoni, H. Bianco-Peled, *Biomacromolecules* **2004**, *5*, 219–223.
[10] R. Fu, L. Liu, W. Huang, P. Sun, *J. Appl. Polym. Sci.* **2003**, *87*, 2253–2261.
[11] A. Lua, T. Yang, *J. Colloid Interface Sci.* **2004**, *274*, 594–601.
[12] J. L. Figueiredo, M. F. R. Pereire, M. A. Freitas, J. J. M. Orafao, *Carbon* **1999**, *37*, 1379–1389.
[13] X. Zhang, J. Golding, I. Burgar, *Polymer* **2002**, *43*, 5791–5796.
[14] V. Budarin, J. H. Clark, S. J. Tavener, *Chem. Commun.* **2004**, 524–525.
[15] a) D. C. H. Hess, G. Burger, H. Musso, *Anqew. Chem.* **1978**, *90*, 645–646; *Angew. Chem. Int. Ed. Engl.* **1978**, *17*, 612–614; b) Y. Okamoto, E. Yashima, *Angew. Chem.* **1998**, *110*, 1072–1095; *Angew. Chem. Int. Ed.* **1998**, *37*, 1021–1043.
[16] H. Angellier, S. Molina-Boisseau, M. N. Belgacem, A. Dufresne, *Langmuir* **2005**, *21*, 2425–2433.
[17] a) M. Abe, K. Kawashima, K. Kozawa, H. Sakai, K. Kaneko, *Langmuir* **2000**, *16*, 5059–5063; b) V. Budarin, J. H. Clark, S. J. Tavener, K. Wilson, *Chem. Commun.* **2004**, 2736–2737.
[18] a) R. S. Mikhail, S. Brunauer, E. E. Bodor, *J. Colloid Interface Sci.* **1968**, *26*, 45–53; b) E. P. Barrett, L. G. Joyner, P. P. Halenda, *J. Am. Chem. Soc.* **1951**, *73*, 373–380; c) P. J. Reucroft, W. H. Simpson, L. A. Jonas, *J. Phys. Chem.* **1971**, *75*, 3526–3531.

 © 2006 Wiley-VCH Verlag GmbH & Co. KGaA, Weinheim

Optical Resolution

DOI: 10.1002/anie.200503054

Hermaphroditic Chirality of a D_2-Symmetric Saddle-Shaped Porphyrin in Multicomponent Spontaneous Optical Resolution: Inclusion Cocrystals with Double-Helical Porphyrin Arrays

*Yukitami Mizuno, Md. Akhtarul Alam, Akihiko Tsuda, Kazushi Kinbara, Kentaro Yamaguchi, and Takuzo Aida**

Spontaneous optical resolution is an interesting chiral-recognition event in which racemic compounds are crystallized to form homochiral assemblies (conglomerates) of individual enantiomers.[1,2] Thus, optically pure compounds are produced without any assistance from chiral environments. However, because the homochiral association event involves a large entropy loss ($RT\ln 2$), only 10% of chiral compounds have been resolved by this crystallization method.[3–5] Herein we report an interesting example of multicomponent spontaneous optical resolution involving two or three chiral components by using a compound with hermaphroditic chirality. Fully substituted porphyrins such as **1** are known to adopt a saddle shape owing to steric repulsion among the neighboring substituents on the porphyrin periphery.[6–9] Thus, porphyrin **1** with two different aryl groups at the adjacent meso positions exhibits molecular chirality (symmetry group D_2).[10–12] However, because of a rapid saddle-to-saddle macrocyclic inversion, **1** frequently switches back and forth between its two enantiomeric forms in solution. Temperature-dependent ^{1}H NMR spectroscopic studies allowed the evaluation of the activation energy for the macrocyclic inversion as 18.1 ± 0.2 kcal mol^{-1} at 110 °C for ordinary saddle-shaped porphyrins.[6] On the other hand, hydrogen-bonding interactions of **1** with chiral carboxylic acids such as (*R*)- or (*S*)-mandelic acid shift the above equilibrium toward the diastereomeric complex with higher thermodynamic stability.[10–12] Thus, **1** can be regarded as a hermaphroditic chiral host,[13,14] as it can accommodate either enantiomeric form of chiral carboxylic acids by stereochemical macrocyclic inversion (Scheme 1). During the course of an X-ray crystallo-

[*] Dr. Y. Mizuno, Dr. Md. A. Alam, Dr. A. Tsuda, Dr. K. Kinbara, Prof. Dr. T. Aida
Department of Chemistry and Biotechnology
School of Engineering, The University of Tokyo
7-3-1 Hongo, Bunkyo-ku, Tokyo 113-8656 (Japan)
Fax: (+81) 3-5841-7310
E-mail: aida@macro.t.u-tokyo.ac.jp
Prof. Dr. K. Yamaguchi[+]
Department of Pharmaceutical Technology
Faculty of Pharmaceutical Sciences at Kagawa Campus
Tokushima Bunri University
Shido, Sanuki, Kagawa 769-2193 (Japan)
[+] Responsible for X-ray crystallographic analysis.

Supporting information for this article is available on the WWW under http://www.angewandte.org or from the author.

WILEY InterScience DISCOVER SOMETHING GREAT
© 2006 Wiley-VCH Verlag GmbH & Co. KGaA, Weinheim

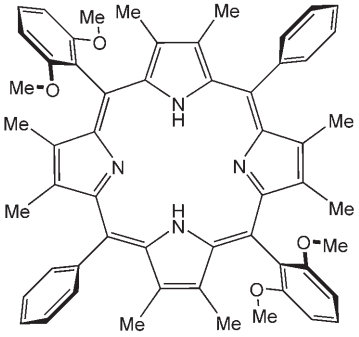

1

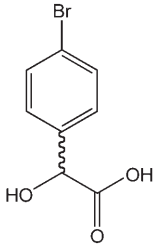

BrMA

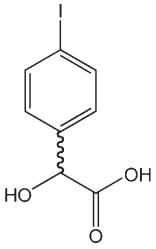

IMA

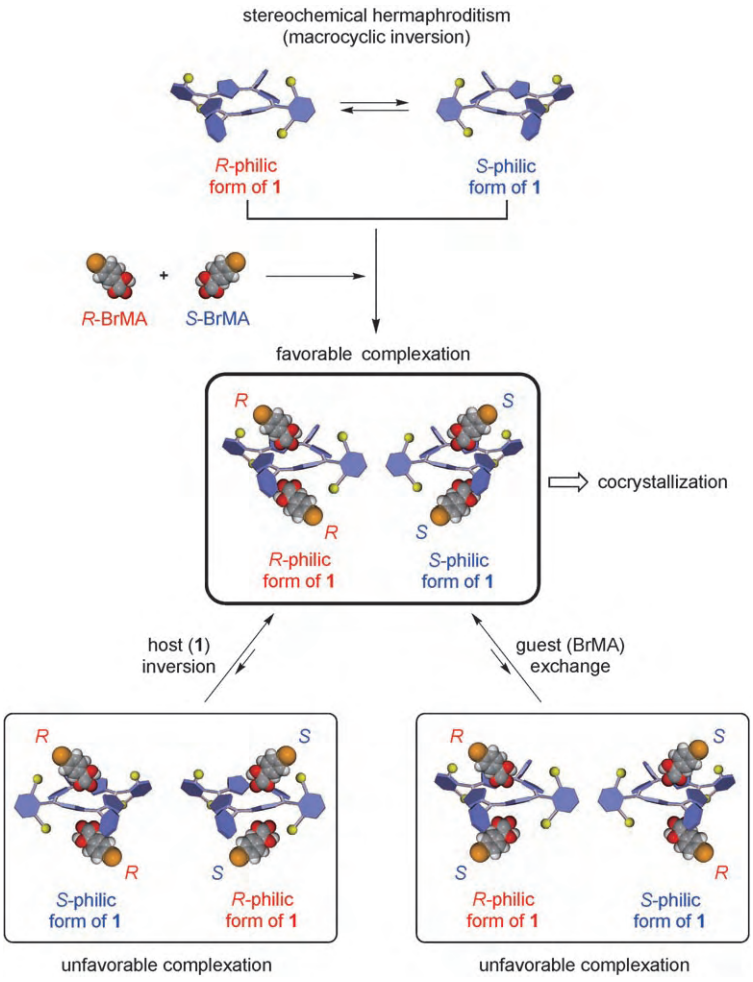

Scheme 1. Schematic representation of asymmetric hydrogen-bonding interactions between **1** and *rac*-BrMA.

graphic study on saddle-shaped chiral porphyrins, we noticed that **1** and racemic mandelic acid derivatives such as bromo- and iodomandelic acids, upon mixing in ethyl acetate (EtOAc), undergo spontaneous binary optical resolution to form solvent-included porous cocrystals consisting of gigantic double-helical porphyrin arrays. Analogous inclusion cocrystals are formed in a chiral ester solvent, with the solvent included in each cocrystal being optically enriched as the third chiral component. We also report results of a study on enantioselective guest inclusion under vapor-diffusion conditions.

When a solution of a mixture of **1** and racemic 4-bromomandelic acid (*rac*-BrMA) (1:2.1) in EtOAc was heated at 80 °C and then allowed to stand at room temperature for 2 days, green-blue prismatic crystals composed of **1** and BrMA formed. The stereochemical profile of this crystallization can be obtained readily with CD spectroscopy, as **1**, upon interaction with chiral carboxylic acids, displays highly enhanced CD bands in the visible region, the signs of which reflect the absolute structures of the guest acids.[10,11]

As the optical activity of **1** is preserved even after the replacement of the interacting chiral with achiral carboxylic acids (chirality memory),[10–12] the optical purity of **1** can be evaluated with CD spectroscopy in, for example, acetic acid (AcOH) without any interfering effects from other existing chiral components. Thus, 10 selected crystals formed from a mixture of **1** and *rac*-BrMA were dissolved in AcOH, and we found that each crystal was optically active and displayed a CD spectral profile that is identical in shape and intensity to that obtained from a reference cocrystal prepared from **1** and either (*R*)- or (*S*)-BrMA (Figure 1a). Therefore, both **1** and BrMA in each crystal are optically resolved (spontaneous binary optical resolution).

Figure 2a shows the structure obtained by single-crystal X-ray crystallography of the complex formed by mixing **1** and *rac*-BrMA in EtOAc. The structure of the cocrystal belongs to the chiral space group *C*2.[15] The porphyrin skeleton clearly adopts a saddle-shaped conformation with the four pyrrole units pointing up and down alternately with respect to the least-squares plane of the porphyrin. Furthermore, the complex involves two BrMA molecules, each hydrogen bonded in a monodentate fashion to the opposing pyrrole NH functionalities in **1**. The BrMA moieties on both sides of **1** are homochiral to one another (*R* configuration in Figure 2a), although the BrMA added is racemic. The phenyl group of each BrMA moiety is orientated toward the least-hindered section of the host molecule, which bears a nonsubstituted phenyl group, whereas the hydrogen atom at the stereogenic center of BrMA points toward the most-hindered section, which contains a bulky 2,6-dimethoxyphenyl group. The BrMA moiety on one side of **1** adopts a *syn* orientation to that on the other, so that the complex takes on a twisted pyramidal shape. Figure 3a shows a crystal-packing diagram of the complex. The crystal appears to consist of pseudohexagonal porphyrin columns, which are packed to form a honeycomb structure through the sharing of each corner with neighboring columns. Interestingly, the side view of the crystal packing (Figure 3b) reveals that each column consists of one-handed double-helical arrays of the saddle-shaped porphyrin. The diagram also indicates that the solvent molecules (red

 © 2006 Wiley-VCH Verlag GmbH & Co. KGaA, Weinheim

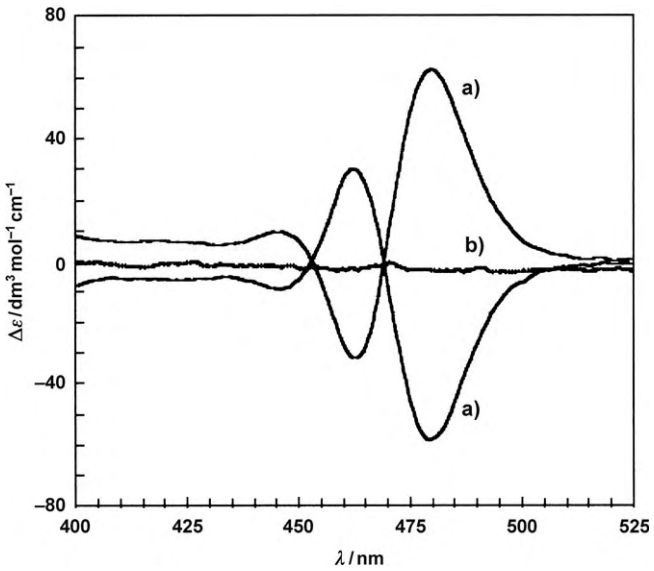

Figure 1. CD spectra of the single crystals of the hydrogen-bonded complexes of **1** with BrMA (1:2) in AcOH at 23 °C, formed upon cocrystallization in a) EtOAc and b) MeCN, with **1**/*rac*-BrMA = 1:2.1.

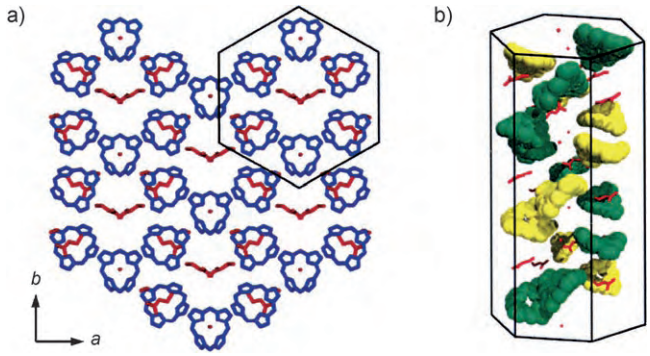

Figure 3. a) Crystal-packing diagram, viewed along the crystallographic *c* axis, of a hydrogen-bonded complex of **1** with BrMA (1:2), formed upon cocrystallization in AcOEt with **1**/*rac*-BrMA = 1:2.1. b) Side view of a porphyrin column in the crystal-packing diagram. BrMA and peripheral substituents of **1** are omitted for clarity. Solvent molecules are in red.

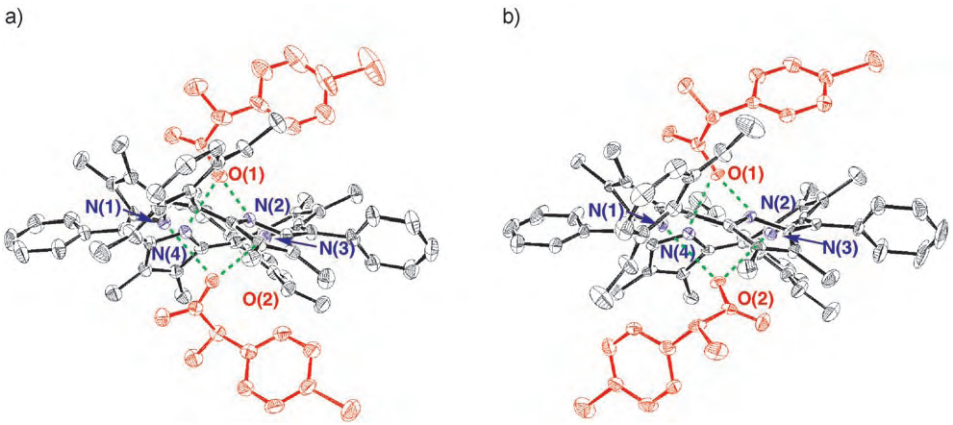

Figure 2. ORTEP diagrams of hydrogen-bonded complexes (1:2) of **1** (black) with BrMA (red), formed upon cocrystallization in a) EtOAc and b) MeCN, with **1**/*rac*-BrMA = 1:2.1 (the structure in a) was extracted from the asymmetric unit containing 1.5 units of the 1:2 complex). Green broken lines represent hydrogen bonds. The hydrogen atoms are omitted for clarity, while the remaining atoms are represented by anisotropic displacement parameter ellipsoids at a 30% probability level. The asymmetric carbon atoms of the mandelate moieties in these diagrams both adopt the *R* configuration. Selected interatomic distances [Å]: a) N(2)–O(1) 2.761(3), N(4)–O(1) 2.865(3), N(1)–O(2) 2.825(3), N(3)–O(2) 2.817(4); b) N(2)–O(1) 2.809(5), N(4)–O(1) 2.817(5), N(1)–O(2) 2.793(5), N(3)–O(2) 2.832(6).

bars) are included in the cocrystal with EtOAc/**1** = 3:2, as determined by ^{1}H NMR spectroscopy.[16] Two molecules of EtOAc are in the central nanoscopic channel of each column at every helical turn, and four such molecules are located within the column wall and shared by the neighboring columns.

As described earlier, the cocrystallization of **1** with *rac*-BrMA can be simplified substantially by taking advantage of the dynamic stereochemical duality of **1** (Scheme 1).[10–12] In general, when a racemic host (*rac*-**H**) binds two molecules of a racemic guest (*rac*-**G**), three association events (events 1–3) that generate six different stereoisomers result. These events are homochiral complexation of **H** with two homochiral **G** molecules to give (*R*)-**H**/((*R*)-**G**)$_2$ and (*S*)-**H**/((*S*)-**G**)$_2$ (event 1), heterochiral complexation of **H** with two homochiral **G** molecules to give (*S*)-**H**/((*R*)-**G**)$_2$ and (*R*)-**H**/((*S*)-**G**)$_2$ (event 2), and heterochiral complexation of **H** with two heterochiral **G** molecules to give (*R*)-**H**/((*R*)-**G**/(*S*)-**G**) and (*S*)-**H**/((*R*)-**G**/(*S*)-**G**) (event 3). In the interaction of **1** with BrMA, event 3, which would form **1**·(*R*)-BrMA·(*S*)-BrMA, does not occur, because the two binding sites of **1** are homochiral to one another, so **1** would be either *R*- or *S*-philic and would not trap both (*R*)- and (*S*)-BrMA together. Besides this stereochemical regulation, **H** has a hermaphroditic chirality and can readily invert its configuration when complex **HG**$_2$ is sterically unfavorable (Scheme 1). Consequently, either event 1 or 2 is preferred. These two regulations operate in the solution containing **1** and *rac*-BrMA and substantially lower the number of chiral species actively involved in the cocrystallization event.

We found that the solvent for cocrystallization significantly affects the optical resolution event. For example, replacing EtOAc with acetonitrile (MeCN) as the solvent resulted in the formation of cocrystals between **1** and *rac*-BrMA that were optically inactive (Figure 1b). Figure 2b shows an ORTEP diagram of the complex formed in MeCN. The structure of the cocrystal belongs to the achiral space group $P\bar{1}$.[15] As with the cocrystal formed in EtOAc (Figure 2a), the saddle-shaped porphyrin is hydrogen bonded to two molecules of BrMA, which are homochiral to one another (*R* configuration in Figure 2b). Furthermore, the orientation of the BrMA moiety relative to the shape of the chiral binding site of **1** is virtually identical to that in the cocrystal formed in EtOAc. However, the BrMA

 © 2006 Wiley-VCH Verlag GmbH & Co. KGaA, Weinheim

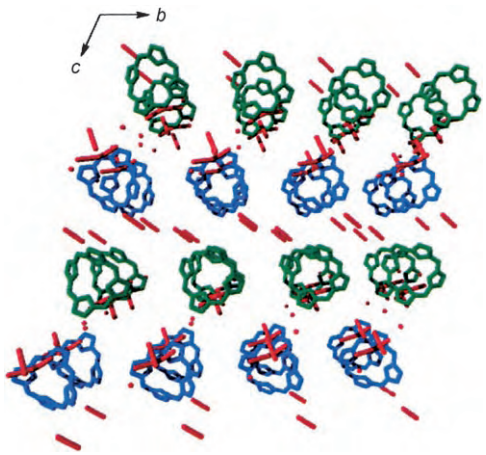

Figure 4. Crystal-packing diagram, viewed along the crystallographic *a* axis (perspective), of a hydrogen-bonded complex of **1** with BrMA (1:2), formed upon cocrystallization in MeCN with **1**/*rac*-BrMA = 1:2.1. BrMA and the peripheral substituents of **1** are omitted for clarity. The saddle-shaped porphyrin skeletons with opposite configurations are in blue and green, and the solvent molecules are in red.

moieties on both sides of **1** adopt an *anti* orientation to one another, thereby making the hydrogen-bonded complex highly symmetrical. Figure 4 shows a crystal-packing diagram of the complex. As with the case in EtOAc, the cocrystal includes MeCN molecules (red bars) with MeCN/**1** = 3:1, as determined by ^{1}H NMR spectroscopy. However, it adopts a lamellar structure consisting of alternately stacked porphyrin layers with opposite enantiomeric forms. Therefore, the cocrystal is racemic, as indicated by the achiral space group $P\bar{1}$.

The structure of the inclusion cocrystal in Figure 3b prompted us to explore the possibility of spontaneous ternary optical resolution, as the crystalline helical channels in the cocrystal may incorporate the third chiral component and allow its optical resolution. Thus, a chiral ester such as ethyl 2-methylbutanoate was chosen as the solvent for the cocrystallization of **1** with mandelic acid derivatives. After numerous trials, we found that **1** combined with racemic 4-iodomandelic acid (*rac*-IMA) undergoes spontaneous optical resolution in racemic ethyl 2-methylbutanoate. Each crystal was optically active, displaying in AcOH an identical CD spectrum to that of a reference **1**/IMA (1:2) complex prepared with either (*R*)- or (*S*)-IMA. ^{1}H NMR spectroscopy of a single crystal of the complex dissolved in $CDCl_3$ indicated that **1**/IMA = 1:2; the spectrum also showed signals due to included ethyl 2-methylbutanoate, with a molar ratio to **1** of 2:1. We dissolved several single crystals of the complex in $CHCl_3$ and subjected these solutions to chiral gas chromatography. Interestingly, the included chiral ester was no longer racemic but enriched in either the *R* or *S* enantiomer. The cocrystal with (*R*)-IMA preferentially included the *R* enantiomer of ethyl 2-methylbutanoate with 44% *ee*; likewise with (*S*)-IMA, the *S* enantiomer was preferentially included.[16] A preliminary crystal-structure analysis indicated that the structure of the cocrystal belongs to the chiral space group $P3_1$.[15,16] Although the solvent molecules are not visible crystallographically due to disordering, the crystal-packing diagram again indicates a honeycomb structure consisting of one-handed double-helical arrays of the saddle-shaped porphyrin. Therefore, ethyl 2-methylbutanoate, the third chiral component, is optically enriched most likely in such helical channels in the cocrystal formed from **1** and IMA.

On the basis of the above observations, we investigated the potential of the inclusion cocrystal of **1** and BrMA, spontaneously resolved in EtOAc (Figure 3), as a chiral organic zeolite for asymmetric separation. Thus, an EtOAc-included single cocrystal of **1** with (*S*)-BrMA was selected and exposed to a vapor of racemic methyl 2-methylbutanoate at 23 °C. Whereas the cocrystal remained glossy and preserved its original appearance, ^{1}H NMR spectroscopy indicated that the solvent molecules initially included in the cocrystal were completely replaced by the chiral ester within 4 h (methyl 2-methylbutanoate/**1** = 3:2).[16] Chiral gas chromatography of a solution of the resulting cocrystal in $CHCl_3$ showed that the newly included chiral guest was enriched in the *S* enantiomer with 50% *ee*. Guest exchange with an inclusion cocrystal prepared with (*R*)-BrMA resulted in preferential incorporation of the opposite enantiomer with comparable enantioselectivity (46% *ee*). Similar results were obtained with other chiral esters such as ethyl 2-methylbutanoate (44% *ee*) and 1-methylpropyl acetate (48% *ee*). Although several synthetic polymers with helical conformations[17–19] perform excellently in chiral separation[20,21] and sensing,[22,23] successful examples of solid materials with helical pores[24–27] are extremely limited, even when chiral solids with nonhelical pores[28] are taken into account.

In conclusion, we have demonstrated a novel example of multicomponent spontaneous optical resolution by taking advantage of the stereochemical hermaphroditism of a D_2-symmetric saddle-shaped chiral porphyrin **1**. The unique stereochemical regulation owing to the hermaphroditic character of **1** substantially decreases the complexity of the crystallization event involving two or three chiral compounds. The hermaphroditic chirality reported herein will give new insight into chiral recognition.[29] Application of the resulting porous cocrystal with a helical element to photosensitized asymmetric catalysis may be an interesting subject worthy of further investigation.

Received: August 27, 2005
Revised: February 17, 2006
Published online: May 3, 2006

Keywords: chiral recognition · chirality · host–guest systems · optical resolution · porphyrinoids

[1] P. Newman, *Optical Resolution Procedures for Chemical Compounds, Vol. 1–3*, Optical Resolution Information Center, New York, **1978**, **1981**, and **1984**.
[2] J. Jacques, A. Collet, S. H. Wilen, *Enantiomers, Racemates, and Resolutions*, Krieger Publishing, Florida, **1994**.
[3] T. Watanabe, S. Hayashi, S. Ouchi, S. Senoo, *Chem. Abstr.* **1974**, *80*, 71099.
[4] C. H. Wong, K. T. Wang, *Tetrahedron Lett.* **1978**, *19*, 3813.

 © 2006 Wiley-VCH Verlag GmbH & Co. KGaA, Weinheim

[5] J. Jacques, M. Leclercq, M. J. Brienne, *Tetrahedron* **1981**, *37*, 1727.
[6] K. M. Barkigia, M. D. Berber, J. Fajer, C. J. Medforth, M. W. Renner, K. M. Smith, *J. Am. Chem. Soc.* **1990**, *112*, 8851.
[7] M. O. Senge, T. P. Forsyth, L. T. Nguyen, K. M. Smith, *Angew. Chem.* **1994**, *106*, 2554; *Angew. Chem. Int. Ed.* **1994**, *33*, 2485.
[8] K. M. Barkigia, J. Fajer, M. D. Berber, K. M. Smith, *Acta Crystallogr. Sect. C* **1995**, *51*, 511.
[9] D. J. Nurco, C. J. Medforth, T. P. Forsyth, M. M. Olmstead, K. M. Smith, *J. Am. Chem. Soc.* **1996**, *118*, 10918.
[10] Y. Furusho, T. Kimura, Y. Mizuno, T. Aida, *J. Am. Chem. Soc.* **1997**, *119*, 5267.
[11] Y. Mizuno, T. Aida, K. Yamaguchi, *J. Am. Chem. Soc.* **2000**, *122*, 5278.
[12] Y. Mizuno, T. Aida, *Chem. Commun.* **2003**, 20.
[13] A. Merlic, J. C. Walsh, D. J. Tantillo, K. N. Houk, *J. Am. Chem. Soc.* **1999**, *121*, 3596.
[14] M. Consuelo Jiménez, C. Dietrich-Buchecker, J.-P. Sauvage, A. De Cian, *Angew. Chem.* **2000**, *112*, 1351; *Angew. Chem. Int. Ed.* **2000**, *39*, 1295.
[15] CCDC-282284 (*C*2), CCDC-282285 ($P\bar{1}$), and CCDC-282286 ($P3_1$) contain the supplementary crystallographic data for this paper. These data can be obtained free of charge from The Cambridge Crystallographic Data Centre at www.ccdc.cam.ac.uk/data_request/cif.
[16] See Supporting Information.
[17] R. J. M. Nolte, A. J. M. van Beijnen, W. Drenth, *J. Am. Chem. Soc.* **1974**, *96*, 5932.
[18] H. Yuki, K. Ohta, Y. Okamoto, K. Hatada, *J. Polym. Sci. Polym. Lett. Ed.* **1977**, *15*, 589.
[19] Y. Okamoto, K. Suzuki, K Ohta, K. Hatada, H. Yuki, *J. Am. Chem. Soc.* **1979**, *101*, 4763.
[20] E. Yashima, C. Yamamoto, Y. Okamoto, *Synlett* **1988**, 344.
[21] Y. Okamoto, E. Yashima, *Angew. Chem.* **1998**, *110*, 1072; *Angew. Chem. Int. Ed.* **1998**, *37*, 1020.
[22] E. Yashima, T. Matsushima, Y. Okamoto, *J. Am. Chem. Soc.* **1995**, *117*, 11596.
[23] E. Yashima, K. Maeda, Y. Okamoto, *Nature* **1999**, *399*, 449.
[24] R. Bishop, *Comprehensive Supramolecular Chemistry*, *Vol.* 6, Elsevier, Oxford, **1996**.
[25] R. Bishop, I. G. Dance, *Top. Curr. Chem.* **1998**, *149*, 137.
[26] L. B. McCusker, Ch. Baerlocher, E. Jahn, M. Bulow, *Zeolites* **1991**, *11*, 308.
[27] T. E. Gier, X. Bu, P. Feng, G. D. Stucky, *Nature* **1998**, *395*, 154.
[28] J. S. Seo, D. Whang, H. Lee, S. I. Jun, J. Oh, Y. J. Jeon, K. Kim, *Nature* **2000**, *404*, 982.
[29] S. N. Black, L. J. Williams, R. J. Davey, F. Moffatt, R. V. H. Jones, D. M. McEwan, D. E. Sadler, *Tetrahedron* **1989**, *45*, 2677.

 © 2006 Wiley-VCH Verlag GmbH & Co. KGaA, Weinheim

Protein–Protein Interactions

DOI: 10.1002/anie.200503965

Discovery of Low-Molecular-Weight Ligands for the AF6 PDZ Domain**

Mangesh Joshi, Carolyn Vargas, Prisca Boisguerin, Annette Diehl, Gerd Krause, Peter Schmieder, Karin Moelling, Volker Hagen, Markus Schade, and Hartmut Oschkinat**

Despite their central role in most regulatory processes and disease mechanisms, protein–protein interactions (PPIs) remain largely unconquered ground for drug discovery and chemical-tool generation. In many cases, these interactions are mediated by protein interaction domains like Src homology 2 (SH2), Src homology 3 (SH3), WW domain, and postsynaptic density/discs large/zona occludens-1 (PDZ).[1] PDZ domains may be considered "drugable" because of a shallow ridge on their surface which is, however, not a proper cavity. Hence, they are good test cases for the development of PPI inhibitors.

PDZ domains comprise ≈90 residues and occur more than 450 times in approximately 250 human proteins. In most cases, they recognize the C terminal four to seven residues of membrane receptors and ion channels,[2–4] although they are also known to bind to internal sequence motifs.[5] Consisting of a six-stranded β-sheet flanked by two α helices, PDZ

[*] Dr. M. Schade
Combinature Biopharm AG
Robert-Roessle-Strasse 10, 13125 Berlin (Germany)
Fax: (+49) 30-94894-038
E-mail: schade@combinature.com

M. Joshi, C. Vargas, Dr. A. Diehl, Dr. G. Krause, Dr. P. Schmieder, Dr. V. Hagen, Prof. Dr. H. Oschkinat
Leibniz-Institut für Molekulare Pharmakologie FMP
Robert-Roessle-Strasse 10, 13125 Berlin (Germany)
Fax: (+49) 30-94793-169
E-mail: oschkinat@fmp-berlin.de

Dr. K. Moelling
Institut für Medizinische Virologie
Universität Zürich
8028 Zürich (Switzerland)

Dr. P. Boisguerin
Institut für Medizinische Immunologie
Charité-Universitätsmedizin Berlin
Hessische Strasse 3–4, 10115 Berlin (Germany)

[**] This work was supported by grants from the European Community (QLK3-2000-00924-SH2 Libraries) and the Deutsche Forschungsgemeinschaft (DFG) (OS 106/4-2). The authors thank Dietmar Leitner for assistance in NMR spectroscopic measurements, Arvid Soderhall and Jens Laettig for their help in molecular dynamics (MD) simulations, Viviane Uryga-Polowy for the MS measurements, and Daniel Geißler for helpful discussions. The structure of the AF6 PDZ domain is deposited in the protein data bank (PDB) under accession code 1XZ9 and the AF6 PDZ-**5 f** complex under accession code 2EXG.

Supporting information for this article is available on the WWW under http://www.angewandte.org or from the author.

WILEY InterScience DISCOVER SOMETHING GREAT
© 2006 Wiley-VCH Verlag GmbH & Co. KGaA, Weinheim

domains bind cognate peptides in an extended conformation whereby the terminal carboxy group is hydrogen bonded with the backbone amides of the highly conserved GLGF loop.[6–8] The protein AF6 (ALL-1 fusion partner on chromosome 6), also known as s-afadin,[9] contains one type II PDZ domain (abbreviated: AF6 PDZ), two N-terminal Ras-association (RA) domains, one forkhead-association (FHA) domain, and one dilute (DIL) domain. AF6 PDZ mediates interactions with a subset of ephrine-receptor protein-tyrosine kinases,[10,11] the poliovirus receptor-related protein PRR2/nectin,[12] the junctional adhesion molecule (JAM),[13] and the breakpoint-cluster-region protein (BCR).[14] It binds target peptides with comparatively low affinities in the 20–150 μM range.[4] When the C-terminal valine of full-length BCR is mutated to Ala, binding to full-length AF6 is abrogated in various cell-based assays.[14]

Herein, we report the identification of novel, low-molecular-weight ligands for the AF6 PDZ domain by NMR spectroscopy-based screening and chemical synthesis. These compounds are active in competition assays and represent building blocks for the design of tight-binding competitors. Furthermore, we have determined the solution structure of AF6 PDZ in complex with the ligand of highest affinity. The synthetic ligand induces the formation of a hydrophobic subpocket in AF6 PDZ that is absent in published structures of both apo and peptide-bound PDZ domains. This unexpected ligand–subpocket interaction redefines the protein's drugability and opens the door to small-molecule modulators for the entire family of PDZ domains.

We selected NMR spectroscopy-based screening as the hit discovery method of choice for the identification of weakly binding small organic frameworks because of its high sensitivity towards weakly binding ligands and unique structural support for a fragment-based lead-generation approach. In the first round of screening, a library of 5000 synthetic compounds was screened against uniformly ^{15}N-labeled protein by using 2D ^{1}H-^{15}N-heteronuclear single quantum correlation (HSQC) experiments. Three chemically distinct classes of binders were identified as indicated by the examples in Figure 1a. Comparison of the three compounds with the structure of the conserved C-terminal valine of natural peptide ligands (Figure 1b) revealed a consistent pharmacophore pattern of one moiety showing at least one hydrogen bond acceptor (red), a moiety showing one hydrogen bond donor (yellow), and a hydrophobic core of variable size. Compound **3** occurs in two tautomeric forms in aqueous solution (Figure 1a) and in organic solvents (Figure 1c), as observed by NMR spectroscopy.

In the second round of screening, initial structure–activity relationships (SAR) were obtained by assaying analogues within the remaining 15000 compounds of our fragment library and further commercially available compounds. Each of the three hit classes showed consistent SAR (data not shown). Hit compound **3** was selected for further optimization because of its comparatively high binding affinity and chemical tractability.

Derivatives of compound **3** were synthesized by condensation of 2-thioxo-4-thiazolidinone with a series of aldehydes according to the procedures described earlier[15,16] (Figure 1c). Some of the condensation products **4** (all *Z* isomers) were reduced to yield the racemates **5**, generating a more flexible linkage between the two ring systems. Normal-phase HPLC and a chiral column (Chiralpak IA, 5 μm, 250 × 4.6 mm^2, Chiral Technologies Europe) were used to separate the enantiomers of **5f**. Although this attempt was initially successful, interconversion produced the racemate again. Aldehydes were chosen to sample hydrophobic moieties of variable sizes in the R^1 position of **4** or **5**, ranging from a small isopropyl group to various substituted and unsubstituted aromatic ring systems (Table 1).

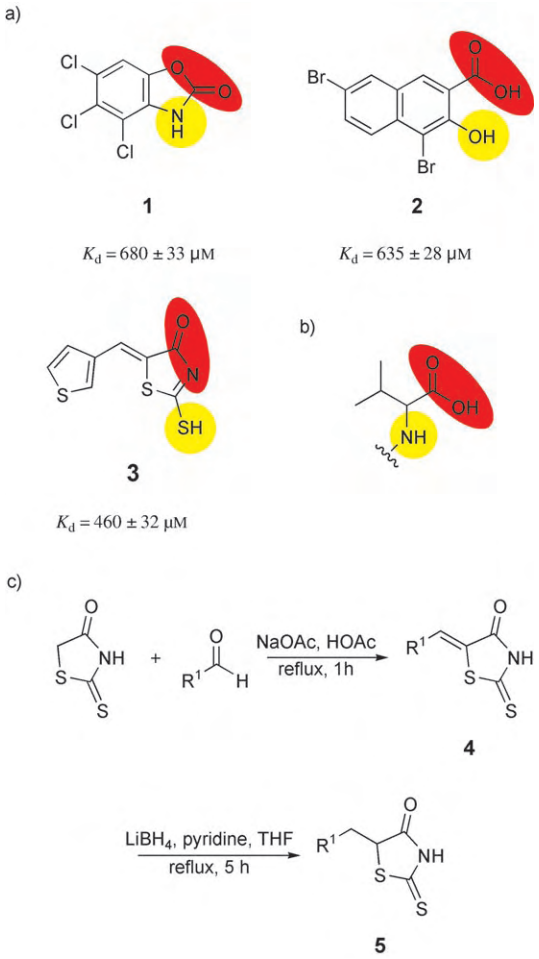

Figure 1. a) Novel ligands for the AF6 PDZ domain as identified by NMR spectroscopy-based screening (H-bond acceptors, red; H-bond donors, yellow). b) Structure of the conserved C-terminal valine of natural peptide ligands. c) Synthesis of 2-thioxo-4-thiazolidinone derivatives (for structures of R^1, see Table 1). Different tautomers owing to different solvents are shown in a) and c).

To monitor the binding activity of the **4** and **5** compound series initially, the chemical shift perturbation (CSP) of Leu25 HN was used. This residue is in the GLGF loop, in contact with the five-membered ring of the ligands (see below), and should hence be in a similar chemical environment in all investigated complexes. In the **4** compound series, the derivatives with a 3-thienyl (**4a**), *i*Pr (**4b**), C_6H_5 (**4c**), or 4-MeC_6H_4 (**4d**) substituent at the R^1 position showed weak chemical-shift changes for Leu25 HN. Compounds **4a** and **4c**

 © 2006 Wiley-VCH Verlag GmbH & Co. KGaA, Weinheim

Table 1: Structure-activity relationship of **4** and **5** compound series.

Compd	Compd[a]	R^1	CSP[b] of Leu 25 HN		Dissociation constant [μM]	
			4	**5**[a]	**4**	**5**[a]
4a	**5a**	3-thienyl	0.20	0.17	460 ± 32	–
4b	–	*i*Pr	0.27	–	–	–
4c	**5c**	C_6H_5	0.17	0.21	680 ± 58	576 ± 40
4d	–	4-MeC_6H_4	0.14	–	–	–
4e	–	3-MeC_6H_4	< 0.02	–	–	–
4f	**5f**	4-$CF_3C_6H_4$	0.50	0.88	348 ± 30	100 ± 12
4g	**5g**	3-$CF_3C_6H_4$	0.21	< 0.02	–	–
4h	**5h**	4-BrC_6H_4	0.24	–	–	–
4i	–	3-indolyl	< 0.02	–	–	–
4j	–	4-PhC_6H_4	< 0.02	–	–	–

[a] Analyzed as racemic mixtures: (–) compound not synthesized or value not determined. [b] Chemical shift perturbation (CSP) in ppm units. CSPs < 0.02 ppm are considered inactive.

showed dissociation constants of 460 ± 32 and 580 ± 62 μM, respectively. Chemical-shift changes below 0.02 ppm were observed for derivatives with 3-MeC_6H_4 (**4e**), the bulky indolyl group (**4i**), and 4-PhC_6H_4 (**4j**) as substituents and were categorized as nonbinding. Interestingly, the 4-$CF_3C_6H_4$ (**4f**)-, 3-$CF_3C_6H_4$ (**4g**)-, and 4-BrC_6H_4 (**4h**)-substituted derivatives showed binding.

Significantly, improved binding to AF6 PDZ was observed when compound **4f** was reduced to **5f**. The *para*-substitution of the phenyl ring in **5** in the R^1 position by a trifluoromethyl (CF_3) is important for binding. In the **5** compound series, however, the 3-$CF_3C_6H_4$-substituted derivative (**5g**) showed negligible CSPs. Taken together, a five-membered ring system with hydrogen bond accepting capacity is critical for activity, and **5** with 4-$CF_3C_6H_4$ substitution in the R^1 position (**5f**) showed the tightest binding of the compounds investigated. By using the racemic mixture of **5f**, we determined a dissociation constant of 100 μM. Assuming that only one of the enantiomers binds preferentially, its dissociation constant may be approximated to 50 μM, which is in the same range as that of the natural peptide ligands.

To demonstrate that **5f** binds competitively to the AF6 PDZ domain, a series of ^{15}N-filtered 1D spectra with increasing amounts of **5f** were recorded on a sample containing equimolar concentrations of U-^{15}N-labeled AF6 PDZ and the natural peptide ligand[10,4] ($_{NH2}$-IQSVEV-$_{COOH}$). Figure 2 shows the result of the titration experiment, in which only signals from the ^{14}N and carbon-bound protons appear. The peptide signal at $\delta = 8.1$ ppm, which vanishes in the presence of the protein, re-emerges with increasing **5f** concentration. In addition, the signals at $\delta =$ 8.3 ppm and $\delta = 7.6$ ppm revert back to the "unbound" state (black arrows). The other signals of the peptide could not be observed as well because of the overlap with the aromatic protons of the protein or **5f** (gray arrows). This experiment proves that the peptide ligand is ejected from the protein's binding groove by **5f**.

To understand the binding mode of compounds **5** at atomic resolution, we determined the solution structure of the complex between AF6 PDZ and **5f** (see the Supporting Information). The structure is well defined by 11.8 inter-residual NOEs per amino acid. The ensemble of the 20 lowest-energy structures has a mean α-carbon root-mean-square deviation (rmsd) of 0.31 ± 0.09 Å for the well-structured regions (residues 11–28, 40–70, 77–95) and 1.21 ± 0.23 Å for all heavy atoms (Table 2). The overall structure of the AF6 PDZ domain in complex with **5f** is similar to other PDZ structures.[6,8,17] The protein has six β strands (βA to βF) and two α helices (αA, αB) (see the Supporting Information).

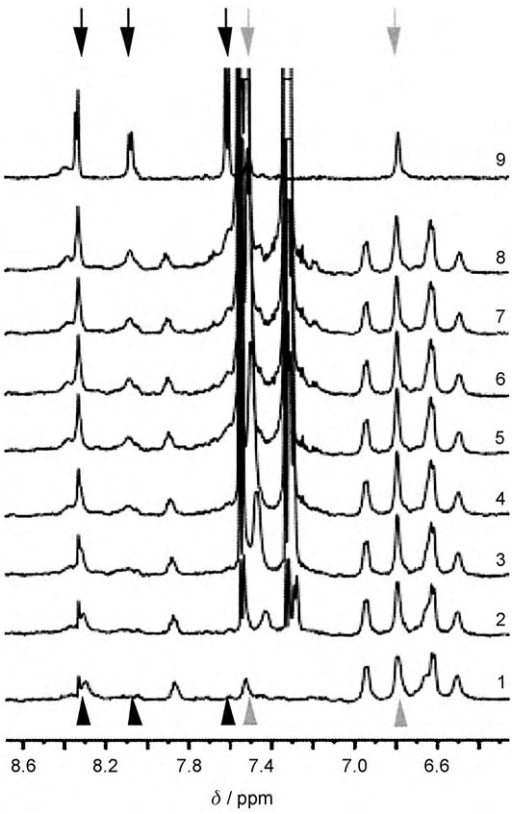

Figure 2. Competition experiment with the AF6 PDZ domain, $_{NH_2}$-IQSVEV-$_{COOH}$ peptide ligand, and **5f**. 1) 100 μM peptide and 100 μM AF6 PDZ domain; 2–8) Spectra recorded at 100, 200, 400, 600, 800, 1000, and 1400 μM concentrations of **5f**, respectively; 9) ^1H NMR spectrum of the peptide (100 μM).

The binding mode of **5f** complexed to AF6 PDZ is defined by 11 intermolecular NOEs obtained from 2D ^{13}C-F2-filtered NOESY and 2D ^{13}C-F2-filtered HMQC-NOESY spectra. Since the signal of 5-H of **5f** overlaps with the water signal, only NOEs to 8-H/12-H and 9-H/11-H, which are degenerate in the bound state, were extracted from the spectra. All 11 intermolecular NOEs occur between these degenerate protons, 8-H/12-H and 9-H/11-H, and the side-chain protons of Met 23, Leu 25, Ile 27, Ala 80, Met 83, and Thr 84. As the thiazolidinone ring did not show NOE restraints, its location was determined by computational docking of the whole molecule utilizing all observed NMR spectroscopic data. By enforcing the 11 intermolecular NOE restraints, we docked the *R* and *S* enantiomers of **5f** into the lowest-energy AF6 PDZ structure in a constrained MD simulation lasting for 2 ns using Amber 8.[20] The tautomeric form of **3** (Figure 1) was chosen for the simulations as the

 © 2006 Wiley-VCH Verlag GmbH & Co. KGaA, Weinheim

Table 2: Structural statistics of AF6 PDZ-**5 f** complex.

Restraints	
total no. of experimental restraints	1518
total no. of NOE restraints	1440
intraresidue ($i=j$)	428
sequential ($\|i-j\|=1$)	390
medium-range ($2\leq\|i-j\|\leq 5$)	151
long-range ($\|i-j\|>5$)	471
no. of H-bond restraints	14
no. of dihedral angle restraints (TALOS)	64
average inter-residual NOEs per residue	12
no. of NOE violations >0.3 Å	0
no. of dihedral angle violations $>5°$	0
$\phi-\psi$ Space (residues)[a,b]	
most favored regions [%]	70.3
additionally allowed regions [%]	22.5
generously allowed regions [%]	6.3
disallowed regions [%]	1.0
rmsd values[c,d]	
Cα	0.31 ± 0.09
heavy atoms	1.21 ± 0.23

[a] Residues considered: 11–95. [b] From Procheck-NMR.[18] [c] Residues considered: 11–17, 25–29, 40–46, 60–66, 69–72, and 77–95. [d] Calculated by using MOLMOL.[19]

experiments were done in aqueous solution. During docking, the backbone of the protein was kept rigid and the side chains of the residues were restrained by using the same distance constraints as in the Cyana structure calculation. The total energy obtained for the complex was significantly higher for the *S* enantiomer than for the *R* enantiomer, suggesting that the *R* enantiomer of **5 f** is the active binder.

The final complex structure shows the 4-$CF_3C_6H_4$ group of **5 f** embedded in a deep hydrophobic pocket surrounded by the side chains of residues Met 23, Leu 25, Ile 27, Ala 80, Met 83, Val 90, and Leu 92 (Figure 3 b and c). N3 and O4 of **5 f** form H-bonds with the backbone HNs of residues Gly 24 and Leu 25, respectively, which belong to the conserved GLGF loop (GMGL in the case of AF6 PDZ). The SH group is involved in hydrophobic interactions. It also explains the lower affinity of compounds **5 a** and **5 c** as compared to **5 f** because of incomplete occupancy of the protein's hydrophobic pocket. The weak binding of **5 g** can be attributed to steric hindrance because the *meta*-substituted ring would require a larger hydrophobic cavity for binding.

To better understand the binding mode of **5 f**, we compared the structures of the AF6 PDZ domain in the ligand-free (see the Supporting Information) and ligand-bound forms. Although the superposition of the structures with the lowest Cyana target function show a good overall agreement with an α-carbon rmsd of 1.25 Å for the β strands, three areas of significant deviation located in αA, αB, and βE were observed. Upon binding of **5 f**, the Cα atom of Gln 76 at the beginning of αA was displaced by 3.3 Å, which results in the widening of the peptide-binding groove (Figure 4 a). In addition, closer inspection of the superimposed structures reveals significant side-chain rearrangements of residues Met 23, Leu 25, and Met 83 and a backbone rearrangement for the residue Ala 80 in the ligand-binding groove to accommodate the bulky 4-$CF_3C_6H_4$ group of **5 f**. The side

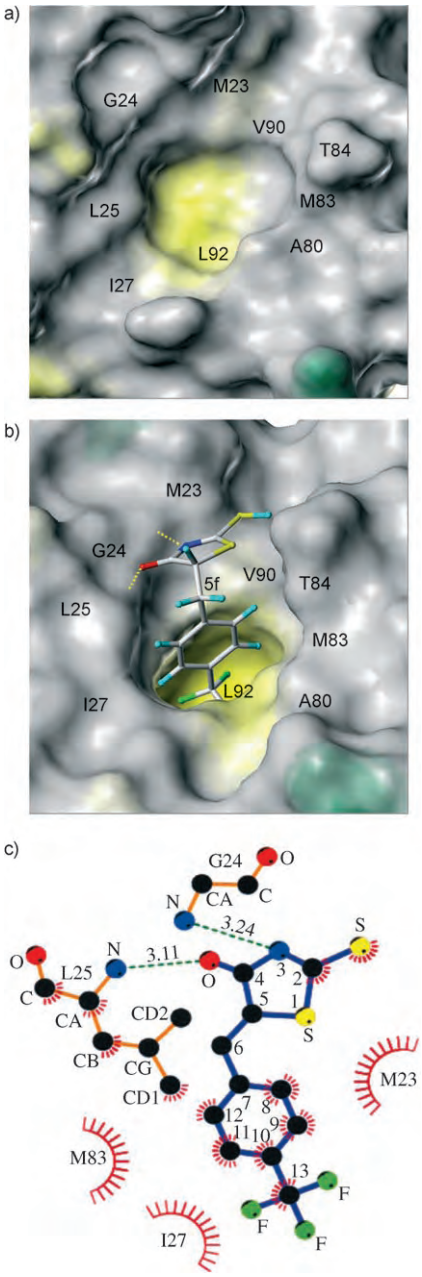

Figure 3. a) Surface representation of the AF6 PDZ domain without ligand, 1XZ9. Surface coloring indicates hydrophobic (yellow) and hydrophilic (green) areas. b) AF6 PDZ domain in complex with **5 f**. Surface coloring indicates hydrophobic (yellow) and hydrophilic (green) areas. The hydrogen bonding interaction between the PDZ domain and **5 f** are shown as yellow-dotted lines. c) Schematic representation of the AF6 PDZ-**5 f** interaction. Hydrogen bonds are shown as green-dotted lines. Hydrophobic interactions are highlighted by red line fences. The Figure was generated by using the program Ligplot.[21]

chains of the other hydrophobic residues lining this pocket (Ile 27, Val 90, and Leu 92) are virtually unchanged. As a consequence, **5 f** triggers an induced-fit rearrangement to shape a new hydrophobic pocket without unbound AF6 PDZ.

To gain insight into the possible interaction between **5 f** and other classes of PDZ domains and to aid the structure-

 © 2006 Wiley-VCH Verlag GmbH & Co. KGaA, Weinheim

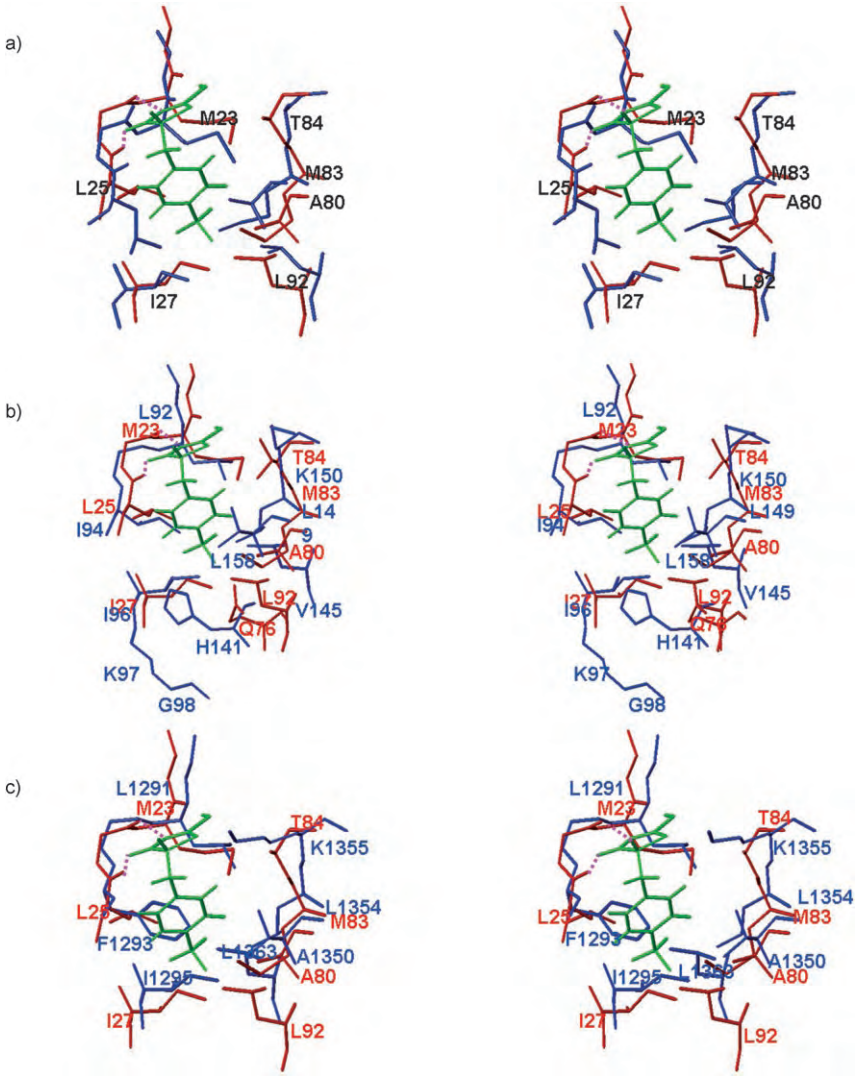

Figure 4. a) Comparison of AF6 PDZ in ligand-free (blue) and ligand-bound (red) state (stereoview). b) Comparison of AF6 PDZ ligand-bound (red) state and syntrophin PDZ domain bound to nNOS β-finger, 1QAV, blue, n-NOS β-finger not shown (stereoview). c) Comparison of AF6 PDZ ligand-bound (red) state and erbin PDZ domain bound to Erbb2 receptor peptide, 1MFG, blue, peptide not shown (stereoview).

based extension of **5f** for developing specific ligands, we compared the structure of AF6 PDZ in the ligand-bound form to the crystal structures of the syntrophin (1QAV)[5] and erbin (1MFG)[22] PDZ domains in complex with their respective ligands. AF6 PDZ in the ligand-bound form superimposes rather well with the two other PDZ domains with rmsd values of 1.7 and 1.5 Å, respectively. In the structure of the syntrophin PDZ domain, the residues homologous to Met 23, Leu 25, Ile 27, Ala 80, Met 83, Thr 84, and Leu 92 adopt similar positions (Figure 4b). Only Leu 149 undergoes a slight side-chain rearrangement to accommodate the 4-$CF_3C_6H_4$ group of **5f**, suggesting that it may interact similarly with **5f**. Indeed, weaker binding of **5f** to the syntrophin PDZ domain ($K_d = 270 \pm 21$ μM) was observed in an NMR spectroscopic screening experiment. In the syntrophin PDZ domain, His 141 narrows the peptide-binding groove at the homologous position of Gln 76 in AF6 PDZ, suggesting that variation of **5f** specifically designed to interact with either His 141 or Gln 76 may be helpful in developing specific ligands for either of the two domains.

In the structure of the erbin PDZ domain, the bulky side chain of Phe 1293, which is homologous to Leu 25 of our AF6 PDZ construct, severely clashes with the CF_3 moiety of **5f** (Figure 4c). As the conformational freedom of the Phe 1293 side chain is limited, specificity may be controlled by the CF_3 group or related moieties. Other residues including the homologues of Ile 27 and Ala 80, which play an important role in the recognition of hydrophobic residues in the −2 position with respect to the C-terminal residue of cognate peptides, show similar orientations, thus being less-promising interaction points for the design of specific ligands.

By using NMR spectroscopic screening, we identified three chemically distinct classes of compounds binding to the challenging PPI target AF6 PDZ. We improved a 2-thioxo-4-thiazolidinone derivative to become a 100-μM K_d ligand with a molecular weight of 291 Da, and determined the solution structure of the *R* enantiomer complexed with AF6 PDZ. The 3D structure reveals a new hydrophobic subpocket formed through induced-fit binding of **5f**. This finding redefines the drugability of PDZ domains and discloses 5-aryl-2-thioxo-4-thiazolidinones and related frameworks as promising candidates for the development of potent and selective small-molecule modulators of individual domains from the large PDZ family.

Experimental Section

All NMR spectroscopic experiments were performed at 295 K on Bruker DRX600 and DMX750 spectrometers in standard configuration by using triple-resonance probes equipped with self-shielded gradient coils. Two samples of 1.5 mM U-^{15}N, ^{13}C-labeled AF6 PDZ with **5f** (1:1 protein/ligand) at pH 6.5 in Na phosphate buffer solution (20 mM) with NaCl (50 mM) and dimethyl sulfoxide (DMSO; 10% v/v) either in D_2O (99.98% v/v) or H_2O/D_2O (90:10% v/v).

Backbone chemical-shift assignments for the complex were achieved as described earlier.[4] Side-chain assignments were obtained from 3D HCCH-COSY, HCCH-TOCSY (100 ms), and ^{13}C-edited NOESY (80 ms) experiments recorded on a sample in D_2O (99.98% v/v); and from ^{15}N-edited NOESY (80 ms) spectra recorded on a sample in H_2O/D_2O (90:10% v/v).[23]

Data were processed by using XWIN-NMR (version 1.3, Bruker BioSpin GmbH, Rheinstetten, Germany) and analyzed by using SPARKY.[24] Structures were calculated from the restraints listed in Table 2 using CYANA.[25] The 20 lowest-energy structures without distance violations greater than 0.3 Å and no angle violations greater

 © 2006 Wiley-VCH Verlag GmbH & Co. KGaA, Weinheim

than 5° were accepted into the final ensemble. A total of 64 dihedral-angle restraints were obtained from backbone chemical shifts by using TALOS.[26] Furthermore, 14 hydrogen-bond restraints were identified from the NOE pattern in the 3D ^{13}C-edited NOESY spectrum.

^{15}N-labeled AF6 PDZ at 50 μM concentration in a 20 mM Na phosphate buffer solution containing NaCl (50 mM), and $[D]_6$DMSO (10% v/v) at pH 7.0 was used for screening experiments. Ligand binding was detected at 300 K by acquiring ^{1}H-^{15}N HSQC spectra in the presence and absence of compounds. Compounds were initially tested at 400 μM each in mixtures of 16 compounds, with subsequent deconvolution to mixtures of 4 compounds at 400 μM each and then to individual compounds. Spectra were acquired with 16 scans and 128 points in the indirect dimension on a Bruker DRX600 spectrometer equipped with a cryoprobe. Chemical-shift mapping of the binding site was achieved by comparing the shifts of protein alone to those of the protein in presence of ligands. Chemical shifts were quantified by using the formula $\Delta\delta = [(\Delta H)^2 + (\Delta N/5)^2]^{1/2}$, in which $\Delta\delta$ is the weighted chemical-shift change, and ΔH and ΔN are the chemical shift changes in the proton and the nitrogen dimensions, respectively. Dissociation constants were obtained for selected compounds by monitoring the chemical shift changes as a function of ligand concentration. Data were fit by using a one-site binding model. A nonlinear least-square optimization was performed by varying the values of K_d and the chemical shift of the fully saturated protein.

Received: November 8, 2005
Revised: January 26, 2006
Published online: May 3, 2006

Keywords: inhibitors · ligand effects · NMR spectroscopy · PDZ domains · protein structures

[1] T. Pawson, P. Nash, *Science* **2003**, *300*, 445 – 452.
[2] Z. Songyang, A. S. Fanning, C. Fu, J. Xu, S. M. Marfatia, A. H. Chishti, A. Crompton, A. C. Chan, J. M. Anderson, L. C. Cantley, *Science* **1997**, *275*, 73 – 77.
[3] B. Z. Harris, W. A. Lim, *J. Cell Sci.* **2001**, *114*, 3219 – 3231.
[4] U. Wiedemann, P. Boisguerin, R. Leben, D. Leitner, G. Krause, K. Moelling, R. Volkmer-Engert, H. Oschkinat, *J. Mol. Biol.* **2004**, *343*, 703 – 718.
[5] B. J. Hillier, K. S. Christopherson, K. E. Prehoda, D. S. Bredt, W. A. Lim, *Science* **1999**, *284*, 812 – 815.
[6] D. A. Doyle, A. Lee, J. Lewis, E. Kim, M. Sheng, R. MacKinnon, *Cell* **1996**, *85*, 1067 – 1076.
[7] M. Cabral, J. H. Petosa, M. J. Sutcliffe, S. Raza, O. Byron, F. Poy, S. M. Marfatia, A. H. Chishti, R. C. Liddington, *Nature* **1996**, *382*, 649 – 652.
[8] J. Schultz, U. Hoffmuller, G. Krause, J. Ashurst, M. J. Macias, P. Schmieder, J. Schneider-Mergener, H. Oschkinat, *Nat. Struct. Biol.* **1998**, *5*, 19 – 24.
[9] R. Prasad, Y. Gu, H. Alder, T. Nakamura, O. Canaani, H. Saito, K. Huebner, R. P. Gale, P. C. Nowell, K. Kuriyama, *Cancer Res.* **1993**, *53*, 5624 – 5628.
[10] B. Hock, B. Böhme, T. Karn, T. Yamamoto, K. Kaibuchi, U. Holtrich, S. Holland, T. Pawson, H. Rubsamen-Waigmann, K. Strebhardt, *Proc. Natl. Acad. Sci. USA* **1998**, *95*, 9779 – 9784.
[11] M. Buchert, S. Schneider, V. Meskenaite, M. T. Adams, E. Canaani, T. Baechi, K. Moelling, C. M. Hovens, *J. Cell Biol.* **1999**, *144*, 361 – 371.
[12] K. Takahashi, H. Nakanishi, M. Miyahara, K. Mandai, K. Satoh, A. Satoh, H. Nishioka, J. Aoki, A. Nomoto, A. Mizoguchi, Y. Takai, *J. Cell Biol.* **1999**, *145*, 539 – 549.
[13] K. Ebnet, C. U. Schulz, M. K. Meyer Zu Brickwedde, G. G. Pendl, D. Vestweber, *J. Biol. Chem.* **2000**, *275*, 27979 – 27988.
[14] G. Radziwill, R. A. Erdmann, U. Margelisch, K. Moelling, *Mol. Cell. Biol.* **2003**, *23*, 4663 – 4672.
[15] G. Bruno, L. Constantino, C. Curinga, R. Maccari, F. Manforte, F. Nicolò, R. Ottanà, M. G. Vigorita, *Bioorg. Med. Chem.* **2002**, *10*, 1077 – 1084.
[16] S. Kukolya, S. Draheim, B. Graves, D. Hunden, J. Pfeil, R. Cooper, J. Ott, F. Counter, *J. Med. Chem.* **1985**, *28*, 1896 – 1903.
[17] N. L. Stricker, K. S. Christopherson, B. A. Yi, P. J. Schatz, R. W. Raab, G. Dawes, D. E. Bassett Jr, D. S. Bredt, M. Li, *Nat. Biotechnol.* **1997**, *15*, 336 – 342.
[18] R. A. Laskowski, J. A. Rullmann, M. W. MacArthur, R. Kaptein, J. M. Thornton, *J. Biomol. NMR* **1996**, *8*, 477 – 486.
[19] R. Koradi, M. Billeter, K. Wüthrich, *J. Mol. Graphics* **1996**, *14*, 29 – 32.
[20] D. A. Case, T. A. Darden, T. E. Cheatham III, C. L. Simmerling, J. Wang, R. E. Duke, R. Luo, K. M. Merz, B. Wang, D. A. Pearlman, M. Crowley, S. Brozell, V. Tsui, H. Gohlke, J. Mongan, V. Hornak, G. Cui, P. Beroza, C. Schafmeister, J. W. Caldwell, W. S. Ross, P. A. Kollman, AMBER 8, University of California, San Francisco**, 2004**.
[21] M. S. Wallace, R. A. Laskowski, J. M. Thornton, *Protein Eng.* **1995**, *8*, 127 – 134.
[22] G. Birrane, J. Chung, J. A. Ladias, *J. Biol. Chem.* **2003**, *278*, 1399 – 1402.
[23] V. Kanelis, J. D. Forman-Kay, L. E. Kay, *IUBMB Life* **2001**, *52*, 291 – 302.
[24] T. D. Goddard, D. G. Kneller, SPARKY 3, *University of California*, *San Francisco* **2003**.
[25] P. Guntert, C. Mumenthaler, K. Wüthrich, *J. Mol. Biol.* **1997**, *273*, 283 – 298.
[26] G. Cornilescu, F. Delaglio, A. Bax, *J. Biomol. NMR* **1999**, *13*, 289 – 302.

 © 2006 Wiley-VCH Verlag GmbH & Co. KGaA, Weinheim

Water Chemistry

DOI: 10.1002/anie.200504159

Magic and Antimagic Protonated Water Clusters: Exotic Structures with Unusual Dynamic Effects**

*N. Jiten Singh, Mina Park, Seung Kyu Min, Seung Bum Suh, and Kwang S. Kim**

Protonated water species are key elements in dissociation and transport phenomena in aqueous chemistry and biological

[*] N. J. Singh, M. Park, S. K. Min, Dr. S. B. Suh, Prof. K. S. Kim
National Creative Research Initiative Center for Superfunctional Materials
Department of Chemistry
Division of Molecular and Life Sciences
Pohang University of Science and Technology
Pohang 790-784 (Korea)
Fax: (+82) 54-279-8137
E-mail: kim@postech.ac.kr

[**] This work was supported by CRI(KOSEF) and BK21. Most calculations were performed on supercomputers at KISTI.

Supporting information for this article is available on the WWW under http://www.angewandte.org or from the author.

© 2006 Wiley-VCH Verlag GmbH & Co. KGaA, Weinheim
InterScience

systems. The investigation of protonated clusters $[H(H_2O)_n]^+$ is essential to understand the nature of protons in nanosized water droplets.[1–8] It has been known for a long time that in mass spectra, magic clusters ($n=21$) appear abundantly and antimagic clusters ($n=22$) appear scarcely or transiently.[4–7] For these clusters, diverse structures have been predicted.[8,9] The magic cluster has been suggested to have an aesthetic geometrical structure, a pentagonal dodecahedron (PD; 5^{12}),[4,5,7,9a] as related to water clathrates that trap methane and other gases in PD water cages.[10] In contrast, no convincing structure has been suggested for the antimagic cluster. Despite recent remarkable experimental progress,[4,5] no model has been successful in explaining the structures of both magic and antimagic clusters. There are few consistencies among experimental and theoretical models, and different empirical potentials predict different structures for these clusters. Therefore, accurate calculations of the magic/antimagic clusters have been called upon to correctly understand many existing experimental data.[11]

Our most accurate results give the answer to the following unresolved controversial issues: 1) why the magic and antimagic clusters exist; 2) whether the proton is inside or on the surface of the cage; 3) whether the proton is strongly bound to a single water molecule (Eigen form; H_3O^+) or is shared between two water molecules (Zundel form; $H_2O\cdots H^+\cdots OH_2$); 4) why a proton moiety is not observed in the IR spectra contrary to the theoretical prediction; 5) whether each spectrum corresponds to a particularly stable structure or many isomers; 6) why the OH stretching peak for AD-type H_d (in which A and D denote proton acceptor and donor, respectively, and H_d denotes a dangling hydrogen atom) is absent for the magic clusters and not appreciably measurable for the antimagic clusters at low temperatures,[5] which is in contrast to the strong AD peaks observed for other clusters; 7) any unknown thermal and dynamic effects of these clusters.

To search for experimentally relevant structures, we considered a number of energetically low-lying structures from those previously reported based on empirical potentials (though not consistent with ab initio results)[8,9] and many topologically different structures generated from our experience with various types of water-containing clusters.[12] Starting with these structures, we generated as many of the refined low-lying structures as possible at the level of the density-functional-based tight-binding theory (DFTB)[13] by using the simulated annealing/cooling method.[14] A more sophisticated basin-hopping method[9] was also employed, which gave consistent results with the above-mentioned method.

Since DFTB results (let alone existing empirical potential results) are not reliable, we refined the energies of the selected low-energy conformers by using Becke-3-Lee-Yang-Parr (B3LYP) calculations with the 6-31+G* basis set followed by the aug-cc-pVDZ$^+$ basis set (in which "+" denotes that the diffuse basis function of the hydrogen atom was removed). Again, Møller–Plesset second-order perturbation (MP2) calculations were performed for more-accurate energies.[15] The lowest-energy and nearly isoenergetic conformers identified with MP2 have been used for Car–Parrinello molecular dynamics (CPMD) simulations. Our experience with hydrogen-bonded clusters indicates that MP2 results are much more consistent with experiments than results obtained with density functional theory (DFT), which occasionally fails to predict realistic structures of water-containing clusters owing to its inability to include dispersion energy.[12] Indeed, for hydrogen-bonded systems, we observe that MP2 results are much more consistent with high-level ab initio calculations such as coupled-cluster theory. In this work, we also note that DFT fails to predict realistic structures, while MP2 explains the experimental data. More concrete results would be obtained at higher levels of ab initio theory.

In the case of the magic cluster of $[NH_4(H_2O)_{20}]^+$,[16] the NH_4^+ ion has four well-balanced, tetrahedrally oriented hydrogen bonds inside the cage and four unbalanced, strained hydrogen bonds on the surface. Thus, we find from our calculations that the cluster with the NH_4^+ ion inside the cage is more stable than the cluster with the NH_4^+ ion on the surface of the cage by about 2 kcal mol^{-1}. Similarly, we find that the magic clusters $[K(H_2O)_{20}]^+$ and $[Cs(H_2O)_{20}]^+$,[16] in which these alkali-metal cations have a coordination number greater than 4, also have internal structures because those cations can be tri- or tetra-coordinated (with strains) on the surface. In contrast, each hydrogen atom of the H_3O^+ ion involves a hydrogen bond as a strong hydrophilic site, whereas the oxygen atom of the H_3O^+ ion behaves as a hydrophobic site due to the three positively charged hydrogen atoms that hinder close approach from other hydrogen atoms towards the oxygen center.[3] Since the H_3O^+ ion and the H_2O molecule favor three and four hydrogen bonds, respectively, clusters are stabilized with a maximized number of hydrogen bonds by having the H_3O^+ ion on the surface and a water molecule inside the cage. Furthermore, in water clusters, an amphiphilic species such as a H_3O^+ ion favors the surface to maximize the polarization-driven binding energy, unless the cluster size is large.

Thus, using the empirical structure–energy relationship obtained from the energies of numerous structures based on the DFTB, B3LYP, MP2, and CPMD calculations, we find a simple and reasonable approach to locate the most-probable lowest-energy structures for these clusters: 1) the H_3O^+ ion tends to be on the surface, and favors a specific-site (S-site) hydrogen atom bonded by three ADD-type water molecules unless the surface has high curvature; 2) water molecules tend to favor four hydrogen bonds (AADD type) and three hydrogen bonds (AAD and ADD types) over two hydrogen bonds (AD, DD, and AA types) unless the increase in strain energy is larger than an additional hydrogen-bond energy gain, which sometimes occurs for an AADD-type hydrogen bond; 3) H_d atoms tend to be maximally distributed with least clustering to minimize the H–H repulsions; 4) the internal water molecule is favored to maximize up to four hydrogen bonds, and its orientation tends to have a strong charge–dipole interaction with the H_3O^+ ion; 5) contiguous long hydrogen-bond relays that have the same helicity as the OH orientations tend to stabilize the cluster with enhanced-polarized hydrogen bonds, and these cyclic hydrogen bonds generate nearly isoenergetic conformational isomers by changing the orientation of the OH helicity.[15]

 © 2006 Wiley-VCH Verlag GmbH & Co. KGaA, Weinheim

The magic cluster $[H(H_2O)_{21}]^+$ has well-packed compact PD structures with nine AAD-type H_d atoms. Seven isoenergetic conformers (within < 0.3 kcal mol^{-1}) are formed with different cyclic OH orientations (Figure 1 a, b); the H_3O^+ ion is on the surface of the cage (21A structures). Based on B3LYP/aug-cc-pVDZ calculations, we found that the surface structure is 5–10 kcal mol^{-1} more stable than the internal structure (i.e., with the H_3O^+ ion inside the cage with ten H_d atoms) because of the presence of one additional hydrogen bond and the polarization effect.[17] In CPMD simulations,[18] when H_3O^+ is put inside a PD at 100 K, the proton is ejected out to the surface in about 1 ps, which is followed by rearrangement toward the S-site in 0.5 ps by the Grotthuss mechanism.

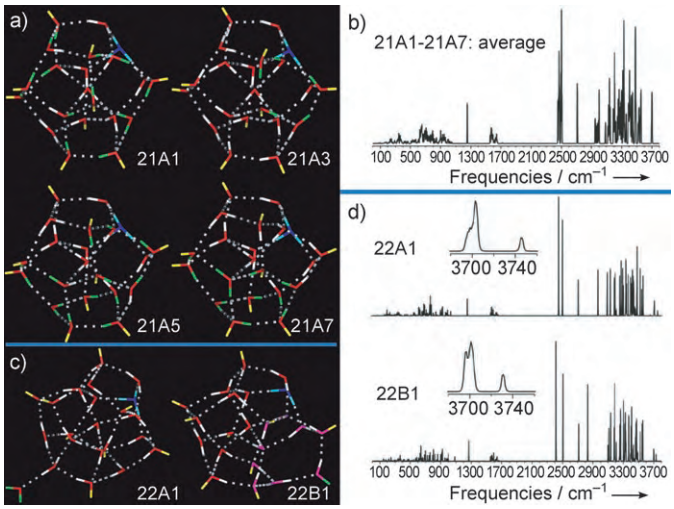

Figure 1. Most-stable conformers of $[H(H_2O)_{21}]^+$ and $[H(H_2O)_{22}]^+$. a) Seven nearly isoenergetic lowest-energy conformers of $[H(H_2O)_{21}]^+$ (only four of which are shown), which have nine ADD-type H_d atoms for the PD (5^{12}) topology with the least-clustered hydrogen bonds; 21A2,4,6 have the opposite helicities to those of 21A1,3,5, respectively; H_d atoms are yellow; cyclic helicity H atoms are green; protonated water molecules have blue O atoms and cyan H atoms. b) Averaged IR spectra of the seven isomers 21A1–21A7. c) Two nearly isoenergetic conformers, 22A1 and 22B1, of $[H(H_2O)_{22}]^+$, which have one A-type H_d (green) and one AD-type H_d (green); O atoms of the six-membered rings are magenta. d) IR spectra of 22A1 and 22B1. The molecular structures were drawn with the POSMOL program.[20]

Based on MP2/aug-cc-pVDZ calculations, we found that the most plausible realistic conformers of $[H(H_2O)_{20}]^+$ have structures with one water molecule being excluded from the surface of the PD structure of $[H(H_2O)_{21}]^+$. They show a strong AD peak, which is in agreement with other experiments.[4,5]

$[H(H_2O)_{22}]^+$ is predicted to have two nearly isoenergetic conformers with intriguing structures arising from one extra water molecule either sitting above or intruded into the PD structure of $[H(H_2O)_{21}]^+$ (Figure 1 c and d): 1) one water molecule (A type) on the top of the surface of the PD structure is singly hydrogen-bonded to one of AAD-type H_d atoms opposite the H_3O^+ ion (22A1); 2) a $5^{10}6^2$ topological structure has nine AAD- and one AD-type H_d atoms (22B1), with one water molecule inserted between two loosely hydrogen-bonded water molecules of the PD structure. These two structures clearly demonstrate why $[H(H_2O)_{21}]^+$ is particularly stable whereas $[H(H_2O)_{22}]^+$ is transient (or less stable) and explains their magic/antimagic natures. This difference in stability is also evidenced from the MP2/aug-cc-pVDZ binding energies with a B3LYP/aug-cc-pVDZ zero-point energy (ZPE) correction for $[H(H_2O)_{20}]^+$, $[H(H_2O)_{21}]^+$, and $[H(H_2O)_{22}]^+$, which are 12.26, 12.29, 12.11 kcal mol^{-1} per water molecule, respectively.

For $[H(H_2O)_{21}]^+$, all three levels of theory—DFTB, B3LYP/aug-cc-pVDZ, and MP2/aug-cc-pVTZ—give the lowest energy for the PD structure among the various structures that we have investigated. However, for $[H(H_2O)_{20}]^+$ and $[H(H_2O)_{22}]^+$, the three levels give different lowest-energy structures. Nevertheless, the potential surface on the local minimum does not vary significantly at the different levels of theory, and hence the three methods give similar frequencies for the same type of structure, which is predicted as a (local) minimum. Thus, for $[H(H_2O)_{20}]^+$ and $[H(H_2O)_{22}]^+$, the spectral study at the CPMD level is only reliable around the local region near the local minimum. However, for $[H(H_2O)_{21}]^+$ the PD structure is particularly stable, and thus the potential surface near the PD structure is reasonably well represented by most theoretical methods. Therefore, for $[H(H_2O)_{21}]^+$, we carried out first-principles CPMD simulations to analyze the thermal and dynamic effects. Nine sets of simulations were performed at 50 to 295 K for 6 ps each.

Figure 2 shows the O–O and O–H radial distribution functions (RDFs) for the last 4 ps sampled, some thermodynamic properties, and snapshots of the $[H(H_2O)_{21}]^+$ cluster at different temperatures. At 195 K, the structure is quite open and is starting to show glassy phenomena (Figure 2 c). The structure at 245 K has on average about 15 H_d atoms; however, it still retains the precluster characteristic of the PD topology. At 270 K the precluster moiety for the formation of the PD topology is completely lost, and the internal water molecule loses its four hydrogen bonds. Thus, the structure starts to have free water molecules, which results in evaporation as evidenced from a peak in the heat capacity (C_v) arising from a phase transition. It was possible to obtain the initial structures before the simulation of the cooling-down process of the CPMD configurations at 245 K (with 15 H_d atoms), but not from those at 270 K (with 18 H_d atoms and one/two freelike water molecules). The simulations also show that the protonated water molecule continues as an Eigen form below 100 K. The percentage of the Zundel form continuously increases with rising temperature, from about 1 % at 125 K to about 20 % at 270 K.

Figure 3 shows the power spectra of the simulations at various temperatures. The AAD- and ADD-type OH_d peaks (≈ 3700 and ≈ 3580 cm^{-1}) are in good agreement with the experimental spectra. As the number of AD-type H_d atoms increases with increasing temperature, the AD peak appears at 3715–3720 cm^{-1} above 170 K and is separated from the AAD peak by about 20 cm^{-1}. The ADD peak is not distinguishable at 50 and 100 K due to the presence of other

 © 2006 Wiley-VCH Verlag GmbH & Co. KGaA, Weinheim

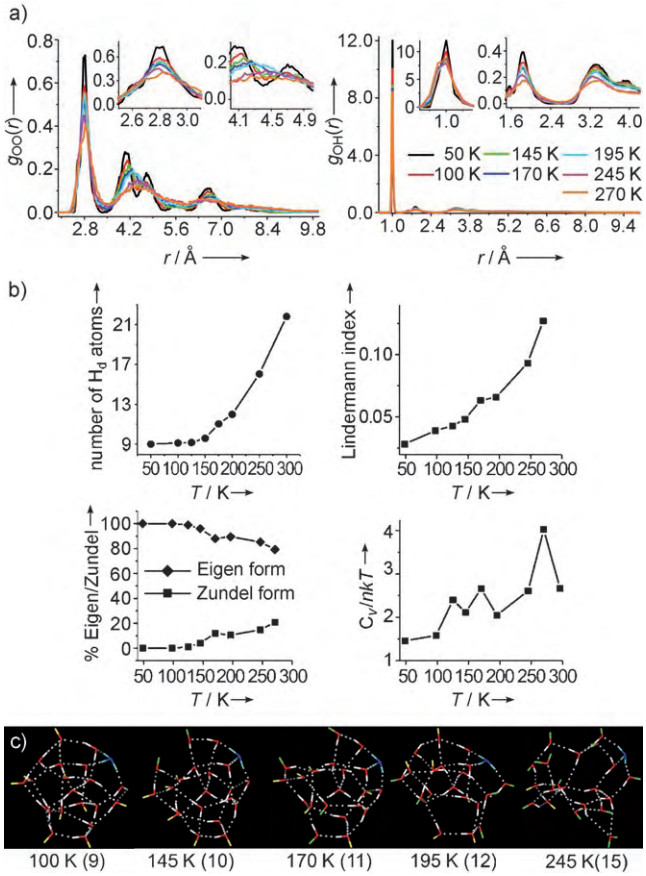

Figure 2. Structural and thermodynamic properties of $[H(H_2O)_{21}]^+$ at various temperatures: a) O–O and O–H RDFs. b) Average number of H_d atoms; Lindemann index; percentage of Eigen and Zundel forms; heat capacity; n = number of atoms. At 145 K, the second and third hydration shells in O–O (4.1, 4.7 Å) and O–H (3.3, 3.9 Å) RDFs start to merge, and from 170 K onwards the two peaks are not distinguishable. The average number of H_d atoms is strongly correlated with the Lindemann index, that is, the root-mean-square deviation of all the interatomic distances. c) Temperature-dependent representative structures (number of H_d atoms in parentheses). The instantaneous structure with ten H_d atoms at 145 K has two AD-type H_d atoms (AAD-type H_d atoms: yellow; AD-type H_d atoms: green).

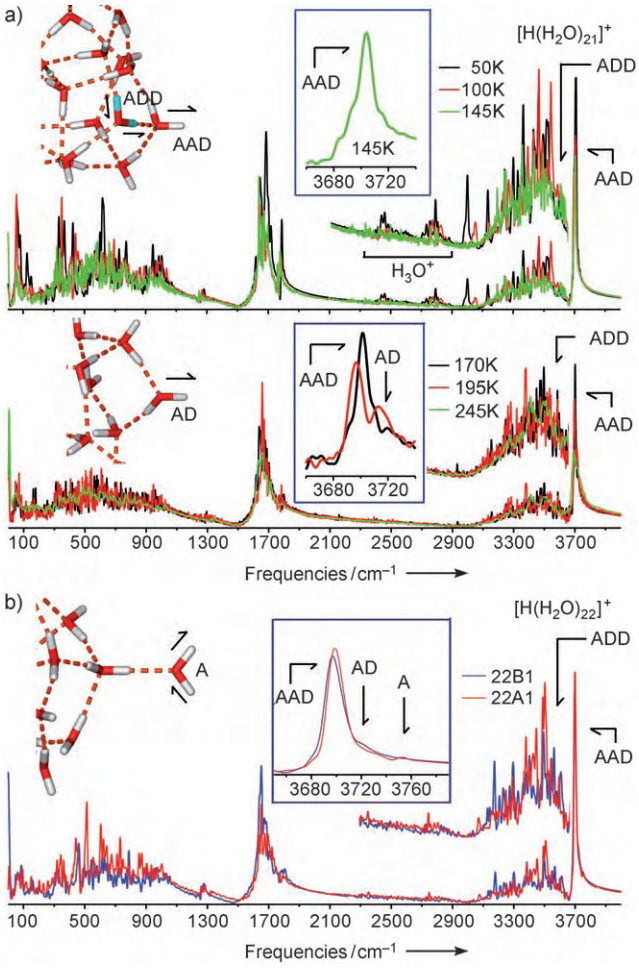

Figure 3. Power spectra of $[H(H_2O)_{21}]^+$ and $[H(H_2O)_{22}]^+$ (frequencies scaled by 1.049). a) $[H(H_2O)_{21}]^+$ at varying temperatures, insets show the expanded spectra to distinguish the AAD and AD peaks. The AAD- and ADD-type OH_d peaks appear at ≈3770 and ≈3580 cm^{-1}, respectively. As the temperature increases, the peaks broaden due to the structural fluctuation and deformation. Despite the presence of configurations with an extra AD-type H_d at 145 K, the AD peak does not appear because of the unusual dynamic effect associated with the flexible potential surface driven by proton mobility as the AD-type OH keeps changing its nature during simulations (towards ADD and AAD types). b) The two most-stable conformers (22A1, 22B1) of $[H(H_2O)_{22}]^+$ at 125 K. A small shoulder at 3724 cm^{-1} corresponds to AD-H_d atoms, and another small peak at 3755 cm^{-1} corresponds to A-H_d atoms, both of which show surprising dynamic effects.

strong peaks nearby, but becomes noticeable as other peaks weaken from 125 K onwards.

The most controversial issue of the spectra is that experiments do not find two key theoretical peaks that correspond to the H_3O^+ ion (≈2500 cm^{-1} and ≈2700 cm^{-1}). As the temperature increases, the peak at about 2500 cm^{-1} rapidly disappears before 100 K, while the peak at about 2750 cm^{-1} slowly diminishes and only this peak represents the unique Eigen feature at about 100 K. Even this peak becomes negligible at 125 K, and eventually disappears above 145 K. As the protonated water molecule on the surface is mostly in the Eigen form at 125 K, the dynamics due to minor fluctuations play a crucial role in defining the vibrational frequencies for the following reason: the energy barrier of a proton transfer from the H_3O^+ moiety in $[H(H_2O)_{21}]^+$ to the hydrogen-bonded oxygen atom in the adjacent water molecule is very low, which is reflected by the high proton mobility. This low barrier arises because each hydrogen atom of the H_3O^+ ion can be electronically shared by oxygen atoms of adjacent water molecules and from electrostatic and polarization effects. Above 125 K, the thermally induced large dynamic motion of the proton on the highly flattened anharmonic-potential-energy surface leads to the complete depletion of the peaks at about 2500 and 2700 cm^{-1}.[15]

The quantum effect for the proton motion is significant. However, the energy barrier of the DFT potential tends to be smaller than that of the more accurate ab initio results. Thus, the zero-point energy correction, which is the dominant quantum effect, is taken into account already (or over-compensated) due partly to the cancellation of errors. The

 © 2006 Wiley-VCH Verlag GmbH & Co. KGaA, Weinheim

underestimated errors in the energy barriers ($> \approx 1$ kcal mol^{-1}) are greater than the small quantum effect (≈ 0.5 kcal mol^{-1} for $[H_9O_4]^+$).[2b] Consequently, the quantum effect is most likely to play a small role compared with the accuracy of the potential surface. Furthermore, the underestimation of the potential barriers in the DFT calculation happens to partially reflect the quantum-tunneling-driven effective barrier for the accurate ab initio potential surface. In this regard, we believe that the CPMD results realistically match the experimental observation. However, any small energy difference would need to be confirmed with more accurate calculations.

The heat capacity C_v (Figure 2b) shows a small peak at about 125 K due to the beginning of Zundel formation, but the IR peak at about 1000 cm^{-1}, which is the unique Zundel feature of the spectrum, cannot be measured. Nevertheless, the peak at around 1800 cm^{-1}, which corresponds to the HOH bending mode of both Eigen and Zundel forms (in contrast to the water-bending mode at ≈ 1700 cm^{-1}) is seen as a very weak proton signature below around 175 K.

Based on our predicted temperature-dependent spectra, we estimate the experimental temperature that produced the IR spectrum of $[H(H_2O)_{21}]^+$ reported by Shin et al. (no peaks for AD-type H_d atoms and H_3O^+, but a distinguishable peak for AAD-type H_d atoms) to be around 150 K,[5] whereas that reported by Miyazaki et al.[4] (a clear AD peak separated from the AAD peak by 20 cm^{-1}) we estimate was taken at around 175 K, which is in agreement with the authors' claim. We note that this latter prediction agrees with a recent experiment of Wu et al.[6]

For $[H(H_2O)_{22}]^+$, the A-type H_d peak (3746 cm^{-1}) in the IR spectra of 22A1 at 0 K and 50 K almost completely disappears in the power spectra at 125 K owing to large thermally induced dynamic motion. This motion is caused by strong anharmonic coupling (which arises from the flexible potential surface and involves the mobility of the hydrogen atom) between the antisymmetric and symmetric vibrational modes of this singly hydrogen-bonded A-type dangling water molecule (A-wat).[15] With increasing temperature, the A-wat outside the PD cage moves widely, and thus the donor hydrogen atom of the AADD-type water molecule that involves the hydrogen bond with the A-wat also moves significantly and affects the potential surface of the A-wat. In this situation, the two OH bonds of the A-wat (even though the bending angle is kept almost constant with only a small variation) can orient randomly through flapping and torsional rotation. Thus, the change in potential for the A-wat affected by the donor hydrogen atom and OH bond of the AADD-type water molecule involves anharmonic coupling of the two OH bonds of the A-wat. Consequently, an increase in temperature leads to a drastic increase in the anharmonic coupling effect,[19] which results in small broad peaks near the difference in value of the two OH frequencies. At higher temperatures, all these peaks disappear.

This unexpected dynamic behavior, which demonstrates the near-complete suppression of the OH peak, is different from the common dynamic effect. In the common dynamic effect, the isolated water monomer has a predefined rigid potential surface for which the corresponding IR peak is simply broadened. This peak reflects the average of the ensemble and does not diminish as each ensemble has a similar frequency and similar intensity. In the power spectra of 22B1 at 125 K, the strong AD-type peak (3724 cm^{-1}) also almost disappears. All previous work has focused in vain on finding structures without AD-type H_d for this antimagic cluster, whereas we find a surprising dynamic effect: that either an A-type or AD-type H_d does exist but the peak is highly suppressed. This finding goes against conventional wisdom and is extremely important as OH peaks of IR spectra have been extensively exploited for the structural identification of diverse hydrogen-bonded clusters.

The present analysis provides answers to previously unresolved problems of magic and antimagic protonated water clusters and accounts for the difference in structure of clusters that have the H_3O^+ ion on the surface compared with those clusters that have internal ions such as Cs^+, K^+, and NH_4^+. Thus, very accurate ab initio calculations are able to predict the right structures. The dynamic effect on the stretching peak of the hydrogen bond would resolve many other problems in this area of cluster chemistry and allow analysis of spectroscopic fingerprints.

Received: November 22, 2005
Revised: February 25, 2006
Published online: May 3, 2006

Keywords: cluster compounds · density functional calculations · molecular dynamics · vibrational spectroscopy · water chemistry

[1] a) J. M. Headrick, E. G. Diken, R. S. Walters, N. I. Hammer, R. A. Christie, J. Cui, E. M. Myshakin, M. A. Duncan, M. A. Johnson, K. D. Jordan, *Science* **2005**, *308*, 1765 – 1769; b) K. R. Asmis, N. L. Pivonka, G. Santambrogio, M. Brümmer, C. Kaposta, D. M. Neumark, L. Wöste, *Science* **2003**, *299*, 1375 – 1377.
[2] a) D. Wei, D. R. Salahub, *J. Chem. Phys.* **1997**, *106*, 6086 – 6094; b) D. Mark, M. Tuckermann, E. J. Hutter, M. Parrinello, *Nature* **1999**, *397*, 601 – 604.
[3] H. M. Lee, P. Tarakeshwar, J. W. Park, M. R. Kolaski, Y. J. Yoon, H.-B. Yi, W. Y. Kim, K. S. Kim, *J. Phys. Chem. A* **2004**, *108*, 2949 – 2958.
[4] M. Miyazaki, A. Fujii, T. Ebata, N. Mikami, *Science* **2004**, *304*, 1134 – 1137.
[5] J.-W. Shin, N. I. Hammer, E. G. Diken, M. A. Johnson, R. S. Walters, T. D. Jaeger, M. A. Duncan, R. A. Christie, K. D. Jordan, *Science* **2004**, *304*, 1137 – 1140.
[6] C.-C. Wu, C.-K. Lin, H.-C. Chang, J.-C. Jiang, J.-L. Kuo, M. L. Klein, *J. Chem. Phys.* **2005**, *122*, 07431519.
[7] a) J. Q. Searcy, J. B. Fenn, *J. Chem. Phys.* **1974**, *61*, 5282 – 5288; b) X. Yang, A. W. Castleman, Jr., *J. Am. Chem. Soc.* **1989**, *111*, 6845 – 6846; c) T. F. Magnera, D. E. David, J. Michl, *Chem. Phys. Lett.* **1991**, *182*, 363 – 370.
[8] a) L. Ojamae, I. Shavitt, S. J. Singer, *J. Chem. Phys.* **1998**, *109*, 5547 – 5564; b) S. S. Iyengak, T. J. F. Day, G. A. Voth, *Int. J. Mass Spectrom.* **2005**, *241*, 197 – 204; c) A. Khan, *Chem. Phys. Lett.* **2000**, *319*, 440 – 450; J.-L. Kuo, M. L. Klein, *J. Chem. Phys.* **2005**, *122*, 02451619.
[9] a) M. P. Hodges, D. J. Wales, *Chem. Phys. Lett.* **2000**, *324*, 279 – 288; b) T. James, D. J. Wales, *J. Chem. Phys.* **2005**, *122*, 134306.
[10] E. D. Sloan, Jr., *Nature* **2003**, *426*, 353 – 359.
[11] T. S. Zwier, *Science* **2004**, *304*, 1119 – 1120.

 © 2006 Wiley-VCH Verlag GmbH & Co. KGaA, Weinheim

[12] a) J. Kim, K. S. Kim, *J. Chem. Phys.* **1998**, *109*, 5886 – 5895; b) H. M. Lee, S. B. Suh, J. Y. Lee, P. Tarakeshwar, K. S. Kim, *J. Chem. Phys.* **2000**, *112*, 9759 – 9772; c) K. S. Kim, P. Tarakeshwar, J. Y. Lee, *Chem. Rev.* **2000**, *100*, 4145 – 4186. d) S. Lee, J. Kim, S. J. Lee, K. S. Kim, *Phys. Rev. Lett.* **1997**, *79*, 2038 – 2041; e) H. M. Lee, S. B. Suh, P. Tarakeshwar, K. S. Kim, *J. Chem. Phys.* **2005**, *122*, 044309.

[13] T. Frauenheim, G. Seifert, M. Elstner, T. Niehaus, C. Köhler, M. Amkreutz, M. Sternberg, Z. Hajnal, A. D. Carlo, S. Suhai, *J. Phys. Condens. Matter* **2002**, *14*, 3049 – 3084.

[14] a) K. S. Kim, M. Dupuis, G. C. Lie, E. Clementi, *Chem. Phys. Lett.* **1986**, *131*, 451 – 456; b) K. S. Kim, *Bull. Korean Chem. Soc.* **1993**, *14*, 18 – 20.

[15] Refer to Supporting Information.

[16] F. Sobott, A. Wattenberg, H.-D. Barth, B. Brutschy, *Int. J. Mass Spectrom.* **1999**, *185–187*, 271 – 279.

[17] Gaussian 03 (Revision A.1), M. J. Frisch, G. W. Trucks, H. B. Schlegel, G. E. Scuseria, M. A. Robb, J. R. Cheeseman, J. A. Montgomery, Jr., T. Vreven, K. N. Kudin, J. C. Burant, J. M. Millam, S. S. Iyengar, J. Tomasi, V. Barone, B. Mennucci, M. Cossi, G. Scalmani, N. Rega, G. A. Petersson, H. Nakatsuji, M. Hada, M. Ehara, K. Toyota, R. Fukuda, J. Hasegawa, M. Ishida, T. Nakajima, Y. Honda, O. Kitao, H. Nakai, M. Klene, X. Li, J. E. Knox, H. P. Hratchian, J. B. Cross, C. Adamo, J. Jaramillo, R. Gomperts, R. E. Stratmann, O. Yazyev, A. J. Austin, R. Cammi, C. Pomelli, J. W. Ochterski, P. Y. Ayala, K. Morokuma, G. A. Voth, P. Salvador, J. J. Dannenberg, V. G. Zakrzewski, S. Dapprich, A. D. Daniels, M. C. Strain, O. Farkas, D. K. Malick, A. D. Rabuck, K. Raghavachari, J. B. Foresman, J. V. Ortiz, Q. Cui, A. G. Baboul, S. Clifford, J. Cioslowski, B. B. Stefanov, G. Liu, A. Liashenko, P. Piskorz, I. Komaromi, R. L. Martin, D. J. Fox, T. Keith, M. A. Al-Laham, C. Y. Peng, A. Nanayakkara, M. Challacombe, P. M. W. Gill, B. Johnson, W. Chen, M. W. Wong, C. Gonzalez, J. A. Pople, Gaussian, Inc., Pittsburgh, PA, **2003**.

[18] Troulller–Martins pseudopotential; BLYP functionals with gradient correction; the energy cutoff value was 90 Ry; time step: 0.1 fs; CPMD code Version 3.7.2, CPMD, Copyright IBM Corp 1990 – 2001, Copyright MPI für Festkörperforschung Stuttgart 1997 – 2001.

[19] L. D. Landau, E. M. Lifshitz, *Mechanics*, Pergamon, 2nd ed., **1969**, pp. 84 – 87.

[20] S. J. Lee, H. Y. Chung, K. S. Kim, *Bull. Korean Chem. Soc.* **2004**, *25*, 1061 – 1064.

 © 2006 Wiley-VCH Verlag GmbH & Co. KGaA, Weinheim

Chemosensors

DOI: 10.1002/anie.200600050

Chemical Sensing with Familiar Devices**

*Daniel Filippini, Adriano Alimelli, Corrado Di Natale, Roberto Paolesse, Arnaldo D'Amico, and Ingemar Lundström**

Computers and mobile phones are ubiquitous devices that are continuously evolving and becoming ever more sophisticated. Eventually, they will constitute a global network of casual terminals that are geographically traceable and able to capture images and sounds of increasing quality. Other target inputs such as odors[1] or (bio)chemical parameters[2–4] are, however, more difficult to detect on such a massive scale, particularly with a generic type of instrumentation. Such a possibility would enable, for example, health diagnostics, environmental monitoring, and food quality assessments on a personalized level and also to feedback determinations of the same parameters to the network. Certainly, it would be a significant advantage if this was feasible as a natural extension of the capabilities of familiar and already well distributed devices.

Here we demonstrate the analytical capabilities of a regular computer screen with a web camera[5,6] for detecting and recognizing different molecules with an inexpensive (and eventually disposable) optical-sensing interface. By using semitransparent spots of porphyrins[7] as sensors we show that is possible to detect detailed and partially disentangled absorption and emission responses resulting from molecules such as amines, CO, and NO_x. The current system is also representative of other sensing approaches that use arrays of fluorescent indicators, and highlights the possibility of analyzing complex response patterns with available means.

Computer screens are not only our main computer interface, they are also widely configurable solid-state light sources.[8] They are capable of displaying confined areas of arbitrary shape, color, and intensity that can be two-dimen-

[*] Dr. D. Filippini, Prof. Dr. I. Lundström
Division of Applied Physics
IFM, Linköping University
58183 Linköping (Sweden)
Fax: (+46) 13-288-969
E-mail: ingemar@ifm.liu.se
Prof. Dr. C. Di Natale, Prof. Dr. A. D'Amico
Dipartimento di Ingegneria Elettronica
Università degli Studi di Roma Tor Vergata
Via del Politecnico 1, 00133 Roma (Italy)
A. Alimelli, Prof. Dr. R. Paolesse
Dipartimento di Scienze e Tecnologie Chimiche
Università degli Studi di Roma Tor Vergata
Via della Ricerca Scientifica, 00133 Roma (Italy)

[**] This work was supported by a grant from the Foundation for Strategic Research, Sweden, which made it possible for I.L. (for five months) and D.F. (for one month) to stay at the University of Rome "Tor Vergata". The work on CSPT is also supported by the Swedish Research Council and the Swedish Agency for Innovation Research.

InterScience
© 2006 Wiley-VCH Verlag GmbH & Co. KGaA, Weinheim

sionally scanned on the screen with 200 μm resolution. All of this is achieved without moving parts and eventually has the possibility of becoming portable, as in the case of LCD displays in cellular phones. It is also true that they are not the natural choice of light sources for analytical purposes; however, they are everywhere and always inherently combined with substantial computing power, and their versatility and processing capabilities allow many of their weaknesses to be overcome. This aspect has been recognized and exploited in the so called computer screen photoassisted technique (CSPT)[5,9,10] for optically characterizing arrays of target indicators.

Here we demonstrate a disposable array of sensing substances that responds with a variety of absorption and emission changes that can be characterized by CSPT. The ability of the system to generate and analyze complex response patterns enables sophisticated determinations using an available and globally disseminated infrastructure (for example, computer sets).

Color arrays are common in biosensing applications,[2,3,11] but there are also examples of optical electronic noses[1,4] and electronic tongues.[12] The research group of Suslick, as well as others, have demonstrated that arrays of porphyrins are a feasible alternative for detecting gases and organic vapors[4,13–16] with minimum instrumentation (for example, reading the responses with flat-bed scanners[17]).[4] Here such a molecular system is chosen because of its rich variety of spectral responses that are used to test the method and to exemplify its possibilities for evaluating fluorescence-labeled assays in general. We thus made experiments on spots of thin layers of (5,10,15,20-tetraphenylporphyrin)zinc ([Zn(tpp)]), (5,10,15,20-tetraphenylporphyrin chloride)iron ([Fe(tppCl)]), and 2,3,17,18-tetraethyl-7,8,12,13-tetraamethyl-*a*,*c*-biladiene dihydrobromide (BD) dispersed in a polyvinylchloride (PVC) matrix and spotted in duplicate on a glass slide (inset in Figure 1 a). The sensing array was exposed to low concentrations of molecules such as NH_3, NO_x, CO, and triethylamine (TEA) in nitrogen.

Computer screens are able to display more than 16 million colors that are formed by different weighted combinations of red, green, and blue primary spectral radiances (RGB colors). During a CSPT measurement a web camera captures the image of the array under an illuminating sequence provided by the screen (a rainbow of 50 colors in this study). From this video stream regions of interest (ROI) are selected (the white circles in Figure 1 a) and used to compose substance fingerprints. The changes in the intensity (average of all the pixels in each ROI) recorded in the channels of the web camera with respect to the intensities recorded in pure nitrogen are shown in Figure 1 a. Signals from the red, green, and blue channel are concatenated in this order, and the fingerprints of all the spots are composed in a single fingerprint of the array (Figure 1 a). The intensity measured, for example, in the red channel of the web camera, for an illuminating color i defined by the triplet (r_i, g_i, b_i) is given by Equation (1).

$$I_{Ri} = \int_{\lambda} [r_i\, R(\lambda) + g_i\, G(\lambda) + b_i\, B(\lambda)]\, S(\lambda, i)\, F_R(\lambda)\, D(\lambda)\, d\lambda \qquad (1)$$

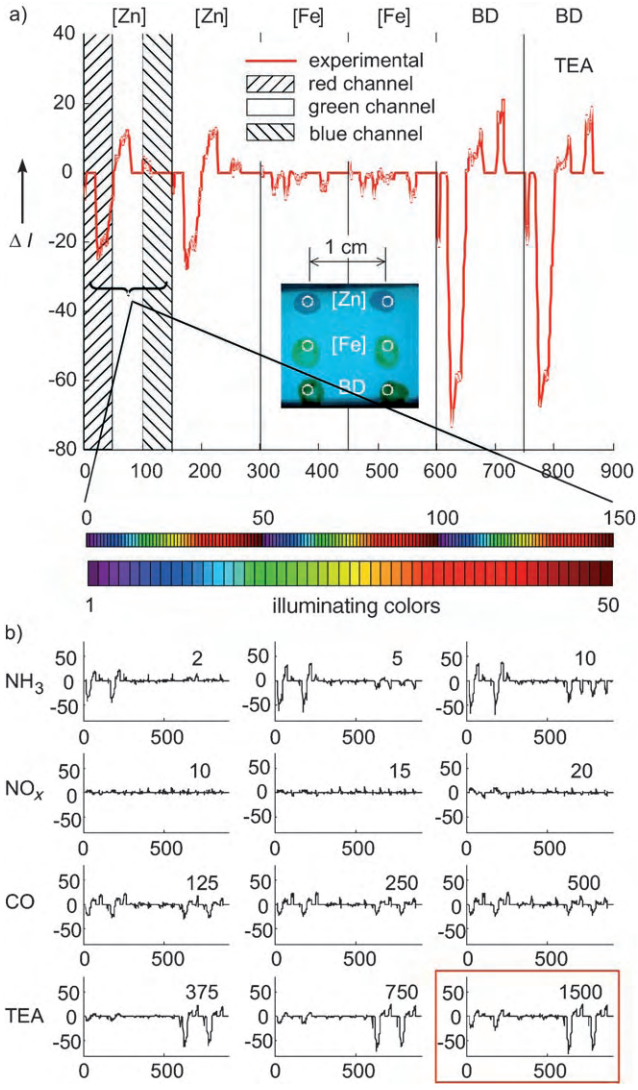

Figure 1. a) CSPT fingerprint of 1500 ppm of triethylamine (TEA). The data correspond to absorption/emission changes of the indicator spots upon exposure to TEA observed as intensity changes in the red, green, and blue channels of the web camera for different screen illuminations. These results were obtained from exposure, at room temperature, of the array to 1500 ppm of TEA in N_2 with the signal of N_2 subtracted. Each spot becomes represented by 50 values in the red channel, 50 values in the green channel, and 50 values in the blue channel. The units on the *y* axis are in "intensity level changes" of the web camera signal (that is, between −255 to +255)). The numbers on the *x* axis identify illuminating colors for the three camera channels and for the six imaged spots. All 900 points were obtained during one single run of the illuminating sequence of 50 colors (ca. 50 s measurement). The inset shows an image of the array at one given color frame ("blue") on the computer screen. The circles illustrate "the regions of interest" (ROIs) used to calculate the average intensity of the light reaching the web camera through the indicator spots. The illuminating sequence used (colors 1–50) as well as the concatenation of the camera channels to construct the fingerprints of a particular spot are shown. b) CSPT fingerprints of a number of molecules at different concentrations obtained with the array of porphyrin spots (inset Figure 1 a). [Zn] = [Zn(tpp)], [Fe] = [Fe(tppCl)], BD = biladiene.

The spectral radiances of the screen primary colors ($R(\lambda)$, $G(\lambda)$, and $B(\lambda)$) are polychromatic sources illuminating the

 © 2006 Wiley-VCH Verlag GmbH & Co. KGaA, Weinheim

tested substance,[6] and represented by $S(\lambda, i)$, which accounts for the substance transmittance $T(\lambda)$ and emission ($E(\lambda,i)$ spectra weighted by the spectral composition of the illumination.

The red, green, and blue filters of the web camera and the spectral response of the detector are represented by $F_R(\lambda)$, $F_G(\lambda)$, $F_B(\lambda)$, and $D(\lambda)$, respectively. Equation (1) summarizes the way that CSPT perceives the excitation emission characteristics of the tested substances when illuminated by the polychromatic light provided by the screen.

Figure 1b collates the response features from different concentrations of target stimuli. The different features of the results in Figure 1b are understood from the corresponding absorption and emission changes of the different porphyrins resulting from the target molecules, and are related to shifts in the absorption and emission peaks, as well as changes in the peak sizes and widths. The ability of CSPT as a method for practical evaluations depends on how well the fingerprints in Figure 1b distinguish different molecules. A simple and efficient way to summarize and compare information in complex signals is to apply principal component analysis (PCA) to the fingerprints.[18,19] Figure 2a shows the first two principal components of the whole set of fingerprints which explain about 80% of the original information. This plot shows the classification of the considered molecules for the different tested concentrations. The biplot representations in Figure 2b and c address the correlation of the classification with the source of the CSPT signals. In these graphics, scores that are 100% correlated with a measuring condition lie in the same direction, while perpendicularly oriented elements are not correlated. Thus, it is possible to identify the CSPT measuring conditions that determine the ability of the CSPT fingerprints to distinguish the different target stimuli. For example, NH_3 detection is mainly correlated with the [Zn(tpp)] response observed in the red channel (Figure 2b), which identifies changes in the emission, whereas the blue channel recognizes CO (Figure 2c). Similarly, the detection of TEA is correlated with the quenching of the BD fluorescence (Figure 2b). From Figure 2 it is also possible to identify a subset of optimum illuminating conditions that could produce a similar result with a shorter color sequence, an important aspect for implementing fast measurements or determination based on mobile phones instead of computer sets.

In this work we selected Zn– and Fe–metal complexes of tpp and a linear tetrapyrrole (BD). In the case of metalloporphyrins, the coordination of the analytes to the metal center is the expected sensing mechanism; aggregation of macrocycles or other matrix effects are ruled out by the dispersion of the porphyrins into the PVC membrane. We selected Zn and Fe complexes because they are representatives of two broad classes of porphyrins according to Gouterman's classification:[7] [Zn(tpp)] represents a "regular" porphyrin, while [Fe(tppCl)] is a typical "irregular" porphyrin. As an important consequence for CSPT applications, [Zn(tpp)] produces fluorescence emission, while [Fe(tppCl)] is a radiationless substance.

In the case of [Zn(tpp)], coordination at the metal center generally induces a red-shift of both the absorbance and emission bands, together with a significant quenching of the fluorescent emission[20] (which is observed as a negative peak in the red channels for a blue illumination, see for example Figure 1a). All these features are well represented in the CSPT results by positive and/or negative peaks arising from

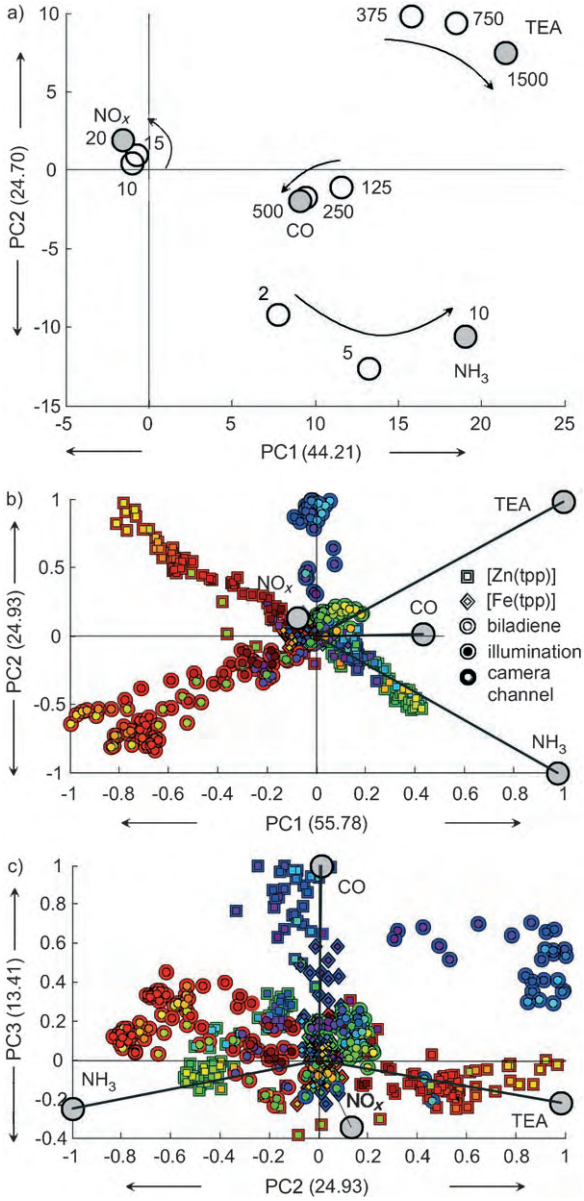

Figure 2. a) Principal component analysis[18] (PCA) of the results in Figure 1b. The intensities in the three channels were made into a data set consisting of 900 points for each measurement and evaluated by standard PCA. The scores plot shows the classification properties of CSPT. The arrows indicate the evolution of the points in the score plot for increasing concentration of the target gases. b) and c) Biplots corresponding to the largest concentrations of the tested gases. The results are shown as PC2 versus PC1, and PC3 versus PC2. In the biplots the contribution from the different colors of the illumination (inner color of the symbols), the camera channels (outer color of the symbols), and the different indicators (□, ◇, and ○ for [Zn(tpp)], [Fe(tppCl)], and BD, respectively) are indicated. The gray circles show the PCA scores of the different molecules. The colored symbols (the loads) indicate the contributions to the scores plot, and thus their relative weight in the classification of the molecules.

 © 2006 Wiley-VCH Verlag GmbH & Co. KGaA, Weinheim

predominant absorption and/or emission responses, respectively. In the case of [Fe(tppCl)], the "irregular" absorbance optical spectrum gave less evident changes in the CSPT responses and this feature, together with the lack of emission, results in smaller responses (Figure 1b). A completely different sensing mechanism should be considered with BD; the linear tetrapyrrole is stable as a dication and its interaction with bases induces significant changes in the molecular structure and consequently in the optical spectra. Loss of a proton leads to the formation of the 22,24-*a*,*b*,*c*-dihydrobilatriene hydrobromide and the loss of a further proton to the corresponding free base, with color changes from red to yellow-orange to green. In solution the formation of the BD free base leads to the formation of corrole by a ring-closure reaction.[21]

In the CSPT measurements we observed an unexpected reversibility of the BD layers upon interaction with TEA or NH_3. Concurrent spectral analysis of a model system suggests that the cyclization reaction does not occur so rapidly in the PVC membranes. From the CSPT results a significant variation in fluorescence after interaction, for example, with amines, even stronger than those obtained with [Zn(tpp)], was expected and corroborated by emission/absorption spectroscopy.

In this study the feasibility of ubiquitous environmental monitoring using an assembly of familiar devices already globally distributed has been demonstrated. This was done with a proven disposable chemical interface but measured with a detail not intuitively expected for the involved instrumentation and not readily available by any other method on the scale considered.

Since it will eventually be possible to run CSPT experiments just through an internet browser, such instrumentation would give a new dimension to environmental monitoring, food quality control, and also medical diagnostics at places where conventional analytical instrumentation would be either too expensive and/or requiring non-available expertise.

The recent introduction of global satellite imaging in search engines,[22] where the location of the user can be detected and placed in the geographical context of the search, is an ongoing vision that could naturally incorporate randomly read environmental or sanitary evaluations performed by the users of CSPT setups. When it is considered that these evaluations can take place everywhere, even in locations inaccessible to remote sensing, for example, inside buildings, they could supply global monitoring with a substantial degree of detail just by exploiting the chemical senses of familiar devices.

Experimental Section

Metalloporphyrins and BD were prepared according to a literature method.[23] The array was prepared by deposition of drops of PVC membrane solutions (1 wt% of porphyrin, PVC/bis(2-ethylhexyl)sebacate (1:2) polymeric matrix) in tetrahydrofuran onto glass slides. Evaporation of the solvent led to the formation of a PVC/porphyrin membrane. Two spots of each porphyrin were made as illustrated in the inset of Figure 1a to test the reproducibility of the method.

The glass slide with the printed sensing array was introduced into a gas cell with glass walls, where it was exposed to controlled concentrations of different gases with the aid of an automatic gas-mixing system.

The measuring procedure used is standard to CSPT experiments and can be found elsewhere[5] and involves a regular LCD screen (Philips 170S4) used as a light source and a Logitech Quickcam pro 4000 operating at a resolution of 320×240 pixels used as the image detector. A sample holder such as that described in Ref. [10] provides a controlled geometry for the measurements, and shields the experiments from ambient illumination.

Software written by us in Matlab commands the measurement procedure (illuminating sequence and video acquisition) and extracts the information (CSPT fingerprints) from manually selected ROIs (white circles in the inset Figure 1a).

Received: January 5, 2006
Published online: May 3, 2006

Keywords: analytical methods · chemosensors · environmental chemistry · porphyrinoids · sensors

[1] J. K. Albert, D. R. Walt, D. S. Gill, T. C. Pearce, *Anal. Chem.* **2001**, *73*, 2501.
[2] *Novel Approaches in Biosensors and Rapid Diagnostic Assays* (Ed.: Z. Liron, A. Bromberg, M. Fisher), Springer, Heidelberg, **2001**.
[3] D. Gershon, *Nature* **2005**, *437*, 1195.
[4] N. A. Rakow, K. S. Suslick, *Nature* **2000**, *406*, 710.
[5] D. Filippini, S. P. S. Svensson, I. Lundström, *Chem. Commun.* **2003**, 2, 240.
[6] D. Filippini, I. Lundström, *Anal. Chim. Acta* **2004**, *512*, 239.
[7] M. Gouterman in *The Porphyrins*, *Vol. III* (Ed.: D. Dolphin), Academic Press, New York, **1979**, p. 1.
[8] E. F. Schubert, J. K. Kim, *Science* **2005**, *308*, 1274.
[9] D. Filippini, I. Lundström, *Appl. Phys. Lett.* **2002**, 81, 3891.
[10] A. Suska, D. Filippini, T. Andersson, I. Lundström, *Biosens. Bioelectron.* **2005**, *21*, 727.
[11] A. Manz, N. Pamme, D. Lossifidis, *Bioanalytical Chemistry*, Imperial College Press, London, **2004**.
[12] T. Mayr, C. Igel, G. Liebsch, I. Klimant, O. Wolfbeis, *Anal. Chem.* **2003**, *75*, 4389.
[13] C. Di Natale, D. Salimbeni, R. Paolesse, A. Macagnano, A. D'Amico, *Sens. Actuators B* **2000**, 65, 220.
[14] M. Salleh, M. , Akrajas, M. Yahaya, *Thin Solid Films* **2002**, *417*, 162.
[15] K. S. Suslick, N. A. Rakow, A. Sen, *Tetrahedron* **2004**, *60*, 11133.
[16] N. A. Rakow, A. Sen, M. C. Janzen, J. B. Ponder, K. S. Suslick, *Angew. Chem.* **2005**, *117*, 4604; *Angew. Chem. Int. Ed.* **2005**, *44*, 4528.
[17] N. C. Birch, D. F. Stickle, *Clin. Chim. Acta* **2003**, 333, 95.
[18] T. Jolliffe, *Principal Component Analysis*, Springer, Heidelberg, **1986**.
[19] R. Johnson, D. Wichern, *Applied Multivariate Statistical Analysis*, Pearson Education, Prentice Hall, New Jersey, **2002**.
[20] a) D. G. Whitten, I. G. Lopp, P. D. Wildes, *J. Am. Chem. Soc.* **1968**, *90*, 7196; b) M. Nappa, J. S. Valentine, *J. Am. Chem. Soc.* **1978**, *100*, 5075.
[21] R. Paolesse in *The Porphyrin Handbook*, *Vol. 2* (Eds.: K. M. Kadish, K. M. Smith, R. Guilard), Academic Press, San Diego, **2000**, p. 201.
[22] http//earth.google.com or http//virtualearth.msn.com.
[23] J. W. Buchler in *The Porphyrins*, *Vol. I* (Ed. D. Dolphin), Academic Press, New York, **1979**, p. 389.

 © 2006 Wiley-VCH Verlag GmbH & Co. KGaA, Weinheim

Multiple Bonds

DOI: 10.1002/anie.200600110

A Quantum Chemical Study of the Quintuple Bond between Two Chromium Centers in [PhCrCrPh]: *trans*-Bent versus Linear Geometry**

Marcin Brynda, Laura Gagliardi,* Per-Olof Widmark, Philip P. Power, and Björn O. Roos*

The recent report of a stable, crystalline compound with a quintuply bonded chromium–chromium core[1] may reopen the debate on the nature of the multiple bonds between transition metals[2] that was initiated by the discovery of a stable, quadruple bond by Cotton et al. in 1964.[3] Although a recent study of a quintuple bond in the uranium dimer[4] U_2 provided strong support for the existence of such bonds, the isolation of the stable [Ar′CrCrAr′] species (Ar′ = 2,6-(2,6-*i*Pr$_2$-C$_6$H$_3$)$_2$-C$_6$H$_3$), which has a planar, *trans*-bent rather than a linear $C_{ipso}Cr{-}CrC_{ipso}$ core and weak temperature-independent paramagnetism, has raised new questions about multiple bonding. Such a *trans*-bent structure was recently predicted for the simple [HCrCrH] dimer by Weinhold and Landis on the basis of DFT calculations and a natural-bond analysis.[5]

The simplest molecule containing a Cr–Cr bond is Cr_2. Its experimental bond length, obtained from laser-induced fluorescence spectroscopy, is 1.679 Å, and this extremely short Cr–Cr bond has a formal bond order of six, although its significance was questioned[6] because of its low dissociation energy (1.53 ± 0.06 eV). According to different theoretical studies, the description of the CrCr interaction in Cr_2 ranges from a sextuple bond,[7–10] through a single bond,[11] to a complete absence of bonding between the chromium atoms.[6]

[*] Dr. M. Brynda, Prof. P. P. Power
Department of Chemistry
University of California, Davis
One Shields Avenue, Davis 95616 CA (USA)
Fax: (+01) 530-752-8995
E-mail: mabrynda@ucdavis.edu
Prof. L. Gagliardi
Département de Chimie Physique
Université de Genève
30, q. E. Ansermet, 1211 Genève (Switzerland)
Fax: (+41) 022-379-6518
E-mail: laura.gagliardi@chiphy.unige.ch
Dr. P.-O. Widmark, Prof. B. O. Roos
Department of Theoretical Chemistry
Chemical Center
P.O. Box 124 S-221 00 Lund (Sweden)

[**] We are grateful to the Petroleum Research Fund administered by the American Chemical Society and the National Science Foundation. B.O.R. and P.-O.W. thank the Swedish Foundation for Strategic Research (SSF) for financial support. L.G. thanks the Swiss National Foundation for financial support.

Supporting information for this article is available on the WWW under http://www.angewandte.org or from the author.

It is now well established that a proper description of the bonding in this species requires a multiconfigurational treatment. A description of the bonding in Cr_2 that is in full agreement with the experimental data was obtained in a recent study.[12] Formally, a sextuple bond is formed, but the effective bond order is only about four because of mixing of excited, less-bonding states into the ground state. Similar behavior was also observed for $[Re_2Cl_8]^{2-}$, in which a formal quadruple bond was found to have a bond order of only about three for similar reasons.[13,14]

The bonding scheme in the [Ar′CrCrAr′] complex resembles that found in the Cr_2 dimer: The interaction of two Cr^I centers with d^5 electron configurations leads to five, rather than six, metal–metal bonding molecular orbitals, along with their antibonding counterparts. The questions that arise are: which electronic configurations dominate the ground-state wave function, and how important is the contribution of the bonding $(\sigma_g)^2(\pi_u)^4(\delta_g)^4$ configuration? The main difference between the bonding in Cr_2 and [Ar′CrCrAr′] lies in the fact that two additional metal–ligand orbital combinations involving the participation of mainly 4s orbitals in the metal–carbon(ligand) bond are present in [Ar′CrCrAr′]. Despite this apparent similarity, the situation in the real complex is more complicated because of the size of the ligands, and also because of the presence of the "indirect" metal–ligand interactions. Because of the presence of the flanking aryl groups in the vicinity of the chromium centers, a weak, but non-negligible interaction occurs.[1] This interaction, along with the large size of the ligand, can lengthen the Cr–Cr bond in the [Ar′CrCrAr′] compound.

We now report the results of a theoretical study of a simplified model compound for [Ar′CrCrAr′], namely [PhCrCrPh] (Ph = phenyl). The complete active space (CAS) self-consistent field (SCF) method[15] was used to generate molecular orbitals and reference functions for subsequent multiconfigurational second-order perturbation calculations of the dynamic correlation energy (CASPT2).[16] Additional DFT calculations were performed on the [PhCrCrPh] model and on the experimentally observed [Ar′CrCrAr′] compound. The results show that the *trans*-bent and linear geometries at the CASPT2 level are essentially degenerate but are separated by an appreciable barrier (Figure 1). Fivefold bonding with filled bonding orbitals $(\sigma_g)^2(\pi_u)^4(\delta_g)^4$ is the predominant configuration in the wave function.

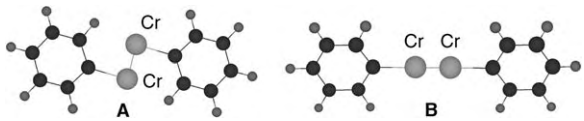

Figure 1. *trans*-Bent (**A**) and linear (**B**) structures of the model [PhCrCrPh] compound optimized at the CASSCF/CASPT2 level.

The most-significant structural parameters for the *trans*-bent (**A**) and linear (**B**) [PhCrCrPh] structures are reported in Table 1. The computed bond distances for the *trans*-bent structure (Cr–Cr = 1.75 Å, Cr–C = 2.018 Å) are somewhat

 WILEY InterScience DISCOVER SOMETHING GREAT © 2006 Wiley-VCH Verlag GmbH & Co. KGaA, Weinheim

Table 1: Bond lengths [Å] and angles [°] of the linear and *trans*-bent structures of [PhCrCrPh] optimized at the CASPT2 level.

[PhCrCrPh]	Cr–Cr	C–Cr	C-Cr-Cr
linear	1.678	2.040	180.0
trans-bent	1.752	2.018	88.4

shorter than the experimentally determined values (Cr–Cr = 1.83, Cr–C = 2.15 Å).[1] As will be shown below, this difference can be attributed to the extra aryl substituents in [Ar′CrCrAr′], which because of steric and electronic factors as well as the presence of an additional Cr–ring interaction weaken both the Cr–Cr and Cr–C bonds somewhat. The application of the same computational methodology to Cr_2 also affords a shorter Cr–Cr bond (1.662 Å) than the experimental value (1.679 Å). We computed the Cr–Cr bond energy by comparing the energy of the complex with that of two CrPh units (with DFT-optimized geometry) and found it to be 76 kcal mol^{-1}. In comparison, the bond energy of Cr_2 is 36 kcal mol^{-1}. The bond in [PhCrCrPh] is thus twice as strong. The reason is most likely that, in Cr_2, the interaction of the 4s is repulsive at equilibrium geometry.

The *trans*-bent planar structure is only 1 kcal mol^{-1} higher in energy than the linear structure. However, the compound [Ar′CrCrAr′] has a *trans*-bent structure, and we presume that this preference is a result of the secondary interaction between the chromium and the flanking ring of the ligand. This behavior is not possible in our model compound. A reaction path between **A** and **B** was determined by interpolating the extreme values of the Cr–Cr bond length, Cr–C bond length, and C-Cr-Cr angle. A barrier of 20 kcal mol^{-1} with respect to the linear structure **B** exists for a Ph-Cr-Cr angle of 131°.

The electronic structures of **A** and **B** were analyzed. The major configuration in both forms has all the bonding orbitals occupied: $(\sigma_g)^2(\pi_u)^4(\delta_g)^4$ with a total weight of 45% in the CASSCF wave function for **A**, which corresponds to a formal quintuple bond. The second dominating configuration has a weight of 9% and corresponds to a double excitation $(\delta_g)^2(\delta_u)^2$. The effective bond order is smaller than five as a result of the large occupation of the antibonding orbitals. It can be estimated as the sum of the occupation numbers of the bonding orbitals, minus the corresponding sum for the antibonding orbitals, divided by two. For the form **A**, we obtained the following occupation numbers (Figure 2): $\sigma_g(1.79)$, $\sigma_u(0.21)$, $\pi_u(3.54)$, $\pi_g(0.46)$, $\delta_g(3.19)$, $\delta_u(0.81)$. These values yield an effective bond order of 3.52. The corresponding number for the linear form **B** is 3.69. The larger number is a reflection of the shorter Cr–Cr bond (see the Supporting Information for a picture of the orbitals of **B** along with the occupation numbers). Although the calculated bond order is less than five, the bond is formally quintuple, because five orbitals and five electrons on each atom are involved in the bonding.

The geometry optimizations of the model [PhCrCrPh] compound were also performed at the DFT level of theory, and yielded a minimum for the linear optimized geometry with a Cr–Cr bond length of 1.560 Å. The single configurational DFT approach typically underestimates the Cr–Cr bond lengths. Optimization of a planar *trans*-bent structure with constrained C_{2h} symmetry led to a second-order transition point with the Cr–Cr bond length of 1.658 Å and a Cr-Cr-C angle of 95.0°. A considerable change in the C-Cr-Cr-C core geometry is observed in the DFT-optimized structure of the [Ar′CrCrAr′] molecule. A wider C-Cr-Cr angle (102.7°) and a net elongation of the Cr–Cr bond (by 0.049 Å relative to the [PhCrCrPh] model) clearly indicate that the bulky terphenyl substituents are responsible for these structural changes. Analysis of the DFT results reveals that two different interactions contribute to such behavior: a repulsive interaction between aryl groups in the terphenyl ligands, and a very weak, bonding interaction of the flanking aryl groups with the chromium atoms.

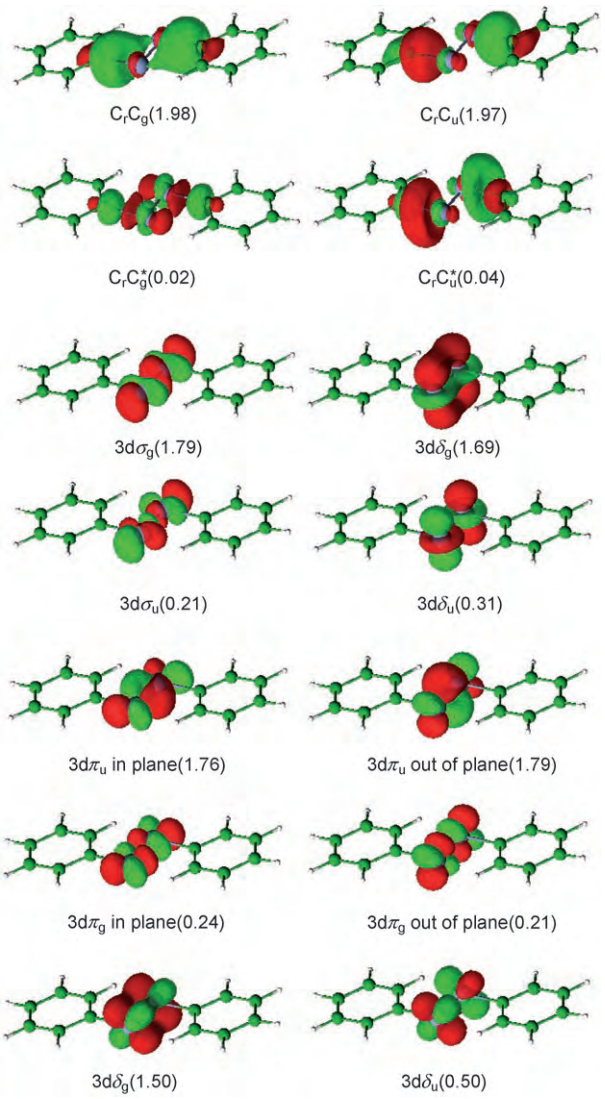

Figure 2. The active molecular orbitals forming the chemical bond between the two chromium centers, and between the chromium centers and the *ipso*-phenyl carbon atoms. The orbital label is given below each orbital, together with the number of electrons occupying the orbital.

 © 2006 Wiley-VCH Verlag GmbH & Co. KGaA, Weinheim

We conclude that a quintuple bond is formed between the Cr atoms in the model compound [PhCrCrPh]. This description is consistent with the pairing of five electrons from each CrPh moiety. The bonding also seems to be stronger than in the formally sixfold bonded chromium dimer Cr_2, which we attribute to the absence of the 4s orbital in the Cr–Cr bond. The geometry of the model compound used in this study is close but not identical to that of the experimentally observed [Ar′CrCrAr′] species. The Cr–Cr bond in [Ar′CrCrAr′] is almost 0.05 Å longer than that in [PhCrCrPh]. When this difference is added to the value of 1.75 Å calculated for [PhCrCrPh] at the CASSCF/CASPT2 level, a Cr–Cr bond length of 1.80 Å results, which is quite close to the experimental value of 1.83 Å. Furthermore, the C-Cr-Cr angle obtained from the DFT-optimized structure (102.7°) of [Ar′CrCrAr′] is identical to the C-Cr-Cr angle determined experimentally in the X-ray structure of this compound. The computed difference in the Cr–Cr bond lengths in [PhCrCrPh] and [Ar′CrCrAr′] is therefore the result of steric repulsion and the extra Cr–ligand bonding that occurs between the metal centers and the flanking aryl groups in the experimental compound. This bonding, even though it is weak, has a significant influence on the structure; it weakens both the Cr–Cr and the Cr–Ph bond.

Further information on this weak interaction can be obtained from DFT calculations, which, because of their monodeterminantal character, cannot properly describe the bonding between the two chromium centers, but can yield important information about the chromium–aryl interaction. The weak chromium–aryl interaction involves mainly chromium centers and the *ipso*-carbon atoms of the flanking aryl groups. This situation bears some resemblance to that observed in chromocene (bis(cyclopentadienyl)chromium(II)) and related derivatives, which have chromium–aryl(centroid) bond lengths in the range 1.60–1.65 Å.[17] In [Ar′CrCrAr′], however, the chromium–aryl(centroid) bond is much longer (2.23 Å). Also, the analysis of the orbital overlaps shows that the chromium–aryl interaction is different and concerns mainly the *ipso*-carbon atom of the flanking aryl group, rather than the whole aryl ring. This situation is a result of the relative positions of the phenyl rings and the Cr center. The "twist" of the flanking aryl group, which causes a pronounced asymmetry, as well as the different orientation of the chromium d orbitals make this interaction weaker than the η^5 complexation observed in chromocene. The DFT calculations suggest that the Cr–C_{ipso} interaction is quite weak and has a value of approximately 1–2 kcal mol^{-1}.

Finally, inspection of the potential-energy surface (PES) scans of the [PhCrCrPh] model (see the Supporting Information) clearly indicates that a *trans*-bent structure is not a minimum but rather a transition point on the PES. Although the size of the bulky terphenyl ligands precluded frequency analysis of the DFT-optimized structure of [Ar′CrCrAr′], we believe that the sterically bulky terphenyl ligands can stabilize the *trans*-bent geometry, and turn a transition point into a minimum in a fashion analogous to that observed in [Ar*PbPbAr*] (Ar* = 2,6-$Ph_2C_6H_3$).[18]

In summary, the number of singly occupied orbitals available for Cr–Cr bonding determines uniquely the formal bond order: six in the chromium dimer, five in the present Cr^{I} compound, and four in Cr^{II} compounds such as $[Cr_2(O_2CMe)_4]$ (Cr–Cr = 1.97 Å,[19] calculated bond length = 1.94 Å).[20]

Experimental Section

Computational details: The CASSCF/CASPT2 calculations were performed by using the software MOLCAS-6.2.[21] The active orbitals were formed by 14 electrons in 14 molecular orbitals (MOs). These orbitals are the two bonding and two antibonding Cr–C MOs and the five bonding and five antibonding Cr–Cr MOs arising as linear combinations of Cr 3d and 4s as well as the phenyl radical orbitals.

Basis sets of the atomic natural-orbital type were used for all atoms. For chromium a basis set developed for relativistic calculations with the Douglas–Kroll–Hess (DKH) Hamiltonian[22,23] was employed. A primitive set 21s15p10d6f4g2h was contracted to 6s5p3d2f1g,[24] whereas basis sets of DZP quality were used for H (7s3p contracted to 2s1p) and C (10s6p3d contracted to 3s2p1d).[25] Scalar relativistic effects were thus included at all levels of theory. Spin-orbit (SO) coupling was not included in the present study. It will have only minor effects on the computed structure for the singlet electronic ground state of the molecule. The CASSCF/CASPT2 method and the basis sets used here have been successful in a number of studies on dimetal compounds such as $[Re_2Cl_8]^{2-}$[14] and the octamethyldimetalates of Cr^{II}, Mo^{II}, and Re^{III}.[13]

An initial geometry optimization was performed both for the planar linear structure (D_{2h} symmetry; Figure 1 **A**) and the planar bent structure (C_{2h} symmetry; Figure 1 **B**) at the DFT level. In the subsequent CASPT2 calculations, only three parameters were re-optimized, namely the Cr–Cr and Cr–Ph bond lengths and the Cr-Cr-Ph angle both for the D_{2h} and C_{2h} structures. The phenyl ring DFT parameters were kept fixed.

DFT calculations were performed by using the zero-order relativistic approximation (ZORA) relativistic Hamiltonian.[26] The geometry optimizations of the model [PhCrCrPh] species were performed with the ADF program[27] in which the ZORA Hamiltonian is combined with Kohn–Sham formalism by using the Becke–Lee–Yang–Paar (BLYP) approximation to the exchange-correlation functional and Slater type orbitals of TZ2P quality. A basis set of TZP quality was used for the optimization of the whole [Ar′CrCrAr′] molecule and the corresponding [PhCrCrPh] model. Vibrational frequencies were analyzed for the minima and the stationary points. The PES scans were performed with fully relaxed geometry (except for the imposed point-group symmetry with a fixed *trans*-bent angle) at each step of the scan. Additional details of DFT calculations are reported in the Supporting Information.

Received: January 11, 2006
Revised: March 15, 2006
Published online: May 3, 2006

Keywords: ab initio calculations · chromium · density functional calculations · metal–metal interactions · multiple bonds

[1] T. Nguyen, A. D. Sutton, M. Brynda, J. C. Fettinger, G. J. Long, P. P. Power, *Science* **2005**, *310*, 844.
[2] F. A. Cotton, C. A. Murillo, R. A. Walton, *Multiple Bonds between Metal Atoms*, 3rd ed. (Eds.: F. A. Cotton, C. A. Murillo, R. A. Walton), Springer, New York, **2005**.
[3] F. A. Cotton, N. F. Curtis, C. B. Harris, B. F. G. Johnson, S. J. Lippard, J. T. Mague, W. R. Robinson, J. S. Wood, *Science* **1964**, *145*, 1305.
[4] L. Gagliardi, B. O. Roos, *Nature* **2005**, *433*, 848.

 © 2006 Wiley-VCH Verlag GmbH & Co. KGaA, Weinheim

[5] F. Weinhold, C. R. Landis, *Valency and Bonding. A Natural Bond Orbital Donor–Acceptor Perspective*, Cambridge University Press, Cambridge, **2005**, p. 556.
[6] M. M. Goodgame, W. A. Goddard III, *J. Phys. Chem.* **1981**, *85*, 215.
[7] C. J. Barden, J. C. Rienstra-Kiracofe, H. F. Schaefer III, *J. Chem. Phys.* **2000**, *113*, 690.
[8] E. A. Boudreaux, E. Baxter, *Int. J. Quantum Chem.* **2001**, *85*, 509.
[9] E. A. Boudreaux, E. Baxter, *Int. J. Quantum Chem.* **2004**, *100*, 1170.
[10] E. A. Boudreaux, E. Baxter, *Int. J. Quantum Chem.* **2005**, *105*, 199.
[11] E. J. Thomas, J. S. Murray, C. J. O'Connor, P. Politzer, *Theochem* **1999**, *487*, 177.
[12] B. O. Roos, *Collect. Czech. Chem. Commun.* **2003**, *68*, 265.
[13] F. Ferrante, L. Gagliardi, B. E. Bursten, A. P. Sattelberger, *Inorg. Chem.* **2005**, *44*, 8476.
[14] L. Gagliardi, B. O. Roos, *Inorg. Chem.* **2003**, *42*, 1599.
[15] B. O. Roos, *Adv. Chem. Phys.* **1987**, 399.
[16] K. Andersson, P. A. Malmqvist, B. O. Roos, A. J. Sadlej, K. Wolinski, *J. Phys. Chem.* **1990**, *94*, 5483.
[17] V. M. Rayon, G. Frenking, *Organometallics* **2003**, *22*, 3304.
[18] Y. Chen, M. Hartmann, M. Diedenhofen, G. Frenking, *Angew. Chem.* **2001**, *113*, 2107; *Angew. Chem. Int. Ed.* **2001**, *40*, 2051.
[19] S. N. Ketkar, M. Fink, *J. Am. Chem. Soc.* **1985**, *107*, 338.
[20] K. Andersson, C. W. Bauschlicher, Jr., B. J. Persson, B. O. Roos, *Chem. Phys. Lett.* **1996**, *257*, 238.
[21] G. Karlstroem, R. Lindh, P.-A. Malmqvist, B. O. Roos, U. Ryde, V. Veryazov, P.-O. Widmark, M. Cossi, B. Schimmelpfennig, P. Neogrady, L. Seijo, *Comput. Mater. Sci.* **2003**, *28*, 222.
[22] M. Douglas, N. M. Kroll, *Ann. Phys.* **1974**, *82*, 89.
[23] B. A. Hess, *Phys. Rev. A* **1986**, *33*, 3742.
[24] B. O. Roos, R. Lindh, P.-A. Malmqvist, V. Veryazov, P.-O. Widmark, *J. Phys. Chem. A* **2005**, *109*, 6575.
[25] K. Pierloot, B. Dumez, P.-O. Widmark, B. O. Roos, *Theor. Chim. Acta* **1995**, *90*, 87.
[26] E. van Lenthe, P. E. S. Wormer, A. van der Avoird, *J. Chem. Phys.* **1997**, *107*, 2488.
[27] ADF-2005.01, SCM, Theoretical Chemistry, Vrije Universiteit, Amsterdam, The Netherlands, http://www.scm.com. For full reference details, see the Supporting Information.

 © 2006 Wiley-VCH Verlag GmbH & Co. KGaA, Weinheim

Water Clusters

DOI: 10.1002/anie.200600254

A Hybrid Water–Chloride Structure with Discrete Undecameric Water Moieties Self-Assembled in a Heptaprotonated Octaamino Cryptand**

*P. S. Lakshminarayanan, Eringathodi Suresh, and Pradyut Ghosh**

Small water clusters are the subject of considerable theoretical and experimental interest as they can lead to an understanding of the structure of bulk water.[1–3] In the past several years, studies on the structural morphologies of water clusters in crystal hydrates have shown that the stabilization of discrete, even-membered water rings such as tetramers,[4] hexamers,[5] octamers,[6] decamers,[7] dodecamers,[8] tetradecamers,[9a] and hexadecamers,[9b] is common within the lattice of a crystal host. Studies on water clusters in different environment have significantly advanced the understanding of the structure of bulk water.[4–10] However, surprisingly little is known of the structural constraints required for stabilizing discrete odd-membered water cluster morphologies of higher nuclearity, even though trimers and pentamers are familiar in crystal hydrates,[11,12] and Férey et al. have isolated an $(H_2O)_{17}$ cluster inside a super-sodalite cage.[13] Here we describe the crystal structure of a discrete, propeller-shaped tricyclic $(H_2O)_{11}$ moiety stabilized by the heptahydrochloride **1** (Figure 1) of the octaamino cryptand $N(CH_2CH_2NHCH_2\text{-}p\text{-}C_6H_4\text{-}CH_2NHCH_2CH_2)_3N$ (L).[14] This study also shows the formation of a hybrid water–chloride structure where chloride encapsulated inside the cryptand cavity is hydrogen-bonded to the undecameric water cluster.

Recently, Mascal et al. have shown that a proper analysis should be done when reporting any new water morphology in a crystal lattice.[15] With this in mind, we performed a Cambridge Structural Database (CSD) search for a propeller-shaped motif having eleven water molecules with the help of the Cambridge Crystallographic Data Centre. Our search algorithm found thirteen matches for the "propeller-shaped" pattern in the CSD.[16] However, in all 13 structures the

[*] P. S. Lakshminarayanan, Dr. E. Suresh, Dr. P. Ghosh
Analytical Science Discipline
Central Salt & Marine Chemicals Research Institute (C.S.I.R.)
Bhavnagar 364002 (India)
Fax: (+91) 278-256-7562
E-mail: pradyut@csmcri.org

[**] We thank Dr. P. K. Ghosh (Director, CSMCRI) for his constant support and encouragement. The authors would also like to thank Dr. J. Chisholm and Dr. L. Infantes of the Cambridge Crystallographic Data Centre and Prof. M. Mascal, UC Davis (USA), for performing a CSD search and for helpful discussions. P.G. gratefully acknowledges the Department of Science and Technology, New Delhi, India (grant no. SR/S1/IC-21/2002) for financial support. P.S.L. acknowledges CSIR, India, for a senior research fellowship.

Supporting Information for this article is available on the WWW under http://www.angewandte.org or from the author.

 © 2006 Wiley-VCH Verlag GmbH & Co. KGaA, Weinheim InterScience

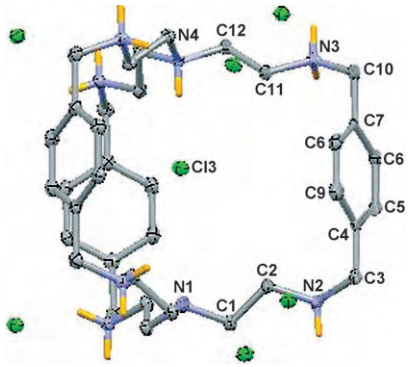

Figure 1. ORTEP diagram of **1**, the heptahydrochloride salt of **L**, with atom numbering scheme (hydrogen atoms attached to the carbon atoms have been omitted for clarity). C gray, Cl green, H yellow, N blue.

propeller-shaped pattern was not discrete but was embedded in an extended water network and our motif cannot be generated with a subset of water molecules included in these crystal structures. To the best of our knowledge, therefore, there is no structural information available for a discrete $(H_2O)_{11}$ cluster or its participation in the stabilization of a supramolecular assembly.[1–13,15,16]

A single crystal of the complex $\mathbf{1}\cdot(H_2O)_{11}$ ($L\cdot 7\,HCl\cdot 11\,H_2O$) was isolated from a methanol/water solution of the white solid that had been obtained upon addition of HCl to an acetonitrile solution of L. In our previous study, protonation of L with HCl in methanol gave the hexaprotonated salt containing disordered water molecules.[17] Complex **1** is expected to facilitate the formation of various water aggregates by forming a hydrogen-bonding network similar to biological systems since it displays different types of amino nitrogen atoms as well as encapsulated and surrounding chloride anions.

X-ray crystallographic analysis revealed that $\mathbf{1}\cdot(H_2O)_{11}$ crystallizes in the hexagonal space group $P6_3$ with two molecules in the unit cell. The chloride anion Cl3 and water molecules O1 and O5 occupy specific positions with C_3 symmetry. The heptaprotonated cryptand also has threefold symmetry, with the C_3 axis bisecting the apical nitrogens N1 and N4 and the hydrogen H4 attached to the bridgehead nitrogen N4. It is interesting to note that Cl3, which is encapsulated within the cryptand cavity, is positioned exactly in the plane of N1, N4, and H4. However, the distances between Cl3 and the bridgehead nitrogen atoms vary considerably (Cl3···N1 3.847 and Cl3···N4 3.059 Å), with a closer approach towards the protonated nitrogen making for a strong intramolecular N–H···Cl^- interaction. A further two chloride anions outside the cryptand cavity are involved in strong inter- and intramolecular H-bonding interactions. Except for the bridgehead nitrogen N1, all other amino nitrogen atoms are protonated and the N–C distances clearly account for the heptaprotoned cryptand moiety (N1–C1 1.4711(17), N2–C2 1.496(2), N2–C3 1.503(2), N3–C11 1.491(2), N3–C10 1.516(2), and N4–C12 1.5060(17) Å).

Eleven water molecules per molecule of **1** in this supramolecular complex form a "propeller-shaped" undecameric water cluster from symmetry-induced tricyclic fused pentameric $(H_2O)_5$ units (O1–O5) around the protonated cryptand host in the solid state (Figure 2a). An ORTEP

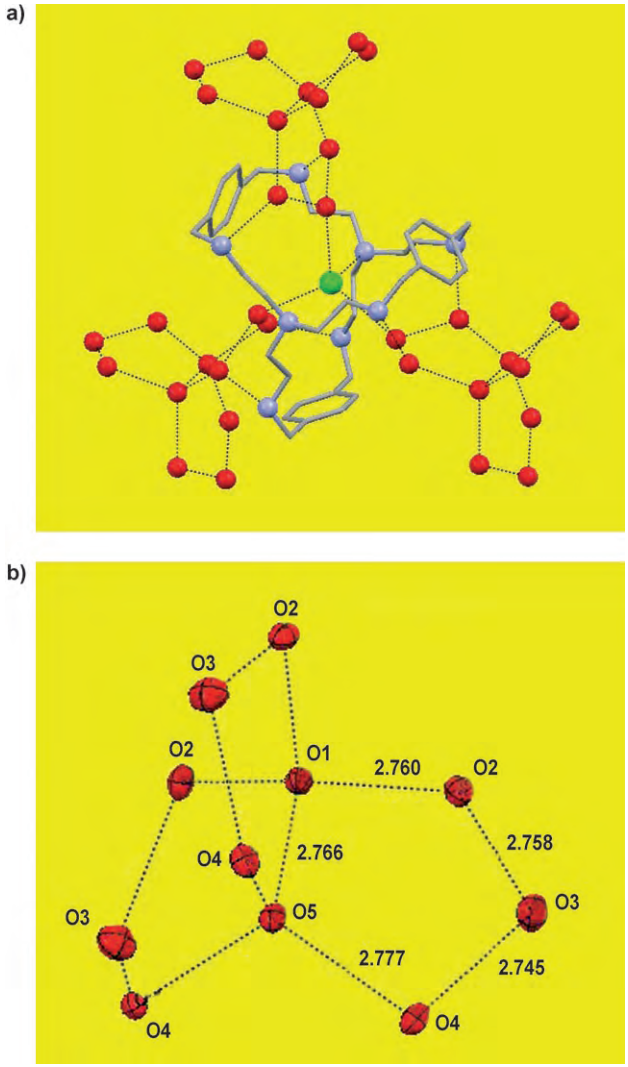

Figure 2. a) Anchoring of the encapsulated chloride (Cl3, green) inside the cryptand cavity by one N–H···Cl^- interaction and three O–H···Cl^- interactions; hydrogen-bonds are represented by dotted lines. C gray, N blue, O red. b) ORTEP diagram of the discrete $(H_2O)_{11}$ cluster. Hydrogen atoms are not depicted.

drawing of one water cluster is shown in Figure 2b. The two water molecules on the threefold axis (O1 and O5) create a fused pentameric unit, which translates into a discrete "propeller-type" arrangement of water molecules around the C_3 axis passing through O1 and O5.The symmetry-related fused pentamers in the $(H_2O)_{11}$ units are strongly held together by O–H···O interactions, with the O···O distance ranging from 2.745 to 2.777 Å (average: 2.761 Å) and the O···O···O angle from 102.03° to 111.20° (average: 106.6°). Ab initio investigations by Sathyamurthy et al. have shown that the most stable geometry for an 11-mer water cluster is a fused pentamer with the eleventh water molecule hydrogen-bonded to one of the corners. These authors also proposed a

 © 2006 Wiley-VCH Verlag GmbH & Co. KGaA, Weinheim

cuboid structure with a missing corner, which has a slightly higher energy than the fused pentameric structure.[18] However, our structural finding is of a discrete C_3 symmetric undecameric water cluster composed of three fused pentameric rings sharing a common edge. The difference between the theoretical prediction and our experimental finding may be due to the various hydrogen-bonding interactions of the water cluster with the cationic host moiety as well as with the surrounding anions, similar to the bound water in biological systems. We also believe that the symmetry of the host cryptand contributes to this unusual morphology of a discrete undecameric water cluster in the lattice.

The encapsulated chloride anion (Cl3) present inside the cryptand cavity forms strong N–H···Cl^- and O–H···Cl^- intramolecular interactions with the protonated apical amino hydrogen H4 and the water hydrogen H3C of the $(H_2O)_{11}$ cluster. Thus, the chloride anion within the cavity makes four contacts—one N–H···Cl^- (N4···Cl3 3.059(3) Å; N4–H4···Cl3 180°) and three O–H···Cl^- (O3···Cl3 3.253(2) Å; O3–H3C···Cl3 170°) intramolecular contacts—with the threefold symmetry-related $(H_2O)_{11}$ units, thereby extending the hydrogen-bonded supramolecular network (Figure 2a).

The hydrogen-bonding interactions of the undecameric water cluster with the surrounding organic moiety and chloride anion are depicted in Figure 3. The centrosymmetric

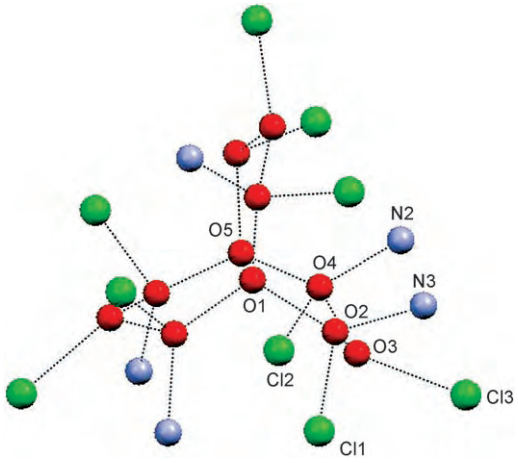

Figure 3. Interaction of $(H_2O)_{11}$ with the cryptand moiety and chloride ions.

water molecules O1 and O5 are only involved in O–H···O hydrogen bonding within the $(H_2O)_{11}$ cluster. In addition to the water cluster formation, O3 is also involved in hydrogen bonding to Cl3, as described earlier, whereas O2 and O4 are involved in one intramolecular O–H···Cl^- interaction with Cl1 and Cl2, respectively, which lie outside the cryptand cavity, and one intermolecular N–H···O interaction with H31 and H22, respectively, of the amino nitrogens N3 and N2 of the surrounding cryptand moiety. Cl1 and Cl2, which occupy a position outside the cryptand cavity, form two strong C–H···Cl^- and one N–H···Cl^- intermolecular hydrogen bond with the heptaprotonated cryptand ligand. Details of these hydrogen-bonding interactions, along with their symmetry codes, are given in the Supporting Information. Thus, Cl1 and Cl2 also make four contacts (one intramolecular hydrogen bond with water hydrogens, two C–H···Cl^- intermolecular contacts with methylene hydrogens, and one N–H···Cl^- contact with the tertiary amino hydrogens of the cryptand).

Figure 4 shows the three-dimensional hydrogen-bonded supramolecular array involving the protonated cryptand moiety, the chloride anion, and the undecameric water

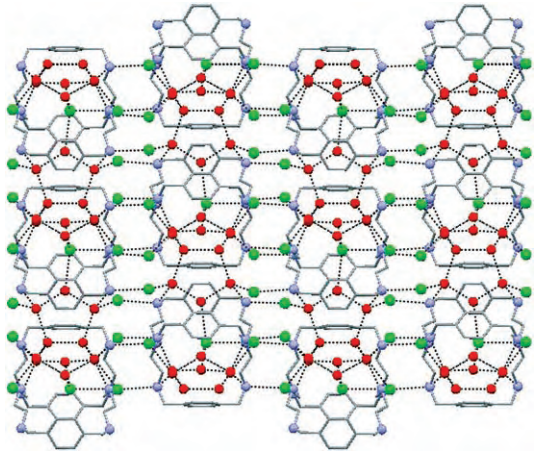

Figure 4. Packing diagram of $\mathbf{1}\cdot(H_2O)_{11}$ viewed down the *b* axis showing various inter- and intramolecular hydrogen-bonding interactions between the discrete $(H_2O)_{11}$ moiety, the chloride ions, and the amino nitrogens of the cryptand.

cluster, along with several of their molecular interactions.

Thermal analysis of $\mathbf{1}\cdot(H_2O)_{11}$ shows that the first weight loss takes place in at 40–140 °C (13.62 %), corresponding to the loss of 7.94 molecules of water. The second weight loss starts at 150 °C and is completed at 260 °C (5.18 %), corresponding to a further 3.02 water molecules.[19] The total loss of 11 water molecules in these two steps can be attributed to the loss of the $(H_2O)_{11}$ cluster. Moreover, the removal of water molecules from the cluster at elevated temperature confirms that most of the water molecules have a strong interaction with heptaprotonated L and the chloride anions, as observed in the single-crystal X-ray studies.

The broad band centered around 3400 cm^{-1} in the FT-IR spectrum of $\mathbf{1}\cdot(H_2O)_{11}$ can be attributed to the O–H stretching frequency of the water cluster as it is similar to the stretching vibration of liquid water.[20] The IR spectrum of the same crystals after heating for six hours at about 140 °C under vacuum (0.1 mm) shows that the broad band has disappeared, thus suggesting the escape of the water cluster from the lattice. Powder X-ray diffraction studies on $\mathbf{1}\cdot(H_2O)_{11}$ before and after expulsion display changes in the diffraction patterns and intensities, which can be attributed to the complete breakdown of the host lattice upon exclusion of water.[19] This sample does not regain its original structure upon exposure to moisture, as determined by IR and TGA studies.

In summary, we have shown that the bound water in the lattice of a supramolecular host having cationic and neutral amine functionalities along with encapsulated and surrounding chloride anions has a discrete tricyclic $(H_2O)_{11}$ cluster

 © 2006 Wiley-VCH Verlag GmbH & Co. KGaA, Weinheim

morphology. This unique, discrete, propeller-shaped undecameric water cluster forms hydrogen bonds with both the host cryptand and surrounding chloride, and also forms strong hydrogen-bonding interactions with the chloride guest inside the host cavity. The present mode of stabilization of an undecameric water cluster morphology and its hydrogen-bonding interactions with the encapsulated chloride has not been predicted theoretically or reported experimentally.

Experimental Section

Compound L was prepared following a procedure reported previously and confirmed by ^{1}H NMR spectroscopy.[14] The complex $\mathbf{1}\cdot(H_2O)_{11}$ was isolated from a methanol/water (4:1) solution of the white solid obtained upon addition of HCl to an acetonitrile solution of L. Colorless crystals suitable for X-ray analysis were grown by slow evaporation of this mixture at room temperature.

^{1}H NMR (200 MHz, D_2O): $\delta = 2.85$ (t, $J(H,H) = 5$ Hz, 12H, NCH_2), 3.33 (t, $J(H,H) = 5$ Hz, 12H, NCH_2CH_2), 4.30 (s, 12H, $ArCH_2$), 7.49 ppm (s, 12H, Ar*H*). ^{13}C NMR (50 MHz, D_2O): $\delta = 45.2$ (NCH_2), 50.0 (NCH_2CH_2), 51.6 ($ArCH_2$), 130.4 (C_{Ar}), 132.4 ppm (CH_{Ar}). C,H,N analysis (%) calcd for $C_{36}H_{83}Cl_7N_8O_{11}$: C 41.09, H 7.95, N 10.65; found: C 41.25, H 7.68, N 10.57.

Crystal data for $\mathbf{1}\cdot(H_2O)_{11}$ were collected at 100 K with a SMART APEX diffractometer equipped with a CCD area detector and a $Mo_{K\alpha}$ radiation source ($\lambda = 0.7107$ Å). A crystal was selected from the mother liquor, immersed in Paratone oil, and then mounted. Data collection, data reduction, and structure solution/refinement were carried out using the software package SMART APEX.[21] Graphics were generated with MERCURY 1.1.1.3.[22] Empirical absorption corrections were performed using equivalent reflections with the program SADABS. The structure was solved by direct methods and refined in a routine manner. Non-hydrogen atoms were treated anisotropically in all cases. Hydrogen atoms attached to the amino nitrogens and some of the water hydrogens were located from the difference Fourier map and refined isotropically. In other cases, the hydrogen atoms were geometrically fixed. We were unable to locate the hydrogen atoms of water molecules O1 and O5, which sit on the threefold axis, from the difference Fourier map. Crystal dimension: $0.32 \times 0.23 \times 0.17$ mm^3; $T = 100(2)$ K; hexagonal, space group $P6_3$; $a = b = 12.4720(4)$, $c = 21.2022(15)$ Å, $V = 2856.2(2)$ Å^3, $Z = 2$, $\rho_{calcd} = 1.219$ g cm^{-3}, $\mu = 0.401$ mm^{-1}, $F(000) = 1116$, 16937 reflections collected of which 4480 were unique, 187 parameters were refined; $R_1 = 0.0318$, $wR_2 = 0.0880$; max./min. residual electron density 0.500/-0.217 e Å^{-3}. CCDC-295431 contains the supplementary crystallographic data for this paper. These data can be obtained free of charge from The Cambridge Crystallographic Data Centre via www.ccdc.cam.ac.uk/data_request/cif.

Received: January 20, 2006
Published online: May 3, 2006

Keywords: anion binding · cryptands · hydrogen bonds · solid-state structures · water clusters

[1] a) R. Ludwig, *Angew. Chem.* **2001**, *113*, 1856; *Angew. Chem. Int. Ed.* **2001**, *40*, 1808; b) N. K. Keutsch, R. J. Saykally, *Proc. Natl. Acad. Sci. USA* **2001**, *98*, 10533; c) M. Henry, *ChemPhysChem* **2002**, *3*, 607.

[2] a) G. A. Jeffrey, *An Introduction to Hydrogen Bonding*, Oxford University Press, Oxford, **1997**; b) P. Ball, *H_2O: A Biography of Water*, Weidenfeld & Nicolson, London, **1999**.

[3] a) K. Liu, M. G. Brown, C. Carter, R. J. Saykally, J. K. Gregory, D. C. Clary, *Nature* **1996**, *381*, 501; b) K. Nauta, R. E. Miller, *Science* **2000**, *287*, 293; c) F. Weinhold, *J. Chem. Phys.* **1998**, *109*, 367; d) J. M. Ugalde, I. Alkorta, J. Elguero, *Angew. Chem.* **2000**, *112*, 733; *Angew. Chem. Int. Ed.* **2000**, *39*, 717; e) F. N. Keutsch, J. D. Cruzan, R. J. Saykally, *Chem. Rev.* **2003**, *103*, 2533.

[4] a) M. Zuhayra, W. U. Kampen, E. Henze, Z. Soti, L. Zsolnai, G. Huttner, F. Oberdorfer, *J. Am. Chem. Soc.* **2006**, *128*, 424; b) S. Supriya, S. Manikumari, P. Raghavaiah, S. K. Das, *New J. Chem.* **2003**, *27*, 218; c) M. T. Ng, T. C. Deivaraj, W. T. Klooster, G. J. McIntyre, J. J. Vittal, *Chem. Eur. J.* **2004**, *10*, 5853.

[5] a) J. N. Moorthy, R. Natarajan, P. Venugopalan, *Angew. Chem.* **2002**, *114*, 3567; *Angew. Chem. Int. Ed.* **2002**, *41*, 3417; b) R. Custelcean, C. Afloroaei, M. Vlassa, M. Polverejan, *Angew. Chem.* **2000**, *112*, 3224; *Angew. Chem. Int. Ed.* **2000**, *39*, 3094; c) S. K. Ghosh, P. K. Bharadwaj, *Inorg. Chem.* **2004**, *43*, 5180.

[6] a) W. B. Blanton, S. W. Gordon-Wylie, G. R. Clark, K. D. Jordon, J. T. Wood, U. Geiser, T. J. Collins, *J. Am. Chem. Soc.* **1999**, *121*, 3551; b) J. L. Atwood, L. J. Barbour, T. J. Ness, C. L. Raston, P. L. Raston, *J. Am. Chem. Soc.* **2001**, *123*, 7192; c) R. J. Doedens, E. Yohannes, M. I. Khan, *Chem. Commun.* **2002**, 62; d) B.-Q. Ma, H.-L. Sun, S. Gao, *Chem. Commun.* **2005**, 2336.

[7] a) L. J. Barbour, G. W. Orr, J. L. Atwood, *Nature* **1998**, *393*, 671; b) L. J. Barbour, G. W. Orr, J. L. Atwood, *Chem. Commun.* **2000**, 859; c) M. Yoshizawa, T. Kusukawa, M. Kawano, T. Ohhara, I. Tanaka, K. Kurihara, N. Niimura, M. Fujita, *J. Am. Chem. Soc.* **2005**, *127*, 2798.

[8] a) S. K. Ghosh, P. K. Bharadwaj, *Angew. Chem.* **2004**, *116*, 3661; *Angew. Chem. Int. Ed.* **2004**, *43*, 3577; b) Q.-Y. Liu, L. Xu, *CrystEngComm* **2005**, *7*, 87.

[9] a) S. K. Ghosh, J. Ribas, M. S. E. Fallah, P. K. Bharadwaj, *Inorg. Chem.* **2005**, *44*, 3856; b) S. K. Ghosh, P. K. Bharadwaj, *Inorg. Chem.* **2004**, *43*, 6887.

[10] a) S. Pal, N. B. Sankaran, A. Samanta, *Angew. Chem.* **2003**, *115*, 1783; *Angew. Chem. Int. Ed.* **2003**, *42*, 1741; b) B.-Q. Ma, H.-L. Sun, S. Gao, *Angew. Chem.* **2004**, *116*, 1398; *Angew. Chem. Int. Ed.* **2004**, *43*, 1374; c) K. Raghuraman, K. K. Katti, L. J. Barbour, N. Pillarsetty, C. L. Barnes, K. V. Katti, *J. Am. Chem. Soc.* **2003**, *125*, 6955; d) C. Janiak, T. G. Scharmann, S. A. Mason, *J. Am. Chem. Soc.* **2002**, *124*, 14010; e) A. Michaelides, S. Skoulika, E. G. Bakalbassis, J. Mrozinski, *Cryst. Growth Des.* **2003**, *3*, 487; f) P. Rodriguez-Cuamatzi, G. Vargas-Diaz, H. Höpfl, *Angew. Chem.* **2004**, *116*, 3103; *Angew. Chem. Int. Ed.* **2004**, *43*, 3041; g) P. S. Lakshminarayanan, E. Suresh, P. Ghosh, *J. Am. Chem. Soc.* **2005**, *127*, 13132; h) N. S. Oxtoby, A. J. Blake, N. R. Champness, C. Wilson, *Chem. Eur. J.* **2005**, *11*, 1; i) B. Sreenivasulu, J. J. Vittal, *Angew. Chem.* **2004**, *116*, 5893; *Angew. Chem. Int. Ed.* **2004**, *43*, 5769.

[11] a) L. Infantes, S. Motherwell, *CrystEngComm* **2002**, *4*, 454; b) L. Infantes, J. Chisholm, S. Motherwell, *CrystEngComm* **2003**, *5*, 480.

[12] a) S. K. Ghosh, P. K. Bharadwaj, *Inorg. Chem.* **2005**, *44*, 5553; b) B.-Q. Ma, H.-L. Sun, S. Gao, *Chem. Commun.* **2004**, 2220; c) L. R. MacGillivray, J. L. Atwood, *J. Am. Chem. Soc.* **1997**, *119*, 2592.

[13] a) L. Beitone, C. Huguenard, A. Gansmüller, M. Henry, F. Taulelle, T. Loiseau, G. Férey, *J. Am. Chem. Soc.* **2003**, *125*, 9102; b) M. Henry, F. Taulelle, T. Loiseau, L. Beitone, G. Férey, *Chem. Eur. J.* **2004**, *10*, 1366.

[14] D. Chen, A. E. Martell, *Tetrahedron.* **1991**, 47, 6895.

[15] M. Mascal, L. Infantes, J. Chisholm, *Angew. Chem.* **2006**, *118*, 36; *Angew. Chem. Int. Ed.* **2006**, *45*, 32.

[16] CSD refcodes of the 13 structures: BUTAHC10, DETHHC20, GIZFEA, IBIDAY, ISAPHM10, KEJQAR, LEWBUK, OBILOA, OKECIQ, PEXQIS, QAFGEJ, UGAQAU, and WEZXOO.

[17] P. S. Lakshminarayanan, D. K. Kumar, P. Ghosh, *Inorg. Chem.* **2005**, *44*, 7540.

 © 2006 Wiley-VCH Verlag GmbH & Co. KGaA, Weinheim

[18] S. Maheshwary, N. Patel, N. Sathyamurthy, A. D. Kulkarni, S. R. Gadre, *J. Phys. Chem. A* **2001**, *105*, 10525.
[19] See Supporting Information.
[20] D. Eisenberg, W. Kauzmann, *The Structure and Properties of Water*, Oxford University Press, Oxford, UK, **1969**.
[21] Bruker AXS: Madison, WI, **1999**.
[22] Mercury 1.1.1.3 supplied with Cambridge Structural Database, CCDC, Cambridge, UK, **2003**.

 © 2006 Wiley-VCH Verlag GmbH & Co. KGaA, Weinheim

Synthetic Methods

DOI: 10.1002/anie.200600910

The Enantioselective Allylation and Crotylation of Sterically Hindered and Functionalized Aryl Ketones: Convenient Access to Unusual Tertiary Carbinol Structures**

*Noah Z. Burns, Blaine M. Hackman, Pui Yee Ng, Ian A. Powelson, and James L. Leighton**

The development of reagents and catalysts for the enantioselective allylation of ketones has been an important goal in asymmetric synthesis for many years. Over the past decade, some important and seminal advances have been recorded, but most of these require the use of potentially toxic tin-based allyl reagents.[1] More recently, Chong,[2] Shibasaki,[3] Soderquist,[4] and Yamamoto[5] have recorded truly remarkable advances. With only a few notable exceptions, however, the scope of reactions that gives useful levels of efficiency and enantioselectivity remains limited to aryl methyl, cyclohexenyl methyl, and *tert*-butyl methyl ketones and structurally related derivatives thereof. There is no current solution at all for the enantioselective allylation of several important classes of ketones, including highly sterically hindered aryl alkyl ketones and diaryl ketones. In addition, only limited success has thus far been recorded in enantioselective ketone crotylation reactions, and no method that can produce both the *syn* and *anti* diastereomers with high levels of diastereo- and enantioselectivity has been reported. Our own recent investigations into the use of strained allylsilanes[6] for enantioselective aldehyde allylations and crotylations[7] prompted us to wonder whether these reagents might be rendered reactive enough for ketone allylation (Scheme 1). Preliminary experiments showed that with either reagent **1** or **2**, no reaction could be induced with acetophenone under a variety of conditions.

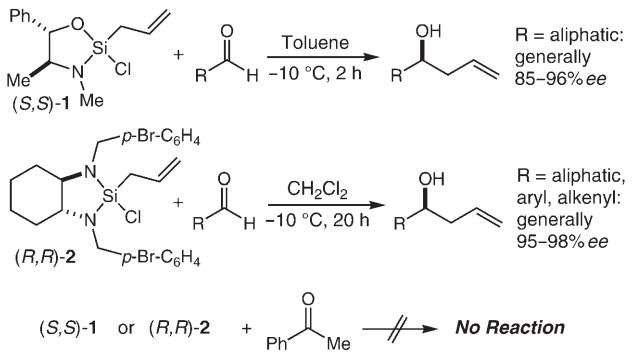

Scheme 1. Asymmetric aldehyde allylation.

Reagent **1** may also be employed for the enantioselective allylation of both aldehyde- and ketone-derived acylhydrazones (Scheme 2).[8] Mechanistic investigations showed that

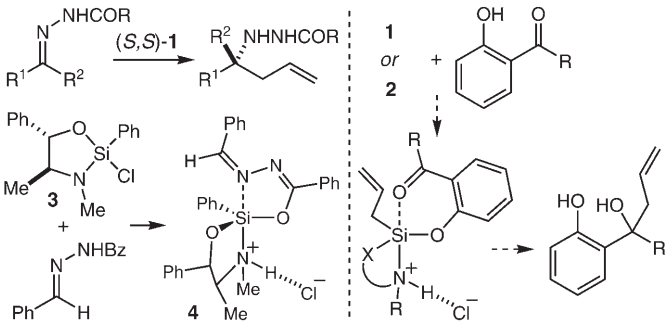

Scheme 2. Proposed hydroxyketone allylation.

the reaction of phenylsilane **3** with the benzoylhydrazone of benzaldehyde gave **4**, as revealed by X-ray crystallography.[8b] Thus, it was discovered that these reactions proceed by covalent attachment of the acyl oxygen atom of the hydrazone to the allylsilane reagent by displacement of the chloride and that the liberated HCl protonates the amino group of the pseudo-ephedrine. The success of the hydrazone allylations may thus be attributed both to their intramolecular reaction pathway and to the presumably significant increase in Lewis acidity of the silane because of the protonation of the amino group. We reasoned that a suitable nucleophile (e.g., phenol) attached to the ketone substrates might mechanistically mimic the acylhydrazones, and therefore we set out to screen such hydroxyketones for reactivity with **1** and **2**.

2′-Hydroxyacetophenone was treated with both **1** and **2**. Although **1** failed to provide a clean reaction, **2** successfully

[*] N. Z. Burns, B. M. Hackman, Dr. P. Y. Ng, I. A. Powelson, Prof. Dr. J. L. Leighton
Department of Chemistry
Columbia University
New York, NY 10027 (USA)
Fax: (+1) 212-932-1289
E-mail: leighton@chem.columbia.edu

[**] Financial support was provided by the National Institutes of Health (GM 58133). N.Z.B. was the recipient of a Pfizer Summer Undergraduate Research Fellowship and an NSF-REU Fellowship. I.A.P. was supported by the Irving Langmuir Scholars Program. We are grateful to Amgen, Merck Research Laboratories, and the Arthur C. Cope Fund for unrestricted research support as well.

Supporting information for this article is available on the WWW under http://www.angewandte.org or from the author.

 © 2006 Wiley-VCH Verlag GmbH & Co. KGaA, Weinheim

allylated the ketone to give tertiary carbinol **5** with encouraging levels of efficiency and enantioselectivity (Scheme 3). After optimization, the product could be obtained in 75% yield and 83% *ee*. Consistent with our mechanistic hypothesis, no allylation products were observed in the reactions of 3′- and 4′-hydroxyacetophenone with **2**. Although the poor performance of **1** is not well understood, we were nevertheless encouraged by the reaction of **2** with 2′-hydroxyacetophenone and undertook a survey of the reaction scope.

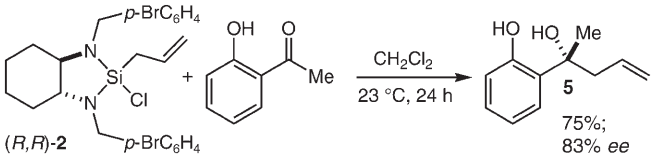

Scheme 3. Asymmetric ketone allylation.

In the hydroxyacetophenone series, substitution of the phenol ring was tolerated with minimal impact on reaction performance (Table 1, entries 1–3). Remarkably, highly sterically hindered ketones could be tolerated as the isopropyl, and even the *tert*-butyl ketone, substrates were not only smoothly allylated but were allylated with improved enantioselectivity (entries 4 and 5). Aryl and heteroaryl ketones were also well tolerated (entries 6–10), thus providing access to enantiomerically enriched diaryl allyl tertiary carbinols. These products are particularly noteworthy in that they would likely be quite difficult to access by allylation of diaryl ketones without recourse to the directing-group strategy employed herein. Indeed, in all previous reports concerning enantioselective ketone allylation, no diaryl ketones have been reported as successful substrates. Thus, the method allows access to truly novel optically active tertiary carbinols, for which there is no obvious alternate approach. Escitalopram, the single enantiomer of the selective serotonin-reuptake inhibitor Celexa, makes the importance of diaryl carbinol derivatives of this type clear. A reasonable entry into systems such as these is demonstrated (entry 10) and further the tolerance of the reaction to extensive functionalization of the aryl rings is shown.

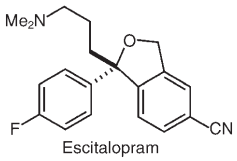

With only two limited exceptions,[3,5] the development of general enantioselective methods for ketone crotylation has proved elusive, and it was thus of interest to examine the corresponding *cis*- and *trans*-crotylsilanes in the present context. Previously reported *cis*-crotylsilane **6**[7c] was found to crotylate 2′-hydroxybenzophenone to give **7** in 63% yield and with excellent diastereo- and enantioselectivity (Scheme 4). The corresponding *trans* crotylsilane **8**[7c] provided **9** in 58% yield and with excellent diastereo- and enantioselectivity. These reactions represent the first method for the highly diastereo- and enantioselective synthesis of both the *syn*- and *anti*-crotyl diastereomers derived from ketones.

Table 1: Enantioselective allylation of 2′-hydroxyphenylketones.

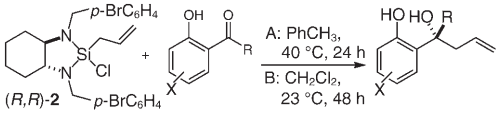

Entry	Conditions	Product	Yield [%]	*ee* [%]
1	A	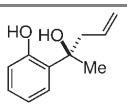	75	83
2	A	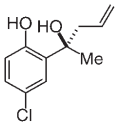	65	81
3	A	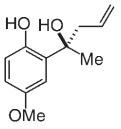	64	82
4	A[a]	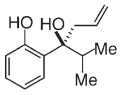	67	88
5	A[a]	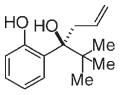	63	93
6	B	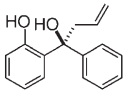	62	93
7	B	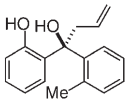	75	94
8	B	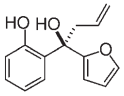	76	88
9	B[a]	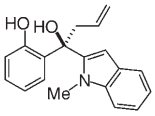	69	95
10	B[b]	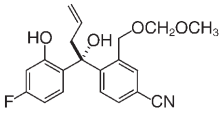	90	90

[a] Reaction time = 48 h. [b] Reaction temperature = 0 °C.

In constructing a mechanistic and stereochemical model for these reactions, the following assumptions, based on the X-ray crystal structure of **4**, were made: 1) The phenol displaces the chloride from the silane, and HCl thus generated protonates one of the amino groups, and 2) the ketone oxygen atom and the protonated amino group occupy apical positions on the trigonal bipyramidal intermediate. Only two such intermediates are possible (**A** and **B**; Scheme 5). In **A**, the indicated steric and electrostatic interactions may plausibly be posited, whereas in **B**, which correctly predicts the observed major enantiomer, no such interactions are present. Further, it is noteworthy that the chairlike transition state depicted in **C** is consistent with the diastereoselectivity observed in the crotylation reactions described in Scheme 4.

 © 2006 Wiley-VCH Verlag GmbH & Co. KGaA, Weinheim

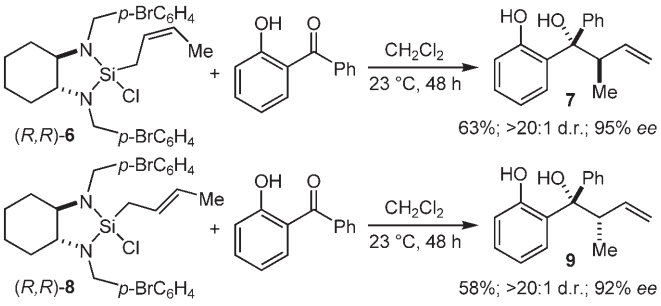

Scheme 4. Enantioselective ketone crotylation.

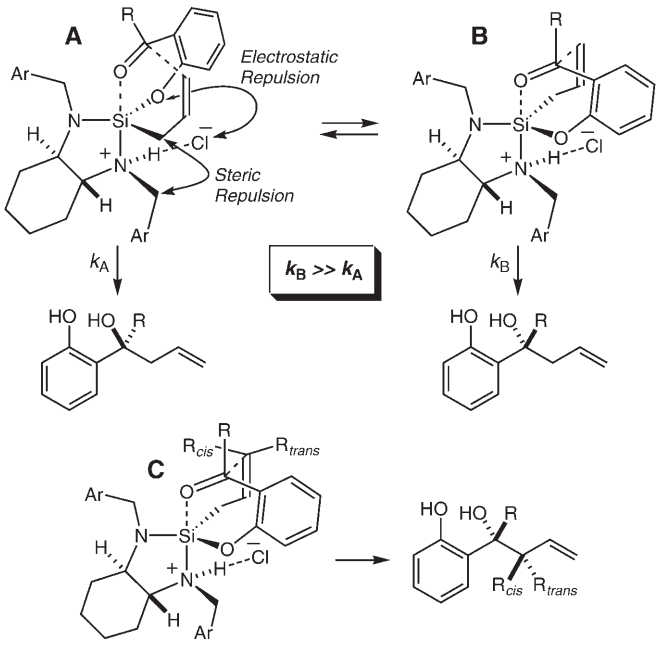

Scheme 5. Mechanistic and stereochemical model.

A simple and convenient method for the enantioselective allylation and crotylation of hydroxyphenylketones has been described. An extraordinary and unprecedented degree of steric hindrance in the ketones is tolerated, and a wide variety of diaryl and heteroaryl ketones are excellent substrates as well, thus leading to structurally novel optically active tertiary carbinols that appear to be otherwise quite difficult to access. In addition, it is further remarkable that the same reagents that are effective for aldehydes are also effective for these ketone allylation and crotylation reactions, despite the fact that the aldehyde and ketone reactions are clearly mechanistically distinct processes. Current goals for this project include the extension of the method to additional classes of ketones and a more detailed understanding of the mechanism.

Experimental Section

General procedure for the enantioselective allylation and crotylation of 2′-hydroxyphenyl ketones: A round-bottomed flask was charged with reagent **2**, **6**, or **8** (1.5 mmol) and toluene or CH_2Cl_2 (5 mL; see Table 1 and Scheme 4). The desired 2′-hydroxyphenyl ketone (1.0 mmol) was then added (neat or as a solution in toluene or CH_2Cl_2 (1 mL)), and the resulting mixture was either cooled to 0 °C, left at ambient temperature, or heated to 40 °C (see Table 1 and Scheme 4). After 24 or 48 h (see Table 1 and Scheme 4), the reaction was quenched by the addition of methanol (3 mL). The mixture was concentrated, and the residue was dissolved in CH_2Cl_2 (10 mL). Water (5 mL) was added, and the layers were separated. The aqueous layer is extracted with CH_2Cl_2 (3 × 10 mL), and the combined organic layers were dried ($MgSO_4$), filtered, and concentrated. Purification of the residue by flash chromatography on silica gel yielded the pure tertiary homoallylic alcohol in the yields and stereoselectivities reported in Table 1 and Scheme 4. See the Supporting Information for full details.

Received: March 8, 2006
Published online: May 3, 2006

Keywords: allylation · allylsilanes · crotylation · enantioselectivity · ketones

[1] a) M. Nakamura, A. Hirai, M. Sogi, E. Nakamura, *J. Am. Chem. Soc.* **1998**, *120*, 5846; b) L. F. Tietze, L. Völkel, C. Wulff, B. Weigand, C. Bittner, P. McGrath, K. Johnson, M. Schäfer, *Chem. Eur. J.* **2001**, *7*, 1304; c) S. Casolari, D. D'Addario, E. Tagliavini, *Org. Lett.* **1999**, *1*, 1061; d) H. Hanawa, S. Kii, K. Maruoka, *Adv. Synth. Catal.* **2001**, *343*, 57; e) K. M. Waltz, J. Gavenonis, P. J. Walsh, *Angew. Chem.* **2002**, *114*, 3849; *Angew. Chem. Int. Ed.* **2002**, *41*, 3697; f) A. Cunningham, S. Woodward, *Synlett* **2002**, 43; g) J. Lu, M.-L. Hong, S.-J. Ji, Y.-C. Teo, T.-P. Loh, *Chem. Commun.* **2005**, 4217.

[2] T. R. Wu, L. Shen, J. M. Chong, *Org. Lett.* **2004**, *6*, 2701.

[3] R. Wada, K. Oisaki, M. Kanai, M. Shibasaki, *J. Am. Chem. Soc.* **2004**, *126*, 8910.

[4] E. Canales, K. G. Prasad, J. A. Soderquist, *J. Am. Chem. Soc.* **2005**, *127*, 11572.

[5] M. Wadamoto, H. Yamamoto, *J. Am. Chem. Soc.* **2005**, *127*, 14556.

[6] For reviews on the chemistry of allylsilanes, see: a) C. E. Masse, J. S. Panek, *Chem. Rev.* **1995**, *95*, 1293; b) L. Chabaud, P. James, Y. Landais, *Eur. J. Org. Chem.* **2004**, 3173.

[7] a) J. W. A. Kinnaird, P. Y. Ng, K. Kubota, K.; X. Wang, J. L. Leighton, *J. Am. Chem. Soc.* **2002**, *124*, 7920; b) K. Kubota, J. L. Leighton, *Angew. Chem.* **2003**, *115*, 976; *Angew. Chem. Int. Ed.* **2003**, *42*, 946; c) B. M. Hackman, P. J. Lombardi, J. L. Leighton, *Org. Lett.* **2004**, *6*, 4375; d) X. Zhang, K. N. Houk, J. L. Leighton, *Angew. Chem.* **2005**, *117*, 960; *Angew. Chem. Int. Ed.* **2005**, *44*, 938.

[8] a) R. Berger, P. M. A. Rabbat, J. L. Leighton, *J. Am. Chem. Soc.* **2003**, *125*, 9596; b) R. Berger, K. Duff, J. L. Leighton, *J. Am. Chem. Soc.* **2004**, *126*, 5686.

 © 2006 Wiley-VCH Verlag GmbH & Co. KGaA, Weinheim

Asymmetric Catalysis

DOI: 10.1002/anie.200600471

Catalytic Enantioselective and Diastereoselective Addition of Aldehyde-Derived Enecarbamates to α-Oxo Aldehydes**

*Ryosuke Matsubara, Nobuyuki Kawai, and Shū Kobayashi**

Catalytic enantioselective aldol reactions have been widely investigated and many successful syntheses have been reported.[1] While most of the studies employed ketones and esters (or their derivatives) as nucleophilic donors, the use of aldehydes as nucleophiles is a challenging topic because side reactions such as self-condensation and further reactions of products take place.[2] Quite recently, Denmark and Ghosh reported the first catalytic diastereo- and enantioselective crossed aldol reactions of aldehydes with trichlorosilyl enolates which are activated by a chiral phosphoramide catalyst.[3] Additionally Northrup and MacMillan have reported proline-catalyzed direct enantioselective crossed aldol reactions between aldehydes, a method which was applied to the facile synthesis of carbohydrates.[4]

In previous publications, we have shown that enamides and enecarbamates may be used as nucleophiles in addition reactions with imines, aldehydes, and ketones.[5] It is especially noteworthy that reactions of enecarbamates afford imine products bearing carbamate N-protecting groups, such as *tert*-butoxycarbonyl (Boc) and benzyloxycarbonyl (Cbz), which may be readily removed to convert those products into other nitrogen-containing compounds. Herein we report asymmetric catalytic addition reactions of aldehyde-derived enecarbamates with aldehydes. The products, in which the aldehyde oxidation level is conserved, were obtained in good yields with high enantioselectivities in the presence of less than 1 mol% of copper(I) catalysts in most cases.

We set about the investigation of this project with enecarbamate **2a** (Scheme 1).[6] Enecarbamates that are derived from aldehydes are rather stable in water and air and they are readily prepared from the corresponding aldehydes (2 steps) or α,β-unsaturated carboxylic acids (1 pot, 4 steps). When the copper(I) catalyst from reference [5b] was employed, **2a** was consumed almost instantaneously, but a complex mixture was obtained and none of the expected products, that is, the aldimine- or aldehyde-type derivatives, were observed after hydrolysis. ^{1}H NMR spectroscopy suggested that the product was a polymeric or oligomeric material. Treatment of this crude material with scandium trifluoromethanesulfonate ($Sc(OTf)_3$) in EtOH/CH_3CN afforded the desired product **3a** in a moderate yield with an excellent *ee* value (see Scheme 1). This result indicates that the crude material obtained in the first reaction includes compounds with the structure of **4a**. However, careful analysis of the products revealed that overreaction had occurred to give compound **5**. In an attempt to suppress the formation of **5**, EtOH was used as a trapping reagent for the initial reactive acylimine product. Under these conditions, product **3a** was obtained without the $Sc(OTf)_3$ treatment, but only in moderate yield (see Scheme 1).[7] The best yield (80%) was observed when *i*PrOH (1 equiv) was employed along with the copper catalyst and the crude product was treated with $Sc(OTf)_3$.

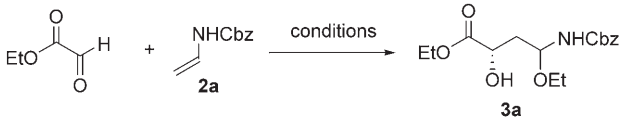

Conditions	Yield [%]	*ee* [%]
$CuClO_4$•$4CH_3CN$ (0.1 mol%), **1** (0.11 mol%), CH_2Cl_2, 0 °C, 1 h, then $Sc(OTf)_3$ (10 mol%), CH_3CN/EtOH, –10 °C, 21 h	45	96
$CuClO_4$•$4CH_3CN$ (0.1 mol%), **1** (0.11 mol%), **EtOH** (2 equiv), CH_2Cl_2, 0 °C, 1 h	42	96
$CuClO_4$•$4CH_3CN$ (0.1 mol%), **1** (0.11 mol%), ***i*PrOH** (1 equiv), CH_2Cl_2, 0 °C, 1 h, then $Sc(OTf)_3$ (10 mol%), CH_3CN/EtOH, –10 °C, 15 h	**80**	92

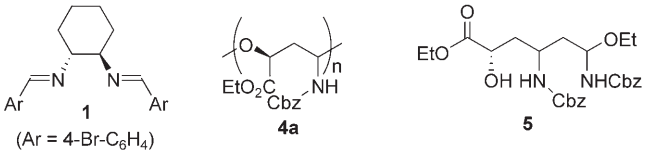

Scheme 1. Reaction of ethyl glyoxylate with aldehyde-derived enecarbamate **2a** to identify the optimal conditions. Compound **4a** is a putative intermediate, compound **5** the overreaction product.

Once the optimal conditions were established, the scope of the reaction was explored (Table 1). Unexpectedly, products of overreaction were not observed even in the absence of alcohol when mono- or disubstituted enecarbamates were used, so in all reactions other than that of entry 1, the alcohol was omitted. It was found that even catalyst loading as low as 0.1 mol% was enough to bring the reaction to completion within 1 h, and the product was obtained with high enantioselectivity (Table 1, entry 1). Phenylglyoxal also performed well in the reaction, with the desired *N*,*O*-acetal being obtained in moderate yield and with an acceptable *ee* value (Table 1, entry 2). The enecarbamate bearing an allyloxycarbonyl protective group on the nitrogen atom was also found to be applicable to this reaction (Table 1, entries 3 and 4). Substituted enecarbamates **2c**–**e**[8] were also acceptable substrates and afforded the corresponding products with good

[*] R. Matsubara, N. Kawai, Prof. Dr. S. Kobayashi
Graduate School of Pharmaceutical Sciences
The University of Tokyo
The HFRE Division, ERATO
Japan Science Technology Agency (JST)
Hongo, Bunkyo-ku, Tokyo 113-0033 (Japan)
Fax: (+81) 3-5684-0634
E-mail: skobayas@mol.f.u-tokyo.ac.jp

[**] This work was partially supported by a Grant-in-Aid for Scientific Research from the Japan Society of the Promotion of Sciences (JSPS).

Supporting information for this article is available on the WWW under http://www.angewandte.org or from the author.

InterScience
© 2006 Wiley-VCH Verlag GmbH & Co. KGaA, Weinheim

Table 1: Cu^{I}-catalyzed addition of enecarbamates **2** to aldehydes.

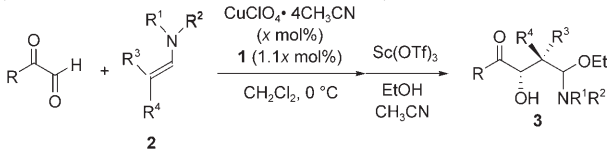

Entry	R	2	R^1, R^2, R^3, R^4	x	t [h]	Yield [%][a]	syn/anti[b]	ee [%][c]
1[d]	OEt	**2a**	H, Cbz, H, H	0.1	1	80	–	92
2[e]	Ph	**2a**		1	1.5	54	–	88
3	OEt	**2b**	H, CO_2All, H, H	0.1	1	50[f]	–	96
4[e]	Ph	**2b**		1	1.5	58	–	91
5	OEt	(*E*)-**2c**	H, Cbz, H, Me	1	5.5	84	12/88	97
6	OEt	(*Z*)-**2c**	H, Cbz, Me, H	1	28	79	92/8	95
7	OEt	(*E*)-**2d**	H, Cbz, H, Et	1	5.5	87	9/91	98
8	OEt	(*Z*)-**2d**	H, Cbz, Et, H	1	28	79	82/18	94
9	OEt	(*E*)-**2e**	H, Cbz, H, Cl	1	24	50[g]	5/95	96
10	OEt	(*Z*)-**2e**	H, Cbz, Cl, H		24	0	–	
11	OEt	**2f**	H, Cbz, Me, Me	5	18	81	–	70
12	OEt	**2f**		1	28	39	–	78
13	OEt	**2g**	Me, Cbz, H, H	5	24	0	–	

[a] Yield of isolated compound **3** unless otherwise noted. [b] The diastereomeric ratio was determined after reduction of **3**; see Supporting Information. [c] *ee* Value of the major diastereomer. [d] *i*PrOH (1 equiv) was added in the copper-catalyzed reaction. [e] **2** was slowly added over 2 h. [f] Yield of toluoylated compound **6**; see Supporting Information. [g] Yield of reduced compound **7**; see Supporting Information. All = allyl group.

yields and high enantioselectivities (Table 1, entries 5–9). It is noteworthy that *anti* and *syn* products were formed stereospecifically from the *E* and *Z* enecarbamates, respectively. Disubstituted enecarbamate **2f** was employed to afford *N*,*O*-acetal **3f** in good yield with modest enantioselectivity (Table 1, entries 11 and 12). The enecarbamate **2g**, which has a tertiary nitrogen atom, did not react with the aldehyde at all, as expected from the results reported previously.[5b,c]

In all cases, the initial products were oligomeric or polymeric (**4**); however, these products could be employed directly in reactions that are typical of *N*,*O*-acetals. For example, allylation proceeded smoothly in the presence of trimethylsilyl trifluoromethanesulfonate (TMSOTf) to give highly functionalized compound **8** in good yield [Eq. (1)].[9] Compound **4c**, prepared from **2c**, was reduced by a combination of triethylsilane (TESH) and TMSOTf to afford aminohydroxy ester **9** in good yield with high selectivity [Eq. (2)].

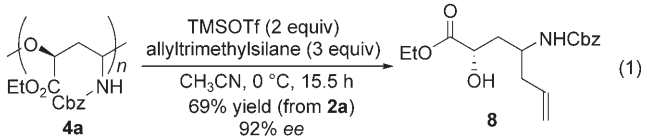

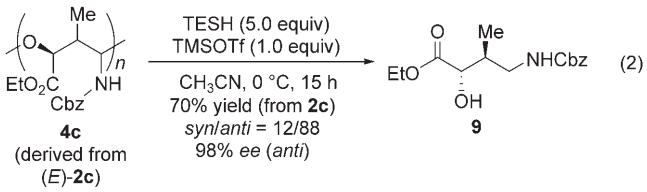

The products obtained have a broad range of applications. The 1,3-amino alcohol motif is present in a number of natural products, and herein we present a catalytic, highly stereoregulated approach to (2*S*,3*S*,4*S*)-3-hydroxy-4-methylproline (HMP, **11**; Scheme 2), which is a nonproteinogenic amino acid known to be a constituent of the elastase inhibitors known as nostopeptins.[10] The reaction of ethyl glyoxylate with (*E*)-**2c** was performed on a 5-mmol scale with 1 mol% of the catalyst. After the reaction mixture was stirred for 3.5 h,followed by treatment with $Sc(OTf)_5$, the resulting product **3c** was isolated in 95% yield (*syn*/*anti* = 12/88, 97% *ee* (*anti*)). The *N*,*O*-acetal **3c** was reduced in high yield by treatment with an excess amount of TESH in the presence of TMSOTf. The resulting alcohol was

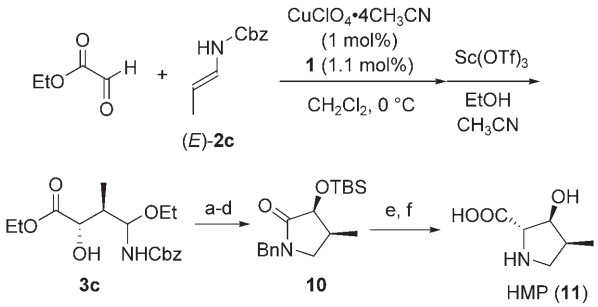

Scheme 2. Total synthesis of HMP (**11**). Reaction Conditions: a) TESH, TMSOTf, 98%; b) TBSOTf, 2,6-lutidine, 93%; c) Pd/C, H_2, AcOH, 87%; d) BnBr, KOH, 18[crown]-6, 86%; e) DIBALH, KCN, 78%; f) *c*HCl; Pd/C, H_2, H_2O, 88%. TBS = *tert*-butyldimethylsilyl, DIBALH = diisobutylaluminum hydride, *c*HCl = concentrated hydrochloric acid.

protected as the TBS ether, and after removal of the Cbz group, cyclization and benzylation gave the desired product **10**.[11] Reductive cyanation of **10** was successfully accomplished according to a reported method[12] and was followed by hydration and deprotection to afford **11**.

In summary, we have demonstrated that enecarbamates derived from aldehydes can react with ethyl glyoxylate in the presence of a chiral catalyst prepared from Cu^{I} and a diimine ligand to give a polymeric structure, which can be converted into the corresponding monomer by treatment with a catalytic amount of $Sc(OTf)_3$ in EtOH. In most cases, less than 1 mol% of the catalyst was enough to complete the reactions and afford the desired products in good yields with high enantioselectivities. Use of *E*-enecarbamates gave *anti* products and *Z*-enecarbamates stereospecifically produced *syn* products. Additionally, the reaction was successfully applied to an

 © 2006 Wiley-VCH Verlag GmbH & Co. KGaA, Weinheim

efficient synthesis of HMP (**11**). Further studies on catalytic asymmetric reactions of aldehyde-derived enecarbamates with less reactive aldehydes are now in progress.

Received: February 4, 2006
Published online: May 3, 2006

Keywords: aldol reaction · asymmetric catalysis · aza-ene reaction · copper · N ligands

[1] For reviews, see: a) M. Limbach, *Chem. Biodiversity* **2005**, *2*, 825; b) C. Palomo, M. Oiarbide, J. M. García, *Chem. Soc. Rev.* **2004**, *33*, 65; c) H. Gröger, E. M. Vogel, M. Shibasaki, *Chem. Eur. J.* **1998**, *4*, 1137; d) S. G. Nelson, *Tetrahedron: Asymmetry* **1998**, *9*, 357; e) R. Mahrwald, *Chem. Rev.* **1999**, *99*, 1095.
[2] a) A. Córdova, W. Notz, C. F. Barbas III, *J. Org. Chem.* **2002**, *67*, 301; b) N. S. Chowdari, D. B. Ramachary, A. Córdova, C. F. Barbas III, *Tetrahedron Lett.* **2002**, *43*, 9591.
[3] S. E. Denmark, S. K. Ghosh, *Angew. Chem.* **2001**, *113*, 4895; *Angew. Chem. Int. Ed.* **2001**, *40*, 4759.
[4] a) A. B. Northrup, D. W. C. MacMillan, *J. Am. Chem. Soc.* **2002**, *124*, 6798; b) A. B. Northrup, D. W. C. MacMillan, *Science* **2004**, *305*, 1752; c) A. Córdova, I. Ibrahem, J. Casas, H. Sundén, M. Engqvist, E. Reyes, *Chem. Eur. J.* **2005**, *11*, 4772; d) A. Córdova, M. Engqvist, I. Ibrahem, J. Casas, H. Sundén, *Chem. Commun.* **2005**, 2047.
[5] a) R. Matsubara, P. Vital, Y. Nakamura, H. Kiyohara, S. Kobayashi, *Tetrahedron* **2004**, *60*, 9769; b) R. Matsubara, Y. Nakamura, S. Kobayashi, *Angew. Chem.* **2004**, *116*, 3320; *Angew. Chem. Int. Ed.* **2004**, *43*, 3258; c) R. Matsubara, Y. Nakamura, S. Kobayashi, *Angew. Chem.* **2004**, *116*, 1711; *Angew. Chem. Int. Ed.* **2004**, *43*, 1679; d) J. S. Fossey, R. Matsubara, P. Vital, S. Kobayashi, *Org. Biomol. Chem.* **2005**, *3*, 2910.
[6] a) D. Hart, A. E. von Dormat, *Bull. Soc. Chim. Belg.* **1956**, *65*, 291; b) J. Wolfrom, R. McFadden, T. Chaney, *J. Org. Chem.* **1961**, *26*, 2597.
[7] For details, see the Supporting Information.
[8] Enecarbamates were synthesized according to: a) T. Mecozzi, M. Petrini, *Synlett* **2000**, 73; b) A. M. Kanazawa, J.-N. Denis, A. E. Greene, *J. Org. Chem.* **1994**, *59*, 1238.
[9] M. Sugiura, H. Hagio, R. Hirabayashi, S. Kobayashi, *J. Am. Chem. Soc.* **2001**, *123*, 12510.
[10] a) T. Okino, S. Qi, H. Matsuda, M. Murakami, K. Yamaguchi, *J. Nat. Prod.* **1997**, *60*, 158; for synthetic approaches to HMP, see: b) N. Kurokawa, Y. Ohfune, *J. Am. Chem. Soc.* **1986**, *108*, 6041; c) D. A. Evans, A. E. Weber, *J. Am. Chem. Soc.* **1987**, *109*, 7151; d) J. Mulzer, R. Becker, E. Brunner, *J. Am. Chem. Soc.* **1989**, *111*, 7500; e) N. Kurokawa, Y. Ohfune, *Tetrahedron* **1993**, *49*, 6195; f) N. Langlois, F. Rakotondradany, *Tetrahedron* **2000**, *56*, 2437; g) W.-H. Meng, T.-J. Wu, H.-K. Zhang, P.-Q. Huang, *Tetrahedron: Asymmetry* **2004**, *15*, 3899.
[11] E. Santaniello, R. Casati, A. Manzocchi, *J. Chem. Soc. Perkin Trans. 1* **1985**, 2389.
[12] a) J.-O. Durand, M. Larchevêque, Y. Petit, *Tetrahedron Lett.* **1998**, *39*, 5743; b) P.-Q. Huang, H.-Y. Huang, *Synth. Commun.* **2004**, *34*, 137.

 © 2006 Wiley-VCH Verlag GmbH & Co. KGaA, Weinheim

Transition-Metal Catalysis

DOI: 10.1002/anie.200600801

With Molecular-Oxygen-Activated Lewis Acids: Dinuclear Molybdenum Complexes for Aza-Diels–Alder Reactions of Acyl Hydrazones**

*Yasuhiro Yamashita, Matthew M. Salter, Kayoko Aoyama, and Shū Kobayashi**

Lewis acids are amongst the most important activating groups in chemistry, and their use is ubiquitous in synthesis. As a result, the last two decades have seen a veritable explosion of interest in the synthesis of Lewis acids based on almost every suitable metal in the Periodic Table and their application as catalysts in a broad range of reactions.[1] In addition to the nature of the metal center, the activity of Lewis acids may be influenced by external factors, such as coordinating additives and variation of the associated counteranion; for example, exchanging a highly coordinating halogen anion for the less nucleophilic triflate anion is frequently used to increase the activity of Lewis acids. Apart from these techniques, however, there are few effective ways of increasing Lewis acidity. We now report a new type of Lewis acid system that is activated by molecular oxygen, which to the best of our knowledge represents the first example of a Lewis acid that is activated in this way. Whilst dinuclear molybdenum compounds [$Mo_2(OAc)_4$] have been investigated as inorganic compounds,[2] their use in synthesis has remained relatively unexplored.[3] Furthermore, we demonstrate that this catalyst mediates the hitherto unknown Diels–Alder reaction of aromatic acyl hydrazones with Danishefsky dienes (Scheme 1).[4]

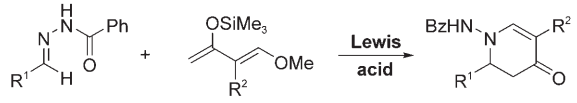

1 (**1a**: R^1=$PhCH_2CH_2$-) + **2** (**2a**: R^2=H; **2b**: R^2=Me) → **3** (**3aa-Ib**)

Scheme 1. Aza-Diels–Alder reaction catalyzed by a Lewis acid.

The aza-Diels–Alder reaction of imines with dienes is an important method for the construction of substituted piper-

[*] Dr. Y. Yamashita, Dr. M. M. Salter, K. Aoyama, Prof. Dr. S. Kobayashi
Graduate School of Pharmaceutical Sciences
The University of Tokyo
Hongo, Bunkyo-ku, Tokyo 113–0033 (Japan)
Fax: (+81) 3-5684-0634
E-mail: skobayas@mol.f.u-tokyo.ac.jp

[**] This work was partially supported by a Grant-in-Aid for Scientific Research from the Japan Society for the Promotion of Science (JSPS).

Supporting information for this article is available on the WWW under http://www.angewandte.org or from the author.

InterScience
© 2006 Wiley-VCH Verlag GmbH & Co. KGaA, Weinheim

idine derivatives. However, some imines are not suitable for use in these reactions owing to their instability, which leads to low yields of the isolated cyclic products. Hydrazones offer a solution to this problem, as they are known to act as stable imine equivalents and the hydrazone N–N bond can be readily cleaved to give amine functionalities.[5] We have previously demonstrated that acyl hydrazones derived from aliphatic aldehydes can function as electrophiles in allylations and Mannich-type reactions in the presence of Lewis acid catalysts, such as $[Sc(OTf)_3]$ (OTf = trifluoromethanesulfonate).[6] However, when we attempted to extend this methodology to the aza-Diels–Alder reactions of hydrazones with Danishefsky dienes, we found that the reaction proceeded only sluggishly in the presence of conventional Lewis acids such as $[Sc(OTf)_3]$, $[Yb(OTf)_3]$, $BF_3{\cdot}OEt_2$, and $ZnCl_2$ (Table 1, entries 1–4). On further investigation, it was discovered that when the catalyst was switched to $[Mo_2(OAc)_4]$, the reaction proceeded smoothly to afford the desired adduct in good yield (entry 5). A screen of common laboratory solvents revealed that acetonitrile and acetone gave the optimum results. The use of other less polar (toluene, CH_2Cl_2, EtOAc) or more polar solvents ($MeNO_2$, dimethylformamide (DMF)) did not lead to any improvement in yield (26–56%).

Whilst delighted by these results, we were concerned by the poor reproducibility of the reaction. After careful examination of the reaction conditions, it was found that molecular oxygen present as a contaminant in the system exerted a profound effect on reactivity (entry 6) and that its exclusion led to a dramatic reduction in yield (entry 7).[7] We therefore deliberately sought to introduce molecular oxygen into the reaction by controlled preparation of the catalytic species, thus the catalyst solution was pretreated with O_2 prior to the addition of the diene.

The effect of varying the molybdenum source was also investigated. Trials showed that use of dinuclear Mo sources with a counterion that has a similar basicity to acetate, such as $[Mo_2(OCOC_5H_{11})_4]$ and $[Mo_2(OCOPh)_4]$, gave very similar results (entries 9 and 10); however, the use of $[Mo_2(OCOCF_3)]$ or $[Mo_2(OTf)_4]$ resulted in complete shutting down of the reaction (entries 11 and 12). Raising the reaction temperature to 40 °C resulted in a marginal improvement in yield, whereas decreasing the catalyst loading to 5 mol% at 40 °C raised the yield still further to 75% (entry 14). The addition of dried 5-Å molecular sieves (MS) to the reaction significantly improved the efficiency of the reaction and afforded the desired adduct in 85% yield (entry 15); however, attempts to decrease the catalyst loading down to 2 mol% resulted in a steep drop in yield (entry 16). It is important to note that use of the mononuclear oxidized molybdenum species (entries 17 and 18) did not promote the reaction at all.[9] This behavior suggests that the catalyst involves a species with at least two metal centers in a well-defined spatial array.[10]

With these results in hand, we turned our attention to the synthetic scope of the reaction (Table 2). Benzoylhydrazones

Table 1: Aza-Diels–Alder reaction of **1a** with **2a** catalyzed by a Lewis acid.[a]

Entry	Catalyst	Solvent	Yield of **3aa** [%]
1[b]	$[Sc(OTf)_3]$	MeCN	–[c]
2[b]	$[Yb(OTf)_3]$	MeCN	8
3[b]	$BF_3{\cdot}OEt_2$	MeCN	22
4[b]	$ZnCl_2$	MeCN	trace amount
5[b]	$[Mo_2(OAc)_4]$	MeCN	69
6	$[Mo_2(OAc)_4]$	MeCN	70
7[d]	$[Mo_2(OAc)_4]$	MeCN	< 10
8[e]	$[Mo_2(OAc)_4]$	acetone	70
9	$[Mo_2(OCOC_5H_{11})]$	MeCN	64
10	$[Mo_2(OBz)_4]$	MeCN	60
11	$[Mo_2(OCOCF_3)_4]$	MeCN	trace amount
12	$[Mo_2(OTf)_4]{\cdot}4$ AcOEt	MeCN	no reaction
13[f]	$[Mo_2(OAc)_4]$	MeCN	71
14[g]	$[Mo_2(OAc)_4]$	MeCN	75
15[g,h]	$[Mo_2(OAc)_4]$	MeCN	85
16[h,i]	$[Mo_2(OAc)_4]$	MeCN	55
17[k]	$[MoO_2]$	MeCN	no reaction
18[k]	$[MoO_3]$	MeCN	no reaction

[a] In the case of the Mo_2 catalysts, the Mo_2 species was freshly prepared from $[Mo(CO)_6]$ according to a literature procedure[8] and stored under Ar in a glove box. For the preparation of the catalyst, the Mo_2 salt (10 mol%) and hydrazone were heated under O_2 at 50 °C for 3 h unless otherwise noted. After addition of the diene, the reaction was carried out under Ar at 20 °C for 24 h. [b] Reaction carried out at room temperature using 20 mol% catalyst with no activation. No precautions to exclude oxygen were taken. [c] Complex mixture. [d] Reaction performed under Ar in degassed MeCN. [e] Treated with O_2 at room temperature. [f] Reaction carried out at 40 °C for 24 h. [g] 5 mol% of catalyst was used at 40 °C for 24 h. [h] Powdered 5-Å MS were added (50 mg/0.4 mmol substrate). [i] 2 mol% of catalyst was used at 40 °C for 24 h. [k] Activated by heating under O_2 at 50 °C for 3 h prior to addition of the hydrazone.

Table 2: Substrate scope in the reaction of hydrazone **1** with Danishefsky diene **2** with nuclear Mo Lewis acid catalysis.[a]

Entry	R^1	Diene	Product	Yield [%][b]
1	$PhCH_2CH_2$ (**1a**)	**2a**	**3aa**	85
2	$PhCH_2CH_2$ (**1a**)	**2b**	**3ab**	86
3	CH_3- (**1b**)	**2a**	**3ba**	88
4	CH_3- (**1b**)	**2b**	**3bb**	77
5	C_3H_7- (**1c**)	**2a**	**3ca**	85
6	C_3H_7- (**1c**)	**2b**	**3cb**	76
7	$C_5H_{11}-$ (**1d**)	**2a**	**3da**	85
8	$C_5H_{11}-$ (**1d**)	**2b**	**3db**	82
9	$C_7H_{15}-$ (**1e**)	**2a**	**3ea**	81
10	$C_7H_{15}-$ (**1e**)	**2b**	**3eb**	70
11	$C_9H_{19}-$ (**1f**)	**2a**	**3fa**	70
12	$C_9H_{19}-$ (**1f**)	**2b**	**3fb**	50
13	*c*-$C_6H_{10}-$ (**1g**)	**2a**	**3ga**	16
14	$(CH_3)_2CHCH_2-$ (**1h**)	**2a**	**3ha**	62
15	$(CH_3)_2CHCH_2-$ (**1h**)	**2b**	**3hb**	73
16	$TBSOCH_2CH_2-$ (**1i**)	**2a**	**3ia**	86
17	$TBSOCH_2CH_2-$ (**1i**)	**2b**	**3ib**	68
18	$TIPSC{\equiv}C-$ (**1j**)	**2a**	**3ja**	84
19	$TIPSC{\equiv}C-$ (**1j**)	**2b**	**3jb**	61
20[c]	C_6H_5- (**1k**)	**2a**	**3ka**	65
21	C_6H_5- (**1k**)	**2b**	**3kb**	72
22[c]	*p*-ClC_6H_4- (**1l**)	**2a**	**3la**	64
23	*p*-ClC_6H_4- (**1l**)	**2b**	**3lb**	42

[a] $[Mo_2(OAc)_4]$ (5 mol%), the hydrazone substrate, and 5-Å MS were mixed in dry MeCN and heated to 50 °C under O_2 atmosphere for 3 h. After addition of the diene in MeCN (final reaction mixture concentration = 0.2 mM), the reaction was carried out at 40 °C under Ar for 24 h. [b] Yield of the isolated product analysis. [c] Conditions: 10 mol% catalyst, reaction time = 72 h. TBS = *tert*-butyldimethylsilyl, TIPS = triisopropylsilyl.

 © 2006 Wiley-VCH Verlag GmbH & Co. KGaA, Weinheim

prepared from non-branched aldehydes performed well in the reaction, thus affording the corresponding 4-piperidenone products in good yields (entries 1–12). However, the introduction of α- or β-branching had a detrimental effect on the efficiency of the reaction (entries 13–15). The mild nature of the procedure was attested to by the observation that a benzylhydrazone bearing a silyloxy functionality could be employed in the reaction without significant deprotection (entries 16 and 17). Additionally, alkynyl hydrazones worked well as they gave the desired adducts in good yields (entries 18 and 19). It should be noted that aryl hydrazones also functioned well in the reaction, although longer reaction times were required to achieve good yields (entries 20–23).

The molecular-oxygen-activated molybdenum catalyst was also found to be effective in other Lewis acid mediated reactions (Scheme 2). Gratifyingly, the Mukaiyama aldol

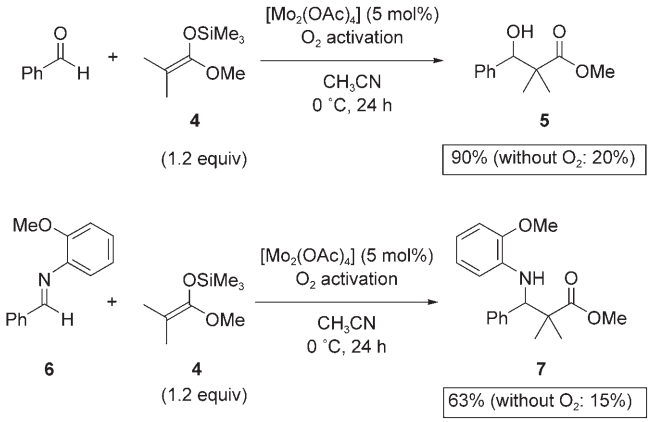

Scheme 2. Mukaiyama aldol and Mannich-type reactions catalyzed by the $[Mo_2(OAc)_4]/O_2$ system.

reaction between benzaldehyde and silyl enol ether **4** proceeded smoothly in the presence of 5 mol% $[Mo_2(OAc)_4]$ to afford the desired β-hydroxy ester **5** in excellent yield. Similarly, the corresponding Mannich-type addition of **4** to *N*-*o*-methoxyphenyl imine **6** was also catalyzed by the oxidized molybdenum system to give β-imino ester **7** cleanly and efficiently. In both cases, it was found that activation of the catalyst by pretreatment with molecular oxygen was essential for an efficient reaction: the corresponding reactions carried out without O_2 activation proceeded to give the products in much lower yields than those observed under the oxygen-activated conditions.

In addition, it was found that the $[Mo_2(OAc)_4]/O_2$ system could also be applied to the catalysis of the Strecker reaction of imine **8** with trimethylsilyl cyanide (TMSCN) to give the corresponding α-cyano imine **9** (Table 3). In these cases as well, the controlled introduction of molecular oxygen was found to be essential for an efficient reaction. Oxidation of freshly prepared $[Mo_2(OAc)_4]$[8] prior to use afforded the desired addition product in very high yield (entry 1), whereas omission of the oxidative conditioning step resulted in a drastic decrease in the efficiency of the reaction (entry 2). Interestingly, the reaction proceeded only very sluggishly in

Table 3: Strecker reaction of (*E*)-*N*-benzylidenebenzenamine (**8**) with TMSCN.

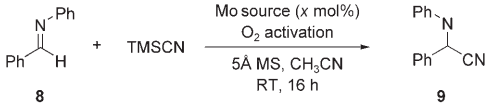

Entry	Mo source	Mo loading [mol%]	O_2 activation[a]	Yield [%][b]
1[c]	$[Mo_2(OAc)_4]$	5	yes	96
2[c]	$[Mo_2(OAc)_4]$	5	no	24
3	$[MoO_2]$	10	yes	18
4	$[MoO_3]$	10	yes	21

[a] Mo source, imine, and MS heated under O_2 for 3 h prior to the addition of TMSCN. [b] Yields of the isolated products. [c] Freshly prepared $[Mo_2(OAc)_4]$ (bright yellow).

the presence of molecular oxygen and the mononuclear $[MoO_x]$ species (entries 3 and 4). This observation further reinforces the hypothesis that a binuclear array of molybdenum centers is responsible for the efficient action of the novel catalyst.

Next, we gave consideration to the structure of the active catalyst species. Our working hypothesis involves an oxidized dinuclear molybdenum species; therefore, as molybdenum complexes are readily oxidized and Cotton et al. reported[10] the preparation and X-ray crystallographic characterization of $[Mo_2(\eta_2\text{-}O_2CCH_3)_2(\mu_2\text{-}DXylF^{2,6})_2(\mu_2\text{-}O_2)]$ (**10**; DXylF = *N*,*N*′-di(2,6-xylylformamidine)), a dinuclear molybdenum complex in which a diamidinate ligand is coordinated to the metal centers and has two bridging oxygen atoms that span the Mo–Mo bond, we examined the species obtained by heating $[Mo_2(OAc)_4]$ with hydrazone **1a** in MeCN by electrospray ionization mass spectroscopy (ESI MS; solvent: MeCN, negative mode). A major peak at *m*/*z* 758 was observed, which corresponds to a molecular formula of $C_{32}H_{30}Mo_2N_4O_6$. By analogy with complex **10**, we tentatively assigned this species as having one of the two possible structures shown in Scheme 3. Moreover, the aza-Diels–Alder reaction pro-

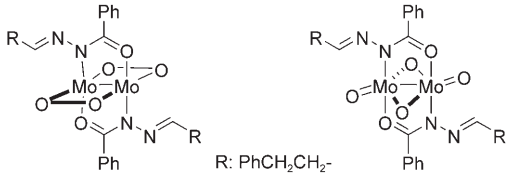

Scheme 3. Plausible structures for the catalytic species formed from $[Mo_2(OAc)_4]$ and hydrazone **1a** under O_2 in MeCN.

ceeded in quite low yield (< 10%) in the presence of 50 mol% $[Mo_2(OAc)_4]$. This result provided further circumstantial evidence for our hypothesis and indicated that the two hydrazone molecules that coordinate to the Mo_2 species were less reactive and that the dimolybdenum–hydrazone complex activates free the hydrazone towards cyclization.

In summary, we have discovered a new type of Lewis acid catalyst based on molybdenum, which relies on activation by molecular oxygen for its function. The novel complex

 © 2006 Wiley-VCH Verlag GmbH & Co. KGaA, Weinheim

catalyzes the aza-Diels–Alder reaction of a range of acyl hydrazones with Danishefsky dienes to afford 4-piperidinones in good yields. Additionally, the same catalyst efficiently mediates Mukaiyama aldol and Mannich-type reactions as well as the addition of TMSCN to imines. In all cases, activation by molecular oxygen was found to be crucial for high catalytic activity; the absence of such activation resulted in a dramatic decrease in efficiency and yield. Further investigations into the synthetic scope of the reaction and catalyst structure are in progress.

Received: March 1, 2006
Published online: May 3, 2006

Keywords: aza-Diels–Alder reaction · homogeneous catalysis · Lewis acids · molybdenum · oxygen activation

[1] *Lewis Acids in Organic Synthesis* (Ed.: H. Yamamoto), Wiley-VCH, Weinheim, **2000**.
[2] a) C. D. Garner in *Comprehensive Coordination Chemistry, Vol. 3* (Eds.: G. Wilkinson, R. D. Gillard, J. A. McCleverty), Pergamon, Oxford, **1987**, chap. 36.3, p. 1301; b) F. H. Jardine, P. S. Sheridan in *Comprehensive Coordination* Chemistry, *Vol. 4* (Eds.: G. Wilkinson, R. D. Gillard, J. A. McCleverty), Pergamon, Oxford, **1987**, chap. 48, p. 901; c) J. L. Eglin in *Comprehensive Coordination Chemistry II*, *Vol. 4* (Eds.: J. A. McCleverty, T. J. Meyer), Pergamon, Oxford, **2004**, chap. 4.9, p. 575.
[3] For organic reactions using molybdenum dimer complexes, see: a) M. McCann in *Catalysis by Di- and Polynuclear Metal Cluster Complexes* (Eds.: A. D. Adams, F. A. Cotton), Wiley-VCH, New York, **1998**, chap. 5, p. 145; for asymmetric hetero Diels–Alder reactions using chiral Rh dimer complexes, see b) M. P. Doyle, I. M. Phillips, W. Hu, *J. Am. Chem. Soc.* **2001**, *123*, 5366; c) M. Valenzuela, M. P. Doyle, C. Hedberg, W. Hu, A. Holmstrom, *Synlett* **2004**, 2425; d) M. P. Doyle, M. Valenzuela, P. Huang, *Proc. Natl. Acad. Sci. USA* **2004**, *101*, 5391; e) R. E. Forslund, J. Cain, J. Colyer, M. P. Doyle, *Adv. Synth. Catal.* **2005**, *347*, 87; f) M. Anada, T. Washio, N. Shimada, S. Kitagaki, M. Nakajima, M. Shiro, S. Hashimoto, *Angew. Chem.* **2004**, *116*, 2719; *Angew. Chem. Int. Ed.* **2004**, *43*, 2665; for a reaction using $[Mo_2(OAc)_4]$ as a stoichiometric Lewis acid, see: g) H. Hirao, Y. Fujihara, S. Tsuno, Y. Ohshiro, T. Agawa, *Chem. Lett.* **1984**, 367.
[4] Y. Yamashita, Y. Mizuki, S. Kobayashi, *Tetrahedron Lett.* **2005**, *46*, 1803.
[5] M. J. Burk, J. E. Feaster, *J. Am. Chem. Soc.* **1992**, *114*, 6266, and also see Ref. [6].
[6] a) H. Oyamada, S. Kobayashi, *Synlett* **1998**, 249; b) S. Kobayashi, T. Furuta, K. Sugita, H. Oyamada, *Synlett* **1998**, 1019; c) S. Kobayashi, Y. Hasegawa, H. Ishitani, H. *Chem. Lett.* **1998**, 1131; d) S. Kobayashi, K. Sugita, H. Oyamada, *Synlett* **1999**, 138; e) K. Manabe, H. Oyamada, K. Sugita, S. Kobayashi, *J. Org. Chem.* **1999**, *64*, 8054; f) O. Okitsu, H. Oyamada, T. Furuta, S. Kobayashi, *Heterocycles* **2000**, *52*, 1143; g) M. Sugiura, S. Kobayashi, *Angew. Chem. Int. Ed.* **2005**, *44*, 5176.
[7] An alternative radical pathway that accounts for C–C bond-forming reactions in the presence of metal catalysts and molecular oxygen can be proposed. We investigated the effect of adding a radical scavenger (2,4,6-tri-*tert*-butylphenol, 20 mol%) to the reaction; almost no effect was observed and the product heterocycle was obtained in 71% yield under the conditions shown in Table 1, entry 14.
[8] A. B. Brignole, F. A. Cotton, *Inorg. Synth.* **1972**, *13*, 81.
[9] The use of monomeric Mo species as Lewis acids has been documented: a) H. Dvořákova, D. Dvořák, J. Šrogi, P. Kocovsky, *Tetrahedron Lett.* **1995**, *36*, 6351; b) A. V. Malkov, I. Baxendale, D. J. Mansfield, P. Kocovsky. *Tetrahedron Lett.* **1997**, 4895; c) A. V. Malkov, I. R. Baxendale, D. Dvořák, D. J. Mansfield, P. Kocovsky, *J. Org. Chem.* **1999**, *64*, 2737; d) A. V. Malkov, S. L. Davis, W. L. Mitchell, P. Kocovsky, *J. Org. Chem.* **1999**, *64*, 2751; e) A. Sakakura, R. Kondon, K. Ishihara, *Org. Lett.* **2005**, *7*, 1974, and references therein.
[10] F. A. Cotton, L. M. Daniels, C. A. Murillo, J. G. Slaton *J. Am. Chem. Soc.* **2002**, *124*, 2878.

 © 2006 Wiley-VCH Verlag GmbH & Co. KGaA, Weinheim

Alkylation

DOI: 10.1002/anie.200600677

Ir- and Ru-Catalyzed Sequential Reactions: Asymmetric α-Alkylative Reduction of Ketones with Alcohols**

Gen Onodera, Yoshiaki Nishibayashi, and Sakae Uemura*

Transition-metal-catalyzed asymmetric reduction of prochiral ketones is one of the most intensive subjects in organic synthesis.[1,2] Among a variety of systems for the catalytic reduction, ruthenium-catalyzed hydrogenation, and transfer hydrogenation of prochiral ketones have been developed and used as reliable synthetic methods to obtain reduced alcohols with a high-to-excellent enantioselectivity.[1,2] We have also reported the enantioselective redox reaction of ketones and alcohols using ruthenium complex $[RuCl_2(PPh_3)(ip\text{-}foxap^{[3]})]$ (**1**) as a catalyst.[4]

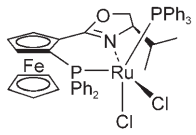

$[RuCl_2(PPh_3)(ip\text{-}foxap)]$ (**1**)

Multiple catalysis in the same medium to obtain the desired products from simple starting materials is one of the most current and important topics in synthetic chemistry.[5,6] Such catalysis

[*] Prof. Dr. Y. Nishibayashi
Institute of Engineering Innovation
The University of Tokyo
Yayoi, Bunkyo-ku, Tokyo, 113-8656 (Japan)
Fax: (+81) 3-5841-1175
E-mail: ynishiba@sogo.t.u-tokyo.ac.jp
G. Onodera, Prof. Dr. S. Uemura
Department of Energy and Hydrocarbon Chemistry
Graduate School of Engineering
Kyoto University
Katsura, Nishikyo-ku, Kyoto, 615-8510 (Japan)

[**] This work was supported by a Grant-in-Aid for Scientific Research for Young Scientists (A; No. 15685006) to Y.N. from the Ministry of Education, Culture, Sports, Science and Technology, Japan.

Supporting information for this article is available on the WWW under http://www.angewandte.org or from the author.

© 2006 Wiley-VCH Verlag GmbH & Co. KGaA, Weinheim

lessens the reaction time and the loss of yield by avoiding the isolation and purification procedure of intermediates required in multistep reactions. The sequential reaction looks easy and simple, but the compatibility between different transition-metal complexes should be established to achieve it.

During our study on the development of novel catalytic transformation using chalcogenolate-bridged diruthenium complexes, we discovered a new type of ruthenium- and platinum- or gold-catalyzed sequential reaction, in which tri- and tetrasubstituted furans, pyrroles, oxazoles, and fused polycyclic products were obtained in good-to-high yields with excellent selectivities from simple and readily available starting compounds.[7] These findings prompted us to further develop useful sequential reactions catalyzed by two different transition-metal complexes. Toward this end, our attention was focused on the iridium-catalyzed α-alkylation of ketones with alcohols[8] and the ruthenium-catalyzed transfer hydrogenation of prochiral ketones[4] because the combination of these two catalytic reactions might realize asymmetric α-alkylative reduction of prochiral ketones with alcohols to obtain optically active alcohols directly with elongation of the carbon skeleton.

A mixture of acetophenone (**2a**) and 1-butanol (**3a**) in the presence of a catalytic amount of [{IrCl(cod)}$_2$] (cod = 1,5-cyclooctadiene; 1 mol%), PPh_3 (4 mol%), and KOH (5 mol%) was heated at 100°C for 4 h and then kept at room temperature for 2 h after the addition of a catalytic amount of **1** (1 mol%) and *i*PrONa (4 mol%) in *i*PrOH. As a result, (*R*)-1-phenyl-1-hexanol (**4aa**) was obtained in 75% yield of the isolated product with 94% *ee* (Scheme 1).

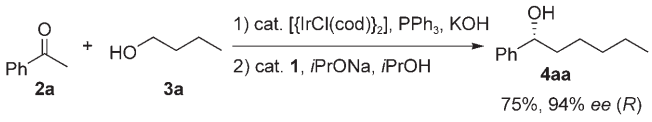

Scheme 1. Asymmetric α-alkylative reduction of a ketone with an alcohol catalyzed by iridium and ruthenium.

Previously, the ruthenium-catalyzed direct synthesis of elongated secondary alcohols through the α-alkylation of ketones with primary alcohols had been reported.[9–11] We tried to develop the enantioselective version of this reaction catalyzed by using only **1**, but a low-to-moderate enantioselectivity was achieved. When the Noyori complexes,[1,2] such as [RuCl(tsdpen)(mesitylene)] (tsdpen = *N*-(*p*-toluenesulfonyl)-1,2-diphenylethanediamine), were used as catalysts in place of **1**, the sequential reaction did not proceed effectively. These results indicate that the compatibility between [{IrCl(cod)}$_2$] and **1** is an essential factor in directly obtaining optically active alcohols with elongation of the carbon skeleton.

Next, reactions of other acetophenones with 1-butanol were investigated by using catalytic amounts of [{IrCl(cod)}$_2$] (1 mol%) and **1** (1 mol%). Typical results are shown in Table 1. The introduction of a methyl group at the *para* or *meta* position of acetophenone did not affect the reactivity and enantioselectivity (entries 2 and 3). Slightly lower yields

Table 1: Reactions of acetophenones **2** with alcohols **3** in the presence of an iridium complex and ruthenium complex **1**.[a]

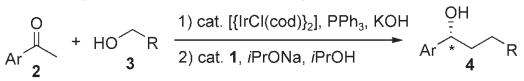

Entry	**2**, Ar	**3**, R	Product	Yield [%][b]	*ee* [%][c]
1	**2a**, Ph	**3a**, *n*Pr	**4aa**	75	94 (*R*)[d]
2	**2b**, 4-MeC_6H_4	**3a**, *n*Pr	**4ba**	72	98
3	**2c**, 3-MeC_6H_4	**3a**, *n*Pr	**4ca**	77	96
4	**2d**, 2-MeC_6H_4	**3a**, *n*Pr	**4da**	52	97
5	**2e**, 4-MeOC_6H_4	**3a**, *n*Pr	**4ea**	57	97 (*R*)[d]
6	**2f**, 4-ClC_6H_4	**3a**, *n*Pr	**4fa**	58	88
7	**2g**, 4-FC_6H_4	**3a**, *n*Pr	**4ga**	15	95
8	**2a**, Ph	**3b**, *i*Pr	**4ab**	51	96 (*R*)[d]
9	**2a**, Ph	**3c**, *n*Bu	**4ac**	77	93 (*R*)[d]
10	**2a**, Ph	**3d**, CH_2CHMe_2	**4ad**	79	96
11	**2a**, Ph	**3e**, Ph	**4ae**	0	–

[a] All reactions of **2** (2.0 mmol) with **3** (6.0 mmol) were carried out in the presence of [{IrCl(cod)}$_2$] (1 mol%), PPh_3 (4 mol%), and KOH (5 mol%) at 100°C for 4 h, and the reaction mixture was kept at room temperature for 2 h by the addition of **1** (1 mol%), *i*PrONa (4 mol%), and *i*PrOH (160 mL). [b] Yield of the isolated product. [c] Determined by HPLC with a chiral column. [d] The absolute configuration was determined by comparison of the value of the optical rotation with that reported in the literature.

of products were observed without loss of optical purity when 2′-methyl- and 4′-methoxyacetophenones were used as substrates (entries 4 and 5). The presence of an electron-withdrawing group, such as a chloro moiety, at the *para* position of acetophenone slightly decreased both the reactivity and the enantioselectivity (entry 6). When 4′-fluoroacetophenone was used as a substrate, only a low yield of product was observed, even for a prolonged reaction time (entry 7).

Various primary alcohols are available as alkylating reagents for ketones. Reactions of acetophenone (**2a**) with 2-methyl-1-propanol, 1-pentanol, and 3-methyl-1-butanol were carried out in the presence of catalytic amounts of [{IrCl(cod)}$_2$] (1 mol%) and **1** (1 mol%) to afford the corresponding α-alkylated alcohols in good yields with a high enantioselectivity (entries 8–10). However, benzyl alcohol could not be employed for this reaction (entry 11).

Although the detailed reaction mechanism is not yet known, it is considered that a primary alcohol is catalytically dehydrogenated by the iridium complex to form the corresponding aldehyde, followed by its base-catalyzed aldol condensation with ketone to afford an α,β-unsaturated ketone, and then iridium-catalyzed hydrogenation to give an α-alkylated ketone. Finally, ruthenium-catalyzed enantioselective transfer hydrogenation of the α-alkylated ketone results in formation of the optically active alcohol with elongation of the carbon skeleton (Scheme 2).

As described above, it is known that the iridium complex [{IrCl(cod)}$_2$] catalytically promotes the α-alkylation of ketones with alcohols.[8] This result indicates that the presence of the iridium complex, PPh_3, and KOH did not interfere with the final reduction step of the ketone intermediate. It is noteworthy that the iridium and ruthenium complexes play their roles independently in each step. The method presented herein provides a useful synthetic route to obtaining optically

 © 2006 Wiley-VCH Verlag GmbH & Co. KGaA, Weinheim

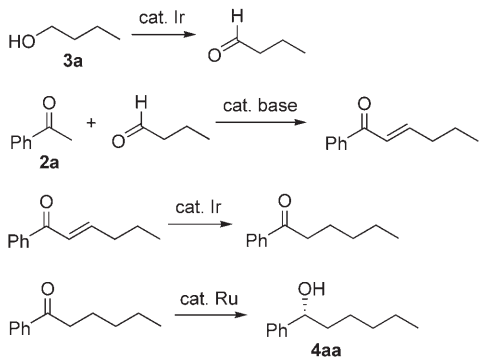

Scheme 2. Plausible reaction pathway.

active alcohols with elongation of the carbon skeleton directly from prochiral ketones and alcohols, in contrast to the conventional asymmetric reduction of prochiral ketones which only gives the simple reduced alcohols.

In summary, we have disclosed that asymmetric α-alkylative reduction of prochiral ketones with primary alcohols catalyzed by both iridium and ruthenium complexes gave the corresponding optically active alcohols with the elongation of the carbon skeleton and with a high enantioselectivity (up to 98% *ee*). The compatibility between iridium and ruthenium complexes is an essential factor in directly obtaining optically active alcohols with elongation of the carbon skeleton. Further investigations involving the broadening of the scope of this sequential reaction system are currently in progress.

Experimental Section

A typical experimental procedure for the reaction of acetophenone (**2a**) with 1-butanol (**3a**) catalyzed by [{IrCl(cod)}$_2$] and [RuCl$_2$(PPh$_3$)(ip-foxap)] (**1**): KOH (5.8 mg, 0.10 mmol), [{IrCl(cod)}$_2$] (13.1 mg, 0.020 mmol), and PPh$_3$ (21.4 mg, 0.082 mmol) under N$_2$ were place in a 20-mL flask. After the addition of **2a** (240.1 mg, 2.0 mmol) and **3a** (445.8 mg, 6.0 mmol), the reaction mixture was kept at 100 °C for 4 h. A solution of *i*PrOH containing *i*PrONa (0.080 mmol) and **1** (18.4 mg, 0.020 mmol) was added to the reaction mixture, and then the reaction mixture was kept at room temperature for 2 h. For the workup, aqueous HCl (1N, 0.5 mL) was added to the reaction mixture. The solvent was concentrated under reduced pressure, and the residue was extracted with water (50 mL) and diethyl ether (3 × 50 mL). The organic solution was dried over anhydrous MgSO$_4$. For isolation, the extract was concentrated under reduced pressure by an aspirator, and the residue was purified by column chromatography on silica gel (EtOAc/*n*-hexane, 10:90) to yield 267.7 mg (1.50 mmol, 75%, 94% *ee*) of (*R*)-1-phenyl-1-hexanol (**4aa**) as a white solid, which was identified by comparison of its spectroscopic data with that in the literature.[9] $[\alpha]_D^{28} = +35.3$ ($c = 1.04$, CHCl$_3$); ^{1}H NMR (CDCl$_3$, 270 MHz) $\delta = 0.85$–0.90 (m, 3H), 1.29–1.43 (m, 6H), 1.71–1.79 (m, 2H), 1.82 (d, 1H, $J = 3.3$ Hz), 4.64–4.70 (m, 1H), 7.24–7.36 ppm (m, 5H); the *ee* value was determined by HPLC analysis with a Chiralcel OD column (eluent: *n*-hexane/2-propanol, 98:2, flow rate: 0.5 mL min^{-1}, column temperature: 30 °C, retention time: 34.72 min (*R*) and 46.60 min (*S*)); the absolute configuration was determined by comparison of the value of the optical rotation with that reported in literature ($[\alpha]_D^{24} = -35.0$ ($c = 0.88$, CHCl$_3$), 92% *ee* (*S*)).[12]

Received: February 21, 2006
Published online: May 3, 2006

Keywords: alkylation · homogeneous catalysis · iridium · reduction · ruthenium

[1] For recent reviews, see: a) R. Noyori, S. Hashiguchi, *Acc. Chem. Res.* **1997**, *30*, 97; b) R. Noyori, T. Ohkuma, *Angew. Chem.* **2001**, *113*, 40; *Angew. Chem. Int. Ed.* **2001**, *40*, 40; c) R. Noyori, *Angew. Chem.* **2002**, *114*, 2108; *Angew. Chem. Int. Ed.* **2002**, *41*, 2008; d) S. E. Clapham, A. Hadzovic, R. H. Morris, *Coord. Chem. Rev.* **2004**, *248*, 2201.

[2] For recent examples, see: a) T. Ohkuma, H. Ooka, S. Hashiguchi, T. Ikariya, R. Noyori, *J. Am. Chem. Soc.* **1995**, *117*, 2675; b) S. Hashiguchi, A. Fujii, J. Takehara, T. Ikariya, R. Noyori, *J. Am. Chem. Soc.* **1995**, *117*, 7562; c) T. Ohkuma, H. Doucet, T. Pham, K. Mikami, T. Korenaga, M. Terada, R. Noyori, *J. Am. Chem. Soc.* **1998**, *120*, 1086; d) Q. Jiang, Y. Jiang, D. Xiao, P. Cao, X. Zhang, *Angew. Chem.* **1998**, *110*, 1203; *Angew. Chem. Int. Ed.* **1998**, *37*, 1100; e) H. Doucet, T. Ohkuma, K. Murata, T. Yokozawa, M. Kozawa, E. Katayama, A. F. England, T. Ikariya, R. Noyori, *Angew. Chem.* **1998**, *110*, 1792; *Angew. Chem. Int. Ed.* **1998**, *37*, 1703; f) M. Bernard, V. Guiral, F. Delbecq, F. Fache, P. Sautet, M. Lemaire, *J. Am. Chem. Soc.* **1998**, *120*, 1441; g) Y. Jiang, Q. Jiang, X. Zhang, *J. Am. Chem. Soc.* **1998**, *120*, 3817; h) D. A. Alonso, P. Brandt, S. J. M. Nordin, P. G. Andersson, *J. Am. Chem. Soc.* **1999**, *121*, 9580; i) C. J. A. Daley, S. H. Bergens, *J. Am. Chem. Soc.* **2002**, *124*, 3680; j) K. Abdur-Rashid, S. E. Clapham, A. Hadzovic, J. N. Harvey, A. J. Lough, R. H. Morris, *J. Am. Chem. Soc.* **2002**, *124*, 15104; k) R. J. Hamilton, C. G. Leong, G. Bigam, M. Miskolzie, S. H. Bergens, *J. Am. Chem. Soc.* **2005**, *127*, 4152.

[3] a) Since the first preparation of optically active ferrocenyloxazolinylphosphines (FOXAPs) by us in 1995,[3b] we have developed many enantioselective reactions catalyzed by various transition-metal complexes bearing FOXAP as a chiral ligand; b) Y. Nishibayashi, S. Uemura, *Synlett* **1995**, 79; c) Y. Nishibayashi, K. Segawa, K. Ohe, S. Uemura, *Organometallics* **1995**, *14*, 5486; d) Y. Nishibayashi, K. Segawa, H. Takada, K. Ohe, S. Uemura, *Chem. Commun.* **1996**, 847; e) Y. Nishibayashi, I. Takei, S. Uemura, M. Hidai, *Organometallics* **1998**, *17*, 3420; f) I. Takei, Y. Nishibayashi, Y. Arikawa, S. Uemura, M. Hidai, *Organometallics* **1999**, *18*, 2271; g) I. Takei, Y. Nishibayashi, Y. Ishii, Y. Mizobe, S. Uemura, M. Hidai, *Chem. Commun.* **2001**, 2360; h) T. Iwata, Y. Miyake, Y. Nishibayashi, S. Uemura, *J. Chem. Soc. Perkin Trans. 1* **2002**, 1548; i) the optically active FOXAP ligand is commercially available from Wako Pure Chemical Industries (Japan) as ip-FOXAP (065-04331).

[4] a) Y. Nishibayashi, I. Takei, S. Uemura, M. Hidai, *Organometallics* **1999**, *18*, 2291; b) Y. Nishibayashi, A. Yamauchi, G. Onodera, S. Uemura, *J. Org. Chem.* **2003**, *68*, 5875.

[5] For recent reviews, see: a) J. M. Lee, Y. Na, H. Han, S. Chang, *Chem. Soc. Rev.* **2004**, *33*, 302; b) J.-C. Wasilke, S. J. Obrey, R. T. Baker, G. C. Bazan, *Chem. Rev.* **2005**, *105*, 1001; c) A. Ajamian, J. L. Gleason, *Angew. Chem.* **2004**, *116*, 3842; *Angew. Chem. Int. Ed.* **2004**, *43*, 3754; d) J.-A. Ma, D. Cahard, *Angew. Chem.* **2004**, *116*, 4666; *Angew. Chem. Int. Ed.* **2004**, *43*, 4566.

[6] For recent examples, see: a) C. J. Kressierer, T. J. J. Müller, *Angew. Chem.* **2004**, *116*, 6123; *Angew. Chem. Int. Ed.* **2004**, *43*, 5997; b) J. Chae, J. Yun, S. L. Buchwald, *Org. Lett.* **2004**, *6*, 4809; c) J. G. Kim, K. M. Waltz, I. F. Garcia, D. Kwiatkowski, P. J. Walsh, *J. Am. Chem. Soc.* **2004**, *126*, 12580; d) H. Lebel, V. Paquet, *J. Am. Chem. Soc.* **2004**, *126*, 11152; e) R. Guo, R. H.

 © 2006 Wiley-VCH Verlag GmbH & Co. KGaA, Weinheim

Morris, D. Song, *J. Am. Chem. Soc.* **2005**, *127*, 516; f) L. Deng, A. J. Giessert, O. O. Gerlitz, X. Dai, S. T. Diver, H. M. L. Davies, *J. Am. Chem. Soc.* **2005**, *127*, 1342; g) D. M. D'Souza, F. Rominger, T. J. J. Müller, *Angew. Chem.* **2005**, *117*, 156; *Angew. Chem. Int. Ed.* **2005**, *44*, 153; h) Y. Yamamoto, H. Hayashi, T. Saigoku, H. Nishiyama, *J. Am. Chem. Soc.* **2005**, *127*, 10804; i) B. A. Seigal, C. Fajardo, M. L. Snapper, *J. Am. Chem. Soc.* **2005**, *127*, 16329.

[7] a) Y. Nishibayashi, M. Yoshikawa, Y. Inada, M. D. Milton, M. Hidai, S. Uemura, *Angew. Chem.* **2003**, *115*, 2785; *Angew. Chem. Int. Ed.* **2003**, *42*, 2681; b) M. D. Milton, Y. Inada, Y. Nishibayashi, S. Uemura, *Chem. Commun.* **2004**, 2712; c) Y. Nishibayashi, M. Yoshikawa, Y. Inada, M. Hidai, S. Uemura, *J. Am. Chem. Soc.* **2004**, *126*, 16066.

[8] K. Taguchi, H. Nakagawa, T. Hirabayashi, S. Sakaguchi, Y. Ishii, *J. Am. Chem. Soc.* **2004**, *126*, 72.

[9] C. S. Cho, B. T. Kim, T.-J. Kim, S. C. Shim, *J. Org. Chem.* **2001**, *66*, 9020.

[10] a) R. Martinez, G. J. Brand, D. J. Ramon, M. Yus, *Tetrahedron Lett.* **2005**, *46*, 3683; b) M. S. Kwon, N. Kim, S. H. Seo, I. S. Park, R. K. Cheedrala, J. Park, *Angew. Chem.* **2005**, *117*, 7073; *Angew. Chem. Int. Ed.* **2005**, *44*, 6913.

[11] A similar one-pot β-alkylation of secondary alcohols with primary alcohols has been reported, see: a) C. S. Cho, B. T. Kim, H.-S. Kim, T.-J. Kim, S. C. Shim, *Organometallics* **2003**, *22*, 3608; b) K. Fujita, C. Asai, T. Yamaguchi, F. Hanasaka, R. Yamaguchi, *Org. Lett.* **2005**, *7*, 4017.

[12] N. A. Salvi, S. Chattopadhyay, *Tetrahedron* **2001**, *57*, 2833.

 © 2006 Wiley-VCH Verlag GmbH & Co. KGaA, Weinheim

Tandem Annulation

DOI: 10.1002/anie.200600408

In(OTf)$_3$-Catalyzed Tandem Nucleophilic Addition and Cyclization of *ortho*-Alkynylarylaldimines to 1,2-Dihydroisoquinolines**

*Reiko Yanada, Shingo Obika, Hideki Kono, and Yoshiji Takemoto**

Indium(III) salts attract considerable attention as water-tolerant and low-toxicity Lewis acids for the activation of C=O and C=N bonds.[1] Their potential as Lewis acid catalysts for fundamental reactions, such as the Diels–Alder,[2a,b] Friedel–Crafts,[2c] Mukaiyama aldol,[2d] and Sakurai–Hosomi allylation reactions,[2e,f] has been extensively investigated over the last decade.[2] Recently, certain indium(III) salts, as well as other transition-metal compounds, were found to have π acidity and to activate C–C multiple bonds by coordination to π electrons.[3] Several InX_3-catalyzed nucleophilic additions of arenes,[4a,b] 1,3-dicarbonyl compounds,[4c,d] and heteroatomic compounds, such as anilines[4e,f] and thiols[4g] to triple bonds, have been reported.[4]

Catalytic dual activation, in which a metal complex exhibits two roles in a single transformation, is of major interest in organic synthesis from the atom-economy and mechanistic points of view.[5] Recently, Shibasaki and coworkers developed an efficient method for catalytic alkynylation of aldehydes and ketones by using the dual activation of a soft nucleophile and a hard electrophile with an indium(III) catalyst.[6] However, to the best of our knowledge, there have been no reports of dual activation of both hard and soft electrophiles by an InX_3 catalyst.

In this context, we are interested in developing InX_3-catalyzed annulation reactions to form 1,2-dihydroisoquinolines,[7] which are known to be versatile intermediates for biologically active natural products, through tandem nucleophilic additions to both imines and C–C triple bonds. Such 6-*endo-dig* cyclizations into quinolines has already been developed by using several transition-metal catalysts.[3c,e–i] We previously reported the diastereoselective allylation of optically active aldimines with an allyl indium reagent prepared in situ [Eq. (1)],[8] and thus planned to develop a tandem

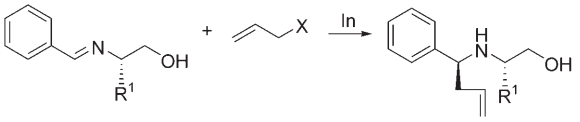

(1)

reaction by using an *ortho*-alkynylarylimine as the starting material, which consists of the nucleophilic addition of an allyl indium reagent to an imine moiety and the intramolecular addition of the resulting amine to the activated C–C triple bond by using an indium salt formed in situ [Eq. (2)]. Herein, we report the efficient synthesis of 1,2-dihydroisoquinolines by an In(OTf)$_3$-catalyzed (OTf = trifluoromethanesulfonate) tandem reaction.

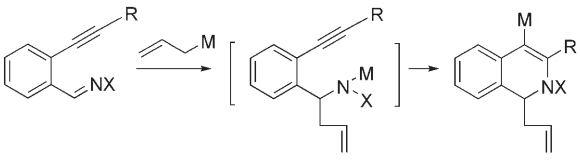

(2)

We first examined the allylation reaction of *ortho*-alkynylarylimine **1a** with several allyl metal reagents. Table 1 shows representative results. Treatment of **1a** with

[*] Dr. R. Yanada, S. Obika, H. Kono, Prof. Y. Takemoto
Graduate School of Pharmaceutical Sciences
Kyoto University
Yoshida, Sakyo-ku, Kyoto 606-8501 (Japan)
Fax: (+81) 75-753-4569
E-mail: takemoto@pharm.kyoto-u.ac.jp

[**] This work was supported by grants from 21st Century COE Program "Knowledge Information Infrastructure for Genome Sciences" and Grant-in-Aid for Scientific Research on Priority Areas from MEXT (17035043), and JSPS. KAKENHI (16390006). S.O. thanks the JSPS for a Fellowship. OTf = trifluoromethanesulfonate.

Supporting information for this article is available on the WWW under http://www.angewandte.org or from the author.

InterScience
© 2006 Wiley-VCH Verlag GmbH & Co. KGaA, Weinheim

Table 1: InX_3-catalyzed tandem reaction of **1a** with allyl metal reagents.

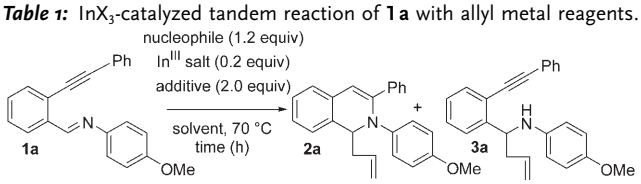

Entry	Nucleophile	In^{III} salt	Additive	Solvent[a]	t [h]	**2a**/**3a** Yield [%]
1	$InBr_2$	–	–	DMF	5	5:90
2	$InBr_2$	$In(OTf)_3$	–	dioxane	48	88:0
3	$SnBu_3$	$In(OTf)_3$	–	1,2-DCE	48	92:0
4	$SnBu_3$	–	–	1,2-DCE	48	0:0[b]
5	$SnBu_3$	$InBr_3$	–	1,2-DCE	60	0:12
6	$SnBu_3$	$In(NTf_2)_3$	–	1,2-DCE	48	91:0
7	$SnBu_3$	$In(OTf)_3$	AcOH	1,2-DCE	48	15:0
8	$SnBu_3$	$In(OTf)_3$	CF_3CH_2OH	1,2-DCE	48	90:0
9	$SnBu_3$	$In(OTf)_3$	H_2O	1,2-DCE	36	85:0
10	$SnBu_3$	$In(OTf)_3$	ArOH[c]	1,2-DCE	6	92:0

[a] 1,2-DCE = 1,2-dichloroethane. [b] Starting material was recovered in 98% yield. [c] ArOH = 2,6-di-*tert*-butyl-4-methoxyphenol.

Table 2: $In(OTf)_3$-catalyzed tandem reaction with various imines.

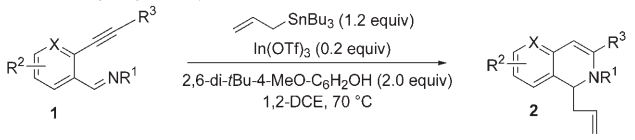

Entry	**1**	R^1	R^2	R^3	X	t [h]	**2**	Yield [%]
1	**1b**	Ph	H	Ph	CH	8	**2b**	91
2	**1c**	Bn[a]	H	Ph	CH	8	**2c**	70
3	**1d**	*i*Bu	H	Ph	CH	7	**2d**	82
4	**1e**	(*R*)-phenylethyl	H	Ph	CH	6	**2e**	85[b]
5	**1f**	*p*-MeO-C_6H_4	5-F	Ph	CH	10	**2f**	87
6	**1g**	*p*-MeO-C_6H_4	5-OMe	Ph	CH	12	**2g**	70
7	**1h**	*p*-MeO-C_6H_4	H	*p*-MeO-C_6H_4	CH	8	**2h**	71
8	**1i**	*p*-MeO-C_6H_4	H	*n*Pr	CH	8	**2i**	89
9	**1j**	*p*-MeO-C_6H_4	H	*p*-CF_3-C_6H_4	CH	8	**2j**	0[c]
10	**1k**	*p*-MeO-C_6H_4	H	Ph	N	8	**2k**	72

[a] Bn = Benzyl. [b] Diastereomeric ratio is 2:1. [c] A complex mixture was obtained.

the allyl indium compound $In(CH_2CHCH_2)Br_2$ in dimethylformamide (DMF) gave the normal allylated product **3a** in 90% yield, accompanied by the formation of 1,2-dihydroisoquinoline **2a** in 5% yield (Table 1, entry 1). We envisaged that the indium(III) salt generated in situ promotes cyclization of the allylated adduct to produce the heterocyclic compound **2a**. In the presence of 20 mol% of $In(OTf)_3$, the predominant product was the cyclic compound **2a**. The best result for this reaction was obtained in dioxane (Table 1, entry 2). Encouraged by this result, we examined the $In(OTf)_3$-catalyzed tandem reaction of **1a** by using allyltributylstannane as a nucleophile. As expected, the reaction gave the same cyclic compound **2a** in 92% yield in 1,2-dichloroethane (Table 1, entry 3). However, we did not obtain **2a** in the absence of $In(OTf)_3$ (Table 1, entry 4). Although the $InBr_3$-catalyzed reaction gave only the allylated compound **3a** in 12% yield, $In(NTf_2)_3$ was a suitable catalyst for the reaction (Table 1, entries 5 and 6). To promote the turnover efficiency of the catalyst, proton sources were added to the reaction system. The addition of 2,6-di-*tert*-butyl-4-methoxyphenol significantly accelerated the tandem cyclization to give **2a** in 92% yield within 6 h,[9] while other additives had no influence on yield and reaction rate (Table 1, entries 7–10). The actual role of the combination of $In(OTf)_3$ and 2,6-di-*tert*-butyl-4-methoxyphenol is not clear; nevertheless, we optimized the reaction conditions for the tandem reaction.

Having established the optimal reaction conditions for the formation of **2a**, we investigated the annulation reaction of various arylimines **1b**–**1k**, which have different substituents (R^1, R^2, and R^3). Representative results are summarized in Table 2. In the reaction of imines derived from aromatic and aliphatic amines **1b**–**1e** with allyltributylstannanes, the desired tandem reaction proceeded smoothly to give the corresponding 1,2-dihydroisoquinolines **2b**–**2e** in good yields and with moderate diastereoselectivity of **2e** (Table 2, entries 1–4).[10] Similarly, both 5-fluoro- and 5-methoxy aldimines **1f** and **1g** provided the desired products, **2f** and **2g**, respectively, in good yields irrespective of the substituent R^2 (Table 2, entries 5 and 6). However, the substituent R^3 on the alkyne carbon atom had a significant effect on this tandem reaction (Table 2, entries 7–9). Although the tandem adducts **2h** and **2i** were obtained by the reaction of imines **1h** and **1i** bearing electron-rich aryl and alkyl groups as the R^3 substituent, the cyclized product **2j** could not be obtained from **1j**, which bears an electron-deficient aryl group (Table 2, entry 9). To extend this reaction for the synthesis of heteroaromatic compounds, we applied this procedure to the imine **1k**, which is a pyridine derivative. It was noteworthy that, despite the presence of a nitrogen atom, the same treatment of **1k** under optimal conditions furnished the corresponding tandem adduct **2k** in 72% yield (Table 2, entry 10).

To investigate the reaction mechanism, ^{13}C NMR spectroscopic studies of **1a** in the presence of 0.4 equivalents of $In(OTf)_3$ in $CDCl_3$ were carried out at room temperature. In the absence of $In(OTf)_3$, the signal corresponding to the imine carbon atom of **1a** appeared at $\delta = 156.77$ ppm and those of the acetylenic carbon atom at $\delta = 95.25$ and 86.40 ppm (Scheme 1A). However, in the presence of $In(OTf)_3$, downfield shifts of the signals corresponding to the imine carbon atom ($\delta = 156.83$ ppm) and acetylenic carbon atom ($\delta = 95.30$ and 86.41; Scheme 1B) were observed.[11] These results support that dual activation of both the imine nitrogen atom and alkyne π electrons by $In(OTf)_3$ occurs, even if it might be a weak interaction.

A proposed mechanism of the tandem reaction is shown in Scheme 2. In path A, allylated amine **b** is formed via $In(OTf)_3$ complex **a**, and the resulting metal amide attacks the alkyne activated by $In(OTf)_3$ in a regiospecific manner, which leads to the formation of 6-*endo*-*dig*-cyclized adduct **c**. Subsequent protonation produces 1,2-dihydroisoquinoline **2**, with regeneration of $In(OTf)_3$. A conceivable alternative pathway is path B, in which the resonance-stabilized iminium

 © 2006 Wiley-VCH Verlag GmbH & Co. KGaA, Weinheim

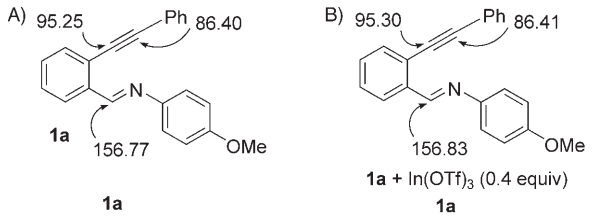

Scheme 1. ^{13}C NMR spectroscopic studies of **1a** in solution with $CDCl_3$. δ values are given in ppm.

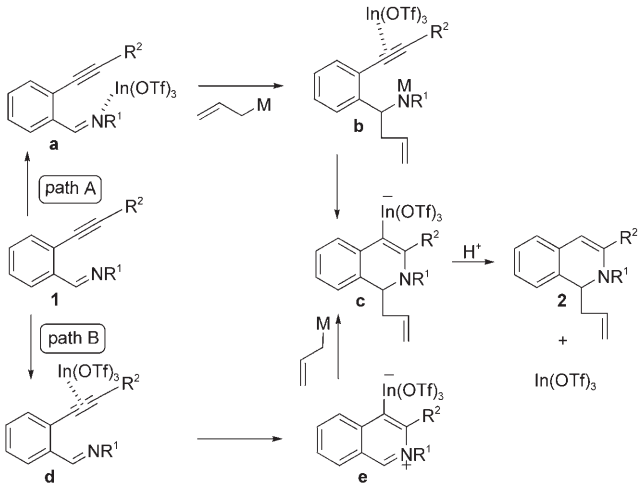

Scheme 2. Proposed mechanism of $In(OTf)_3$-catalyzed tandem addition and cyclization reaction.

ion **e**,[5b] formed by nucleophilic attack of the imine nitrogen atom at the indium-coordinated alkyne **d**, is trapped by the allyl metal species to give **2** via the same intermediate **c**. We examined the cyclization of the protonated compound of intermediate **b** under similar reaction conditions, but almost all the starting material was recovered, which indicates that protonation of compound **b** did not occur during the nucleophilic addition of the allyl metal reagent to imine **1**.

We next examined the tandem reaction of **1a–c** with other nucleophiles. Selected examples are listed in Table 3. The reaction of **1a** with methallylstannane and crotylstannane proceeded smoothly to give the corresponding dihydroisoquinolines **4a** and **4b**, respectively, in good yields (Table 3, entries 1 and 2). In contrast to these results, $In(OTf)_3$-catalyzed Mannich-type reactions (imino–aldol reactions) of **1a** with ketene silyl acetal afforded only the addition adduct **5a** but not the desired cyclized product (Table 3, entry 3). However, this problem could be overcome by changing the nitrogen-protecting groups of imine **1**. Although phenylimine **1b** did not provide the cyclized adduct at all, benzylimine **1c** underwent the tandem reaction with ketene silyl acetal to give rise to the desired product **4c** as a single product (Table 3, entries 4 and 5). As the Mannich-type reaction of **1c** did not required 2,6-di-*tert*-butyl-4-methoxyphenol to accelerate the tandem reaction, these reactions were carried out without the additive. In addition, not only ketene silyl acetals but also silyl enol ethers worked well, with the reaction yielding the

Table 3: $In(OTf)_3$-catalyzed tandem reaction with various nucleophiles.

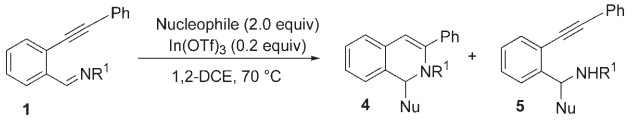

Entry	**1**	R^1	Nucleophile	*t* [h]	**4**	Yield [%]	**5**	Yield [%]
1[a]	**1a**	*p*-MeO-C_6H_4	$SnBu_3$	6	**4a**	89		0
2[a]	**1a**	*p*-MeO-C_6H_4	$SnBu_3$	6	**4b**	80		0
3	**1a**	*p*-MeO-C_6H_4	Me, Me, OMe, OTMS	8		0	**5a**	68
4	**1b**	Ph	Me, Me, OMe, OTMS	7		0	**5b**	82
5	**1c**	Bn	Me, Me, OMe, OTMS	9	**4c**	90		0
6	**1c**	Bn	OMe, OTMS	12	**4d**	88		0
7	**1c**	Bn	Ph, OTMS	12	**4e**	78		0
8	**1c**	Bn	Me, OTMS	12	**4f**	87		0
9	**1b**	Ph	$MeNO_2$	10	**4g**	89		0
10	**1b**	Ph	$CH_2(CN)_2$	24	**4h**	69		0

[a] 2,6-Di-*tert*-butyl-4-methoxyphenol was used as additive.

corresponding cyclic compounds **4d–4f** in high yields (Table 3, entries 6–8). Finally, we treated imine **1b** with activated methylene compounds, such as nitromethane and malononitrile. These reactions also proceeded smoothly to give the desired 1,2-dihydroisoquinolines **4g** and **4h** in good yields (Table 3, entries 9 and 10).

In conclusion, starting from *ortho*-alkynylarylimine, we have developed an $In(OTf)_3$-catalyzed tandem reaction for the one-pot synthesis of 1,2-dihydroisoquinolines bearing several substituents at C1. In this reaction, $In(OTf)_3$ activates both the imine and alkyne groups to the addition of various nucleophiles and for the subsequent intramolecular cyclization. The method described herein should be applicable to a wide range of nucleophiles and various alkynes and enable the synthesis of more complex heterocycles. Further studies in this area are in progress.

Received: January 31, 2006
Published online: May 3, 2006

Keywords: alkynes · cyclization · homogeneous catalysis · indium · nucleophilic addition

[1] For recent reviews, see a) T.-P. Loh, G.-L. Chua, *J. Synth. Org. Chem. Jpn.* **2005**, *63*, 1137–1146, and references therein; b) S. Araki, T. Hirashita, *Main Group Metals in Organic Synthesis*, VCH, Weinheim, **2004**, p. 323–386, and references therein; c) K. K. Chauhan, C. G. Frost, *J. Chem. Soc. Perkin Trans.* 1 **2000**, 3015–3019; d) C.-J. Li, T.-H. Chan, *Tetrahedron* **1999**, *55*, 11149–11176; e) P. Cintas, *Synlett* **1995**, 1087–1096.

[2] a) Y.-C. Teo, T.-P. Loh, *Org. Lett.* **2005**, *7*, 2539–2541; b) G. Babu, P. T. Perumal, *Tetrahedron Lett.* **1998**, *39*, 3225–3228; c) T. Miyai, Y. Onishi, A. Baba, *Tetrahedron Lett.* **1998**, *39*, 6291–6294; d) T.-P. Loh, L.-L. Wei, *Tetrahedron Lett.* **1998**, *39*,

 © 2006 Wiley-VCH Verlag GmbH & Co. KGaA, Weinheim

323 – 326; e) G. K. Friestad, C. S. Korapala, H. Ding, *J. Org. Chem.* **2006**, *71*, 281 – 289; f) Y. Onishi, T. Ito, M. Yasuda, A. Baba, *Eur. J. Org. Chem.* **2002**, 1578 – 1581; allylation of carbonyl compounds with allyltributylstannanes: g) Y.-U. Teo, J.-D. Goh, T.-P. Loh, *Org. Lett.* **2005**, *7*, 2743 – 2745; h) J. Lu, S.-J. Ji, Y.-C. Teo, T.-P. Loh, *Org. Lett.* **2005**, *7*, 159 – 161; i) J. A. Marshall, K. W. Hinkle, *J. Org. Chem.* **1995**, *60*, 1920 – 1921; other reactions: j) S. Harada, S. Handa, S. Matsunaga, M. Shibasaki, *Angew. Chem.* **2005**, *117*, 4439 – 4442; *Angew. Chem. Int. Ed.* **2005**, *44*, 4365 – 4368; k) R. Yanada, S. Obika, Y. Kobayashi, T. Inokuma, M. Oyama, K. Yanada, Y. Takemoto, *Adv. Synth. Catal.* **2005**, *347*, 1632 – 1642; l) R. Yanada, S. Obika, M. Oyama, Y. Takemoto, *Org. Lett.* **2004**, *6*, 2825 – 2828; m) A. P. Dobbs, S. J. J. Guesné, S. Martinović, S. J. Coles, M. B. Hursthouse, *J. Org. Chem.* **2003**, *68*, 7880 – 7883; n) Y. Onishi, D. Ogawa, M. Yasuda, A. Baba, *J. Am. Chem. Soc.* **2002**, *124*, 13690 – 13691; o) Y. S. Cho, H. Y. Kim, J. H. Cha, A. N. Pae, H. Y. Koh, J. H. Choi, M. H. Chang, *Org. Lett.* **2002**, *4*, 2025 – 2028; p) M. Yasuda, Y. Onishi, M. Ueba, T. Miyai, A. Baba, *J. Org. Chem.* **2001**, *66*, 7741 – 7744.

[3] a) N. Asao, C. S. Chan, K. Takahashi, Y. Yamamoto, *Tetrahedron* **2005**, *61*, 11322 – 11326; b) S. Mori, M. Uerdingen, N. Krause, K. Morokuma, *Angew. Chem.* **2005**, *117*, 4795 – 4798; *Angew. Chem. Int. Ed.* **2005**, *44*, 4715 – 4719; c) M. Ohtaka, H. Nakamura, Y. Yamamoto, *Tetrahedron Lett.* **2004**, *45*, 7339 – 7341; d) B. Witulski, C. Alayrac, L. Tevzadze-Saeftel, *Angew. Chem.* **2003**, *115*, 4392 – 4396; *Angew. Chem. Int. Ed.* **2003**, *42*, 4257 – 4260; e) Q. Huang, R. C. Larock, *J. Org. Chem.* **2003**, *68*, 980 – 988; f) G. Dai, R. C. Larock, *J. Org. Chem.* **2003**, *68*, 920 – 928; g) Q. Huang, J. A. Hunter, R. C. Larock, *J. Org. Chem.* **2002**, *67*, 3437 – 3444; h) K. R. Roesch, H. Zhang, R. C. Larock, *J. Org. Chem.* **2001**, *66*, 8042 – 8051; i) K. R. Roesch, R. C. Larock, *Org. Lett.* **1999**, *1*, 553 – 556; j) K. R. Roesch, R. C. Larock, *J. Org. Chem.* **1998**, *63*, 5306 – 5307.

[4] a) T. Tsuchimoto, H. Matsubayashi, M. Kaneko, E. Shirakawa, Y. Kawakami, *Angew. Chem.* **2005**, *117*, 1360 – 1364; *Angew. Chem. Int. Ed.* **2005**, *44*, 1336 – 1340; b) T. Tsuchimoto, K. Hatanaka, E. Shirakawa, Y. Kawakami, *Chem. Commun.* **2003**, 2454 – 2455; c) M. Nakamura, K. Endo, E. Nakamura, *Org. Lett.* **2005**, *7*, 3279 – 3281; d) M. Nakamura, K. Endo, E. Nakamura, *J. Am. Chem. Soc.* **2003**, *125*, 13002 – 13003; e) N. Sakai, K. Annaka, T. Konakahara, *Tetrahedron Lett.* **2006**, *47*, 631 – 634; f) N. Sakai, K. Annaka, T. Konakahara, *Org. Lett.* **2004**, *6*, 1527 – 1530; g) M. Weïwer, L. Coulombel, E. Duñach, *Chem. Commun.* **2006**, 332 – 334; other substrates: h) K. Miura, N. Fujisawa, A. Hosomi, *J. Org. Chem.* **2004**, *69*, 2427 – 2430; i) G. Abbiati, A. Arcadi, G. Bianchi, S. D. Giuseppe, F. Marinelli, E. Rossi, *J. Org. Chem.* **2003**, *68*, 6959 – 6966; j) N. Sakai, M. Hirasawa, T. Konakahara, *Tetrahedron Lett.* **2003**, *44*, 4171 – 4174; k) T. Tsuchimoto, T. Maeda, E. Shirakawa, Y. Kawakami, *Chem. Commun.* **2000**, 1573 – 1574.

[5] Recently, Yamamoto reported an elegant AgOTf-catalyzed nucleophilic cyclization to give *ortho*-alkynylarylaldimines: a) N. Asao, S. Yudha, T. Nogami, Y. Yamamoto, *Angew. Chem.* **2005**, *117*, 5662 – 5664; *Angew. Chem. Int. Ed.* **2005**, *44*, 5526 – 5528; b) N. T. Patil, Y. Yamamoto, *J. Org. Chem.* **2004**, *69*, 5139 – 5142; c) S. Mondal, T. Nogami, N. Asao, Y. Yamamoto, *J. Org. Chem.* **2003**, *68*, 9496 – 9498; d) S. Kamijo, Y. Yamamoto, *J. Org. Chem.* **2003**, *68*, 4764 – 4771; e) N. Asao, T. Nogami, K. Takahashi, Y. Yamamoto, *J. Am. Chem. Soc.* **2002**, *124*, 764 – 765.

[6] a) R. Takita, K. Yakura, T. Ohshima, M. Shibasaki, *J. Am. Chem. Soc.* **2005**, *127*, 13760 – 13761; b) N. Sakai, R. Kanada, M. Hirasawa, T. Konakahara, *Tetrahedron* **2005**, *61*, 9298 – 9304; c) R. Takita, Y. Fukuta, R. Tsuji, T. Ohshima, M. Shibasaki, *Org. Lett.* **2005**, *7*, 1363 – 1366.

[7] a) A. M. Taylor, S. L. Schreiber, *Org. Lett.* **2006**, *8*, 143 – 146; b) J. Chen, X. Chen, M. Bois-Choussy, J. Zhu, *J. Am. Chem. Soc.* **2006**, *128*, 87 – 89; c) S. Kwon, A. G. Myers, *J. Am. Chem. Soc.* **2005**, *127*, 16796 – 16797; d) P. Magnus, K. S. Matthews, *J. Am. Chem. Soc.* **2005**, *127*, 12476 – 12477; e) E. Ullah, S. Rotzoll, A. Schmidt, D. Michalik, P. Langer, *Tetrahedron Lett.* **2005**, *46*, 8997 – 8999; f) P. Magnus, K. S. Matthews, V. Lynch, *Org. Lett.* **2003**, *5*, 2181 – 2184; g) J. D. Scott, R. M. Williams, *J. Am. Chem. Soc.* **2002**, *124*, 2951 – 2956; h) J. D. Scott, R. M. Williams, *Angew. Chem.* **2001**, *113*, 1511 – 1513; *Angew. Chem. Int. Ed.* **2001**, *40*, 1463 – 1465; i) F. Diaba, C. L. Houerou, M. Grignon-Dubois, B. Rezzonico, P. Gerval, *Eur. J. Org. Chem.* **2000**, 2915 – 2921; j) F. Diaba, I. Lewis, M. Grignon-Dubois, S. Navarre, *J. Org. Chem.* **1996**, *61*, 4830 – 4832; k) M. E. Flanagan, R. M. Williams, *J. Org. Chem.* **1995**, *60*, 6791 – 6797.

[8] R. Yanada, A. Kaieda, Y. Takemoto, *J. Org. Chem.* **2001**, *66*, 7516 – 7518.

[9] The combination of lanthanum triflate and benzoic acid effectively accelerates the allylation of imines with allyltributylstannane: H. C. Aspinall, J. S. Bissett, N. Greeves, D. Levin, *Tetrahedron Lett.* **2002**, *43*, 323 – 325.

[10] The same results were obtained on allylation reactions of imines with allyl metal species: a) G. Alvaro, D. Savoia, M. R. Valentinetti, *Tetrahedron* **1996**, *52*, 12571 – 12586; b) A. Bocoum, C. Boga, D. Savoia, A. Umani-Ronchi, *Tetrahedron Lett.* **1991**, *32*, 1367 – 1370.

[11] The same downfield shifts were reported in reference [5e] for *ortho*-alkynylaldehyde with $Pd(OAc)_2$.

 © 2006 Wiley-VCH Verlag GmbH & Co. KGaA, Weinheim

Nanostructures

DOI: 10.1002/anie.200600239

Platinum-Functionalized Octahedral Silica Nanocages: Synthesis and Characterization**

*Xiong Wen Lou, Chongli Yuan, Qing Zhang, and Lynden A. Archer**

The preparation of hollow inorganic micro- and nanostructures has attracted consistent research efforts in the last few years.[1–22] The technological importance of these hollow particles are well-demonstrated in a myriad of applications, including their use as nanoscale chemical reactors, efficient catalysts, drug-delivery carriers, photonic building blocks, and energy-storage media.[1–17] The general approach for the preparation of hollow particles involves the use of various

[*] X. W. Lou, C. Yuan, Q. Zhang, Prof. Dr. L. A. Archer
School of Chemical and Biomolecular Engineering
Cornell University
Ithaca, NY 14853-5201 (USA)
Fax: (+1) 607-255-9166
E-mail: laa25@cornell.edu

[**] We are grateful to the National Science Foundation (DMR-0404278) for supporting this study. Facilities available through the Cornell Center for Materials Research (CCMR), a Materials Research Science and Engineering Center of the National Science Foundation (DMR-0079992), were used for this study.

© 2006 Wiley-VCH Verlag GmbH & Co. KGaA, Weinheim
WILEY InterScience DISCOVER SOMETHING GREAT

removable templates, including hard structures such as narrow size-distribution silica[1,2] and polymer–latex spheres,[7–9] as well as soft ones, for example, emulsion droplets,[10] micelles,[11] and even gas bubbles.[12] More-novel approaches based on the Kirkendall effect[14,15,19] and galvanic replacement[16] are also employed to construct hollow particles. Nonetheless, the geometry of hollow structures obtained from these approaches is primarily spherical.

The construction of hollow particles with other well-defined shapes is still a significant challenge to materials scientists. Several recent efforts devoted to the synthesis of nonspherical hollow micro- and nanostructures have produced promising results. Sun and Xia constructed single-crystal cubic Au/Ag-alloy nanoboxes with Ag nanocubes as sacrificial templates,[16a] as well as Pd nanoboxes by utilizing a simple and elegant corrosion-based method.[17] PbTe nanoboxes were synthesized by using a one-pot solvothermal route.[18] Highly symmetric 18-faceted polyhedral nanocages of Cu_7S_4 were prepared by treating precursor cubic Cu_2O nanocrystals with thiourea at 90 °C.[19] Furthermore, Yang and Zeng reported a one-pot solution synthesis of polycrystalline hollow SnO_2 octahedra in relatively high yield, based on the 2D aggregation of nanocrystallites.[20] Most recently, single-crystal octahedral Cu_2O nanocages were prepared through a one-pot catalytic solution process,[21] and hollow polyaniline with octahedral morphology was also prepared with presynthesized octahedral Cu_2O templates.[22]

Despite these successes, a simple general strategy for the synthesis of nonspherical hollow particles is preferred. Herein we propose a potentially general approach towards the facile synthesis of hollow particles with octahedral and other (e.g. cubic) morphology. We demonstrate the concept by preparing octahedral silica nanocages. Silica is chosen because of the intrinsic simplicity of its sol-gel chemistry.[8,9,23]

The synthetic strategy is as follows: $[H_2PtCl_6]$ is added to a mixture of ethanol/H_2O/ammonia containing tetraethylorthosilicate (TEOS) and aminopropyltrimethoxysilane (APS) to form a yellow precipitate of $[(NH_4)_2PtCl_6]$ instantaneously. This is followed by surface functionalization in situ with the amino groups from APS, which plays an important role in the subsequent deposition of silica on the $[(NH_4)_2PtCl_6]$ quasi-template (see below). This quasitemplate method has several important advantages over conventional template strategies. First, the quasitemplates, though insoluble in the original ethanol/H_2O reaction mixture, are easily removed by washing with water. Moreover, the template is generated in situ, which renders presynthesized hard templates unnecessary, thus allowing structures with a wider range of sizes and of extremely high purity to be synthesized readily. Furthermore, the quasitemplate itself is the precursor to noble-metal nanoparticles, which can lead to controlled Pt-functionalized products by simple calcination.

Figure 1 shows some silica nanostructures produced by the above procedure. The materials depicted were obtained after intensive washing with water to produce better TEM visualization. Even after several cycles of washing, we found that trace amounts of the Pt precursor remained. From the low-magnification image (Figure 1 d), it is apparent that the main reaction product is the targeted octahedral silica nanocages, with a much smaller amount of featureless silica particles (dark spots in the figure) produced by homogeneous nucleation. Although the morphological yield of octahedral structures was high (> 90 %), the size of these structures spanned a wide range, from 200 nm to 1.5 μm, with the vast majority in the range of 500 nm to 1 μm. Control experiments without APS produced a much lower yield of octahedral silica structures, thus underscoring its importance in the synthesis. The octahedral morphology of the silica structures can be clearly seen in the high-magnification images (Figure 1 a, c), with all eight facets being equilateral triangles. Figure 1 e shows a high-magnification field-emission scanning-electron-microscopy (FESEM) image, which again confirms unambiguously that the particles are indeed octahedral and hollow. Interestingly, twinning of two octahedra (Figure 1 b) through edge- or plane-sharing is often observed as reported for other octahedral particles.[20–22]

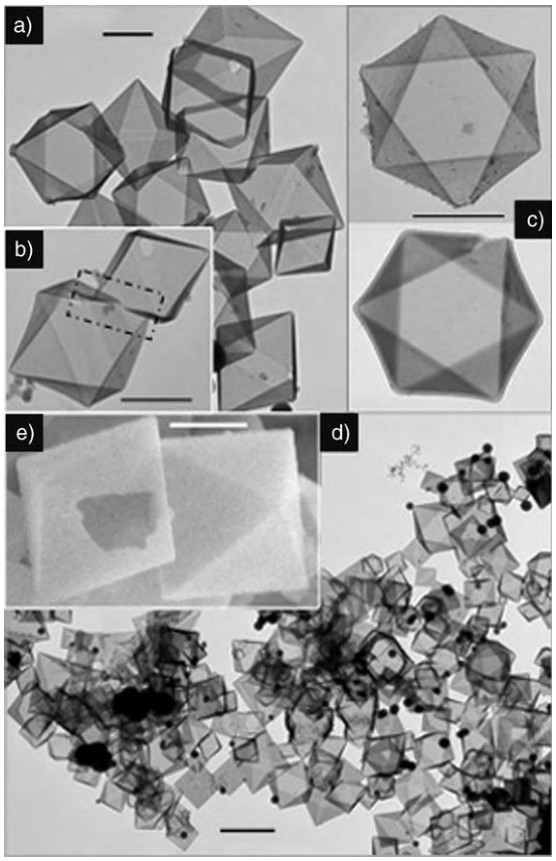

Figure 1. a)–d) TEM images and e) FESEM image of octahedral silica nanostructures after intensive washing with water. b) Two plane-sharing twinned octahedra; c) two free-standing octahedra clearly showing that each plane is an equilateral triangle; d) typical low-magnification overall view of octahedra, in which the darker spots are silica spheres; e) a perfect octahedron and a broken hollow octahedron. The scale bar in d) is 2 μm, all the rest are 500 nm.

Figure 2 shows the powder XRD patterns of the product (washed only with ethanol) a) before and b) after calcination at 450 °C. All peaks in a) and b) can be indexed undisputedly to cubic $[(NH_4)_2PtCl_6]$ (JCPDS card 07-0218) and cubic Pt (JCPDS card 04-0802), respectively. The elemental composi-

 © 2006 Wiley-VCH Verlag GmbH & Co. KGaA, Weinheim

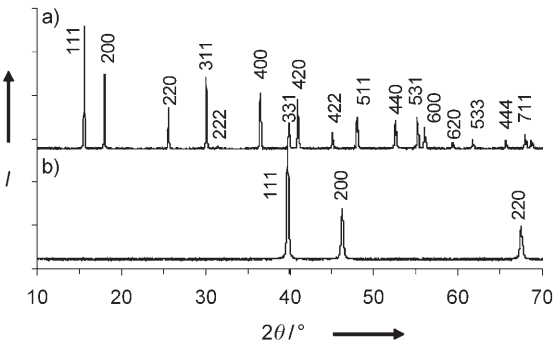

Figure 2. XRD patterns of the same product a) before and b) after calcination at 450 °C for 1 h. The product was washed with ethanol only.

tions of the products were confirmed with energy-dispersive X-ray (EDX) analysis (see below). Thermogravimetric analysis (TGA) revealed a sharp weight loss at 300–350 °C, which corresponds to the decomposition of $[(NH_4)_2PtCl_6]$ to form metallic Pt. The products after calcination were further examined with TEM. It was found that the octahedral morphology remained essentially intact (Figure 3). The wall thickness was 20–40 nm as estimated from Figure 3c and e.

Another interesting observation is that depending on the amount of Pt precursor that remains in the product after washing, the size and distribution of the Pt nanoparticles trapped inside the octahedral nanocages can be controlled. For example, when the $[(NH_4)_2PtCl_6]$ was partially removed by washing with water before calcination, the resultant Pt nanoparticles were relatively small (< 100 nm) and uniformly distributed on the interior walls (Figure 3a–c). In contrast, without prior removal by washing with water, the Pt precursor decomposed to form a few big particles (Figure 3e, f), which appeared to congregate around one apex of the structures (Figure 3e). In this way, controlled functionalization with Pt in the interior of nanocages could be achieved. Furthermore, it is well-known that the silica shell formed through the Stöber process is highly porous, evidence for which is provided in this case by the easy removal of $[(NH_4)_2PtCl_6]$ in water.[8,9,23] These pores could serve as percolated channels that connect the interior cavity and exterior space for potential applications such as nanoreactors.[4,5,20]

Detailed composition characterization was carried out with EDX analysis and converged-beam electron diffraction (CBED). Measurements based on nanostructures that contain a small number of Pt nanoparticles are particularly revealing because they facilitate spatially resolved characterization of the composition of individual units. Specifically, EDX spectra were collected from different locations within the nanostructures (Figure 4). From the EDX spectrum (Figure 4b) corresponding to spot 1 (Figure 4a, b inset), it is clear that the bright mushroomlike particle in the dark-field TEM image (Figure 4a, marked with a white square) is composed of Pt, and that these particles are trapped inside a silica cage, with their crystalline nature confirmed by CBED (Figure 4a inset). If the X-ray beam is positioned slightly off spot 1 (i.e. spot 2 or any other dark area within the nanostructure, e.g. spot 3), the EDX spectrum (Figure 4c) shows much stronger silica bands and no hint of Pt, thus indicating that the material is locally composed of silica.

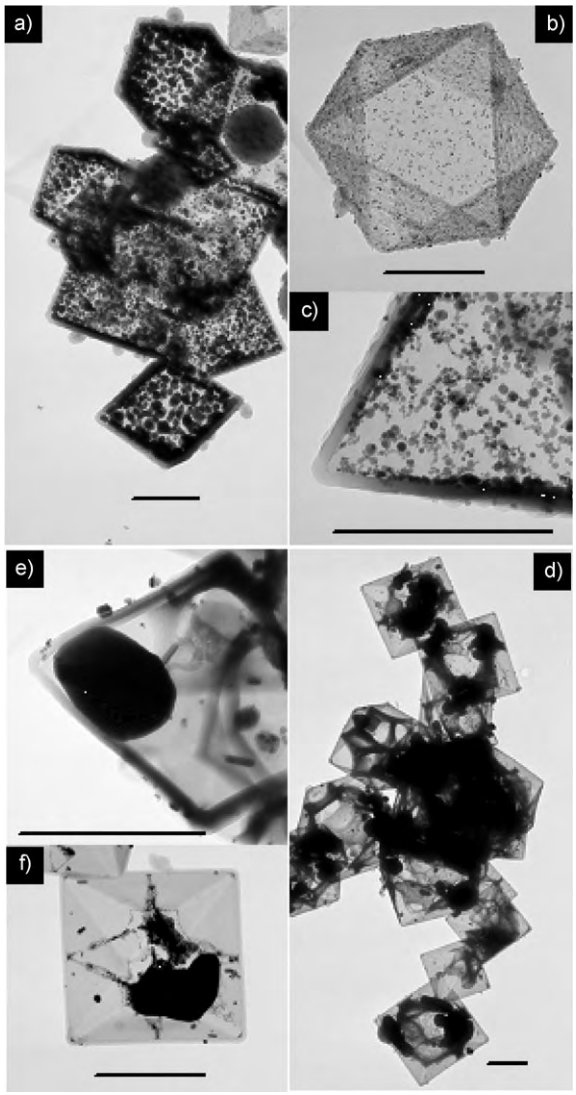

Figure 3. TEM images of Pt-functionalized silica nanocages. a)–c) The Pt precursor in the product was partially removed by washing with water prior to calcination; d)–f) the product was washed with ethanol only so that no Pt precursor was removed before calcination. All scale bars are 500 nm.

To understand further the proposed mechanism by which octahedral nanocages are formed, several control experiments were conducted. For example, if mixture B (silica precursor; see Experimental Section) was not added, only microsized $[(NH_4)_2PtCl_6]$ octahedra were formed (Figure 5a). The octahedral shape may therefore be intrinsically attributed to its cubic crystal structure, for which the formation of {111} surface planes is favorable.[20,21] The inset in Figure 5a reveals another important feature: Most of the surface of the eight {111} planes of larger crystals (about 10 μm) is absent. This is likely due to inefficient monomers during rapid crystal growth, which leads to preferential growth at the edges. On the other hand, smaller crystals (< 5 μm) have only some hexagonal windows on their {111} planes, which may even be

 © 2006 Wiley-VCH Verlag GmbH & Co. KGaA, Weinheim

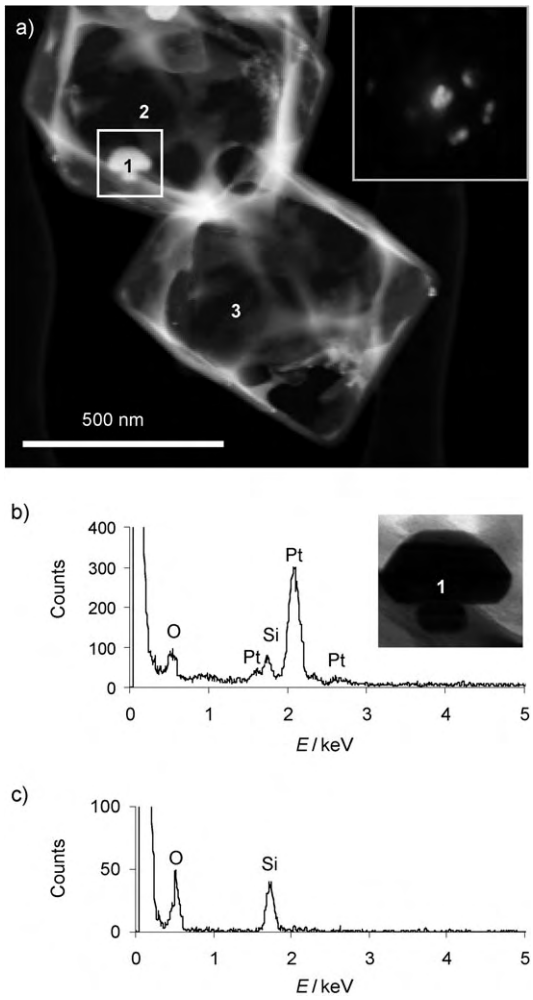

Figure 4. a) Dark-field TEM image; the inset shows a typical CBED pattern with clear diffraction spots from small Pt nanoparticles; b) EDX spectrum collected from spot 1 in a); the inset shows a magnified bright-field TEM image of spot 1; c) typical EDX spectrum collected from a dark area such as spot 2 and spot 3 in a).

completely closed to form perfect octahedra. The crystal-growth behavior could be largely altered in the presence of silica sols and the functionalizing APS; the formation of larger octahedral skeletons is inhibited, whereas the growth of small perfect octahedra is favored. To gain more insight, we also reversed the sequence in which mixture B and $[H_2PtCl_6]$ were introduced. The product consisted of large skeleton-like octahedra, many small perfect octahedra, and a significant fraction of silica spheres (Figure 5b). Notably, the large octahedron is assembled from six small octahedra, which may provide clues about the prevention of growth of larger octahedra and the origin of twinning between the individual structures.

Although the construction scheme reported herein is a one-step process, successful preparation of octahedral nanocages of a particular size or range of sizes is evidently the result of fine-tuning many other experimental conditions such as the hydrolysis rate of TEOS and the amount of APS required for optimal deposition. The proposed facile strategy for the preparation of octahedral nanostructures can be

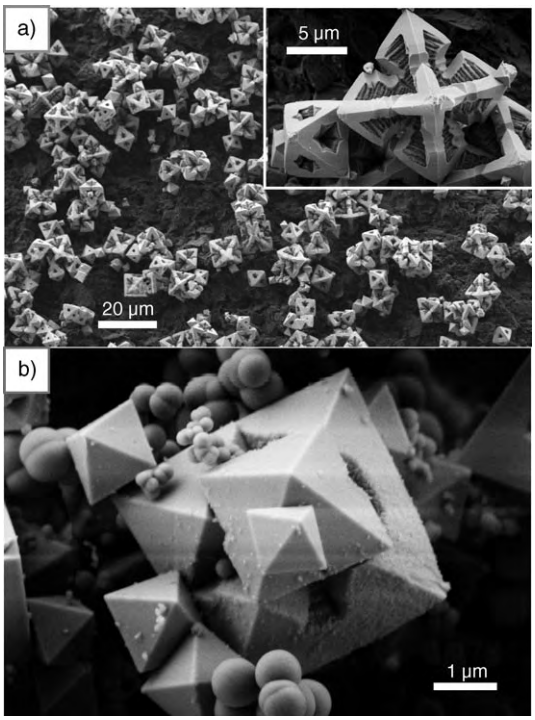

Figure 5. FESEM images of $[(NH_4)_2PtCl_6]$ microcrystals a) produced without adding mixture B (silica precursor) and b) obtained by reversing the order in which mixture B and $[H_2PtCl_6]$ were added (see Experimental Section).

extended to other polyhedra and materials such as metal oxides. Our continual effort is directed towards the construction of polyhedral nanocages for TiO_2, ZrO_2, and composites.

In summary, octahedral silica nanocages have been prepared by a facile one-step approach, which also enabled controlled functionalization with Pt in the cavities. The strategy is based on mediated deposition of silica on simultaneously generated salt quasitemplates, which can be simply removed by washing with water. By suitable optimization of the sol-gel chemistry, the growth mechanism can, in principle, be implemented in the synthesis of hollow polyhedra of many other materials.

Experimental Section

Mixture A, composed of absolute ethanol (58.5 g), deionized water (10 g), and ammonia (29.6%, 3 g), and mixture B, composed of TEOS (99%, 3 mL; Aldrich) and APS (0.4 mL; Gelest), were prepared as stock solutions. Pt-functionalized octahedral silica nanocages were synthesized by APS-assisted deposition of silica on insoluble quasi-templates generated in situ. Mixture B (20 μL) and hydrogen hexachloroplatinate(IV) solution (8 wt% in H_2O, 300 μL; Aldrich) were added successively to mixture A (2 mL) within about 3 s under vigorous magnetic stirring; a yellow precipitate was formed instantaneously. The resulting mixture was quickly vortexed for 10 s and kept under static conditions for 1 h. The solid product was harvested by centrifugation and washed with ethanol, deionized water, and again with ethanol, before being vacuum-dried at room temperature. The yellow $[(NH_4)_2PtCl_6]$ is insoluble in ethanol but soluble in water, so the amount of Pt in the final product can be controlled by the number of washing cycles with water. The dried product was calcined at 450 °C for 1 h to give Pt-functionalized octahedral silica nanocages.

 © 2006 Wiley-VCH Verlag GmbH & Co. KGaA, Weinheim

Products were characterized with powder XRD analysis (Scintag PAD X, $Cu_{K\alpha}$, $\lambda = 1.5406$ Å), EDX spectroscopy (JEOL 8900 EPMA Microprobe), TEM (JEOL-1200EX, 120 kV), ultrahigh-vacuum scanning TEM (100 kV) equipped with EDX analysis and CBED, and FESEM (LEO 1550, 3 kV).

Received: January 19, 2006
Published online: April 28, 2006

Keywords: nanocages · nanostructures · platinum · silica · template synthesis

[1] a) F. Caruso, R. A. Caruso, H. Möhwald, *Science* **1998**, *282*, 1111; b) F. Caruso, *Adv. Mater.* **2001**, *13*, 11.
[2] Y. F. Zhu, J. L. Shi, W. H. Shen, X. P. Dong, J. W. Feng, M. L. Ruan, Y. S. Li, *Angew. Chem.* **2005**, *117*, 5213; *Angew. Chem. Int. Ed.* **2005**, *44*, 5083.
[3] S. W. Kim, M. Kim, W. Y. Lee, T. Hyeon, *J. Am. Chem. Soc.* **2002**, *124*, 7642.
[4] H. P. Liang, H. M. Zhang, J. S. Hu, Y. G. Guo, L. J. Wan, C. L. Bai, *Angew. Chem.* **2004**, *116*, 1566; *Angew. Chem. Int. Ed.* **2004**, *43*, 1540.
[5] a) J. Li, H. C. Zeng, *Angew. Chem.* **2005**, *117*, 4416; *Angew. Chem. Int. Ed.* **2005**, *44*, 4342; b) H. G. Yang, H. C. Zeng, *J. Phys. Chem. B* **2004**, *108*, 3492.
[6] Q. Liu, H. Liu, M. Han, J. Zhu, Y. Liang, Z. Xu, Y. Song, *Adv. Mater.* **2005**, *17*, 1995.
[7] a) M. Yang, J. Ma, C. Zhang, Z. Yang, Y. Lu, *Angew. Chem.* **2005**, *117*, 6885; *Angew. Chem. Int. Ed.* **2005**, *44*, 6727; b) Z. Z. Yang, Z. W. Niu, Y. F. Lu, Z. B. Hu, C. C. Han, *Angew. Chem.* **2003**, *115*, 1987; *Angew. Chem. Int. Ed.* **2003**, *42*, 1943.
[8] Y. Lu, J. McLellan, Y. N. Xia, *Langmuir* **2004**, *20*, 3464.
[9] X. W. Lou, C. Yuan, E. Rhoades, Q. Zhang, L. A. Archer, *Adv. Funct. Mater.*, in press.
[10] H. G. Yang, H. C. Zeng, *Angew. Chem.* **2004**, *116*, 5318; *Angew. Chem. Int. Ed.* **2004**, *43*, 5206.
[11] C. I. Zoldesi, A. Imhof, *Adv. Mater.* **2005**, *17*, 924.
[12] Q. Peng, Y. Dong, Y. Li, *Angew. Chem.* **2003**, *115*, 3135; *Angew. Chem. Int. Ed.* **2003**, *42*, 3027.
[13] X. Sun, Y. Li, *Angew. Chem.* **2004**, *116*, 3915; *Angew. Chem. Int. Ed.* **2004**, *43*, 3827.
[14] Y. D. Yin, R. M. Rioux, C. K. Erdonmez, S. Hughes, G. A. Somorjai, A. P. Alivisatos, *Science* **2004**, *304*, 711.
[15] J. Yang, L. Qi, C. Lu, J. Ma, H. Cheng, *Angew. Chem.* **2005**, *117*, 604; *Angew. Chem. Int. Ed.* **2005**, *44*, 598.
[16] a) Y. G. Sun, Y. N. Xia, *Science* **2002**, *298*, 2176; b) Y. Sun, B. Mayers, Y. Xia, *Adv. Mater.* **2003**, *15*, 641.
[17] Y. Xiong, B. Wiley, J. Chen, Z. Y. Li, Y. Yin, Y. Xia, *Angew. Chem.* **2005**, *117*, 8127; *Angew. Chem. Int. Ed.* **2005**, *44*, 7913.
[18] W. Wang, B. Poudel, D. Wang, Z. F. Ren, *Adv. Mater.* **2005**, *17*, 2110.
[19] H. Cao, X. Qian, C. Wang, X. Ma, J. Yin, Z. Zhu, *J. Am. Chem. Soc.* **2005**, *127*, 16024.
[20] H. G. Yang and H. C. Zeng, *Angew. Chem.* **2004**, *116*, 6056; *Angew. Chem. Int. Ed.* **2004**, *43*, 5930.
[21] C. Lu, L. Qi, J. Yang, X. Wang, D. Zhang, J. Xie, J. Ma, *Adv. Mater.* **2005**, *17*, 2562.
[22] Z. Zhang, J. Sui, L. Zhang, M. Wan, Y. Wei, L. Yu, *Adv. Mater.* **2005**, *17*, 2854.
[23] W. Stöber, A. Fink, E. Bohn, *J. Colloid Interface Sci.* **1968**, *26*, 62.

 © 2006 Wiley-VCH Verlag GmbH & Co. KGaA, Weinheim

Nanotechnology

DOI: 10.1002/anie.200504390

Fluorescent Quantum Dots with Boronic Acid Substituted Viologens To Sense Glucose in Aqueous Solution**

*David B. Cordes, Soya Gamsey, and Bakthan Singaram**

Since their development in the 1980s, fluorescent quantum-dot semiconductor nanoparticles have increasingly replaced traditional organic fluorophores in applications such as biomolecule tagging, tissue imaging, and ion sensing.[1–6] Interest in fluorescent quantum dots (QDs) derives from their broad absorption, narrow emission, intense brightness, and good photostability relative to organic dyes.[7] Surprisingly, despite the large and diverse set of fluorescence-based sensing systems for glucose,[8–11] no methods for glucose detection that utilize inherently fluorescent QDs have been reported.[12] Previously, we demonstrated a very general two-component glucose-sensing system in which glucose modulates the ability of a boronic acid substituted viologen quencher/receptor to quench the fluorescence of anionic organic dyes.[13–15] Signal modulation occurs when glucose binds to the boronic acid receptor moiety, which at pH 7.4 exists in its trigonal neutral form in the absence of glucose.[16] Formation of the more-acidic glucose boronate ester shifts the acid–base equilibrium of the boronic acid towards its anionic tetrahedral "-ate" form. These electronic and/or steric changes, which have been confirmed with ^{11}B NMR spectroscopy, cause a decrease in the quenching interaction between viologen and fluorophore and result in an increase in fluorescence. This two-component approach to glucose sensing allows considerable flexibility in choosing the quencher/receptor and fluorophore components depending on the particular requirements of the sensing application. For example, fluorophore components may be selected to provide any one of a range of desired excitation or emission wavelengths, whereas a particular quencher/receptor may be chosen for reasons of its monosaccharide-binding selectivity. Herein we show that some of the advantages of QDs can be realized in our two-component system to sense changes in glucose concentration in aqueous solution. The putative mechanism for glucose sensing with quantum dots and

[*] D. B. Cordes, S. Gamsey, Prof. B. Singaram
Department of Chemistry and Biochemistry
University of California, Santa Cruz
1156 High Street, Santa Cruz, CA 95064 (USA)
Fax: (+1) 831-459-2935
E-mail: singaram@chemistry.ucsc.edu

[**] We thank GluMetrics, Inc., operating through the UC BioStar Industry–University Cooperative Research program (grant bio04-10458), for continual financial support.

Supporting information for this article is available on the WWW under http://www.angewandte.org or from the author.

© 2006 Wiley-VCH Verlag GmbH & Co. KGaA, Weinheim

boronic acid substituted viologen quenchers/receptors is shown in Scheme 1.

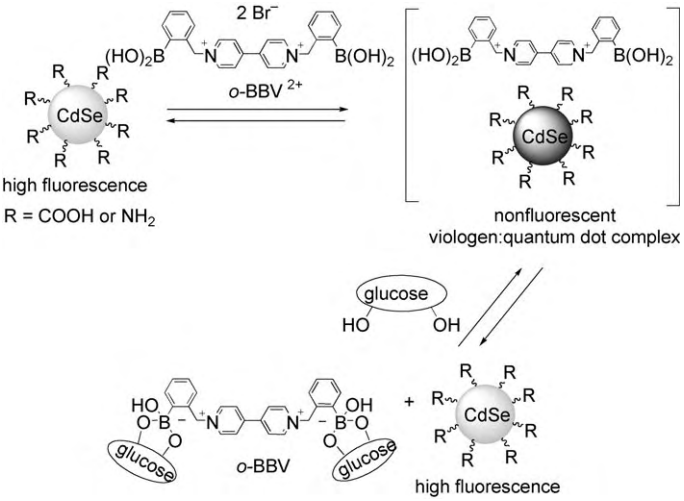

Scheme 1. Putative mechanism for glucose sensing with fluorescent QDs.

Typically, fluorescent QDs are constructed from inorganic semiconductor core materials such as CdTe and CdSe, coated with an insulating shell material such as ZnS, and further treated to provide the desired surface chemistry. For the preparation of water-soluble core–shell QDs, surface functionalization with phosphonate, carboxy, or amine groups is often employed. The particular surface chemistry allows the QDs to bind to molecules of interest such as proteins and also determines their solubility, aggregation behavior, and sensitivity to quenching processes. Several groups have observed quenching of QD fluorescence with methyl viologen (MV^{2+}).[1,17–19] The process is believed to occur through excited-state electron transfer from the QD to the viologen, thus resulting in reduction of the viologen to $MV^{\bullet+}$. Our previous studies showed that viologens were extremely efficient in statically quenching the fluorescence of many organic dyes through complex formation with the fluorophore.[13,14] We reasoned that the fluorescence of core–shell QDs that bear polar surface groups such as carboxy and amine groups might be similarly quenched through complex formation with our boronic acid substituted viologen quenchers.

To test our hypothesis, we examined two sets of commercially available core–shell CdSe QDs coated with ZnS, which were identically prepared except for their surface functionalization; one set was prepared with carboxy groups on the surface, the other with amine groups.[20] Both sets had a fairly narrow fluorescence emission centered at 604 nm. We found that these QDs indeed functioned in our system in a manner similar to that of organic dyes: they showed a decrease in fluorescence upon the introduction of viologen quencher. To our delight, we also found a robust fluorescence recovery when glucose was added to the quenched QD solutions (Figure 1).

The sensitivity of both QD sets to fluorescence quenching by the boronic acid substituted viologen *o*-BBV^{2+} was

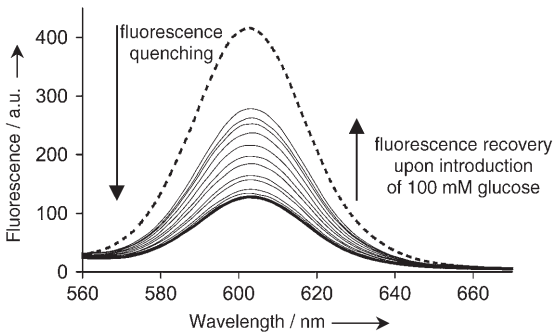

Figure 1. Characteristic fluorescence response upon introduction of quencher followed by glucose to amine-functionalized QD solution (5×10^{-8} M) at pH 7.4. Final quencher/QD (*o*-BBV^{2+}/NH_2 QD) ratio for this data = 50:1, final glucose concentration = 100 mM. The dashed line indicates unquenched fluorescence, the bold line indicates fluorescence after introduction of quencher.

determined in an aqueous solution at pH 7.4 (Figure 2). We found that the fluorescence of both the carboxy- and amine-substituted QDs were sensitive to quenching by *o*-BBV^{2+},

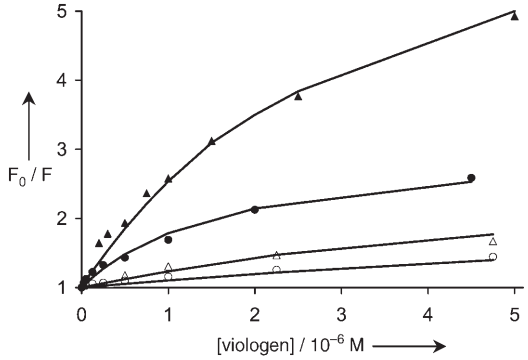

Figure 2. Stern–Volmer plot showing the quenching of the fluorescence of amine- and carboxy-substituted QDs (5×10^{-8} M) at pH 7.4 by *o*-BBV^{2+} and BV^{2+}. ▲ COOH QDs with *o*-BBV^{2+}, ● NH_2 QDs with *o*-BBV^{2+}, △ COOH QDs with BV^{2+}, ○ NH_2 QDs with BV^{2+}.

with the carboxy-substituted QDs showing a stronger sensitivity to quenching than the amine-substituted dots. Quenching experiments conducted at various temperatures showed that quenching was more efficient at lower temperatures, thus indicating a static quenching mechanism that involves complex formation between QD and viologen quencher.[21] We found that the fluorescence of both sets of QDs was also similarly quenched by simple unsubstituted benzyl viologen (BV^{2+}), though to a lesser degree than with *o*-BBV^{2+}, which suggests that the boronic acids may play some role in the quenching process. Control quenching experiments with 3-nitrophenylboronic acid showed that, on its own, the boronic acid produces insignificant quenching (less than 2% of that observed with *o*-BBV^{2+}).[21] Significantly, although we were unable to determine the degree of ionization of the surface groups, the carboxy-substituted dots are expected to exist primarily in their anionic form at pH 7.4, whereas the amine dots are most likely to be neutral. We speculate that the

 © 2006 Wiley-VCH Verlag GmbH & Co. KGaA, Weinheim

enhanced sensitivity of the carboxy-substituted QDs is due to electrostatic attraction between the cationic viologen quencher and the anionic surface groups on the QD.

Surprisingly, we observed uncharacteristic profiles for our quenching studies compared with previous observations in which Stern–Volmer analysis gave linear or superlinear plots. All our plots in the study of QD fluorescence quenching showed negative deviations from linearity. Such downward deviations were observed by several other groups studying fluorescence quenching of core–shell QDs.[22] Such a profile may indicate the presence of multiple fluorescence pathways, some of which are less efficiently quenched than others, or it may reflect limited accessibility of the quencher to the surface. Regardless of these differences in quenching behavior, both sets of QDs examined in this study successfully detected changes in glucose concentration. As expected, the QDs quenched with BV^{2+}, which does not contain boronic acids, showed no fluorescence recovery when glucose was added.

Previous studies showed that the choice of an appropriate quencher/fluorophore ratio was critical for a strong and linear signal response across the physiological range of glucose concentrations ($\approx$2.5–20 mM).[13,14] When experimenting with several different quencher/QD ratios, we observed generally the same behavior as with traditional organic dyes, in which higher ratios tended to give larger, more-linear fluorescence signals in response to the introduction of glucose (Figure 3).

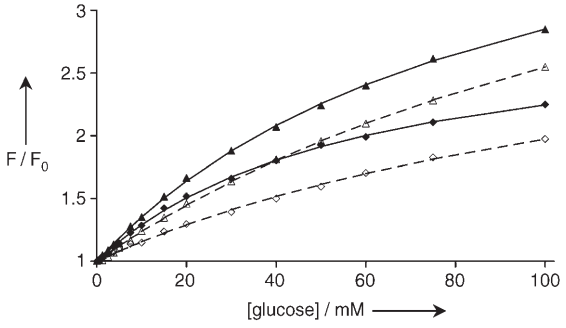

Figure 3. Glucose-response curves obtained from *o*-BBV^{2+}-fluorescence-quenched amine- and carboxy-substituted QDs (5×10^{-8} M) at pH 7.4. ▲ NH_2 QDs 1000:1, ◆ NH_2 QDs 50:1, △ COOH QDs 1000:1, ◇ COOH QDs 50:1.

We screened both sets of QDs for glucose response at quencher/QD ratios of 50:1, 200:1, 500:1, and 1000:1. For both amine- and carboxy-substituted QDs, we obtained optimal results with quencher/QD = 1000:1. While the fluorescence-signal response is modest in the physiological range, this application of QDs allows a large signal response and a considerable degree of recovery of the initial unquenched QD fluorescence after the introduction of glucose (100 mM) (Figure 3).

Studies are currently underway to examine further the use of QDs in two-component sensing systems for the detection of monosaccharides and other analytes.

Experimental Section

The fluorescent QDs (CdSe/ZnS Fort Orange COOH-functionalized QDs, CdSe/ZnS Fort Orange NH_2-functionalized QDs) were acquired from Evident Technologies as buffered aqueous stock solutions (7.76 nmols mL^{-1}). All data were analyzed with Solver (nonlinear least-squares curve fitting) in Microsoft Excel.

Fluorescence emission: All studies were carried out in buffer solution (pH 7.4) prepared with water purified by a Nanopure ultrafiltration system. The buffer solution (pH 7.4, ionic strength 0.1) was freshly prepared with KH_2PO_4 and Na_2HPO_4. The QD stock solutions were diluted in a quartz cuvette (path = 1 cm) with phosphate buffer (pH 7.4) to afford solutions (5×10^{-8} M) with a total volume of 2 mL. Fluorescence spectra were acquired with a Perkin–Elmer LS50-B luminescence spectrometer, except for temperature studies, which were conducted on a Varian Cary Eclipse fluorescence spectrophotometer. Studies were carried out at 22 °C without the exclusion of air, with the exception of temperature-dependent quenching experiments.[21] Excitation was performed with a slit width of 15 nm and a wavelength of 460 nm. The emission slit was set at 20 nm, and fluorescence emission was taken as the area under the emission curve from 560 to 670 nm, with peak emission for both sets of QDs at 604 nm. For fluorescence-titration experiments, the volume added did not exceed 3 % of the total, and the absorbance for all fluorescence measurements was below 0.1.

Fluorescence quenching: A quartz cuvette filled with QD solution (2 mL, 5×10^{-8} M in pH 7.4 buffer) was irradiated at 460 nm. The emission of the unquenched solution was obtained, then aliquots of *o*-BBV^{2+} quencher (0.001 M) were added, the solution was gently shaken for 60 s, and the new fluorescence was measured. Fluorescence intensity was taken as the area under the emission curve. Temperature-dependent quenching studies were conducted at 15, 25, and 65 °C with amine-functionalized QDs. Stern–Volmer constants were calculated by fitting the data to [Eq. (1)], where F_o is the initial unquenched fluorescence, F is the fluorescence in the presence of quencher, V is the dynamic quenching constant, K_S is the static quenching constant, [Q] is the quencher concentration.

$$\frac{F_o}{F} = \frac{V K_S [Q]}{1 + K_S [Q]} \quad (1)$$

Fluorescence glucose sensing: A quartz cuvette filled with QD solution (2 mL, 5×10^{-8} M in pH 7.4 buffer) was irradiated at 460 nm. The emission of the unquenched solution was obtained, then the solution was quenched with *o*-BBV^{2+}, and the new emission was measured. Aliquots of concentrated glucose solution (2.5 M, pH adjusted in buffer to 7.4) were then added, the mixture was gently shaken for 60 s, and the new fluorescence was measured. Fluorescence intensity was taken as the area under the emission curve. Apparent glucose-binding constants were calculated by fitting the data to the [Eq. (2)], where F_{calcd} is the calculated fluorescence intensity, F_{min} is the initial fluorescence intensity of the quenched dye, F_{max} is the calculated intensity at which the fluorescence increase reaches its maximum, K is the apparent binding constant, and [glucose] is the concentration of glucose.[23]

$$F_{calcd} = \frac{F_{min} + F_{max} K [\text{glucose}]}{1 + K [\text{glucose}]} \quad (2)$$

Received: December 10, 2005
Published online: April 28, 2006

Keywords: boronic acids · fluorescence · glucose · quantum dots · sensors · viologens

 © 2006 Wiley-VCH Verlag GmbH & Co. KGaA, Weinheim

[1] D. Ishii, K. Kinbara, Y. Ishida, N. Ishii, M. Okochi, M. Yohda, T. Aida, *Nature* **2003**, *423*, 628.
[2] D. R. Larson, W. R. Zipfel, R. M. Williams, S. W. Clark, M. P. Bruchez, F. W. Wise, W. W. Webb, *Science* **2003**, *300*, 1434.
[3] W. C. W. Chan, D. J. Maxwell, X. H. Gao, R. E. Bailey, M. Y. Han, S. M. Nie, *Curr. Opin. Biotechnol.* **2002**, *13*, 40.
[4] W. C. W. Chan, S. M. Nie, *Science* **1998**, *281*, 2016.
[5] C. M. Niemeyer, *Angew. Chem.* **2001**, *113*, 4254; *Angew. Chem. Int. Ed.* **2001**, *40*, 4128.
[6] M. Green, *Angew. Chem.* **2004**, *116*, 4221; *Angew. Chem. Int. Ed.* **2004**, *43*, 4129.
[7] M. Bruchez, M. Moronne, P. Gin, S. Weiss, A. P. Alivisatos, *Science* **1998**, *281*, 2013.
[8] R. J. McNichols, G. L. Cote, *J. Biomed. Opt.* **2000**, *5*, 5.
[9] T. D. James, S. Shinkai, *Host–Guest Chem.* **2002**, *218*, 159.
[10] H. S. Cao, M. D. Heagy, *J. Fluoresc.* **2004**, *14*, 569.
[11] J. C. Pickup, F. Hussain, N. D. Evans, O. J. Rolinski, D. J. S. Birch, *Biosens. Bioelectron.* **2005**, *20*, 2555.
[12] Nonfluorescent semiconductor particles have been used as platforms for glucose-sensing systems; for examples, see: K. Aslan, J. Zhang, J. R. Lakowicz, C. D. Geddes, *J. Fluoresc.* **2004**, *14*, 391 and references therein.
[13] D. B. Cordes, S. Gamsey, Z. Sharrett, A. Miller, P. Thoniyot, R. A. Wessling, B. Singaram, *Langmuir* **2005**, *21*, 6540.
[14] D. B. Cordes, A. Miller, S. Gamsey, Z. Sharrett, P. Thoniyot, R. Wessling, B. Singaram, *Org. Biomol. Chem.* **2005**, *3*, 1708.
[15] J. T. Suri, D. B. Cordes, F. E. Cappuccio, R. A. Wessling, B. Singaram, *Angew. Chem.* **2003**, *115*, 6037; *Angew. Chem. Int. Ed.* **2003**, *42*, 5857.
[16] Y. Nambu, K. Yamamoto, T. Endo, *J. Chem. Soc. Chem. Commun.* **1986**, *7*, 574.
[17] S. Logunov, T. Green, S. Marguet, M. A. El-Sayed, *J. Phys. Chem. A* **1998**, *102*, 5652.
[18] Y. Nosaka, H. Miyama, M. Terauchi, T. Kobayashi, *J. Phys. Chem.* **1988**, *92*, 255.
[19] D. Duonghong, E. Borgarello, M. Gratzel, *J. Am. Chem. Soc.* **1981**, *103*, 4685.
[20] T. Nagase, E. Nakata, S. Shinkai, I. Hamachi, *Chem. Eur. J.* **2003**, *9*, 3660.
[21] See Supporting Information for details.
[22] C. Landes, C. Burda, M. Braun, M. A. El-Sayed, *J. Phys. Chem. B* **2001**, *105*, 2981.
[23] C. R. Cooper, T. D. James, *J. Chem. Soc. Perkin Trans. 1* **2000**, 963.

 © 2006 Wiley-VCH Verlag GmbH & Co. KGaA, Weinheim

Palladium-Catalyzed Hydrogenation

DOI: 10.1002/anie.200600263

A Highly Enantioselective, Pd–TangPhos-Catalyzed Hydrogenation of *N*-Tosylimines**

*Qin Yang, Gao Shang, Wenzhong Gao, Jingen Deng, and Xumu Zhang**

Although significant progress has been made in the catalytic asymmetric reduction of ketones and olefins over the last few decades,[1] the asymmetric reduction of imines remains a major challenge.[2] Enantioselective reductive amination with organocatalysts has recently been reported,[3] and a number of transition-metal-based catalysts, such as those containing Rh,[4] Ru,[5] Ti,[6] Zr,[6d] and Ir,[7] have been applied to the asymmetric hydrogenation of imines. However, this method has been less successful than the hydrogenation of other substrates. The main obstacles in solving the problems in this hydrogenation approach include different enantioselectivities for *E* and *Z* isomers of acyclic imines,[6b,c,8] the instability of some imines prepared from ketones, and the inhibitory effect of the amine products on the metal catalysts. In order to solve these problems, *N*-tosylimines were selected as the hydrogenation substrates since they are relatively stable and can be easily obtained from the corresponding ketones exclusively as the *E* isomer.[9] In addition, the strongly electron-withdrawing character of the tosyl group reduces the inhibitory effect of the reduction product on the catalysts, which might lead to higher reactivity. These advantages of *N*-tosylimines as substrates prompted us to look for a good reduction catalyst for the substrates. To the best of our knowledge, the asymmetric hydrogenation of *N*-tosylimines has rarely been explored, and the best result reported so far is the 84% *ee* reported by the Charette group using a Ru–Binap catalyst.[9] In our search for effective hydrogenation catalysts for the reduction of *N*-tosylimines, we have explored this trans-

[*] Q. Yang, G. Shang, Dr. W. Gao, Prof. X. Zhang
Department of Chemistry
The Pennsylvania State University
104 Chemistry Building, University Park, PA 16802 (USA)
Fax: (+1) 814-863-8403
E-mail: xumu@chem.psu.edu
Q. Yang, Prof. J. Deng
Key Laboratory of Asymmetric Synthesis & Chirotechnology of Sichuan Province and
Union Laboratory of Asymmetric Synthesis
Chendu Institute of Organic Chemistry
Chinese Academy of Sciences
Chengdu 610041 (China)
and
Graduate School of the Chinese Academy of Science
Beijing (China) Department of Chemistry

[**] This work was supported by the National Institutes of Health (GM58832).

Supporting Information for this article is available on the WWW under http://www.angewandte.org or from the author.

InterScience
© 2006 Wiley-VCH Verlag GmbH & Co. KGaA, Weinheim

formation with many transition-metal-containing catalysts, in particular Rh, Ru, Ir, and Pd complexes.

Palladium complexes have been extensively employed as catalysts for a wide range of reactions, especially for carbon–carbon and carbon–heteroatom coupling reactions.[10] Although heterogeneous Pd/C catalysts have been used extensively in imine reductions, there are only a few reports of Pd-catalyzed homogeneous and asymmetric hydrogenation. The first asymmetric hydrogenation of imino esters was described by Amii with a $Pd(OCOCF_3)_2$–Binap complex that gave up to 90% *ee*.[11] However, the substrate scope of this system was limited to fluoro-substituted compounds. Raja and Thomas have reported a heterogeneous palladium-catalyzed asymmetric hydrogenation of α-ketoesters,[12] and, very recently, the Zhou group disclosed their results on the hydrogenation of functionalized ketones using $Pd(OCOCF_3)_2$ and Me-DuPhos as catalyst, with a best result of 92% *ee*.[13]

Our group has developed a series of diphosphane ligands, such as TangPhos, DuanPhos, Binapine, and C_n-Tunephos (Scheme 1), which we have successfully employed in the asymmetric hydrogenation of a wide range of substrates.[14] The electron-donating rigid TangPhos ligand was found to be particularly good for highly enantioselective hydrogenation reactions; therefore we anticipated that the combination of Pd precursors with TangPhos could lead to outstanding results in the asymmetric hydrogenation of imines. Here we present our preliminary results on the Pd–TangPhos-catalyzed hydrogenation of *N*-tosylimines, which occurs with up to >99% *ee* and complete conversion.

Our initial study began with *N*-tosylimine (**1a**) as the model substrate and a rhodium complex of a chiral diphosphane as the catalyst. A number of catalytic systems were tested; the results are summarized in Table 1. First, we investigated the asymmetric hydrogenation of **1a** using the Rh–TangPhos complex **A**, which has been proved to be an efficient hydrogenation catalyst for a number of substrates. Up to 91% *ee* was observed (Table 1, entry 1). Other Rh complexes with chiral diphosphane ligands, such as **B** and **C**, also provided good enantioselectivities (Table 1, entries 2 and 3). A systematic study of the hydrogenation of **1a** was then performed to screen the reaction conditions. The hydrogenation with Rh–(*R*,*R*)-Et-DuPhos (**D**) or Rh–(*R*,*R*)-Met-DuPhos (**E**) proceeded with high conversions; however, the *ee* values of the products were relatively low (63% and 68%, respectively; Table 1, entries 4 and 5). To our delight, the best result was obtained with the Pd–TangPhos complex **L** (up to 99% *ee* and >99% conversion; Table 1, entry 14). In contrast, complexes **I** and **J** did not show any reactivity. These results imply that the weakly coordinating $CF_3CO_2^-$ ion in complex **L** might play an important role in this transformation (Table 1, entries 9 and 10).

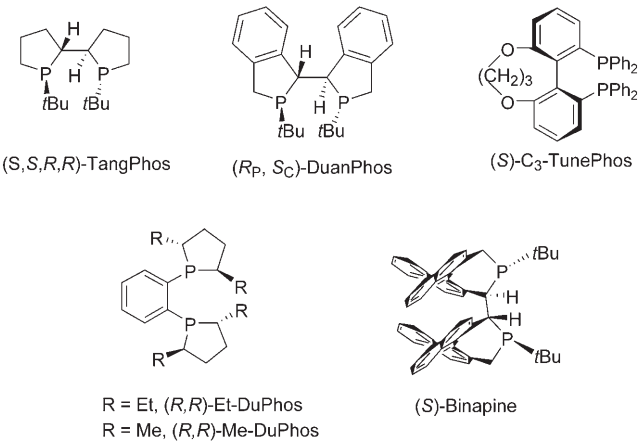

Scheme 1. Structure of ligands for asymmetric hydrogenation.

The effect of reaction temperature and hydrogen pressure on the enantioselectivity and reactivity of the hydrogenation was also tested. We found that both the conversion and the *ee* decreased at a lower hydrogen pressure (Table 1, entry 12). A lower temperature only resulted in a lower conversion; the enantioselectivity remained the same (Table 1, entry 13). Further studies indicated that changing the solvent had no significant effect on the enantioselectivities and conversions (Table 1, entries 15–18).

To demonstrate the efficiency of this Pd–TangPhos catalyst, a series of substituted *N*-tosylimines **1** were synthesized from readily available starting materials according to

Table 1: Enantioselective hydrogenation of *N*-tosylimine **1a**.[a]

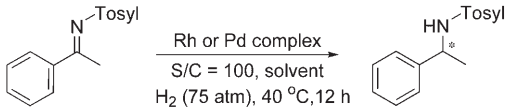

1a **2a**

Entry	Cat. precursor	Ligand	Complex	Solvent	Conv. [%][b]	*ee* [%][c]
1	$[Rh(cod)_2]BF_4$	(*S*,*S*,*R*,*R*)-TangPhos	**A**	CH_2Cl_2	>99	91
2	$[Rh(cod)_2]BF_4$	(R_P,S_C)-DuanPhos	**B**	CH_2Cl_2	>99	82
3	$[Rh(cod)_2]BF_4$	S_P-Binapine	**C**	CH_2Cl_2	>99	88
4	$[Rh(cod)_2]BF_4$	(*R*,*R*)-Et-DuPhos	**D**	CH_2Cl_2	>99	63
5	$[Rh(cod)_2]BF_4$	(*R*,*R*)-Me-Duphos	**E**	CH_2Cl_2	>99	68
6	$[Rh(cod)_2]BF_4$	(*S*)-C_3-Tunephos	**F**	CH_2Cl_2	>99	94
7	$Pd(OCOCF_3)_2$	(*S*)-Binapine	**G**	CH_2Cl_2	15	n.a.
8	$Pd(OCOCF_3)_2$	(*S*)-C_3-Tunephos	**H**	CH_2Cl_2	65	n.a.
9	$Pd(OAc)_2$	(*S*,*S*,*R*,*R*)-TangPhos	**I**	CH_2Cl_2	n.r.	n.a.
10	$[Pd(MeCN)]Cl_2$	(*S*,*S*,*R*,*R*)-TangPhos	**J**	CH_2Cl_2	n.r.	n.a.
11	$[Pd(MeCN)_4](BF_4)_2$	(*S*,*S*,*R*,*R*)-TangPhos	**K**	CH_2Cl_2	>99	98
12[d]	$Pd(OCOCF_3)_2$	(*S*,*S*,*R*,*R*)-TangPhos	**L**	CH_2Cl_2	60	93
13[e]	$Pd(OCOCF_3)_2$	(*S*,*S*,*R*,*R*)-TangPhos	**L**	CH_2Cl_2	75	99
14	$Pd(OCOCF_3)_2$	(*S*,*S*,*R*,*R*)-TangPhos	**L**	CH_2Cl_2	>99	99
15	$Pd(OCOCF_3)_2$	(*S*,*S*,*R*,*R*)-TangPhos	**L**	MeOH	>99	99
16	$Pd(OCOCF_3)_2$	(*S*,*S*,*R*,*R*)-TangPhos	**L**	*i*PrOH	>99	98
17	$Pd(OCOCF_3)_2$	(*S*,*S*,*R*,*R*)-TangPhos	**L**	toluene	>99	98
18	$Pd(OCOCF_3)_2$	(*S*,*S*,*R*,*R*)-TangPhos	**L**	EtOAc	>99	96

[a] cod = 1,5-cyclooctadiene, n.r. = no reaction, n.a. = not analyzed. [b] Conversions (in %) were determined by ^{1}H NMR spectroscopy of the crude reaction mixture. [c] Enantiomeric excesses were determined by chiral HPLC. [d] The reaction was carried out under 20 atm hydrogen pressure. [e] The reaction was carried out at 24 °C.

© 2006 Wiley-VCH Verlag GmbH & Co. KGaA, Weinheim

the procedures reported in the literature.[15] The Pd–TangPhos-catalyzed hydrogenation of **1** under optimized conditions was then performed; the results are summarized in Table 2. Both electron-donating and electron-withdrawing

Table 2: Pd-catalyzed asymmetric hydrogenation of *N*-tosylimines **1**.

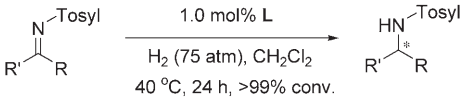

Entry	R′ in **1**	R	Prod.	*ee* [%][a]	Config.[b]
1	C_6H_5 (**1a**)	CH_3	**2a**	99	*R* (+)
2	4-$CH_3C_6H_4$ (**1b**)	CH_3	**2b**	96	(+)
3	4-FC_6H_4 (**1c**)	CH_3	**2c**	99	(+)
4	4-$CH_3OC_6H_4$ (**1d**)	CH_3	**2d**	99	(+)
5	3-$CH_3OC_6H_4$ (**1e**)	CH_3	**2e**	>99	(+)
6	2-naphthyl (**1f**)	CH_3	**2f**	>99	(+)
7	1-naphthyl (**1g**)	CH_3	**2g**	99	(−)
8	4-ClC_6H_4 (**1h**)	CH_3	**2h**	99	(+)
9	3-ClC_6H_4 (**1i**)	CH_3	**2i**	>99	(+)
10	C_6H_5 (**1j**)	C_2H_5	**2j**	93	*R* (+)
11	*t*Bu (**1k**)	CH_3	**2k**	98	*R* (+)
12	cyclopropyl (**1l**)	CH_3	**2l**	75	(+)

[a] Enantiomeric excesses were determined by chiral HPLC. [b] The absolute configuration was determined by comparison of the sign of the optical rotation with the reported data.[16]

substituents on the aryl unit of the imines gave excellent enantioselectivities (96–99% *ee*; Table 2, entries 1–9). The *ee* value decreased from 99% to 93% when a methyl group was replaced by an ethyl group (Table 2, entry 10). The doubly alkyl substituted *N*-tosylimines **1k** and **1l** were also used as substrates. Up to 98% *ee* was achieved for the *tert*-butyl-substituted imine **1k** (Table 2, entry 11), while a lower *ee* was observed with **1l** (75% *ee*; Table 2, entry 12). It is worth noting that the Pd–TangPhos-catalyzed hydrogenation of cyclic imines **1m** and **1n** also proceeded with high enantioselectivities (98% and 94% *ee*, respectively) to produce α-aminotetralin (**2m**) and α-aminindanes (**2n**), respectively, which are important structural motifs in biologically active compounds [Eq. (1)]. Surprisingly, we found that *N*-tosyli-

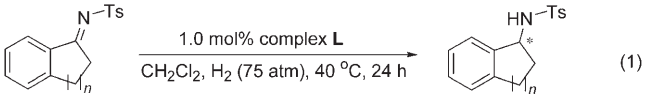

(1)

mines **1l, 1m**, and **1n** could be prepared from the corresponding ketones and readily available *p*-toluenesulfonamide in one step in up to 75% yield. The feasibility of this method for the synthesis of other *N*-tosylimine substrates is still under investigation.

Substituted sultams are important chiral auxiliaries that were first introduced in 1990 by Oppolzer[17] and have since been successfully applied to a number of asymmetric transformations. Asymmetric hydrogenation of the corresponding *N*-tosylimine is one of their most widely used synthetic transformations. To examine the efficiency of the Pd–TangPhos catalysts on this transformation, compound **1o** was synthesized and hydrogenated with complex **L** to give the methyl-substituted sultam **2o** with good enantioselectivity [Eq. (2)].[17] To examine the synthetic potential of this

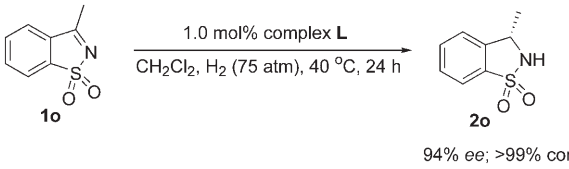

(2)

methodology, a reductive cleavage of the tosyl group in **2a** was performed according to a literature procedure.[18] (*R*)-α-Methylbenzylamine was obtained in 92% yield with retention of the previous *ee*.

In conclusion, we have developed an efficient Pd-catalyzed asymmetric hydrogenation of *N*-tosylimines, which are stable and can be prepared from aromatic, aliphatic, and cyclic ketones exclusively with the *E* configuration. A highly enantioselective hydrogenation of *N*-tosylimines has been achieved in the presence of $Pd(OCOCF_3)_2$–TangPhos, with enantioselectivities of up to 99% *ee* and conversions of more than 99%. However, a relatively high hydrogen pressure and catalytic loading are important limitations of this work. Further studies to improve the turnover number and characterize the catalytic species are underway and will be reported in due course.

Experimental Section

General hydrogenation procedure: $Pd(OCOCF_3)_2$ (3.3 mg, 0.01 mmol) and (*S*,*S*,*R*,*R*)-TangPhos (3.4 mg, 0.012 mmol) were dissolved in degassed acetone in a Schlenk tube under N_2. After stirring the solution at room temperature for 0.5 h, the solvent was removed under vacuum to give the complex as a brown solid. The solid was dissolved in degassed dichloromethane (10 mL) in a glovebox and divided equally between 10 vials. To each vial, substrate (0.1 mmol, S/C = 100) was then added to the catalyst solution and the resulting mixture was transferred to an autoclave, which was charged with H_2 (75 atm). The autoclave was stirred at 40 °C for 12–24 h, before cooling it to room temperature and carefully releasing the H_2. The solvent was then evaporated and the residue was purified by column chromatography to give the corresponding hydrogenation product, which was then analyzed directly by HPLC to determine the enantiomeric excess.

Received: January 21, 2006
Published online: May 3, 2006

Keywords: asymmetric catalysis · enantioselectivity · hydrogenation · imines · palladium

[1] a) *Comprehensive Asymmetric Catalysis, Vol. 1* (Eds.: E. N. Jacobsen, A. Pfaltz, H. Yamamoto), Springer, Berlin, **1999**; b) T. Ohkuma, M. Kitamura, R. Noyori in *Catalytic Asymmetric Synthesis* (Ed.: I. Ojima), Wiley, New York, **2000**; c) R. Noyori,

 © 2006 Wiley-VCH Verlag GmbH & Co. KGaA, Weinheim

T. Ohkuma, *Angew. Chem.* **2001**, *113*, 40 – 75; *Angew. Chem. Int. Ed.* **2001**, *40*, 40 – 73.

[2] For reviews, see: a) Q. C. Zhu, R. O. Hutchins, *Org. Prep. Proced. Int.* **1994**, *26*, 193 – 236; b) S. Kobayashi, H. Ishitani, *Chem. Rev.* **1999**, *99*, 1069 – 1094; c) M. J. Palmer, M. Wills, *Tetrahedron: Asymmetry* **1999**, *10*, 2045 – 2061; d) H.-U. Blaser, F. Spindler in *Comprehensive Asymmetric Catalysis*, *Vol. 1* (Eds.: E. N. Jacobsen, A. Pfaltz, H. Yamamoto), Springer, Berlin, **1999**, pp. 247 – 265; e) H.-U. Blaser, C. Malan, B. Pugin, F. Spindler, H. Steiner, M. Studer, *Adv. Synth. Catal.* **2003**, *345*, 103 – 151; f) F. Spindler, H.-U. Blaser in *Transition Metals for Organic Synthesis*, *Vol. 2*, 2nd ed. (Eds.: M. Beller, C. Bolm), Wiley-VCH, Weinheim, **2004**, pp. 113 – 123.

[3] a) R. I. Storer, D. E. Carrera, Y. Ni, D. W. C. MacMillan, *J. Am. Chem. Soc.* **2006**, *128*, 84 – 86, and references therein; b) S. Hoffmann, A. M. Seayad, N. List, *Angew. Chem.* **2005**, *117*, 7590 – 7593; *Angew. Chem. Int. Ed.* **2005**, *44*, 7424 – 7427; c) M. Rueping. E. Sugiono, C. Azap, T. Theissmann, M. Bolte, *Org. Lett.* **2005**, *7*, 3781 – 3783; d) R. Kadyrov, T. H. Riermeier, *Angew. Chem.* **2003**, *115*, 5630 – 5632; *Angew. Chem. Int. Ed.* **2003**, *42*, 5472 – 5474.

[4] a) S. Vastag, J. Bakos, S. Totos, N. E. Takach, R. B. King, B. Heil, L. Marko, *J. Mol. Catal.* **1984**, *22*, 283 – 287; b) M. J. Burk, J. E. Feaster, *J. Am. Chem. Soc.* **1992**, *114*, 6266 – 6267; c) J. Mao, D. C. Baker, *Org. Lett.* **1999**, *1*, 841 – 843.

[5] a) N. Uematsu, A. Fujii, S. Hashiguchi, T. Ikariya, R. Noyori, *J. Am. Chem. Soc.* **1996**, *118*, 4916 – 4917; b) C. J. Cobley, J. P. Henschke, *Adv. Synth. Catal.* **2003**, *345*, 195 – 201.

[6] a) C. A. Willoughby, S. L. Buchwald, *J. Am. Chem. Soc.* **1992**, *114*, 7562 – 7564; b) C. A. Willoughby, S. L. Buchwald, *J. Am. Chem. Soc.* **1994**, *116*, 8952 – 8965; c) X. Verdaguer, U. E. W. Lange, S. L. Buchwald, *Angew. Chem.* **1998**, *110*, 1174 – 1178; *Angew. Chem. Int. Ed.* **1998**, *37*, 1103 – 1107; d) M. Ringwald, R. Stürmer, H. H. Brintzinger, *J. Am. Chem. Soc.* **1999**, *121*, 1524 – 1527; e) M. C. Hansen, S. L. Buchwald, *Org. Lett.* **2000**, *2*, 713 – 715.

[7] For some recent publication see: a) R. Sablong, J. A. Osborn, *Tetrahedron Lett.* **1996**, *37*, 4937 – 4940; b) S. Kainz, A. Brinkmann, W. Leitner, A. Pfaltz, *J. Am. Chem. Soc.* **1999**, *121*, 6421 – 6429; c) D. Xiao, X. Zhang, *Angew. Chem.* **2001**, *113*, 3533 – 3536; *Angew. Chem. Int. Ed.* **2001**, *40*, 3425 – 3428; d) F. Menges, A. Pfaltz, *Adv. Synth. Catal.* **2002**, *344*, 40 – 44; e) X.-B. Jiang, A. J. Minnaard, B. Hessen, B. L. Feringa, A. L. L. Duchateau, J. G. O. Andrien, J. A. F. Boogers, J. G. de Vries, *Org. Lett.* **2003**, *5*, 1503 – 1506; f) A. Trifonova, J. S. Diesen, C. J. Chapman, P. G. Andersson, *Org. Lett.* **2004**, *6*, 3825 – 3827; g) C. Moessner, C. Bolm, *Angew. Chem.* **2005**, *117*, 7736 – 7739; *Angew. Chem. Int. Ed.* **2005**, *44*, 7564 – 7567.

[8] C. G. McCarty in *Chemistry of the Carbon-Nitrogen Double Bond* (Ed.: S. Patai), Wiley-Interscience, London, **1970**, pp. 363 – 364.

[9] A. B. Charette , A. Giroux, *Tetrahedron Lett.* **1996**, *37*, 6669 – 6672.

[10] Palladium Reagents: a) R. F. Heck, *Organic Synthesis*, Academic Press, New York, **1985**; b) E. Negishi, *Handbook of Organopalladium Chemistry for Organic Synthesis*, Wiley, Hoboken, **2002**; c) *J. Organomet. Chem.* **2003**, *687*, 209 – 590 (special issue "Palladium Chemistry in 2003: Recent Developments"); d) J. Tsuji, *Palladium Reagents and Catalysis*, Wiley, Chichester, **2004**; e) L. F. Tietze, H. Ila, H. P. Bell, *Chem. Rev.* **2004**, *104*, 3453 – 3516.

[11] a) H. Abe, H. Amii, K. Uneyama, *Org. Lett.* **2001**, *3*, 313 – 315; b) A. Suzuki, M. Mae, H. Amii, K. Uneyama, *J. Org. Chem.* **2004**, *69*, 5132 – 5134.

[12] a) R. Raja, J. M. Thomas, M. D. Jones, B. F. G. Johnson, D. E. W. Vaughan, *J. Am. Chem. Soc.* **2003**, *125*, 14982 – 14983; b) P. Nanayakkara, H. Alper, *Chem. Commun.* **2003**, *18*, 2384 – 2385.

[13] Y.-Q. Wang, S.-M. Lu, Y.-G. Zhou, *Org. Lett.* **2005**, *7*, 3235 – 3238.

[14] a) W. Tang, X. Zhang, *Chem. Rev.* **2003**, *103*, 3029 – 3070, and references therein; b) W. Tang, X. Zhang, *Angew. Chem.* **2002**, *114*, 1682 – 1684; *Angew. Chem. Int. Ed.* **2002**, *41*, 1612 – 1614.

[15] J. L. G. Ruano, J. Alemán, M. B. Cid, A. Parra, *Org. Lett.* **2005**, *7*, 179 – 182.

[16] a) H. Yamada, T. Kawate, A. Nishida, M. Nakagawa, *J. Org. Chem.* **1999**, *64*, 8821 – 8828; b) T. Soeta, K. Nagai, H. Fujihara, M. Kuriyama, K. Tomioka, *J. Org. Chem.* **2003**, *68*, 9723 – 9727.

[17] a) W. Oppolzer, M. Wills, C. Starkemann, G. Bernardinelli, *Tetrahedron Lett.* **1990**, *31*, 4117 – 4120; b) W. Oppolzer, M. Wills, M. J. Kelly, M. Signer, J. Blagg, *Tetrahedron Lett.* **1990**, *31*, 5015 – 5018; c) W. Oppolzer, I. Rodriguez, C. Starkemann, E. Walther, *Tetrahedron Lett.* **1990**, *31*, 5019 – 5022.

[18] S. Ji, L. B. Gortle, A. Waring, A. Battisti, S. Bank, W. D. Closson, P. Wriede, *J. Am. Chem. Soc.* **1967**, *89*, 5311 – 5312.

 © 2006 Wiley-VCH Verlag GmbH & Co. KGaA, Weinheim

Thermoelectric Materials

DOI: 10.1002/anie.200600865

High Thermoelectric Figure of Merit and Nanostructuring in Bulk p-type $Na_{1-x}Pb_mSb_yTe_{m+2}$**

*Pierre F. P. Poudeu, Jonathan D'Angelo, Adam D. Downey, Jarrod L. Short, Timothy P. Hogan, and Mercouri G. Kanatzidis**

Thermoelectric materials are special types of semiconductors that function as "heat pumps" and as heat-to-electricity converters. Thermoelectric power generation allows for small size, high reliability, and quiet operation. Efficient thermoelectric-based heat-to-electricity converters require higher performance materials than are currently available.[1,2] Direct conversion of heat to electricity could be achieved with solid-state devices based on thermoelectric materials. These devices could play an important role in future energy production, conversion, management, and utilization. When a temperature gradient is created across a thermoelectric

[*] Dr. P. F. P. Poudeu, Prof. M. G. Kanatzidis
Department of Chemistry
Michigan State University
East Lansing, MI 48824 (USA)
Fax: (+1) 517-353-1793
E-mail: kanatzid@cem.msu.edu

J. D'Angelo, A. D. Downey, J. L. Short, Prof. T. P. Hogan
Department of Electrical and Computer Engineering
Michigan State University
East Lansing, MI 48824 (USA)

[**] Financial support from the Office of Naval Research (MURI program) is gratefully acknowledged.

Supporting information for this article is available on the WWW under http://www.angewandte.org or from the author.

© 2006 Wiley-VCH Verlag GmbH & Co. KGaA, Weinheim

module, a voltage is generated, owing to the Seebeck effect. This voltage can be used to drive an external load.[3] Currently, there is a strong scientific and technological drive to identify new materials with enhanced thermoelectric figures of merit $ZT=(\sigma S^2/\kappa)T$ (where σ is the electrical conductivity, S the thermopower or Seebeck coefficient, κ the thermal conductivity, and T the temperature). The numerator σS^2 is called the power factor PF. Several classes of materials are currently under investigation, including complex chalcogenides,[4] doped PbTe and its solid solutions, such as $Pb_{1-x}Sn_xTe$,[5,6] superlattice thin films,[7,8] and quantum-dot superlattices.[9–11] Also of interest are skutterudites,[12,13] metal oxides,[14] and intermetallic clathrates.[15–17] The superlattice thin-film structures of Bi_2Te_3/Sb_2Te_3 grown from chemical vapor deposition,[18] and of $PbSe_{0.98}Te_{0.02}$/PbTe formed by molecular beam epitaxy (MBE)[11,19,20] have figures of merit greater than $ZT=2$ (at approximately 300 and 550 K, respectively). The MBE-grown thin films $PbSe_{0.98}Te_{0.02}$/PbTe are n-type materials and contain pyramid-shaped "nanodots" of PbSe of uniform size (approximately 20 nm), which form spontaneously inside a matrix of PbTe.[11,19,20] Because energy-conversion applications require materials in large quantities, we seek bulk analogues of these systems with similar figures of merit.

A recent contribution to these efforts was the discovery of the n-type Ag-based tellurides $AgSbTe_2$/PbTe, which can exhibit high figures of merit ($ZT\approx1.7$ at 700 K) when properly doped.[21,22] To construct a fully functioning optimal thermoelectric device, both n- and p-type materials are needed. To date, there is no p-type counterpart to $AgSbTe_2$/PbTe with similar performance. The highest figure of merit reported for p-type bulk materials ($ZT\approx1.2$ at 700 K) is exhibited by the so-called TAGS system (based on Te, Ag, Ge, and Sb: $(GeTe)_{1-x}((Ag_2Te)_{1-y}(Sb_2Te_3)_y)_x$).[23] These Ge-containing materials, though more efficient than PbTe, have found limited use, owing to their high cost and to a low-temperature phase transition. Recently, we described the p-type materials $Ag(Pb_{1-y}Sn_y)_mSbTe_{2+m}$, which show outstanding thermoelectric properties, reaching a maximum figure of merit of $ZT\approx1.45$ at 630 K.[24]

Herein, we report that the Ag-free system $Na_{1-x}Pb_mSb_yTe_{m+2}$, with appropriate combinations of m, y, and x, achieves record-high ZT values for a p-type bulk thermoelectric material. The effect of the composition on the thermoelectric properties is profound. We show that the high performance of these materials derives mainly from a low thermal conductivity. High-resolution transmission electron microscopy (HRTEM) demonstrates pervasive nanostructuring in $Na_{1-x}Pb_mSb_yTe_{m+2}$, which may be the root cause for the remarkably low thermal conductivity.[25] The $Na_{1-x}Pb_mSb_yTe_{m+2}$ system was selected for study because it should be naturally prone to create Na,Sb-rich clusters in the lattice. The distribution of Na^+ and Sb^{3+} ions in the Pb^{2+} sublattice cannot be random, as would be demanded by a solid solution, because Coulombic forces alone tend to drive the system to clustering at the nanoscale, thereby lowering the overall energy.[26] The results described herein are in agreement with long-standing theoretical predictions that nanostructuring in semiconductors would lead to enhanced thermoelectric figures of merit.[25,27] The $Na_{1-x}Pb_mSb_yTe_{m+2}$ materials could find applications in devices for power generation from a wide variety of hot sources, for example, vehicle exhausts, coal-burning installations, or electric power utilities.

$Na_{1-x}Pb_mSb_yTe_{m+2}$ ($y\le1$) samples (see Supporting Information for synthesis details[28]) exhibit p-type conduction from 300 to 700 K. Ingots with the composition $Na_{0.95}Pb_{19}SbTe_{21}$ ($m=19$, $x=0.05$, $y=1$) exhibit an electrical conductivity of $\sigma=1422\ S\,cm^{-1}$ with a positive thermopower of $S=105\ \mu V\,K^{-1}$ at room temperature. This leads to the relatively high power factor of $PF=15.6\ \mu W\,cm^{-1}\,K^{-2}$. The temperature dependence of the electrical conductivity and the thermopower of $Na_{0.95}Pb_{19}SbTe_{21}$ are shown in Figure 1 A.

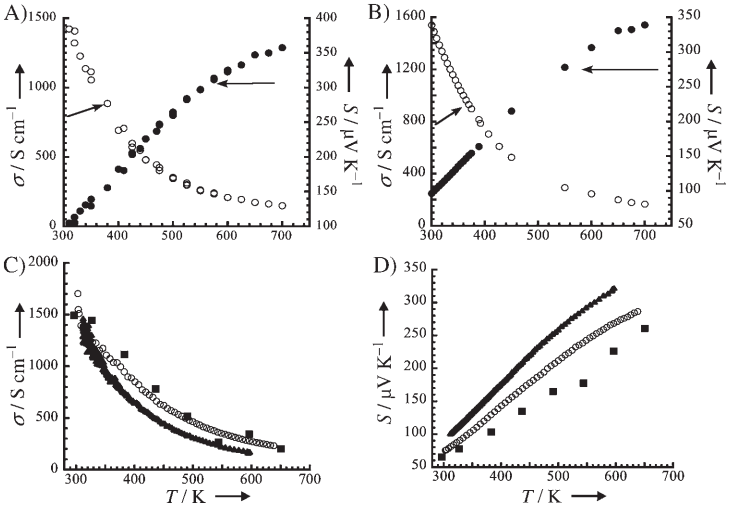

Figure 1. Temperature dependence of the electrical conductivity σ (○) and the Seebeck coefficient S (●) for A) $Na_{0.95}Pb_{19}SbTe_{21}$ and B) $Na_{0.95}Pb_{20}SbTe_{22}$. Temperature dependence of C) the electrical conductivity σ and D) the Seebeck coefficient S for $Na_{0.8}Pb_{20}Sb_yTe_{22}$ with $y=0.4$ (■), 0.6 (○), and 0.8 (▲). The conductivity and thermopower measurements were performed simultaneously on samples of typical size $7\times5\times4\ mm^3$. See Supporting Information for measurement details.[28]

The conductivity decreases with increasing temperature, which is consistent with degenerate semiconductors, and reaches $\sigma=150\ S\,cm^{-1}$ at 700 K. However, the thermopower increases rapidly to $S=357.6\ \mu V\,K^{-1}$ at 700 K, yielding a much higher power factor of $PF=19\ \mu W\,cm^{-1}\,K^{-2}$.

For samples of composition $Na_{0.95}Pb_{20}SbTe_{22}$ ($m=20$, $x=0.05$, $y=1$), an electrical conductivity of $\sigma=1541\ S\,cm^{-1}$ and a thermopower of $S=96\ \mu V\,K^{-1}$ were measured, which result in a power factor of $PF=14.2\ \mu W\,cm^{-1}\,K^{-2}$ at 300 K. As observed for $Na_{0.95}Pb_{19}SbTe_{21}$, the electrical conductivity decreases rapidly with rising temperature (Figure 1 B). At 700 K, the conductivity is $\sigma=165\ S\,cm^{-1}$ and the thermopower is $S=339\ \mu V\,K^{-1}$, yielding a power factor of $PF=19\ \mu W\,cm^{-1}\,K^{-2}$. Therefore, the electrical performance (power factor) of $Na_{1-x}Pb_mSb_yTe_{m+2}$ samples remains almost

 © 2006 Wiley-VCH Verlag GmbH & Co. KGaA, Weinheim

unchanged upon small variation of m for a constant Na/Sb ratio.

To study the influence of the Na/Sb ratio on the properties of the materials, samples with compositions $Na_{0.8}Pb_{20}Sb_yTe_{22}$, ($m = 20$, $x = 0.2$, $y = 0.4$, 0.6, 0.8) were examined. As shown in Figure 1C, the electrical conductivity increases slightly with decreasing Sb content. The drop in conductivity with rising temperature is more pronounced as the Na/Sb ratio decreases. The room-temperature Seebeck coefficient of the $Na_{0.8}Pb_{20}Sb_yTe_{22}$ samples tends to increase with decreasing Na/Sb ratio (Figure 1D). As the temperature increases, a more substantial divergence is observed in the thermopower plots, which suggests higher performance at high temperatures with decreasing Na/Sb ratio. From Figure 2A, we can

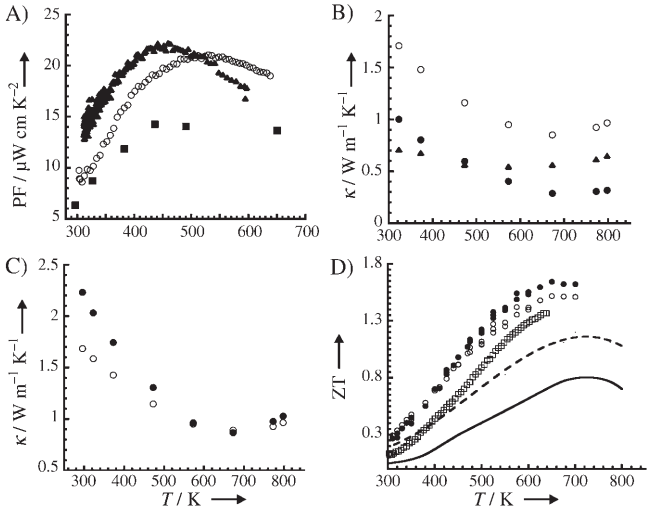

Figure 2. A) Temperature dependence of the power factor $PF = \sigma S^2$ for $Na_{0.8}Pb_{20}Sb_yTe_{22}$ with $y = 0.4$ (■), 0.6 (○), and 0.8 (▲). B) Temperature dependence of the thermal conductivity κ of $Na_{0.95}Pb_{20}SbTe_{22}$ (○), showing the lattice κ_{latt} (▲) and carrier κ_{el} (●) contributions. See text for details. C) Temperature dependence of the thermal conductivity κ of $Na_{0.95}Pb_{19}SbTe_{21}$ (○) and $Na_{0.8}Pb_{20}Sb_{0.6}Te_{22}$ (●). D) Temperature dependence of the thermoelectric figure of merit ZT for $Na_{0.95}Pb_{20}SbTe_{22}$ (●), $Na_{0.95}Pb_{19}SbTe_{21}$ (○), and $Na_{0.8}Pb_{20}Sb_{0.6}Te_{22}$ (□), compared to those of the state-of-the-art p-type materials PbTe (solid line) and TAGS (dashed line). See Supporting Information for measurement details.[28]

see that the power factor of the $Na_{0.8}Pb_{20}Sb_yTe_{22}$ materials at room temperature increases with decreasing Na/Sb ratio. The highest power factor of $PF = 22\ \mu W\,cm^{-1}\,K^{-2}$ is found for the sample with Na/Sb = 1 ($y = 0.8$) at 450 K. At 600 K, the sample with $y = 0.6$ showed a power factor of $PF = 19.5\ \mu W\,cm^{-1}\,K^{-2}$, which is the highest among the $Na_{1-x}Pb_mSb_yTe_{m+2}$ samples for this temperature.

The temperature dependence of the thermal conductivity of $Na_{0.95}Pb_{20}SbTe_{22}$, along with the lattice and carrier contributions to the thermal conductivity, are plotted in Figure 2B. At room temperature, the total thermal conductivity of the sample is $\kappa = 1.8\ W\,m^{-1}\,K^{-1}$, which is approximately 22% lower than the typical value of $\kappa = 2.3\ W\,m^{-1}\,K^{-1}$ reported for p-type PbTe.[29] The thermal conductivity decreases with increasing temperature, reaching a minimum of $\kappa = 0.85\ W\,m^{-1}\,K^{-1}$ at 675 K, and then increasing slightly from 675 to 800 K. The lattice thermal conductivity κ_{latt} was determined by subtracting the electronic contribution κ_{el} as calculated using the Wiedemann–Franz law ($\kappa_{el} = L\sigma T$, where $L \approx 2.45 \times 10^{-8}\ W\,\Omega\,K^{-2}$ is the Lorenz number) from the total thermal conductivity (that is, $\kappa_{latt} = \kappa - \kappa_{el}$). The value of $\kappa_{latt} = 0.74\ W\,m^{-1}\,K^{-1}$ at 300 K is only one third of that of PbTe ($\kappa_{latt} = 2.2\ W\,m^{-1}\,K^{-1}$).[6] Below 500 K, the thermal conductivity is mostly due to the electronic contribution, whereas above 500 K, the lattice contribution dominates. The $Na_{0.95}Pb_{19}SbTe_{21}$ and $Na_{0.80}Pb_{20}Sb_{0.6}Te_{22}$ samples also show low thermal conductivities with a temperature dependence similar to that of $Na_{0.95}Pb_{20}SbTe_{22}$ (Figure 2C). For both samples, the thermal conductivity drops very rapidly with rising temperature and reaches a minimum value of $\kappa = 0.85\ W\,m^{-1}\,K^{-1}$ near 700 K. The lattice contribution reaches a minimum of $\kappa_{latt} = 0.55\ W\,m^{-1}\,K^{-1}$, which approaches the values reported for the superlattice thin films of $PbSe_{0.98}Te_{0.02}$/PbTe ($\kappa_{latt} \approx 0.35\ W\,m^{-1}\,K^{-1}$).[11,20]

In Figure 2D, the figures of merit for the $Na_{1-x}Pb_mSb_yTe_{m+2}$ samples calculated from the above data are compared to those of the state-of-the-art p-type TAGS and PbTe-based materials. $Na_{0.95}Pb_{20}SbTe_{22}$ outperforms both systems at their individual temperatures of maximum ZT (near 700 K). At 300 K, the figure of merit of $Na_{0.95}Pb_{20}SbTe_{22}$ ($ZT \approx 0.25$) is already four times larger than that of doped p-type PbTe and 1.3 times larger than that of TAGS. More interestingly, the figure of merit of $Na_{0.95}Pb_{20}SbTe_{22}$ rises dramatically with temperature, reaches $ZT = 1$ near 475 K, and then reaches $ZT \approx 1.7$ at 650 K. The figure of merit is above $ZT = 1$ over a temperature range of approximately 300 K. This is one of the widest temperature ranges of high thermoelectric efficiency reported for a single material. Likewise, the figures of merit of $Na_{0.95}Pb_{19}SbTe_{22}$ and $Na_{0.8}Pb_{20}Sb_{0.6}Te_{22}$ reach their highest values of $ZT \approx 1.5$ and 1.4 at 650 and 640 K, respectively.

Why do the $Na_{1-x}Pb_mSb_yTe_{m+2}$ materials exhibit such good thermoelectric properties? The key characteristic is their exceptionally low thermal conductivity. The thermal conductivity of a material is typically reduced by large mass-fluctuation disorder in one atomic position of its crystal structure (random-alloy disorder, point defects, and grain boundaries). However, the large drop observed here may suggest the existence of additional mechanisms. Recently, it has been suggested that nanostructuring in bulk samples could produce strong phonon scattering.[25] While the conventional disorder condition is very likely present in our samples, the presence of nanostructuring can only be probed through a detailed examination of the structure at the atomic scale. Thus, we performed HRTEM on numerous pieces of various $Na_{1-x}Pb_mSb_yTe_{m+2}$ ingots.

HRTEM images of $Na_{0.95}Pb_{20}SbTe_{22}$ samples, for example, revealed frequent nanoscale features thought to be favorable for phonon scattering. In Figure 3A, two distinct domains with notably different atomic spacings, which have cocrystallized at the nanoscale, can be seen. The corresponding fast Fourier transforms (FFTs) of the two domains in the HRTEM image reveal a doubling of the periodicity in one direction for domain (a) with respect to the cubic spacing of domain (b),

 © 2006 Wiley-VCH Verlag GmbH & Co. KGaA, Weinheim

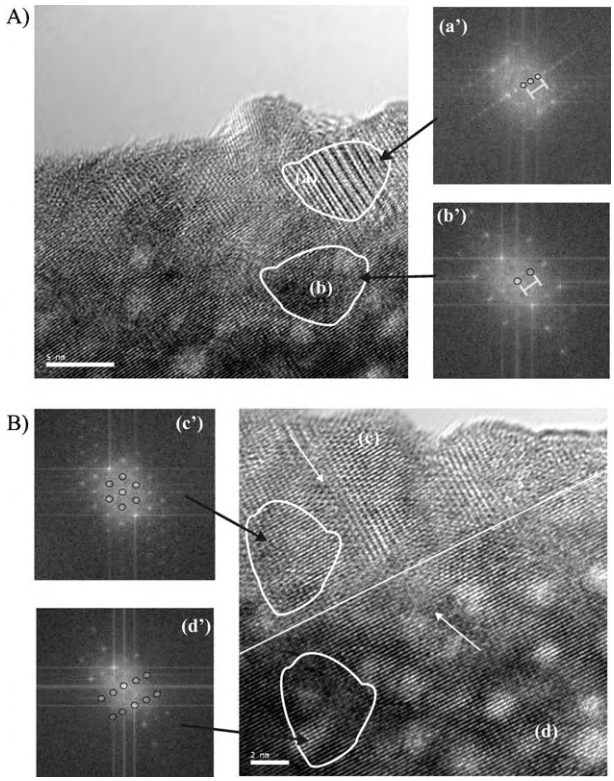

Figure 3. A) HRTEM image (left; scale bar: 5 nm) of a selected part of a $Na_{0.95}Pb_{20}SbTe_{22}$ sample, showing the coexistence of domains (a) and (b) with different features. The corresponding FFTs (a′) and (b′) (right) indicate that in one direction the periodicity of domain (a) is doubled compared to that of domain (b) (spacing indicated). B) HRTEM image (right; scale bar: 2 nm) of a selected part of a $Na_{0.95}Pb_{20}SbTe_{22}$ sample, consisting of two areas (c) and (d). The corresponding FFTs (c′) and (d′) (left) reveal that area (c) has a [111] orientation and area (d) a [011] orientation. The white arrows in the HRTEM image indicate crystal boundaries between domains of similar orientation. The white line across the HRTEM image, which divides the two areas, is drawn over one atomic row and traverses domains of type (c) and (d), without a shift in atomic row. See Supporting Information for measurement details.[28]

which surrounds domain (a). The nanocrystal domains of type (a) have compositions rich in Na and Sb. Figure 3B shows another area of nanoscale inhomogeneity elsewhere in the sample, in which two areas (c) and (d) have different orientations, [111] and [011], as revealed by the corresponding FFTs. The arrows indicate crystal boundaries between domains of similar orientation. Both domains are coherently grown; this feature is called endotaxy and is important in preserving facile charge transport through the sample, owing to reduced scattering.[2,22] This growth process creates interfaces between Na,Sb-rich, and Pb-rich regions. The Pb-rich regions are indicated by the slightly larger lattice spacing evident in the images (PbTe (NaCl type, $Fm\bar{3}m$) has a larger lattice spacing than $NaSbTe_2$).

The abundance of nano-interfaces is also apparent in the larger-area view shown in Figure 4, in which the degree of dispersity of the nanocrystals can be better assessed. The nanostructuring of $Na_{0.95}Pb_{20}SbTe_{22}$ is a key feature, whose impact on the properties of the material needs to be further

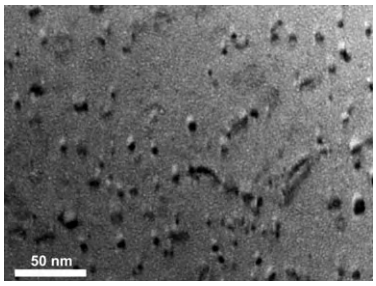

Figure 4. A low magnification TEM image of a $Na_{0.95}Pb_{20}SbTe_{22}$ sample, showing the evenly dispersed nanoscale features.

understood. To unequivocally support our view that this nanostructuring is largely responsible for the large drop observed in the lattice thermal conductivity in this system, we need the solid-solution version of these materials. The stabilization of real solid solutions of $Na_{1-x}Pb_mSb_yTe_{m+2}$, however, was not possible in our hands. Instead, we can compare the lattice thermal conductivity of $Na_{0.95}Pb_{20}SbTe_{22}$ with those of the well-known solid solutions of $PbTe_{1-x}Se_x$ and $Pb_{1-x}Sn_xTe$ for $x = 0.1$.[30,31] This x value represents the same degree of alloying of foreign atoms in the PbTe lattice for all three systems. Given the similar masses of the Sb, Se, and Sn atoms, we can expect that a true solid solution of composition $NaPb_{20}SbTe_{22}$ (that is, $(NaSbTe_2)(PbTe)_{20}$) for the same alloy fraction would produce a similar phonon scattering to those of $PbTe_{0.9}Se_{0.1}$ and $Pb_{0.9}Sn_{0.1}Te$. This hypothesis is, in fact, supported by the very similar lattice thermal conductivities of $\kappa_{latt} = 1.35$ and $1.44\ W m^{-1} K^{-1}$ for $PbTe_{0.9}Se_{0.1}$ and $Pb_{0.9}Sn_{0.1}Te$, respectively (Figure 5). Therefore, we expect a true solid solution of composition $NaPb_{20}SbTe_{22}$ to have

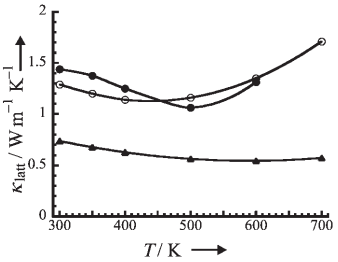

Figure 5. Comparison of the lattice thermal conductivity κ of $PbTe_{0.9}Se_{0.1}$ (○), $Pb_{0.9}Sn_{0.1}Te$ (●), and $Na_{0.95}Pb_{20}SbTe_{22}$ (▲). Data for $PbTe_{0.9}Se_{0.1}$ and $Pb_{0.9}Sn_{0.1}Te$ adapted from the literature.[30,31]

a comparable lattice thermal conductivity ($\kappa_{latt} \approx 1.4\ W m^{-1} K^{-1}$), but in contrast, we observe only half this value for $Na_{0.95}Pb_{20}SbTe_{22}$ (Figure 5). Thus, we can provide no other explanation for the reduced thermal conductivity of the $Na_{1-x}Pb_mSb_yTe_{m+2}$ materials, but to assign a significant role to the nanostructuring present in the samples.

Received: March 6, 2006
Published online: April 28, 2006

Keywords: lead · nanostructures · semiconductors · tellurides · thermoelectric materials

 © 2006 Wiley-VCH Verlag GmbH & Co. KGaA, Weinheim

[1] *Thermoelectric Materials 2003–Research and Applications* (Eds.: G. S. Nolas, J. Yang, T. P. Hogan, D. C. Johnson), MRS Proceedings **2004**, *793*, references therein.
[2] G. Chen, M. S. Dresselhaus, G. Dresselhaus, J.-P. Fleurial, T. Caillat, *Int. Mater. Rev.* **2003**, *48*, 45 – 66.
[3] C. Wood, *Rep. Prog. Phys.* **1988**, *51*, 459 – 539.
[4] M. G. Kanatzidis, *Semicond. Semimetals* **2000**, *69*, 51 – 100.
[5] Z. M. Dashevsky, P. Dariel, S. Shusterman, *Semicond. Phys. Quantum Electron. Optoelectron.* **2000**, *3*, 181 – 184.
[6] M. Orihashi, Y. Noda, L.-D. Chen, T. Goto, T. Hirai, *J. Phys. Chem. Solids* **2000**, *61*, 919 – 923.
[7] R. Venkatasubramanian, T. Colpitts, E. Watko, M. Lamvik, N. El-Masry, *J. Cryst. Growth* **1997**, *170*, 817 – 821.
[8] T. C. Harman, D. L. Spears, M. J. Manfra, *J. Electron. Mater.* **1996**, *25*, 1121 – 1127.
[9] T. C. Harman, D. L. Spears, M. P. Walsh, *J. Electron. Mater.* **1999**, *28*, L1 – L4.
[10] T. C. Harman, P. J. Taylor, D. L. Spears, M. P. Walsh, *18th International Conference on Thermoelectrics* **1999**, 280 – 284.
[11] T. C. Harman, P. J. Taylor, M. P. Walsh, B. E. LaForge, *Science* **2002**, *297*, 2229 – 2232.
[12] C. Uher, *Semicond. Semimetals* **2000**, *69*, 139 – 253.
[13] B. C. Sales, D. Mandrus, R. K. Williams, *Science* **1996**, *272*, 1325 – 1328.
[14] I. Terasaki, Y. Ishii, D. Tanaka, K. Takahata, Y. Iguchi, *Jpn. J. Appl. Phys. Part 2* **2001**, *40*, L65 – L67.
[15] B. C. Sales, B. C. Chakoumakos, J. W. Sharp, D. Mandrus, *J. Solid State Chem.* **1999**, *146*, 528 – 532.
[16] G. S. Nolas, G. A. Slack, S. B. Schujman, *Semicond. Semimetals* **2001**, *69*, 255 – 300.
[17] S. Latturner, X. Bu, N. Blake, H. Metiu, G. Stucky, *J. Solid State Chem.* **2000**, *151*, 61 – 64.
[18] R. Venkatasubramanian, E. Siivola, T. Colpitts, B. O'Quinn, *Nature* **2001**, *413*, 597 – 602.
[19] H. Beyer, J. Nurnus, H. Bötner, A. Lambrecht, T. Roch, G. Bauer, *Appl. Phys. Lett.* **2002**, *80*, 1216 – 1218.
[20] J. C. Caylor, K. Coonley, J. Stuart, T. Colpitts, R. Venkatasubramanian, *Appl. Phys. Lett.* **2005**, *87*, 023105.
[21] K. F. Hsu, S. Loo, F. Guo, W. Chen, J. S. Dyck, C. Uher, T. Hogan, E. K. Polychroniadis, M. G. Kanatzidis, *Science* **2004**, *303*, 818 – 821.
[22] E. Quarez, K.-F. Hsu, R. Pcionek, N. Frangis, E. K. Polychroniadis, M. G. Kanatzidis, *J. Am. Chem. Soc.* **2005**, *127*, 9177 – 9190.
[23] E. Skrabeck, D. S. Trimmer, *CRC Handbook of Thermoelectrics* (Ed.: D. M. Rowe), CRC, Boca Raton, **1995**, p. 267.
[24] J. Androulakis, K. F. Hsu, R. Pcionek, H.-J. Kong, C. Uher, J. J. D'Angelo, A. Downey, T. Hogan, M. G. Kanatzidis, *Adv. Mater.* **2006**, in press.
[25] A. Khitun, K. L. Wang, G. Chen, *Nanotechnology* **2000**, *11*, 327 – 331.
[26] K. Hoang, K. Desai, S. D. Mahanti, *Phys. Rev. B* **2005**, *72*, 064102.
[27] D. Hicks, M. S. Dresselhaus, *Phys. Rev. B* **1993**, *47*, 12727 – 12731.
[28] Supporting Information available: synthesis procedures, measurement details, thermal-diffusivity, density, and specific-heat data, TEM sample-preparation procedure.
[29] A. F. Ioffe, *Semiconductor Thermoelements and Thermoelectric Cooling*, Infoserach, London, **1957**.
[30] E. D. Devyatkova, V. V. Tikhonov, *Sov. Phys.-Solid State* **1965**, *7*, 1427 – 1431.
[31] M. Orihashi, Y. Noda, L.-D. Chen, T. Hirai, *Mater. Trans. JIM* **2000**, *41*, 1196 – 1201.

 © 2006 Wiley-VCH Verlag GmbH & Co. KGaA, Weinheim

Asymmetric Synthesis

DOI: 10.1002/anie.200600470

Construction of Enantiomerically Enriched Tertiary α-Hydroxycarboxylic Acid Derivatives by Phase-Transfer-Catalyzed Asymmetric Alkylation of Diaryloxazolidin-2,4-diones**

*Takashi Ooi, Kazuhiro Fukumoto, and Keiji Maruoka**

The direct alkylation of enolates is an important method for the formation of carbon–carbon bonds in synthetic organic chemistry. The concept of diastereoselective alkylation by using chiral auxiliaries has played a dominant role over the past three decades for rigorously controling the stereochemistry. The establishment of systems useful for a broad range of substrates has resulted in chiral auxillaries attaining a preeminent position in the field.[1] On the other hand, complementary catalytic variants have been much less developed despite their practical and fundamental importance.[2] In contrast to the recent emergence of highly efficient transition-metal-catalyzed processes for asymmetric allylations,[2,3] arylations,[2] and vinylations[4] of enolates, reliable protocols for catalytic enantioselective alkylation involving sp^3-hybridized electrophiles, such as alkyl halides, are still restricted.[2,5,6] Although chiral phase-transfer catalysis has made a significant contribution to this area,[2,6] the major drawback of this strategy is that it is only effective for a limited pool of substrates. In particular it has limited applicability in accessing enantioenriched carbonyl compounds of high value which possess quaternary α-carbon stereocenters.[7] Our approach toward this largely unsolved problem utilizes 3,5-diaryloxazolidin-2,4-diones **2** as novel oxygen-containing substrates that undergo highly enantioselective alkylation under mild phase-transfer conditions in the presence of the N-spiro chiral quaternary ammonium bromide **1e** as catalyst (Scheme 1).[8] This substrate–catalyst combination provides a new and practical entry to a wide range of tertiary α-hydroxy-α-aryl carboxylic acid derivatives.[9,10]

The requisite 3,5-diaryloxazolidin-2,4-diones **2** can be readily prepared from racemic α-hydroxy esters by sequential treatment with 1,1′-carbonyldiimidazole (CDI) and an appro-

[*] Dr. T. Ooi, K. Fukumoto, Prof. K. Maruoka
Department of Chemistry
Graduate School of Science
Kyoto University
Sakyo, Kyoto, 606-8502 (Japan)
Fax: (+81) 75-753-4041
E-mail: maruoka@kuchem.kyoto-u.ac.jp

[**] This work was partially supported by the Mitsubishi Chemical Corporation Fund and a Grant-in-Aid for Scientific Research on Priority Areas "Advanced Molecular Transformation of Carbon Resources" from the Ministry of Education, Culture, Sports, Science, and Technology, Japan.

Supporting information for this article is available on the WWW under http://www.angewandte.org or from the author.

 © 2006 Wiley-VCH Verlag GmbH & Co. KGaA, Weinheim

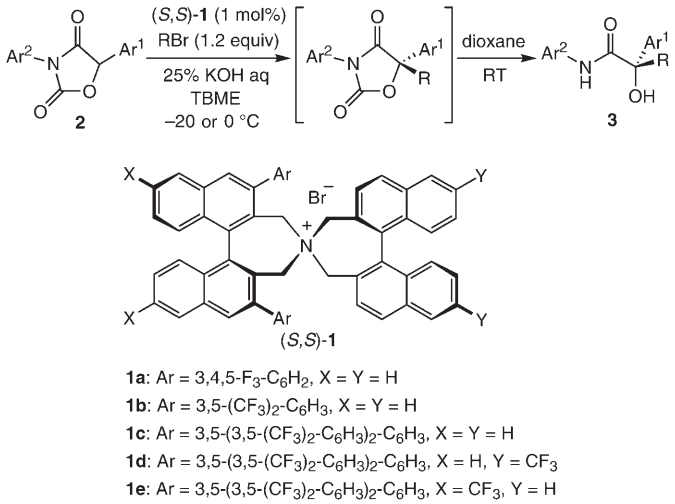

Scheme 1. Enantioselective alkylation of 3,5-diaryloxazolidin-2,4-diones **2** by phase-transfer catalysis of (*S*,*S*)-**1** to afford optically active tertiary α-hydroxy amides **3**.

priate aromatic amine (Ar^2NH_2) in CH_2Cl_2.[11] The feasibility of the stereoselective alkylation of **2** was examined under typical liquid–liquid phase-transfer conditions with 3,5-diphenyloxazolidin-2,4-dione (**2a**, $Ar^2 = Ph$) as a representative substrate and chiral quaternary ammonium bromide (*S*,*S*)-**1a**[12a,b] as the catalyst. The reaction of **2a** ($Ar^2 = Ph$) with benzyl bromide (1.2 equiv) in the presence of **1a** (1 mol%) in toluene/50% aqueous solution of KOH was found to proceed at 0°C, and TLC analysis confirmed the consumption of all the substrate **2a** after 18 h. Subsequent addition of dioxane and continuous stirring of the reaction mixture at room temperature for 1 h facilitated the one-pot partial hydrolysis to directly afford the corresponding tertiary α-hydroxy amide **3a** ($Ar^2 = Ph$) in 79% yield, albeit with low enantiomeric excess (19% *ee*; Table 1, entry 1). Switching the 3,3′-aromatic substituent (Ar) to a 3,5-bis(trifluoromethyl)phenyl group (**1b**)[12c] resulted in a diminished yield with a similar degree of enantioselectivity (entry 2). To our surprise, however, a dramatic improvement in the selectivity was attained in the reaction with **1c** (which has radially disposed 3,5-bis[3,5-bis(trifluoromethyl)phenyl]phenyl moieties) as a catalyst,[12d,e] and furnished **3a** ($Ar^2 = Ph$) in 85% yield and with 91% *ee* (entry 3).

We then focused on modifying the catalyst further by introducing an electron-withdrawing trifluoromethyl group at the 6,6′-positions of each binaphthyl subunit. Evaluation of the performance of the new chiral ammonium bromides **1d** and **1e** revealed the superiority of **1e** (entries 4 and 5); the phase-transfer-catalyzed benzylation of **2a** ($Ar^2 = Ph$) in the presence of **1e** gave the desired **3a** ($Ar^2 = Ph$) with 96% *ee*. Although the electronic nature of the aryl group (Ar^2) on the nitrogen atom of **2a** subtly affected the enantioselectivity and reaction efficiency (entries 6 and 7), we observed a beneficial effect of using ethereal solvents such as cyclopentyl methyl ether (CPME) and *tert*-butyl methyl ether (TBME). Substantial rate acceleration and virtually complete stereochemical control were achieved by using TBME (entries 8 and 9). It should be noted that the decreased chemical yield stems from hydrolysis prior to the alkylation because of the increased polarity of the solvent, which was overcome by reducing the concentration of the base to an aqueous solution of 25% KOH (entry 10).

With optimized conditions in hand, the scope of this new asymmetric enolate alkylation protocol was thoroughly investigated, and the representative results are summarized in Table 2.[13] In general, 1 mol% of **1e** with 1.2 equivalents of alkyl halide was sufficient for smooth alkylation, and in some cases the reaction was performed at lower temperature to enable the catalyst to achieve its full stereocontrol. A series of benzylic bromides of different steric and electronic properties were tolerated, thus allowing the preparation of structurally diverse, enantioenriched α-alkyl mandelic acid derivatives (entries 1–5). Construction of stereogenic quaternary carbon centers bearing allylic and propargylic substituents on **2** can also be achieved in a similar manner (entries 6–8). Both

Table 1: Optimization of the phase-transfer-catalyzed asymmetric benzylation of **2a** using (*S*,*S*)-**1** as the catalyst.[a]

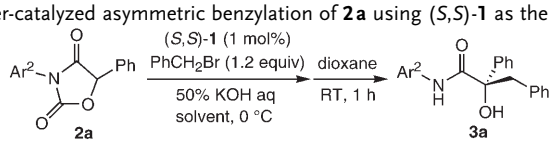

Entry	Catalyst	**2a** (Ar^2)	Solvent	*t* [h]	Yield[b] [%]	*ee*[c] [%]
1	**1a**	Ph	PhMe	18	79	19
2	**1b**	Ph	PhMe	20	65	19
3	**1c**	Ph	PhMe	19	85	91
4	**1d**	Ph	PhMe	20	83	92
5	**1e**	Ph	PhMe	19	87	96
6	**1e**	*p*-F-C_6H_4	PhMe	18	84	87
7	**1e**	*p*-MeO-C_6H_4	PhMe	17	81	94
8	**1e**	Ph	CPME	3	69	92
9	**1e**	Ph	TBME	5	75	99
10[d]	**1e**	Ph	TBME	7	82	99

[a] Unless otherwise specified, the reaction was carried out with 1.2 equiv of benzyl bromide in the presence of (*S*,*S*)-**1** (1 mol%) in a mixture of organic solvent and a 50% aqueous solution of KOH at 0°C for the given reaction time, after which dioxane was added and stirring was continued at room temperature for 1 h. [b] Yield of isolated product. [c] The enantiopurity of α-hydroxy amide **3a** was determined by HPLC analysis on a chiral stationary phase (DAICEL Chiralpak AS-H) with hexane/2-propanol as the solvent. The absolute configuration was deduced from that of **3g**. [d] Aqueous 25% KOH solution was used as a base.

 © 2006 Wiley-VCH Verlag GmbH & Co. KGaA, Weinheim

Table 2: Catalytic asymmetric alkylation of 3-phenyl-5-aryloxazolidin-2,4-dione (**2**) under phase-transfer conditions.[a]

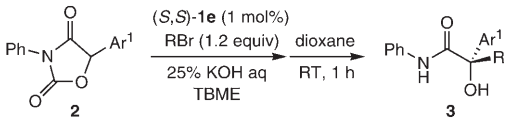

Entry	**2** (Ar^1)	RBr	T [°C]	t [h]	Yield[b] [%]	*ee*[c,d] [%]	Product
		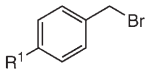					
1	Ph (**2a**)	R^1 = Me	0	9	83	94	**3b**
2	Ph (**2a**)	R^1 = F	−20	23	81	97	**3c**
3	Ph (**2a**)	R^1 = Ph	0	8	80	94	**3d**
4	Ph (**2a**)	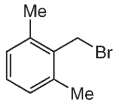	0	10	76	94	**3e**
5	Ph (**2a**)	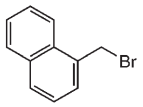	−20	22	80	96	**3f**
6	Ph (**2a**)	$CH_2{=}CHCH_2Br$	0	7	83	95	**3g**
7	Ph (**2a**)	$CH_2{=}C(Me)CH_2Br$	−20	24	80	97	**3h**
8	Ph (**2a**)	$CH{\equiv}CCH_2Br$	0	9	81	86	**3i**
9	*p*-F-C_6H_4	$PhCH_2Br$	0	6	76	90	**3j**
10	*p*-MeO-C_6H_4	$PhCH_2Br$	−20	23	87	90	**3k**
11	2-furyl	$PhCH_2Br$	0	7	81	94	**3l**
12	2-thienyl	$PhCH_2Br$	−20	24	81	99	**3m**

[a] The reaction was carried out with 1.2 equiv of alkyl halide and 1 mol% of **1e** in a mixture of TBME and an aqueous 25% KOH solution under the given reaction conditions. [b] Yield of isolated product. [c] The enantiomeric excess of **3** was determined by HPLC analysis on a chiral stationary phase. [d] The absolute configuration of **3g** was assigned to be *S* by comparison of the optical rotation with the reported value after amide hydrolysis[13] (see Scheme 2).

electron-withdrawing and electron-donating substituents on **2** were also tolerated (entries 9 and 10). Moreover, the catalytic asymmetric quaternization of **2** possessing a heteroaromatic group as Ar^1 was feasible, and excellent enantioselectivity was observed (entries 11 and 12).

The tertiary α-hydroxy amide **3** thus obtained can be cleanly converted into the corresponding α-hydroxycarboxylic acid by simple treatment with KOH in ethylene glycol at 150 °C as shown in Scheme 2, and no loss in the enantiomeric excess of **4** was confirmed by HPLC analysis after further derivatization to its methyl ester **5**. The absolute configuration of **4** was assigned to be *S* by comparison of the optical rotation with the literature value.[14]

In conclusion, we have successfully introduced a new catalyst **1e** for realizing catalytic, highly enantioselective alkylation of substrates **2** under mild phase-transfer conditions. This system represents the first example of the catalytic asymmetric alkylation of glycolates that establishes stereogenic quaternary carbon centers, and offers direct access to various optically active tertiary α-hydroxy acids and their derivatives. These compounds are an important class of chiral building blocks, in particular for the preparation of complex biologically active substances.[15] Further investigations on expanding the scope of our approach in terms of both the nucleophiles and electrophiles are currently underway.

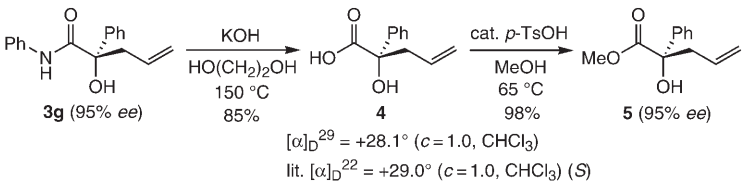

Scheme 2. Conversion of tertiary α-hydroxy amide **3g** into the corresponding α-hydroxy acid **4** and ester **5**.

Received: February 4, 2006
Published online: May 3, 2006

Keywords: alkylation · asymmetric synthesis · phase-transfer catalysis · synthetic methods

[1] For reviews, see: a) D. A. Evans in *Asymmetric Synthesis*, *Vol. 3* (Ed.: J. D. Morrison), Academic Press, New York, **1983**, chap. 1, p. 83; b) A. I. Meyers in *Asymmetric Synthesis*, *Vol. 3* (Ed.: J. D. Morrison), Academic Press, New York, **1983**, chap. 3, p. 213; see also: c) W. Oppolzer, R. Moretti, S. Thomi, *Tetrahedron Lett.* **1989**, *30*, 5603; d) A. G. Myers, B. H. Yang, H. Chen, L. McKinstry, D. J. Kopecky, J. L. Gleason, *J. Am. Chem. Soc.* **1997**, *119*, 6496; e) A. Job, C. F. Janeck, W. Bettray, R. Peters, D. Enders, *Tetrahedron* **2002**, *58*, 2253.

[2] For reviews, see: a) D. L. Hughes in *Comprehensive Asymmetric Catalysis*, *Vol. 3* (Eds.: E. N. Jacobsen, A. Pfaltz, H. Yamamoto), Springer, Berlin, **1999**, chap. 3, p. 1273; b) D. L. Hughes in *Comprehensive Asymmetric Catalysis, Supplement*, *Vol. 1* (Eds.: E. N. Jacobsen, A. Pfaltz, H. Yamamoto), Springer, Berlin, **2004**, p. 161.

[3] For a recent review, see: B. M. Trost, C. Lee in *Catalytic Asymmetric Syntheses*, 2nd ed. (Ed.: I. Ojima), Wiley-VCH, New York, **2000**, chap. 8E, p. 593; for recent notable achievements, see: a) D. C. Behenna, B. M. Stoltz, *J. Am. Chem. Soc.* **2004**, *126*, 15044; b) B. M. Trost, J. Xu, *J. Am. Chem. Soc.* **2005**, *127*, 2846.

[4] A. Chieffi, K. Kamikawa, J. Åhman, J. M. Fox, S. L. Buchwald, *Org. Lett.* **2001**, *3*, 1897.

[5] a) M. Imai, A. Hagihara, H. Kawasaki, K. Manabe, K. Koga, *J. Am. Chem. Soc.* **1994**, *116*, 8829; b) N. Vignola, B. List, *J. Am. Chem. Soc.* **2004**, *126*, 450; for recent significant advances, see: c) A. G. Doyle, E. N. Jacobsen, *J. Am. Chem. Soc.* **2005**, *127*, 62; d) D. A. Evans, R. J. Thomson, *J. Am. Chem. Soc.* **2005**, *127*, 10506.

[6] For recent representative reviews on asymmetric phase-transfer catalysis, see: a) T. Shioiri in *Handbook of Phase-Transfer Catalysis* (Eds.: Y. Sasson, R. Neumann), Blackie Academic & Professional, London, **1997**, chap. 14, p. 462; b) M. J. O'Donnell in *Catalytic Asymmetric Syntheses*, 2nd ed. (Ed.: I. Ojima), Wiley-VCH, New York, **2000**, chap. 10, p. 727; c) T. Shioiri, S. Arai, In *Stimulating Concepts*

 © 2006 Wiley-VCH Verlag GmbH & Co. KGaA, Weinheim

in Chemistry (Eds.: F. Vogtle, J. F. Stoddart, M. Shibasaki), Wiley-VCH, Weinheim, **2000**, p. 123; d) M. J. O'Donnell, *Aldrichimica Acta* **2001**, *34*, 3; e) K. Maruoka, T. Ooi, *Chem. Rev.* **2003**, *103*, 3013; f) M. J. O'Donnell, *Acc. Chem. Res.* **2004**, *37*, 506; g) B. Lygo, B. I. Andrews, *Acc. Chem. Res.* **2004**, *37*, 518.

[7] T. Ooi, K. Maruoka in *Quaternary Stereocenters-Challenges and Solutions for Organic Synthesis* (Eds.: J. Christoffers, A. Baro), Wiley-VCH, Weinheim, **2005**, chap. 10, p. 265; for recent excellent general reviews, see: a) C. J. Douglas, L. E. Overman, *Proc. Natl. Acad. Sci. USA* **2004**, *101*, 5363; b) J. Christoffers, A. Baro, *Adv. Synth. Catal.* **2005**, *347*, 1473.

[8] For a recent impressive study on phase-transfer-catalyzed asymmetric alkylation of α-alkoxyacetophenone derivatives, see: a) M. B. Andrus, E. J. Hicken, J. S. Stephens, *Org. Lett.* **2004**, *6*, 2289; b) M. B. Andrus, E. J. Hicken, J. S. Stephens, D. K. Bedke, *J. Org. Chem.* **2005**, *70*, 9470.

[9] For other powerful strategies for catalytic asymmetric synthesis of tertiary α-hydroxycarboxylic acid derivatives, see, for example: a) D. P. Curran, S.-B. Ko, *J. Org. Chem.* **1994**, *59*, 6139; b) Y. Hamashima, M. Kanai, M. Shibasaki, *J. Am. Chem. Soc.* **2000**, *122*, 7412; c) E. F. DiMauro, M. C. Kozlowski, *J. Am. Chem. Soc.* **2002**, *124*, 12669; d) K. Funabashi, M. Jachmann, M. Kanai, M. Shibasaki, *Angew. Chem.* **2003**, *115*, 5529; *Angew. Chem. Int. Ed.* **2003**, *42*, 5489; e) B. M. Trost, K. Dogra, M. Franzini, *J. Am. Chem. Soc.* **2004**, *126*, 1944.

[10] For leading contributions utilizing stoichiometric amounts of chiral sources, see: a) F. A. Davis, M. C. Weismiller, *J. Org. Chem.* **1990**, *55*, 3715; b) S. V. Pansare, R. G. Ravi, *Tetrahedron* **1998**, *54*, 14549; c) A. Loupy, D. A. Monteux, *Tetrahedron* **2002**, *58*, 1541, and references therein.

[11] For a recent report on the preparation and synthetic utility of N-substituted oxazolidin-2,4-diones, see: T. Kurz, K. Widyan, *Tetrahedron* **2005**, *61*, 7247.

[12] a) T. Ooi, M. Takeuchi, M. Kameda, K. Maruoka, *J. Am. Chem. Soc.* **2000**, *122*, 5228; b) T. Ooi, M. Kameda, K. Maruoka, *J. Am. Chem. Soc.* **2003**, *125*, 5139; c) T. Ooi, T. Miki, M. Taniguchi, M. Shiraishi, M. Takeuchi, K. Maruoka, *Angew. Chem.* **2003**, *115*, 3926; *Angew. Chem. Int. Ed.* **2003**, *42*, 3796; d) T. Ooi, M. Kameda, M. Taniguchi, K. Maruoka, *J. Am. Chem. Soc.* **2004**, *126*, 9685; e) T. Ooi, S. Fujioka, K. Maruoka, *J. Am. Chem. Soc.* **2004**, *126*, 11790.

[13] Unfortunately, the present system was not effective for less reactive electrophiles; for example, the attempted methylation of **2a** with methyl iodide (10 equiv) under otherwise similar conditions afforded **3** ($Ar^1 = Ph$, $R = Me$) in 45% yield with 36% *ee*. In addition, alkylation with alkyl halides such as ethyl iodide and butyl iodide gave only O-alkylation product.

[14] H. Moorlag, R. M. Kellogg, M. Kloosterman, B. Kaptein, J. Kamphuis, H. E. Schoemaker, *J. Org. Chem.* **1990**, *55*, 5878.

[15] a) S. Hanessian, *Total Synthesis of Natural Products. The Chiron Approach*, Pergamon Press, New York, **1983**, chap. 2; b) G. M. Coppola, H. F. Schuster, *α-Hydroxy Acids in Enantioselective Syntheses*, Wiley-VCH, Weinheim, **1997**; see also Refs. [9a] and [10c].

†

 © 2006 Wiley-VCH Verlag GmbH & Co. KGaA, Weinheim

Nonlinear Optics

DOI: 10.1002/anie.200504581

Hydrogen-Bond-Directed Head-to-Tail Orientation of Dipolar Merocyanine Dyes: A Strategy for the Design of Electrooptical Materials**

Frank Würthner, Johann Schmidt, Matthias Stolte, and Rüdiger Wortmann**

Merocyanine dyes are undoubtedly among the best chromophores for nonlinear optical (NLO)[1] and photorefractive (PR) applications.[2] For no other π-conjugated systems can the dipole moment μ, polarizability α and hyperpolarizabilities β and γ be better optimized by proper donor–acceptor substitution according to established structure–property relationships.[1–3] Nevertheless, exploitation of optimized molecular properties at the macroscopic level remains a challenge. For technologically promising polymer composite materials, optimized molecular properties μ, α, β, and γ must be transformed into optimized macroscopic susceptibilities by appropriate orientation of the dipolar dyes by an external electric field.[4] However, the efficiency of this field-induced poling approach is hampered by the thermodynamically favored antiparallel aggregation of dipolar dyes to give dimers with extinguished dipole moments (Figure 1 a).[5,6] This kind of H-aggregated dimer has been established as the predominant supramolecular species arising from push–pull chromophores[6] in NLO and PR materials at the required high concentrations (> 20 wt %), while the desirable parallel orientation (Figure 1 b) has not been realized to date in a thermodynamically equilibrated system.[7,8]

Here we introduce a supramolecular approach in which a receptor is employed to orient two merocyanine dyes in the desirable head-to-tail parallel fashion through multiple hydrogen bonding. As we show by electrooptical absorption (EOA) spectroscopy,[9] collective alignment of such a hydrogen-bonded complex in an electric field affords a markedly improved degree of dye orientation.

To demonstrate the feasibility of the concept outlined in Figure 1 c, two merocyanine dyes are required that contain complementary receptor units of sufficient strength to

[*] Prof. Dr. F. Würthner, J. Schmidt
Institut für Organische Chemie
Universität Würzburg
Am Hubland, 97074 Würzburg (Germany)
Fax: (+49) 931-888-4756
E-mail: wuerthner@chemie.uni-wuerzburg.de
M. Stolte, Prof. Dr. R. Wortmann†
Physikalische Chemie
Technische Universität Kaiserslautern
Erwin-Schrödinger-Straße, 67663 Kaiserslautern (Germany)
[†] Deceased on March 13, 2005.

[**] We gratefully acknowledge financial support for this work by the Volkswagen Foundation within the priority program "Complex Materials" and initial contributions to this project by Dr. Sheng Yao.

 WILEY InterScience DISCOVER SOMETHING GREAT © 2006 Wiley-VCH Verlag GmbH & Co. KGaA, Weinheim

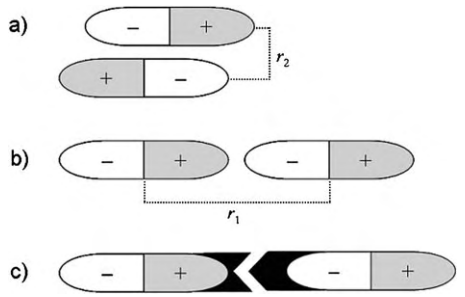

Figure 1. Supramolecular structures formed by self-assembly of dipolar dyes. For typical dyes with $(r_1/r_2) > 2^{1/3}$ the antiparallel arrangement (a) is preferred over the more desirable parallel orientation (b) according to predictions based on electrostatic interactions in the dipole approximation.[8] A concept for the realization of a parallel arrangement by taking advantage of a supramolecular receptor unit is depicted in (c).

facilitate hydrogen bond directed self-assembly at micromolar concentrations. It appeared to us that an ideal choice might be a combination of the Hamilton receptor[10] and barbituric acids, because the latter units are present as electron acceptors in many merocyanine dyes. Scheme 1 outlines our strategy to connect merocyanine dyes in a rigid fashion to the Hamilton receptor.

In the first step, 5-aminoisophthalic acid (**1**) was treated with dehydroacetic acid **2** to give pyridone hydrochloride **3**,[11] which was subsequently transformed into its diethyl ester derivative **4**. Reaction of diester **4** with lithiated 2,6-diaminopyridine (**5**) afforded diamide **6**, which can be easily acylated with butanoyl chloride to give pyridone-bearing Hamilton receptor **7**. This pyridone is only moderately reactive towards nucleophiles, but it did react with barbituric acid **8** to provide the desired receptor-functionalized merocyanine **9** in moderate yield.[12]

Two design features make this dye-appended receptor **9** particularly promising for the realization of a thermodynamically favored parallel arrangement of two dipolar dyes (Scheme 2): 1) The Hamilton receptor is well-positioned at the "head" of one merocyanine dye. Strong and directional intermolecular forces provided by six hydrogen bonds to the "tail" of another merocyanine dye should make the parallel head-to-tail assembly thermodynamically preferable to electrostatically driven antiparallel aggregation; 2) two methyl groups at the *ortho* positions of the dihydropyridine ring result in an almost orthogonal orientation of the two planes of the merocyanine dye and its Hamilton receptor (and to the dye complexed with the Hamilton receptor as well). This geometry is expected to be important in diminishing the propensity towards antiparallel aggregation for the even more dipolar hydrogen-bonded complex **9**·**10**.

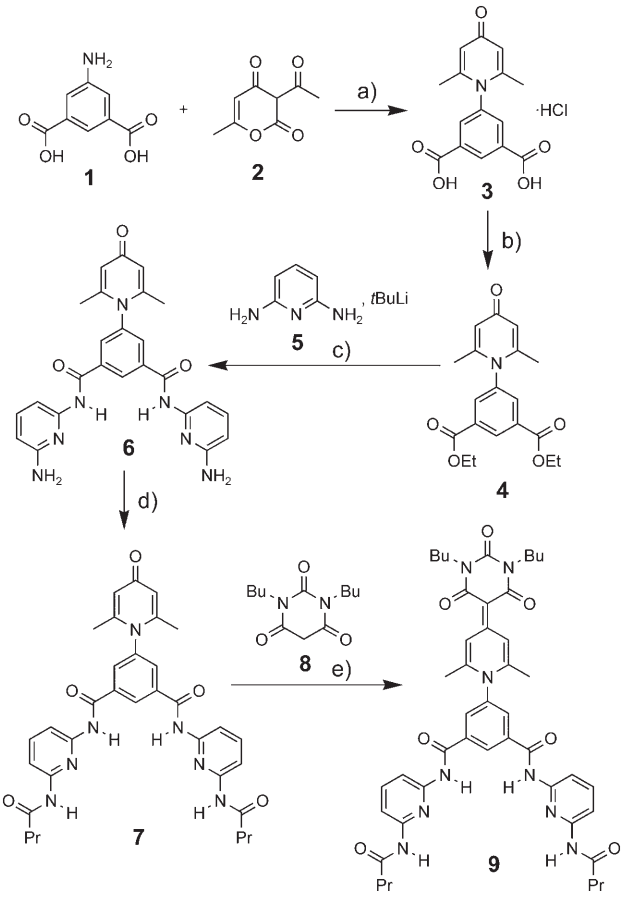

Scheme 1. Synthesis of merocyanine dyes bearing a Hamilton receptor. a) HCl/H_2O, 110 °C, 15 h, 53 %; b) EtOH, H_2SO_4, toluene, reflux, 6 h, 82 %; c) THF, RT, 20 h, 55 %; d) C_3H_7COCl, Et_3N, THF, RT, 20 h, 78 %; e) Ac_2O, AcOH, 105 °C, 4 h, 22 %.

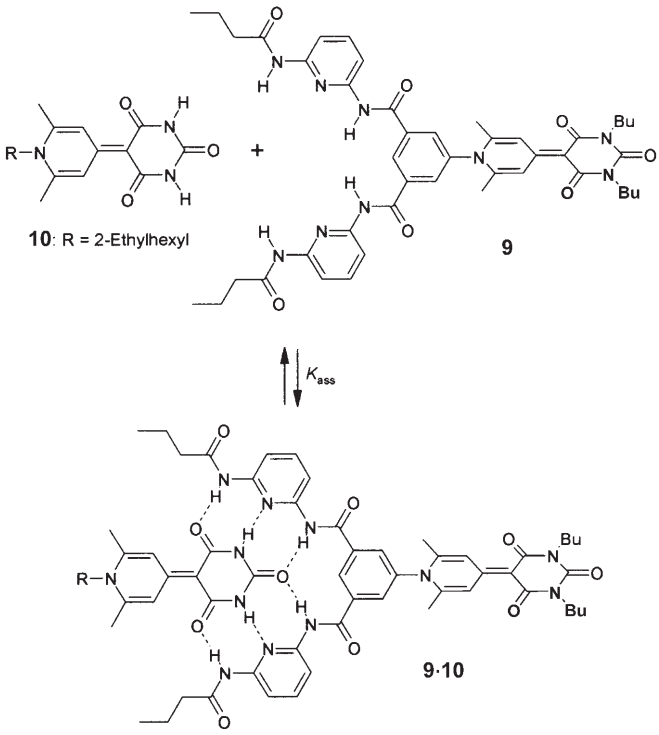

Scheme 2. Hydrogen bond directed complexation of merocyanine **10** with the Hamilton receptor of merocyanine **9**.

 © 2006 Wiley-VCH Verlag GmbH & Co. KGaA, Weinheim

At an equimolar stoichiometry of the Hamilton receptor functionalized merocyanine **9** and complementary barbituric acid merocyanine **10**,[13] clear evidence for the formation of a 1:1 complex **9·10** (Scheme 2) was obtained by ^{1}H NMR spectroscopy. Formation of hydrogen bonds became evident from pronounced downfield shifts of all hydrogen-bonded protons, that is, the NH protons of barbituric acid **10** shift from $\delta = 7.30$ to $\delta = 11.93$ ppm in **9·10** (all values in $CDCl_3$), and the two NH protons of the diacylpyridine units of Hamilton receptor **9** shift from $\delta = 7.55$ and 8.38 ppm to $\delta =$ 10.52 and 10.63 ppm, respectively. Owing to the high binding strength provided by six hydrogen bonds, complexation could even be realized in hydrogen-bond acceptor solvents such as dioxane at a millimolar concentration. Notably, saturation of all hydrogen-bond donor and acceptor sites within complex **9·10** resulted in a twisted geometry and remarkable solubility of this highly dipolar complex even in weakly polar solvents such as toluene, in which individual dyes **9** and **10** are poorly soluble.[14]

To obtain more profound information on the binding strength in solvents that are suitable for EOA measurements (chloroform, dioxane, toluene), titration experiments were performed. Due to dynamic broadening of all signals for hydrogen-bonded NH protons during titration of **10** with **9** (or vice versa), the extent of complexation was assessed from the downfield shift of the protons at the 3,5-positions of the dihydropyridine unit of **10** (Figure 2). Well-defined binding

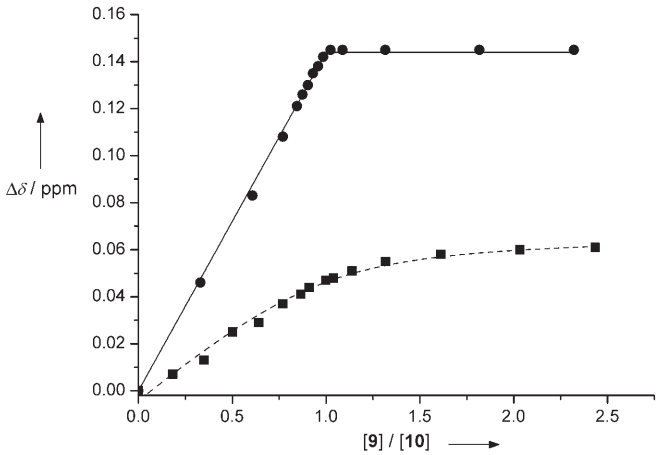

Figure 2. ^{1}H NMR titration data for protons H-3,5 of merocyanine **10** (1×10^{-3} M) on addition of merocyanine **9** in [D_8]dioxane (■) and $CDCl_3$ (●) at 298 K, and binding isotherms calculated by nonlinear regression analysis.

isotherms in [D_8]dioxane and $CDCl_3$ are indicative of 1:1 complex stoichiometry and significantly higher binding strength for the complex in $CDCl_3$. Nonlinear least-square regression analysis afforded values for the binding constant of $K = (9 \pm 3) \times 10^3\ M^{-1}$ in [D_8]dioxane and $K > 10^6\ M^{-1}$ in $CDCl_3$. Even higher binding constants can be expected in less polar aromatic and aliphatic solvents,[15] but binding isotherms could not be determined in such solvents by ^{1}H NMR titration due to insufficient solubility of free dyes **9** and **10**.[16]

The UV/Vis absorption spectrum of complex **9·10** exhibits two absorption maxima at 380.4 and 389.7 nm which can be attributed to its two components, that is, chromophores **10** ($\lambda = 379.8$ nm) and **9** ($\lambda = 396.4$ nm) (Figure 3). Another

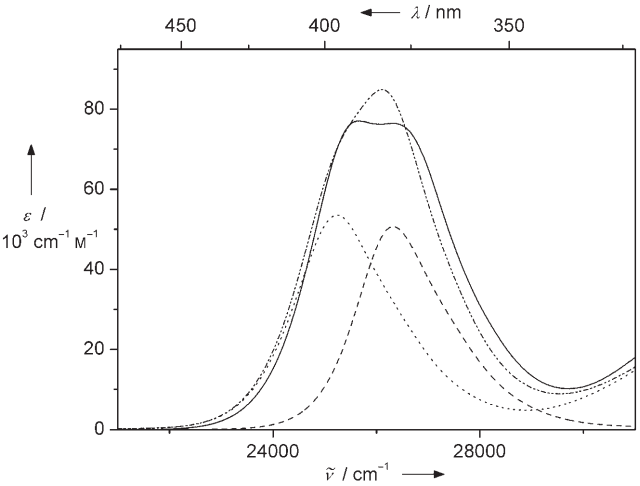

Figure 3. UV/Vis absorption spectra of merocyanines **10** (-----) and **9** (•••••), and their complex **9·10** (——), as well as the calculated sum of the spectra of **9** and **10** (–•–•) in toluene at 298 K (ca. 10^{-6} M).

indication for simple additive behavior of the two dye building blocks is given by the integral absorption I_A, which is proportional to the square of the electric transition dipole moment μ_{ag}. Thus, I_A for complex **9·10** is equal to the sum of the individual parts I_A(**9**) and I_A(**10**) (Table 1). Nevertheless, a

Table 1: Dipole moments of the ground (μ_g) and excited states (μ_a) derived from UV/Vis and EOA measurements on **9**, **10**, and **9·10** and integral absorption I_A of their CT transitions in toluene at $T = 298$ K.

	9	**10**	**9·10**
μ_g [D]	8.5 ± 0.1	10.4 ± 0.1	18.3 ± 0.1
μ_a [D]	4.5 ± 0.4	7.0 ± 0.2	13.6 ± 0.2
I_A [$m^2\,mol^{-1}$]	552	435	984

closer look at the molar decadic absorption coefficients ε reveals a small mutual interaction between the two building blocks. Thus, the maximum of the calculated sum of the spectra of **9** and **10** is higher and the band width is smaller in comparison to the experimental spectrum of the complex (Figure 3). This variation of the band structure can be attributed to hydrogen bond directed polarization of merocyanine **10** and weak exciton coupling between the two chromophores in the complex.

The most sophisticated technique for obtaining reliable information on dipole moments of the ground and excited states is the determination of $L(\varphi,\tilde{\nu})$ [Eq. (1)] of a dilute

$$L(\varphi,\tilde{\nu}) = \frac{\varepsilon^E(\varphi,\tilde{\nu}) - \varepsilon(\tilde{\nu})}{\varepsilon(\tilde{\nu})} \frac{1}{E^2} \qquad (1)$$

solution of compounds in an electric field E by EOA

 © 2006 Wiley-VCH Verlag GmbH & Co. KGaA, Weinheim

spectroscopy.[9] The direct measurement of the very small absorption difference $\varepsilon^{E}(\varphi,\tilde{\nu})-\varepsilon(\tilde{\nu})$ is carried out with linearly polarized light that is polarized parallel ($\varphi=0°$) and perpendicular ($\varphi=90°$) to the applied electric field E (Figure 4);

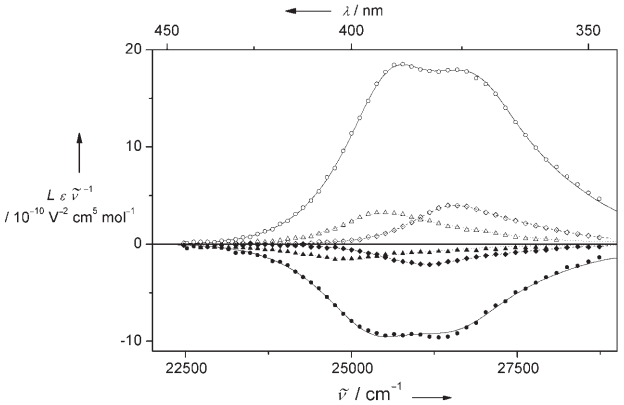

Figure 4. Measured data points of the EOA spectra $L(\varphi)\varepsilon\tilde{\nu}^{-1}$ for $\varphi=0°$ (△, ◇, ○) and $\varphi=90°$ (▲, ◆, ●) as well as multilinear regression curves (•••••, -----, ——) of merocyanines **9** (△, ▲, •••••) and **10** (◇, ◆, -----) and their complex **9·10** (○, ●, -----) in toluene ($T=298$ K, $E\approx 4\times10^{6}$ V m^{-1}, ca. 10^{-6} M).

$\varepsilon^{E}(\varphi,\tilde{\nu})$ is the molar decadic absorption coefficient of the solution in an externally applied field.

For dyes **9** and **10** as well as complex **9·10**, Figure 4 shows increased absorbance when the light beam is polarized parallel to the direction of the electric field (open symbols) and decreased absorbance when it is polarized perpendicular to the direction of the electric field (filled symbols). Significantly, for complex **9·10** the observed effect is far more pronounced than for the individual dyes. To explain this observation, it should be taken into account that for highly dipolar chromophores like **9** and **10** and the associate **9·10**, $L\varepsilon\tilde{\nu}^{-1}$ is mainly determined by the square of the ground-state dipole moment μ_g. Consequently, the fact that $L\varepsilon\tilde{\nu}^{-1}$ for complex **9·10** is more than four times larger than the sum of the $L\varepsilon\tilde{\nu}^{-1}$ of **9** and **10** (Figure 4) unequivocally confirms cooperative orientation of these dyes in the electric field.

The quantitative evaluation of the optical and electro-optical data provides ground-state dipole moments μ_g, excited-state dipole moments μ_a, and the integral absorption I_A for **9**, **10** and **9·10** (Table 1). These results corroborate the qualitative conclusion for the collective orientation and our predictions for a geometry of **9·10** in which all moments seem to be approximately parallel to each other and to the longest axis of the head-to-tail assembly of two chromophores as well. Also, the excited-state dipole moments μ_a, determined through $L\varepsilon\tilde{\nu}^{-1}$ due to the shift of the absorption band, gives a further hint for cooperative orientation of the two chromophores in complex **9·10**. This will be discussed in detail in a forthcoming paper.

In summary, this work introduces the first supramolecular architecture in which two dipolar dyes are assembled in a head-to-tail fashion by multiple hydrogen bonds with summation of their dipole moments. In this geometry a cooperative alignment of the two dyes in the complex becomes possible in an external electric field with an unprecedented degree of dye alignment for this type of chromophore. We intend to apply this concept to optimized NLO and PR chromophores and to design self-complementary merocyanine dye building blocks that afford supramolecular polymers[17] with improved nonlinear optical and photorefractive properties.

Received: December 23, 2005
Revised: February 20, 2006
Published online: May 3, 2006

Keywords: chromophores · dyes/pigments · hydrogen bonds · nonlinear optics · supramolecular chemistry

[1] a) J. J. Wolff, R. Wortmann, *Adv. Phys. Org. Chem.* **1999**, *32*, 121–217; b) T. Verbiest, S. Houbrechts, M. Kauranen, K. Clays, A. Persoons, *J. Mater. Chem.* **1997**, *7*, 2175–2189.

[2] F. Würthner, R. Wortmann, K. Meerholz, *ChemPhysChem* **2002**, *3*, 17–31.

[3] a) S. Dähne, *Chimia* **1991**, *45*, 288–296; b) S. R. Marder, C. B. Gorman, F. Meyers, J. W. Perry, G. Bourhill, J.-L. Brédas, B. M. Pierce, *Science* **1994**, *263*, 511–514; c) M. Barzoukas, M. Blanchard-Desce, R. Wortmann, *Proc. SPIE-Int. Soc. Opt. Eng.* **1999**, *3623*, 194–204; d) S. Beckmann, K.-H. Etzbach, P. Krämer, K. Lukaszuk, R. Matschiner, A. J. Schmidt, P. Schuhmacher, R. Sens, G. Seybold, R. Wortmann, F. Würthner, *Adv. Mater.* **1999**, *11*, 536–541.

[4] a) D. M. Burland, R. D. Miller, C. A. Walsh, *Chem. Rev.* **1994**, *94*, 31–75; b) L. R. Dalton, A. W. Harper, B. Wu, R. Ghosn, J. Laquindanum, Z. Liang, A. Hubbel, C. Xu, *Adv. Mater.* **1995**, *7*, 519–540.

[5] a) L. R. Dalton, A. W. Harper, B. H. Robinson, *Proc. Natl. Acad. Sci. USA* **1997**, *94*, 4842–4847; b) Y. V. Pereverzev, O. V. Prezhdo, L. R. Dalton, *ChemPhysChem* **2004**, *5*, 1821–1830.

[6] a) R. Wortmann, U. Rösch, M. Redi-Abshiro, F. Würthner, *Angew. Chem.* **2003**, *115*, 2126–2129; *Angew. Chem. Int. Ed.* **2003**, *42*, 2080–2083; b) F. Würthner, S. Yao, T. Debaerdemaeker, R. Wortmann, *J. Am. Chem. Soc.* **2002**, *124*, 9431–9447; c) F. Würthner, S. Yao, *Angew. Chem.* **2000**, *112*, 2054–2057; *Angew. Chem. Int. Ed.* **2000**, *39*, 1978–1981.

[7] Hydrogen bond directed NLO-active solid-state material prepared by vapor-phase deposition have been reported: a) C. Cai, M. M. Bösch, Y. Tao, B. Müller, Z. Gan, A. Kündig, C. Bosshard, I. Liakatas, M. Jäger, H. P. Günter, *J. Am. Chem. Soc.* **1998**, *120*, 8563–8564; b) P. Zhu, H. Kang, A. Facchetti, G. Evmenenko, P. Dutta, T. J. Marks, *J. Am. Chem. Soc.* **2003**, *125*, 11496–11497. For an amorphous solid state material formed by hydrogen bond directed self-assembly, see: H. Saadeh, L. Wang, L. Yu, *J. Am. Chem. Soc.* **2000**, *122*, 546–547.

[8] According to electrostatic considerations, for spherical molecules the parallel orientation (Figure 1b) is favored. However, for typical flat and elongated dye molecules the antiparallel side-on association (Figure 1a) is preferred due to the smaller intermolecular distance: C. P. J. M. van der Vorst, S. J. Picken in *Polymers as Electrooptical and Photooptical Active Media* (Ed.: V. P. Shibaev), Springer, Berlin, **1996**, pp. 173–211.

[9] a) W. Liptay in *Excited States, Vol. 1* (Ed.: E. C. Lim), Academic Press, New York, **1974**, pp. 129–229; b) R. Wortmann, K. Elich, S. Lebus, W. Liptay, P. Borowicz, A. Grabowska, *J. Phys. Chem.* **1992**, *96*, 9724–9730.

[10] a) S. K. Chang, A. D. Hamilton, *J. Am. Chem. Soc.* **1988**, *110*, 1318–1319. For recent applications of the Hamilton receptor for

 © 2006 Wiley-VCH Verlag GmbH & Co. KGaA, Weinheim

the organization of dyes, see: b) Y. Molard, D. M. Bassani, J.-P. Desvergne, P. N. Horton, M. B. Hursthouse, J. H. R. Tucker, *Angew. Chem.* **2005**, *117*, 1096 – 1099; *Angew. Chem. Int. Ed.* **2005**, *117*, 1072 – 1075; c) A. Dirksen, U. Hahn, F. Schwanke, M. Nieger, J. N. H. Reek, F. Vögtle, L. De Cola, *Chem. Eur. J.* **2004**, *10*, 2036 – 2047.

[11] It is noteworthy that aniline **1** was too unreactive to undergo condensation with pyrrylium salts according to standard procedures: A. R. Katritzky, O. Rubio, M. Szajda, B. Nowak-Wydra, *J. Chem. Res. Synop.* **1984**, 234 – 235.

[12] All compounds were characterized by NMR spectroscopy, mass spectrometry, and elemental analysis. Data for **9**: M.p. 321–322 °C. ^{1}H NMR (CD_3OD, 400 MHz, 298 K): $\delta = 0.98$ (t, $^3J =$ 7.3 Hz, 6H; CH_3), 1.01 (t, $^3J = 7.4$ Hz, 6H; CH_3), 1.38 (sext, $^3J =$ 7.5 Hz, 4H; CH_2), 1.63 (quint, $^3J = 7.4$ Hz, 4H; CH_2), 1.74 (sext, $^3J = 7.4$ Hz, 4H; CH_2), 2.33 (s, 6H; CH_3), 2.40 (t, $^3J = 7.5$ Hz, 4H; CH_2), 3.99 (t, $^3J = 7.5$ Hz, 4H; CH_2), 7.74 (dd, $^3J = 7.5$, $^4J =$ 0.9 Hz, 2H; H_{pyr}), 7.81 (t, $^3J = 8.0$ Hz, 2H; H_{pyr}), 7.98 (dd, $^3J =$ 7.5, $^4J = 0.9$ Hz, 2H; H_{pyr}), 8.29 (d, $^4J = 1.6$ Hz, 2H; H_{aryl}), 8.84 (t, $^4J = 1.6$ Hz, 1H; H_{aryl}), 8.91 ppm (s, 2H; $H_{dihydropyr}$). MS (FAB, 3-NBA): m/z 832 (10.78 %) $[M+H]^+$. Elemental analysis (%) calcd for $C_{45}H_{53}N_9O_7 \cdot CH_3OH$ (863.43): C 63.95, H 6.65, N 14.59; found: C 63.75, H 6.33, N 14.63.

[13] a) F. Eiden, *Arch. Pharm.* **1960**, 404 – 414; b) F. Eiden, P. Peter, *Arch. Pharm.* **1964**, 1 – 10.

[14] The solubility of **9** and **10** in toluene was sufficient to obtain UV/Vis and EOA spectra at a concentration of about 10^{-6} M.

[15] F. Würthner, C. Thalacker, A. Sautter, W. Schärtl, W. Ibach, O. Hollricher, *Chem. Eur. J.* **2000**, *6*, 3871 – 3885.

[16] A value for the binding constant in toluene of $K > 10^8$ M^{-1} could be estimated from fluorescence titration experiments for the related 1:1 complex of **10** with a Hamilton receptor lacking the appended merocyanine chromophore.

[17] a) L. Brunsveld, B. J. B. Folmer, E. W. Meijer, R. P. Sijbesma, *Chem. Rev.* **2001**, *101*, 4071 – 4097. For recent work on multiple hydrogen bond directed formation of polar structures, see: b) M. Ikeda, T. Nobori, M. Schmutz, J.-M. Lehn, *Chem. Eur. J.* **2005**, *11*, 662 – 668; c) A. J. Preston, J. C. Gallucci, J. R. Parquette, *Chem. Commun.* **2005**, 3280 – 3282.

 © 2006 Wiley-VCH Verlag GmbH & Co. KGaA, Weinheim

Photoisomerization

DOI: 10.1002/anie.200504364

Optical Switching of Self-Assembly: Micellization and Micelle–Hollow-Sphere Transition of Hydrogen-Bonded Polymers**

*Xikui Liu and Ming Jiang**

One attractive goal of supramolecular chemistry is to control molecular self-assembly by an external stimulus. Temperature and pH are the stimuli that have been studied primarily, although light irradiation is regarded as the most reliable external stimulus as it involves only photochemical processes, which are energy-saving and easily controllable. The isomerization of photochromic groups, particularly azobenzene groups, is a well-known photochemical process that has been extensively studied.[1] Clearly, when azobenzene groups are incorporated into the building-block molecules, light-induced changes in the structure of the photochromic groups will affect their self-assembly behavior as the two isomers possess different properties. Most work in this field deals with small-molecule systems containing azobenzene photochromic units.[2] However, the use of photoisomerization as a stimulus-responsive procedure in the construction of polymeric self-assembly systems has been largely unexploited.

Recently, Zhao et al.[3] achieved reversible morphological changes in micelles of block copolymers containing azobenzene mesogens, induced by exposure to UV and visible light. Harada et al.[4] constructed a photoresponsive hydrogel system based on molecular recognition between cyclodextrin and azobenzene units. Hatton et al.[5] obtained the light-controlled gelation of hydrophobically modified poly(acrylic acid) and a surfactant containing azobenzene groups. Fréchet et al.[6] reported a micellar system sensitive to infrared light through a two-photon photoreaction. An ABA-type triblock copolymer film with azobenzene groups in the side chains was found to possess a reversible photocontrolled 2D microphase separation.[7] Clearly, it still remains a great challenge to explore reversible optical switching in the construction of various polymeric self-assembly systems.

In recent years our group has succeeded in developing "block-copolymer-free" strategies to construct polymeric micelles and hollow spheres by interpolymer-specific interactions.[8] We are now able to use homopolymers, random

[*] Dr. X. Liu, Prof. M. Jiang
Department of Macromolecular Science and
The Key Laboratory of Molecular Engineering of Polymers
Fudan University
Shanghai 200433 (P.R. China)
Fax: (+86) 21-6564-0293
E-mail: mjiang@fudan.edu.cn

[**] The National Natural Science Foundation of China (NNSFC, Project No. 50333010) is acknowledged for supporting this research.

Supporting information for this article is available on the WWW under http://www.angewandte.org or from the author.

WILEY InterScience DISCOVER SOMETHING GREAT
© 2006 Wiley-VCH Verlag GmbH & Co. KGaA, Weinheim

copolymers, and oligomers as building blocks to construct noncovalently connected micelles (NCCMs), in which core and shell are connected by hydrogen bonding only. Some of these NCCMs are highly sensitive to changes in temperature and pH.[8c,d] Herein, we report significant progress in the construction of NCCMs driven by the photoinduced isomerization of azobenzene groups incorporated into the polymer building blocks. Furthermore, reversible transition between micelles and hollow spheres is also achieved by the photoinduced isomerization.

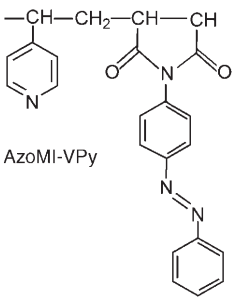

Our photocontrollable self-assembly system contains a polymer pair comprising poly(4-phenylazomaleinanil-*co*-4-vinylpyridine) (AzoMI-VPy) and polybutadiene with a terminal carboxy group (CPB). The AzoMI-VPy synthesized by free-radical polymerization[9] contains azobenzene side groups that serve as photoresponsive units and pyridine residues as proton acceptors. The CPB with terminal carboxy groups as hydrogen-bonding donors was obtained by the free-radical polymerization of butadiene initiated by succinic peroxide.[10a]

Mixing of AzoMI-VPy and CPB in various ratios in their common solvent, toluene, is expected to give a soluble interpolymer complex through hydrogen bonding between the pyridyl and carboxy groups. Such complexation between these proton-donor and proton-acceptor groups was reported in our previous publications.[10] The transparent toluene solutions of the AzoMI-VPy/CPB interpolymer complex were then irradiated with UV light at room temperature and the process was monitored by UV/Vis spectroscopy. As shown in Figure 1, the absorption of *trans*-azobenzene (π–π^* transition) becomes progressively weaker with increasing irradiation wavelength, with the peak shifting from about 330 to about 325 nm, while the absorption band near 440 nm (n–π^* transition of *cis*-azobenzene) grows gradually stronger.

This result indicates isomerization of the *trans*-azobenzene group into *cis*-azobenzene.[3a,11] Meanwhile, this UV irradiation makes the solution turn faintly blue and opalescent, which indicates the formation of polymeric assemblies. AzoMI-VPy/CPB solutions over a broad range of composition and undergoing UV exposure for 30 min were studied by dynamic light scattering (DLS). The results (Table 1) showed that assembled particles with a diameter around 250 nm appeared in the solution. The UV-induced particles possess a relatively narrow size distribution; for example, a low polydispersity index (PDI) is obtained when the molar ratio of pyridyl units to carboxy units (AzoMI-VPy/CPB) is in the range from 1.0:0.4 to 1.0:1.0.

Scanning electron microscopy (SEM) revealed spherical particles with diameters around 200 nm in the UV-irradiated solutions (Figure 2A), in agreement with the DLS results. To obtain an insight into the structure of the aggregate, we also carried out transmission electron microscopy (TEM) experiments. As shown in Figure 2B, the aggregates are spherical with diameters around 100 nm, much smaller than the values from SEM and DLS. This difference may be caused by the low shell-to-background contrast as a result of the low chain density of the solvated CPB chains. This conjecture finds support from the TEM image shown in Figure 2C, which shows that when the sample is stained with RuO_4, the particle size reaches about 180 nm as a result of the CPB shell becoming visible. This core–shell structure can further be revealed by the ^{1}H NMR spectrum of AzoMI-VPy/CPB (1.0:0.5) in deuterated toluene (see Supporting Information). The intensity ratio of the −CH= signal of CPB to that of the *o*-H of the azobenzene moiety of AzoMI-VPy is 13:1 when the two polymers are dissolved and form a soluble complex. After UV irradiation the ratio is dramatically increased to 96:1, as the proton signals of AzoMI-VPy drop sharply while those of the CPB remain unchanged. This finding demonstrates that in the micelles, the CPB chains remained soluble and formed the micellar shells, while the AzoMI-VPy chains aggregated and formed cores with low chain mobility.

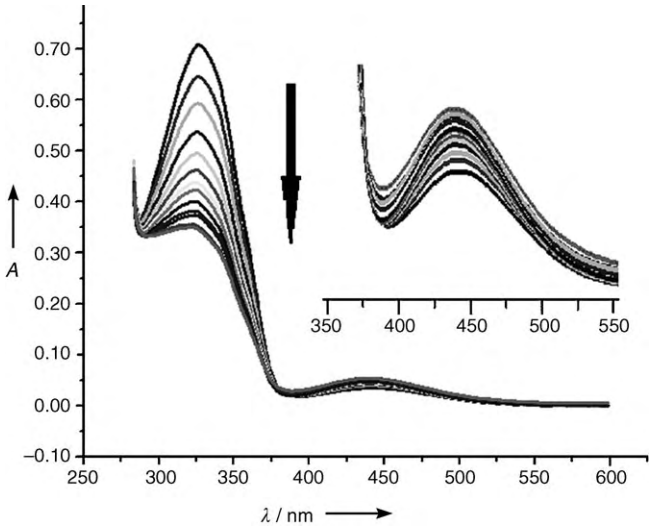

Figure 1. UV/Vis spectra of AzoMI-VPy/CPB (1.0:0.5) solutions, from the top down (visible part enlarged in insert, from the bottom up), for UV irradiation for 0, 3, 6, 9, 12, 15, 18, 21, 24, 27, 30, 33, and 36 min.

On the basis of the above results, we may rationalize the photoinduced formation of micelles as follows. The AzoMI-VPy with azobenzene units in the *trans* conformation can be dissolved in nonpolar toluene. Under UV irradiation, the azobenzene units isomerize into the *cis* isomer with a higher polarity (Scheme 1), and thus the AzoMI-VPy tends to precipitate in the nonpolar toluene solvent.[9a,12] However, driven by the hydrogen bonding between the end carboxy group in CPB and the pyridyl group in AzoMI-VPy, the CPB chains may gather around the AzoMI-VPy aggregates and

Table 1: Characteristic data of the UV-induced micelles for various AzoMI-VPy/CPB molar ratios, measured by DLS.

ratio	1.0:0.1	1.0:0.2	1.0:0.3	1.0:0.4	1.0:0.5	1.0:0.6	1.0:0.7	1.0:0.8	1.0:0.9	1.0:1.0
D_h [nm]	211	216	217	236	231	230	258	256	253	212
PDI [$\mu_2/\langle\Gamma\rangle^2$]	0.50	0.28	0.19	0.17	0.080	0.025	0.12	0.12	0.046	0.13

© 2006 Wiley-VCH Verlag GmbH & Co. KGaA, Weinheim

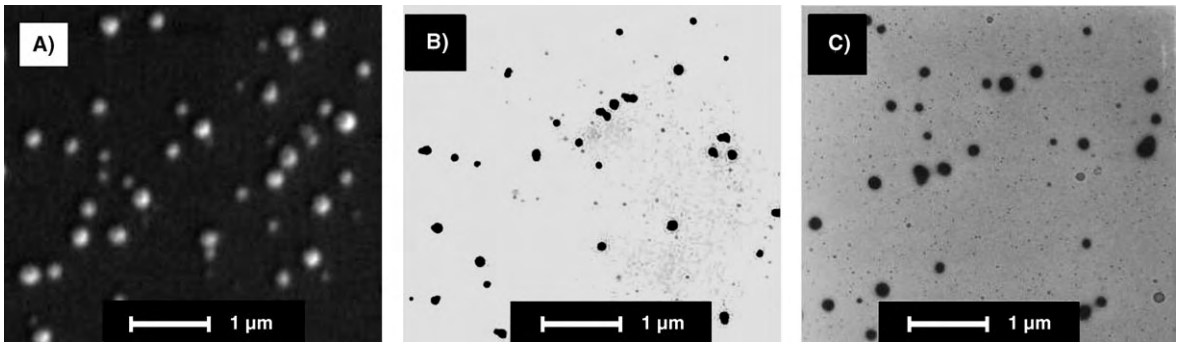

Figure 2. Morphology of UV-induced micelles of AzoMI-VPy/CPB (1.0:0.5) observed by SEM (A) and TEM (B) unstained; C) stained with RuO_4).

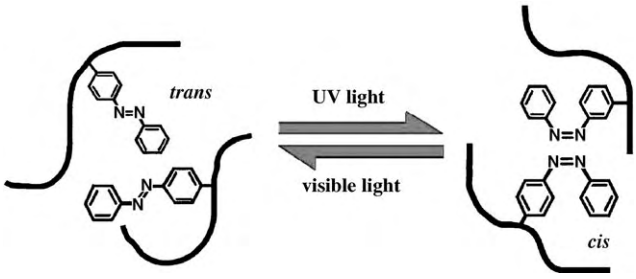

Scheme 1. Illustration of the UV-induced isomerization of azobenzene groups attached to polymer chains.

consequently stabilize them, thus forming stable core–shell micelles. The micellar structure in this case clearly differs from that of micelles of block copolymers, as the CPB shell and AzoMI-VPy core are linked by hydrogen bonding instead of covalent bonding; hence our appellation "noncovalently connected micelles".[8a]

When the solutions of UV-induced micelles were irradiated by visible light they turned transparent within a couple of minutes, which indicates dissociation of the micelles. The UV/Vis spectra showed that in this process, the *cis*-azobenzene groups returned to their *trans* state (Figure 3A). As the *trans* form of azobenzene is thermodynamically more stable, the *cis*-to-*trans* isomerization can be achieved thermally as well.[13] We obtained the UV/Vis spectrum of the micelle solution at 40 °C in the dark as a function of time. As shown in Figure 3B, over 30 min only a very small proportion of the azobenzene molecules in the *cis* form thermally reverted to the *trans* form, as the absorbance increased merely from 0.35 to 0.37 (A1 to B1). In contrast, under visible light the isomerization was almost complete within 3 min (A1 to A2), with the absorbance increasing to 0.70 and staying at that value with further irradiation. Clearly, under our experimental conditions, isomerization from the *cis* to the *trans* conformation was predominantly photoinduced.

A solution of the soluble complex is transparent whereas a micellar solution scatters light strongly, and thus a change in the turbidity of the solution is a good indicator of micellization or demicellization. As shown in Figure 4, the reversible changes in the turbidity of the solution caused by alternate UV and visible light irradiation proved that the micellization is a completely photoinduced reversible process.

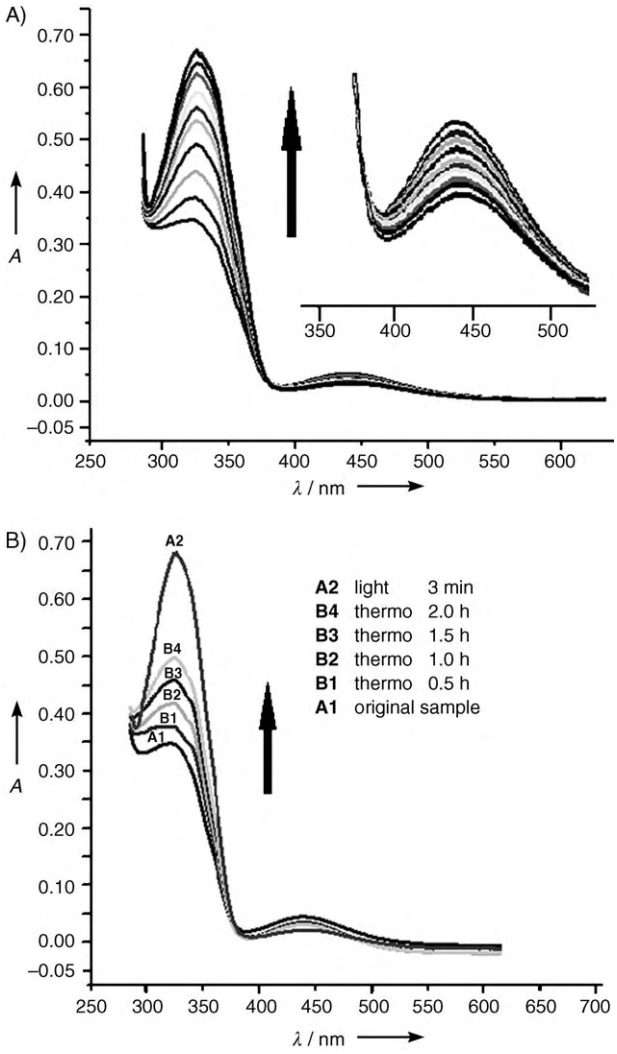

Figure 3. UV/Vis spectra A) of AzoMI-VPy/CPB (1.0:0.5) solutions, from the bottom up (visible part enlarged in the insert, from the top down), for visible light irradiation for 0, 20, 40, 60, 80, 100, 120, 140, 160, 180, and 200 s; B) showing visible-light and thermal (treatment at 40 °C) recovery.

Furthermore, the structure of the micelles induced by UV irradiation can be fixed simply through core cross-linking of the pyridyl groups with 1,4-diiodobutene at room temper-

 © 2006 Wiley-VCH Verlag GmbH & Co. KGaA, Weinheim

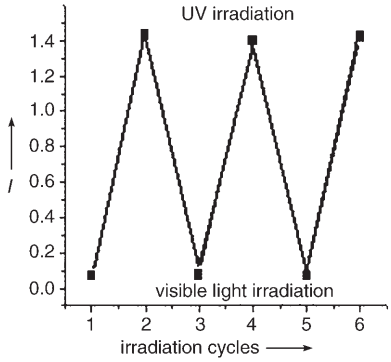

Figure 4. Turbidity of the AzoMI-VPy/CPB (1.0:0.5) solution under alternate UV and visible light irradiation.

ature for 48 h.[14] As a control example, a micelle solution without the cross-linker was treated under the same conditions. After irradiation with visible light for 5 min, micellar structures were still maintained in the cross-linked sample, whereas the micelles were totally dissociated in the control sample and the solution turned transparent. Moreover, DLS revealed a dramatic increase in the size of the core-cross-linked micelles from 250 to about 900 nm under irradiation by visible light (Figure 5A). This remarkable size expansion of the micelles can be attributed to isomerization of the azobenzene from the *cis* to the *trans* state, which gives the cross-linked AzoMI-VPy chains a much higher affinity to the solvent, thus making them greatly swelled.

In TEM experiments, the spheres irradiated with visible light showed a clear contrast between a dark periphery and a gray central part (Figure 5B), typical of hollow spheres.[15,16]. When the solution was again irradiated with UV light, the hollow spheres collapsed and returned to micelles with diameters of about 250 nm (measured by DLS; Figure 5A) as the *trans* isomer reverted to the *cis* isomer. The DLS measurements also indicate that the transition between micelles and hollow spheres induced by alternate UV and visible light irradiation is reversible (Figure 5A). Thus, optical switching of the micelle–hollow-sphere transition was achieved.

As summarized in Figure 6, we have demonstrated that reversible optical switching of self-assembly can be achieved by the incorporation of azobenzene units into one of the polymeric building blocks, with the aid of the hydrogen-bonding interaction between the polymer pair of AzoMI-VPy and CPB. First, the AzoMI-VPy/CPB can form "graftlike" interpolymer complexes in toluene thanks to the hydrogen-bonding interaction between carboxylic acid and pyridine. The complex is soluble in toluene when the azobenzene units of AzoMI-VPy are in the *trans* conformation. Then under UV irradiation, the azobenzene units are transformed into the polar *cis* conformation and thus make the AzoMI-VPy chains aggregate. However, macroscopic precipitation is inhibited by the soluble CPB chains surrounding the AzoMI-VPy aggregates through hydrogen-bonding interactions. Thus, core–shell micelles are formed with a volume about 250 nm across. Upon irradiation with visible light, the micelles are quickly disassociated into a transparent interpolymer complex as the azobenzene *cis* form returns to the *trans* form.

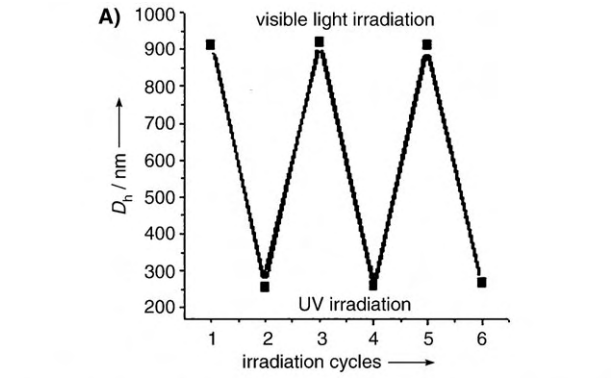

Figure 5. A) $\langle D_h \rangle$ of the micelle–hollow-sphere transition of an AzoMI-VPy/CPB (1.0:0.5) solution after cross-linking under alternate UV and visible light irradiation. B) TEM image of visible-light-induced hollow spheres of cross-linked AzoMI-VPy/CPB (1.0:0.5) micelles.

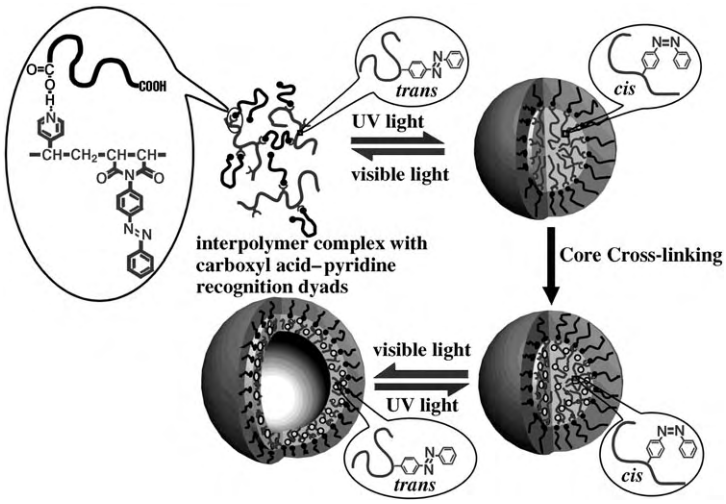

Figure 6. Illustration of the reversible photoinduced micellization and micelle–hollow-sphere transition of hydrogen-bonded polymers.

 © 2006 Wiley-VCH Verlag GmbH & Co. KGaA, Weinheim

The UV-light-induced micelles can be readily cross-linked by the pyridyl units reacting with 1,4-diiodobutene. The core-cross-linked micelles respond to light irradiation with reversible and remarkable morphological changes: visible light causes the formation of hollow spheres as a result of intense swelling of the core as the *cis*-azobenzene turns into the *trans* form, while UV light causes the hollow spheres to return to micelles as a result of isomerization in the opposite direction. In short, we have achieved reversible optical switching of micellization and the micelle–hollow-sphere transition in a system containing common, readily prepared polymers.

Experimental Section

Polymer synthesis: CPB was prepared by the free-radical polymerization of butadiene initiated by succinic peroxide in solution. Most of the resultant polybutadiene chains carried carboxy groups at both ends because of the dominance of the combination termination of the propagating free radicals. The carboxy content determined by chemical titration was 0.561 mmol g^{-1}, and hence the calculated number-average molecular weight was 3565. The PDI obtained by gel permeation chromatography (GPC) with polystyrene standards was 2.85. AzoMI-VPy was synthesized by the free-radical polymerization of 4-vinylpyridine (10.0 mmol) and 4-phenylazomaleinanil (10.0 mmol) in 1,4-dioxane (20 mL) at 70 °C for 24 h in a 100-mL round-bottomed flask fitted with a nitrogen bubbler, with azobisisobutyronitrile as initiator (0.03 g, 0.2 mmol). The copolymer was isolated by precipitation into a fivefold excess of cold methanol, washed with methanol, and dried at 40 °C under reduced pressure. The number-average molecular weight was 1984 and the PDI obtained by GPC analysis with polystyrene standards was 2.39.

UV and visible light exposure: UV irradiation was carried out with a 300-W high-pressure mercury lamp coupled with UV filters (<360 nm). Irradiation by visible light was performed using a 200-W incandescent light bulb (>440 nm).

The fixation of micelles through core cross-linking was performed by adding an equivalent of 1,4-diiodobutene, based on the pyridine units in the micellar solution, and stirring the mixture at room temperature for 48 h in the dark.

Measurements: A Malvern Autosizer 4700 laser-light-scattering spectrometer, equipped with a multi-τ digital time correlator and a solid-state laser as light source, was used. All the DLS measurements were carried out at (25.0 ± 0.1) °C and at a scattering angle of 90°. UV/Vis spectra were recorded on a Perkin-Elmer Lamda 35 UV/Vis spectrophotometer. The turbidity of the micellar solutions was measured at 700 nm, which was far from the absorption of the azobenzene chromophore.

TEM experiments were performed on a Philips CM 120 electron microscope at an accelerating voltage of 80 kV. The specimens were prepared by placing the micelle solution (5 μL) on a copper grid and allowing it to dry in a desiccator. SEM was conducted with a Tescan 5136 MM scanning electron microscope. Samples were prepared by placing the micelle solution (5 μL) on freshly cleaved mica and allowing it to dry in a desiccator.

The molecular weights of the polymers were measured by Agilent 1100 size-exclusion chromatography with THF as the eluent. The ^{1}H NMR measurements were performed on a Bruker DMX500 spectrometer in dimethyl sulfoxide (or toluene) with tetramethylsilane as an internal reference.

Received: December 8, 2005
Revised: March 9, 2006
Published online: April 28, 2006

Keywords: isomerization · micelles · optical switching · polymers · self-assembly

[1] a) S. Hecht, *Small* **2005**, *1*, 26; b) S. Yagai, T. Karatsu, A. Kitamura, *Chem. Eur. J.* **2005**, *11*, 4054; c) L. Frkanec, M. Jokic, J. Makarevic, K. Wolsperger, M. Zÿinic, *J. Am. Chem. Soc.* **2002**, *124*, 9716; d) T. Kawasaki, M. Tokuhiro, N. Kimizuka, T. Kunitake, *J. Am. Chem. Soc.* **2001**, *123*, 6792.

[2] a) T. Kunitake, N. Nakashima, M. Shimomura, Y. Okahata, K. Kano, T. Ogawa, *J. Am. Chem. Soc.* **1980**, *102*, 6644; b) H. Sakai, Y. Orihara, H. Kodashima, A. Matsumura, T. Ohkubo, K. Tsuchiya, M. Abe, *J. Am. Chem. Soc.* **2005**, *127*, 13454; c) D. Faure, J. Gravier, T. Labrot, B. Desbat, R. Oda, D. M. Bassani, *Chem. Commun.* **2005**, 1167; d) M. Han, M. Hara, *J. Am. Chem. Soc.* **2005**, *127*, 10951; e) S. Yagai, T. Nakajima, K. Kishikawa, S. Kohmoto, T. Karatsu, A. Kitamura, *J. Am. Chem. Soc.* **2005**, *127*, 11134.

[3] a) G. Wang, X. Tong, Y. Zhao, *Macromolecules* **2004**, *37*, 8911; b) X. Tong, G. Wang, A. Soldera, Y. Zhao, *J. Phys. Chem. B* **2005**, *109*, 20281.

[4] a) I. Tomatsu, A. Hashidzume, A. Harada, *Macromolecules* **2005**, *38*, 5223; b) Y. Takashima, T. Nakayama, M. Miyauchi, Y. Kawaguchi, H. Yamaguchi, A. Harada, *Chem. Lett.* **2004**, *33*, 890.

[5] C. T. Lee, K. A. Smith, T. A. Hatton, *Macromolecules* **2004**, *37*, 5397.

[6] A. P. Goodwin, J. L. Mynar, Y. Ma, G. R. Fleming, J. M. J. Fréchet, *J. Am. Chem. Soc.* **2005**, *127*, 9952.

[7] S. Kadota, K. Aoki, S. Nagano, T. Seki, *J. Am. Chem. Soc.* **2005**, *127*, 8266.

[8] For example, see: a) D. Y. Chen, M. Jiang, *Acc. Chem. Res.* **2005**, *38*, 494; b) H. W. Duan, D. Y. Chen, M. Jiang, W. J. Gan, S. J. Li, M. Wang, J. Gong, *J. Am. Chem. Soc.* **2001**, *123*, 12097; c) H. J. Dou, M. Jiang, H. S. Peng, D. Y. Chen, Y. Hong, *Angew. Chem.* **2003**, *115*, 1554; *Angew. Chem. Int. Ed.* **2003**, *42*, 1516; d) Y. W. Zhang, M. Jiang, J. X. Zhao, X. W. Ren, D. Y. Chen, G. Z. Zhang, *Adv. Funct. Mater.* **2004**, *14*, 695.

[9] a) A. Shulkin, H. D. H. Stover, *Macromolecules* **2003**, *36*, 9836; b) M. A. Noordegraaf, J. G. J. Kuiper, A. T. M. Marcelis, E. J. R. Sudholter, *Macromol. Chem. Phys.* **1997**, *198*, 3681.

[10] a) M. Wang, G. Z. Zhang, D. Y. Chen, M. Jiang, S. Y. Liu, *Macromolecules* **2001**, *34*, 7172; b) S. Y. Liu, Q. M. Pan, J. W. Xie, M. Jiang, *Polymer* **2000**, *41*, 6919; c) H. Peng, D. Chen, M. Jiang, *Langmuir* **2003**, *19*, 10989.

[11] a) A. Desponds, R. Freitag, *Langmuir* **2003**, *19*, 6261; b) T. Okada, Y. Watanabe, M. Ogawa, *J. Mater. Chem.* **2005**, *15*, 987.

[12] M. Irie, W. Schnabel, *Macromolecules* **1985**, *18*, 394.

[13] B. Klaussner, D. Nees, F. Schmid, T. Wolff, *J. Colloid Interface Sci.* **1994**, *162*, 481.

[14] R. Saito, K. Ishizu, *Polymer* **2001**, *38*, 225.

[15] F. T. Liu, A. Eisenberg, *J. Am. Chem. Soc.* **2003**, *125*, 15059.

[16] On prolonging the cross-linking time to far more than 48 h, microspheres without a central cavity were observed by TEM. In our opinion, the strengthening of the cross-linking reaction enabled the reaction to occur in the center as well as the periphery of the core. Thus, slightly swollen micelles instead of hollow spheres were obtained (see Supporting Information).

 © 2006 Wiley-VCH Verlag GmbH & Co. KGaA, Weinheim

Oligosaccharide Synthesis

DOI: 10.1002/anie.200600433

Orthogonal Glycosylation Reactions on Solid Phase and Synthesis of a Library Consisting of a Complete Set of Fucosyl Galactose Isomers**

Osamu Kanie, Isao Ohtsuka, Takuro Ako, Shusaku Daikoku, Yoshimi Kanie, and Rumiko Kato*

The development of efficient methods for accessing synthetic oligosaccharides with diverse structures is essential to our understanding of the involvement of such molecules in biological phenomena.[1] Recent efforts directed toward the synthesis of complex glycoconjugates have made it possible to control the stereo- and regiospecificity of glycosylation reactions in solution- and solid-phase organic synthesis.[2–10] Current syntheses, however, can not be applied directly to the combinatorial chemistry of carbohydrates, for which the synthetic protocols must be extremely simple.[11] Various approaches to the creation of an oligosaccharide library have been described,[11–14] however, there are no reports of successful multiple glycosylation reactions that occur at every hydroxy-group position of a monosaccharide acceptor in a position-specific manner. We describe herein the synthesis of a complete disaccharide library with an L-fucosyl-D-galactose (Fuc-Gal) sequence with three parameters, namely, the anomeric configuration of the Fuc and Gal residues and the linkage position (Table 1). The library was synthesized on the basis of an orthogonal glycosylation strategy. The potential of this approach for solid-phase oligosaccharide synthesis is also illustrated with a focus on overall efficiency. The particular Fuc-Gal sequence used was chosen because αFuc(1→2)βGal is an O-blood-type epitope and also relates to the Le^b antigen, which has been reported to act as a ligand of *Helicobacter pylori*. Thus, a library may provide important information for the potential treatment of ulcers.

In planning the synthesis of an oligosaccharide library, we focused on the efficiency of the overall process. It was necessary to minimize the number of 1) types of protecting groups used and 2) reaction steps in the synthesis. To fulfill the first criterion, a benzyl group was chosen as the sole protecting group, with the exception of protection, when needed, at the connecting position to the resin.[15] To satisfy the second criterion, we chose to combine the use of an orthogonal glycosylation strategy[16] with solid-phase chemistry.[17–19] In the orthogonal glycosylation method, reaction starts from the nonreducing terminus. In this way, the formation of the deletion sequence is suppressed without the need for capping reactions, as has been described for glycal chemistry, because the by-products can not serve as glycosylating agents in the next cycle.[5] At the final stage of glycosylation, a hydrophobic tag was introduced to facilitate rapid isolation of the final product(s) after the deprotection reactions.[20–22]

Table 1: Anomeric configurations and linkage positions of library compounds **1**–**16**.

Fuc		Gal	Compound
Anomeric configuration	Linkage position	Anomeric configuration	
α	2	α	**1**
β	2	α	**2**
α	2	β	**3**[a]
β	2	β	**4**
α	3	α	**5**
β	3	α	**6**
α	3	β	**7**
β	3	β	**8**
α	4	α	**9**
β	4	α	**10**
α	4	β	**11**
β	4	β	**12**
α	6	α	**13**
β	6	α	**14**
α	6	β	**15**
β	6	β	**16**

[a] Synthesis was reported in reference [21].

In our strategy, the position of the interglycosidic linkage is fixed and the anomeric configuration is randomized to avoid formation of a highly complex mixture that would make isolation extremely difficult.[11] The glycosyl fluorides **17**–**20** were synthesized from the corresponding phenylthioglycosides of galactopyranose[23] by protection of a hydroxy group with a chloroacetyl group (ClAc), conversion of the phenylthio group into a fluoride substituent by treatment with *N*,*N*-diethylaminosulfur trifluoride, and removal of the ClAc group.[24] The synthesis of a disaccharide library was carried out with **17**–**20**, which contain orthogonal leaving groups, and a fucosyl donor in the form of the phenylthioglycoside **21** (Scheme 1). The phenylthio group was activated chemoselectively over glycosyl fluoride with dimethyl(methylthio)sulfonium trifluoromethanesulfonate (DMTST)[25,26] to yield disaccharides in generally good yields (TLC analysis). Individual anomers in the disaccharide mixtures **22**–**25** were not isolated at this stage, to avoid the unnecessary loss of some anomers. The disaccharide fractions were collected as mixtures by gel-permeation chromatography. The mixtures were then used as the glycosyl donors and treated with *n*-octanol in the presence of hafnocene bis(trifluoromethanesulfonate) $[Cp_2Hf(OTf)_2]$.[27–30] An *n*-octyl group was introduced at the reducing-end anomeric position to facilitate the removal of

[*] Dr. O. Kanie, Dr. I. Ohtsuka, T. Ako, S. Daikoku, Dr. Y. Kanie, R. Kato
Mitsubishi Kagaku Institute of Life Sciences (MITILS)
11 Minamiooya, Machida-shi, Tokyo 194-8511 (Japan)
Fax: (+81) 42-724-6317
E-mail: kokanee@libra.ls.m-kagaku.co.jp

[**] Financial support provided by Mitsubishi Chemical Co. (MCC) and the Key Technology Research Promotion Program of the New Energy and Industrial Development Organization (NEDO), Ministry of Economy, Trade, and Industry (METI) of Japan is gratefully acknowledged.

Supporting information for this article is available on the WWW under http://www.angewandte.org or from the author.

 © 2006 Wiley-VCH Verlag GmbH & Co. KGaA, Weinheim

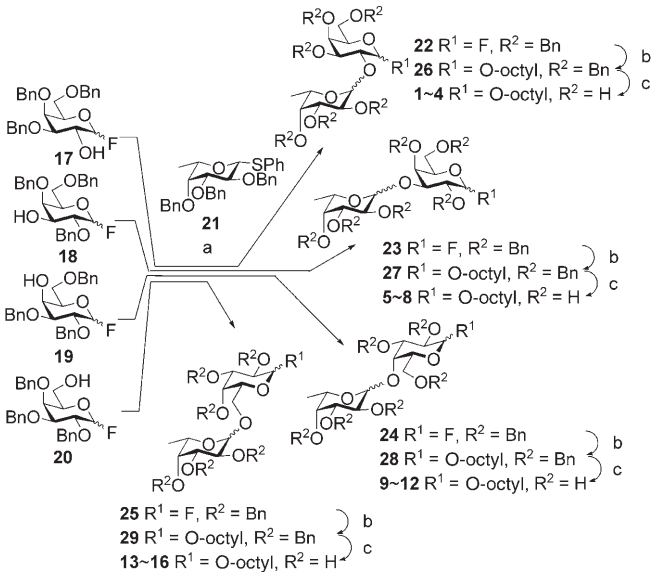

Scheme 1. a) DMTST, MS-AW300, $C_2H_4Cl_2/CH_3CN$ (1:1), 0°C, 4 h; b) *n*-octanol, $[Cp_2Hf(OTf)_2]$, MS-AW300, $C_2H_4Cl_2/CH_3CN$ (1:1), −20°C, 4 h; c) H_2, Pd/C, MeOH. Bn = benzyl.

hydrophilic by-products after complete deprotection. This approach is considered particularly useful in solid-phase synthesis.[20] The octyl glycosides **26**–**29** were subjected to hydrogenation and purified roughly by using a C18 cartridge column (Sep-Pak). Ideally, only compounds with an octyl group were collected at this stage (compounds with 2-, 3-, 4-, and 6-linked Fuc-Gal were isolated in 58, 49, 65, and 68% yield, respectively, over three steps). Finally, anomeric mixtures were separated by HPLC with a C18 column to give the individual anomers **1**–**16**. Chemical shifts and coupling constants for the anomeric positions, retention times, and compound ratios are summarized in Table 2.[24,31]

Such a library might be used to obtain information regarding the specificities of various enzymes, especially in connection with methods of structural elucidation.[32] A preliminary assay of a library of 16 compounds with an α(1→2)-"specific" fucosidase from *Corynebacterium*[33,34] revealed that several compounds: **1** (0.5), **3** (4.0), **5** (1.0), **7** (1.2) and **15** (0.7), were accepted as substrates. (The numbers in parentheses indicate the hydrolysis rate relative to that of αFuc(1→2)βGal(1→4)Glc.) Compound **1** with an α-Gal moiety was found unexpectedly to undergo very slow hydrolysis, as well as α(1→3)-linked **5** and **7**, and α(1→6)-linked **15**. Although no information regarding the structure of this particular enzyme is available, it is possible that the 2-OH group of Gal in **5** and **7** may occupy the same space as the 3-OH group in **3** and the reference compound. The presence of these groups may not be essential, as PNP-fucoside (*p*-nitrophenyl α-fucoside) is a better substrate, but they do not

Table 2: Properties of compounds **1**–**16**.

	Fuc		Gal		t_R[b] [min]	Ratio of anomers[c]
	δ [ppm][a]	J [Hz][a]	δ [ppm][a]	J [Hz][a]		
1	5.05	3.6	5.02	3.5	73.3	12.0
2	4.45	7.9	5.08	3.7	46.4	1.0
3[21]	5.26	3.6	4.62	7.9	93.3	37.0
4	4.67	7.8	4.54	7.3	49.0	21.0
5	5.13	4.0	4.94	3.7	87.4	1.0
6	4.67	7.8	4.97	3.8	140	1.0
7	5.15	3.9	4.43	7.4	74.2	1.7
8	4.49	7.8	4.42	8.0	123	1.6
9	5.12	4.0	4.94	3.1	62.4	1.0
10	4.33	7.8	4.95	3.2	49.8	3.1
11	5.14	3.9	4.41	7.9	54.4	7.8
12	4.31	7.7	4.41	7.9	36.9	4.2
13	4.94	3.3	4.90	3.6	39.7	1.0
14	4.38	7.9	4.91	3.7	78.7	1.9
15	4.93	3.9	4.38	7.9	46.9	6.4
16	4.39	7.9	4.39	7.9	82.7	15.0

[a] NMR spectra (500 MHz) were recorded in D_2O at 298 K (DOH: δ = 4.768 ppm). [b] Retention time was measured by LC–MS; for conditions and chromatograms, see the Supporting Information. [c] Ratios of anomers were estimated from the LC–MS spectra on the basis of the assumption that in each case both anomers were ionized similarly. The ratio of the major isomer to the minor isomer of the same sequence is given.

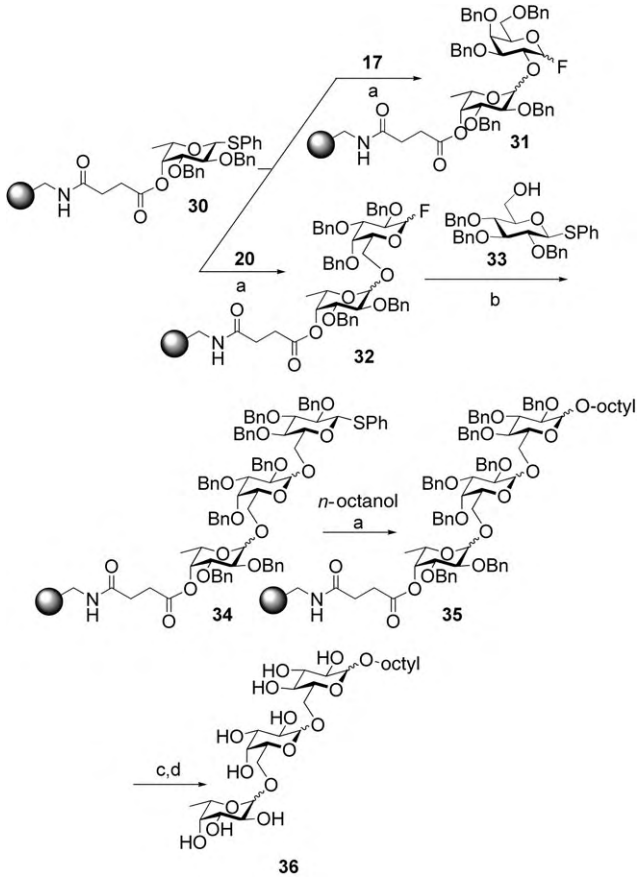

Scheme 2. a) DMTST, $C_2H_4Cl_2/CH_3CN$ (1:1), −30→0°C (2.5°C h^{-1}); b) $[Cp_2Hf(OTf)_2]$, $C_2H_4Cl_2/CH_3CN$ (1:1), −15→0°C (1.25°C h^{-1}); c) NaOMe/MeOH/$C_2H_4Cl_2$; d) H_2, $Pd(OH)_2$/C, MeOH/EtOAc (1:1).

 © 2006 Wiley-VCH Verlag GmbH & Co. KGaA, Weinheim

interfere with binding or catalysis. Interference by aglycons in α-linked Gal moieties with the surface of the protein may be responsible for the difference in the observed activity.

Having confirmed the eligibility of the orthogonal-glycosylation protocol in a library synthesis, we next investigated a combined method with solid-phase chemistry. Studies with potential orthogonal glycosyl donors attached to a solid support have been reported, but only single glycosylation reactions were carried out.[17–19] We conducted solid-phase reactions in which the glycosyl donor was linked to a bead through a succinyl ester (see **30**; Scheme 2).[24] Glycosylation with the acceptors **17** and **20**, which contain a secondary and a primary hydroxy group, respectively, proceeded smoothly to give the resin-bound disaccharides **31** and **32**, each of which consists of a mixture of anomers.[35] The excellent performance of the reactions was confirmed by the formation of disaccharides (determined by ESI MS) upon the treatment of a few beads with methanolic NaOMe (Figure 1 A).[36] The disaccharide fluoride **32** thus obtained was subjected to a further glycosylation reaction with **33**, which has a hydroxy group at C6 and a phenylthio group at C1, in the presence of $[Cp_2Hf(OTf)_2]$, to give **34** (Figure 1 B). Compound **34** underwent glycosylation with *n*-octanol readily with DMTST as a promoter. (For MS analysis of the trisaccharide, see Figure 1 C.) After hydrogenolysis, the anomeric mixture **36** was obtained in 33 % yield (five steps) by using a Sep-Pak column, which removed all accumulated by-products (Figure 1 D). The incorporation of a hydrophobic tag in the final step on the solid support is important, as then only the compounds with that tag are isolated. The yield of the glycosylation reaction in this solid-phase synthesis (glycosylation at the primary hydroxy group) was 72 %, which is comparable to that of the solution reaction (76 %).[37]

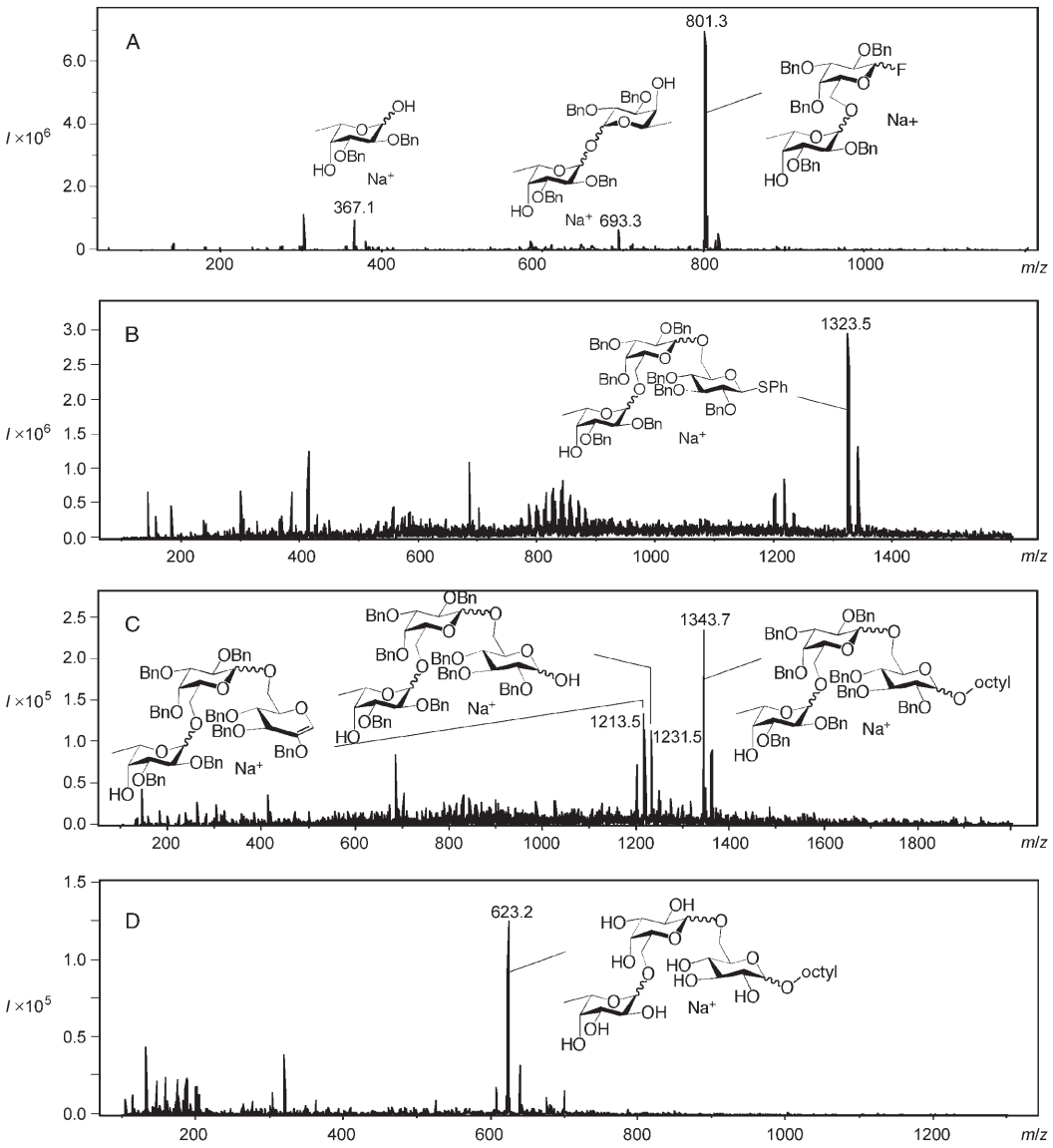

Figure 1. Mass spectra of glycosylation products. Spectra of the A) disaccharide, B) trisaccharide, C) octyl trisaccharide, and D) deprotected octyl trisaccharide **36** after purification by using a Sep-Pak C18 cartridge column.

In summary, we synthesized a library consisting of a complete set of structural isomers with Fuc-Gal sequences as octyl glycosides. Furthermore, in an assay of the library compounds, unexpected substrate specificity of fucosidase was discovered. The successful extension of an orthogonal-glycosylation protocol to solid-phase synthesis and the demonstration of a result comparable to that observed for the solution reaction suggest the potential usefulness of the present method in future combinatorial oligosaccharide synthesis.

Received: February 1, 2006
Published online: April 28, 2006

Keywords: chemoselectivity · compound libraries · glycosylation · oligosaccharides · solid-phase synthesis

[1] A. Varki, *Glycobiology* **1993**, *3*, 97–130.
[2] H. Paulsen, *Angew. Chem.* **1982**, *94*, 184–201; *Angew. Chem. Int. Ed. Engl.* **1982**, *21*, 155–175.
[3] R. R. Schmidt, *Angew. Chem.* **1986**, *98*, 213–236; *Angew. Chem. Int. Ed. Engl.* **1986**, *25*, 212–235.

 © 2006 Wiley-VCH Verlag GmbH & Co. KGaA, Weinheim

[4] G.-J. Boons, *Tetrahedron* **1996**, *52*, 1095 – 1121.
[5] S. J. Danishefsky, K. F. McClure, J. T. Randolph, R. B. Ruggeri, *Science* **1993**, *260*, 1307 – 1309.
[6] O. J. Plante, E. R. Palmacci, P. H. Seeberger, *Science* **2001**, *291*, 1523 – 1527.
[7] *Solid Support Oligosaccharide Synthesis and Combinatorial Carbohydrate Libraries* (Ed.: P. H. Seeberger), Wiley-Interscience, New York, **2001**, and references therein.
[8] T. Kanemitsu, O. Kanie, *Comb. Chem. High Throughput Screening* **2002**, *5*, 339 – 360.
[9] Y. Ito, S. Manabe, *Curr. Opin. Chem. Biol.* **1998**, *2*, 701 – 708.
[10] L. Yan, C. M. Taylor, R. Goodnow, Jr., D. Kahne, *J. Am. Chem. Soc.* **1994**, *116*, 6953 – 6954.
[11] O. Kanie, F. Barresi, Y. Ding, J. Labbe, A. Otter, L. S. Forsberg, B. Ernst, O. Hindsgaul, *Angew. Chem.* **1995**, *107*, 2912 – 2915; *Angew. Chem. Int. Ed. Engl.* **1995**, *34*, 2720 – 2722.
[12] R. Liang, L. Yan, J. Loebach, M. Ge, Y. Uozumi, K. Sekanina, N. Horan, J. Gildersleeve, C. Thompson, A. Smith, K. Biswas, W. C. Still, D. Kahne, *Science* **1996**, *274*, 1520 – 1522.
[13] G.-J. Boons, B. Heskamp, F. Hout, *Angew. Chem.* **1996**, *108*, 3053 – 3056; *Angew. Chem. Int. Ed. Engl.* **1996**, *35*, 2845 – 2847.
[14] M. Izumi, Y. Ichikawa, *Tetrahedron Lett.* **1998**, *39*, 2079 – 2082.
[15] T. Kanemitsu, C.-H. Wong, O. Kanie, *J. Am. Chem. Soc.* **2002**, *124*, 3591 – 3599.
[16] O. Kanie, Y. Ito, T. Ogawa, *J. Am. Chem. Soc.* **1994**, *116*, 12073 – 12074.
[17] L. O. Kononov, Y. Ito, T. Ogawa, *Tetrahedron Lett.* **1997**, *38*, 1599 – 1602.
[18] T. Doi, M. Sugiki, H. Yamada, T. Takahashi, J. A. Porco, Jr., *Tetrahedron Lett.* **1999**, *40*, 2141 – 2144.
[19] J. Ferguson, C. Marzabadi, *Tetrahedron Lett.* **2003**, *44*, 3573 – 3577.
[20] M. M. Palcic, L. D. Heerze, M. Pierce, O. Hindsgaul, *Glycoconjugate J.* **1988**, *5*, 49 – 63.
[21] T. Lowary, O. Hindsgaul, *Carbohydr. Res.* **1993**, *249*, 163 – 195.
[22] U. J. Nilsson, E. J.-L. Fournier, O. Hindsgaul, *Bioorg. Med. Chem.* **1998**, *6*, 1563 – 1575.
[23] K. Suzuki, I. Ohtsuka, T. Kanemitsu, T. Ako, O. Kanie, *J. Carbohydr. Chem.* **2005**, *24*, 219 – 236.
[24] I. Ohtsuka, T. Ako, R. Kato, S. Daikoku, S. Koroghi, T. Kanemitsu, O. Kanie, *Carbohydr. Res.* **2006**, in press.
[25] M. Ravenscroft, R. M. G. Roberts, J. G. Tillett, *J. Chem. Soc. Perkin Trans. 2* **1982**, 1569 – 1572.
[26] P. Fügedi, P. J. Garegg, *Carbohydr. Res.* **1986**, *149*, C9 – C12.
[27] K. Suzuki, H. Maeta, T. Matsumoto, G. Tsuchihashi, *Tetrahedron Lett.* **1988**, *29*, 3571 – 3574.
[28] K. Suzuki, H. Maeta, T. Matsumoto, *Tetrahedron Lett.* **1989**, *30*, 4853 – 4856.
[29] K. C. Nicolaou, T. J. Caulfield, H. Kataoka, N. A. Stylianides, *J. Am. Chem. Soc.* **1990**, *112*, 3693 – 3695.
[30] Y. Ito, S. Nunomura, S. Shibayama, T. Ogawa, *J. Org. Chem.* **1992**, *57*, 1821 – 1831.
[31] HRMS values obtained for compounds **1**–**16** were within the generally tolerated range.
[32] C. J. Edge, T. W. Rademacher, M. R. Wormald, R. B. Parekh, T. D. Butters, D. R. Wing, R. A. Dwek, *Proc. Natl. Acad. Sci. USA* **1992**, *89*, 6338 – 6342.
[33] A. Sano, T. Sakai, K. Hayakawa, I. Kato, *Glycoconjugate J.* **1991**, *8*, 271.
[34] K. Yamashita, K. Totani, Y. Iwaki, M. Kuroki, Y. Matsuoka, T. Endo, A. Kobata, *J. Biol. Chem.* **1989**, *264*, 17873 – 17881.
[35] Solid-phase reactions were carried out in the absence of molecular sieves to avoid problems such as clogging and/or resin breakdown.
[36] The yield of the solid-phase reaction was not determined at each step. Instead, the overall yield was calculated after deprotection and Sep-Pak purification. Experimental details and the structural assignments of all anomers will be reported elsewhere.
[37] The calculation was based on the assumption of a quantitative yield for the hydrogenolysis and 90% yield for the cleavage reaction. Calculations were based on the data obtained for O6-linked saccharides.

 © 2006 Wiley-VCH Verlag GmbH & Co. KGaA, Weinheim

Quinone Complexes

DOI: 10.1002/anie.200600414

A η^4-Dithio-*para*-benzoquinone Metal Complex**

*Jamal Moussa, Daniel A. Lev, Kamal Boubekeur, Marie Noelle Rager, and Hani Amouri**

Although the chemistry of *para*-benzoquinone is well documented,[1] very little is known about the related dithio-*para*-benzoquinone. Unlike benzoquinones, the sulfur analogues are highly reactive owing to their instability, making their handling and isolation in pure form a difficult task. Thus, examples of isolated thioquinones are scarce, the parent compound **1** (Scheme 1) has only been generated and characterized spectroscopically at low temperature (10 K) in an argon matrix.[2] Oda and co-workers reported the synthesis of 2,6-di-*tert*-butyl-1-thio-1,4-benzoquinone, where the presence of two *tert*-butyl groups at the 2- and 6-positions offers steric protection and increases the stability of the monothiobenzoquinone.[3] More recently Cava and co-workers

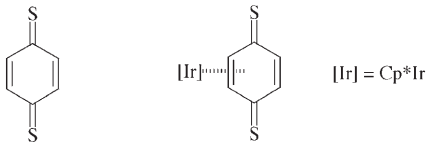

1 **4**

Scheme 1.

[*] J. Moussa, Pr. K. Boubekeur, Dr. H. Amouri
Laboratoire de Chimie Inorganique et Matériaux Moléculaires
UMR CNRS 7071; Université Pierre et Marie Curie
4 place Jussieu, case 42, 75252 Paris Cedex 05 (France)
Fax: (+33) 1–4427–3841
E-mail: amouri@ccr.jussieu.fr

Dr. M. N. Rager
NMR Services de l'Ecole Nationale Supérieure de Chimie de Paris
11 rue Pierre et Marie Curie, 75231 Paris Cedex 05 (France)

Dr. D. A. Lev
Northwestern University School of Law
357 East Chicago Avenue, Chicago, IL 60611 (USA)

[**] This work was supported by the CNRS and by the Université Pierre et Marie Curie which we gratefully acknowledge.

WILEY InterScience DISCOVER SOMETHING GREAT
© 2006 Wiley-VCH Verlag GmbH & Co. KGaA, Weinheim

reported the synthesis of dithioanthraquinone analogue in 16% yield after several steps: first annelation of thiophene rings to benzoquinone produced the anthraquinone analogue, and subsequent treatment with Lawesson's reagent and/or Davy reagent for 18 h produced the mono- and the dithioanthraquinone analogues.[4] These procedures illustrate the difficulty in isolating and stabilizing thioquinones.

In contrast, we report herein a rational synthetic procedure to isolate and fully characterize the first stable η^4-dithio-*para*-benzoquinone complex **4** (Scheme 1). The parent compound **1** was obtained as the iridium complex [Cp*Ir(η^4-$C_6H_4S_2$)] (**4**; Cp* = C_5Me_5) which was fully characterized including the first X-ray structure of **1** as a metal complex.

In a previous work we reported the first example of metal stabilized *ortho*-quinone methide, and showed that the {Cp*Ir} fragment can stabilize this highly reactive intermediate through η^4-coordination to the internal diene moiety of the simple quinone methide.[5] Pursuing our research in the "stabilization of reactive intermediates",[6] we discovered that {Cp*Ir} can also stabilize the elusive dithio-*para*-benzoquinone intermediate. Our synthetic approach is completely different than that reported for the quinone methide. It involves the synthesis of the complex [Cp*Ir(η^6-$C_6H_4Cl_2$)-$[BF_4]_2$ (**3**), substitution of the chlorides by (HS^{-1}), and deprotonation by a base, to provide **4** in high yield (Scheme 2).

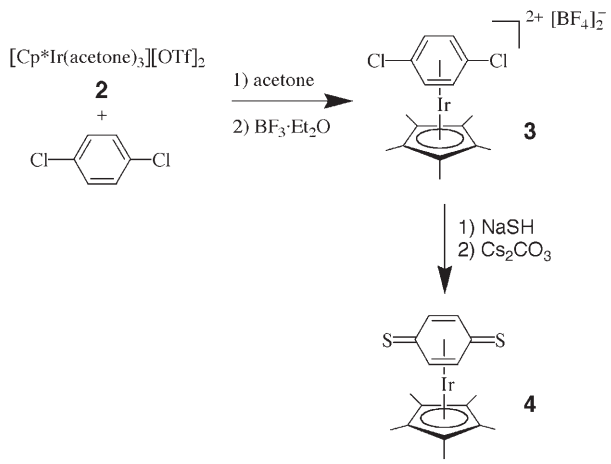

Scheme 2.

Treatment of an excess of 1,4-dichlorobenzene with the solvated iridium complex $[Cp^*Ir(acetone)_3][OTf]_2$ (**2**; OTf = $[CF_3SO_3]^-$) and then with $BF_3{\cdot}Et_2O$ solution gave **3** in 80% yield as a white microcrystalline complex. This air and moisture sensitive compound was completely characterized. The ^1H NMR spectrum recorded in CD_3NO_2, showed two singlets at $\delta = 7.82$ ppm, attributed to the aromatic protons, and at $\delta = 2.48$ ppm, attributed to the methyl protons of {Cp*Ir}. The ^{19}F NMR spectrum showed a singlet at −153.6 ppm designated to free BF_4 anion.[7] Further the IR spectrum also showed an intense band at 1083 cm^{-1} attributed to BF_4 anions. The ^{13}C NMR spectrum is in accord with the proposed formula (see Experimental Section). We then treated the white powder complex **3** with an excess of dried NaSH in CH_3CN for 20 min. Subsequent deprotonation with Cs_2CO_3 provided the neutral η^4-dithio-*para*-benzoquinone complex **4** which was obtained as orange microcrystalline material, analytically pure, and stable under argon. The IR spectrum recorded in KBr displayed a sharp band at 1096 cm^{-1} that we attribute to C=S vibration. This thiocarbonyl stretching frequency is lower than that of the free monothio-1,4-benzoquinone (1141 cm^{-1}).[3] Such a trend has been observed for the C=O vibration in the related free and metallated 1,4-benzoquinone.[8] The IR data for dithio-*para*-benzoquinone complexes have not been reported before.

The structure of **4** was confirmed by a single-crystal X-ray diffraction study. Crystals of **4** were grown by vapor diffusion of diethyl ether into a solution of the complex in CH_2Cl_2.[9] Complex **4** crystallizes with one molecule of CH_2Cl_2 in the monoclinic unit cell with space group $P2_1/m$. The asymmetric unit consists of three half complexes (I, II and III; Figure 1a) and one quarter molecule of CH_2Cl_2. Complexes I, II, and III are generated by the crystallographic mirror plane. Further, the CH_2Cl_2 molecule lies also on the plane of symmetry and occupies four sites (25% occupation) in the unit cell. Molecules I and II show π–π interactions between a) the {Cp*Ir} moiety of molecule I and the η^4-$C_6H_4S_2$ unit of II (d = 3.565(4) Å and $\alpha = 21.30(12)°$) and b) the {Cp*Ir} moiety of molecule II and the η^4-$C_6H_4S_2$ unit of complex I (d = 3.631(3) Å and $\alpha = 17.69(15)°$) providing a one-dimensional supramolecular chain (Figure 1b). The distance between the closest sulfur atoms of two independent molecules II and III is 4.23 Å, suggesting absence of an interatomic contact (sum of van der Waals radii of sulfur is 3.7 Å).[10] The structure of **4** clearly shows the {Cp*Ir} moiety is coordinated to only four diene carbons of the π-thioquinone ligand (Figure 1c). The average values of the Ir–C1 and Ir–C4 distances are longer (2.367, 2.358 Å) than those of the diene subunit (Ir–C3, Ir–C2: average bond lengths 2.206, 2.214 Å) in molecules I–III. Further, the η^4-thioquinone ligand acquires a boat-like conformation with the thioquinoid carbon atoms bent out the diene plane by $\theta = 8.22(0.7)°$ and $\theta = 8.21(0.4)°$ in molecule I, in molecule II the two dihedral angles are θ = 8.49(0.6)°, $\theta = 7.69(0.3)°$ and in molecule III $\theta = 12.94$ (0.8) and $\theta = 10.04(1.1)$. These angle values are smaller than those reported for the analogous iridium benzoquinone complex ($\theta = 16°$).[8a] The average C–S bond lengths for the three independent molecules are 1.719, 1.705, and 1.710 Å, which gives an overall average of 1.711 Å and characteristic of a partial double bond character (see below). This bond length is shorter than simple C–S bond of 1.796 Å reported for 1,4-benzenedithiol[11] and of 1.766 Å for 4,4′-biphenyldithiol[12] but comparable to C=S bonds of 1.674–1.702 Å reported for thiourea compounds.[13] To our knowledge this is the first X-ray structure of the parent thioquinone complex.

Protonation of a suspension of **4** in CH_3CN by $HBF_4{\cdot}Et_2O$, resulted in a rapid color change, giving rise to a light yellow solution. Reaction work up allowed the isolation of the related dithiophenol complex [Cp*Ir(η^6-HSC_6H_4SH)]$[BF_4]_2$ (**5**) in 93% yield as a pale yellow microcrystalline solid. Compound **5** was characterized by spectroscopic data (^1H NMR, IR). For instance the ^1H NMR of **5** recorded in CD_3CN

 © 2006 Wiley-VCH Verlag GmbH & Co. KGaA, Weinheim

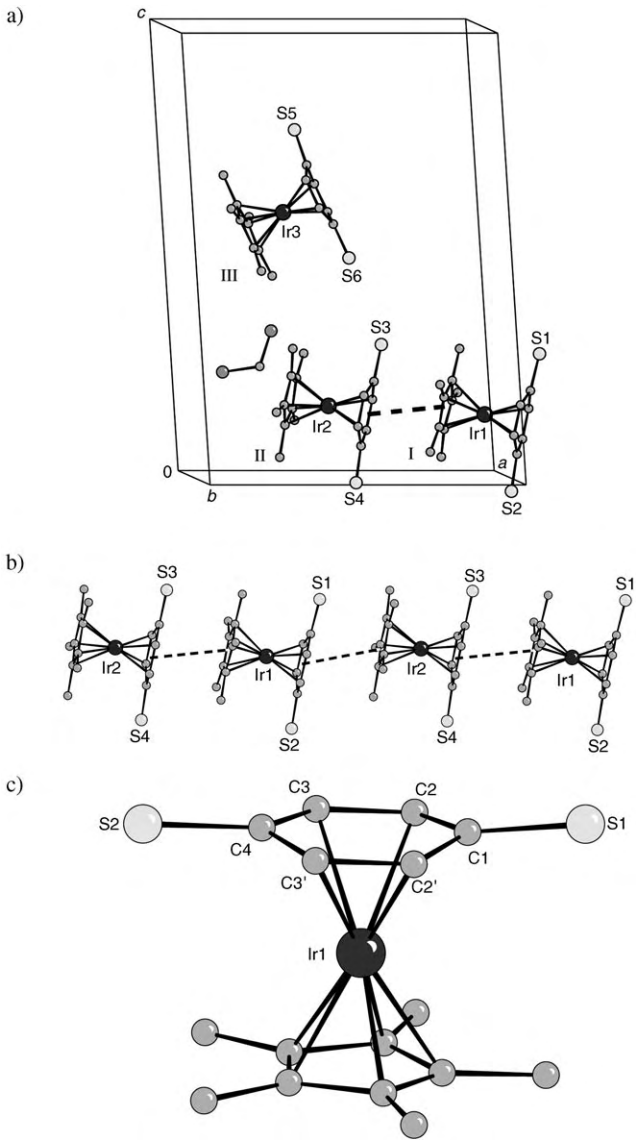

Figure 1. X-ray molecular structure of $[Cp^*Ir(\eta^4\text{-}C_6H_4S_2)]$ (**4**). a) Unit cell of **4** showing the three independent molecules (I, II, III) of the asymmetric unit. b) 1 D supramolecular chain formed through π–π contacts between molecules I and II. c) Selected bond lengths [Å] and angles [°] for **4** molecule I: Ir1–C1 2.353(8) , Ir1–C2 2.210(6), Ir1–C3 2.219(5), Ir1–C4 2.346(7), C1–S1 1.726(10), C4–S2 1.713(9); C2-C1-C2′ 114.2(9), C3-C4-C3′ 115.0(8). Dashed lines indicates π–π interactions.

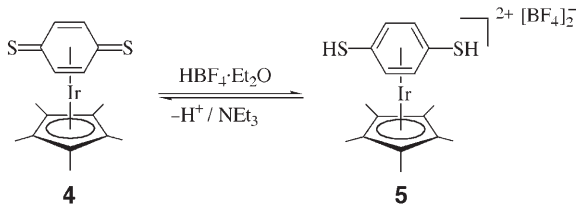

Scheme 3.

showed a singlet at $\delta = 1.98$ ppm attributed to the methyl protons of the {Cp*Ir} fragment and another singlet at $\delta =$ 7.15 ppm assigned to the aromatic protons that integrates to four protons. Upon treatment of the NMR-tube sample of **5** in CD_3CN with NEt_3, the starting material **4** was recovered (Scheme 3).

To understand the role of {Cp*Ir} in stabilization of the short-lived *para*-dithiobenzoquinone, we have taken an ab initio computational approach employing the hybrid density functional theory (DFT) B3LYP method.[14] Previous computational studies have examined related organic compounds, notably the *para*-benzodithiyl radical anion and *ortho*-dithiobenzoquinone.[15] This study is the first computational analysis of a *para*-dithiobenzoquinone metal complex. Initially, we examined the electronic structure of the geometry of **4** determined from the X-ray diffraction experiments. These calculations were performed at the B3LYP/LANL2DZ** level.[14] For comparison, we performed similar calculations at the B3LYP/cc-pVTZ level on the free *para*-dithiobenzoquinone ligand **1**, in the same geometry as in the metal complex except without the {Cp*Ir} fragment. The advantage of calculating the electronic structure of **1** in the same geometry it adopts when complexed to the metal in **4** is to obtain a more accurate picture of the role of the {Cp*Ir} fragment in stabilizing the reactive compound. Minimization of the energy of **1** in geometric space further revealed that the ligand geometry is a local minimum for **1**.

The atomic charge densities for **4** and **1** are summarized in Table 1. Population analyses according to standard Mulliken analysis and natural population analysis (NPA) were performed on both **4** and **1**. It is immediately apparent that the two methods assign drastically different charges to the iridium center, differing by more than one electronic charge unit. Such a behavior has also been observed for the iridium *ortho*-quinone methide complexes.[16] The distribution of charge on the *para*-dithiobenzoquinone ligand is more consistent in the two calculation methods. However, the NPA method assigns more total negative charge to the ligand and approximately 0.1 additional electronic charge units on each sulfur atom. The difference between Mulliken and NPA analyses for **1** is less pronounced than for **4**, but a significant difference in the distribution of charge between the sulfur atoms and the *ipso* carbon atoms arises. Mulliken analysis of the self consistent

Table 1: Charge density in *para*-dithiobenzoquinones **4** and **1**.

Atom	**4**		**1**	
	Mulliken	NPA	Mulliken	NPA
Ir	−0.4618	0.5777	–	–
C1	−0.2760	−0.2076	0.0134	−0.1447
C2	0.1511	0.0312	0.0659	0.0368
C6[a]	0.1526	0.0302	0.0659	0.0368
C3	0.1511	0.0358	0.0569	0.0501
C5[a]	0.1503	0.0362	0.0569	0.0501
C4	−0.2584	−0.2219	0.0207	−0.1530
S1	−0.1469	−0.2752	−0.1415	0.0573
S2	−0.1495	−0.2652	−0.1382	0.0667
Σ[b]	−0.2257	−0.8365	0	0

[a] As a result of the symmetry plane in complex **4** C5 and C6 denote C3′ and C2′, respectively. [b] Sum of electronic charge on *para*-dithiobenzoquinone ligand.

 © 2006 Wiley-VCH Verlag GmbH & Co. KGaA, Weinheim

field (SCF) density results in slightly positively charged carbon atoms and in sulfur atoms with excess electron density that is comparable to that in **4**. However, NPA assigns the positive charge to the sulfur atoms and the negative charge to the *ipso* carbon atoms.

Generally, stabilization of the reactive *para*-dithiobenzoquinone species is accomplished by π-backbonding from d orbitals on the metal to the ligand π* orbitals. Mulliken population analysis reveals a net increase in the electron count of the ligand by 0.2, while according to NPA this value is about 0.8. This situation results in lengthening of the C2–C3 and C3′–C2′ bonds in **4,** and of the corresponding bonds C2–C3 and C5–C6 in **1**, by about 0.1 Å relative to calculated dithiobenzoquinone bond lengths.[15b] The atomic orbital analysis phase of the NPA reveals an occupancy for the degenerate iridium d_{xy} and d_{yz} orbitals of 1.368 and 1.216, respectively. This occupation represents a deficiency in these orbitals of about 0.4–0.5 electrons relative to the other iridium d orbitals. The additional electron density is almost entirely localized on the thiocarbonyl group, resulting in a C=S bond length of 1.72 Å that is intermediate between the values 1.77 and 1.62 which are typical of single and double CS bonds.[17] For comparison, the radical *para*-benzodithiyl anionic species also has a net gain of one electron in the ring, in which the radical anion is almost entirely located on the sulfur atoms.[15a] The similarity between this compound and **4** is further supported by the thiocarbonyl bond stretching frequency, which is 1096 cm^{-1} for **4** and 1081 cm^{-1} for the radical anion. The calculated C=S bond length, 1.70 Å, for the radical anion is also longer than would be expected for a typical double bond. In contrast, the calculated bond lengths in the free neutral ligand are 1.62 Å for C=S, 1.33 Å for C=C, and 1.46 for C–C, and the calculated C=S bond stretching frequency is 1123 cm^{-1}.[15a] These results are identical to those calculated for the *ortho*-substituted compound.[15]

Natural bond orbital (NBO) analysis supports localization of backbonding electron density on the C=S bonds. The results of this analysis are summarized in Table 2. The occupancy of the carbon–carbon π bonds in the ligand decrease upon binding to the iridium center. However, this decrease is more than compensated by an increase in electron density around the thiocarbonyl bonds. The NBO analysis confirms that the C=S bond is no longer formally a double bond, but the total occupancy of electrons around each thiocarbonyl bond increases by approximately 0.8 electrons when **1** complexes with the {Cp*Ir} fragment. This result is also consistent with the data obtained for the radical *para*-benzodithiyl anion, wherein the additional electron is localized on sulfur 3p orbitals.

In conclusion, we report the first isolation and complete characterization of an unsubstituted dithiobenzoquinone. This isolation is only possible through the use of the {Cp*Ir} moiety which stabilizes the elusive intermediate by forming an η^4-complex. The NMR spectroscopy data, IR stretching frequencies, and X-ray diffraction data support stabilization of this reactive species by metal-to-ligand π backbonding. Computational analyses using density functional theory confirm a net transfer of about 0.8 units of electron density to the π* ligand LUMO. This additional electron density is largely localized around the thiocarbonyl bonds, resulting in a reduction in C=S bond order as well as the anticipated decrease in C=C bond order. This result provides further confirmation of the versatility of the {Cp*Ir} fragment in stabilizing reactive π systems. We intend to use complex **4** as an organometallic linker in a similar way to the related benzoquinone metal complex[18] to construct novel supramolecular coordination polymers.

Table 2: Occupancy of natural bond orbitals calculated with an occupancy threshold of 1.50.

Bond	**4**		**1**	
	BD = 1	BD = 2	BD = 1	BD = 2
C1–S1	1.9725	–[a]	1.9827	1.7826[b]
C4–S2	1.9754	–[c]	1.9850	1.7921[d]
C1–C2	1.9680	–	1.9849	–
C2–C3	1.9621	1.5285	1.9764	1.7383
C3–C4	1.9682	–	1.9859	–
C4–C5[e]	1.9682	–	1.9859	–
C5–C6[e]	1.9622	1.5282	1.9764	1.7383
C1–C6[e]	1.9680	–	1.9849	–

[a] According to this analysis of **4**, C1 has a nonbonding 2p orbital with an occupancy of 0.9836 and S1 has three nonbonding lone pairs with occupancies of 1.9772, 1.9236, and 1.5679. [b] S1 has two lone pairs in the free ligand with occupancies of 1.9865 and 1.9398. [c] According to this analysis of **4**, C4 has a nonbonding 2p orbital with an occupancy of 0.9872 and S2 has three nonbonding lone pairs with occupancies of 1.9764, 1.9201, and 1.5590. [d] S2 has two lone pairs in the free ligand with occupancies of 1.9858 and 1.9368. [e] As a result of the symmetry plane in complex **4** C5 and C6 denote C3′ and C2′, respectively. BD = two-centered bond.

Experimental Section

All experimental manipulations were carried out under argon using Schlenk tube techniques. The ^1H and ^{13}C and ^{19}F NMR spectra were recorded in CD_2Cl_2, CD_3CN, and CD_3NO_2 using a Bruker Avance 400 NMR spectrometer at 400.13 and 100.61 and 376.45 MHz respectively. IR spectra were recorded from KBr discs on a Bio-Rad FT-IR spectrometer FTS 165. All calculations were carried out using the Gaussian 03 program package.[14] All structures were first computed at the B3LYP level using the LANL2DZ basis set as it is implemented in the Gaussian programs. This basis set uses the effective core potential of Hay and Wadt to describe the core electrons of the metal atom, Ir (341/321/21). The valence electrons of the metal atom in addition to those of H, C, and S are treated by the Dunning–Huzinaga double-ζ basis set (D95). These basis sets were augmented by the addition of a single polarization function to all H, C, S, and Ir atoms, designated in the text as LANL2DZ**.

3 : A solution of $AgCF_3SO_3$ (520 mg, 2 mmol) in acetone (10 mL) was added to $[\{Cp^*Ir(\mu\text{-}Cl)Cl\}_2]$ (400 mg, 0.5 mmol) in acetone (5 mL) and rapidly gave a white precipitate of AgCl. The reaction mixture was stirred for 15 min then the resulting yellow solution of $[Cp^*Ir(acetone)_3][BF_4]_2$ (**2**) was filtered under argon into a dry Schlenk tube containing 1,4-dichlorobenzene (1.45 g, 10 mmol) and the solvent was removed under vacuum. $BF_3{\cdot}Et_2O$ (2 mL) was added to the yellow residue which immediately decolorized. The mixture was stirred for 30 min at room temperature, then diethyl ether (60 mL) was added. Compound **3** precipitated as a white microcrystalline air sensitive powder which was collected by filtration and washed several times with diethyl ether (20 mL) and dried under vacuum. Yield: 80 %. (515 mg, 0.8 mmol). Elemental analysis (%) calcd for $C_{16}H_{19}IrB_2Cl_2F_8$ (648 g mol^{-1}): C 29.65, H, 2.96; found: C

 © 2006 Wiley-VCH Verlag GmbH & Co. KGaA, Weinheim

27.39, H 2.96. ^{1}H NMR (400 MHz, CD_3NO_2): $\delta = 2.48$ (s, 15 H, Cp*), 7.82 (s, 4 H, aromatic) ppm. ^{13}C{^{1}H}NMR (100 MHz, CD_3NO_2): $\delta =$ 8.3 (s, CH_3, Cp*), 108.5 (s, C_{ring}, Cp*), 99.4 (s, CH, aromatic), 114.9 (s, CCl, aromatic) ppm. ^{19}F NMR (376 MHz, CD_3NO_2): $\delta = -153.6$ (s, BF_4) ppm. IR (KBr disk): ν(B–F) 1083 cm^{-1}.

4 : A solution of **3** (340 mg, 0.52 mmol) in CH_3CN (10 mL) was added to a suspension of dried HSNa (360 mg, 6.0 mmol) in CH_3CN (5 mL) and the mixture was stirred for 20 min at room temperature then the solvent was r'emoved by evaporation under vacuum. The residue was extracted by CH_2Cl_2 (20 mL) and filtered through celite into Cs_2CO_3 (325 mg, 1 mmol) and the mixture was stirred for further 1 h. After filtration through celite, CH_2Cl_2 was evaporated under vacuum. Compound **4** was obtained as an orange microcrystalline powder (238 mg, 0.49 mmol). Yield: 95 %. M.p. 160 °C (decomp.) Elemental analysis (%) calcd for $C_{16}H_{19}IrS_2{\cdot}H_2O$ (486 g mol^{-1}): C 39.57, H 4.36, S 13.20; found: C 38.96, H 4.32, S 13.24. ^{1}H NMR (400 MHz, CD_2Cl_2): $\delta = 1.91$ (s, 15 H, Cp*), 5.96 (s, 4 H, aromatic) ppm. ^{13}C{^{1}H} NMR (100 MHz, CD_2Cl_2): $\delta = 7.1$ (s, CH_3, Cp*), 96.25 (s, C_{ring}, Cp*), 91.8 (s, CH, aromatic), 148.1 (s, C=S, aromatic) ppm. IR (KBr disk): ν(C=S) 1096 cm^{-1}.

Received: January 31, 2006
Published online: May 3, 2006

Keywords: coordination modes · iridium · quinones · reactive intermediates · structure elucidation

[1] S. Patai and Z. Rappoport, *The Chemistry of the Quinonoid Compounds*, Wiley, New York, 2nd ed., **1988**.
[2] H. Bock, S. Mohmand, T. Hirabayashi, G. Maier, H. P. Reisenauer *Chem. Ber.* **1983**, *116*, 273 – 281.
[3] R. Suzuki, K. Matsumoto, H. Kurata, M. Oda *Chem. Commun.* **2000**, 1357 – 1358.
[4] Y. A. Jackson, D. Rajagopal, J. Bendolph, M. Guillory, M. V. Lakshmikantham, J. Yang, M. P. Cava *Org. Lett.* **2003**, *5*, 1883 – 1885.
[5] H. Amouri, J. Le Bras, *Acc. Chem. Res.* **2002**, *35*, 501 – 510, and references therein.
[6] a) W. H. Hersh, R. G. Bergman *J. Am. Chem. Soc.* **1981**, *103*, 6992 – 6994; b) A. Vigalok, D. Milstein *J. Am. Chem. Soc.* **1997**, *119*, 7873 – 7874; c) D. B. Grotjahn, G. A. Bikzhanova, L. S. B. Collins, T. Concolino, K.-C. Lam, A. L. Rheingold *J. Am. Chem. Soc.* **2000**, *122*, 5222 – 5223; d) Q. Zheng, J. A. Gladysz *J. Am. Chem. Soc.* **2005**, *127*, 10508 – 10509.
[7] a) E. F. Mooney, *An Introduction to ^{19}F NMR spectroscopy*, Heyden&Son, Universities Press, Belfast, **1970**, chap. 6, p. 63; b) H. Amouri, M. N. Rager, F. Cagnol, J. Vaissermann *Angew. Chem.* **2001**, *113*, 3748 – 3750; *Angew. Chem. Int. Ed.* **2001**, *40*, 3636 – 3638; c) H. Amouri, L. Mimassi, M. N. Rager, B. E. Mann, C. Guyard-Duhayon, L. Raehm *Angew. Chem.* **2005**, *117*, 4619 – 4622; *Angew. Chem. Int. Ed.* **2005**, *44*, 4543 – 4546.
[8] a) J. Le Bras, H. Amouri, J. Vaissermann *Organometallics* **1998**, *17*, 1116 – 1121; b) J. Moussa, C. Guyard-Duhayon, P. Herson, H. Amouri, M. N. Rager, A. Jutand *Organometallics* **2004**, *23*, 6231 – 6238.
[9] Crystal data for **4**. Orange crystals: $C_{48}H_{57}Ir_3S_6{\cdot}1/2CH_2Cl_2$, monoclinic, $P2_1/m$, $a = 4.5450(5)$, $b = 9.92730(11)$, $c =$ 20.6380(3) Å, β=94.271(4)°, $V = 2775.8(5)$ Å^3, $Z = 2$, $T =$ 250(2) K, $\mu = 7.476$ mm^{-1}, 33263 reflections measured, 8342 independent ($R_{int} = 0.0413$), 6364 observed [$I = 2\sigma(I)$], 321 parameters, final R indices R_1 [$I = 2\sigma(I)$] = 0.0335 and wR_2 (all data) = 0.0956, GOF on $F^2 = 1.027$, max/min residual electron densit $y = 1.31/-1.34$ e Å^{-3}. A single crystal of the very moisture sensitive compound **4** was selected rapidly, mounted onto a glass fiber, and transferred in a cold nitrogen gas stream. Intensity data were collected with a Bruker-Nonius Kappa-CCD with graphite-monochromated Mo-Kα radiation. Unit-cell parameters determination, data collection strategy and integration were carried out with the Nonius EVAL-14 suite of programs (A. J. M. Duisenberg, L. M. J. Kroon-Batenburg, A. M. M. Schreurs, *J. Appl. Crystallogr.* **2003**, *36*, 220). The structure was solved by direct methods using the SHELXS-86 program (G. M. Sheldrick, University of Göttingen, **1986**) and refined anisotropically by full-matrix least-squares methods using the SHELXL-97 software package (G. M. Sheldrick, University of Göttingen, Germany, **1997**). CCDC-293581 (**4**) contains the supplementary crystallographic data for this paper. These data can be obtained free of charge from the Cambridge Crystallographic Data Centre via www.ccdc.cam.ac.uk/data request/cif.
[10] a) A. Bondi *J. Phys. Chem.* **1964**, *68*, 441 – 451; b) S.-Y. Kwon, J.-H. Cho, H.-I. Lee, U. Lee, D.-Y. Noh *Inorg. Chem. Commun.* **2001**, *8*, 510 – 512.
[11] T. Ohashi, E. Kobayashi, T. Jinbo, J. Furukawa *J. Polym. Sci. A. Polym. Chem.* **1997**, *35*, 1621 – 1625.
[12] M. Ratajczak-Sitarz, A. Katrusiak, Z. Kaluski, J. Garbarczyk, *Acta. Cryst. C*, **1987**, *43*, 2389 – 2391.
[13] T. K. Venkatachalam, E. Sudbeck, F. M. Uckun *J. Mol. Struct.* **2005**, *751*, 41 – 54.
[14] Gaussian 03, Revision C.01, M. J. Frisch, G. W. Trucks, H. B. Schlegel, G. E. Scuseria, M. A. Robb, J. R. Cheeseman, J. A. Montgomery, Jr., T. Vreven, K. N. Kudin, J. C. Burant, J. M. Millam, S. S. Iyengar, J. Tomasi, V. Barone, B. Mennucci, M. Cossi, G. Scalmani, N. Rega, G. A. Petersson, H. Nakatsuji, M. Hada, M. Ehara, K. Toyota, R. Fukuda, J. Hasegawa, M. Ishida, T. Nakajima, Y. Honda, O. Kitao, H. Nakai, M. Klene, X. Li, J. E. Knox, H. P. Hratchian, J. B. Cross, C. Adamo, J. Jaramillo, R. Gomperts, R. E. Stratmann, O. Yazyev, A. J. Austin, R. Cammi, C. Pomelli, J. W. Ochterski, P. Y. Ayala, K. Morokuma, G. A. Voth, P. Salvador, J. J. Dannenberg, V. G. Zakrzewski, S. Dapprich, A. D. Daniels, M. C. Strain, O. Farkas, D. K. Malick, A. D. Rabuck, K. Raghavachari, J. B. Foresman, J. V. Ortiz, Q. Cui, A. G. Baboul, S. Clifford, J. Cioslowski, B. B. Stefanov, G. Liu, A. Liashenko, P. Piskorz, I. Komaromi, R. L. Martin, D. J. Fox, T. Keith, M. A. Al-Laham, C. Y. Peng, A. Nanayakkara, M. Challacombe, P. M. W. Gill, B. Johnson, W. Chen, M. W. Wong, C. Gonzalez, and J. A. Pople, Gaussian, Inc., Wallingford CT, 2004.
[15] a) G. N. R. Tripathi, D. M. Chipman, R. H. Schuler, D. A. Armstrong *J. Phys. Chem.* **1995**, *99*, 5264 – 5268; b) M. Mann, J. Fabian *Int. J. Quant. Chem.* **1996**, *60*, 859 – 874.
[16] D. A. Lev, D. B. Grotjahn, H. Amouri *Organometallics* **2005**, *24*, 4232 – 4240.
[17] F. H. Allen, O. Kennard, D. G. Watson, L. Brammer, A. G. Orpen, R. Taylor *J. Chem. Soc. Perkin Trans. 2.* **1987**, *12*, S1 – S19.
[18] J. Moussa, K. Boubekeur, H. Amouri *Eur. J. Inorg. Chem.* **2005**, 3808 – 3810.

 © 2006 Wiley-VCH Verlag GmbH & Co. KGaA, Weinheim

Carbocyclic Carbenes

DOI: 10.1002/anie.200503589

A Carbocyclic Carbene as an Efficient Catalyst Ligand for C–C Coupling Reactions**

Wolfgang A. Herrmann, Karl Öfele, Sabine K. Schneider, Eberhardt Herdtweck, and Stephan D. Hoffmann*

Dedicated to Professor Richard F. Heck on the occasion of his 75th birthday

Starting from the prototypes **I** and **II**[1] N-heterocyclic carbenes (NHCs) have proved to be efficient control ligands in organometallic homogeneous catalysis.[2–4] It could not have foreseen, but they are beginning to displace the classical organophosphanes as ligands. Metal complexes of NHCs generally have greater thermal and acid stability of their metal complexes; they frequently exhibit higher catalytic activities, are amenable to a broad range of structure variation, and are also successful as immobilized variants.[2] Prominent examples of their application are the activation of haloarenes and olefin metathesis.[2,4] We have now found that, as a control ligand, the simple, carbocyclic carbene **III** (cycloheptatrienylidene, CHT) is comparable with or even superior to the well-established NHCs. We describe this here with the example of the palladium complexes.

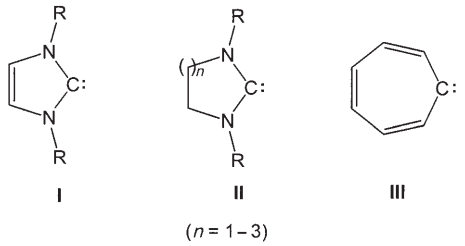

In a short reaction sequence 1,1-dichloro- and 1,1-dibromocycloheptatrienes (**1a** and **1b,** respectively) were transformed in good yield with palladium black into the mononuclear carbene complexes **4** and **5** by way of the binuclear complexes **2a**,**b** (π-allyl) and **3a**,**b** (σ,π-carbene) (Scheme 1). Complexes **4** and **5** were formed almost quantitatively when intermediates **2** and **3** were not isolated. The intermediate **2a** may be isolated by interruption of the reaction at an early stage, but it rearranges into the carbene complex **3a** during the further course of the reaction and during workup. The π-allyl complex **2a** and the carbene complex **4** were characterized by X-ray crystallography (Figures 1 and 2).[5,6] The constitution of the complex compounds in solution was established spectroscopically

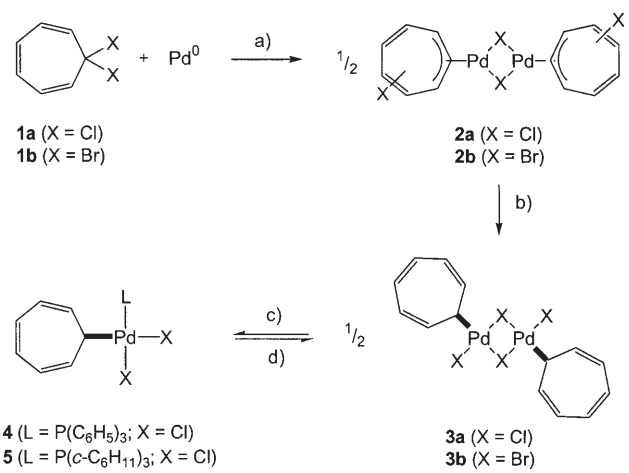

Scheme 1. Synthesis of CHT–palladium complexes: a) CH_2Cl_2, −10 °C; b) 40 °C (X = Cl) or 25 °C (X = Br); c) in C_6H_6, 1 equiv L = $P(C_6H_5)_3$ or $P(c\text{-}C_6H_{11})_3$; d) DMSO, ca. 150 °C.

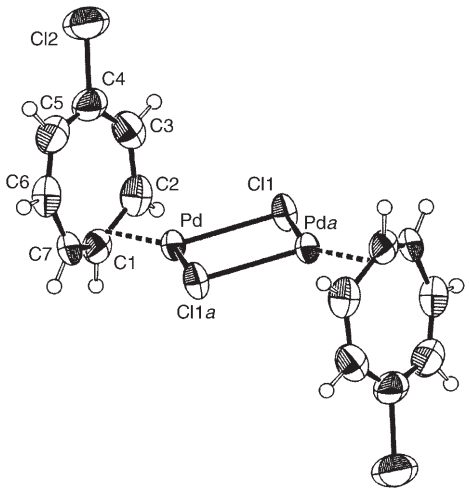

Figure 1. ORTEP drawing of **2a** in the crystal; thermal ellipsoids set at 50% probability. Selected bond lengths [Å] and angles [°]: Pd–Cl1 2.4588(9), Pd–Cl1*a* 2.4545(10), Pd–C1 2.073(4), Pd–C2 2.183(5), Pd–C7 2.179(4), Pd–Cg 1.870, C1–C2 1.415(6), C1–C7 1.385(6), C2–C3 1.450(7), C3–C4 1.353(7), C4–C5 1.402(7), C5–C6 1.328(6), C6–C7 1.433(6); Cl1-Pd-Cl1*a* 87.58(3), Pd-Cl1-Pd*a* 92.42(3), Cl1-Pd-Cg 134.10, Cl1*a*-Pd-Cg 136.80. Symmetry operations for the equivalent atom positions *a*: −*x*, 1−*y*, 1−*z*. Cg defines the mass center of the allylic system C1, C2, and C7.

[*] Prof. Dr. W. A. Herrmann, Dr. K. Öfele, Dipl.-Chem. S. K. Schneider, Dr. E. Herdtweck
Lehrstuhl für Anorganische Chemie
Technische Universität München
Lichtenbergstrasse 4, 85747 Garching (Germany)
Fax: (+49) 89-289-13473
E-mail: lit@arthur.anorg.chemie.tu-muenchen.de
Dr. S. D. Hoffmann
Lehrstuhl für Anorganische Chemie
mit Schwerpunkt Neue Materialien
Technische Universität München
Lichtenbergstrasse 4, 85747 Garching (Germany)

[**] This work was supported by the Deutsche Forschungsgemeinschaft and the Fonds der Chemischen Industrie (fellowship for S.K.S.).

 © 2006 Wiley-VCH Verlag GmbH & Co. KGaA, Weinheim

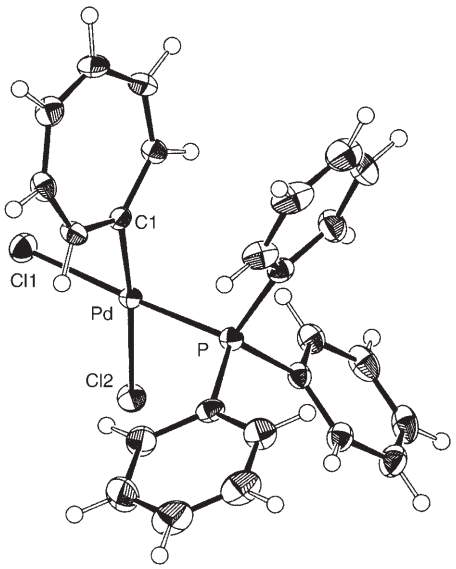

Figure 2. ORTEP drawing of **4** in the crystal; thermal ellipsoids set at 50% probability. Selected bond lengths [Å] and angles [°]: Pd–C1 1.968(2), Pd–Cl1 2.3697(6), Pd–Cl2 2.3884(7), Pd–P 2.2483(6); Cl1-Pd-Cl2 91.83(2), Cl1-Pd-P 175.89(2), Cl1-Pd-C1 85.14(7), Cl2-Pd-P 92.27(2), Cl2-Pd-C1 174.55(6), P-Pd-C1 90.76(7).

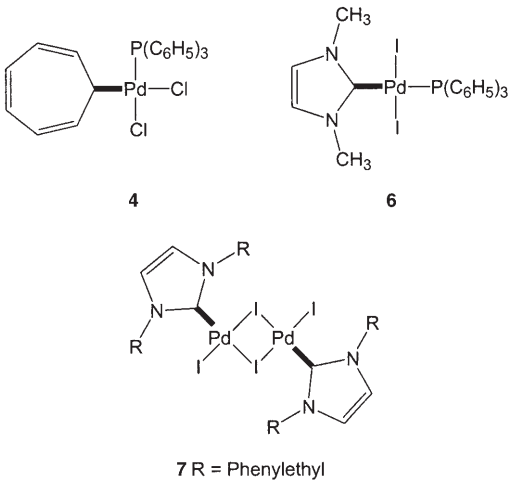

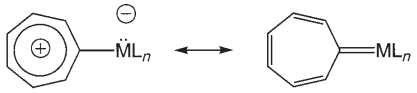

Scheme 2. Mesomeric resonance structures of CHT(6π)–metal complexes.

(see the Experimental Section). The bromo derivative **2b** reacts immediately to form the carbene complex **3b** and therefore cannot be isolated.

The C–C bonds of the cyclocarbene in complex **4** are almost all the same length (1.39 ± 0.02 Å), which suggests extensive 6π delocalization similar to that of the cycloheptatrienyl cation. The delocalization of the π system includes the carbene p orbital similar to that in the NHC ligands **I** and **II** so that π(M→C) backbonding contributes only minimally to the stabilization of the CHT complexes. Hence the cycloheptatrienylium resonance form (**a** in Scheme 2) is also favored in the literature for the low-valent metal complexes.[7] This is in agreement with the Pd–C distance in **4** which at 1.968(2) Å lies in the range typical for the NHCs **I** and **II**.[1,2] Clearly the C_7H_6 carbene is essentially a σ-donor ligand.

We used the route shown in Scheme 1 to prepare palladium complexes of cycloheptatrienylidene for the first time. This synthesis did not require special precursors for air- and temperature-sensitive metal(0) complexes such as $[Pt\{P(C_6H_5)_3\}_3]$ as was previously described by Jones et al.[8] Since our method has several steps (π-allyl intermediate!), we avoid formation of heptafulvalene, which would occur from the reductive coupling of the ligand precursor.[7a]

The carbocyclic carbene complex **4** gave good results in numerous variants of the Heck and Suzuki coupling reactions.[9] Thus *p*-bromoacetophenone and *n*-butyl acrylate underwent C–C coupling at 145 °C with only 10^{-4} mol% of catalyst **4**, which corresponds to turnover numbers (TON) of the order of 10^6 at turnover frequencies (TOF) of $\geqslant 10^3\,h^{-1}$ (Table 1, entry 1). Reaction of bromobenzene was also achieved (10^{-1} mol% cat) in 90% yield and with TON ≈ 10^4 (Table 1, entry 2). In all examples of the Heck coupling reaction investigated the NHC reference catalyst **6**[10] was inferior (Figure 3a). Unlike the NHC catalyst **6**, **4** did not require an induction period.

An analogous picture emerges for typical Suzuki coupling reactions (Figure 3b). With catalyst **4** (10^{-3} mol%) bromobenzene underwent quantitative coupling with phenylboronic

Table 1: Catalyzed Heck coupling.

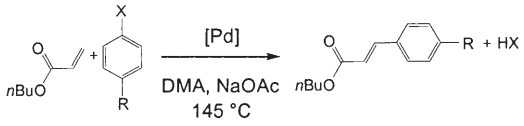

Entry	R	X	Cat.	PR'_3	mol% Pd	*t* [h]	Conv. [%][a]	Yield [%][a]	TON
1	$C(O)CH_3$	Br	**4**	–	10^{-4}	14	100	100	10^6
2	H	Br	**4**	–	0.1	14	92	90	9000
3	OCH_3	Br	**4**	–	0.1	14	43	42	420
4	OCH_3	Br	**4**	–	1	14	59	58	58
				–		35	66	65	65
				–		104	91	89	89
5	$C(O)CH_3$	Cl	**4**	–	1[b]	14	30	28	28
				–		35	63	58	58
				–		104	81	76	76
6	$C(O)CH_3$	Cl	**3a**	PCy_3	1[b]	14	76	75	75

[a] GC yield with diethylene glycol di-*n*-butyl ether as the internal standard. [b] Addition of $[nBu_4N]Br$ (0.2 equiv.), $T = 150$ °C.

 © 2006 Wiley-VCH Verlag GmbH & Co. KGaA, Weinheim

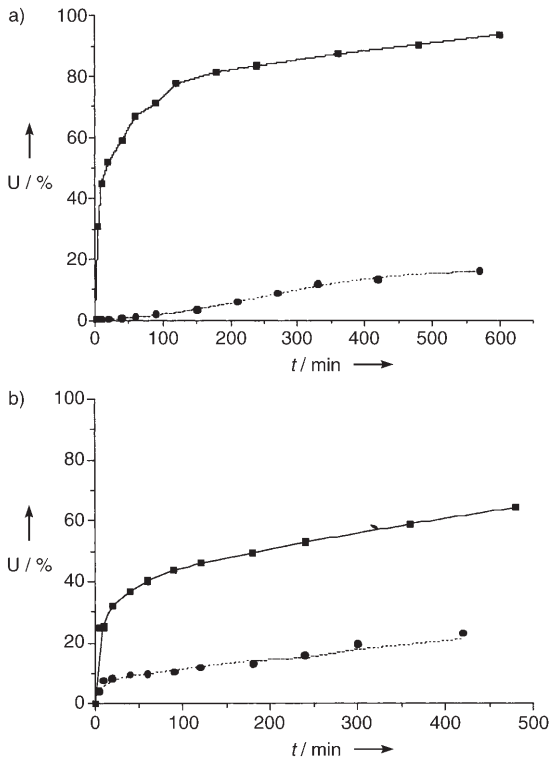

Figure 3. Conversion(U)–time(*t*) plot for the a) Heck coupling of bromobenzene with *n*-butyl acrylate and the b) Suzuki coupling of *p*-bromoanisole with phenylboronic acid; in each case catalysts **4** (■, ——; 0.1 mol%) and **6** (●, •••••; 0.1 mol%) are compared.

acid at 130°C and the conversion rates (TON) were of the order of 10^4 to 10^6; with chloroarenes TONs of up to $>10^3$ were achieved, for example with *p*-chloroacetophenone (Table 2, entry 4). Once again catalyst **6** does not approach the carbocyclic variant **4**.

In Suzuki coupling reactions with chloroarenes catalyst **5** was more effective than the most active NHC–phosphane system previously known, which is produced in situ from **7** and PCy_3 (Table 2, entries 5–8).[10] Better results for chloroarenes were found previously only with optimized in situ catalysts derived from $Pd(OAc)_2$ or $[Pd_2(dba)_3]$ (dba = *trans*,-*trans*-dibenzylideneacetone) and imidazolium salts, the structures of which were not defined.[11]

Table 2: Catalyzed Suzuki coupling.

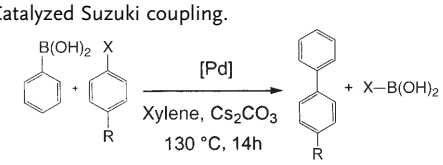

Entry	R	X	Cat.	PR′$_3$	mol% Pd	Yield [%][a]	TON
1	H	Br	**4**	–	10^{-3}[b]	100	10^5
2	H	Br	**4**	–	10^{-4}[b]	89	8.9×10^5
3	OCH_3	Br	**4**	–	0.01[b]	43	4300
4	$C(O)CH_3$	Cl	**4**	–	0.01	11	1100
5	H	Cl	**3a**	PCy_3	1	100	100
6	H	Cl	**7**	$+PCy_3$[10]	1	42	42
7	OCH_3	Cl	**3a**	PCy_3	1	93	93
8	OCH_3	Cl	**7**	$+PCy_3$[10]	1	69[c]	69

[a] GC yield with diethylene glycol di-*n*-butyl ether as the internal standard. [b] K_2CO_3 as base. [c] Yield after 32 h.

With respect to their ready synthesis and high thermal and air stability, the catalyst complexes of cycloheptatrienylidene are at least comparable to the NHC complexes. The tremendous robustness of the CHT catalysts is demonstrated inter alia in that the complex **4** used in the catalyst experiments could be subjected to temperatures of more than 145°C over five days without a trace of decomposition. Complex **3a** can even be purified by stirring with concentrated HCl.

We attribute the efficiency of the new class of catalysts essentially to a low metal coordination achieved with high thermal stability such that the metal–carbene unit is retained in the catalytic cycle. Whether and to what extent the carbon–metal bond determines the catalytic properties is the subject of kinetic and quantum mechanical investigations. The catalysts may be widely varied both constitutionally and structurally. It is expected above all that the substituents at positions 2 and 7 next to the carbene center exercise a far greater effect on the metal environment than is the case in the NHC five-membered-ring system. In that way we hope to solve the problem of the Heck coupling of deactivated chloroarenes which have failed with all known, molecularly defined, homogeneous catalysts.[12]

Experimental Section

2a: Pd black (1.0 g, 9.40 mmol) and **1a** (1.47 g, 9.13 mmol) were stirred in 25 mL of dichloromethane for 6 h at −10°C. The suspension was filtered through a D4 frit, the residue was rinsed with dichloromethane (6×20 mL), and the combined rinses were concentrated under reduced pressure to a volume of 20 mL. The solution was cooled to −18°C, and the resulting red-brown crystals were filtered off and dried in vacuo. Yield: 0.21 g (9%). ^{1}H NMR (399.8 MHz, CD_2Cl_2): $\delta = 6.39$ (m, 2H), 5.59 (m, 2H), 5.30 ppm (m, 2H); $^{13}C\{^1H\}$ NMR (100.5 MHz, CD_2Cl_2): $\delta = 116.2$, 101.7, 89.5 ppm; elemental analysis (%) calcd for $C_{14}H_{12}Cl_4Pd_2$: C 31.43, H 2.26, Pd 39.78; found: C 31.76, H 2.31, Pd 39.36.

3a: Pd black (1.45 g, 13.63 mmol) and **1a** (2.15 g, 13.35 mmol) were stirred in dichloromethane (30 mL) for 24 h at −10°C. The product mixture was then extracted in two portions for 24 h in a small Soxhlet apparatus with 50 mL of boiling dichloromethane in each case. The combined extracts were concentrated under reduced pressure to 40 mL and cooled to −18°C. The precipitated orange-colored crystals were filtered off, washed with dichloromethane (10 mL), and dried in vacuo. Yield: 2.25 g (64%). M.p. 150–160°C (decomp). ^{1}H NMR (399.8 MHz, [D$_6$]DMSO): $\delta = 5.36$ (m, 2H), 5.22 (m, 2H), 5.03 ppm (d, J = 12.0 Hz, 2H); $^{13}C\{^1H\}$ NMR (100.5 MHz, [D$_6$]DMSO): $\delta = 185.8$ (s, carbene C), 140.2, 135.4, 133.8; IR (Nujol): $\tilde{\nu} = 346$ (terminal halogen atom), 313, 282 cm^{-1} (bridging halogen atoms). Elemental analysis (%) calcd for $C_{14}H_{12}Cl_4Pd_2$: C 31.43, H 2.26, Pd 39.78; found: C 30.96, H 2.31, Pd 39.08.

4: A solution of complex **3a** (0.45 g, 0.815 mmol) and $P(C_6H_5)_3$ (0.44 g, 1.68 mmol) in C_6H_6 (20 mL) was first warmed to 80°C with stirring and then stirred for a further 20 h at 25°C. The resulting yellow microcrystalline needles were filtered off, washed with C_6H_6 (5×10 mL), purified by recrystallization from CH_3CN, and dried in vacuo. Yield: 0.80 g (93%). MS (FAB-MS): *m*/*z*: 493 $[M-Cl]^+$ (100). Elemental analysis (%) calcd for $C_{25}H_{21}Cl_2PdP$: C 56.68, H 4.00, Pd 20.09; found: C 56.42, H 3.79, Pd 19.5. Compound **4** was obtained almost quantitatively when, as described in the above method, **1a** was first allowed to react with Pd black in dichloromethane at −10°C and

 © 2006 Wiley-VCH Verlag GmbH & Co. KGaA, Weinheim

48 h at room temperature, and then with PPh_3 in C_6H_6 at 80 °C and 24 h at room temperature.

Catalyzed reactions: a) Heck coupling: A Schlenk flask that had been evacuated and filled with argon several times was charged with sodium acetate (3.0 mmol), aryl halide (2.0 mmol), and the internal standard diethylene glycol di-*n*-butyl ether (100 mg). Then *n*-butyl acrylate (3 mmol) and degassed *N*,*N*-dimethylacetamide (DMA; 2 mL) were added, and the reaction mixture was heated to 145 °C. When the reaction temperature had been reached the catalyst solution was added against stream of argon. At the end of the reaction the reaction solution was cooled to 25 °C, treated with 1N aq. HCl (1 mL), and extracted with dichloromethane (3 × 2 mL). The organic phase was dried over $MgSO_4$. Conversions and yields were determined by GC analysis.

b) Suzuki coupling: A Schlenk flask that had been evacuated and filled with argon several times was charged with potassium or cesium carbonate (3.0 mmol), aryl halide (2.0 mmol), phenylboronic acid (2.4 mmol), and the internal standard diethylene glycol di-*n*-butyl ether (100 mg). Then degassed xylene (2 mL) was added, and the reaction mixture was heated to 130 °C. When the reaction temperature had been reached the catalyst solution was added against a stream of argon. At the end of the reaction the reaction solution was cooled to 25 °C, treated with water (3 mL), and extracted with diethyl ether (3 × 2 mL). The organic phase was dried over $MgSO_4$. Conversions and yields were determined GC analysis.

Catalyst solutions for the catalysts **4** and **6**: A solution of catalyst (0.02 mmol) in DMA (10 mL) was stored in the freezer. The concentration was selected such that 0.1 mL of the solution corresponds to a catalyst/substrate ratio of 0.01 mol% catalyst. For experiments with extremely low catalyst concentrations the catalyst solution was diluted further. Catalyst solutions for the catalysts **5** and **7**: The solutions were prepared by stirring the phosphane with **3a** or **7** (P/Pd ratio 1:1) in DMA (0.5 mL) for 10 min at 25 °C.

Received: October 11, 2005
Published online: May 3, 2006

Keywords: C–C coupling · carbenes · carbocycles · homogeneous catalysis · palladium

[1] a) W. A. Herrmann, M. Elison, J. Fischer, C. Köcher, G. R. J. Artus, *Angew. Chem.* **1995**, *107*, 2602; *Angew. Chem. Int. Ed. Engl.* **1995**, *34*, 2371; b) W. A. Herrmann, C. Köcher, *Angew. Chem.* **1997**, *109*, 2256; *Angew. Chem. Int. Ed. Engl.* **1997**, *36*, 2162; c) D. Bourissou, O. Guerret, F. P. Gabbaï, G. Bertrand, *Chem. Rev.* **2000**, *100*, 39.

[2] Review article : a) W. A. Herrmann, *Angew. Chem.* **2002**, *114*, 1342; *Angew. Chem. Int. Ed.* **2002**, *41*, 1290; b) W. A. Herrmann, T. Weskamp, V. P. W. Böhm, *Adv. Organomet. Chem.* **2002**, *48*, 1.

[3] Since the first publication on C–C coupling reactions catalyzed by NHC complexes[1a] in 1995 more than 200 original publications from 15 research groups have appeared.

[4] a) W. A. Herrmann, J. Fischer, M. Elison, C. Köcher, K. Öfele (Hoechst AG), DE 4447066.5A1, **1996**, EP 0721953A1, **1996** [*Chem. Abstr.* **1996**, *125*, 143019y]; b) W. A. Herrmann, J. Fischer, M. Elison, C. Köcher (Hoechst AG), DE 4447068.1A1, **1996**, EP 0719758A1, **1996**, US 5.703.269, **1997** [*Chem. Abstr.* **1996**, *125*, 167571y]; c) W. A. Herrmann, M. Elison, J. Fischer, C. Köcher (Celanese GmbH), DE 4447067.3A1, **1996**, EP 0719753A1, **1995** [*Chem. Abstr.* **1996**, *125*, 167338c]; d) W. A. Herrmann (Hoechst AG), DE 4447070.3A1, **1996**, EP 0721951A1, **1996** [*Chem. Abstr.* **1996**, *125*, 143016v]; e) W. A. Herrmann, C. Köcher, L. Goossen (Hoechst AG), DE 1961090.8A1, **1997**, EP 888308, **1997**, WO 9734875, **1997** [*Chem. Abstr.* **1997**, *127*, 318962v]; f) W. A. Herrmann, H.-C. Militzer, U. Scholz, C. Gstöttmayr (Bayer AG), EP 1308157A1, **2003**.

[5] X-ray crystal structure analysis of **2a**: $C_{14}H_{12}Cl_4Pd_2$, $M_r = 534.88$, red fragment ($0.03 \times 0.20 \times 0.51$ mm^3), triclinic, $P\bar{1}$, $a = 5.0196(6)$, $b = 7.2075(8)$, $c = 11.5141(15)$ Å, $\alpha = 86.792(10)$, $\beta = 80.650(10)$, $\gamma = 80.080(9)°$, $V = 404.72(9)$ Å^3, $Z = 1$, $\rho_{calcd} = 2.195$ g cm^{-3}, $F_{000} = 256$, $\mu = 2.886$ mm^{-1}. The preliminary investigation and data collection were carried out with a IPDS-2T diffractometer (Stoe & Cie) at the window of a rotating-anode generator (NONIUS FR591) with $Mo_{K\alpha}$ radiation (graphite monochromator, $\lambda = 0.71073$ Å) at 293 K in the range of $4.53° < \Theta < 25.35°$. 5867 Reflections integrated with TWIN program, data LP-corrected, and corrected for decomposition, starting from the scaling. Numerical absorptions correction ($T_{min} = 0.544$, $T_{max} = 0.812$) after optimization of the crystal form. All 1168 independent reflections ($R_{int} = 0.039$) [1081: $I_o > 2\sigma(I_o)$] used for the refinement of the 102 parameters, structure solution by direct methods and difference Fourier syntheses. All non-hydrogen atoms refined with anisotropic displacement parameters, hydrogens at calculated positions with a C–H distance of 0.93 Å and $U_{iso(H)} = 1.2\,U_{eq(C)}$ refined, structure refinement (method of least squares on $\Sigma w(F_o^2 - F_c^2)^2$) converged with $R1 = 0.0206$ [$I_o > 2\sigma(I_o)$], $wR2 = 0.0492$ [all data], GOF = 1.041, and shift/error ratio < 0.001. The final difference Fourier map showed only small deviations ($\Delta e_{min/max} = +0.31/-0.30$ e Å^{-3}). Smaller extinction effects were corrected with SHELXL-97 (G. M. Sheldrick, SHELXL-97, Program for Refinement of Crystal Structures, Universität Göttingen, **1997**) [$\varepsilon = 0.013(2)$]. The molecule lies on an inversion center. The resulting partial disorder [0.830(4):0.170(4)]of the chlorine atoms C12/C13 was observed and resolved. CCDC-683874 contains the detailed crystallographic data for this publication. The data may be obtained free of charge from the Cambridge Crystallographic Data Centre under www.ccdc.cam.ac.uk/data_request/cif.

[6] X-ray crystal structure analysis of **4**·CH_3CN: $C_{27}H_{24}Cl_2NPPd$, $M_r = 570.76$, yellow needles ($0.05 \times 0.10 \times 0.66$ mm^3), triclinic, $P\bar{1}$ (No. 2), $a = 9.7796(2)$, $b = 10.5189(2)$, $c = 12.5658(3)$ Å, $\alpha = 99.2431(7)$, $\beta = 93.8821(6)$, $\gamma = 90.2501(6)°$, $V = 1272.79(5)$ Å^3, $Z = 2$, $\rho_{calcd} = 1.489$ g cm^{-3}, $F_{000} = 576$, $\mu = 1.017$ mm^{-1}. $R1 = 0.0290$ [$I_o > 2\sigma(I_o)$], $wR2 = 0.0555$ [all data], GOF = 1.116, shift/error ratio < 0.001. CCDC-603873 contains the detailed crystallographic data for this publication. The data may be obtained free of charge from the Cambridge Crystallographic Data Centre under www.ccdc.cam.ac.uk/data_request/cif.

[7] a) N. T. Allison, Y. Kawada, W. M. Jones, *J. Am. Chem. Soc.* **1978**, *100*, 5224; b) P. E. Riley, R. E. Davis, N. T. Allison, W. M. Jones, *Inorg. Chem.* **1982**, *21*, 1321.

[8] a) Z. Lu, K. A. Abboud, W. M. Jones, *J. Am. Chem. Soc.* **1992**, *114*, 10991; b) Z. Lu, W. M. Jones, W. R. Winchester, *Organometallics* **1993**, *12*, 1344.

[9] Current literature, e.g. a) W. A. Herrmann, K. Öfele, D. von Preysing, S. K. Schneider, J. *Organomet. Chem.* **2003**, *687*, 229; b) W. A. Herrmann in *Applied Homogeneous Catalysis with Organometallic Compounds*, 2nd ed. (Eds.: B. Cornils, W. A. Herrmann), Wiley-VCH, Weinheim, **2002**, p. 591–598; W. A. Herrmann in *Applied Homogeneous Catalysis with Organometallic Compounds*, 2nd ed. (Eds.: B. Cornils, W. A. Herrmann), Wiley-VCH, Weinheim, **2002**, p. 775–793; W. A. Herrmann in *Applied Homogeneous Catalysis with Organometallic Compounds*, 2nd ed. (Eds.: B. Cornils, W. A. Herrmann), Wiley-VCH, Weinheim, **2002**, p. 822–828.

[10] W. A. Herrmann, V. P. W. Böhm, C. W. K. Gstöttmayer, M. Grosche, C.-P. Reisinger, T. Weskamp, J. *Organomet. Chem.* **2001**, *617–618*, 616.

[11] G. A. Grasa, M. S. Viciu, J. Huang, C. Zhang, M. L. Trudell, S. P. Nolan, *Organometallics*, **2002**, *21*, 2866.

[12] A. F. Littke, G. C. Fu, *J. Am. Chem. Soc.* **2001**, *123*, 6989.

 © 2006 Wiley-VCH Verlag GmbH & Co. KGaA, Weinheim

Structure Elucidation

DOI: 10.1002/anie.200504525

Siphonazole, an Unusual Metabolite from *Herpetosiphon* sp.

*Markus Nett, Özlem Erol, Stefan Kehraus, Matthias Köck, Anja Krick, Ekaterina Eguereva, Edith Neu, and Gabriele M. König**

Bacteria are an impressive source of biologically active secondary metabolites. To date, however, only a relatively small number of bacterial taxa—actinomycetes, bacilli, pseudomonads, and myxobacteria—has entered natural product chemistry studies.

Studies on molecular phylogeny have clearly demonstrated that the diversity of microbial populations in natural habitats far exceeds former anticipations. Many of the less well characterized groups evolved independently from other lineages. These taxa show a number of phenotypic idiosyncrasies, and it can be expected that their secondary metabolism differs from that of other bacteria as well.

We have directed our interest towards the phylum Chloroflexi which branched off early from the eubacterial stem and is represented by Gram-negative gliding bacteria with an unusual cell-wall composition.[1]

Sequence analysis of this phylum shows that the genus *Herpetosiphon* has noticeable deviations in highly conserved sites in its ribosomal RNA. Thus it appears to be a rather rapidly evolving line that is moving away from its thermophilic ancestors.[2] Although *Herpetosiphon* strains can be isolated from many habitats, at present little is known about the secondary metabolism of this genus.

Screening of ten different *Herpetosiphon* strains by NMR- and LC-MS-based techniques led to the discovery of an unusual metabolite comprising a styrene residue, two oxazole rings connected through a C_2 bridge, and an unprecedented amide-bonded *N*-penta[2,4]diene side chain. Even though some structural elements resemble those of myxobacterial metabolites, the overall composition makes this compound the first member of a new structural class. Here we report the structure elucidation and biosynthesis of the novel compound siphonazole.

The producing strain was cultivated at 28 °C in shaked flasks containing a peptone medium which had been supplemented with amberlite resin (XAD-16). After extraction of the adsorber resin with acetone, the more hydrophilic by-products were removed by partition between 60 % aqueous methanol and dichloromethane. Chromatography of the dichloromethane layer on silica gel and final purification by RP-HPLC yielded 31 mg of siphonazole (**1**) and 1 mg of the dimethoxy derivative **2**.

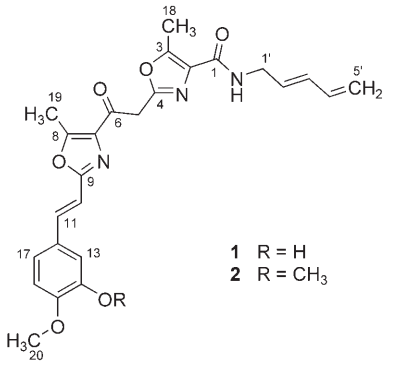

1 R = H
2 R = CH_3

The molecular ion of **1** ($m/z = 463.1743$) in the HR-EI mass spectrum was consistent with the elemental composition $C_{25}H_{25}N_3O_6$. The 1D ^{13}C NMR spectrum recorded in [D_4]methanol, however, revealed only 24 signals. In [D_6]acetone and [D_6]dimethylsulfoxide, where no keto–enol tautomerism occurs, we were able to detect the missing carbon signal (C-5) at $\delta = 40.0$ ppm. A DEPT experiment showed this signal to correspond to a methylene group.

Both the C_6H_3-CH=CH partial structure and the unsaturated aliphatic side chain were deduced from $^1H,^1H$-COSY and $^1H,^{13}C$-HMBC data (Table 1). The *para*-methoxylation pattern of the styrene residue was confirmed by a selective NOESY experiment. The presence of an amide function in the aliphatic side chain was evident from key fragments in the EI mass spectrum with signals at $m/z = 67$ and 396 as well as $m/z = 82$ and 381 which can be traced back to an allylic cleavage and an α cleavage of the carbonyl group, respectively (Figure 1, see HR-EIMS data for **1**).

The structure of the central part of the molecule, which comprises two methyl oxazole rings, was solved by $^1H,^{15}N$ long-range couplings (Figure 2). Correlations between H-10 and H-11 and the resonance of the nitrogen atom at $\delta =$ 249 ppm indicated the presence of an oxazole ring connected to the styrene moiety.[3] A weak correlation from $H_{(3)}$-19 to the same nitrogen atom as well as $^1H,^{13}C$-HMBC data enabled the identification of C-7 and C-8 as the two remaining carbon atoms of this oxazole ring. The second methyl oxazole part was concluded from $^1H,^{15}N$ long range couplings from $H_{(2)}$-5 and $H_{(3)}$-18 to the nitrogen resonance at $\delta = 251$ ppm. $^1H,^{13}C$ long-range couplings from $H_{(3)}$-19 to C-6 and from $H_{(2)}$-5 to both C-4 and C-6 led to the identification of the C_2 bridge linking the two oxazole rings.

The location of the methyl groups on the oxazole rings was assigned on the basis of ^{13}C NMR chemical shifts and verified with selective INEPT experiments.[4] By using a C,H coupling constant of 7 Hz ($^3J_{C,H}$), polarization was transferred

[*] M. Nett, Ö. Erol, Dr. S. Kehraus, Dr. A. Krick, E. Eguereva, E. Neu, Prof. Dr. G. M. König
Institute for Pharmaceutical Biology
University of Bonn
Nussallee 6, 53115 Bonn (Germany)
Fax: (+49) 228-73-3250
E-mail: g.koenig@uni-bonn.de
Priv.-Doz. Dr. M. Köck
Alfred Wegener Institute for Polar and Marine Research
Am Handelshafen 12, 27570 Bremerhaven (Germany)

Supporting information for this article is available on the WWW under http://www.angewandte.org or from the author.

 © 2006 Wiley-VCH Verlag GmbH & Co. KGaA, Weinheim

Table 1: NMR spectral data for siphonazole (**1**) in $(CD_3)_2CO$.

C no.	δ_C	δ_H, mult., int., J [Hz]	COSY correlations	HMBC correlations ($^1H \rightarrow ^{13}C$, $^1H \rightarrow ^{15}N$)
1	161.9			
2	130.5			
3	153.7			
4	156.7			
5	40.0	4.42, s, 2 H		C-4, 6, N-3
6	190.0			
7	135.2			
8	155.9			
9	159.9			
10	111.4	6.83, d, 1 H, 16.4	H-11	C-9, 11, 12, N-2
11	138.1	7.43, d, 1 H, 16.4	H-10	C-9, 10, 12, 13, 17, N-2
12	129.4			
13	113.9	7.21, d, 1 H, 2.2	H-17	C-11, 14, 15, 17
14	147.8			
15	150.0			
16	112.3	6.98, d, 1 H, 8.3	H-17	C-12, 14, 15
17	121.3	7.13, dd, 1 H, 8.3 ($J_{16,17}$), 2.2 ($J_{13,17}$)	H-13, H-16	C-11, 13, 15
18	11.5	2.58, s, 3 H		C-1, 2, 3, N-3
19	12.2	2.62, s, 3 H		C-6, 7, 8, N-2
20	56.2	3.88, s, 3 H		C-15
1′	40.6	4.00, d, 2 H, 5.9	H-2′	C-1, 2′, 3′, N-1
2′	131.8	5.79, dt, 1 H, 15.2 ($J_{2',3'}$), 5.9 ($J_{1',2'}$)	H-1′, 3′	C-1′, 4′, N-1
3′	132.7	6.21, dd, 1 H, 15.2, 10.5 ($J_{3',4'}$)	H-2′, 4′	C-1′, 5′
4′	137.5	6.35, ddd, 1 H, 16.9 ($J_{4',5'a}$) , 10.5, 10.3 ($J_{4',5'b}$)	H-3′, 5′a, 5′b	C-2′
5′	116.9	a 5.15, dd, 1 H, 16.9, 2.0 ($J_{5'a,5'b}$)	H-4′, 5′b	C-3′, 4′
		b 5.01, dd, 1 H, 10.3, 2.0	H-4′, 5′a	C-3′

N no.	δ_N	δ_H, mult., int., J [Hz]	COSY correlations	HMBC correlations ($^1H \rightarrow ^{13}C$)
1	108	7.58, t, 1 H, 5.9		C-1, 1′
2	249			
3	251			

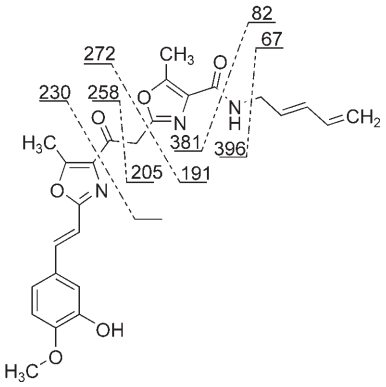

Figure 1. Key fragments of **1** in the EI mass spectrum.

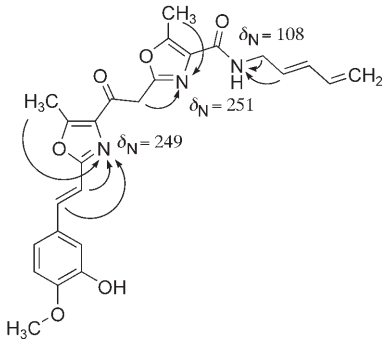

Figure 2. ^1H,^{15}N long-range correlations in **1**.

from $H_{(3)}$-19 to a quaternary carbon atom resonating at $\delta =$ 135.2 ppm (C-7). Similarly, the carbon atom at position 2 was excited upon irradiation at the resonance frequency of $H_{(3)}$-18. The configuration of the double bonds was derived from the size of the vicinal proton coupling constants (see Table 1).

The structural elements present in siphonazole (**1**) led to the expectation that different metabolic pathways would be involved in its biosynthesis. The styrene moiety was suspected to originate from phenylalanine-derived cinnamic acid. Subsequent condensation with threonine would result in the formation of the first methyl-substituted oxazole ring. The next step in the biosynthetic progress would be an unusual extension of the heterocycle with acetate followed by another condensation catalyzed by nonribosomal peptide synthetase (NRPS) and cyclization with threonine. Two pathways seemed possible for the formation of the aliphatic side chain: a C_5N unit could be produced from a lysine precursor. However, such a unit tends to be found as a piperidine ring system as a result of an intramolecular Mannich reaction.[5] Therefore, the side chain was presumed to originate from glycine and propionate.

^{13}C labeling experiments were carried out to verify the biosynthesis of **1** (Table 2). Feeding studies with [1-^{13}C]acetate resulted in the incorporation of the label at positions 4, 9, 11, 2′, and 4′ of **1**. No ^{13}C enrichment of the aromatic carbon atoms of the C_6H_3-CH=CH unit was observed. Since the styrene moiety carries a hydroxylation pattern characteristic of shikimic acid derived metabolites, the formation of the phenyl ring from acetic acid units was definitely excluded.

The labeling of C-9 and C-11 was also not consistent with the incorporation of phenylalanine-derived cinnamic acid. After conversion through the tricarboxylic acid cycle and gluconeogenesis, [1-^{13}C]acetate enters the shikimate pathway as [1-^{13}C]phosphoenolate are required for the biosynthesis of phenylalanine, the incorporation of phenylalanine-derived cinnamic acid would result exclusively in a ^{13}C enrichment in carbon C-9 of **1**. The reason for this is that a decarboxylative aromatization occurs after the Claisen rearrangement of chorismic acid into prephenic acid which results in the loss of one of the labeled carbon atoms. On the basis of the observed labeling pattern and the different enrichment in C-9 and C-11, we postulate benzoic acid (or a hydroxylated/methoxylated derivative) as the starter unit in

 © 2006 Wiley-VCH Verlag GmbH & Co. KGaA, Weinheim

Table 2: ^{13}C enrichment in siphonazole (**1**) after feeding of [1-^{13}C]acetate (A), [1,2-$^{13}C_2$]acetate (B), [1-^{13}C]glycine (C), [1,2-$^{13}C_2$,^{15}N]glycine (D), and [*methyl*-^{13}C]methionine (E).[a]

C no.	A	B	C	D	E
1	1.2	1.2	1.2	1.1	1.0
2	1.0	1.1	1.1	1.2	1.2
3	1.1	1.0	1.2	1.1	1.0
4	**6.1**	**5.8(64)**	1.0	1.2	1.2
5	0.6	**4.0(64)**	0.8	0.9	1.0
6	1.0	1.1	1.1	1.2	1.2
7	1.0	0.9	1.1	1.0	1.3
8	0.9	1.0	1.2	1.2	1.2
9	**6.4**	**6.0(81)**	1.1	1.4	1.1
10	0.8	**4.3(81)**	0.9	1.0	1.2
11	**3.0**	**2.3**	0.9	1.0	1.1
12	0.8	1.2	1.1	1.1	1.2
13	0.7	1.1	0.8	0.9	1.0
14	0.8	1.0	0.9	1.0	1.1
15	1.3	1.2	1.1	1.2	1.0
16	1.0	1.0	1.0	1.0	1.0
17	0.9	1.3	0.8	1.0	1.0
18	1.2	1.2	1.2	1.2	1.2
19	1.0	1.2	1.1	1.0	1.0
20	0.9	0.8	1.0	**2.9**	**18.4**
1′	0.9	1.0	0.9	**8.8(46)**	1.2
2′	**2.2**	**2.2**	**17.4**	**10.9(46)**	1.2
3′	1.1	**9.6(54)**	1.0	1.2	1.3
4′	**10.1**	**8.8(54)**	1.7	1.7	1.8
5′	1.2	**9.7**	1.3	1.4	1.5

[a] All signals were referenced to the integral of the ^{13}C-16 signal. Coupling constants (in Hz) are set in parenthesis. The numbers in boldface efer to the unequivocal incorporation of the corresponding precursor.

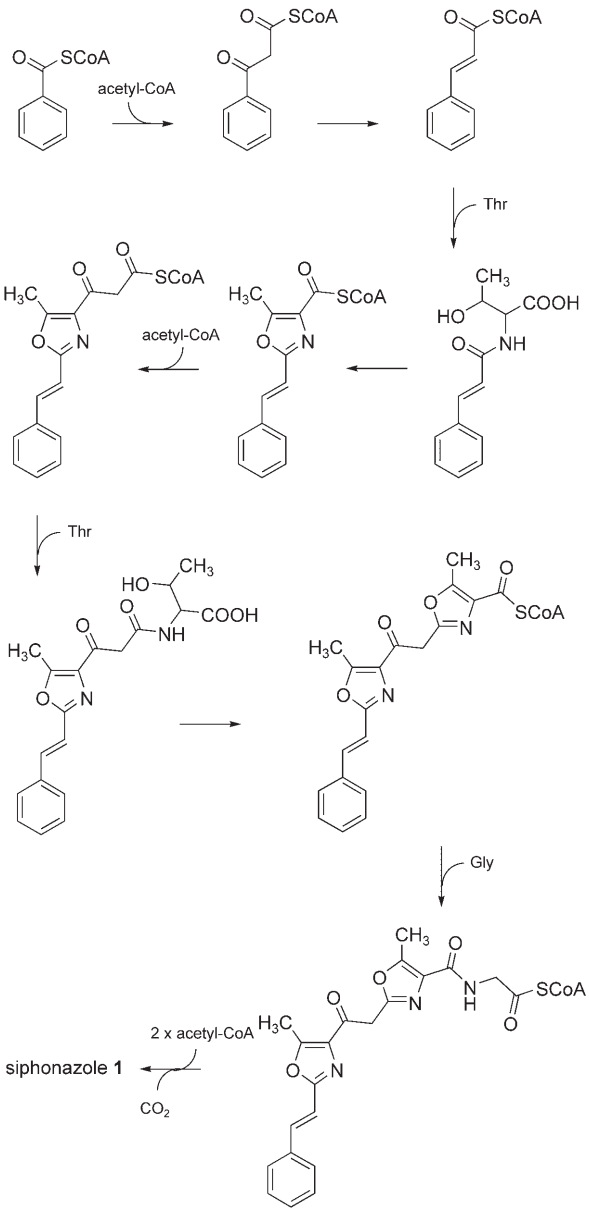

Scheme 1. Postulated biosynthesis of the siphonazole skeleton.

the biosynthesis of **1**.[6] This building block is extended to a phenylpropane unit by condensation with acetyl-CoA (Scheme 1).

Corroboration of our hypothesis for the construction of the side chain comes from the labeling of C-2′ by [1-^{13}C]acetate. This incorporation arises from an intensive metabolism via [1-^{13}C]oxaloacetate (tca cycle) and [1-^{13}C]-3-phosphoglycerate (gluconeogenesis) to [1-^{13}C]glycine. This finding was further confirmed by the clear incorporation of [1-^{13}C]glycine at position 2′ as well as of intact [$^{13}C_2$,^{15}N]glycine in the side chain.[7,8]

Unexpectedly, feeding with [1-^{13}C]propionate gave no ^{13}C enrichment at C-5′ (data not shown). In contrast the ^{13}C NMR spectrum of the [1,2-$^{13}C_2$]acetate-labeled compound showed all three carbon atoms (C-3′, C-4′, and C-5′) in the side chain to be enriched. Moreover, a clear homonuclear coupling between C-3′ and C-4′ was observed. As C-5′ had not been labeled in the previous experiment with [1-^{13}C]acetate, the last acetate unit must have been decarboxylated after its incorporation. Feeding with [*methyl*-^{13}C]methionine resulted in an ^{13}C enrichment in position 20 as expected.

The structure and biosynthesis of siphonazole (**1**) are remarkable in many respects. Whereas the formation of natural products by the combined polyketide synthase (PKS)/NRPS systems appears to be quite common in the eubacterial domain, only very few metabolites derived from cinnamic acid have been described. This observation has been traced back to the inability of many bacteria to convert phenylalanine directly into cinnamic acid. Compared to plants, most prokaryotes lack the required phenylalanine ammonia lyase.[9] While some bacteria presumably have evolved alternative pathways leading to cinnamic acid (for example, from benzoic acid), most of them have not. In consequence, reports on compounds displaying both a cinnamate unit and structural elements of a polyketide with incorporated amino acids are rarely found in the literature. Exceptions are metabolites that were isolated from myxobacteria such as the crocacins, phenalamides, and phenoxane (**3**).[10,11]

From a biosynthetic point of view, only the latter exhibits high similarities to siphonazole (**1**). Even though no data on labeling studies of **3** are available, the biosynthesis presumably proceeds through an alternating integration of building

 © 2006 Wiley-VCH Verlag GmbH & Co. KGaA, Weinheim

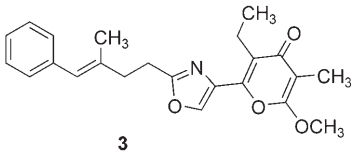

3

blocks that are derived from the shikimate, polyketide, and amino acid metabolism as well.

Our findings indicate the presence of a complex biosynthetic machinery in a deep-rooted bacterium which is phylogenetically (16S rDNA) distinct from myxobacteria.[12] Identification and analysis of the genes governing the biosynthesis of siphonazole (**1**) are currently in progress. These data will enable the production of novel hybrid structures by combinatorial biosynthesis.

Experimental Section

The producing strain (no. 060) was isolated from a mud sample of the intertidal region. The strain was confirmed as *Herpetosiphon* sp. by 16S rDNA sequencing. Stock cultures are kept at −80 °C.

Isolation of **1** and **2**: Cultivation was performed in ten 5-L Erlenmeyer flasks, each containing a peptone medium (MD1 medium supplemented with 0.2% glucose; 1.5 L) with 2% XAD-16 (Fluka, Germany). The flasks were inoculated with a preculture (MD1 medium; 100 mL) and shaken on a rotary shaker (140 rpm) at 28 °C for seven days. At the end of the cultivation, the bacterial cells and adsorber resin were separated from the culture broth by centrifugation and extracted ten times with acetone (300 mL). After removal of the solvent, the residue (7.08 g) was suspended in 60% aqueous methanol (250 mL) and extracted three times with dichloromethane (100 mL). The dichloromethane layers were combined and concentrated (1.87 g). Separation of this extract by column chromatography over silica gel (Merck, 63–200 μm; 30 g) by consecutively employing dichloromethane, ethyl acetate, acetone, and methanol as eluents gave four fractions of 200 mL each. ^{1}H NMR spectroscopic analysis indicated the EtOAc fraction to be of further interest. After evaporation of the solvent, this fraction (257 mg) was subjected to semipreparative RP-HPLC (column: Eurospher-100 C_{18}, 5 μm, 250 × 8 mm (Knauer), eluent: methanol/water 75:25, flow rate: 2.5 mL min^{-1}, detection: UV absorption). The retention times of **1** and **2** were 14.6 and 20.3 minutes, respectively.

Biosynthetic studies: Labeled compounds (500 mg [1-^{13}C]acetate, 500 mg [1,2-$^{13}C_2$]acetate, 500 mg [1-^{13}C]glycine, 250 mg [1,2-$^{13}C_2$, ^{15}N]glycine, 500 mg [*methyl*-^{13}C]methionine, all dissolved in 10 mL H_2O) were obtained from Cambridge Isotope Laboratories or ISOTEC. All feeding experiments were conducted in 5-L Erlenmeyer flasks containing peptone medium (1.5 L) and 2% XAD-16. Labeled precursors were added at the time of inoculation.

NMR spectra were recorded at 300 K on a Bruker Avance 300 DPX or Bruker Avance 500 DRX spectrometer with $(CD_3)_2CO$, CD_3OD, or $(CD_3)_2SO$ as the solvent and internal standard. ^{1}H,^{15}N-HMBC spectra were referenced externally to urea.

For the determination of the incorporation yield ^{13}C spectra were recorded with the inverse-gated decoupling pulse sequence in the presence of 0.05 M [Cr(acac)$_3$] (acac = acetylacetanoate) as a relaxation reagent.[13]

1: white solid; UV/Vis (MeOH): λ_{max} (log ε) = 225 (4.54), 334 nm (4.11); IR (ATR): $\tilde{\nu}$ = 2925, 1724, 1688, 1650, 1590, 1511, 1441, 1272, 1132, 1025, 762 cm^{-1}; ^{1}H NMR: see Table 1; ^{13}C NMR: see Table 1; EIMS *m*/*z* (%): 463 (100), 448 (4), 422 (6), 396 (14), 381 (12), 354 (6), 339 (6), 309 (13), 300 (17), 272 (4), 258 (14), 230 (10), 205 (4), 191 (32), 188 (19), 177 (11), 161 (11), 146 (6), 82 (32), 67 (12); HR EIMS (*m*/*z*): found: 463.1743, calcd: 463.1743 for $[C_{25}H_{25}N_3O_6]$; found: 396.1199, calcd: 396.1196 for $[C_{20}H_{18}N_3O_6]$; found: 381.1087, calcd: 381.1087 for $[C_{20}H_{17}N_2O_6]$; found: 272.0927, calcd: 272.0923 for $[C_{15}H_{14}NO_4]$; found: 258.0763, calcd: 258.0766 for $[C_{14}H_{12}NO_4]$; found: 230.0817, calcd: 230.0817 for $[C_{13}H_{12}NO_3]$; found: 205.0981, calcd: 205.0977 for $[C_{11}H_{13}N_2O_2]$; found: 191.0814, calcd: 191.0821 for $[C_{10}H_{11}N_2O_2]$; found: 82.0680, calcd: 82.0657 for $[C_5H_8N]$; found: 67.0534, calcd: 67.0548 for $[C_5H_7]$.

2: white solid; UV/Vis (MeOH): λ_{max} (log ε) = 227 (4.38), 334 nm (4.14); IR (ATR): $\tilde{\nu}$ = 2923, 1710, 1690, 1651, 1592, 1513, 1357, 1265, 1140, 1024, 806 cm^{-1}; ^{1}H NMR (300 MHz, $(CD_3)_2CO$, reference: δ = 2.04 ppm): δ = 2.58 (s, $H_{(3)}$-18), 2.62 (s, $H_{(3)}$-19), 3.84 (s, $H_{(3)}$-20), 3.90 (s, $H_{(3)}$-21), 4.00 (d, J = 5.9 Hz, $H_{(2)}$-1′), 4.41 (s, $H_{(2)}$-5), 5.01 (dd, J = 10.3, 2.0 Hz, H-5′b), 5.15 (dd, J = 16.9, 2.0 Hz, H-5′a), 5.79 (dt, J = 15.2, 5.9 Hz, H-2′), 6.21 (dd, J = 15.2, 10.5 Hz, H-3′), 6.35 (ddd, J = 16.9, 10.5, 10.3 Hz, H-4′), 6.92 (d, J = 16.4 Hz, H-10), 6.98 (d, J = 8.3 Hz, H-16), 7.20 (dd, J = 8.3, 2.2 Hz, H-17), 7.37 (d, J = 2.2 Hz, H-13), 7.47 ppm (d, J = 16.4 Hz, H-11); ^{13}C NMR (75 MHz, $(CD_3)_2CO$, reference: δ = 29.8 ppm): δ = 11.5 (C-18), 12.2 (C-19), 40.0 (C-5), 40.6 (C-1′), 56.1 (C-20, C-21), 110.4 (C-13), 111.5 (C-10), 112.4 (C-16), 116.9 (C-5′), 122.6 (C-17), 129.0 (C-12), 130.5 (C-2), 131.9 (C-2′), 132.7 (C-3′), 135.2 (C-7), 137.6 (C-4′), 138.1 (C-11), 150.7 (C-14), 151.9 (C-15), 153.7 (C-3), 155.9 (C-8), 156.7 (C-4), 160.0 (C-9), 161.9 (C-1), 190.0 ppm (C-6); EIMS *m*/*z* (%): 477 (100), 436 (6), 410 (14), 395 (12), 368 (8), 353 (4), 337 (7), 323 (14), 314 (14), 286 (7), 275 (16), 272 (10), 244 (11), 202 (38), 191 (58), 175 (15), 82 (33), 67 (7); HR EIMS (*m*/*z*): found: 477.1911, calcd: 477.1900 for $[C_{26}H_{27}N_3O_6]$.

Received: December 20, 2005
Published online: May 3, 2006

Keywords: biosynthesis · herpetosiphon · natural products · siphonazole · structure elucidation

[1] G. M. Garrity, J. G. Holt in *Bergey's Manual of Systematic Bacteriology*, *Vol. 1*, 2nd ed. (Ed.: G. M. Garrity), Springer, New York, **2001**, p. 427.
[2] H. Oyaizu, B. Debrunner-Vossbrinck, L. Mandelco, J. A. Studier, C. R. Woese, *Syst. Appl. Microbiol.* **1987**, *9*, 47–53.
[3] L. Stefaniak, *Bull. Acad. Pol. Sci. Ser. Sci. Chim.* **1978**, *26*, 291–302.
[4] A. Bax, J. A. Ferretti, N. Nashed, D. M. Jerina, *J. Org. Chem.* **1985**, *50*, 3029–3034.
[5] P. M. Dewick in *Medicinal Natural Products—A Biosynthetic Approach*, 2nd ed., Wiley, Chichester, **2002**, p. 307.
[6] In many bacteria 4-hydroxybenzoic acid is produced directly from chorismic acid by elimination of pyruvic acid. Metabolism of [1-^{13}C]acetate yields an incorporation of the label in the carboxy carbon atom of benzoic acid, which corresponds to C-11 of siphonazole (**1**).
[7] Although [1-^{13}C]serine is an intermediate in the conversion of [1-^{13}C]acetate into [1-^{13}C]glycine, only an incorporation of the latter was demonstrated in **1** after incubation with [1-^{13}C]acetate. Furthermore, feeding experiments utilizing [1-^{13}C]glycine and [1,2-$^{13}C_2$,^{15}N]glycine gave no evidence for the incorporation of isotopically labeled serine, which is known to result from glycine degradation. For these reasons, serine was excluded as a possible precursor of the oxazole rings in **1**.
[8] The incorporation of label from [1,2-$^{13}C_2$,^{15}N]glycine at C-20 can be traced back to cleavage of a glycine residue to yield N^5,N^{10}-[*methylene*-^{13}C]tetrahydrofolate and a subsequent transfer of the labeled methylene group onto methionine.
[9] H. B. Bode, R. Müller, *Plant Physiol.* **2003**, *132*, 1153–1161.
[10] R. Jansen, P. Washausen, B. Kunze, H. Reichenbach, G. Höfle, *Eur. J. Org. Chem.* **1999**, 1085–1089.

 © 2006 Wiley-VCH Verlag GmbH & Co. KGaA, Weinheim

[11] E. Jurkiewicz, R. Jansen, B. Kunze, W. Trowitzsch-Kienast, E. Forche, H. Reichenbach, G. Höfle, G. Hunsmann, *Antiviral Chem. Chemother.* **1992**, *3*, 189 – 193.
[12] N. R. Krieg, G. M. Garrity in *Bergey's Manual of Systematic Bacteriology*, *Vol. 1*, 2nd ed. (Ed.: G. M. Garrity), Springer, New York, **2001**, p. 16.
[13] S. Berger, S. Braun in *200 and More NMR Experiments*, Wiley-VCH, Weinheim, **2004**, pp. 318 – 320.

 © 2006 Wiley-VCH Verlag GmbH & Co. KGaA, Weinheim

Copper Dioxygen Compounds

DOI: 10.1002/anie.200600351

Crystallographic Characterization of a Synthetic 1:1 End-On Copper Dioxygen Adduct Complex**

Christian Würtele, Ekaterina Gaoutchenova, Klaus Harms, Max C. Holthausen, Jörg Sundermeyer,* and Siegfried Schindler**

Dedicated to Professor Kurt Dehnicke on the occasion of his 75th birthday

Synthetic bioinorganic copper dioxygen complexes have attracted great interest in the past decades because of their prominent role as oxidants in biochemistry and catalysis. Recent advances in this field form a basis to correlate the pronounced structural diversity of known complexes with the resulting differences in reactivity as oxidants.[1–3] Many of these studies have been concerned with the fine tuning of ligand properties to stabilize the various copper oxygen compounds that occur as intermediates in the formation of reactive species and which are largely responsible for the oxidation activity.[2,3] The collective picture arising from these studies can be discussed within a general mechanistic framework of oxygen binding to copper complexes (Scheme 1, charges are omitted)[1–4] analogous to a scheme recently proposed for iron complexes.[5]

While ample literature exists on the coordination chemistry and reactivity of 2:1 Cu/O_2 species,[2,3,6,7] the characterization of 1:1 Cu/O_2 complexes is complicated by the intrinsic tendency of these species to dimerize in solution or to decompose after irreversible ligand oxidation. Accordingly, to date only three crystallographically characterized examples for 1:1 Cu/O_2 complexes exist, all exhibiting a side-on (η^2) coordination mode.[8–12] End-on copper dioxygen adduct complexes have been proposed as reactive intermediates in the catalytic cycle of mononuclear copper enzymes, such as peptidylglycine α-hydroxylating monooxygenase (PHM) or dopamine β-monooxygenase (DβH).[2,3] And indeed, very recently the existence of such a species could be demonstrated by X-ray crystallography for a precatalytic PHM complex.[13] Yet, in the bioinorganic regime all attempts to isolate and characterize a synthetic analogue of the first step in Scheme 1, that is, the formation of an end-on 1:1 Cu/O_2 complex, failed to date.

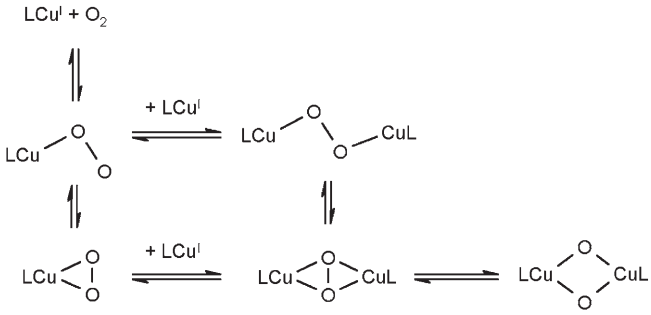

Scheme 1.

With tripodal tetradentate tren (tris(2-aminoethyl)amine) or tmpa (tris[(2-pyridyl)methyl]amine) ligands, such complexes are short-lived and could only be detected as transient species at low temperatures using stopped-flow UV/Vis spectroscopy.[1–3,14–16] In related studies we showed, however, that the high reactivity of the transient species can be moderated by use of sterically more demanding ligands with stronger N-donor character, such as Me_6tren.[15] This success led us to employ the sterically congested superbasic[17] tren derivative tris(tetramethylguanidino)tren (TMG_3tren)[18] as a ligand and in a recent study we were eventually able to obtain a stable 1:1 Cu/O_2 adduct at low temperatures (Scheme 2).[19]

Most remarkably—and in striking contrast to former experiments with other tren derivatives, for which only irreversible oxidation reactions were observed upon warming—we found that the formation of the $Cu–O_2$ adduct is

[*] C. Würtele, Prof. Dr. S. Schindler
Institut für Anorganische und Analytische Chemie
Justus-Liebig-Universität Gießen
Heinrich-Buff-Ring 58, 35392 Gießen (Germany)
Fax: (+49) 641-993-4149
E-mail: siegfried.schindler@chemie.uni-giessen.de
E. Gaoutchenova, Dr. K. Harms, Prof. Dr. J. Sundermeyer
Fachbereich Chemie
Philipps-Universität Marburg
Hans-Meerwein-Strasse, 35032 Marburg (Germany)
Fax: (+49) 6421-282-8917
E-mail: jsu@chemie.uni-marburg.de
Prof. Dr. M. C. Holthausen
Institut für Anorganische und Analytische Chemie
Johann Wolfgang Goethe-Universität Frankfurt
Max-von-Laue Strasse 7, 60438 Frankfurt am Main (Germany)
Fax: (+49) 69-798-29260
E-mail: max.holthausen@chemie.uni-frankfurt.de

[**] The authors gratefully acknowledge financial support from the Deutsche Forschungsgemeinschaft (Schwerpunktprogramm 1118). Dr. Michael Serafin (University of Gießen), Dr. Olaf Walter (Forschungszentrum Karlsruhe), and Dr. Frank Hampel (University of Erlangen-Nürnberg) are acknowledged for their kind hospitality and their help to introduce C.W. to the details of crystal-structure analysis in nontrivial situations.

Supporting information for this article is available on the WWW under http://www.angewandte.org or from the author.

 © 2006 Wiley-VCH Verlag GmbH & Co. KGaA, Weinheim

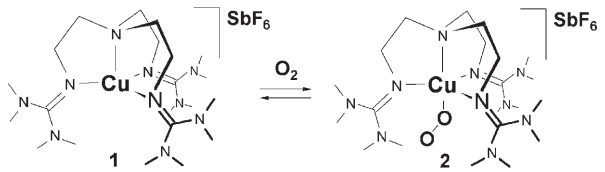

Scheme 2. Reversible binding of dioxygen to $[TMG_3trenCu]^+$.

reversible: warming of the intensely green solution of the adduct complex to room temperature caused release of dioxygen (colorless solution), while cooling of the sample led to back formation of the $Cu–O_2$ adduct (see Supporting Information). Warming/cooling cycles can be repeated many times without any evidence of major decomposition reactions. The progress of this reaction can readily be monitored by UV/Vis, NMR, or resonance Raman spectroscopy.[19]

Different from other amine or imine tren derivatives the TMG_3tren ligand easily forms stable complexes with copper(I) and with copper(II) ions as shown by crystallographic studies.[18] This stability is supported by the results of additional electrochemical investigations we performed with the $[CuTMG_3tren]^+$ complex: using cyclic voltammetry we observed reversible redox behavior in acetone ($-0.024/+0.140$ V against AgCl). Of note is that in crystals of $[Cu(TMG_3tren)]^+$ obtained from an acetonitrile solution, no solvent molecule is coordinated as an additional ligand. Even more remarkable is that in $[Cu(TMG_3tren)]Cl$ the chloride anion only functions as counterion and does not coordinate to the copper(I) ion as would be expected.[18] However, to investigate the general possibility of adding additional ligands we treated the copper(I) complex with CO in acetone at low temperatures. While it was not possible to isolate the corresponding carbonyl complex as a solid to date, we could detect its formation by IR spectroscopy (IR band at 2057 cm^{-1}, acetone solution, −80 °C).

For the present species we were also able to monitor the formation of the superoxo complex using low-temperature IR-spectroscopy ($\tilde{\nu}_{O-O} = 1122\ cm^{-1}$, acetone solution, −80 °C). This finding confirms the results of our previous resonance Raman measurements ($\tilde{\nu}_{O-O} = 1117\ cm^{-1}$). Based on the almost perfect match between experiment and quantum chemical results for the O–O stretching frequencies we excluded the presence of a side-on coordination mode and we felt safe to assign a stable 1:1 end-on $Cu–O_2$ adduct, which is best described as an end-on superoxo-copper(II) species.[19] Yet, erroneous characterizations of 1:1 $Cu-O_2$ adduct complexes and recent discussions on the assignment of end-on superoxo-copper(II) complexes in the literature[19–21] made it clear that only a crystal structure of this complex would allow for the unambiguous characterization of such a 1:1 end-on $Cu-O_2$ adduct.[1–3] In spite of the observed stability of the $Cu–O_2$ adduct formed, numerous attempts to obtain crystals of this compound failed. However, after systematic modifications of the crystallization conditions we are now able to present the missing link, a high-quality crystal structure of $[Cu(TMG_3tren)O_2]SbF_6$ (Figure 1).

Perfectly in line with our previous quantum chemical characterization[22] the dioxygen in $[Cu(TMG_3tren)O_2]SbF_6$ is

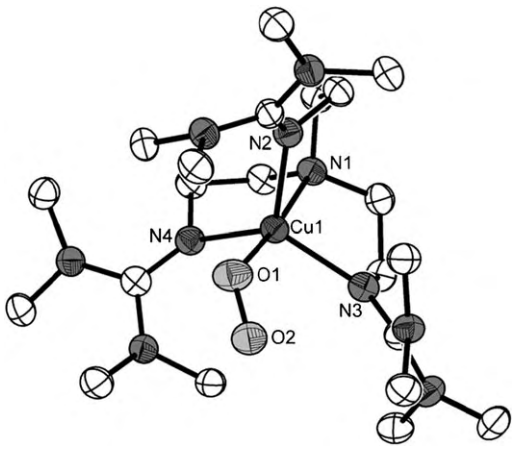

Figure 1. Molecular structure of $[TMG_3trenCu(O_2)]^+$. ORTEP plot with thermal ellipsoids set at 50% probability (hydrogen atoms, the acetone solvent molecules present in the crystal lattice, and the 6% disorder position of O2A are not shown). Selected bond lengths [Å] and angles [°]: O1–O2 1.280(3), O1–Cu1 1.927(2), O2–Cu1 2.842(7); O2-O1-Cu1 123.53(2).

coordinated to Cu1 in an end-on fashion as an axial ligand in the trigonal-bipyramidal complex. The O1–O2 bond is 1.280(3) Å and the O2-O1-Cu1 angle is 123.53(18)°. This geometry is consistent with the recent X-ray results on the copper dioxygen complex in PHM[13] in which the crystal structure, determined to 1.85 Å resolution, showed an end-on coordination mode to a mononuclear copper ion in the precatalytic enzyme complex with an O–O bond of 1.23 Å and an Cu-O-O angle of 110°.

Our present results clearly demonstrate that end-on coordination of O_2 to copper ions can lead to quite stable intermediates, which lends support to their assumed role as important intermediates in catalytic oxidation reactions. The end-on copper superoxide species most likely represents the primary adduct formed in the interaction of Cu^I ions with dioxygen molecules preceding the formation of other key copper dioxygen species shown in Scheme 1. The resolution of the crystal structure of $[Cu(TMG_3tren)(O_2)]SbF_6$ reported herein is excellent, and of far superior to that of other end-on superoxo transition-metal complexes presented to date. Hence this complex represents a key intermediate with which to correlate spectroscopic and structural features of mononuclear end-on superoxo copper complexes in the future.

Experimental Section

Cyclic voltammetry experiments were performed with a Princeton BAS Model 263 instrument, using a 1 mM solution of the copper(I) complex (tetraphenylborate as anion) in acetone. Electrodes employed were glassy carbon (working electrode), AgCl (reference electrode), and a platinum wire (auxiliary electrode). Ferrocene was used as an internal reference (0.450/0.580 V). IR-spectroscopy in solution was performed using a Nicolet 510 P FT-IR Spectrometer equipped with a low-temperature cell (RIEC) and CaF_2 windows (0.1 mm)

1: Under the inert conditions of a glove box TMG_3tren (0.6 g, 1.4 mmol) was dissolved in acetonitrile (4 mL) to which of a solution

 © 2006 Wiley-VCH Verlag GmbH & Co. KGaA, Weinheim

of $[Cu(CH_3CN)_4]SbF_6$ (0.6 g, 1.3 mmol) in acetonitrile (6 mL) was added. The complex $[Cu(TMG_3tren)]SbF_6$ was precipitated by addition of diethyl ether (approximately 40 mL). The light yellow solid was filtered and washed with diethyl ether. Yield: 0.637 g (70%).

2: Under inert conditions $[Cu(TMG_3tren)]SbF_6$ was dissolved in a very small amount of acetone, cooled to −55 °C and then oxidized with pure, dry dioxygen for 5 minutes. The green solution obtained was then kept at −80 °C for one week leading to intensely green crystals of the end-on superoxo complex, $[Cu(TMG_3tren)O_2]SbF_6$, suitable for X-ray structural characterization: Some material was taken under inert conditions from the crystallization flask kept at −80 °C and put into precooled perfluorpolyether oil. A suitable crystal was selected under the microscope using a cryostated loop, it was shock frozen using liquid nitrogen and mounted on the diffractometer which was equipped with a cooling device. For the measurement conditions see the Supporting Information.

A refinement using a first data set collected at 173 K showed a threefold 75:15:10 disorder of the end-on coordinated superoxide ligand and a very short O–O bond length of approximately 1.1 Å (unpublished results). In contrast, refinement on the data set obtained at 100 K showed only a minor disorder of 94:0:6 (see Supporting Information). The O–O bond length converges to 1.280(2) Å. Because of the small occupation factor, the geometric parameters involving the second position of oxygen disorder are not reliable. The highest residual electron density remained in the region of the SbF_6 anion.

CCDC 287898 (**1**) contains the supplementary crystallographic data for this paper. These data can be obtained free of charge from The Cambridge Crystallographic Data Centre via www.ccdc.cam.ac.uk/data_request/cif.

Received: January 26, 2006
Published online: May 3, 2006

Keywords: bioinorganic chemistry · copper · crystal structure · dioxygen ligands · tripodal ligands

[1] L. Q. Hatcher, K. D. Karlin, *J. Biol. Inorg. Chem.* **2004**, *9*, 669.
[2] E. A. Lewis, W. B. Tolman, *Chem. Rev.* **2004**, *104*, 1047.
[3] L. M. Mirica, X. Ottenwaelder, T. D. P. Stack, *Chem. Rev.* **2004**, *104*, 1013.
[4] S. Schindler, *Eur. J. Inorg. Chem.* **2000**, 2311.
[5] S. V. Kryatov, E. Rybak-Akimova, S. Schindler, *Chem. Rev.* **2005**, *105*, 2175.
[6] L. J. Que, W. B. Tolman, *Angew. Chem.* **2002**, *114*, 1160; *Angew. Chem. Int. Ed.* **2002**, *41*, 1114.
[7] E. I. Solomon, P. Chen, M. Metz, S.-K. Lee, A. E. Palmer, *Angew. Chem.* **2001**, *113*, 4702; *Angew. Chem. Int. Ed.* **2001**, *40*, 4570.
[8] K. Fujisawa, M. Tanaka, Y. Moro-oka, N. Kitajima, *J. Am. Chem. Soc.* **1994**, *116*, 12079.
[9] D. J. E. Spencer, N. W. Aboelella, A. M. Reynolds, P. L. Holland, W. B. Tolman, *J. Am. Chem. Soc.* **2002**, *124*, 2108.
[10] P. Chen, D. E. Root, C. Campochiaro, K. Fujisawa, E. I. Solomon, *J. Am. Chem. Soc.* **2003**, *125*, 466.
[11] N. W. Aboelella, S. V. Kryatov, B. F. Gherman, W. W. Brennessel, V. G. Young, Jr., R. Sarangi, E. V. Rybak-Akimova, K. O. Hodgson, B. Hedman, E. I. Solomon, C. J. Cramer, W. B. Tolman, *J. Am. Chem. Soc.* **2004**, *126*, 16896.
[12] A. M. Reynolds, B. F. Gherman, C. J. Cramer, W. B. Tolman, *Inorg. Chem.* **2005**, *44*, 6989.
[13] S. T. Prigge, B. A. Eipper, R. E. Mains, L. M. Amzel, *Science* **2004**, *304*, 864.
[14] M. Weitzer, M. Schatz, F. Hampel, F. W. Heinemann, S. Schindler, *J. Chem. Soc. Dalton Trans.* **2002**, *5*, 686.
[15] M. Weitzer, S. Schindler, G. Brehm, S. Schneider, E. Hörmann, S. Jung, S. Kaderli, A. D. Zuberbühler, *Inorg. Chem.* **2003**, *42*, 1800.
[16] C. X. Zhang, S. Kaderli, M. Costas, E.-I. Kim, Y.-M. Neuhold, K. D. Karlin, A. D. Zuberbühler, *Inorg. Chem.* **2003**, *42*, 1807.
[17] The term superbasic refers to neutral guanidine ligands, that have a p$K(BH^+)$ value more than six orders of magnitude higher than that of the most basic tertiary amines. Typically they are used as ligands for protons ("proton sponges"); see: V. Raab, J. Kipke, R. M. Gschwind, J. Sundermeyer, *Chem. Eur. J.* **2002**, *8*, 1682.
[18] V. Raab, J. Kipke, O. Burghaus, J. Sundermeyer, *Inorg. Chem.* **2001**, *40*, 6964.
[19] M. Schatz, V. Raab, S. P. Foxon, G. Brehm, S. Schneider, M. Reiher, M. C. Holthausen, J. Sundermeyer, S. Schindler, *Angew. Chem.* **2004**, *116*, 4460; *Angew. Chem. Int. Ed.* **2004**, *43*, 4360.
[20] B. A. Jazdzeweski, A. M. Reynolds, P. L. Holland, V. G. Young, Jr., S. Kaderli, A. D. Zuberbühler, W. B. Tolman, *J. Biol. Inorg. Chem.* **2003**, *8*, 381.
[21] K. Komiyama, H. Furutachi, S. Nagatomo, A. Hashimoto, H. Hayashi, S. Fujinami, M. Suzuki, T. Kitagawa, *Bull. Chem. Soc. Jpn.* **2004**, *77*, 59.
[22] Please note that in our earlier study[19] we erroneously reported an angle α(Cu-O-O) of 132.2° in Figure 3—the correct value, however, is α(Cu-O-O) = 121.4°.

 © 2006 Wiley-VCH Verlag GmbH & Co. KGaA, Weinheim

Nucleophilicity Scales

DOI: 10.1002/anie.200600542

Towards a General Scale of Nucleophilicity?**

*Thanh Binh Phan, Martin Breugst, and Herbert Mayr**

Dedicated to Professor Dieter Enders on the occasion of his 60th birthday

The development of quantitative scales of nucleophilicity has intrigued chemists for more than 50 years.[1] The optimistic start in the 1950s, which delivered the Swain–Scott equation [Eq. (1)][2] and the Edwards equation[3] was followed by a period of disillusionment in the 1960s, when more and more factors were identified which had to be considered for a quantitative description of nucleophilicity.[4]

[*] Dr. T. B. Phan, M. Breugst, Prof. Dr. H. Mayr
Department Chemie und Biochemie
Ludwig-Maximilians-Universität München
Butenandtstrasse 5–13 (Haus F), 81377 München (Germany)
Fax: (+49) 89-2180-77717
E-mail: herbert.mayr@cup.uni-muenchen.de

[**] Financial support by the Deutsche Forschungsgemeinschaft (Ma673/21-1) and the Fonds der Chemischen Industrie is gratefully acknowledged. We thank F. Brotzel and Dr. A. R. Ofial for helpful discussions.

Supporting information for this article is available on the WWW under http://www.angewandte.org or from the author.

© 2006 Wiley-VCH Verlag GmbH & Co. KGaA, Weinheim

$$\lg(k/k_{H_2O}) = s'_E n$$
n = nucleophilicity constant ($n_{H_2O} = 0$) (1)
s'_E = sensitivity of electrophile ($s'_{CH_3Br} = 1$)[5]

The culmination of the pessimistic view was reached in 1968, when Pearson reported that the reactivities of nucleophiles towards *trans*-$[Pt(py)_2Cl_2]$ (py = pyridine) did not correlate with any of the nucleophilicity parameters known at that time and finally concluded: "*At present it is not possible to predict quantitatively the rates of nucleophilic displacement reactions if a number of substrates of widely varying properties are considered.*"[6]

Only four years later, Ritchie reported a correlation of astonishing simplicity [Eq. (2)],[7] which claims that the relative reactivities of a variety of nucleophiles toward carbocations and diazonium ions can be described by a single, electrophile-independent nucleophilicity parameter N_+.

$$\lg(k/k_o) = N_+ \quad (2)$$

The impact of this so-called constant selectivity relationship has significantly been augmented by the work of Kane-Maguire and Sweigart et al. who showed that Equation (2) holds also for the reactions of cationic metal π-complexes with a variety of nucleophiles.[8,9]

The most extensive nucleophilicity scale,[10,11] presently available, has been derived from the rate constants of the reactions of benzhydrylium ions with alkenes, arenes, enol ethers, ketene acetals,[12] enamines,[13] allyl element compounds,[14] transition-metal π-complexes,[15] diazoalkanes,[16] and delocalized carbanions[17–19] (π-nucleophiles), amines,[20] alcohols,[21] alkoxides,[22] phosphanes,[23] inorganic anions[24–27] (*n*-nucleophiles), and a variety of hydrides[28–31] (σ-nucleophiles); these rate constants were subjected to a least-squares minimization on the basis of Equation (3)[10,11] in which k is the second-order rate constant at 20 °C and E is a nucleophile-independent electrophilicity parameter.

$$\lg k = s_N(E + N) \quad (3)$$

It has been shown that the electrophile-independent nucleophile-specific N and s_N parameters[5] derived in this way can be employed for predicting the rates of reactions of the corresponding nucleophiles with carbocations,[10,11] cationic metal-π-complexes,[10,11] as well as electron-deficient alkenes[32] and arenes.[33,34] Their applicability to S_N2 type reactions has not yet been examined.

Recently, we have found that the nucleophilicity parameters N for aqueous and alcoholic solvents, which we derived from the rates of decay of benzhydrylium ions in these solvents,[21] correlate linearly with Kevill's N_T parameters.[35] Because the N_T parameters reflect the rates of solvolysis of the *S*-methyldibenzothiophenium ion (**1**) in the corresponding solvents, that is, the rates of S_N2 reactions, we were prompted to examine whether the nucleophilicity parameters N and s_N derived from Equation (3) are generally applicable to bimolecular nucleophilic substitutions. We now demonstrate that this is the case for a variety of substrates and suggest a general correlation equation which includes Equations (1)–(3) as special cases.

The reactions of **1** with nucleophiles proceed with changes in the UV spectrum as exemplified in Figure 1 for the reaction of **1** with the azide ion. The decrease of the absorbance at 271 nm owing to the consumption of **1** is accompanied by the increase of the absorbances at 285 nm and 325 nm as a result of the formation of dibenzothiophene (**2**).

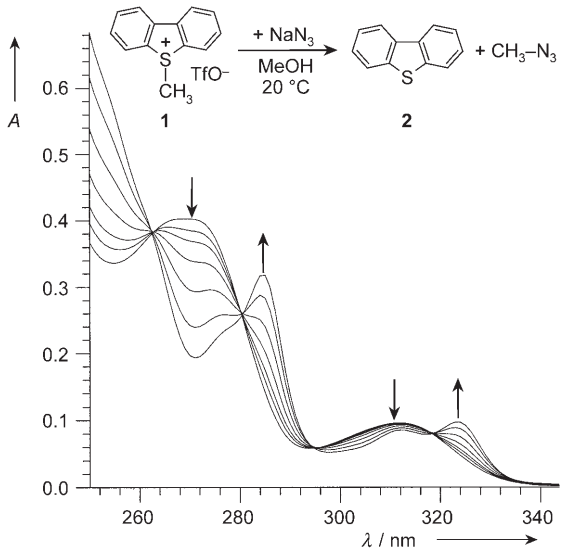

Figure 1. UV spectra during the reaction of **1** with sodium azide (in MeOH, 20 °C) at $t = 0$, 1, 2, 4, 8, 16, and 47 min; $[\mathbf{1}]_0 = 6.05 \times 10^{-5}$ M, $[N_3^-]_0 = 3.51 \times 10^{-3}$ M.

As the nucleophiles were generally employed in high excess over **1**, first-order rate constants k_{obs} [Eq. (4)] can be derived from the exponential decay of [**1**] (absorbance at 271 nm). The formation of product **2** can be monitored by the exponential increase of the absorbances at 285 and 325 nm.

$$d[\mathbf{1}]/dt = -k_{obs}[\mathbf{1}] \quad (4)$$

The least-squares fits of the time-dependent absorbances A to the single-exponential function $A_t = A_0 \exp(-k_{obs} t) + C$ (for 271 nm) and $A_t = A_{end}[1 - \exp(-k_{obs} t)] + C$ (for 285 and 325 nm) gave rise to identical first-order rate constants $k_{obs} = 1.83 \times 10^{-3}\ s^{-1}$ at any of these three wavelengths (Figure 2). Details of the kinetic investigations are given in the Supporting Information.

As indicated by Equation (5), the second-order rate constants k_2 for the reactions of **1** with the nucleophiles listed in Table 1 were obtained from the slopes of k_{obs} versus [Nu] plots.

$$k_{obs} = k_2[Nu] + k_{MeOH} \quad (5)$$

The small values of the intercepts of these plots (see Supporting Information) indicate that the competing reaction of **1** with the solvent methanol is negligible. This observation

 © 2006 Wiley-VCH Verlag GmbH & Co. KGaA, Weinheim

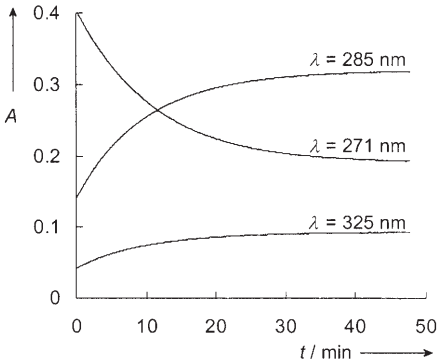

Figure 2. Monitoring of the reaction of **1** with sodium azide depicted in Figure 1 at three different wavelengths (methanol, 20 °C).

is in accord with the first-order rate constant for the reaction of **1** with methanol (Table 1), which was reported by Kevill[36] and which is corroborated in this work.

For several nucleophiles used in this work, N and s_N parameters were not available. These parameters were derived from the kinetics of the reactions of the corresponding nucleophiles with the benzhydrylium reference electrophiles,[10] following the procedure described in the literature.[22] For technical reasons, these reactions could not be studied in pure methanol and were performed in the presence of 9% acetonitrile (see footnotes of Table 1). Details of the kinetic experiments are given in the Supporting Information.

Figure 3 shows that the correlation of $(\lg k)/s_N$ versus N for the reactions of the sulfonium ion **1** with C-, N-, O-, and P-nucleophiles, which covers 20 units of the logarithmic nucleophilicity scale, is linear with a slope of 0.6. Although the relevance of the benzhydrylium-based parameters N and s_N for this S_N2 reaction is thus demonstrated, the non-unity slope indicates that Equation (3) is not applicable because variation of the nucleophiles affects the reactivities toward **1** by only 60% of the amount that is observed in the reactions with benzhydrylium ions (slope = 1.00).

A similar correlation is found for the reactions of different types of charged and neutral nucleophiles with iodomethane in methanol (Figure 4).

While the paucity of data in a narrow reactivity range do not allow a discussion of the slope of the graph in Figure 4, it can be seen that in both correlations (Figures 3 and 4) the absolute deviations from the correlation lines are generally smaller than one order of magnitude despite the large variety of nucleophiles employed. It can thus be deduced that the order of nucleophilicities toward electrophilic C_{sp^3} and C_{sp^2} centers is not fundamentally different.

This conclusion may be surprising because the contrasting reactivity orders $CN^- > HO^- > N_3^-$ (towards CH_3Br) and $CN^- < HO^- < N_3^-$ (towards Ar_3C^+) have been considered as an indication that nucleophilicities toward C_{sp^3} and C_{sp^2} centers are controlled by different factors.[41] It should be noted, however, that CN^- and HO^- are of similar reactivity toward both types of electrophiles, and it is only N_3^- which deviates significantly (Table 2).

In agreement with our findings, more comprehensive comparisons had already come to the conclusion that nucleophilicities toward C_{sp^3} and C_{sp^2} centers are closely related. Bunting and co-workers, for example, reported that the rate constants of the reactions of about 60 amines with methyl *p*-nitrosulfonates correlate linearly with the corresponding reactivities toward 4-vinylpyridinium ions.[44] Analogous orders of nucleophilicities toward carbocations and haloalkanes have also been claimed by Richard and co-workers[45] who noted that only N_3^- and α-effect nucleophiles deviate strongly from the linear correlation between Ritchie's N_+ and Swain and Scott's n constants (Figure 5).

These reports and preliminary data for S_N2 reactions with further haloalkanes[46] indicate that the benzhydryl-cation-

Table 1: Rate constants for the reactions of **1** with nucleophiles (in methanol, 20 °C).

Nucleophiles	N	s_N	k
$(MeO_2C)_2CH^-$	18.24[a]	0.644[a]	1.41×10^{1} [b,c]
$(NC)_2CH^-$	18.21[a]	0.686[a]	1.13×10^{1} [b,c]
pyrrolidine	15.97[d]	0.627[d]	1.25[b]
piperidine	15.63[d]	0.644[d]	1.16[b]
morpholine	15.40[d]	0.643[d]	9.9×10^{-1} [b,e]
azide	14.54[f]	0.822[f]	5.08×10^{-1} [b]
methoxide	14.51[g]	0.680[g]	1.50[b]
diethanolamine	13.71[d]	0.670[d]	2.92×10^{-1} [b]
hydrazine	13.47[d]	0.702[d]	3.24×10^{-1} [b]
benzylamine	13.46[d]	0.624[d]	2.25×10^{-1} [b]
n-propylamine	13.41[d]	0.657[d]	2.01×10^{-1} [b]
ethanolamine	13.23[d]	0.646[d]	1.91×10^{-1} [b]
hydroxylamine	12.23[d]	0.663[d]	1.07×10^{-1} [b]
imidazole	10.41[d]	0.696[d]	1.09×10^{-2} [b]
2,2,2-trifluoroethylamine	10.20[d]	0.917[d]	1.02×10^{-2} [b]
trimethylphosphite	9.04[d]	0.698[d]	1.80×10^{-3} [b]
methanol	7.54[h,i]	0.92[h,i]	7.23×10^{-5} [j]
ethanol	7.44[h,i]	0.90[h,i]	1.14×10^{-4} [j]
propan-1-ol	7.05[h,k]	0.80[h,k]	8.50×10^{-5} [l]
80E20W[m]	6.68[h,i]	0.85[h,i]	4.84×10^{-5} [j]
propan-2-ol	6.49[h,k]	0.96[h,k]	6.42×10^{-5} [l]
60E40W[m]	6.28[h,i]	0.87[h,i]	1.99×10^{-5} [j]
40E60W[m]	5.81[h,i]	0.90[h,i]	8.91×10^{-6} [j]
80A20W[m]	5.77[h,n]	0.87[h,n]	2.06×10^{-5} [j]
90A10W[m]	5.70[h,n]	0.85[h,n]	2.14×10^{-5} [j]
20E80W[m]	5.54[h,i]	0.94[h,i]	3.32×10^{-6} [j]
water	5.20[h,i]	0.89[h,i]	2.03×10^{-6} [j]
40T60W[m]	3.77[h,i]	0.88[h,i]	8.97×10^{-7} [j,o]
60T40W[m]	3.42[h,i]	0.90[h,i]	5.11×10^{-7} [j,p]
90T10W[m]	2.93[h,i]	0.88[h,i]	1.36×10^{-7} [j,q]
2,2,2-trifluoroethanol	1.23[h,i]	0.92[h,i]	5.66×10^{-9} [j]

[a] From reference [37]. [b] Second-order rate constant [$M^{-1}s^{-1}$], this work; see Supporting Information. [c] In 91/9 (v/v) methanol/acetonitrile. [d] Reactivity parameters N and s_N refer to second-order rate constants in 91/9 (v/v) methanol/acetonitrile, this work; see Supporting Information. [e] Only two data points were available for the determination of k [$M^{-1}s^{-1}$]. [f] In 91/9 (v/v) methanol/acetonitrile, from ref. [38]. [g] In 91/9 (v/v) methanol/acetonitrile, from ref. [22]. [h] Reactivity parameters N and s_N refer to first-order rate constants. [i] From ref. [21]; [j] First-order rate constants in [s^{-1}] at 25.1 °C, from ref. [36]. [k] Reactivity parameters of 91/9 (v/v) alcohol/acetonitrile mixtures, from ref. [22]. [l] First-order rate constant in [s^{-1}], this work, for details see Supporting Information. [m] Mixtures of solvents are given as (v/v); solvents: A = acetone, E = ethanol, T = 2,2,2-trifluoroethanol, W = water. [n] From ref. [39]. [o] Rate constant for 50T50W (w/w) [= 42T58W (v/v)]. [p] Rate constant for 70T30W (w/w) [= 63T37W (v/v)]. [q] Rate constant for 90T10W (w/w) [= 87T13W (v/v)].

 © 2006 Wiley-VCH Verlag GmbH & Co. KGaA, Weinheim

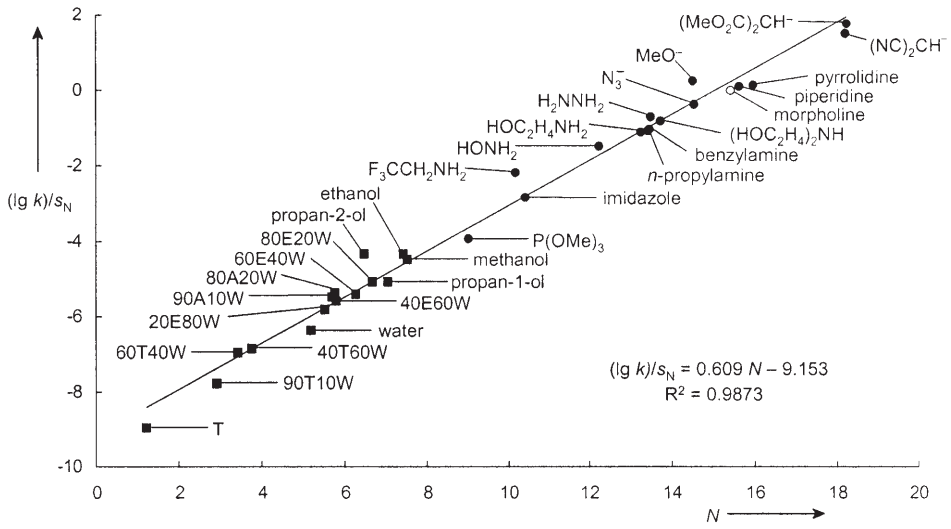

Figure 3. Correlation of $(\lg k)/s_N$ for the reactions of **1** with various solvents and with solutions of nucleophiles in methanol versus the nucleophilicity parameters N. Nucleophile-specific parameters s_N and N as well as rate constants k (■ in s^{-1}, ● and ○ in $M^{-1}s^{-1}$) from Table 1; the rate constant for morpholine (○) was not used for the correlation; mixtures of solvents are given as v/v; solvents: A = acetone, E = ethanol, T = 2,2,2-trifluoroethanol, W = water.

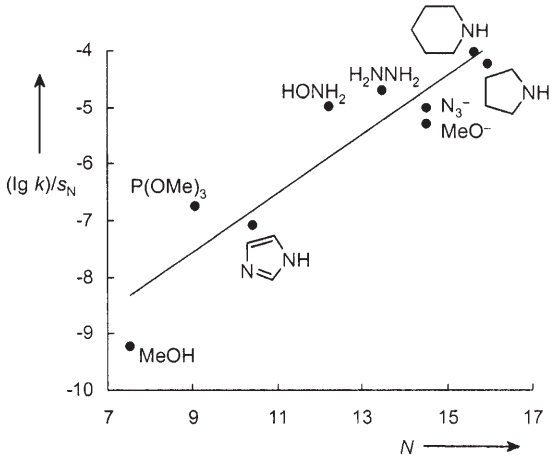

Figure 4. Reactions of iodomethane with methanol and with solutions of various nucleophiles in methanol (N and s_N parameters from Table 1; rate constants of the reactions with iodomethane at 25 °C from ref. [6, 40]). In ref. [6] the rate constant for the reaction of $P(OMe)_3$ with iodomethane is reported to be of lower reliability than the other rate constants.

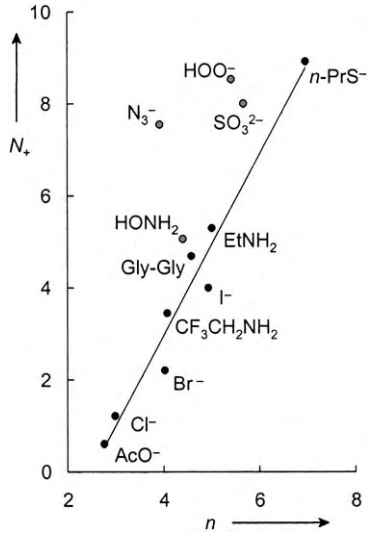

Figure 5. Correlation between Ritchie N_+ and Swain–Scott n parameters (from ref. [45]); entries for the azide ion and for α-effect nucleophiles (○) were not considered for the correlation.

Table 2: Swain–Scott (n) and Ritchie (N_+) nucleophilicity constants of the cyanide, hydroxide, and azide ions in water.

Nucleophiles	$n(CH_3Br)$[a]	N_+ (Ar_3C^+)[b]
CN^-	5.10	4.12
HO^-	4.20	4.75
N_3^-	4.00	7.54

[a] From ref. [42]; [b] From ref. [43].

based nucleophilicity parameters N and s_N are also suitable for many S_N2 type reactions. We, therefore, suggest extending Equation (3) by an electrophile-specific parameter s_E to arrive at the general Equation (6) (see Scheme 1), which includes the empirical correlations given in Equations (1)–(3) as special cases.[47]

If only reactions of nucleophiles with carbocations are considered, the electrophile-specific slope parameter s_E becomes 1 and Equation (6) transforms into Equation (3) (Scheme 1, left). We have already discussed that Equation (3) simplifies to Ritchie's constant selectivity relationship [Eqs. (2a) or (2)] if only reactions of carbocations with nucleophiles of $s_N \approx 0.6$, for example, CN^-, HO^-, MeO^-, RNH_2 are considered.[20] Water, originally selected as the reference nucleophile of the Ritchie relationship,[7] was later reported to deviate from the constant selectivity relationship in Equation (2).[43,48] We have recently shown that this deviation is due to the slope parameter $s_N(H_2O) = 0.89$[21] which differs from those of the other nucleophiles studied by Ritchie. Note, however, that other groups of reactions, for example, reactions of terminal alkenes ($s_N = 1$) with carbocations ($s_E = 1$) also constitute discrete sets of constant selectivity relationships which can be described by Equation (2).[49]

The Swain–Scott equation [Eq. (1)] was derived from rate constants for S_N2 reactions of haloalkanes and related compounds with n-nucleophiles of $s_N \approx 0.6$. Substitution of this value into Equation (6) yields Equation (1a) which is equivalent to the Swain–Scott relationship (Scheme 1, right).

While it is tempting to consider Equation (6) as *the* equation for describing polar organic reactivity, it should be emphasized that the scope and limitations of Equation (6)

 © 2006 Wiley-VCH Verlag GmbH & Co. KGaA, Weinheim

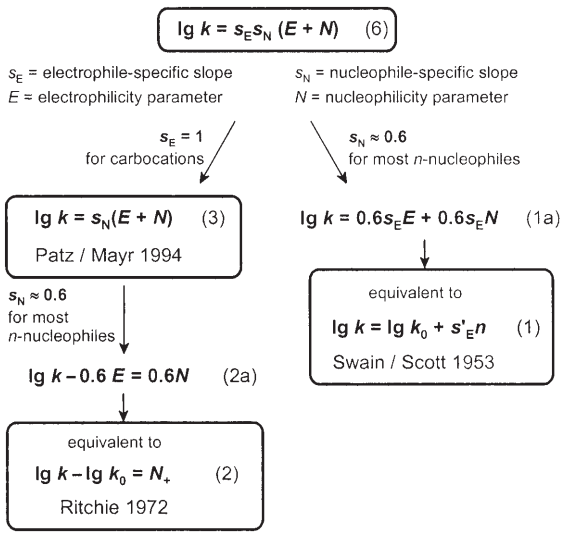

Scheme 1. General equation [Eq. (6)] for electrophile–nucleophile combinations and its relation to other more specialized correlation equations.

have not yet been explored. As the nucleophilicity parameters N and s_N have been derived from reactions with carbon electrophiles whereas the electrophilicity parameters E and s_E have been derived from reactions with carbon nucleophiles, Equation (6) should only be applied to reactions where at least one of the reaction centers in either electrophile or nucleophile is carbon. Even then, deviations are to be expected, if stabilizing or destabilizing geminal substituent interactions are created or destroyed in the transition state. Thus, carboxonium ions react faster with alcohols than predicted by Equations (3) or (6) (anomeric product stabilization).[50] On the other hand, Ritchie's observation that the N_+ parameters for heteronucleophiles defined by Equation (2) are also applicable to reactions with diazonium ions[7,43,51] indicates that in certain cases Equation (6) may also hold for combinations of heteroelectrophiles with heteronucleophiles.

We hope that the possibility to describe a large variety of organic reactions by a single empirical correlation [Eq. (6)] will stimulate further activities to unveil the physical basis of electrophilicity and nucleophilicity.

Received: February 9, 2006
Published online: April 28, 2006

Keywords: kinetics · linear free energy relationships · nucleophiles · reaction mechanisms · reactivity scales

[1] *Nucleophilicity* (Eds.: M. Harris, S. P. McManus), American Chemical Society, Washington, DC, **1987**, *(Adv. Chem. Ser. 215)*.
[2] C. G. Swain, C. B. Scott, *J. Am. Chem. Soc.* **1953**, *75*, 141 – 147.
[3] a) J. O. Edwards, *J. Am. Chem. Soc.* **1954**, *76*, 1540 – 1547; b) J. O. Edwards, *J. Am. Chem. Soc.* **1956**, *78*, 1819 – 1820.
[4] J. F. Bunnett, *Annu. Rev. Phys. Chem.* **1963**, *14*, 271 – 290; see also reference [1].
[5] In the original literature, s'_E in Equation (1) and s_N in Equation (3) are both termed *s*. Because use of the same symbol for different properties would lead to confusion herein, we have modified the symbols used in the literature.
[6] R. G. Pearson, H. Sobel, J. Songstad, *J. Am. Chem. Soc.* **1968**, *90*, 319 – 326.
[7] a) C. D. Ritchie, *Acc. Chem. Res.* **1972**, *5*, 348 – 354; b) C. D. Ritchie, P. O. I. Virtanen, *J. Am. Chem. Soc.* **1972**, *94*, 4966 – 4971.
[8] L. A. P. Kane-Maguire, E. D. Honig, D. A. Sweigart, *Chem. Rev.* **1984**, *84*, 525 – 543.
[9] R. D. Pike, D. A. Sweigart, *Coord. Chem. Rev.* **1999**, *187*, 183 – 222.
[10] a) H. Mayr, T. Bug, M. F. Gotta, N. Hering, B. Irrgang, B. Janker, B. Kempf, R. Loos, A. R. Ofial, G. Remennikov, H. Schimmel, *J. Am. Chem. Soc.* **2001**, *123*, 9500 – 9512; b) For a comprehensive listing of nucleophilicity parameters N and electrophilicity parameters E, see http://www.cup.uni-muenchen.de/oc/mayr/DBintro.html.
[11] a) H. Mayr, M. Patz, *Angew. Chem.* **1994**, *106*, 990 – 1010; *Angew. Chem. Int. Ed. Engl.* **1994**, *33*, 938 – 957; b) H. Mayr, B. Kempf, A. R. Ofial, *Acc. Chem. Res.* **2003**, *36*, 66 – 77; c) H. Mayr, A. R. Ofial in *Carbocation Chemistry* (Eds.: G. A. Olah, G. K. S. Prakash), Wiley, Hoboken, NJ, **2004**, chap. 13, pp. 331 – 358; d) H. Mayr, A. R. Ofial, *Pure Appl. Chem.* **2005**, *77*, 1807 – 1821.
[12] a) T. Tokuyasu, H. Mayr, *Eur. J. Org. Chem.* **2004**, 2791 – 2796; b) A. D. Dilman, H. Mayr, *Eur. J. Org. Chem.* **2005**, 1760 – 1764.
[13] a) A. D. Dilman, S. L. Ioffe, H. Mayr, *J. Org. Chem.* **2001**, *66*, 3196 – 3200; b) B. Kempf, N. Hampel, A. R. Ofial, H. Mayr, *Chem. Eur. J.* **2003**, *9*, 2209 – 2218.
[14] F. Dulich, K.-H. Müller, A. R. Ofial, H. Mayr, *Helv. Chim. Acta* **2005**, *88*, 1754 – 1768.
[15] a) H. Mayr, K.-H. Müller, *Collect. Czech. Chem. Commun.* **1999**, *64*, 1770 – 1779; b) H. Mayr, O. Kuhn, C. Schlierf, A. R. Ofial, *Tetrahedron* **2000**, *56*, 4219 – 4229.
[16] T. Bug, M. Hartnagel, C. Schlierf, H. Mayr, *Chem. Eur. J.* **2003**, *9*, 4068 – 4076.
[17] a) R. Lucius, H. Mayr, *Angew. Chem.* **2000**, *112*, 2086 – 2089; *Angew. Chem. Int. Ed.* **2000**, *39*, 1995 – 1997; b) R. Lucius, R. Loos, H. Mayr, *Angew. Chem.* **2002**, *114*, 97 – 102; *Angew. Chem. Int. Ed.* **2002**, *41*, 91 – 95.
[18] T. Bug, T. Lemek, H. Mayr, *J. Org. Chem.* **2004**, *69*, 7565 – 7576.
[19] T. Bug, H. Mayr, *J. Am. Chem. Soc.* **2003**, *125*, 12980 – 12986.
[20] S. Minegishi, H. Mayr, *J. Am. Chem. Soc.* **2003**, *125*, 286 – 295.
[21] S. Minegishi, S. Kobayashi, H. Mayr, *J. Am. Chem. Soc.* **2004**, *126*, 5174 – 5181.
[22] T. B. Phan, H. Mayr, *Can. J. Chem.* **2005**, *83*, 1554 – 1560.
[23] B. Kempf, H. Mayr, *Chem. Eur. J.* **2005**, *11*, 917 – 927.
[24] R. Loos, S. Kobayashi, H. Mayr, *J. Am. Chem. Soc.* **2003**, *125*, 14126 – 14132.
[25] A. A. Tishkov, H. Mayr, *Angew. Chem.* **2005**, *117*, 145 – 148; *Angew. Chem. Int. Ed.* **2005**, *44*, 142 – 145.
[26] S. Minegishi, R. Loos, S. Kobayashi, H. Mayr, *J. Am. Chem. Soc.* **2005**, *127*, 2641 – 2649.
[27] A. A. Tishkov, U. Schmidhammer, S. Roth, E. Riedle, H. Mayr, *Angew. Chem.* **2005**, *117*, 4699 – 4703; *Angew. Chem. Int. Ed.* **2005**, *44*, 4623 – 4626.
[28] H. Mayr, G. Lang, A. R. Ofial, *J. Am. Chem. Soc.* **2002**, *124*, 4076 – 4083.
[29] H. Mayr, N. Basso, G. Hagen, *J. Am. Chem. Soc.* **1992**, *114*, 3060 – 3066.
[30] H. Mayr, N. Basso, *Angew. Chem.* **1992**, *104*, 1103 – 1105; *Angew. Chem. Int. Ed. Engl.* **1992**, *31*, 1046 – 1048.
[31] M. A. Funke, H. Mayr, *Chem. Eur. J.* **1997**, *3*, 1214 – 1222.
[32] T. Lemek, H. Mayr, *J. Org. Chem.* **2003**, *68*, 6880 – 6886.

 © 2006 Wiley-VCH Verlag GmbH & Co. KGaA, Weinheim

[33] a) F. Terrier, S. Lakhdar, R. Goumont, T. Boubaker, E. Buncel, *Chem. Commun.* **2004**, 2586 – 2587; b) F. Terrier, S. Lakhdar, T. Boubaker, R. Goumont, *J. Org. Chem.* **2005**, *70*, 6242 – 6253.
[34] G. Ya. Remennikov, B. Kempf, A. R. Ofial, K. Polborn, H. Mayr, *J. Phys. Org. Chem.* **2003**, *16*, 431 – 437.
[35] D. N. Kevill in *Advances in Quantitative Structure-Property Relationship*, *Vol. 1* (Ed.: M. Charton), JAI, Greenwich, **1996**, pp. 81 – 115.
[36] D. N. Kevill, S. W. Anderson, *J. Org. Chem.* **1991**, *56*, 1845 – 1850.
[37] T. B. Phan, H. Mayr, *Eur. J. Org. Chem.* **2006**, in press.
[38] T. B. Phan, H. Mayr, *J. Phys. Org. Chem.* **2006**, in press.
[39] B. Denegri, S. Minegishi, O. Kronja, H. Mayr, *Angew. Chem.* **2004**, *116*, 2353 – 2356; *Angew. Chem. Int. Ed.* **2004**, *43*, 2302 – 2305.
[40] For the reaction of MeOH with MeI at 25 °C, the first-order rate constant $k = 3.3 \times 10^{-9}\ s^{-1}$ from ref. [6] as well as $N = 7.54$ and $s_N = 0.92$ from ref. [21] were used.
[41] a) A. Pross in *Theoretical and Physical Principles in Organic Reactivity*, Wiley, New York, **1995**, p. 232; b) S. Hoz in *Nucleophilicity* (Eds.: M. Harris, S. P. McManus), American Chemical Society, Washington, DC, **1987**, pp. 181 – 194.
[42] J. Koskikallio, *Acta Chem. Scand.* **1969**, *23*, 1477 – 1489.
[43] C. D. Ritchie, *Can. J. Chem.* **1986**, *64*, 2239 – 2250.
[44] J. W. Bunting, J. M. Mason, C. K. M. Heo, *J. Chem. Soc. Perkin Trans.* 2 **1994**, 2291 – 2300.
[45] J. P. Richard, M. M. Toteva, J. Crugeiras, *J. Am. Chem. Soc.* **2000**, *122*, 1664 – 1674.
[46] T. B. Phan, H. Mayr, unpublished results.
[47] Because s_E and E are nucleophile independent, and s_N and N are electrophile independent, Equation (6) is equivalent to $\lg k = s_N E' + s_E N'$, where $E' = s_E E$ and $N' = s_N N$. For the same reasons discussed for Equation (3) (see ref. [11]), the parameters E' and N' are less convenient in practical use. Hence, we prefer to use the version of Equation (6) shown in Scheme 1.
[48] a) C. D. Ritchie, *J. Am. Chem. Soc.* **1975**, *97*, 1170 – 1179; b) C. D. Ritchie, M. Sawada, *J. Am. Chem. Soc.* **1977**, *99*, 3754 – 3761; c) C. D. Ritchie, J. E. Van Verth, P. O. I. Virtanen, *J. Am. Chem. Soc.* **1982**, *104*, 3491 – 3497; d) C. D. Ritchie, *J. Am. Chem. Soc.* **1984**, *106*, 7187 – 7194.
[49] H. Mayr, *Angew. Chem.* **1990**, *102*, 1415 – 1428; *Angew. Chem. Int. Ed. Engl.* **1990**, *29*, 1371 – 1384.
[50] a) *The Anomeric Effect and Associated Stereoelectronic Effects* (Ed.: G. R. J. Thatcher), *ACS Symp. Ser.* **1993**, *539*; b) E. Juaristi, G. Cuevas, *Tetrahedron* **1992**, *48*, 5019 – 5087.
[51] C. D. Ritchie, P. O. I. Virtanen, *J. Am. Chem. Soc.* **1972**, *94*, 1589 – 1594.

 © 2006 Wiley-VCH Verlag GmbH & Co. KGaA, Weinheim

Protein Folding

DOI: 10.1002/anie.200600008

Details of the Partial Unfolding of T4 Lysozyme on Quartz Using Site-Directed Spin Labeling**

*Kerstin Jacobsen, Wayne L. Hubbell, Oliver P. Ernst, and Thomas Risse**

The adsorption of proteins at solid surfaces, which has been investigated intensively during the last three decades, has been triggered largely by the technological interest in the development of biocompatible materials for implants and engineered tissue.[1–4] One of the main challenges in the development of these materials is the suppression of inflammatory responses caused by the uptake and concomitant denaturing of proteins at the surface of the materials. A variety of strategies have been explored to circumvent this problem.[5–10] However, insight into the microscopic details of the interaction of proteins with solid surfaces is rather scarce.[11–14] The problem is complex owing to the large number of rather weak interactions that determine the native protein fold. This structure is perturbed by interactions of the protein with a surface leading to the structural changes in the adsorbed state. An important piece of information to gain insight into this problem on the microscopic level is the structure of the protein in the adsorbed state. Yet, the number of experimental techniques for obtaining this information for adsorbed proteins is very restricted. The application of the classical methods for protein structure analysis, namely, crystallography and NMR spectroscopy, to adsorbed proteins is up to now limited to special cases (e.g. Refs. [15,16]). Surface-sensitive variants of vibrational (ATR-IR, Raman, SFG) spectroscopy,[17–21] fluorescence spectroscopy,[22–24] circular dichroism,[25–27] surface force measurements[28] and microscopy,[29] and neutron reflectivity[30,31] have been used to study structural changes of adsorbed proteins, providing

[*] Dr. K. Jacobsen, Dr. T. Risse
Fritz Haber Institute of the Max Planck Society
Department of Chemical Physics
Faradayweg 4–6, 14195 Berlin (Germany)
Fax: (+49) 30-8413-4316
E-mail: risse@fhi-berlin.mpg.de
Prof. Dr. W. L. Hubbell
Jules Stein Eye Institute and
Department of Chemistry and Biochemistry
University of California
Los Angeles, 90095-7008 (USA)
Dr. O. P. Ernst
Institut für medizinische Physik und Biophysik
Charité – Universitätsmedizin Berlin
Schumannstrasse 20/21, 10098 Berlin (Germany)

[**] T.R. and K.J. thank Prof. H.-J. Freund for his support of this work. K.J. thanks the Studienstiftung des deutschen Volkes for a fellowship. The work was supported by Max Planck Society, the U.S. National Institutes of Health grant EY05216 (W.L.H.), the Jules Stein Professorship Endowment (W.L.H.), and the Deutsche Forschungsgemeinschaft SFB 449 (O.P.E.).

WILEY InterScience DISCOVER SOMETHING GREAT
© 2006 Wiley-VCH Verlag GmbH & Co. KGaA, Weinheim

global statements on changes in secondary and tertiary structure or information on special chromophores. However, detailed information on the level of the backbone fold could not be obtained.

Here we show that the extension of the site-directed spin labeling (SDSL) technique to the investigation of proteins adsorbed to planar surfaces allows the determination of adsorption-induced conformational changes on the level of the backbone fold. The small globular protein T4 lysozyme (T4L) adsorbed to a quartz surface is used as an example.

SDSL has become a powerful tool for monitoring the structure and dynamics of both soluble and membrane proteins.[32–34] The technique involves the introduction of a nonnative spin-labeled side chain at a specific residue in the amino acid sequence using cysteine substitution followed by a selective coupling with a nitroxide spin label. Recently, the method was extended to the investigation of proteins adsorbed to planar lipid bilayers.[35,36] In those studies, protein adsorption with conservation of the secondary structure was demonstrated, and methods to elucidate the orientation of the protein or of secondary structural elements were developed. In contrast to the zwitterionic lipid bilayers in those studies, the quartz surface is negatively charged at neutral pH[37] while T4L carries a net positive charge under these conditions. Therefore, the protein–surface interaction is expected to be increased on the quartz surface, and a more severe perturbation of the protein structure is expected. The proposed conformations of lysozymes adsorbed on quartz surfaces, based on data from a variety of methods, differ substantially, and include the native conformation,[28,31] a conformation with extended β-sheet content,[20] a partially unfolded conformation,[22,29] and a completely unfolded state[22] (Figure 1).

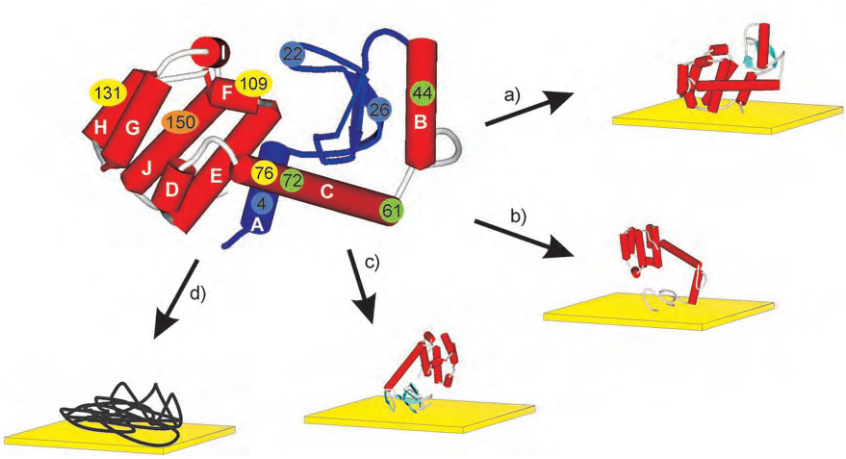

Figure 1. Models for T4 lysozyme adsorped to a quartz surface. a) intact, b) partial unfolding of the N-terminal region, c) β-sheet formation, d) complete unfolding. The highlighted residues were used to evaluate the structure in the adsorbed state.

The differences cannot be rationalized simply by differences in the experimental conditions, which were similar in each case (low ionic strength).

Here we describe the conformation of T4 lysozyme adsorbed on quartz at neutral pH and high salt concentration (0.5 M NaCl). Under these conditions the electrostatic contribution to the interaction between the positively charged protein and the negatively charged surface is screened to a large extent. We address the effect of the electrostatic contribution on the structure of the protein by comparison to experiments performed at low ionic strength, which was shown to have little effect on the structure in solution. Spin labels were introduced at ten different positions throughout the protein (Figure 1). EPR spectra recorded in solution can be compared directly to those obtained after adsorption to extract structural information. This comparison is justified by a lack of angular dependence of the EPR spectra observed for the adsorbed state.

The EPR spectra acquired for these mutants can be classified into two main groups, the first of which show virtually no change of the EPR line shape upon adsorption. This group, consisting of mutants 76R1,[*] 109R1, and 131R1 (residues shown in yellow in Figure 1), is represented by the spectra of residue 131 shown in Figure 2a. From the conservation of the EPR line shape, which encodes information on the local environment of the residue as well as backbone dynamics, and the lack of angular dependence, it can be concluded that the corresponding secondary structure elements are conserved, but there is no macroscopic alignment with respect to the quartz surface. A local microscopic disorder of the spin label can be excluded on the basis of previous experiments on supported lipid bilayers showing a macroscopic orientation of the molecule with the same local environment as probed by the spin label.[35] The finding of a random lysozyme orientation on the quartz surface is in line with a sum frequency generation study, which did not give any evidence for a macroscopic alignment of adsorbed hen egg white (HEW) lysozyme.[17]

For members of the second group, consisting of mutants 4R1, 22R1, and 26R1 (residues shown in blue in Figure 1), the line shape for the adsorbed state is drastically different from that in solution. It is particularly interesting to note that each residue has an almost identical line shape in the adsorbed state, although the local environment in the native fold and thus the EPR spectrum of each in solution are quite different. Residue 22 is located in a flexible β-turn, residue 4 is located in the short N-terminal helix, and residue 26 is located in the center of the β-sheet. Figure 2 shows the spectra in solution (upper row) for the two extremes on the mobility scale, namely, mutants 22R1 and 4R1. These are compared to the spectra measured in the adsorbed state (lower row). The solution spectra clearly reflect the difference in the local environment, while the EPR spectra in the adsorbed state are very similar and characterized by a coexistence of

[*] Spin-labeled mutants are designated by giving the residue position with a suffix R1 to indicate the spin-labeled side chain.

 © 2006 Wiley-VCH Verlag GmbH & Co. KGaA, Weinheim

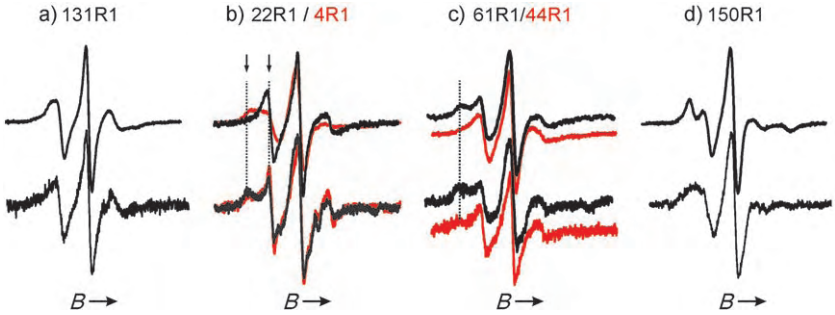

Figure 2. Typical EPR spectra for each set of mutants in solution (upper row) and in the adsorbed state (lower row). The sweep width is 100 G.

broad as well as sharp components, which can be understood as a superposition of a small fraction of a very mobile component and a majority of an immobilized component.

In addition to these two groups, a transition group is observed, which is characterized by slight changes of the line shape upon adsorption (mutants 72R1, 61R1, and 44R1; residues shown in green in Figure 1). For example, for 61R1 (see Figure 2c) and 72R1 (data not shown) the effect is very small. Only a small increase of the spectral breadth is observed, which indicates a slight decrease of local mobility. The change for residue 44 is more prominent (Figure 2c); here, a second more immobile component appears in the spectrum indicating that the environment of this residue is more strongly perturbed by the adsorption process. The spectra of 150R1 (Figure 2d) show a rather strong change in line shape; however, this change is due to a special situation which will be discussed in more detail below.

The extraction of structural information in SDSL relies on the fact that the dynamics of the spin-labeled side chain is uniquely determined by the local environment and the backbone dynamics of the secondary structure element.[38,39] Thus, changes of the EPR line shape directly reflect alterations of the local environment of the side chain. The very similar line shapes in the adsorbed state for mutants 4R1, 22R1, and 26R1, consisting of a broad immobile and a small variable fraction of a very sharp mobile component (arrows in Figure 2b), can be understood by the unfolding of this part of the protein upon interaction with the quartz surface. This would explain the similarity of the spectra of the adsorbed state for all three mutants which is explained by a similar range of local environments found within the ensemble. The similarity is not likely a result of a new folded structure which—by pure coincidence—has the very same local environment for all three residues. The broad immobile component of the spectrum can be explained by an interaction of the spin label with the surface or adjacent unfolded parts of protein. The sharp mobile component is interpreted to arise from segments of the unfolded region extending into solution, and in equilibrium with the adsorbed state. The high mobility of this component, as compared to rather flexible regions in the native fold such as the β-turn, can be understood by the lack of secondary or tertiary structure restraints. The equilibrium constant strongly favors the adsorption and varies slightly for the different residues.

In a previous investigation, we emphasized the sensitivity of the tertiary contact site 150R1, located in the C-terminal helix bundle, to surface-induced structural changes.[35] To understand the spectral change for 150R1 observed in this study (Figure 2d), it is important to realize that the unique spectrum in solution arises from a highly anisotropic motion imposed by numerous hydrophobic contacts of the side chain with the adjacent helix G and a hydrogen bond to the nitroxide ring.[40] Thus, the spectrum is very sensitive to slight modifications of the helix packing, as already observed to some extent when T4L was adsorbed to a solid-supported DOPC bilayer.[35] The EPR spectrum of 150R1 in T4L adsorbed on quartz is in line with the expectations for a solvent-exposed helical site lacking tertiary contacts. Thus, the spectral change observed upon adsorption of 150R1 is interpreted as a repacking of the helix bundle (G–J). However, the secondary structure of the helices is likely to be retained.

The line shape analysis of the EPR spectra shows that the N-terminal part of T4L, namely helix A and the adjacent β-sheet, unfolds upon adsorption on a quartz surface at high ionic strength as indicated by the blue region of the protein in Figure 1. On the other hand, spin labels located in the C-terminal region of T4L (namely in helices H and F and the C-terminal half of helix C) indicate a conserved secondary structure. It is of interest that the unfolded part of the protein has residues known to be involved in substrate binding.[41] Furthermore, an unfolding of the active site is consistent with the loss of enzymatic activity of T4L adsorbed to quartz.[42] As a result of the unfolding of helix A and the β-sheet, changes are expected for secondary structure elements in close contact with these regions. In particular, helix B and the N-terminal part of helix C should be influenced by these changes. These are indeed the regions where small changes of the local environment were observed. This behavior may be compared to unfolding of T4L induced by guanidium hydrochloride.[43] In this case, a thermodynamically more stable C-terminal domain (helices A, D–J) and an N-terminal domain of inferior stability (the β-sheet and helix B) have been identified. It is interesting to note that the low thermodynamic stability of the β-sheet inferred from guanidinium-induced unfolding correlates with unfolding at the quartz surface. However, the correlation does not hold for helices A and B. This is not surprising, because of the different mechanisms of unfolding in each case.

Electrostatic interactions have been proposed to dominate the protein–surface interaction, because of their opposite charges.[44] The observed partial unfolding of the protein contradicts this idea, because it is the C-terminal part that contains the higher positive charge density. It is commonly accepted that protein–surface interactions are governed by the balance between electrostatic, hydrophobic, and van der Waals interactions. For the experimental condition used here this balance is not in favor of the electrostatic interaction owing to screening of the 0.5 M NaCl buffer. This balance may

 © 2006 Wiley-VCH Verlag GmbH & Co. KGaA, Weinheim

easily be tuned in favor of the electrostatic contribution by a reduction of the ionic strength of the buffer solution. Experiments at low ionic strength show strong changes of the line shape for residues located in the C-terminal region of the protein, indicating that this region also takes part in the adsorption to the surface. Thus, one can conclude that the partial unfolding observed at high ionic strength is not primarily driven by electrostatic interactions. In analogy to a recent thermodynamic analysis of the interaction of HEW lysozyme with quartz, we conclude that hydrophobic interactions play an important role for this interaction.[22]

In the present study we have applied the SDSL technique to monitor structural changes of a protein adsorbed to a solid surface. For the particular example, namely T4L adsorption on quartz, we provide direct evidence for a partial unfolding of the N-terminal region around the enzymatic active site which is presumably driven by hydrophobic interactions. These results emphasize the capabilities of SDSL to study the interaction of proteins with solid surfaces: It clearly shows the potential of the method to elucidate the structure and dynamics of proteins interacting with surfaces on the level of the backbone fold hardly achieved by other techniques for proteins of arbitrary size.

Experimental Section

The cysteine-free pseudo-wild-type T4L gene containing the substitutions C45T and C97A was kindly provided by F. W. Dahlquist (University of Orgeon). The cloning, expression, purification, and spin labeling of the ten T4L mutants investigated (F4C, E22C, T26C, S44, D61C, D72C, D76C, T109C, V131C, I150C) was performed as reported previously.[35] Proteins were adsorbed at the precleaned inner surfaces of an aqueous EPR flat cell (Bruker ER160FC-Q). The cleaning procedure included treatment in chloroform for 12 h followed by rinsing sequentially with chloroform, acetone, ethanol, and water, and sonication in an ethanol/water bath. Prior to use, the cells were baked in a furnace at 600 °C for 12 h. Adsorption took place in a buffer containing 0.01 M $NH_4H_2PO_4$, 0.01 M $(NH_4)_2HPO_4$, and 0.5 M NaCl at pH 7.4. After an adsorption time of 4 h, residual protein solution was removed by washing the cell with 15 times the cell volume. EPR spectroscopy was performed on a Bruker EMX spectrometer fitted with a spherical SHQ (super-high-Q) resonator (Bruker, Karlsruhe). All spectra were acquired using 2-mW incident microwave power and appropriate modulation amplitude to avoid line broadening. To reduce the global tumbling of the protein in solution, solution spectra were recorded in 30% w/v sucrose.[38] Sucrose at this concentration does not affect the rotational mobility of the side chain.[45]

Received: January 2, 2006
Published online: May 3, 2006

Keywords: enzymes · EPR spectroscopy · mutagenesis · protein folding · structure elucidation

[1] B. Kasemo, *Surf. Sci.* **2002**, *500*, 656.
[2] D. G. Castner, B. D. Ratner, *Surf. Sci.* **2002**, *500*, 28.
[3] M. Mrksich, *Curr. Opin. Colloid Interface Sci.* **1997**, *2*, 83.
[4] T. A. Horbett, J. L. Brash, *ACS Symp. Ser.* **1995**, *602*.
[5] R. G. Chapman, E. Ostuni, S. Takayama, R. E. Holmlin, L. Yan, G. M. Whitesides, *J. Am. Chem. Soc.* **2000**, *122*, 8303.
[6] R. Langer, D. A. Tirrell, *Nature* **2004**, *428*, 487.
[7] P. Kingshott, H. J. Griesser, *Curr. Opin. Solid State Mater. Sci.* **1999**, *4*, 403.
[8] V. Vogel, G. Baneyx, *Annu. Rev. Biomed. Eng.* **2003**, *5*, 441.
[9] B. D. Ratner, S. J. Bryant, *Annu. Rev. Biomed. Eng.* **2004**, *6*, 41.
[10] S. F. Badylak, *Transp. Immunol.* **2004**, *12*, 367.
[11] P. Harder, M. Grunze, R. Dahint, G. M. Whitesides, P. E. Laibinis, *J. Phys. Chem. B* **1998**, *102*, 426.
[12] K. Feldman, G. Hahner, N. D. Spencer, P. Harder, M. Grunze, *J. Am. Chem. Soc.* **1999**, *121*, 10134.
[13] K. Glasmastar, C. Larsson, F. Hook, B. Kasemo, *J. Colloid Interface Sci.* **2002**, *246*, 40.
[14] E. E. Ross, T. Spratt, S. C. Liu, L. J. Rozanski, D. F. O'Brien, S. S. Saavedra, *Langmuir* **2003**, *19*, 1766.
[15] S. J. Opella, F. M. Marassi, *Chem. Rev.* **2004**, *104*, 3587.
[16] A. Brisson, G. Mosser, R. Huber, *J. Mol. Biol.* **1991**, *220*, 199.
[17] G. Kim, M. Gurau, J. Kim, P. S. Cremer, *Langmuir* **2002**, *18*, 2807.
[18] A. Sethuraman, G. Belfort, *Biophys. J.* **2005**, *88*, 1322.
[19] J. Wang, Z. Paszti, M. A. Even, Z. Chen, *J. Phys. Chem. B* **2004**, *108*, 3625.
[20] A. Ball, R. A. L. Jones, *Langmuir* **1995**, *11*, 3542.
[21] D. H. Murgida, P. Hildebrandt, *Acc. Chem. Res.* **2004**, *37*, 854.
[22] C. Czeslik, R. Winter, *Phys. Chem. Chem. Phys.* **2001**, *3*, 235.
[23] C. Czeslik, *Z. Phys. Chem.* **2004**, *218*, 771.
[24] S. M. Daly, T. M. Przybycien, R. D. Tilton, *Langmuir* **2003**, *19*, 3848.
[25] P. Billsten, M. Wahlgren, T. Arnebrant, J. McGuire, H. Elwing, *J. Colloid Interface Sci.* **1995**, *175*, 77.
[26] M. H. Tian, W. K. Lee, M. K. Bothwell, J. McGuire, *J. Colloid Interface Sci.* **1998**, *200*, 146.
[27] M. Karlsson, L. G. Martensson, B. H. Jonsson, U. Carlsson, *Langmuir* **2000**, *16*, 8470.
[28] J. C. Froberg, T. Arnebrant, J. McGuire, P. M. Claesson, *Langmuir* **1998**, *14*, 456.
[29] D. T. Kim, H. W. Blanch, C. J. Radke, *Langmuir* **2002**, *18*, 5841.
[30] G. Jackler, R. Steitz, C. Czeslik, *Langmuir* **2002**, *18*, 6565.
[31] T. J. Su, J. R. Lu, R. K. Thomas, Z. F. Cui, J. Penfold, *J. Colloid Interface Sci.* **1998**, *203*, 419.
[32] W. L. Hubbell, A. Gross, R. Langen, M. A. Lietzow, *Curr. Opin. Struct. Biol.* **1998**, *8*, 649.
[33] W. L. Hubbell, D. S. Cafiso, C. Altenbach, *Nat. Struct. Biol.* **2000**, *7*, 735.
[34] G. E. Fanucci, K. A. Coggshall, N. Cadieux, M. Kim, R. J. Kadner, D. S. Cafiso, *Biochemistry* **2003**, *42*, 1391.
[35] K. Jacobsen, S. Oga, W. L. Hubbell, T. Risse, *Biophys. J.* **2005**, *88*, 4351.
[36] T. Risse, W. L. Hubbell, J. M. Isas, H. T. Haigler, *Phys. Rev. Lett.* **2003**, *91*.
[37] P. L. Edmiston, S. S. Saavedra, *Biophys. J.* **1998**, *74*, 999.
[38] H. S. McHaourab, M. A. Lietzow, K. Hideg, W. L. Hubbell, *Biochemistry* **1996**, *35*, 7692.
[39] L. Columbus, W. L. Hubbell, *Trends Biochem. Sci.* **2002**, *27*, 288.
[40] M. Fleissner, D. Cascio, W. L. Hubbell, unpublished results.
[41] R. Kuroki, L. H. Weaver, B. W. Matthews, *Science* **1993**, *262*, 2030.
[42] C. K. Bower, Q. Xu, J. McGuire, *Biotechnol. Bioeng.* **1998**, *58*, 658.
[43] M. Llinas, B. Gillespie, F. W. Dahlquist, S. Marqusee, *Nat. Struct. Biol.* **1999**, *6*, 1072.
[44] J. McGuire, V. Krisdhasima, M. V. Wahlgren, T. Arnebrant in *Proteins at interfaces II*, *Vol. 602* (Eds.: T. A. Horbett, J. L. Brash), American Chemical Society, Washington, **1995**.
[45] R. Langen, K. Cai, C. Altenbach, H. G. Khorana, W. L. Hubbell, *Biochemistry* **1999**, *38*, 7918.

 © 2006 Wiley-VCH Verlag GmbH & Co. KGaA, Weinheim

Protein NMR Spectroscopy

DOI: 10.1002/anie.200600328

Ultrahigh Resolution in Proton Solid-State NMR Spectroscopy at High Levels of Deuteration**

*Veniamin Chevelkov, Kristina Rehbein, Anne Diehl, and Bernd Reif**

Structure investigations of biological solids by high- resolution magic-angle spinning (MAS) solid-state NMR spectroscopy has rapidly progressed in the last few years and resulted in complete structure elucidation of several peptides and small proteins.[1–4] Successful spectral assignment and determination of structural constraints in isotopically enriched materials (mostly ^{13}C, ^{15}N) is, however, still limited by resolution and sensitivity. A gain in sensitivity in solid-state NMR (ssNMR) experiments can in principle be achieved using direct proton detection. This technique makes use of the high gyromagnetic ratio γ of protons, a property which however, leads to broad resonance lines. Several approaches have been suggested to achieve line narrowing. Application of windowed homonuclear decoupling schemes[5,6] yield a rescaled ^1H line width on the order of 140–400 Hz, but require large receiver bandwidths, which allows radio-frequency (RF) noise to fold into the spectral region which finally compromises overall sensitivity. In addition, the applied pulse sequences scale the ^1H chemical shift. In recent years, high-speed (35–60 kHz) MAS instrumentation has become available.[7–9] However, even at these high spinning rates, fully protonated samples still have homogeneously broadened lines (>500 Hz).

Alternatively, ^1H line narrowing could be achieved by isotopic spin dilution at moderate (10–20 kHz) MAS frequencies.[10–14] Dilution is achieved by perdeuteration of the sample and subsequent back-exchange of deuterons by protons. In these experiments, the ^1H line width of most of the resonances is typically on the order 150–250 Hz or 80–150 Hz in the absence and in the presence of homonuclear ^1H,^1H decoupling, respectively. This labeling strategy allows, in addition the determination of long-range H^N–H^N distances,[12,15,16] detection of dynamic water molecules in the protein structure[16,17] and the characterization of protein side-chain dynamics.[18,19]

Herein, we demonstrate that a further increase in the degree of deuteration by using a 10:90 H_2O:D_2O mixture for recrystallization results in significant narrowing of the proton line width without loss in sensitivity. A ^1H line width on the order of 17–35 Hz can be achieved at moderate spinning frequencies (8–24 kHz) without application of homonuclear decoupling. The experiments are carried out using a perdeuterated, ^{15}N-enriched microcrystalline sample of the SH3 domain from chicken α-spectrin. To our knowledge, this strategy yields the most dispersed ^1H correlation spectra in the solid state reported to date.

Figure 1 represents a comparison of the 2D-^1H,^{15}N correlation spectra for the reference sample (Figure 1B, D) and the H^N dilute sample (Figure 1A, C). The ^1H-detected experiments (Figure 1A at 400 MHz, Figure 1C at 600 MHz) and the ^{15}N-detected experiments (Figure 1B at 400 MHz, Figure 1D at 600 MHz) were acquired using the NMR pulse sequence shown in Figure 4A and Figure 4B, respectively (see also the Experimental Section). The spinning frequency for the ^1H experiments was set to 13 kHz and 10 kHz for the ^{15}N experiments. For clarity, Figure 1B and D are displayed such that the proton dimension appears on the horizontal axis. The proton line width is not sensitive to moderate changes in the spinning rate under homonuclear dipolar decoupling,[6,20] if broadening conditions which arise from interference between MAS and the periodicity of the decoupling sequence are avoided.[20] Clearly, the resolution in the proton dimension is clearly improved for the H^N dilute sample yielding a fully resolved ^{15}N–^1H correlation spectrum of the protein even at 400 MHz.Figure 2 shows the ^1H line-width dependence as a function of the rotor period for selected residues. We find that the line width is inversely proportional to the spinning rate. This result is in agreement with previous studies which show that in the fast-spinning regime the residual dipolar line width depends linearly on the rotational frequency.[7,21] In an investigation of protonated alanine which was embedded in a deuterated alanine matrix, Rienstra and co-workers found that the slope of the MAS-dependent ^1H line width depends only on the average proton concentration in the sample.[22] The slope varies from 6728 Hz ms^{-1} to 970 Hz ms^{-1} depending on the degree of protonation. We observe in our studies a slope of 80.8 Hz ms^{-1} and of 144 Hz ms^{-1} for G51H^N and A56H^N, respectively. In spin systems that behave purely inhomogeneous (based on the criteria of Maricq and Waugh[23]), the line width should not depend on the MAS rotational frequency, if ω_r is comparable or larger than the size of the interaction. Non-zero slopes of the spinning-frequency dependence of the line width indicate therefore that ^1H,^1H dipolar couplings are not totally suppressed despite the high level of deuteration. The fitted lines in Figure 2 have non-vanishing y-intercepts, implying that line broadening cannot be removed even at infinite MAS rates. The inherent transverse relaxation time T_2, sample heterogeneity, static-field inhomogenity (ca. 7 Hz, based on the ^1H line width of a water sample which was used for shimming the probe) might be responsible for this observation. Given the observed resolution, major hardware improvements, especially in view of the ^2H lock system will be required in the future. We attribute differences in the line widths, y intercepts, and slopes for different residues to site-to-site variations in the local proton density and to local backbone dynamics.[24,25]

[*] V. Chevelkov, K. Rehbein, Dr. A. Diehl, Prof. Dr. B. Reif
Leibniz-Institut für Molekulare Pharmakologie (FMP)
Robert-Rössle-Strasse 10, 13125 Berlin (Germany)
Fax: (+49) 30-9479-3199
E-mail: reif@fmp-berlin.de

[**] This research was supported by the DFG grant Re1435. The authors are grateful to H. Oschkinat for his continuous support for this project and stimulating disscusions.

Supporting information for this article is available on the WWW under http://www.angewandte.org or from the author.

InterScience
© 2006 Wiley-VCH Verlag GmbH & Co. KGaA, Weinheim

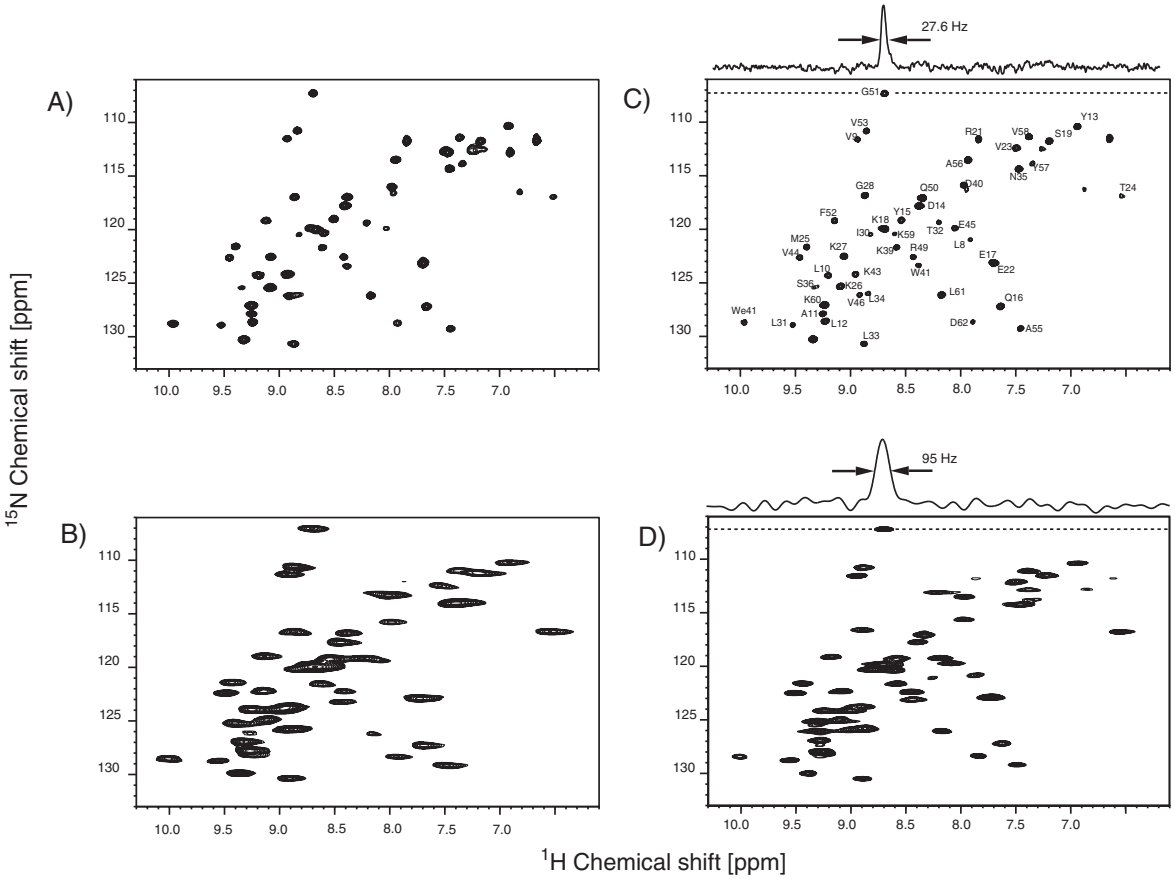

Figure 1. A,C) ^{1}H-detected 2D ^{15}N–^{1}H correlation spectra of the H^N dilute sample (deuterated SH3, 10% ^{1}H at labile proton positions) recorded at 400 MHz (A) and 600 MHz (C). (64 scans per increment; $t_1^{max}(^{15}N) = 26.4$ ms; $t_2^{max}(^{1}H) = 100.0$ ms; total experimental time = 3.8 h.) B,D) ^{15}N-detected 2D ^{15}N–^{1}H correlation experiments for the reference sample (deuterated SH3, 100% ^{1}H at labile proton positions) recorded at 400 MHz (B) 600 MHz (D). (8 scans per increment; $t_1^{max}(^{1}H) = 17.2$ ms; $t_2^{max}(^{15}N) = 37.0$ ms; total experimental time = 0.6 h). Acquisition of more increments in the indirect ^{1}H dimension did not result in a higher resolution in the ^{1}H dimension. All spectra were apodized using a 5 Hz lorentzian broadening in both dimensions.

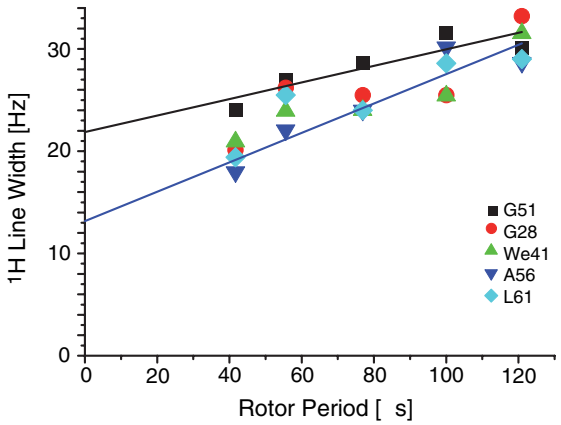

Figure 2. Dependence of the ^{1}H line width on the inverse MAS spinning frequency for selected residues in perdeuterated H^N dilute SH3.

While the ^{1}H line width for the H^N dilute sample is on the order of 17–35 Hz, the effective line width of the reference sample under phase-modulated Lee–Goldberg (PMLG) conditions amounts to 80–150 Hz taking chemical shift scaling resulting from PMLG into account. The resolution in the proton dimension is therefore improved by a factor of 4–5. The ^{15}N line width in both experiments is on the order of 20–30 Hz, and is limited by the acquisition time employed. In case of the ^{15}N detected experiment, two pulsed phase modulation (TPPM) decoupling is applied during 30–37 ms in each scan. This irradiation induces significant sample heating, which reduces the life time of the sample even under good cooling conditions in case of short repetition delays.[26] The ^{1}H-detected NMR experiments presented herein for the H^N dilute sample do not require homonuclear or heteronuclear decoupling, thus, reducing sample heating, set-up time, and possible experimental missettings. In addition, the proposed scheme does not require rescaling of the proton chemical shift, which is often problematic when spectra are acquired with homonuclear decoupling.

Figure 3 shows the experimental data for the ^{1}H T_1 measurements. ^{1}H T_1 times were found to be equal to 0.98 s (reference sample) and 1.76 s (H^N dilute sample), respectively. The H^N dilute sample has an unexpectedly short inversion recovery time T_1, allowing a recycle delay of 2.2 s,

 © 2006 Wiley-VCH Verlag GmbH & Co. KGaA, Weinheim

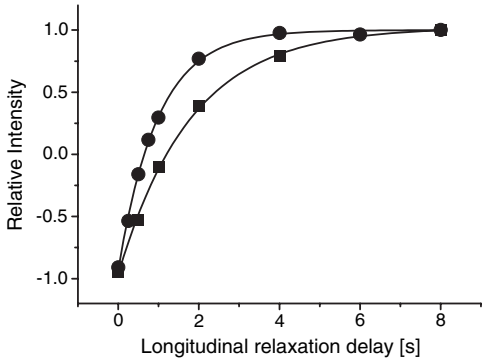

Figure 3. Experimental data for a ^{1}H inversion recovery experiment of $^1H^N$ bulk signal of the H^N dilute (■; ^{1}H $T_1 = 1.76$ s) and the reference sample (●; ^{1}H $T_1 = 0.98$ s).

while for the reference sample a repetition delay of 2.3 s was used to allow for dissipation of heat and to avoid sample degradation.

The improvement in ^{1}H line width is achieved by dilution of the proton spin density by a factor of 10. This results in a decrease of the Boltzman magnetization in the same proportion and in an increase of the longitudinal ^{1}H T_1 relaxation time. These drawbacks in sensitivity are compensated by using protons for detection which yields a gain in sensitivity by a factor of 5–9.[21] In addition, the ^{1}H line width is decreased by approximately a factor of 4. The signal-to-noise ratio for the ^{15}N- and ^{1}H-detected experiments amount to 10.4:1 and 25.3:1, respectively (determined for a ^{1}H cross section through the cross peak G51, as indicated in Figure 1C and D). Taking into account the different amount of material and experimental time, the normalized signal-to-noise ratio for the H^N dilute sample is reduced by only a factor of 1.2 compared to the reference sample. The experiments therefore demonstrate that a high degree of deuteration leads to ultra-high-resolution proton spectra, which could not be achieved to date despite many attempts to improve homonuclear decoupling schemes and the development of fast MAS technologies. We expect that this labeling approach will enable a straight forward assignment strategy, making an additional backbone nucleus available for resonance dispersion.

Experimental Section

The employed 2D pulse scheme using proton detection is illustrated in Figure 4A. Effective suppression of the dominant water resonance was achieved by modification of the constant time (CT) experiment suggested by Zilm and co-workers.[14] After magnetization transfer from ^{1}H to ^{15}N, polarization is stored along the z-axis during a variable delay ($\tau - t_1/2$), which precedes and follows the ^{15}N evolution period t_1. Two variable delays are required to achieve J decoupling in the indirect dimension and to keep the experiment constant time with respect to water magnetization. The fixed delay τ_w (60–120 ms) which follows the CT period, is optimized for water signal suppression. After back-transfer of magnetization to ^{1}H, magnetization is acquired using Waltz-16 ($\omega_1 = 1.6$ kHz) for heteronuclear scalar decoupling.[14]

Figure 4B shows the pulse sequence which was employed for the ^{15}N-detected ^{1}H–^{15}N correlation spectra. PMLG-9[27] was implemented in the indirect ^{1}H evolution period to achieve ^{1}H–^{1}H dipolar decoupling ($\omega_1 = 81$ kHz). A 180° pulse on the ^{15}N channel is applied in the center of t_1 for heteronuclear J decoupling. During ^{15}N detection, TPPM proton decoupling was applied using a RF field of $\omega_1 = 90$ kHz.

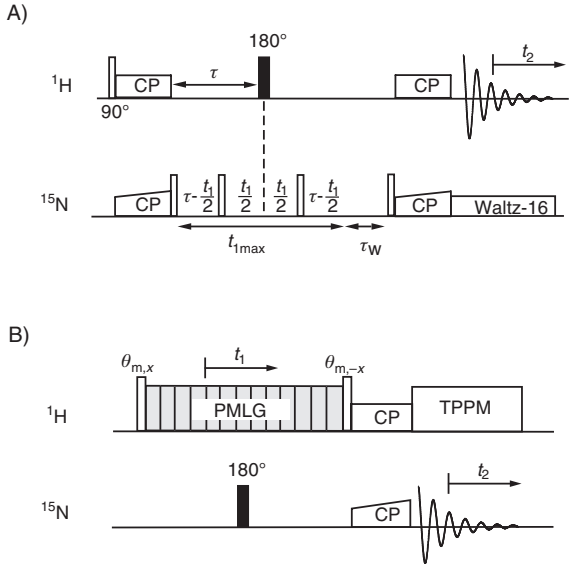

Figure 4. Pulse sequences employed for A) ^{1}H-detected and B) ^{15}N-detected ^{15}N–^{1}H correlation experiments. CP = cross polarization.

Received: January 25, 2006
Published online: April 28, 2006

Keywords: line widths · magic-angle spinning · predeuteration · proteins · solid-state NMR spectroscopy · structure elucidation

[1] F. Castellani, B.-J. van Rossum, A. Diehl, M. Schubert, K. Rehbein, H. Oschkinat, *Nature* **2002**, *420*, 98.
[2] C. M. Rienstra, L. Tucker-Kellogg, C. P. Jaroniec, M. Hohwy, B. Reif, M. T. McMahon, B. Tidor, T. Lozano-Pérez, R. G. Griffin, *Proc. Natl. Acad. Sci. USA* **2002**, *99*, 10260.
[3] S. G. Zech, A. J. Wand, A. E. McDermott, *J. Am. Chem. Soc.* **2005**, *127*, 8618.
[4] A. Lange, S. Becker, K. Seidel, K. Giller, O. Pongs, M. Baldus, *Angew. Chem.* **2005**, *117*, 2125; *Angew. Chem. Int. Ed.* **2005**, *44*, 2089.
[5] E. Vinogradov, P. K. Madhu, S. Vega, *Chem. Phys. Lett.* **2002**, *354*, 193.
[6] A. Lesage, D. Sakellariou, S. Hediger, B. Elena, P. Charmont, S. Steuernagel, L. Emsley, *J. Magn. Reson.* **2003**, *163*, 105.
[7] C. Filip, S. Hafner, I. Schnell, D. E. Demco, H. W. Spiess, *J. Chem. Phys.* **1999**, *110*, 423.
[8] Y. Ishii, R. Tycko, *J. Magn. Reson.* **2000**, *142*, 199.
[9] M. Ernst, M. A. Meier, T. Tuherm, A. Samoson, B. H. Meier, *J. Am. Chem. Soc.* **2004**, *126*, 4764.
[10] A. E. McDermott, F. J. Creuzet, A. C. Kolbert, R. G. Griffin, *J. Magn. Reson.* **1992**, *98*, 408.
[11] L. Zheng, K. W. Fishbein, R. G. Griffin, J. Herzfeld, *J. Am. Chem. Soc.* **1993**, *115*, 6254.
[12] B. Reif, C. P. Jaroniec, C. M. Rienstra, M. Hohwy, R. G. Griffin, *J. Magn. Reson.* **2001**, *151*, 320.
[13] V. Chevelkov, B. J. van Rossum, F. Castellani, K. Rehbein, A. Diehl, M. Hohwy, S. Steuernagel, F. Engelke, H. Oschkinat, B. Reif, *J. Am. Chem. Soc.* **2003**, *125*, 7788.

 © 2006 Wiley-VCH Verlag GmbH & Co. KGaA, Weinheim

[14] E. K. Paulson, C. R. Morcombe, V. Gaponenko, B. Dancheck, R. A. Byrd, K. W. Zilm, *J. Am. Chem. Soc.* **2003**, *125*, 15831.
[15] B. Reif, B. J. van Rossum, F. Castellani, K. Rehbein, A. Diehl, H. Oschkinat, *J. Am. Chem. Soc.* **2003**, *125*, 1488.
[16] E. K. Paulson, C. R. Morcombe, V. Gaponenko, B. Dancheck, R. A. Byrd, K. W. Zilm, *J. Am. Chem. Soc.* **2003**, *125*, 14222.
[17] V. Chevelkov, K. Faelber, A. Diehl, U. Heinemann, H. Oschkinat, B. Reif, *J. Biomol. NMR* **2005**, *31*, 295.
[18] M. Hologne, K. Faelber, A. Diehl, B. Reif, *J. Am. Chem. Soc.* **2005**, *127*.
[19] M. Hologne, Z. Chen, B. Reif, *J. Magn. Reson.* **2006**, *179*, 20.
[20] E. Vinogradov, P. K. Madhu, S. Vega, *Chem. Phys. Lett.* **2000**, *329*, 207.
[21] B. Reif, R. G. Griffin, *J. Magn. Reson.* **2003**, *160*, 78.
[22] D. H. Zhou, D. T. Graesser, W. T. Franks, C. M. Rienstra, *J. Magn. Reson.* **2006**, *178*, 297.
[23] M. M. Maricq, J. S. Waugh, *J. Chem. Phys.* **1979**, *70*, 3300.
[24] N. Giraud, A. Böckmann, A. Lesage, F. Penin, M. Blackledge, L. Emsley, *J. Am. Chem. Soc.* **2004**, *126*, 11422.
[25] N. Giraud, M. Blackledge, M. Goldman, A. Böckmann, A. Lesage, F. Penin, L. Emsley, *J. Am. Chem. Soc.* **2005**, *127*, 18190.
[26] J. A. Stringer, C. E. Bronnimann, C. G. Mullen, D. H. H. Zhou, S. A. Stellfox, Y. Li, E. H. Williams, C. M. Rienstra, *J. Magn. Reson.* **2005**, *173*, 40.
[27] E. Vinogradov, P. K. Madhu, S. Vega, *Chem. Phys. Lett.* **1999**, *314*, 443.

 © 2006 Wiley-VCH Verlag GmbH & Co. KGaA, Weinheim

Cover Picture

Duhee Bang, Brad L. Pentelute, and Stephen B. H. Kent*

Convergent chemical ligation enables the more efficient total synthesis of protein molecules. S. B. H. Kent and co-workers describe in their Communication on page 3985 ff. how the two halves of the target peptide chain can be synthesized by kinetically controlled chemical ligation of unprotected peptide segments. A final native chemical ligation step then gives the full-length polypeptide chain, which folds with high efficiency to give the synthetic protein molecule. (The artwork for the coverpicture was prepared by David Boerema.)

Metallabenzenes
The Review by M. M. Haley and C. W. Landorf on page 3914 ff. concerns metallabenzenes. Structural and NMR spectroscopic properties are as much a focus as the reactivity of metallabenzenes and the mechanisms of their syntheses.

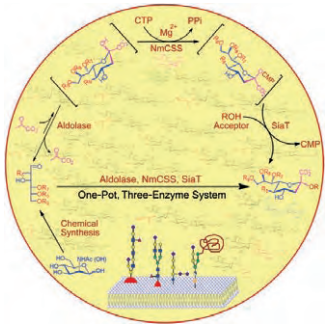

Chemoenzymatic Synthesis
Sialic acid exists in 50 structurally distinct forms in naturally occurring structures. X. Chen et al. describe in their Communication on page 3938 ff. how sialosides with natural and non-natural sialic acid forms have been prepared.

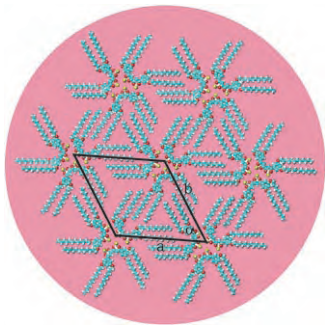

cis–trans Isomerization
In their Communication on page 3996 ff., L.-J. Wan et al. describe how thermal annealing transforms the molecular symmetry of an adlayer from lamellar to hexagonal which causes a *trans*-to-*cis* isomerization of the molecules within the adlayer.

Contents

VIP *The following Communications have been judged by at least two referees to be "very important papers" and will be published online at www.angewandte.org soon:*

*A. Narayanaswamy, H. Xu, N. Pradhan, X. Peng**
Single-Crystal Nanoflowers with Different Chemical Compositions and Physical Properties Grown by Limited Ligand Protection

J. L. Alonso, E. Cocinero, A. Lesarri, M. E. Sanz, J. López*
The Glycine–Water Complex

*A. Tao, P. Sinsermsuksakul, P. Yang**
Polyhedral Silver Nanocrystals with Distinct Scattering Signatures

J. van Bokhoven, C. Louis, J. Miller, M. Tromp, O. Safonova, P. Glatzel*
Activation of Oxygen on Gold–Alumina Catalysts: In situ High-Energy Resolution Fluorescence and Time-Resolved X-ray Spectroscopy

M. Brynda, R. Herber, P. Hitchcock, M. Lappert,* I. Nowik, P. Power,* A. Protchenko, A. Ruzicka, J. Steiner*
Higher Nuclearity Group 14 Metalloid Clusters: $[Sn_9\{Sn(NRR')\}_6]$ (R = 2,6-*i*$Pr_2C_6H_3$; R′ = $SiMe_3$ or $SiMe_2Ph$)

*O. Guillén-Villafuerte, G. García, B. Anula, E. Pastor, M. Blanco, M. A López-Quintela, A. Hernández-Creus, G. Planes**
Assembly of Subnanometric 2D Pt Nanoislands in Parallel Rows on Au(111) by Self-Assembly of Pt Clusters

News

Organic Chemistry: Mayr Awarded ____ **3902**

Catalysis: Basset and Rothenberg Honored ____ **3902**

Books

Engineering the Genetic Code — Nediljko Budisa — *reviewed by G. J. Palm* ____ **3903**

Highlights

Green Solvents

M. Avalos, R. Babiano, P. Cintas,* J. L. Jiménez, J. C. Palacios ____ **3904 – 3908**

Greener Media in Chemical Synthesis and Processing

When two solids make a liquid: The phenomenon is reproduced every winter when salt is spread on icy roads. Upon mixing certain solids, a variety of low-freezing and biodegradable liquids result (see picture). These eutectic mixtures offer a greener alternative to conventional ionic liquids and organic solvents.

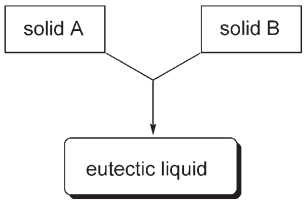

Organocatalysis

S. J. Connon* ____ **3909 – 3912**

Chiral Phosphoric Acids: Powerful Organocatalysts for Asymmetric Addition Reactions to Imines

Loaded with potential: The enormous potential of chiral phosphoric acids (see formulae) as promoters of novel, highly enantioselective addition reactions to imines under mild conditions has recently been recognized. The use of such catalysts has brought about the development of a number of new asymmetric reactions for the synthesis of amine-based chiral building blocks.

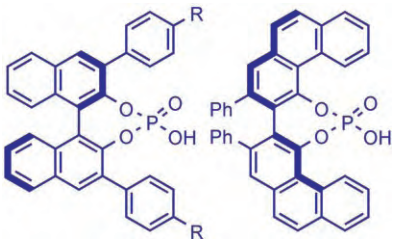

WILEY InterScience DISCOVER SOMETHING GREAT
© 2006 Wiley-VCH Verlag GmbH & Co. KGaA, Weinheim

Reviews

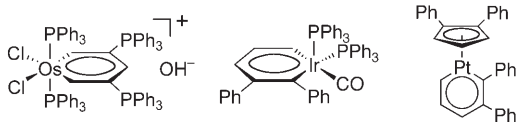

Chemical chameleons—with regard to properties normally associated with aromaticity—aptly describe metallabenzenes (see scheme for examples), as they exhibit delocalized bonding, possess downfield ^{1}H NMR chemical shifts, and form arene-coordination complexes, but are often distinctly nonplanar, undergo [4+2] cycloaddition reactions, and rearrange to form cyclopentadiene complexes. This Review describes their synthesis, chemistry, and unusual physical properties.

Metallabenzenes

C. W. Landorf, M. M. Haley* **3914 – 3936**

Recent Advances in Metallabenzene Chemistry

Communications

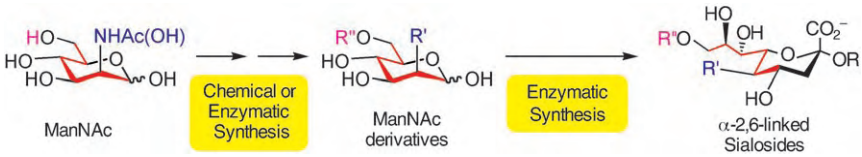

Just relax: A one-pot, three-enzyme chemoenzymatic synthetic approach is highly efficient for obtaining complex sialosides that contain diverse naturally occurring sialic acid modifications. α-2,6-Linked sialosides containing twelve naturally occurring sialic acid forms and seven non-natural sialic acid forms have been obtained.

Enzyme Catalysis

H. Yu, S. Huang, H. Chokhawala, M. Sun, H. Zheng, X. Chen* **3938 – 3944**

Highly Efficient Chemoenzymatic Synthesis of Naturally Occurring and Non-Natural α-2,6-Linked Sialosides: A *P. damsela* α-2,6-Sialyltransferase with Extremely Flexible Donor–Substrate Specificity

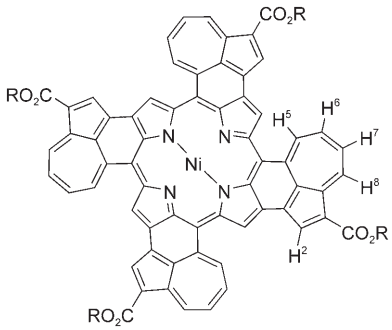

Extending conjugation: Azulene-fused porphyrins (see example) are synthesized through the oxidation of *meso*-(4-azulenyl)porphyrins with $FeCl_3$. The azulene-fused strategy allowed highly π-conjugated porphyrinic electronic systems, which are promising two-photon absorption pigments, to be realized.

Porphyrinoids

K. Kurotobi, K. S. Kim, S. B. Noh, D. Kim,* A. Osuka* **3944 – 3947**

A Quadruply Azulene-Fused Porphyrin with Intense Near-IR Absorption and a Large Two-Photon Absorption Cross Section

For the USA and Canada:
ANGEWANDTE CHEMIE International Edition (ISSN 1433-7851) is published weekly by Wiley-VCH PO Box 191161, D 69451 Weinheim, Germany. Air freight and mailing in the USA by Publications Expediting Inc. 200 Meacham Ave., Elmont, NY 11003. Periodicals postage paid at Jamaica NY 11431. US POSTMASTER: send address changes to *Angewandte Chemie*, Wiley-VCH, 111 River Street, Hoboken, NJ 07030. Annual subscription price for institutions: US$ 5685/5168 (valid for print and electronic / print or electronic delivery); for individuals who are personal members of a national chemical society prices are available on request. Postage and handling charges included. All prices are subject to local VAT/sales tax.

© 2006 Wiley-VCH Verlag GmbH & Co. KGaA, Weinheim

The best in chemistry –

for more than a hundred years

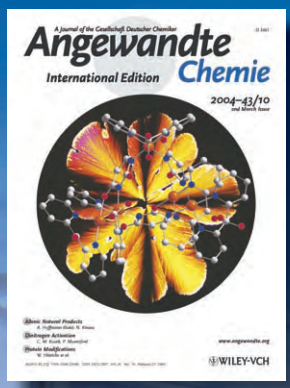

A Journal of the Gesellschaft Deutscher Chemiker

Angewandte
International Edition Chemie

www.angewandte.org

1888: ***The beginning of a success story***

Constant Innovations

1962: *First issue of the International Edition*
1976: *Graphical abstracts*
1979: *Cover pictures*
1988: *Centenary of Angewandte*
1989: *Routine use of color*
1991: *New section: Highlights*
1992: *Computerized editorial tracking system*
1995: *Internet service for readers*
1998: *Regular press service; full-text online*
2000: *New section: Essays; EarlyView: Communications available online ahead of the printed version*
2001: *New section: Minireviews*
2002: *Online submission of manuscripts*
2003: *Weekly publication; new section: News; new layout*
2004: *Backfiles (1962-1997); ManuscriptXpress: Online system for authors and referees*

Angewandte's advisors...

Manfred Reetz
Max-Planck-Institut für Kohlenforschung, Mülheim

*»**Angewandte Chemie** is extremely well-balanced in providing various types of information to the academic and industrial chemical community. If you inadvertently miss an issue, the mishap will catch up with you sooner or later.«*

***Angewandte Chemie International Edition** is a journal of the German Chemical Society (GDCh)*

GDCh

WILEY InterScience® DISCOVER SOMETHING GREAT

WILEY-VCH

1881404_gu

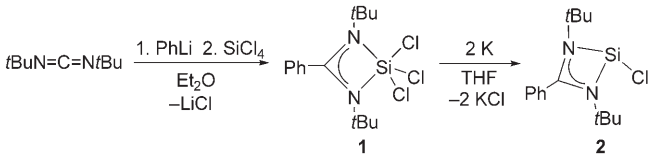

The single life: The reaction of [PhC(N*t*Bu)$_2$]SiCl$_3$ (**1**) with potassium afforded the monomeric chlorosilylene [PhC(N*t*Bu)$_2$]SiCl (**2**). The X-ray crystal structure of **2** has been determined and natural-bond-orbital analysis carried out.

Silicon Chemistry

C.-W. So, H. W. Roesky,* J. Magull, R. B. Oswald ——— **3948 – 3950**

Synthesis and Characterization of [PhC(N*t*Bu)$_2$]SiCl: A Stable Monomeric Chlorosilylene

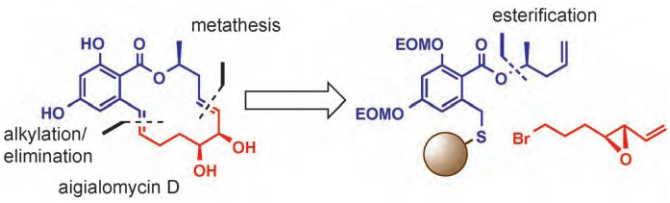

On solid ground: Despite no obvious resemblance to adenosine analogues, the family of resorcylic macrolides contains a high proportion of kinase and ATPase inhibitors. A solid-phase total synthesis of aigialomycin D extends the diversity of this class of natural product. Aigialomycin was found to inhibit CDK1/5 and GSK. EOM = ethoxymethyl.

Natural Products

S. Barluenga, P.-Y. Dakas, Y. Ferandin, L. Meijer, N. Winssinger* — **3951 – 3954**

Modular Asymmetric Synthesis of Aigialomycin D, a Kinase-Inhibitory Scaffold

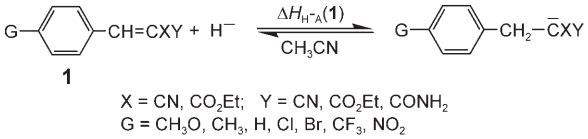

Choosing a suitable hydride reducing agent and thermodynamic analysis of reduction mechanisms is facilitated by experimental hydride affinities ΔH_{H^-A}, which are reported herein for 28 polarized olefins **1** in acetonitrile (see scheme). The method should also be applicable to ketones, aldehydes, and imines.

Hydride Affinities

X.-Q. Zhu,* M. Zhang, Q.-Y. Liu, X.-X. Wang, J.-Y. Zhang, J.-P. Cheng* ——— **3954 – 3957**

A Facile Experimental Method To Determine the Hydride Affinity of Polarized Olefins in Acetonitrile

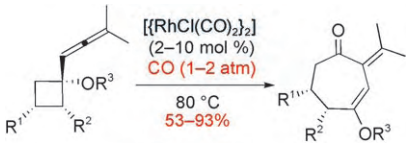

Ever expanding: A Rh^I-catalyzed C–C activation reaction of allenylcyclobutanes generates intermediate metallacycles that can be trapped with CO to produce a new [6+1] reaction. Functionalized monocyclic and bicyclic cycloheptenones are obtained in good-to-excellent yields with this [6+1] higher-order carbonylative cycloaddition reaction.

Cycloadditions

P. A. Wender,* N. M. Deschamps, R. Sun ——— **3957 – 3960**

Rh^I-Catalyzed C–C Bond Activation: Seven-Membered Ring Synthesis by a [6+1] Carbonylative Ring-Expansion Reaction of Allenylcyclobutanes

Directed delivery: Chiral methylenecyclopropanes were prepared from cyclopropene derivatives upon reaction with Grignard reagents. A higher-order dependence of the reaction on the concentration of the Grignard reagent was revealed, and based on this finding, it was possible to reverse the regioselectivity of the process (see scheme; MEM = methoxyethoxymethyl).

Synthetic Methods

Z. Yang, X. Xie, J. M. Fox* — **3960 – 3962**

Diastereoselective Synthesis of Methylenecyclopropanes from Chiral Cyclopropene Derivatives

© 2006 Wiley-VCH Verlag GmbH & Co. KGaA, Weinheim

Contents

Synthetic Methods

S. Simaan, A. Masarwa, P. Bertus, I. Marek* ——— **3963 – 3965**

Enantiomerically Pure Cyclopropenylcarbinols as a Source of Chiral Alkylidenecyclopropane Derivatives

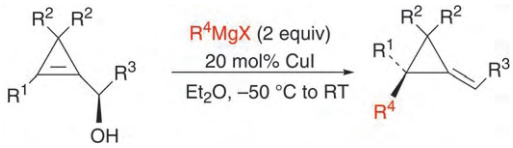

The straightforward approach: The copper-catalyzed carbomagnesiation reaction of chiral cyclopropenylcarbinol derivatives, obtained through kinetic resolution of secondary allylic alcohols, leads to the preparation of enantiomerically pure alkylidenecyclopropane derivatives. The reaction mechanism is composed of a *syn* carbometalation followed by a *syn* elimination reaction.

Microporous Materials

Y.-P. Xu,* Z.-J. Tian, S.-J. Wang, Y. Hu, L. Wang, B.-C. Wang, Y.-C. Ma, L. Hou, J.-Y. Yu, L.-W. Lin ——— **3965 – 3970**

Microwave-Enhanced Ionothermal Synthesis of Aluminophosphate Molecular Sieves

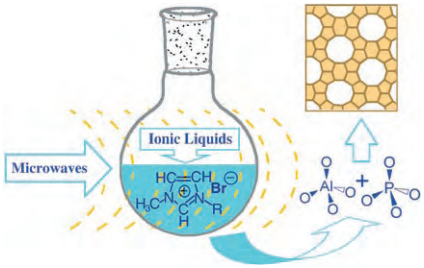

Fast and safe: The combination of microwaves and ionic liquids provides a new method for the preparation of aluminophosphate molecular sieves (see picture). This method has the advantage of enabling the synthesis to be carried out at ambient pressures and results in a rapid crystallization and high structural selectivity.

Nanoparticle Assemblies

Q. Zhou, X. Li, Q. Fan, X. Zhang, J. Zheng* ——— **3970 – 3973**

Charge Transfer between Metal Nanoparticles Interconnected with a Functionalized Molecule Probed by Surface-Enhanced Raman Spectroscopy

Good vibrations: Metal–molecule–metal nanosystems are fabricated by the self-assembly of gold and silver nanoparticles interconnected with 4-aminothiophenol (PATP) molecules (see picture). The b_2 vibrational modes of the PATP molecules are greatly enhanced by near-infrared excitation, as a result of charge transfer between the metal nanoparticles coupled with the vibrations of the PATP molecules.

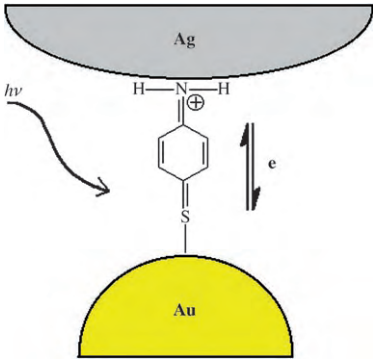

Homogeneous Catalysis

D. Banerjee, A. L. Markley, T. Yano, A. Ghosh, P. B. Berget, E. G. Minkley, Jr., S. K. Khetan, T. J. Collins* ——— **3974 – 3977**

"Green" Oxidation Catalysis for Rapid Deactivation of Bacterial Spores

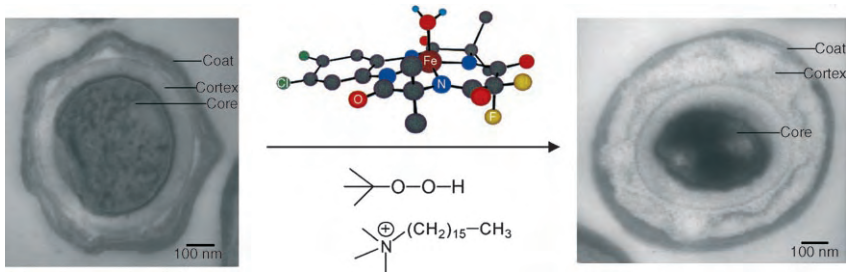

A view to a kill: Iron(III)-coordinated tetraamide macrocyclic ligands (see example) activate peroxides in water in the presence of a cationic surfactant to rapidly deactivate spores of the common anthrax surrogate, *Bacillus atrophaeus*. A 99.99999% kill can be achieved in 15 min at pH 10 and room temperature with *tert*-butyl hydroperoxide (see TEM images).

© 2006 Wiley-VCH Verlag GmbH & Co. KGaA, Weinheim

It's under control: In the presence of an artificial double-hydrophilic block copolymer, poly(ethylene glycol)-*b*-poly(L-glutamic acid), highly monodisperse vaterite microspheres crystallize from a mixture of *N*,*N*-dimethylformamide and water (see picture). Varying the ratio of the solvents can control the morphology of the $CaCO_3$ crystals.

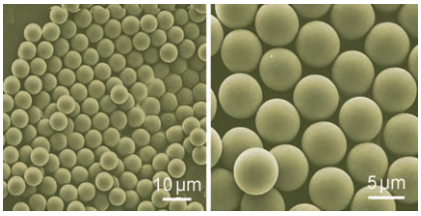

Polymorphism

X.-H. Guo, S.-H. Yu,*
G.-B. Cai ——— **3977 – 3981**

Crystallization in a Mixture of Solvents by Using a Crystal Modifier: Morphology Control in the Synthesis of Highly Monodisperse $CaCO_3$ Microspheres

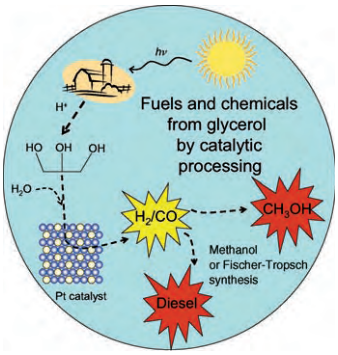

Lean and green: Glycerol can be catalytically converted into synthesis gas at relatively low temperatures. The combination of this process with Fischer–Tropsch and methanol-synthesis steps offers a new strategy for the production of liquid fuels and chemicals from renewable resources.

Biofuels

R. R. Soares, D. A. Simonetti,
J. A. Dumesic* ——— **3982 – 3985**

Glycerol as a Source for Fuels and Chemicals by Low-Temperature Catalytic Processing

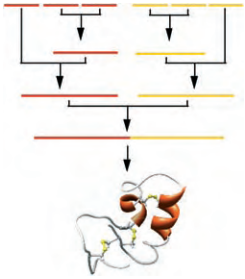

Converging on the goal: New chemistry enables the key Cys-peptide-("thioester) intermediate to be extended by ligation at either the N or C termini in a controlled fashion. This approach forms the basis for a set of novel tactics for the fully convergent synthesis of proteins by the chemical ligation of multiple peptide segments.

Protein Total Synthesis VIP

D. Bang, B. L. Pentelute,
S. B. H. Kent* ——— **3985 – 3988**

Kinetically Controlled Ligation for the Convergent Chemical Synthesis of Proteins

Free at last: Two free dithiocarbenes, a dithianylidene and a di-*n*-propyldithiocarbene generated thermally from the respective dialkylthiooxadiazoline precursors, are characterized and their reactivity examined. (The picture shows a cut through the C_s plane of the [1,3]dithian-2-ylidene, thus revealing the carbene sp^2 orbital.)

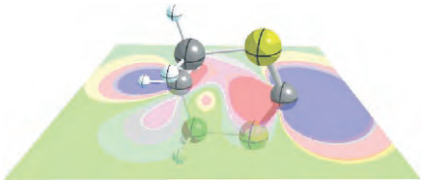

Heterocyclic Carbenes

P. R. Schreiner,* H. P. Reisenauer,
J. Romanski, G. Mloston ——— **3989 – 3992**

[1,3]Dithian-2-ylidene

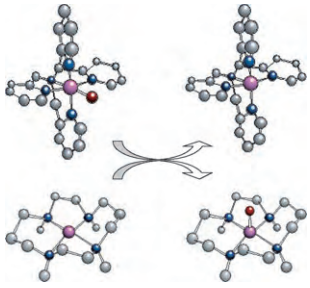

Completing the move: The intermetal transfer of an oxygen atom from nonheme iron(IV)–oxo to iron(II) complexes (see example, purple: Fe, red: O, blue: N, gray: C) has been unambiguously evidenced spectrophotometrically, mass spectrometrically, and electrochemically. The transfer of the oxygen atom was found to be dependent on the oxidizing power of the iron(IV)–oxo complexes.

Enzyme Models

C. V. Sastri, K. Oh, Y. J. Lee, M. S. Seo, W. Shin, W. Nam* ——— **3992 – 3995**

Oxygen-Atom Transfer between Mononuclear Nonheme Iron(IV)–Oxo and Iron(II) Complexes

© 2006 Wiley-VCH Verlag GmbH & Co. KGaA, Weinheim

Contents

cis–trans Isomerization

D. Rohde, C.-J. Yan, H.-J. Yan, L.-J. Wan* ——— **3996 – 4000**

From a Lamellar to Hexagonal Self-Assembly of Bis(4,4′-(*m*,*m*′-di(dodecyloxy)phenyl)-2,2′-difluoro-1,3,2-dioxaborin) Molecules: A *trans*-to-*cis*-Isomerization-Induced Structural Transition Studied with STM

Lick into shape: Molecular adlayer symmetry can be transformed from lamellar to hexagonal through a thermal-annealing process which causes a *trans*-to-*cis* isomerization of the molecules within the adlayer. Different temperatures resulted in the formation of pure *trans*- and *cis*-isomer adlayers on the surface.

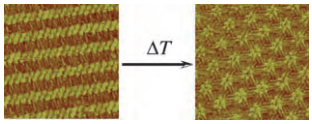

Analytical Techniques

C. Amatore,* S. Arbault, Y. Chen, C. Crozatier, F. Lemaître, Y. Verchier ——— **4000 – 4003**

Coupling of Electrochemistry and Fluorescence Microscopy at Indium Tin Oxide Microelectrodes for the Analysis of Single Exocytotic Events

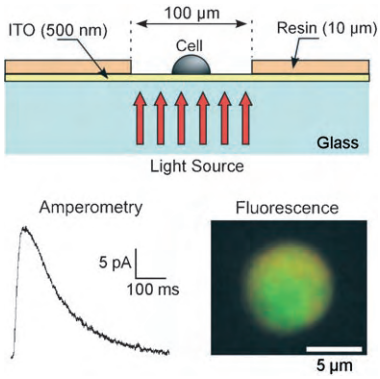

One-off analysis: Quantitative, kinetic, and spatial monitoring of single biological events involving vesicular secretion such as exocytosis may be achieved by combining electrochemistry with fluorescence microscopy at indium tin oxide (ITO) transparent microelectrodes. This method paves the way for real-time tracking of the intracellular fate of vesicles while monitoring precisely their dynamics of fusion.

Crystal Engineering

K.-T. Youm, M. G. Kim, J. Ko,* M.-J. Jun* ——— **4003 – 4007**

A Noninterpenetrating Three-Dimensional $4^6 6^9$ Iron(II) Coordination Polymer Built with a Trigonal-Antiprismatic Iron(III) Metalloligand

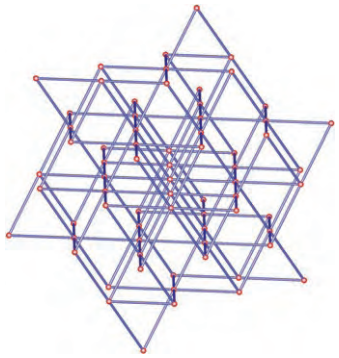

A second coordination sphere of six N_{exo} atoms in a trigonal-antiprismatic arrangement allows the metalloligand $[Fe^{III}(L)_2]^+$ (red spheres, L = hydrotris(1,2,4-triazolyl)borate) to assemble with $Rh_2(OAc)_4$ linear spacers (blue rods) in an unprecedented noninterpenetrating 3D framework with $4^6 6^9$ topology. The metalloligand is reduced to the iron(II) state during the reaction by the borate ligand.

Glycoproteins

G. J. L. Bernardes, D. P. Gamblin, B. G. Davis* ——— **4007 – 4011**

The Direct Formation of Glycosyl Thiols from Reducing Sugars Allows One-Pot Protein Glycoconjugation

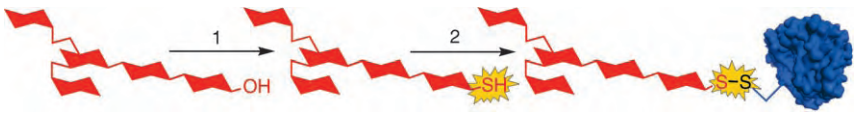

Sweet and easy: A one-pot method consisting of direct thionation (1) followed by thiol-mediated chemoselective ligation (2) can be used for site-selective protein glycosylation. This procedure, which uses the Lawesson reagent, has been shown to be fully compatible with unprotected sugars, the products of which can be directly used in a selenenylsulfide protein glycosylation strategy.

© 2006 Wiley-VCH Verlag GmbH & Co. KGaA, Weinheim

Seeing the light: Upon binding to a complementary nucleic acid, a metal-complex–DNA conjugate releases copper(II) ions that activate the precatalyst 1,10-phenanthroline (phen) and amplify the primary signal through catalytic production of a fluorescent dye (DCF). This combination of allosteric signal transduction and catalytic signal amplification imitates biological signaling cascades. tpy = 2,2′:6′,2″-terpyridine.

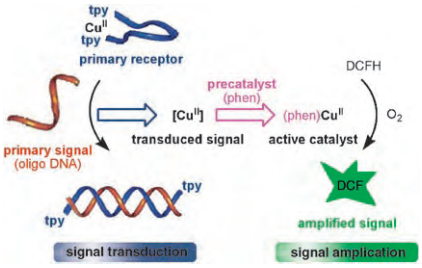

Allosteric Signal Transduction

N. Graf, M. Göritz, R. Krämer* ——— **4013 – 4015**

A Metal-Ion-Releasing Probe for DNA Detection by Catalytic Signal Amplification

Take the strain: Despite extreme ring strain and reactivity, the heterocycles **2**, which are easily obtained from azides **1** and detectable by NMR spectroscopy, can be converted stereoselectively by novel addition and cycloaddition reactions.

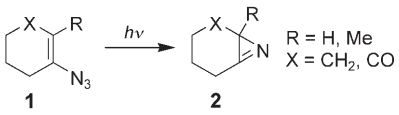

Strained Molecules

K. Banert,* B. Meier ——— **4015 – 4019**

Synthesis and Reactions of Highly Strained 2,3-Bridged 2*H*-Azirines

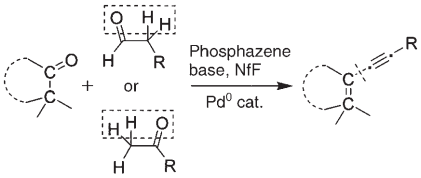

Ultimate coupling partners: Widely available enolizable aldehydes and ketones undergo Sonogashira cross-coupling with other carbonyl compounds to give conjugated enynes in a newly devised general method (see scheme; NfF = nonafluorobutane-1-sulfonyl fluoride). The synthetic protocol comprises at least four operating steps, which are carried out in one pot using common reagents, catalysts, and additives.

Multistep One-Pot Syntheses

I. M. Lyapkalo,* M. A. K. Vogel ——— **4019 – 4023**

A General and Versatile Method for a C–C Cross-Coupling Synthesis of Conjugated Enynes: One-Pot Sequence Starting from Carbonyl Compounds

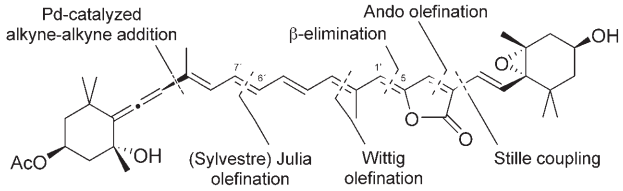

Light work: The light-harvesting marine C_{37} carotenoid peridinin was synthesized from (+)-diethyl tartrate and (−)-actinol. Key transformations were the differential reduction of an ester-containing Weinreb amide, an *E*-selective olefination by an Ando-type bromophosphonate, the *anti*-selective β-elimination establishing the $C^{1'}{=}C^{5}$ bond *Z* selectively, and a *cis*→*trans* isomerization of the $C^{6'}{=}C^{7'}$ bond (see picture).

Total Synthesis

T. Olpp, R. Brückner* ——— **4023 – 4027**

Total Synthesis of the Light-Harvesting Carotenoid Peridinin

© 2006 Wiley-VCH Verlag GmbH & Co. KGaA, Weinheim

Contents

Water Clusters

Z. Sun, C.-K. Siu, O. P. Balaj, M. Gruber, V. E. Bondybey,* M. K. Beyer* _____ **4027 – 4030**

Proton Transfer in Ionic Water Clusters

How waterlike are ionic water clusters? Clusters with 10 to 100 water molecules are frequently used as model systems for reactions in aqueous solution. Concerted proton transfer, a key feature of liquid water, can be probed by observing the formation of HDO when D_2O is used as a reactant (see scheme). Mass spectrometry shows that proton transfer occurs in $H(H_2O)_n^+$, whereas the individual water molecules stay intact in $(H_2O)_n^-$ and $O_2(H_2O)_n^-$.

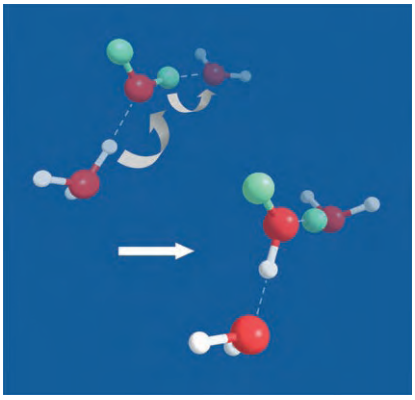

WILEY InterScience® DISCOVER SOMETHING GREAT

"**Hot Papers**" are chosen by the Editors for their importance in a rapidly evolving field of high current interest. A preview with the graphical abstracts of these articles can be found on the *Angewandte Chemie* homepage in Wiley InterScience at www.angewandte.org.

All articles in *Angewandte Chemie* are published online several weeks ahead of print. They are found under the "**EarlyView**" link on the journal's homepage in Wiley InterScience.

Service

Keywords _____ *4032*

Authors _____ *4033*

Preview _____ *4035*

Corrigendum

Catalytic Enantioselective Hydrogenolysis of [$Cr(CO)_3$(5,8-Dibromonaphthalene)]

E. P. Kündig,* P. D. Chaudhuri, D. House, G. Bernardinelli _____ **1092–1095**

Angew. Chem. Int. Ed. **2006**, *45*

DOI 10.1002/anie.200502688

The paragraph that begins at the bottom of the first column on page 1093 should start: "Checking if incomplete dba dissociation in [$Pd(dba)_2$] was part of the problem, we turned to [CpPd(allyl)] and [(Trost ligand (**6**))Pd(allyl)][OTf] ($Cp = C_5H_5$, $OTf = CF_3SO_3^-$) as catalyst precursors.[13]"

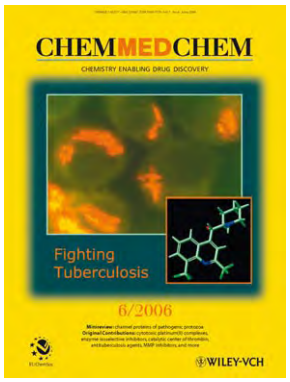

For more information on ChemMedChem see www.chemmedchem.org

© 2006 Wiley-VCH Verlag GmbH & Co. KGaA, Weinheim

Contents

Corrigendum

Catalytic Enantioselective Hydrogenolysis of [$Cr(CO)_3$(5,8-Dibromonaphthalene)]

E. P. Kündig,* P. D. Chaudhuri, D. House, G. Bernardinelli _____ **1092–1095**

Angew. Chem. Int. Ed. **2006**, *45*

DOI 10.1002/anie.200502688

The paragraph that begins at the bottom of the first column on page 1093 should start: "Checking if incomplete dba dissociation in [$Pd(dba)_2$] was part of the problem, we turned to [CpPd(allyl)] and [(Trost ligand (**6**))Pd(allyl)][OTf] (Cp = C_5H_5, OTf = $CF_3SO_3^-$) as catalyst precursors.[13]"

 © 2006 Wiley-VCH Verlag GmbH & Co. KGaA, Weinheim

Awarded...

H. Mayr Receives Liebig Medal

Herbert Mayr (Ludwig-Maximilians-Universität München, LMU) was awarded the Liebig Medal of the German Chemical Society (Gesellschaft Deutscher Chemiker, GDCh). Mayr was honored for his work on reaction kinetics, in particular in organic chemistry. His group has developed a reactivity scale that describes reactions between electrophiles and nucleophiles.[1a] The scale already stretches over 24 orders of magnitude, and will soon extend by another 12. Mayr believes that this scale will lead to a better understanding and easier planning of organic syntheses. He recently described the development of a general scale of nucleophilicity in *Angewandte Chemie*.[1b]

H. Mayr

Mayr studied chemistry at the LMU München. After completing his PhD in 1974 under the guidance of R. Huisgen, he spent a year as a postdoctoral researcher with G. A. Olah in Cleveland (OH, USA). He carried out his habilitation from 1976 to 1981 at the Universität Erlangen-Nürnberg. In 1984, he accepted a professorship at the Medizinische Universität Lübeck. In 1991 he moved to the Technische Universität Darmstadt, and five years later he returned to the LMU.

J.-M. Basset and G. Rothenberg Receive Rylander Awards

The Organic Reactions Catalysis Society awarded the Paul N. Rylander Awards for 2005 and 2006 to Jean-Marie Basset and Gadi Rothenberg, respectively, during the 21st Conference on Catalysis of Organic Reactions in Orlando (FL, USA) in April.

J.-M. Basset

Basset (Ecole Supérieure Chimie Physique Electronique de Lyon, CPE) was recognized for his work on organometallic chemistry at interfaces and especially in catalysis. He wrote a Review on bridging the gap between heterogeneous and homogeneous catalysis which appeared in *Angewandte Chemie* in 2003.[2b] He also recently compared therein the role of surface versus molecular siloxy ligands in well-defined olefin metathesis catalysts.[2b]

Basset completed his PhD in 1969 under the guidance of M. Prettre (Institut de Recherche sur la Catalyse, Lyon; IRC) and then worked as a postdoctoral researcher at the University of Toronto (W. Graydon) and at Imperial College (G. Wilkinson). He returned to Lyon to join the Université C. Bernard as an assistant professor and was later appointed the Deputy Director of the IRC. He founded the Surface Organometallic Chemistry group in 1983 at the CPE, where he has been Scientific Director since 1994. Basset is a member of the Académie des Sciences (Paris).

Rothenberg (University of Amsterdam) studied chemistry at the Hebrew University of Jerusalem and obtained his PhD there in 1999 under the guidance of Y. Sasson. He then spent two years at the University of York in the group of J. Clark. His research at the University of Amsterdam involves the theoretical and experimental development of heterogeneous and homogeneous catalysts. He recently described in *ChemPhysChem* the use of microwave-susceptible oxidation catalysts to obtain clean diesel power, and reported in *Angewandte Chemie* on the leaching of palladium nanoclusters in catalyzed C–C coupling reactions. Rothenberg, together with Hubert de Jonge (Sorbisense), was recently awarded the Bayer Crop Science Innovation Award 2006.

G. Rothenberg

[1] a) H. Mayr, M. Patz, *Angew. Chem.* **1994**, *106*, 990; *Angew. Chem. Int. Ed. Engl.* **1994**, *33*, 938; b) T. B. Phan, M. Breugst, H. Mayr, *Angew. Chem.* **2006**, *118*, 3954; *Angew. Chem. Int. Ed.* **2006**, *45*, 3869.

[2] a) C. Copéret, M. Chabanas, R. Petroff Saint-Arroman, J.-M. Basset, *Angew. Chem.* **2003**, *115*, 1648; *Angew. Chem. Int. Ed.* **2003**, *42*, 156; b) F. Blanc, C. Copéret, J. Thivolle-Cazat, J.-M. Basset, A. Lesage, L. Emsley, A. Sinha, R. R. Schrock, *Angew. Chem.* **2006**, *118*, 1238; *Angew. Chem. Int. Ed.* **2006**, *45*, 1216.

[3] a) J. Beckers, L. M. van der Zande, G. Rothenberg, *ChemPhysChem* **2006**, *7*, 747; b) M. B. Thathagar, J. E. ten Elshof, G. Rothenberg, *Angew. Chem.* **2006**, *118*, 2956; *Angew. Chem. Int. Ed.* **2006**, *45*, 2886.

DOI: 10.1002/anie.200601931

InterScience © 2006 Wiley-VCH Verlag GmbH & Co. KGaA, Weinheim

Green Solvents

DOI: 10.1002/anie.200504285

Greener Media in Chemical Synthesis and Processing**

Martín Avalos, Reyes Babiano, Pedro Cintas, José L. Jiménez, and Juan C. Palacios*

Keywords:
eutectic solvents · green chemistry · ionic liquids · polarity

It is hoped that a greener approach will be adopted in both academic and industrial chemistry in the 21st century. A series of green principles has become well established[1] and can be summarized conveniently as follows: a) environmentally benign strategies (e.g. catalytic systems, atom-economy protocols, or use of renewable raw materials), b) activation techniques (e.g. microwaves or ultrasound) that accelerate certain transformations, thereby avoiding the formation of side products,[2] and c) less-hazardous solvents.[3] The last criterion would ideally be fulfilled by water or, better yet, by solvent-free reactions that do not involve any further solvent-based workup.[4]

Prominent among polar fluids are salts of 1,3-dialkylimidazolium cations,[5] which may generate a wide variety of room-temperature ionic liquids (RTILs) with weakly coordinating anions. Their "greenness" is usually linked to a negligible vapor pressure, thus they have the potential to replace more-volatile organic solvents in chemical processes.[6] The non-innocent behavior of ILs under certain conditions that causes decomposition of both cations and anions has also been described.[7] Moreover, the toxicology of ILs remains unclear and further studies are required to assess their sustainability.[8,9]

Greener alternatives would be mixtures composed of biodegradable constituents that exist as liquids over a large range of temperatures yet exhibit high thermal and chemical stabilities. One such emerging low-freezing liquid results when choline chloride and urea are combined in a molar ratio of 1:2.[10] The resulting liquid freezes at 12 °C, which is indeed remarkable when it is considered that the pure precursors melt at 302 °C and 133 °C, respectively. Formation of this liquid phase is guided by the same principle that governs the melting point of ionic compounds: The larger the ions and the smaller the charge, the less energy is needed to break the bond, which causes a depression of the freezing point. Whilst alkaline and alkaline-earth halides (e.g. NaCl, NH_4Cl, or $CaCl_2$) are fluids at only very high temperatures,[11] large quaternary ammonium ions are more difficult to fit into a lattice. As a result of the lower lattice energy, such ionic substances may exist as liquids at ambient temperatures. Like conventional ILs, the choline chloride/urea mixture exhibits non-flammability and conductivity, although to distinguish RTILs from such mixtures the term "deep eutectic solvent" has now been adopted for the latter.[12] In this context, the reactivity of two solids, once thought to be controlled solely by diffusion, often proceeds through the formation of a liquid (melt) phase.[13]

A eutectic mixture of choline chloride and urea dissolves a wide range of transition-metal oxides,[14] a fact that could be exploited for industrial use, such as in the recovery and extraction of metals from mineral ores. Eutectic mixtures with large depressions of freezing point can equally be obtained from metal halides and choline chloride or other quaternary ammonium halides.[15–17] Ionic liquids composed of choline chloride and $ZnCl_2$ (or $SnCl_2$) in a molar ratio of 1:2 show interesting catalytic properties, and, moreover, such solvent systems are not moisture-sensitive and can be recycled without appreciable decrease in activity.[18] For example, Diels–Alder cycloadditions occur smoothly in this mixture at room temperature (Scheme 1), although the accelerating effect results from the Lewis acid. These reactions catalyzed by zinc-containing choline chloride are two-phase processes: The dienophile dissolves in the ionic mixture, whereas the less-polar diene remains in a separate phase. At the end, the product also forms a separate phase on top of the ionic solvent, thereby allowing easy separation.[19]

A variety of synthetically useful transformations can be conducted in a similar way. The Fischer indole annula-

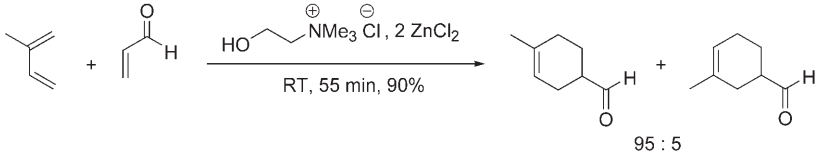

Scheme 1. Diels–Alder cycloadditions in eutectic mixtures.[19]

[*] Dr. M. Avalos, Dr. R. Babiano, Dr. P. Cintas, Dr. J. L. Jiménez, Dr. J. C. Palacios
Departamento de Química Orgánica
Facultad de Ciencias-UEX
06071 Badajoz (Spain)
Fax: (+34) 924-271-149
E-mail: pecintas@unex.es

[**] This work was performed under the auspices of the Spanish Network of Sustainable Chemistry (REQS). We thank the Ministry of Education and Science (grants BQU2003-05946 and BQU2005-07676) for financial assistance.

InterScience
© 2006 Wiley-VCH Verlag GmbH & Co. KGaA, Weinheim

tion proceeded with one equivalent of a 1:2 mixture of choline chloride and $ZnCl_2$, and the products could be easily recovered by sublimation from the ionic liquid.[20] Exclusive formation of 2,3-disubstituted regioisomers was observed with substrates derived from alkyl methyl ketones (Scheme 2). A supported heterogeneous catalyst composed of choline hydroxide on MgO was shown to be an excellent catalyst for aldol reactions between aldehydes and ketones.[21] This system exhibited better catalytic efficiency than other common basic catalysts and is more ecologically compatible.

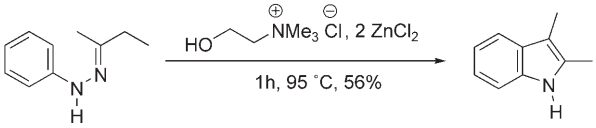

Scheme 2. Fischer indole annulation.[20]

As choline-based ionic liquids dissolve not only metal salts but also hydrogen-bonded substrates, transformations of certain organic compounds, such as unprotected sugars and even cellulose (Scheme 3), can advantageously be carried out. For example, selective acylation of primary hydroxy groups in cellulose was reported.[22]

The fact that eutectic liquids may be generated from choline chloride and metal salts provides a promising outlook for two relevant electrochemical processes: electropolishing and electroplating.[12] In the former a metal is removed, representing a way of increasing resistance to corrosion in certain materials such as stainless steel. Abbott et al. demonstrated that an environmentally friendly eutectic mixture of choline chloride and ethylene glycol dissolves metal cations on the surface of the steel to form a complex that can further be precipitated and filtered.[23] The eutectic fluid and the metal particles can also be recycled, in contrast to the polluting acid-based technology presently employed. In electroplating, the opposite process, a metal is deposited onto a surface, such as in the massive industry of chromium electroplating. To this end, electrolysis of an ionic liquid containing choline chloride and chromium(III) chloride hexahydrate in a 1:2 molar ratio that freezes at 14 °C deposits a crack-free coating of chromium with high current efficiency.[15] This fluid is much less toxic than Cr^{VI} salts in acid media. Moreover, hydrogen production is negligible as no aqueous solutions are involved.

A more innovative application of choline-based eutectic mixtures was recently disclosed by Morris and co-workers.[24] They showed that choline chloride/urea as well as imidazolium-containing ionic liquids act as the solvent and the template for the synthesis of microporous crystalline zeolites and that the resulting framework depends on the type of ionic mixture employed as well as the presence of other ions and water (Scheme 4). Thus, 3-ethyl-1-methyl-imidazolium bromide provided four different aluminophosphate zeotypes. On heating at 150 °C, a novel structure of formula $(C_6H_{11}N_2)_3[Al_8(PO_4)_{10}H_3]$ consisting of hexagonal prismatic units was obtained. The pores contain the imidazolium templates that counterbalance the negative charge resulting from terminal P–O bonds. The eutectic mixture based on choline chloride and urea gave rise to another novel framework of formula $(NH_4)_3[Al_2(PO_4)_3]$ in which ammonium ions, released by partial decomposition of the urea, template the aluminophosphate zeolite and balance the ionic charge. Further experiments revealed that NH_4^+ ions can also be interchanged with other metal cations such as Cu^{II}.

Addition of fluoride ion or excess water to the ionic mixtures also resulted in condensed zeotypes with channel structures.[24] Owing to the lack of volatility of the ionic solvents, some syntheses could be conducted in open vessels, thus avoiding safety risks of hydrothermal reactions in sealed vessels. Moreover, the authors noted that the ionic liquids dissolved the raw materials at the reaction temperature, thus confirming that formation of zeolites occurs by crystallization from solution and not by a solid-to-solid reaction. The eutectic mixture of choline chloride and urea was similarly used for the synthesis and crystallization of coordination polymers such as $(NH_4)[Zn(O_3PCH_2CO_2)]$, in which ammonium ions direct the structure of the framework.[25]

Besides urea, other hydrogen-bond donors form eutectic complexes with a quaternary ammonium cation, which enables the formation of related green solvents. For instance, choline chloride forms room-temperature eutectic solvents with carboxylic acids, although a significant depression of freezing point is observed only with low-molecular-weight acids.[26] The lowest melting point of these antifreeze mixtures may occur at different eutectic compositions. Although the minimum freezing point occurs when the ratio of salt to hydrogen-bond donor is 1:2 for the choline chloride/urea mixture, polyfunctional molecules form a eutectic mixture at lower ratios. Thus, oxalic acid

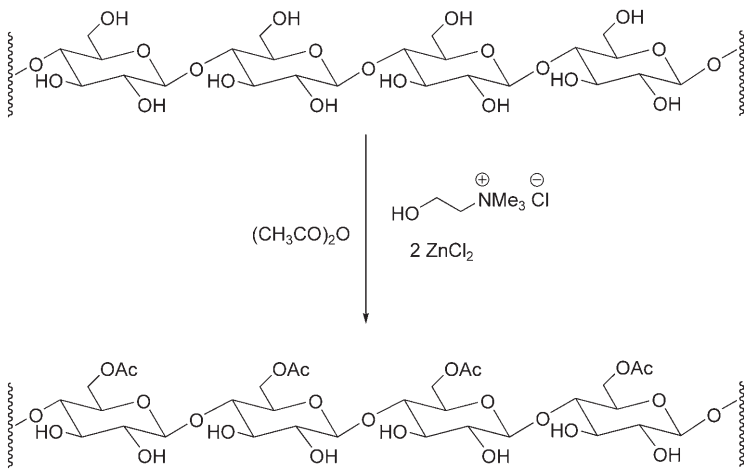

Scheme 3. Selective acylation of primary hydroxy groups in cellulose.[22]

© 2006 Wiley-VCH Verlag GmbH & Co. KGaA, Weinheim

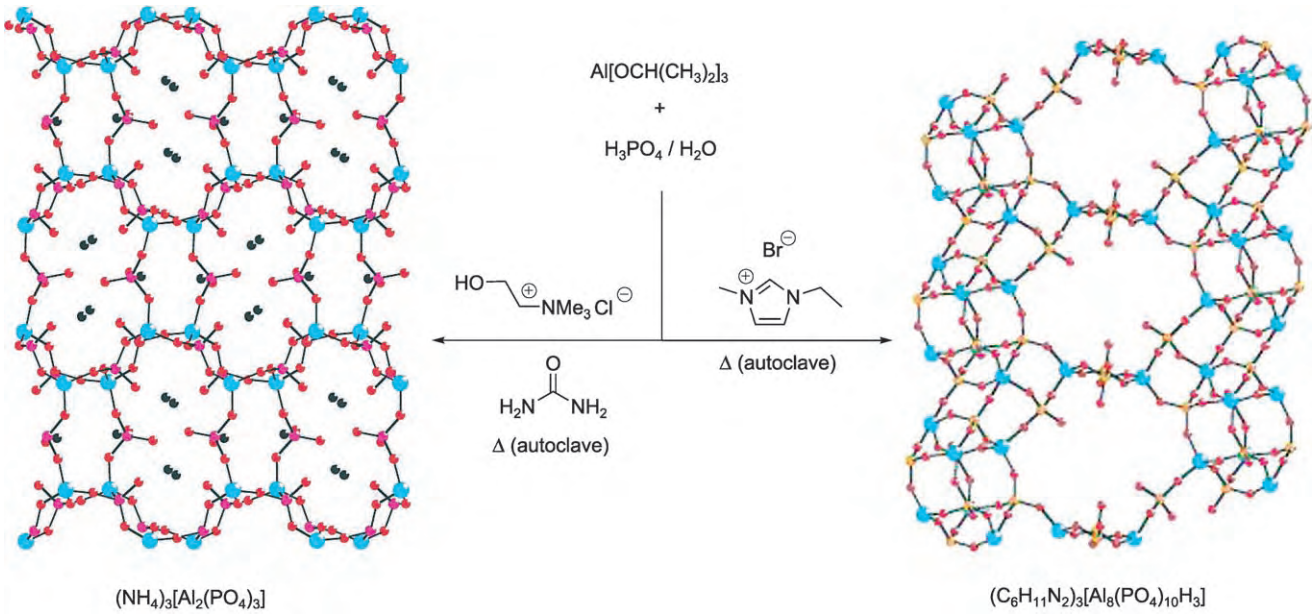

Scheme 4. Syntheses of novel zeolite analogues by using ionic mixtures as both solvents and structure-directing agents. Al blue; O red; P pink-red (left) or yellow (right). The ammonium ions present in the pores of the first zeotype are represented as black spheres. Adapted from reference [24].

(H_2OCCO_2H) forms a eutectic mixture at 50 mol% acid and, as expected, citric acid (a tricarboxylic derivative) forms a eutectic mixture at 30–35 mol% acid. In contrast, phenylacetic or phenylpropionic acids reveal their eutectics at 67 mol% acid, similar to that of the choline chloride/urea mixture.

Some properties of these mixtures, including data for refractive indexes, which are related to the polarizability of the medium, are summarized in Table 1. Notably, these values are similar to those of conventional ionic liquids. The surface tensions are larger than those of most organic solvents, although they are comparable to those of imidazolium-based ionic liquids. The surface tension of the eutectic formed from choline chloride and Cr^{III} chloride has a value similar to that of molten salts such as KBr. Low-freezing liquids can also be generated from mixtures of fatty acids such as lauric acid/myristic acid or lauric acid/palmitic acid in different molar ratios. These materials exhibit good thermal properties and are suitable for energy storage and solar-heating applications.[27]

Low-melting eutectic mixtures from sugars, so-called "sweet solutions", can be generated from commercially available sugars (e.g. glucose, fructose, or sorbitol), urea, and an inorganic salt ($CaCl_2$ or NH_4Cl).[28] The three-component mixture is significantly green, yet clear and viscous solutions can only be obtained between 65 °C and 75 °C. Notably, this depression avoids a common drawback of sugars upon heating at higher temperatures, namely browning with concomitant formation of caramel. "Sweet" eutectics were employed as media for Diels–Alder reactions with similar results to those obtained using ILs and supercritical CO_2. Despite their inherent chirality, no asymmetric induction was observed. This solvent system is as polar as *N*,*N*-dimethylformamide (DMF) and could potentially replace toxic, high-boiling solvents.[35]

Table 1: Properties of some eutectics formed with choline chloride.

Molecular donor [mol%]	M.p. [°C]	Refractive index	Surface tension [10^{-3} N m^{-1}]
urea (67)	12	1.504	52.02
malonic acid (50)	10	1.478	65.68
oxalic acid (50)	34	1.480	–
citric acid (30–35)	69	1.502	–
phenylacetic acid (67)	25	1.526	41.86
phenylpropionic acid (67)	20	1.522	–
$CrCl_3 \cdot 6H_2O$ (67)	14	1.547	77.68
anhydrous $ZnCl_2$ (67)	23–25	–	50.90
anhydrous $SnCl_2$ (67)	43–45	–	–

Elsewhere, the search for ionic fluids devoid of toxic anions culminated in the preparation of a benign system with reversible polarity control. The liquid is a mixture of 1,8-diazabicyclo-[5.4.0]undec-7-ene (DBU) and 1-hexanol.[29] When CO_2 is bubbled through the liquid, the DBU salt of 1-hexylcarbonate is generated. Bubbling of an inert gas, such as N_2 or Ar, removes the CO_2, and the ionic liquid reverts to the nonpolar state (Scheme 5). Both processes occur at ambient temperature, although the reverse step proceeds faster at 50 °C. The nonionic liquid is as nonpolar as $CHCl_3$, whereas the ionic phase is as polar as DMF or a carboxylic acid. Thus, *n*-decane is miscible with the

 © 2006 Wiley-VCH Verlag GmbH & Co. KGaA, Weinheim

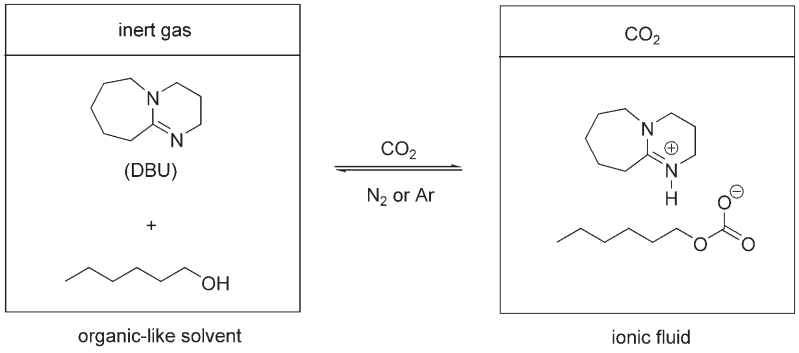

Scheme 5. Reversible polarity control in a eutectic mixture of DBU and 1-hexanol.[29]

DBU/alcohol mixture under N_2 and before exposure to CO_2. The alkane, however, separates out after bubbling CO_2.

Nature reminds us that living organisms may offer biologically inspired alternatives; they have developed molecular tools, through natural selection, to lower the freezing point of their body fluids, thus allowing their survival in extreme environments or simply allowing them to remain active in the cold winter. Some insects use dimethyl sulfoxide as an antifreeze; other organisms live in briny pools, such as in Antarctica, containing about one molecule of calcium chloride for every two water molecules and do not freeze until −45 °C. In this environment there is likely to be a microflora that continues the metabolism at least down to −23 °C.[30] More sophisticated strategies use antifreeze proteins (AFPs), which were first discovered in fishes and versions of which are now known in bacteria, plants, and insects.[31] AFPs work by binding to the surfaces of ice crystals as they start to form, inhibiting further growth.[32] A recent study described a species of snow flea, a wingless insect, that has developed two glycine-rich proteins, which are among the most effective AFPs ever observed, lowering the freezing point of its body fluids by nearly 6 °C. These proteins are also quite different from the threonine-rich AFPs found in two other insects, the beetle and the moth.[33] These findings shed light on the evolution of AFPs in organisms and could be instrumental in developing protein-based antifreeze agents with applications ranging from cryosurgery to frost-resistant crops.[34]

Chemistry and biology, as well as other applied sciences, will almost certainly benefit from molecular systems that serve as greener reaction media and scaffolds for low-temperature applications.

Published online: May 19, 2006

[1] P. T. Anastas, J. C. Warner, *Green Chemistry: Theory and Practice*, Oxford University Press, Oxford, **1998**.

[2] a) *Microwaves in Organic Synthesis* (Ed.: A. Loupy), Wiley-VCH, Weinheim, **2002**; b) T. J. Mason, P. Cintas, *Handbook of Green Chemistry and Technology* (Eds.: J. Clark, D. Macquarrie), Blackwell, Oxford, **2002**, pp. 372–396.

[3] *Green Reaction Media in Organic Synthesis* (Ed.: K. Mikami), Blackwell, Oxford, **2005**.

[4] "Organic Solid State Reactions": *Topics in Current Chemistry Series, Vol. 254* (Ed.: F. Toda), Springer, Heidelberg, **2005**.

[5] There are some conceptual problems associated with the term "polar solvents" in the case of 1,3-dialkylimidazolium salts as they comprise both donor and acceptor sites. Moreover, these systems are far from being homogeneous solvents and are better described as hydrogen-bonded polymeric superstructures. This pattern is maintained to a great extent in the liquid phase, and even in the gas phase. For an overview, see: J. Dupont, *J. Braz. Chem. Soc.* **2004**, *15*, 341–350.

[6] a) *Ionic Liquids in Synthesis* (Eds.: P. Wasserscheid, T. Welton), Wiley-VCH, Weinheim, **2002**; b) N. Jain, A. Kumar, S. Chauhan, S. M. S. Chauhan, *Tetrahedron* **2005**, *61*, 1015–1060; c) for ILs based on naturally occurring substances, see: S. T. Handy, *Chem. Eur. J.* **2003**, *9*, 2938–2944.

[7] J. Dupont, J. Spencer, *Angew. Chem.* **2004**, *116*, 5408–5409; *Angew. Chem. Int. Ed.* **2004**, *43*, 5296–5297.

[8] a) M. T. García, N. Gathergood, P. J. Scammells, *Green Chem.* **2005**, *7*, 9–14; b) R. P. Swatloski, J. D. Holbrey, R. D. Rogers, *Green Chem.* **2003**, *5*, 361–363; c) B. Jastorff, R. Störmann, J. Ranke, K. Mölter, F. Stock, B. Oberheitmann, W. Hoffmann, J. Hoffmann, M. Nüchter, B. Ondruschka, J. Filser, *Green Chem.* **2003**, *5*, 136–142.

[9] A recent study points to potential damage by ionic liquids to the aquatic environment, even at lower exposure concentrations than other organic pollutants; see: C. Pretti, C. Chiappe, D. Pieraccini, M. Gregori, F. Abramo, G. Monni, L. Intorre, *Green Chem.* **2006**, *8*, 238–240.

[10] A. P. Abbott, G. Capper, D. L. Davies, R. K. Rasheed, V. Tambyrajah, *Chem. Commun.* **2003**, 70–71.

[11] K. S. Pitzer, *Acc. Chem. Res.* **1990**, *23*, 333–338.

[12] M. Freemantle, *Chem. Eng. News* **2005**, *12*, 36–38.

[13] G. Rothenberg, A. P. Downie, C. L. Raston, J. L. Scott, *J. Am. Chem. Soc.* **2001**, *123*, 8701–8708.

[14] A. P. Abbott, G. Capper, D. L. Davies, R. K. Rasheed, P. Shikotra, *Inorg. Chem.* **2005**, *44*, 6497–6499.

[15] A. P. Abbott, G. Capper, D. L. Davies, R. K. Rasheed, *Chem. Eur. J.* **2004**, *10*, 3769–3774.

[16] A. P. Abbott, G. Capper, D. L. Davies, R. K. Rasheed, *Inorg. Chem.* **2004**, *43*, 3447–3452.

[17] V. Lecocq, A. Graille, C. C. Santini, A. Baudouin, Y. Chauvin, J. M. Basset, L. Arzel, D. Bouchou, B. Fenet, *New J. Chem.* **2005**, *29*, 700–706.

[18] A. P. Abbott, G. Capper, D. L. Davies, H. L. Munro, R. K. Rasheed, V. Tambyrajah, *Chem. Commun.* **2001**, 2010–2011.

[19] A. P. Abbott, G. Capper, D. L. Davies, R. K. Rasheed, V. Tambyrajah, *Green Chem.* **2002**, *4*, 24–26.

[20] R. C. Morales, V. Tambyrajah, P. R. Jenkins, D. L. Davies, A. P. Abbott, *Chem. Commun.* **2004**, 158–159.

[21] S. Abelló, F. Medina, X. Rodríguez, Y. Cesteros, P. Salagre, J. E. Sueiras, D. Tichit, B. Coq, *Chem. Commun.* **2004**, 1096–1097.

[22] A. P. Abbott, T. J. Bell, S. Handa, B. Stoddart, *Green Chem.* **2005**, *7*, 705–707.

[23] A. P. Abbott, G. Capper, B. G. Swain, D. A. Wheeler, *Trans. Inst. Met. Finish.* **2005**, *83*, 51–53.

[24] E. R. Cooper, C. D. Andrews, P. S. Wheatley, P. B. Webb, P. Wormald, R. E. Morris, *Nature* **2004**, *430*, 1012–1016.

 © 2006 Wiley-VCH Verlag GmbH & Co. KGaA, Weinheim

[25] J.-H. Liao, P.-C. Wu, Y.-H. Bai, *Inorg. Chem. Commun.* **2005**, *8*, 390–392.
[26] A. P. Abbott, D. Boothby, G. Capper, D. L. Davies, R. K. Rasheed, *J. Am. Chem. Soc.* **2004**, *126*, 9142–9147.
[27] A. Sari, *Appl. Therm. Eng.* **2005**, *25*, 2100–2107.
[28] G. Imperato, E. Eibler, J. Niedermaier, B. König, *Chem. Commun.* **2005**, 1170–1172.
[29] P. G. Jessop, D. J. Heldebrant, X. Li, C. A. Eckert, C. L. Liotta, *Nature* **2005**, *436*, 1102.
[30] *The New Encyclopaedia Britannica*, *15th ed.*, *Vol. 22*, Encyclopaedia Britannica Inc., Chicago, IL, **1990**, p. 990.
[31] a) K. V. Ewart, Q. Lin, C. L. Hew, *Cell. Mol. Life Sci.* **1999**, *55*, 271–283; b) C.-H. C. Cheng, L. Chen, *Nature* **1999**, *401*, 443–444; c) G. L. Fletcher, C. L. Hew, P. L. Davies, *Annu. Rev. Physiol.* **2001**, *63*, 359–390.
[32] N. J. Reeves, J. S. Evans, *J. Phys. Chem. A* **1997**, *101*, 6665–6669.
[33] L. A. Graham, P. L. Davies, *Science* **2005**, *310*, 461.
[34] G. L. Fletcher, S. V. Goddard, Y. L. Wu, *CHEMTECH* **1999**, *29*, 17–28.
[35] A very recent study reported bulk fusion when imidazole and menthol are mixed at room temperature, resulting from stabilizing hydrogen-bonding interactions; see: R. Hiraoka, H. Watanabe, M. Senna, *Tetrahedron Lett.* **2006**, *47*, 3111–3114. In a different approach, Kanakubo et al. reported melting point depression of ILs confined in nanostructures—remarkably, such a depletion is proportional to the inverse of the pore size; see: M. Kanakubo, Y. Hiehima, K. Minami, T. Aizawa, H. Nanjo, *Chem. Commun.* **2006**, 1828–1830.

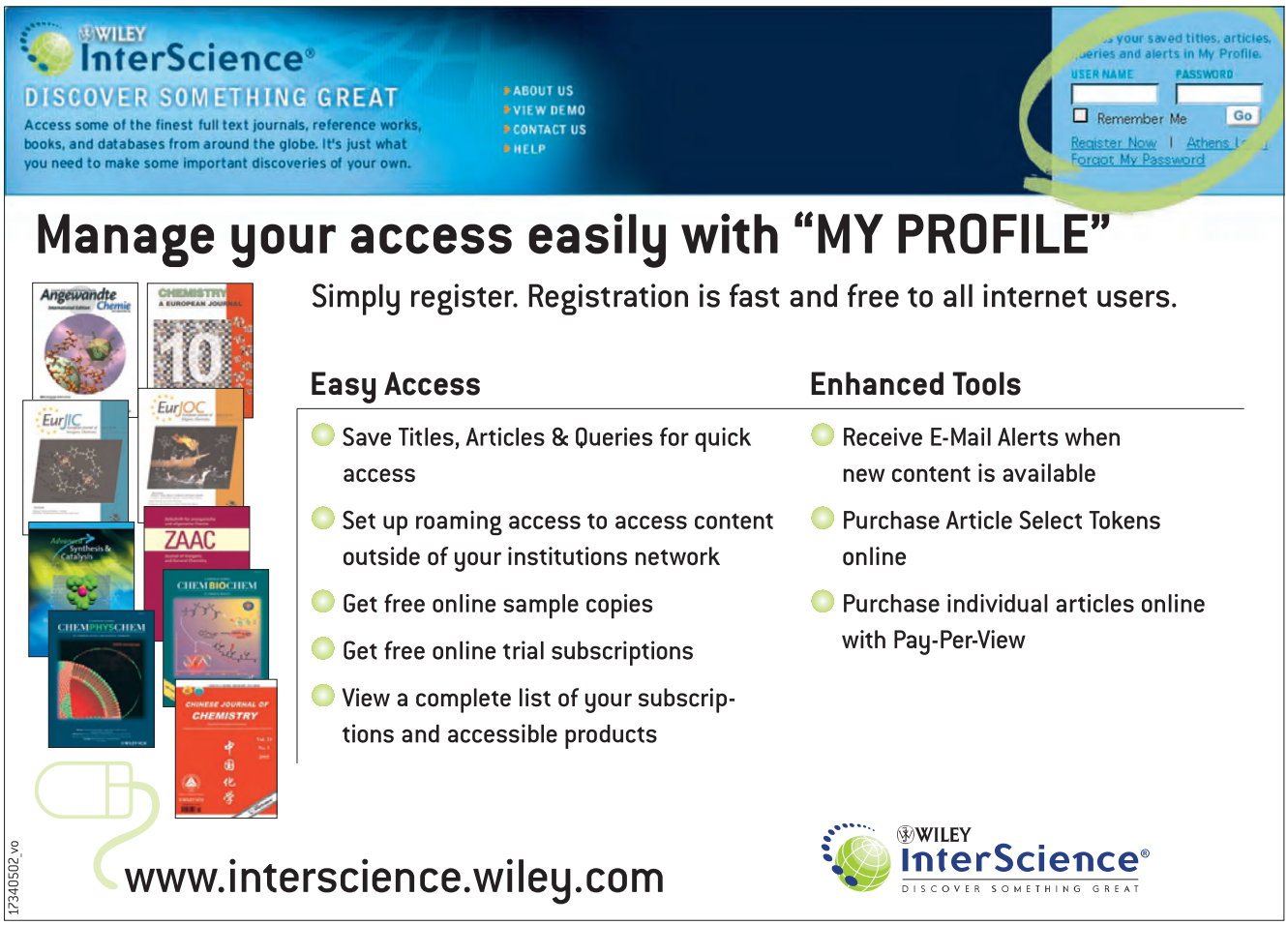

 © 2006 Wiley-VCH Verlag GmbH & Co. KGaA, Weinheim

Organocatalysis

DOI: 10.1002/anie.200600529

Chiral Phosphoric Acids: Powerful Organocatalysts for Asymmetric Addition Reactions to Imines

*Stephen J. Connon**

Dedicated to Prof. Siegfried Blechert on the occasion of his 60th birthday

Keywords:
amines · asymmetric synthesis · enantioselectivity · organocatalysis · phosphorus

Although the use of small organic molecules for the promotion of enantioselective transformations was first attempted almost a century ago,[1] the past decade has witnessed such an explosion of growth in this domain that asymmetric organocatalysis is, with some justification, often considered an emerging field of significant contemporary importance.[2] Several of the advances in this area are a result of the realization that reactions known to be susceptible to general acid catalysis involving prochiral substrates can be potentially carried out with high levels of stereoinduction in the presence of a chiral Brønsted acid (Scheme 1). The underlying concept is simple: since general acid catalysis[3] presupposes the participation of the acidic promoter (to some extent) in the reaction transition state (TS), one can thus aspire towards the design of catalysts capable of stabilizing the TS of a rate-determining, stereocenter-forming reaction step by partial proton transfer/hydrogen bonding while effectively preventing access to a single prochiral substrate face—thereby allowing an addition/cycloaddition reaction (for example) to occur in a stereoselective fashion.[4,5]

In this context, it is perhaps unsurprising that addition reactions to imines have proven an attractive target for asymmetric Brønsted acid organocatalysis,[2,4] as: a) nucleophilic addition to imines generally results in an increase in basicity at the heteroatom in the TS, b) both the electrophilicity and hydrogen-bond-accepting ability of the imine substrate can be modulated through the choice of N-protecting group, and c) the enantioenriched, protected amine products are often of high synthetic utility as chiral precursors to molecules of pharmaceutical and biological interest. To date, several efficient and selective Brønsted acid analogues (including bifunctional Brønsted acid/base systems) that catalyze a range of imine-addition processes previously demonstrated to be amenable to promotion by chiral metal(-ion)-based catalysts have been reported. Such processes include asymmetric Strecker (catalysts **1a–d**, Scheme 1),[6] Mannich (**1e** and **6**),[6f,7] aza-Henry (nitro-Mannich, **2–4**),[8] aza-Baylis–Hillman (**5**),[9] Pictet–Spengler (**6**),[10] and hydrophosphonylation (**1d**)[11] reactions.

In 2004, the research groups of Akiyama[12] and Terada[13] independently reported the development of a new class

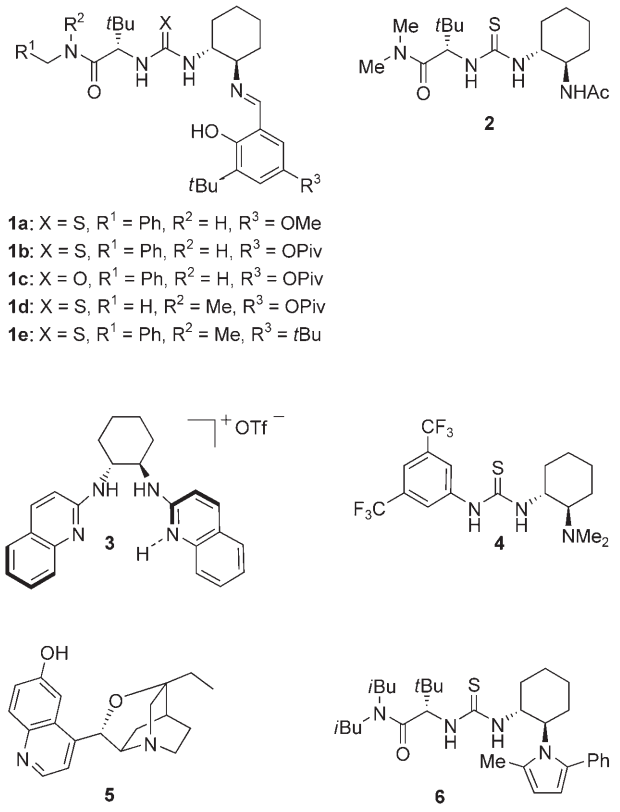

Scheme 1. Representative Brønsted acid catalysts for addition reactions to imines. Piv = pivaloyl, Ac = acetyl, OTf = trifluoromethanesulfonate.

[*] Dr. S. J. Connon
Centre for Synthesis and Chemical Biology
Department of Chemistry
University of Dublin
Trinity College, Dublin 2 (Ireland)
Fax: (+353) 1-671-2826
E-mail: connons@tcd.ie

© 2006 Wiley-VCH Verlag GmbH & Co. KGaA, Weinheim

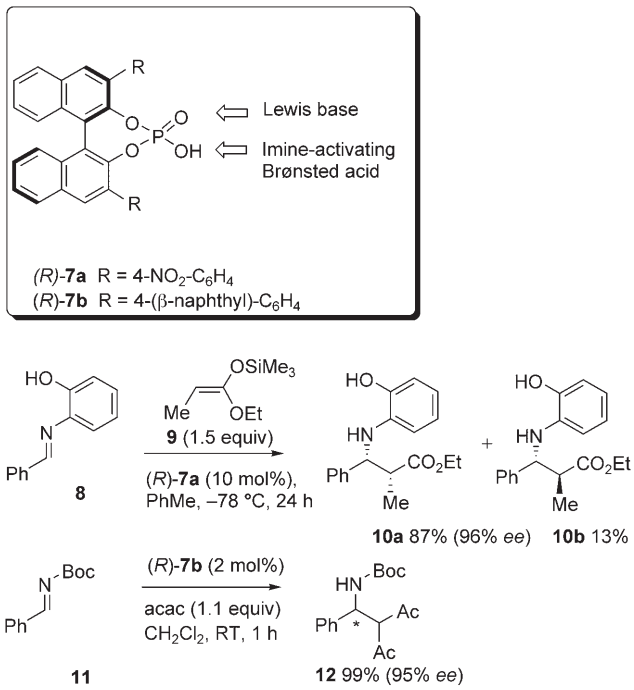

Scheme 2. Prototype phosphoric acid catalysts for Mannich-type reactions. Boc = *tert*-butoxycarbonyl, acac = acetylacetone

of chiral phosphoric Brønsted acid catalyst ((*R*)-**7a**,**b**, Scheme 2). These axially chiral materials represented a departure in terms of the design principle from the highly successful (thio)urea-based catalysts **1**,**2**,**4**, and **6**. Compounds (*R*)-**7a**,**b** are conformationally rigid and rely on a single proton (of considerable acidity[14]) and axially chiral substituents for the transfer of stereochemical information to the substrate, while the presence of the Lewis basic phosphoryl moiety in proximity to the acidic proton potentially allows for bifunctional catalysis (that is, simultaneous activation of both electrophilic and nucleophilic reaction components). Compounds (*R*)-**7a**,**b** were found to promote the efficient and selective catalysis of Mannich-type reactions between *N*-aryl- and *N*-Boc-substituted imines with silyl ketene acetals[12] and acetyl acetone,[13] respectively (Scheme 2).[15] The excellent catalytic activity of (*R*)-**7a**,**b** is illustrated by the compatibility of (protected) internal enol nucleophiles (such as **9**) in these reactions.

Following these seminal studies, it soon became clear that chiral phosphoric acids possessed tremendous potential for application in the development of novel asymmetric processes for which no catalytic strategies (either metal-ion-based or organocatalytic) were previously available. As part of a research program directed at the development of new catalytic addition reactions to imines, Antilla and co-workers[16] discovered that a range of potentially biologically relevant, orthogonally protected aminals could be prepared through a conceptually novel Brønsted acid catalyzed addition of protected amines (*N*-acyl, -formyl, -mesyl, -tosyl) to *N*-Boc-protected imines. Among the wide range of identified efficacious acidic promoters of the reaction was phenyl phosphinic acid (**13**), which prompted the development of an asymmetric variant of this novel transformation catalyzed by either (*S*)-**7c** or the (*S*)-VAPOL-derived compound (*S*)-**14** (Scheme 3). The latter phosphoric acid exhibited outstanding activity and selectivity in the addition of aryl sulfonamides (the sulfonamide moiety was required for high levels of stereoinduction) to a variety of aromatic *N*-Boc-protected imines such as **11**. The product aminals such as **16** were found to be susceptible to neither decomposition nor racemization upon storage in solution over several days. While the scope of the reaction was found to be general for a variety of aromatic *N*-Boc-protected imines, the transformation of analogous aliphatic imines was not reported.

MacMillan and co-workers recently reported examples of an organocatalytic, asymmetric reductive-amination reaction.[17,18] Prompted by the remarkable paucity of catalytic strategies for this reaction of almost unparalleled synthetic utility for the enantioselective synthesis of chiral amine derivatives, MacMillan and co-workers first attempted the reductive coupling of acetophenone (**17**) with anisidine (**18**) in the presence of the Hantzsch ester reductant **19** and a selection of benchmark

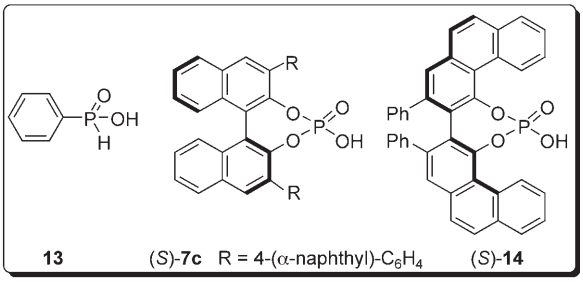

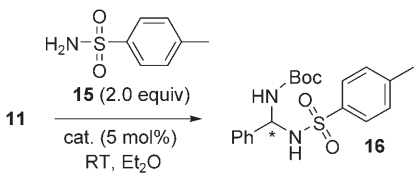

Catalyst	*t*	yield [%]	*ee* [%]
(*S*)-**7c**	24 h	99	71
(*S*)-**14**	1 h	95	94

Scheme 3. The first (asymmetric) catalytic imine-amidation reaction.

chiral Brønsted acid catalysts (Scheme 4). Although the bifunctional catalyst **2** and TADDOL **21** were inactive, the phosphoric acid derivative (*R*)-**7d** gave a poor yield of **20** with moderate selectivity. Subsequent optimization of the catalyst structure and reaction

 © 2006 Wiley-VCH Verlag GmbH & Co. KGaA, Weinheim

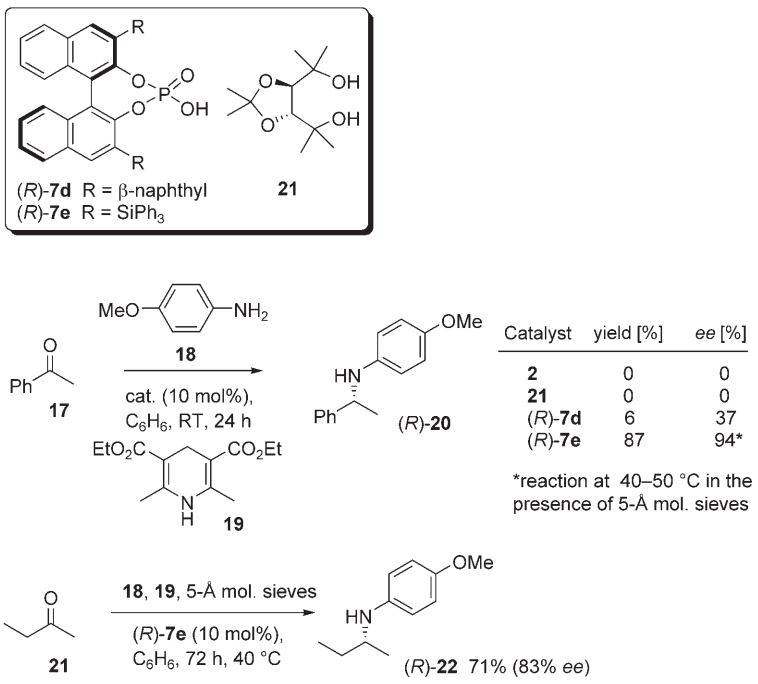

Scheme 4. The first asymmetric organocatalytic reductive amination.

conditions (the removal of in situ formed H_2O proved crucial) resulted in the efficient and highly enantioselective reductive coupling of **17** and **18** catalyzed by (*R*)-**7e**. The reaction was found to be applicable to the enantioselective coupling of a range of aromatic amines and either aromatic or aliphatic ketones; however, experimental, computational, and X-ray crystallographic studies indicated that the imine substrate for the reduction reaction must be derived from a methyl ketone—substituents larger than methyl shield the "open" *si* face of the catalyst-bound (activated) imine in the stereocenter-forming reaction TS. Nonetheless, this biomimetic methodology—which requires neither high pressures nor high temperatures—undoubtedly represents a breakthrough in catalytic asymmetric synthesis, and although the specificity for methyl ketones curtails general utility somewhat, this can be taken advantage of in the enantioselective reductive amination of highly challenging substrates such as ethyl methyl ketone (**21**, Scheme 4).

Terada and co-workers have recently developed two novel asymmetric organocatalytic reactions that they propose exploit the bifunctional nature of the phosphoric acid moiety.[19] In one interesting application, it was posited that an assisted deprotonation (**A**, Scheme 5) of the adduct from the Brønsted acid catalyzed reaction of *N*-acyl imine **23a** with α-diazoester **24** would prevent aziridination (**B**, Scheme 5), which is the usual fate of such intermediates in the absence of a suitable base, and allow the isolation of synthetically useful enantioenriched, protected α-diazo-β-amino acid derivatives. Exploratory studies involving the achiral phosphoric acid **26** verified this hypothesis and allowed the development of an efficient asymmetric analogue catalyzed by (*R*)-**7f** (Scheme 5). Bulky ester substituents and electron-rich *N*-acyl moieties proved optimal, and both facile reduction ($N_2 \rightarrow H$) and diastereoselective oxidation ($N_2 \rightarrow OH$, *anti*/*syn* > 99:1) of products such as (*S*)-**25** were demonstrated.[19]

The same research group also very recently disclosed an asymmetric organocatalytic version[20] of a recently discovered copper-catalyzed asymmetric addition of enamine derivatives to activated imines that was reported by Kobayashi and co-workers in 2004.[21] Speculating that phosphoric acid derivatives

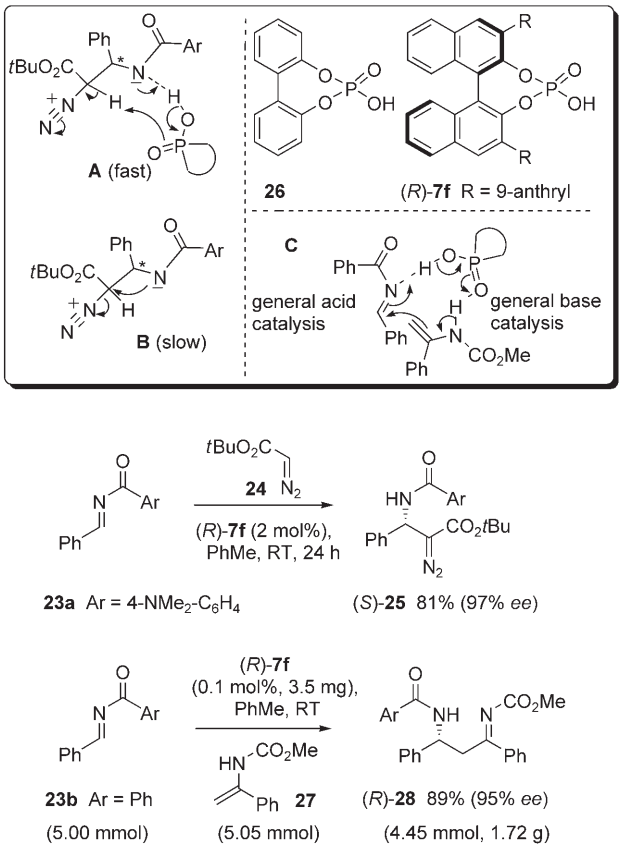

Scheme 5. The first asymmetric organocatalytic additions of α-diazoesters and enecarbamates to imines.

© 2006 Wiley-VCH Verlag GmbH & Co. KGaA, Weinheim

could facilitate the reaction between enecarbamates and protected imines by bifunctional acid/base catalysis (**C**, Scheme 5), the authors found that low loadings of (*R*)-**7f** (substrate/catalyst = 1000:1) could effectively promote the addition of **27** to **23b** to furnish (*R*)-**28** with excellent enantioselectivity in an efficient process which could be readily carried out on a gram scale. Subsequent diastereoselective (74% *de*) reduction of (*R*)-**28** afforded the corresponding orthogonally protected *anti*-1,3-diamine derivative in high yield.[20]

In summary, the advent of chiral strong Brønsted acid catalysts of general type **7** has resulted in a significant expansion of the scope of asymmetric nucleophilic-addition reactions to imine substrates and has accelerated the growth of an already swiftly expanding frontier of research in organic chemistry. In less than two years, the use of these catalysts has allowed the discovery of several completely novel asymmetric (organocatalytic) reactions for the synthesis of useful amine-based chiral building blocks. Therefore, as the process of elucidating the precise mode of action of these materials (on a reaction-by-reaction basis) begins and progresses, one can readily anticipate further rapid advances in terms of both catalyst design and the expansion of substrate scope—to the benefit of all those interested in enantioselective synthesis.

[1] First examples of organocatalytic kinetic resolution: a) G. Bredig, K. Fajans, *Ber. Dtsch. Chem. Ges.* **1908**, *41*, 752; b) K. Fajans, *Z. Phys. Chem.* **1910**, *73*, 25; for the first organocatalytic asymmetric synthesis, see: c) G. Bredig, P. S. Fiske, *Biochem. Z.* **1912**, *46*, 7.

[2] Reviews: a) S. Jayasree, B. List, *Org. Biomol. Chem.* **2005**, *3*, 719; b) P. I. Dalko, L. Moisan, *Angew. Chem.* **2004**, *116*, 5248; *Angew. Chem. Int. Ed.* **2004**, *43*, 5138; c) *Acc. Chem. Res.* **2004**, *37*(8).

[3] For instructive discussions of general acid catalysis: a) W. P. Jencks, *Chem. Rev.* **1972**, *72*, 705; b) W. P. Jencks, *Acc. Chem. Res.* **1976**, *9*, 425; c) W. P. Jencks, *Acc. Chem. Res.* **1980**, *13*, 161.

[4] Reviews: a) S. J. Connon, *Chem. Eur. J.* **2006**, DOI: 10.1002/chem.200501076; b) M. S. Taylor, E. N. Jacobsen, *Angew. Chem.* **2006**, *118*, 1550; *Angew. Chem. Int. Ed.* **2006**, *45*, 1520; c) Y. Takemoto, *Org. Biomol. Chem.* **2005**, *3*, 4299; d) P. M. Pihko, *Angew. Chem.* **2004**, *116*, 2110; *Angew. Chem. Int. Ed.* **2004**, *43*, 2062; e) P. R. Schreiner, *Chem. Soc. Rev.* **2003**, *32*, 289.

[5] For a discussion of the use of chiral Brønsted acid catalysts in conjunction with Lewis acids and other additives, see: H. Yamamoto, K. Futatsugi, *Angew. Chem.* **2005**, *117*, 1958; *Angew. Chem. Int. Ed.* **2005**, *44*, 1924.

[6] a) M. S. Sigman, E. N. Jacobsen, *J. Am. Chem. Soc.* **1998**, *120*, 4901; b) M. S. Sigman, P. Vachal, E. N. Jacobsen, *Angew. Chem.* **2000**, *112*, 1336; *Angew. Chem. Int. Ed.* **2000**, *39*, 1279; c) J. T. Su, P. Vachal, E. N. Jacobsen, *Adv. Syn. Catal.* **2000**, *343*, 197; d) P. Vachal, E. N. Jacobsen, *Org. Lett.* **2000**, *2*, 867; e) P. Vachal, E. N. Jacobsen, *J. Am. Chem. Soc.* **2002**, *124*, 10012; f) A. G. Wenzel, M. P. Lalonde, E. N. Jacobsen, *Synlett* **2003**, 1919.

[7] a) A. G. Wenzel, E. N. Jacobsen, *J. Am. Chem. Soc.* **2002**, *124*, 12964; b) M. S. Taylor, N. Tokunaga, E. N. Jacobsen, *Angew. Chem.* **2005**, *117*, 6858; *Angew. Chem. Int. Ed.* **2005**, *44*, 6700.

[8] a) T. Okino, S. Nakamura, T. Furukawa, Y. Takemoto, *Org. Lett.* **2004**, *6*, 625; b) B. M. Nugent, R. A. Yoder, J. N. Johnson, *J. Am. Chem. Soc.* **2004**, *126*, 3418; c) T. P. Yoon, E. N. Jacobsen, *Angew. Chem.* **2005**, *117*, 470; *Angew. Chem. Int. Ed.* **2005**, *44*, 466.

[9] S. Kawahara, Y. Iwabuchi, S. Hatakeyama, *Org. Lett.* **2003**, *5*, 3103.

[10] M. S. Taylor, E. N. Jacobsen, *J. Am. Chem. Soc.* **2004**, *126*, 10558.

[11] G. D. Joly, E. N. Jacobsen, *J. Am. Chem. Soc.* **2004**, *126*, 4102.

[12] T. Akiyama, J. Itoh, K. Yokota, K. Fuchibe, *Angew. Chem.* **2004**, *116*, 1592; *Angew. Chem. Int. Ed.* **2004**, *43*, 1566.

[13] D. Uraguchi, M. Terada, *J. Am. Chem. Soc.* **2004**, *126*, 5356.

[14] The pK_a value of diethyl phosphate is 1.39: L. D. Quin, *A Guide to Organophosphorus Chemistry*, Wiley, New York, **2000**, chap. 5.

[15] Shortly thereafter, analogues of **7a**,**b** were shown to serve as highly effective promoters of both aza-Friedel–Crafts-type alkylation reactions of furan and imine hydrophosphonylations; see: a) D. Uraguchi, K. Sorimachi, M. Terada, *J. Am. Chem. Soc.* **2004**, *126*, 11804; b) T. Akiyama, H. Morita, J. Itoh, K. Fuchibe, *Org. Lett.* **2005**, *7*, 2583.

[16] G. B. Rowland, H. Zhang, E. B. Rowland, S. Chennamadhavuni, Y. Wang, J. C. Antilla, *J. Am. Chem. Soc.* **2005**, *127*, 15696.

[17] R. I. Storer, D. E. Carrera, Y. Ni, D. W. C. MacMillan, *J. Am. Chem. Soc.* **2006**, *128*, 84.

[18] a) For seminal work on the phosphoric acid catalyzed reduction of preformed imines, see: M. Rüping, E. Sugiono, C. Azap, T. Theissmann, M. Bolte, *Org. Lett.* **2005**, *7*, 3781; b) for a similar study, which includes an example of a prototype reductive amination protocol, see: S. Hoffmann, A. M. Seayad, B. List, *Angew. Chem.* **2005**, *117*, 7590; *Angew. Chem. Int. Ed.* **2005**, *44*, 7424; c) phosphoric acids have also been utilized recently in asymmetric Pictet-Spengler reactions: J. Seayad, A. M. Seayad, B. List, *J. Am. Chem. Soc.* **2006**, *128*, 1086; d) for a short review of organocatalytic asymmetric reduction of α,β-unsaturated aldehydes, see: H. Adolfsson, *Angew. Chem.* **2005**, *117*, 3404; *Angew. Chem. Int. Ed.* **2005**, *44*, 3340.

[19] D. Uraguchi, K. Sorimachi, M. Terada, *J. Am. Chem. Soc.* **2005**, *127*, 9360.

[20] M. Terada, K. Machioka, K. Sorimachi, *Angew. Chem.* **2006**, *118*, 2312; *Angew. Chem. Int. Ed.* **2006**, *45*, 2254.

[21] R. Matsubara, Y. Nakamura, S. Kobayashi, *Angew. Chem.* **2004**, *116*, 1711; *Angew. Chem. Int. Ed.* **2004**, *43*, 1679.

 © 2006 Wiley-VCH Verlag GmbH & Co. KGaA, Weinheim

M. M. Haley and C. W. Landorf

DOI: 10.1002/anie.200504358

Metallabenzenes

Recent Advances in Metallabenzene Chemistry

*Christopher W. Landorf and Michael M. Haley**

Keywords:
aromaticity · iridium · metallacycles · osmium · platinum · ruthenium

Dedicated to Professor Peter Vollhardt on the occasion of his 60th birthday

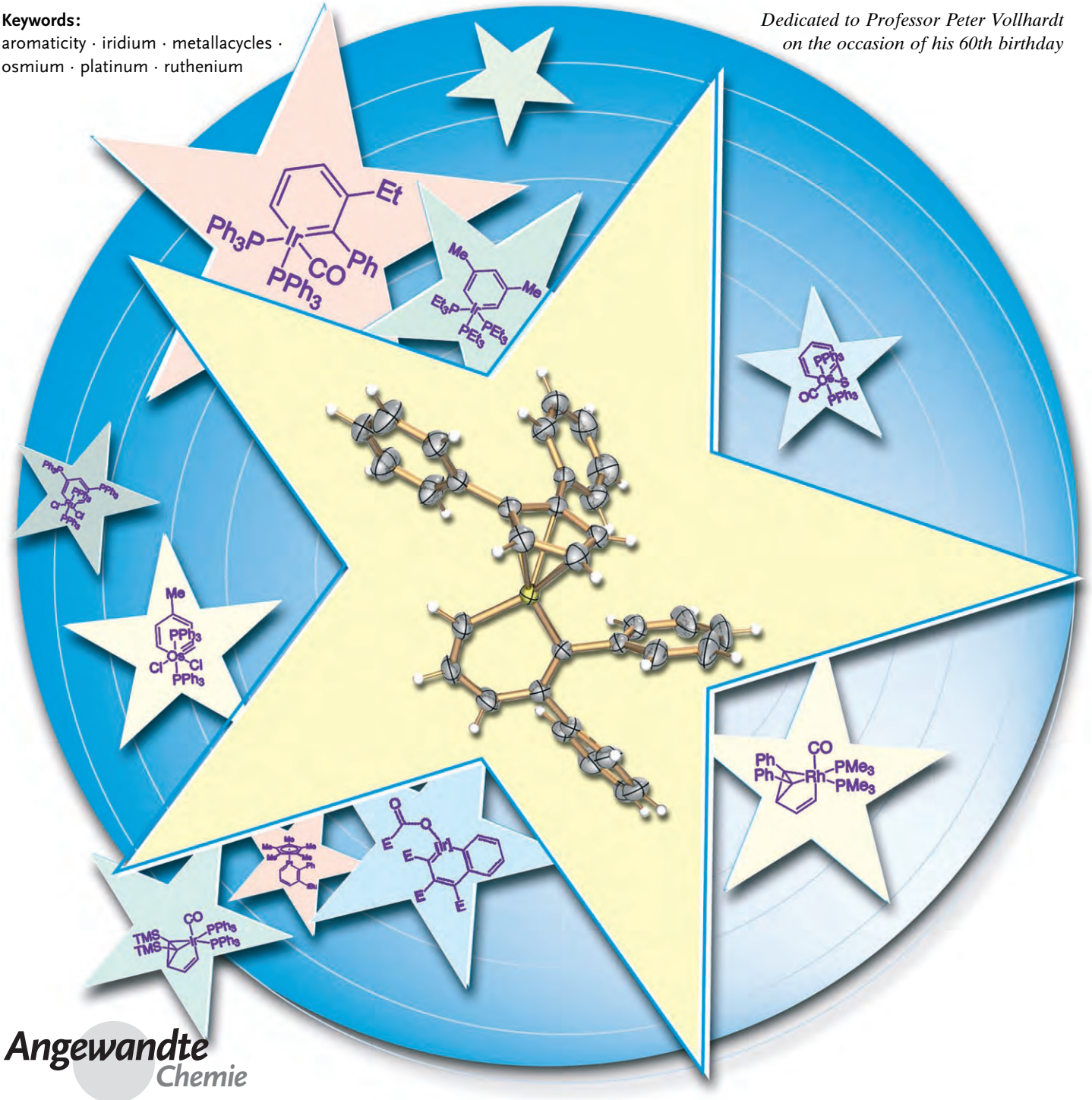

© 2006 Wiley-VCH Verlag GmbH & Co. KGaA, Weinheim

Research into aromatic metallacycles, though discussed in the literature over the last quarter century, has undergone a major expansion since 2000. A wide variety of new metallabenzenes, encompassing new synthetic methods and new metal centers, is now available. New aromatic metallacycle topologies (iridanaphthalene, osmabenzynes) have been isolated and characterized. The first metallabenzene valence isomers (iridabenzvalenes, rhodabenzvalenes) and constitutional isomers (isoosmabenzenes) are now known. This review discusses the synthesis, chemistry, and physical properties of these intriguing aromatic compounds.

From the Contents

1. Introduction	3915
2. Historical Perspectives	3916
3. Osmium	3917
4. Ruthenium	3921
5. Iridium	3924
6. Rhodium	3932
7. Platinum	3932
8. Conclusions	3934

1. Introduction

Ever since Kekulé proposed a cyclic six-membered ring with rapidly alternating single and double bonds to describe the structure and stability of benzene, chemists have been debating the nature of aromaticity and "aromatic" molecules.[1,2] New aromatic molecules are constantly being synthesized, some of which continue to stretch and expand our definition of this concept. How does one qualify an aromatic compound?[1–3] An undergraduate chemist is usually taught that a compound is either aromatic, antiaromatic, or non-aromatic based on the Hückel $[4n+2]$ π-electron rule, but it does not take much imagination to think of a compound that does not neatly fall into one of these categories. These "intermediate" compounds may exhibit some properties normally associated with aromaticity, such as downfield ^{1}H NMR signals, but completely lack other facets, such as stability towards dienophiles. For these reasons, it is risky to attempt to define aromaticity in fixed terms. Instead, it may be best to remove arguments that attempt to rigidly define the concept of "aromaticity" by considering the characteristics commonly attributed to aromaticity separately.[3]

The replacement of a CH group within a benzenoid ring with an isolobal heteroatomic fragment is well-known and exemplified by molecules such as pyridine, phosphabenzene, pyrillium, and thiabenzene.[4–6] Benzenoid aromatic compounds of even heavier elements such as silicon and gallium are also known.[5–8] Where the lines begin to blur is with one of these classes of "intermediate" compounds known as metallabenzenes. Metallabenzenes are six-membered metallacycles analogous to benzene for which one CH unit has been replaced by an isolobal transition-metal fragment $\{ML_n\}$.[9,10] These metallacycles differ from regular aromatic compounds in that the π bonding requires involvement of the metal d orbitals since the metal p orbitals participate in σ bonding to the ligands. Thorn and Hoffmann were the first to consider the application of the Hückel rule to metallabenzenes.[11] In their analysis, four electrons come from the p orbitals in the five-carbon backbone, while two electrons come from the filled d_{xz} orbital of the metal fragment; therefore, metallabenzenes obey the Hückel definition of aromaticity. Nonetheless, with such a fundamental difference in bonding, one cannot but wonder how incorporation of the d orbitals might affect the aromaticity and thus stability, reactivity, properties, etc. of the resultant compounds.

In the quarter century since Thorn and Hoffmann's initial proposal, over 30 varieties of metalla-aromatic species have been synthesized and/or characterized. Although most of these metallacycles have been isolated examples, a majority exhibit properties normally associated with aromatic systems, such as relatively deshielded proton resonances in the ^{1}H NMR spectrum.[12] Whereas the ring protons in metallabenzenes are also deshielded, the anisotropy of the metal center can severely affect this analysis, especially at the position *ortho* to the metal.[9] NICS (Nucleus Independent Chemical Shift) calculations have often been invoked to determine the aromaticity of a compound;[13] however, NICS values are also subject to the anisotropy of metal centers.[14]

Structurally, bond lengths and ring planarity can be analyzed to determine if the molecule in question is aromatic.[15] An aromatic ring typically exhibits bond lengths intermediate between a single and double bond, and this property holds true to a reasonable extent for all metallabenzenes characterized to date. The bulkiness of the metal fragment, however, tends often to distort the six-membered ring from planarity.

Unique reactions such as electrophilic aromatic substitution (EAS) are occasionally invoked to demonstrate aromaticity. Owing in part to the reactivity of the metal center, EAS reactions have rarely been observed for metallabenzenes.[9,16] Another reaction unique to aromatic compounds is the formation of arene-coordination complexes. For metallabenzenes, these complexes are formed readily and often stabilize metallacycles that would otherwise be too short-lived to be observed.[9,17,18]

[*] C. W. Landorf, Prof. Dr. M. M. Haley
Department of Chemistry
University of Oregon
Eugene, OR 97403-1253 (USA)
Fax: (+1) 541-346-0487
E-mail: haley@uoregon.edu

© 2006 Wiley-VCH Verlag GmbH & Co. KGaA, Weinheim

Aromatic compounds are often noted for their stability and lack of reactivity under ordinary conditions. Metallabenzenes, however, undergo some very unusual reactions that are unheard of for classically aromatic compounds. For example, cycloadditions with dienophiles and rearrangements to form cyclopentadienyl complexes suggest that these molecules are not as aromatic—that is, as stable—as their all-carbon analogues.[9,17,19–22]

While metallabenzenes have been known since 1982[23] and were the subject of an excellent review in early 2001,[9] these metallacycles have been synthesized at an ever-increasing pace over the last few years. More importantly, new aromatic topologies (metallabenzynes, metallanaphthalenes) as well as new, versatile syntheses of such metallacycles have begun to emerge. As opposed to being an all-encompassing document, this review will highlight the numerous advances from 2000 on. We will focus predominantly on the syntheses and properties of metallabenzenes and related aromatics where one metal atom and five carbon atoms comprise the metallacycle. Some attention will be paid to metal-coordinated metallabenzenes, for which the uncoordinated metallabenzenes, specifically of the 4d metals, were until very recently not known. Although there are numerous examples of hetero-metallabenzenes, such as a metallathiabenzene, that are worthy of inclusion, they do not fall under the scope of this review.[24,25]

2. Historical Perspectives

Originally postulated to be a stable species by Thorn and Hoffman in their seminal paper in 1979,[11] the first unambiguous isolation of a metallabenzene was reported by Roper and co-workers in 1982.[23,26] Through inspiration from the synthesis of metallacyclopentadienes from the [2+2+1] cycloaddition of alkynes with transition-metal complexes, arene **1** was isolated from the formal [2+2+2] cycloaddition of two ethyne molecules to $[Os(CO)(CS)(PPh_3)_3]$. The ^1H NMR spectrum of the resulting six-membered metallacycle exhibited a peak at $\delta = 13.95$ ppm and several overlapping peaks at $\delta = 7.28$ ppm. The unusual peak at $\delta = 13.95$ ppm was attributed to the proton *ortho* to the metal, and its deshielding was attributed to the anisotropy of the metal. Since the effects of the metal are expected to drop sharply as the distance from the metal center increases, the three peaks at $\delta = 7.28$ resonated in the typical range for aromatic protons. Additionally, C–C bond-length alternation was shown to be negligible by X-ray crystallography.

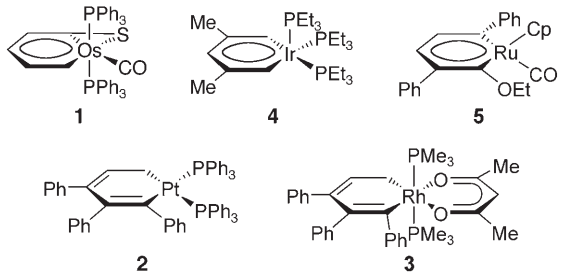

Work reported by Hughes and co-workers in 1986 demonstrated the first use of vinylcyclopropenes to give six-membered metallacycles. Platinacyclohexadiene **2** could be made from treating $[Pt(\eta^2\text{-}C_2H_4)(PPh_3)_2]$ with 1,2,3-triphenyl-3-vinylcycloprop-1-ene.[27] A year later this group reported that reaction of the same vinylcyclopropene with $[MCl(PMe_3)_2]$ (M = Rh, Ir) also produced the corresponding metallacyclohexadienes, one of which was crystallographically characterized as the acetylacetonate (acac) complex **3**.[28] On heating, these metallacyclohexadienes were found to generate 1,2,3-triphenylcyclopentadiene. Recent studies have demonstrated that elimination to form cyclopentadienyl complexes is a common decomposition pathway of metallabenzenes, although other pathways could be responsible for this transformation.[22]

In 1989, Bleeke et al. reported the synthesis of the first stable iridabenzene **4** utilizing 2,4-dimethylpentadienide as a source for the carbon backbone.[17,29] Using the resultant iridabenzene as a starting point, the Bleeke group extensively examined the chemistry of such complexes.[17] When exposed to EAS conditions, it was found that the electrophiles react preferentially with the electron-rich metal center. Additionally, it was found that when exposed to dienophiles, these iridabenzenes behave more like cyclohexatrienes and undergo cycloaddition reactions.[19,20,30]

The first ruthenabenzene **5** to be observed spectroscopically was reported by Jones, Allison, and co-workers in 1995.[31] Utilizing a method similar to what Ferede and Allison had previously reported for a suspected ferrabenzene,[32] a

Michael M. Haley was born in 1965 in Lake Charles, LA. After growing up in Tulsa, Oklahoma, he carried out his Bachelor's and Ph.D. studies with Prof. W. E. Billups at Rice University. In 1991 he received an NSF Postdoctoral Fellowship to work with Prof. K. P. C. Vollhardt at the University of California, Berkeley. In 1993 he joined the faculty at the University of Oregon where he is currently Professor of Chemistry and member of the Materials Science Institute. His current research focuses on the chemistry of dehydroannulenes and dehydrobenzoannulenes, metallabenzenes, and other novel aromatic systems.

Christopher W. Landorf was born in Summit, New Jersey in 1972. After receiving his B.S. degree in chemistry at Iowa State University in 1995, he studied at Southern Illinois University at Carbondale where he investigated the synthesis of hydrogen-bonded liquid crystals and earned his M.S. degree in chemistry in 2001. He is currently completing his Ph.D. studies at the University of Oregon under the direction of Professor Haley investigating platina- and iridabenzenes.

 © 2006 Wiley-VCH Verlag GmbH & Co. KGaA, Weinheim

^{13}C NMR spectrum of the ^{13}C-enriched complex exhibited a label-enhanced singlet at $\delta = 291$ ppm, which was attributed to the ring carbon atom in the {RuC(OEt)} moiety. Complex **5** subsequently decomposed above −50 °C to an η^1-cyclopentadienyl complex.[31] Additionally, a similar reaction sequence was proposed to proceed through a ruthenaphenanthrene complex, although no direct observation of the metallaphenanthrene was made. This was the first, and to date remains one of the very few, second-row metalla-aromatic molecules to be reported.

3. Osmium

3.1. Osmabenzenes

The first metallabenzene to be isolated and characterized was osmabenzene **1**.[23,26] Recently, van der Boom, Martin, and co-workers calculated the energies of the various transition states in the formation of **1** by using model **6** as the starting complex to prepare **7** (Scheme 1).[33] Their study

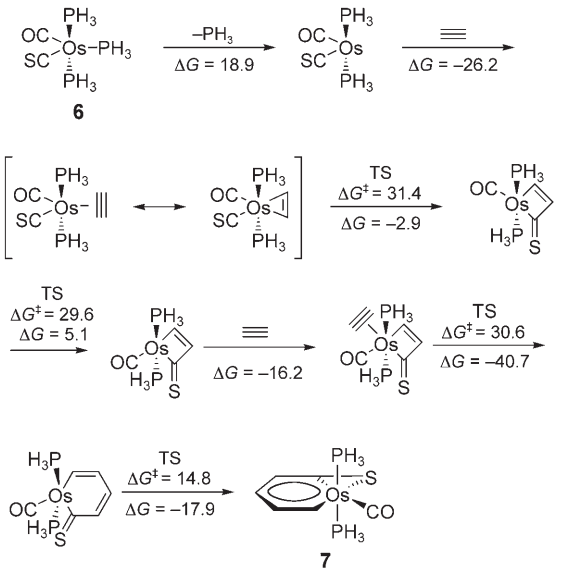

Scheme 1. Calculated pathway to osmabenzene by Roper and co-workers. [23,26] Energies are given in kcal mol^{-1}. TS = transition state.

revealed that the first step in osmabenzene formation is loss of a phosphine ligand, followed by coordination to an acetylene molecule. The lowest-energy pathway was found to proceed by migratory insertion of the CS ligand into the σ bond of the osmacyclopropene (Dewar–Chatt–Duncanson model).[34] The first insertion step opens up another coordination site for a second equivalent of acetylene, but the pathway leading to the resulting osmabenzene requires that the CO ligand rearranges to a position *cis* to the thiocarbonyl ligand prior to coordination with a second equivalent of acetylene. Coordination followed by insertion leads to the 2-osma-3,5-cyclohexadiene-1-thione, which then rearranges to afford osmabenzene **7**.

The hypothetical reaction involving migratory insertion of CO instead of CS was also studied.[33] In addition to higher transition-state energies, it was found that the final step, rearrangement of the 2-osma-3,5-cyclohexadiene-1-one to the osmabenzene, would not take place owing to the strain in the resulting three-membered ring. The larger size of the sulfur atom reduces the ring strain sufficiently to allow formation of **7**.

While the structural properties of metallabenzenes are clearly consistent with the "aromatic" label, it is less clear with regard to the chemistry of these compounds since most metallabenzenes tend to react in ways that are atypical of conventional aromatic molecules.[9,17] Recently, however, the first demonstration of electrophilic aromatic substitution was observed for osmabenzene **8** (Scheme 2).[16] The nitration of **8**

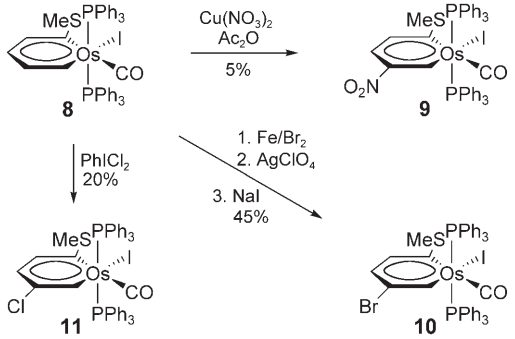

Scheme 2. Electrophilic aromatic substitution of osmabenzene **8**.

was achieved with a solution of $Cu(NO_3)_2$ in Ac_2O. Analysis of the resultant purple crystals showed that nitration had occurred on the position *para* to the thioether to give **9**. Similarly, the addition of Br_2 and Fe powder to a solution of **8** resulted in bromination at the *para* position of the metallacycle to give **10** (partial exchange of the osmium-bound iodide was also observed). Chlorination of **8** with $PhICl_2$ gave the corresponding metallacycle **11**. Since electrophilic substitution occurred at the position predicted by the directing effects of the thioether, it is unclear what, if any, the directing effects of the metal fragment are.

A second pathway to stable osmabenzenes was reported by Jia and co-workers in 2004.[35] This group found that reaction of $[OsCl_2(PPh_3)_3]$ with 1,4-pentadiyn-3-ol led to the isolation of metallacycle **12**, the phosphonium salt of an osmabenzene. The mechanism proposed for formation of this unusual species involves the substitution of a coordinated phosphine ligand with an η^2-coordinated alkyne to give species **13** (Scheme 3). This step is followed by addition of the phosphine at the 2-position on the coordinated alkyne to afford intermediate **14**, which could be isolated. A second molecule of PPh_3 then attacks the resulting coordinated alkyne to give intermediate **15**, which then eliminates a hydroxide ion to yield osmabenzene **12**. Treatment of **12** with excess PMe_3 and Bu_4NCl furnished osmabenzene **16**.

Spectroscopic characterization of **12** displayed the characteristic downfield shift of the *ortho* proton in the ^1H NMR spectrum at $\delta = 23.13$ ppm. This shift is significantly farther

© 2006 Wiley-VCH Verlag GmbH & Co. KGaA, Weinheim

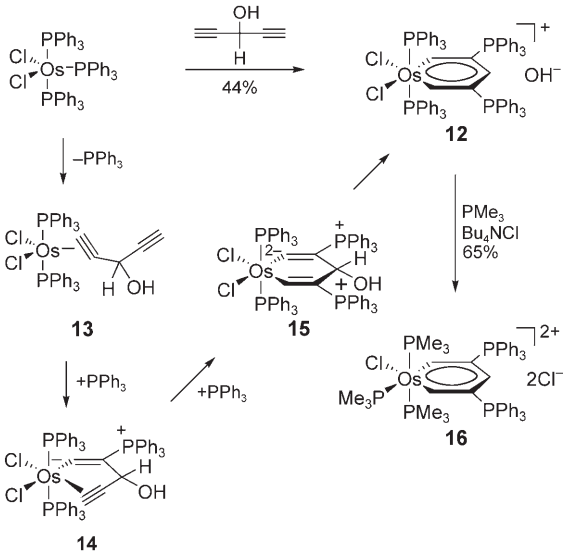

Scheme 3. Synthesis of osmabenzene **12**.

downfield from the *ortho* proton in **1**, which resonates at $\delta =$ 13.95 ppm.[23,26] The lower-field signal in **12** could, in part, be explained by the electron-deficient phosphonium substituents on the ring. The *para* proton gave a signal at $\delta = 8.57$ ppm. Once again, compared to **1** ($\delta = 7.28$ ppm), the shift is comparatively deshielded. A similar trend was observed for the *ortho* and *para* carbons in the ^{13}C NMR spectrum, in which the respective signals were observed at $\delta = 239.7$ and 160.5 ppm. The *meta* carbon is shifted upfield ($\delta = 112.7$ ppm) relative to benzene ($\delta = 128.4$ ppm).

An X-ray diffraction analysis of **12** revealed that the metallacycle is a planar ring structure similar to osmabenzene **1**, except that the Os–C bond lengths are shorter than in **1** (1.97 Å vs. 2.00 Å). Contributing resonance structures **12c** and **12d** may explain this difference (Scheme 4). The mean

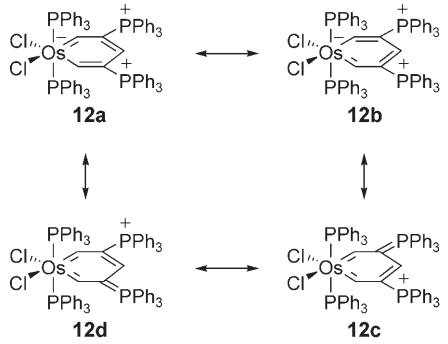

Scheme 4. Resonance contributors for osmabenzene **12**.

deviation from the least-squares plane of the ring is 0.075 Å. All C–C bond lengths are intermediate between bond lengths typical for single and double bonds, which range from 1.363 Å to 1.448 Å. Two of the contributing resonance structures (**12c** and **12d**) are not cyclically conjugated. Comparison of the P–C bond lengths, however, shows that the P–$C_{osmabenzene}$ and P–C_{phenyl} bond lengths are similar, thus indicating that these two resonance structures are not major contributors to the overall structure.

Nucleophiles other than PPh_3 were also found to react with intermediate **14** to produce osmabenzenes.[35] Addition of NaI to a solution of **14** gave iodobenzene **17** (Scheme 5).

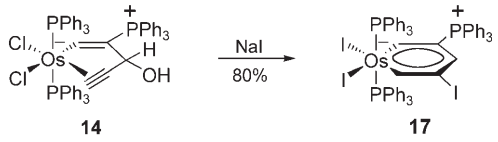

Scheme 5. Synthesis of iodoosmabenzene **17**.

The *ortho* protons of **17** resonate at $\delta = 20.1$ ppm (OsC*H*Cl) and $\delta = 19.0$ ppm (OsC*H*CPPh$_3$) and the *para* proton resonates at $\delta = 8.1$ ppm in the ^{1}H NMR spectrum. This upfield shift in resonances in comparison to analogous protons in cationic **12** reflects the electronic effects of having one phosphonium group fewer.

Similar reactivity was observed upon treatment of [$OsBr_2(PPh_3)_3$] with 1,4-pentadiyn-3-ol, which formed intermediate **18**. Subsequent treatment with PPh_3 produced osmabenzene **19** after metathesis with Bu_4NBr (Scheme 6).[35]

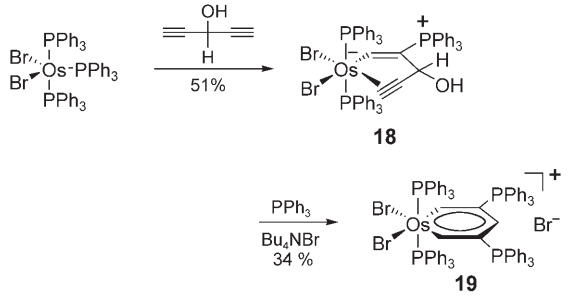

Scheme 6. Synthesis of osmabenzene **19**.

3.2. Osmabenzynes

Addition of strong bases such as KNH_2 to a solution of chlorobenzene produces benzyne, a well-known but transient species.[3a,36] Benzyne is a relative of benzene with two neighboring sp-hybridized carbons. The six-membered ring puts enormous strain on the ordinarily linear carbon–carbon triple bond, thus making this species extremely unstable.[37] For this reason, it seems almost unthinkable that a metallabenzyne could be isolated and fully characterized.

In 2001, the Jia group was able nonetheless to isolate the first stable osmabenzyne **20** (Scheme 7).[38–40] Treatment of [$OsCl_2(PPh_3)_3$] with an excess of trimethylsilylacetylene in wet benzene produced a brown solution, from which **20** was isolated in 30% yield. As confirmed by X-ray structural analysis, **20** contains an essentially planar six-membered metallacycle with a maximum deviation from the least-squares plane of 0.047 Å. The Os–C(sp) bond length is

 © 2006 Wiley-VCH Verlag GmbH & Co. KGaA, Weinheim

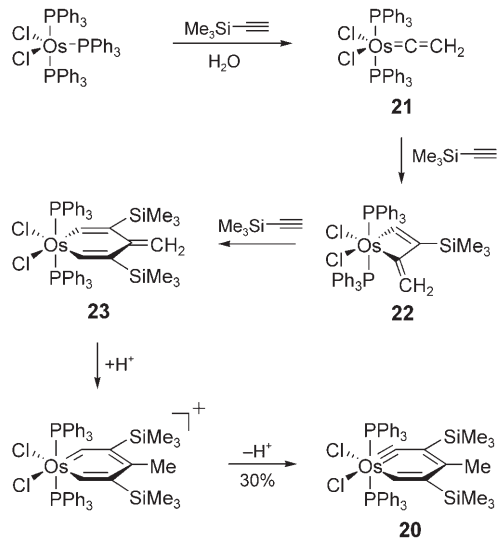

Scheme 7. Proposed mechanism for the synthesis of osmabenzyne **20**.

1.815 Å, shorter than that observed in both **1** and **12**, but longer than that for typical osmium–carbyne complexes. The ring C–C bond lengths range from 1.376 to 1.420 Å. Not surprisingly, the Os–C(sp^2) bond length is 1.939 Å, only slightly shorter than those in the osmabenzenes (see Section 3.1).

A possible mechanism for the formation of osmabenzyne **20** is given in Scheme 7. Initial formation of a vinylidene complex followed by hydrolysis of the trimethylsilyl group should produce **21**. Subsequent [2+2] cycloaddition with a second equivalent of trimethylsilylacetylene would afford cyclobutene **22**. The remaining ring carbons then come from insertion of a third equivalent of trimethylsilylacetylene to give the six-membered metallacycle **23**, which aromatizes by protonation at the terminal methylene group and subsequently loses a proton at the carbon atom *ortho* to the Os center to furnish aryne **20**.

The sole aromatic proton on the benzyne ring of **20** resonates at $\delta = 13.83$ ppm, a value very similar to those of the osmabenzenes.[9,23,38] In the ^{13}C NMR spectrum, the sp carbon atom resonates at $\delta = 306.6$ ppm. The remaining *ortho* carbon atom produces a signal at $\delta = 227.8$ ppm. The carbon atoms *meta* to the metal center produce signals at $\delta = 136.1$ and 113.0 ppm, and the *para* carbon atom resonates at $\delta =$ 188.6 ppm.

Initially, it may seem surprising that such a metallacycle might be stable; however, there are several factors that likely contribute to the stability of this species. The main reason for the instability of benzyne is the strain placed on the two sp carbon atoms by constricting the bond angles from 180° to 127°.[41,42] With 2-butyne as a model, calculations showed that going from linear **24** to constrained **25** leads to a 51.8 kcal mol^{-1} increase in energy. In a metallabenzyne, one of the sp-hybridized carbon atoms is replaced by a 14-electron transition-metal fragment. For this metal unit, the optimized Me-[Os]≡CMe angle in the acyclic fragment **26** ([Os] = $OsCl_2(PH_3)_2$) was calculated to be 93.8°. In the osmabenzyne model

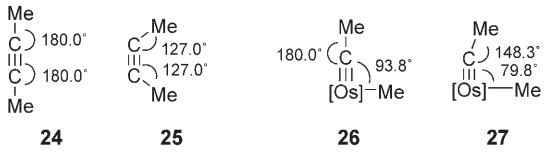

24 **25** **26** **27**

27 ([Os] = $OsCl_2(PH_3)_2$), this angle is constricted to 79.8°, and the optimal [Os]≡C-C_{Me} angle of 180° is constricted to 148.3°. The resulting increase in energy on going from **26** to **27** was only 9.6 kcal mol^{-1}.

Several additional osmabenzynes have been synthesized by derivatizing **20** (Scheme 8).[43] Reaction with two equivalents of aqueous HBF_4 first led to substitution of one chloride

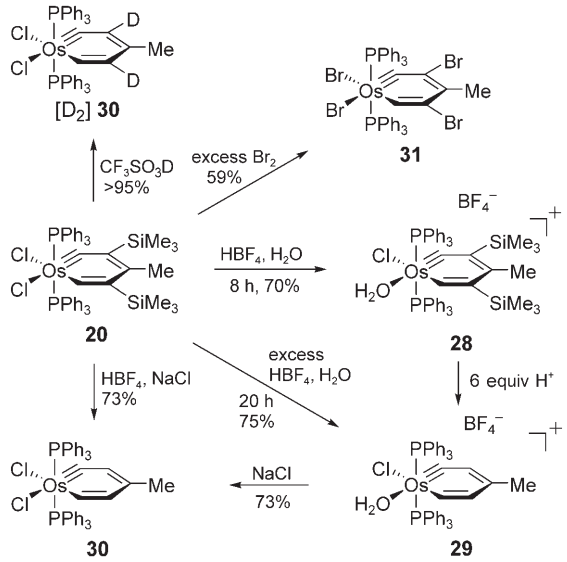

Scheme 8. Derivatization of osmabenzyne **20**.

ion with water to produce the osmabenzyne salt **28**. The mechanism probably involves loss of one of the chloride ligands followed by trapping of the resultant cation with water. Reaction of the salt with six equivalents of acid resulted in hydrolysis of the trimethylsilyl groups to give cationic complex **29**. When **20** was treated with acid and NaCl, or when NaCl was added to the hydrolyzed complex **29**, the neutral species **30** was produced. Reaction of either **20** or **30** with deuterated triflic acid resulted in quantitative, regiospecific deuteration of the β-carbon atoms. Similarly to normal silylarenes, treatment of **20** with Br_2 resulted in bromodesilylation to give tetrabromide **31**.[43]

Attempts to synthesize osmabenzynes directly from [$OsCl_2(PPh_3)_3$] and other terminal alkynes have not been successful.[44,45] The proposed intermediate metallacyclobutene **22** (Scheme 7) was not isolable; however, cycloaddition of vinylidene **32** with phenylacetylene produced the related compound **33** (Scheme 9).[46] Based on NMR and structural data, this compound is best described as an η^3-allenylcarbene complex with three contributing resonance forms.

Reaction of **33** with phenylacetylene resulted mainly in polymerization and/or produced a mixture of species. Only a

 © 2006 Wiley-VCH Verlag GmbH & Co. KGaA, Weinheim

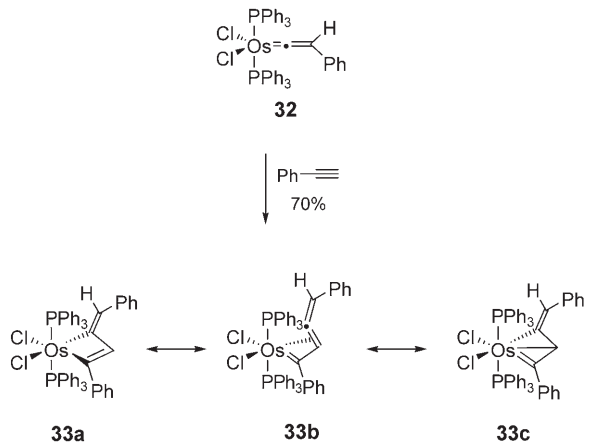

Scheme 9. Synthesis and contributing resonance structures of allenylcarbene complex **33**.

trace of osmabenzyne could be observed. Interestingly, when the reaction was carried out in the presence of NEt_3, osmabenzyne **34** was produced as the major product after a day, thus suggesting that an acetylide intermediate may be involved in the formation of the osmabenzyne. This hypothesis was tested by treating **33** with [(PPh_3)AuC≡CPh] in the presence of $HNEt_3Cl$, which quickly proceeded to form osmabenzyne **34**. Exposure of **33** to three other gold acetylides under analogous conditions produced metallabenzynes **35**–**37** (Scheme 10).[46]

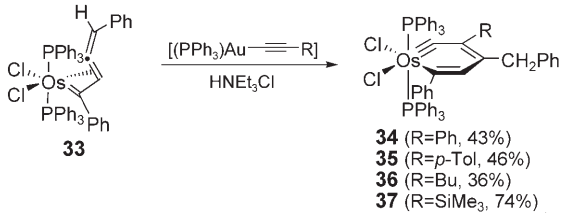

Scheme 10. Synthesis of a series of osmabenzynes.

The mechanism for formation of these complexes is still not completely known.[46] Reaction of **33** with [(PPh_3)AuC≡CR] may initially produce the osmium–acetylide complexes [$OsCl(C{\equiv}CR)(=CPh\text{-}\eta^2\text{-}CH{=}C{=}CHPh)(PPh_3)_2$]. Alternatively, the gold acetylide may coordinate to the osmium–allenylcarbene complexes. The β-carbon atom of the acetylide attacks the γ-carbon atom of the allenyl carbene in the cyclization reaction. It is unclear if the cyclization reaction takes place before or after protonation of the terminal CHPh group. This newer work calls into question the mechanism outlined in Scheme 7; however, direct comparison may not be valid, as phenylacetylene and trimethylsilylacetylene can often exhibit different modes of reactivity with metal complexes.

3.3. Isoosmabenzene

The tautomer of benzene 1,2,4-cyclohexatriene (isobenzene) is a highly reactive, short-lived species proposed as a key intermediate in Diels–Alder reactions of enynes.[47] Interestingly though, like the metallabenzynes, isometallabenzenes have proven to be isolable compounds. Reaction of **38** with phenylacetylene and $HBF_4{\cdot}OEt_2$ produces the alkenyl–alkynyl–carbyne complex **39** (Scheme 11), which

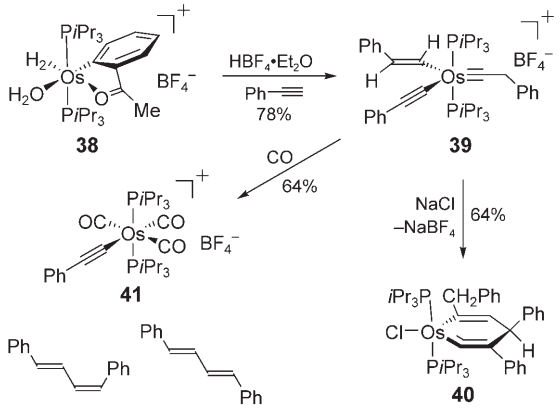

Scheme 11. Synthesis of isoosmabenzene **40**.

decomposes in solution at temperatures above −30 °C. In the presence of excess NaCl, the decomposition process is controlled and produces isoosmabenzene **40** in 64 % yield.[48]

The mechanism involved in producing **40** probably starts with migration of the α-alkenyl carbon atom to the α-carbyne carbon atom. Next, the β-alkynyl carbon atom couples with the β-alkenyl carbon atom. In the presence of CO instead of Cl^-, it was found that the carbyne is destabilized so that (*E*,*Z*)- and (*E*,*E*)-1,4-diphenyl-1,3-butadiene and the alkynyl–tricarbonyl osmium complex **41** are isolated.

3.4. Osmabenzofuran

Consistent with the mechanism calculated by Martin, van der Boom, and co-workers,[33] Elliott and Roper have found that the reaction of diphenylacetylene with [$Os(CS)(CO)(PPh_3)_3$] produces the alkyne-substituted complex **42** and an osmacyclohexadienethione.[49] Unlike in the case calculated for acetylene, a second equivalent of diphenylacetylene does not add to generate the osmabenzene. Reaction of **42** with methyl propiolate, an activated acetylene, does indeed afford a metallacycle.[50] Interestingly, an osmabenzene did not result from insertion of the thiocarbonyl into the ring, but instead a second equivalent of methyl propiolate inserted to create the bicyclic species **43** (Scheme 12; the numbering scheme is used in Table 1). This molecule is best described as an osmabenzofuran in which the Os center is shared by both rings. Reaction of **43** with ethanolic HCl results in transesterification of the free ester functionality to afford **44** while leaving the metal-bound ester unchanged. Reaction of **43** with pyridinium tribromide results in bromination at C6 to give

 © 2006 Wiley-VCH Verlag GmbH & Co. KGaA, Weinheim

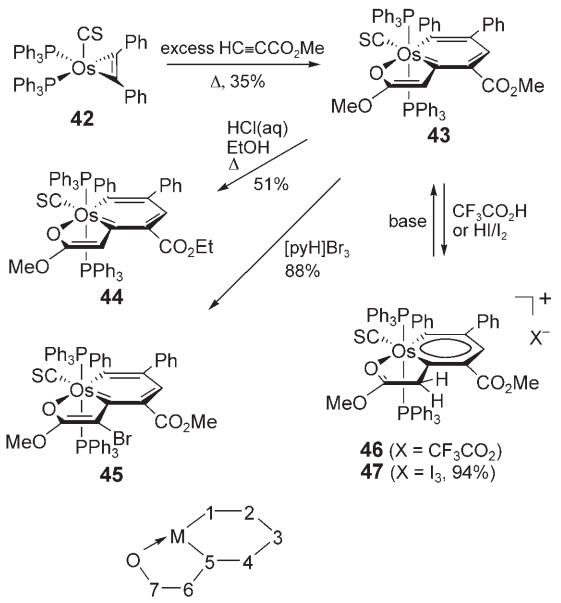

Scheme 12. Synthesis of osmabenzofurans **43–45** and osmabenzenes **46–47**.

45. Finally, C6 can also be protonated with either trifluoroacetic acid or HI/I_2 to generate complexes **46** and **47**, respectively. While the triiodide salt **47** could be isolated, attempts to isolate **46** only resulted in regeneration of **43**. The reversible nature of this reaction at C6 is strikingly similar to recent iridabenzene chemistry reported by Chin et al. (see Section 5.2).[51,52]

Three resonance structures account for the overall bonding picture in these complexes. Structures **43a** and **43b** (Scheme 13) account for the aromatic character of these

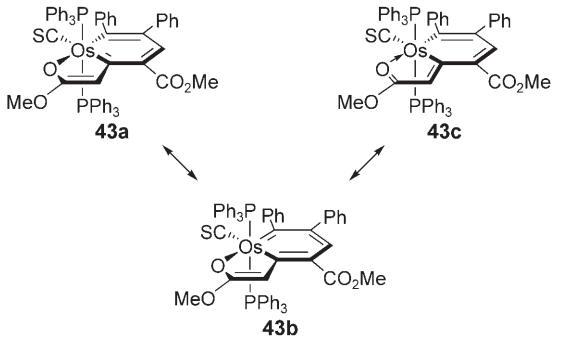

Scheme 13. Contributing resonance structures of **43**.

molecules, while structure **43c** contains an osmacyclohexadiene system.[50] The crystal structures of compounds **43–45** show, unlike in other metallabenzenes, that there is some apparent bond alternation (Table 1). The C1–C2, C3–C4, and C5–C6 bonds are all shorter than the C2–C3 and C4–C5 bonds. This bond alternation suggests that the dominant contributing resonance structure may be **43c**; however, the C5–C6 and the C6–C7 bonds are similar enough in length to suggest that resonance forms **43a** and **43b** also contribute

Table 1: Bond lengths for osmabenzofurans **43–45**, osmabenzene **47**, and structurally related Ru (**48**) and Fe (**49**) complexes.

	43	**44**	**45**	**47**	**48**	**49**
M	Os	Os	Os	Os	Ru	Fe
M-C1	2.068	2.068	2.055	1.996	2.003	1.908
M-C5	2.142	2.162	2.135	2.103	2.107	1.994
M-O	2.218	2.232	2.234	2.221	2.26	2.073
C1-C2	1.367	1.406	1.389	1.45	1.367	1.364
C2-C3	1.442	1.45	1.433	1.374	1.448	1.43
C3-C4	1.359	1.38	1.368	1.438	1.34	1.366
C4-C5	1.436	1.466	1.438	1.375	1.477	1.467
C5-C6	1.371	1.375	1.363	1.507	1.369	1.363
C6-C7	1.416	1.424	1.438	1.495	1.442	1.421
C7-O	1.333	1.264	1.244	1.226	1.239	1.242

significantly. In all of these complexes, the *trans* influence of the thiocarbonyl ligand lengthens the Os–C5 bond.

The X-ray structure for cationic complex **47** reveals deviations from the trends in the neutral series. In this structure, C1–C2, C3–C4, and C5–C6 have bond lengths that are larger than the C2–C3 and C4–C5 bond lengths (Table 1). Additionally, the Os–C5 bond is slightly shortened. This combination of structural features suggests that **47** has significantly more delocalization than **43–45**. Consistent with this observation is the downfield shift of the ^1H NMR resonance signal of the *ortho* proton upon acidification with HI/I_2 or CF_3CO_2H (from $\delta = 6.99$ ppm for **43** to $\delta = 8.36$ ppm for **46**).

Similar Ru (**48**) and Fe (**49**) complexes have been reported previously but were not initially recognized as

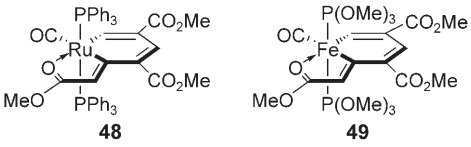

metallabenzofurans.[53–56] These molecules are structurally quite similar to **43–45**. It is interesting to note that the authors did not report these complexes as aromatic, though they do have some characteristics suggesting that delocalization is present. Nonetheless, bond alternation is more pronounced in **48** and **49** (Table 1) and thus these may be borderline cases of metalla-aromatic compounds.

4. Ruthenium

While osmium has been shown to be involved in a number of thermally stable metalla-aromatic compounds, the same cannot be said about chemically similar ruthenium. Most of the ruthenabenzenes that have been synthesized are either short-lived at room temperature or can be isolated only if coordinated to a transition-metal center to which some of the electron density can be donated.[18,31] This stability trend between the 4d and 5d metallabenzenes is generally true, in

 © 2006 Wiley-VCH Verlag GmbH & Co. KGaA, Weinheim

that the 4d metals do not usually produce isolable metallabenzenes while the 5d metals do.

4.1. Coordinated Ruthenabenzenes

One recent example of a metal-coordinated ruthenabenzene was reported by Bruce et al.[57] The authors found that when the Ru cluster **50** was mixed with two equivalents of HC≡CFc in CH_2Cl_2 (Scheme 14), complex **51** was formed in 10% yield, as identified by X-ray crystallography. The Ru–C(sp^2) bond lengths in the metallacycle are 2.083 and 2.054 Å, and the C–C bond lengths within the ring range from 1.407 to 1.437 Å. The C-Ru-C angle is 88.4°, and the remaining ring angles lie between 120.8 and 128.4°. Despite the structural similarities to previous metallabenzenes, the two protons *meta* to the metal resonate as a singlet at 5.31 ppm in the ^{1}H NMR spectrum. Similar upfield shifts for metal-coordinated arenes are commonly observed.[9,34] The mechanism for formation of ruthenabenzene **51** probably involves double insertion of HC≡CFc into the Ru–C bonds of the complex and subsequent loss of water.

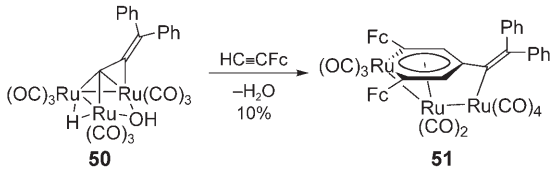

Scheme 14. Synthesis of ruthenium-coordinated ruthenabenzene **51**. Fc = ferrocenyl.

Jia obtained the triple-decker ruthenabenzene **52** by treating [Cp*Ru(H_2O)(nbd)]BF_4 (**53**; nbd = norbornadiene) with sodium formate to produce first the binuclear Ru cluster **54** (Scheme 15). This cluster was then treated with HBF_4, and the resultant solution was allowed to stand for several days at room temperature to give ruthenabenzene **52**.[58] The initial complex **54** is probably produced by C–C bond cleavage of the norbornadiene ligand and subsequent elimination to produce the bridging vinylcyclopentadiene ligand. Protonation of **54** leads to the intermediate complex **55**, which rearranges to form the triple-decker ruthenabenzene **52**, as well as ruthenacene **56** and the triple-decker complex **57**. While the details of these rearrangements are not well understood, it is interesting since it must involve C–C bond activation under mild conditions.

X-ray diffraction revealed that the six-membered ruthenacycle of **52** is η^6-bonded to the lower Ru center but only η^5-bonded to the upper Ru center. The bridging hydride ligand allows the Ru center of the ring to maintain its 18-electron count. The C–C bonds of the metallacycle range between 1.358 and 1.463 Å with no significant bond alternation while

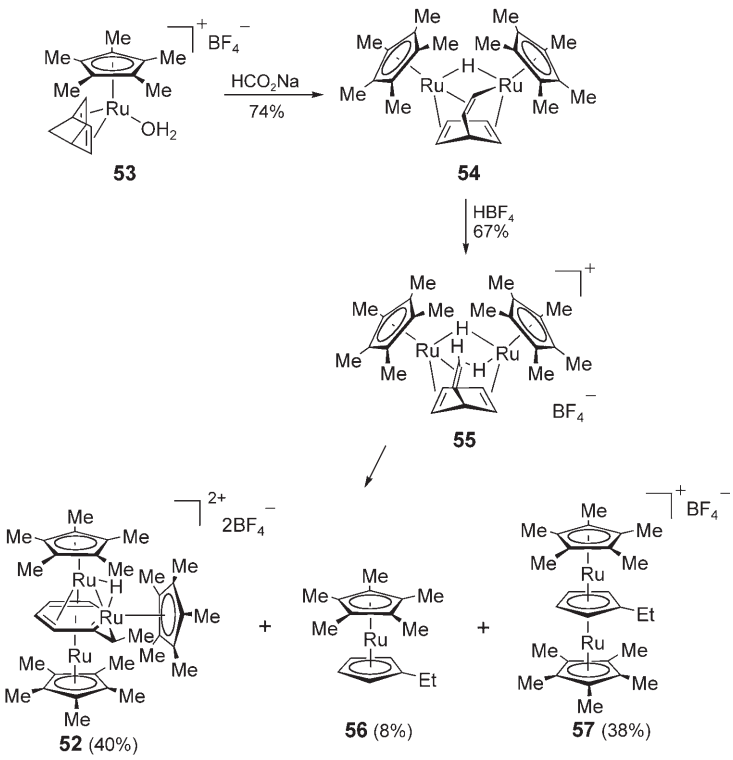

Scheme 15. Synthesis of triple-decker ruthenabenzene **52**.

the Ru-C(sp^2) bond lengths are 2.043 and 2.055 Å. The C(sp^2)-Ru-C(sp^2) angle is 82.2°, and the remaining ring angles range between 120.4 and 132.9°. As in the previously described coordinated ruthenabenzene **51**, the ^{1}H NMR spectrum of **52**, with signals ranging from $\delta = 5.26$ to 8.20 ppm, exhibits signals shifted upfield from those of other metallabenzenes.

Other examples of metal-coordinated ruthenabenzenes are the homoleptic Ru sandwich complexes **58** and **59** reported by Salzer, Kaupp, and co-workers (Scheme 16).[59] These complexes were produced by treating pentadienyl sandwich complexes with two equivalents of [$Ru_3(CO)_{12}$]. Interestingly, reaction with only one equivalent of [$Ru_3(CO)_{12}$] afforded pentadienyl ruthenabenzene complex **60** in very low yield. Complex **58** produced signals at $\delta =$ 6.23 ppm (*para*) and $\delta = 5.62$ ppm (*ortho*) in the ^{1}H NMR spectrum. The related complex **59** produced a signal at $\delta =$ 5.39 ppm for the protons *ortho* to the metal center. In both **58** and **59**, the most stable conformation is fully eclipsed with the ring plane tilted 18.2° (**58**) toward one another at the side of the metals, such that the ring plane is defined by the four *ortho* and *meta* carbon atoms. The Ru atoms in the metallacycles of **58** are bent slightly away from each other by 14.3° and 16.3° with Ru–Ru distances (3.38 Å) between the rings that are smaller than the sum of the van der Waals radii. These structural features indicate that there is more than a superficial relationship between them. Reaction of **58** with HBF_4 produced unstable complex **61**, which revealed a ^{1}H NMR resonance ($\delta = -16.89$ ppm) typical for a metal hydride.

 © 2006 Wiley-VCH Verlag GmbH & Co. KGaA, Weinheim

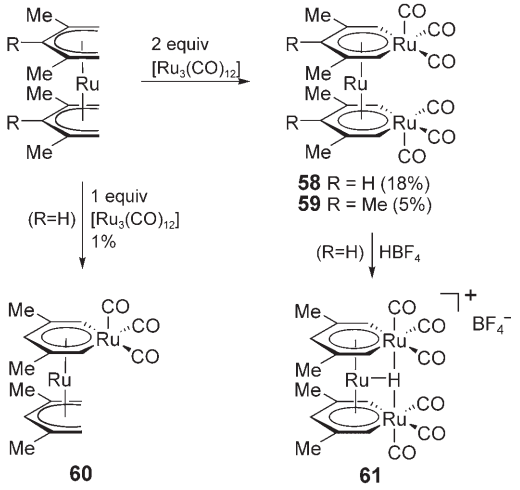

Scheme 16. Synthesis of ruthenabenzene complexes **58**–**61**.

4.2. Ruthenabenzenes Revisited

Early work by Hughes and Robinson suggested that ruthenium would be a good candidate for producing metallabenzenes from vinylcyclopropene derivatives.[60] The Dartmouth group demonstrated that mixing 3-vinylcyclopropenes with either [Cp*RuCl(cod)] or [{Cp*Ru(μ^3-Cl)}$_4$] produced ruthenacenes such as **62** (Scheme 17) which are potential

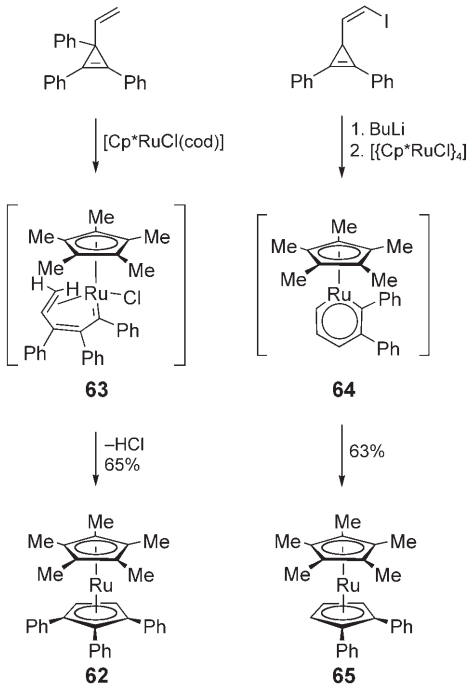

Scheme 17. Reactions of vinylcyclopropenes with ruthenium complexes. cod = cyclooctadiene; Cp* = C_5Me_5.

decomposition products of ruthenabenzenes. It was presumed that these complexes were formed by loss of HCl from the intermediate olefin complexes such as **63** and subsequent carbene insertion to produce the new cyclopentadienyl ligands. Our group has recently generated a similar result via a lithiated vinylcyclopropene.[61] Based on related chemistry from our lab (see below), ruthenabenzene **64** is presumed as an unstable intermediate which undergoes facile carbene insertion to give **65**.

Given the instability of **5** and the elusiveness of **64**, it would seem that synthetic efforts to prepare an isolable metallabenzene of a 4d metal which is not coordinated to another metal fragment would be futile. Very recently, Jia, Xia, and co-workers proved this theory wrong by isolating the first stable ruthenabenzene by a method analogous to the synthesis of **12**. Treatment of [$RuCl_2(PPh_3)_3$] with 1,4-pentadiyn-3-ol, PPh_3, and Bu_4NCl afforded cationic ruthenabenzene **66** in 55% yield (Scheme 18).[62] This complex can

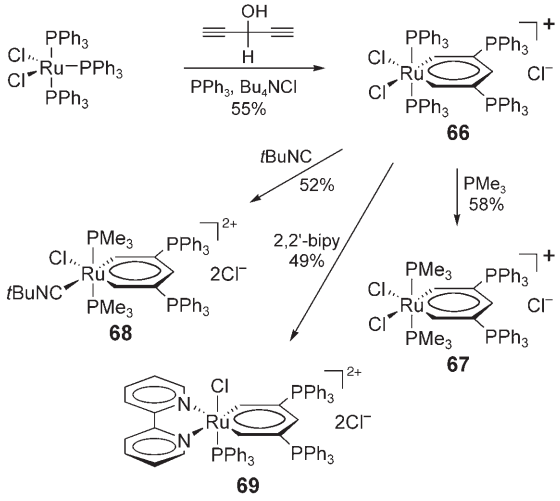

Scheme 18. Synthesis and derivatization of stable ruthenabenzene **66**. 2,2′-bipy = 2,2′-bipyridine.

also be produced directly from $RuCl_3 \cdot 3H_2O$, PPh_3, and 1,4-pentadiyn-3-ol in 20% yield. Metallacycle **66** is stable in air at temperatures up to 100 °C. The authors attribute this unusual stability to the bulky phosphine substituents and/or ligands.

Complex **66** has similar spectral characteristics to other metallabenzenes. The *ortho* proton resonates in the ^{1}H NMR spectrum at $\delta = 17.5$ ppm, which is reasonably expected for a Ru carbene. The *para* proton appears in the aromatic region at $\delta = 8.2$ ppm. The carbon atoms *ortho*, *meta*, and *para* to the metal center resonate at $\delta = 284.3$, 108.3, and 146.0 ppm, respectively, in the ^{13}C NMR spectrum. Confirmation of this structure was provided by X-ray diffraction, which showed that **66** is basically planar with only small deviations (0.043 Å) from the root-mean-square plane defined by the six-membered metallacycle. The electrons in the ruthenacycle are fully delocalized with the C–C bond lengths ranging from 1.378 to 1.395 Å, thus showing no significant bond alternation.

Derivatization of **66** afforded three additional ruthenabenzene complexes (Scheme 18). Reaction with PMe_3 resulted in substitution of the metal-bound phosphines to produce **67**. The ligand sphere could also be modified by reaction of **66** with *t*BuNC, resulting in **68** in which one

 © 2006 Wiley-VCH Verlag GmbH & Co. KGaA, Weinheim

chlorine ion is exchanged for the isonitrile. Complex **69** could be produced by reaction of **66** with 2,2′-bipyridine. The structural and spectroscopic properties of **67** and **68** are analogous to those of **66**; however, the solid-state structure of **69** reveals that the Ru atom is situated outside of the plane of the ring (defined by the five carbon atoms) by 0.672 Å. Nonetheless, **69** retains its aromaticity, as the *para* proton resonates at $\delta = 8.2$ ppm and the C–C and Ru–C bond lengths indicate delocalization.

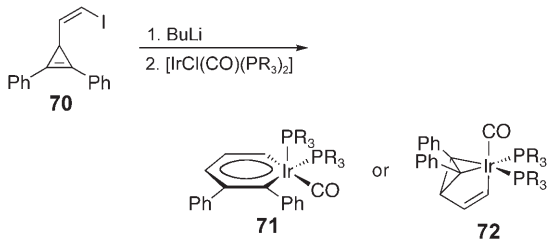

Scheme 19. Iridabenzene synthesis from a nucleophilic 3-vinylcyclopropene.

5. Iridium

One of the earliest metallabenzenes to be isolated and characterized was iridabenzene **4**, which Bleeke et al. synthesized by the reaction of 2,4-dimethylpentadienide with $[IrCl(PEt_3)_3]$.[17,29] A number of iridabenzene derivatives could be prepared from **4**; for example, reactions with phosphines that are more electron-rich usually resulted in substitution of one or more PEt_3 ligand, depending on the sterics of the ligand. Carbon monoxide could substitute one ligand at room temperature, while at reflux a second equivalent would insert into the metallacycle to produce an iridium–phenoxide complex. Reaction with bromine or iodine resulted in oxidation of the Ir center rather than electrophilic aromatic substitution.[9,29]

A key step in the synthesis of **4** is deprotonation of an intermediate iridacyclohexadiene.[17,29] This deprotonation was not found to occur when using $[IrCl(PMe_3)_3]$ as the metal source.[63] As a result, synthesis of an iridabenzene was only feasible from $[IrCl(PEt_3)_3]$, such that all additional metallacycle examples must be derived from **4**.

5.1. Iridabenzenes from Nucleophilic 3-Vinylcyclopropenes

Recently, our group reported the direct synthesis of a series of iridabenzenes from nucleophilic 3-vinylcyclopropenes.[64–68] In this case, several different ligands and metal complexes were used to produce a variety of structurally related iridabenzenes. This method of synthesis, which was inspired by the aforementioned studies from Hughes and co-workers, is derived from the well-known reactivity of cyclopropenes to form vinyl carbenes.[69] For a bond-fixed "Kekulé" structure of a metallabenzene, the ring can be seen as a vinyl carbene that is tethered to the metal center by a vinyl σ bond. Retrosynthetic analysis suggested that a (*Z*)-3-(2-iodoethenyl)cyclopropene such as **70** would be a good synthon for iridabenzenes like **71** (Scheme 19). Lithium–halogen exchange of vinyl iodide **70** and subsequent addition of Vaska's complex resulted in the isolation of iridabenzene **71a** (R = Ph).[64] When less bulky phosphines were used, the σ-vinyl/η^2-cyclopropene complex **72** (for example, R = Me) was isolated. This "iridabenzvalene", a valence isomer of **71**, then could be converted into the corresponding iridabenzene in nearly quantitative yield either by heating in solution or by treatment with Ag^I salts.[65]

Varying the phosphine ligand gave insight into the factors determining which isomer would be isolated (Table 2).[67]

Table 2: Product ratios for the synthesis of iridabenzenes **71** with various phosphines.

Cmpd	Phosphine	∢ [°][a]		Yield [%]		
			71:72[b]	**71**	**72**	**72→71**
71a	PPh_3	145	100:0	66	–	–
71b	PMe_3	118	0:100	–	54	97
71c	PMe_2Ph	122	2:98	58	–	–
71d	PEt_3	132	0:100	–	51	95
71e	$PMePh_2$	136	30:70	56	–	–
71f	$PiBu_3$	143	35:65	49	–	–
71g	$P(p\text{-}MeOC_6H_4)_3$	145	100:0	61	–	–

[a] Cone angle, reference [70]. [b] Initial product ratio, determined by ^1H NMR spectroscopy.

Phosphines with smaller cone angles[70] tended to afford more of the iridabenzvalene product. Comparison of PMe_3 and $PiBu_3$ shows that the smaller PMe_3 ligand forms 100% iridabenzvalene, while the larger $PiBu_3$ forms only 65%. Additionally, ligands possessing electron-rich groups resulted in an initial product ratio favoring the iridabenzvalene. For example, while PPh_3 led to exclusive formation of the iridabenzene, $PiBu_3$ led to an initial product ratio of about 2:1 iridabenzvalene to iridiabenzene. Since the cone angles on these two ligands are 145 and 143°, respectively, it is likely that electronic effects are primarily responsible for this difference. Steric effects, which seem to be secondary in this study, do eventually come into play as a solution of the $PiBu_3$ product mixture in C_6D_6 does convert to all iridabenzene over eight hours at room temperature, while a solution of the PMe_3 iridabenzvalene in C_6D_6 is stable indefinitely at room temperature.

There are two potential mechanisms for the formation of iridabenzene **71** from iridabenzvalene **72** (Scheme 20).[33,67,68] One pathway begins by dissociation of the cyclopropene from the metal center and subsequent oxidative addition to generate Dewar benzene **74**, which quickly rearranges into **71**. Evidence for this pathway lies in the ability of donor solvents to rapidly increase the rate of isomerization. Similar types of reactivity with cyclopropenes have been reported by Hughes and co-workers.[71,72] In these cases the intermediate metallacyclobutenes were isolated from the reaction of perfluorinated cyclopropenes with transition-metal complexes. Additionally, a metal-assisted mechanism has been proposed for the opening of 3,3-diphenylcyclopropenes, as based on the isolation of an iridium-coordinated iridacyclobutene.[73]

 © 2006 Wiley-VCH Verlag GmbH & Co. KGaA, Weinheim

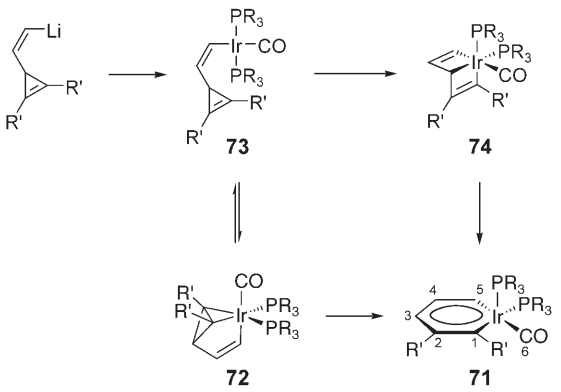

Scheme 20. Proposed mechanisms for formation of iridabenzenes and valence isomers from a nucleophilic 3-vinylcyclopropene (R′ = Ph). For the purpose of calculations, R = R′ = H. The numbering scheme is used in Table 3.

Recent DFT calculations reported by van der Boom, Martin, and co-workers, however, suggest that the more feasible pathway is through direct rearrangement of the iridabenzvalene by twisting of the iridacyclopropane ring into the planar metallacycle.[33] For the purpose of these calculations, an Ir complex **73** for which R = R′ = H was used. Under these circumstances, two isomers of **73** were distinguishable by the orientation of the cyclopropene ring. The *syn* isomer, in which the cyclopropene ring is oriented towards the Ir center, gave a calculated energy of 1.8 kcal mol^{-1} higher than the *anti* isomer. When this lower-energy σ complex is defined as having an energy of zero, the transition state to iridabenzvalene **72** carries an energy of only 3.5 kcal mol^{-1}. The iridabenzvalene itself lies in an energy well at −23.1 kcal mol^{-1}. From the iridabenzvalene, a barrier of 39.5 kcal mol^{-1} was found in forming the iridabenzene **71** directly. While no transition state was found for the formation of Dewar benzene **74**, its energy was calculated to be 38.3 kcal mol^{-1} above the iridabenzvalene, thus suggesting that the Dewar benzene model would be considerably higher in energy.

None of the experimental evidence so far indicates definitively either the Dewar benzene or the direct-insertion pathway. While the calculations are generally reliable, they may not take into account any associative mechanism(s) in which the solvent may play a role. Since the calculations were only able to approximate solvation effects by using the polarized continuum model, no direct interactions such as solvent coordination or a metal-assisted mechanism would be predicted. It is also possible that no one of these mechanisms operates to the exclusion of the others.

In addition to isolating iridabenzenes with different phosphine ligands, we have successfully synthesized a number of iridabenzenes with different ring substituents from unsymmetrically substituted cyclopropene precursors.[66,68] As in the previous work, iridabenzvalenes such as **75** and **79** are formed in addition to iridabenzenes depending not on the phosphine, but on the nature of the R group. In certain cases, isomerization to the iridabenzene was found to be highly regioselective, forming the *ortho*-phenyl isomer **76** over the *meta*-phenyl isomer **77**. In addition to the iridacycles, cyclopentadienyl complexes such as **78** and **81** were also isolated. As in previous examples, these complexes are thought to come from migratory carbene insertion of the corresponding iridacycle.

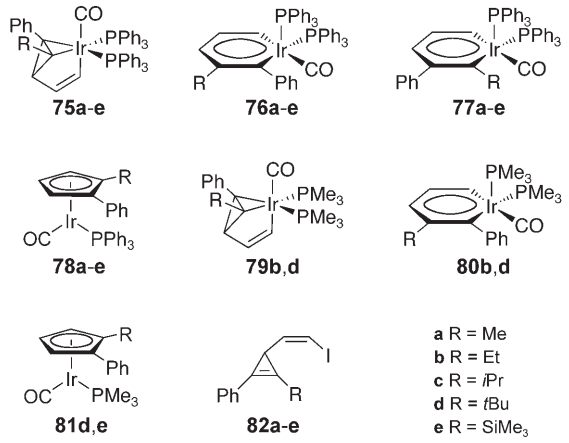

The series derived from 1-alkyl-2-phenylcyclopropenes **82a–d** proved to be the best "behaved" of the various systems explored, with **82d** allowing easy access for complete study of the iridabenzene manifold.[68] Reaction of lithiated **82d** with Vaska's complex furnished iridabenzvalene **75d** (Scheme 21).

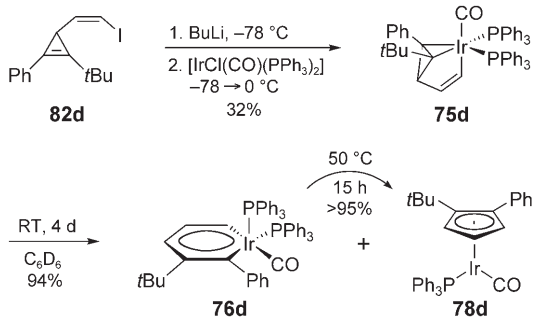

Scheme 21. Synthesis of *t*Bu/Ph-substituted iridacycles.

Although stable in the solid state, solutions of **75d** in C_6D_6 at 20 °C immediately began to isomerize, which after four days afforded a 3:1 mixture of iridabenzene **76d** and cyclopentadienyl complex **78d** in 94 % combined yield. The regiochemistry of **76d** was confirmed by X-ray analysis to be the *meta*-*t*Bu isomer, and none of the corresponding *ortho*-*t*Bu regioisomer **77d** was detected. Unlike **71a–g**, **76d** proved to be extremely labile as it converted quantitatively into **78d** in C_6D_6 solution at 50 °C. The kinetics of the rearrangement were shown to be first-order with respect to **76d**.

Initially, it was presumed that the *ortho*-*t*Bu regioisomer **77d** had quickly rearranged and thus was the source of **78d**. To test this theory, kinetic studies on the isomerization of **75d** and **76d** to the cyclopentadienyl complex **78d** were performed. The data showed that at 20 °C the rate of isomerization of **76d** to **78d** was faster than the corresponding rate of isomerization of **75d** to **78d**. This was taken to mean that the

 © 2006 Wiley-VCH Verlag GmbH & Co. KGaA, Weinheim

cyclopentadienyl complex **78d** originated by the rearrangement of the *meta*-*t*Bu isomer **76d** and not from *ortho*-*t*Bu isomer **77d**. It therefore appears that the valence isomerization of unsymmetrical iridabenzvalene **75d** to iridabenzene **76d** is highly regioselective.

Reactions of Vaska's complex with cyclopropenes **82a–c** showed the influence of alkyl substituent on both the formation of **75** and its transformation to **76**. ^{1}H NMR spectroscopy showed that each crude reaction mixture was composed of the corresponding iridabenzvalene and iridabenzene. Iridabenzvalenes **75a–c** were not isolated from the reaction mixture because of their relatively rapid isomerization to **76a–c**, which were isolated in about 25–30% yield. After eight hours and 30 hours at 20°C in C_6D_6 solution, **75a**,**b** and **75c**, respectively, had isomerized completely to **76a–c**, and very minor amounts of the *ortho*-alkyl regioisomer **77a–c** were detected by NMR spectroscopy of the crude reaction mixtures. Unlike **76d**, solutions of **76a–c** were stable for over 48 hours at 75°C.

In contrast, reaction of vinylcyclopropenes **82b,d** with the less bulky and more electron-rich complex [IrCl(CO)-$(PMe_3)_2$] yielded the corresponding iridabenzvalenes **79b,d** as the only products, which were stable at 20°C. Isomerization at 75°C converted **79b** completely into the *meta*-Et regioisomer **80b** over four hours. Under the same conditions, however, the *t*Bu analogue **79d** gave a mixture composed of unreacted iridabenzvalene, iridabenzene **80d**, and cyclopentadienyl complex **81d** in a ratio of 5:10:1, as well as partial decomposition. Prolonged heating of this mixture led to complete decomposition to unidentified materials. Interestingly, evidence for formation of the *ortho*-alkyl regioisomer of **80** was never observed; thus, the lower steric hindrance of PMe_3 than PPh_3 does not decrease the regioselectivity of the isomerization. The influence of the Et and *t*Bu substituents on the stability and isomerization rate of **79** is similar to that observed for the corresponding PPh_3 analogues **75**. Additionally, the greater stability of *meta*-*t*Bu substituted **80d** compared to the corresponding PPh_3 analogue **76d** indicates that the PMe_3 ligand does stabilize the iridabenzene. Regarding the whole "alkyl" series, the trend of the isomerization rate of alkyl-substituted iridabenzvalenes to iridabenzenes is **75a** = **75b** > **75c** > **75d** > **79b** > **79d**, which is in agreement with the increase in both electronic-donating ability and steric hindrance of the alkyl group as well as with increased electronic-donating ability and/or reduced steric hindrance of the phosphine ligand. On the other hand, iridabenzene stability is ordered as **80b** > **76a** = **76b** = **76c** > **80d** > **76d**, indicating that a decrease in steric hindrance of the alkyl group as well as a decrease in electronic-donating ability and/or sterics of the phosphine ligand enhance the stability of the iridabenzene.

Replacement of the alkyl group with a trimethylsilyl unit, as in **82e**, furnished interesting but more perplexing results. In this case, the reaction of the lithiated vinylcyclopropene with Vaska's complex furnished a 47% yield of a mixture of **75e**, **77e**, and **78e** in a 10:2:3 ratio (Scheme 22). Iridabenzvalene **75e** and cyclopentadienyl **78e** were isolated cleanly by treatment of the purified mixture with MeI or by heat, respectively; unfortunately, pure iridabenzene **77e** could not be isolated. In contrast to **75a–d**, the Ph/$SiMe_3$-substituted

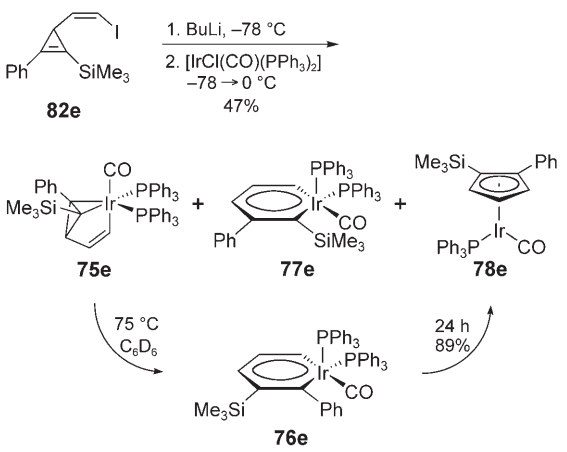

Scheme 22. Synthesis of Ph/$SiMe_3$-substituted complexes **75e–78e**.

iridabenzvalene **75e** is stable at room temperature. Heating a solution of pure **75e** to 75°C, however, did not lead to isomerization of **77e** as expected, but instead afforded the *meta*-silyl regioisomer **76e** (confirmed by ^{1}H,^{29}Si gHMQC NMR experiments). While **76e** is more stable than the *ortho*-silyl isomer **77e**, it also undergoes carbene migratory insertion to give complex **78e**. It is reasonable to suspect that the *ortho*-silyl isomer **77e** is also an intermediate in the isomerization of **75e** to **78e**; however, **77e** was not detected by ^{1}H NMR during the isomerization of **75e**.

These results suggest that regioisomers **76** and **77** are formed by different mechanisms. One possible pathway is that the initial σ-vinyl complex **83** forms an intermediate such as **84** (Scheme 23, R = $SiMe_3$). This intermediate is plausible for R = $SiMe_3$ since the carbocation would be stabilized by both the α-Ph and the β-$SiMe_3$ moieties. Subsequent cleavage of the three-membered ring could then lead to the selective formation of iridabenzene **77e**. Possibly a result of steric congestion by the bulky trimethylsilyl group, **77e** easily undergoes carbene migratory insertion and subsequent dissociation of PPh_3 to give cyclopentadienyl complex **78e**. The lower stability to **84** which results from the corresponding alkyl groups essentially shuts down this pathway and thus leads to detection of **77a–c** only by NMR. Instead, the major pathway consists of concerted opening of **75** to yield **76**. Nonetheless, the exact origin of this preferential pathway to furnish regioisomer **76** is still uncertain and is subject to further interpretation and debate.

One additional system studied by our group is derived from the bis(trimethylsilyl)cyclopropene **85**. By employment of the usual synthetic method with Vaska's complex, **86** could be isolated in 40% yield (Scheme 24).[74] Compound **86** has proven to be one of the most stable iridabenzvalenes isolated to date, requiring prolonged heating at 75°C to isomerize/rearrange to cyclopentadienyl complex **87** in essentially quantitative yield. Unfortunately, iridabenzene **88** has not been detected in this process, though its intermediacy is presumed based on the related studies. Incorporation of two trimethylsilyl groups seems to have two effects: the σ-

 © 2006 Wiley-VCH Verlag GmbH & Co. KGaA, Weinheim

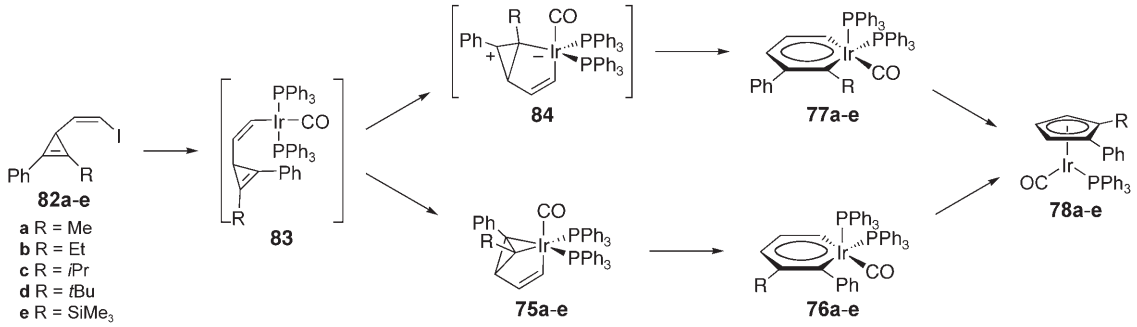

Scheme 23. Proposed mechanism for isomerization/rearrangement to **78**.

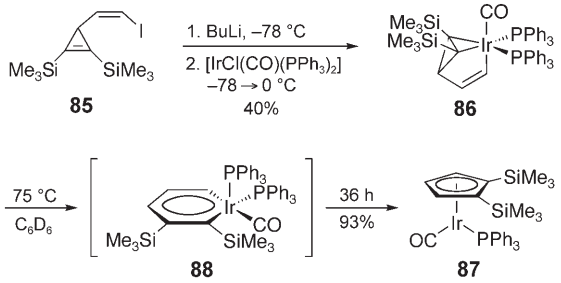

Scheme 24. Synthesis of bis(trimethylsilyl) complexes **86** and **87**.

donating ability of the Si atoms appears to stabilize the formation of iridabenzvalene, yet the π-accepting nature of the Si atoms destabilizes the corresponding iridabenzenes. Ongoing computational efforts tend to support this hypothesis.[75]

5.1.1. *Spectroscopic Properties*

The synthesis of a family of structurally related iridabenzenes has allowed for detailed comparison of their spectroscopic properties. All the iridabenzenes are easily identified by the NMR resonance of the proton *ortho* to the metal, which varies between $\delta = 10.41$ ppm for **71a** and $\delta = 11.30$ ppm for **71d** (Table 3).[67] The downfield shift of these characteristic resonances is attributed to the anisotropy of the neighboring metal. This effect quickly dissipates for the protons *meta* and *para* to the metal center ($\delta = 7.38$–7.90 ppm and $\delta = 7.69$–8.78 ppm, respectively). These latter two resonances are more in line with aromatic ring currents in electron-withdrawn systems such as pyridine. Interestingly, in C_6D_6 the *meta* and *para* protons are 0.1–0.5 ppm downfield compared to the same protons in CD_2Cl_2, but the analogous comparison of the *ortho* proton shows that it generally resonates 0.1–0.2 ppm upfield in C_6D_6.

The ^{13}C NMR spectra demonstrate similar anisotropy trends (Table 3). Carbon atoms neighboring the Ir center resonate between $\delta = 174$ and 190 ppm with the resonance of the phenyl-substituted carbon atom C1 appearing generally downfield from unsubstituted C5. The remaining carbons resonate in the standard aromatic region. While the resonating frequency of the carbon atom *meta* to the metal center remains relatively unaffected by changes to the ligand sphere of **71** ($\Delta\delta < 1.4$ ppm), carbon atoms C5 (*ortho*) and C3 (*para*)

Table 3: Selected NMR data for iridabenzenes **71**, **76**, and **80**.[a]

Compound	Phosphine	Substituent	$\delta(^1H)$ [ppm]			$\delta(^{13}C)$ [ppm]						$\delta(^{31}P)$ [ppm]
		R	H3	H4	H5	C1	C2	C3	C4	C5	C6	
71a[b]	PPh_3	Ph	7.99	7.69	10.41	187.60	141.93	139.99	127.76	187.43	201.09	16.44
71a[c]	PPh_3	Ph	8.44	7.79	10.79	187.74	142.83	141.16	127.64	187.49	203.26	17.88
71b[b]	PMe_3	Ph	7.75	7.49	11.10	189.25	140.49	135.53	128.65	176.58	189.44	−40.54
71b[c]	PMe_3	Ph	8.25	7.91	11.00	189.95	141.49	136.74	129.06	176.04	189.44	−40.27
71c[b]	PMe_2Ph	Ph	7.82	7.53	11.05	188.56	140.53	136.49	128.85	179.68	190.77	−26.90
71d[b]	PEt_3	Ph	7.69	7.40	11.30	189.87	140.53	135.67	128.07	176.45	192.36	−2.08
71e[b]	$PMePh_2$	Ph	7.98	7.66	10.93	187.36	141.47	137.61	128.37	181.93	197.14	−5.20
71f[b]	$PiBu_3$	Ph	7.71	7.51	10.89	190.54	141.45	136.14	128.01	177.28	194.09	−0.29
71g[b]	$P(p\text{-}MeOC_6H_4)_3$	Ph	7.96	7.38	10.43	188.51	141.70	138.92	128.50	187.11	198.18	13.01
76a[c]	PPh_3	Me	8.30	7.75	10.62	187.46	140.47	133.93	129.07	183.92	204.97	18.03
76b[c]	PPh_3	Et	8.29	7.79	10.61	187.31	140.84	139.99	129.48	184.95	204.17	18.65
76c[c]	PPh_3	*i*Pr	8.41	7.86	10.60	187.65	145.52	—[d]	129.85	185.52	203.90	18.79
76d[c]	PPh_3	*t*Bu	8.69	7.83	10.54	186.68	145.61	138.89	129.63	186.55	208.32	18.24
76e[c]	PPh_3	$SiMe_3$	8.78	—[d]	10.85	188.00	141.37	137.15	128.95	188.93	—[e]	17.13
80b[c]	PMe_3	Et	8.13	7.90	10.92	188.83	138.55	135.38	129.70	174.20	181.02	−38.56
80d[c]	PMe_3	*t*Bu	8.46	7.88	10.87	—[e]	—[e]	—[e]	—[e]	—[e]	—[e]	−38.79

[a] Atom labeling as shown in Scheme 20. [b] In CD_2Cl_2. [c] In C_6D_6. [d] Resonance obscured by other signals. [e] Resonance not assigned.

 © 2006 Wiley-VCH Verlag GmbH & Co. KGaA, Weinheim

vary considerably. Replacement of an alkyl group with a phenyl group on the phosphine results in a deshielding of the *para* carbon atom C3 ($\Delta\delta = 4.5$ ppm) and the *ortho* carbon atom C5 ($\Delta\delta = 11$ ppm). The resonance of the carbonyl group varies in a similar way (C6: $\Delta\delta = 11.5$ ppm). The substituted carbon atom C1 does not show this dependence on the ligand sphere ($\Delta\delta = -1.4$ ppm) and actually shifts in the opposite direction. For the "alkyl" series **76**/**80**, replacement of PPh_3 with PMe_3 on the Ir center leads to an upfield shift of the resonances for C3 ($\Delta\delta = -5.5$ ppm), C5 ($\Delta\delta = -10.8$ ppm), and C6 ($\Delta\delta = -23.2$ ppm), which can be rationalized in terms of electronic influences. The stronger donating ability of PMe_3 compared to PPh_3 results in a more electron-rich metal center, which in turn increases the electron density of the iridabenzene ring and thus results in the upfield carbon shifts. On the other hand, these effects are much smaller for C1 ($\Delta\delta = -1.5$ ppm), C2 ($\Delta\delta = -1.4$ ppm), and C4 ($\Delta\delta = -0.2$ ppm).

The ^{31}P NMR spectra reveal sharp singlets for the phosphines, even when samples were cooled to −80 °C, thus demonstrating that the axial and basal phosphines exchange rapidly in solution by the well-known Berry pseudorotation process. ^{31}P-^{13}C coupling is observed for the substituted carbon atom C1 but not for the unsubstituted C5. This observation demonstrates that while the ligand sphere in solution is dynamic, the smaller CO ligand spends a disproportionate amount of time near substituted C1, probably as a result of steric crowding. Analogous behavior was demonstrated previously by Bleeke et al. through careful correlation of ^{31}P-^{1}H coupling constants in a similar system.[17]

The ^{1}H NMR signals of the other species observed in these studies offer a quick and easy diagnostic handle. For the iridabenzvalenes, the bridgehead cyclopropyl proton appears as a characteristic broad singlet in the range of $\delta = 3.2$–3.8 ppm. Two complex multiplets in the ranges $\delta = 6.0$–6.8 ppm and $\delta = 6.7$–7.2 ppm (the latter was sometimes obscured by additional peaks from Ph groups) correspond to the alkene resonances H4 and H5, respectively. For cyclopentadienyl complexes, sharp signals for the three ring hydrogens appear around $\delta = 4.2$–5.4 ppm. The unreacted lithiated vinylcyclopropene that is protonated in the reaction work up has a characteristic signal (ddd) that appears at about $\delta = 6.0$–6.2 ppm. Thus, by ^{1}H NMR analysis, it is relatively easy to ascertain what products are present in the crude reaction mixtures.

5.1.2. *Solid-State Structures*

X-ray diffraction studies of five iridabenzenes synthesized in our group illustrate some key structural features of metallabenzenes. The molecular structure of **76b** is shown in Figure 1. Comparison of the bond lengths and bond angles of **71a,d** and **76a**,**b**,**d** is given in Table 4. The metallacycles possess a distorted coordination geometry that can be classified as somewhere between square pyramidal and trigonal bipyramidal. The C–C bond lengths in the central ring (1.334–1.427 Å) are essentially equal and thus can be regarded as evidence of delocalization of the π-electrons. The mean C–C bond lengths are very close and range from 1.383 to 1.392 Å. The Ir–C1 and Ir–C5 bond lengths (average: 2.02 Å) are intermediate between typical Ir–C single- and double-bond lengths. The metallacycles are basically planar (sum of bond angles: 719.1–720.0°) with the Ir center tilted out of the five-carbon backbone from 1.2° (**76a**) up to 6.4° (**71d**). The X-ray analyses verify that the alkyl groups of **76a**,**b**,**d** are at the *meta* position to the Ir center, thus in agreement with the spectroscopic assignments. Contrary to our expectations based on reactivity, the bulky *t*Bu group does not induce greater torsion strain in the iridabenzene ring of **76d**, at least not in the solid state.

The solid-state structures of the iridabenzvalenes are also of considerable interest. The molecular structure of **75d** is shown in Figure 2, and selected bond lengths and bond angles

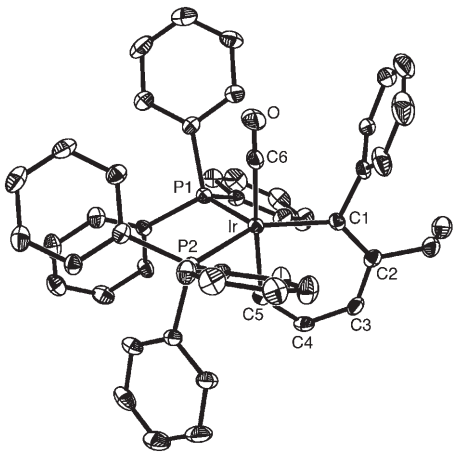

Figure 1. Molecular structure of iridabenzene **76b**. The thermal ellipsoids are set at 25% probability.

Table 4: Selected bond lengths [Å] and bond angles [°] from X-ray structural analyses of iridabenzenes.

	71a	**71d**	**76a**	**76b**	**76d**
Ir-C1	2.021	2.047	2.020	2.029	2.054
Ir-C5	2.025	2.004	2.012	2.023	2.000
C1-C2	1.409	1.427	1.423	1.413	1.407
C2-C3	1.410	1.372	1.335	1.390	1.382
C3-C4	1.377	1.386	1.382	1.393	1.427
C4-C5	1.334	1.381	1.408	1.360	1.343
∅(C-C)	1.383	1.392	1.387	1.389	1.390
Ir-C1-C2	128.8	127.1	129.1	130.0	130.8
C1-C2-C3	123.6	123.1	123.5	122.1	119.5
C2-C3-C4	124.2	127.9	125.9	126.2	128.2
C3-C4-C5	125.5	122.5	126.6	124.3	123.9
C4-C5-Ir	130.7	130.4	126.4	130.3	130.2
C1-Ir-C5	86.9	88.1	88.5	87.0	87.4
sum of angles	719.7	719.1	720.0	719.9	720.0
C5-Ir-C6	165.0	167.8	172.5	171.8	172.1
P1-Ir-P2	99.2	104.8	102.5	102.4	105.6
P1-Ir-C1	112.6	101.9	119.8	121.0	137.5
P2-Ir-C1	148.2	153.0	137.7	136.3	116.5
tilt angle[a]	3.7	6.4	1.7	1.2	1.4

[a] The angle between the C1-Ir-C5 plane and the C1-C2-C3-C4-C5 plane.

 © 2006 Wiley-VCH Verlag GmbH & Co. KGaA, Weinheim

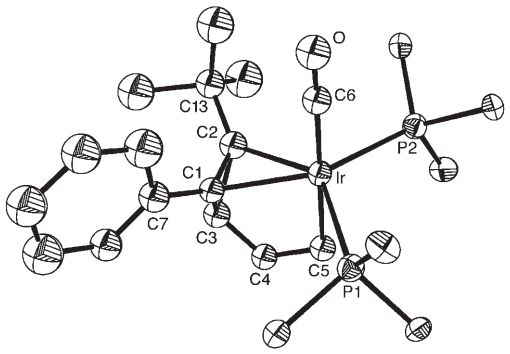

Figure 2. Molecular structure of iridabenzvalene **75d**. Thermal ellipsoids are set at 30% probability. Only the *ipso* carbon atoms of the PPh_3 ligands are shown.

of **72b**,**d**, **75d**, and **86** are given in Table 5. The iridabenzvalenes possess a torsion trigonal-bipyramidal coordination sphere composed of a carbonyl ligand, the cyclopropene double bond (bound in η^2 mode), two phosphine ligands, and

Table 5: Selected X-ray bond lengths [Å] and bond angles [°] for iridabenzvalenes.

	72b	72d	75d	86
Ir-P1	2.306	2.330	2.353	2.367
Ir-P2	2.318	2.326	2.353	2.381
Ir-C1	2.146	2.172	2.189	2.173
Ir-C2	2.143	2.159	2.220	2.189
Ir-C5	2.095	2.092	2.184	2.074
C1-C2	1.447	1.440	1.405	1.446
C1-C3	1.529	1.519	1.555	1.539
C2-C3	1.526	1.533	1.566	1.543
C3-C4	1.466	1.481	1.401	1.457
C4-C5	1.322	1.328	1.375	1.330
C1-Ir-C2	39.4	38.8	37.1	38.7
C5-Ir-C6	178.9	176.5	174.0	172.6
P1-Ir-P2	104.1	109.4	110.4	106.5
P1-Ir-C1	109.4	106.5	100.5	105.0
P2-Ir-C2	105.9	104.0	109.8	109.2
dihedral angle[a]	110.4	109.9	108.8	108.4
dihedral angle[b]	116.3	116.2	120.2	129.6

[a] Angle between the C1-C2-C3 plane and the Ir-C1-C2 plane. [b] Angle between the C1-C2-C3 plane and the C7-C1-C2-C13 plane.

the σ-vinyl ligand around the Ir atom. The Ir–C1 and Ir–C2 bond lengths (2.143–2.220 Å) are typical of Ir–C single bonds. The C1–C2 bond lengths (1.405–1.447 Å) are characteristic of transition-metal–olefin complexes that have significant back-bonding contribution from the metal center, that is, metallacyclopropanes. The longer Ir–C bond lengths, the shorter C1–C2 bond length, and the smaller C1-Ir-C2 bond angle in **75d** all suggest that the η^2 interaction of the cyclopropene π bond with the Ir center is considerably weaker than in the analogous complexes listed in Table 5. This weaker bonding is corroborated by the fact that **75d** isomerizes at room temperature to **76d** whereas the other iridabenzvalenes are stable under similar conditions (see Section 5.1).

5.2. Iridabenzenes by [2+2+1] Cycloaddition

C–C bond-forming reactions of alkynes with transition-metal complexes is an area of considerable interest because of the synthetic utility in assembling highly conjugated organic products.[76] One common intermediate in such reactions is a metallacyclopentadiene. During recent investigations, Chin et al. found that reaction of $[Ir(CO)(NCMe)(PPh_3)_2]^+$ with two equivalents of acetylene and subsequent addition of an equivalent of a terminal arylacetylene, produced alkynyl iridacyclopentadienes such as **89** (Scheme 25).[77] Upon acidification with HBF_4, **89** rearranged cleanly into iridacyclohexadiene **90**, the product of a formal [2+2+1] alkyne cyclization. Treatment of **90** with Lewis bases such as CO and MeCN caused the aryl group to rotate outward to a position *trans* to the Ir center to afford **91** and **92**, respectively. Although zwitterionic iridabenzene resonance structures such as **90′** and **91′** were invoked to help explain these types of rearrangements, metalla-aromatic species were not observed.[76]

More recently though, Chin and Lee found that if MeCN is present during acidification of **90** with HBF_4, cationic iridabenzene **93** is then isolated.[51] ^{1}H NMR analysis of **93** is consistent with the classification of this compound as an iridabenzene. The proton *ortho* to the Ir center in **93** (Ar = Ph) resonates at $\delta = 13.99$ ppm, considerably downfield from where the corresponding proton resonates in **90** (R = H, $\delta =$ 6.64 ppm). On going from **90** (R = Me) to **93** (Ar = *p*-Tol), a similar trend is observed for the protons *meta* to the Ir center: from $\delta = 5.79$ ppm and $\delta = 5.55$ ppm to $\delta = 6.88$ ppm and $\delta =$ 7.3–7.6 ppm (with overlapping signals from PPh_3), respectively.

Unique to **93** is its ability to reversibly react with weak Lewis bases such as CO and Et_3N to form iridacyclohexadiene complexes **91** and **92**, respectively.[51] It is particularly unusual that MeCN (ordinarily a more labile ligand) would replace the carbonyl ligand on conversion of **91** back into **93**. The facile interconversion of cyclohexadienes **91** and **92** and iridabenzene **93** supports the presumed intermediacy of iridabenzenes in the original studies.[76] This reactivity could be a result of the amphiprotic benzylic carbon atom connected to the carbon atom *ortho* to the Ir center. Resonance structures **90′** and **91′** could at least partly explain this behavior. While the ^{1}H NMR data of the iridacyclohexadienes suggest that **91′** is not a dominant resonance structure, it may increase the lability of the CO ligand by reducing the ability of the Ir center to backbond efficiently. Additional evidence for the amphiprotic nature of the benzylic carbon atom is found on treatment of **90** with HCl, which protonates this carbon atom and cleanly produces iridabenzene **94**.[51] This unusual reactivity parallels that observed in the previously mentioned osmabenzofuran studies (see Section 3.4).[50]

The addition of an arylacetylene to (η^2-acetato)iridacycle **95** produced an unexpected difference in the key intermediate that nonetheless led to iridabenzene synthesis.[52] Unlike **89**, the alkynyl(buta-1,3-dien-1-yl)iridium complex **96** was isolated in this experiment (Scheme 26). Addition of triflic acid to a $CHCl_3$ solution of **96** furnished cationic iridabenzene **97**,

 © 2006 Wiley-VCH Verlag GmbH & Co. KGaA, Weinheim

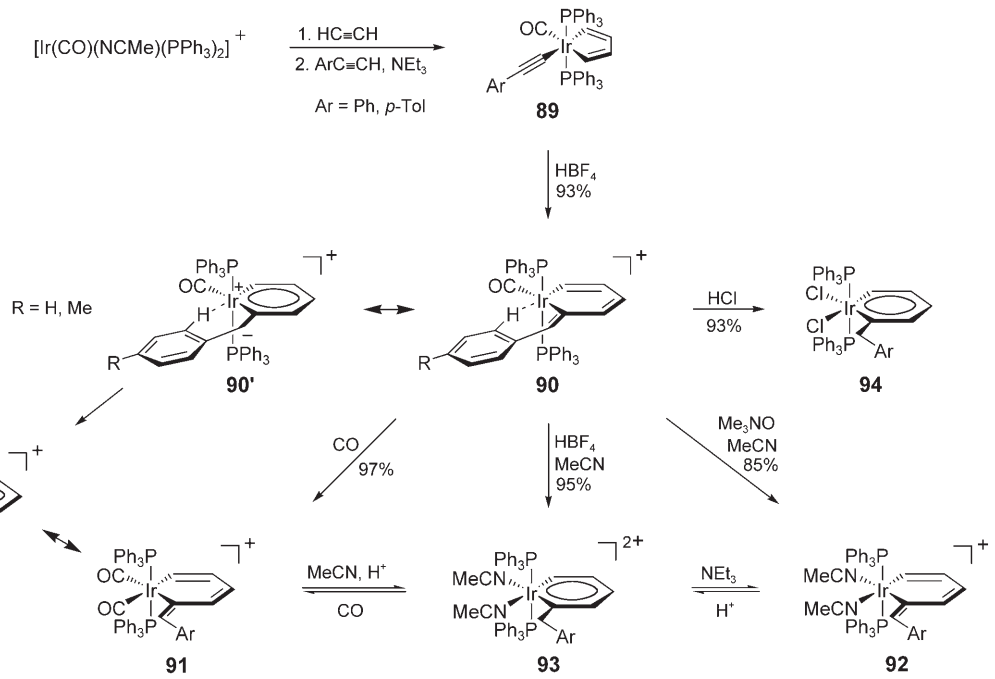

Scheme 25. Formation of iridabenzenes by [2+2+1] cycloaddition.

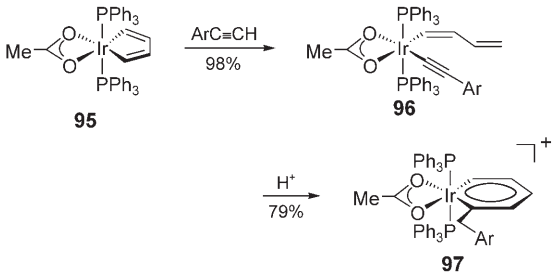

Scheme 26. Formation of iridabenzene **97**. Ar = Ph, *p*-Tol.

which was characterized as its OTf^- salt by NMR and IR spectroscopy and by elemental analysis. Iridabenzene **97** could also be produced by displacement of both MeCN ligands in complex **93** when it was treated with NaOAc.[51,52]

The probable mechanism for the formation of **97** from **96** involves proton attack on the β-carbon atom of the alkynyl group in **96** to give a cationic alkylidene, which is then attacked at the α-carbon atom by the terminal diene. Tautomerization of the resulting iridacycle affords **97**. Deuterium-labeling studies corroborate this hypothesis. Reaction of **96** with D^+ produces iridabenzene [6-D]-**97** (here, C6 is the benzylic carbon). Similarly, reaction of **95** with deuterated acetylene and subsequently with D^+ produced [4,6-D_2]-**97**, thus confirming that it is the terminal carbon atom of the diene that attacks the α-carbon atom of the alkylidene complex. This chemistry is related to the known reactions of alkynyl complexes with H^+ which lead to C–C coupling with neighboring unsaturated ligands.[76,77]

Paneque, Poveda, and co-workers have recently reported an interesting variation of the [2+2+1] protocol by the coupling of an alkene and an iridacyclopentadiene.[78] Reaction of diene **98** with propene at 60 °C furnished iridabenzene **99** (Scheme 27). It is believed that **99** results from the coordination of the alkene and subsequent isomerization to the propylidene species **100**, in which the propylidene ligand undergoes carbene migratory insertion into the iridacyclopentadiene moiety. Subsequent α-hydride elimination from **101** produces iridabenzene **99**. Support for this mechanism is provided by the reaction of **99** with MeCN to yield a 6:1 kinetic mixture of **102** and **103**. These two products are explained by hydride migration back to the six-membered ring. Upon heating, **102** rearranges to the more thermodynamically favored isomer **103**, likely via **99**, which is similar to reactivity first observed by Hughes et al. in their studies of the reaction of 3-vinylcyclopropenes with Ir complexes.[79]

Replacement of **98** with the related diene complex **104** illustrates the subtleties of the system, as this analogous reaction affords iridabenzene **105**, which bears a Me group bound to the Ir center.[78] As before, the first step in the mechanism is alkene coordination; however, to explain the different outcome, a 1-methylethylidene unit must be favored over the linear propylidene in the previous example. Carbene migratory insertion would then be followed by the unusual α-methyl elimination to give iridabenzene **105**. Even more surprisingly, the reaction with MeCN completely reverses the process, such that loss of propene regenerates the original iridacyclopentadiene ring in **106**.

X-ray structure analyses of **99** and **105** reveal two interesting features. First, the molecules are decidedly nonplanar, with the Ir centers deviating 0.57 and 0.70 Å out of the plane defined by the five C atoms of each iridacycle. Second, the molecules both exhibit a surprising degree of bond alternation. In contrast to most metallabenzenes, the differences between the "single" and "double" bonds in the two

 © 2006 Wiley-VCH Verlag GmbH & Co. KGaA, Weinheim

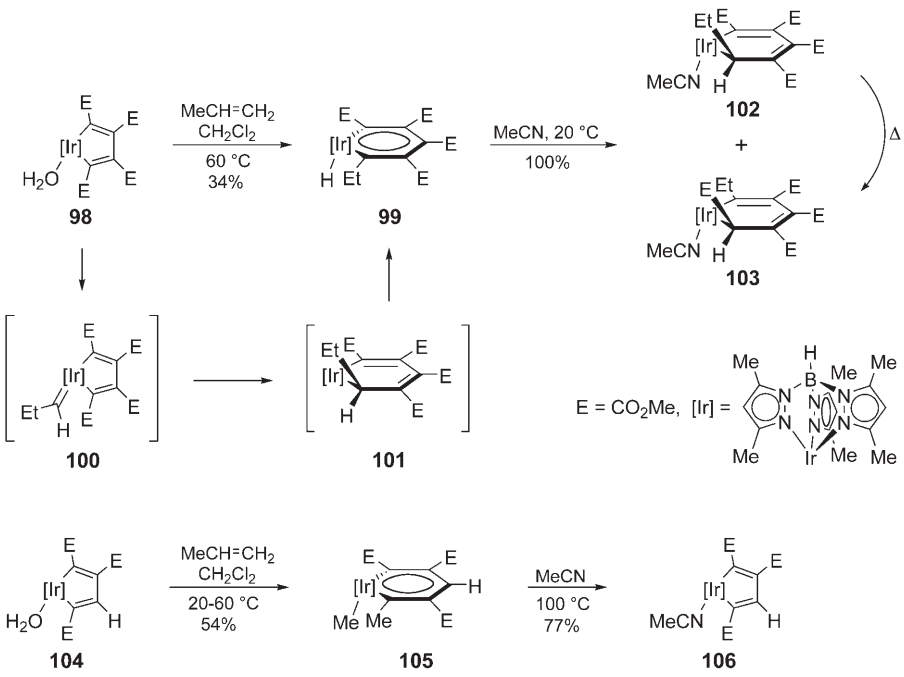

Scheme 27. Formation of iridabenzenes **99** and **105**.

structures are on the order of 0.040–0.057 and 0.21–0.36 Å for **99** and **105**, respectively. These features reflect the diminished aromaticity of these iridabenzenes and thus could explain in part the unusual reactivity noted above.

5.3. Iridanaphthalene

Although the existence of higher homologues of metallabenzenes had only been inferred from their decomposition products and the comparable reactivity of the metallabenzene analogues, one of the most exciting developments in recent years is the isolation and characterization of iridanaphthalene **107** by Paneque et al.[80] Synthesis of **107** begins by treating **108** with dimethyl acetylenedicarboxylate (DMAD), which yields isomeric iridacycloheptatrienes **109** and **110** (Scheme 28).[81] Even though no intermediates could be detected, these products are likely produced by initial insertion of one molecule of DMAD into one of the Ir–C_{aryl} bonds. C–H activation of the *ortho* proton in the resulting phenylalkenyl ligand and subsequent reductive elimination of benzene would lead to an iridacyclopentadiene complex. Insertion of a second equivalent of DMAD into either Ir–C bond and coordination of an adventitious water molecule would result in **109** or **110**. Oxidation of isomer **109** with *t*BuOOH produces the coordinated oxoacetyl product **111**. If excess *t*BuOOH is added, then iridanaphthalene **107** is produced.[80] Conversion of **111** into **107** likely starts as a simple Baeyer–Villiger oxidation of the oxoacetyl group. The newly generated O–$C_{aliphatic}$ bond in **112** can then be cleaved irreversibly to form **107**.

Structurally, the iridanaphthalene framework of **107** is similar to naphthalene in many respects. The bond lengths in the six-membered carbocycle are within 0.02 Å of those in naphthalene. The Ir atom is tilted somewhat out of the plane of the metallacycle carbon atoms by 0.76 Å. The two Ir–C bond lengths (1.930 and 1.981 Å) are intermediate between single- and double-bond lengths and are in good agreement with those in Ir^{III} metallabenzenes. Spectroscopically, the aromatic protons of **107** resonate between $\delta =$ 6.60 and 8.12 ppm and are increasingly deshielded the nearer they are to the metal center. While no protons are attached directly to the primary metallacycle, ^{13}C NMR spectroscopy demonstrates the typical anisotropic effects of the metal, as the outside C atom produces a signal at $\delta =$ 255.0 ppm, and the bridging C atom gives a signal at $\delta = 177.9$ ppm.

Column chromatography of **107** on silica gel results in the destruction of its aromaticity and affords **113**

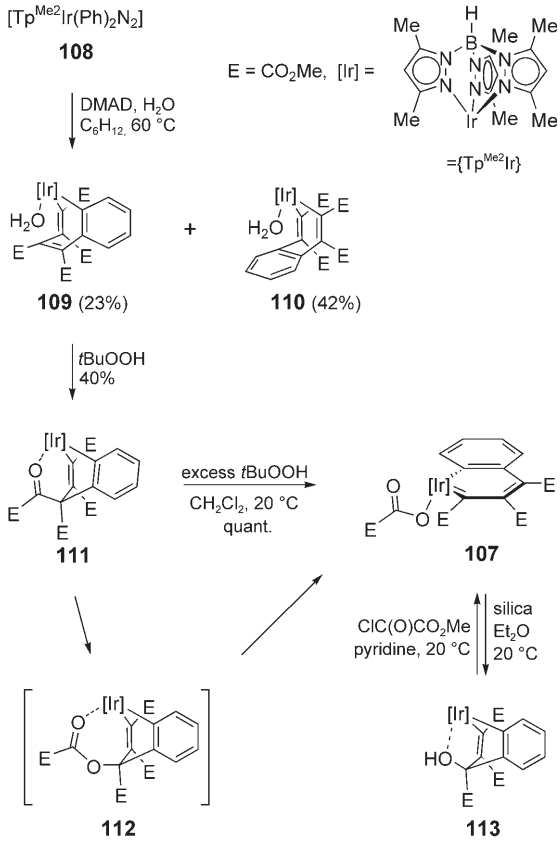

Scheme 28. Synthesis of iridanaphthalene **107**.

(Scheme 28),[80] thus reminiscent of an internal "neutral" Jackson–Meisenheimer complex.[82] Hydrolysis of the carboxylate ligand in **107** would result in an intermediate hydroxyl complex, which likely undergoes intramolecular nucleophilic

 © 2006 Wiley-VCH Verlag GmbH & Co. KGaA, Weinheim

attack at the γ-carbon atom to furnish **113**. Reaction of this new complex with $ClC(O)CO_2Me$ in the presence of pyridine regenerates the iridanaphthalene, thus proving the viability of the proposed final step in the initial formation of **107**.

Similar to the method used to generate iridanaphthalene **107**, treatment of **114** with excess *t*BuOOH produced iridabenzene **115** (Scheme 29).[80] When Thorn and Hoffman

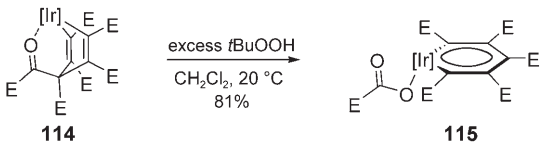

114 **115**

Scheme 29. Synthesis of iridabenzene **115**.

first predicted the stability of metallabenzenes, it was suggested that because of the low-lying LUMO of the $C_5R_5^-$ fragment, π donors, especially those *ortho* and *para* to the metal, would be most suited for stabilizing the metallabenzene.[11] Although a number of metallabenzenes have been synthesized with π donors *ortho* to the metal fragment,[23,31] iridanaphthalene **107** and iridabenzenes **99**, **105**, and **115** are the first examples of metalla-aromatic species substituted with electron-withdrawing groups, namely CO_2Me. Other examples of metallabenzenes bearing electron-withdrawing groups include the phosphonium-substituted osmabenzenes and ruthenabenzenes reported by Jia,[35,62] but these moieties are located on the less influential *meta* positions.

6. Rhodium

As with other 4d transition metals, uncoordinated rhodabenzenes are probably unstable, and no rhodabenzene has yet been reported. Reaction of lithiated cyclopropene **70** with the Rh analogue of Vaska's complex provided spectroscopic evidence of a rhodabenzene, but all attempts to isolate the material furnished either uncharacterizable decomposition products or very low yields of cyclopentadienyl complexes similar to **78**.[83] However, analogous reaction with $[RhCl(CO)(PMe_3)_2]$ resulted in the isolation of rhodabenzvalene **116** (Scheme 30).[84] Solutions of this complex decomposed at room temperature to an unidentified mixture of products, but at −30 °C are stable for several weeks.

X-ray data of a crystal of **116** which was kept at low temperature showed that, while most bond lengths and bonds angles were similar to those of **72b**, the main differences between the two structures were a consequence of the differing binding affinities for the cyclopropene π bond.

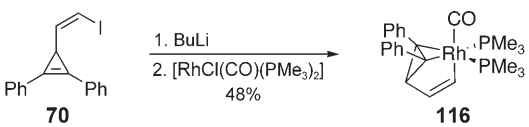

70 **116**

Scheme 30. Synthesis of rhodabenzvalene **116**.

Second-row metals are known to backbond less efficiently. This was reflected in a shorter C1–C2 bond length (1.414 in **116** vs. 1.447 Å in **72b**). The dihedral angle between the plane of the three-membered ring and the plane formed by the phenyl *ipso* carbon atoms and the cyclopropene double bond was greater (119.3° in **116** vs. 115.8° in **72b**). The weaker coordination also translated into a much larger P1-M-P2 angle, which was nearly 7° larger in **116**. Formation of the η^2-cyclopropene–rhodium moiety was unique, as oxidative addition to the strained σ bond had been the exclusive reactivity observed in previous studies of cyclopropenes with Rh complexes. Equally rare was the σ-vinyl Rh^I linkage as such complexes generally display poor thermal stability and require sterically demanding ligands for stabilization. Given these facts, successful preparation of **116** was attributed to the synergistic combination of intramolecular π bonding of the cyclopropene unit and σ-vinylic linkage to the Rh atom, both of which in turn inhibit decomposition of the other respective moiety.

In 1999, Hughes et al. reported the reaction of a 3-vinylcyclopropene with the $\{RhCl(PMe_3)_2\}$ fragment to furnish isomeric complexes **117** and **118**. In solution, a third

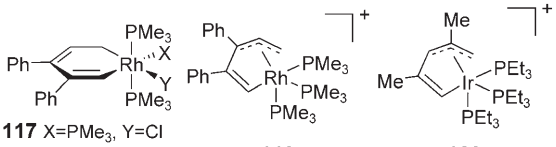

117 X=PMe_3, Y=Cl
118 X=Cl, Y=PMe_3 **119** **120**

compound, **119**, was detected.[85] There is a striking similarity between cation **119** and **120**,[29] the precursor to Bleeke's iridabenzene **4**, which suggested that deprotonation may lead to a rhodabenzene. Complex **119**, however, either decomposed or failed to react with several strong bases.

The inability to isolate a rhodabenzene is congruent with the DFT calculations reported by van der Boom, Martin, and co-workers.[22,33] According to their computations, after initial phosphine loss, the hypothetical rhodabenzene $[C_5H_5Rh(PH_3)_3]$ has a barrier of 20.5 kcal mol^{-1} for decomposition to the cyclopentadienyl complex, while the analogous decomposition of the corresponding iridabenzene gives a much higher barrier of 44.4 kcal mol^{-1}. For that reason it can be expected that, in the absence of stabilizing functionalities, rhodabenzenes are too reactive to be isolated.

7. Platinum

The most recent transition metal to be incorporated into stable metallabenzene complexes is platinum.[86,87] Using the same chemistry that was used to prepare iridabenzenes, we reported the synthesis of platinabenzene **121** by the addition of lithiated **70** to $[PtCl_2(cod)]$, albeit in only 7% yield (Scheme 31).[86] One particularly intriguing aspect of this reaction is that both the metallacycle and cyclopentadienyl moiety are derived from the starting 3-vinylcyclopropene.

 © 2006 Wiley-VCH Verlag GmbH & Co. KGaA, Weinheim

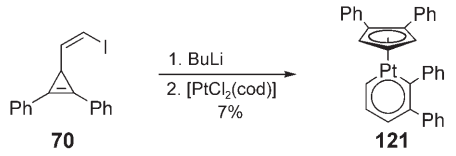

Scheme 31. Synthesis of the first platinabenzene **121**.

Based on related experiments (see below), it is possible that formation of the cyclopentadienyl ligand results from the decomposition of an intermediate platinabenzene before addition of the second equivalent of lithiated **70**. In addition to being the first platinabenzene, this example demonstrates the versatility of the 3-vinylcyclopropene approach to metallabenzenes, as this is the first method that has produced stable metallabenzenes for more than one transition metal, while Jia's 1,4-pentadiyn-3-ol cyclization route now represents a second such method (see Sections 3.1 and 4.2).

After this initial success, attempts were made to synthesize platinabenzenes by using an "asymmetric" $[L_2Pt(X)Y]$ complex in which only ligand X would be substituted for the vinylcyclopropene unit while Y would remain unchanged. In the following step, Y could then be cleaved from the σ-vinyl compound, thus allowing for coordination of the cyclopropene double bond. Depending on stability, either the resultant cationic platinabenzvalene or rearranged products like a cationic platinabenzene would be expected. Addition of lithiated **70** to $[Pt(Me)I(PEt_3)_2]$ resulted in displacement of the primary leaving group, I^-, and thus formation of σ-vinyl complex **122** (Scheme 32).[88] Given that Pt^{II} is found preferentially in a square-planar geometry, it is not surprising that the cyclopropene moiety does not coordinate to afford a platinabenzvalene. Protonolysis of **122** with HBF_4 opened a coordination site by removal of the secondary leaving group, Me^-. Similarly, substitution with chloride to give **123** and subsequent Cl^- abstraction with $TlPF_6$ generated the analogous reactive 14-electon Pt^{II} species. In both cases, only complex **124** was isolated. This complex is an interesting molecule itself, which in the solid state possesses a slipped Cp ring with η^3 coordination. Since platinabenzene intermediates were suspected, protonolysis was performed at −60 °C with trifluoroacetic acid to yield the *cis* complex **125**. While **125** was stable at low temperatures, warming to room temperature resulted in the production of a 3:2 mixture of **124**-O_2CCF_3 and the *trans* isomer of **125**. Even though monitoring the reaction by ^{1}H NMR spectroscopy provided no direct evidence for a platinabenzene, it is reasonable to assume the intermediacy of unstable cationic platinabenzenes such as **126**, which readily undergo carbene migratory insertion to give Cp complexes like **124**.

The results of the above two studies suggested that the next set of experiments should begin with a Cp unit already affixed to the Pt center. Reaction of [Cp*Pt(CO)Cl][89] with the lithiated vinylcyclopropene **70** resulted only in trace amounts of platinabenzene, recovered Pt starting complex, and the protonated vinylcyclopropene. A more labile leaving group was next examined, and thus, the new complex [Cp*Pt(CO)I] was synthesized from the known platinum dimer $[\{Cp^*Pt(CO)\}_2]$.[87,89] Reaction of lithiated **70** with [Cp*Pt(CO)I] afforded a mixture of σ complex **127a** and platinabenzene **128a** (Scheme 33). Solutions of pure **127a** in C_6D_6 rearrange over 2–3 days at room temperature to give quantitative conversion to **128a**. Presumably, **128a** is formed by metathesis of the iodide with the lithiated vinylcyclopropene and subsequent loss of CO with fast rearrangement to the platinabenzene. Unlike in the case with iridium, monitoring this process by ^{1}H NMR spectroscopy did not provide evidence for an intermediate platinabenzvalene. Extension of this chemistry has also led to phenyl(alkyl)platinabenzenes

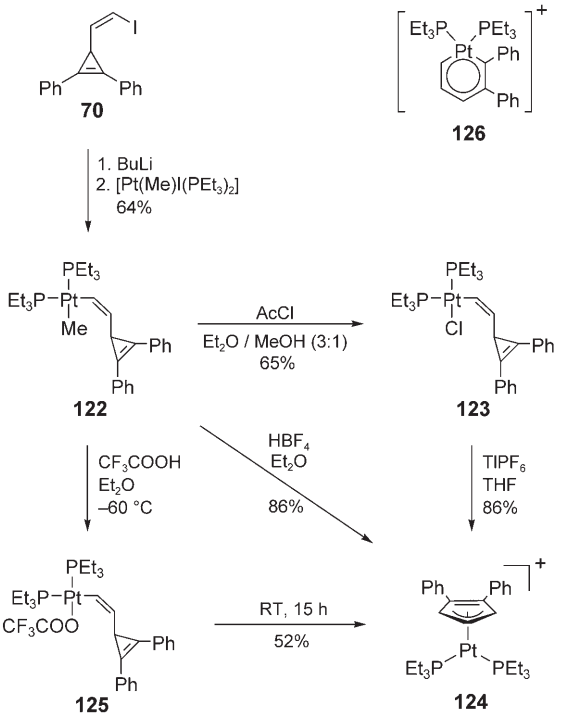

Scheme 32. Unsuccessful attempts at the synthesis of platinabenzenes.

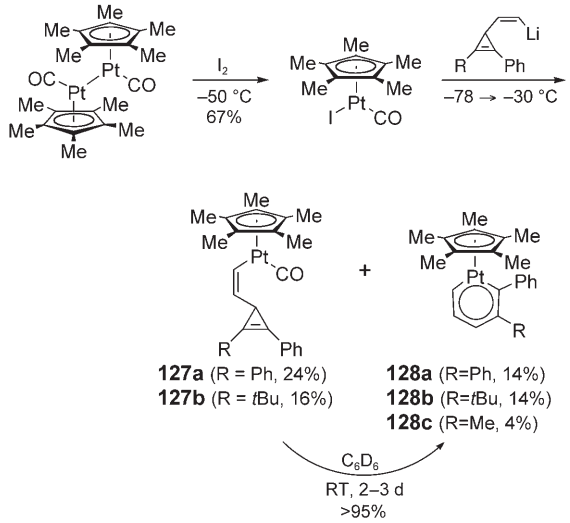

Scheme 33. Synthesis of platinabenzenes **128**.

 © 2006 Wiley-VCH Verlag GmbH & Co. KGaA, Weinheim

128b,c. Additional examples are currently under investigation along with general studies of platinabenzene reactivity.[61]

The NMR spectroscopic data for **121** and **128** are similar to those of other metallabenzenes. The proton *ortho* to the Pt atom produces a ^{195}Pt-coupled signal at $\delta = 12.76$ ppm for **121** and in the range $\delta = 11.83$–12.09 ppm for **128a–c**. The upfield shift for the latter complexes illustrates the greater contribution of electron density by Cp* to the metal center. The *meta* and *para* protons produce signals in the ranges $\delta =$ 7.4–7.6 and 8.2–8.5 ppm, respectively. Two ^{13}C NMR signals in the ranges $\delta = 200$–204 and 188–195 ppm are attributed to the phenyl-substituted and unsubstituted *ortho* carbon atoms, respectively.

The solid-state structures of the platinacycles are of considerable interest. The molecular structure of **128b** is shown in Figure 3, and selected bond lengths and angles for

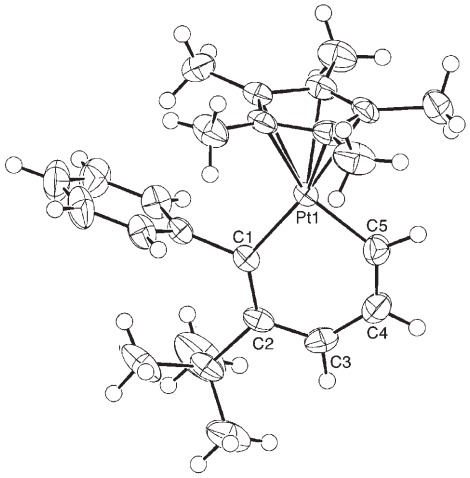

Figure 3. Molecular structure of platinabenzene **128b**. Thermal ellipsoids are set at 30% probability.

121 and **128a,b** are given in Table 6. Unlike most metallabenzenes, the platinabenzenes have planar structures (for **121**: deviation from mean plane 0.02 Å, sum of angles 720°).

Table 6: Selected X-ray bond lengths [Å] and bond angles [°] for platinabenzenes.

	121	128a	128b
Pt-C1	1.959	1.951	1.975
Pt-C5	1.929	1.937	1.926
C1-C2	1.387	1.401	1.406
C2-C3	1.392	1.395	1.389
C3-C4	1.381	1.364	1.387
C4-C5	1.364	1.387	1.350
∅(C-C)	1.382	1.387	1.383
Pt-C1-C2	129.2	129.2	129.8
C1-C2-C3	122.6	122.3	124.1
C2-C3-C4	124.8	125.2	126.9
C3-C4-C5	124.1	124.5	119.8
C4-C5-Pt	130.0	128.9	129.8
C1-Pt-C5	89.3	89.7	89.4
sum of angles	720.0	719.8	719.8

The Pt–C bond lengths are 1.926–1.937 and 1.951–1.975 Å, which compare well with Pt–C bond lengths in other Pt^{II} carbene complexes. The C–C bond lengths in the metallacycle have an average of 1.382–1.387 Å with no appreciable bond alternation. The Cp ring in each system is η^5-coordinated to the Pt center (Pt–C_{Cp} bond lengths: 2.257–2.342 Å).

Van der Boom, Martin, and co-workers also performed calculations on the stability of several platinabenzene complexes.[22,33] Based on their results, the cyclopentadienyl ligand does stabilize the platinabenzene by increasing the energy barrier for the occurrence of carbene migratory insertion. In the case of $[C_5H_5Pt(PH_3)_2]^+$, the computational analogue of **126**, the transition state to forming $[(\eta^5\text{-Cp})Pt(PH_3)_2]^+$ was only 24.0 kcal mol^{-1}, which corroborates the experimental results shown in Scheme 32. For the Cp complex $[C_5H_5PtCp]$, the computational analogue of **121**, the energy of the transition state for forming $[(\eta^3\text{-Cp})_2Pt]$ was considerably higher (45.9 kcal mol^{-1}). De Proft and Geerlings recently utilized the isomerization method to predict the aromatic stabilization energy of the platinabenzene ring in the model system $[Pt(C_5H_3Me_2)(\eta^3\text{-}C_5H_3Me_2)]$.[90] They obtained a calculated value of 23.4 kcal mol^{-1}, approximately two thirds of the aromatic stabilization energy calculated for benzene. Based on these computational results, it is not surprising that platinabenzenes such as **121** and **128** are stable even at elevated temperatures.

8. Conclusions

Aromaticity is a concept that many chemists take for granted as well-defined. In fact, like so many things in chemistry, the truth is multifaceted and thus considerably more complicated. Metallabenzenes and their higher analogues display a number of contradictory behaviors that place them in a delicate gray area between aromatic and nonaromatic. While their structures are in general planar and exhibit negligible bond alternation, they also undergo [4+2] cycloadditions as if they were simple metallacyclohexatrienes. The NMR spectroscopic properties suggest that the ring substituents are deshielded; however, this could simply be an effect of the transition metal. Unlike benzene, many metallabenzenes rearrange readily to form cyclopentadienyl complexes. Like benzene, they readily form η^6-metal complexes, through which the metallabenzenes are in fact clearly stabilized.

Over the last few years, the field of metalla-aromatics has expanded significantly. Several new methods to generate metallabenzenes have been developed. In addition to synthesis from nucleophilic 3-vinylcyclopropenes, they can be prepared from a number of alkyne precursors by generally unrelated mechanisms. For the first time, a metallanaphthalene has been isolated and characterized. Platinum has now been added to the list of transition metals capable of yielding a metallabenzene. At the current rate of progress, there is little doubt that the coming years will be equally exciting for metallabenzene chemistry.

 © 2006 Wiley-VCH Verlag GmbH & Co. KGaA, Weinheim

We would like to thank the University of Oregon graduate and undergraduate students and postdoctoral associates who made our work on metallabenzene chemistry possible. The National Science Foundation and the University of Oregon are gratefully acknowledged for support of this research. We also thank Profs. John Bleeke, Guochen Jia, Warren Roper, and James Wright, our colleagues in the field, for stimulating discussions and helpful advice, and for sharing results prior to publication.

Received: December 8, 2005

[1] M. K. Cyranski, T. M. Krygowski, A. R. Katritzky, P. von R. Schleyer, *J. Org. Chem.* **2002**, *67*, 1333 – 1338.
[2] J. A. N. F. Gomes, R. B. Mallion, *Chem. Rev.* **2001**, *101*, 1349 – 1383.
[3] a) P. J. Garratt, *Aromaticity*, Wiley, New York, **1986**; b) V. I. Minkin, M. N. Glukhovtsev, B. Ya. Simkin, *Aromaticity and Antiaromaticity*, Wiley, New York, **1994**; c) *Chem. Rev.* **2001**, *101*, 1115 – 1566 (special issue on aromaticity); d) *Chem. Rev.* **2005**, *105*, 3433 – 3947 (special issue on delocalization).
[4] a) L. Nyulaszi, *Chem. Rev.* **2001**, *101*, 1229 – 1246; b) Y.-Z. Huang, S.-Y. Yang, X.-Y. Li, *J. Organomet. Chem.* **2004**, *689*, 1050 – 1056.
[5] A. J. Ashe, *Acc. Chem. Res.* **1978**, *11*, 153 – 157.
[6] P. Jutzi, *Angew. Chem.* **1975**, *87*, 269 – 283; *Angew. Chem. Int. Ed. Engl.* **1975**, *14*, 232 – 245.
[7] A. J. Ashe, S. Al-Ahmad, J. W. Kampf, *Angew. Chem.* **1995**, *107*, 1479 – 1481; *Angew. Chem. Int. Ed. Engl.* **1995**, *34*, 1357 – 1359.
[8] a) A. Shinohara, N. Takeda, T. Sasamori, T. Matsumoto, N. Tokitoh, *Organometallics* **2005**, *24*, 6141 – 6146; b) Y. Mizuhata, T. Sasamori, N. Takeda, N. Tokitoh, *J. Am. Chem. Soc.* **2006**, *128*, 1050 – 1051.
[9] J. R. Bleeke, *Chem. Rev.* **2001**, *101*, 1205 – 1227.
[10] Recent minireviews: a) G. He, H. Xia, G. Jia, *Chin. Sci. Bull.* **2004**, *49*, 1543 – 1550; b) L. J. Wright, *J. Chem. Soc. Dalton Trans.* **2006**, 1821 – 1827.
[11] D. L. Thorn, R. Hoffmann, *Nouv. J. Chim.* **1979**, *3*, 39 – 45.
[12] R. H. Mitchell, *Chem. Rev.* **2001**, *101*, 1301 – 1315.
[13] a) P. von R. Schleyer, C. Maerker, A. Dransfeld, H. Jiao, N. J. R. van E. Hommes, *J. Am. Chem. Soc.* **1996**, *118*, 6317 – 6318; b) Z. Chen, C. S. Wannere, C. Corminboeuf, R. Puchta, P. von R. Schleyer, *Chem. Rev.* **2005**, *105*, 3842 – 3888.
[14] a) P. von R. Schleyer, B. Kiran, D. V. Simion, T. S. Sorensen, *J. Am. Chem. Soc.* **2000**, *122*, 510 – 513; b) H. Wadepohl, M. E. Castano, *Chem. Eur. J.* **2003**, *9*, 5266 – 5273.
[15] T. M. Krygowski, M. K. Cyranski, *Chem. Rev.* **2001**, *101*, 1385 – 1419.
[16] C. E. F. Rickard, W. R. Roper, S. D. Woodgate, L. J. Wright, *Angew. Chem.* **2000**, *112*, 766 – 768; *Angew. Chem. Int. Ed.* **2000**, *39*, 750 – 752.
[17] J. R. Bleeke, R. Behm, Y.-F. Xie, M. Y. Chiang, K. D. Robinson, A. M. Beatty, *Organometallics* **1997**, *16*, 606 – 623.
[18] W. Lin, S. R. Wilson, G. S. Girolami, *Organometallics* **1997**, *16*, 2356 – 2361.
[19] J. R. Bleeke, R. Behm, Y.-F. Xie, T. W. Clayton, Jr., K. D. Robinson, *J. Am. Chem. Soc.* **1994**, *116*, 4093 – 4094.
[20] M. A. Iron, J. M. L. Martin, M. E. van der Boom, *J. Am. Chem. Soc.* **2003**, *125*, 11 702 – 11 709.
[21] M. A. Iron, J. M. L. Martin, M. E. van der Boom, *Chem. Commun.* **2003**, 132 – 133.
[22] M. A. Iron, J. M. L. Martin, M. E. van der Boom, *J. Am. Chem. Soc.* **2003**, *125*, 13 020 – 13 021.
[23] G. P. Elliott, W. R. Roper, J. M. Waters, *J. Chem. Soc. Chem. Commun.* **1982**, 811 – 813.
[24] J. R. Bleeke, P. V. Hinkle, M. Shokeen, *Organometallics* **2004**, *23*, 4139 – 4149.
[25] J. Chen, V. G. Young, Jr., R. J. Angelici, *Organometallics* **2002**, *21*, 5951 – 5961.
[26] G. P. Elliot, N. M. McAuley, W. R. Roper, *Inorg. Synth.* **1989**, *26*, 184 – 189.
[27] N. A. Grabowski, R. P. Hughes, B. S. Jaynes, A. L. Rheingold, *J. Chem. Soc. Chem. Commun.* **1986**, 1694 – 1695.
[28] J. W. Egan, Jr., R. P. Hughes, A. L. Rheingold, *Organometallics* **1987**, *6*, 1578 – 1581.
[29] J. R. Bleeke, Y.-F. Xie, W.-J. Peng, M. Chiang, *J. Am. Chem. Soc.* **1989**, *111*, 4118 – 4120.
[30] J. R. Bleeke, R. Behm, A. M. Beatty, *Organometallics* **1997**, *16*, 1103 – 1105.
[31] J. Yang, W. M. Jones, J. K. Dixon, N. T. Allison, *J. Am. Chem. Soc.* **1995**, *117*, 9776 – 9777.
[32] R. Ferede, N. T. Allison, *Organometallics* **1983**, *2*, 463 – 465.
[33] M. A. Iron, A. C. B. Lucassen, H. Cohen, M. E. van der Boom, J. M. L. Martin, *J. Am. Chem. Soc.* **2004**, *126*, 11 699 – 11 710.
[34] R. Crabtree, *The Organometallic Chemistry of the Transition Metals*, 3rd ed., Wiley, New York, **2001**, p. 116.
[35] H. Xia, G. He, H. Zhang, T. B. Wen, H. H. Y. Sung, I. D. Williams, G. Jia, *J. Am. Chem. Soc.* **2004**, *126*, 6862 – 6863.
[36] M. B. Smith, J. March, *March's Advanced Organic Chemistry*, 5th ed., Wiley, New York, **2001**, pp. 854 – 855.
[37] An example of an even more strained metallacyclopentyne has been reported: N. Suzuki, N. Alhara, H. Takahara, T. Watanabi, M. Iwasaki, M. Saburi, D. Hashizumi, T. Chihara, *J. Am. Chem. Soc.* **2004**, *126*, 60 – 61.
[38] T. B. Wen, Z. Y. Zhou, G. Jia, *Angew. Chem.* **2001**, *113*, 2005 – 2008; *Angew. Chem. Int. Ed.* **2001**, *40*, 1951 – 1954.
[39] W. R. Roper, *Angew. Chem.* **2001**, *113*, 2506 – 2507; *Angew. Chem. Int. Ed.* **2001**, *40*, 2440 – 2441.
[40] G. Jia, *Acc. Chem. Res.* **2004**, *37*, 479 – 486.
[41] S. M. Ng, X. Huang, T. B. Wen, G. Jia, Z. Lin, *Organometallics* **2003**, *22*, 3898 – 3904.
[42] S.-Y. Yang, X.-Y. Li, Y.-Z. Huang, *J. Organomet. Chem.* **2002**, *658*, 9 – 14.
[43] T. B. Wen, S. M. Ng, W. Y. Hung, Z. Y. Zhou, M. F. Lo, L.-Y. Shek, I. D. Williams, Z. Lin, G. Jia, *J. Am. Chem. Soc.* **2003**, *125*, 884 – 885.
[44] T. B. Wen, S.-Y. Yang, Z. Y. Zhou, Z. Lin, C.-P. Lau, G. Jia, *Organometallics* **2000**, *19*, 3757 – 3761.
[45] T. B. Wen, Z. Y. Zhou, M. F. Lo, I. D. Williams, G. Jia, *Organometallics* **2003**, *22*, 5217 – 5225.
[46] T. B. Wen, W. Y. Hung, H. H. Y. Sung, I. D. Williams, G. Jia, *J. Am. Chem. Soc.* **2005**, *127*, 2856 – 2857.
[47] a) B. Engels, J. C. Shöneboom, A. F. Münster, S. Groetsch, M. Christl *J. Am. Chem. Soc.* **2002**, *124*, 287 – 297; b) R. P. Johnson, *Chem. Rev.* **1989**, *89*, 1111 – 1124.
[48] P. Barrio, M. A. Esteruelas, E. Oñate, *J. Am. Chem. Soc.* **2004**, *126*, 1946 – 1947.
[49] G. P. Elliott, W. R. Roper, *J. Organomet. Chem.* **1983**, *250*, C5 – C8.
[50] G. R. Clark, P. M. Johns, W. R. Roper, L. J. Wright, *Organometallics* **2006**, *25*, 1771 – 1777.
[51] C. S. Chin, H. Lee, *Chem. Eur. J.* **2004**, *10*, 4518 – 4522.
[52] C. S. Chin, H. Lee, M.-S. Eum, *Organometallics* **2005**, *24*, 4849 – 4852.
[53] U. Grössmann, H.-U. Hund, H. W. Bosch, H. Schmalle, H. Berke, *J. Organomet. Chem.* **1991**, *408*, 203 – 218.
[54] M. I. Bruce, B. C. Hall, B. W. Skelton, E. R. T. Tiekink, *Aust. J. Chem.* **2000**, *53*, 99 – 107.
[55] H. Yamazaki, K. Aoki, *J. Organomet. Chem.* **1976**, *122*, C54 – C58.
[56] R. Birk, U. Grössmann, H.-U. Hund, H. Berke, *J. Organomet. Chem.* **1988**, *345*, 321 – 329.

© 2006 Wiley-VCH Verlag GmbH & Co. KGaA, Weinheim

[57] M. I. Bruce, N. N. Zaitseva, B. W. Skelton, A. H. White, *J. Chem. Soc. Dalton Trans.* **2002**, 1678 – 1686.
[58] S. H. Liu, W. S. Ng, H. S. Chu, T. B. Wen, H. Xia, Z. Y. Zhou, C. P. Lau, G. Jia, *Angew. Chem.* **2002**, *114*, 1659 – 1661; *Angew. Chem. Int. Ed.* **2002**, *41*, 1589 – 1591.
[59] U. Effertz, U. Englert, F. Podewils, A. Salzer, T. Wagner, M. Kaupp, *Organometallics* **2003**, *22*, 264 – 274.
[60] R. P. Hughes, D. J. Robinson, *Organometallics* **1989**, *8*, 1015 – 1019.
[61] C. L. Landorf, M. M. Haley, unpublished results.
[62] H. Zhang, H. Xia, G. He, T. B. Wen, L. Gong, G. Jia, *Angew. Chem.* **2006**, *118*, 2986 – 2989; *Angew. Chem. Int. Ed.* **2006**, *45*, 2920 – 2923.
[63] J. R. Bleeke, *Acc. Chem. Res.* **1991**, *24*, 271 – 277.
[64] R. D. Gilbertson, T. J. R. Weakley, M. M. Haley, *J. Am. Chem. Soc.* **1999**, *121*, 2597 – 2598.
[65] R. D. Gilbertson, T. J. R. Weakley, M. M. Haley, *Chem. Eur. J.* **2000**, *6*, 437 – 441.
[66] H.-P. Wu, S. Lanza, T. J. R. Weakley, M. M. Haley, *Organometallics* **2002**, *21*, 2824 – 2826.
[67] R. D. Gilbertson, T. L. S. Lau, S. Lanza, H.-P. Wu, T. J. R. Weakley, M. M. Haley, *Organometallics* **2003**, *22*, 3279 – 3289.
[68] H.-P. Wu, T. J. R. Weakley, M. M. Haley, *Chem. Eur. J.* **2005**, *11*, 1191 – 1200.
[69] K. C. Bishop, *Chem. Rev.* **1976**, *76*, 461 – 486.
[70] C. A. Tolman, *Chem. Rev.* **1977**, *77*, 313 – 348.
[71] R. P. Hughes, M. E. King, D. J. Robinson, J. M. Spotts, *J. Am. Chem. Soc.* **1989**, *111*, 8919 – 8920.
[72] R. C. Hemond, R. P. Hughes, D. J. Robinson, A. L. Rheingold, *Organometallics* **1988**, *7*, 2239 – 2241.
[73] R. T. Li, S. T. Nguyen, R. H. Grubbs, J. W. Ziller, *J. Am. Chem. Soc.* **1994**, *116*, 10032 – 10040.
[74] H.-P. Wu, S. Lanza, T. J. R. Weakley, M. M. Haley, unpublished results.
[75] Z. Lin, personal communication.
[76] a) C. S. Chin, G. Won, D. Chong, M. Kim, H. Lee, *Acc. Chem. Res.* **2002**, *35*, 218 – 225; b) C. S. Chin, M. Kim, H. Lee, S. Noh, K. M. Ok, *Organometallics* **2002**, *21*, 4785 – 4793.
[77] C. S. Chin, H. Lee, M. Oh, *Organometallics* **1997**, *16*, 816 – 818.
[78] E. Alvarez, M. Paneque, M. L. Poveda, N. Rendon, *Angew. Chem.* **2006**, *118*, 488 – 491; *Angew. Chem. Int. Ed.* **2006**, *45*, 474 – 477.
[79] R. P. Hughes, H. A. Trujillo, J. A. Egan, Jr., A. L. Rheingold, *J. Am. Chem. Soc.* **2000**, *122*, 2261 – 2271.
[80] M. Paneque, C. M. Posadas, M. L. Poveda, N. Rendon, V. Salazar, E. Onate, K. Mereiter, *J. Am. Chem. Soc.* **2003**, *125*, 9898 – 9899.
[81] E. Alvarez, M. Gomez, M. Paneque, C. M. Posadas, M. L. Poveda, N. Rendon, L. L. Santos, S. Rojas-Lima, V. Salazar, K. Mereiter, C. Ruiz, *J. Am. Chem. Soc.* **2003**, *125*, 1478 – 1479.
[82] F. Terrier, *Chem. Rev.* **1982**, *82*, 77 – 152.
[83] R. D. Gilbertson, H.-P. Wu, M. M. Haley, unpublished results.
[84] H.-P. Wu, T. J. R. Weakley, M. M. Haley, *Organometallics* **2002**, *21*, 4320 – 4322.
[85] R. P. Hughes, H. A. Trujillo, J. W. Egan, Jr., A. L. Rheingold, *Organometallics* **1999**, *18*, 2766 – 2772.
[86] V. Jacob, T. J. R. Weakley, M. M. Haley, *Angew. Chem.* **2002**, *114*, 3620 – 3623; *Angew. Chem. Int. Ed.* **2002**, *41*, 3470 – 3473.
[87] C. W. Landorf, V. Jacob, T. J. R. Weakley, M. M. Haley, *Organometallics* **2004**, *23*, 1174 – 1176.
[88] V. Jacob, T. J. R. Weakley, M. M. Haley, *Organometallics* **2002**, *21*, 5394 – 5400.
[89] N. M. Boag, *Organometallics* **1988**, *7*, 1446 – 1449.
[90] F. De Proft, P. Geerlings, *Phys. Chem. Chem. Phys.* **2004**, *6*, 242 – 250.

 © 2006 Wiley-VCH Verlag GmbH & Co. KGaA, Weinheim

Communications

DOI: 10.1002/anie.200600572

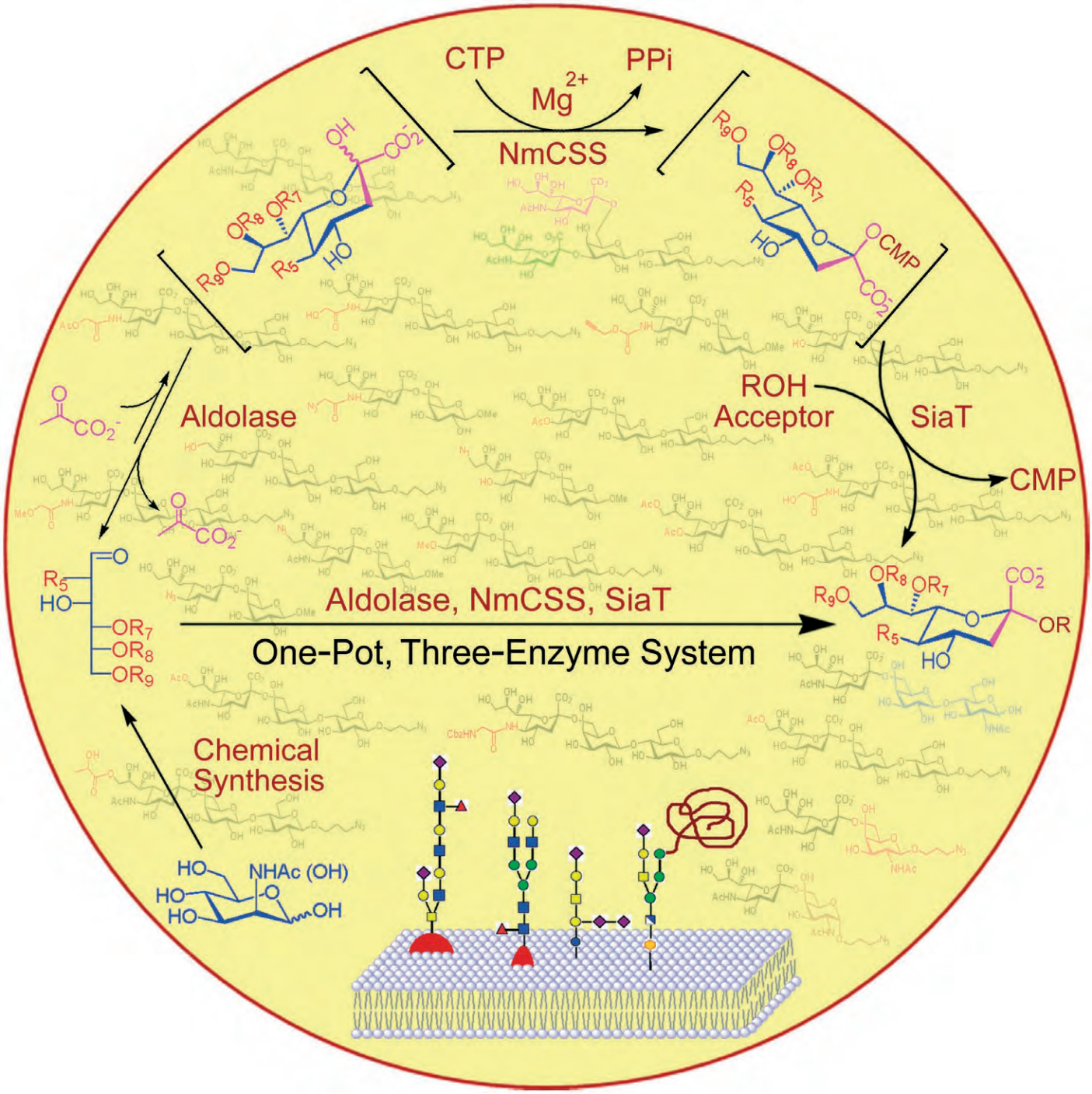

α-2,6-Linked sialosides that contain both natural and non-natural sialic acid forms have been prepared through a one-pot, three-enzyme chemoenzymatic synthesis. In the Communication on the following pages, X. Chen and co-workers show that relaxed substrate specificity of biosynthetic enzymes is the key.

WILEY InterScience DISCOVER SOMETHING GREAT
© 2006 Wiley-VCH Verlag GmbH & Co. KGaA, Weinheim

Enzyme Catalysis

DOI: 10.1002/anie.200600572

Highly Efficient Chemoenzymatic Synthesis of Naturally Occurring and Non-Natural α-2,6-Linked Sialosides: A *P. damsela* α-2,6-Sialyltransferase with Extremely Flexible Donor–Substrate Specificity**

*Hai Yu, Shengshu Huang, Harshal Chokhawala, Mingchi Sun, Haojie Zheng, and Xi Chen**

Sialic acids are a family of α-keto acids with a nine-carbon backbone. They have been predominantly found as terminal carbohydrate units on glycoproteins and glycolipids of vertebrates or as components of capsular polysaccharides and lipooligosaccharides of pathogenic bacteria.[1] Sialic acid containing structures play pivotal roles in many physiologically and pathologically important processes, including cellular recognition and communication, bacterial and viral infection, and tumor metastasis, etc.[1] Currently, more than 50 structurally distinct forms of sialic acids have been found in nature,[1] more than 15 of which have been found on human red-blood-cell (RBC) surfaces, saliva proteins, and gastrointestinal mucins.[2] Three basic forms of sialic acids (Figure 1)

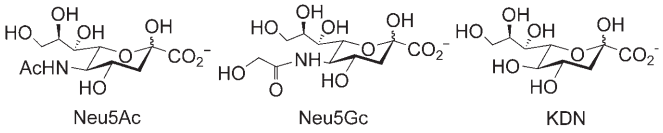

Figure 1. Three basic forms of naturally occurring sialic acids. Ac = acetyl.

are *N*-acetylneuraminic acid (Neu5Ac), *N*-glycolylneuraminic acid (Neu5Gc), and deaminoneuraminc acid (KDN). Based on these three forms, single or multiple substitutions can occur at the hydroxyl group on C4, C5, C7, C8, and/or C9 positions, including O-acetylation and the less frequent O-methylation, O-lactylation, O-sulfation, and O-phosphorylation (Figure 2).[1]

Modifications of sialic acids and cell-surface presentation of modified sialic acids are species and tissue specific. They

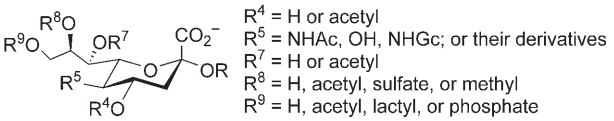

Figure 2. Naturally occurring sialic acid modifications.

are developmentally regulated and are believed to be closely related to their biological functions.[1] Nevertheless, a clear understanding of the mechanism and the significance of nature's sialic acid structural diversity is currently missing. This is mainly owing to the difficulties in obtaining homogenous sialosides or sialylglycoconjugates, especially those that contain diverse naturally occurring sialic acid modifications. These structures are extremely difficult to isolate in homogenous forms from natural sources[3] and chemical sialylation remains challenging.[4] Although sialyltransferase-catalyzed synthesis offers great advantages,[5] it suffers from the low expression level and the narrow substrate specificity of many sialyltransferases, especially those from mammalian sources.[6] Current chemical[4,7] and enzymatic[5,8] sialylation activities have been focusing on structures containing non-natural sialic acid derivatives and a limited number of natural sialic acid forms (e.g. Neu5Ac, Neu5Gc, KDN, Neu5Ac8Me, and Neu5,9Ac_2).[3–9] Further development of the synthetic methodology, thus, is required to obtain structurally defined naturally occurring sialosides for better understanding of their biological roles.

Sialic acid modifications, such as O-acetylation, O-methylation, O-lactylation, and O-sulfation, are believed to occur after the formation of sialylglycoconjugates or polysialic acids in mammals,[10] group C *meningococci*,[11] and *E. coli*.[12] There is indication, however, that O-acetylation may occur on free Neu5 Ac in the biosynthesis of Group B *Streptococcus* (GBS) capsular polysaccharide.[10b] Only a few enzymes involved in the sialic acid modifications have been discovered, including 9-*O*-acetyltransferases from rat liver,[10a] bovine submandibular gland,[13] *E. coli* K1,[1b,14] and *C. jejuni*;[15] 4-*O*-acetyltransferases from guinea-pig liver[16] and equine submandibular gland;[17] a sialic acid 8-*O*-methyltransferase from starfish *A. rubens*.[18] Cytidine monophosphate (CMP)-Neu5 Ac hydroxylase[19] and *C. jejuni* 9-*O*-acetyltransferase[15] are the only proteins in this category that have ever been cloned. Owing to the unavailability of these sialic acid modifying enzymes, it is impractical to synthesize naturally occurring sialosides by totally following their biosynthetic pathways.

Instead of nature's way of introducing sialic acid modifications after oligosaccharide formation, we have established a highly efficient and convenient one-pot, three-enzyme chemoenzymatic approach for the synthesis of sialosides containing naturally occurring as well as non-natural sialic acid modifications at C5, C7, C8, and/or C9. In this method, sialic acid modifications can be chemically introduced at the very beginning, onto the six-carbon sugar precursors (ManNAc or mannose) of sialic acids. These ManNAc or mannose analogues can then be directly converted to the corresponding sialosides in one pot by using three enzymes, including a sialic acid aldolase, a CMP-sialic acid synthetase, and a sialyltransferase without the isolation of intermediates

[*] Dr. H. Yu, S. Huang, H. Chokhawala, M. Sun, H. Zheng, Prof. Dr. X. Chen
Department of Chemistry
University of California, Davis
One Shields Avenue, Davis, CA 95616 (USA)
Fax: (+1) 530-752-8995
E-mail: chen@chem.ucdavis.edu

[**] The authors thank Prof. Ajit Varki for providing plasmids containing the *P. damsela* α-2,6-sialyltransferase gene in a TOPO vector. This work was supported by Mizutani Foundation for Glycoscience and NIH R01M076360.

Supporting information for this article is available on the WWW under http://www.angewandte.org or from the author.

 © 2006 Wiley-VCH Verlag GmbH & Co. KGaA, Weinheim

(Scheme 1). Depending on the type of the sialyltransferase used, α-2,3- or α-2,6-linked sialosides can be synthesized conveniently. Combining the diversity of organic synthesis and the highly efficient, regio- and stereoselective enzymatic approaches, this chemoenzymatic system is an attractive synthetic method for complex sialic acid containing structures.

Two major challenges for highly effective chemoenzymatic synthesis are 1) the availability and efficiency of biosynthetic enzymes; and 2) the extent of substrate modification that can be tolerated by the enzymes. We have successfully found solutions for synthesizing complex sialosides by matching these two challenges.

Previously, we reported the high-level expression of a recombinant sialic acid aldolase from *E. coli* K-12 and a CMP-sialic acid synthetase from *N. meningitidis* (NmCSS).[20] Both enzymes have flexible substrate specificity. They have been used successfully in one-pot, two-enzyme preparative syntheses of CMP-sialic acid derivatives[20] and one-pot, three-enzyme syntheses of α-2,3-linked sialoside libraries.[21] To prepare α-2,6-linked sialosides with naturally occurring or non-natural sialic acid modifications, we investigated the donor–substrate specificity of a recombinant *Photobacterium damsela* α-2,6-sialyltransferase (Pd2,6ST) and explored its application in the one-pot, three-enzyme synthesis.

Pd2,6ST was the first bacterial α-2,6-sialyltransferase that has ever been cloned.[22] The isolation of this sialyltransferase was firstly reported in 1996.[23] Subsequently, its extremely flexible acceptor–substrate specificity was described.[8c,24] No study, however, has been reported on the donor–substrate specificity of this enzyme.

To facilitate the protein purification, a truncated Pd2,6ST encoding for amino acid residues 16–497 of the full-length protein was cloned into a pET15b vector and expressed as a N-His_6-tagged protein. The recombinant Pd2,6ST was purified by a nickel-nitrilotriacetic acid (Ni-NTA) agarose affinity column. The tolerance of donor–substrate modification of the purified Pd2,6ST was firstly tested by TLC analysis (EtOAc/MeOH/H_2O/HOAc = 4:2:1:0.1) in the one-pot, three-enzyme system shown in Scheme 1, in which CMP-sialic acid derivatives were generated in situ from sialic acid precursors catalyzed by the aldolase and NmCSS. For sialosides that do not contain O-acetyl or O-lactyl groups, reactions were typically performed in a tris(hydroxymethyl)aminomethane (Tris)-Cl buffer solution at pH 8.5 for 2–10 h at 25 °C. When this condition was used for the synthesis of sialosides containing O-acetyl groups, de-O-acetylation was observed. Therefore, a Tris-Cl buffer solution (pH 7.5) with a lower pH value was used for synthesizing sialosides containing O-acetylated or O-lactylated sialic acid residues to avoid the hydrolysis of the esters. After observing the product formation on TLC, preparative scale syntheses were carried out. Sialoside products were purified by gel filtration chromatography and characterized by NMR spectroscopy and HRMS.

As shown in Table 1, by using 3-azidopropyl lactoside **20** as an acceptor for Pd2,6ST, naturally occurring α-2,6-linked sialosides containing Neu5Ac or its C5-substituted analogues (**26**–**32**) were firstly synthesized in 75–99 % yields (Table 1, entries a–g) from ManNAc, mannose, or their C2-modified analogues (**1**–**7**) as sialic acid precursors. 5-*O*-Acetyl-KDN (KDN5Ac) (the sialic acid form in **29**) has been found on the eggs of *Rana temporaria*, *Rana arvalis*, and *Pleurodeles waltii*;[2b] 5-*O*-methyl-KDN (KDN5Me) (the sialic acid form in **30**) has been observed in *Sinorhizobium fredii*;[25] *N*-acetylglycolyl-neuraminic acid (Neu5GcAc) (the sialic acid form in **31**) has been detected in rat peritoneal macrophages.[26]

Naturally occurring α-2,6-linked sialosides containing a C9-substituted Neu5Ac or KDN (**33**–**35**) were synthesized in 72–84 % yields (Table 1, entries h–j) from the corresponding C6-modified ManNAc or mannose (**8**–**10**). 9-*O*-Acetylation has been found in nearly all higher animals and certain bacteria and is believed to play a pivotal role in modulating various biological processes.[27] For example, 9-*O*-acetyl-*N*-acetylneuraminic acid (Neu5,9Ac_2) (the sialic acid form in **33**) is an essential determinant of the cell surface receptors for the influenza C virus, but prevents the recognition of influenza A and B viruses.[28] It is also presented in an antigenic ganglioside found in developing rat embryonic cells.[29] 9-*O*-Lactyl-Neu5Ac (Neu5Ac9Lt) (the sialic acid form in **34**) has been found in bovine submandibular gland glycoprotein[30] and human RBC membranes.[2a] 9-*O*-Acetyl-KDN (KDN9Ac) (the sialic acid form in **35**) has been found in *O. nerka adonis* polysialoglycoproteins.[31]

Naturally occurring α-2,6-linked sialosides containing disubstituted sialic acid residues **36** and **37** have also been synthesized successfully in 78 % and 65 % yields (Table 1, entries k and l), respectively. 9-*O*-Acetyl-Neu5Gc (Neu9-

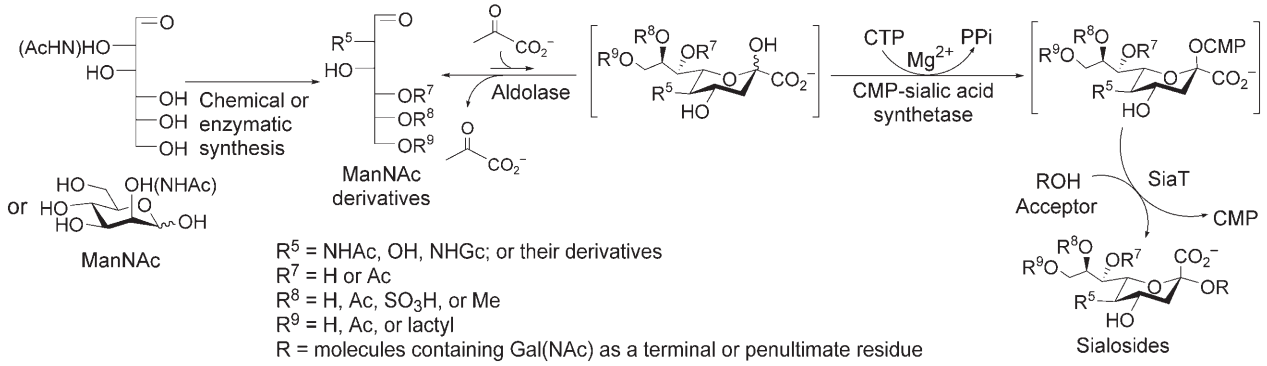

Scheme 1. An efficient chemoenzymatic approach for the synthesis of sialosides containing sialic acid modifications. PPi = inorganic pyrophosphate, SiaT = sialyltransferase.

 © 2006 Wiley-VCH Verlag GmbH & Co. KGaA, Weinheim

Table 1: Synthesis of α-2,6-linked sialosides using the one-pot, three-enzyme system shown in Scheme 1.[a]

Entry	Donor Precursors	Acceptor	Product	Yield [%]
a	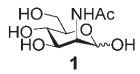 **1**	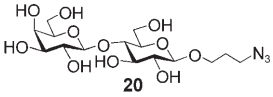 **20**	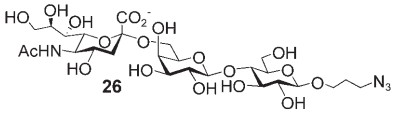 **26**	**98**
b	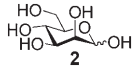 **2**	**20**	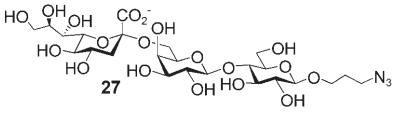 **27**	**97**
c	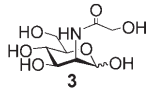 **3**	**20**	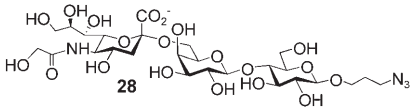 **28**	**95**
d	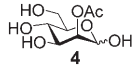 **4**	**20**	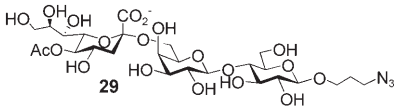 **29**	**75**
e	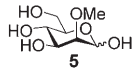 **5**	**20**	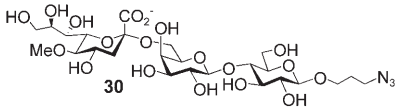 **30**	**76**
f	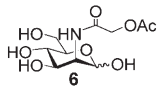 **6**	**20**	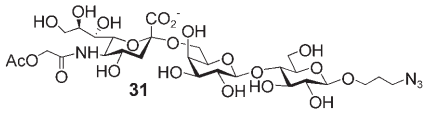 **31**	**87**
g	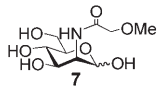 **7**	**20**	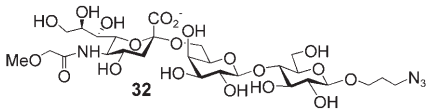 **32**	**99**
h	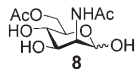 **8**	**20**	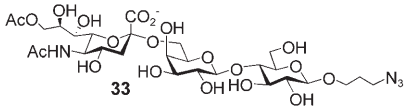 **33**	**84**
i	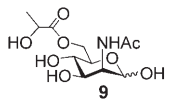 **9**	**20**	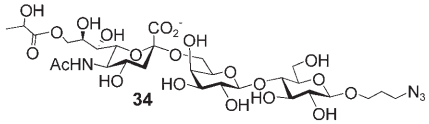 **34**	**72**
j	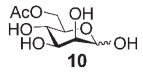 **10**	**20**	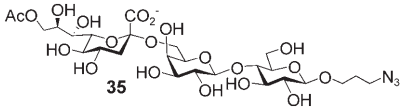 **35**	**75**
k	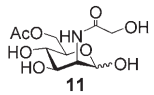 **11**	**20**	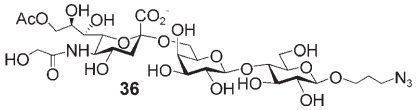 **36**	**78**
l	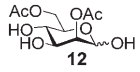 **12**	**20**	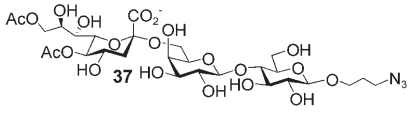 **37**	**65**
m	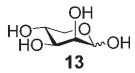 **13**	**20**	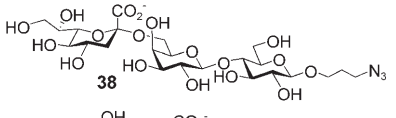 **38**	**92**
n	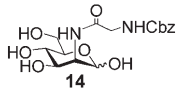 **14**	**20**	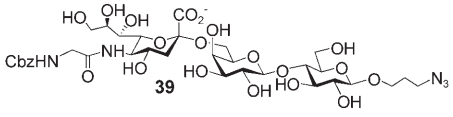 **39**	**99**
o	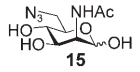 **15**	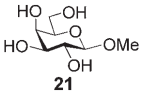 **21**	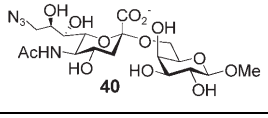 **40**	**93**

© 2006 Wiley-VCH Verlag GmbH & Co. KGaA, Weinheim

Table 1: (Continued)

Entry	Donor Precursors	Acceptor	Product	Yield [%]
p	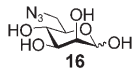 **16**	**21**	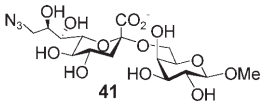 **41**	**91**
q	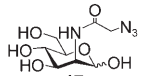 **17**	**21**	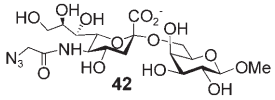 **42**	**90**
r	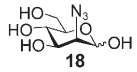 **18**	**21**	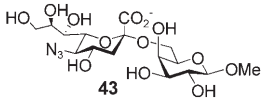 **43**	**86**
s	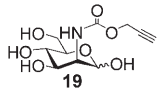 **19**	**21**	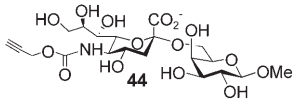 **44**	**87**
t	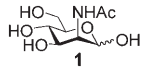 **1**	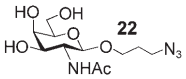 **22**	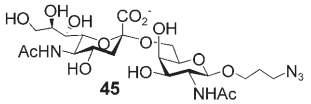 **45**	**87**
u	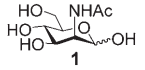 **1**	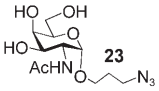 **23**	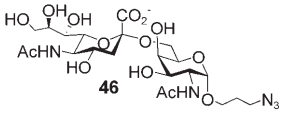 **46**	**61**
v	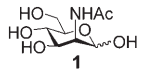 **1**	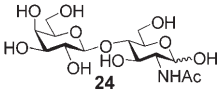 **24**	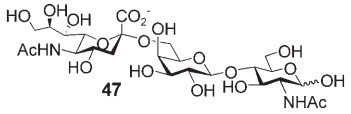 **47**	**92**
w	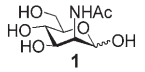 **1**	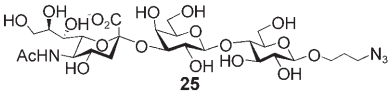 **25**	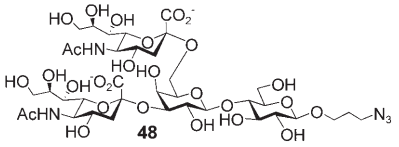 **48**	**91**

[a] All reactions were carried out in preparative (50–150 mg) scales.

Ac5Gc) (the sialic acid form in **36**) has been found in bovine submandibular gland glycoprotein.[30] 5,9-Di-*O*-acetyl-KDN (KDN5,9Ac_2) (the sialic acid form in **37**) has also been found in nature.[1a]

By using the same 3-azidopropyl lactoside **20** as the acceptor for Pd2,6ST, non-natural sialosides containing a 4,6-bis-*epi*-KDO (**38**) and an *N*-(benzyloxycarboxyamido) glycinylamido-neuraminic acid (NeuGlyCbz) (**39**) were successfully synthesized in high yields (Table 1, entries m and n). The successful synthesis of the KDO analogue containing trisaccharide **38** demonstrates that Pd2,6ST can transfer sialic acids with carbon backbones shorter than nine carbons to galactoside with high efficiency. Furthermore, a bulky benzyloxycarbonyl (Cbz) group at C9 of the sialic acid residue of the donor does not affect the activity of Pd2,6ST. This further demonstrates the extremely flexible donor–substrate specificity of this enzyme.

By using GalβOMe (**21**) as an acceptor for Pd2,6ST, α-2,6-linked sialosides containing sialic acid modified with non-natural substitutents (**40**–**44**), such as an azido or an acetylene group, were also synthesized in excellent yields (86–93%) from C2- or C6-modified ManNAc or mannose that bears azide or alkyne functional groups **15**–**19**. The resulting sialosides tagged with an azide or alkyne group can be easily linked to other molecules through a Staudinger ligation[32] or click chemistry.[33]

Acceptor specificity of the recombinant Pd2,6ST was explored by using an *N*-acetyl-β-galactosaminide **22**, an *N*-acetyl-α-galactosaminide **23**, an α-galactoside (methyl-α-D-galactopyranoside), β-galactosides **20**, **21**, and **24**, and an α-2,3-linked sialoside **25**. Similar to that reported previously,[8c,23] Pd2,6ST showed a much broader acceptor specificity compared to mammalian sialyltransferases.[24] The recombinant Pd2,6ST could use both α- or β-linked GalNAc derivatives. Furthermore, β-galactosides and α-2,3-linked sialosides were all excellent acceptors for the sialyltransferase. In contrast to that reported,[23] however, α-galactosides were not acceptors for the enzyme.

In conclusion, we have demonstrated that the recombinant *P. damsela* α-2,6-sialyltransferase does not only have relaxed acceptor–substrate specificity, but also extremely flexible donor–substrate specificity. We have also proved the practical application of the one-pot, three-enzyme chemoenzymatic approach in effective preparative-scale synthesis of diverse sialosides with naturally or non-naturally occurring sialic acid modifications. This system can be easily extended

 © 2006 Wiley-VCH Verlag GmbH & Co. KGaA, Weinheim

to large-scale synthesis. Sialyltransferases, together with sialic acid aldolases and CMP-sialic acid synthetases, are important tools for simple and efficient preparation of sialoside libraries. These structurally defined synthetic sialosides will be essential standards for developing analytical methods. They are key probes to elucidate the biological significance of nature's sialic acid diversity, the biosynthetic and degradation pathways of structurally modified sialic acids, and their involvement in the physiological and pathological processes of human and other vertebrates. The synthetic sialosides are also important ligands for identifying specific lectins and producing specific antibodies, which in turn, are vital tools in histochemical studies of organ- and species-specific presentation of modified sialic acids.

Experimental Section

Preparative scale (50–150 mg) synthesis: Reactions were typically carried out in a 50 mL centrifuge tube of Tris-Cl buffer solution (10 mL, 100 mM; pH 8.5 or pH 7.5) containing an acceptor (lactose, GalNAc, or galactose derivatives, 50–100 mg), ManNAc or mannose derivatives (1.5 equiv), sodium pyruvate (7.5 equiv), cytidine-5′-triphosphate (CTP; 1.5 equiv), $MgCl_2$ (20 mM), aldolase, NmCSS, and Pd2,6ST. The reaction mixture was incubated at 25 °C for 12 h with shaking (120 rpm). After adding the same volume of ice-cold methanol to stop the reaction, insoluble material was removed by centrifugation. The supernatant was concentrated by rotor evaporation and purified by Bio-Gel P2 gel filtration chromatography. Lyophilized sialoside products were characterized by NMR spectroscopy and HRMS.

Received: February 13, 2006

Keywords: carbohydrates · chemoenzymatic synthesis · enzyme catalysis · sialic acids · transferases

[1] a) T. Angata, A. Varki, *Chem. Rev.* **2002**, *102*, 439–469; b) R. Schauer, *Glycoconjugate J.* **2000**, *17*, 485–499.

[2] a) C. Robbe, C. Capon, E. Maes, M. Rousset, A. Zweibaum, J. P. Zanetta, J. C. Michalski, *J. Biol. Chem.* **2003**, *278*, 46337–46348; b) J. P. Zanetta, A. Pons, M. Iwersen, C. Mariller, Y. Leroy, P. Timmerman, R. Schauer, *Glycobiology* **2001**, *11*, 663–676.

[3] M. D. Chappell, R. L. Halcomb, *J. Am. Chem. Soc.* **1997**, *119*, 3393–3394.

[4] a) G. J. Boons, A. V. Demchenko, *Chem. Rev.* **2000**, *100*, 4539–4566; b) M. J. Kiefel, M. von Itzstein, *Chem. Rev.* **2002**, *102*, 471–490.

[5] a) M. Izumi, C. H. Wong, *Trends Glycosci. Glycotechnol.* **2001**, *13*, 345; b) J. Thiem, W. Treder, *Angew. Chem.* **1986**, *98*, 1100–1101; *Angew. Chem. Int. Ed. Engl.* **1986**, *25*, 1096–1097; c) D. H. Joziasse, W. E. Schiphorst, D. H. Van den Eijnden, J. A. Van Kuik, H. Van Halbeek, J. F. Vliegenthart, *J. Biol. Chem.* **1987**, *262*, 2025–2033; d) C. Unverzagt, S. Kelm, J. C. Paulson, *Carbohydr. Res.* **1994**, *251*, 285–301; e) M. Gilbert, A.-M. Cunningham, D. C. Watson, A. Martin, J. C. Richards, W. W. Wakarchuk, *Eur. J. Biochem.* **1997**, *249*, 187–194.

[6] a) K. M. Koeller, C. H. Wong, *Nature* **2001**, *409*, 232–240; b) H. J. Gross, R. Brossmer, *Eur. J. Biochem.* **1988**, *177*, 583–589; c) H. H. Higa, J. C. Paulson, J. Weinstein, *J. Biol. Chem.* **1985**, *260*, 8838–8849; d) Y. Kajihara, T. Ebata, K. Koseki, H. Kodama, H. Matsushita, H. Hashimoto, *J. Org. Chem.* **1995**, *60*, 5732–5735.

[7] a) S. J. Danishefsky, J. R. Allen, *Angew. Chem.* **2000**, *112*, 882–912; *Angew. Chem. Int. Ed.* **2000**, *39*, 836–863; b) C. D. Meo, A. V. Demchenko, G. J. Boons, *J. Org. Chem.* **2001**, *66*, 5490–5497; c) V. Martichonok, G. M. Whitesides, *J. Org. Chem.* **1996**, *61*, 1702–1706; d) H. Kondo, Y. Ichikawa, C. H. Wong, *J. Am. Chem. Soc.* **1992**, *114*, 8748–8750.

[8] a) O. Blixt, K. Allin, L. Pereira, A. Datta, J. C. Paulson, *J. Am. Chem. Soc.* **2002**, *124*, 5739–5746; b) C. H. Wong, R. L. Halcomb, Y. Ichikawa, T. Kajimoto, *Angew. Chem.* **1995**, *107*, 569–593; *Angew. Chem. Int. Ed. Engl.* **1995**, *34*, 521–546; c) Y. Kajihara, T. Yamamoto, H. Nagae, M. Nakashizuka, T. Sakakibara, I. Terada, *J. Org. Chem.* **1996**, *61*, 8632–8635.

[9] a) Y. Ichikawa, J. L. C. Liu, G. J. Shen, C.-H. Wong, *J. Am. Chem. Soc.* **1991**, *113*, 6300–6302; b) E. C. Rodriguez, L. A. Marcaurelle, C. R. Bertozzi, *J. Org. Chem.* **1998**, *63*, 7134–7135; c) S. A. Kalovidouris, O. Blixt, A. Nelson, S. Vidal, W. B. Turnbull, J. C. Paulson, J. F. Stoddart, *J. Org. Chem.* **2003**, *68*, 8485–8493; d) T. K. Mong, H. K. Lee, S. G. Duron, C. H. Wong, *Proc. Natl. Acad. Sci. USA* **2003**, *100*, 797–802.

[10] a) C. Butor, S. Diaz, A. Varki, *J. Biol. Chem.* **1993**, *268*, 10197–10206; b) A. L. Lewis, V. Nizet, A. Varki, *Proc. Natl. Acad. Sci. USA* **2004**, *101*, 11123–11128; c) C. Traving, R. Schauer, *Cell. Mol. Life Sci.* **1998**, *54*, 1330–1349.

[11] W. F. Vann, T. Y. Liu, J. B. Robbins, *J. Bacteriol.* **1978**, *133*, 1300–1306.

[12] H. H. Higa, C. Butor, S. Diaz, A. Varki, *J. Biol. Chem.* **1989**, *264*, 19427–19434.

[13] V. Vandamme-Feldhaus, R. Schauer, *J. Biochem.* **1998**, *124*, 111–121.

[14] H. H. Higa, A. Varki, *J. Biol. Chem.* **1988**, *263*, 8872–8878.

[15] R. S. Houliston, H. P. Endtz, N. Yuki, J. Li, H. C. Jarrell, M. Koga, A. Van Belkum, M.-F. Karwashki, W. W. Wakarchuk, M. Gilbert, *J. Biol. Chem.* **2006**, *281*, 11480–11486.

[16] M. Iwersen, V. Vandamme-Feldhaus, R. Schauer, *Glycoconjugate J.* **1998**, *15*, 895–904.

[17] J. Tiralongo, H. Schmid, R. Thun, M. Iwersen, R. Schauer, *Glycoconjugate J.* **2000**, *17*, 849–858.

[18] A. Kelm, L. Shaw, R. Schauer, G. Reuter, *Eur. J. Biochem.* **1998**, *251*, 874–884.

[19] T. Kawano, S. Koyama, H. Takematsu, Y. Kozutsumi, H. Kawasaki, S. Kawashima, T. Kawasaki, A. Suzuki, *J. Biol. Chem.* **1995**, *270*, 16458–16463.

[20] H. Yu, H. Yu, R. Karpel, X. Chen, *Bioorg. Med. Chem.* **2004**, *12*, 6427–6435.

[21] H. Yu, H. Chokhawala, R. Karpel, H. Yu, B. Wu, J. Zhang, Y. Zhang, Q. Jia, X. Chen, *J. Am. Chem. Soc.* **2005**, *127*, 17618–17619.

[22] T. Yamamoto, M. Nakashizuka, I. Terada, *J. Biochem.* **1998**, *123*, 94–100.

[23] T. Yamamoto, M. Nakashizuka, H. Kodama, Y. Kajihara, I. Terada, *J. Biochem.* **1996**, *120*, 104–110.

[24] a) T. Yamamoto, H. Nagae, Y. Kajihara, I. Terada, *Biosci. Biotechnol. Biochem.* **1998**, *62*, 210–214; b) T. Endo, S. Koizumi, K. Tabata, S. Kakita, A. Ozaki, *Carbohydr. Res.* **2001**, *330*, 439–443; c) C.-F. Teo, T.-S. Hwang, P.-H. Chen, C.-H. Hung, H.-S. Gao, L.-S. Chang, C.-H. Lin, *Adv. Synth. Catal.* **2005**, *347*, 967–972.

[25] A. M. Gil-Serrano, M. A. Rodriguez-Carvajal, P. Tejero-Mateo, J. L. Espartero, J. Thomas-Oates, J. E. Ruiz-Sainz, A. M. Buendia-Claveria, *Biochem. J.* **1998**, *334*, 585–594.

[26] A. Kluge, G. Reuter, H. Lee, B. Ruch-Heeger, R. Schauer, *Eur. J. Cell Biol.* **1992**, *59*, 12–20.

[27] A. Varki, *Glycobiology* **1992**, *2*, 25–40.

[28] a) H. H. Higa, G. N. Rogers, J. C. Paulson, *Virology* **1985**, *144*, 279–282; b) G. Herrler, R. Rott, H. D. Klenk, H. P. Muller, A. K. Shukla, R. Schauer, *Embo J.* **1985**, *4*, 1503–1506.

 © 2006 Wiley-VCH Verlag GmbH & Co. KGaA, Weinheim

[29] D. A. Cheresh, R. A. Reisfeld, A. P. Varki, *Science* **1984**, *225*, 844 – 846.
[30] a) G. Reuter, R. Pfeil, S. Stoll, R. Schauer, J. P. Kamerling, C. Versluis, J. F. Vliegenthart, *Eur. J. Biochem.* **1983**, *134*, 139 – 143; b) P. Stehling, M. Gohlke, R. Fitzner, W. Reutter, *Glycoconjugate J.* **1998**, *15*, 339 – 344.
[31] M. Iwasaki, S. Inoue, F. A. Troy, *J. Biol. Chem.* **1990**, *265*, 2596 – 2602.
[32] E. Saxon, C. R. Bertozzi, *Science* **2000**, *287*, 2007 – 2010.
[33] a) C. W. Tornøe, M. Meldal in *Peptides: The Wave of the Future* (Eds.: M. Lebl, R. A. Houghten), American Peptide Society and Kluwer Academic, San Diego, **2001**, pp. 263 – 264; b) C. W. Tornøe, C. Christensen, M. Meldal, *J. Org. Chem.* **2002**, *67*, 3057 – 3064; c) H. C. Kolb, M. G. Finn, K. B. Sharpless, *Angew. Chem.* **2001**, *113*, 2056 – 2075; *Angew. Chem. Int. Ed.* **2001**, *40*, 2004 – 2021; d) F. Fazio, M. C. Bryan, O. Blixt, J. C. Paulson, C. H. Wong, *J. Am. Chem. Soc.* **2002**, *124*, 14397 – 14402.

 © 2006 Wiley-VCH Verlag GmbH & Co. KGaA, Weinheim

Porphyrinoids

DOI: 10.1002/anie.200600892

A Quadruply Azulene-Fused Porphyrin with Intense Near-IR Absorption and a Large Two-Photon Absorption Cross Section**

Kei Kurotobi, Kil Suk Kim, Su Bum Noh, Dongho Kim, and Atsuhiro Osuka**

Considerable efforts have been continuously devoted to the exploration of extensively π-conjugated porphyrins in light of their potential applications in optoelectronic devices, sensors, photovoltaic devices, and so forth.[1–3] Recently, some of these conjugated porphyrins have been shown to exhibit large two-photon absorption (TPA) cross sections as a promising attribute.[4] The great promise of conjugated porphyrins relies on their flexible electronic systems, which are susceptible to peripheral modifications. An effective synthetic strategy is to fuse an aromatic segment directly onto the periphery of the porphyrin unit to expand a conjugated electronic system that is forced to take a planar conformation favorable for π conjugation.[5] Among such aromatic-fused porphyrins, Scott and co-workers reported an *anti*-bisnaphthoazulene-8-one-fused–Cu^{II} porphyrin that exhibited a Q-band-like absorption band at 1204 nm and a very small electrochemical HOMO–LUMO gap (1.17 V) as the most π-expanded example of a monomeric porphyrin.[5d] In this fusion strategy, azulene may be an effective aromatic segment because of the unique dipolar and polarizable electronic property that arises from its nonalternant hydrocarbon nature.[6] Previously, we prepared a series of directly linked *meso*-azulenylporphyrins, except for one bearing a 4-azulenyl group, and found that 1- and 6-azulenyl groups actually served as electron-donating and electron-withdrawing substituents, respectively, toward a Zn^{II} porphyrin, but the influence of such singly linked azulenyl groups upon the electronic system of the porphyrin are only small.[7]

Herein, we employed 4-azulenylporphyrin as a precursor of azulene-fused porphyrin targets, as the electron-rich 3-position of the azulene, which is directed toward the porphyrin, may be used for an oxidative ring-closing reaction. It has been reported that 1-methoxycarbonyl-4-formylazulene (**3a**) was prepared from 1-methoxycarbonyl-4-methylazulene (**1a**) by selective dibromination at the 4-methyl group followed by oxidation,[8] but treatment of **1a** with *N*-bromosuccinimide (NBS) led to predominant bromination at the 3-position in our hands. Therefore, aldehyde **3a** was prepared via enamine **2a** from **1a**.[9] Treatment of **1a** with *N*,*N*-dimethylformamide (DMF) dimethylacetal in DMF at 140 °C gave **2a**, which was oxidized to **3a** with $NaIO_4$ in 81% yield in two steps. Dipyrromethane **4a** was prepared by the condensation reaction of **3a** with excess pyrrole in 94% yield (Scheme 1).

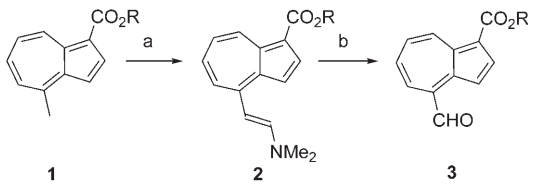

Scheme 1. Synthesis of **3** (R = Me (**a**), octyl (**b**), 2,4,6-tri-*tert*-butylphenyl (**c**)). a) $Me_2NCH(OMe)_2$, DMF, 140 °C; b) $NaIO_4$, THF/H_2O.

Ni^{II}–5-(4-azulenyl)porphyrin **6** was prepared from the cross-condensation of dipyrromethanes **4a** and **5** with 3,5-di(*tert*-butyl)benzaldehyde followed by Ni^{II}-ion insertion in 16% yield, and Ni^{II}–5,15-bis(4-azulenyl)porphyrin **7** was prepared from **4a** and 3,5-di(*tert*-butyl)benzaldehyde in 16% yield. ^1H NMR spectrum of **7** displays two sets of signals in a 1:1 ratio, thus indicating the presence of two atropisomers. Ni^{II}–5,10,15,20-tetrakis(4-azulenyl)porphyrin

[*] K. S. Kim, S. B. Noh, Prof. Dr. D. Kim
Center for Ultrafast Optical Characteristics Control and
Department of Chemistry
Yonsei University, Seoul 120-749 (Korea)
Fax: (+82) 2-2123-2434
E-mail: dongho@yonsei.ac.kr
Dr. K. Kurotobi, Prof. Dr. A. Osuka
Department of Chemistry
Graduate School of Science
Kyoto University
and
Core Research for Evolutional Science and Technology (CREST)
Japan Science and Technology Agency
Sakyo-ku, Kyoto 606-8502 (Japan)
Fax: (+81) 75-753-3970
E-mail: osuka@kuchem.kyoto-u.ac.jp

[**] This work was partly supported by a Grant-in-Aid (B) (No. 17350017) from the Ministry of Education, Culture, Sports, Science, and Technology, Japan (A.O.) and the Star Faculty Program of the Ministry of Education, Korea for Human Resources (D.K.). We thank Shinetsu Igarashi and Kenji Yoza (Bruker, Japan) for the X-ray analysis.

Supporting information for this article is available on the WWW under http://www.angewandte.org or from the author.

InterScience
© 2006 Wiley-VCH Verlag GmbH & Co. KGaA, Weinheim

8a was prepared from **3a** under Lindsey conditions[10] in 12% yield as a mixture of atropisomers. Structural determination of these azulenylporphyrins were mainly based on ^{1}H NMR spectroscopic, MALDI-TOF mass-spectrometric, and UV/Vis absorption spectroscopic analysis. The structure of the Cu^{II} complex of **6** [Cu(**6**)] was confirmed by X-ray diffraction analysis (Figure 1),[11] which showed that the 4-azulenyl group is linked to the porphyrin ring with a C–C bond length of 1.505 Å and a dihedral angle of 81°, similar to other *meso*-azulenylporphyrins.[7]

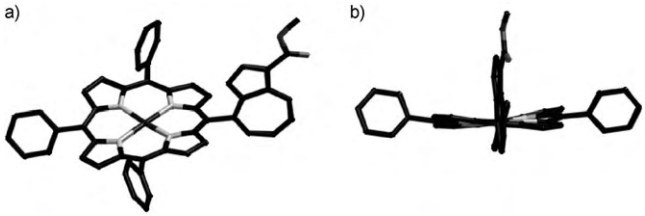

Figure 1. X-ray crystal structure of [Cu(**6**)]. a) Oblique view, b) side view. The *tert*-butyl groups and hydrogen atoms have been omitted for clarity.

Attempted oxidative ring-closing reaction of **6** with $AgPF_6$[12] did not cause any conversion, but the use of 2,3-dichloro-5,6-dicyano-*p*-benzoquinone (DDQ)/$[Sc(OTf)_3]$[2d] (Tf = trifluoromethanesulfonyl) as a stronger oxidant gave rise to a complicated mixture. In the meantime, we found that treatment of **6** with $FeCl_3$[13] under mild conditions (5 min, room temperature) afforded azulene-fused porphyrin **9** in 63% yield. A double ring-closing reaction of **7** was performed under similar conditions to regioselectively provide only the *anti* isomer **10** in 84% yield. Curiously, the *syn* isomer was not detected at all. This result suggested that the regiochemistry of the second ring-closing reaction is strongly influenced by the preformed azulene-fused structure at the opposite side. The symmetric *anti* structure of **10** is indicated by its simple ^{1}H NMR spectrum, which exhibits a single set of signals for the *meso* aryl protons, *para* protons ($\delta = 7.83$ ppm), and *ortho* protons ($\delta = 7.91$ ppm). A fourfold ring-closing reaction of **8a** was attempted with $FeCl_3$ under similar conditions; however, a complicated mixture was yielded. Separation of this mixture turned out to be quite difficult as a result of its extremely low solubility. We thus changed substrates to more soluble porphyrins **8b** and **8c**,[14] which were prepared from **3b** and **3c**, respectively, through the same synthetic route used for **8a**. Although the similar treatment of **8b** with $FeCl_3$ also led to an intractable mixture of low solubility, porphyrin **8c** was cleanly transformed into quadruply azulene-fused porphyrin **11** as a major product in 60% yield. The product **11** showed its parent-ion peak at *m*/*z* 2017.0052, calculated for $C_{136}H_{140}N_4O_8Ni$ *m*/*z* 2017.0057 in the high-resolution electrospray ionization TOF mass spectrum. In line with the symmetric structure, the ^{1}H NMR spectrum of **11** was quite simple and featured a single set of signals for the azulene protons ($\delta = 8.74$, 8.64, 8.45, 7.93, and 9.89 ppm for H^2, H^5, H^6, H^7, and H^8, respectively; Scheme 2) and a singlet at $\delta =$ 9.12 ppm for the pyrrolic β-protons. Furthermore, X-ray diffraction analysis confirmed the structure, in which the four azulene moieties are fused to the central porphyrin ring in a symmetric manner to constitute an overall coplanar structure, which exhibits strong ruffling with a mean deviation of 0.81 Å

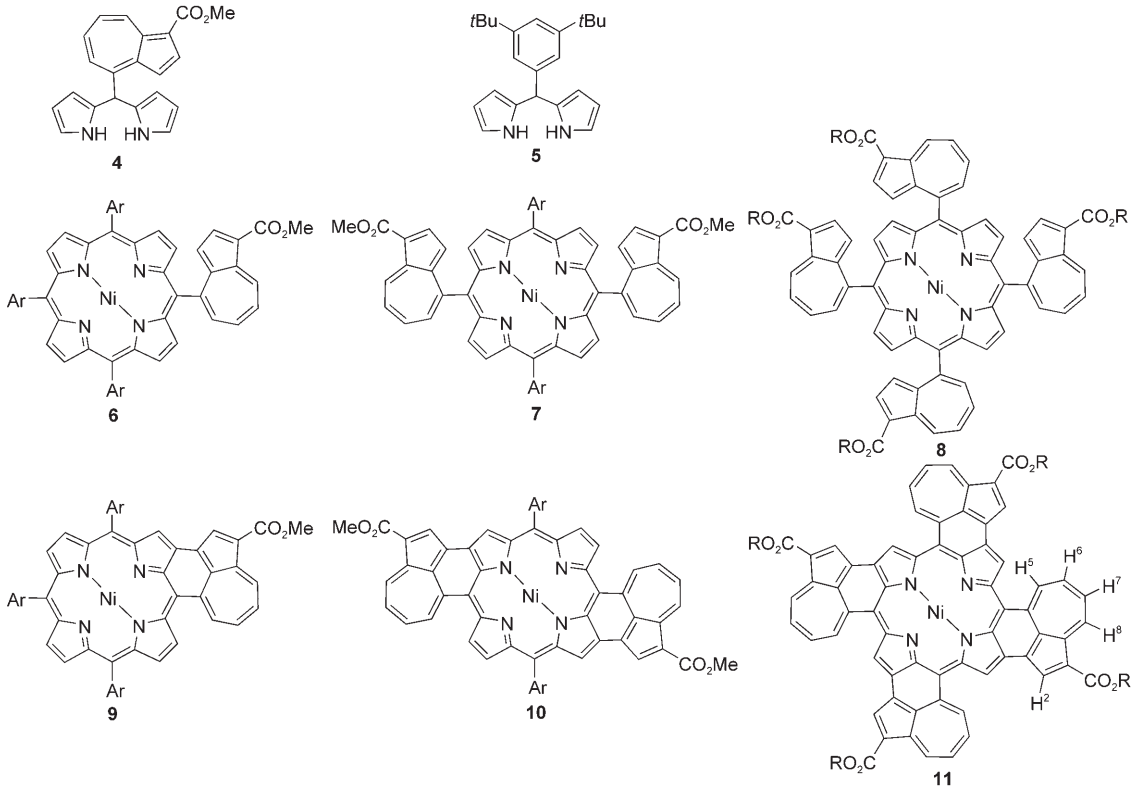

Scheme 2. Compounds studied herein. R = Me (**8a**), octyl (**8b**), 2,4,6-*tert*-butylphenyl (**8c**, **11**).

© 2006 Wiley-VCH Verlag GmbH & Co. KGaA, Weinheim

with respect to the porphyrin macrocyclic plane of 24 atoms (Figure 2).[15] The Ni–N bond lengths are 1.863, 1.877, 1.893, and 1.894 Å between the Ni center and N(1)–N(4), respectively. The opposite halves are bent with 120.9 and 111.6° dihedral angles.

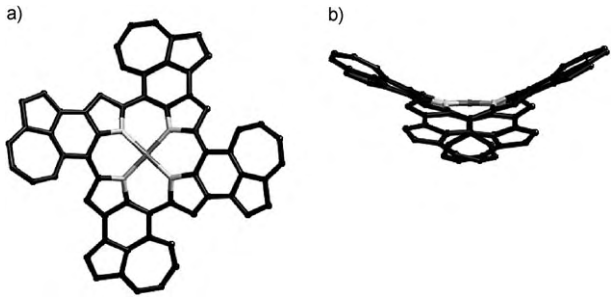

Figure 2. X-ray crystal structure of **11**. a) Top view, b) side view. The ester groups and hydrogen atoms have been omitted for clarity.

The absorption spectra of **6**–**8** exhibit slightly red-shifted, broadened Soret and Q bands. Such trends become larger upon an increase in the number of azulenyl groups; the Soret bands are observed at 422, 426, and 437 nm for **6**–**8**, respectively, and Q(1,0) bands are intensified in the order of **6** < **7** < **8** (Figure 3a). In sharp contrast, the azulene-fused structure causes more profound impacts in the electronic system of the porphyrin. The absorption spectrum of **9** shows a broad Soret band at 467 nm with a shoulder at 526 nm and a quite broad Q band that reaches around 1000 nm; the absorption spectrum of **10** shows a split Soret band at 487 and 545 nm and red-shifted, intense Q bands at 763, 898, and 1014 nm with roughly equal intensities; and the quadruply azulene-fused porphyrin **11** exhibits a drastically perturbed absorption spectrum with bands at 684 and 1136 nm, which cover the whole visible and near-IR regions up to approximately 1200 nm (Figure 3b). To the best of our knowledge, this large bathochromic shift is, as a monomeric porphyrin, comparable to the largest one reported by Scott and coworkers.[5d] Interestingly, the spectral shapes of the Q-band shape are considerably distorted for symmetry-broken fused porphyrins **9** and **10**, whereas that of the C_2-symmetric **11** restores a typical vibrational structure common to normal porphyrins.

As the very low-energy absorption band for **11** suggested a very small HOMO–LUMO gap, cyclic voltammetric studies were performed in benzonitrile (Table 1). The first oxidation potential ($E_{ox,1}$) and the first reduction potential ($E_{red,1}$) of **6** were positively shifted by introduction of an electron-withdrawing 4-azulenyl group relative to those of Ni^{II}–5,10,15,20-tetrakis(3,5-di-*tert*-butylphenyl)porphyrin (Ni–TDBPP). The separation of $E_{ox,1}$ and $E_{red,1}$ was decreased dramatically for **9** (1.58 V) relative to **6** (2.27 V), and such a decrease was more significant for **10** (1.23 V) and **11** (1.01 V), thus reflecting the increased expanded π-electronic systems.

Table 1: Redox potentials in benzonitrile (versus ferrocene/ferrocenium; in V).

Compound	$E_{ox,1}$	$E_{ox,2}$	$E_{red,1}$	$E_{red,2}$	$E_{ox,1}-E_{red,1}$
6	0.65		−1.62		2.27
9	0.38	0.55	−1.20	−1.58	1.58
10	0.25	0.47	−0.98	−1.27	1.23
11	0.13	0.33	−0.88	−1.05	1.01
Ni–TDBPP	0.61		−1.73		2.34

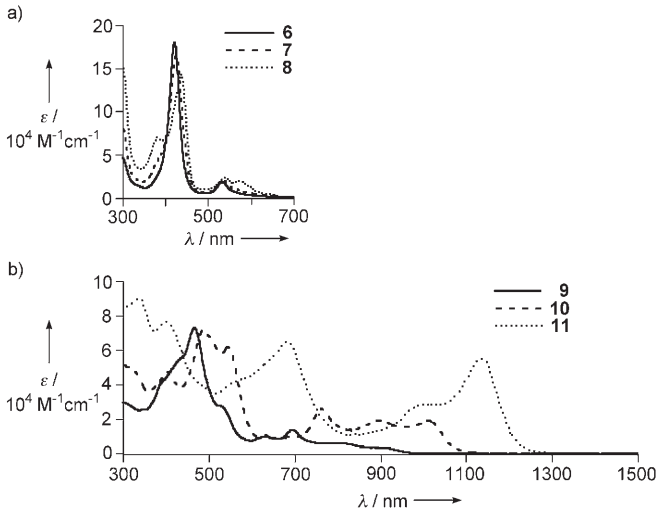

Figure 3. a) UV/Vis absorption spectra of **6**–**8**. b) UV/Vis–near IR absorption spectra of **9**–**11**.

We investigated the excited-state dynamics by transient absorption measurements (see the Supporting Information). The time-resolved spectroscopic investigations revealed that the photoexcited states of **9**–**11** decay biexponentially with fast decay components of 1–2-ps time constants and relatively slow components. The contribution of a long-lived ($\approx$1.4 ns) component to the decay of photoexcited **11** is significant, thus indicating that the porphyrin $^1(\pi,\pi^*)$ state is largely responsible for the deactivation process. On the other hand, the photoexcited dynamics of **9** are very fast, mainly governed by an approximately 1-ps decay component. This feature is attributable to the decay of the (d,d) state, formed by unoccupied d orbitals of the central Ni^{II} in the porphyrin ring, as it has been well established that the (d,d) state acts as a quenching state in the energy relaxation dynamics of photoexcited Ni^{II} porphyrins.[16] The decay of photoexcited **10** shows an intermediate behavior between **9** and **11**, thus suggesting a competition between the $^1(\pi,\pi^*)$ and (d,d) states. In other words, while the low-lying (d,d) state remains at the relatively same energy, the position of the porphyrin-ring $^1(\pi,\pi^*)$ state in energy changes dramatically as the π-conjugation pathway increases from **9** to **11**.

The TPA cross-section values were measured by an open-aperture Z-scan method[17] with wavelength-tunable 130-fs pulses at a 5-kHz repetition rate generated from a femtosecond Ti:sapphire regenerative amplifier system. Pulses of sufficiently high power readily afford the power density enough for the TPA process without tight focusing, which eliminates unwanted nonlinear effects, such as self-focusing and white-light continuum generation. The maximum TPA

 © 2006 Wiley-VCH Verlag GmbH & Co. KGaA, Weinheim

cross section $\sigma^{(2)}$ values are 340 GM at 1200 nm for **1a**, 2050 GM at 1200 nm for **10**, and 7170 GM at 1380 nm for **11**, respectively. In addition, the TPA spectra of **11** in the 1300–1450-nm region indicate that two-photon allowed states should exist near 680–700 nm (see the Supporting Information). In the case of **11**, a highly notable enhancement of the $\sigma^{(2)}$ value in comparison with those of **9** and **10** demonstrates that the expansion of π conjugation by incorporating azulene-fused structures is the overriding factor in increasing the $\sigma^{(2)}$ value. The enlargement of azulene-fused structures gives rise to a very effective π-electron conjugation pathway throughout the porphyrin moiety.[4f]

In summary, the azulene-fused porphyrins, **9**, **10**, and **11** were synthesized through the oxidation of *meso*-(4-azulenyl)-porphyrins **6**, **7**, and **8c**, respectively, with $FeCl_3$. The azulene-fused strategy allowed the realization of highly π-conjugated porphyrinic electronic systems, which are promising TPA pigments.

Received: March 8, 2006
Published online: May 9, 2006

Keywords: azulenes · fused-ring systems · optical properties · porphyrinoids · two-photon absorption

[1] a) M. J. Crossley, P. L. Burn, *J. Chem. Soc. Chem. Commun.* **1987**, 39; b) M. J. Crossley, P. L. Burn, *J. Chem. Soc. Chem. Commun.* **1991**, 1569; c) M. J. Crossley, L. J. Govenlock, J. K. Prashar, *J. Chem. Soc. Chem. Commun.* **1995**, 2379; d) N. Kobayashi, M. Numao, R. Kondo, S. Nakajima, T. Osa, *Inorg. Chem.* **1991**, *30*, 2241; e) L. Jaquinod, O. Siri, R. G. Khoury, K. M. Smith, *Chem. Commun.* **1998**, 1261; f) M. G. H. Vicente, M. T. Cancilla, C. B. Lebrilla, K. M. Smith, *Chem. Commun.* **1998**, 2355; g) M. G. H. Vicente, L. Jaquinod, K. M. Smith, *Chem. Commun.* **1999**, 1771; h) H. L. Anderson, *Chem. Commun.* **1999**, 2323.

[2] a) K. Sugiura, T. Matsumoto, S. Ohkouchi, Y. Naitoh, T. Kawai, Y. Takai, K. Ushiroda, Y. Sakata, *Chem. Commun.* **1999**, 1957; b) A. Tsuda, A. Nakano, H. Furuta, H. Yamochi, A. Osuka, *Angew. Chem.* **2000**, *112*, 572; *Angew. Chem. Int. Ed.* **2000**, *39*, 558; c) A. Tsuda, H. Furuta, A. Osuka, *Angew. Chem.* **2000**, *112*, 2649; *Angew. Chem. Int. Ed.* **2000**, *39*, 2549; d) A. Tsuda, A. Osuka, *Science* **2001**, *293*, 79; e) A. Tsuda, H. Furuta, A. Osuka, *J. Am. Chem. Soc.* **2001**, *123*, 10304; f) A. Tsuda, Y. Nakamura, A. Osuka, *Chem. Commun.* **2003**, 1096.

[3] a) H. Aihara, L. Jaquinod, D. J. Nurco, K. M. Smith, *Angew. Chem.* **2001**, *113*, 3547; *Angew. Chem. Int. Ed.* **2001**, *40*, 3439; b) M. Nath, J. C. Huffman, J. M. Zaleski, *J. Am. Chem. Soc.* **2003**, *125*, 11484; c) K. Tan, L. Jaquinod, R. Paolesse, S. Nardis, C. D. Natale, A. D. Carlo, L. Prodi, M. Montalti, N. Zaccheroni, K. M. Smith, *Tetrahedron* **2004**, *60*, 1099; d) J. D. Spence, T. D. Lash, *J. Org. Chem.* **2000**, *65*, 1530.

[4] a) T. E. O. Screen, J. R. G. Thorne, R. G. Denning, D. G. Bucknall, H. L. Anderson, *J. Am. Chem. Soc.* **2002**, *124*, 9712; b) T. E. O. Screen, J. R. G. Thorne, R. G. Denning, D. G. Bucknal, H. L. Anderson, *J. Mater. Chem.* **2003**, *13*, 2796; c) H. T. Uyeda, Y. Zhao, K. Wostyn, I. Asselberghs, K. Clays, A. Persoons, M. J. Therien, *J. Am. Chem. Soc.* **2002**, *124*, 13806; d) K. Ogawa, A. Ohashi, Y. Kobuke, K. Kamada, K. Ohta, *J. Am. Chem. Soc.* **2003**, *125*, 13356; e) C. Ikeda, Z. S. Yoon, M. Park, H. Inoue, D. Kim, A. Osuka, *J. Am. Chem. Soc.* **2005**, *127*, 534; f) D. Y. Kim, T. K. Ahn, J. H. Kwon, D. Kim, T. Ikeue, N. Aratani, A. Osuka, M. Shigeiwa, S. Maeda, *J. Phys. Chem. A* **2005**, *109*, 2996; g) Y. Inokuma, N. Ono, H. Uno, D. Y. Kim, S. B. Noh, D. Kim, A. Osuka, *Chem. Commun.* **2005**, 3782; h) T. K. Ahn, K. S. Kim, D. Y. Kim, S. B. Noh, N. Aratani, C. Ikeda, A. Osuka, D. Kim, *J. Am. Chem. Soc.* **2006**, *128*, 1700.

[5] a) H. J. Callot, E. Schaetfer, R. Cromer, F. Metz, *Tetrahedron* **1990**, *46*, 5253; b) L. Barloy, D. Dolphin, D. Dupre, T. Wijesekera, *J. Org. Chem.* **1994**, *59*, 7976; c) S. Richeter, C. Jeandon, J.-P. Gisselbrecht, R. Ruppert, H. J. Callot, *J. Am. Chem. Soc.* **2002**, *124*, 6168; d) H. S. Gill, M. Harmjanz, J. Santamaria, I. Finger, M. J. Scott, *Angew. Chem.* **2004**, *116*, 491; *Angew. Chem. Int. Ed.* **2004**, *43*, 485; e) O. Yamane, K. Sugiura, H. Miyasaka, K. Nakamura, T. Fujimoto, K. Nakamura, T. Kaneda, Y. Sakata, M. Yamashita, *Chem. Lett.* **2004**, *33*, 40; f) S. Fox, R. W. Boyle, *Chem. Commun.* **2004**, 1322; g) A. N. Cammidge, P. J. Scaife, G. Berber, D. L. Hughes, *Org. Lett.* **2005**, *7*, 3413; h) D. Shen, C. Liu, Q. Chen, *Chem. Commun.* **2005**, 4982; i) E. Hao, F. R. Fronczek, M. G. H. Vicente, *J. Org. Chem.* **2006**, *71*, 1233.

[6] a) K.-P. Zeller, *Methoden der Organishen Chemie* (Houben-Weyl), *Vol. V/2c* (Ed.: H. Krof), Georg Themie, Stuttgart, **1985**, p. 127; b) R. S. H. Liu, A. E. Asato, *J. Photochem. Photobiol. C* **2003**, *4*, 179; c) azuliporphyrins were reported by S. R. Graham, D. A. Colby, T. D. Lash, *Angew. Chem.* **1997**, *109*, 867; *Angew. Chem. Int. Ed. Engl.* **1997**, *36*, 839; d) D. A. Colby, T. D. Lash, *Chem. Eur. J.* **2002**, *8*, 5397.

[7] K. Kurotobi, A. Osuka, *Org. Lett.* **2005**, *7*, 1055.

[8] U. Siegel, R. Mues, R. Dönig, T. Eicher, M. Blechschmidt, H. Becker, *Phytochemistry* **1992**, *31*, 1671.

[9] M. G. Vetelino, J. W. Coe, *Tetrahedron Lett.* **1994**, *35*, 219.

[10] J. S. Lindsey, I. C. Schreiman, H. C. Hsu, P. C. Kearney, A. M. Marguerettaz, *J. Org. Chem.* **1987**, *52*, 827.

[11] Crystallographic data for [Cu(**6**)]: $C_{76}H_{81}Cl_6CuN_4O_2$, $M_r = 1358.69$, monoclinic, space group $P2_1/n$, $Z = 4$, $a = 19.2311(15)$, $b = 10.0770(8)$, $c = 36.129(3)$ Å, $b = 98.146(2)°$, $V = 6930.8(9)$ Å^3, $D_{calcd} = 1.302$ g cm^{-3}, $T = 90(2)$ K, crystal size $0.70 \times 0.40 \times 0.30$ mm^3, $R = 0.0996$ ($I > 2\sigma(I)$), $Rw = 0.2661$, GOF = 1.044. CCDC-600204 contains the supplementary crystallographic data for this paper. These data can be obtained free of charge from The Cambridge Crystallographic Data Centre via www.ccdc.cam.ac.uk/data_request/cif.

[12] a) A. Osuka, H. Shimidzu, *Angew. Chem.* **1997**, *109*, 93; *Angew. Chem. Int. Ed. Engl.* **1997**, *36*, 135; b) N. Aratani, A. Osuka, Y. H. Kim, D. H. Jeong, D. Kim, *Angew. Chem.* **2000**, *112*, 1517; *Angew. Chem. Int. Ed.* **2000**, *39*, 1458.

[13] M. Müller, C. Kübel, K. Müllen, *Chem. Eur. J.* **1998**, *4*, 2099.

[14] The porphyrins **8b** and **8c** were prepared from **3b** and **3c** and pyrrole in 10 and 12% yields, respectively, by using the methods developed by Lindsey.[10] The formylazulenes **3b** and **3c** were prepared by a similar route using **3a** (see the Supporting Information).

[15] Crystallographic data for **11**: $C_{136}H_{140}N_4NiO_8$, $M_r = 2017.23$, monoclinic, space group $P2_1/c$, $Z = 8$, $a = 26.6423(14)$, $b = 42.798(2)$, $c = 26.3773(14)$ Å, $b = 104.820(2)°$, $V = 29076(3)$ Å^3, $D_{calcd} = 0.922$ g cm^{-3}, $T = 90(2)$ K, crystal size $0.55 \times 0.40 \times 0.35$ mm^3, $R = 0.0888$, $Rw = 0.2465$, GOF = 1.030. CCDC-600205 contains the supplementary crystallographic data for this paper. These data can be obtained free of charge from The Cambridge Crystallographic Data Centre via www.ccdc.cam.ac.uk/data_request/cif. Solvent molecules contained in the lattice were severely disordered and could not be resolved. The program SQUEEZE[18a] in PLATON[18b] was used to remove the solvent density.

[16] D. Kim, C. Kirmaier, D. Holten, *Chem. Phys.* **1983**, *75*, 305.

[17] M. Sheik-Bahae, A. A. Said, T.-H. Wei, D. G. Hagan, E. W. van Stryland, *IEEE J. Quantum Electron.* **1990**, *26*, 760.

[18] a) P. V. Sluis, A. L. Spek, *Acta Crystallogr. Sect. A* **1990**, *46*, 194; b) A. L. Spek, *Acta Crystallogr. Sect. A* **1990**, *46*, c34.

 © 2006 Wiley-VCH Verlag GmbH & Co. KGaA, Weinheim

Silicon Chemistry

DOI: 10.1002/anie.200600647

Synthesis and Characterization of [PhC(N*t*Bu)$_2$]SiCl: A Stable Monomeric Chlorosilylene**

Cheuk-Wai So, Herbert W. Roesky, Jörg Magull, and Rainer B. Oswald*

Dedicated to Professor Karl Otto Christe on the occasion of this 70th birthday

The chemistry of gaseous silicon dichloride has attracted much attention over recent decades owing to its carbene-like properties.[1] Gaseous silicon dichloride can be prepared by the reaction of silicon with silicon tetrachloride at high temperatures; however, it is unstable at room temperature and polymerizes to insoluble perchloropolysilene $(SiCl_2)_n$.[2] Therefore, gaseous silicon dichloride is not suitable for the preparation of chlorosilylene of composition RSiCl. Until now no such compounds have been synthesized and structurally characterized. In contrast, heavier Group 14 metal chlorocarbene analogues are well known and their reactivities have been extensively investigated.[3] Nevertheless, stable silylene complexes $(Me_5C_5)_2Si$[4] and $[(SiMe_3)C(PMe_2)_2]_2Si$,[5] as well as N-heterocyclic silylene compounds,[6] have been isolated and structurally characterized. Herein, we describe the preparation and characterization of a donor-stabilized chlorosilylene complex [PhC(N*t*Bu)$_2$]SiCl.

The reaction of *tert*-butylcarbodiimide (*t*BuN=C=N*t*Bu) with one equivalent of PhLi in Et_2O followed by treatment with $SiCl_4$ afforded [PhC(N*t*Bu)$_2$]$SiCl_3$ (**1**; Scheme 1). Compound **1** was obtained as colorless crystalline solid in 47% yield and its structure confirmed by NMR spectroscopic, EI mass-spectrometric, and elemental analysis. A similar amidinato silicon trichloride [PhC(NSiMe$_3$)$_2$]$SiCl_3$ was synthesized by the reaction of LiN(SiMe$_3$)$_2$ with PhCN and $SiCl_4$.[7]

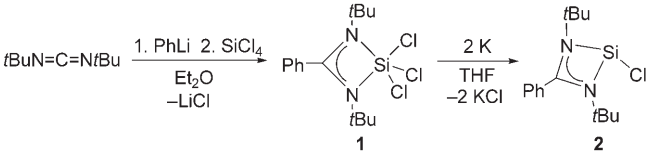

Scheme 1. Synthesis of **2**.

Treatment of **1** with two equivalents of potassium in THF for 17 h afforded the novel monomeric chlorosilylene [PhC(N*t*Bu)$_2$]SiCl (**2**) in 10% yield. Compound **2** is the first example of a system stable at room temperature that contains a Si^{II}–Cl bond. The coordination number of the silicon atom in **2** is comparable to that in $(Me_5C_5)_2Si$[4] and $[(SiMe_3)C(PMe_2)_2]_2Si$.[5] It is suggested that **2** is stabilized kinetically by the sterically hindered amidinate ligand. Similar amidinato complexes of heavier Group 14 metal carbene analogues, such as [MeC(NC$_6$H$_{11}$)$_2$][N(SiMe$_3$)$_2$]Ge,[8] [*p*-PhC$_6$H$_4$C(NSiMe$_3$)$_2$]$_2$Sn,[9] and [MeC(NSiMe$_3$)$_2$]$_2$Pb[9] have been reported.

Compound **2** was isolated as a colorless crystalline solid with good solubility in solvents such as diethyl ether, toluene, and THF; furthermore, it is stable in solution or the solid state at room temperature in an inert atmosphere. It has been characterized by elemental analysis, spectroscopic methods, and X-ray studies. The ^{1}H and ^{13}C NMR spectra of **2** displayed one set of resonances that result from the amidinate ligand. The resonances show an upfield shift relative to those of **1**. The shift is probably due to the lower oxidation state of the silicon center in **2**. The ^{29}Si NMR spectrum of **2** exhibits one singlet ($\delta = 14.6$ ppm), which lies between two-coordinate silicon in Si[N(*t*Bu)CHCHN(*t*Bu)] ($\delta = 78.3$ ppm) and four-coordinate silicon in Si[N(*t*Bu)CHCHN(*t*Bu)]Cl_2 ($\delta = -40.7$ ppm).[6a] Moreover, it shows a downfield shift relative to that of five-coordinate silicon in **1** ($\delta = -98.6$ ppm).

The molecular structure of **2** with an atom-numbering scheme is shown in Figure 1. Compound **2** is the first example of a monomeric heteroleptic silylene.[10] The amidinate ligand is bonded in a *N*,*N*′-chelate fashion to the silicon center and

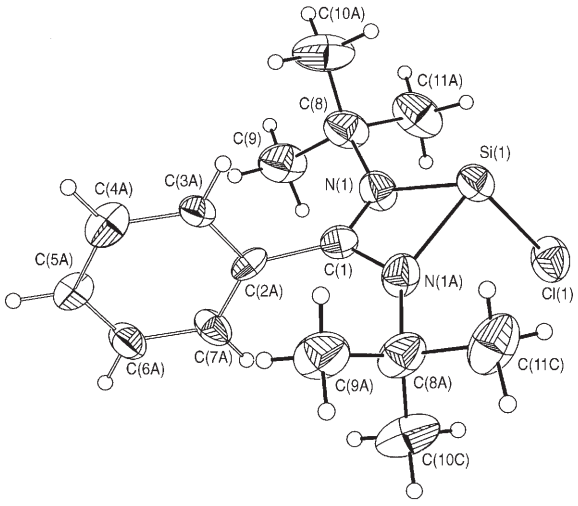

Figure 1. Molecular structure of **2**. Selected bond lengths [Å] and angles [°]: N(1)-Si(1) 1.870(2), N(1A)-Si(1) 1.917(2), Si(1)-Cl(1) 2.156(1), N(1)-C(1) 1.333(2), N(1A)-C(1) 1.333(2); N(1)-Si(1)-N(1A) 68.35(8), N(1)-Si(1)-Cl(1) 95.82(6), N(1A)-Si(1)-Cl(1) 96.56(6), C(1)-N(1)-Si(1) 91.86(10), N(1)-C(1)-N(1A) 105.94(18).

[*] Dr. C.-W. So, Prof. Dr. H. W. Roesky, Prof. Dr. J. Magull
Institut für Anorganische Chemie
Universität Göttingen
Tammannstrasse 4, 37077 Göttingen (Germany)
Fax: (+49) 551-393-373
E-mail: hroesky@gwdg.de
Dr. R. B. Oswald
Institut für Physikalische Chemie
Universität Göttingen
Tammannstrasse 6, 37077 Göttingen (Germany)

[**] This work was supported by the Göttinger Akademie der Wissenschaften. C.-W.S. thanks the Alexander von Humboldt Stiftung for a research fellowship.

Supporting information for this article is available on the WWW under http://www.angewandte.org or from the author.

InterScience
© 2006 Wiley-VCH Verlag GmbH & Co. KGaA, Weinheim

displays a trigonal pyramidal geometry. The sum of the bond angles at the silicon center is 260.73°, which is significantly smaller than that of 330.0° in the tetra-coordinated silylene $[(SiMe_3)C(PMe_2)_2]_2Si$.[5] This geometry is consistent with a stereoactive lone pair at the silicon center. The four-membered Si(1)-N(1)-C(1)-N(1A) ring is planar, and the phenyl group is orthogonally arranged to this plane. The Si(1)–Cl(1) bond length (2.156(1) Å) is in good agreement with the electron-diffraction data of gaseous silicon dichloride (2.083 Å).[11] The Si^{II}–Cl bond length in **2** is also similar to that in $(SiCl_2)_n$ (2.120(9) and 2.088(9) Å).[12] The C–N bond lengths in **2** (C(1)–N(1): 1.333(2) Å; C(1)–N(1A): 1.333(2) Å) are the same and are approximately intermediate between the C–N double and C–N(sp^2) single bond lengths. This geometry shows considerable delocalization throughout the NCN backbone of the ligand. The N(1)-Si(1)-N(1A) angle (68.35(8)°) in **2** is comparable to that in $[MeC(NiPr)_2]_2SiCl_2$ (68.8(1) and 69.0(1)°).[13] The Si(1)–N(1) bond length (1.870(2) Å) is slightly longer than the Si–N_{amide} bond length in a silicon(IV) complex $(C_5H_3N$-6-Me-2-$NSiMe_3)SiCl_3$ (1.753(5) Å).[14]

According to the crystallographic data, there is a complicated binding situation among the four-membered Si(1)-N(1)-C(1)-N(1A) ring, silicon center, and the chlorine atom. Compound **2** was investigated by means of quantum chemical calculations. The molecule was first fully optimized with the DFT-variant B3L YP[15] as implemented in the Gaussian G03[16] program suite employing a basis set including diffuse and polarization functions termed 6-31 + G(2pd,3df).[17] The calculated structural parameters (C(1)-N(1A): 1.339 Å; C(1)-N(1): 1.339 Å; N(1A)-Si(1): 1.893 Å; N(1)-Si(1): 1.893 Å; C(1)-N(1A)-Si(1): 91.59°; N(1A)-Si(1)-N(1): 68.95°; C(8 A)-N(1A)-Si(1): 134.22°; N(1A)-Si(1)-Cl(1): 100.09°) are in good agreement with the crystallographic data. The natural-bond-orbital (NBO)[18] analysis shows that the C(1)–N(1) bond is formed by $sp^{1.59}$ hybrids on the nitrogen centers and $sp^{3.89}$ hybrids on the carbon atom, with the nitrogen atoms contributing 63% of the electronic density. The situation for the Si–N bonds is completely different because the nitrogen atom contributes 85% to the bond, with an orbital having s character, and the silicon atom contributes to this bond with a pure p orbital. The highly acute bond angle is a direct result of this s–p-orbital overlapping. The Si–Cl bond is made up of a nearly pure p orbital on the silicon atom and a p-rich hybrid on the chlorine atom. The dominant p character of the orbitals involved in these bonds gives the possibility for a strongly delocalized situation as shown in Figure 2.

In summary, a novel monomeric chlorosilylene complex has been prepared and fully characterized. Compound **2** can serve as functionalized silylene in metathesis reactions, thus possibly leading to a new era in silicon(II) chemistry. Moreover, the corresponding RCCl compound is not known so far.

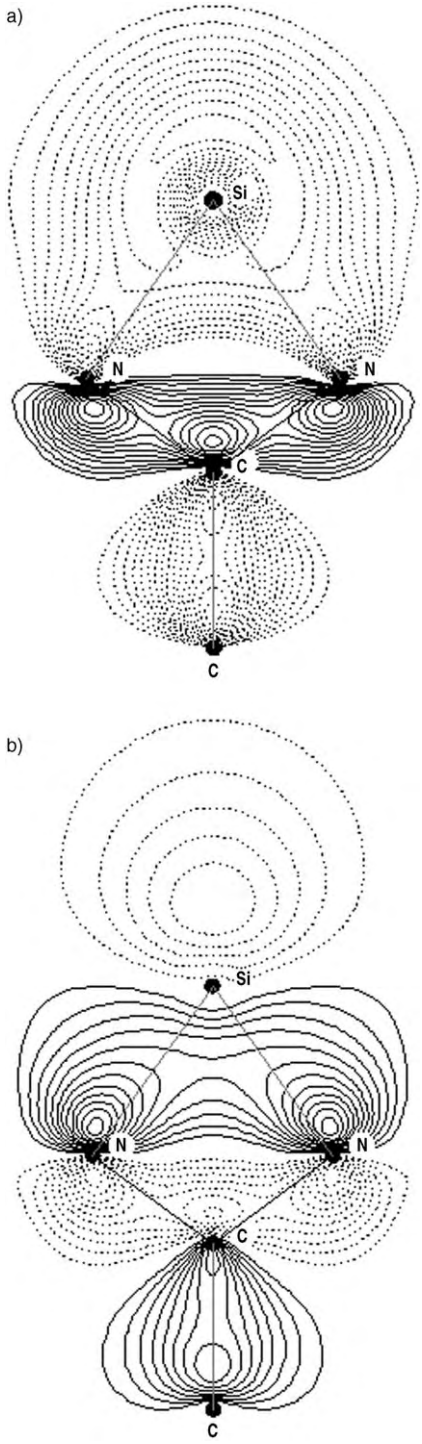

Figure 2. Contour level plots of two binding molecular orbitals (a, b) with different line styles that represent the phase of wave function. For clarity, the remaining atoms have been omitted.

Experimental Section

All manipulations were carried out in an inert atmosphere of dinitrogen using standard Schlenk techniques and in a dinitrogen filled glove box.

1: PhLi (7.2 mL, 13.0 mmol, 1.8 M in cyclohexane/Et_2O (7:3)) was added to a solution of *t*BuN=C=N*t*Bu (2.5 mL, 13.0 mmol) in Et_2O (80 mL) at −78 °C. The solution was raised to ambient temperature and stirred for 1 h. $SiCl_4$ (1.6 mL, 14.0 mmol) was added to this solution at −78 °C. The resulting yellow suspension was stirred overnight at ambient temperature. The precipitate was filtered, and the filtrate was concentrated under reduced pressure until colorless crystals of **1** (2.23 g, 47.0%) were obtained. M.p. 178 °C; elemental

 © 2006 Wiley-VCH Verlag GmbH & Co. KGaA, Weinheim

analysis (%) calcd for $C_{15}H_{23}Cl_3N_2Si$: C 49.24, H 6.34, N 7.66; found: C 49.07, H 6.14, N 7.61; ^{1}H NMR (200 MHz, C_6D_6, 25 °C): $\delta = 1.17$ (s, 18H, *t*Bu), 6.68–6.85 ppm (m, 5H, Ph); $^{13}C\{^1H\}$ NMR (126 MHz, C_6D_6, 25 °C): $\delta = 31.7$ (CMe_3), 56.5 (CMe_3), 127.9, 128.1, 128.2, 128.5, 130.2, 131.9 (Ph), 171.9 ppm (NCN); $^{29}Si\{^1H\}$ NMR (99 MHz, C_6D_6, 25 °C): $\delta = -98.6$ ppm; EI MS: *m*/*z*: 366 [M^+], 329 [M^+−Cl].

2: THF (80 mL) was added to a mixture of **1** (1.98 g, 5.41 mmol) and finely divided potassium (0.43 g, 11.0 mmol) at ambient temperature. The resulting red mixture was stirred for 17 h. The solvent was then removed in vacuo, and the residue was extracted with toluene (50 mL). The insoluble precipitate was filtered off, and the red filtrate was concentrated to yield colorless crystals of **2** (0.16 g, 10.0 %). M.p. 159 °C; elemental analysis (%) calcd for $C_{15}H_{23}ClN_2Si$: C 61.10, H 7.87, N 9.51; C 60.95, H 7.64, N 9.35; ^{1}H NMR (300 MHz, C_6D_6, 25 °C): $\delta = 1.08$ (s, 18H, *t*Bu), 6.78–7.05 ppm (m, 5H, Ph); $^{13}C\{^1H\}$ NMR (75 MHz, C_6D_6, 25 °C): $\delta = 31.4$ (CMe_3), 53.7 (CMe_3), 127.4, 127.9, 128.4, 129.8, 133.0 (Ph), 166.7 ppm (NCN); $^{29}Si\{^1H\}$ NMR (60 MHz, C_6D_6, 25 °C): $\delta = 14.6$; EI-MS: *m*/*z*: 295 [M^+], 231 [M^+−Si−Cl].

Received: February 17, 2006
Published online: May 3, 2006

Keywords: carbene homologues · halides · N ligands · silicon · silylenes

[1] a) P. L. Timms, *Acc. Chem. Res.* **1973**, *6*, 118–123; b) P. L. Timms, *Inorg. Chem.* **1968**, *7*, 387–389.
[2] M. Schmeisser, P. Voss, *Z. Anorg. Allg. Chem.* **1964**, *334*, 50–56.
[3] a) Y. Ding, Q. Ma, H. W. Roesky, R. Herbst-Irmer, I. Usón, M. Noltemeyer, H.-G. Schmidt, *Organometallics* **2002**, *21*, 5216–5220; b) Y. Ding, H. Hao, H. W. Roesky, M. Noltemeyer, H.-G. Schmidt, *Organometallics* **2001**, *20*, 4806–4811; c) Y. Ding, H. W. Roesky, M. Noltemeyer, H.-G. Schmidt, P. P. Power, *Organometallics* **2001**, *20*, 1190–1194; d) L. W. Pineda, V. Jancik, H. W. Roesky, D. Neculai, A. M. Neculai, *Angew. Chem.* **2004**, *116*, 1443–1445; *Angew. Chem. Int. Ed.* **2004**, *43*, 1419–1421; e) Y. Ding, Q. Ma, I. Usón, H. W. Roesky, M. Noltemeyer, H.-G. Schmidt, *J. Am. Chem. Soc.* **2002**, *124*, 8542–8543; f) W.-P. Leung, C.-W. So, Y.-S. Wu, H.-W. Li, T. C. W. Mak, *Eur. J. Inorg. Chem.* **2005**, 513–521; g) P. B. Hitchcock, M. F. Lappert, M. Layh, *Inorg. Chim. Acta* **1998**, *269*, 181–190; h) I. Saur, G. Rima, K. Miqueu, H. Gornitzka, J. Barrau, *J. Organomet. Chem.* **2003**, *672*, 77–85; i) A. Akkari, J. J. Byrne, I. Saur, G. Rima, H. Gornitzka, J. Barrau, *J. Organomet. Chem.* **2001**, *622*, 190–198; j) J. Barrau, G. Rima, T. El-Amraoui, *J. Organomet. Chem.* **1998**, *561*, 167–174; k) L. Pu, M. M. Olmstead, P. P. Power, B. Schiemenz, *Organometallics* **1998**, *17*, 5602–5606; l) L. Pu, B. Twamley, P. P. Power, *Organometallics* **2000**, *19*, 2874–2881; m) L. Pu, A. D. Philips, A. F. Richards, M. Stender, R. S. Simons, M. M. Olmstead, P. P. Power, *J. Am. Chem. Soc.* **2003**, *125*, 11626–11636; n) B. E. Eichler, P. P. Power, *J. Am. Chem. Soc.* **2000**, *122*, 8785–8786; o) L. Pu, B. Twamley, P. P. Power, *J. Am. Chem. Soc.* **2000**, *122*, 3524–3525; p) C. Stanciu, S. S. Hino, M. Stender, A. F. Richards, M. M. Olmstead, P. P. Power, *Inorg. Chem.* **2005**, *44*, 2774–2780; q) H. V. R. Dias, Z. Wang, *J. Am. Chem. Soc.* **1997**, *119*, 4650–4655; r) A. E. Ayers, D. S. Marynick, H. V. R. Dias, *Inorg. Chem.* **2000**, *39*, 4147–4151.
[4] P. Jutzi, D. Kanne, C. Krüger, *Angew. Chem.* **1986**, *98*, 163–164; *Angew. Chem. Int. Ed. Engl.* **1986**, *25*, 164.
[5] H. H. Karsch, U. Keller, S. Gamper, G. Müller, *Angew. Chem.* **1990**, *102*, 297–298; *Angew. Chem. Int. Ed. Engl.* **1990**, *29*, 295–296.
[6] a) M. Denk, R. Lennon, R. Hayashi, R. West, A. V. Belyakov, H. P. Verne, A. Haaland, M. Wagner, N. Metzler, *J. Am. Chem. Soc.* **1994**, *116*, 2691–2692; b) B. Gehrhus, M. F. Lappert, J. Heinicke, R. Boese, D. Bläser, *J. Chem. Soc. Chem. Commun.* **1995**, 1931–1932; c) J. Heinicke, A. Oprea, M. K. Kindermann, T. Karpati, L. Nyulászi, T. Veszprémi, *Chem. Eur. J.* **1998**, *4*, 541–545.
[7] H. W. Roesky, B. Meller, M. Noltemeyer, H.-G. Schmidt, U. Scholz, G. M. Sheldrick, *Chem. Ber.* **1988**, *121*, 1403–1406.
[8] S. R. Foley, C. Bensimon, D. S. Richeson, *J. Am. Chem. Soc.* **1997**, *119*, 10359–10363.
[9] U. Kilimann, M. Noltemeyer, F. T. Edelmann, *J. Organomet. Chem.* **1993**, *443*, 35–42.
[10] Crystal data for **2** ($C_{15}H_{23}ClN_2Si$): $M_r = 294.89$; $a = 14.2675(11)$, $b = 10.8409(11)$, $c = 11.9518(9)$ Å; $\alpha = 90$, $\beta = 114.926(5)$, $\gamma = 90°$; $V = 1676.4(2)$ Å^3; $Z = 4$; space group *C*2/*c* (monoclinic); $T = 133(2)$ K; $\lambda = 0.71073$ Å; $\mu = 0.290$ mm^{-1}; $\rho_{calc} = 1.168$ g cm^{-3}; $2\theta_{max} = 24.74°$; $F(000) = 632$; 8610 measured reflections, 1416 independent and 1253 observed reflections ($I > 2\sigma(I)$); $R1 = 0.0382$, $wR2 = 0.1020$; largest diff. peak and hole 0.242/−0.158 e Å^{-3}. The crystal data were collected on a Stoe Image Plate IPDS II System. The structure was solved by direct phase determination (SHELXS-97)[19] and refined for all data by full-matrix least squares methods on F^2. All non-hydrogen atoms were subjected to anisotropic refinement. The hydrogen atoms were generated geometrically and allowed to ride on their respective parent atoms; they were assigned appropriate isotopic thermal parameters and included in the structure-factor calculations. CCDC-297194 contains the supplementary crystallographic data for this paper. These data can be obtained free of charge from The Cambridge Crystallographic Data Centre via www.ccdc.cam.ac.uk/data_request/cif.
[11] I. Hargittai, G. Schultz, J. Tremmel, N. D. Kagramanov, A. K. Maltsev, O. M. Nefedov, *J. Am. Chem. Soc.* **1983**, *105*, 2895–2896.
[12] J. R. Koe, D. R. Powell, J. J. Buffy, S. Hayase, R. West, *Angew. Chem.* **1998**, *110*, 1514–1515; *Angew. Chem. Int. Ed.* **1998**, *37*, 1441–1442.
[13] H. H. Karsch, P. A. Schlüter, M. Reisky, *Eur. J. Inorg. Chem.* **1998**, 433–436.
[14] C. Jones, P. C. Junk, S. G. Leary, N. A. Smithies, J. W. Steed, *Inorg. Chem. Commun.* **2002**, *5*, 533–536.
[15] a) C. Lee, W. Yang, R. G. Parr, *Phys. Rev. B* **1988**, *37*, 785–789; b) B. Miehlich, A. Savin, H. Stoll, H. Preuss, *Chem. Phys. Lett.* **1989**, *157*, 200–206.
[16] Gaussian 03, Revision C.02, M. J. Frisch et al.; see the Supporting Information.
[17] a) R. Ditchfield, W. J. Hehre, J. A. Pople, *J. Chem. Phys.* **1971**, *54*, 724–728; b) P. C. Hariharan, J. A. Pople, *Theo. Chim. Acta* **1973**, *28*, 213–218; c) V. A. Rassolov, M. A. Ratner, J. A. Pople, P. C. Redfern, L. A. Curtiss, *J. Comput. Chem.* **2001**, *22*, 976–984.
[18] a) J. P. Foster, F. Weinhold, *J. Am. Chem. Soc.* **1980**, *102*, 7211–7218; b) A. E. Reed, F. Weinhold, *J. Chem. Phys.* **1985**, *83*, 1736–1740; c) A. E. Reed, L. A. Curtiss, F. Weinhold, *Chem. Rev.* **1988**, *88*, 899–926.
[19] G. M. Sheldrick, *SHELXS-97*, Program for Crystal Structure Refinement, University of Göttingen, Göttingen, Germany, **1997**.

 © 2006 Wiley-VCH Verlag GmbH & Co. KGaA, Weinheim

Natural Products

DOI: 10.1002/anie.200600593

Modular Asymmetric Synthesis of Aigialomycin D, a Kinase-Inhibitory Scaffold**

*Sofia Barluenga, Pierre-Yves Dakas, Yoan Ferandin, Laurent Meijer, and Nicolas Winssinger**

Dedicated to K. C. Nicolaou on the occasion of his 60th birthday

Aigialomycin D (**1**) was isolated[1] together with the known hypothemycin[2,3] (**2**) from the mangrove fungus *Aigialus*

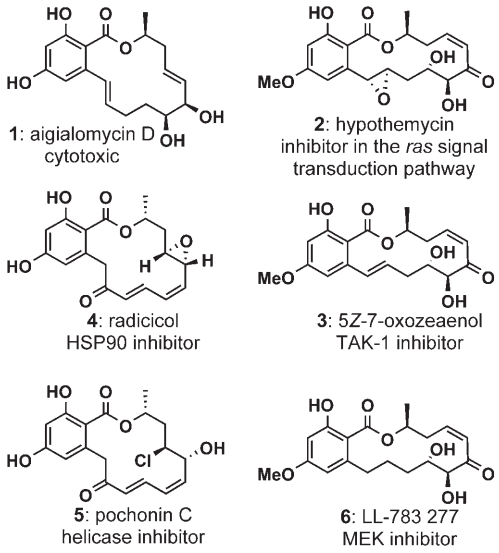

parvus in Thailand. Both these natural products were found to be low-concentration (μM) inhibitors of the malaria parasite *Plasmodium falciparum* and are also cytotoxic. An elegant synthesis of aigialomycin D was reported by Danishefsky and co-workers utilizing a late-stage Diels–Alder reaction to build the aromatic ring.[4] Our interest in the resorcyclides[5–8] comes from the observation that there are several potent kinase inhibitors amongst this relatively small class of natural products.[9] Indeed, 5*Z*-7-oxozeaenol (**3**) is an inhibitor of TAK-1,[10] structurally related LL-783277 (**6**) is a MEK inhibitor,[11] and hypothemycin has been reported to inhibit the *ras* signaling pathway.[12] Structurally related radicicol (**4**) and pochonin C (**5**), on the other hand, do not inhibit a specific kinase but rather a specific ATPase (HSP90[13] and HSV-helicase,[14] respectively). Despite the lack of structural similarity between radicicol and ATP, radicicol was found to bind to the ATP-binding site of HSP90.[15]

The high potential to find new ATPase or kinase inhibitors amongst this class of natural products[16,17] coupled to the interest in inhibitions of these two enzyme classes from a therapeutic as well as a chemical genomic perspective[18,19] led us to seek a modular diversity-oriented synthesis amenable to preparation of libraries extending beyond the naturally available compounds. The retrosynthetic disconnections are shown in Scheme 1. A key point is the use of the

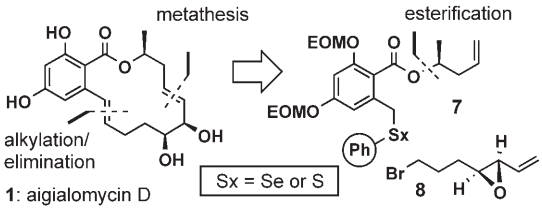

Scheme 1. Retrosynthetic analysis. EOM = ethoxymethyl.

thio- or selenoether at the benzylic position (see **7**) which should facilitate alkylation chemistry and provide a potential attachment point for immobilization. The macrocycle would be formed by a metathesis reaction, and the diol moiety was anticipated to originate from *trans* epoxide **8**, which can be obtained by Sharpless asymmetric epoxidation. The key intermediate **8** was prepared in four steps from commercially available products (Scheme 2). Thus, cross-metathesis of 5-bromopentene (**9**) with unprotected 1,4-butenediol in the presence of the second-generation Hoveyda–Grubbs catalyst[20] afforded the allylic alcohol **10** in excellent yield and *E*/*Z* ratio (>25:1). This is a convenient alternative to the conventional sequence involving formation of an aldehyde, Horner–Wadsworth–Emmons olefination, and reduction with DIBAL to *trans* allylic alcohols.[21,22] Sharpless epoxidation of allylic alcohol **10** followed by oxidation with SO_3·py and Wittig olefination afforded the epoxide **8** in 62% overall yield. The epoxide could be converted into the protected diol **11** by $Sc(OTf)_3$-catalyzed opening of the epoxide[6] followed by protection with an acetonide group.

The aromatic portion **7** was obtained through a three-step sequence starting with Mitsunobu esterification[5,23] of the unprotected benzoic acid **12** followed by protection of both phenol groups (Scheme 3). The selenide was introduced at the benzylic position by deprotonation with LDA followed by addition of diphenyldiselenide (59% yield over three steps). Compound **7** was efficiently alkylated with either bromide **8** or **11** to yield the metathesis precursor **13** and **14**, respectively.

[*] Dr. S. Barluenga, P.-Y. Dakas, Prof. N. Winssinger
Institut de Science et Ingénierie Supramoléculaires
Université Louis Pasteur
8 allée Gaspard Monge, 67000 Strasbourg (France)
Fax: (+33) 3-9024-5112
E-mail: winssinger@isis.u-strasbg.fr
Y. Ferandin, Dr. L. Meijer
C.N.R.S., UMR7150 & UPS2682, Station Biologique
Place G. Teissier, B.P. 74, 29682 Roscoff cedex (France)

[**] This project was partly supported by grants from the ARC (3683 to N.W.), the EEC (FP6-2002-Life Sciences & Health, PRO-KINASE Research Project to L.M. and MIRG-CT-2004-505317 to N.W.), and the Human Frontier Science Program (HFSP 0080/2003 to N.W.). A MENRT fellowship (P.-Y.D.) is also gratefully acknowledged. The authors thank Niels Reichardt for preliminary work on this project.

Supporting information for this article is available on the WWW under http://www.angewandte.org or from the author.

© 2006 Wiley-VCH Verlag GmbH & Co. KGaA, Weinheim

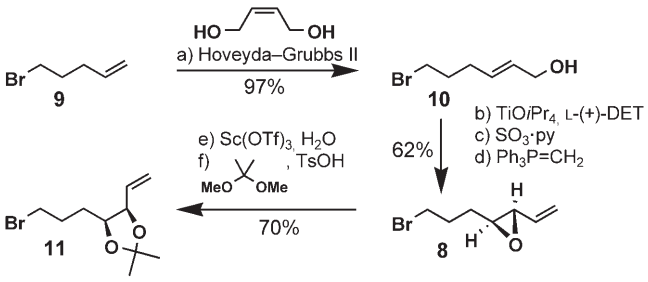

Scheme 2. Synthesis of key intermediates **8** and **11**. a) **9** (1.0 equiv), 2-buten-1,4-diol (2.0 equiv), Hoveyda–Grubbs catalyst II (0.01 equiv), CH_2Cl_2, 23 °C, 4 h, 97%; b) L-(+) diethyl tartrate (0.12 equiv), Ti(O*i*Pr)$_4$ (0.1 equiv), *t*BuOOH (1.52 equiv), CH_2Cl_2, −40 °C, 30 min; then, **10** (1.0 equiv), −24 °C, 12 h, 85%; c) SO_3·py (3.47 equiv), CH_2Cl_2/DMSO, 0 °C, 30 min; d) $Ph_3P{=}CH_2$ (1.8 equiv), THF, −10 °C, 10 min, 70% over two steps; e) Sc(OTf)$_3$ (0.2 equiv), THF/H_2O (10:1), 23 °C, 2.5 h, 100%; f) dimethoxypropane (10 equiv), TsOH·H_2O (0.05 equiv), CH_2Cl_2, 23 °C, 12 h, 70%. Grubbs–Hoveyda catalyst II = 1,3-(bis-(mesityl)-2-imidazolidinylidene)dichloro-(*o*-isopropoxyphenylmethylene)ruthenium; DET = diethyl tartrate; Tf = trifluoromethanesulfonyl; Ts = *p*-toluenesulfonyl.

Treatment of **14** with second-generation Grubbs catalyst[24,25] under equilibrating conditions[26] (80 °C for 12 h) afforded the macrocycle with $E/Z > 10{:}1$. This macrocycle was then treated with H_2O_2 to oxidize and eliminate the selenide, thus affording compound **15** in 77% overall yield. Interestingly, inversing the sequence of reaction (oxidation/elimination of the selenide followed by the metathesis on the triene) gave rise to a significant amount of the undesired six-membered ring product from the cyclization with the benzylic alkene. Global deprotection of the acetonide and EOM groups afforded aigialomycin D (**1**)[27] in a total of 10 steps and 21% overall yield. When the diol was masked as an epoxide, macrocycle **16** was obtained in excellent yield starting from diene **13** through the same sequence (RCM, selenide oxidation/elimination). Interestingly, in this case, the order of reaction could be inversed without observing the competing ring-closure corresponding to the six-membered ring (the geometry of the *trans* epoxide favors macrocyclization). However, Lewis or protic acid ($ScOTf_3$, TsOH, TFA, HFIP) mediated opening of the epoxide failed to yield the desired 1,2-*cis*-diol and led in all cases to an S_N2' opening to afford **17a** or **18a**. Although the epoxide **16** could not be converted into aigialomycin D, this diverging reaction pathway proved to be quite general and could be carried out with different nucleophiles such as NaN_3 or KCN to obtain **17b** and **c**, respectively. Deprotection of the EOM ethers (PS-SO_3H, MeOH) from **17a–c** or concomitant epoxide opening/deprotection with different alcohols (MeOH, EtOH, *i*PrOH) in the presence of sulfonic acid resin from **16** afforded aigialomycin analogues **18a–f**.

In the interest of streamlining the synthesis, the phenyl selenide was replaced by a polymer-bound thioether. The required thiol resin was prepared in a similar fashion as previously reported[28] from 3-hydroxythiophenol rather than 4-hydroxyphenol to avoid the deactivating effect of a *para*-phenol (Scheme 4). The chemistry leading to aigialomycin was found to be equally efficient on solid phase as in solution.

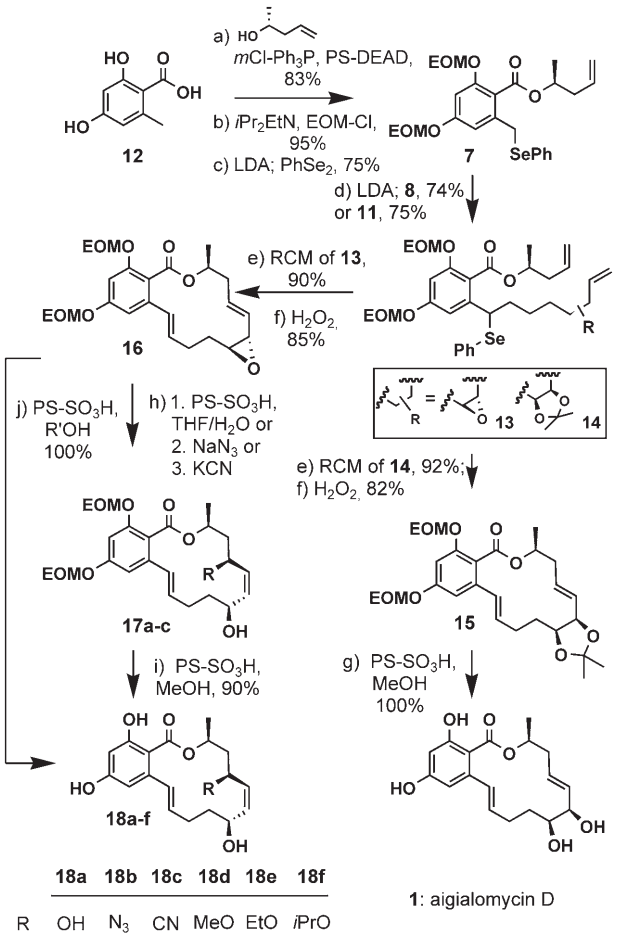

Scheme 3. Total synthesis of aigialomycin D (**1**) and divergent synthetic pathways. a) PS-DEAD (2.5 equiv, 1.3 mmol g^{-1}), (*R*)-(+)-penten-2-ol (1.0 equiv), *m*-ClPh_3P (2.0 equiv), CH_2Cl_2, 23 °C, 0.5 h, 83%; b) *i*Pr_2EtN (4.0 equiv), EOMCl (4.0 equiv), TBAI (cat.), DMF, 80 °C, 5 h, 95%; c) LDA (2.0 equiv), THF, −78 °C; then $(PhSe)_2$ (0.9 equiv), 2 h, 75%; d) LDA (2.0 equiv), **8** or **11** (1.0 equiv), THF/HMPA (10:1), −78 °C, 20 min, 74% (**8**) and 75% (**11**); e) Grubbs II catalyst (0.05 equiv), toluene, 80 °C, 12 h, 90% (from **13**) and 92% (from **14**); f) H_2O_2 (2.0 equiv), THF, 23 °C, 3 h, 82% (**15**) and 85% (**16**); g) PS-SO_3H (9.0 equiv, 3.2 mmol g^{-1}), MeOH, 50 °C, 2 h, quant.; h) 1. PS-SO_3H (10.0 equiv, 2.9 mmol g^{-1}), THF/H_2O (1:1); 45 °C, 16 h, quant.; or 2. NaN_3 (5 equiv), PS-SO_3H (0.1 equiv, 2.9 mmol g^{-1}), DMF, 65 °C, 12 h, 83%; or 3. KCN (5 equiv), PS-SO_3H (0.1 equiv, 2.9 mmol g^{-1}), DMF, 65 °C, 12 h, 89%; i) PS-SO_3H (10.0 equiv, 2.9 mmol g^{-1}), MeOH, 45 °C, 3 h, >90%; j) PS-SO_3H (10.0 equiv, 2.9 mmol g^{-1}), R'OH, 45 °C, 3 h, quant. PS = polymer-supported; DEAD = diethyl azodicarboxylate; TBAI = tetrabutylammonium iodide; DMF = *N*,*N*-dimethylformamide; LDA = lithium diisopropylamide; HMPA = hexamethylphosphoramide.

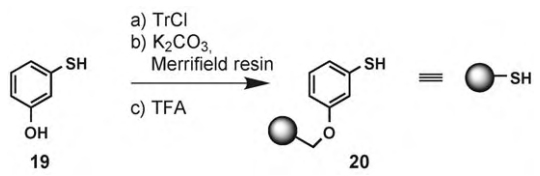

Scheme 4. Conversion of Merrifield resin into a thiophenol resin (**20**). a) TrCl (1.0 equiv), pyridine (1.0 equiv), CH_2Cl_2, 23 °C, 12 h, 100%; b) K_2CO_3 (2.0 equiv), PS-CH_2Cl (1.0 equiv), DMF, 50 °C, 12 h, 100%; c) TFA/CH_2Cl_2/Et_3SiH (9:10:1), 23 °C, 1 h, 100%. Tr = triphenylmethyl; TFA = trifluoroacetic acid.

 © 2006 Wiley-VCH Verlag GmbH & Co. KGaA, Weinheim

Unprotected ester **21**[29] was loaded onto a thiophenol resin **20**, and the phenols were protected as EOM ethers (Scheme 5). Alkylation of the polymer-bound thioether with a variety of alkyl bromides yielded the desired metathesis precursors **23a–e**. Interestingly, initial attempts to carry out the ring-closing metathesis under the conditions successfully used in solution failed. However, excellent yields were attained in CH_2Cl_2 solvent at 120 °C using microwave irradiation for 75 min. As the catalyst is short-lived at that temperature, it was added in three portions of 6 mol%. Notably, oligomer products were not observed under these conditions (the loading was calculated to be 0.33 mmol g^{-1}).

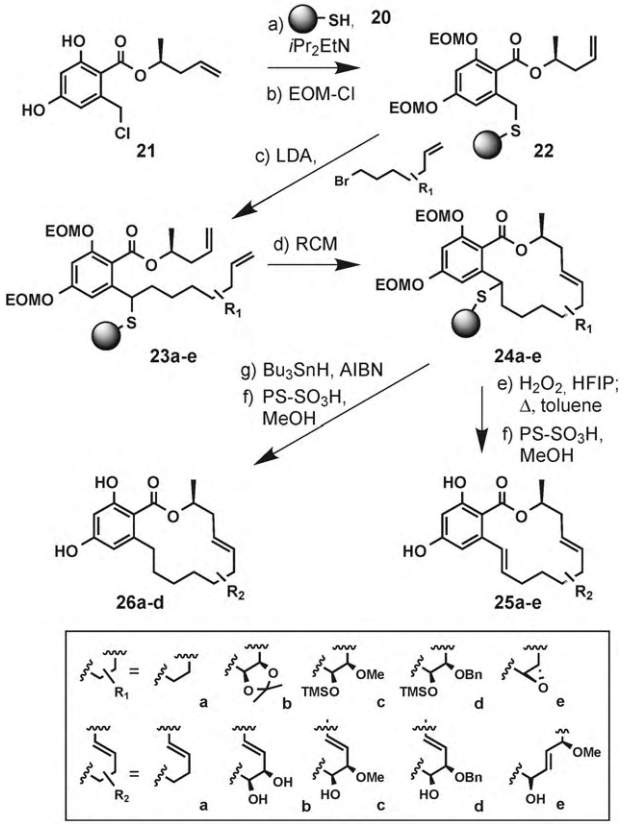

Scheme 5. Diversity-oriented synthesis of aigialomycin D (**1**) and analogues. a) PS-SH (1.0 equiv, 0.6–0.8 mmol g^{-1}), **21** (1.1 equiv), *i*Pr_2EtN (1.0 equiv), DMF, 60 °C, 12 h, 82% (by mass gain considering 0.8 mmol g^{-1} for PS-SH); b) DBU (4.0 equiv), EOMCl (4.0 equiv), TBAI (cat.), DMF, 23 °C, 12 h, ≈96% (by mass gain considering 0.8 mmol g^{-1} for PS-SH); 80% over two steps (by radical cleavage, AIBN (cat), *n*Bu_3SnH (5.0 equiv), toluene, 150 °C, microwave, 10 min); c) LDA (6.0 equiv), R^1Br (2.0 equiv), THF/HMPA (10:1), −78 °C, 20 min, ≈quant. (by radical cleavage (AIBN (cat.), Bu_3SnH (5.0 equiv), toluene, 150 °C, microwave, 10 min) and by oxidation/elimination (H_2O_2 (4.0 equiv), CH_2Cl_2/HFIP (1:1), 23 °C, 12 h; then toluene, 80 °C, 3 h); d) Grubbs II catalyst (3×0.06 equiv), CH_2Cl_2, 120 °C, microwave, 25 min, 100% (by radical cleavage, AIBN (cat.), Bu_3SnH (5.0 equiv), toluene, 150 °C, microwave, 10 min); e) H_2O_2 (4.0 equiv), CH_2Cl_2/HFIP (1:1), 23 °C, 12 h; then toluene, 80 °C, 3 h, >90%; f) PS-SO_3H (10.0 equiv, 2.9 mmol g^{-1}), MeOH, 45 °C, 3 h, >90%; g) AIBN (cat), Bu_3SnH (5.0 equiv), toluene, 150 °C, microwave, 10 min; >98%. DBU = 1,8-diazabicyclo[5.4.0]undec-7-ene; TBAI = tetrabutylammonium iodide; AIBN = 2,2′-azobisisobutyronitrile; HFIP = hexafluoropropanol.

The compounds were released from the resin by using both an oxidation (H_2O_2, HFIP)[30]/elimination and free-radical cleavages (Bu_3SnH, AIBN) followed by global deprotection with sulfonic acid resin to obtain aigialomycin D (**25b**) and its analogues **25a**,**c–e** as well as dihydroaigialomycin and its analogues **26a–d** (**25e** is identical to **18d**).

Aigialomycin D (**1**) and selected analogues obtained by the described chemistry were tested for their activity against a panel of kinases.[31] As shown in Table 1, aigialomycin D was found to inhibit CDK1/cyclin B and CDK5/p25 at 5.7 and 5.8 μM, respectively, as well as GSK-3 at 14 μM but much less PfGSK-3, the *Plasmodium* homologue of GSK-3 (Table 1).[32] Importantly, the acetonide-protected aigialomycin D or compounds with a different relative arrangement of the hydroxy groups and the olefin (**18a** and **b**) showed no activity. As previously reported,[4] we confirmed that aigialomycin D is not an inhibitor of HSP90. These results show that aigialomycin D is not an indiscriminate ATP antagonist. The lack of activity of aigialomycin against HSP90 may be rationalized by the very high energetic penalty of adopting the required conformation to fit in the ATP-binding pocket of HSP90.

Table 1: Biological activity of aigialomycin D (**1**) and selected analogues.

	IC 50 [μM]			
Compound/kinase	CDK1	CDK5	GSK3	PfGSK3
1	5.7	5.8	14	100
1–acetonide	>100	64	70	>100
18a	>100	>100	>100	>100
18b	>100	>100	>100	>100

In conclusion, we have developed a flexible polymer-supported synthesis of aigialomycin D amenable to the preparation of libraries extending beyond the diversity of the analogues accessible from natural sources. The reported chemistry extends the utility of the thioether resin for the solid-phase synthesis of natural-product libraries. It is unlikely that the antimalarial activity of aigialomycin D can be attributed to PfGSK-3 inhibition; however, its cytotoxicity in human cells may be attributed to CDK/GSK-3 inhibition. The fact that aigialomycin D inhibits selected kinases further supports the hypothesis that the resorcyclides constitute a promising scaffold for ATP antagonism/kinase inhibition and may be a valuable class of compounds for chemical genetics.

Received: February 14, 2006
Published online: May 9, 2006

Keywords: natural products · protein kinase inhibitors · solid-phase synthesis · total synthesis

[1] M. Isaka, C. Suyarnsestakorn, M. Tanticharoen, P. Kongsaeree, Y. Thebtaranonth, *J. Org. Chem.* **2002**, *67*, 1561.
[2] T. Agatsuma, A. Takahashi, C. Kabuto, S. Nozoe, *Chem. Pharm. Bull.* **1993**, *41*, 373.
[3] M. S. R. Nair, S. T. Carey, J. C. James, *Tetrahedron* **1981**, *37*, 2445.
[4] X. Geng, S. J. Danishefsky, *Org. Lett.* **2004**, *6*, 413.

 © 2006 Wiley-VCH Verlag GmbH & Co. KGaA, Weinheim

[5] S. Barluenga, P. Lopez, E. Moulin, N. Winssinger, *Angew. Chem.* **2004**, *116*, 3449; *Angew. Chem. Int. Ed.* **2004**, *43*, 3467.
[6] S. Barluenga, E. Moulin, P. Lopez, N. Winssinger, *Chem. Eur. J.* **2005**, *11*, 4935.
[7] E. Moulin, S. Barluenga, N. Winssinger, *Org. Lett.* **2005**, *7*, 5637.
[8] E. Moulin, V. Zoete, S. Barluenga, M. Karplus, N. Winssinger, *J. Am. Chem. Soc.* **2005**, *127*, 6999.
[9] A Scifinder search for 14-membered resorcyclic lactones resulted in 22 isolated macrolides (monocillin I–IV, hypothemycin, LL-Z1640-1/4, LL-283–277, LL-283–290, zearalenone, pochonin A–F, and aigialomycins A–E).
[10] J. Ninomiya-Tsuji, T. Kajino, K. Ono, T. Ohtomo, M. Matsumoto, M. Shiina, M. Mihara, M. Tsuchiya, K. Matsumoto, *J. Biol. Chem.* **2003**, *278*, 18485.
[11] A. Dombrowski, R. Jenkins, S. Raghoobar, G. Bills, J. Polishook, F. Pelaez, B. Burgess, A. Zhao, L. Huang, Y. Zhang, M. Goetz, *J. Antibiot.* **1999**, *52*, 1077.
[12] H. Tanaka, K. Nishida, K. Sugita, T. Yoshioka, *Jpn. J. Cancer Res.* **1999**, *90*, 1139.
[13] T. W. Schulte, S. Akinaga, S. Soga, W. Sullivan, B. Stensgard, D. Toft, L. M. Neckers, *Cell Stress Chaperones* **1998**, *3*, 100.
[14] V. Hellwig, A. Mayer-Bartschmid, H. Mueller, G. Greif, G. Kleymann, W. Zitzmann, H.-V. Tichy, M. Stadler, *J. Nat. Prod.* **2003**, *66*, 829.
[15] S. M. Roe, C. Prodromou, R. O'Brien, J. E. Ladbury, P. W. Piper, L. H. Pearl, *J. Med. Chem.* **1999**, *42*, 260.
[16] F. J. Dekker, M. A. Koch, H. Waldmann, *Curr. Opin. Chem. Biol.* **2005**, *9*, 232.
[17] R. Breinbauer, I. R. Vetter, H. Waldmann, *Angew. Chem.* **2002**, *41*, 3002; *Angew. Chem. Int. Ed.* **2002**, *41*, 2879.
[18] S. L. Schreiber, *Bioorg. Med. Chem.* **1998**, *6*, 1127.
[19] S. Shang, D. S. Tan, *Curr. Opin. Chem. Biol.* **2005**, *9*, 248.
[20] S. B. Garber, J. S. Kingsbury, B. L. Gray, A. H. Hoveyda, *J. Am. Chem. Soc.* **2000**, *122*, 8168.
[21] K. C. Nicolaou, C. V. C. Prasad, P. K. Somers, C. K. Hwang, *J. Am. Chem. Soc.* **1989**, *111*, 5330.
[22] G. Stork, K. Zhao, *J. Am. Chem. Soc.* **1990**, *112*, 5875.
[23] D. L. Hughes, R. A. Reamer, J. J. Bergan, E. J. J. Grabowski, *J. Am. Chem. Soc.* **1988**, *110*, 6487.
[24] A. K. Chatterjee, J. P. Morgan, M. Scholl, R. H. Grubbs, *J. Am. Chem. Soc.* **2000**, *122*, 3783.
[25] M. Scholl, S. Ding, C. W. Lee, R. H. Grubbs, *Org. Lett.* **1999**, *1*, 953.
[26] C. W. Lee, R. H. Grubbs, *Org. Lett.* **2000**, *2*, 2145.
[27] The spectral characteristics of synthetic aigialomycin D were found to be identical to those of natural aigialomycin D (NMR spectra were kindly provided by Dr. Isaka, NSTDA, Thailand).
[28] C. H. Tai, H. C. Wu, W. R. Li, *Org. Lett.* **2004**, *6*, 2905.
[29] See Experimental Section for its preparation.
[30] K. S. Ravikumar, J.-P. Begue, D. Bonnet-Delpon, *Tetrahedron Lett.* **1998**, *39*, 3141.
[31] S. Leclerc, M. Garnier, R. Hoessel, D. Marko, J. A. Bibb, G. L. Snyder, P. Greengard, J. Biernat, Y. Z. Wu, E. M. Mandelkow, G. Eisenbrand, L. Meijer, *J. Biol. Chem.* **2001**, *276*, 251.
[32] E. Droucheau, A. Primot, V. Thomas, D. Mattei, M. Knockaert, C. Richardson, P. Sallicandro, P. Alano, A. Jafarshad, B. Baratte, C. Kunick, D. Parzy, L. Pearl, C. Doerig, L. Meijer, *Biochim. Biophys. Acta* **2004**, *1697*, 181.

 © 2006 Wiley-VCH Verlag GmbH & Co. KGaA, Weinheim

Hydride Affinities

DOI: 10.1002/anie.200600536

A Facile Experimental Method To Determine the Hydride Affinity of Polarized Olefins in Acetonitrile**

Xiao-Qing Zhu, Min Zhang, Qiao-Yun Liu, Xiao-Xiao Wang, Jian-Yu Zhang, and Jin-Pei Cheng**

Reductions of various unsaturated compounds, such as olefins, alkynes, ketones, aldehydes, and imines in solution by hydride reagents ($NaBH_4$, $LiAlH_4$, NADH, etc.) to the corresponding saturated compounds are fundamental reactions[1] that have been extensively applied in organic syntheses.[2] The thermodynamics and kinetics of reduction of unsaturated compounds are not only dependent on the hydride-donating ability (hydricity) of the hydride reagents, but also on the hydride-accepting ability (hydride affinity) of the unsaturated compounds (hydride acceptors). Hence, the hydride affinity of unsaturated compounds should be an important clue to select suitable reducing agents for their efficient reduction and to perform detailed thermodynamic analyses on the reduction mechanisms. Examination of past publications on this subject shows that, although much attention has been paid to determining hydricity of reducing agents (hydride donors) and the hydricity values of many reducing agents have been accurately determined,[3] no reports have been made on the determination of hydride affinity of unsaturated organic compounds, especially in solution. The main reason could be that the state free energy or state enthalpy of the free hydride anion in solution is not available, and this strictly limits the experimental methods that can be efficiently applied for the direct determination of the hydride affinities of unsaturated compounds in solution. Several years ago, we embarked on a major project to experimentally determine the hydride affinity scale of various unsaturated compounds in organic solvents. Herein we report a facile and efficient experimental method to determine the hydride affinity of polarized olefins **1** in acetonitrile.

[*] Prof. Dr. X.-Q. Zhu, M. Zhang, Q.-Y. Liu, X.-X. Wang, J.-Y. Zhang, Prof. Dr. J.-P. Cheng
Department of Chemistry and the
State Key Laboratory of Elemento-Organic Chemistry
Nankai University
Tianjin 300071 (P.R. China)
Fax: (+86) 22-2350-2458
E-mail: xqzhu@nankai.edu.cn

[**] X.-Q.Z. is grateful for financial support from the Ministry of Science and Technology of China (Grant No. 2004CB719905), the National Natural Science Foundation of China (Grant Nos. 20272027, 20472038, and 20421202), and Natural Science Fund of Tianjin (Grant No. 033804311).

Supporting information for this article is available on the WWW under http://www.angewandte.org or from the author.

WILEY InterScience DISCOVER SOMETHING GREAT
© 2006 Wiley-VCH Verlag GmbH & Co. KGaA, Weinheim

The hydride affinity of olefins **1** [$\Delta H_{H^-A}(\mathbf{1})$] is defined in this work as the enthalpy change in the reaction of olefin **1** with free hydride ion to form carbanion **2** at 25 °C [Eq. (1)].

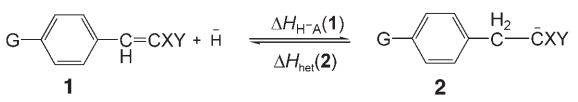

(1)

According to the definition of hydride affinity of **1** [Eq. (2)], it is clearly difficult to directly determine the hydride affinity of the olefins [$\Delta H_{H^-A}(\mathbf{1})$] in solution by an experimental method because the enthalpy of the free hydride ion in solution is not available.

$$\Delta H_{H^-A}(\mathbf{1}) = H(\mathbf{2}) - [H(H^-) + H(\mathbf{1})] \quad (2)$$

However, examining Equation (1) shows that the hydride affinity of olefins is simply equal to the heterolytic C_β–H bond dissociation energy of the corresponding carbanion **2** of **1** [$\Delta H_{het}(\mathbf{2})$] by switching the sign [Eq. (5)]. This grants efficient and facile access to determining the hydride affinity of olefins **1** in solution according to the enthalpy change in the reaction of the corresponding carbanion **2** with the strong hydride acceptor *N*-methylacridinium [$AcrH^+$; Eqs. (3) and (4)]. In

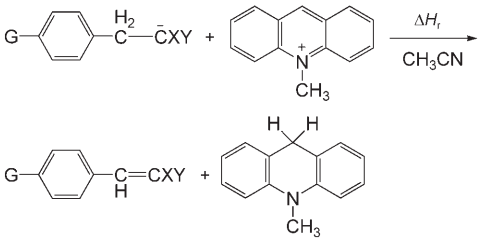

(3)

Equation (5), ΔH_r is the enthalpy change of the reaction [Eq. (3)], which can be obtained by titration calorimetry;[5] $\Delta H_{het}(AcrH_2)$ is the heterolytic C9–H bond dissociation energy of 9,10-dihydroacridine ($AcrH_2$) in solution, which we have determined previously.[5]

$$\Delta H_r = \Delta H_{het}(\mathbf{2}) - \Delta H_{het}(AcrH_2) \quad (4)$$

$$\Delta H_{H^-A}(\mathbf{1}) = -\Delta H_{het}(\mathbf{2}) = -[\Delta H_r + \Delta H_{het}(AcrH_2)] \quad (5)$$

Herein, the hydride affinity scales of four types of polarized olefins **1a–d**, which have been extensively applied in organic syntheses,[6] were examined in acetonitrile solution. The hydride affinities of **1a–d** are summarized in Table 1. The enthalpy changes of the reactions of **2a–d** with $AcrH^+$ [Eq. (3)] and the standard redox potentials of the relevant species are listed in the Supporting Information.

As the reductions of olefins **1** by hydride ions could involve multistep hydride-transfer mechanism, such as e^-–H^+–e^-, e^-–H, H–e^-, and so on (Scheme 1),[7] it is evident that the hydrogen affinity of olefins **1**, $\Delta H_{HA}(\mathbf{1})$, as well as proton affinity and hydrogen affinity of the corresponding radical carbanion of the olefins $\mathbf{1}^{\bullet-}$, $\Delta H_{PA}(\mathbf{1}^{\bullet-})$ and $\Delta H_{HA}(\mathbf{1}^{\bullet-})$, are also very important for elucidating the reduction mech-

Table 1: Hydride and hydrogen affinities of olefins **1**, as well as proton affinities and hydrogen affinities of the radical anions $\mathbf{1}^{\bullet-}$ in acetonitrile [kcal mol^{-1}].[a]

G	$\Delta H_{H^-A}(\mathbf{1})$[b]	$\Delta H_{HA}(\mathbf{1})$[c]	$\Delta H_{PA}(\mathbf{1}^{\bullet-})$[d]	$\Delta H_{HA}(\mathbf{1}^{\bullet-})$[e]
1a (X = CN, Y = CN)				
CH_3O	−60.4	−42.6	−25.3	−70.1
CH_3	−60.6	−42.7	−24.1	−69.0
H	−61.0	−42.6	−22.8	−68.1
Cl	−61.6	−42.8	−20.4	−66.2
Br	−61.5	−42.7	−20.1	−65.9
CF_3	−62.6	−43.2	−16.6	−63.0
NO_2	−63.0	−43.0	−13.5	−60.5
1b (X = CN, Y = CO_2Et)				
CH_3O	−58.1	−40.9	−27.4	−71.6
CH_3	−58.4	−41.0	−26.5	−70.8
H	−59.0	−41.3	−24.9	−69.6
Cl	−59.4	−41.2	−22.6	−67.8
Br	−59.5	−41.3	−22.7	−67.8
CF_3	−60.3	−41.5	−19.0	−64.8
NO_2	−60.8	−41.6	−15.8	−61.9
1c (X = CN, Y = $CONH_2$)				
CH_3O	−55.1	−38.6	−30.2	−73.7
CH_3	−55.3	−38.6	−28.9	−72.5
H	−55.7	−38.7	−26.9	−70.8
Cl	−56.6	−39.2	−24.4	−68.8
Br	−56.7	−39.2	−24.5	−68.9
CF_3	−57.2	−39.1	−20.8	−65.7
NO_2	−57.7	−39.1	−17.7	−63.2
1d (X = CO_2Et, Y = CO_2Et)				
CH_3O	−52.8	−36.9	−31.6	−74.4
CH_3	−53.1	−37.0	−30.7	−73.8
H	−53.7	−37.3	−29.1	−72.5
Cl	−54.2	−37.4	−27.0	−70.8
Br	−54.3	−37.5	−27.8	−71.0
CF_3	−55.0	−37.6	−23.8	−68.2
NO_2	−55.7	−37.8	−21.6	−66.4

[a] Relative uncertainties were estimated to be smaller than or close to 1 kcal mol^{-1} in each case. [b] $\Delta H_{H^-A}(\mathbf{1})$ was estimated from Equation (5), taking $\Delta H_{het}(AcrH_2) = 81.1$ kcal mol^{-1} from reference [5]. [c] Estimated from Equation (6) with $E^\circ(H^{0/-}) = -1.137$ V vs. Fc^+/Fc^0 (Fc = ferrocen).[9] [d] Estimated from Equation (7) with $E^\circ(H^{+/0}) = -2.307$ V vs. Fc^+/Fc^0.[9] [e] Estimated from Equation (8) with $E^\circ(H^{+/0}) = -2.307$ V vs. Fc^+/Fc^0.

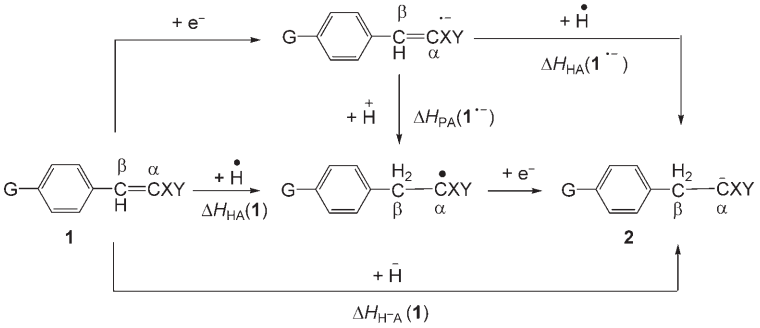

Scheme 1. Possible pathways of the reduction of **1** by hydride.

 © 2006 Wiley-VCH Verlag GmbH & Co. KGaA, Weinheim

anism. In this work, their values were also estimated according to Equations (6)–(8), which were derived from appropriate thermodynamic cycles (see Supporting Information).[8] The results are also summarized in Table 1.

$$\Delta H_{HA}(\mathbf{1}) = \Delta H_{H^-A}(\mathbf{1}) - F[E^o(H^{0/-}) - E^o(\mathbf{2}^{0/-})] \quad (6)$$

$$\Delta H_{PA}(\mathbf{1}^{\cdot-}) = \Delta H_{H^-A}(\mathbf{1}) + F[E^o(\mathbf{1}^{0/-}) - E^o(H^{0/-})] - F[E^o(H^{+/0}) - E^o(\mathbf{2}^{0/-})] \quad (7)$$

$$\Delta H_{HA}(\mathbf{1}^{\cdot-}) = \Delta H_{H^-A}(\mathbf{1}) - F[E^o(H^{0/-}) - E^o(\mathbf{1}^{0/-})] \quad (8)$$

Table 1 shows that the hydride affinities of olefins **1** in acetonitrile range from −60.4 to −63.0 kcal mol^{-1} for **1a**, from −58.1 to −60.8 kcal mol^{-1} for **1b**, from −55.1 to −57.7 kcal mol^{-1} for **1c**, and from −52.8 to −55.7 kcal mol^{-1} for **1d**. The hydride affinities of olefins **1** decrease in the order **1a** > **1b** > **1c** > **1d**.[10] Among the 28 olefins, **1a** (G = NO_2) is the strongest oxidant (ΔH_{H^-A} = −63.0 kcal mol^{-1}) and the easiest to reduce; **1d** (G = CH_3O) should be the weakest oxidant (ΔH_{H^-A} = −52.8 kcal mol^{-1}) and the most difficult to reduce.

The hydride affinities of olefins **1**[10] are much smaller than those of the corresponding primary benzylic carbonium ions in acetonitrile solution (e.g., −106, −112, −118, and −121 kcal mol^{-1} for 4-$CH_3OC_6H_4CH_2^+$, 4-$MeC_6H_4CH_2^+$, $C_6H_5CH_2^+$, and 4-$ClC_6H_4CH_2^+$, respectively),[11] but slightly smaller than or close to that of NAD^+ models (NADH = nicotinamide adenine dinucleotide) in acetonitrile (e.g., −64.2 kcal mol^{-1} for BNA^+ and −66.9 to −72.6 kcal mol^{-1} for (G)PNA^+; G = CH_3O, CH_3, H, Cl, Br, and CF_3),[4] which indicates that olefins **1**, like the NAD^+ models, are not strong hydride acceptors. Thus, if these olefins are to be efficiently reduced, only stronger reducing agents such as $NaBH_3(CN)$ (ΔH_{het}(B–H) = 45.0 kcal mol^{-1} in acetonitrile)[12] should be chosen. Weak reducing agents, such as *N*-benzyl-1,4-dihydronicotinamide (BNAH) and *N*-phenyl-1,4-dihydronicotinamide (PNAH), can not be used to reduce them in nonprotic solvents, as is well supported by experimental results.

Examining reaction (1) shows that, unlike the reduction of benzylic carbonium ions by hydride, the reduction of olefins **1** by hydride does not only involve the formation of a new C–H σ bond to release energy, but also dissociation of one C=C π bond to consume energy. Hence, the magnitude of the olefin hydride affinities should be equal to the heterolytic dissociation energy of the newly formed C–H σ bond minus the heterolytic dissociation energy of the broken C=C π bond. Thus, it is easy to understand why the hydride affinity scale of olefins **1** is much smaller than that of the corresponding primary benzylic carbonium ions, since the hydride affinities of the primary benzylic carbonium ions do not involve the heterolytic dissociation energy of the broken C=C π bond.

From the same viewpoint, we also can explain why the hydride affinity scale of olefins **1** is close to or slightly smaller than that of NAD^+ models in the same solvent: The reason is that the reduction of the NAD^+ models by hydride, like the reduction of the olefins, also involves dissociation of one π bond in the pyridine ring. This leads to the valuable prediction that the hydride affinities of carbonyl compounds such as ketones and aldehydes should all be close to those of the corresponding olefins **1** in the same solvent.

In Table 1, the hydrogen affinities of olefins **1** in acetonitrile range from −42.6 to −43.0 kcal mol^{-1} for **1a**, from −40.9 to −41.6 kcal mol^{-1} for **1b**, from −38.6 to −39.1 kcal mol^{-1} for **1c** and from −36.9 to −37.8 kcal mol^{-1} for **1d**. These values are all close to or slightly larger than the average hydrogen affinities of typical olefins in the gas phase (−35.2 kcal mol^{-1}),[13] which means that the hydrogen affinities of olefins **1** determined in this work should be reasonable and reliable, and the same should hold true for their hydride affinities in acetonitrile. The hydrogen affinities of olefins **1** are smaller than the corresponding hydride affinities by about 18 kcal mol^{-1}, that is, olefins **1** should prefer hydride to the neutral hydrogen atom.

Proton and hydrogen affinities of the radical anions of olefins (**1**$^{\cdot-}$) in acetonitrile range from −25.3 to −13.5 and from −70.1 to −60.5 kcal mol^{-1} for **1**$^{\cdot-}$, from −27.4 to −15.8 and from −71.6 to −61.9 kcal mol^{-1} for **1b**$^{\cdot-}$, from −30.2 to −17.7 and from −73.7 to −63.2 kcal mol^{-1} for **1c**$^{\cdot-}$, and from −31.6 to −21.6 and from −74.4 to −66.4 kcal mol^{-1} for **1d**$^{\cdot-}$, respectively (Table 1). Thus, the proton affinities of radical anions **1**$^{\cdot-}$ are much smaller than the corresponding hydrogen affinities, by about 45 kcal mol^{-1}, which suggests that these radical anions are strong acceptors of the neutral hydrogen atom but weak proton acceptors. Conceivably, if reduction of olefins **1** by a hydride donor were initiated by single-electron transfer, hydrogen-atom transfer in the second step to the formed **1**$^{\cdot-}$ should be much easier than proton transfer to the same radical anion. Since the hydrogen-atom affinities of **1**$^{\cdot-}$ all are large (−60.5 to −74.4 kcal mol^{-1}), hydrogen-atom transfer could be extremely fast and possibly diffusion-controlled. We conclude that the e^-–H$^{\cdot}$ sequence of hydride transfer should be most likely among the possible multistep mechanisms for reduction of olefins **1** by hydride if the reactions were initiated by single-electron transfer.

The effect of the α substituents X and Y on the hydride affinity ΔH_{H^-A}(**1**) (slope of −17.7, see Supporting Information) is much larger than that of the remote substituent G (slope of −2.56). Electron-withdrawing groups increase the hydride affinity, while electron-donating groups decrease it, that is, the hydride affinities of olefins **1** are mainly dependent on the stability of carbanions **2**, since α-Y(X) is closer to the center of negative charge than G. By using a similar method, the effects of α-substituents X and Y and remote substituent G on ΔH_{HA}(**1**), ΔH_{PA}(**1**$^{\cdot-}$), and ΔH_{HA}(**1**$^{\cdot-}$) can also easily be elucidated (see Supporting Information).

In summary, the hydride affinities of 28 polarized olefins **1** in acetonitrile were determined by an experimental method, while the hydrogen-atom affinities of **1** and the proton affinity and hydrogen-atom affinity of the radical anions **1**$^{\cdot-}$ were estimated by using thermodynamic cycles according to Hess' law. These thermodynamic data should be very valuable when choosing suitable reducing agents for olefins and carrying out detailed thermodynamic analysis of the reduction mechanism. This paper not only reports the hydride affinities of polarized olefins in solution for the first time, but also offers a facile and efficient experimental method to determine the hydride affinities of unsaturated organic compounds such as ketones,

 © 2006 Wiley-VCH Verlag GmbH & Co. KGaA, Weinheim

aldehydes, and imines in solution, which have also not yet been reported. The detailed hydride affinities of some imines will be disclosed in a forthcoming paper.

Received: February 9, 2006
Published online: May 3, 2006

Keywords: alkenes · calorimetry · hydrides · radical anions · thermodynamics

[1] a) H. Zimmerman, I. Zimmerman, *Elements of Organic Chemistry*, Benziger Bruce & Glencoe, London, **1977**; b) L. G. Wade, Jr., *Organic Chemistry*, Pearson Education, New York, **2003**.

[2] a) J. March, *Advanced Organic Chemistry*, Wiley, New York, **1985**, p. 809; b) H. O. House, *Modern Synthetic Reactions*, Benjamin Cummings Publishing, Reading, MA, **1972**, p. 45.

[3] a) A. Hajos, *Complex Hydrides*, Elsevier, New York, **1979**; b) W. W. Ellis, J. W. Raebiger, C. J. Curtis, J. W. Bruno, D. L. DuBois, *J. Am. Chem. Soc.* **2004**, *126*, 2738 – 2743; c) C. J. Curtis, A. Miedaner, W. W. Ellis, D. L. DuBois, *J. Am. Chem. Soc.* **2002**, *124*, 1918; d) W. W. Ellis, A. Miedaner, C. J. Curtis, D. H. Gibson, D. L. DuBois, *J. Am. Chem. Soc.* **2002**, *124*, 1926; e) T.-Y. Cheng, B. S. Brunschwig, R. M. Bullock, *J. Am. Chem. Soc.* **1998**, *120*, 13121 – 13137.

[4] Carbanions **2** were prepared by deprotonation of the parent compounds with KH. Reactions of **2** with *N*-methylacridinium ($AcrH^+$) in acetonitrile solution give the corresponding olefins **1** and $AcrH_2$ quantitatively [Eq. (3)], which were identified by MS and ^1H NMR spectroscopy. The reaction enthalpy change ΔH_r can be directly determined by titration calorimetry, since the combination of carbanions **2** with $AcrH^+$ in acetonitrile is not only fast, but also quantitative, and hence thoroughly suitable for titration calorimetry.

[5] X.-Q. Zhu, H.-R. Li, Q. Li, T. Ai, J.-Y. Lu, Y. Yang, J.-P. Cheng, *Chem. Eur. J.* **2003**, *9*, 871 – 880.

[6] a) S. J. Garden, C. R. W. Guimaraes, M. B. Correa, C. A. F. Oliveira, A. da C. Pinto, R. B. de Alencastro, *J. Org. Chem.* **2003**, *68*, 8815; b) B. C. Ranu, S. Samanta, *Tetrahedron* **2003**, *59*, 7901; c) B. C. Ranu, S. Samanta, *Tetrahedron Lett.* **2002**, *43*, 7405; d) B. C. Ranu, J. Dutta, S. K. Guchhait, *Org. Lett.* **2001**, *3*, 2603; e) A. Sommer, H. Stamm, *Liebigs Ann. Chem.* **1992**, *2*, 99; f) B.-L. Zhang, X.-Q. Zhu, J.-Y. Lu, J.-Q. He, P. G. Wang, J.-P. Cheng, *J. Org. Chem.* **2003**, *68*, 3295.

[7] X.-Q. Zhu, Y.-C. Liu, *J. Org. Chem.* **1998**, *63*, 2786 – 2787.

[8] Note that we used the term free-energy change ΔG_{et} to replace the enthalpy change ΔH_{et} in Equations (6)–(8) for the electron-transfer processes. The justification of this treatment is that entropies associated with electron transfer are negligible, as verified by Arnett et al.: E. M. Arnett, K. Amarnath, N. G. Harvey, J.-P. Cheng, *J. Am. Chem. Soc.* **1990**, *112*, 344 – 355.

[9] D. D. M. Wayner, V. D. Parker, *Acc. Chem. Res.* **1993**, *26*, 287 – 294.

[10] Unless specified, the magnitude of the hydride affinity in this paper indicates the absolute value rather than the pure mathematical values (negative values) for the sake of convention.

[11] J.-P. Cheng, K. L. Handoo, V. D. Parker, *J. Am. Chem. Soc.* **1993**, *115*, 2655.

[12] W. W. Ellis, R. Ciancanelli, S. M. Miller, J. W. Raebiger, M. R. DuBois, D. L. DuBois, *J. Am. Chem. Soc.* **2003**, *125*, 12230 – 12236.

[13] T. L. Brown, Jr., H. E. LeMay, B. E. Bursten, *Chemistry the Central Science*, Prentice Hall, New York **2000**, p. 289.

 © 2006 Wiley-VCH Verlag GmbH & Co. KGaA, Weinheim

Cycloadditions

DOI: 10.1002/anie.200600806

Rh^{I}-Catalyzed C–C Bond Activation: Seven-Membered Ring Synthesis by a [6+1] Carbonylative Ring-Expansion Reaction of Allenylcyclobutanes**

Paul A. Wender, Nicole M. Deschamps, and Robert Sun*

The transition-metal-catalyzed activation of carbon–carbon (C–C) sigma bonds represents an important and fundamental challenge in organometallic chemistry that has the potential to broaden how we approach problems in organic synthesis.[1] We have previously shown that transition metals can be used to catalyze the strain-assisted C–C bond activation of vinylcyclopropanes (VCPs) to produce organometallic intermediates that can be intercepted with various trapping agents to afford new two-, three-, and four-component cycloadditions. Representative examples include the [5+2] cycloaddition of VCPs and π systems (Scheme 1a);[2] the [5+2+1] cycloaddition of VCPs, alkynes (and allenes), and CO;[2c,3] and the [5+1+2+1] cycloaddition of VCPs, alkynes, and CO,[4] thus providing new routes to seven-, eight-, and nine-membered rings and their derivatives.[5] Whereas the extension of this five-carbon VCP chemistry to simple six-carbon vinylcyclobutanes has failed thus far (Scheme 1c), the metal-catalyzed activation of the C–C bond of vinylcyclobutanones has been successful, thus leading to a new [6+2] cycloaddition for the formation of eight-membered rings (Scheme 1b).[6,7]

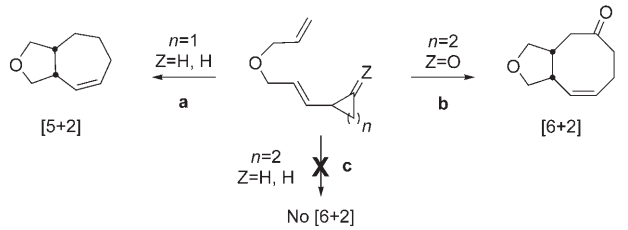

Scheme 1. [5+2], [6+2], and attempted [6+2] reactions.

To explore whether vinylcyclobutanes could be activated for use as six-carbon components in metal-catalyzed reactions, we examined the reaction of 1-siloxy-1-vinylcyclobu-

[*] Prof. P. A. Wender, N. M. Deschamps, R. Sun
Department of Chemistry
Department of Molecular Pharmacology
Stanford University
Stanford, CA 94305-5080 (USA)
Fax: (+1) 650-725-0259
E-mail: wenderp@stanford.edu

[**] This research was supported by the National Science Foundation (CHE-040638). Fellowship support from Eli Lilly and Company (R.S. and N.M.D.) is gratefully acknowledged.

Supporting information for this article is available on the WWW under http://www.angewandte.org or from the author.

© 2006 Wiley-VCH Verlag GmbH & Co. KGaA, Weinheim

tane **1** (Scheme 2) with Rh^I catalysts. Although we had previously shown that similar siloxy-substituted (and alkoxy-substituted) VCPs are more reactive than their non-oxygenated counterparts in metal-catalyzed [5+2] cycloaddi-

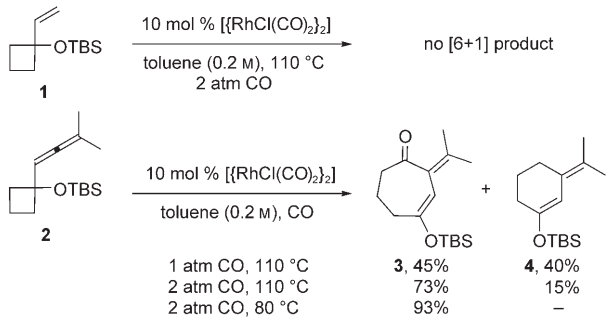

Scheme 2. Attempted [6+1] reaction of **1** and [6+1] reaction of **2**. TBS = *tert*-butyldimethylsilyl.

tions,[8] the corresponding 1-siloxy-1-vinylcyclobutane **1** was unreactive. Given that the requisite C–C cleavage process would likely be assisted by metal coordination to the π system and that allenes are often better coordinators than alkenes, the reaction of 1-siloxy-1-allenylcyclobutane **2** was examined. In contrast to vinylcyclobutane **1**, allenylcyclobutane **2** reacted readily through a metal-catalyzed C–C activation process and, in the presence of CO, produced both six- and seven-membered ring products (Scheme 2).[9] We describe herein our studies on this new class of metal-catalyzed C–C activation reactions and its incorporation into a new method for seven-membered ring synthesis through a carbonylative ring expansion reaction, a formal [6+1] cycloaddition.[10]

Our initial studies revealed that activation of **2** could be achieved with $[\{RhCl(CO)_2\}_2]$ (10 mol%) in toluene in the presence of CO (1 atm) to give cycloheptenone **3** in 45% yield along with the cycloisomerization product, cyclohexene **4**, in 40% yield (Scheme 2). Increasing the CO pressure to 2 atmospheres, improved the mode selectivity of the reaction, thus giving **3** and **4** in 73 and 15% yields, respectively. Significantly, decreasing the reaction temperature to 80 °C decoupled the competing pathways, thus resulting in a completely selective and highly efficient trapping reaction to give **3** in 93% yield. Interestingly, although $[IrCl(CO)(PPh_3)_2]$ was the catalyst of choice in the [5+1] reaction of allenylcyclopropanes,[10] no reaction was obtained with **2** under the analogous reaction conditions.

As depicted in Scheme 3, this reaction putatively proceeds through pre-coordination of the Rh^I center to the double bond of the allene that is proximal to the cyclobutane **2a**. This step leads to the metallacycle **2b** after insertion into the adjacent C–C bond. Reductive elimination affords the cycloisomerized cyclohexene **4**.[11] A competing CO insertion step, which is apparently favored at lower temperature followed by reductive elimination provides the [6+1] cycloadduct **3**. Metallacycles **2b** and **2c**/**2d** represent new reactive intermediates that could potentially be points of divergence to new classes of higher-order cycloaddition reactions.[7b,c]

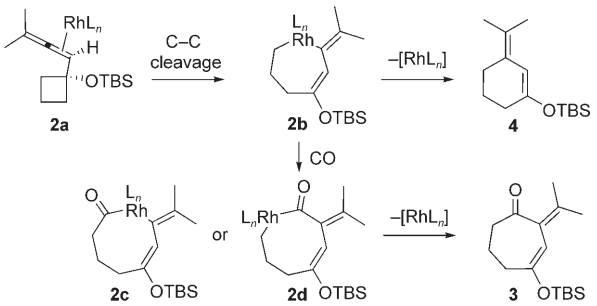

Scheme 3. Mechanistic proposal for the [6+1] reaction.

Studies on the scope of this new [6+1] reaction indicate that it can be used to synthesize various functionalized cycloheptenones (Table 1). Of the solvents surveyed, including 1,4-dioxane, 1,2-dichloroethane, 1,1,2,2-tetrachloroethane, toluene, and *m*-xylene, aromatic solvents gave higher yields of the [6+1] products. Processes that required longer reaction times were carried out in *m*-xylene to minimize solvent loss. Monocyclic allenylcyclobutane **2** reacts to give a 93% yield of the cycloheptenone **3**. The substituted allenylcyclobutanes **5** and **8** react to give cycloheptenones **6**, **7**, and **9**. With the exception of **2**, better results were obtained using only 1 atmosphere of CO for the [6+1] reactions. In the case of **5**, two regioisomeric products were obtained, **6** which results from cleavage of the less-substituted C–C bond and **7** which results from cleavage of the more-substituted C–C bond. The benzyloxy-substituted allenylcyclobutane gave only **9**, the product that results from cleavage of the less-substituted C–C bond. Attempts to achieve a [6+1] reaction with allenylcyclobutane **10**, which has only one methyl group at the double bond distal to the cyclobutane have thus far been unsuccessful with Rh^I catalysts.[12]

Given the potential of this process for access to the core ring systems of natural and non-natural targets containing seven-membered rings (e.g., Scheme 4),[13] the reactions of various allenyl-substituted [*n*.2.0] bicycles were also investigated. The cycloadducts **12** and **14**, which incorporate a himachalane core, were obtained in excellent yield using only 2 mol% of catalyst and a substrate concentration of 0.5 M (Table 1). A comparison of the [6+1] reactions of **11** and **13** illustrates that the replacement of the methoxyethyl protecting group with a benzyl group has a negligible effect on yield; however, a longer reaction time is required, thus possibly reflecting a chelating effect for the former group. It is noteworthy that the reaction proceeds with exclusive cleavage of the more-substituted bond in these cases. In contrast, the [6+1] reaction of **15**, which contains an angular methyl group, gave the bicyclo[5.4.0]undecenone product **16**, which arises from cleavage of the less-substituted bond in moderate yield. Interestingly, the bicyclo[3.2.0]heptane substrate **17** afforded the regioisomers **18** and **19** in a 3:4 ratio with a combined yield of 56%, both of which possess the bicyclo[5.3.0]decane system of pseudoguaianes, guaianes, tiglianes, daphnanes, and other natural products. The norbornene-derived substrate **20** provided only regioisomer **21**, which results from cleavage of the less-substituted C–C bond in 85% yield.

 © 2006 Wiley-VCH Verlag GmbH & Co. KGaA, Weinheim

Table 1: [6+1] Reaction of allenylcyclobutanes.

Substrate		Conditions[a]	*t*	Product(s)		Yield [%][b]
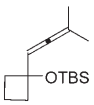	**2**	A	24	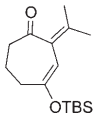	**3**	93
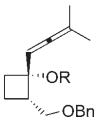	**5**[b]	B	44	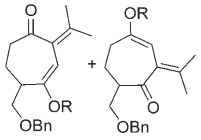	**6**+**7**	70 (5:1)
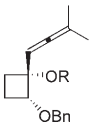	**8**[b]	C	48	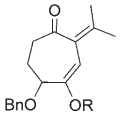	**9**	55
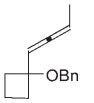	**10**	D	48	decomposition		
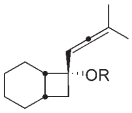	**11**[b]	E	11	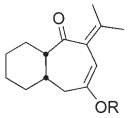	**12**	89
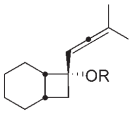	**13**[c]	E	22	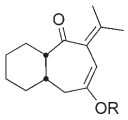	**14**	90
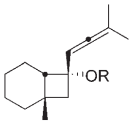	**15**[b]	B	20	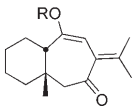	**16**	53
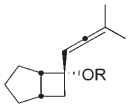	**17**[b]	F	40	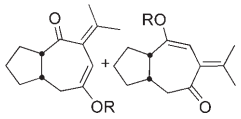	**18**+**19**	56 (3:4)
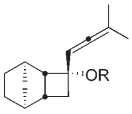	**20**[b]	C	44	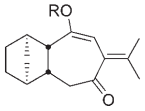	**21**	85

[a] A: [{RhCl(CO)$_2$}$_2$] (10 mol%), toluene (0.1 M), CO (2 atm), 80°C; B: [{RhCl(CO)$_2$}$_2$] (2 mol%), *m*-xylene (0.5 M), CO (1 atm), 80°C; C: [{RhCl(CO)$_2$}$_2$] (10 mol%), *m*-xylene (0.1 M), CO (1 atm), 80°C; D: [{RhCl(CO)$_2$}$_2$] (10 mol%), toluene (0.1 M), CO (1 atm), 80°C; E: [{RhCl(CO)$_2$}$_2$] (2 mol%), toluene (0.5 M), CO (1 atm), 80°C; F: [{RhCl(CO)$_2$}$_2$] (10 mol%), *m*-xylene (0.1 M), CO (1 atm), 95°C. [b] R = (CH$_2$)$_2$OCH$_3$. [c] R = Bn.

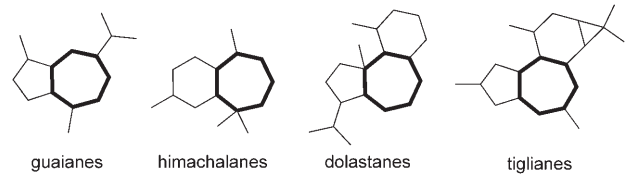

Scheme 4. Representative natural product skeletons.

In summary, we have shown that allenylcyclobutanes undergo Rh^{I}-catalyzed C–C activation to generate intermediate metallacycles that can be trapped with CO to produce cycloheptenones in good to excellent yields. This novel [6+1] cycloaddition offers a new route to functionalized cycloheptenones that would be difficult to produce conventionally, including those corresponding to the bicyclo[5.4.0] and -[5.3.0] cores of a wide range of natural products. Further studies on the scope and applications of this reaction and the trapping of these intermediates to produce higher order cycloadditions are in progress.

Experimental Section

Allenylcyclobutane **11** (41 mg, 0.163 mmol) was weighed into an oven-dried test tube equipped with a magnetic stir bar. The substrate was dissolved in toluene (0.33 mL), and [{RhCl(CO)$_2$}$_2$] (1.3 mg, 0.0033 mmol) was added in one portion. The test tube was capped with a rubber septum. The resulting yellow solution was stirred in an atmosphere of CO (balloon, 1 atm) vented to a bubbler through an outlet needle for 15 min. The outlet needle was removed and the test tube was partially immersed into a thermostat-controlled oil bath preheated to 80°C. The reaction mixture was stirred for 11 h, at which time TLC analysis indicated that the starting material was consumed. The solution was cooled to room temperature and was purified by column chromatography on silica gel (Et$_2$O/pentane, gradient elution: 5:95→10:90). Product-containing fractions were combined and concentrated to give **12** (40.3 mg, 89%) as a colorless oil. The compounds were chromatographically homogeneous.

Received: March 1, 2006
Published online: May 9, 2006

Keywords: C–C activation · carbonylation · cycloaddition · cyclobutanes · rhodium

[1] For reviews on the metal-mediated C–C sigma-bond activation reactions, see: a) R. H. Crabtree, *Chem. Rev.* **1985**, *85*, 245–269; b) M. Murakami, Y. Ito in *Topics in Organometallic Chemistry*, *Vol. 3* (Ed.: S. Murai), Springer, New York, **1999**, pp. 97–129; c) B. Rybtchinski, D. Milstein, *Angew. Chem.* **1999**, *111*, 918–932; *Angew. Chem. Int. Ed.* **1999**, *38*, 870–883.

[2] For the first examples, see: a) P. A. Wender, H. Takahashi, B. Witulski, *J. Am. Chem. Soc.* **1995**, *117*, 4720–4721; b) P. A. Wender, H. Rieck, M. Fuji, *J. Am. Chem. Soc.* **1998**, *120*, 10976–10977; for some recent examples, see: c) H. A. Wegner, A. de Meijere, P. A. Wender, *J. Am. Chem. Soc.* **2005**, *127*, 6530–6531; d) P. A. Wender, T. J. Williams, *Angew. Chem.* **2002**, *114*, 4732–4735; *Angew. Chem. Int. Ed.* **2002**, *41*, 4550–4553; e) P. A. Wender, J. A. Love, T. J. Williams, *Synlett* **2003**, 1295–1298.

[3] P. A. Wender, G. G. Gamber, R. D. Hubbard, L. Zhang, *J. Am. Chem. Soc.* **2002**, *124*, 2876–2877.

[4] P. A. Wender, G. G. Gamber, R. D. Hubbard, S. M. Pham, L. Zhang, *J. Am. Chem. Soc.* **2005**, *127*, 2836–2837.

[5] For reviews, see: a) P. A. Wender, G. G. Gamber, T. J. Williams in *Modern Rhodium-Catalyzed Organic Reactions* (Ed.: P. A. Evans), Wiley-VCH, Weinheim, **2005**, pp. 263–299; b) P. A.

 © 2006 Wiley-VCH Verlag GmbH & Co. KGaA, Weinheim

Wender, J. L. Baryza, S. E. Brenner, M. O. Clarke, G. G. Gamber, J. C. Horan, T. C. Jessop, C. Kan, K. Pattabiraman, T. J. Williams, *Pure Appl. Chem.* **2003**, *75*, 143 – 155; c) P. A. Wender, F. C. Bi, G. G. Gamber, F. Gosselin, R. D. Hubbard, M. J. C. Scanio, R. Sun, T. J. Williams, L. Zhang, *Pure Appl. Chem.* **2002**, *74*, 25 – 31; d) P. A. Wender, J. A. Love in *Advances in Cycloadditions* (Ed.: M. Harmata), JAI Press, Stamford, CT, **1999**, pp. 1 – 45.

[6] P. A. Wender, A. G. Correa, Y. Sato, R. Sun, *J. Am. Chem. Soc.* **2000**, *122*, 7815 – 7816.

[7] For studies related to Rh^I insertion into cyclobutanone, see: a) M. Murakami, H. Amii, K. Shigeto, Y. Ito, *J. Am. Chem. Soc.* **1996**, *118*, 8285 – 8290; for recent examples, see: b) M. Murakami, T. Itahashi, Y. Ito, *J. Am. Chem. Soc.* **2002**, *124*, 13976 – 13977; c) T. Matsuda, A. Fujimoto, M. Ishibashi, M. Murakami, *Chem. Lett.* **2004**, *33*, 876 – 877.

[8] P. A. Wender, C. M. Barzilay, A. J. Dyckman, *J. Am. Chem. Soc.* **2001**, *123*, 179 – 180.

[9] For [5+1] reactions of vinylcyclopropanes, see: a) $[Fe(CO)_5]$, S. Sarel, *Acc. Chem. Res.* **1978**, *11*, 204 – 211; b) D. F. Taber, K. Kanai, Q. Jiang, G. Bui, *J. Am. Chem. Soc.* **2000**, *122*, 6807 – 6808; c) $[Co_2(CO)_8]$ and $[\{RhCl(CO)_2\}_2]$, T. Kurahashi, A. de Meijere, *Synlett* **2005**, 2619 – 2622.

[10] For an Ir^I-catalyzed [5+1] reaction of allenylcyclopropanes, see: a) M. Murakami, K. Itami, M. Ubukata, I. Tsuji, Y. Ito, *J. Org. Chem.* **1998**, *63*, 4 – 5; for a $[Co_2(CO)_8]$-mediated [5+1] reaction of allenylcyclopropanols, see: b) N. Iwasawa, Y. Owada, T. Matsuo, *Chem. Lett.* **1995**, 115 – 116.

[11] For a Rh^I-catalyzed rearrangement of allenylcyclopropanes to cyclopentenes, see: M. Hayashi, T. Ohmatsu, Y.-P. Meng, K. Saigo, *Angew. Chem.* **1998**, *110*, 877 – 879; *Angew. Chem. Int. Ed.* **1998**, *37*, 837 – 839.

[12] A steric requirement may be necessary to promote binding of the metal to the double bond proximal to the cyclobutane ring. Similar steric requirements have been observed in a) the carbonylative rearrangement reaction of allenylethers, see: P. A. Wender, N. M. Deschamps, R. Sun, *Can. J. Chem.* **2005**, *83*, 838 – 842; b) the [5+1] reaction of allenylcyclopropanes, see reference [9]; and c) the Rh^I-catalyzed [4+1] reaction of vinylallenes and CO, see: M. Murakami, K. Itami, Y. Ito, *Angew. Chem.* **1995**, *107*, 2943 – 2946; *Angew. Chem. Int. Ed. Engl.* **1995**, *34*, 2691 – 2694.

[13] For examples of guaianes and himachalanes, see: a) B. M. Frago, *Nat. Prod. Rep.* **2003**, *20*, 392 – 413; for examples of dolastanes, see: b) C. B. Rao, G. Trimurtulu, D. V. Rao, S. C. Bobzin, D. M. Kushlan, D. J. Faulkner, *Phytochemistry* **1991**, *30*, 1971 – 1976; for examples of tiglianes, see: c) G. Krauter, C.-W. Von Der Lieth, R. Schmidt, E. Hecker, *Eur. J. Biochem.* **1996**, *242*, 417 – 427; d) P. A. Wender, K. D. Rice, M. E. Schnute, *J. Am. Chem. Soc.* **1997**, *119*, 7897 – 7898.

 © 2006 Wiley-VCH Verlag GmbH & Co. KGaA, Weinheim

Synthetic Methods

DOI: 10.1002/anie.200600531

Diastereoselective Synthesis of Methylenecyclopropanes from Chiral Cyclopropene Derivatives**

*Zhe Yang, Xiaocong Xie, and Joseph M. Fox**

Described herein is a new method for the preparation of chiral methylenecyclopropanes from cyclopropene derivatives and Grignard reagents. Methylenecyclopropanes[1] have broad utility for the rapid generation of molecular complexity through a number of reactions that are enabled by their considerable strain energy (ca. 40 kcal mol^{-1}).[2] Of particular utility is the growing body of stereospecific transformations of methylenecyclopropanes.[1,3] A limitation for the chemistry of methylenecyclopropanes is that there are few preparations of enantiomerically enriched derivatives.[4] The utility of methylenecyclopropanes would be greatly enhanced by a common intermediate approach that provides access to a range of enantiomerically enriched derivatives. Herein, conditions for the selective synthesis of methylenepropanes from chiral cyclopropene precursors[5] are reported, thus providing access to diverse types of highly functionalized methylenecyclopropanes that possess chiral quaternary centers. The cyclopropene precursors are readily available in enantiomerically enriched form.[5b–d]

The discovery that Grignard reagents can convert cyclopropenes into methylenecyclopropanes was serendipitous and resulted from an attempt to use the directed cyclopropene carbometallation reaction to prepare **2** (Scheme 1).[6] Organ-

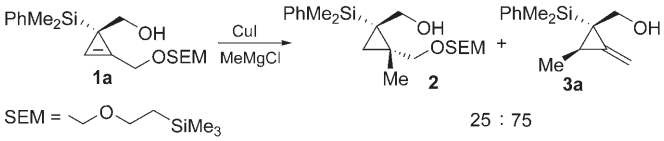

Scheme 1. Precedent for synthesis of methylenecyclopropanes.

ometallic and metal-hydride reagents normally add to 1-alkylcyclopropenes by introducing the nucleophile to the more substituted side of the multiple bond.[6] The unusual reversal of regioselectivity to produce **3a** suggested a pathway

[*] Dr. Z. Yang, X. Xie, Prof. Dr. J. M. Fox
Department of Chemistry and Biochemistry
University of Delaware
Brown Laboratories
Newark, DE 19716 (USA)
Fax: (+1) 302-831-6335
E-mail: jmfox@udel.edu

[**] This work was supported by NIH grant GM068640-01A1.

Supporting information for this article is available on the WWW under http://www.angewandte.org or from the author.

InterScience
© 2006 Wiley-VCH Verlag GmbH & Co. KGaA, Weinheim

for the diastereoselective synthesis of functionalized methylenecyclopropanes.[7,8]

By following the result in Scheme 1, it was found that changing the Grignard counterion from chloride to bromide can alter the regioselectivity to favor exclusive formation of the methylenecyclopropane. Under the optimized conditions (Table 1), the directed reaction proceeded with excellent

Table 1: Synthesis of methylenecyclopropanes from chiral cyclopropenes.[a]

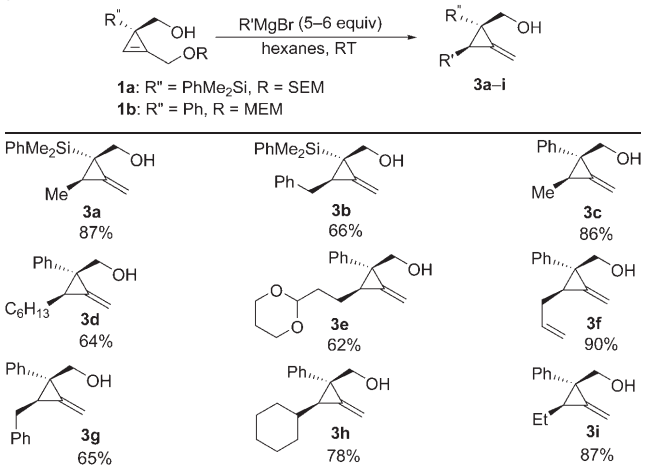

[a] All reactions gave a single isomer (d.r. > 95%) as determined by ^{1}H NMR spectroscopic analysis. Percentages represent yields of isolated product as the average of two runs.

regio- and diastereoselectivity. Methyl-, alkyl- (1° or 2°), allyl-, and benzylmagnesium halides were suitable nucleophiles, and the MEM and SEM ethers (MEM = methoxyethoxymethyl; SEM = 2-(trimethylsilyl)ethoxymethyl) proved to be superior to methyl ethers in terms of both regio- and diastereoselectivity.[9] In contrast to our previous system for cyclopropene carbometallation,[6a] CuI was not needed for the reactions to form methylenecyclopropanes. The precursors for this chemistry are readily available in enantiomerically enriched form. Thus, 3-hydroxymethylcyclopropenes **1a** and **1b** were prepared by a straightforward sequence of $[Rh_2(dosp)_4]$-catalyzed enantioselective cyclopropenation[5b] (70 and 82% *ee*, respectively) and reduction with DIBAL (dosp = (*N*-dodecylbenzenesulfonyl)prolinate; DIBAL = diisobutylaluminum hydride). Furthermore, it was demonstrated that **1b** could easily be resolved to enantiomeric purity by a method that we have described previously.[5d]

The dependence of selectivity on the counterion suggested that the reaction rates might have a higher-order dependence on the concentration of the Grignard reagent. Therefore, reactions of metalated **1b** with varying amounts of MeMgBr were studied (Table 2). Reactions were quenched after one hour (prior to completion). While detailed kinetic analysis was complicated by the heterogeneous nature of the reaction, it was clear that the reaction had a higher-order dependence on the concentration of the Grignard reagent. Only an isomeric diene side product **4** was observed in the reaction of metalated **1b** with a single equivalent of MeMgBr.

Table 2: Higher-order dependence on MeMgBr for product formation.[a]

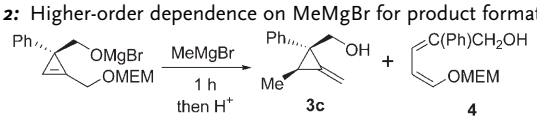

MeMgBr	Conversion [%]	Yield of **3c** [%]	Yield of **4** [%]
1 equiv	40	ca. 0	27
2 equiv	40	20	9
4 equiv	60	43	4

[a] Yields and conversions were measured by ^{1}H NMR spectroscopy; reactions were conducted at 23 °C and quenched after one hour (prior to completion).

Allowing this reaction to continue overnight did not result in the formation of methylenecyclopropane **3c**. Although the mechanism of the isomerization is unclear at this point, the formation of the diene was suppressed and the yield of **3c** increased when the amount of MeMgBr was increased to two equivalents. The ratio of **3c**:**4** was further increased to 10:1 when the amount of MeMgBr was increased to four equivalents.

The results in Table 2 suggest that the magnesium center may serve a second role as a Lewis acid in the reactions of cyclopropenes with Grignard reagents. The addition of $MgBr_2$ did not have an effect on the rate of the reaction,[10] thus suggesting that an alkyl magnesium species serves as the Lewis acid. We hypothesized that coordination of the magnesium center by the MEM ether group influences the regioselectivity. For substrates that lack a coordinating oxygen atom (that is, 1-(*n*-alkyl)cyclopropenes), it is established that delivery of the nucleophile occurs at the more substituted carbon atom.[6b] Accordingly, it was speculated that a sterically demanding trityl ether group would disfavor metal coordination and restore the "normal" regioselectivity. A working hypothesis of the interactions leading to this difference is shown in Scheme 2. Although only two metal

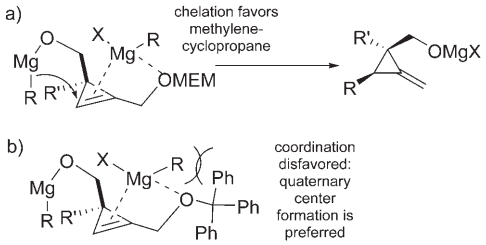

Scheme 2. a) Plausible model for chelation-controlled nucleophilic delivery. b) Replacement of the MEM group by a trityl group is expected to prevent coordination and reverse regioselectivity.

centers are shown in Scheme 2, a mechanism that is higher-order with respect to concentration of magnesium cannot be ruled out. Regardless, the major roles for magnesium (nucleophilic delivery and Lewis acid activation) are conveyed by Scheme 2, which proves to be a useful and predictive model for chelation control of regioselectivity. Thus, efficient reversal of regioselectivity was observed when trityl ether **5** (Scheme 3) was used instead of the corresponding MEM ether **1b**. The best results were obtained when catalytic CuI

 © 2006 Wiley-VCH Verlag GmbH & Co. KGaA, Weinheim

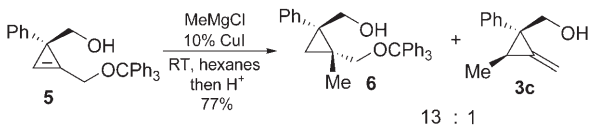

Scheme 3. Reversal of regioselectivity starting from trityl ether **5**.

was included, but the formation of **6** still predominated (4.5:1 ratio of **6**:**3c**) under conditions that were identical to those used to form **3c** from **1b** as described in Table 1.

In summary, general conditions were described for the regio- and diastereoselective synthesis of methylenecyclopropanes from common intermediate precursors. The reaction is counterion-dependent and requires more than one equivalent of Grignard reagent. These observations suggested a Lewis acidic role for the magnesium reagent. This hypothesis was subsequently used to design experiments that reverse the regioselectivity of the nucleophilic delivery. Efforts are currently being made to apply these reactions in target-directed synthesis.

Received: February 9, 2006
Published online: May 9, 2006

Keywords: chirality · diastereoselectivity · regioselectivity · small ring systems · strained molecules

[1] Reviews on methylenecyclopropanes: a) A. Brandi, A. Goti, *Chem. Rev.* **1998**, *98*, 589; b) M. S. Baird, T. Schmidt in *Carbocyclic Three-Membered Ring Compounds* (Ed.: A. de Meijere) Georg Thieme, Stuttgart, **1996**, p. 114; c) M. Lautens, W. Klute, W. Tam, *Chem. Rev.* **1996**, *96*, 49; d) A. Brandi, S. Cicchi, F. M. Cordero, A. Goti, *Chem. Rev.* **2003**, *103*, 1213; e) P. Binger, H. M. Buch, *Top. Curr. Chem.* **1987**, *135*, 77; f) B. M. Trost, *Angew. Chem.* **1986**, *98*, 1; *Angew. Chem. Int. Ed. Engl.* **1986**, *25*, 1.

[2] a) R. D. Bach, O. Dmitrenko, *J. Am. Chem. Soc.* **2004**, *126*, 4444; b) K. B. Wiberg, *Angew. Chem.* **1986**, *98*, 312; *Angew. Chem. Int. Ed. Engl.* **1986**, *25*, 312.

[3] Selected examples of stereospecific transformations of methylenecyclopropanes: a) M. Lautens, Y. Ren, P. H. M. Delanghe, *J. Am. Chem. Soc.* **1994**, *116*, 8821; b) R. J. Boffey, W. G. Whittingham, J. D. Kilburn, *J. Chem. Soc. Perkin Trans. 1* **2001**, 487.

[4] Key references to enantiomerically enriched methylcyclopropanes: a) E. Zohar, A. Stanger, I. Marek, *Synlett* **2005**, 2239, and reference [9] therein; b) M. Lautens, P. H. M. Delanghe, *J. Am. Chem. Soc.* **1994**, *116*, 8526; c) M. Lautens, P. H. M. Delanghe, *J. Org. Chem.* **1993**, *58*, 5037; d) A. de Meijere, L. Wessjohann, *Synlett* **1990**, 20; e) B. Achmatowicz, M. M. Kabat, J. Krajewski, J. Wicha, *Tetrahedron* **1992**, *48*, 10201; f) S. Ramaswamy, K. Prasad, O. Repic, *J. Org. Chem.* **1992**, *57*, 6344; g) J. E. Baldwin, R. M. Adlington, D. Beddington, A. T. Russell, *J. Chem. Soc. Chem. Commun.* **1992**, 1249; h) T. Chevtchouk, J. Ollivier, J. Salaün, *Tetrahedron: Asymmetry* **1997**, *8*, 1005.

[5] a) M. P. Doyle, M. Protopopova, P. Müller, D. Ene, E. A. Shapiro, *J. Am. Chem. Soc.* **1994**, *116*, 8492; b) H. M. L. Davies, G. H. Lee, *Org. Lett.* **2004**, *6*, 1233; c) L.-a. Liao, F. Zhang, O. Dmitrenko, R. D. Bach, J. M. Fox, *J. Am. Chem. Soc.* **2004**, *126*, 4490; d) L.-a. Liao, F. Zhang, N. Yan, J. A. Golen, J. M. Fox, *Tetrahedron* **2004**, *60*, 1803; e) L.-a. Liao, N. Yan, J. M. Fox, *Org. Lett.* **2004**, *6*, 4937; f) S. Chuprakov, M. Rubin, V. Gevorgyan, *J. Am. Chem. Soc.* **2005**, *127*, 3714; g) Y. Lou, M. Horikawa, R. A. Kloster, N. A. Hawryluk, E. J. Corey, *J. Am. Chem. Soc.* **2004**, *126*, 8916.

[6] a) L.-a. Liao, J. M. Fox, *J. Am. Chem. Soc.* **2002**, *124*, 14322; recent reviews on addition of organometallic reagents to cyclopropenes: b) J. M. Fox, N. Yan, *Curr. Org. Chem.* **2005**, *9*, 719; c) M. Nakamura, H. Isobe, E. Nakamura, *Chem. Rev.* **2003**, *103*, 1295; recent examples of regio- and stereoselective hydrometallation reactions of cyclopropenes: d) E. Zohar, I. Marek, *Org. Lett.* **2004**, *6*, 341; e) M. Rubina, M. Rubin, V. Gevorgyan, *J. Am. Chem. Soc.* **2004**, *126*, 3688, and references therein.

[7] Methylenecyclopropanes had previously been prepared by base-promoted isomerization of cyclopropenes. Variants of that reaction involve capture by electrophiles.[4a,7c] The method presented here is distinct because it involves nucleophilic addition to the alkene. For isomerization approaches to cyclopropenes, see references [4a], [6c], and: a) R. Köster, S. Arora, P. Binger, *Angew. Chem.* **1969**, *81*, 642; *Angew. Chem. Int. Ed. Engl.* **1969**, *8*, 205; b) M. Vincens, C. Dumont, M. Vidal, *Tetrahedron* **1981**, *37*, 2683; c) A. Padwa, M. W. Wannamaker, *Tetrahedron* **1991**, *47*, 6139; d) M. Vidal, M. Vincens, P. Arnaud, *Bull. Soc. Chim. Fr.* **1972**, 665; e) A. A. Formanovskii, L. I. Leonova, N. I. Yakushkina, M. Bakhbukh, Y. K. Grishin, I. G. Bolesov, *Zh. Org. Khim.* **1977**, *13*, 1883; A. A. Formanovskii, L. I. Leonova, N. I. Yakushkina, M. Bakhbukh, Y. K. Grishin, I. G. Bolesov, *J. Org. Chem. USSR (Engl. Transl.)* **1977**, *13*, 1745.

[8] There was a single example of palladium-catalyzed nucleophilic substitution on a cyclopropenyl methyl ester to give a methylenecyclopropane in 27% yield (as the minor regioisomer of the reaction); see: a) H. Nüske, S. Bräse, A. de Meijere, *Synlett* **2000**, 1467. Recently, a report appeared that describes the addition of soft nucleophiles to a chiral cyclopropene with a bromine atom at the allylic position. Complementary to the work reported here, the facial control in that work is determined by steric considerations; see: b) R. A. Weatherhead-Kloster, E. J. Corey, *Org. Lett.* **2006**, *8*, 171.

[9] The reaction of **1** (where R = Me, R′ = Ph; see Table 1) with MeMgBr still gave **3c** as the major product (ca. 55%), but with significant contamination by the diasteromeric product (ca. 15%) and two regioisomeric products (ca. 30%).

[10] A reaction was conducted that was similar to the second entry in Table 2, with the modification that four equivalents of $MgBr_2$ were added. After one hour, the reaction was quenched, and the yield of the corresponding methylenecyclopropane was measured to be 16% by analysis of the crude product by ^{1}H NMR spectroscopy.

 © 2006 Wiley-VCH Verlag GmbH & Co. KGaA, Weinheim

Synthetic Methods

DOI: 10.1002/anie.200600556

Enantiomerically Pure Cyclopropenylcarbinols as a Source of Chiral Alkylidenecyclopropane Derivatives**

*Samah Simaan, Ahmad Masarwa, Philippe Bertus, and Ilan Marek**

Over the past few decades, racemic cyclopropene and alkylidenecyclopropane (ACP) derivatives have been established as powerful tools in synthetic chemistry. Indeed, on one hand, cyclopropene derivatives can be readily transformed into more complex molecules by hydro- or carbometalation reactions[1] on the strained internal double bond,[2] whereas ACP derivatives have proven their usefulness by their unique reactivity with transition-metal catalysts.[3] These catalyzed transformations, also based on the release of the high level of strain, can be performed either on the distal or proximal bonds of the three-membered ring and the *exo*-alkylidene moiety.[4] Despite this mounting interest, the synthesis of enantiomerically pure cyclopropenes, particularly 1,2-disubstituted (internal) cyclopropenes and chiral ACPs are still in their infancy.[5] In the course of our study on the functionalization of cyclopropenyl derivatives, we have recently shown that cyclopropenylcarbinols (readily prepared in a one-pot operation from 1,1,2-trihalogenocyclopropane[6]) are regio- and diastereoselectively reduced with $LiAlH_4$ in Et_2O into cyclopropylcarbinols as single *trans* isomers (Scheme 1, path A).[1a] Herein, we document the first preparation of racemic and then enantiomerically pure ACPs **2** from cyclopropenylcarbinol derivatives **1** (Scheme 1, path B) through a copper-catalyzed addition of various Grignard reagents. In our initial investigations, the regio- and stereochemistry of the reaction was first checked on racemic cyclopropenylcarbinol derivatives **1a**–**h**, and the results reported in Table 1 fulfilled our expectations.

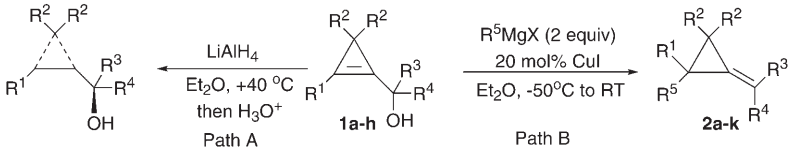

Scheme 1. General preparation of ACPs.

Table 1: Synthesis of ACP derivatives.

Entry	Substrate	R^1	R^2	R^3	R^4	R^5	ACP	E/Z[a]	Yield [%][b]
1	**1a**	CH_3	H	C_2H_5	C_2H_5	C_4H_9	**2a**	–	76
2	**1a**	CH_3	H	C_2H_5	C_2H_5	C_6H_5	**2b**	–	81
3	**1b**	CH_3	H	C_6H_5	C_6H_5	C_6H_5	**2c**	-	61
4	**1c**	C_4H_9	H	C_6H_5	C_6H_5	C_6H_5	**2d**	–	62
5	**1d**	C_4H_9	H	*i*Pr	H	CH_3	**2e**	100:0	82
6	**1e**	CH_3	H	*i*Pr	H	C_4H_9	**2e**	100:0	91
7	**1f**	CH_3	H	C_6H_5	H	C_4H_9	**2f**	97:3	70
8	**1f**	CH_3	H	C_6H_5	H	C_6H_5	**2g**	87:13	66
9	**1f**	CH_3	H	C_6H_5	H	CH_3	**2h**	92:8	81
10	**1f**	CH_3	H	C_6H_5	H	C_2H_5	**2i**	96:4	72
11	**1g**	CH_3	H	Ar[c]	H	C_2H_5	**2j**	95:5	88
12	**1h**	H	CH_3	*p*-tol	H	CH_3	**2k**	12:88	91

[a] Determined on crude NMR spectroscopic and gas-chromatographic analysis. [b] Yield of isolated product after purification by column chromatography. [c] Ar = *p*-BrC_6H_4.

In all experiments, ACPs were obtained in good-to-excellent yields which resulted from a formal copper-catalyzed S_N2' reaction of alkyl and aryl magnesium halides R^5MgX (X = Br, I) with the free allylic alcohol **1a**–**h**. Tertiary and secondary alcohol derivatives (Table 1, entries 1–4 and 5–12, respectively) led similarly to ACP derivatives. Substituents on the double bond of the cyclopropenyl ring (R^1) can be either alkyl groups (entries 1–11) or a hydrogen atom (entry 12). The same is true for substituent R^2. Substituents R^3 and R^4 can be either alkyl, aryl, or hydrogen groups. When secondary alcohols were used (R^3 = alkyl or aryl, R^4 = H; entries 5–12), the fate of the stereochemistry of the double bond was raised. In all these experiments, we always found that the unique or major isomer was *E* configured (in entry 12, the configuration of the double bond was identical but the configuration of the product became *Z* because of the interconversion of substituents R^1 and R^2).[7] Without a copper salt, the reaction did not proceed.

With a straightforward method for the preparation of ACPs from cyclopropenylcarbinol derivatives in hand, we then turned our attention to their asymmetric synthesis. Considering that cyclopropenylcarbinols are strained allylic alcohols, we envisaged the enantiomerically enriched preparation of the ACPs to be through the Sharpless kinetic resolution (Scheme 2).[8] When the racemic allylic alcohol **1f** (Table 2, entry 1) was subjected to the epoxidation reaction conditions using (*R*,*R*)-(+)-diethyl tartrate as the chiral ligand, we were pleased to observe, despite the highly reactive nature of the strained double bond, a very efficient kinetic resolution at −20 °C. Only one enantiomer is epoxi-

[*] Dr. S. Simaan, A. Masarwa, Prof. I. Marek
The Mallat Family Laboratory of Organic Chemistry
Department of Chemistry
Institute of Catalysis Science and Technology
The Lise Meitner-Minerva Center for Computational Quantum Chemistry
Technion-Israel Institute of Technology, Haifa 32000 (Israel)
Fax: (+972) 4-829-3709
E-mail: chilanm@tx.technion.ac.il
Dr. P. Bertus
UMR 6519
Reactions selectives et Applications
CNRS Université de Reims Champagne-Ardenne
BP 1039, 51687 Reims Cedex 2 (France)

[**] This research was supported by the German–Israeli Project Cooperation (DIP-F.6.2), the Fund for the Promotion of Research at the Technion, and a fellowship from the Lady Davis Foundation. The authors thank Prof. Amnon Stanger for his great help in the determination of absolute configuration by computational methods. I.M. is holder of the Sir Michael and Lady Sobell Academic Chair.

 © 2006 Wiley-VCH Verlag GmbH & Co. KGaA, Weinheim

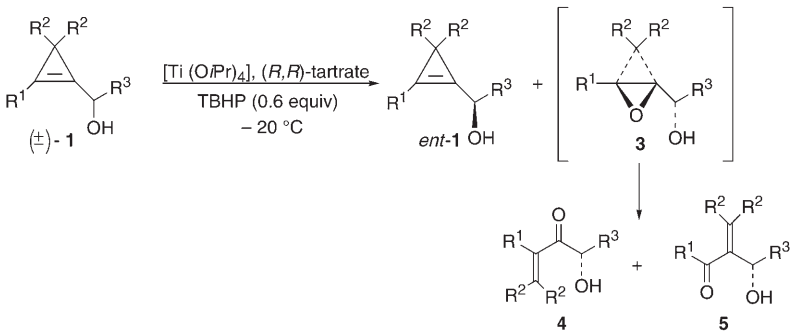

Scheme 2. Kinetic resolution of cyclopropenylcarbinol derivatives. TBHP = *tert*-butyl hydroperoxide.

Table 2: Kinetic resolution of cyclopropenylcarbinol derivatives.

Entry	R^1	R^2	R^3	Products	Yield [%][b]	*ee* [%][a]
1	CH_3	H	C_6H_5	**1f**	46	99
2	CH_3	H	*p*-BrC_6H_4	**1g**	44	99
3	C_4H_9	H	C_6H_5	**1i**	44	99
4	CH_3	H	$CH_2CH_2C_6H_5$	**1j**	42	96
5	CH_3	CH_3	C_6H_5	**1k**	47	99
6	CH_3	CH_3	$CH_2CH_2C_6H_5$	**1l**	40	95

[a] Yield of the isolated product after kinetic resolution and purification by column chromatography. [b] Enantiomeric excess was determined by gas-chromatographic analysis on chiral column (cyclodextrin B; see the Supporting Information).

dized to lead to the putative unstable chiral 2-oxabicyclo-[1.1.0]butane **3**.

Two enantiomerically pure α,β-unsaturated ketols **4** and **5**, formed in equal amounts (each in 22–25% yield of isolated product) as a result of the isomerization of the oxabicyclobutane by cleavage of the two pheripheral σ bonds.[9] Oxabicyclobutanes have been postulated several times to be intermediates in various thermal[10a] and photochemical reactions.[10b] In none of these cases, however, were oxabicyclobutanes detected. Although we were also not able to isolate this intermediate, the Sharpless kinetic resolution implies that the corresponding oxabicyclobutane was formed as a reactive intermediate. The remaining non-oxidized products, namely, the cyclopropenylcarbinols **1** were obtained with very high enantiomeric excess and yields (95–99% *ee* and 40–47% yield of isolated product). The scope of the kinetic resolution is broad, as several different alkyl groups can be present either on the double bond of the cyclopropenyl unit ($R^1 = CH_3$ and C_4H_9) or on the cyclopropene ring itself ($R^2 = H$ or CH_3; Table 2, entries 1–4 and 5 and 6, respectively).

Aryl and alkyl groups can be interchangeably used as secondary substituents at the allylic position, although the enantiomeric excess is slightly higher when R^3 is an aryl group (99% *ee*; entries 1–3 and 5) relative to an alkyl group (≈95% *ee*; entries 4 and 6). Following the strategy we described in Scheme 1, path B for the preparation of ACPs from cyclopropenylcarbinols, alcohols **1f**,**g** were treated with various Grignard reagents in the presence of 20 mol% of CuI (Scheme 3 and Table 3). The reaction proceeds with an

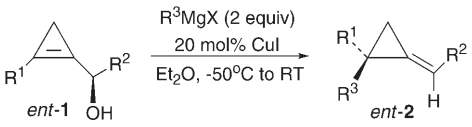

Scheme 3. Preparation of enantiomerically pure ACPs.

excellent transfer of chirality from chiral cyclopropenylcarbinol to ACP regardless of the nature of the alkyl magnesium halides (R^3 = aryl or alkyl; Table 3, entries 1–4).

The absolute configuration of **2j** was determined as *S* by using both computational methods[11] and X-ray analysis of functionalized **2j** (see the Supporting Information).

Table 3: Enantioselective preparation of ACPs.

Entry	Substrate	R^1	R^2	R^3	Product	*E*/*Z*	Yield [%][a]	*ee* [%][b]
1	**1f**	CH_3	C_6H_5	C_6H_5	**2g**	87:13	66	97
2	**1f**	CH_3	C_6H_5	C_4H_9	**2f**	97:3	70	97
3	**1f**	CH_3	C_6H_5	C_2H_5	**2i**	96:4	72	95
4	**1g**	CH_3	*p*-BrC_6H_4	C_2H_5	**2j**	97:3	88	99

[a] Yield of isolated product after purification by column chromatography. [b] Enantiomeric excess of the *E* isomer was determined by gas-chromatographic analysis on chiral column (cyclodextrin B; see the Supporting Information).

The absolute configurations of the starting cyclopropenylcarbinol **1g** and the final ACP **2j** imply an overall *syn* S_N2' displacement of the alcohol moiety. Starting at −50 °C, the stirred mixture was slowly warmed to room temperature and carefully followed by analysis of hydrolyzed aliquots. Under these conditions, we were able to isolate the addition products (after hydrolysis of aliquots of [Cu(**6**)]). These cyclopropyl–metal complexes ([Cu(**6**)] or **6**MgX) disappear in favor of the ACP **2**, which is obtained in good yield. As the deprotonation of the alcohol precedes the addition, the most stable conformer of the cyclopropenylcarbinolate is given in Scheme 4, with the smallest substituent (hydrogen) at the pre-existing orientation "inside" and the aryl group "outside", away from the allylic methyl substituent (minimum 1,3-strain). Thus, this catalytic reaction proceeds through a *syn* addition/*syn* elimination mechanism (Scheme 4).

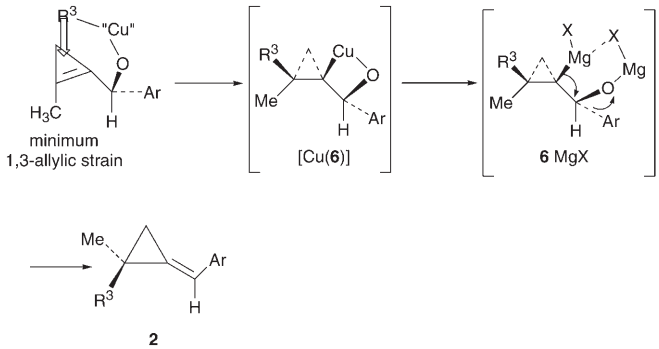

Scheme 4. Mechanistic hypothesis for the overall *syn* S_N2 process.

 © 2006 Wiley-VCH Verlag GmbH & Co. KGaA, Weinheim

In conclusion, the copper-catalyzed carbomagnesiation reaction of chiral cyclopropenylcarbinol derivatives, obtained through the kinetic resolution of secondary allylic alcohols, leads to a straightforward, new preparation of enantiomerically pure alkylidenecyclopropane derivatives.

Received: February 10, 2006
Published online: April 20, 2006

Keywords: cyclopropanes · elimination · Grignard reagents · homogeneous catalysis · strained molecules

[1] Recent hydro- and carbometalation reactions of cyclopropenes: a) E. Zohar, I. Marek, *Org. Lett.* **2004**, *6*, 341; b) E. Zohar, M. Ram, I. Marek, *Synlett* **2004**, 1288; c) J. M. Fox, N. Yan, *Curr. Org. Chem.* **2005**, *9*, 719; d) M. Rubin, V. Gevorgyan, *Synthesis* **2004**, 796; e) M. Rubina, M. Rubin, V. Gevorgyan, *J. Am. Chem. Soc.* **2002**, *124*, 11566; f) M. Rubina, M. Rubin, V. Gevorgyan, *J. Am. Chem. Soc.* **2003**, *125*, 7198; g) M. Rubina, M. Rubin, V. Gevorgyan, *J. Am. Chem. Soc.* **2004**, *126*, 3688; h) L. A. Liao, J. M. Fox, *J. Am. Chem. Soc.* **2002**, *124*, 14322; i) M. Nakamura, H. Isobe, E. Nakamura, *Chem. Rev.* **2003**, *103*, 1295; j) I. Nakamura, G. B. Bajracharya, Y. Yamamoto, *J. Org. Chem.* **2003**, *68*, 2297; k) S. Araki, T. Tanaka, T. Hirashita, J.-i. Setsune, *Tetrahedron Lett.* **2003**, *44*, 8001.

[2] R. D. Bach, O. Dmitrenko, *J. Am. Chem. Soc.* **2004**, *126*, 4444.

[3] For reviews, see: a) A. Brandi, A. Goti, *Chem. Rev.* **1998**, *98*, 589; b) M. Lautens, W. Klute, W. Tam, *Chem. Rev.* **1996**, *96*, 49; c) A. Brandi, S. Cicchi, F. Cordero, A. Goti, *Chem. Rev.* **2003**, *103*, 1213; d) I. Nakamura, Y. Yamamoto, *Adv. Synth. Catal.* **2002**, *344*, 111; e) B. M. Trost, *Angew. Chem. Int. Ed. Engl.* **1986**, *25*, 1; f) Methods of Organic Chemistry, *Houben-Weyl*, *Vol. E17*, (Ed.: A. de Meijere), Thieme, Stuttgart, **1996**.

[4] P. Binger, U. Schuchardt, *Chem. Ber.* **1981**, *114*, 3313.

[5] For chiral cyclopropenes, see: a) L. A. Liao, F. Zhang, N. Yan, J. A. Golen, J. M. Fox, *Tetrahedron* **2004**, *60*, 1803; b) L. A. Liao, F. Zhang, O. Dmitrenko, R. D. Bach, J. M. Fox, *J. Am. Chem. Soc.* **2004**, *126*, 4490; c) L. A. Liao, N. Yan, J. M. Fox, *Org. Lett.* **2004**, *6*, 4937; d) M. K. Pallerla, J. M. Fox, *Org. Lett.* **2005**, *7*, 3593; e) M. Isaka, E. Nakamura, *J. Am. Chem. Soc.* **1990**, *112*, 7428; f) K. Kubota, M. Nakamura, M. Isaka, E. Nakamura, *J. Am. Chem. Soc.* **1993**, *115*, 5867; g) Y. Lou, T. P. Remarchuk, E. J. Corey, *J. Am. Chem. Soc.* **2005**, *127*, 14223; h) Y. Lou, M. Horikawa, R. A. Kloster, N. A. Hawryluk, E. J. Corey, *J. Am. Chem. Soc.* **2004**, *126*, 8916; for chiral ACPs, see: i) E. Zohar, A. Stanger, I. Marek, *Synlett* **2005**, 2239; j) M. Lautens, P. H. M. Delanghe, *J. Am. Chem. Soc.* **1994**, *116*, 8526; k) M. Lautens, Y. Ren, P. Delanghe, P. Chiu, S. Ma, J. Colucci, *Can. J. Chem.* **1995**, *73*, 1251; l) M. Lautens, P. H. M. Delanghe, *J. Org. Chem.* **1993**, *58*, 5037; m) A. de Meijere, L. Wessjohann, *Synlett* **1990**, 20; n) S. Ramaswany, K. Prasad, O. Repic, *J. Org. Chem.* **1992**, *57*, 6344; o) B. Achmatowicz, M. M. Kabat, J. Krajewski, J. Wicha, *Tetrahedron* **1992**, *48*, 10201; p) J. E. Baldwin, R. M. Adlington, D. Beddington, A. T. Russell, *J. Chem. Soc. Chem. Commun.* **1992**, 1249; q) T. Nemoto, M. Ojika, Y. Sakagami, *Tetrahedron Lett.* **1997**, *38*, 5667.

[6] a) M. S. Baird, W. Nethercott, *Tetrahedron Lett.* **1983**, *24*, 605; b) M. S. Baird, H. H. Hussain, *Tetrahedron* **1987**, *43*, 215; c) A. R. Al-Dulayymi, M. S. Baird, *J. Chem. Soc. Perkin Trans. 1* **1994**, 1547.

[7] The stereochemistry of **2j** was determined and assigned by analogy with the other reaction products; see the Supporting Information and also: T. Harada, H. Wada, A. Oku, *J. Org. Chem.* **1995**, *60*, 5370.

[8] Y. Gao, R. M. Hanson, J. M. Klunder, S. Y. Ko, H. Masamune, K. B. Sharpless, *J. Am. Chem. Soc.* **1987**, *109*, 5765.

[9] a) J. Ciabattoni, P. J. Kocienski, *J. Am. Chem. Soc.* **1969**, *91*, 6534; b) J. Ciabattoni, P. J. Kocienski, *J. Am. Chem. Soc.* **1971**, *93*, 4902; c) L. E. Friedrich, R. A. Fiato, *J. Am. Chem. Soc.* **1974**, *96*, 5783; d) P. J. Kocienski, J. Ciabattoni, *J. Org. Chem.* **1974**, *39*, 388; e) L. E. Friedrich, R. A. Fiato, *J. Org. Chem.* **1974**, *39*, 416; f) L. E. Friedrich, N. L. de Vera, Y-S. P. Lam, *J. Org. Chem.* **1978**, *43*, 34; g) J. K. Crandall, W. W. Conover II, *J. Org. Chem.* **1978**, *43*, 1323; h) B. M. Branan, X. Wang, P. Jankowski, J. Wicha, L. A. Paquette, *J. Org. Chem.* **1994**, *59*, 6874.

[10] a) S. Marmor, M. M. Thomas, *J. Org. Chem.* **1967**, *32*, 252; b) E. J. Corey, J. D. Bass, R. Le Mahieu, R. B. Mitra, *J. Am. Chem. Soc.* **1964**, *86*, 5570; c) H. E. Zimmerman, R. G. Lewis, J. J. McCullough, A. Padwa, S. W. Staley, M. Semmelhack, *J. Am. Chem. Soc.* **1966**, *88*, 1965.

[11] a) P. L. Polavarapu, *Chirality* **2002**, *14*, 768; b) C. Forzato, G. Furlan, P. Nitti, G. Pitacco, D. Marchesan, S. Coriani, E. Valentin, *Tetrahedron: Asymmetry* **2005**, *16*, 3011.

 © 2006 Wiley-VCH Verlag GmbH & Co. KGaA, Weinheim

Microporous Materials

DOI: 10.1002/anie.200600054

Microwave-Enhanced Ionothermal Synthesis of Aluminophosphate Molecular Sieves**

Yun-Peng Xu, Zhi-Jian Tian, Shao-Jun Wang, Yue Hu, Lei Wang, Bing-Chun Wang, Ying-Chong Ma, Lei Hou, Jia-You Yu, and Li-Wu Lin*

Molecular sieves are crystalline or amorphous materials with uniform micropores or mesopores.[1–3] They are effective separation materials and are the most important catalysts in industry because of their special structures and acidities.[3,4]

[*] Dr. Y.-P. Xu, Prof. Z.-J. Tian, L. Wang, B.-C. Wang
Laboratory of Natural Gas Utilization and Application Catalysis
Dalian Institute of Chemical Physics
Chinese Academy of Sciences
Dalian 116023 (P.R. China)
Fax: (+86) 411-843-79151
E-mail: xuyp@dicp.ac.cn

Prof. S.-J. Wang, Y. Hu, Y.-C. Ma, L. Hou, Prof. J.-Y. Yu
Department of Chemical Engineering
Dalian Institute of Light Industry
Dalian 116034 (P.R. China)

Prof. Z.-J. Tian, Prof. L.-W. Lin
State Key Laboratory of Catalysis
Dalian Institute of Chemical Physics
Chinese Academy of Sciences
Dalian 116023 (P.R. China)

[**] Financial support from PetroChina Company Ltd. (Grant Nos. W050508-03-03 to Y.-P.X. and Z.-J.T.) and State Key Projects for Basic Research & Development, China (Grant No. 2003CB615805 to S.-J.W.) is gratefully acknowledged. We thank Prof. Mark Schlossman, University of Illinois, for useful discussions.

Supporting information for this article is available on the WWW under http://www.angewandte.org or from the author.

© 2006 Wiley-VCH Verlag GmbH & Co. KGaA, Weinheim

The synthesis of molecular sieves is usually conducted in water or other polar solvents in a sealed container under hydrothermal or solvothermal conditions.[2,3] Many effective methods have been developed for the synthesis of molecular sieves during the last century,[2,3] with one of them being microwave dielectric heating synthesis.[5] Microwaves are a form of electromagnetic energy, and microwave dielectric heating is known popularly as a domestic cooking method, but it is also widely used in organic synthesis, analytical chemistry, polymer curing, and inorganic synthesis.[6] In contrast to conventional heating, the heating effect of microwaves is caused by dielectric loss from the irradiated sample.[5] Microwave heating has been used in the hydrothermal synthesis of molecular sieves,[7,8] and highlighted the advantages of fast crystal growth and high selectivity obtained relative to conventional heating.[5] However, hydrothermal synthesis under microwave heating has safety concerns because of the high temperatures required ($>100\,^{\circ}C$) and autogenous pressure. Moreover, organic templates used in the synthesis of molecular sieves tend to decompose under microwave irradiation at high temperatures, which impairs the structure-directing function of the templates.[5] These drawbacks limit the utilization of microwaves in the hydrothermal synthesis of molecular sieves.

Recently, Morris and co-workers reported a novel method for the synthesis of molecular sieves known as ionothermal synthesis,[9] which has attracted the interest of other researchers.[10–12] In ionothermal synthesis, molecular sieves are synthesized in an ionic liquid, which is different from hydrothermal and solvothermal synthesis which employs a molecular liquid.[9] The predominant advantages of the ionothermal synthesis of molecular sieves are that a separate organic template is not required and the synthesis can be carried out at ambient pressure. Ionic liquids are special molten salts typically containing organic cations and inorganic anions.[13,14] They have a low melting point ($<100\,^{\circ}C$), relatively low viscosity, high electric and thermal stability, are good solvents for a wide range of organic and inorganic materials, and, importantly, have negligible vapor pressure.[13,14] These characteristics enable ionic liquids to be widely used as a "green" solvent, functional solvent, or catalyst in organic synthesis,[15,16] inorganic preparation,[17,18] electrochemistry,[19,20] as well as other areas.[21,22] Ionic liquids have been proven to be good media for absorbing microwaves,[23,24] so there is a possibility to combine the "green" solvent aspect of ionic liquids with the "green" chemistry aspect of microwave irradiation to yield a new synthesis method. Very recently Zhu et al. reported a new microwave-assisted ionic liquid method (MAIL) for the fast, controlled synthesis of nonporous nanomaterials.[25] This is a good example of combining microwaves and ionic liquids for inorganic synthesis.

Here we report the ionothermal synthesis of molecular sieves under microwave heating—namely, the microwave-enhanced ionothermal synthesis of molecular sieves—which combines the advantages of both microwave heating and ionothermal synthesis. The synthesis of a series of aluminophosphate molecular sieves by this process demonstrates the advantages of a rapid crystal growth rate, high product selectivity, and low pressure. The method overcomes the drawbacks of the hydrothermal synthesis of molecular sieves by microwave heating, including safety concerns, and provides a new way to synthesize molecular sieves.

The microwave-enhanced ionothermal synthesis was carried out in a microwave reaction system, and the crystallization reaction was conducted in an open round-bottom glass flask under microwave irradiation. The effects of different heating methods (conventional and microwave dielectric) on the ionothermal synthesis of molecular sieves were investigated.

In contrast to microwave-heating hydrothermal synthesis of molecular sieves, the use of ionic liquids allows the synthesis with microwave heating to be conducted under low pressure and safe conditions. The crystallization of the molecular sieves during the ionothermal synthesis is carried out in an open flask at $150\,^{\circ}C$. Under the conditions of hydrothermal synthesis, the pressure can reach 476 KPa at this temperature. Therefore, a pressure-resistant vessel such as a metal autoclave would be needed in hydrothermal synthesis, but this is not suitable for microwave dielectric heating. Teflon and other microwave-transparent polymers are widely used to make autoclaves for microwave heating, but they become flexible at high temperatures and cannot withstand the high pressure. This may lead to a serious safety concern, which limits the utilization of microwave dielectric heating at high pressures. The use of an ionic liquid such as 1-ethyl-3-methylimidazolium bromide ([emim]Br) addresses this problem, since it has negligible vapor pressure and high stability at $150\,^{\circ}C$ or even higher temperatures.[14] In addition, ionic liquids have high polarity and electric conductivity. Both dipolar polarization losses and conduction losses occur[23] when ionic liquids are irradiated by microwaves which generate heat. Ionic liquids readily absorb microwaves and can be heated rapidly;[23] therefore, ionic liquids are the ideal solvent for the safe synthesis of molecular sieves by microwave irradiation.

Ionothermal synthesis has been shown to be an effective method for the preparation of aluminophosphate molecular sieves.[9] AEL-type aluminophosphate molecular sieves ($AlPO_4$-11 and SAPO-11) were successfully synthesized in [emim]Br under ionothermal conditions.[9,26] The microwave-enhanced ionothermal synthesis in the same ionic liquid produced the same type of aluminophosphate molecular sieve (AEL, PDF-410556), nevertheless the crystallization time was much shorter than that with conventional heating. The X-ray diffraction (XRD) patterns of AEL-type aluminophosphate molecular sieves prepared with microwave heating and conventional heating ionothermal processes are shown in Figure 1. The effect of crystallization time on the growth of the AEL molecular sieves under microwave and conventional heating is shown in Figure 2. Complete crystallization required several hours under conventional heating as shown in Figure 2b, while the yield of solid product decreased with increasing time (Table 1). However, the crystallization of the molecular sieve under microwave heating was completed within tens of minutes (Figure 2a) and the yield of solid product increased within the crystallization time investigated (Table 1). We can conclude from these results that microwave heating led to a more rapid growth of crystalline molecular

 © 2006 Wiley-VCH Verlag GmbH & Co. KGaA, Weinheim

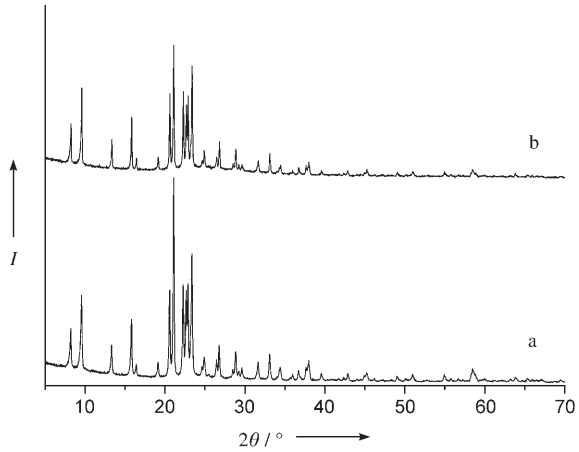

Figure 1. XRD patterns of the aluminophosphate molecular sieves (AEL type) prepared by ionothermal synthesis: a) with 24 h of conventional heating and b) with 20 minutes of microwave heating. Synthesis conditions: 150 °C, ambient pressure, ionic liquid: [emim]Br.

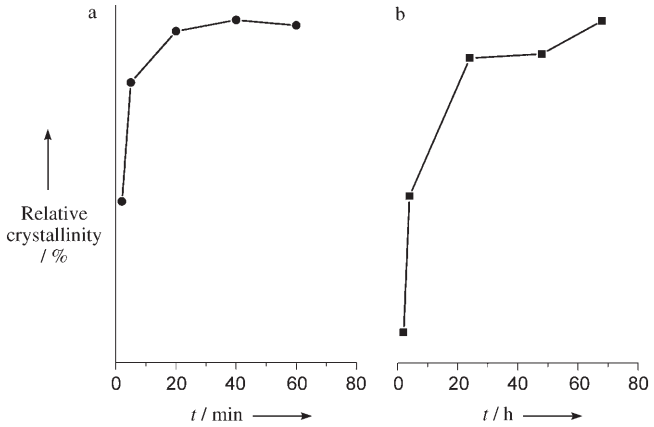

Figure 2. Relative crystallinities of aluminophosphate molecular sieves (AEL type) prepared by ionothermal synthesis as a function of time: a) with microwave heating and b) with conventional heating. Synthesis conditions: 150 °C, ambient pressure, ionic liquid: [emim]Br.

Table 1: Crystallinities and yields of molecular sieve (AEL-type) samples synthesized by ionothermal processes.[a]

Sample	IL[b]:P:Al:F:Si	Heating mode	*t* [min]	Relative crystallinity [%]	Solid product yield [%]
CH-1	40:3:1:0.8:0	conventional	240	48.8	103
CH-2	40:3:1:0.8:0	conventional	1440	89.1	75.3
CH-3	40:3:1:0.8:0	conventional	4080	100	62.9
MW-1	40:3:1:0.8:0	microwave	2	47.0	26.3
MW-2	40:3:1:0.8:0	microwave	20	96.7	47.1
MW-3	40:3:1:0.8:0	microwave	60	98.4	62.7
MW-4	40:3:1:1.6:0	microwave	20	144.3	10.9
MWS-1	40:3:1:0.8:0.25	microwave	60	25.1	74.0
MWS-2	40:3:1:1.6:0.25	microwave	60	100	17.2

[a] Synthesis conditions: 150 °C, ambient pressure, ionic liquid [emim]Br. [b] Ionic liquid [emim]Br.

sieve compared with that by conventional heating during ionothermal synthesis. The rapid crystallization under microwave heating also produced a different morphology of the AEL molecular sieve crystallines (Figure 3). Samples obtained by conventional heating have needlelike features; however, samples synthesized by microwave heating consist primarily of cuboidlike crystallites. In ionothermal synthesis,

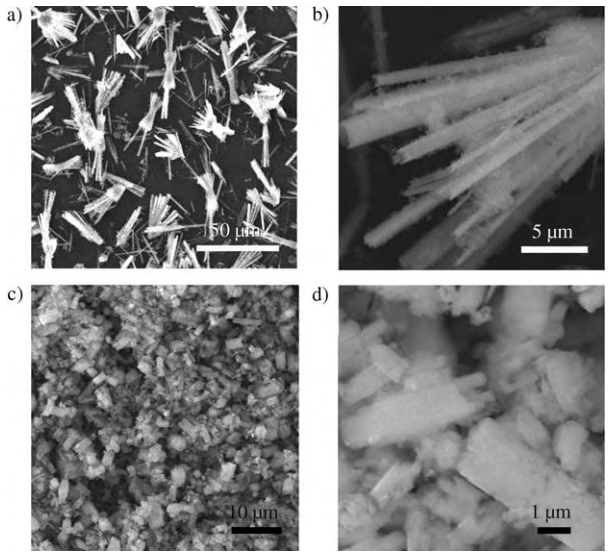

Figure 3. SEM micrographs of aluminophosphate molecular sieves (AEL type) prepared by ionothermal synthesis: a), b) samples after 68 h crystallization with conventional heating; c), d) samples after 20 minutes crystallization with microwave heating. Synthesis conditions: 150 °C, ambient pressure, ionic liquid: [emim]Br.

crystallites grow in an optimal direction as a result of the ionic liquid environment[25] and form needlelike morphologies. However, under microwave heating, rapid crystallization weakens the optimal directional growth which leads to the formation of cuboidlike crystallites.

The rapid crystallization of molecular sieves during microwave-enhanced ionothermal synthesis is probably a consequence of local superheating. The growth of the molecular sieve generally consists of three periods:[3,5] 1) digestion and equilibration of reactants, 2) crystal nucleation, and 3) crystal growth. Earlier experimental evidence from hydrothermal synthesis showed that local superheating induced by microwaves could facilitate the reagent digestion to hasten the equilibration of the reactants between the liquid and solid phases.[5–7] Therefore, crystal nucleation and crystal growth would be faster with microwave heating than with conventional thermal heating hydrothermal synthesis. The local superheating effect of microwaves is caused mainly by the heterogeneity of the reaction mixtures used in hydrothermal synthesis, which leads to several different energy-loss mechanisms coexisting in the bulk phase of hydrothermal synthesis mixtures used in microwave irradiation.[5] In microwave-enhanced ionothermal synthesis, the situation is similar to the microwave-enhanced hydrothermal synthesis. Ionic liquids have high polarity and good conductivity and can be heated effectively by microwaves.[23] Ionothermal synthesis mixtures are cloudy liquids and have noticeable heterogeneity. Thus, it is likely that the different energy-loss mechanisms will coexist in ionothermal synthesis, which will lead to local

 © 2006 Wiley-VCH Verlag GmbH & Co. KGaA, Weinheim

superheating effects by the microwaves. Therefore, the digestion of reagents will be facilitated and a rapid crystallization rate will be obtained in microwave-enhanced ionothermal synthesis. The product yields obtained with microwave heating is lower than that obtained from ionothermal synthesis with conventional heating (Table 1). The results imply that more reactant exists in the liquid phase under microwave heating than under conventional heating and provides evidence that microwaves facilitate the digestion of the reactant. Therefore, the crystallization during microwave-enhanced ionothermal synthesis is faster than with conventional heating.

Fluoride plays an important role in ionothermal synthesis and affects both the yield of the crystalline product and its crystallinity. Thus, the effect on crystallization of adding HF to the synthesis mixtures with microwave heating was investigated. Table 1 shows that the product yield increased from 10.9% to 47.1% when the ratio of HF was decreased from 1.6:1 to 0.8:1 (molar ratio of F:Al in the synthesis mixtures). The crystallinity of the AEL structure produced increased as the amount of HF was increased (Figure 4).

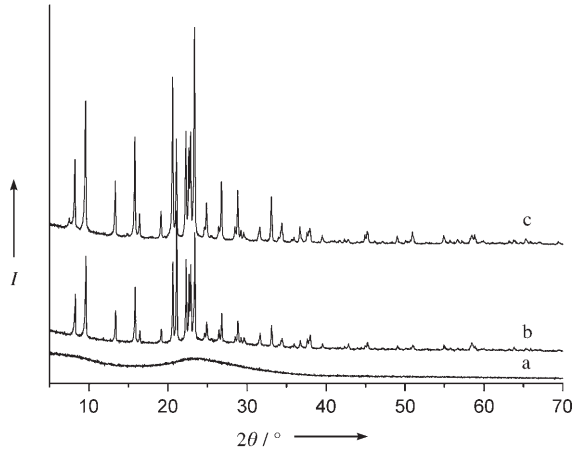

Figure 4. XRD patterns of aluminophosphate molecular sieves (AEL type) prepared by microwave-enhanced ionothermal synthesis with different amounts of HF additive. Molar ratio of F:Al in the synthesis mixtures: a) 0:1, b) 0.8:1, c) 1.6:1. Synthesis conditions: 150°C, 20 min, ambient pressure, ionic liquid [emim]Br.

However, no aluminophosphate molecular sieves were formed without the addition of HF, although the yield of solid products of Al species could reach nearly 100%. The results indicate that the presence of fluoride was a key factor in the formation of AEL-type aluminophosphate molecular sieves. However, excessive fluoride decreases the yield of crystalline products in ionothermal synthesis. Previous literature reports show that fluoride displays the same effect in hydrothermal synthesis.[27,28] It is widely accepted that fluoride reacts with the reagent to form soluble fluoride species that remain in the solution after crystallization[28] and are incorporated with difficulty into the crystalline phase of the molecular sieve. Thus, the yield of the solid product was low when fluoride was involved in the crystallization process. As in the microwave-enhanced ionothermal synthesis, microwaves facilitate the process of digestion and equilibration of reactants during crystallization, as discussed above.[5] Furthermore, according to our results, it seems unlikely that the anion of the ionic liquid (Br^- in the ionic liquid [emim]Br) participated in the digestion period of the molecular sieve crystallization since no AEL-type structure formed after crystallization and the yield of the solid product was almost 100%. Therefore, it seems likely that microwaves enhanced the reaction of F^- ions with Al species, namely, enhanced the digestion of the reactant into the liquid phase, as well as facilitated the formation of the molecular sieve structure during ionothermal synthesis.

In the ionothermal synthesis of aluminophosphate molecular sieves, the introduction of a silicon source (e.g. tetraethyl orthosilicate (TOES)) into the synthesis mixture can result in the formation of AEL-type silicoaluminophosphate molecular sieves (SAPO-11). The molar compositions of the reagents used in the synthesis mixtures are shown in Table 1. The incorporation of silicon into the framework of the molecular sieves is an important indication of the formation of AEL-type silicoaluminophosphate molecular sieves. We used ^{29}Si NMR spectroscopy, energy-dispersive X-ray spectroscopy (EDX), and temperature-programed desorption of ammonia (NH_3-TPD) to determine that Si was incorporated into the framework of the AEL molecular sieves (see the Supporting Information).

In contrast to the ionothermal synthesis of AEL aluminophosphate molecular sieves, the introduction of Si into the synthesis mixtures hindered the crystallization of the AEL structure. Figure 5a shows that the crystallinity was very low after one hour of microwave irradiation at 150°C when TOES was added to the reactions. Under the same reaction conditions the crystallization was almost complete in the absence of Si. The digestion and incorporation of the Si materials into the molecular sieve framework has a close relationship with the amount of fluoride in the synthesis mixtures. It seems that competition between the Si and Al

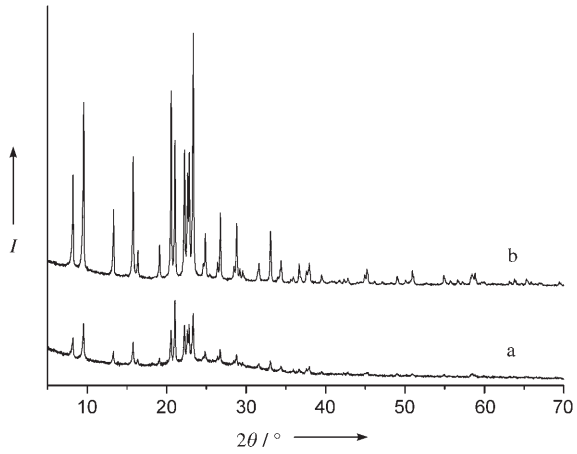

Figure 5. XRD patterns of silicoaluminophosphate molecular sieves (AEL type) prepared by microwave-enhanced ionothermal synthesis with different amounts of HF additive amount. Molar ratio of F:Al in the synthesis mixtures: a) 0.8:1, b) 1.6:1. Synthesis conditions: 150°C, 60 min, ambient pressure, ionic liquid [emim]Br.

 © 2006 Wiley-VCH Verlag GmbH & Co. KGaA, Weinheim

species to react with F^- ions may exist in the crystallization, which has a negative effect on the growth of the AEL molecular-sieve structure. To verify this supposition, twice the amount of HF was added into the reaction. As expected, the AEL structure obtained had a higher crystallinity when microwave irradiation was used (Figure 5b). However, the crystalline yield was very low (decreasing from 74.0% to 17.2%) because of the high degree of digestion of Si and Al materials as a consequence of the large amount of F^- ions.

In a conventional heating ionothermal synthesis process, in addition to the formation of AEL-type molecular sieves, other by-products are produced[26] (Figure 6a), whose structures are similar to chabazite. However, when microwave heating was used, the product was nearly pure AEL-type molecular sieve (Figure 6b). The high structural selectivity of microwave synthesis may be related to the local superheating by the microwaves. The growth of AEL-type molecular sieves may be facilitated under such conditions. Therefore, the high crystallization rate of AEL-type molecular sieves under microwave heating depressed the growth of other by-products.

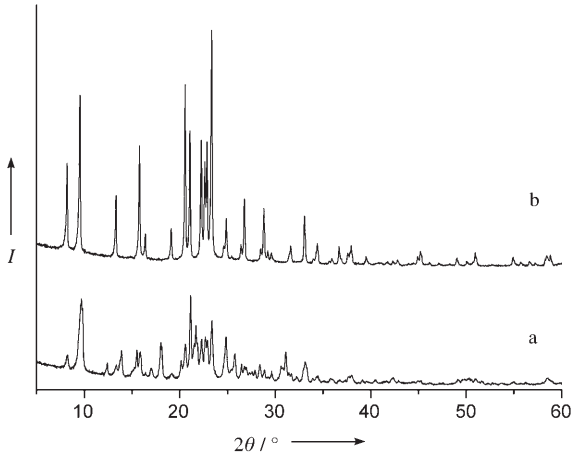

Figure 6. XRD patterns of silicoaluminophosphate molecular sieves (AEL type) prepared by ionothermal synthesis: a) with 68 h of conventional heating and b) with 60 min of microwave heating. Synthesis conditions: 150°C, ambient pressure, ionic liquid [emim]Br.

We also investigated another ionic liquid, 1-butyl-3-methylimidazolium bromide ([bmim]Br), as an ionothermal synthesis medium during microwave heating. The results showed that [bmim]Br led to the formation of mixtures of AEL ($AlPO_4$-11, PDF-410556) and AFI ($AlPO_4$-5, PDF-410044) aluminophosphate molecular sieves (Figure 7). The crystallinity of the AFI structure decreases with reaction time, while the AEL structure displays the opposite trend.

The ionic liquid plays a dual role in the ionothermal synthesis of molecular sieves: solvent and template.[9] The size of the cation in the ionic liquids is very important for determining the structure of the molecular sieves. The imidazolium cation $[bmim]^+$ is larger than $[emim]^+$. Thus, the AFI structure formed with $[bmim]^+$ has a 12-ring channel (7.3×7.3 Å)[29] that is larger than the AEL structure formed with $[emim]^+$ which has a 10-ring channel (6.5×4.0 Å).[30] This

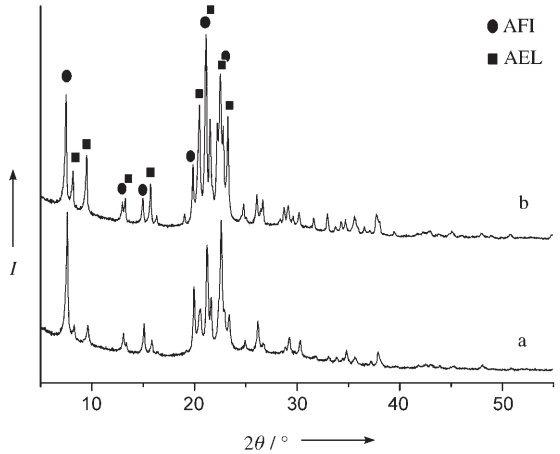

Figure 7. XRD patterns of mixture of aluminophosphate molecular sieves (AEL and AFI types) prepared by microwave-enhanced ionothermal synthesis in [bmim]Br with different crystallization times: a) 10 min; b) 40 min. Synthesis conditions: 150°C, ambient pressure.

result implies a relationship between the cation size of the ionic liquid and the structure of the molecular sieve formed during ionothermal synthesis, which means that a templating effect of the ionic liquid may exist during ionothermal synthesis. Further work on the synthesis of AFI-type aluminophosphate molecular sieves in [bmim]Br is now underway.

In summary, microwave-enhanced ionothermal synthesis is a novel method to prepare molecular sieves. Its advantages are its fast crystallization rate, low synthesis pressure, and high structural selectivity. Ionic liquids are "green" solvents with immeasurably low vapor pressure and good stability. They are also appropriate templates for porous materials and good microwave absorbers that are suitable for microwave dielectric heating. The method reported here will lead to a very promising future for the preparation of molecular sieves by microwave heating.

Experimental Section

Typical preparation of reaction mixtures for ionothermal synthesis: Ionic liquid ([emim]Br or [bmim]Br; 40.0 g) and H_3PO_4 (1.8 g; 85 wt% in water) were mixed in a round-bottom flask, then heated to 100°C with continuous stirring for 10 min. $[Al\{OCH(CH_3)_2\}_3]$ (1.06 g) and an appropriate amount of HF (40 wt% in water) were added separately to the above mixtures. When the target product was silicoaluminophosphate molecular sieve a certain amount of tetraethyl orthosilicate (TEOS) was then introduced to the liquid mixtures. The molar ratio of ionic liquid to Al in the synthesis mixtures was around 40:1. A small amount of water accompanying the H_3PO_4 and HF existed in the synthesis mixtures at the beginning of synthesis. The final reaction mixtures were stirred at 100°C for 20 min and then were heated to 150°C under microwave irradiation or conventional heating for crystallization of the molecular sieves.

Microwave-enhanced ionothermal synthesis of aluminophosphate and silicoaluminophosphate molecular sieves: The final reaction mixtures prepared at 100°C were placed in a microwave reaction system and heated to 150°C at about 20 K min^{-1} and kept under ambient pressure for 2–60 min. The microwave reaction system of MARS5 made by CEM Co. (2.45 GHz, maximum power of 1200 W) was used in the experiment. An RPT-300 plus temperature

 © 2006 Wiley-VCH Verlag GmbH & Co. KGaA, Weinheim

control sensor was used to measure and control the reaction temperature in the round-bottom flask. The resulting products were washed thoroughly with acetone and water after the synthesis mixtures had cooled to room temperature. The yield of the crystalline product was calculated on the basis of the theoretical amount of $AlPO_4$ in the synthesis mixtures.

Conventional electric heating ionothermal synthesis of aluminophosphate and silicoaluminophosphate molecular sieves: The final reaction mixtures prepared at 100 °C were heated to 150 °C within about 30 min in an oil bath and kept for an appropriate time for crystallization of the molecular sieves. Treatment of the resultant products and calculation of the yield of the solid product are the same as for the microwave heating process.

Sample characterization: The samples were characterized by X-ray diffraction (XRD) and scanning electron microscopy (SEM). XRD patterns were recorded on a Philips instrument (model CX' Pert PRO, Cu_K radiation, nickel filter, $\lambda = 1.5404$ Å, operating at 40 kV, 40 mA, and with a 2θ scanning speed of $5° \, min^{-1}$). The sample morphology was examined by SEM (JEOL JSN-6460 LV model).

Received: January 6, 2006
Published online: May 9, 2006

Keywords: ionic liquids · ionothermal synthesis · microporous materials · microwaves

[1] D. W. Breck, *Zeolite Molecular Sieves*, Wiley, New York, **1974**.
[2] R. Szostak, *Molecular Sieves—Principles of Synthesis and Identification*, 1st ed., Van Nostrand Reinhold, New York, **1989**, 2nd ed., Blackie, London, **1998**.
[3] C. S. Cundy, P. A. Cox, *Chem. Rev.* **2003**, *103*, 663.
[4] R. A. van Santen, X. Rozanska, *Adv. Chem. Eng.* **2001**, 28,399.
[5] C. S. Cundy, *Collect. Czech. Chem. Commun.* **1998**, *63*,1699.
[6] S. A. Galema, *Chem. Soc. Rev.* **1997**, *26*, 233.
[7] A. Arafat, J. C. Jansen, A. R. Ebaid, H. van Bekkum, *Zeolites* **1993**, *13*, 162.
[8] X. Xu, W. Yang, J. Liu, L. Lin, *Adv. Mater.* **2000**, *12*, 195.
[9] E. R. Cooper, C. D. Andrews, P. S. Wheatley, P. B. Webb, P. Wormald, R. E. Morris, *Nature* **2004**, *430*, 1012.
[10] E. R. Parnham, R. E. Morris, *J. Am. Chem. Soc.* **2006**, *128*, 2204.
[11] J. H. Liao, P. C. Wu, Y. H. Bai, *Inorg. Chem. Commun.* **2005**, *8*, 390.
[12] E. R. Parnham, P. S. Wheatley, R. E. Morris, *Chem. Commun.* **2006**, 380.
[13] P. Wasserscheid, W. Keim, *Angew. Chem.* **2000**, *112*, 3926; *Angew. Chem. Int. Ed.* **2000**, *39*, 3772.
[14] T. Welton, *Chem. Rev.* **1999**, *99*, 2071.
[15] J. A. Boon, J. A. Levisky, J. L. Pflug, J. S. Wilkes, *J. Org. Chem.* **1986**, *51*, 480.
[16] Y. Chauvin, B. Gilbert, I. Guibard, *J. Chem. Soc. Chem. Commun.* **1990**, 1715.
[17] M. Antonietti, D. Kuang, B. Smarsly, Y. Zhou, *Angew. Chem.* **2004**, *116*, 5096; *Angew. Chem. Int. Ed.* **2004**, *43*, 4988.
[18] Y. Zhou, J. H. Schattka, M. Antonietti, *Nano Lett.* **2004**, *4*, 477.
[19] T. B. Scheffler, C. L. Hussey, K. R. Seddon, C. M. Kear, P. D. Armitage, *Inorg. Chem.* **1983**, *22*, 2099.
[20] T. M. Laher, C. L. Hussey, *Inorg. Chem.* **1983**, *22*, 3247.
[21] D. Appleby, C. L. Hussey, K. R. Seddon, J. E. Turp, *Nature* **1986**, *323*, 614.
[22] F. Shi, J. Peng, Y. Deng, *J. Catal.* **2003**, *219*, 372.
[23] J. Hoffmann, M. Nüchter, B. Ondruschka, P. Wasserscheid, *Green Chem.* **2003**, *5*, 296.
[24] N. E. Leadbeater, H. M. Torenius, *J. Org. Chem.* **2002**, *67*, 3145.
[25] Y. Zhu, W. Wang, R. Qi, X.-L. Hu, *Angew. Chem.* **2004**, *116*, 1434; *Angew. Chem. Int. Ed.* **2004**, *43*, 1410.
[26] Y. Xu, Z. Tian, Z. Xu, B. Wang, P. Li, S. Wang, Y. Hu, Y. Ma, K. Li, Y. Liu, J. Yu, L. Lin, *Chin. J. Catal.* **2005**, *26*, 446.
[27] P. A. Barrett, M. A. Camblor, A. Corma, R. H. Jones, L. A. Villaescusa, *J. Phys. Chem. B* **1998**, *102*, 4147.
[28] S. I. Zones, R. J. Darton, R. Morris, S. J. Hwang, *J. Phys. Chem. B* **2005**, *109*, 652.
[29] J. M. Bennett, J. P. Cohen, E. M. Flanigen, J. J. Pluth, J. V. Smith, *ACS Symp. Ser.* **1983**, *218*, 109.
[30] J. M. Bennett, J. W. Richardson, Jr., J. J. Pluth, J. V. Smith, *Zeolites* **1987**, *7*, 160.

 © 2006 Wiley-VCH Verlag GmbH & Co. KGaA, Weinheim

Nanoparticle Assemblies

DOI: 10.1002/anie.200504419

Charge Transfer between Metal Nanoparticles Interconnected with a Functionalized Molecule Probed by Surface-Enhanced Raman Spectroscopy**

*Qun Zhou, Xiaowei Li, Qiang Fan, Xingxia Zhang, and Junwei Zheng**

The assembly of nanosized metal particles with functionalized molecules is a rapidly emerging field of great fundamental and practical interest because of the prospective applications in nanoelectronic devices.[1] The charge transfer (CT) properties of individual particles are dependent on the particle size and the distance between the particles. Importantly, the activation energy for electron transfer between the particles can be varied by the structure of the interconnecting molecule. In particular, tunneling CT may occur for particles covalently linked with π-conjugated molecules.[2] Recent progress in surface-enhanced Raman spectroscopy (SERS) has made single-molecule detection possible, which is of considerable interest to the communities concerned with nanomaterials, analytical chemistry, and single-molecule spectroscopy. An enhancement factor of approximately 10^{11} has been estimated at the junctions between the closely spaced nanoparticles, as a result of the electromagnetic (EM) enhancement mechanism.[3] The CT mechanism has also been suggested to play an important role in single-molecule SERS.[4] Herein, we investigate the Raman scattering of molecules in the assembled structures of metal nanoparticles.

The present study is of interest from two points of view. First, by using layer-by-layer (LBL) self-assembly, a molec-

[*] Prof. Q. Zhou, X. Li, Q. Fan, X. Zhang, Prof. J. Zheng
Department of Chemistry
Suzhou University
Suzhou 215006 (P.R. China)
Fax: (+86) 512-6588-0089
E-mail: jwzheng@suda.edu.cn

[**] Financial support from the Nature Science Foundation of China (Nos. 20473056, 20073028) and the State Key Laboratory of Organic Synthesis of Jiangsu Province is gratefully acknowledged.

WILEY InterScience DISCOVER SOMETHING GREAT
© 2006 Wiley-VCH Verlag GmbH & Co. KGaA, Weinheim

ular-scale gap can be spontaneously formed between the metal nanoparticles through interconnecting functionalized 4-aminothiophenol (PATP) molecules, which is a typical "push–pull"-type molecule with the electron-donating and electron-accepting groups connected by a conjugated π system. Second, SERS measurements were performed with near-IR excitation (1064 nm), which is far away from the surface plasmon resonance of the metal nanoparticles. This strategy may distinctly demonstrate the CT behavior of metal contacts, which play a significant role in metal–molecule–metal nanosystems.

The LBL assembly of the metal nanoparticles is illustrated in Figure 1 A. The protonated pyridine groups of polyvinylpyridine (PVP) derivatized on a glass slide provided the active sites for the adsorption of negatively charged gold

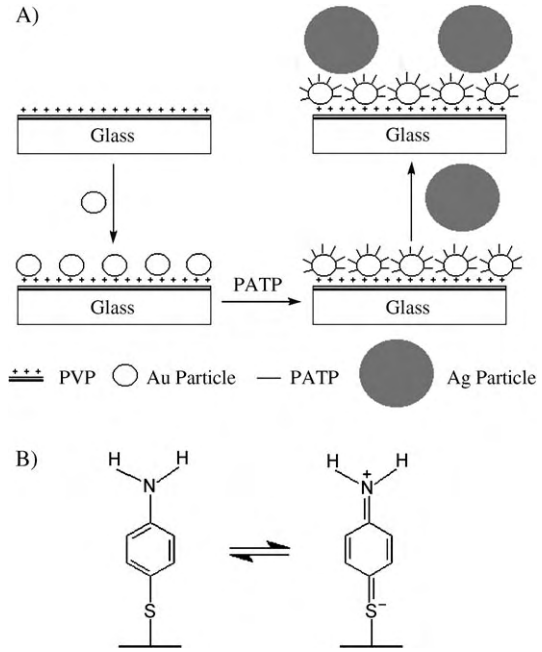

Figure 1. Illustration of A) the assembly of gold and silver nanoparticles and B) the resonance structures of the adsorbed PATP molecule.

nanoparticles. A layer of gold nanoparticles ($\approx$30 nm in diameter) was assembled on the surface by electrostatic interaction. PATP molecules were then adsorbed on the surface of the assembled gold nanoparticles through the formation of Au–S bonds. Similar to *p*-nitroaniline,[5] the PATP molecule possesses two resonance structures: the benzenoid and quinonoid forms (Figure 1 B). In the quinonoid form, it can further interact electrostatically or covalently with silver nanoparticles. As a result, a layer of silver nanoparticles ($\approx$100 nm in diameter) can be assembled on top of the gold nanoparticle layer.

Scanning electron microscopy (SEM) images of the surface morphologies of the single and double assemblies of the metal nanoparticles are shown in Figure 2. As can be seen, the gold nanoparticles were uniformly assembled into a submonolayer structure on the PVP-derivatized glass surface. Most of the particles existed separately as a result of the

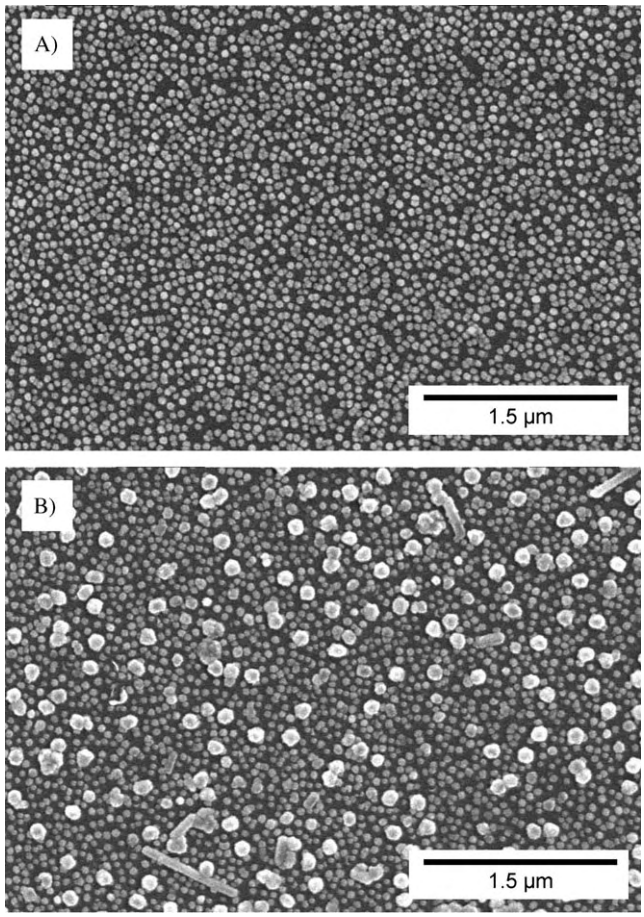

Figure 2. SEM images of A) gold nanoparticle and B) gold/PATP/silver assemblies.

electrostatic repulsion because of their negative charge. No apparent change in the assembled structure of the nanoparticles was observed after the adsorption of PATP, which indicates that the PATP molecules adsorbed on the surface of the individual gold nanoparticles did not disturb the distribution of the particles on the slide surface. The second layer of metal nanoparticles is distinguishable after the assembly of the silver nanoparticles (Figure 2 B). A single silver nanoparticle may be attached to several underlying gold nanoparticles because of the difference in the particle size.

As a result of the dipole–dipole EM interaction between the particles,[6] the surface plasmon resonance (SPR) of the gold nanoparticles shifted from 527 nm for the particles in the colloid (Figure 3, curve a) to 531 nm for the particles immobilized on the surface of the PVP-derivatized glass slide (Figure 3, curve b). The adsorption of the PATP molecules on the gold nanoparticles caused negligible spectral change. Further assembly of a layer of silver nanoparticles resulted in the appearance of the SPR band of the silver nanoparticles at 432 nm, along with the SPR band of the gold nanoparticles (Figure 3, curve c). However, a shift of the SPR of the gold nanoparticles to 528 nm was observed. This shift could result from either EM interaction of the metal particles in different layers, or CT through the linked PATP molecules, as demonstrated by SERS.

 © 2006 Wiley-VCH Verlag GmbH & Co. KGaA, Weinheim

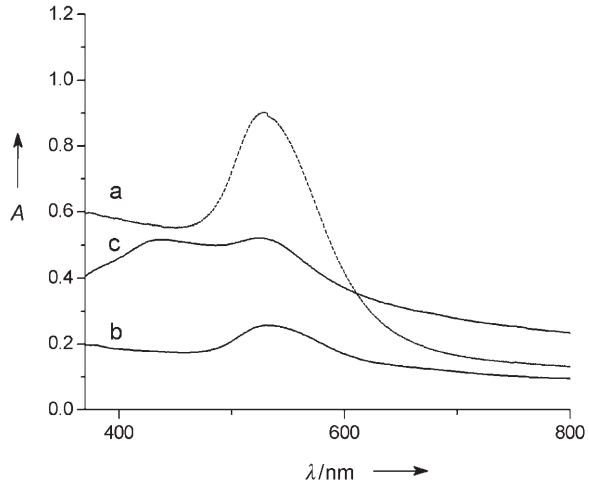

Figure 3. Extinction spectra of a) a gold colloid, b) the gold nanoparticle assembly, and c) the gold/PATP/silver assembly.

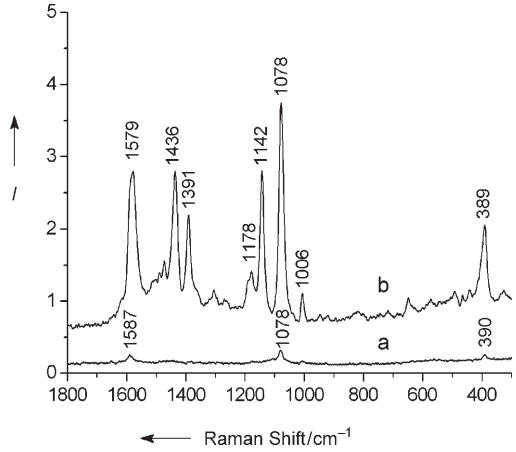

Figure 4. Surface-enhanced Raman spectra of PATP molecules a) adsorbed on the assembled gold nanoparticles and b) interconnected in the gold/PATP/silver assembly.

In most of the SERS studies, the difficulty in experimentally gaining deep insight into the enhancement associated with the CT mechanism is that the chemical enhancement is normally inextricably linked with the EM enhancement. For example, in a recent SERS study of the assembly of silver nanoparticles interconnected with symmetric 1,4-benzenedithiol molecules, Moskovits and Jeong[7] demonstrated a large SERS enhancement of the interconnecting molecules as a result of the strong local EM field produced in the interstitial regions between the neighboring nanoparticles. However, the contribution from the CT mechanism was not described in their study. It is probable that the EM mechanism, which is strongly related to the SPR of the metal particles in the visible spectral region, is the main factor responsible for the overall SERS enhancement under their experimental conditions (with excitation at 514 nm). In the present study, we measured the surface-enhanced Raman spectra with excitation at 1064 nm, which is far away from the SPR bands of the nanoparticles in the assemblies. Therefore, the Raman spectral features obtained under our experimental conditions may be largely associated with the CT effect.

The surface-enhanced Raman spectra of the PATP molecules adsorbed on the gold nanoparticle assembly and cross-linked in the layers of the gold and silver nanoparticles are shown in Figure 4. The PATP molecules on the gold nanoparticles exhibited three major bands at 1587, 1078, and 390 cm^{-1} (Figure 4, curve a), which are the a_1 modes of the PATP molecule.[8] Interestingly, the assembly of the layer of silver nanoparticles caused a large increase in the intensity of the spectrum (Figure 4, curve b). In particular, in addition to the bands observed in curve a of Figure 4, additional bands appeared at 1142, 1391, 1436, and 1579 cm^{-1}. These new bands were assigned to the nontotally symmetric b_2 vibrational modes of the PATP molecule.[8] The selective enhancement of the b_2 modes (Figure 4, curve b) cannot be explained by the EM mechanism.

According to the surface-selection role of the EM model, the SERS enhancement order for the vibrational modes of molecules with C_{2v} symmetry should be $b_1 = b_2 > a_2$ for molecules with a standing-up orientation, and $a_2 = b_1 > b_2$ for molecules with a lying-down orientation, respectively. In Figure 4, curve b, only the b_2 modes among the three vibrational modes are enhanced. The possibility of a difference between bonding geometries in the assembly structures is also excluded, because no noticeable difference in the frequencies of the a_1 modes was observed in the two spectra. Therefore, we consider that the b_2 modes are enhanced by the CT mechanism through the Herzberg–Teller contribution.[9] That is, the enhancement of the b_2 modes of PATP is associated with CT between the metal nanoparticles and the adsorbed molecules, and is dependent on the degree of matching between the energy level of the adsorbed molecules and the metal nanoparticles, and the extent of the CT. On the other hand, curve a in Figure 4 indicates that there is no clear enhancement of the b_2 modes on the assembled gold nanoparticles alone. Our previous study also indicated that only slight enhancement of the b_2 modes of the PATP molecules can be obtained on assembled silver nanoparticles under 1064-nm excitation conditions.[10] In other words, the individual nanoparticles of the two metals cannot provide such a large enhancement of the b_2 modes as that observed in curve b of Figure 4; such a large enhancement should be related to the particular assembly structure of the gold and silver nanoparticles.

The assembly of the nanoparticles through the PATP molecules (Figure 1 A) generated an exactly asymmetric metal–molecule–metal nanosystem. Accordingly, the CT model of the "donor–bridge–acceptor" system may be applicable to the present nanosystem.[2] In this case, dynamic CT between the particles could occur through coupling with the vibrations of the bridging molecules, as the energy levels of the metal nanoparticles match the HOMO and LUMO energy levels of the molecules under excitation by light. The selective enhancement of the b_2 modes of the PATP molecules may be indicative of such a CT process. The work function of silver ($\approx$4.3 eV) is lower than that of gold ($\approx$5.0 eV),[11] and therefore we consider that the overall CT could be from silver to gold by tunneling through the interconnecting PATP molecules.

 © 2006 Wiley-VCH Verlag GmbH & Co. KGaA, Weinheim

Furthermore, the quinonoid form of the adsorbed PATP may play a very important role in the CT process in this system, because the CT direction is parallel to the dipolar direction of the PATP molecule, which may be favorable to the overall CT process between the metal nanoparticles. To verify this point, the nanoparticles were assembled inversely, with the silver nanoparticles as the first layer and the gold nanoparticles as the second. The surface-enhanced Raman spectrum of the PATP molecules adsorbed on the silver nanoparticle assembly (Figure 5, curve a) is comparable to that reported previously.[10] Importantly, the assembly of the gold nanoparticles on the silver nanoparticle layer did not result in an enhancement of the b_2 modes of the interconnecting PATP molecules (Figure 5, curve b), because the possible

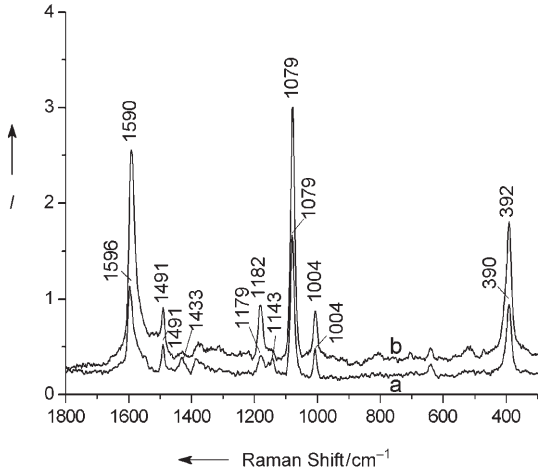

Figure 5. Surface-enhanced Raman spectra of PATP molecules a) adsorbed on the assembled silver nanoparticles and b) interconnected in the silver/PATP/gold assembly.

CT from silver to gold is opposite to the dipolar direction of the PATP molecule. The enhancement of the a_1 modes at 1590, 1079, and 392 cm^{-1} in curve b of Figure 5 could be related to the enhancement of the EM field between the metal particles. Notably, the EM mechanism, as demonstrated by Moskovits and Jeong,[7] should also contribute to the overall SERS enhancement in the present study, as a result of the broad SPR of the assembled metal nanoparticles. Further theoretical analysis is necessary for a better understanding of the CT mechanism in this particular system.

In summary, a metal–molecule–metal nanosystem has been fabricated by the self-assembly of gold and silver nanoparticles interconnected with PATP molecules. The b_2 vibrational mode in the surface-enhanced Raman spectrum of the interconnecting PATP molecules, which is characteristic of CT between the metal nanoparticles and PATP molecules, is likely greatly enhanced by CT from the silver to gold nanoparticles by tunneling through the PATP molecules. The CT process is dependent on the dipolar direction of the PATP molecules. Together with the SPR data for the metal nanoparticle assemblies, the greatly enhanced SERS signal of the interconnecting PATP molecules may demonstrate the importance of the contribution of the CT mechanism in single-molecule SERS.

Experimental Section

Gold and silver colloids were prepared according to literature protocols.[12] The metal nanoparticles were assembled on glass slides according to the following procedure. The surface of the glass was derivatized by immersing the slides in a solution of PVP (5 wt%) in ethanol. After washing with ethanol and water, the slides were immersed in a colloidal solution of silver or gold nanoparticles for 6 h. The slides covered with a surface layer of metal nanoparticles were then immersed in a solution of PATP in ethanol (1 mM) for 3 h. After adsorption of the PATP molecules, the slides were transferred into a colloidal solution of gold or silver nanoparticles to allow the assembly of the second layer of metal nanoparticles.

The extinction spectra were measured on a Shimadzu UV-3150 spectrometer. The surface morphologies of the samples were measured on a Hitachi 7350G scanning electron microscope. The surface-enhanced Raman spectra were measured on a Nicolet 960 FT-Raman spectrometer equipped with a liquid-nitrogen-cooled Ge detector and a Nd:VO_4 laser (1064 nm) as excitation source. The laser power used was about 300 mW at the samples. The spectral resolution was 4 cm^{-1} at the excitation wavelength.

Received: December 13, 2005
Revised: March 8, 2006

Keywords: charge transfer · gold · nanoparticles · self-assembly · silver

[1] a) X. D. Cui, A. Primak, A. Zarate, J. Tomfohr, O. F. Sankey, A. L. Moore, T. A. Moore, D. Gust, G. Harris, S. M. Lindsay, *Science* **2001**, *294*, 571 – 574; b) A. Nitzan, M. A. Ratner, *Science* **2003**, *300*, 1384 – 1389; c) C. Lee, Y. Kang, K. Lee, *Curr. Appl. Phys.* **2002**, *2*, 39 – 45.
[2] a) D. M. Adams, L. Brus, C. E. D. Chidsey, S. Creager, C. Creutz, C. R. Kagan, P. V. Kamat, M. Lieberman, S. Lindsay, R. A. Marcus, R. M. Metzger, M. E. Michel-Beyerle, J. R. Miller, M. D. Newton, D. R. Rolison, O. Sankey, K. S. Schanze, J. Yardley, X. Zhu, *J. Phys. Chem. B* **2003**, *107*, 6668 – 6697; b) V. Torma, O. Vidoni, U. Simon, G. Schmid, *Eur. J. Inorg. Chem.* **2003**, 1121 – 1127.
[3] H. Xu, J. Azipurua, M. Kall, P. Apell, *Phys. Rev. E* **2000**, *62*, 4318 – 4324.
[4] a) A. Otto, *J. Raman Spectrosc.* **2005**, *36*, 497 – 509; b) J. Jiang, K. Busnick, M. Maillard, L. Brus, *J. Phys. Chem. B* **2003**, *107*, 9964 – 9972; c) W. E. Doering, S. Nie, *J. Phys. Chem. B* **2002**, *106*, 311 – 317.
[5] M. Muniz-Miranda, N. Neto, *Colloids Surf. A* **2004**, *249*, 79 – 84.
[6] a) W. Rechberger, A. Hohenau, A. Leitner, J. R. Krenn, B. Lamprecht, F. R. Aussenegg, *Opt. Commun.* **2003**, *220*, 137 – 141; b) C. L. Haynes, A. D. McFarland, L. Zhao, R. P. Van Duyne, G. C. Schatz, L. Gunnarsson, J. Prikulis, B. Kasemo, M. Käll, *J. Phys. Chem. B* **2003**, *107*, 7337 – 7342.
[7] M. Moskovits, D. H. Jeong, *Chem. Phys. Lett.* **2004**, *397*, 91 – 95.
[8] a) M. Osawa, N. Matsuda, K. Yoshii, I. Uchida, *J. Phys. Chem.* **1994**, *98*, 12702 – 12707; b) L. Cao, P. Diao, L. Tong, T. Zhu, Z. Liu, *ChemPhysChem* **2005**, *6*, 913 – 918.
[9] J. R. Lombardi, R. L. Birke, T. Lu, J. Xu, *J. Phys. Chem.* **1986**, *90*, 4174 – 4180.
[10] J. Zheng, X. Li, R. Gu, T. Lu, *J. Phys. Chem. B* **2002**, *106*, 1019 – 1023.
[11] I. G. Hill, J. Schwartz, A. Kahn, *Org. Electron.* **2000**, *1*, 5 – 13.
[12] a) P. C. Lee, D. Mesel, *J. Phys. Chem.* **1982**, *86*, 3391 – 3395; b) D. D. Evanoff, Jr., G. Chumanov, *J. Phys. Chem. B* **2004**, *108*, 13948 – 13956.

 © 2006 Wiley-VCH Verlag GmbH & Co. KGaA, Weinheim

Homogeneous Catalysis

DOI: 10.1002/anie.200504511

"Green" Oxidation Catalysis for Rapid Deactivation of Bacterial Spores**

*Deboshri Banerjee, Andrew L. Markley, Toshihiro Yano, Anindya Ghosh, Peter B. Berget, Edwin G. Minkley, Jr., Sushil K. Khetan, and Terrence J. Collins**

Under environmental stress, the vegetative cells of certain Gram-positive bacteria such as lethal *Bacillus anthracis* form metabolically dormant spores, which can survive indefinite periods of starvation and desiccation as well as withstand UV radiation, chemical assault, and elevated temperatures.[1] Spore hardiness derives from two structurally complex and chemically robust encapsulating layers: the proteinaceous coat[2] and the peptidoglycan cortex.[3] These protective barriers envelop the inner core compartment that contains dehydrated cytoplasm and the cellular components until nutrients are encountered in the environment to stimulate spore germination.[4] Additionally, the protective walls include two membranes: the inner membrane surrounding the core and the outer membrane lying between the cortex and coat.[5]

B. anthracis spores are considered to be among the most difficult biological warfare and terrorism (BWT) agents to destroy.[6,7] Better lines of defense against such agents are crucially needed. Ideally, decontamination technologies would rapidly deactivate BWT pathogens in diverse scenarios while being nontoxic, user friendly, materials compatible, and environmentally benign.[8] An effective chemical decontamination system presumably must breach the aggregate protective casing swiftly to irreversibly damage critical components. Several oxidation-based chemical approaches have been successfully investigated for the deactivation of bacterial spores, including chlorine dioxide,[9] vaporized hydrogen peroxide,[9] oxone,[10] and the activation of hydrogen peroxide by bicarbonate.[11] These processes involve stoichiometric quantities of the respective oxidants and exhibit varied levels of efficacy and materials compatibility.

Herein, we describe a relatively innocuous catalytic sporicidal system. Minute concentrations of the Fe–tetra-amido macrocyclic ligand ([Fe(taml)]) activator[12,13] **1** (Scheme 1) activate hydrogen peroxide or *tert*-butyl hydroperoxide (TBHP) in aqueous solutions of simple composition under ambient conditions to deactivate spores of the non-infectious anthrax surrogate *Bacillus atrophaeus* (ATCC 9372). The process incorporates numerous desirable properties including the attainment of a 10^7-fold reduction in the viable bacterial spore population in 15 minutes—an important criterion in the pursuit of a superior spore decontamination technology.[8,14]

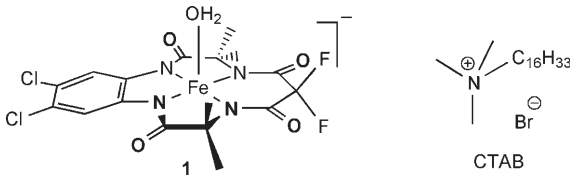

Scheme 1. The principal [Fe(taml)] activator used in this study (**1**), and the cationic surfactant cetyltrimethylammonium bromide (CTAB).

The resistance of Bacillus spores to enzymatic and chemical treatments has been attributed partly to the presence of protein disulfide cross-linkages in the spore coat.[5,11,15,16] The **1**/H_2O_2 system ruptures the disulfide bond of cysteine, $>90\,\%$ of which was converted into cysteic acid within 1 h (pH 10.0, 25 °C) compared to $<5\,\%$ with H_2O_2 alone. This result suggested the system would fracture the coat and render other spore components vulnerable to destructive chemistries.

B. atrophaeus bacteria were cultured at 32 °C (12 h) in brain heart infusion (BHI) broth and were then transferred to BHI agar plates containing $MnCl_2$ (0.002 %). The plates were incubated at 32, 37, and 42 °C for approximately 4 weeks to obtain spores at different temperatures. The mixture of spores and unaltered vegetative bacterial cells on the BHI plates were suspended in sterile distilled water and heated (80 °C, 20 min) to kill vegetative cells, thus leaving only viable spores.

The *B. atrophaeus* spores were dispersed well in a buffered solution (0.1 M Na_2CO_3/0.1 M $NaHCO_3$, pH 9.9 ± 0.1) containing the cationic surfactant cetyltrimethylammonium bromide (CTAB), a quaternary ammonium compound (QAC). QACs are known to be antimicrobials because of their ability to disrupt microbial cellular membranes,[15,17] but are not independently sporicidal. However, we found that CTAB significantly enhances the sporicidal activity of [Fe(taml)]/peroxide toward *B. atrophaeus* spores. CTAB was used at 0.03 %, in slight excess of its critical micelle concentration.

The initial *B. atrophaeus* spore population was about 10^8 colony-forming units per mL (CFU mL^{-1}). The spores were treated with [Fe(taml)]/peroxide (H_2O_2 or TBHP) and CTAB

[*] D. Banerjee, A. L. Markley, A. Ghosh, Dr. S. K. Khetan, Prof. T. J. Collins
Department of Chemistry
Carnegie Mellon University
4400 Fifth Avenue, Pittsburgh, PA 15213 (USA)
Fax: (+1) 412-268-1061
E-mail: tc1u@andrew.cmu.edu
T. Yano
Molecular Materials Science Department
3-3-138 Sugimoto, Sumiyoshi-ku
Osaka 558–8585 (Japan)
Dr. P. B. Berget, Dr. E. G. Minkley, Jr.
Department of Biological Sciences
Carnegie Mellon University
4400 Fifth Avenue, Pittsburgh, PA 15213 (USA)

[**] This material is based upon work supported in part by the NSF (CHE-0211605 COLLINS-SGER), the US Army Research Office (DAAD-19-03-1-0165), and the Eden-Hall Foundation. We thank Joseph Suhan for obtaining the electron micrographs reported here. D.B. and A.G. thank the Teresa and H. John Heinz III Foundation for Teresa Heinz Scholars for Environmental Research awards.

WILEY InterScience DISCOVER SOMETHING GREAT
© 2006 Wiley-VCH Verlag GmbH & Co. KGaA, Weinheim

at 25 °C in pH 10.0 buffer. The reactions with H_2O_2 were quenched with catalase (from *Aspergillus niger*, Sigma). In reactions with TBHP, residual TBHP was removed by centrifugation (14 000 × g, 60 s) of the reaction mixtures and the spore pellets were washed twice with sterile phosphate-buffered saline (PBS, pH 7.4). Spore suspensions, both treated and untreated, were diluted serially (10^1–10^7-fold dilutions in PBS, pH 7.4), and a 100 μL aliquot from each tube was plated on BHI agar plates. Colonies were counted after incubating the plates overnight at 37 °C from which the reduction in the population of viable spores accompanying deactivation was determined. The plates were also observed for 72 h to monitor the growth of any new colonies.[18]

Spores of *B. atrophaeus* (grown at 32 °C) were treated with H_2O_2 and CTAB at pH 10.0 in the absence and presence of **1** for 1 h. The presence of **1** improved the deactivation factor from $< 2 \log_{10}$ kill with H_2O_2 (0.5 M, 1.7 %) to a $3 \log_{10}$ (or 99.9 %) kill (**1**, 10 μM; H_2O_2, 0.5 M, 1.7 %; CTAB, 0.03 %). This could be improved to a $5 \log_{10}$ kill (1 h) by increasing the concentration of H_2O_2 (0.85 M, 3 %); the control with 0.85 M H_2O_2 resulted in an approximately $4 \log_{10}$ kill. At higher peroxide concentrations, the kill rate increased. Higher peroxide concentrations also increase concerns over the safety of human exposure and materials compatibility. Increasing the concentrations of **1** did not enhance spore killing, a feature that we believe derives from the appreciable catalase-like activity of **1**. Therefore, we explored *tert*-butyl hydroperoxide (TBHP) as an alternative oxidant, since it is less hydrophilic than H_2O_2 and could thus result in an increased peroxide concentration at the spores. It is less susceptible to catalase-like decompositions than H_2O_2,[19] and in vitro studies have been found to show substantial DNA-cleaving activity.[20] TBHP is also one of only two organic peroxides that the U.S. Department of Transportation certifies for tank car shipment.[14]

The dependence of spore deactivation on TBHP concentration was studied in the presence of CTAB with and without **1** (Figure 1 a). A $7.8 \log_{10}$ kill was achieved in 1 h with **1** (10 μM), TBHP (0.5 M), and CTAB (0.03 %; Figure 1 b). Treatment of the spores with **1**/TBHP but without CTAB resulted in an approximately $3 \log_{10}$ reduction (Figure 1 b). The $5 \log_{10}$ enhancement of the sporicidal activity of **1**/TBHP by CTAB is noteworthy. In contrast with the H_2O_2 case, higher concentrations of **1** were found to accelerate spore deactivation (Figure 2 a). Increasing the concentration of **1** from 10 to 15 μM resulted in a $7.8 \log_{10}$ reduction in just 35 min. At [**1**] = 25 μM, added in 3 aliquots over 10 minutes, a $6 \log_{10}$ reduction was achieved in 15 minutes. At [**1**] = 50 μM, added in 5 equal aliquots over 10 minutes, with the same amount of TBHP (0.5 M) and increased CTAB (0.05 %), a $7 \log_{10}$ kill in 15 minutes was achieved (Figure 2 b).

Spores prepared at higher temperatures exhibited greater resistance to deactivation, a phenomenon attributed to subtle differences in the coat proteins.[21] These results are presented in Table 1.

[Fe(taml)] activators show highest reactivity at pH 10.0, the pH value used for all the prior results. However, decontamination under near-neutral pH conditions could be useful for protecting sensitive materials when rapid decontamination might be less critical. At pH 8.0 (0.1 M KH_2PO_4), a $7 \log_{10}$ kill of *B. atrophaeus* spores (prepared at 32 °C) was attained in 5 hours by employing **1** (50 μM added in 5 aliquots) and 0.5 M TBHP with CTAB (0.03 %).

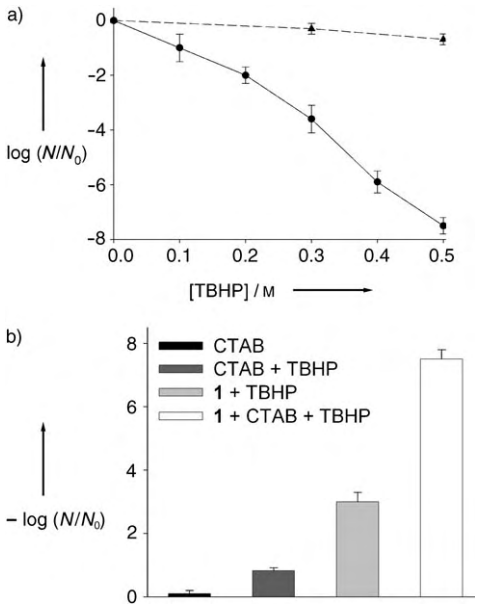

Figure 1. a) Deactivation of *B. atrophaeus* spores in 1 h at various concentrations of TBHP in the presence (●) of **1** (10 μM) and without **1** (▲). b) Bar chart showing spore deactivation in 1 h with different components of the [Fe(taml)]/peroxide system using **1** (10 μM) and TBHP (0.5 M). All the experiments were conducted in the presence of 0.03 % CTAB. N_0 = initial number of spores, N = number of surviving spores at a given time, and N/N_0 = fraction of surviving spores at the same time.

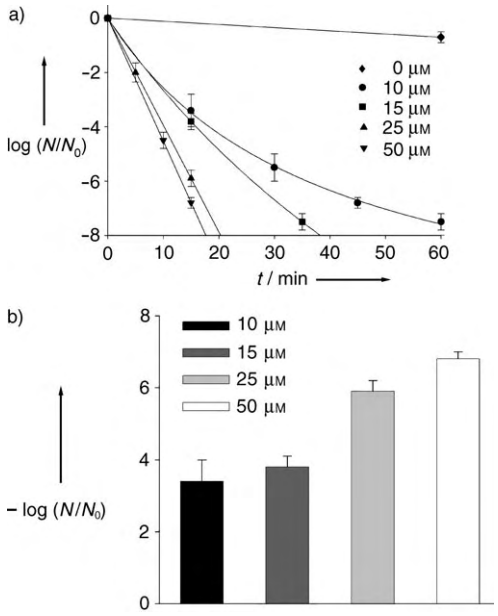

Figure 2. a) Time dependence of the deactivation of *B. atrophaeus* spores with various concentrations of **1**. b) Bar chart showing levels of deactivation achieved in 15 min with different concentrations of **1**. The experiments were conducted in the presence of 0.5 M TBHP and 0.03 % CTAB (except in the case of 50 μM [Fe(taml)], where the CTAB concentration used was 0.05 %).

 © 2006 Wiley-VCH Verlag GmbH & Co. KGaA, Weinheim

Table 1: Rate of deactivation of *B. atrophaeus* spores prepared at 32, 37 and 42 °C.

B. atrophaeus spores prepared at	Reduction in the number of spores		
	15 min	60 min[c]	90 min[c]
32 °C	$7\log_{10}$[a]	$7.8\log_{10}$	–
37 °C	$7\log_{10}$[b]	$5.5\log_{10}$	$7\log_{10}$
42 °C	–	$4.5\log_{10}$	$5.5\log_{10}$

[a] **1** (50 μM), TBHP (0.5 M), and CTAB (0.05 %). [b] **1** (60 μM), TBHP (0.5 M), and CTAB (0.05 %). [c] **1** (10 μM), TBHP (0.5 M), and CTAB (0.03 %).

The role of oxygen-based free radicals as probable biocides is well documented in the literature and bactericidal/sporicidal activities of TBHP through a free-radical mechanism have been reported.[22,23] An HPLC analysis of the supernatant solution from the suspension containing deactivated spores revealed the presence of acetone (and dipicolinic acid, see below). Control experiments revealed that reaction between **1** and TBHP produce significant amounts of acetone. The formation of acetone suggested that *tert*-butoxyl radicals (*t*BuO•) form during the reaction: one path of their decomposition involves the formation of the methyl radical and acetone.[24] *tert*-Butoxyl radicals have been reported to yield bactericidal activity.[24] This bactericidal activity is in addition to that of the "membrane-active" CTAB.

In the late stage of sporulation pyridine-2,6-dicarboxylic acid (dipicolinic acid, DPA) accumulates within the highly dehydrated spore core.[25] The HPLC quantitation of DPA in the supernatant solution from deactivated spores (prepared at 32 °C) was estimated to be 10 ± 2 % of the total spore core depot, based on the amount of DPA released from otherwise untreated spores on heating at 100 °C for 20 minutes.[26] The deactivated spores still appeared bright under a phase-contrast microscope. Heating these spores at 85 °C (a sublethal temperature for healthy spores) for 30 minutes led to release of the remaining DPA from the spore core (85 ± 5 %). Such release of DPA from the core has been attributed to damage incurred to the inner membrane during oxidative treatment.[27] The structural changes induced in *B. atrophaeus* spores before and after treatment with **1**/TBHP and CTAB are revealed in the transmission electron micrographs[28] in Figure 3. After treatment with **1**/TBHP and CTAB, the outermost spore layer appeared less punctate, the core was appreciably compressed, and the cortex layer was enlarged.

This work shows that [Fe(taml)]/peroxide oxidation can rapidly deactivate bacterial spores. The inherent robustness of the [Fe(taml)] activators under oxidizing conditions and their high catalytic activity with peroxides allow relatively simple compositions to render the bacterial spores incapable of germination and reproduction. The incorporation of CTAB plays a significant role in enhancing the sporicidal activity of **1**/TBHP relative to **1**/H_2O_2, as the membrane-disruptive action of CTAB apparently potentiates the biocidal activity produced by **1**/peroxide. Preliminary toxicity tests indicate that [Fe(taml)] complexes and their decomposition products are relatively nontoxic.[13] Thus, these studies demonstrate that [Fe(taml)]/peroxide systems show considerable promise for providing a superior decontamination technology for real-world applications.

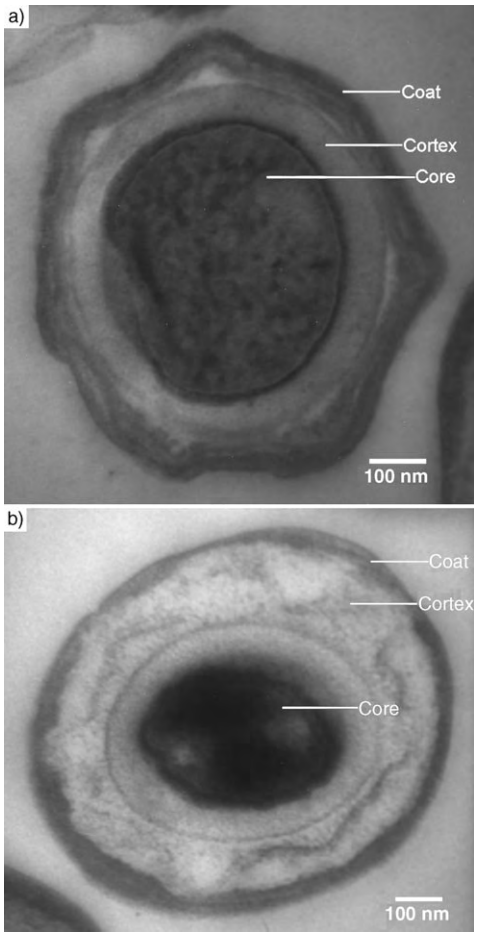

Figure 3. TEM images of *B. atrophaeus* spores a) before and b) after treatment with **1**/TBHP (10 μM/0.5 M) and CTAB (0.03 %) for 1 h.

Received: December 19, 2005
Revised: April 1, 2006
Published online: May 4, 2006

Keywords: green chemistry · homogeneous catalysis · iron · peroxides · spore deactivation

[1] W. L. Nicholson, N. Munakata, G. Horneck, H. J. Melosh, P. Setlow, *Microbiol. Mol. Biol. Rev.* **2000**, *64*, 548 – 572.
[2] V. G. R. Chada, E. A. Sanstad, R. Wang, A. Driks, *J. Bacteriol.* **2003**, *185*, 6255 – 6261.
[3] D. L. Popham, *Cell. Mol. Life Sci.* **2002**, *59*, 426 – 433.
[4] A. Moir, B. M. Corfe, J. Behravan, *Cell. Mol. Life Sci.* **2002**, *59*, 403 – 409.
[5] A. O. Henriques, C. P. Moran, Jr., *Methods* **2000**, *20*, 95 – 110.
[6] A. Watson, D. Keir, *Epidemiol. Infect.* **1994**, *113*, 479 – 490.
[7] H. Liu, N. H. Bergman, B. Thomason, S. Shallom, A. Hazen, J. Crossno, D. A. Rasko, J. Ravel, T. D. Read, S. N. Peterson, J. Yates III, P. C. Hanna, *J. Bacteriol.* **2004**, *186*, 164 – 178.
[8] "U.S. Department of Defense, Chemical and Biological Defense Program: Annual Report to Congress" to be found under http://www.acq.osd.mil/cp/reports.html, **2005**.

 © 2006 Wiley-VCH Verlag GmbH & Co. KGaA, Weinheim

[9] E. A. S. Whitney, M. E. Beatty, T. H. Taylor, Jr., R. Weyant, J. Sobel, M. J. Arduino, D. A. Ashford, *Emerging Infect. Dis.* **2003**, *9*, 623 – 627.
[10] E. Raber, R. McGuire, *J. Hazard. Mater.* **2002**, *93*, 339 – 352.
[11] M. E. Tadros, M. D. Tucker (Sandia Corporation, USA), Eur. Pat. Appl. Ep, **2002**, p. 46.
[12] T. J. Collins, *Acc. Chem. Res.* **2002**, *35*, 782 – 790.
[13] S. S. Gupta, M. Stadler, C. A. Noser, A. Ghosh, B. Steinhoff, D. Lenoir, C. P. Horwitz, K.-W. Schramm, T. J. Collins, *Science* **2002**, *296*, 326 – 328.
[14] J. Brown, R. C. Hodge in *Joint Service Scientific Conference on Chemical and Biological Defense Research*, Towson, MD, **2003**.
[15] G. McDonnell, A. D. Russell, *Clin. Microbiol. Rev.* **1999**, *12*, 147 – 179.
[16] H.-S. Kim, D. Sherman, F. Johnson, A. I. Aronson, *J. Bacteriol.* **2004**, *186*, 2413 – 2417.
[17] P. Gilbert, L. E. Moore, *J. Appl. Microbiol.* **2005**, *99*, 703 – 715.
[18] The treated spores were subjected to a range of revival techniques. Of most significance, the viability of treated spores is not increased by inclusion of lysozyme in the plates, a recovery technique that helps to revive spores treated in other ways that are not truly "dead" but only damaged: P. Setlow, University of Connecticut, personal communication.
[19] D. H. R. Barton, V. N. Le Gloahec, H. Patin, F. Launay, *New J. Chem.* **1998**, *22*, 559 – 563.
[20] R. A. Shane, K. U. Ingold, *Chem. Res. Toxicol.* **2002**, *15*, 1324 – 1329.
[21] E. Melly, P. C. Genest, M. E. Gilmore, S. Little, D. L. Popham, A. Driks, P. Setlow, *J. Appl. Microbiol.* **2002**, *92*, 1105 – 1115.
[22] T. Akaike, K. Sato, S. Ijiri, Y. Miyamoto, M. Kohno, M. Ando, H. Maeda, *Arch. Biochem. Biophys.* **1992**, *294*, 55 – 63.
[23] S. Y. Shin, R. E. Marquis, *Arch. Microbiol.* **1994**, *161*, 184 – 190.
[24] T. Ichinohe, M. Miyajima, Y. Noguchi, M. Ito, M. Kimura, T. Koyama, K. Hanabusa, A. Hachimori, H. Shirai, *J. Porphyrins Phthalocyanines* **1998**, *2*, 101 – 106.
[25] M. Paidhungat, B. Setlow, A. Driks, P. Setlow, *J. Bacteriol.* **2000**, *182*, 5505 – 5512.
[26] W. L. Nicholson, P. Setlow in *Molecular Biological Methods for Bacillus* (Eds.: C. R. Harwood, S. M. Cutting), Wiley, New York, **1990**, pp. 391 – 450.
[27] S. B. Young, P. Setlow, *J. Appl. Microbiol.* **2004**, *96*, 289 – 301.
[28] Spores were fixed in 2% glutaraldehyde, followed by 1% osmium tetroxide buffered with PBS. After washing the spores with distilled water and ethanol solutions of increasing strength (50%, 70%, 95%, and 100%), they were placed overnight in a 1:1 mixture of LR White resin and propylene oxide. The mixture was then replaced with 100% LR White resin and the spores were sliced into sections (100 nm thick). Thin sections were stained with 1% uranyl acetate and Reynold's lead citrate, and viewed on a Hitachi 7100 transmission electron microscope. Digital images were obtained using AMT Advantage 10 CCD Camera System and NIH Image software.

 © 2006 Wiley-VCH Verlag GmbH & Co. KGaA, Weinheim

Polymorphism

DOI: 10.1002/anie.200600029

Crystallization in a Mixture of Solvents by Using a Crystal Modifier: Morphology Control in the Synthesis of Highly Monodisperse $CaCO_3$ Microspheres**

Xiao-Hui Guo, Shu-Hong Yu, and Guo-Bing Cai*

Bio-inspired morphosynthesis of inorganic and inorganic/organic composite materials by using a self-organized organic superstructure, organic additives, and/or templates with special functionalization patterns has attracted considerable attention.[1,2] One of the most intensively investigated systems is calcium carbonate, which is not only one of the most abundant biomaterials in nature but also has industrial application as a filler in paints, plastics, rubber, and paper.[3] Bio-inspired synthesis of crystals with complex forms that mimic natural biominerals in the presence of an organic template or additives has been intensively developed over the years.[2,4–6] Proteins were extracted from mollusc shell layers and used for the conformation-dependent control of the morphology of calcium carbonate.[6,7] Furthermore, self-assembled two-dimensional protein layers can play a key role in biomineralization. For example, a polypeptide structure may be associated with the $CaCO_3$ polymorph or morphology, in which the transformation of aragonite and calcite is coupled with the altering of a secondary structure of the polypeptide used.[8,9] Moreover, the sequences and conformation of proteins or mineral tissues were also used for the mediation of nucleation and crystal structure of calcium carbonate.[10]

In 1998, a class of so-called double-hydrophilic block copolymers (DHBCs) was introduced for the controlled crystallization of various compounds.[11] Nanocrystalline building blocks can be stabilized, at least temporarily, and

[*] X.-H. Guo, Prof. Dr. S.-H. Yu, G.-B. Cai
Division of Nanomaterials and Chemistry
Hefei National Laboratory for Physical Sciences at Microscale
School of Chemistry and Materials
University of Science and Technology of China
Hefei 230026 (P.R. China)
Fax: (+86) 551-360-3040
E-mail: shyu@ustc.edu.cn

[**] We acknowledge the special funding support from the Centurial Program of the Chinese Academy of Sciences, the National Natural Science Foundation of China (NSFC, Nos. 20325104, 20321101, 50372065) and the Scientific Research Foundation for the Returned Overseas Chinese Scholars, the Specialized Research Fund for the Doctoral Program (SRFDP) of Higher Education State Education Ministry, the Partner Group of the Chinese Academy of Sciences, and the Max Planck Society. We genuinely thank PD. Dr. habil. H. Cölfen and Prof. Dr. M. Antonietti for donating the block copolymers and for the long-standing and enjoyable collaboration in the area of biomimetic mineralization.

Supporting information for this article is available on the WWW under http://www.angewandte.org or from the author.

© 2006 Wiley-VCH Verlag GmbH & Co. KGaA, Weinheim

then used for mesoscale transformation into complex morphologies.[5,12–14] The controlled synthesis and crystallization of $CaCO_3$ by using DHBCs has been intensively investigated.[15] Choi and Kim found in certain biological systems that the secondary structures of peptides can affect the structure of $CaCO_3$ as the transition from aragonite into calcite is related to the denaturing of an antiparallel β sheet.[16] Moreover, DHBCs with adjustable secondary structures, such as poly(ethylene glycol)-*b*-poly(L-glutamic acid), PEG(*m*)-*b*-pGlu(*n*), have been used to control the growth of $CaCO_3$ in aqueous solution.[17] Previously, crystallization of calcium carbonate under the control of DHBCs has been mainly carried out in nonionic water (NIW). DHBC-controlled crystallization in a mixture of solvents can lead to entirely new results because of the variation in mineral solubility, precipitation kinetics, solution properties, and aggregation of the polymer in the solvent mixture. However, this new system has not yet been thoroughly investigated.

Mineralization reactions in alcohol, ethanol, 2-propanol, and diethylene glycol have seldom been explored, and only $CaCO_3$ crystals with morphologies such as elongated spheres or inhomogeneous aggregated structures have been obtained.[5,18] In recent years, several research groups have focused on the use of the solvent to control the crystal growth of $CaCO_3$ and other compounds.[19] Vaterite microspheres can be produced in the presence of starburst dendrimers[20] and PEG(*m*)-*b*-pGlu(*n*),[17] but the vaterite spheres obtained thus far are not monodisperse. To date, a precisely controlled synthesis of highly monodisperse $CaCO_3$ spheres has not been achieved in a pure-water system.

Monodisperse particles have numerous important applications in ceramics, catalysis, pigments, recording materials, medical diagnostics, and many other areas. Thus, the exploration of rational routes for their synthesis has been a challenge.[21] Herein, we present a precisely controlled synthesis of highly monodisperse $CaCO_3$ microspheres by a slow gas–liquid diffusion reaction with an artificial peptide-type block copolymer, PEG(110)-*b*-pGlu(6), as a crystal-growth

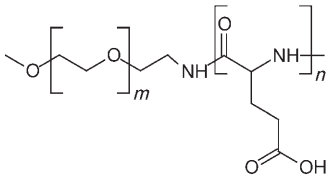

PEG (110)-*b*-pGlu(6), $m = 110$, $n = 6$

modifier in a mixture of solvents. The synergistic effect of PEG-*b*-pGlu and the solvent mixture on the growth of calcium carbonate has been investigated. The results demonstrate that the ratio of solvent used has significant influence on the morphology and polymorph of $CaCO_3$ crystals in the presence of this DHBC.

N,*N*-dimethylformamide (DMF) and other solvents, such as THF, *n*-propanol, ethanol, and 1,4-dioxane have been applied as the mineralization media for the crystallization of $CaCO_3$. The $CaCO_3$ samples obtained from different types of solvent mixtures are indexed as vaterite or a mixture of calcite and vaterite (see Supporting Information). Figure 1a shows that the $CaCO_3$ particles crystallized in pure DMF are almost polyhedral. From a mixture of DMF and methanol, the formed particles are made up of layers of rectangles with

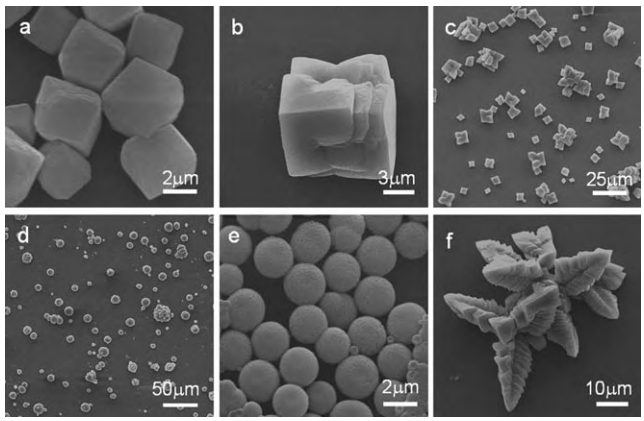

Figure 1. SEM images of $CaCO_3$ particles obtained from different solvent mixtures (volume ratios): a) Pure DMF; b) DMF:methanol = 5:1; c) DMF:THF = 5:1; d) DMF:*n*-propanol = 5:1; e) DMF:ethanol = 5:1; f) DMF:1,4-dioxane = 5:1. [PEG-*b*-pGlu] = 1 g L^{-1}. A solution of $CaCl_2$ was added to the solvent mixtures and the crystallization was allowed to proceed for 3 days at room temperature.

small cavities at the center of each face (Figure 1b). In a mixture of DMF and THF, there are calcium carbonate crystals similar in shape to those obtained in the DMF/methanol mixture (Figure 1c). However, the $CaCO_3$ particles are mostly aggregates of oblong blocks with small cavities in the center of the crystal surfaces. Nearly spherical aggregates and spherical particles (vaterite phase) are obtained from a mixture of DMF and *n*-propanol (Figure 1d). Relatively uniform microspheres with rough surfaces are obtained from a mixture of DMF and ethanol (Figure 1e). Surprisingly, multibranched hierarchical structures form in a mixture of DMF and 1,4-dioxane (Figure 1f). These results demonstrate that the combination of a block copolymer and a mixture of solvents can provide an effective tool for controlled morphogenesis of $CaCO_3$.

$CaCO_3$ microsphere arrays obtained from a DMF/NIW mixture with a polymer concentration of 1.0 g L^{-1} are highly monodisperse (Figure 2a). High-magnification SEM (Figure 2b) reveals the smooth surface of the microspheres with diameters ranging from 5.3 to 6.0 μm. Similar results are obtained in a mixture of DMF and ethanol, as shown in Figure 2c, but the vaterite microspheres obtained have a rough surface and are smaller and range from 1.5 to 2.4 μm in diameter (Figure 2d). However, these microspheres are not stable and transform into rhombohedral calcite over prolonged reaction times (see Supporting Information).

To further examine the effects of DMF/NIW mixtures on controlled crystallization and modification of the $CaCO_3$ particles, a series of experiments was carried out by varying the volume ratio of the solvents, crystallization time, and polymer concentration (Figures 2 and 3). Decreasing the volume ratio of DMF:NIW to 1:7 results in the formation of

 © 2006 Wiley-VCH Verlag GmbH & Co. KGaA, Weinheim

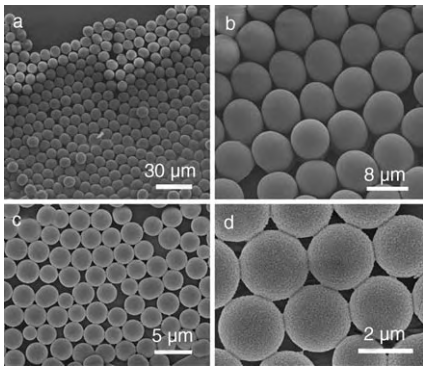

Figure 2. SEM images of $CaCO_3$ microspheres obtained from different solvent mixtures (volume ratios): a) DMF:NIW = 1:1; b) magnified SEM image of (a); c) DMF:ethanol = 5:1; d) magnified FESEM image of (c). [PEG-*b*-pGlu] = 1 g L^{-1}. A solution of $CaCl_2$ was added to the solvent mixtures and the crystallization was allowed to proceed for 3 days at room temperature.

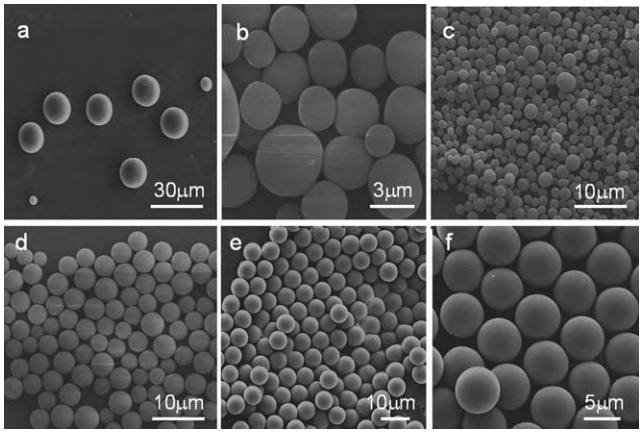

Figure 3. SEM images of $CaCO_3$ microspheres obtained in DMF/NIW with different volume ratios: a) 1:7; b) 1:3; c) 1:5; d) 1:2; e) 1:1.4; f) magnified SEM image of (e). [PEG-*b*-pGlu] = 1 g L^{-1}. A solution of $CaCl_2$ was added to the solvent mixtures and the crystallization was allowed to proceed for 3 days at room temperature.

$CaCO_3$ microspheres of mainly two sizes (Figure 3a). There is a broad size distribution when the volume ratio of DMF:NIW is 1:3 (Figure 3b). When the volume ratio of DMF:NIW is 1:5, $CaCO_3$ particles tend to transform into slightly deformed quasi-spheres or ellipsoids, which have a broad size distribution (Figure 3c). Further decreasing the volume ratio of DMF:NIW to 1:2 results in the microspheres having a broader size distribution (Figure 3d) A ratio of DMF:NIW of 1:1 results in the $CaCO_3$ particles being well-defined monodisperse spheres that tend to form an array similar to that shown in Figure 2b and a similar result is found for a DMF:NIW ratio of 1:1.4 (Figure 3e,f). Figure 4 shows the diameter distribution of microspheres obtained under different volume ratios of DMF to NIW. The microspheres obtained from DMF/NIW mixtures with volume ratios of 1:1.4 and 1:1 display narrow size distributions (Figure 4c,d). However, changing the volume ratio of DMF:NIW from 1:7 to 1:2 results in a broadening of the size distribution (Figure 4a,b and Table 1).

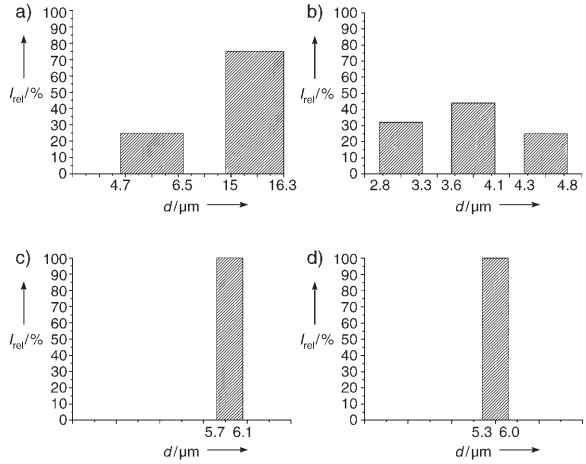

Figure 4. Size distributions of $CaCO_3$ microspheres produced under different conditions (*d*: diameter): The volume ratios of DMF:NIW are: a) DMF:NIW = 1:7; b) DMF:NIW = 1:2; c) DMF:NIW = 1:1.4; d) DMF:NIW = 1:1.

Table 1: Crystallization of vaterite particles.

DMF:NIW (v/v)	Polymorph	Particle distribution	Particle shape
1:7	vaterite	inhomogeneous	spheres
1:5	vaterite	inhomogeneous	spheres
1:3	vaterite	inhomogeneous	spheres and ellipsoids
1:2	vaterite	inhomogeneous	spheres
1:1.4	vaterite	monodisperse	spheres
1:1	vaterite + calcite[a]	monodisperse	spheres

[a] Trace of calcite phase present in this sample.

Figure 5 shows the X-ray diffraction (XRD) patterns of the as-prepared products obtained in DMF/NIW mixtures with different volume ratios when the other experimental

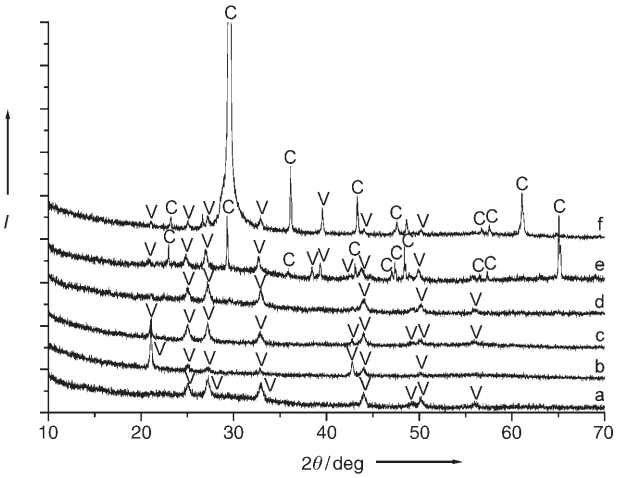

Figure 5. XRD patterns of $CaCO_3$ particles obtained in DMF/NIW with different volume ratios after mineralization for 7 days. a) 1:7; b) 1:5; c) 1:2; d) 1:1.4; e) 1:1; f) pure DMF. [PEG-*b*-pGlu] = 1.0 g L^{-1}. A solution of $CaCl_2$ was added to the solvent mixtures. V denotes vaterite and C denotes calcite.

 © 2006 Wiley-VCH Verlag GmbH & Co. KGaA, Weinheim

conditions were kept constant. All reflection peaks of $CaCO_3$ particles can be easily indexed as vaterite for volume ratios ranging from 1:7 to 1:1.4 (Figure 5a–d). The broadening diffraction peaks indicate that the produced vaterite microspheres are composed of small nanoparticles. A trace amount of calcite phase is present when the volume ratio is 1:1 (Figure 5e). In pure DMF, the dominant phase is calcite although the vaterite phase is present (Figure 5f). These data are different from those reported previously, which show that modification of calcite occurs only in pure water.[17b] Furthermore, metastable vaterite is stable for more than two months in a DMF/NIW mixture.

It was reported that a short block of glutamic acid, such as PEG-*b*-pGlu, can be used to precipitate a mixture of calcite and vaterite particles with irregular morphology, and that only the peptide block length of $n = 10$ produces vaterite spheres.[17] However, the results obtained here with mixtures of solvents are remarkably different from those reported previously for a pure-water system.[17]

The formation of monodisperse vaterite microspheres in a DMF/NIW mixture in the presence of PEG-*b*-pGlu is related to the secondary conformation of the polymer and its aggregated state adopted in the solvent mixture as well as to the effect of the solvent mixture itself.[16,19] Because of the different solvent properties of DMF and NIW, different volume ratios of them will have an influence on the polymer's solution properties, including the polymer conformation. A suitable mixture of DMF and NIW favors the dissolution of PEG-*b*-pGlu and alters its self-assembly process. The aggregates of PEG-*b*-PGlu in DMF/NIW mixtures are relatively uniform nanospheres with diameters of 100–150 nm as observed by TEM either in the absence or presence of Ca^{2+} ions (see Supporting Information). Clearly, such spherical aggregates of the block copolymer in the solvent mixture play a crucial role in controlling the nucleation and growth process of uniform vaterite microspheres.

Vaterite is transformed into thermodynamically stable calcite within a few days under the appropriate conditions.[22] Stable spherical vaterite particles can also be produced in the presence of a carboxylate-terminated dendrimer.[20] We propose that such particles can be stabilized by the aggregated framework of PEG-*b*-pGlu formed in DMF/NIW solution: PEG-*b*-pGlu associates with calcium ions to form strong Ca–O bonds thus preventing the dissolution of vaterite particles, as reported recently in the case of a mineralization reaction by using a native peptide, pelovaterin, extracted from eggshells of a soft-shelled turtle.[23] This viewpoint is also consistent with the recent findings that carboxylate block copolymers were able to initiate vaterite nucleation from stable supersaturated solutions through binding of the calcium ions at the ionized carboxylic groups.[20] However, the hydrogen-bonding interactions between peptide chains in PEG-*b*-pGlu and DMF/NIW mixed solvents, of PEG-*b*-pGlu itself, or between DMF and NIW could also attribute to the polymorph transformation from amorphous into vaterite as recently found by using acidic peptides that contain poly(carboxylate) ligands as crystal modifiers.[24]

Thermogravimetric analysis (TGA) was performed to examine the weight percentage of polymer in the superstructure microspheres, which was 5.7 wt% (see Supporting Information) and indicates that the polymer is enclosed within the microspheres. Time-dependent TEM observation in the early stage of the vaterite microsphere formation was performed and shows that after 10 min of mineralization, amorphous aggregated nanoparticles have formed, which grow and transform into single-crystalline spherical vaterite nanospheres within 30 min of mineralization (See Supporting Information). This growth process is different from the reported "sphere–rod–dumbbell–sphere" growth scenarios found in water with other DHBC additives, but has a similar aggregation-based mechanism.[12b] Microspheres were broken by ultrasound, and the broken parts were composed of small nanoparticles with diameters of about 15–20 nm (see Supporting Information), which is consistent with diameters calculated by the Scherer equation based on the broadening diffraction peaks of the XRD pattern (Figure 5d). SEM observation of the inner structure of a broken microsphere also revealed that they are indeed composed of small nanoparticles (see Supporting Information).

According to the LaMer model,[25] uniform particle growth occurs if the uniform primary particles form in solution below a critical supersaturation point. The size of the primary nanoparticles observed in the inner structures of the microspheres and the calculated size from the XRD pattern based on the Scherer equation are smaller than those observed in the early stage of mineralization, for example, after 30 min, which suggests either that the primary nanoparticles nucleate and then secondary nucleation occurs on the nanoparticle surface because it is energetically favored or that nanoparticles are nucleated in solution and then aggregate on the already existing seeds of about 100–200 nm in diameter (see Supporting Information).

We propose that polymer aggregates sequester Ca^{2+} ions and thus serve as localized nucleation centers due to the high local concentration of Ca^{2+} ions after the addition of a source of CO_3^{2-} ions, which is consistent with observations during hydroxyapatite whiskers growth in the presence of aggregates of PEO-*b*-PMAA-C_{12} [PEO is poly(ethylene oxide), PMAA is poly(methacrylic acid)].[11c] Important to the formation of highly monodisperse microparticles is the fact that the long solvating PEG blocks, with respect to the pGlu blocks, are mainly distributed on the outside of the aggregates and can stabilize the forming vaterite microparticles, thus preventing the microparticles from aggregating as demonstrated previously in a comprehensive study of PEO-*b*-PMAA and PMAA as additives for the mineralization of $CaCO_3$.[12a] Ostwald ripening also contributes to the formation of such uniform microspheres in the latter stages of mineralization.

In summary, we have demonstrated that PEG(110)-*b*-pGlu(6) can effectively mediate the controlled crystallization of $CaCO_3$ in a suitable mixture of solvents. Highly monodisperse vaterite microspheres can be produced by using a suitable volume ratio of DMF/NIW and by taking advantage of the synergistic effects of the block copolymer and the solvent mixture. Clearly, the solvent mixture plays a key role in controlling the growth, polymorphism, and shape of the $CaCO_3$ mineral. The detailed mechanism for the formation of such highly monodisperse vaterite microspheres mineralized

 © 2006 Wiley-VCH Verlag GmbH & Co. KGaA, Weinheim

in such a complex mixed-solvent system under the control of a block copolymer is not clear yet. The highly uniform $CaCO_3$ microspheres produced may have applications as an excellent template for polyelectrolyte multilayer capsules and biomimetic photon crystals in devices. Furthermore, this mixed-solvent approach may open a new general route for the crystallization of minerals with high quality and structure specialty.

Experimental Section

All chemicals were of analytical grade. Ammonium carbonate and calcium chloride were purchased from the Shanghai Chemical Reagent Company and used as received without further purification. PEG-*b*-pGlu (PEG = 700 g mol^{-1}, pGlu = 770 g mol^{-1}) was synthesized as described elsewhere.[17] The polymer was purified by exhaustive dialysis before being used in the crystallization of calcium carbonate.

All glassware (glass bottle and small pieces of glass substrates) was cleaned and subjected to ultrasound in a bath containing ethanol for 5–10 min, then rinsed with NIW (18.2 Ω cm^{-1}) and further soaked in a mixture of NIW/HNO_3(65%)/H_2O_2 (volume ratio of 1:1:1), then rinsed with NIW, and finally dried with acetone. The mineralization experiments were carried out as described by Addadi et al.[26] The precipitation of $CaCO_3$ was carried out in a 10-mL glass bottle. A stock solution of $CaCl_2$ (0.1M) was freshly prepared in boiled NIW.

In a typical synthesis, polymer (6 mg) was added to the solvent mixture (6 mL), then a solution of $CaCl_2$ (0.6 mL, 0.1M) was injected into the vigorously stirring mixture. The reaction vessel was covered with parafilm, which was punctured with three needle holes, and placed in a closed desiccator at room temperature ((25 ± 3) °C). Three glass bottles (10 mL) filled with crushed ammonium carbonate and covered with parafilm punctured with three needle holes were also placed in the desiccator. After a set period of time, the parafilm was removed and the precipitate rinsed with NIW and ethanol and allowed to dry at room temperature. For the time-dependent crystallization experiments, copper TEM grids (3 mm in diameter) were put at the bottom of a glass bottle with the carbon film exposed to the solution. The copper grids and glass were then removed after a set period, allowed to dry in air, and directly used for TEM and SEM observation.

Samples on glass substrates were examined after being sputtered with gold for SEM on a BYBY-1010A microscope and field-emission SEM on a JSM-6700F microscope. The products were characterized by XRD, recorded on a (Philips X′ Pert Pro Super) diffractometer with $Cu_{K\alpha}$ radiation (λ = 1.541874 Å). TEM imaging and electron diffraction were performed with an H-800 electron microscope operating at 200 keV. TGA was carried out on a Diamond TG/DTA thermal analyzer (Perkin Elmer) with a heat rate of 10 K min^{-1} in a nitrogen atmosphere.

Received: January 4, 2006
Revised: March 14, 2006
Published online: May 4, 2006

Keywords: block copolymers · crystal growth · peptides · polymorphism · solvent effects

[1] a) S. Mann, *Angew. Chem.* **2000**, *112*, 3532; *Angew. Chem. Int. Ed.* **2000**, *39*, 3392; b) L. A. Estroff, A. D. Hamilton, *Chem. Mater.* **2001**, *13*, 3227.
[2] D. B. Deoliveira, R. A. Laursen, *J. Am. Chem. Soc.* **1997**, *119*, 10627.
[3] E. Dalas, P. Klepetsanis, P. G. Koutsoukos, *Langmuir* **1999**, *15*, 8322.
[4] a) G. A. Ozin, *Acc. Chem. Res.* **1997**, *30*, 17; b) S. W. Weiner, L. Addadi, *J. Mater. Chem.* **1997**, *7*, 689; c) T. Kato, A. Sugawara, N. Hosoda, *Adv. Mater.* **2002**, *14*, 869; d) F. C. Meldrum, *Int. Mater. Rev.* **2003**, *48*, 187; e) H. Cölfen, S. Mann, *Angew. Chem.* **2003**, *115*, 2452; *Angew. Chem. Int. Ed.* **2003**, *42*, 2350.
[5] For reviews, see: a) S. H. Yu, H. Cölfen, *J. Mater. Chem.* **2004**, *14*, 2124, and references therein; b) H. Cölfen, S. H. Yu, *MRS Bull.* **2005**, *30*, 727, and references therein; c) H. Cölfen, *Macromol. Rapid Commun.* **2001**, *22*, 219.
[6] G. Falini, S. Albeck, L. Addadi, *Science* **1996**, *271*, 67.
[7] A. M. Belcher, X. H. Wu, R. J. Christensen, P. K. Hansma, G. D. Stucky, D. E. Morse, *Nature* **1996**, *381*, 56.
[8] N. J. Reeves, J. S. Evans, *J. Phys. Chem. B* **1997**, *101*, 6665.
[9] G. Falini, M. Gazzano, A. Ripamonti, *J. Cryst. Growth* **1994**, *137*, 577.
[10] G. K. Hunter, *Curr. Opin. Solid State Mater. Sci.* **1996**, *1*, 430.
[11] a) M. Sedlak, M. Antonietti, H. Cölfen, *Macromol. Chem. Phys.* **1998**, *199*, 247; b) H. Cölfen, M. Antonietti, *Langmuir* **1998**, *14*, 582; c) M. Antonietti, M. Breulmann, C. Göltner, H. Cölfen, K. K. Wong, D. Walsh, S. Mann, *Chem. Eur. J.* **1998**, *4*, 2493.
[12] a) H. Cölfen, L. M. Qi, *Chem. Eur. J.* **2001**, *7*, 106; b) S. H. Yu, H. Cölfen, M. Antonietti, *J. Phys. Chem. B* **2003**, *107*, 7396; c) S. H. Yu, H. Cölfen, A. W. Xu, *Cryst. Growth Des.* **2004**, *4*, 33; d) S. F. Chen, S. H. Yu, T. X. Wang, J. Jiang, H. Cölfen, B. Hu, B. Yu, *Adv. Mater.* **2005**, *17*, 1461; e) Y. X. Gao, S. H. Yu, H. P. Cong, J. Jiang, A. W. Xu, W. F. Dong, H. Cölfen, *J. Phys. Chem. B*, **2006**, *110*, 6432.
[13] a) S. H. Yu, H. Cölfen, K. Tauer, M. Antonietti, *Nat. Mater.* **2005**, *4*, 51; b) S. H. Yu, H. Cölfen, J. Hartmann, M. Antonietti, *Chem. Eur. J.* **2002**, *8*, 2937.
[14] a) D. B. Zhang, L. M. Qi, J. M. Ma, H. M. Cheng, *Chem. Mater.* **2002**, *14*, 2450; b) L. M. Qi, H. Cölfen, M. Antonietti, *Angew. Chem.* **2000**, *112*, 617; *Angew. Chem. Int. Ed.* **2000**, *39*, 604.
[15] a) T. X. Wang, H. Cölfen, M. Antonietti, *J. Am. Chem. Soc.* **2005**, *127*, 3246; b) H. Endo, D. Schwahn, H. Cölfen, *J. Chem. Phys.* **2004**, *120*, 9410; c) H. Cölfen, *Curr. Opin. Colloid Interface Sci.* **2003**, *8*, 23.
[16] C. S. Choi, Y. W. Kim, *Biomaterials* **2000**, *21*, 213.
[17] a) P. Kašparová, *PhD Thesis*, Postdam, **2002**; b) P. Kašparová, M. Antonietti, H. Cölfen, *Colloids Surf. A* **2004**, *250*, 153.
[18] a) F. Manoli, E. Dalas, *J. Cryst. Growth* **2000**, *218*, 359; b) L. M. Qi, J. M. Ma, *Chem. J. Chin. Univ.* **2002**, *23*, 1595.
[19] a) S. R. Dickinson, K. M. Mcgrath, *J. Mater. Chem.* **2003**, *13*, 928; b) G. Falini, M. Gazzano, A. Ripamonti, *Chem. Commun.* **1996**, 1037; c) K. S. Seo, C. Han, J. H. Wee, J. K. Park, J. W. Ahn, *J. Cryst. Growth* **2005**, *276*, 680; d) S. F. Chen, S. H. Yu, B. Yu, *Chem. Eur. J.* **2004**, *10*, 3050; S. F. Chen, S. H. Yu, J. Jiang, F. Q. Li, Y. K. Liu, *Chem. Mater.* **2006**, *18*, 122.
[20] K. Naka, Y. Tanaka, Y. Chujo, *Langmuir* **2002**, *18*, 3655.
[21] For reviews, see: a) E. Matijević, *Chem. Mater.* **1993**, *5*, 412; b) E. Matijević, *Langmuir* **1994**, *10*, 8.
[22] a) A. Richter, D. Petzold, H. Hofmann, B. Ulrich, *Chem. Tech.* **1996**, *48*, 271; b) N. Nassrallah-Aboukais, A. Boughriet, J. Laureyns, A. Aboukais, J. C. Fischer, H. R. Langelin, M. Wartel, *Chem. Mater.* **1998**, *10*, 238.
[23] R. Lakshminarayanan, E. O. C. Jin, X. J. Loh, R. M. Kini, S. Valiyaveettil, *Biomacromolecules* **2005**, *6*, 1429.
[24] K. Takahashi, A. Kobayashi, M. Doi, S. Adachi, T. Taguchi, *J. Mater. Chem.* **2005**, *15*, 2178.
[25] V. K. LaMer, *Ind. Eng. Chem.* **1962**, *54*, 1270; V. K. LaMer, R. Dinegar, *J. Am. Chem. SOC.* **1950**, *72*, 4847.
[26] S. Weiner, S. Albeck, L. Addadi, *Chem. Eur. J.* **1996**, *2*, 278.

 © 2006 Wiley-VCH Verlag GmbH & Co. KGaA, Weinheim

Biofuels

DOI: 10.1002/anie.200600212

Glycerol as a Source for Fuels and Chemicals by Low-Temperature Catalytic Processing**

*Ricardo R. Soares, Dante A. Simonetti, and James A. Dumesic**

In this era of diminishing petroleum reserves, it is imperative that industrialized society should develop ways to utilize more effectively the abundant and renewable biomass resources available to provide new sources of energy and chemical intermediates.[1] To this end, various processes have been developed to convert biomass and biomass-derived molecules into specialty chemicals (methanol), light alkanes (C_1–C_6), liquid fuels (ethanol and C_7–C_{15} alkanes), and synthesis gas.[2] As a new direction, we show herein that glycerol can be converted over platinum-based catalysts into gas mixtures of H_2 and CO (synthesis gas) at temperatures from 498 to 620 K. These temperatures are lower than those for conventional gasification of biomass (e.g. 800–1000 K).[3,4] Synthesis gas can be used to produce fuels and chemicals; therefore, the endothermic conversion of glycerol into synthesis gas can be combined with exothermic Fischer–Tropsch and methanol syntheses to provide low-temperature and energy-efficient routes for the production of these compounds. The glycerol used can be sourced from waste glycerol streams that are currently generated as by-products from the production of biodiesel. This heat-integrated catalytic process could also be a less energy-intensive alternative to current methods of converting carbohydrates into fuel-grade ethanol.

Synthesis gas production methods for conventional Fischer–Tropsch plants require either an O_2 plant or a large Fischer–Tropsch reactor to process the synthesis-gas stream diluted with N_2 from air, thereby increasing the capital costs of such facilities.[5] Furthermore, Hamelinck et al. showed that nearly 50% of the cost of producing Fischer–Tropsch liquids from biomass is related to capital cost,[6] of which 50% stems from biomass gasification, gas cleaning, and synthesis-gas processing. The method we present herein may allow for economic operation of a small-scale Fischer–Tropsch reactor by producing an undiluted H_2/CO gas mixture. Indeed, our method reduces the capital cost of the Fischer–Tropsch plant by eliminating the O_2 plant or biomass gasifier and subsequent gas-cleaning steps.

The conversion of glycerol into CO and H_2 takes place by Equation (1). The endothermic enthalpy change of this

$$C_3O_3H_8 \rightarrow 3\,CO + 4H_2 \quad (1)$$

reaction (350 kJ mol^{-1}) corresponds to about 24% of the heating value of the glycerol (−1480 kJ mol^{-1}). The heat generated by Fischer–Tropsch conversion of the CO and H_2 to liquid alkanes such as octane (−412 kJ mol^{-1}) corresponds to about 28% of the heating value of the glycerol. Thus, combining these two reactions results in the following exothermic process, with an enthalpy change (−63 kJ mol^{-1}) that is about 4% of the heating value of the glycerol:

$$C_3O_3H_8 \rightarrow \frac{7}{25}C_8H_{18} + \frac{19}{25}CO_2 + \frac{37}{25}H_2O \quad (2)$$

One source of glycerol for our catalytic process is the low-value waste stream from the transesterification of plant oils[1,7] and animal fat[1] in the production of biodiesel. This waste contains glycerol in water at high concentrations (e.g. 80%).[8] The current production levels of biodiesel in the United States and Europe are 1×10^8 and 2×10^9 L year^{-1}, respectively, and are expected to double in the near future.[8,9] Selling waste glycerol solution can lower the production costs of biodiesel by 6%.[10] The production of methanol from this glycerol is an attractive alternative that could help alleviate the burden of low-value waste glycerol and decrease the production costs of biodiesel by lowering the dependence on natural-gas-derived methanol.

Glycerol can also be produced by fermentation of sugars such as glucose, either directly[11] or as a by-product of the industrial conversion of lignocellulose into ethanol.[12] This form of ethanol production in the U.S. is expected to increase to 30×10^9 L year^{-1} by 2020 (three times the expected increase in ethanol production from corn over the same period);[13] this growing industry may be a major biofuel provider in the future. Technical and economic analyses show that the co-production of glycerol with ethanol lowers production costs and increases profit margins.[11,14–16] The process pathways that generate liquid fuels and chemicals from glycerol are outlined in the Supporting Information.

Although the fermentation of glucose produces ethanol at concentrations of about 5 wt% in water, it can be carried out to produce glycerol at concentrations of at least 25 wt%.[11] This higher concentration of glycerol decreases the energy costs required to remove water from the oxygenated hydrocarbon fuel. Indeed, distillation is one of the most energy-intensive steps involved in the production of fuel-grade ethanol from glucose.[17,18] For example, the energy required to vaporize a 5-wt% aqueous solution of ethanol (as an estimate of the energy of distillation) is 1680 kJ mol^{-1}, which

[*] D. A. Simonetti, Prof. J. A. Dumesic
Department of Chemical and Biological Engineering
University of Wisconsin
Madison, WI 53706 (USA)
Fax: (+1) 608-262-5434
E-mail: dumesic@engr.wisc.edu
R. R. Soares
Universidade Federal de Uberlândia
Faculdade de Engenharia Química
Uberlândia, MG 38408-100 (Brazil)

[**] This work was supported by the Office of Basic Energy Sciences, U.S. Department of Energy (DOE), and we acknowledge a post-doctoral grant from CAPES–Brazil for R.R.S. We thank Edward L. Kunkes for help with catalyst preparation and characterization. We thank Randy D. Cortright and Manos Mavrikakis for discussions throughout this project.

Supporting information for this article is available on the WWW under http://www.angewandte.org or from the author.

InterScience DISCOVER SOMETHING GREAT
© 2006 Wiley-VCH Verlag GmbH & Co. KGaA, Weinheim

corresponds to 1.4 times the lower heating value of the ethanol product ($-1241\ kJ\,mol^{-1}$). In contrast, the energy required to vaporize a 25-wt% aqueous solution of glycerol ($531\ kJ\,mol^{-1}$) corresponds to 0.33 times the lower heating value of the liquid-alkane products ($-1418\ kJ\,mol^{-1}$, assuming octane as the product molecule and utilizing the enthalpy change in Equation (2)). Detailed energy calculations are presented in the Supporting Information.

Figure 1 shows results for the gas-phase conversion of glycerol into synthesis gas over supported Pt catalysts at 623 K and atmospheric pressure with a feed solution of glycerol in water (30 wt%). This concentration is similar to that reported by Gong et al.[11] Moreover, the energy required to separate the glycerol from water is similar to that of vaporizing the solution and condensing the water after the glycerol has reacted. Catalysts consisting of Pt supported on Al_2O_3, ZrO_2, CeO_2/ZrO_2, and MgO/ZrO_2 exhibited deactivation during time-on-stream, whereas the Pt/C catalyst showed stable conversion of glycerol into synthesis gas for at least 30 h (Figure 1 a). The catalyst with the most acidic support, Pt/Al_2O_3, showed a period of apparently stable catalytic activity, followed by a period of rapid catalyst deactivation. Because the reactor initially operates at 100% conversion, glycerol is present only in the upstream portion of the catalyst bed in the tubular reactor, and a deactivation front moves from the reactor inlet to the outlet as olefinic species are formed from glycerol on acid sites associated with alumina, followed by deposition of coke from these species on the Pt surface sites. The most basic catalyst support, MgO/ZrO_2, showed rapid deactivation for all times-on-stream. The most stable oxide-supported catalyst appears to be Pt on CeO_2/ZrO_2; however, the performance of this catalyst is inferior to that of Pt supported on carbon.

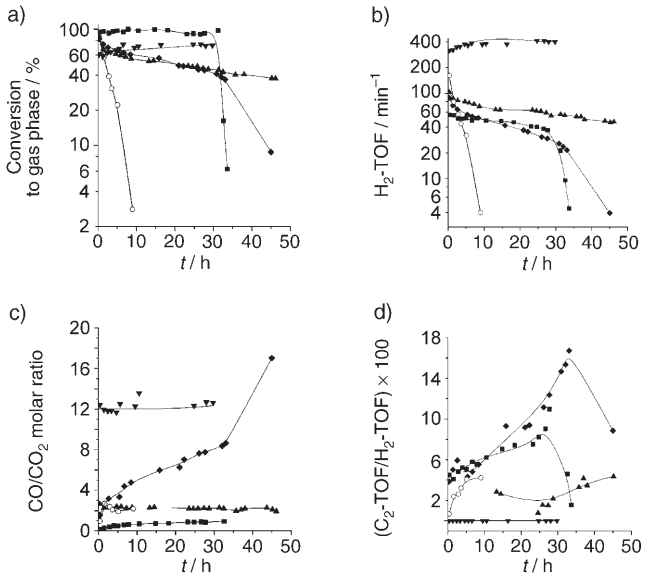

Figure 1. Performance of supported Pt catalysts. Variation with time-on-stream of a) percentage glycerol conversion to gas-phase products, b) H_2-turnover frequency, c) CO/CO_2 molar ratio, and d) C_2-TOF/H_2-TOF ratio for Pt catalysts supported on Al_2O_3 (■), CeO_2/ZrO_2 (▲), C (▼), ZrO_2 (◆), and MgO/ZrO_2 (○). Percentage conversion to gas phase is calculated as [(C atoms in gas-phase product stream)/(total C atoms into reactor as feed)]×100. Reactions were carried out at 1 bar and 623 K with aqueous glycerol feed solution (30 wt%) over oxide-supported Pt catalysts (1.0 g) or Pt/C catalyst (0.060 g) and a feed rate of $0.32\ cm^3\,min^{-1}$. See Supporting Information for further experimental details.

The different deactivation profiles displayed in Figure 1 for the various catalysts suggest that the support plays an important role in the deactivation process. Figure 1 d shows the rate of formation of C_2-hydrocarbons (ethane and ethylene) normalized to the rate of H_2 production for the various supported Pt catalysts. Negligible amounts of C_2-hydrocarbons were formed on the Pt/C catalyst. In contrast, catalysts consisting of Pt supported on the various oxides formed measurable amounts of C_2-hydrocarbons, and the C_2-TOF/H_2-TOF ratio (TOF = turnover frequency) increased with time-on-stream. This behavior suggests that one of the modes of catalyst deactivation is caused by dehydration on the oxide catalyst supports, which leads to the formation of unsaturated hydrocarbon species that form carbonaceous deposits on the Pt surface, thereby decreasing the rate of H_2 production and increasing the C_2-TOF/H_2-TOF ratio.

Table 1: Experimental data for catalytic processing of glycerol into synthesis gas under various conditions.

Conditions		Conversion into gas phase [%]	H_2-TOF [min^{-1}]	H_2/CO	CO/CO_2	CH_4/H_2
Feed flow rate [$cm^3\,min^{-1}$][a]	0.08	68	111	1.6	5.7	0.038
	0.16	71	241	1.4	8.8	0.036
	0.32	64	373	1.3	12	0.045
	0.64	39	449	1.3	17	0.038
Glycerol concentration [wt%][b]	20	64	265	1.4	8.7	0.025
	30[c]	50	285	1.3	14	0.032
	50	26	267	1.2	37	0.050
T [K][d]	573	17	104	1.31	90	0.037
	623	54	335	1.31	17	0.027
	673	100	600	1.33	11	0.027
	673[e]	72	450	1.38	–	–
	723	61	419	1.68	4.6	0.019
	723[e]	43	300	1.83	–	–

For these studies of reaction kinetics, 0.060 g of 5 wt% Pt/C was used. [a] Glycerol feed 30 wt%, 623 K, 1 bar. [b] Feed flow rate $0.32\ cm^3\,min^{-1}$, 623 K, 1 bar. [c] Point taken after 2 h time-on-stream. [d] Glycerol feed 30 wt%, $0.32\ cm^3\,min^{-1}$, 1 bar. [e] Point taken after 3 h time-on-stream.

The H_2/CO ratio for the product stream from the Pt/C catalyst is approximately 1.3:1 (Table 1), which is in agreement with the stoichiometry of Equation (1). In contrast, the H_2/CO ratios obtained over the other catalysts were higher than 1.5:1, which indicates some contribution from water–gas shift (WGS). This behavior is demonstrated more clearly by the CO/CO_2 ratio (Figure 1 c). The initial CO/CO_2 ratio for Pt/C is 12:1, whereas for the other catalysts it is less than 3:1. Thus, it appears that the WGS reaction is facilitated by the

 © 2006 Wiley-VCH Verlag GmbH & Co. KGaA, Weinheim

presence of the oxide support, as reported in other studies of WGS over supported metal catalysts.[19–21]

Reaction conditions (Table 1) that result in lower conversions of glycerol (i.e. higher flow rates of the glycerol feed (30 wt%) and higher glycerol concentrations at constant feed flow rate) lead to higher CO/CO_2 ratios. This behavior suggests that the primary reaction in glycerol conversion is the formation of CO and H_2, and the production of CO_2 by WGS is a secondary reaction. Therefore, water acts primarily as a diluent in the production of synthesis gas from glycerol, thus leading to higher conversions (Table 1). The important consequence of this behavior is that it is possible to adjust the space velocity of the catalytic process to ensure that the conversion of glycerol is complete, while simultaneously controlling the H_2/CO ratio for the Fischer–Tropsch synthesis step. We note that the rate of methane formation remained low for all of the conditions in Table 1.

The results in Table 1 show that the rate of H_2 production passes through a maximum with respect to reaction temperature at constant-feed conditions. The rate increases with increasing temperature from 573 to 623 K (with an activation energy of about 70 kJ mol^{-1}). However, although the rate of hydrogen production increases further when the temperature is initially increased to 673 K, the Pt/C catalyst eventually undergoes deactivation at this higher temperature. We suggest that at high temperatures, dehydration is fast relative to H_2 formation, thus leading to catalyst deactivation.

Figure 2a and b show the performance of the Pt/C catalyst under different pressures (1 and 20 bar) for the 30-wt% glycerol feed, and at different glycerol feed concentrations (30 and 50 wt%) at a pressure of 1 bar. The catalyst showed good stability for at least 48 h time-on-stream for both the higher glycerol feed concentration (50 wt%) and the higher reaction pressure (20 bar). It also showed excellent stability for converting a 30-wt% glycerol feed into synthesis gas at 20 bar, with a H_2/CO ratio ($\approx$2:1) that is appropriate for Fischer–Tropsch[22] or methanol synthesis.[23]

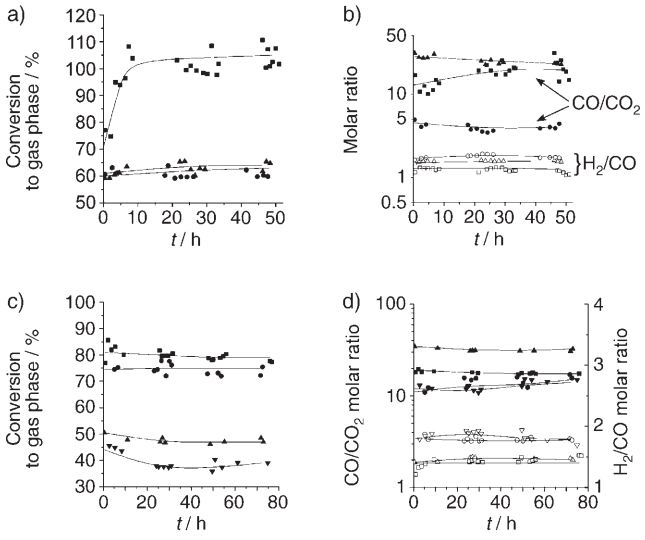

Figure 2. Performance of carbon-supported Pt and Pt-bimetallic catalysts under various process conditions. Variation with time-on-stream of a) percentage glycerol conversion to gas-phase products and b) molar ratios for conversion of 30 wt% glycerol at 1 bar (■), 50 wt% at 1 bar (▲), and 30 wt% at 20 bar (●) over 0.090 g Pt/C at 623 K. Variation with time-on-stream of c) percentage glycerol conversion to gas-phase products and d) CO/CO_2 (filled symbols) and H_2/CO (empty symbols) molar ratios for conversion of 30 wt% glycerol at 1 bar over Pt–Ru/C at 548 K (triangles; 0.435 g catalyst) and 573 K (squares; 0.513 g catalyst) and over Pt–Re/C at 498 K (inverted triangles; 0.535 g catalyst) and 523 K (circles; 0.535 g catalyst). A feed rate of 0.16 cm^3 min^{-1} for a) and b) and 0.08 cm^3 min^{-1} for c) and d) was used.

To allow the efficient combination of the endothermic conversion of glycerol into synthesis gas with the exothermic Fischer–Tropsch or methanol-synthesis steps, the former should be performed at the lowest-possible temperature. In doing so, flexibility in the Fischer–Tropsch materials used (e.g, Co-based versus Fe-based catalysts) becomes possible. Therefore, we carried out studies of glycerol conversion into synthesis gas at 498–573 K. The catalytic conversion of polyols to H_2, CO_2, and CO involves the preferential cleavage of C–C bonds as opposed to C–O bonds,[24,25] and Pt-based catalysts are particularly active and selective for this process. Under these reaction conditions, the surface is covered primarily by adsorbed CO species;[26] therefore, a strategy for a catalyst that converts polyols into synthesis gas and is active at low temperatures is to facilitate the desorption of CO, thereby suppressing the subsequent WGS step and improving the turnover of the catalytic cycle by regenerating vacant surface sites. Accordingly, we require materials that possess the catalytic properties of Pt with respect to selective cleavage of C–C versus C–O bonds, but that have less exothermic enthalpy changes for CO adsorption; Pt–Ru and Pt–Re alloy catalysts fit this description.[27,28]

Figure 2c and d show that the percentage conversion of glycerol and the product-gas ratios remained constant for at least 72 h time-on-stream at these low temperatures over Pt–Ru and Pt–Re (atomic ratio 1:1) bimetallic catalysts. The overall carbon balances for these runs came to within 10%. The main condensable organic compound in the effluent streams of the catalysts was unconverted glycerol, with smaller amounts of ethylene glycol, methanol, hydroxypropanone, and ethanol. These results demonstrate that the conversion of glycerol to synthesis gas can, in fact, be accomplished at temperatures well within the ranges employed for Fischer–Tropsch and methanol syntheses,[22,23,29] thus allowing for the efficient combination of these processes. Moreover, the H_2/CO ratio can be adjusted by adding a WGS functionality (see Supporting Information).

We have presented a low-temperature catalytic route for converting glycerol into H_2/CO gas mixtures that are suitable for combination with Fischer–Tropsch and methanol syntheses. This new route opens new opportunities for use with processes that produce polyols, such as glycerol through fermentation of carbohydrate feedstocks, at high concentrations in water.

Received: January 18, 2006
Published online: May 9, 2006

Keywords: biomass · gas-phase reactions · heterogeneous catalysis · liquid fuels · synthesis gas

 © 2006 Wiley-VCH Verlag GmbH & Co. KGaA, Weinheim

[1] D. L. Klass, *Biomass for Renewable Energy, Fuels, and Chemicals*, Academic Press, San Diego, **1998**.
[2] J. O. Metzger, *Angew. Chem.* **2006**, *118*, 710 – 713; *Angew. Chem. Int. Ed.* **2006**, *45*, 696 – 698.
[3] M. Asadullah, S. Ito, K. Kunimori, M. Yamada, K. Tomishige, *Environ. Sci. Technol.* **2002**, *36*, 4476 – 4481.
[4] R. L. Bain, D. C. Dayton, D. L. Carpenter, S. R. Czernik, C. J. Feik, R. J. French, K. A. Magrini-Bair, S. D. Phillips, *Ind. Eng. Chem. Res.* **2005**, *44*, 7945 – 7956.
[5] C. H. Bartholomew, R. J. Farrauto, *Fundamentals of Industrial Catalytic Processes*, Wiley, Hoboken, **2006**.
[6] C. N. Hamelinck, A. P. C. Faaij, H. den Uil, H. Boerrigter, *Energy* **2004**, *29*, 1743 – 1771.
[7] J. M. Encinar, J. F. González, A. Rodríguez-Reinares, *Ind. Eng. Chem. Res.* **2005**, *44*, 5491 – 5499.
[8] J. Van Gerpen, *Fuel Process. Technol.* **2005**, *86*, 1097 – 1107.
[9] K. Bozbas, *Renew. Sust. Ener. Rev.*, in press.
[10] M. J. Haas, A. J. McAloon, W. C. Yee, T. A. Foglia, *Bioresour. Technol.* **2006**, *97*, 671 – 678.
[11] C. S. Gong, J. X. Du, N. J. Cao, G. T. Tsao, *Appl. Biochem. Biotechnol.* **2000**, *84*, 543 – 560.
[12] "Carbohydrate Economy Bulletin", to be found under http://www.carbohydrateeconomy.org/library/admin/uploadedfiles/Carbohydrate_Economy_Bulletin_Volume_1_Numb_3.htm, **2000**.
[13] P. L. Rogers, Y. J. Jeon, C. J. Svenson, *Process Saf. Environ. Prot.* **2005**, *83*, 499 – 503.
[14] C. E. Wyman, *Biotechnol. Prog.* **2003**, *19*, 254 – 262.
[15] J. J. Bozell, R. Landucci (Eds.), *Alternative Feedstocks Program Technical and Economic Assessment: Thermal/Chemical and Bioprocessing Components*, U.S. Department of Energy, Washington D.C., **1993**, pp. 1 – 196.
[16] R. Landucci, B. J. Goodman, C. E. Wyman, *Appl. Biochem. Biotechnol.* **1994**, *45–46*, 677 – 696.
[17] H. Shapouri, J. A. Duffield, M. Wang, (report no. 814, Office of the Chief Economist, U. S. Department of Agriculture; available at http://www.usda.gov/oce/reports/energy/aer-814.pdf) **2002**.
[18] D. Pimentel, T. W. Patzek, *Nat. Resour. Res.* **2005**, *14*, 65 – 76.
[19] A. Basinska, L. Kepinski, F. Domka, *Appl. Catal. A* **1999**, *183*, 143 – 153.
[20] R. J. Gorte, S. Zhao, *Catal. Today* **2005**, *104*, 18 – 24.
[21] F. Esch, S. Fabris, L. Zhou, T. Montini, C. Africh, P. Fornasiero, G. Comelli, R. Rosei, *Science* **2005**, *309*, 752 – 755.
[22] E. Iglesia, S. C. Reyes, R. J. Madon, S. L. Soled, *Adv. Catal.* **1993**, *39*, 221 – 302.
[23] K. A. Pokrovski, M. D. Rhodes, A. T. Bell, *J. Catal.* **2005**, *235*, 368 – 377.
[24] R. D. Cortright, R. R. Davda, J. A. Dumesic, *Nature* **2002**, *418*, 964 – 967.
[25] R. Alcala, M. Mavrikakis, J. A. Dumesic, *J. Catal.* **2003**, *218*, 178 – 190.
[26] R. He, R. R. Davda, J. A. Dumesic, *J. Phys. Chem. B* **2005**, *109*, 2810 – 2820.
[27] E. Christoffersen, P. Liu, A. Ruban, H. L. Skriver, J. K. Norskov, *J. Catal.* **2001**, *199*, 123 – 131.
[28] J. Greely, M. Mavrikakis, *Nat. Mater.* **2004**, *3*, 810 – 815.
[29] A. P. Steynberg, R. L. Espinoza, B. Jager, A. C. Vosloo, *Appl. Catal. A* **1999**, *186*, 41 – 54.

 © 2006 Wiley-VCH Verlag GmbH & Co. KGaA, Weinheim

DOI: 10.1002/anie.200600702

Kinetically Controlled Ligation for the Convergent Chemical Synthesis of Proteins**

*Duhee Bang, Brad L. Pentelute, and Stephen B. H. Kent**

In the past decade, total chemical synthesis has proved to be a robust and reproducible method for making proteins of defined tertiary structure and full biological activity.[1–5] This success has been made possible by the introduction of chemical ligation methods based on the chemoselective reaction of unprotected peptides under mild conditions in aqueous solution.[6] Our objective is the fully convergent synthesis of proteins from four or more peptide segments using modern native chemical ligation methods. Convergent synthesis is inherently parallel and is thus more efficient.[7] In a convergent approach, the two halves of the target sequence are prepared from multiple peptide segments and condensed in a final step to give the full-length polypeptide chain. In the fully convergent strategy reported herein for the chemical synthesis of a target polypeptide chain, novel synthetic routes are used to make the two halves of the target polypeptide chain. Thus, the left half of the target polypeptide is made by sequential C-to-N ligations in the presence of a potentially reactive thioester moiety at the C terminus, while the right half of the target sequence is made by unprecedented sequential ligations in the N-to-C direction.

Native chemical ligation, the thioester-mediated covalent joining of unprotected peptide segments at a cysteine residue,[8] is the most practical and most widely used chemoselective ligation method. Until now, most synthetic proteins have been prepared from just two peptide segment building blocks. Recent improvements have been focused on the preparation of proteins by sequential ligation of three or four peptide segments.[2,3,5,9,10] For syntheses involving multiple segments, existing strategies for the use of native chemical ligation are suitable only for sequential ligations towards the N terminus from a C-terminal Cys peptide segment. An N-terminal Cys residue can be reversibly protected (PG = protecting group) to give PG-Cys-peptide 1-($^{\alpha}$thioester), so that reaction with Cys-peptide 2 gives only the desired PG-Cys-peptide 1-peptide 2; removal of the protecting group to give

[*] Dr. D. Bang, B. L. Pentelute, Prof. S. B. H. Kent
Department of Chemistry
Institute for Biophysical Dynamics
Center for Integrative Science
The University of Chicago
929 East 57th Street, Chicago, IL 60637 (USA)
Fax: (+1) 773-702-0439
E-mail: skent@uchicago.edu

[**] This work was supported by funding from the DOE GTL program (grant DE-FG02-04ER63786 to S.B.K).

Supporting information for this article is available on the WWW under http://www.angewandte.org or from the author.

© 2006 Wiley-VCH Verlag GmbH & Co. KGaA, Weinheim
InterScience

Cys-peptide 1-peptide 2 enables the synthesis to be continued by sequential ligation towards the N terminus of the target polypeptide chain.[3] No corresponding set of chemical tactics currently exists for protecting the thioester moiety of a peptide-(α-thioester), thus preventing not only N-to-C sequential assembly of the peptide segments by native chemical ligation but also fully convergent protein synthesis using this chemistry.[11]

Herein, we report an approach based on the novel principle of "kinetically controlled ligation" that enables a highly practical, fully convergent strategy for the synthesis of a target protein. The major challenge was to control the intrinsic dual reactivity of a bifunctional Cys-peptide 2-(α-thioester) under native chemical ligation reaction conditions so that it would react with a peptide 1-(α-thioester) to yield only a single product (see Scheme 1 A).[12] Like most researchers who use native chemical ligation, until now we have routinely prepared relatively unreactive peptide-(α-$COSCH_2CH_2CO$)-Leu (i.e. alkyl) thioesters.[13] Typically, native chemical ligation of such a peptide-(α-thioalkylester) and a Cys-peptide has been carried out in the presence of thiophenol as a catalyst; the reactive species is assumed to be the peptide-(α-thiophenylester).[14] We conjectured that a preformed peptide-(α-thiophenylester) would react with a Cys-peptide so much faster than a standard peptide-(α-thioalkylester) that, in the same solution under competitive reaction conditions in the absence of exogenous thiophenol, this large rate difference (see Supporting Information) would make the standard peptide-(α-thioalkylester) effectively unreactive. This turned out to be the case.

To present concrete examples of the chemical challenges involved in the fully convergent synthesis of a protein from

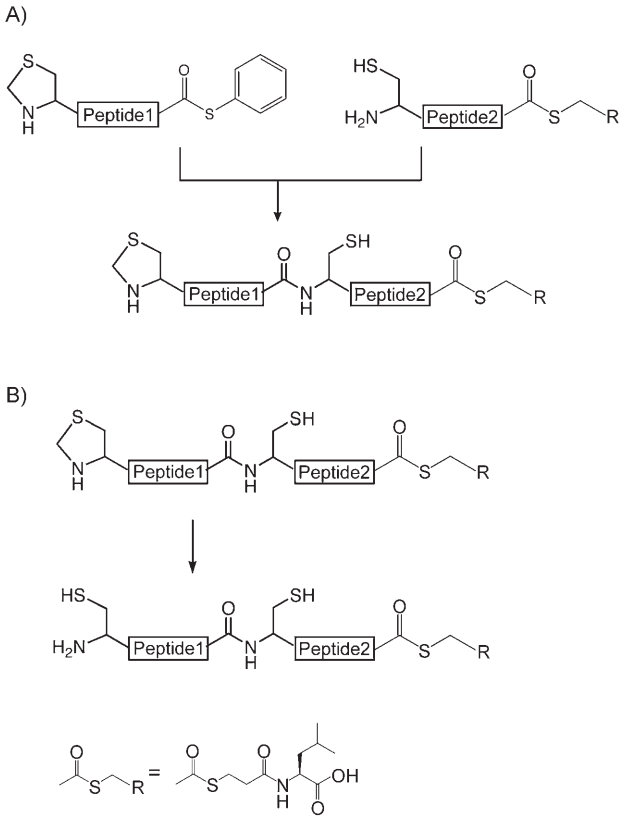

Scheme 1. Key steps in a convergent synthesis using native chemical ligation. A) Kinetically controlled reaction of a peptide-(α-thiophenylester) with a Cys-peptide-(α-thioalkylester) to give a single ligation product. B) The conversion of a Thz-peptide-(α-thioalkylester) into a Cys-peptide-(α-thioalkylester), without damage to the thioalkylester moiety.

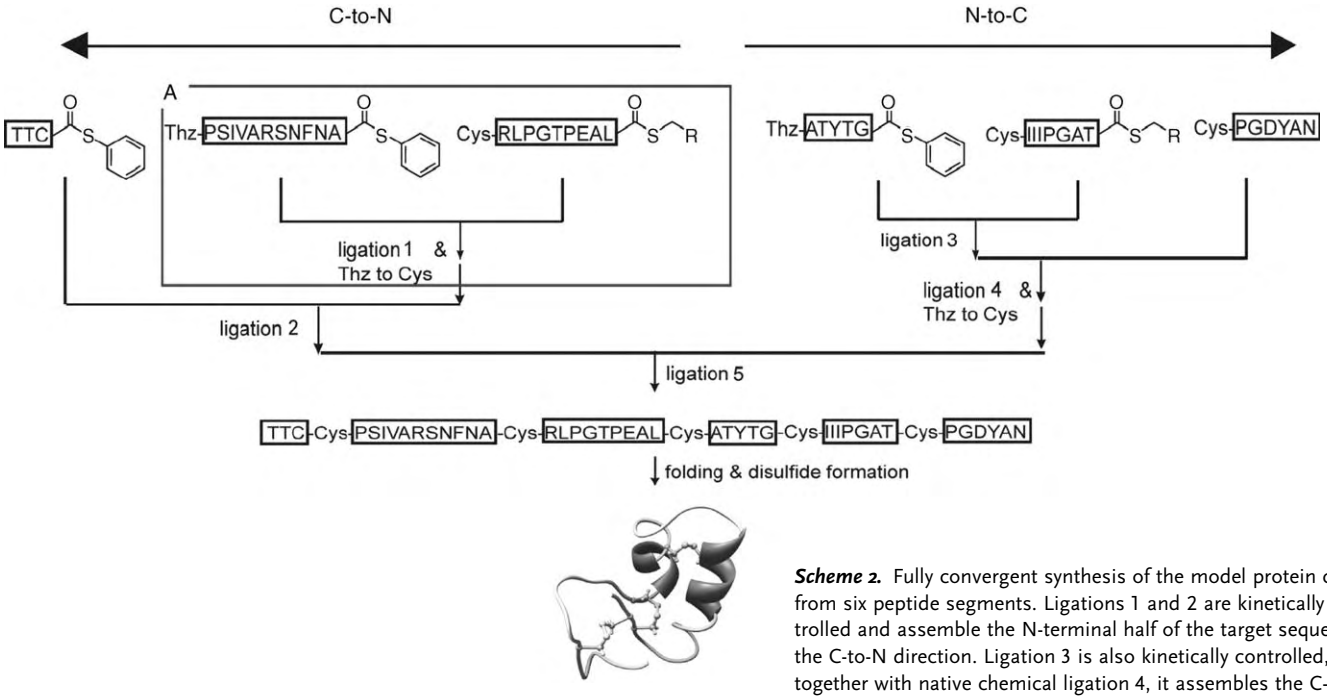

Scheme 2. Fully convergent synthesis of the model protein crambin from six peptide segments. Ligations 1 and 2 are kinetically controlled and assemble the N-terminal half of the target sequence in the C-to-N direction. Ligation 3 is also kinetically controlled, and together with native chemical ligation 4, it assembles the C-terminal half of the molecule in the N-to-C direction. Ligation 5 is the final native chemical ligation of the two halves of the target molecule 46-residue polypeptide, which is folded to give the protein crambin.

 © 2006 Wiley-VCH Verlag GmbH & Co. KGaA, Weinheim

multiple peptide segments and to illustrate how we were able to effectively address those challenges, we undertook a synthesis of the model protein crambin from six peptide segments.[3,15–17] The sequence of the target molecule and the synthetic design are shown in Scheme 2.

The efficacy of our kinetic-control strategy for determining the outcome of a ligation reaction is shown in ligation 1 in the crambin synthesis (see Scheme 2, box A), with the reaction of Thz-Pro-Ser-Ile-Val-Ala-Arg-Ser-Asn-Phe-Asn-Ala-(α-thiophenylester) with Cys-Arg-Leu-Pro-Gly-Thr-Pro-Glu-Ala-Leu-(α-thioalkylester) in aqueous buffer (pH 6.8) in the absence of added thiophenol (see Figure 1 A and B). The ligation reaction was complete in one hour and gave the desired product Thz-Pro-Ser-Ile-Val-Ala-Arg-Ser-Asn-Phe-Asn-Ala-Cys-Arg-Leu-Pro-Gly-Thr-Pro-Glu-Ala-Leu-(α-thioalkylester) in near-quantitative yield. Only trace amounts of by-products from undesired reaction of the alkyl

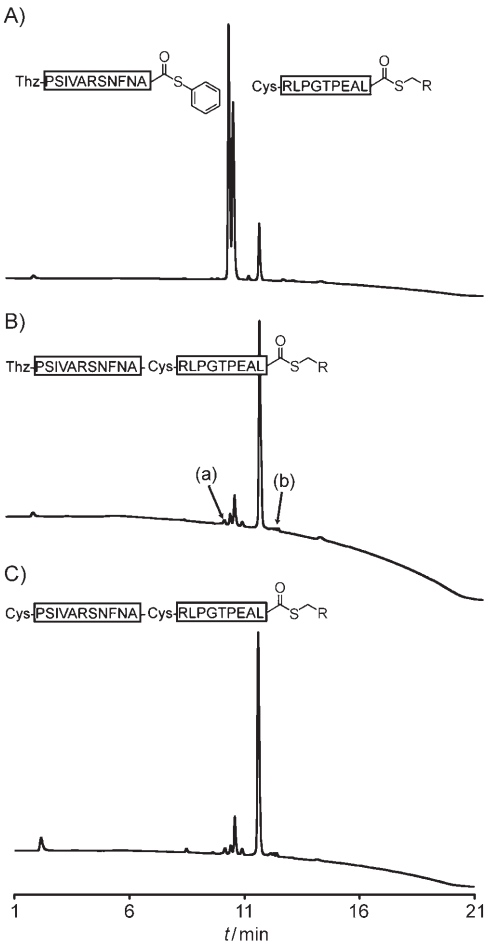

Figure 1. Analytical HPLC traces of the kinetically controlled ligation of [Thz4–Ala15]-(α-thiophenylester) and [Cys16–Leu25]-(α-thioalkylester). A) $t < 1$ min, B) $t = 1$ h. The ligation gave almost exclusively the [Thz4–Leu25]-(α-thioester). In part (B), arrow (a) indicates cyclized by-product (cyclic (Cys16–Leu25); the two peaks eluting just after this by-product are residual reactants), and arrow (b) indicates the by-product [Thz4–Leu25]–[Cys16–Leu25]-(α-thioalkylester). C) Conversion of [Thz4–Leu25]-(α-thioalkylester) into [Cys4–Leu25]-(α-thioalkylester) using 0.2 M methoxyamine hydrochloride added directly to the ligation reaction mixture. The reaction was complete in two hours.

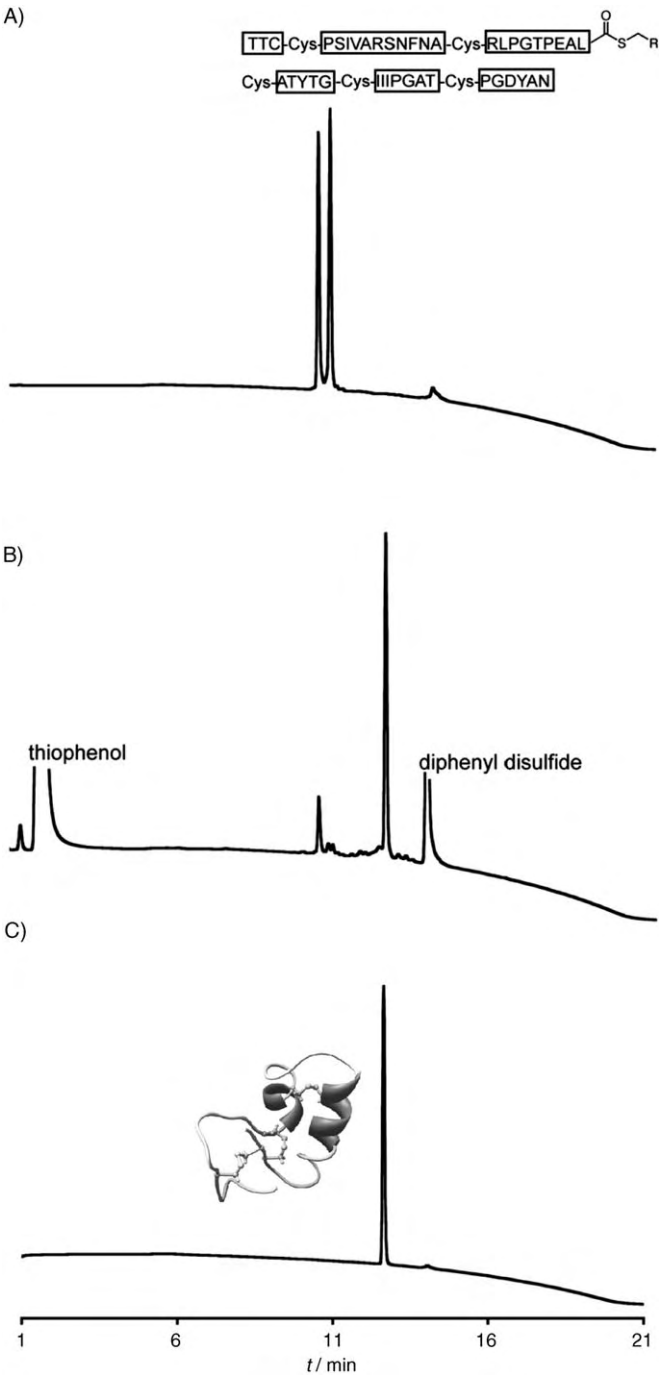

Figure 2. Analytical HPLC traces corresponding to the final step in the fully convergent synthesis of crambin, namely the native chemical ligation of the two halves of the target polypeptide chain [Thr1–Leu25]-(α-thioalkylester) and [Cys26–Asn46]. Trace (A) shows the starting point (i.e. before the addition of thiophenol). Overnight reaction under standard native chemical ligation conditions gave the full-length crambin polypeptide, which was then folded without purification. Trace (B) shows the total crude products from folding and disulfide formation of the unpurified full-length polypeptide ligation product obtained upon dilution to 1 M guanidinium hydrochloride in the presence of 8 mM Cys and 1 mM cystine. The correctly folded crambin molecule was formed in near-quantitative yield in 1 h. Trace (C) shows the folded crambin molecule after purification by preparative HPLC (observed mass: 4702.0 ± 0.8 Da; calculated mass: 4702.4 Da, as expected for three disulfides). Reverse-phase HPLC analyses were performed on a Vydac C4 column using a linear gradient (1–61%) of buffer B in buffer A over 15 min (buffer A: 0.1% trifluoroacetic acid (TFA) in water; buffer B: 0.08% TFA in acetonitrile). Disulfide bridges were not determined.

 © 2006 Wiley-VCH Verlag GmbH & Co. KGaA, Weinheim

thioester were formed (see Figure 1B): cyclized by-product (<1.5%) and oligomer (≪1%). Similar results were obtained for the two other kinetically controlled ligations in the crambin synthesis (Scheme 2, ligations 2 and 3; see also Supporting Information).

The other key chemical transformation for the use of native chemical ligation in a fully convergent synthesis is to be able to convert a Thz-peptide-(α-thioalkylester) into a Cys-peptide-(α-thioalkylester) (Scheme 1B). This transformation was accomplished by treatment with 0.2 M methoxyamine hydrochloride. The thioester moiety was unaffected during the quantitative conversion from the Thz-peptide-(α-thioalkylester) into the Cys-peptide-(α-thioalkylester) (compare the products shown in Figure 1C with the starting mixture in Figure 1B).

The last step in the convergent synthesis was the native chemical ligation of the two halves of the polypeptide chain, followed by folding and disulfide formation, which gave the synthetic crambin protein in good yield (see Figure 2).

Several aspects of the kinetically controlled ligation reactions used in the convergent synthesis of crambin are worthy of comment. Ligation 2 (Scheme 2) involves reaction of a peptide-thiophenylester that contains an internal Cys residue with a free thiol group. In this instance, the presence of a free thiol did not interfere with the formation of the desired product (see Supporting Information); however, the ligation product underwent internal cyclization with the C-terminal thioester to form a thiolactone, which could be readily converted into a thioalkyl ester (see Supporting Information). The nature of the C-terminal amino acid residue in a peptide-(α-thioester) affects the relative reactivity of that peptide in native chemical ligation: hindered C-terminal amino acids such as Ile, Thr, or Val are much less reactive than, for example, a C-terminal Ala-(α-thioester). This needs to be taken into account in the design of a convergent synthesis and can be used to advantage to help control the outcome of the reaction as we have done in the example presented herein. We have also successfully used kinetically controlled ligation to join two peptides, both of which have a C-terminal alanine (i.e. ligation of a peptide-Ala-(α-thiophenylester) to a Cys-peptide-Ala-(α-thioalkylester)), with results that are comparable to those shown here (data not shown).

The new tactics and chemistries described herein are a major advance in the chemical synthesis of proteins. We are successfully using fully convergent synthesis based on kinetically controlled ligation for an increasing number of protein targets, including erythropoietin, the HIV-1 protease, and a KChIP accessory protein. We believe that kinetically controlled ligation will form the basis for a truly practical convergent chemical synthesis of proteins.[18]

Received: February 23, 2006
Published online: April 26, 2006

Keywords: kinetics · native chemical ligation · peptides · protein synthesis

[1] P. E. Dawson, S. B. Kent, *Annu. Rev. Biochem.* **2000**, *69*, 923–960.
[2] G. G. Kochendoerfer, S. Y. Chen, F. Mao, S. Cressman, S. Traviglia, H. Shao, C. L. Hunter, D. W. Low, E. N. Cagle, M. Carnevali, V. Gueriguian, P. J. Keogh, H. Porter, S. M. Stratton, M. C. Wiedeke, J. Wilken, J. Tang, J. J. Levy, L. P. Miranda, M. M. Crnogorac, S. Kalbag, P. Botti, J. Schindler-Horvat, L. Savatski, J. W. Adamson, A. Kung, S. B. Kent, J. A. Bradburne, *Science* **2003**, *299*, 884–887.
[3] D. Bang, S. B. Kent, *Angew. Chem.* **2004**, *116*, 2588–2592; *Angew. Chem. Int. Ed.* **2004**, *43*, 2534–2538.
[4] D. Bang, G. I. Makhatadze, V. Tereshko, A. A. Kossiakoff, S. B. Kent, *Angew. Chem.* **2005**, *117*, 3920–3924; *Angew. Chem. Int. Ed.* **2005**, *44*, 3852–3856.
[5] Z. Wu, J. Alexandratos, B. Ericksen, J. Lubkowski, R. C. Gallo, W. Lu, *Proc. Natl. Acad. Sci. USA* **2004**, *101*, 11587–11592.
[6] M. Schnölzer, S. B. Kent, *Science* **1992**, *256*, 221–225.
[7] J. B. Hendrickson, *J. Am. Chem. Soc.* **1977**, *99*, 5439–5450.
[8] P. E. Dawson, T. W. Muir, I. Clark-Lewis, S. B. Kent, *Science* **1994**, *266*, 776–779.
[9] D. Bang, S. B. Kent, *Proc. Natl. Acad. Sci. USA* **2005**, *102*, 5014–5019.
[10] L. E. Canne, P. Botti, R. J. Simon, Y. Chen, E. A. Dennis, S. B. Kent, *J. Am. Chem. Soc.* **1999**, *121*, 8720–8727.
[11] G. Casi, D. Hilvert, *Curr. Opin. Struct. Biol.* **2003**, *13*, 589–594.
[12] Under native chemical ligation reaction conditions, the Cys-peptide 2-(α-thioester) will itself undergo multiple reactions to form cyclic (Cys-peptide 2), Cys-peptide 2-Cys-peptide 2-(α-thioester), and other oligomerization and cyclization products. See: a) L. Zhang, J. P. Tam, *J. Am. Chem. Soc.* **1997**, *119*, 2363–2370; b) T. C. Evans, J. Benner, M.-Q. Xu, *J. Biol. Chem.* **1999**, *274*, 18359–18363.
[13] T. M. Hackeng, J. H. Griffin, P. E. Dawson, *Proc. Natl. Acad. Sci. USA* **1999**, *96*, 10068–10073.
[14] P. E. Dawson, M. J. Churchill, M. R. Ghadiri, S. B. H. Kent, *J. Am. Chem. Soc.* **1997**, *119*, 4325–4329.
[15] M. M. Teeter, J. A. Mazer, J. J. L'Italien, *Biochemistry* **1981**, *20*, 5437–5443.
[16] C. Jelsch, M. M. Teeter, V. Lamzin, V. Pichon-Pesme, R. H. Blessing, C. Lecomte, *Proc. Natl. Acad. Sci. USA* **2000**, *97*, 3171–3176.
[17] D. Bang, N. Chopra, S. B. Kent, *J. Am. Chem. Soc.* **2004**, *126*, 1377–1383.
[18] H. J. Musiol, S. Dong, M. Kaiser, R. Bausinger, A. Zumbusch, U. Bertsch, L. Moroder, *ChemBioChem* **2005**, *6*, 625–628.

 © 2006 Wiley-VCH Verlag GmbH & Co. KGaA, Weinheim

Heterocyclic Carbenes

DOI: 10.1002/anie.200600669

[1,3]Dithian-2-ylidene**

Peter R. Schreiner, Hans Peter Reisenauer, Jaroslaw Romanski, and Grzegorz Mloston*

Dedicated to Professor Dieter Seebach

While many 1,3-heterocarbenes (RX-C-XR) substituted with X = N,N/N,O/N,S/P,Si/P,P and others have been well characterized and proven to be far more stable than anticipated, dithioalkyl carbenes, such as title compound **1**, are practically unknown.[1] Bisalkylthiocarbenes were suggested as reaction intermediates in the reactions of the respective orthothioformiates with a strong base[2] and in the decomposition of *p*-toluenesulfonylhydrazone salts.[3,4] The difficulty of the preparation of **1** and related dithiocarbenes is the unavailability of the respective diazo precursors. Even trapping of hitherto unobserved 2-diazodithiane (**2**) proved difficult as the product mixtures from the reactions with various electrophilic olefins were dominated by the formal carbene dimer of **1**, bis(1,3-dithianylidene) (**3**).[5] This class of tetrathioethylene[6] is quite important for various electronic applications, but they could alternatively form from the reactions of the carbene intermediates with the respective precursor carbanions.[7] The intermediacy of **4** in the equilibrium with tris(phenylthio)-methyl lithium was inferred from the observed typical carbene trapping reactions[8] and from kinetic measurements of the decomposition of the carbenoid in solution.[9] Probably the closest one has come to a spectroscopically identifiable dithiocarbene is with λ^6-sulfaacetylene **5**, which can be formally depicted as a zwitterion or a λ^3-sulfinylcarbene (Scheme 1).[10]

Important synthetic advances were made by generating dithiocarbenes from bis(alkylsulfanyl)oxadiazoline whose thermal decompositions and reactions with suitable electrophiles gave the formal carbene adducts (namely, dithioacetals) in good yields.[11–13] However, the free carbenes could not be characterized. Another reason for the unavailability of

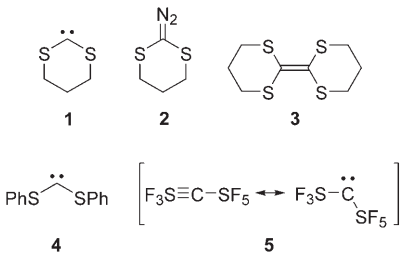

1 2 3 4 5

Scheme 1. Title compound **1**, its diazo precursor **2**, dimerization product **3**, bis(phenylthio)carbene **4** (not observed), and sulfaacetylene **5** with its carbene resonance form.

dithiocarbenes is the much lower π-donor ability[14] of sulfur relative to nitrogen for the stabilization of the carbene center (see below). As the dialkylthiooxadiazoline route apparently proved successful for the generation of dithiocarbene intermediates, we prepared known derivative **6**[13] (3,4-diaza-2,2-dimethyl-1-oxa-6,10-dithiaspiro[4.5]dec-3-ene; Scheme 2) to study its thermal and photochemical decomposition under matrix isolation conditions. This synthesis builds on the successful preparation of dioxycarbene precursors.[15]

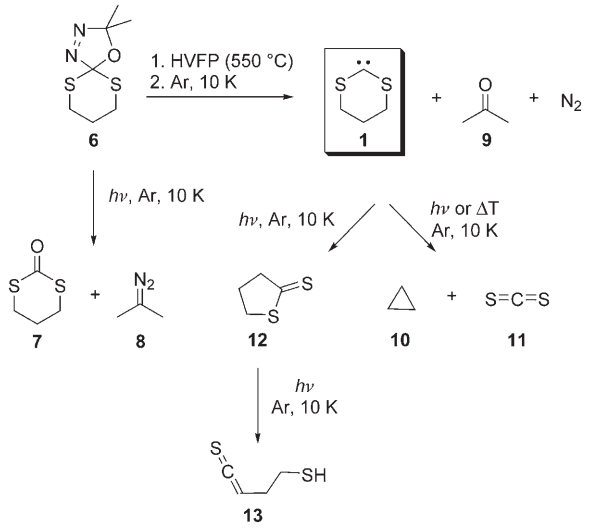

6 1 9 7 8 12 10 11 13

Scheme 2. Photochemical and thermal decomposition of **6**, and photochemical reactions of **1**.

Compound **6**, which is, in contrast to earlier reports,[13] stable at room temperature, indeed shows the decomposition behavior we had hoped for (Scheme 2). Remarkably, the photochemical and thermal decomposition reactions of **6** are entirely different and complementary. Irradiation (λ_{max} = 313 nm) of **6** did not give **1** but instead gave 1,3-dithiane-2-on (**7**) and 2-diazopropane (**8**), as evident from comparisons with authentic samples and from the agreement with the DFT-computed vibrational frequencies. Carbene **1** was ge nerated thermally through high-vacuum flash pyrolysis (HVFP) in a quartz tube at 550 °C and was trapped in an argon matrix at 10 K.

Carbene **1** shows strong absorption bands at 278 and 220 nm and a very weak band at around 390 nm (Figure 1).

[*] Prof. Dr. P. R. Schreiner, Dr. H. P. Reisenauer
Institut für Organische Chemie
Justus-Liebig Universität
Heinrich-Buff-Ring 58, 35392 Gießen (Germany)
Fax: (+49) 641-9934309
E-mail: prs@org.chemie.uni-giessen.de
Dr. J. Romanski, Prof. Dr. G. Mloston
University of Lodz
Section of Heteroorganic Compounds
Narutowicza 68, 90136 Lodz (Poland)

[**] This work was supported by the DAAD (University Partnership between Lodz and Justus-Liebig University). J.R. and G.M. acknowledge financial support by the Polish State Committee for Scientific Research (Grant No. 4T09A04625).

Supporting information for this article is available on the WWW under http://www.angewandte.org or from the author.

 © 2006 Wiley-VCH Verlag GmbH & Co. KGaA, Weinheim

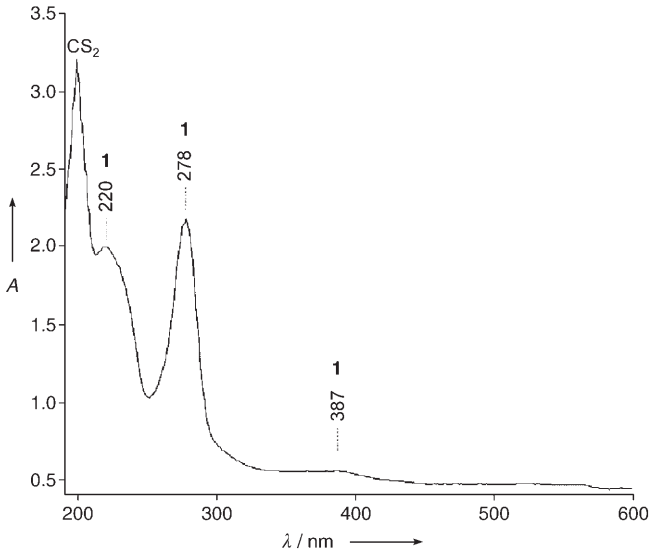

Figure 1. UV spectrum of carbene **1** at 10 K (Ar matrix).

The long-wavelength absorption stems from the HOMO–LUMO transition, whereas the intense absorptions originate from combinations of excitations. Irradiation of the matrix with wavelengths $\lambda > 385$, 280, and 254 nm leads to complete disappearance of the observed UV bands. The IR absorptions (Figure 2) parallel these findings and also vanish completely

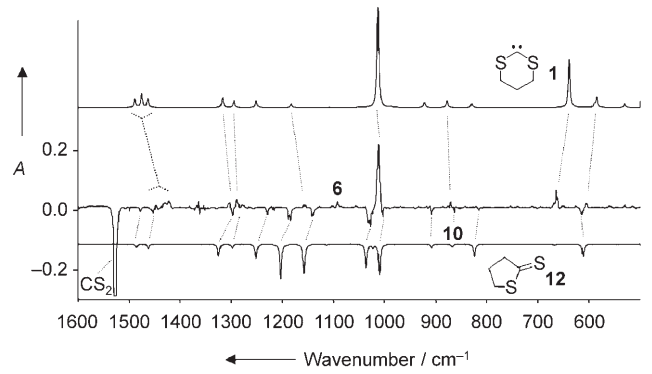

Figure 2. IR spectra of carbene **1** and dithiolactone **12** at 10 K (Ar matrix). The experimental difference spectrum is in the middle and the computed (B3LYP/6-311 + G(d,p)) spectra above (for **1**) and below (for **12**).

upon irradiation at the above wavelengths. IR spectra before and after irradiation allow the assignment of the IR bands of **1**. To evaluate the magnitude of matrix effects on the vibrational frequencies, we also generated **1** in an N_2 matrix for comparison (Table 1); the differences are rather small. The IR absorptions also agree very well with the computations at B3LYP and MP2 with a 6-311 + G(d,p) basis set (unscaled). The intense symmetric and asymmetric S-C-S bond vibrations at 1011.8 and 664.7 cm^{-1} are particularly indicative of carbene **1**. The C_s optimized geometry (we use the B3LYP geometry for our discussion; the MP2 structure is very similar (see the Supporting Information)) indicates a short S^1–C^2 ($=S^3$–C^2) bond length of 1.665 Å ($\sphericalangle$S-C-S = 126.3°) as opposed to the S^1–C^6 ($=S^3$–C^4) bond length of 1.870 Å; the S–C^2 ($=$S–C^2) bond length in dithiane is 1.827 Å ($\sphericalangle$S-C-S = 115.4°). A comparison with the C=S bond length in CS_2 of 1.560 Å reveals that the double-bond character between the carbene center and the sulfur π-donor atoms is significant (see below).

Table 1: Measured and computed (unscaled) IR absorption frequencies of **1**.

Symm., type[a]	Position [cm^{-1}] (Intensity [km mol^{-1}])			
	Computation, 6-311 + G(d,p)		Experiment	
	MP2	B3LYP	Ar matrix	N_2 matrix
a″, rd	120.1 (0.0)	129.8 (0.0)		
a′, rd	287.6 (4.9)	265.4 (3.9)		
a″, rd	349.1 (1.9)	347.2 (2.3)		
a′, rd	386.4 (3.1)	367.7 (2.4)		
a′, rd	392.5 (3.3)	380.1 (2.4)		
a′, rd	549.5 (2.0)	530.1 (2.7)		
a′, CS-ss	638.1 (8.0)	584.9 (6.7)	606.8 (w)	607.7 (w)
a″, CS-as	657.3 (1.3)	590.0 (2.2)		
a′, SCS-ss	683.3 (33.3)	638.9 (31.2)	664.7 (m)	665.3 (m)
a″, CH_2-r	840.8 (1.5)	829.7 (2.4)		
a′, CCC-s	907.5 (6.2)	878.1 (4.3)	879.7 (w)	872.3 (w)
a′, CCC-s	949.2 (1.0)	922.3 (3.2)		
a′, CH_2-r	1016.8 (0.4)	987.7 (0.6)		
a″, SCS-as	1056.0 (122.1)	1013.3 (64.5)	1011.8 (s)	1008.8 (s)
a″, CCC-s	1089.0 (3.3)	1049.0 (0.3)		
a″, CH_2-t	1134.7 (0.1)	1107.7 (0.2)		
a″, CH_2-t	1203.8 (0.9)	1182.8 (2.3)		
a′, CH_2-t	1272.5 (4.5)	1251.4 (4.2)		
a′, CH_2-w	1334.5 (4.3)	1295.1 (4.1)	1288.9 (w)	1290.1 (w)
a″, CH_2-w	1342.2 (8.7)	1317.4 (6.3)	1302.7 (w)	
a″, CH_2-w	1393.2 (0.0)	1380.0 (0.0)		
a″, CH_2-sc	1466.8 (3.6)	1463.6 (5.5)		
a′, CH_2-sc	1479.9 (9.3)	1475.8 (8.8)	1422.4 (w)	
a′, CH_2-sc	1497.3 (5.0)	1488.7 (5.5)		
a′, CH-s	3074.9 (18.9)	3020.7 (25.2)		
a″, CH-s	3085.7 (11.9)	3044.8 (7.7)		
a′, CH-s	3086.5 (16.3)	3046.8 (12.4)		
a′, CH-s	3128.3 (12.1)	3062.7 (26.9)		
a″, CH-s	3152.1 (4.7)	3100.6 (6.8)		
a′, CH-s	3156.1 (12.4)	3104.4 (18.4)		

[a] rd = ring deformation; ss/as = symmetric/asymmetric stretch; r = rocking; t = twisting; w = wagging; sc = scissoring; s = stretch.

Irradiation of **1** leads both to CS_2 and cyclopropane (**10**), which are also the main products from pyrolysis at 700 °C. These products are in line with the earlier findings that both the five-membered ring analogue of **6**[13] and the respective tosylhydrazone sodium salt[4] readily gave ethylene and the remaining stable fragments. Hence, this CS_2 extrusion reaction may also be viewed as the dithio analogue of the well known Corey–Winter method for the preparation of olefins from vicinal diols through the reaction with thiophosgen and phospane-induced loss of CO_2.[16] Formal thio-Wolff rearrangement of **1** gives dithiolactone **12**, which rearranges upon irradiation at 300 nm probably to thioketene **13** (IR absorption at 1772 cm^{-1}).

We examined the reactivity of **1** by condensing the pyrolysis products on a cooling finger without a stabilizing matrix at 80 K. We found that upon warming **1** is perfectly stable up to 100 K, whereas, at 120 K the UV and IR bands slowly decrease ($t_{1/2} \approx 45$ min) and disappear completely after

 © 2006 Wiley-VCH Verlag GmbH & Co. KGaA, Weinheim

17 h. Upon warming to room temperature, we identified the known dimer[6] **3** by GC–MS. The stability of **1** relative to cyclohexenylidene (**14**) and several heterocarbenes (**15**–**18**) can also be estimated by the homodesmotic equation depicted in Scheme 3. As expected, nitrogen is the best π donor,[14] thus

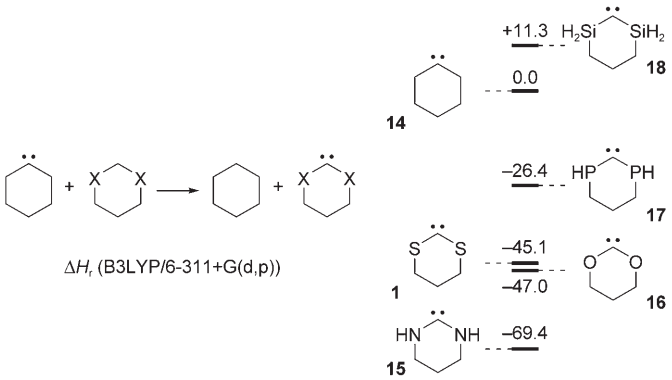

Scheme 3. Stabilization enthalpies of 1,3-dihetereo-2-ylidenes.

making **15** by far the most stable carbene in this series. Although surprising at first glance, the energy difference between dioxocarbene **16** and dithiocarbene **1** is negligible (1.9 kcal mol^{-1}), but this is in line with the findings for oxo- and thio-substituted carbenium ions that also are similarly stabilized by these heteroatoms.[17] This finding is striking because the difference in the stabilization between dinitrogen- and diphosphorous-substituted 1,3-heterocarbenes **15** and **17**, respectively, is very large (43.0 kcal mol^{-1}). Saturated disilacarbene **18** is actually destabilized relative to cyclohexenylidene **14** owing to the less effective hyperconjugation of Si–H versus C–H and the appreciable σ-donor character of the electropositive silicon atom.

As for the other six-membered heterocarbenes, the electronic structure of **1** is characterized by several high-lying orbitals that describe the sp^2-type lone pair of electrons (HOMO) on the carbon atom and highly delocalized π-type MOs, such as HOMO-3 (Figure 3), which emphasizes the stabilizing power of the heteroatoms. As a consequence, the triplet state is far above the singlet ($\Delta E_{ST} = -33.8$ kcal mol^{-1} at B3LYP/6-311 + G(d,p)) and dithiocarbenes are expected to behave as nucleophiles.

We also attempted the preparation of the corresponding five-membered cyclic dithiocarbene **20** (Scheme 4), but noticed, in agreement with earlier findings, that the precursor

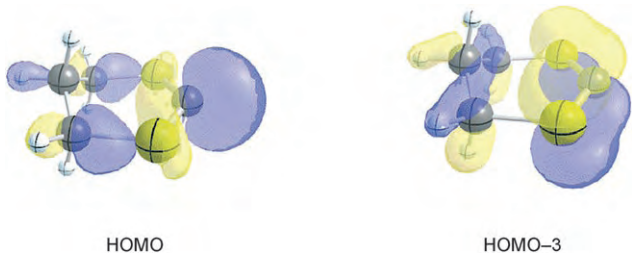

Figure 3. Selected high-lying molecular orbitals (B3LYP/6-311 + G(d,p)) of carbene **1**; sulfur atoms in yellow, carbon atoms in black.

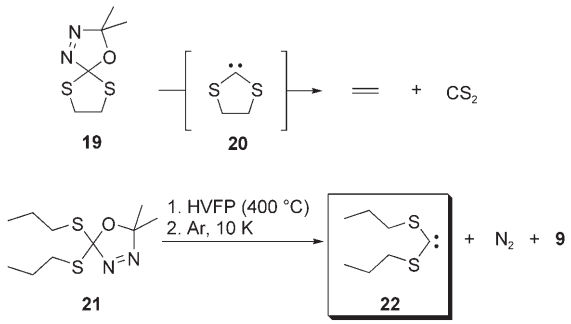

Scheme 4. Other dialkyl dithiocarbenes and their precursors.

19[13] is far more labile than **6**. Thermal treatment of **19** and co-condensation on an Ar matrix as before at 10 K only showed IR signals that correspond to ethylene and CS_2. The Corey–Winter-type CS_2 extrusion reaction apparently is quite facile for these small cyclic dithiocarbenes, so we turned our attention to the preparation of an di-*n*-alkyldithiocarbene that should not readily decompose into CS_2 and two alkyl fragments. Following the same protocol, the preparation of **21** was straightforward (Scheme 4).[11] Indeed, HVFP and co-condensation of the pyrolysis products on an Ar matrix gives the novel di-*n*-propyldithiocarbene **22**.

As with **1**, carbene **22** can be identified by comparison of experimental and computed IR absorptions (Figure 4) and by

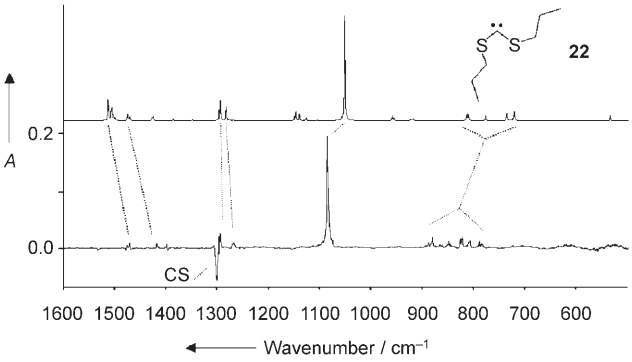

Figure 4. IR spectra of carbene **22** and CS at 10 K (Ar matrix): experimental-difference spectrum (bottom) versus the computed (B3LYP/6-311 + G(d,p)) spectrum above (for *cis*,*trans*-**22**).

the strong band observed at 300 nm in the UV spectrum. The IR spectra of **1** and **22** compare well and both show a characteristic absorption just above 1000 cm^{-1} (**22** = 1039.9 cm^{-1}). Irradiation of **22** with $\lambda = 313$ nm for 17 min leads to its disappearance and generation of CS; hence, the decomposition path is different from that of **1** (see above).

In summary, we have presented the first experimental IR and UV spectroscopic characterization of two dithiocarbenes, dithianylidene **1** and di-*n*-propyldithiocarbene **22**, generated thermally from the respective dialkylthiooxadiazoline precursors. Carbene **1** is considerably less stable than the exceptionally stable nitrogen-substituted analogues and dimerizes at temperatures above 100 K; its stability is comparable to that of the dioxo analogue. The photochem-

 © 2006 Wiley-VCH Verlag GmbH & Co. KGaA, Weinheim

istry of **1** is interesting, as it formally represents the dithiophotochemical variation of the practical Corey–Winter reaction.

Experimental Section

Matrix isolation experiments.: Compounds **6**, **19**, and **21** were subjected to HVFP at 400–700 °C (empty quartz tube, inner diameter: 8 mm, length of heating zone: 50 mm). The products thus formed were trapped immediately thereafter on a cold (10 K) CsI (or BaF_2) window together with a large excess of Ar or N_2. These matrices were examined with FT-IR and UV/Vis spectroscopy. The spectra and additional information are collected in the Suppporting Information.

Computations: Geometries were fully optimized at the B3LYP[18] and MP2[19] levels of theory with a 6-311 + G(d,p) basis set including frequency analyses to disclose the nature of all stationary points (Nimag = 0 for minima and 1 for transition structures). All computations utilized the Gaussian03 program package.[20] The *xyz* coordinates and the energies of all computed species are collected in the Supporting Information.

Received: February 20, 2006
Published online: May 10, 2006

Keywords: computational chemistry · dialkyldithiocarbenes · dithianes · matrix isolation · sulfur

[1] G. Bertrand in *Reactive Intermediates* (Eds.: R. A. Moss, M. S. Platz, M. Jones, Jr.), Wiley-Interscience, Hoboken, New Jersey, **2004**, pp. 329; D. Bourissou, O. Guerret, F. P. Gabbad', G. Bertrand, *Chem. Rev.* **2000**, *100*, 39; K. Seppelt, *Angew. Chem.* **1991**, *103*, 399; *Angew. Chem. Int. Ed. Engl.* **1991**, *30*, 361; W. A. Herrmann, C. Köcher, *Angew. Chem.* **1997**, *109*, 2256; *Angew. Chem. Int. Ed. Engl.* **1997**, *36*, 2162.
[2] J. Hine, R. P. Bayer, G. G. Hammer, *J. Am. Chem. Soc.* **1962**, *84*, 1751; R. M. Carlson, P. M. Helquist, *Tetrahedron Lett.* **1969**, 173.
[3] U. Schöllkopf, E. Wiskott, *Angew. Chem.* **1963**, *75*, 725; *Angew. Chem. Int. Ed. Engl.* **1963**, *2*, 485.
[4] D. M. Lemal, E. H. Banitt, *Tetrahedron Lett.* **1964**, 245.
[5] D. Seebach, A. K. Beck, B. Graf, K. H. Geiss, H. Daum, *Chem. Ber.* **1972**, *105*, 3280; L. Benati, G. Calestani, D. Nanni, P. Spagnolo, M. Volta, *Tetrahedron* **1997**, *53*, 9269; L. Benati, G. Calestani, P. C. Montevecchi, P. Spagnolo, *J. Chem. Soc. Chem. Commun.* **1995**, 1999.
[6] D. L. Coffen, J. Q. Chambers, D. R. Williams, P. E. Garrett, N. D. Canfield, *J. Am. Chem. Soc.* **1971**, *93*, 2258.
[7] W. Kirmse, *Carbene Chemistry*, 2nd ed., Academic Press, New York, **1971**.
[8] D. Seebach, *Angew. Chem.* **1967**, *79*, 468; *Angew. Chem. Int. Ed. Engl.* **1967**, *6*, 442.
[9] D. Seebach, A. K. Beck, *J. Am. Chem. Soc.* **1969**, *91*, 1540.
[10] R. Gerhardt, T. Grelbig, J. Buschmann, P. Luger, K. Seppelt, *Angew. Chem.* **1988**, *100*, 1592; *Angew. Chem. Int. Ed. Engl.* **1988**, *27*, 1534; B. Pötter, K. Seppelt, *Angew. Chem.* **1984**, *96*, 138; *Angew. Chem. Int. Ed. Engl.* **1984**, *23*, 150.
[11] J. H. Rigby, S. Laurent, *J. Org. Chem.* **1999**, *64*, 1766.
[12] J. H. Rigby, M. D. Danca, *Tetrahedron Lett.* **1999**, *40*, 6891.
[13] J. H. Rigby, S. Laurent, W. T. Dong, M. D. Danca, *Tetrahedron* **2000**, *56*, 10101.
[14] P. v. R. Schleyer, *Pure Appl. Chem.* **1987**, *59*, 1647.
[15] H. Zhou, G. Mloston, J. Warkentin, *Org. Lett.* **2005**, *7*, 487; M. Dawid, G. Mloston, J. Warkentin, *Chem. Eur. J.* **2002**, *8*, 2184; M. Dawid, G. Mloston, D. L. Reid, J. Warkentin, *Can. J. Chem.* **2003**, *81*, 1025.
[16] E. J. Corey, R. A. E. Winter, *J. Am. Chem. Soc.* **1963**, *85*, 2677.
[17] J. Kapp, C. Schade, A. M. El-Nahasa, P. v. R. Schleyer, *Angew. Chem.* **1996**, *108*, 2373; *Angew. Chem. Int. Ed. Engl.* **1996**, *35*, 2236.
[18] A. D. Becke, *J. Chem. Phys.* **1993**, *98*, 5648.
[19] C. Møller, M. S. Plesset, *Phys. Rev.* **1934**, *46*, 618.
[20] Gaussian 03 (Revision A.1), M. J. Frisch, G. W. Trucks, H. B. Schlegel, G. E. Scuseria, M. A. Robb, J. R. Cheeseman, J. A. Montgomery, Jr., T. Vreven, K. N. Kudin, J. C. Burant, J. M. Millam, S. S. Iyengar, J. Tomasi, V. Barone, B. Mennucci, M. Cossi, G. Scalmani, N. Rega, G. A. Petersson, H. Nakatsuji, M. Hada, M. Ehara, K. Toyota, R. Fukuda, J. Hasegawa, M. Ishida, T. Nakajima, Y. Honda, O. Kitao, H. Nakai, M. Klene, X. Li, J. E. Knox, H. P. Hratchian, J. B. Cross, C. Adamo, J. Jaramillo, R. Gomperts, R. E. Stratmann, O. Yazyev, A. J. Austin, R. Cammi, C. Pomelli, J. W. Ochterski, P. Y. Ayala, K. Morokuma, G. A. Voth, P. Salvador, J. J. Dannenberg, V. G. Zakrzewski, S. Dapprich, A. D. Daniels, M. C. Strain, O. Farkas, D. K. Malick, A. D. Rabuck, K. Raghavachari, J. B. Foresman, J. V. Ortiz, Q. Cui, A. G. Baboul, S. Clifford, J. Cioslowski, B. B. Stefanov, G. Liu, A. Liashenko, P. Piskorz, I. Komaromi, R. L. Martin, D. J. Fox, T. Keith, M. A. Al-Laham, C. Y. Peng, A. Nanayakkara, M. Challacombe, P. M. W. Gill, B. Johnson, W. Chen, M. W. Wong, C. Gonzalez, J. A. Pople, Gaussian, Inc., Pittsburgh, PA, **2003**.

 © 2006 Wiley-VCH Verlag GmbH & Co. KGaA, Weinheim

Enzyme Models

DOI: 10.1002/anie.200504422

Oxygen-Atom Transfer between Mononuclear Nonheme Iron(IV)–Oxo and Iron(II) Complexes**

*Chivukula V. Sastri, Kyungeun Oh, Yoon Jin Lee, Mi Sook Seo, Woonsup Shin, and Wonwoo Nam**

High-valent iron(IV)–oxo species have been implicated as the key reactive intermediates in the catalytic oxidation of organic substrates by mononuclear nonheme iron enzymes and their model compounds.[1] Recently, such nonheme iron(IV)–oxo species were observed directly in enzymatic and biomimetic reactions.[2–5] For example, an intermediate with a high-spin iron(IV)–oxo unit was identified and proposed as an active oxidant in the catalytic cycle of

[*] Dr. C. V. Sastri,[+] K. Oh,[+] Y. J. Lee,[+] Dr. M. S. Seo, Prof. Dr. W. Nam
Department of Chemistry
Division of Nano Sciences
Center for Biomimetic Systems
Ewha Womans University, Seoul 120-750 (Korea)
Fax: (+82) 2-3277-4441
E-mail: wwnam@ewha.ac.kr
Prof. Dr. W. Shin
Department of Chemistry and Interdisciplinary Program of Integrated Biotechnology
Sogang University, Seoul 121-742 (Korea)
[+] These authors contributed equally to this work.

[**] This research was supported by the Korea Science and Engineering Foundation through the Creative Research Initiative Program.

WILEY InterScience DISCOVER SOMETHING GREAT
© 2006 Wiley-VCH Verlag GmbH & Co. KGaA, Weinheim

E. coli taurine, namely in α-ketoglutarate dioxygenase (TauD).[2,3] In biomimetic studies, mononuclear nonheme iron(IV)–oxo complexes bearing tetradentate N4 and pentadentate N5 ligands were synthesized and characterized by various spectroscopic techniques including X-ray crystallography.[4,5] The iron(IV)–oxo species have shown reactivities in a variety of oxidation reactions such as alkane hydroxylation,[4c,5b,c] olefin epoxidation,[4b,5b,c] alcohol oxidation,[4h] and the oxidation of sulfides,[4e,i] dihydroanthracene,[4f,k] and PPh_3.[4a,e,j,5c]

Very recently, Golubkov and Gross reported the transfer of a nitrogen atom between manganese complexes of salen (*N*,*N*′-bis(salicylidene)ethylenediamine dianion), porphyrin, and corrole ligands.[6] Prior to this work, intermetal transfer of a nitrogen atom was well documented in metalloporphyrin (M = Mn and Cr) reactions.[7] In addition to the transfer of nitrogen atoms, the transfer of oxygen atoms between high-valent metal-oxo and metal complexes has also been demonstrated.[7,8] In the case of iron porphyrins, the reaction of iron(IV)–oxo and iron(II) porphyrins resulted in the generation of μ-oxo-bridged iron(III) porphyrin dimers (that is, incomplete intermetal transfer of an oxygen atom) [Eq. (1),

$$[(\mathrm{Porp})\mathrm{Fe^{IV}}{=}\mathrm{O}] + [\mathrm{Fe^{II}}(\mathrm{Porp})] \rightarrow [(\mathrm{Porp})\mathrm{Fe^{III}}\text{-}\mathrm{O}\text{-}\mathrm{Fe^{III}}(\mathrm{Porp})] \quad (1)$$

Porp = porphyrin].[7a,9] Although the oxidation of organic substrates by nonheme iron(IV)–oxo complexes has been demonstrated recently, the intermetal transfer of oxygen atoms between nonheme iron complexes has never been explored previously. Herein, we report that in contrast to iron porphyrins,[9] nonheme iron(IV)–oxo complexes transfer their oxygen atom to iron(II) complexes, thus affording the corresponding iron(II) and iron(IV)–oxo complexes (that is, complete intermetal transfer of an oxygen atom occurs)[7a] [Eq. (2)].

$$[(\mathrm{L_1})\mathrm{Fe^{IV}}{=}\mathrm{O}]^{2+} + [\mathrm{Fe^{II}}(\mathrm{L_2})]^{2+} \rightarrow [\mathrm{Fe^{II}}(\mathrm{L_1})]^{2+} + [(\mathrm{L_2})\mathrm{Fe^{IV}}{=}\mathrm{O}]^{2+} \quad (2)$$

The oxygen-atom transfer reactions were carried out by adding nonheme iron(II) complexes to in situ generated nonheme iron(IV)–oxo complexes in CH_3CN at 25 °C. The addition of $[Fe^{II}(tmc)]^{2+}$ to the solution of $[(N4Py)Fe^{IV}{=}O]^{2+}$ (**1**) afforded changes in the absorption spectra which are consistent with the transfer of an oxygen atom from **1** (λ_{max} at 695 nm) to $[Fe^{II}(tmc)]^{2+}$ [Eq. (3)], thereby producing

$$[(\mathrm{N4Py})\mathrm{Fe^{IV}}{=}\mathrm{O}]^{2+}\ (\mathbf{1}) + [\mathrm{Fe^{II}}(\mathrm{tmc})]^{2+} \rightarrow [\mathrm{Fe^{II}}(\mathrm{N4Py})]^{2+} + [(\mathrm{tmc})\mathrm{Fe^{IV}}{=}\mathrm{O}]^{2+}\ (\mathbf{2}) \quad (3)$$

$[(tmc)Fe^{IV}{=}O]^{2+}$ (**2**; λ_{max} at 820 nm) and $[Fe^{II}(N4Py)]^{2+}$ (λ_{max} at 450 nm; Figure 1; see the Supporting Information for nonheme ligand structures).[10] Well-defined isosbestic points were observed at 570 and 790 nm. The reaction was complete within 20 minutes, and an increase in the concentration of the reactants diminished the reaction time (data not shown). The latter results indicate the reaction to be first order in each of the reactants. In contrast, the intermediate **2** remained intact upon addition of $[Fe(N4Py)]^{2+}$, thus indicating that the transfer of an oxygen atom from **2** to $[Fe(N4Py)]^{2+}$ does not occur [namely, the reverse reaction of Eq. (3) does not occur].

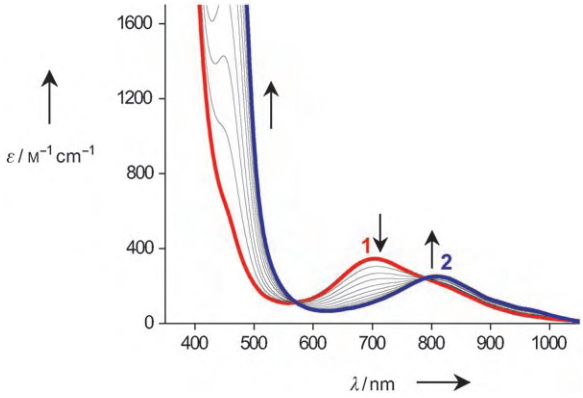

Figure 1. UV/Vis spectral changes showing the formation of **2** (blue) upon addition of 4 equiv $[Fe(tmc)(CF_3SO_3)_2]$ (2 mM, diluted in 50 μL CH_3CN) to the solution of $[(N4Py)Fe^{IV}{=}O]^{2+}$ (**1**, 0.5 mM; red) in CH_3CN (2 mL) at 25 °C.

The transfer of an oxygen atom between nonheme iron complexes was also evidenced by changes in the electrospray ionization mass spectra of the reaction solution recorded at different times (Figure 2). Mixing equimolar amounts of $[Fe(tmc)]^{2+}$ and **1**-^{18}O resulted in a decrease in the signals corresponding to $[Fe(tmc)]^{2+}$ (*m*/*z* 461) and **1**-^{18}O (*m*/*z* 590) with a concomitant increase in the signals corresponding to **2**-^{18}O (*m*/*z* 479) and $[Fe(N4Py)]^{2+}$ (*m*/*z* 572). Such mass spectral

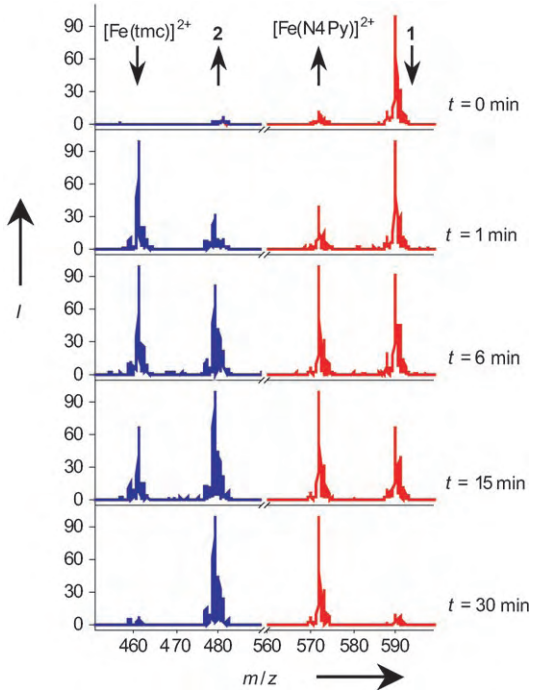

Figure 2. Changes in the electrospray ionization mass spectra in the reactants $[Fe^{II}(tmc)(CF_3SO_3)]^+$ (*m*/*z* 461) and $[Fe^{IV}(N4Py)(^{18}O)(CF_3SO_3)]^+$ (**1**-^{18}O; *m*/*z* 590) as well as the products $[Fe^{IV}(tmc)(^{18}O)(CF_3SO_3)]^+$ (**2**-^{18}O; *m*/*z* 479) and $[Fe^{II}(N4Py)(CF_3SO_3)]^+$ (*m*/*z* 572) in the reaction of equimolar amounts of $[Fe^{II}(tmc)]^{2+}$ (0.5 mM) and $[(N4Py)Fe^{IV}{=}O]^{2+}$ (**1**; 0.5 mM) in CH_3CN at 25 °C.

 © 2006 Wiley-VCH Verlag GmbH & Co. KGaA, Weinheim

changes strongly demonstrate the transfer of an oxygen atom from **1** to $[Fe(tmc)]^{2+}$ which results in the formation of $[Fe(N4Py)]^{2+}$ and **2** [Eq. (3)]. Furthermore, the observation of the ^{18}O transfer from **1** to **2** indicates that molecular oxygen was not involved in the oxygen atom transfer reaction.

Further evidence for the transfer of an oxygen atom was obtained by electrochemical methods. First, cyclic and differential pulse voltammograms (CV and DPV) of nonheme iron(II) complexes $[Fe(N4Py)]^{2+}$ and $[Fe^{II}(tmc)(N_3)]^+$ as well as their iron(IV)–oxo complexes **1** and $[Fe^{IV}(tmc)(O)(N_3)]^+$ (**2**-N_3) were recorded. The $[Fe(N4Py)]^{2+}$ and $[Fe^{II}(tmc)(N_3)]^+$ complexes exhibit reversible and quasireversible redox waves for the Fe^{III}/Fe^{II} couple at +0.64 and +0.35 V, respectively (see the Supporting Information). We then attempted to identify voltammetric responses corresponding to the iron(IV)–oxo species, by carrying out titration experiments by adding different amounts of PhIO to solutions of the iron(II) complexes. Incremental addition of PhIO to the solution of $[Fe^{II}(tmc)(N_3)]^+$ resulted in a decrease in an oxidation peak at +0.35 V for the $[Fe^{III}(tmc)(N_3)]^{2+}/[Fe^{II}(tmc)(N_3)]^+$ couple with a proportionate increase in a new reduction peak at −0.63 V (Figure 3a). The new reduction peak is irreversible in nature, and the increase in the peak current was proportional to the amount of **2**-N_3 formed in the reaction of $[Fe^{II}(tmc)(N_3)]^+$ and PhIO (see UV/Vis spectral data in Figure 3b).[4j] Furthermore, the addition of PPh_3 to the solution of **2**-N_3 resulted in the reduction peak at −0.63 V disappearing and the regeneration of the redox wave at +0.35 V which corresponds to the $[Fe^{III}(tmc)(N_3)]^{2+}/[Fe^{II}(tmc)(N_3)]^+$ couple (data not shown); the disappearance of **2**-N_3 is the result of the oxygenation of PPh_3.[4j] On the basis of the results described above, we conclude that the irreversible wave at −0.63 V results from the reduction of **2**-N_3.[11–13] Similarly, we found that the reduction peak of **1** appears at −0.44 V (see the Supporting Information for the CV and DPV traces of **1** and **2**-N_3).[13] The transfer of an oxygen atom from **1** to $[Fe^{II}(tmc)(N_3)]^+$ was followed by monitoring the changes in the DPV trace of the reactant (**1**) and the product (**2**-N_3) in the reaction solution [Eq. (3)]. Addition of $[Fe^{II}(tmc)(N_3)]^+$ to the solution of **1** resulted in the peak current at −0.44 V corresponding to **1** disappearing gradually, whereas the reduction peak current at −0.63 V corresponding to **2**-N_3 increased (Figure 4). The decrease and increase in the peak

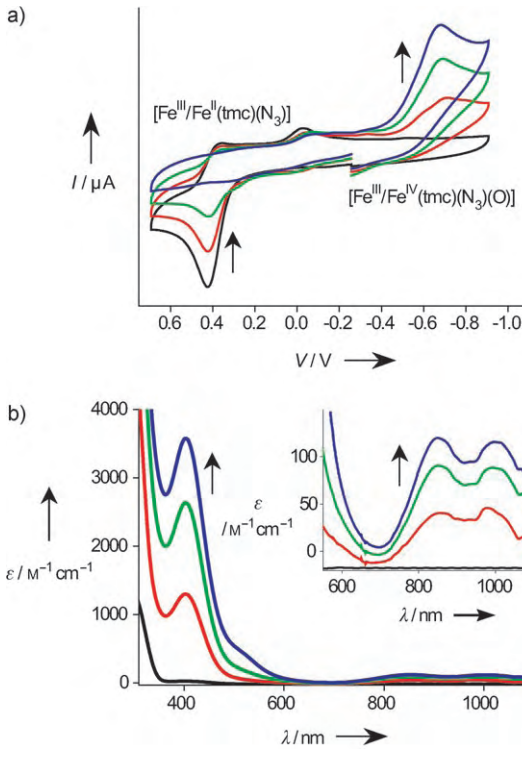

Figure 3. a) Cyclic voltammograms and b) UV/Vis spectral changes for the conversion of $[Fe^{II}(tmc)(N_3)]^+$ into $[Fe^{IV}(tmc)(N_3)(O)]^+$ (**2**-N_3) upon addition of different amounts of PhIO. Reaction conditions: PhIO (black, 0 equiv; red, 0.4 equiv; green, 0.8 equiv; blue, 1.2 equiv) was added to a reaction solution containing $[Fe^{II}(tmc)(N_3)]^+$ (1 mM) and tetrabutylammonium hexafluorophosphate (nBu_4NPF_6, 0.1 M) in CH_3CN at 25 °C.

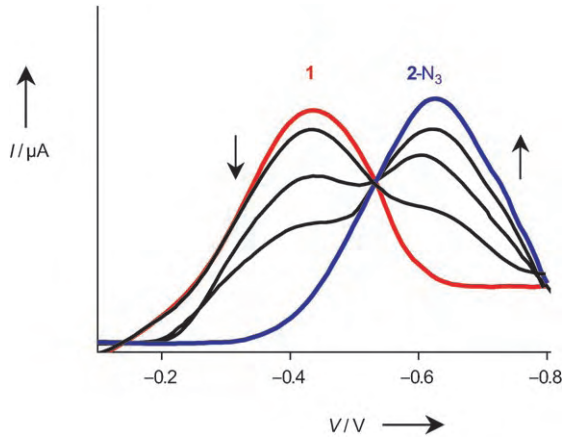

Figure 4. Differential pulse voltammograms of **1** (red) and **2**-N_3 (blue) upon addition of $[Fe^{II}(tmc)(N_3)]^+$ (1 mM) to a reaction solution containing **1** (1 mM) and nBu_4NPF_6 (0.1 M) in CH_3CN at 25 °C.

currents of **1** and **2**-N_3, respectively, demonstrate again that the oxo group of **1** was transferred to $[Fe^{II}(tmc)(N_3)]^+$, thus giving rise to the formation of **2**-N_3.

The transfer of an oxygen atom was also examined between $[(Bn\text{-}tpen)Fe^{IV}{=}O]^{2+}$ (**3**)[10] and $[Fe^{II}(tmc)]^{2+}$ as well as between **3** and $[Fe^{II}(N4Py)]^{2+}$. Addition of $[Fe^{II}(tmc)]^{2+}$ (2.0 mM) to the solution of **3** (0.5 mM) in CH_3CN at 25 °C resulted in changes in the electronic absorption spectra, namely the disappearance of **3** and the formation of **2** [Eq. (4)] (data not shown). Addition of $[Fe^{II}(N4Py)]^{2+}$ to the

$$[(Bn\text{-}tpen)Fe^{IV}{=}O]^{2+}\ (\mathbf{3}) + [Fe^{II}(tmc)]^{2+} \rightarrow [Fe^{II}(Bn\text{-}tpen)]^{2+} + [(tmc)Fe^{IV}{=}O]^{2+}\ (\mathbf{2}) \quad (4)$$

solution of **3** resulted in the disappearance of **3** and the concomitant formation of **1** in the electronic absorption and ESI mass spectra [Eq. (5); see the Supporting Information].

$$[(Bn\text{-}tpen)Fe^{IV}{=}O]^{2+}\ (\mathbf{3}) + [Fe^{II}(N4Py)]^{2+} \rightarrow [Fe^{II}(Bn\text{-}tpen)]^{2+} + [(N4Py)Fe^{IV}{=}O]^{2+}\ (\mathbf{1}) \quad (5)$$

In contrast, the reverse reactions such as the transfer of an oxygen atom from **2** to $[Fe^{II}(Bn\text{-}tpen)]^{2+}$ and from **1** to

 © 2006 Wiley-VCH Verlag GmbH & Co. KGaA, Weinheim

$[Fe^{II}(Bn\text{-}tpen)]^{2+}$ did not take place [that is, the reverse reactions of Eqs. (4) and (5)]. The transfer of an oxygen atom was not observed between **2**-X (X = CH_3CN and N_3^-) and $[Fe^{II}(tmc)(X)]$. The latter results may be ascribed to the fact that the accessibility of an iron(II) ion toward an iron(IV)–oxo group is not favorable because of a steric interaction between the tmc ligands of the iron complexes.[4a,g]

In conclusion, we have reported the first example of the transfer of an oxygen atom between mononuclear nonheme iron complexes. The transfer of an oxygen atom from iron(IV)–oxo to iron(II) complexes was clearly evidenced by spectrophotometric, ESI mass spectrometric, and voltammetric techniques. The results (summarized in Scheme 1)

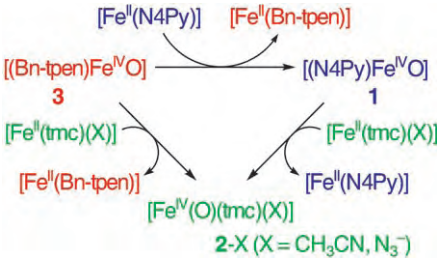

Scheme 1. Summary of the transfer of an oxygen atom between nonheme iron(IV)–oxo and iron(II) complexes.

show that the transfer of the oxygen atom was dependent on the oxidizing power of the iron(IV)–oxo complexes; the oxidizing power of iron(IV)–oxo complexes was determined to be in the order **3** > **1** > **2** in the oxidation of organic substrates.[4c,h,j] Detailed investigations of mechanistic aspects (e.g., complete transfer of an oxygen atom in nonheme iron models versus incomplete transfer in iron porphyrins)[8,9] and kinetic parameters of the transfer from nonheme iron(IV)–oxo to iron(II) complexes are currently underway.

Received: December 13, 2005
Revised: April 2, 2006
Published online: May 10, 2006

Keywords: coordination modes · enzyme models · iron · N ligands · oxygen

[1] a) M. M. Abu-Omar, A. Loaiza, N. Hontzeas, *Chem. Rev.* **2005**, *105*, 2227–2252; b) A. Decker, E. I. Solomon, *Curr. Opin. Chem. Biol.* **2005**, *9*, 152–163; c) S. V. Kryatov, E. V. Rybak-Akimova, *Chem. Rev.* **2005**, *105*, 2175–2226; d) A. S. Borovik, *Acc. Chem. Res.* **2005**, *38*, 54–61; e) M. Costas, M. P. Mehn, M. P. Jensen, L. Que, Jr., *Chem. Rev.* **2004**, *104*, 939–986.

[2] a) J. M. Bollinger, Jr., J. C. Price, L. M. Hoffart, E. W. Barr, C. Krebs, *Eur. J. Inorg. Chem.* **2005**, 4245–4254; b) R. P. Hausinger, *Crit. Rev. Biochem. Mol. Biol.* **2004**, *39*, 21–68.

[3] a) J. C. Price, E. W. Barr, B. Tirupati, J. M. Bollinger, Jr., C. Krebs, *Biochemistry* **2003**, *42*, 7497–7508; b) J. C. Price, E. W. Barr, T. E. Glass, C. Krebs, J. M. Bollinger, Jr., *J. Am. Chem. Soc.* **2003**, *125*, 13008–13009; c) D. A. Proshlyakov, T. F. Henshaw, G. R. Monterosso, M. J. Ryle, R. P. Hausinger, *J. Am. Chem. Soc.* **2004**, *126*, 1022–1023; d) P. J. Riggs-Gelasco, J. C. Price, R. B. Guyer, J. H. Brehm, E. W. Barr, J. M. Bollinger, Jr., C. Krebs, *J. Am. Chem. Soc.* **2004**, *126*, 8108–8109.

[4] a) J.-U. Rohde, J.-H. In, M. H. Lim, W. W. Brennessel, M. R. Bukowski, A. Stubna, E. Münck, W. Nam, L. Que, Jr., *Science* **2003**, *299*, 1037–1039; b) M. H. Lim, J.-U. Rohde, A. Stubna, M. R. Bukowski, M. Costas, R. Y. N. Ho, E. Münck, W. Nam, L. Que, Jr., *Proc. Natl. Acad. Sci. USA* **2003**, *100*, 3665–3670; c) J. Kaizer, E. J. Klinker, N. Y. Oh, J.-U. Rohde, W. J. Song, A. Stubna, J. Kim, E. Münck, W. Nam, L. Que, Jr., *J. Am. Chem. Soc.* **2004**, *126*, 472–473; d) J.-U. Rohde, S. Torelli, X. Shan, M. H. Lim, E. J. Klinker, J. Kaizer, K. Chen, W. Nam, L. Que, Jr., *J. Am. Chem. Soc.* **2004**, *126*, 16750–16761; e) S. O. Kim, C. V. Sastri, M. S. Seo, J. Kim, W. Nam, *J. Am. Chem. Soc.* **2005**, *127*, 4178–4179; f) J.-U. Rohde, L. Que, Jr., *Angew. Chem.* **2005**, *117*, 2295–2298; *Angew. Chem. Int. Ed.* **2005**, *44*, 2255–2258; g) E. J. Klinker, J. Kaizer, W. W. Brennessel, N. L. Woodrum, C. J. Cramer, L. Que, Jr., *Angew. Chem.* **2005**, *117*, 3756–3760; *Angew. Chem. Int. Ed.* **2005**, *44*, 3690–3694; h) N. Y. Oh, Y. Suh, M. J. Park, M. S. Seo, J. Kim, W. Nam, *Angew. Chem.* **2005**, *117*, 4307–4311; *Angew. Chem. Int. Ed.* **2005**, *44*, 4235–4239; i) C. V. Sastri, M. S. Seo, M. J. Park, K. M. Kim, W. Nam, *Chem. Commun.* **2005**, 1405–1407; j) C. V. Sastri, M. J. Park, T. Ohta, T. A. Jackson, A. Stubna, M. S. Seo, J. Lee, J. Kim, T. Kitagawa, E. Münck, L. Que, Jr., W. Nam, *J. Am. Chem. Soc.* **2005**, *127*, 12494–12495; k) M. R. Bukowski, K. D. Koehntop, A. Stubna, E. L. Bominaar, J. A. Halfen, E. Münck, W. Nam, L. Que, Jr., *Science* **2005**, *310*, 1000–1002.

[5] a) C. A. Grapperhaus, B. Mienert, E. Bill, T. Weyhermüller, K. Wieghardt, *Inorg. Chem.* **2000**, *39*, 5306–5317; b) V. Balland, M.-F. Charlot, F. Banse, J.-J. Girerd, T. A. Mattioli, E. Bill, J.-F. Bartoli, P. Battioni, D. Mansuy, *Eur. J. Inorg. Chem.* **2004**, 301–308; c) M. Martinho, F. Banse, J.-F. Bartoli, T. A. Mattioli, P. Battioni, O. Horner, S. Bourcier, J.-J. Girerd, *Inorg. Chem.* **2005**, *44*, 9592–9596.

[6] a) G. Golubkov, Z. Gross, *J. Am. Chem. Soc.* **2005**, *127*, 3258–3259; b) G. Golubkov, Z. Gross, *Angew. Chem.* **2003**, *115*, 4645–4648; *Angew. Chem. Int. Ed.* **2003**, *42*, 4507–4510.

[7] a) R. H. Holm, *Chem. Rev.* **1987**, *87*, 1401–1449; b) L. K. Woo, *Chem. Rev.* **1993**, *93*, 1125–1136.

[8] a) J. A. Hays, C. L. Day, V. G. Young, Jr., L. K. Woo, *Inorg. Chem.* **1996**, *35*, 7601–7607; b) L. K. Woo, J. A. Hays, J. G. Goll, *Inorg. Chem.* **1990**, *29*, 3916–3917.

[9] a) A. L. Balch, Y.-W. Chan, R.-J. Cheng, G. N. La Mar, L. Latos-Grazynski, M. W. Renner, *J. Am. Chem. Soc.* **1984**, *106*, 7779–7785; b) D.-H. Chin, G. N. La Mar, A. L. Balch, *J. Am. Chem. Soc.* **1980**, *102*, 5945–5947.

[10] Abbreviations used: tmc 1,4,8,11-tetramethyl-1,4,8,11-tetraazacyclotetradecane; N4Py *N*,*N*-bis(2-pyridylmethyl)-*N*-bis(2-pyridyl)methylamine; Bn-tpen *N*-benzyl-*N*,*N*′,*N*′-tris(2-pyridylmethyl)ethane-1,2-diamine.

[11] For some examples of the electrochemical studies of high-valent iron(IV)–oxo porphyrins, see: a) K. M. Kadish, E. V. Caemelbecke, G. Royal in *The Porphyrin Handbook*, *Vol. 8* (Eds.: K. M. Kadish, K. M. Smith, R. Guilard), Academic Press, New York, **2000**, chap. 55, pp. 1–111; b) W. A. Lee, T. S. Calderwood, T. C. Bruice, *Proc. Natl. Acad. Sci. USA* **1985**, *82*, 4301–4305; c) J. T. Groves, J. A. Gilbert, *Inorg. Chem.* **1986**, *25*, 123–125; d) C. Swistak, X. H. Mu, K. M. Kadish, *Inorg. Chem.* **1987**, *26*, 4360–4366.

[12] The redox potentials of compound II, $[(Porp)Fe^{IV}{=}O]$, of heme-containing peroxidases have been reported: a) M. T. Green, J. H. Dawson, H. B. Gray, *Science* **2004**, *304*, 1653–1656; b) Y. Hayashi, I. Yamazaki, *J. Biol. Chem.* **1979**, *254*, 9101–9106.

[13] We only observed the reduction of the iron(IV)–oxo complexes and did not identify the products and reaction pathways during the electrochemical reduction. Detailed electrochemical studies of mononuclear nonheme iron(IV)–oxo species are underway and will be presented elsewhere.

 © 2006 Wiley-VCH Verlag GmbH & Co. KGaA, Weinheim

cis–trans Isomerization

DOI: 10.1002/anie.200600725

From a Lamellar to Hexagonal Self-Assembly of Bis(4,4′-(*m*,*m*′-di(dodecyloxy)phenyl)-2,2′-difluoro-1,3,2-dioxaborin) Molecules: A *trans*-to-*cis*-Isomerization-Induced Structural Transition Studied with STM**

*Dirk Rohde, Cun-Ji Yan, Hui-Juan Yan, and Li-Jun Wan**

Self-assembly or self-organization of molecules on solid surfaces is of ever increasing importance in chemistry and material science and plays an important role in the "bottom-up" strategy used in nanofabrication.[1] With the development in preparing supramolecular assemblies and molecular nanostructures, the precise control of the structure of two-dimensional (2D) molecular assemblies attracts increasing attention.[2] As a result of these studies, it is known that the common method to change the structure of a self-assembly is to modify the molecular chemical structure.[3] Furthermore, the molecular ordering can be tuned to a certain extent by using different types of substrates[4] and by employing different film-growth conditions.[5] On the other hand, a promising approach to form a 2D adlayer is to exert external stimuli such as light irradiation, heating, chemical treatment, or electric and/or magnetic fields.[6] Finally, it is possible to manipulate molecules and molecular structures on surfaces with an STM tip.[7]

The well-established STM technique has been successfully used to study the structure of self-assembled monolayers (SAMs) and their ordering, molecular orientation, intermolecular reaction, and structural transformation.[2–7] For example, the light-induced *cis*/*trans* isomerization of azobenzene derivatives has been intensively investigated by STM in the past.[8] However, as the *trans*-to-*cis* isomerization does not occur in adlayers of azobenzene derivatives, the isomerization is typically initiated in solution, followed by the adsorption of the *cis* molecules on the substrate. Because the molecular assemblies of *cis* isomers of azobenzene adlayers are not stable, the *cis*-isomer domains disappear quickly and only *trans*-isomer domains are observed.[8a,9] Recently, in situ light-induced *cis*-to-*trans* isomerization of stilbene on Ag/Ge(111) surfaces was demonstrated.[10] In this particular case, the *cis*-isomer domains formed spontaneously and simultaneously along with the *trans*-isomer domains from the gas phase. The *cis*-isomer domains are metastable and can be transformed to *trans*-isomer domains by brief exposure to 248-nm UV-light radiation. The attempt to induce the *cis*-to-*trans* isomerization by thermal annealing was unsuccessful.[10] It is known that the isomerization on surfaces originates from the energetically unstable *cis* isomer and leads to the energetically stable *trans* isomer. To the best of our knowledge, there are no previous STM reports on thermally induced *cis*-to-*trans* isomerization on surface-adsorbed molecules. Although a few papers have described thermally induced changes in the morphology of adlayers of various molecules, no significant changes in the molecular structure were observed.[6b,11]

Recently, we have synthesized a series of connected two-core dioxaborines (DOBs) that were substituted with dodecyloxy groups. DOBs possess interesting and potentially beneficial properties such as electron transport in electronic devices, for example, organic light emitting diodes.[12] The molecular structure of bis(4,4′-(*m*,*m*′-di(dodecyloxy)phenyl)-2,2′-difluoro-1,3,2-dioxaborine, **4** is shown in Figure 1. The

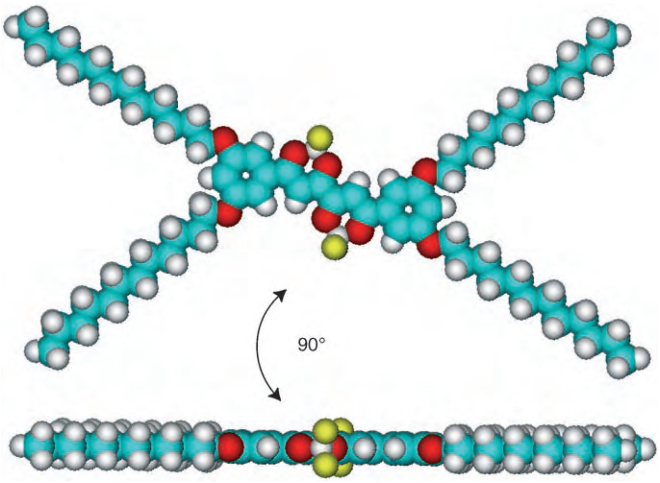

Figure 1. Top and side views of molecule **4** calculated by using the Gaussian program.

molecule was synthesized by conversion of the corresponding tetraketone **3** with $BF_3{\cdot}Et_2O$ in acetic acid/toluene. The tetraketone **3** was obtained by a classical Claisen condensation from *m*,*m*′-di(dodecyloxy)-acetophenone and oxalic acid ethyl esters with sodium hydride in toluene.[13] Scheme 1 simply describes the synthesis process and shows that the molecule has four dodecyloxy groups. The presence of the dodecyl chains among the molecules may produce unusual and unexpected effects on the assembly structure at HOPG surfaces.

AUSTIN model 1 semiempirical quantum chemical method (AM1) structure optimization of the molecular geometry by using the Gaussian program shows that bis-(4,4′-(*m*,*m*′-di(dodecyloxy)phenyl)-2,2′-difluoro-1,3,2-dioxaborine) is in a planar conformation with an achiral C_{2h} symmetry. The details can be seen in the top side views in

[*] Dr. D. Rohde, C.-J. Yan, Dr. H.-J. Yan,[+] Prof. Dr. L.-J. Wan
Beijing National Laboratory for Molecular Sciences
Institute of Chemistry
Chinese Academy of Sciences (CAS)
Beijing 100080 (China)
Fax: (+86) 10-6255-8934
E-mail: wanlijun@iccas.ac.cn
[+] Also in Graduate School of CAS, Beijing, China

[**] Financial support from the Natural Science Foundation of China (Nos. 20575070, 20121301, and 20520140277), the National Key Project on Basic Research (No. 2002CCA03100), and Chinese Academy of Sciences is gratefully acknowledged. The authors thank Prof. C.L. Bai for discussion.

InterScience
© 2006 Wiley-VCH Verlag GmbH & Co. KGaA, Weinheim

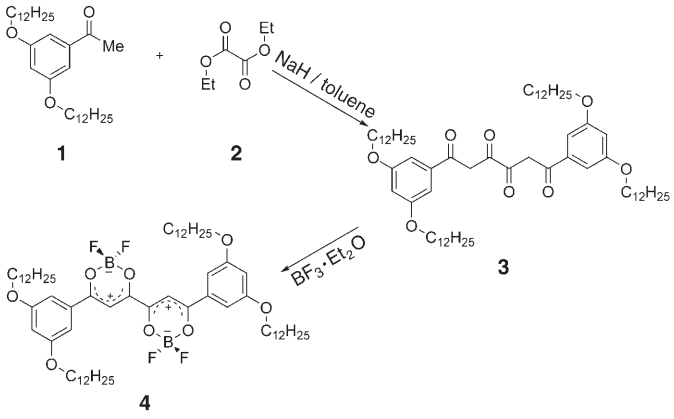

Scheme 1. Synthesis and chemical structure of bis(4,4′-(*m*,*m*′-di(dodecyloxy)phenyl)-2,2′-difluoro-1,3,2-dioxaborine).

Figure 1. The two DOB moieties have a dihedral angle of 180°. The molecule exists in a *trans* conformation. The two outer phenyl groups are arranged in the same plane as the DOB moieties and with a dihedral angle of 0°.

A theoretical calculation of the binding energy of a single molecule in the gas phase with different dihedral angles between the DOB moieties, as illustrated in Figure 2,

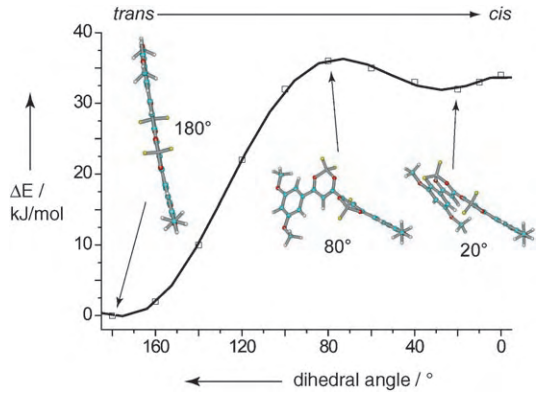

Figure 2. Theoretical calculation of structures and energy variations for the rotation about the central bond of bis(4,4′-(*m*,*m*′-di-(methoxy)phenyl)-2,2′-difluoro-1,3,2-dioxaborine) in the gas phase.

confirms that the *cis* isomer of molecule **4** is energetically unstable and has a higher energy than that of the *trans* isomer. However, the energy barrier of the isomerization is much lower than that for azobenzene[14] or stilbene.[15] This lower energy barrier may allow the DOB molecules to change their conformation by thermal stimulation. In a differential scan calorimetric (DSC) experiment on solid bulk material of **4**, a *trans*-to-*cis* transition was found at 132 °C. The computations also indicated that the most stable conformation is not the planar *cis* isomer but the *gauche cis* isomer with a dihedral angle of about 20° as shown in Figure 2. NMR spectropic investigations and absorption measurements in solution gave no indication of a *cis*/*trans* isomerization (see the Experimental Section). In solution, the *trans* isomer dominates and occupies the global energy minimum of molecule **4**. However, the most stable isomer of molecule **4** that is adsorbed on a solid surface such as on highly oriented pyrolytic graphite (HOPG) is as of yet unknown.

Herein, we report the results of self-assembly on HOPG surfaces. Molecular-symmetry breaking and chiral assemblies were observed on the SAMs. Self-assembly symmetry can be tuned from lamellar to hexagonal through a thermal-annealing process. This transformation, for the first time, was found to be owing to the *trans*-to-*cis* isomerization of the molecules within the adlayer. Although thermodynamically unstable in solution, the *cis* isomer was stabilized through adsorption onto the HOPG surface.

Figure 3a shows a large-scale STM image of the 2D molecular assembly on HOPG. Several domains larger than 50 nm are seen in the scanning area. Each domain consists of highly ordered molecular rows. The molecules in the domains form a lamellar structure with aligned bright spots as shown in

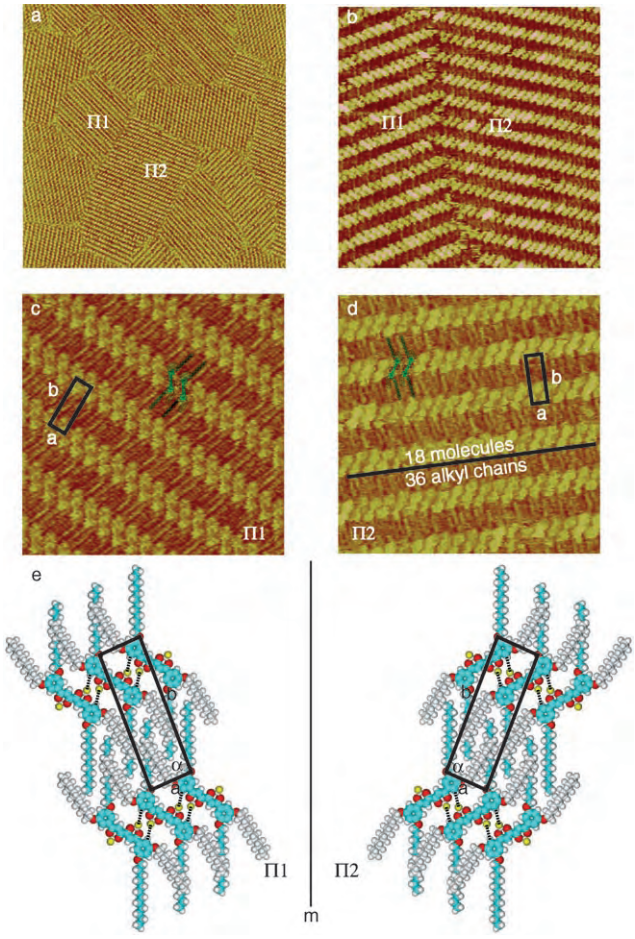

Figure 3. a) A large-scale STM image of molecular assembly with a scanning area of 203×203 nm^2. Tunneling conditions: I_{set} = 422 pA, V_{bias} = 512 mV. b) STM image with a domain boundary between ∏1 and ∏2. The scanning area is 38.2×38.2 nm^2. Tunneling conditions: I_{set} = 434 pA, V_{bias} = 487 mV. c) High-resolution STM image showing domain ∏1. The image size is 15.6×15.6 nm^2. Tunneling conditions: I_{set} = 511 pA, V_{bias} = 671 mV. d) High-resolution STM image showing domain ∏2. The image size is 19.7×19.7 nm^2. Tunneling conditions: I_{set} = 531 pA, V_{bias} = 372 mV. e) Structural models for domains ∏1 and ∏2. The out-of-plane alkyl chains are illustrated in light gray.

 © 2006 Wiley-VCH Verlag GmbH & Co. KGaA, Weinheim

Figure 3b. Because π-conjugated systems are well known to give a high contrast in STM images,[16] the bright rows were identified as the π-conjugated backbones of the molecules. The distance between the bright rows is about 3.3 nm. A careful analysis of the image in Figure 3b reveals that there are two types of domains, labeled $\prod 1$ and $\prod 2$, that appear like mirror images. The high-resolution STM images in Figure 3c,d show that the dodecyl chains are arranged in a comblike fashion between the neighboring bright π-conjugated backbones. Because of the large packing density, not all dodecyl chains can find room to adsorb on the surface. This large packing density is thought to be owing to the intermolecular reaction through hydrogen bonding between adjacent molecules (shown as black dashed lines in Figure 3e). When we count the alkyl chains and the π-conjugated groups in a lamella, as an example, we find only half as many alkyl chains as expected in Figure 3d. This finding suggests a packing model in which every other alkyl chain is not adsorbed on the HOPG surface. On the basis of the adlayer symmetry and intermolecular distances, a unit cell for the self-assembly in domains $\prod 1$ and $\prod 2$ is outlined in Figure 3c,d, respectively. Figure 3e is a structural model for the molecular arrangements of domain $\prod 1$ and $\prod 2$ in Figures 3c,d. In the packing model shown in the left column of Figure 3e and corresponding to the domain $\prod 1$, the out-of-plane alkyl chains are illustrated in light grey. These alkyl chains are positioned out of the plane of the molecule and can not be detected by STM.[17] The alkyl chains may not exist as illustrated in the model (oriented in a certain direction) owing to significant thermally induced motion and disorder. From STM results, a unit cell of the assembly on HOPG is defined with the parameters of $a = 0.98 \pm 0.2$ nm, $b = 3.34 \pm 0.2$ nm, and $\alpha = 95 \pm 2°$. The molecular arrangement in domain $\prod 2$ is the same as that in domain $\prod 1$. The model is shown in the right column of Figure 3e. After careful observation, it is found that the adsorption of the molecules on the HOPG surface causes breaking of the molecular symmetry. Compared with the two molecular domains $\prod 1$ and $\prod 2$, the molecules exist in an axial chirality. It is well known that adsorption can cause a chiral discrimination[2,18] and that achiral molecules can form enantiomerically pure, chiral, 2D assemblies on solid surfaces.[11b,19] For the particular molecule discussed here, the driving force for the symmetry breaking is the hydrogen bonding between the molecules, that is, between the fluorine atoms of the BF_2 group and the hydrogen in the *ortho* position of the phenyl ring. The chirality of the two domains is illustrated with a mirror plane, m, in Figure 3e.

When the HOPG substrate is heated to 100 °C, an increase in domain size is observed. After annealing for 10 minutes, the domains grew larger than the STM scanning area of 600 × 600 nm^2. Figure 4a is a typical large scale STM image showing the feature of the adlayer. The adlayer consists of ordered molecular rows. The results indicate that a stable and uniform molecular assembly exists after an annealing process. This therefore provides a simple method for surface modification and molecular manipulation.

After heating the HOPG substrate at 130 °C, small regions like domain Θ in Figure 4b with a different ordering feature appear in the assembly. The new domain Θ shows a hexagonal

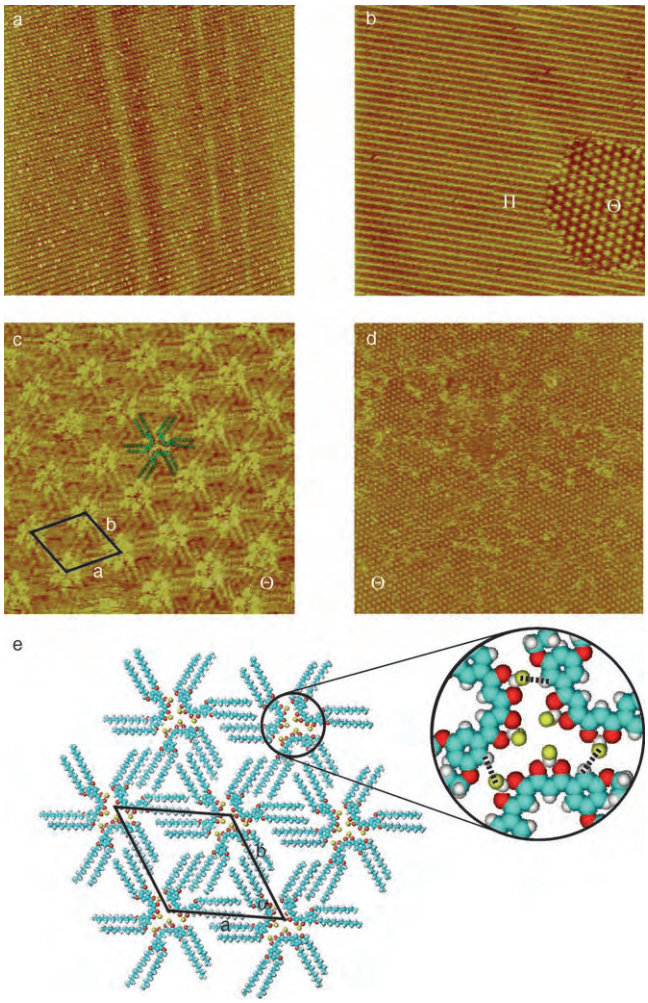

Figure 4. a) A large-scale STM image of the molecular assembly after thermal annealing at 100 °C for 10 min. The scanning area is 200 × 200 nm^2. Tunneling conditions: $I_{set} = 363$ pA, $V_{bias} = 567$ mV. b) A large-scale STM image after thermal annealing at 130 °C. The scanning area is 100 × 100 nm^2. Tunneling conditions: $I_{set} = 422$ pA, $V_{bias} = 539$ mV. c) High-resolution STM image showing domain Θ. The image size is 19.6 × 19.6 nm^2. Tunneling conditions: $I_{set} = 376$ pA, $V_{bias} = 529$ mV. d) A large-scale STM image of the adlayer after thermal annealing at 150 °C. The image size is 200 × 200 nm^2. Tunneling conditions: $I_{set} = 433$ pA, $V_{bias} = 644$ mV. e) Structural model for domain Θ determined from the STM images.

symmetry with bright spots rather than the previous lamellar structure in the domain $\prod$ in Figure 3 and Figure 4b. The domains Θ can be as large as 50 nm. The high-resolution STM image in Figure 4c reveals the details of the hexagonal structure. Although a thermal drift in recording the image can be seen in Figure 4c, it is clear that each of the bright spots in the domain Θ consists of three molecules. However, the geometry of the molecular structure with *trans*-connected DOB moieties, as shown in Figure 1, does not allow for such a molecular arrangement. Instead, domain Θ is composed of the *cis* isomer of the molecules. The hydrogen bonding between the molecules is responsible for the formation of the trimers. An enlarged inset in Figure 4e shows the details of the trimers. The possible hydrogen bonding in the trimer is

 © 2006 Wiley-VCH Verlag GmbH & Co. KGaA, Weinheim

indicated by black dashed lines. The hydrogen bonding is considered to exist between the fluorine atoms of the BF_2 group and the hydrogen in the *ortho* position of the phenyl ring. From the adlayer symmetry and intermolecular distances, a unit cell for the assembly is outlined in Figure 4c. Figure 4e shows a structural model for the molecular assembly shown in Figure 4c. The unit cell dimensions are $a = 3.92 \pm 0.2$ nm, $b = 3.92 \pm 0.2$ nm, $\alpha = 60 \pm 5°$. The model is in good agreement with the observed results from STM images.

A size increase in these hexagonal domains was observed when the adlayer was heated to 150 °C. Finally, the hexagonal structure covers the entire substrate surface. Figure 4d is a typical STM image of the new phase. Some molecular clusters can be seen in the image indicating the starting of the molecular desorption from the HOPG surface. However, until this temperature, the retransformation from *cis* isomers to *trans* isomers was not observed. The in-solution unstable *cis* isomers can stably exist on HOGP surface owing to the molecule–molecule and molecule–substrate interactions. The hexagonal arrangement of the *cis* isomers in domain Θ allows all dodecyl chains to adsorb on the HOPG surface resulting in a more stable assembly and stronger adsorption. The adsorption of those dodecyl chains which were previously not adsorbed on the surface releases sufficient energy to thermodynamically favor domain Θ. Therefore, the hexagonal assembly is stabilized by the adsorption and is remarkably stable and still clearly observable without noticeable changes after several months.

The self-assembly of *cis*/*trans*-conformation molecules was well reported. The conformational change does not occur in all assemblies as can be seen from the differences between azobenzene/stilbene[8a,9,10] and DOB molecules. There are several important factors that influence the *cis*/*trans* transformation; First, the substrate is very important, on Au and Ag surfaces, the interaction between the molecule and the substrate would be usually stronger than that on HOPG surfaces. Second, the difference in molecular structure is also important to the transformation as it is not possible that just one DOB changes its conformation in close-packed assemblies. All DOB molecules in the assembly changed their conformation from *trans* to *cis*, however, the details on the transformation are not clear. For example, it is not clear whether all molecules change in uniform steps or the transformation is translated by a process of disorder to order. As thermal drift is so heavy, no STM imaging can be carried out during thermal annealing. As a guess, we propose that the transformation is through a process of disorder to order and results in the adsorption of all molecules on the HOPG surface in a *cis* conformation.

In summary, we have studied the adsorption behavior of bis(4,4′-(*m*,*m*′-di(dodecyloxy)phenyl)-2,2′-difluoro-1,3,2-dioxaborine) on HOPG surfaces. It was found that the structure of the adlayer can be converted from lamellar to hexagonal through a thermal-annealing process. The hydrogen bonding between the molecules causes a break in molecular symmetry upon adsorption onto the surface and results in chiral assemblies from achiral molecules that were previously clearly observed by STM. For the first time, a thermally induced *trans*-to-*cis* isomerization of adsorbed molecules was observed and the thermodynamically stable *cis*-isomer adlayers were created. Although thermodynamically unstable in solution, the *cis* isomers become remarkably stable when adsorbed on the HOPG surface. By using only thermal stimulation at different temperatures, we have obtained pure *trans*- and *cis*-isomer adlayers. The results of this research are significant in the study of self-assembly and molecular architecture on solid surfaces.

Experimental Section

A solution of *m*,*m*′-di(dodecyloxy)acetophenone (0.02 mol), diethyl oxalic acid ester (0.01 mol), and sodium hydride (0.6 g) in toluene (300 mL)was stirred and heated for 10 h. After cooling down to room temperature, the solution was added to a mixture of water/ice/acetic acid (1:1:1). The organic layer was separated, washed with water, dried over Mg_2SO_4, and then concentrated. The precipitated product was then isolated by filtration. For purification, the product was recrystallized from toluene/hexane (1:1).

1,6-Bis(*m*,*m*′-di(dodecyloxy)phenyl)hexane-1,3,4,6-tetraone) (**3**): yellow crystalline product, yield: 81 %; mp. 62–67 °C; ^{1}H NMR (400 MHz, $CDCl_3$): $\delta = 1.26$ (m, 76H; CH_3, CH_2), 1.46 (quin, 8H; CH_2), 1.79 (quin, 8H; CH_2), 3.94 (t, 8H; CH_2), 6.66 (s, 2H; CH), 7.06 (s, 2H; CH), 7.12 (s, 4H; CH), 15.54 ppm (s, 2H; OH); elemental analysis (%) calcd for $C_{66}H_{110}O_8$: C 76.9, H 10.6; found: C 76.7, H 10.7.

To a boiled solution of **3** in acetic acid, the $BF_3{\cdot}Et_2O$ adduct was added as the limiting reagent. After addition, the solution was boiled for two minutes. The product crystallized from the cooling solution and was isolated by filtration. The product was then recrystallized several times from dry toluene to purify.

Bis(4,4′-(*m*,*m*′-di(dodecyloxy)phenyl)-2,2′-difluoro-1,3,2-dioxaborine) (**4**): orange crystalline product, yield: 95 %; mp. 122 °C (DSC); UV/Vis (toluene): $\lambda_{max.} = 435$ nm; Fluorescence (toluene): $\lambda_{fluoro.} = 500$ nm; ^{1}H NMR (400 MHz, $CDCl_3$): $\delta = 1.27$ (m, 76H; CH_3, CH_2), 1.47 (m, 8H; CH_2), 1.82 (quin, 8H; CH_2), 4.03 (t, 8H; CH_2), 6.88 (s, 2H; CH), 7.32 (s, 4H; CH), 7.55 ppm (s, 2H; CH); elemental analysis (%) calcd for $C_{66}H_{108}O_8B_2F_4$: C 70.3, H 9.5; found: C 70.2, H 9.5.

Molecule **4** was dissolved in toluene (HPLC grade, Aldrich) with a concentration of less than 10^{-4} M. A drop of the solution was then deposited on a freshly cleaved surface of HOPG (quality ZYB, Digital Instruments) and dried in air prior to STM imaging. The samples were imaged by STM in ambient conditions. The experiments were performed on a Nanoscope III SPM (Digital Instruments, Santa Barbara, USA). STM tips were made from mechanically cut Pt/Ir wire (90/10). All STM images were recorded in the constant current mode. The specific-tunneling conditions are given in the legends of Figure 3 and 4. All images are shown without further processing such as low-pass and Fourier transformation.

The theoretical calculations were performed for molecules in the gas phase by using GAUSSIAN 03 (Gaussian Inc., Pittsburgh, USA) and MATERIALS STUDIO 3.1 (Accelrys, San Diego, USA). The packing models for the various self-assemblies were build by HYPERCHEM (Hypercube Inc., Florida, USA) program packages.

Received: February 24, 2006
Published online: May 4, 2006

Keywords: chirality · Hydrogen bonds · isomerization · scanning probe microscopy · self-assembly

 © 2006 Wiley-VCH Verlag GmbH & Co. KGaA, Weinheim

[1] a) J. M. Lehn, *Proc. Natl. Acad. Sci. USA* **2002**, *99*, 4763; b) G. M. Whitesides, M. Boncheva, *Proc. Natl. Acad. Sci. USA* **2002**, *99*, 4769.

[2] a) S. Fujii, U. Akiba, M. Fujihira, *Chem. Commun.* **2001**, *17*, 1688; b) S. Yoshimoto, E. Tsutsumi, Y. Honda, Y. Murata, M. Murata, K. Komatsu, O. Ito, K. Itaya, *Angew. Chem.* **2004**, *116*, 3106; *Angew. Chem. Int. Ed.* **2004**, *43*, 3044; c) G. B. Pan, J. M. Liu, H. M. Zhang, L. J. Wan, Q. Y. Zheng, C. L. Bai, *Angew. Chem.* **2003**, *115*, 2853; *Angew. Chem. Int. Ed.* **2003**, *42*, 2747; d) S. De Feyter, F. C. De Schryver, *J. Phys. Chem. B* **2005**, *109*, 4290.

[3] a) A. Haran, D. H. Waldeck, R. Naaman, E. Moons, D. Cahen, *Science* **1994**, *263*, 948; b) H. B. Fang, L. C. Giancarlo, G. W. Flynn, *J. Phys. Chem. B* **1999**, *103*, 5712.

[4] a) J. V. Barth, J. Weckesser, C. Cai, P. Günter, L. Bürgi, O. Jeandupeux, K. Kern, *Angew. Chem.* **2000**, *112*, 1285; *Angew. Chem. Int. Ed.* **2000**, *39*, 1230; b) J. R. Gong, L. J. Wan, Q. H. Yuan, C. L. Bai, H. Jude, P. J. Stang, *Proc. Natl. Acad. Sci. USA* **2005**, *102*, 971; c) Q. H. Yuan, L. J. Wan, H. Jude, P. J. Stang, *J. Am. Chem. Soc.* **2005**, *127*, 16279.

[5] a) R. Yamada, H. Wano, K. Uosaki, *Langmuir* **2000**, *16*, 5523; b) J. Lu, Q. D. Zeng, C. Wang, L. J. Wan, C. L. Bai, *Chem. Lett.* **2003**, *32*, 856.

[6] a) L. P. Xu, C. J. Yan, L. J. Wan, S. G. Jiang, M. H. Liu, *J. Phys. Chem. B* **2005**, *109*, 14773; b) C. J. Li, Q. D. Zeng, Y. H. Liu, L. J. Wan, C. Wang, C. R. Wang, C. L. Bai, *ChemPhysChem* **2003**, *4*, 857; c) L. J. Scherer, L. Merz, E. C. Constable, C. E. Housecroft, M. Neuburger, B. A. Hermann, *J. Am. Chem. Soc.* **2005**, *127*, 4033; d) L. J. Wan, H. Noda, C. Wang, C. L. Bai, M. Osawa, *ChemPhysChem* **2001**, *2*, 617; e) J. D. Mougous, A. J. Brackley, K. Foland, R. T. Backer, D. L. Patrick, *Phys. Rev. Lett.* **2000**, *84*, 2742.

[7] Q. M. Xu, M. J. Han, L. J. Wan, C. Wang, C. L. Bai, B. Dai, J. L. Yang, *Chem. Commun.* **2003**, 2874.

[8] a) P. Vanoppen, P. C. M. Grim, M. Rücker, S. De Feyter, G. Moessner, S. Valiyaveettil, K. Müllen, F. C. De Schryver, *J. Phys. Chem.* **1996**, *100*, 19636; b) G. Z. Yang, Q. D. Zeng, L. J. Wan, C. L. Bai, *Chin. Sci. Bull.* **2003**, *48*, 1952.

[9] a) P. C. M. Grim, P. Vanoppen, M. Rücker, S. De Feyter, S. Valiyaveettil, G. Moessner, K. Müllen, F. C. De Schryver, *J. Vac. Sci. Technol. B* **1997**, *15*, 1419; b) J. Jin, W. Yang, Y. Li, L. Li, Y. Zhao, L. Jiang, T. Li, *New J. Chem.* **2003**, *27*, 1463.

[10] C. S. Tsai, J. K. Wang, R. T. Skodje, J. C. Lin, *J. Am. Chem. Soc.* **2005**, *127*, 10788.

[11] a) L. Pan, Q. Zeng, J. Lu, D. Wu, S. Xu, Z. Tan, L. J. Wan, C. Wang, C. L. Bai, *Surf. Sci.* **2004**, *559*, 70; b) F. Vidal, E. Delvigne, S. Stepanow, N. Lin, J. V. Barth, K. Kern, *J. Am. Chem. Soc.* **2005**, *127*, 10101; c) P. Samori, H. Engelkamp, P. A. J. de Witte, A. E. Rowan, R. J. M. Nolte, J. P. Rabe, *Adv. Mater.* **2005**, *17*, 1265; d) S. N. Magonov, N. A. Yerina, *Langmuir* **2003**, *19*, 500.

[12] a) J. Fabian, H. Hartmann, *J. Phys. Org. Chem.* **2004**, *17*, 359; b) B. Domercq, C. Grasso, J.-L. Maldonado, M. Halik, S. Barlow, S. R. Marder, B. Kippelen, *J. Phys. Chem. B* **2004**, *108*, 8647.

[13] a) A. Hunze, A. Kanitz, W. Rogler, H. Hartmann, D. Rohde, WO 02/065600 [*Chem. Abstr.* **2003**, *137*, 187010]; b) J. M. Halm, J. H. DeLorme, *Photogr. Sci. Eng.* **1979**, *23*, 252.

[14] H. Rau in *Photochemistry and Photophysics*, *Vol. 2* (Ed.: J. Rebek), CRC, Boca Raton, FL, **1990**, p. 119.

[15] a) D. H. Waldeck, *Chem. Rev.* **1991**, *91*, 415; b) W. G. Han, T. Lovell, T. Liu, L. Noodleman, *ChemPhysChem* **2002**, *3*, 167.

[16] A. J. Fisher, P. E. Blöchl, *Phys. Rev. Lett.* **1993**, *70*, 3263.

[17] a) P. Zell, F. Mögele, U. Ziener, B. Rieger, *Chem. Commun.* **2005**, 1294; b) J. Zhang, A. Gesquière, M. Sieffert, M. Klapper, K. Müllen, F. C. De Schryver, S. De Feyter, *Nano Lett.* **2005**, *5*, 1395; c) S. De Feyter, A. Gesquière, P. C. M. Grim, F. C. De Schryver, S. Valiyaveettil, C. Meiners, M. Sieffert, K. Müllen, *Langmuir* **1999**, *15*, 2817.

[18] a) H. B. Fang, L. C. Giancarlo, G. W. Flynn, *J. Phys. Chem. B* **1998**, *102*, 7311; b) M. D. Ward, *Nature* **2003**, *426*, 615; c) M. O. Lorenzo, C. J. Baddeley, C. Muryn, R. Raval, *Nature* **2000**, *404*, 376.

[19] a) N. Katsonis, A. Marchenko, D. Fichou, *J. Am. Chem. Soc.* **2003**, *125*, 13682; b) C. J. Li, Q. D. Zeng, P. Wu, S. L. Xu, C. Wang, Y. H. Qiao, L. J. Wan, C. L. Bai, *J. Phys. Chem. B* **2002**, *106*, 13262.

 © 2006 Wiley-VCH Verlag GmbH & Co. KGaA, Weinheim

Analytical Techniques

DOI: 10.1002/anie.200600510

Coupling of Electrochemistry and Fluorescence Microscopy at Indium Tin Oxide Microelectrodes for the Analysis of Single Exocytotic Events**

Christian Amatore, Stéphane Arbault, Yong Chen, Cécile Crozatier, Frédéric Lemaître, and Yann Verchier*

Exocytosis of secretory vesicles is an essential process for communication between cells and organs in complex living systems. Following appropriate stimulation, vesicles containing bioactive molecules (neurotransmitters, peptides, hormones, etc.) at high concentration are transported via the cytoskeleton to eventually dock and fuse with the cell membrane, thus resulting in the release of their contents into the extracellular medium.[1] The four main steps of exocytosis,[2,3] particularly the intermediate phase of the fusion pore, are controlled by multiple biological[1] and physicochemical factors.[4,5] Over the past 20 years, several important methods have been developed for the investigation of exocytotic processes in single living cells with individual resolution of single secretory events. These methods are based either on electrical measurements[6,7] (that is, electrophysiological or electrochemical) or on optical detection.[8] Among them, amperometry at microelectrodes[3,4,9] and fluorescence microscopy (including observation in an evanescent wave field)[8,10] appear to be currently two of the most powerful techniques. They are in fact complementary, since each one provides an extremely precise way to monitor specific steps of

[*] Prof. C. Amatore, Dr. S. Arbault, Prof. Y. Chen, C. Crozatier, Dr. F. Lemaître, Y. Verchier
Ecole Normale Supérieure
UMR CNRS-ENS-UPMC 8640 PASTEUR
Département de Chimie
24 rue Lhomond, 75231 Paris cedex 05 (France)
Fax: (+33) 144-323-263
E-mail: Christian.Amatore@ens.fr

[**] This work was financially supported by the ENS, CNRS, and Université Pierre et Marie Curie, Paris 6, as well as by the French Ministry of Research (MRT). The MRT (Y.V.) and DGA (C.C.) are thanked for supporting PhD grants.

WILEY InterScience DISCOVER SOMETHING GREAT
© 2006 Wiley-VCH Verlag GmbH & Co. KGaA, Weinheim

the whole event. The first method enables accurate investigation of the dynamics of release (kinetics and quantum of charge) from individual vesicles once fusion begins. Conversely, the second technique provides precious data concerning the status of the vesicles before and during fusion (displacements, docking location, geometric area of fusion). Consequently, combining both techniques should afford a mighty tool for studies of single secretory events, with the aim of correlating both sources of information and enabling a complete analysis in situ of each event from predocking to full release.

We report here the analysis of exocytosis at single adrenal chromaffin cells on transparent indium tin oxide (ITO) microelectrodes that allow a simultaneous observation of fluorescence and amperometric measurements on stained cells (Figure 1). The methodology was applied to neuroendocrine cells but may be transposed to any adherent or immobilized secretory cell (neurons, granulocytes, lymphocytes, pancreatic β cells, etc.) that emits electroactive compounds through vesicular release. This study is aimed at demonstrating that both techniques may be coupled without introducing severe difficulties to each other. Coupling with evanescent wave measurements will require implementation of the current device onto adequate ITO-coated optical prisms rather than onto optical flat windows as documented here, and access to an evanescent wave microscope rather than a epifluorescent microscope as used here. However, we believe that the results presented here establish that the optical quality of the present device will enable such work to be implemented in further work.

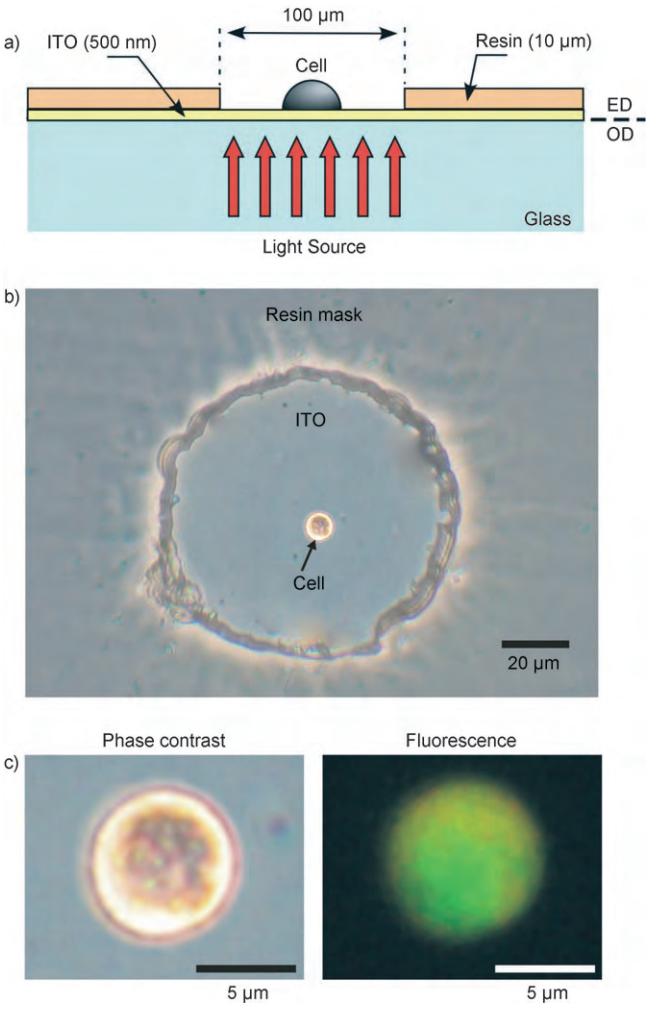

Figure 1. a) Schematic vertical cross-section of an ITO microelectrode. The electrochemical detection (ED) is performed on the ITO surface (upper part of the device) while the optical detection (OD) is obtained through the glass and ITO (lower part). b) Photograph (inverted microscopy) of a chromaffin cell adhering to an ITO microelectrode (100 µm diameter); the insulating resin appears as the dark gray external area. c) Close-up image obtained using phase contrast (left) or fluorescence (right) microscopy of the same cell preincubated with acridine orange and adhering onto the ITO surface.

Optical (for example, fluorescence) detection requires coverslips or slides with excellent optical properties (low refraction index), and a surface suitable for cell adhesion or immobilization through appropriate chemical modification. Conversely, amperometry requires an excellent electrical conductivity for a direct electrochemical detection of electroactive species secreted by the cell. ITO-coated glass slides possessed this set of requirements.[11] For example, thin films of ITO (typically 500 nm thickness) offer an excellent active surface for the electrochemical oxidation of epinephrine (Figure 2a), the main catecholamine released by chromaffin cells. Fluxes of catecholamines emitted during exocytotic events are in the range of 1000 molecules per ms.[4] A precise amperometric monitoring thus requires detection with a very high signal/noise ratio. This is achieved by restricting the active electrochemical surface to at most a few times the surface area of a single cell. This ensures the minimization of non-Faradaic information, such as noise of capacitive origin, while allowing a quantitative collection of released molecules. ITO-coated slides were thus insulated by a thin photoresist layer (10 µm thickness) through which circular openings (40–300-µm diameter wells) were created by photolithography (Figure 1a).

The root-mean-square (rms) noise detected on such micrometric surfaces of ITO by amperometry under experimental conditions appropriate for the analysis of living cells was typically 0.5 pA[12] and reached 0.3 pA for the smallest electrode diameters.

An aliquot of chromaffin cells in culture medium was deposited into a well of poly(dimethylsiloxane) (PDMS) positioned over an ITO microelectrode. The reduced aliquot volume and microelectrode dimensions meant that only one to two individual cells generally adhered to the free ITO surface (Figure 1b). Such isolated cells were left to adhere for at least 20 minutes before being stimulated by injecting a 2 mM barium solution in its vicinity with a micropipette. The ensuing secretion (Figure 2b) of catecholamines was followed by amperometry at the oxidation potential of +650 mV versus Ag/AgCl (Figure 2c). It is noteworthy that the data were obtained for secretion at the basal pole of each single cell, namely, under usual conditions for observation of cell fluorescence and for working with evanescent waves techniques.

The frequency of exocytosis was 3 Hz on average (Figure 2b), thus allowing the monitoring of numerous ampero-

 © 2006 Wiley-VCH Verlag GmbH & Co. KGaA, Weinheim

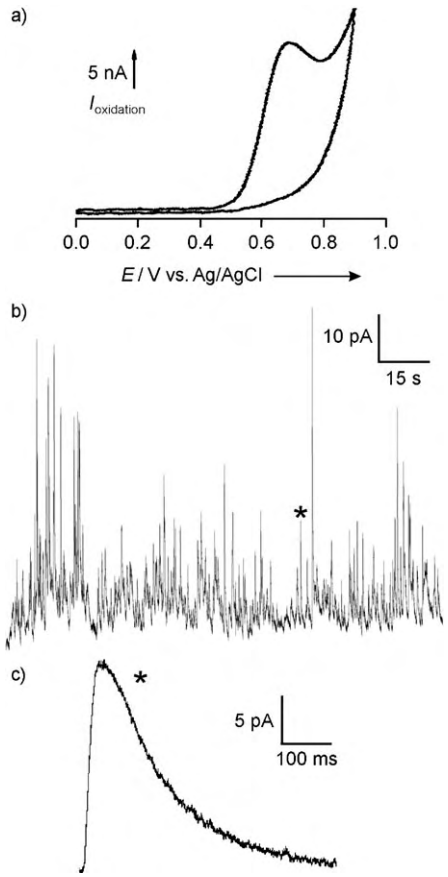

Figure 2. a) Cyclic voltammogram (initial potential: 0 V versus Ag/AgCl; sweep rate = 20 mVs^{-1}) of epinephrine (50 μM) in vitro in phosphate-buffered saline (PBS) buffer/$HClO_4$ (0.1 M) solution on an ITO microelectrode (well diameter = 40 μm) at 25 °C. b) Amperometric trace (E = 650 mV versus Ag/AgCl) corresponding to the exocytosis of a single chromaffin cell on an ITO microelectrode. Secretion was triggered by injection of a barium solution (2 mM). c) A representative spike from the trace (see labeling by asterisk in (b)) corresponding to a single vesicular event.

metric spikes. Each isolated spike (Figure 2c) was analyzed according to the method we and others have described previously.[12,13] The mean values of the main quantitative and kinetic parameters (Q, I_{max}, t_{20-90}, $t_{1/2}$) are summarized in Table 1. Clearly, the charges and maximum currents measured herein as well as the experimental reproducibility are in good agreement with those obtained at carbon microelectrodes in previous studies on cells from the same origin. Interestingly, it appears however that the kinetics of vesicle fusion are slower under the present conditions of analysis at the basal pole of the cells than at the apical one. This difference does not represent intrinsic differences in the kinetics of the electrochemical oxidation of catecholamines as demonstrated by in vitro experiments performed at each type of electrode (that is, carbon and ITO) but probably stems from specific molecular and physicochemical conditions at different exocytosis sites.[8] Thus, these studies show unambiguously that the electrochemical monitoring of exocytosis is feasible and reproducible on ITO microelectrodes with a similar accuracy as obtained with carbon microelectrodes.

Table 1: Mean values (± S.D.) of quantitative and kinetic parameters of amperometric spikes (n = 245).[a]

Q [fC]	I_{max} [pA]	t_{20-90} [ms]	$t_{1/2}$ [ms]
1745 ± 106	19.8 ± 1.2	19.3 ± 0.9	72.6 ± 2.5

[a] Detected during exocytosis of chromaffin cells (n = 5) on the surface of ITO microelectrodes.

Furthermore, fluorescent microscopy may be achieved at these same ITO microelectrodes simultaneously to amperometry. Prior to experiments, chromaffin cells were thus stained with acridine orange, a classical fluorescent probe known to accumulate into acidic compartments such as the secretion granules.[14,15] As evidenced in Figure 1c, the green fluorescence was easily observed through the ITO surface. Some granules appeared as green spots while other substructures appeared as orange areas (less acidic compartments), thereby establishing that the optical spectrum on ITO is large enough to record subtle differences in the granules. These studies will be extended to other fluorescent probes such as FM1-43 or green fluorescent proteins (GFPs)[14] and to different ITO surfaces.[11]

In this study, we have established the validity of the coupling between two essential analytical techniques that are among the most efficient for the direct and real-time analysis of biological exocytotic phenomena. The simultaneous optical and electrochemical detection of exocytotic events was shown to be feasible on the same transparent ITO material. The present procedure displays all the required qualities for the association of electrochemical techniques with total internal reflection fluorescence microscopy (TIRFM). This coupling should afford a comprehensive view about the "life" of a secretory vesicle before and after its fusion with the cell membrane together with a precise kinetic monitoring of the released material. Potential applications of this methodology include studies of other key biological processes involving secretion (cell communication, immune defense, oxidative stress, etc.) and especially its integration into microfluidic systems for parallel analyses on multiple cells.

Experimental Section

Bovine chromaffin cells were prepared by collagenase digestion of the medulla of adrenal glands obtained from a local slaughterhouse (Meaux, France). Cells were purified and isolated by using previously described methods.[12,16] Cells were used from the third to the eighth day after preparation.

Classical glass slides (75 mm × 25 mm × 1 mm) for microscopic observation were coated with a film of ITO (500 nm thickness; ACM, Villiers Saint Frédéric, France) to afford a material of low electrical resistance (20 ohms per square) and low refraction index (1.52). Micrometric disk surfaces of ITO were delimited by photolithography by two steps: first, an insulating resin (SPR220, MicroChem Corp., Newton, MA) was spin coated onto the whole ITO surface to form a film with an average thickness of 10 μm. Then, the film was exposed to a UV light through a mask made of a laser-printed transparency. After development of the resin, patterns of circular openings of 40 to 300 μm were obtained in the photoresist. Slabs of poly(dimethylsiloxane) (PDMS, 5 mm thickness) with holes punched through (10 mm diameter) were used as wells positioned over the ITO microelectrodes for solution, microcapillary, and reference electrode positioning.

 © 2006 Wiley-VCH Verlag GmbH & Co. KGaA, Weinheim

The PDMS slabs were obtained by heating a mixture (weight ratio 10:1) of PDMS prepolymer (RTV 615 A) and its curing agent (RTV 615B, General Electric Silicones, Waterford, NY) for 1 h at 80 °C. The PDMS slab offers the advantage of immediately adhering and of being easily removable from the insulating resin delimiting ITO microelectrodes.

About 1 mL of an isotonic physiological saline solution (154 mM NaCl, 4.2 mM KCl, 0.7 mM $MgCl_2$, 11.2 mM glucose, 10 mM HEPES, pH 7.4) containing cells (at most 3×10^5) was injected into a well of PDMS lying on an ITO microelectrode. The cells were allowed to seed for 20 to 30 min at room temperature. In general, only one to two cells adhered to the surface of each ITO disk. A glass microcapillary (10–20 μm diameter) was then positioned with a micromanipulator (MHW-103, Narishige, Tokyo, Japan) at a distance of 20 to 30 μm from the single cell located in the well and used to inject (Femtojet injector, Eppendorf, Hamburg, Germany) a stimulating solution (2 mM $BaCl_2$ in Locke buffer supplemented with 0.7 mM $MgCl_2$, without carbonates) towards the cell surface for 10 s. This configuration allowed the stimulation of one cell at a time and to study its response. All chemicals were from Sigma–Aldrich (St-Louis, MO). Experiments were conducted at room temperature (22 ± 1 °C).

Amperometric detection of exocytosis at ITO microelectrodes was achieved at +0.65 V versus an Ag/AgCl reference electrode using a commercially available picoamperometer (model AMU-130, Radiometer Analytical Instruments, Copenhagen, DK), for which the adjustable time response was set at 1 ms. The output was digitized at 10 kHz, displayed in real-time, and stored on a computer (Powerlab-4SP A/D converter and software Chart 5.0, ADinstruments, Colorado Springs, CO) without any subsequent digital filtering. Each amperometric trace obtained during cell secretion was analyzed according to previously described methods.[12] The characteristics of each spike, that is, the maximum oxidation current I_{max} (pA), the total electrical charge Q (fC), the half-width $t_{1/2}$ (ms), and the rise time t_{20-90} (the delay between $I = 20\%$ of I_{max} and $I = 90\%$ of I_{max} in ms), were determined using home-made software.[12] All values are reported as the mean ± SD considering Gaussian-type distributions of the data.

Voltammograms (sweep rate 20 mV s^{-1}) of 50 μM epinephrine in a phosphate-buffered saline/$HClO_4$ (0.1M) solution were recorded in vitro with the same ITO microelectrodes with a different potentiostat (EI400, Ensman Instruments, Bloomington, IN).

For the fluorescence experiments, chromaffin cells were preincubated for 30 to 60 min in culture flasks containing DMEM/F12 medium supplemented with 10 mM acridine orange (Molecular Probes Inc., Eugene, OR). The cells were then washed, resuspended in isotonic saline solution, and allowed to seed on the ITO microelectrode surface. Acridine orange labeling was detected on an inverted microscope (Axiovert-135, Carl Zeiss, Germany) equipped with a Zeiss filter set 10 (excitation filter BP 450-490, BS 510, emission filter BP 515-565). Pictures of the fluorescent cells were taken with a 4 mega pixels camera (power shot A80, Canon, Japan) directly connected to the microscope body.

Received: February 7, 2006
Published online: May 9, 2006

Keywords: analytical methods · electrochemistry · exocytosis · fluorescence · indium–tin oxide

[1] R. D. Burgoyne, A. Morgan, *Physiol. Rev.* **2003**, *83*, 581 – 632.
[2] G. A. de Toledo, R. Fernandez Chacon, J. M. Fernandez, *Nature* **1993**, *363*, 554 – 558.
[3] T. J. Schroeder, J. A. Jankowski, K. T. Kawagoe, R. M. Wightman, C. Lefrou, C. Amatore, *Anal. Chem.* **1992**, *64*, 3077 – 3083.
[4] C. Amatore, S. Arbault, I. Bonifas, Y. Bouret, M. Erard, M. Guille, *ChemPhysChem* **2003**, *4*, 147 – 154.
[5] C. Amatore, Y. Bouret, E. R. Travis, R. M. Wightman, *Angew. Chem.* **2000**, *112*, 2028 – 2031; *Angew. Chem. Int. Ed.* **2000**, *39*, 1952 – 1955.
[6] M. Lindau, G. A. de Toledo, *Biochim. Biophys. Acta* **2003**, *1641*, 167 – 173.
[7] G. Dernick, L. W. Gong, L. Tabares, G. A. de Toledo, M. Lindau, *Nat. Methods* **2005**, *2*, 699 – 708.
[8] D. Zenisek, J. A. Steyer, W. Almers, *Nature* **2000**, *406*, 849 – 854.
[9] R. M. Wightman, J. A. Jankowski, R. T. Kennedy, K. T. Kawagoe, T. J. Schroeder, D. J. Leszczyszyn, J. A. Near, E. J. Diliberto, O. H. Viveros, *Proc. Natl. Acad. Sci. USA* **1991**, *88*, 10754 – 10758.
[10] M. Oheim, *Biophys. J.* **2004**, *87*, 1403 – 1405.
[11] I. Zudans, J. R. Paddock, H. Kuramitz, A. T. Maghasi, C. M. Wansapura, S. D. Conklin, N. Kaval, T. Shtoyko, D. J. Monk, S. A. Bryan, T. L. Hubler, J. N. Richardson, C. J. Seliskar, W. R. Heineman, *J. Electroanal. Chem.* **2004**, *565*, 311 – 320.
[12] C. Amatore, S. Arbault, I. Bonifas, Y. Bouret, M. Erard, A. G. Ewing, L. A. Sombers, *Biophys. J.* **2005**, *88*, 4411 – 4420.
[13] E. V. Mosharov, D. Sulzer, *Nat. Methods* **2005**, *2*, 651 – 658.
[14] D. Perrais, I. C. Kleppe, J. W. Taraska, W. Almers, *J. Physiol.* **2004**, *560*, 413 – 428.
[15] F. Schapper, J. T. Goncalves, M. Oheim, *Eur. Biophys. J.* **2003**, *32*, 635 – 643.
[16] B. G. Livett, *Physiol. Rev.* **1984**, *64*, 1103 – 1161.

 © 2006 Wiley-VCH Verlag GmbH & Co. KGaA, Weinheim

Crystal Engineering

DOI: 10.1002/anie.200503992

A Noninterpenetrating Three-Dimensional $4^6 6^9$ Iron(II) Coordination Polymer Built with a Trigonal-Antiprismatic Iron(II) Metalloligand**

Kyoung-Tae Youm, Min Gyu Kim, Jaejung Ko, and Moo-Jin Jun**

Research into three-dimensional (3D) coordination polymers and other relevant materials has been intensively pursued in order to develop their physical properties for use in the fields

[*] Dr. K.-T. Youm, Prof. Dr. M.-J. Jun
Department of Chemistry
Yonsei University
Seoul 120-749 (Korea)
Fax: (+82) 2-364-7050
E-mail: mjjun@yonsei.ac.kr
Dr. M. G. Kim
Pohang Accelerator Laboratory
Pohang University of Science and Technology
Pohang 790-784 (Korea)
Prof. Dr. J. Ko
Departments of Chemistry
Korea University
Chochiwon, Chugnam 339-700 (Korea)

[**] This work was financially supported by the Korean Science and Engineering Foundation (Grant No. RO1-2001-00053).

Supporting information for this article is available on the WWW under http://www.angewandte.org or from the author.

© 2006 Wiley-VCH Verlag GmbH & Co. KGaA, Weinheim

of transport, storage, separation, optics, and magnetism.[1] When manipulating multidimensional coordination polymers, good control over the structure is of great importance, so that the assembled components form the desired architectures.[2] Recently, novel metalloligands have been investigated as a means for controlling the assembly of building blocks by manipulating their structural properties.[3,4] The metalloligand should have a second coordination sphere comprised of *exo*-oriented donor atoms and *endo*-oriented donor atoms that complete the first coordination sphere of an unsaturated transition-metal moiety.[4] The geometric orientation of the second coordination sphere of the metalloligand depends on the preferred geometry of the metal ions and the nature of the ligands bearing the multifunctional groups.

The development of well-designed metalloligands is highly demanding, especially when coordination polymers with specific topologies are desired. To the best of our knowledge, only a few types of metalloligands have been so far been reported (i.e., linear,[3,5] trigonal,[4,6] and square-planar[7]) despite their great potential for fabricating specific topologies. We have focused on synthesizing novel metalloligands and their subsequent incorporation into new functional coordination polymers. Herein we present the novel metalloligand $[Fe^{III}(\mathbf{L})_2]ClO_4\cdot 2\,MeCN$ (**1**·2 MeCN) as a molecular building block. The noninterpenetrating 3D coordination polymer framework of $[Fe^{II}(\mathbf{L})_2][Rh_2(OAc)_4]_3\cdot x\,\mathbf{S}$ (**2**·*x* **S**) was characterized by single-crystal X-ray structure analysis (**L** = hydrotris(1,2,4-triazolyl)borate anion, **S** = solvent).[8]

Reaction of K**L**[9] with $Fe^{III}(ClO_4)_3\cdot x\,H_2O$ in MeCN yielded orange **1**·2 MeCN. Six N_{endo} atoms of two **L** complete the first coordination sphere in the terdentate mode. As a result, the iron center adopts a slightly distorted octahedral geometry (Figure 1). The magnetic moment of **1**·2 MeCN, about 1.5 μ_B in the temperature range 5–300 K, implies that iron(III) is in a low-spin state (the spin-only value of the low-spin d^5 system is 1.7 μ_B). The average Fe–N_{endo} bond length of 1.95 Å is comparable to those of the low-spin $Fe^{III}N_6$ complexes $[Fe^{III}(phen)_3](ClO_4)_3$ (phen = 1,10-phenanthroline)[10] (1.974 Å) and $[Fe^{III}(tacn)_2]Cl_3\cdot 5\,H_2O$ (tacn = 1,4,7-triazacyclononane)[11] (1.99 Å). The intrinsic structure of **L**

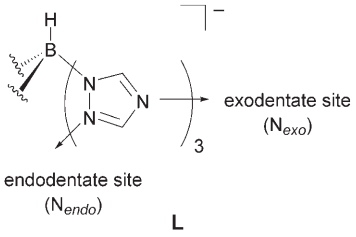

means that the orientation of the lone-pair electrons of the N_{exo} atoms does not coincide with that of the N_{endo}–Fe^{II} bonds in **1**, and hence the arrangement of the free N_{exo} atoms is not octahedral but trigonal-antiprismatic. Thus, the N_{exo} atoms are located at the vertices of a trigonal-antiprismatic building block. All free N_{exo} atoms can interact with appropriate linkers, such as a transition metal ion or an unsaturated metal complex, to afford a variety of multidimensional coordination polymers. While neutral complexes $[M^{II}(\mathbf{L})_2]$[9,12] (M = Fe, Co, Ni, Cu, Zn) have similar structural properties to **1**, their use as trigonal-antiprismatic metalloligands suffers from extremely low solubility. On the other hand, metalloligand **1** has the advantage of good solubility in MeCN and CH_3NO_2. Interestingly, in MeCN solution, **1** is easily reduced to the magenta iron(II) species $[Fe^{II}(\mathbf{L})_2]$, due to the strong reducing power of the borate ligand; similar transformations were observed for $[Fe^{III}(Tp)_2]^+$ (Tp = hydrotris(pyrazolyl)borate anion).[9] The addition of hydroquinone drastically facilitates the reduction of **1** in MeCN solution. The iron(III) state of **1** is somewhat more stable in the solid state. In short, the facile reduction of **1** and its good solubility make it very useful for assembling $[Fe^{II}(\mathbf{L})_2]$ moieties as potential spin-crossover sites in a series of coordination polymers that may show unique spin-transition behavior.[12]

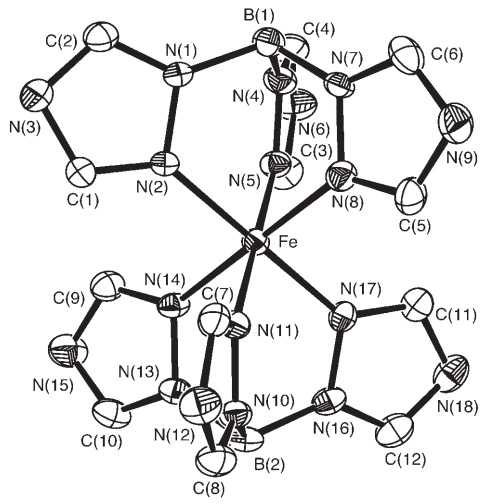

Figure 1. X-ray structure of the $[Fe(\mathbf{L})_2]^+$ cation in **1**. The Fe–N_{endo} bond lengths range from 1.943(3) to 1.955(3) Å. N_{exo} atoms are at the vertices of a trigonal antiprism.

In pursuit of a novel topology built by trigonal-antiprismatic metalloligand **1**, we obtained the neutral noninterpenetrating 3D coordination polymer **2**·*x* **S** (**S** = MeCN and $CHCl_3$) by reaction of **1** with paddle-wheel-shaped dirhodium tetraacetate ($Rh_2(OAc)_4\cdot 2\,MeOH$ or $Rh_2(OAc)_4\cdot 2\,py$). Single-crystal X-ray structure analysis revealed that **2**·*x* **S** crystallizes in the highly symmetric cubic space group $Ia\bar{3}d$ (No. 230). The framework results from the assembly of a dirhodium complex as a linear spacer[5d,13] and an iron(II) metalloligand acting as a six-connected uninode (Figure 2).

In **2**, the iron center adopts an octahedral geometry with an Fe–N_{endo} distance of 2.007(3) Å, which is somewhat longer than that of **1**. This implies that the iron(III) metalloligand is reduced to $[Fe^{II}(\mathbf{L})_2]$, which retains its trigonal-antiprismatic geometry. All of the N_{exo} atoms are coordinated to axial sites of dirhodium moieties at a distance of 2.255(4) Å. The topology of **2** is related to a body-centered cubic structure, which has an eight-connected node in view of the occupation of the node in the lattice. If the symmetry was not taken into account, the unit cell of **2** could be considered to be comprised of eight body-centered cubic subunits, of which all lattice points are occupied by Fe^{II} nodes. If all the connections

 © 2006 Wiley-VCH Verlag GmbH & Co. KGaA, Weinheim

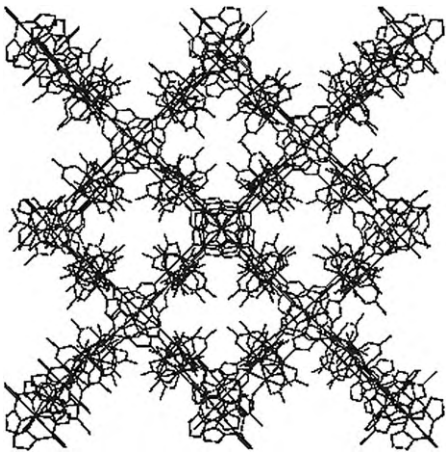

Figure 2. Perspective view of 3D noninterpenetrating framework of **2** along the crystallographic *a*/*b*/*c* axis. Hydrogen atoms are omitted for clarity.

between the nodes were intact, then an eight-connected framework could appear, like that found in CsCl. However, because the Fe^{II} node has six N_{exo} atoms that adopt a trigonal-antiprismatic binding arrangement, two *trans* connections should be omitted from the eight-connected nodes in a manner that preserves the cubic symmetry (Figure 3a).

Then, the noninterpenetrating 3D framework of **2** is formed, which is composed of six-connected nodes. Each iron(II) center is linked to six adjacent ones at a distance of 15.077(2) Å through two triazole rings of **L** and one $Rh_2(OAc)_4$ unit. The framework of **2** can be defined as $4^6 6^9$ net by considering the iron centers as topological uninodes (Figure 3b), though the resulting 3D net resembles the α-polonium structure viewed along all the crystallographic axes. To the best of our knowledge, this topology has never been realized before. In general, homogeneous six-connected nodes adopting octahedral geometry afford well-known primitive cubic nets,[14] which allows the α-polonium net to be described as a $4^{12}6^3$ topology.

The 3D framework of **2** cannot be sustained out of the mother liquor. The XRD pattern of the dried solid collapses due to easy escape of solvent molecules **S** from **2**·*x***S**, so that we could not determine the exact number of solvent molecules per iron center accommodated within the framework voids. Thus, all contributions of the disordered MeCN and $CHCl_3$ molecules were subtracted from the observed data in the diffraction pattern by using SQUEEZE in PLATON.[15] By this procedure a good framework geometry was obtained.

To inquire into the oxidation state of the iron center in dried solid **2**, we investigated the X-ray absorption structure (XAS) of **1**, **2**, and $[Fe^{II}(\mathbf{L})_2]$[9] at the Fe K-edge (Figure 4). The pre-edge absorption peaks corresponding to the 1s→3d transition provide parameters such as oxidation states, site symmetry, and covalent bond strength.[16,17] The 1s→3d pre-edge feature of **1** is very similar to that of the low-spin $[Fe^{III}(Tp)_2]^+$ complex, in which the $^2T_{2g}$ ground state has a $(t_{2g})^1(e_g)^4$ hole configuration with two allowed one-electron excited configurations (7113.6 eV). This is consistent with the results of magnetic measurements. Consequently, **1** is confirmed as a low-spin iron(III) complex. On the other hand, the

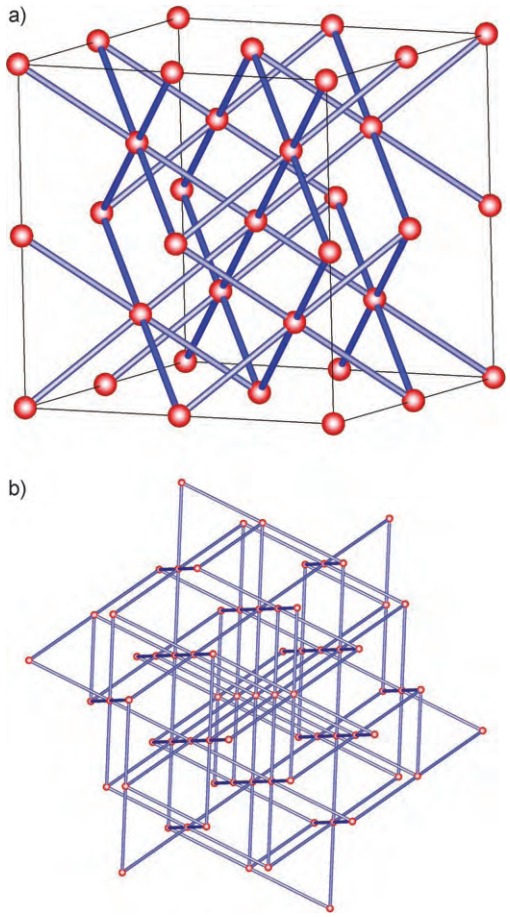

Figure 3. a) Bonding mode of the six-connected Fe^{II} nodes (red spheres) of **2** in the unit cell. b) Schematic representation of 3D noninterpenetrating six-connected framework assigned as $4^6 6^9$ topology in **2**. $Rh_2(OAc)_4$ linear spacers are represented by blue rods.

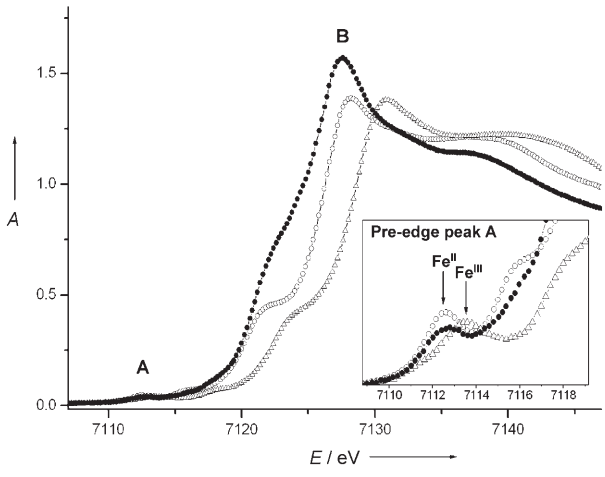

Figure 4. Fe K-edge XANES spectra of **1**·2MeCN (△), **2** (●), and $[Fe(\mathbf{L})_2]$ (○). The inset shows an expanded view of the 1s→3d transition in the pre-edge region.

single 1s→3d pre-edge absorption peak (7112.8 eV) of **2** appears to be similar to that of low-spin $[Fe^{II}(\mathbf{L})_2]$ (7112.6 eV). This can be assigned as the allowed electric quadrupole transition feature corresponding to the transition

 © 2006 Wiley-VCH Verlag GmbH & Co. KGaA, Weinheim

from the $^1A_{1g}$ ground state with an electronic hole configuration of $(e_g)^4$ to the ^2E_g excited state with $(e_g)^3$ as a pre-edge feature of a low-spin iron(II) complex.[16] Despite the collapse of the framework, the iron centers are still firmly confined by six N_{endo} atoms, and all N_{exo} atoms are coordinated to dirhodium moieties. This is because the decrease in peak **A** and the increase in peak **B** of **2** in intensity with respect to $[Fe^{II}(\mathbf{L})_2]$ indicate that the local structure around the octahedral iron centers of **2** is more centrosymmetric than that of $[Fe^{II}(\mathbf{L})_2]$, and less 3d–4p orbital mixing occurs.

Variable-temperature magnetic susceptibility measurements revealed that **2** shows an incomplete spin transition. For octahedral iron(II) complexes with an N_6 environment, a spin transition between the high- and low-spin states has been reported.[18] The $\chi_M T$ value expected for a full high-spin iron(II) ion could not be observed within the temperature limits (5–380 K). The spin transition was found to be gradual and incomplete without any thermal hysteresis for both increasing and decreasing temperature, which is the usual observation for mononuclear iron(II) complexes of substituted 1,2,4-triazole ligands.[19] It also is indicative of a lack of "cooperativity" caused by the collapse of the crystal lattice. At the highest temperature (380 K), the $\chi_M T$ value of 1.72 $cm^3 K mol^{-1}$ is much smaller than the theoretical spin-only $\chi_M T$ value of 3.0 $cm^3 K mol^{-1}$ for a high-spin $Fe^{II}N_6$ set.[20] The highest molar fraction of a high-spin state γ_{HS} is estimated to be 0.57. However, below 340 K low-spin states predominate over high-spin states, which corresponds to the finding that the 1s→3d pre-edge feature of **2** is very similar to that of the low-spin iron(II) complex $[Fe^{II}(\mathbf{L})_2]$ at ambient temperature. The $\chi_M T$ value decreases gradually, reaching about 0.47 $cm^3 K mol^{-1}$ at 100 K, and remains constant down to 15 K. Below 15 K the $\chi_M T$ value falls, which may be attributed to the zero-field splitting of the residual high-spin state. However, the predominance of a low-spin state at a low temperature is also confirmed by crystallographic evidence: the Fe^{II}–N bond length of 2.007(3) Å in **2** at 150 K is comparable to that of low-spin $[Fe^{II}(\mathbf{L})_2]$ (1.99 Å) rather than with that of high-spin iron(II) complex $[Fe^{II}(Tp^{3,5Me2})_2]$ (2.172 Å, $Tp^{3,5Me2}$ = hydrotris(3,5-dimethylpyrazolyl)borate anion).[21]

In summary, we have demonstrated incorporation of trigonal-antiprismatic metalloligand **1** in an unprecedented noninterpenetrating 3D $4^6 6^9$ coordination polymer. The ease of reduction and good solubility of **1**·2 MeCN facilitates incorporation of $[Fe^{II}(\mathbf{L})_2]$ as a potential spin-crossover moiety in a 3D net showing spin transition. Taking advantage of **1**·2 MeCN as a metalloligand, we are seeking to obtain stable multidimensional coordination polymers in order to establish a correlation of structural properties with magnetic properties.

Experimental Section

Caution! Perchlorate salts of metal complexes with organic ligands are potentially explosive and should be handled with care.

1·2 MeCN: A solution of K**L** (0.512 g, 2 mmol) in methanol (30 mL) was added dropwise to a solution of $Fe(ClO_4)_3 \cdot x H_2O$ (0.354 g, 1 mmol) in MeOH (40 mL). The reaction mixture was stirred vigorously for 4 h. The resultant orange precipitate was separated by filtration and recrystallized from MeCN/$CHCl_3$ to afford orange crystals (0.393 g, 58.7%). C,H,N analysis (%) calcd for $C_{16}H_{20}B_2ClFeN_{20}O_4$: C 28.71, H 3.01, N 41.85; found: C 28.41, H 2.88, N 42.03; IR (KBr): $\tilde{\nu}$ = 2565 (w, ν_{BH}), 2020 (w, ν_{MeCN}), 1146, 1110, 1086 cm^{-1} (s, ν_{ClO_4}).

2: Method A: A solution of **1**·2 MeCN (0.017 g, 0.025 mmol) in MeCN (5 mL) was carefully layered over a solution of $Rh_2(OAc)_4$·2 py (0.045 g, 0.075 mmol) in $CHCl_3$ (5 mL) in a test tube. After 2 d, red crystals of **2**·x**S** had separated, which lost their crystallinity once out of the mother liquor (0.043 g, 47.4%). C,H,N analysis (%) calcd for $C_{36}H_{50}B_2FeN_{18}O_{24}Rh_6$ (vacuum-dried solid): C 23.84, H 2.78, N 13.90; found: C 24.01, H 2.55, N 14.37; IR (KBr): $\tilde{\nu}$ = 2528 cm^{-1} (w, ν_{BH}).

Method B: A solution of **1**·2 MeCN (0.034 g, 0.05 mmol) in MeCN (5 mL) was carefully layered in a test tube with a solution of $Rh_2(OAc)_4$·2 MeOH (0.076 g, 0.15 mmol) in MeCN/$CHCl_3$ (4:1, 5 mL). Red crystals separated after 2 d.

Fe K-edge X-ray absorption spectra were recorded on the Electrochemistry beam line (BL7C1) of the Pohang Accelerator Laboratory (PAL) with a ring current of 120–170 mA at 2.5 GeV. An Si(111) monochromator crystal was used, detuned to 85% in intensity, to eliminate high-order harmonics. The data were collected in transmission mode with gas-filled (85% N_2, 15% Ar) ionization chambers as detectors. Energy calibration was carried out for all measurements by placing Fe foil in front of the third ion chamber and thus assigning the first inflection point to 7112 eV.

Magnetic measurements on a vacuum-dried sample of **2** were carried out with a Quantum Design MPMS-5 SQUID magnetometer in the temperature range 5–380 K at the Korean Basic Science Institute (KBSI) with an applied magnetic field of 0.5 T. Molar susceptibilities χ_M were corrected for diamagnetic contributions χ_D, that is, -246.44×10^{-6} $cm^3 mol^{-1}$ for **1**·2 MeCN and -353.44×10^{-6} $cm^3 mol^{-1}$ for **2**.[22]

Received: November 10, 2005
Revised: March 6, 2006
Published online: May 4, 2006

Keywords: crystal engineering · iron · magnetic properties · N ligands · X-ray absorption spectroscopy

[1] a) O. M. Yaghi, M. O'Keeffe, N. W. Ockwig, H. K. Chae, M. Eddaoudi, J. Kim, *Nature* **2003**, *423*, 705–714; b) M. Munakata, L. P. Wu, T. Kuroda-Soda, *Adv. Inorg. Chem.* **1999**, *46*, 173–304; c) B. Moulton, M. J. Zaworotko, *Curr. Opin. Solid State Mater. Sci.* **2002**, *7*, 117–123; d) H. K. Chae, D. Y. Siberio-Pérez, J. Kim, Y. Go, M. Eddaoudi, A. J. Matzger, M. O'Keeffe, O. M. Yaghi, *Nature* **2004**, *427*, 523–527; e) D. N. Dybtsev, H. Chun, S. H. Yoon, D. Kim, K. Kim, *J. Am. Chem. Soc.* **2004**, *126*, 32–33; f) X.-J. Zheng, L.-P. Jin, S.-Z. Lu, *Eur. J. Inorg. Chem.* **2002**, 3356–3363.

[2] a) B. Moulton, M. J. Zaworotko, *Chem. Rev.* **2001**, *101*, 1629–1658; b) S. R. Batten, R. Robson, *Angew. Chem.* **1998**, *110*, 1558–1595; *Angew. Chem. Int. Ed.* **1998**, *37*, 1460–1494; c) P. J. Hagrman, D. Hagrman, J. Zubieta, *Angew. Chem.* **1999**, *111*, 2798–2848; *Angew. Chem. Int. Ed.* **1999**, *38*, 2638–2684; d) B. F. Abrahams, B. F. Hoskins, R. Robson, *J. Am. Chem. Soc.* **1991**, *113*, 3606–3607.

[3] a) S.-I. Noro, S. Kitagawa, M. Yamashita, T. Wada, *Chem. Commun.* **2002**, 222–223; b) R. Kitaura, G. Onoyama, H. Sakamoto, R. Matsuda, S.-I. Noro, S. Kitagawa, *Angew. Chem.* **2004**, *116*, 2738–2741; *Angew. Chem. Int. Ed.* **2004**, *43*, 2684–2687.

[4] K.-T. Youm, S. Huh, Y. J. Park, S, Park, M. G. Choi, M. J. Jun, *Chem. Commun.* **2004**, 2384–2385.

 © 2006 Wiley-VCH Verlag GmbH & Co. KGaA, Weinheim

[5] a) A. Kamiyama, T. Noguchi, T. Kajiwara, T. Ito, *Angew. Chem.* **2000**, *112*, 3260 – 3262; *Angew. Chem. Int. Ed.* **2000**, *39*, 3130 – 3132; b) Y. B. Dong, M. D. Smith, H. C. zur Loye, *Inorg. Chem.* **2000**, *39*, 1943 – 1949; c) Y. B. Dong, M. D. Smith, H. C. zur Loye, *Angew. Chem.* **2000**, *112*, 4441 – 4443; *Angew. Chem. Int. Ed.* **2000**, *39*, 4271 – 4273; d) C. T. Chapman, D. M. Ciurtin, M. D. Smith, H.-C. zur Loye, *Solid State Sci.* **2002**, *4*, 1187 – 1191.

[6] F. Lambert, J.-P. Renault, C. Policar, J. Morgenstern-Badarau, M. Cesario, *Chem. Commun.* **2000**, 35 – 36.

[7] a) B. F. Abrahams, B. F. Hoskins, D. M. Michail R. Robson, *Nature* **1994**, *369*, 727 – 729; b) L. Carlucci, G. Ciani, F. Porta, D. M. Proserpio, L. Santagostini, *Angew. Chem.* **2002**, *114*, 1987 – 1991; *Angew. Chem. Int. Ed.* **2002**, *41*, 1907 – 1911; c) Y. Diskin-Posner, I. Goldberg, *Chem. Commun.* **1999**, 1961 – 1962; d) L. Carlucci, G. Ciani, D. M. Proserpio, F. Porta, *Angew. Chem.* **2003**, *115*, 331 – 336; *Angew. Chem. Int. Ed.* **2003**, *42*, 317 – 322.

[8] Crystal data for **1**·2 MeCN: $C_{16}H_{20}B_2Cl_3FeN_{20}O_4$, orthorhombic, $P2_12_12_1$ (no. 19), $a = 8.7139(2)$, $b = 12.412(2)$, $c = 25.618(5)$ Å, $V = 2770.8(9)$ Å^3, $Z = 4$, $\rho_{calcd} = 1.605$ g cm^{-1}, $\mu = 0.707$ mm^{-1}, $T = 233(2)$ K, 14766 reflections were recorded of which 5161 were unique ($R_{int} = 0.0467$). All hydrogen atoms were placed in idealized positions, and all other atoms were refined anisotropically by a full-matrix least-squares method on F^2 to give $R1 = 0.0421$ ($I > 2\sigma(I)$), $wR2 = 0.0744$, GOF = 0.975, max./min. residual electron density 0.325/−0.407 e Å^{-3}, Flack parameter 0.038(2). Crystal data for **2**·*x* **S**: $C_{36}H_{50}B_2FeN_{18}O_{24}Rh_6$ (including only well-ordered atoms), cubic, $Ia\bar{3}d$ (no. 230), $a = 34.8205(6)$ Å, $V = 42218.7(1)$ Å^3, $Z = 16$, $\rho_{calcd} = 1.141$ g cm^{-1}, $\mu = 1.100$ mm^{-1}, $T = 150(1)$ K, 27878 reflections were recorded, of which 3119 were unique ($R_{int} = 0.043$). Disordered model crystallographic refinement converged at $R1 = 0.1101$ and $wR2 = 0.2828$ ($I > 2\sigma(I)$). After subtracting the contribution of all disordered solvent molecules to the diffraction pattern from the observed data by SQUEEZE in PLATON, final $R1 = 0.0409$ and $wR2 = 0.1149$ ($I > 2\sigma(I)$), GOF = 1.094, and max./min. residual electron density 0.589/−0.453 e Å^{-3} were obtained. CCDC-220728 and -220729 contain the supplementary crystallographic data for this paper. These data can be obtained free of charge from The Cambridge Crystallographic Data Centre via www.ccdc.cam.ac.uk/data_request/cif.

[9] C. Janiak, *Chem. Ber.* **1994**, *127*, 1379 – 1385.

[10] J. Baker, L. M. Engelhardt, B. N. Figgis, A. H. White, *J. Chem. Soc. Dalton Trans.* **1975**, 530 – 534.

[11] C. A. Boeyens, A. G. S. Forbes, R. D. Hancock, K. Wieghardt, *Inorg. Chem.* **1985**, *24*, 2926 – 2931.

[12] a) C. Janiak, T. G. Scharmann, J. C. Green, R. P. G. Parkin, M. J. Kolm, E. Riedel, W. Mickler, J. Elguero, R. M. Claramunt, D. Sanz, *Chem. Eur. J.* **1996**, *2*, 992 – 1000; b) C. Janiak, T. G. Scharmann, T. Bräuniger, J. Holubová, M. Nádvornik, *Z. Anorg. Allg. Chem.* **1998**, *624*, 769 – 774.

[13] F. A. Cotton, T. L. Felthouse, *Inorg. Chem.* **1981**, *20*, 600 – 608.

[14] a) S.-I. Noro, S. Kitagawa, M. Kondo, K. Seki, *Angew. Chem.* **2000**, *112*, 2161 – 2164; *Angew. Chem. Int. Ed.* **2000**, *39*, 2081 – 2084; b) M. Eddaoudi, D. B. Moler, H. L. Li, B. L. Chen, T. M. Reineke, M. O'Keeffe, O. M. Yaghi, *Acc. Chem. Res.* **2001**, *34*, 319 – 330.

[15] A. L. Spek, PLATON, A Multipurpose Crystallographic Tool, Utrecht University, Utrecht, **2003**.

[16] a) T. E. Westre, P. Kennepohl, J. G. DeWitt, B. Hedman, K. O. Hodgson, E. I. Solomon, *J. Am. Chem. Soc.* **1997**, *119*, 6297 – 6313; b) C. Hannay, M.-J. Hubin-Franskin, F. Grandjean, V. Briois, J.-P. Itié, A. Polian, S. Trofimenko, G. J. Long, *Inorg. Chem.* **1997**, *36*, 5580 – 5588.

[17] a) V. Briois, P. Sainctavit, G. J. Long, F. Grandjean, *Inorg. Chem.* **2001**, *40*, 912 – 918; b) M.-L. Boillot, J. Zarembowitch, J.-P. Itié, A. Polian, E. Bourdet, J. G. Haasnoot, *New J. Chem.* **2002**, *26*, 313 – 322.

[18] a) E. König, *Prog. Inorg. Chem.* **1987**, *35*, 527 – 622; b) P. Gütlich, Y. Garcia, H. A. Goodwin, *Chem. Soc. Rev.* **2000**, *29*, 419 – 427.

[19] a) K. H. Sugiyarto, D. C. Craig, A. D. Rae, H. A. Goodwin, *Aust. J. Chem.* **1993**, *46*, 1269 – 1290; b) P. J. Kumkeler, P. J. van Koningsbruggen, J. P. Cornelissen, A. N. van der Horst, A. M. van der Kraan, A. J. Haasnoot, J. Reedijk, *J. Am. Chem. Soc.* **1996**, *118*, 2190 – 2197; c) A. F. Stassen, M. D. Vos, P. J. van Koningsbruggen, F. Renz, J. Ensling, H. Kooijman, A. J. Spek, J. G. Haasnoot, P. Gütlich, J. Reedijk, *Eur. J. Inorg. Chem.* **2000**, 2231 – 2237.

[20] E. Breuning, M. Ruben, J.-M. Lehn, F. Renz, Y. Garcia, V. Ksenofantov, P. Gütlich, E. Wegelius, K. Rissanen, *Angew. Chem.* **2000**, *112*, 2563 – 2566; *Angew. Chem. Int. Ed.* **2000**, *39*, 2504 – 2507.

[21] a) J. D. Oliver, D. F. Mullica, B. B. Hutchinson, W. O. Milligan, *Inorg. Chem.* **1980**, *19*, 165 – 169; b) J. A. Real, M. C. Muñoz, J. Faw, X. Solans, *Inorg. Chem.* **1997**, *36*, 3008 – 3013; c) D. L. Reger, C. A. Little, V. G. Young, Jr., M. Pink, *Inorg. Chem.* **2001**, *40*, 2870 – 2574.

[22] R. L. Carlin, *Magnetochemistry*, Springer, Heidelberg, **1986**.

 © 2006 Wiley-VCH Verlag GmbH & Co. KGaA, Weinheim

Glycoproteins

DOI: 10.1002/anie.200600685

The Direct Formation of Glycosyl Thiols from Reducing Sugars Allows One-Pot Protein Glycoconjugation**

*Gonçalo J. L. Bernardes, David P. Gamblin, and Benjamin G. Davis**

Glycoconjugates have become essential tools for the investigation of many biological processes,[1] and it is now well established that protein and lipid-bound carbohydrate units play essential roles in cell signaling regulation,[2] cellular differentiation,[3] and immune response.[4] In recent years, glycosyl thiols have become useful building blocks for the synthesis of certain glycoconjugates that may be considered to be analogues of glycopeptides and glycoproteins.[5–8] Their use has allowed specific glycosylation of peptides to form S-linked glycopeptides through alkylation[6] or conjugate-addition strategies.[7] Moreover, we have demonstrated that a combi-

[*] G. J. L. Bernardes, Dr. D. P. Gamblin, Dr. B. G. Davis
Chemistry Research Laboratory
Department of Chemistry
University of Oxford
Mansfield Road, Oxford, OX1 3TA (UK)
Fax: (+44) 1865-275-652
E-mail: Ben.Davis@chem.ox.ac.uk

[**] We gratefully acknowledge the Fundação para a Ciência e a Tecnologia, Portugal for the award of a doctoral fellowship (G.J.L.B., grant BD/16997/2004), and the EPRSC (D.P.G.). We also thank Katie J. Doores and Dr. Graeme Horne for helpful discussions, and Alister French and Norberto Reis for graphics.

Supporting information for this article is available on the WWW under http://www.angewandte.org or from the author.

© 2006 Wiley-VCH Verlag GmbH & Co. KGaA, Weinheim

nation of site-directed mutagenesis followed by thiol-mediated chemoselective ligation can be used for site-selective protein glycosylation. In this two-step strategy (Glyco–SeS),[8] a cysteine residue is incorporated into the desired position within the protein backbone; the free thiol in the side chain of this cysteine is subsequently converted into a selenenylsulfide following exposure to phenylselenenyl bromide. This activated protein, upon the addition of a glycosyl thiol, is converted directly into the corresponding homogenous glycoprotein.

Given this value of such glycosyl thiols and their other potential uses, for example, as precursors[9] to widely used thioglycosides[10] and glycosyldisulfide[11] donors, it is all the more surprising that methods for producing these compounds are somewhat protracted and that until now no ready and general direct method for their preparation exists. Furthermore, thioglycosides and their resulting glycoconjugates often demonstrate increased chemo- and enzymatic stability and are tolerated by most biological systems.[12] Indeed, gold salts of thioaldoses[12b] are used in the treatment of rheumatoid arthritis and have recently been identified as potential blockers of transformed growth of lung-cancer cells.[12c]

The most frequently employed method for the synthesis of glycosyl thiols **1** involves the treatment of glycosyl halides **2** with a sulphur nucleophile (either thiourea[13] or potassium thioacetate) in acetone,[14] followed by mild hydrolysis (Scheme 1).[15,16] Other methods include the use of anomeric

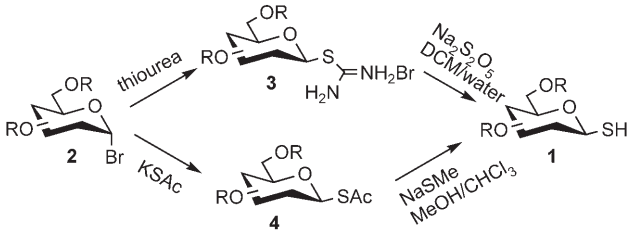

Scheme 1. Current approaches for the synthesis of glycosyl thiols. DCM = dichloromethane.

acetates under Lewis acidic conditions[17] and the Birch reduction of anomeric thiobenzyl.[18] Defaye et al. have described the preparation of glucosyl thiols from D-glucose typically in yields of $< 30\,\%$ by bubbling hydrogen sulfide into a solution of the deprotected sugar in hydrogen fluoride.[19] However, this procedure requires special precautions and generates a complex mixture of products.

We considered that a direct method of thiol formation in combination with Glyco–SeS[8] would allow a one-pot protein glycosylation method that could utilize sugars directly isolated from natural sources (Scheme 2).[20] With the goal of finding a more efficient strategy for the direct synthesis of glycosyl thiols, we speculated that a reagent that operated through a concerted Lewis acid activation and displacement might allow chemo- and regioselective thionation of C1 in the presence of other, perhaps unprotected, functionalities. However, to date, no such reagent or method exists. Such a C1-selective thionation might be considered mechanistically in two ways as shown in Scheme 3.

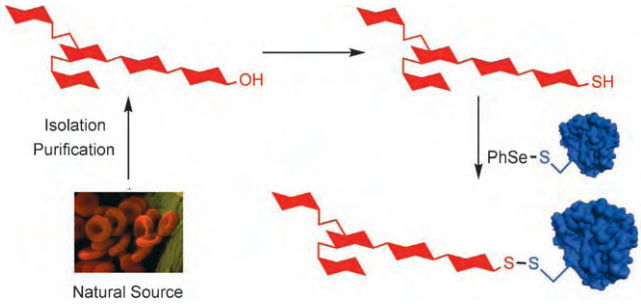

Scheme 2. One-pot protein glycosylation with reducing sugars isolated from natural sources.

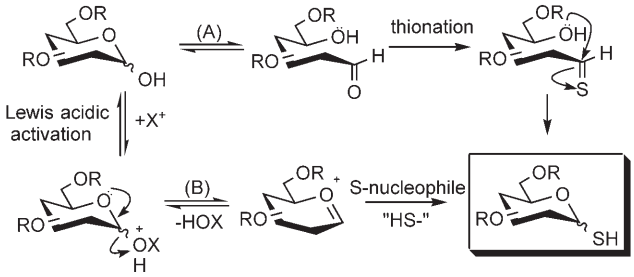

Scheme 3. Two possible mechanisms for the direct formation of glycosyl thiols from reducing sugars through path A) open chain or path B) an oxacarbenium ion intermediate.

The mechanism of Lawesson's reagent[21] (LR) suggests that it might service either pathway, acting potentially as both an oxaphilic electrophile and a sulphur source. This reagent has been extensively used for the efficient conversion of a wide variety of carbonyl functions into their corresponding thiocarbonyl functionalities.[22] Moreover, an earlier report had highlighted a rare single use of LR in the conversion of a benzylic alcohol into the corresponding thiol,[23] thereby suggesting potential utility in S_N1 or S_N1-like pathways. Therefore, owing to the enhanced reactivity of the anomeric hydroxy group in S_N1-like processes, it was thought that this

Table 1: Optimization of direct thionation reaction conditions.

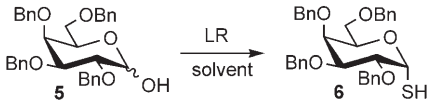

Entry	Equiv LR	T [°C]	t [h]	Solvent[a]	Yield [%]
1A	2	RT	48	dioxane	no reaction
1B	0.6	80	5	dioxane	56
1C	1.2	80	2.5	dioxane	83
1D	2	80	2	dioxane	58
1E	1.2	reflux	2	dioxane	84
1F	2	RT	48	toluene	no reaction
1G	0.6	80	5	toluene	54
1H	1.2	80	2.5	toluene	70
1I	1.2	reflux	2	toluene	75
1J	1.2	RT	48	acetonitrile	14
1K	0.6	80	5	acetonitrile	49
1L	1.2	80	2.5	acetonitrile	62

[a] Reactions conducted in anhydrous solvents (5 mL for a 200 mg scale reaction) and under an atmosphere of argon. Bn = benzyl.

© 2006 Wiley-VCH Verlag GmbH & Co. KGaA, Weinheim

procedure might proceed in an analogous fashion with sugar substrates. This approach appeared attractive for several reasons: 1) allowing direct formation of the anomeric thiosugars in one step from the corresponding anomeric alcohols; 2) application to differently protected and to unprotected sugars and 3) the possibility for direct site-selective glycosylation of proteins with sugars isolated from natural sources in just two steps and in one pot (Scheme 2).

Initial investigations (Table 1) used reducing sugar **5** as a test substrate. Encouragingly, a first attempt (Table 1, entry B) performed in anhydrous toluene at 80 °C by using 0.6 equivalents of LR for 5 h directly afforded thiogalactopyranose **6** in 54 % yield as a single α-anomer. Fortunately, 1-thiohexoses do not mutarotate under basic or neutral conditions.[24] Following this initial success, reaction conditions were optimized with respect to solvent system, temperature, reaction time, and equivalents of LR (Table 1). It was observed that prolonged reaction times and large excesses of LR were detrimental, resulting in the generation of numerous side products. Optimum conditions used anhydrous dioxane at 80 °C or above over a period of 2–3 h with 1.2 equivalents of LR affording **6** in a yield of 83–84 % (Table 1, entries C and E). Although yields in toluene were nearly comparable (Table 1, entry I), the use of more-polar dioxane opened up the exciting possibility of using deprotected sugars, which are not soluble in toluene or acetonitrile.

Next we explored the scope and limitations of this LR-mediated protocol (Table 2), demonstrating that this procedure is quite general and is applicable for the preparation of a variety of differently protected 1-thiosugars, including for the

Table 2: Direct formation of glycosyl thiols using Lawesson's reagent.[a]

Entry	Substrate[b]		T [°C]	t	Equiv LR	Glycosyl thiol		Yield[c]
1	see Table 1							
2	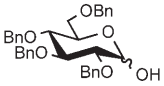	**7**	80	2.5 h	1.2	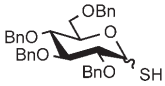	**8**	82 % α/β 2:1
3	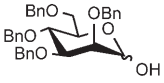	**9**	80	2 h	1.2	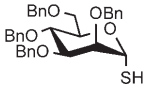	**10**	80 % α anomer only
4	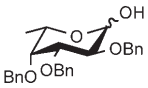	**11**	80	1 h	1.2	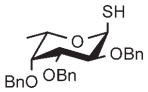	**12**	78 % α anomer only
5	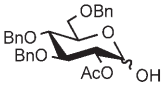	**13**	80	3 h	1.2	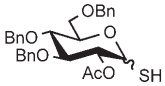	**14**	82 % α/β 1:5
6	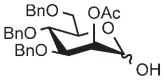	**15**	80	3 h	1.2	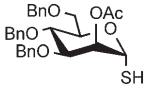	**16**	85 % α anomer only
7	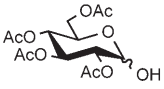	**17**	80 110 110	3 h 24 h 72 h	1.2 1.5 2	no product formed 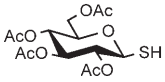	**18**	– 32 % (63 %) β anomer only 41 % (68 %) β anomer only
8	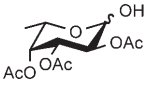	**19**	80 110	2.5 h 24 h	1.2 1.5	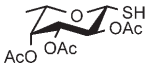	**20**	43 % (65 %) β anomer only 47 % (69 %) β anomer only
9	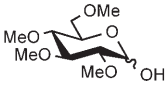	**21**	80	2.5 h	1	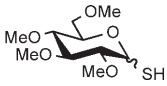	**22**	75 % α/β 2:5
10	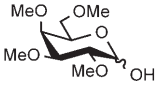	**23**	80	1 h	1	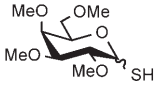	**24**	77 % α/β 2:1
11	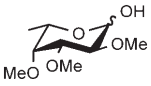	**25**	80	45 min	1	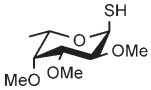	**26**	85 % α anomer only
12	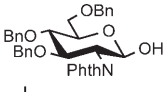	**27**	80	4.5 h	1.2	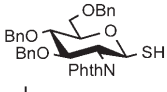	**28**	82 % β anomer only
13	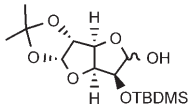	**29**	80	4 h	1.2	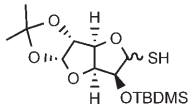	**30**	74 % 3:1

[a] Reactions conducted in anhydrous dioxane under an atmosphere of argon; see the Supporting Information for details. [b] All substrates were synthesized according to literature procedures; see the Supporting Information for details [c] Parentheses indicate yield based on recovered starting material. TBDMS = dimethyl-1,1-dimethylethyl-silyl, Phth = phthalimidyl.

 © 2006 Wiley-VCH Verlag GmbH & Co. KGaA, Weinheim

direct conversion of sugars fully protected with benzyl and methyl ether (78–85%). Partially *O*-benzyl-protected sugars with an *O*-acetyl function at C-2 were also converted to the corresponding glycosyl thiols in good yields (82–85%). Lower yields were observed on deactivated, so called disarmed,[25] systems such as acetylated sugars (41–43%); however, the starting material was largely recovered and could be recycled (yields based on recovered starting material 63–69%). Nitrogen functionality at C-2 in the form of phthalimide (Table 2, entry 12), and base and acid-labile protecting groups, such as silyl groups and acetonides (Table 2, entry 13), remained stable under the reaction conditions, thereby expanding the functional-group tolerance significantly.

Finally, application of this methodology to unprotected sugars was investigated (Table 3). The optimized conditions were applied to unprotected sugars, and after 48 h the formation of the desired thiol product and corresponding disulfide species was observed. Chromatographic separation of these from the LR decomposition products proved cumbersome and was exacerbated by further disulfide formation.[26] Two strategies were adopted to aid in isolation. First, an acetylation–deacetylation protocol afforded the corresponding glycosyl thiols **31a–c** in fair yields (Table 3). Alternatively, treatment with tributylphosphine (solution in

Table 3: Synthesis of glycosyl thiols from unprotected sugars.

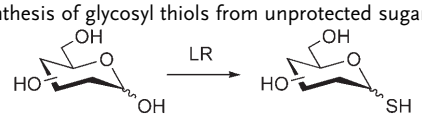

Entry	Substrate	product		Yield A[a]	Yield B[b]
1	Glc	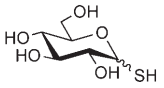	**31a**	61% α/β 1:9	71% α/β 1:6
2	Man	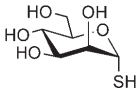	**31b**	48% α anomer	63% α anomer
3	Gal	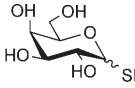	**31c**	58% α/β 1:8	70% α/β 1:4

[a] Protocol A: 1) LR (1.5 equiv), anhydrous dioxane, 110°C. 2) Ac_2O, pyridine. 3) NaOMe, MeOH. [b] Protocol B: 1) LR (1.5 equiv), anhydrous dioxane, 110°C. 2) Bu_3P, MeOH/$CHCl_3$; see the Supporting Information for full details.

Table 4: Two-step strategy for direct protein conjugation from deprotected reducing sugars through LR and Glyco–SeS.[8]

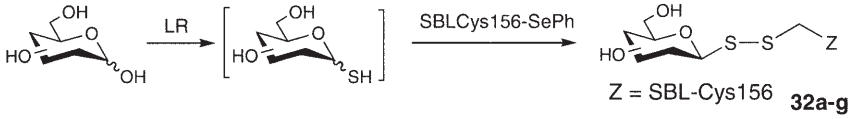

Sugar	Thiol product[a]	Protein product[b]		Conversion [%][c]	ESI-MS Found (calcd)
Glc	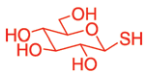	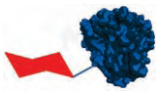	**32a**	>95	27066 (27064)
Man	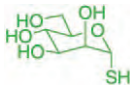	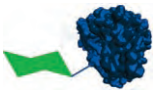	**32b**	>95	27064 (27064)
Gal	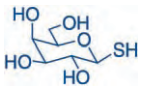		**32c**	>95	27064 (27064)
Lactose (Galβ1,4Glc)	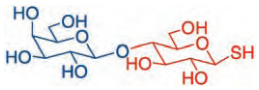		**32d**	>95	27234 (27225)
Maltopentaose ($Glc\alpha1,4)_4Glc$	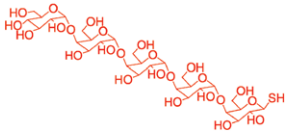		**32e**	>95	27722 (27711)
Galabiose (Gaα1,4Gal)	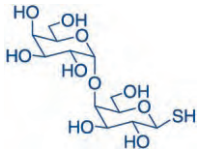		**32f**	>95	27224 (27225)
(Xylα1,3Glc)	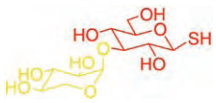		**32g**	>95	27194 (27194)

[a] Typically, LR (1.2 equiv) was added to a solution of the deprotected sugar in anhydrous dioxane and left to stir at 110°C for 48 h; see the Supporting Information for more details. [b] Typically, crude thiol (20–50 equiv), in water, was added to preactivated SBLS156C-SePh in CHES (70 mM), MES (5 mM), $CaCl_2$ (2 mM); pH 9.5. After 30 min at RT, the reaction was analyzed by LC–MS; [c] Conversion determined by ESI-MS.

© 2006 Wiley-VCH Verlag GmbH & Co. KGaA, Weinheim

$CHCl_3$/MeOH) reduced the resulting disulfides allowing the direct isolation of pure unprotected glycosyl thiols **31a–c** in 63–71% yields (Table 3). These results importantly demonstrated application to unprotected sugars providing a method to prepare glycosyl thiols suitable for protein glycosylation.

Following this key result, it was envisaged that our newly developed thionation procedure would offer a direct route from free sugars to glycoproteins by using our protein glycosylation strategy (Scheme 2). A variety of representative, free sugars (Table 4), including those isolated from N-(galabiose Galα1,4Gal)[27] and O-linked (Xylα1,3Glc) glycoproteins,[28] were treated with LR after the optimized conditions.[29] The subsequent addition of these sugars to a selenenylsulfide-activated single-cysteine mutant protein[8] (subtilisin *Bacillus lentus*, SBLS156C), gave complete conversion to the corresponding glycoproteins (Table 4).

In summary, we have established that Lawesson's reagent may be used in a direct and general manner for the preparation of glycosyl thiols from the corresponding anomeric lactols/reducing sugars. Notably, this procedure has also been shown to be fully compatible with unprotected sugars, the products of which can be directly used in our selenenylsulfide-mediated protein glycosylation strategy.[8] The result is a one-pot method for direct protein glycosylation. Further investigations into the use of LR are currently being explored by this laboratory.

Received: February 21, 2006
Published online: May 4, 2006

Keywords: carbohydrates · glycoproteins · glycosyl thiols · lawesson reagent · protein modifications

[1] a) A. Varki, *Glycobiology* **1993**, *3*, 97–130; b) R. A. Dwek, *Chem. Rev.* **1996**, *96*, 683–720; c) P. M. Rudd, T. Elliot, P. Cresswell, I. A. Wilson, R. A. Dwek, *Science* **2001**, *291*, 2370–2376; d) B. G. Davis, *Chem. Rev.* **2002**, *102*, 579–601; e) J. B. Lowe, J. D. Marth, *Annu. Rev. Biochem.* **2003**, *72*, 643–691; f) K. J. Doores, D. P. Gamblin, B. G. Davis, *Chem. Eur. J.* **2006**, *12*, 656–665.

[2] a) A. Helenius, M. Aebi, *Science* **2001**, *291*, 2364–2369; b) R. Kannagi, *Curr. Opin. Struct. Biol.* **2002**, *12*, 599–608.

[3] K. Nishiwaki, Y. Kubota, Y. Chigira, S. K. Roy, M. Suzuki, M. Schvarzstein, Y. Jigami, N. Hisamoto, K. Matsumoto, *Nat. Cell Biol.* **2004**, *6*, 31–37.

[4] J. B. Lowe, *Cell* **2001**, *104*, 809–812.

[5] a) B. G. Davis, R. C. Lloyd, J. B. Jones, *J. Org. Chem.* **1998**, *63*, 9614–9615; b) W. M. Macindoe, A. H. van Oijen, G.-J. Boons, *Chem. Commun.* **1998**, 847–848; c) B. G. Davis, M. A. T. Maughan, M. P. Green, A. Ullman, J. B. Jones, *Tetrahedron: Asymmetry* **2000**, *11*, 245–262; d) B. G. Davis, *Chem. Commun.* **2001**, 351–352; e) D. P. Gamblin, P. Garnier, S. J. Ward, N. J. Oldham, A. J. Fairbanks, B. G. Davis, *Org. Biomol. Chem.* **2003**, *1*, 3642–3644; f) G. M. Watt, J. Lund, M. Levens, V. S. K. Kolli, R. Jefferis, G.-J. Boons, *Chem. Biol.* **2003**, *10*, 807–814; g) P. M. Rendle, A. Seger, J. Rodrigues, N. J. Oldham, R. R. Bott, J. B. Jones, M. M. Cowan, B. G. Davis, *J. Am. Chem. Soc.* **2004**, *126*, 4750–4751; h) T. Hotchkiss, H. B. Kramer, K. J. Doores, D. P. Gamblin, N. J. Oldham, B. G. Davis, *Chem. Commun.* **2005**, 4264–4266.

[6] a) S. Knapp, D. S. Myers, *J. Org. Chem.* **2002**, *67*, 2995–2999; b) X. Zhu, K. Pachamuthu, R. R. Schmidt, *J. Org. Chem.* **2003**, *68*, 5641–5651; c) X. Zhu, R. R. Schmidt, *Chem. Eur. J.* **2004**, *10*, 875–887; d) D. A. Thayer, N. Y. Henry, M. C. Galan, C. H. Wong, *Angew. Chem.* **2005**, *117*, 4672–4675; *Angew. Chem. Int. Ed.* **2005**, *44*, 4596–4599.

[7] a) Y. Zhu, W. A. van der Donk, *Org. Lett.* **2001**, *3*, 1189–1192; b) Y. Zhu, M. D. Gieselman, H. Zhou, O. Averin, W. A. van der Wonk, *Org. Biomol. Chem.* **2003**, *1*, 3304–3315.

[8] D. P. Gamblin, P. Garnier, S. van Kasteren, N. J. Oldham, A. J. Fairbanks, B. G. Davis, *Angew. Chem.* **2004**, *116*, 846–851; *Angew. Chem. Int. Ed.* **2004**, *43*, 828–833.

[9] M. M. Ponpipom, W. K. Hagmann, L. A. O'Grady, J. J. Jackson, D. D. Wood, H. J. Zweerink, *J. Med. Chem.* **1990**, *33*, 861–867.

[10] P. J. Garegg, *Adv. Carbohydr. Chem. Biochem.* **1997**, *52*, 179–205.

[11] a) B. G. Davis, S. J. Ward, P. M. Rendle, *Chem. Commun.* **2001**, 189–190; b) E. J. Grayson, S. J. Ward, A. L. Hall, P. M. Rendle, D. P. Gamblin, A. S. Batsanov, B. G. Davis, *J. Org. Chem.* **2005**, *70*, 9740–9754.

[12] a) B. Capon, *Chem. Rev.* **1969**, *69*, 407–498; b) S. T. Crooke, R. M. Snyder, T. R. Butt, D. J. Ecker, H. S. Allaudeen, B. Monia, C. K. Mirabelli, *Biochem. Pharmacol.* **1986**, *35*, 3423–3431; c) M. Stallings-Mann, L. Jamieson, R. P. Regala, C. Weems, N. R. Murray, A. P. Fields, *Cancer Res.* **2006**, *66*, 1767–1774.

[13] a) Y. C. Lee, C. P. Stowell, M. J. Krantz, *Biochemistry* **1976**, *15*, 3956–3963; b) Y. C. Lee, C. P. Stowell, *Methods Enzymol.* **1982**, *83*, 278–288.

[14] J. M. MacDougall, X. D. Zhang, W. E. Polgar, T. V. Khroyan, L. Toll, J. R. Cashman, *J. Med. Chem.* **2004**, *47*, 5809–5815.

[15] a) B. D. Johnston, B. M. Pinto, *J. Org. Chem.* **2000**, *65*, 4607–4617; b) O. B. Wallace, D. M. Springer, *Tetrahedron Lett.* **1998**, *39*, 2693–2694.

[16] W. Koenigs, E. Knorr, *Ber. Dtsch. Chem. Ges.* **1901**, *34*, 957–981.

[17] F. M. Ibatulin, K. A. Shabalin, J. V. Jänis, A. G. Shavva, *Tetrahedron Lett.* **1998**, *39*, 7961–7964.

[18] S. A. Holick, L. Anderson, *Carbohydr. Res.* **1974**, *34*, 208–213.

[19] In one instance a yield of 67% was reported for this method. However the use of HF and H_2S requires special precautions and is not mild or convenient; see: J. Defaye, A. Gadelle, C. Pedersen, *Carbohydr. Res.* **1991**, *217*, 51–58.

[20] J. B. L. Damm, J. P. Kamerling, G. W. K. van Dedem, J. F. G. Vliegenthart, *Glycoconjugate J.* **1987**, *4*, 129–144.

[21] a) B. S. Pedersen, S. Scheibye, W. H. Nilson, S. -O. Lawesson, *Bull. Soc. Chim. Belg.* **1978**, *87*, 223–228; b) T. B. Rauchfuss, G. A. Zank, *Tetrahedron Lett.* **1986**, *27*, 3445–3448.

[22] a) M. P. Cava, M. I. Levinson, *Tetrahedron* **1985**, *41*, 5061–5087; b) M. Jesberger, T. P. Davis, L. Barner, *Synthesis* **2003**, 1929–1958.

[23] a) T. Nishio, *J. Chem. Soc. Chem. Commun.* **1989**, 205–206; b) T. Nishio, *J. Chem. Soc. Perkin Trans. 1* **1993**, 1113–1117.

[24] W. Schneider, H. Leonhardt, *Ber. Dtsch. Chem. Ges.* **1929**, *62*, 1384–1389.

[25] D. R. Mootoo, P. Konradsson, U. Udodong, B. Fraser-Reid, *J. Am. Chem. Soc.* **1988**, *110*, 5583–5584.

[26] Reaction of crude product with DMF and the use of activated carbon in an attempt to remove the excess of Lawesson's reagent failed.

[27] N. Susuki, K. H. Khoo, C. M. Chen, H. C. Chen, Y. C. Lee, *J. Biol. Chem.* **2003**, *278*, 46293–46246–46306.

[28] a) H. Nishimura, S. I. Kawabata, W. Kisiel, S. Hase, T. Itenaka, T. Takao, Y. Shimonishi, S. Iwanaga, *J. Biol. Chem.* **1989**, *264*, 20320–20325; b) K. Fukase, S. Hase, T. Itenaka, S. Kusumoto, *Bull. Chem. Soc. Jpn.* **1992**, *65*, 436–445.

[29] The crude thiol aldoses could be extracted after the reaction following partition between DCM and water.

 © 2006 Wiley-VCH Verlag GmbH & Co. KGaA, Weinheim

Allosteric Signal Transduction

DOI: 10.1002/anie.200504319

A Metal-Ion-Releasing Probe for DNA Detection by Catalytic Signal Amplification**

*Nora Graf, Mareike Göritz, and Roland Krämer**

Chemical and physical signals are very efficiently enhanced in biological systems and rapidly converted into a biochemical response by signal cascades which combine several signal transduction and catalytic amplification steps. Signal amplification by catalysis has been used in the development of highly sensitive analytical detection schemes. Many powerful assays rely on enzymatic amplification, for example, the widely applied heterogeneous ELISA test (enzyme-linked immunosorbent assay). The design of bioinspired amplification strategies involving chemical catalysts is an emerging research field.[1] An example is a chloride sensor in which the analyte is an allosteric[2] regulator and activates a synthetic catalyst.[3] In a sensing assay developed by Anslyn and co-workers,[4] a metal-ion analyte (the primary signal) interacts with a macrocyclic receptor by replacing another, bound-metal ion. The latter (the transduced signal) assembles as a cofactor with a precatalyst into the active, signal-amplifying organometallic catalyst.

Our new sensing concept relies on a unique allosteric transduction of the primary signal (a DNA oligonucleotide) into a metal-ion signal (Scheme 1). The metal ion functions as a cofactor and activates a chemical redox catalyst, which converts a nonfluorescent substrate into a fluorescent product. This approach is more flexible in so far as a structural similarity between the primary and transduced signals is no longer essential. The PCR-independent, amplified catalytic detection of nucleic acid sequences has recently gained considerable interest, with a focus on enzyme- and ribozyme-based techniques.[5]

The primary receptor in Scheme 1 is the 20 mer DNA **1** with 2,2′:6′,2″-terpyridine (tpy) attached to both termini (Scheme 2). The synthesis of **1** and 3′-mono(tpy)-DNA **2** is described elsewhere.[6]

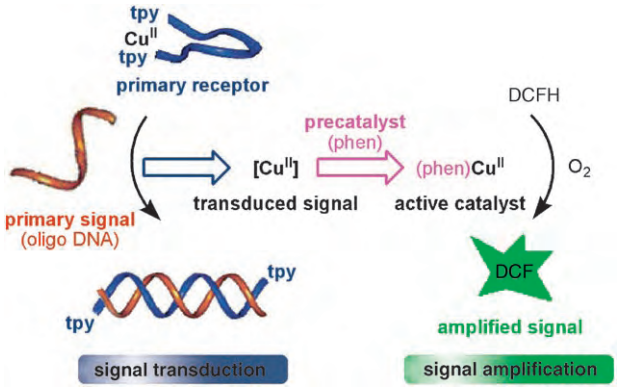

Scheme 1. Detection of DNA **3** (primary signal) by allosteric signal transduction and catalytic amplification with formation of the fluorescent dye DCF. See text for abbreviations.

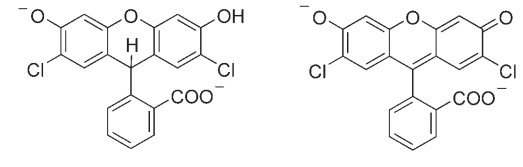

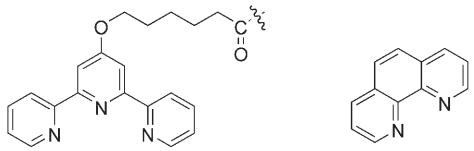

1: 5′-**tpy**d(ATCGTTACCAAAGCATCGTA)**tpy**
2: 5′-d(ATCGTTACCAAAGCATCGTA)**tpy**
3: 5′-d(TACGATGCTTTGGTAACGAT)
4: 5′-d(TACGATGCTTTGGTAA**T**GAT)

Scheme 2. Structures of DCFH, DCF, conjugated tpy, and phen. Sequences of oligonucleotide-terpyridine conjugates **1** and **2**, of complementary DNA **3** and mismatch DNA **4**.

Coordination of Cu^{II} ions by both terpyridine moieties in **1** is evident by UV spectrophotometric titration, a characteristic EPR signal ($g_{par} = 2.23$, $A_{par} = 156$ G), and destabilization of a hybrid of **1** with short complementary DNA (see the Supporting Information). Excess 1,10-phenanthroline (phen), a high-affinity Cu^{II} chelator (complex formation constant $\log K = 9.2$[7] for [Cu^{II}(phen)] versus $\log K = 9.1$ for [Cu^{II}(tpy)][8]), does not extract the metal ion from the copper(II) complex of **1**. However, the intensity of the UV band at 320 nm of the copper(II)-coordinated tpy decreases spontaneously when complementary 20 mer-DNA **3** is added to the **1**-Cu/phen mixture (see the Supporting Information), and after one minute no further changes in absorbance are observed. Apparently, formation of the rigid **1**:**3** DNA double helix disrupts intramolecular bis(chelation) and destabilizes the **1**–Cu interaction.

The catalytic module of the nucleic acid detection assay comprises the bidentate chelator and precatalyst 1,10-phenanthroline (phen), its cofactor copper(II), the nonfluorescent substrate 2′,7′-dichlorodihydrofluorescein (DCFH), dioxygen from air as an oxidant, and cysteamine ($H_2NCH_2CH_2SH$) as a reducing cosubstrate. A plausible pathway for the formation

[*] N. Graf, Dr. M. Göritz, Prof. Dr. R. Krämer
Anorganisch-Chemisches Institut
Universität Heidelberg
Im Neuenheimer Feld 270, 69120 Heidelberg (Germany)
Fax: (+49) 6221-54-8599
E-mail: roland.kraemer@urz.uni-heidelberg.de

[**] N.G. and M.G. thank Baden-Württemberg for financial support (Landesgraduiertenstipendien). These authors contributed equally to this work.

Supporting information for this article is available on the WWW under http://www.angewandte.org or from the author.

© 2006 Wiley-VCH Verlag GmbH & Co. KGaA, Weinheim

of the fluorescent product 2′,7′-dichlorofluorescein (DCF) includes the [Cu(phen)]-promoted generation of H_2O_2 from cysteamine and O_2, followed by [Cu(phen)]-catalyzed H_2O_2 oxidation of DCFH to DCF.[9] Although it is likely that this reaction also involves the formation of OH radicals or other aggressive oxygen species,[10] no significant cleavage of oligo-DNA is detectable by HPLC under assay conditions (see the Supporting Information). We suggest that DCFH functions as an antioxidant and protects DNA from degradation. DCFH has been used as a fluorogenic probe to monitor the concentration of reactive oxygen species in living cells.[11]

Formation of the product DCF was monitored by following the increase in the relative fluorescence intensity at 523 nm with time (dI_{rel}/dt). Figure 1a illustrates the sequence selectivity, and Figure 1b the sensitivity of the assay. Reagent concentrations were optimized for a high signal-to-background ratio.

Although oxidation of DCFH by **1**-Cu in the presence of excess phen is very slow, the rate increases dramatically in the presence of complementary DNA **3**. The activity is about two thirds that of a "DNA-free" phen/Cu^{II} mixture, thus indicating formation of the active [Cu(phen)] catalyst.[12] In contrast to **1**-Cu, a **2**/Cu/phen mixture displays significant catalytic activity in the absence of complementary DNA (Figure 1a). This observation indicates facile extraction of Cu^{II} ions from the complex with mono(tpy)-DNA **2** and confirms the significant stabilization of **1**-Cu by intramolecular bischelation. The method is sensitive to single base mismatches: the rate of DCF formation in the presence of DNA **4** (C/T mismatch) is only slightly above the background level. At a low concentration of **1**-Cu, complementary DNA **3** is detectable at 5 nM (250 fmol; Figure 1b).

After 12 h reaction time, the fluorescence of the **1**+**3** mixture (Figure 1a) can even be detected by the naked eye (Figure 2). Turnover numbers of 20 and 5 have been determined relative to copper(II) and analyte DNA **3**, respectively.

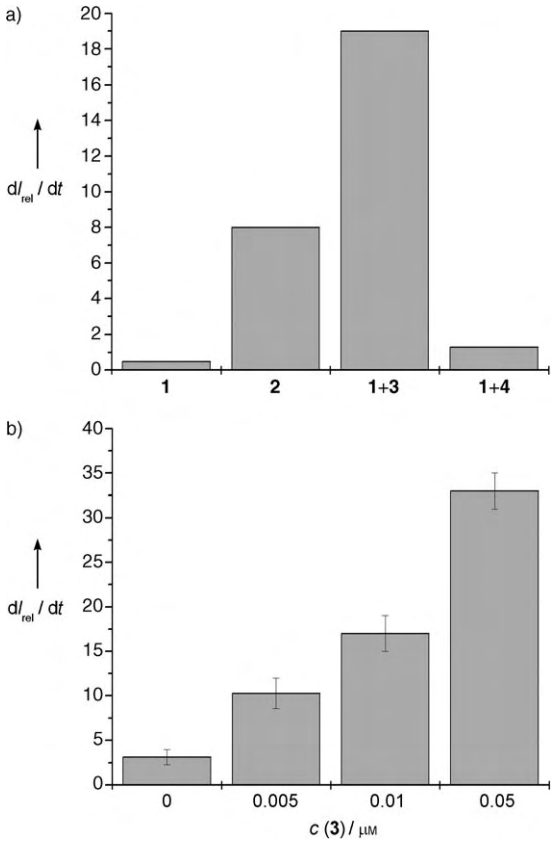

Figure 1. Increase in the relative fluorescence intensity from the initial level (0–10 min) with time (dI_{rel}/dt, $\lambda_{ex}=503$ nm, $\lambda_{em}=523$ nm): pH 7 (10 mM 3-(*N*-morpholino)propanesulfonic acid (MOPS) buffer) 25 °C, DCFH (10 μM), cysteamine (100 μM), NaCl (0.1 M) as well as a) 5 μM phen, 0.5 μM $CuSO_4$, and 2 μM of the indicated DNA oligonucleotide(s) or b) 0.2 μM phen, 0.02 μM $CuSO_4$, 0.05 μM **1**, and various amounts of **3**.

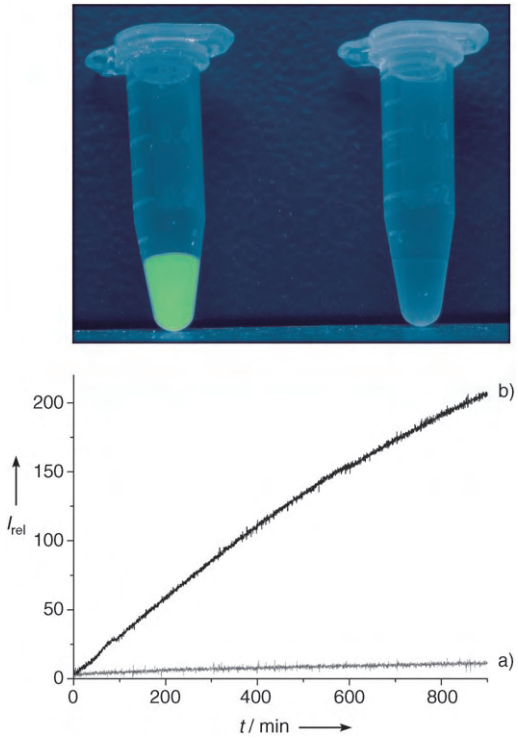

Figure 2. Top: Reaction solutions containing DNA **1** (right) and **1**+**3** (left) under UV light after 12 h (for the conditions see Figure 1a). Bottom: Increase in the relative fluorescence intensity with time: a) DNA **1**, b) DNA **1**+**3**.

Our prototypical DNA sensor does not approach the low detection limits of some reported systems[5a–e] since the sensitivity is limited to the nanomolar range by uncatalyzed background oxidation of the fluorogenic substrate DCFH. In addition, the low catalytic turnover rate ($2\ h^{-1}$) limits the efficiency of the signal amplification. The catalytic module must be optimized to achieve better sensitivity and more effective amplification. The signal-to-background ratio could be slightly improved from 3:1 to 5:1 at lowest target DNA concentrations when the precatalyst phen was replaced by 5-amino-1,10-phenanthroline. We are currently exploring alternative chemical and biochemical catalytic systems, such as the activation of apoenzymes by their metal-ion cofactors.

 © 2006 Wiley-VCH Verlag GmbH & Co. KGaA, Weinheim

In conclusion we have described a homogeneous-phase chemical method for DNA detection which combines an allosteric signal transduction with a catalytic amplification step. The system resembles the initial steps of biological signal cascades such as hormone action. For example, the primary chemical signal adrenaline is (in a simplified scheme) allosterically transduced by a membrane receptor, thus resulting in the activation and release of receptor-associated G protein. The latter then combines with adenylate cyclase and activates this enzyme for catalytic generation of cAMP from ATP. Such biological cascades can be a source of inspiration for the design of artificial, modular detection systems which amplify chemical signals strongly and rapidly.

Received: December 5, 2005
Revised: February 24, 2006
Published online: May 9, 2006

Keywords: allostery · copper · DNA · fluorescence · signal amplification

[1] L. Zhu, E. V. Anslyn, *Angew. Chem.* **2006**, *118*, 1208 – 1215; *Angew. Chem. Int. Ed.* **2006**, *45*, 1190 – 1196.
[2] For a comprehensive overview on synthetic allosteric receptors and catalysts, see: L. Kovbasyuk, R. Krämer, *Chem. Rev.* **2004**, *104*, 3161 – 3187.
[3] N. C. Gianneschi, S. T. Nguyen, C. A. Mirkin, *J. Am. Chem. Soc.* **2005**, *127*, 1644 – 1645.
[4] Q. Wu, E. V. Anslyn, *J. Am. Chem. Soc.* **2004**, *126*, 14682 – 14683; see also L. Zhu, V. M. Lynch, E. V. Anslyn, *Tetrahedron* **2004**, *60*, 7267 – 7275.
[5] Heterogeneous enzyme-based methods: a) F. Patolsky, Y. Weizmann, I. Willner, *J. Am. Chem. Soc.* **2002**, *124*, 770 – 772; b) F. Patolsky, E. Katz, I. Willner, *Angew. Chem.* **2002**, *114*, 3548 – 3552; *Angew. Chem. Int. Ed.* **2002**, *41*, 3398 – 3402; c) T. Niazov, V. Pavlov, Y. Xiao, R. Gill, I. Willner, *Nano Lett.* **2004**, *4*, 1683 – 1687; d) F. Patolysky, R. Gill, Y. Weizmann, T. Mokari, U. Banin, I. Willner, *J. Am. Chem. Soc.* **2003**, *125*, 13918 – 13919; homogeneous enzyme-based methods: e) A. Saghatelian, K. M. Guckian, D. A. Thayer, M. R. Ghadiri, *J. Am. Chem. Soc.* **2003**, *125*, 344 – 345; f) V. Pavlov, B. Shlyahovsky, I. Willner, *J. Am. Chem. Soc.* **2005**, *127*, 6522 – 6523; g) P. Simon, C. Dueymes, M. Fontecave, J.-L. Décout, *Angew. Chem.* **2005**, *117*, 2824 – 2827; *Angew. Chem. Int. Ed.* **2005**, *44*, 2764 – 2767; Ribozyme-based: h) M. N. Stojanovic, P. de Prada, D. W. Landry, *ChemBioChem* **2001**, *2*, 411 – 415; i) S. Sando, T. Sasaki, K. Kanatani, Y. Aoyama, *J. Am. Chem. Soc.* **2003**, *125*, 15720 – 15721; j) J. S. Hartig, I. Gruene, S. H. Najafi-Shoushtari, M. Famulok, *J. Am. Chem. Soc.* **2004**, *126*, 722 – 723; k) S. Sando, A. Narita, K. Abe, Y. Aoyama, *J. Am. Chem. Soc.* **2005**, *127*, 5300 – 5301; catalysis templated by nucleic acids: l) Z. Ma, J. S. Taylor, *Proc. Natl. Acad. Sci. USA* **2000**, *97*, 11159 – 11163; m) J. Brunner, A. Mokhir, R. Krämer, *J. Am. Chem. Soc.* **2003**, *125*, 12410 – 12411.
[6] M. Göritz, R. Krämer, *J. Am. Chem. Soc.* **2005**, *127*, 18016 – 18017.
[7] P. Mitchell, H. Sigel, *J. Am. Chem. Soc.* **1978**, *100*, 1564 – 1570.
[8] A. Odani, H. Masuda, K. Inukai, O. Yamauchi, *J. Am. Chem. Soc.* **1992**, *114*, 6294 – 6300.
[9] Copper-promoted formation of H_2O_2 from O_2 and cysteamine: T. Kamidate, I. Kuniya, T. Segawa, H. Watanabe, *Chem. Lett.* **1992**, 887 – 890. Copper-catalyzed oxidation of DCFH to DCF in the presence of O_2 and reducing agents: D. E. Ryan, J. Holzbecher, *Int. J. Environ. Anal. Chem.* **1971**, *1*, 159 – 168. Both reaction types show a complicated dependence of rate on the copper concentration. We found that phen/copper(II) is a much more efficient catalyst than free copper(II) ions for the oxidation of DCFH.
[10] D. S. Sigman, D. R. Graham, V. D'Aurora, A. M. Stern, *J. Biol. Chem.* **1979**, *254*, 12269 – 12272; B. C. Bales, T. Kodama, Y. N. Weledji, M. Pitié, B. Meunier, M. M. Greenberg, *Nucleic Acids Res.* **2005**, *33*, 5371 – 5379.
[11] See for example: S. L. Hempel, G. R. Buettner, Y. Q. O'Malley, D. A. Wessels, D. M. Flaherty, *Free Radical Biol. Med.* **1999**, *27*, 146 – 159.
[12] For simplicity, we denote the active species [Cu(phen)], although both [Cu(phen)] and $[Cu(phen)_2]$ are expected to form and catalyze the oxidation of DCFH (see the Supporting Information). The catalytic activities of the in situ prepared complexes $[Cu(tpy)_2]$ and [Cu(tpy)] are negligible. A 1:1:1 mixture of tpy, phen, and Cu^{II} in the absence of any DNA has only 10% of the activity of a 1:1 phen/Cu mixture under the reaction conditions indicated for Figure 1a.

 © 2006 Wiley-VCH Verlag GmbH & Co. KGaA, Weinheim

Strained Molecules

DOI: 10.1002/anie.200600483

Synthesis and Reactions of Highly Strained 2,3-Bridged 2*H*-Azirines**

Klaus Banert and Barbara Meier*

Strained compounds are of special interest because of their increased energy content and the enhanced reactivity that frequently results from this. The already considerable ring strain of simple cyclopropenes (ca. 54 kcal mol^{-1}) is significantly increased if the three-membered ring is incorporated into the bicyclic framework **1** (Scheme 1).[1] It should be possible to transfer this concept from the hydrocarbons **1** to the heterocycles **3**.[2,3] The 2,3-bridged azirine **3d**, which is easily obtainable from azide **2d** by photolysis or thermolysis, can be distilled in vacuo,[4] whereas the more unstable compound **4** could be characterized only in solution.[5] Until now, the even more strained azirine **3b** and many similar bridged azirines bearing a six-membered ring can be generated only in situ and detected by trapping reactions.[4a,6] Thus,

[*] Prof. Dr. K. Banert, Dr. B. Meier
Lehrstuhl für Organische Chemie
Technische Universität Chemnitz
Strasse der Nationen 62, 09111 Chemnitz (Germany)
Fax: (+49) 371-531-1839
E-mail: klaus.banert@chemie.tu-chemnitz.de

[**] Reactions of Unsaturated Azides, Part 19. This work was supported by the Fonds der Chemischen Industrie. We thank Dr. M. Hagedorn, Dr. F. Köhler, and Dr. J. Lehmann for support with spectroscopic investigations. Part 18: J. R. Fotsing, M. Hagedorn, K. Banert, *Tetrahedron* **2005**, *61*, 8904–8909.

Supporting information for this article is available on the WWW under http://www.angewandte.org or from the author.

© 2006 Wiley-VCH Verlag GmbH & Co. KGaA, Weinheim

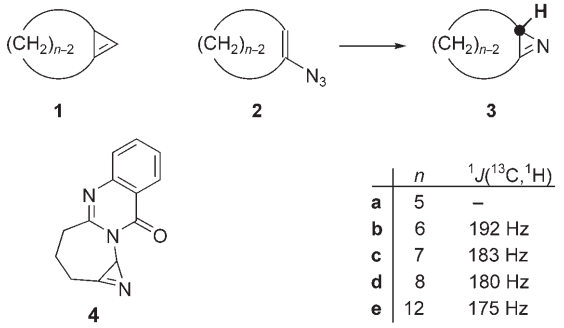

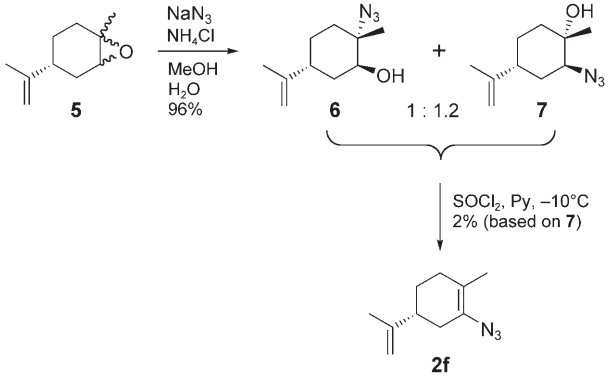

Scheme 1.

the prospect of spectroscopically characterizing **3b** in solution appears to be gloomy, especially as the ^{1}H NMR data of the analogous short-lived hydrocarbon **1b** were obtained even at −90 °C only partially.[7]

We now report the heterocycles **3b**, **3c**, **3e**, **3f**, and **3h–j** (Table 2), which have been analyzed spectroscopically for the first time, as well as some further 2,3-bridged azirines. The highly strained title compounds undergo several addition and cycloaddition reactions that are not possible for simple 2*H*-azirines.[2]

To produce the corresponding azirines, we prepared first the necessary vinyl azides[8] **2c**,[9] **2d**,[4b,c] and **2e**[9] by using Hassner's method,[10] that is, by electrophilic addition of iodine azide, generated in situ, to cycloalkenes followed by base-induced elimination of hydrogen iodide. In the case of five- and six-membered rings, it is well-known[4b,c,11–13] that this method does not lead to vinyl azides, but rather to allyl azides. Thus, we switched over to Zbiral's[11b] sequence for the synthesis of **2a** and **2b**. Neither route was successful in the synthesis of 1-azido-2-methylcycloalkenes such as **2f**, **2g**, and **2h** (Scheme 2). The dehydration with thionyl chloride of a mixture of the regioisomeric azidoalcohols **6**[14] and **7**,[14] which could be easily synthesized from the inexpensive limonene oxide **5**, was problematic and led only to a very low yield of **2f**. However, the formal addition of iodine azide to 1-methylcycloalkenes **8g**,**h** assisted by cerium(IV) ammonium nitrate (CAN)[15] and the subsequent treatment of **9g**,**h** with potassium *tert*-butylate gave somewhat better yields of the desired vinyl azides **2g**,**h**.

When a solution of the azide **2b** in anhydrous $CDCl_3$ or [D_8]toluene was irradiated at −50 °C with a mercury high-pressure lamp, surprisingly the bridgehead azirine **3b** could be detected even at room temperature by its IR as well as ^{1}H NMR and ^{13}C NMR data (Table 1).[16] However, a rapid subsequent reaction led to the formation of the dimer **11b**, and this product was quickly oxidized to **12b** when oxygen was not excluded rigorously (Table 2).[17] Addition of tetrachloro-1,4-benzoquinone caused instantaneous transformation of **11b** to **12b**. If photolysis of **2b** is performed in $CDCl_3$ or [D_8]toluene saturated with water, the dimerization **3b**→**11b** is accelerated so strongly that the intermediate **3b** can no longer be observed by NMR spectroscopy. We assume that even traces of water act as a catalyst and initiate the reaction sequence shown in Scheme 3. The less strained bridgehead azirine **3c** dimerizes considerably slower than **3b** (3 months,

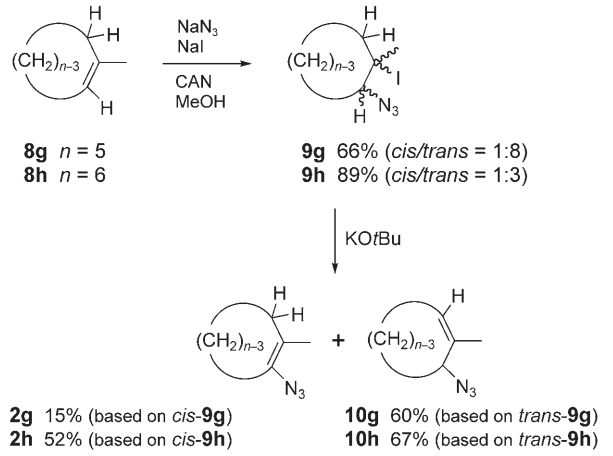

Scheme 2.

Table 1: Selected physical data of 2,3-bridged 2*H*-azirines **3b** and **3c**.[a]

3b: IR ($CDCl_3$): $\tilde{\nu}$ = 1743 cm^{-1} (C=N); ^{1}H-NMR ($CDCl_3$, −40 °C): δ = 1.01 (ddddd, ^2J = 14.0, ^3J = 9.9, 8.9, 4.7, 2.6 Hz, 1 H, 4-H$_{endo}$), 1.28 (ddddd, ^2J = 14.7, ^3J = 5.5, 4.7, ^4J = 1.1, ^3J = 0.6 Hz, 1 H, 5-H$_{endo}$), 1.41 (ddddd, ^2J = 14.0, ^3J = 7.3, 5.5, 5.0, 2.6 Hz, 1 H, 4-H$_{exo}$), 1.54 (dddddd, ^2J = 12.6, 7.3, 6.9, 5.0, 2.6, ^4J = 1.1 Hz, 1 H, 3-H$_{endo}$), 1.64 (dddd, ^2J = 14.7, ^3J = 8.9, 5.0, 3.8, 1 H, 5-H$_{exo}$), 1.82 (ddddd, ^2J = 12.6, ^3J = 9.9, 7.6, 7.1, 2.6 Hz, 1 H, 3-H$_{exo}$), 2.28 (dd, ^3J = 3.8, 0.6 Hz, 1 H, 6-H), 2.84 (ddd, ^2J = 12.7, ^3J = 7.1, 6.9 Hz, 1 H, 2-H$_{exo}$), 3.24 ppm (ddd, ^2J = 12.7, ^3J = 7.6, 5.0 Hz, 1 H, 2-H$_{endo}$); ^{13}C-NMR ($CDCl_3$, −40 °C): δ = 21.39 (t, C-4), 23.85 (t, C-3), 25.96 (d, $^1J_{C,H} \approx$ 192 Hz, C-6), 27.27 (t, C-2), 28.33 (t, C-5), 179.04 ppm (s, C-1).

3c: Colorless liquid; IR ($CDCl_3$): $\tilde{\nu}$ = 1764 cm^{-1} (C=N); ^{1}H NMR ($CDCl_3$): δ = 0.87 (m, 1 H), 1.27 (m, 1 H), 1.41 (m, 1 H), 1.54 (m, 1 H), 1.66–1.76 (m, 3 H), 2.07 (m, 1 H), 2.13 (m, 1 H), 2.79 (m, 1 H, 2-H), 3.00 ppm (m, 1 H, 2-H); ^{13}C NMR ($CDCl_3$): δ = 26.37 (t), 27.46 (t), 27.82 (t), 28.02 (t), 28.96 (d, $^1J_{C,H}$ = 183 Hz C-7), 31.53 (t), 175.35 ppm (s, C-1).

[a] The data of the other bridgehead azirines and those of other new compounds are summarized in the Supporting Information. ^{1}H NMR: 300 MHz, ^{13}C NMR: 75 MHz. The assignment of NMR signals and the measurement of coupling constants were performed with the help of ^{1}H,^{1}H double-resonance experiments, ^{1}H NMR NOE difference spectra, ^{1}H,^{1}H COSY experiments, ^{13}C,^{1}H shift correlations, DEPT135, GATED, and 2D *J*-resolved experiments, as well as spectrum simulation in the case of **3b**. The vicinal coupling constants found for **3b** correlate with the H-C-C-H torsion angles, which were calculated semiempirically (MOPAC), with the Karplus relationship.

 © 2006 Wiley-VCH Verlag GmbH & Co. KGaA, Weinheim

Table 2: Generation and successive reactions of 2,3-bridged 2*H*-azirines **3**.

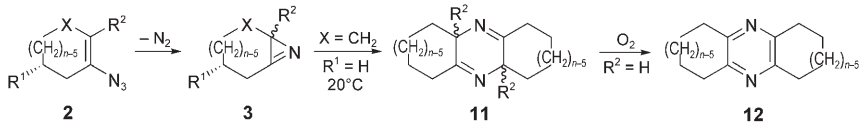

2 **3** **11** **12**

	Substrate **2**				Yield[a] of **3** [%] after photolysis	Yield[a] of **3** [%] after thermolysis	Yield of **11** [%]	Yield[a] of **12** [%]
	n	R^1	R^2	X				
2a	5	H	H	CH_2	0 ($CDCl_2F$, −120 °C)	n.i.[b]	n.d.[b]	45[c]
2b	6	H	H	CH_2	83 ($CDCl_3$, −50 °C)	0 ($CDCl_3$, 80 °C)	n.m.[b]	49[d]
2c	7	H	H	CH_2	91 ($CDCl_3$, −50 °C)	85 ($CDCl_3$, 80 °C)	n.d.	54[d]
2e[e]	12	H	H	CH_2	100 ($CDCl_3$, −50 °C)	96 ($CDCl_3$, 80 °C)	0	0
2f	6	$CMe=CH_2$	Me	CH_2	94[f] ($CDCl_3$, −50 °C)	n.i.	n.i.	–
2g	5	H	Me	CH_2	0 (CD_2Cl_2, −80 °C)	n.i.	65[c,g,h]	–
2h	6	H	Me	CH_2	85 ($CDCl_3$, −50 °C)	n.i.	52[a,d,i]	–
2i	6	H	H	C=O	22[j] (CD_2Cl_2, −80 °C)	n.i.	0	0
2j	6	H	Me	C=O	65 ($CDCl_3$, −50 °C)	n.i.	0	–

[a] Yield based on ^{1}H NMR standard. [b] n.i. = reaction not investigated, n.d. = compound not detected because of rapid oxidation to **12**, n.m. = yield not measured. [c] Yield based on azide **2**. [d] Yield based on azirine **3**. [e] Mixture of (*Z*)-**2e**/(*E*)-**2e** = 2.5:1. [f] 1:1 mixture of diastereomers. [g] Yield based on isolated products. [h] Mixture of diastereomers (60:40). [i] Mixture of diastereomers (ca. 5:1). [j] 47% **2i** was recovered; prolonged irradiation led to destruction of **3i**.

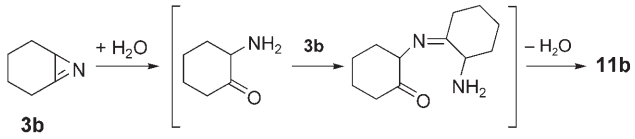

Scheme 3.

20 °C, 54% yield of **12c**). Moreover, we were not able to observe the corresponding reaction of **3e**. The azirines **3i**,**j** generated from azides **2i**,**j**[6f,g] did not form pyrazines analogous to **11** and **12**, but decomposed by unknown subsequent reactions.

The significantly increased ring strain for **3b** relative to **3c** is demonstrated by the $^1J(^{13}C,^1H)$ NMR coupling constants of the C–H unit at the bridgehead (Scheme 1). Consequently, **3b** is distinctly more reactive than the azirine **3c**, which can also be observed, similarly to **3e**, after thermolysis in solution (Table 2) and which can be isolated after flash vacuum pyrolysis (300 °C, 2×10^{-4} Torr) in 78% yield. In contrast, it was not possible to remove the solvent from a solution of photochemically generated **3b** without complete destruction. Furthermore, no trace of **3b** could be detected by monitoring the thermolysis of a solution of **2b** in chloroform or cyclohexane by NMR spectroscopy,[16] whereas flash vacuum pyrolysis led to low yields of **3b**. Comparison of the properties of **3b** with those of **3h** and of **3i** with those of **3j** shows that an additional methyl group at the bridgehead increases the kinetical stability of the azirines significantly.

Our attempts to detect azirines bridged by a five-membered ring, such as **3a**, **3g**, or **3k**, by spectroscopy directly led at best to strongly broadened NMR signals of the starting materials even after irradiation and measurement at low temperatures (Table 2 and Scheme 4). Nevertheless, the photolyzed solutions yielded definite products after thawing. The azides **2a** and **2g** gave the pyrazine derivatives **12a** and **11g**, respectively (Table 2), and we were able to isolate the nitrile **15k** as well as the azo compound **16k** after photolysis of **2k** and workup by chromatography (Scheme 4). The diradical intermediates shown in Scheme 4 could possibly play a role in the formation of **15k** and **16k**; thus, the difficulties in detecting azirine **3k** by NMR spectroscopy may result not only from its short lifetime.

As a result of their increased ring strain, 2,3-bridged azirines such as **3b**, **3c**, and **3h** can undergo addition and cycloaddition reactions that are not possible for simple 2*H*-azirines. Whereas alkyl- or aryl-substituted azirines do not react with cyclopentadiene,[2b] the corresponding Diels–Alder reactions of **3b** and **3c**

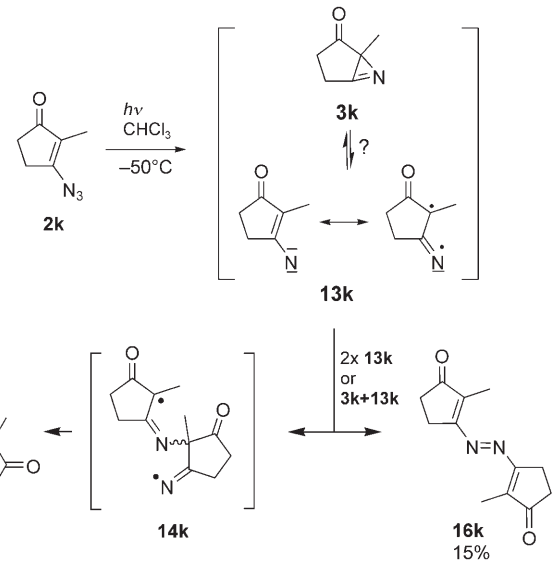

Scheme 4.

were successful under mild conditions (1 h, −50 °C for **17b** and 4 days, 20 °C for **17c**, Scheme 5). Of the four imaginable diastereomeric [4+2] cycloadducts (*exo,exo*; *endo,exo*; *exo,endo*; *endo,endo*), we isolated always the *exo,endo* stereoisomer **17**, which has the cyclopentadiene added to the *exo* side of the bridgehead azirine to form a 5-azanorbornene with an attached three-membered ring in the *endo* position. The addition of hydrogen cyanide to the highly strained azirines takes place already at −50 °C and leads to good yields of the aziridines **18b**,**c**,**h**. The less strained 2,3-bridged heterocycle **3e** does not undergo addition of hydrogen cyanide even after 7 days at 90 °C.[18] However, the photolysis of the azide **2l**[19] in the presence of hydrogen cyanide can be used to gain evidence for the highly strained

 © 2006 Wiley-VCH Verlag GmbH & Co. KGaA, Weinheim

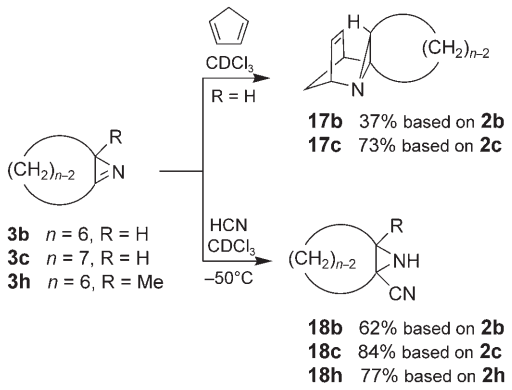

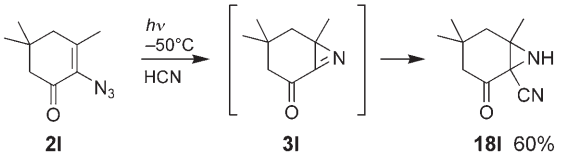

Scheme 5.

bridgehead azirine **3l**, which is not detectable by NMR spectroscopy. The trapping product **18l** proves the particularly short-lived intermediate **3l**, in which the azirine unit is further destabilized by the electron-withdrawing carbonyl group.

The reaction of simple 2*H*-azirines with diazo compounds to give allyl azides via 1,2,3-triazabicyclo[3.1.0]hex-2-enes (compared with **19** in Table 3) has been known for more than forty years.[20] The 1,3-dipolar cycloaddition of the starting materials proceeds relatively slowly at room temperature relative to the fragmentation of the postulated intermediate to yield the final products. Hence, short-lived 1,2,3-triazabicyclo[3.1.0]hex-2-enes, which were also discussed as intermediates of the rearrangement of allyl azides,[21] could not be proved spectroscopically until now.

Table 3: Treatment of 2,3-bridged 2*H*-azirines with diazomethane.

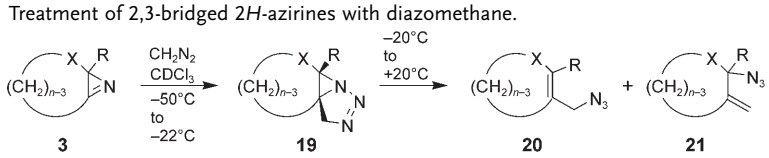

	Substrate **3**			Max. yield[a] of **19** [%]	Yield[a,b] of **20** + **21** [%]	Initial ratio **20**/**21**[c]	**20**/**21** after equilibration
	n	R	X				
3b	6	H	CH_2	89	89	4:1 (−20 °C)	4:1
3c	7	H	CH_2	97	84 (62)[d]	1:1 (−20 °C)	2:1
3d	8	H	CH_2	< 8	96 (78)[d]	2:1 (0 °C)	5:1
3j	6	Me	C=O	86	85 (37)[d]	1:0 (−20 °C)	1:0

[a] Yield based on ^{1}H NMR standard. [b] Yield based on **3**. [c] At low temperature. [d] Values in brackets correspond to the yields of isolated products **20** + **21** based on the precursor **2**.

At −50 °C, the highly strained bridgehead azirines **3b** and **3j** react instantaneously with diazomethane by *exo* addition to give the tricyclic compounds **19b** and **19j**, respectively (Table 3). These tricyclic compounds, as well as **19c**, could be characterized by their ^{1}H and ^{13}C NMR data. The analogous transformations of **3c** or the less reactive azirine **3d** required 1 h at −40 °C and 4 days at −22 °C, respectively. The intermediates **19** decomposed already at −20 °C to yield the allyl azides[22] **20** and **21**, hence **19d** especially was always present only in small proportions. We observed that at low temperatures, at which the rearrangement of allyl azides (equilibration of **20** and **21**) had not yet begun, **20b–d** as well as **21b–d** formed from **19b–d**. Consequently, **19** reacts not only by cleavage of the two C–N bonds of the three-membered ring, but also by cycloreversion of the five-membered ring.

Highly strained 2,3-bridged 2*H*-azirines can also be converted in the presence of ketenes, acyl isocyanates, or nitrile oxides. We will report on these remarkable reactions elsewhere.

Received: February 6, 2006
Revised: March 10, 2006
Published online: May 9, 2006

Keywords: azides · cycloaddition · dimerization · nitrogen heterocycles · strained molecules

[1] W. E. Billups, M. M. Haley, G.-A. Lee, *Chem. Rev.* **1989**, *89*, 1147–1159.
[2] Reviews on 2*H*-azirines: a) J. Backes in *Houben-Weyl*, *Vol. E16c* (Ed.: D. Klamann), Thieme, Stuttgart, **1992**, pp. 321–369; b) V. Nair in *The Chemistry of Heterocyclic Compounds, Small-Ring Heterocycles*, *Vol. 42*, *Part 1* (Ed.: A. Hassner), Wiley, New York, **1983**, pp. 215–332; c) W. H. Pearson, B. W. Lian, S. C. Bergmeier in *Comprehensive Heterocyclic Chemistry II*, *Vol. 1A* (Ed.: A. Padwa), Pergamon, New York, **1996**, pp. 1–60; d) F. Palacios, A. N. Ochoa de Retana, E. Martinez de Marigorta, J. M. de los Santos, *Eur. J. Org. Chem.* **2001**, 2401–2414; e) T. L. Gilchrist, *Aldrichimica Acta* **2001**, *34*, 51–55; f) K. M. L. Rai, A. Hassner in *Advances in Strained and Interesting Organic Molecules*, *Vol. 8* (Ed.: B. Halton), Jai, Greenwich, **2000**, pp. 187–257.
[3] For the ring strain in 2*H*-azirines, see: E.-U. Würthwein, T. Hergenröther, H. Quast, *Eur. J. Org. Chem.* **2002**, 1750–1755.
[4] a) A. Hassner, F. W. Fowler, *J. Am. Chem. Soc.* **1968**, *90*, 2869–2875; b) A. Hassner, F. W. Fowler, *Tetrahedron Lett.* **1967**, *8*, 1545–1548; c) B. Rose, D. Schollmeyer, H. Meier, *Liebigs Ann.* **1997**, 409–412.
[5] R. S. Atkinson, M. J. Grimshire, *J. Chem. Soc. Perkin Trans. 1* **1986**, 1215–1224.
[6] a) K. M. L. Rai, A. Hassner in *Comprehensive Heterocyclic Chemistry II*, *Vol. 1A* (Ed.: A. Padwa), Elsevier, Oxford, **1996**, pp. 61–96, and references therein; b) J. Laue, G. Seitz, *Liebigs Ann.* **1996**, 645–648; c) M. Drögemüller, R. Jautelat, E. Winterfeldt, *Angew. Chem.* **1996**, *108*, 1669–1671; *Angew. Chem. Int. Ed. Engl.* **1996**, *35*, 1572–1574; d) M. Drögemüller, T. Flessner, R. Jautelat, U. Scholz, E. Winterfeldt, *Eur. J. Org. Chem.* **1998**, 2811–2831; e) E. Haak, E. Winterfeldt, *Synlett* **2004**, 1414–1418; f) Y. Tamura, Y. Yoshimura, T. Nishimura, S. Kato, Y. Kita, *Tetrahedron Lett.* **1973**, *14*, 351–354; g) Y. Tamura, S. Kato,

 © 2006 Wiley-VCH Verlag GmbH & Co. KGaA, Weinheim

Y. Yoshimura, T. Nishimura, Y. Kita, *Chem. Pharm. Bull.* **1974**, *22*, 1291 – 1296; h) S. Senda, K. Hirota, T. Asao, K. Maruhashi, *J. Am. Chem. Soc.* **1978**, *100*, 7661 – 7664; i) D. S. Pearce, M. J. Locke, H. W. Moore, *J. Am. Chem. Soc.* **1975**, *97*, 6181 – 6186; j) M. Zaidlewicz, I. G. Uzarewicz, *Heteroat. Chem.* **1993**, *4*, 73 – 77.

[7] W. E. Billups, G.-A. Lee, B. E. Arny, K. H. Whitmire, *J. Am. Chem. Soc.* **1991**, *113*, 7980 – 7984.

[8] Reviews on vinyl azides: a) K. Banert in *Houben-Weyl*, *Vol. E15* (Eds.: H. Kropf, E. Schaumann), Thieme, Stuttgart, **1993**, pp. 818 – 875; b) A. Hassner in *Azides and Nitrenes* (Ed.: E. F. V. Scriven), Academic Press, Orlando, **1984**, pp. 35 – 76.

[9] Treatment of 1-azido-2-iodocycloheptane with KO*t*Bu followed by separation by chromatography gave **2c** (31 %) as well as 3-azidocycloheptene (25 %). Hassner's route afforded **2e** (73 % overall yield from cyclododecene) as a yellow oil.

[10] A. Hassner, *Acc. Chem. Res.* **1971**, *4*, 9 – 16.

[11] a) A. Hassner, F. W. Fowler, *J. Org. Chem.* **1968**, *33*, 2686 – 2691; b) J. Schweng, E. Zbiral, *Justus Liebigs Ann. Chem.* **1978**, 1089 – 1095.

[12] From cyclohexene, we obtained by using Hassner's route 3-azidocyclohexene along with a portion of **2b** $\leq$ 1 %; see the contrast to reference [13].

[13] a) F. Müller, Dissertation, Universität Münster, **1992**; b) F. Müller, J. Mattay, *Angew. Chem.* **1992**, *104*, 207 – 208; *Angew. Chem. Int. Ed. Engl.* **1992**, *31*, 209 – 210; c) F. Müller, J. Mattay, *Chem. Ber.* **1993**, *126*, 543 – 549.

[14] C. E. Davis, J. L. Bailey, J. W. Lockner, R. M. Coates, *J. Org. Chem.* **2003**, *68*, 75 – 82.

[15] V. Nair, T. G. George, V. Sheeba, A. Augustine, L. Balagopal, L. G. Nair, *Synlett* **2000**, 1597 – 1598.

[16] Our spectroscopic data of the four azirines **3b–e** (Table 1 and Supporting Information) and the properties found for **3b** differ very clearly from the statements in reference [13] (e.g., see the data of **3c** and **3e** in reference [13c] for correct data of **3d**, see also reference [4a,c]).

[17] Alternative syntheses for **11b**,**h** and **12a**,**b**,**c**: a) R. K. Grasselli, D. D. Suresh, D. R. Bridgeman, US Patent US4379925A, **1983** [*Chem. Abstr.* **1983**, *99*, 88228]; b) D. G. Farnum, G. R. Carlson, *Synthesis* **1972**, 191 – 192; c) T. Kobayashi, S.-Y. Yamamoto, H. Kato, *Bull. Chem. Soc. Jpn.* **1997**, *70*, 1193 – 1197; d) C. Herzig, J. Gasteiger, *Chem. Ber.* **1981**, *114*, 2348 – 2354; e) T. Kobayashi, S.-Y. Yamamoto, H. Kato, *Bull. Chem. Soc. Jpn.* **1997**, *70*, 1193 – 1197; f) H. E. Baumgarten, F. A. Bower, *J. Am. Chem. Soc.* **1954**, *76*, 4561 – 4564; g) J.-X. Chen, J.-P. Jiang, W.-X. Chen, T.-Y. Kao, *Heterocycles* **1991**, *32*, 2339 – 2342.

[18] For the addition of exactly one equivalent of HCN to 2-methylene-2*H*-azirines, see: K. Banert, M. Hagedorn, E. Knözinger, A. Becker, E.-U. Würthwein, *J. Am. Chem. Soc.* **1994**, *116*, 60 – 62.

[19] M. Mizuno, T. Shioiri, *Tetrahedron Lett.* **1999**, *40*, 7105 – 7108.

[20] a) A. L. Logothetis, *J. Org. Chem.* **1964**, *29*, 3049 – 3052; b) V. Nair, *J. Org. Chem.* **1968**, *33*, 2121 – 2123 und V. Nair, *J. Org. Chem.* **1968**, *33*, 4316; c) T. C. Gallagher, R. C. Storr, *Tetrahedron Lett.* **1981**, *22*, 2909 – 2912; d) K. Banert, M. Hagedorn, C. Liedtke, A. Melzer, C. Schöffler, *Eur. J. Org. Chem.* **2000**, 257 – 267; e) T. M. V. D. Pinho e Melo, A. L. Cardoso, C. S. B. Gomes, A. M. d'A. Rocha Gonsalves, *Tetrahedron Lett.* **2003**, *44*, 6313 – 6315.

[21] A. Gagneux, S. Winstein, W. G. Young, *J. Am. Chem. Soc.* **1960**, *82*, 5956 – 5957.

[22] Alternative syntheses for **20b**,**d** and **21b**: a) E. Maxa, E. Zbiral, G. Schulz, E. Haslinger, *Justus Liebigs Ann. Chem.* **1975**, 1705 – 1720; b) R. C. Hayward, G. H. Whitham, *J. Chem. Soc. Perkin Trans. 1* **1975**, 2267 – 2270.

 © 2006 Wiley-VCH Verlag GmbH & Co. KGaA, Weinheim

DOI: 10.1002/anie.200504594

A General and Versatile Method for C–C Cross-Coupling Synthesis of Conjugated Enynes: One-Pot Sequence Starting from Carbonyl Compounds**

Ilya M. Lyapkalo and Michael A. K. Vogel*

In light of the pivotal role of the carbonyl group in organic synthesis,[1] new general transformations of the carbonyl compounds are always of particular importance. This is why the relatively recent discovery of transition-metal-catalyzed reactions of alkenyl triflates, readily available from enolizable carbonyl precursors, immediately found widespread application.[2] Following this line of research, alkenyl 1,1,2,2,3,3,4,4,4-nonafluorobutane-1-sulfonates (hereinafter referred to alkenyl nonaflates) were introduced and advantageously employed as a useful alternative to the triflates in Heck,[3] Negishi,[4] Stille,[5] and Sonogashira[6] coupling reactions.

Routinely, the coupling protocols consist of two steps that include O-sulfonylation of the starting carbonyl compounds, followed by Pd-catalyzed C–C cross-coupling of the isolated alkenyl perfluoroalkanesulfonate leading to the desired products. Alternatively, Reissig and co-workers established that isolation and purification of the alkenyl nonaflates is not necessary for the subsequent coupling reaction provided that the nonaflates are generated from trimethylsilyl enol ethers and the mild sulfonylating reagent nonafluorobutane-1-sulfonyl fluoride (NfF)[7] under catalysis by fluoride ion. This resulted in the development of a general, one-pot transformation of trimethylsilyl enol ethers into 1,3-dienes by in situ generation of alkenyl nonaflates followed by Heck reactions.[8] However, it requires an extra step to obtain the requisite trimethylsilyl enolates from the ultimate precursors, ketones or aldehydes. This requirement serves to highlight a major challenge in the development of general and straightforward coupling methods, namely, the conversion of carbon-

[*] Dr. I. M. Lyapkalo
Institute of Chemical & Engineering Sciences
1 Pesek Road, Jurong Island, Singapore 627833 (Singapore)
Fax: (+65) 6316-6184
E-mail: ilya_lyapkalo@ices.a-star.edu.sg
M. A. K. Vogel
Freie Universität Berlin
Institut für Chemie—Organische Chemie
Takustrasse 3, 14195 Berlin (Germany)

[**] We thank Prof. H.-U. Reissig (Freie Universität Berlin, Germany) and Prof. B. Cox (AstraZeneca, Macclesfield, UK) for useful discussions. Financial support by the Agency for Science Technology and Research (A*STAR Singapore) and by the Alexander von Humboldt Foundation is most gratefully acknowledged. We are indebted to Bayer AG for the generous donation of nonafluorobutane-1-sulfonyl fluoride.

Supporting information for this article is available on the WWW under http://www.angewandte.org or from the author.

 © 2006 Wiley-VCH Verlag GmbH & Co. KGaA, Weinheim InterScience

yl compounds to the alkenyl nonaflates, combined with the subsequent C–C cross-coupling step in a one-pot operation.

Here we report a novel general method for the synthesis of conjugated enynes based on the Sonogashira reaction, with both components originating from widely available carbonyl compounds, whereby the generated alkenyl nonaflate and alkyne intermediates interact smoothly under Pd^0 catalysis to give the anticipated cross-coupling products in an one-pot reaction sequence.

To achieve a clean conversion of the starting materials **1**–**3** to the mixture of a cyclic nonaflate and a terminal alkyne (Scheme 1), we needed to find a base that would not react

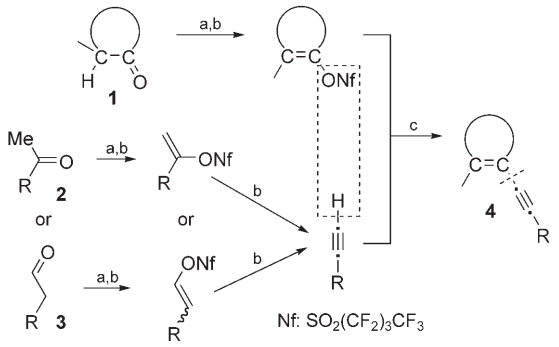

Scheme 1. One-pot synthesis of the enynes **4** starting from cyclic ketones **1** and methyl ketones **2** or aldehydes **3**. a) NfF; b) base; c) iPr_2NH (excess), $Pd(OAc)_2$ (5 mol%), PPh_3 (10 mol%), CuI (10 mol%), LiCl, 24 h at 25 °C, or 17 h at 45–47 °C, or 5–6 h at 60 °C.

with NfF but be strong enough to provide α-deprotonation of the carbonyl substrates and effect E2 elimination of NfOH from the intermediate alkenyl nonaflates at ambient or subambient temperatures. Since lithium amide bases are known to react with NfF readily, even at low temperature,[9] we turned our attention to metal-free nitrogen bases. After extensive experimentation,[10] we found that (*tert*-butylimino)tris(1-pyrrolidinyl)phosphorane[11] (hereinafter referred to as P_1 base) and 1-(*tert*-butylimino)-1,1,3,3,3-pentakis(dimethylamino)-1λ^5,3λ^5-diphosphazene (P_2 base[12]), commercially available representatives of the family of phosphazene bases, were particularly successful (Figure 1).

When combined with NfF in dry aprotic solvent, the P bases effect clean and complete conversion of cyclic and acyclic ketones to the cyclic nonaflate and the respective alkyne intermediates which can be observed by ^{1}H NMR spectroscopy of the crude reaction mixtures. The one-pot reaction sequence culminates in Sonogashira coupling of these intermediates to give high yields of the desired products **4a**–**e** (Table 1, entries 1–5).

The metal-free noncoordinating P_1 base provided perfect regioselectivity control in favor of the deprotonation at the position most remote to the ring nitrogen[14] of **1c** leading exclusively to the product **4d** (Table 1, entry 4). However, the

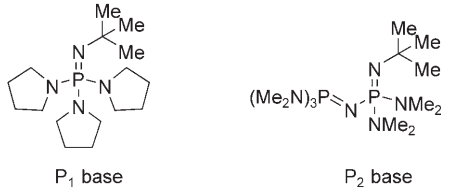

Figure 1. Phosphazene bases employed for generation of alkenyl nonaflates and terminal alkynes from the carbonyl compounds **1**–**3**.

Table 1: Reaction conditions and yields of the products **4** according to Scheme 1.

Entry	Cyclic ketone **1**	Ketone **2** or aldehyde **3**	Reaction conditions[a]	Product **4** (Yield [%])
1	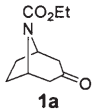 **1a**	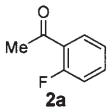 **2a**	A, 17 h	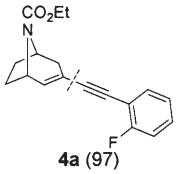 **4a** (97)
2	**1a**	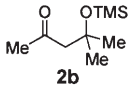 **2b**	A, 24 h	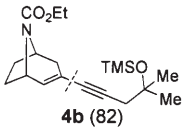 **4b** (82)
3	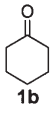 **1b**	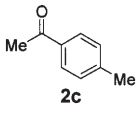 **2c**	A, 24 h	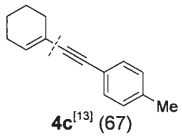 **4c**[13] (67)
4	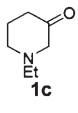 **1c**	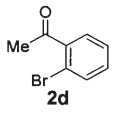 **2d**	A, 24 h	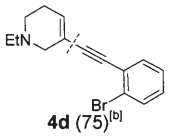 **4d** (75)[b]
5	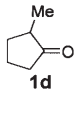 **1d**	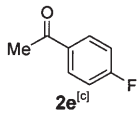 **2e**[c]	1) B then 2) A, 17 h	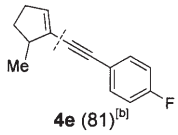 **4e** (81)[b]
6	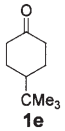 **1e**	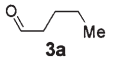 **3a**	A, 24 h	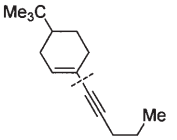 **4f** (83)
7	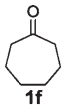 **1f**	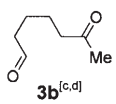 **3b**[c,d]	1) A, 36 h then 2) A, 17 h	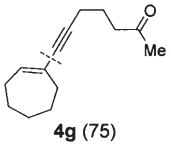 **4g** (75)
8	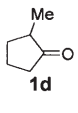 **1d**	**3b**[c,d]	1) B then 2) A, 17 h	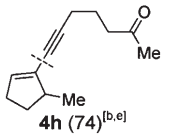 **4h** (74)[b,e]

[a] Nonaflation/elimination conditions: A (P_1 base, NfF, DMF, 0 °C to 25 °C), B (P_2 base, NfF, THF, −78 °C to 25 °C, 4.5 h); for the Sonogashira coupling, see step c in Scheme 1. [b] >95:<5 selectivity in favor of the kinetically controlled double-bond regioisomer shown. [c] The component was added to the reaction mixture under the conditions 2 *after* the complete conversion of the cyclic ketone **1** to the nonaflate (^{1}H NMR control) under the conditions (1). [d] Added at −10 °C. [e] 1.2:1 mixture of the tri- (**4h**) and tetrasubstituted C–C double-bond regioisomers was obtained under the conditions specified in the entry 7.

 © 2006 Wiley-VCH Verlag GmbH & Co. KGaA, Weinheim

P_1 base was not regioselective in the deprotonation of **1d** with regard to the α-methine and α-methylene positions (Table 1, footnote [e]). Fortunately, the regioselectivity was dramatically improved when the much stronger P_2 base was employed under the kinetically controlled conditions, resulting in the enynes **4e** and **4h** bearing the less substituted double bonds (Table 1, entries 5 and 8).

Aldehydes proved to be a promising source of terminal alkynes. In all cases, clean conversions were observed (entries 6–8 in Table 1, entry 3 in Table 2). Moreover, aldehydes are more acidic and react much faster than ketones, which enables the highly selective reaction of the aldehyde moiety in the presence of the unprotected keto group in the 6-oxo-heptanal **3b** (entries 7 and 8). To our knowledge, one-step formation of C–C triple bond by elimination of H_2O from aldehydes is unprecedented.[15,16]

Acyclic nonaflates are unsuccessful as cross-coupling components when generated directly from carbonyl compounds using phosphazene bases, because of their ease of elimination to give alkynes.[17] However, a modification of the protocol made it possible to obtain cross-coupling products from the combination of both acyclic carbonyl precursors. We realized that the highly reactive soluble fluoride sources phosphazenium fluorides [P base]H^+F^-, generated during the course of the alkyne formation from the compounds **2** and **3**, could be used to selectively produce the appropriate (acyclic) nonaflate[7b] (Scheme 2). Thus, the nonaflates required for the coupling products **6** were routinely generated in situ by simple addition of the trimethylsilyl enol ethers **5** to reaction mixtures containing the appropriate excess of NfF after the completion of the alkyne formation (Table 2), that is, when free phosphazene bases were no longer present. Remarkably, under these conditions the fluoride ion effects desilylation and nonaflation of the trimethylsilyl enol ether moiety in a highly selective manner, without appreciably affecting fragile trimethylsilyl alcohol protection[18] (Table 2, entries 2 and 3). The subsequent Sonogashira coupling resulted in good yields of the desired products **6a–c**. Noteworthy, the product **6a** is produced with almost complete retention of the *Z* configuration of the double bond originating from the parent enol ether **5a**.[19]

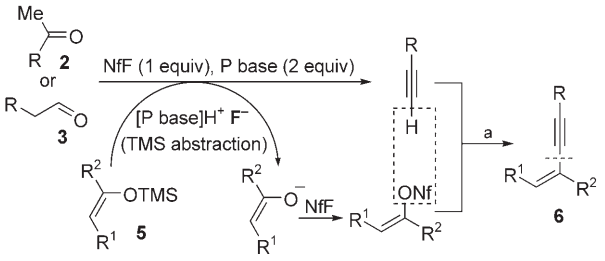

Scheme 2. One-pot synthesis of the acyclic enynes **6** employing trimethylsilyl enolates **5**. a) iPr_2NH (excess), $Pd(OAc)_2$ (5 mol%), PPh_3 (10 mol%), CuI (10 mol%), LiCl, 17–24 h at 25 °C.

Table 2: Reaction conditions and yields of the products **6** according to Scheme 2.

Entry	Ketone **2** or aldehyde **3**	Reaction conditions[a]	TMS enolate **5**	Product **6** (Yield [%])
1	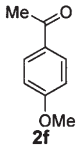 **2f**	A, 17 h	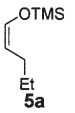 **5a**	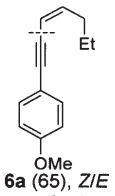 **6a** (65), *Z*/*E* >40 : 1
2	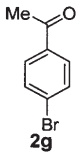 **2g**	B	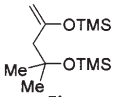 **5b**	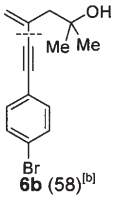 **6b** (58)[b]
3	**3c**	B	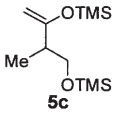 **5c**	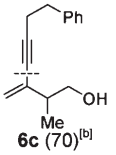 **6c** (70)[b]

[a] For the conversions to the alkynes: A (P_1 base, NfF, DMF, 0 °C to 25 °C), B (P_2 base, NfF, THF, −78 °C to 25 °C, 4.5 h); for the Sonogashira coupling, see a) in Scheme 2. [b] Obtained and characterized as free alcohols after the TMS deprotection.

In conclusion, the method represents a straightforward, general, and versatile approach to highly diverse conjugated enynes, starting from readily available carbonyl precursors. Relatively low nucleophilicity, in combination with high basicity, makes phosphazene bases compatible with NfF, thereby permitting clean formation of alkenyl nonaflates under the "internal quench" conditions.[20] Furthermore, neither phosphazene bases nor their salts impede the bimetallic catalytic cycle of the subsequent Sonogashira reaction. The operational simplicity of our one-pot protocol and a wide selection of commercially available carbonyl compounds permit a flexible, convergent approach towards a variety of conjugated enynes. It should open up new and interesting opportunities for the synthesis of target products containing conjugated enyne[21] or enediyne fragments and exhibiting very promising antibiotic, antitumor, and other biological activities.[2d,22]

Experimental Section

Typical procedure for the one-pot synthesis of enynes: Synthesis of **4a** (entry 1, Table 1): Predried LiCl[23] (0.127 g, 3.00 mmol) was placed into a reaction flask equipped with a three-way tap and a magnetic stirrer coated with teflon, and was heated to ca. 250–300 °C with a heat gun under high vacuum for a few minutes. After the LiCl had cooled down under an atmosphere of dry argon, DMF (2 mL), *N*-ethoxycarbonyl tropinone (**1a**) (0.395 g, 2.00 mmol), 2-fluoroacetophenone (**2a**) (0.345 g, 2.50 mmol), and NfF (1.495 g, 4.95 mmol) were added successively. The reaction mixture was cooled down to 10 °C under vigorous stirring, and P_1 base (2.406 g, 7.70 mmol) was added dropwise within 2–3 min. After completion of the nonaflation and elimination steps (17 h at RT, ^{1}H NMR monitoring), iPr_2NH (3 mL) was added, followed by solid PPh_3 (0.052 g, 0.20 mmol), CuI

 © 2006 Wiley-VCH Verlag GmbH & Co. KGaA, Weinheim

(0.038 g, 0.20 mmol), and $Pd(OAc)_2$ (0.022 g, 0.10 mmol) (all together in one lot), and the reaction mixture was stirred at 60 °C for 5.5 h. It was then subjected to aqueous workup (benzene/water; in other cases usually *t*BuOMe/water or hexane/water), the two-phase mixture was filtrated carefully through a pad of celite and the aqueous phase re-extracted with benzene. The combined organic layers were dried (Na_2SO_4), the solvent was then removed under vacuum, and the residue was subjected to column chromatography (silica gel, gradient elution (1. hexane, 2. benzene/hexane 1:4, 3. benzene/hexane 1:1, 4. benzene) to give pure **4a** (0.579 g, 97% yield) as a yellow oil. ^{1}H NMR (C_6D_6, 500 MHz, 75 °C): $\delta = 1.05$ (t, $J = 7.1$ Hz, 3H, Me), 1.29–1.36 (br m, 1H), 1.55 (ddd, $J = 11.8$, 9.0, 2.8 Hz, 1H), 1.64 (m_c, 1H), 1.77 (ddddd, $J = 12.5$, 12.5, 8.0, 2.8, 1.7 Hz, 1H), 1.83 (br d, $J =$ 17 Hz, 1H), 2.99 (br d, $J = 17$ Hz, 1H) (all CH_2), 4.06 (dq, $J = 10.8$, 7.1 Hz, 1H), 4.09 (dq, $J = 10.8$, 7.1 Hz, 1H) (both OCH_2), 4.29 (br s, 1H, CHN), 4.37 (br s, 1H, CHN), 6.29 (ddd, $J = 5.3$, 1.9, 1.8 Hz, 1H, CH=C), 6.68 (td, $J = 7.6$, 1.3 Hz, 1H), 6.74 (ddd, $J = 9.5$, 8.3, 1.3 Hz, 1H), 6.78–6.73 (m, 1H), 7.25 ppm (td, $J = 7.4$, 1.8 Hz, 1H) (all CH_{Ar}); ^{13}C (C_6D_6, 125.8 MHz, 75 °C): $\delta = 14.8$ (q, Me), 29.9, 34.5, 38.2 (all br t, CH_2), 52.4, 53.7 (both d, CHN), 61.0 (t, OCH_2), 82.8 (s, C=C), 95.0 (d, $^3J_{^{13}C,^{19}F} = 3.2$ Hz, C=C), 112.8 (d, $^2J_{^{13}C,^{19}F} = 15.7$ Hz, C_{Ar}), 115.7 (dd, $^2J_{^{13}C,^{19}F} = 21.0$ Hz), 124.1 (dd, $^3J_{^{13}C,^{19}F} = 3.8$ Hz), 129.9 (dd, $^3J_{^{13}C,^{19}F} =$ 7.9 Hz), 133.6 (dd, $^4J_{^{13}C,^{19}F} = 1.3$ Hz) (all CH_{Ar}), 118.6 (br s, *C*=CH), 139.7 (br d, C=*CH*), 154.4 (s, C=O), 163.2 ppm (d, $^1J_{^{13}C,^{19}F} = 251.6$ Hz, C-F); IR (film): $\tilde{\nu} = 3060$–3035 cm^{-1} (=C-H), 2980–2835 (C-H), 2210 (C=C), 1700 (C=O), 1620–1490 (C=C); MS (EI, 80 eV): m/z (%) = 300 (M^++1, 21), 299 (M^+, 100), 271 ([$M^+ - C_2H_4$], 37), 270 ([$M^+ - C_2H_5$], 91), 242 ([$M^+ - C_2H_5 - CO$], 45), 226 ([$M^+ - C_2H_5 - CO_2$], 28), 198 ([$M^+ - CO_2Et - C_2H_4$], 85), 183 ([$M^+ - CO_2Et - C_2H_4 - NH$], 10), 29 ($C_2H_5^+$, 44); C,H,N analysis (%): calcd for $C_{18}H_{18}FNO_2$ (299.4): C 72.22, H 6.06, N 4.68; found C 71.91, H 5.95, N 4.64.

Received: December 27, 2005
Published online: May 9, 2006

Keywords: C–C coupling · cross-coupling · enynes · homogeneous catalysis · phosphazene bases

[1] *"The chemistry of carbonyl compounds is virtually the backbone of synthetic organic chemistry"*: J. D. Roberts, M. C. Caserio, *Basic Principles of Organic Chemistry*, Benjamin, New York, **1965**, p. 426.

[2] a) W. J. Scott, J. E. McMurry, *Acc. Chem. Res.* **1988**, *21*, 47–54; b) K. Ritter, *Synthesis* **1993**, 735–762; c) S. Cacchi, *Pure Appl. Chem.* **1996**, *68*, 45–52; d) R. Brückner, J. Suffert, *Synlett* **1999**, 657–679.

[3] a) K. Voigt, P. von Zezschwitz, K. Rosauer, A. Lansky, A. Adams, O. Reiser, A. de Meijere, *Eur. J. Org. Chem.* **1998**, 1521–1534; b) S. Bräse, *Synlett* **1999**, 1654–1656.

[4] F. Bellina, D. Ciucci, R. Rossi, P. Vergamini, *Tetrahedron* **1999**, *55*, 2103–2112.

[5] A. Wada, Y. Ieki, M. Ito, *Synlett* **2002**, 1061–1064.

[6] a) J. Suffert, A. Eggers, S. W. Scheuplein, R. Brueckner, *Tetrahedron Lett.* **1993**, *34*, 4177–4180; b) T. Okauchi, T. Yano, T. Fukamachi, J. Ichikawa, T. Minami, *Tetrahedron Lett.* **1999**, *40*, 5337–5340.

[7] a) R. Zimmer, M. Webel, H.-U. Reissig, *J. Prakt. Chem.* **1998**, *340*, 274–277, and references therein; b) I. M. Lyapkalo, M. Webel, H.-U. Reissig, *Eur. J. Org. Chem.* **2002**, 1015–1025.

[8] a) M. Webel, H.-U. Reissig, *Synlett* **1997**, 1141–1142; b) I. M. Lyapkalo, M. Webel, H.-U. Reissig, *Eur. J. Org. Chem.* **2002**, 3646–3658; c) I. M. Lyapkalo, J. Hogermeier, H.-U. Reissig, *Tetrahedron* **2004**, *60*, 7721–7729.

[9] The reaction results in the anticipated nonafluorobutane-1-sulfonamides: I. M. Lyapkalo, H.-U. Reissig, A. Schaefer, A. Wagner, *Helv. Chim. Acta* **2002**, *85*, 4206–4215.

[10] Trialkylamines are not basic enough to promote the nonaflation, whereas DBU gives low conversions as a result of the side reaction with NfF. The results will be reported in a subsequent full account.

[11] R. Schwesinger, J. Willaredt, H. Schlemper, M. Keller, D. Schmitt, H. Fritz, *Chem. Ber.* **1994**, *127*, 2435–2454. It has the highest basicity ($pK_a = 28.35$ in MeCN) of the commercially available P_1 bases.

[12] a) Commercially available as a 2 M solution in THF ($pK_a = 33.49$ in MeCN); b) According to the primary classification given by Schwesinger, the subscript designates the number of P atoms in the molecule. For the synthesis and properties of P_2 or higher order phosphazene bases, see: R. Schwesinger, H. Schlemper, C. Hasenfratz, J. Willaredt, T. Dambacher, T. Breuer, C. Ottaway, M. Fletschinger, J. Boele, H. Fritz, D. Putzas, H. W. Rotter, F. G. Bordwell, A. V. Satish, G. Z. Ji, E. M. Peters, K. Peters, H. G. von Schnering, L. Walz, *Liebigs Ann.* **1996**, 1055–1082 and references therein.

[13] S. Chang, S. H. Yang, P. H. Lee, *Tetrahedron Lett.* **2001**, *42*, 4833–4836.

[14] T. Imahori, Y. Kondo, *J. Am. Chem. Soc.* **2003**, *125*, 8082–8083.

[15] For the relevant multistep methods known to date, see a) M. Shibasaki, Y. Torisawa, S. Ikegami, *Tetrahedron Lett.* **1982**, *23*, 4607–4610; b) L. A. Paquette, S. Hormuth, C. J. Lovely, *J. Org. Chem.* **1995**, *60*, 4813–4821; c) T. Matsuura, S. Yamamura, Y. Terada, *Tetrahedron Lett.* **2000**, *41*, 2189–2192.

[16] Preliminary investigations show that the nonaflation/elimination protocol is applicable to a wide range of carbonyl compounds, leading to terminal or internal alkynes or allenes, depending on the stereoelectronic effects of the substituents in the carbonyl substrate. The results will be reported in due course.

[17] In our attempts to generate the nonaflates from isopropyl methyl ketone or benzyl methyl ketone using P_2 base (1 equiv) and NfF under the kinetic conditions, we could detect only mixtures of the alkyne and the starting material, which clearly indicates that nonaflation is the rate-determining step.

[18] ^{1}H NMR analyses of the reaction mixtures towards the end of the final coupling step indicated that the Me_3SiO group at sp^3-hybridized carbon centers of the coupling products remained intact, which should warrant the stability of the most frequently used alcohol silyl protecting groups, such as *t*BuMe$_2$Si, *t*BuPh$_2$Si, or Et$_3$Si, under our reaction conditions.

[19] Trimethylsilyl enolate **5a** was obtained as an 8:92 *E*/*Z* mixture by silylation of the freshly distilled pentanal with Me_3SiCl/NaI/*i*Pr$_2$NEt in MeCN at −45 °C to 5 °C. The pure *Z* isomer was then isolated by preparative HPLC (68% yield).

[20] E. J. Corey, A. W. Gross, *Tetrahedron Lett.* **1984**, *25*, 495–498.

[21] The antimycotic agent terbinafine (Lamisil) manufactured by Novartis Pharmaceuticals is perhaps most prominent example of a widely applied drug bearing an eneyne structural motif; for other interesting bioactive compounds, see: a) L. Garlaschelli, E. Magistrali, G. Vidari, O. Zuffardi, *Tetrahedron Lett.* **1995**, *36*, 5633–5636; b) H.-J. Zhang, K. Sydara, G. T. Tan, C. Ma, B. Southavong, D. D. Soejarto, J. M. Pezzuto, H. H. S. Fong, *J. Nat. Prod.* **2004**, *67*, 194–200.

[22] J. W. Grissom, G. U. Gunawardena, D. Klingberg, D. Huang, *Tetrahedron* **1996**, *52*, 6453–6518, and references therein.

[23] Since $Pd(OAc)_2$ was used as a uniform source of catalytic Pd in our method, LiCl was considered as an additive for in situ generation of $[Pd(PPh_3)_2Cl_2]$ from $Pd(OAc)_2$ and PPh_3 at the outset of the cross-coupling step. $[Pd(PPh_3)_2Cl_2]$ is one of the most frequently used precatalysts for the Sonogashira reaction of alkenyl sulfonates: a) S. W. Scheuplein, K. Harms, R. Brueckner, J. Suffert, *Chem. Ber.* **1992**, *125*, 271–278; b) L.

 © 2006 Wiley-VCH Verlag GmbH & Co. KGaA, Weinheim

Castedo, A. Mourino, L. A. Sarandeses, *Tetrahedron Lett.* **1986**, *27*, 1523 – 1526; c) L. Castedo, J. L. Mascarenas, A. Mourino, L. A. Sarandeses, *Tetrahedron Lett.* **1988**, *29*, 1203 – 1206; d) M. Moniatte, M. Eckhardt, K. Birckmann, R. Brueckner, J. Suffert, *Tetrahedron Lett.* **1994**, *35*, 1965 – 1968; e) J. Suffert, E. Abraham, S. Raeppel, R. Brueckner, *Liebigs Ann.* **1996**, 447 – 456; f) A. L. Braga, D. J. Emmerich, C. C. Silveira, T. L. C. Martins, O. E. D. Rodrigues, *Synlett* **2001**, 369 – 370; g) P. E. Tessier, N. Nguyen, M. D. Clay, A. G. Fallis, *Org. Lett.* **2005**, *7*, 767 – 770.
However, we did not carry out a specific study on the LiCl effect.

 © 2006 Wiley-VCH Verlag GmbH & Co. KGaA, Weinheim

Total Synthesis

DOI: 10.1002/anie.200600502

Total Synthesis of the Light-Harvesting Carotenoid Peridinin**

*Thomas Olpp and Reinhard Brückner**

Peridinin (**1**) is the major light-harvesting pigment of planktonic dinoflagellates[1] conspicuously present in harmful algae blooms ("red tides").[2] Peridinin is distinguished by its antitumor activity,[3] and it is one of the most abundantly biosynthesized carotenoids on earth.[4] There are more than 700 naturally occurring carotenoids,[5] but the butenolide ring is almost unique to peridinin (**1**).[6] The biosynthesis of ist C_{37} framework is not yet understood.[7]

A century after its first isolation[8] and a decade after its structure elucidation,[9] peridinin (**1**) became a target of total synthesis. Ito et al.[10] as well as Katsumura et al.[11] have synthesized the natural product, while de Lera's group, collaborating with us, prepared its allene epimer.[12] Here we describe the third total synthesis of **1**. It is strategically novel and promises to lead to other natural[6] or related non-natural butenolide-containing carotenoids.

With an emphasis on convergency, our retrosynthetic analysis traced back peridinin (**1**) to the three building blocks **2** ("allenylsulfone"), **3** ("alkenylstannane"), and **4** ("oxobromoacrylate") (Scheme 1). Compound **4** was designed to yield, after acetal cleavage and lactonization, a 3-alkenyl-5-(α-hydroxyalkyl)butenolide. Subsequent *anti*-selective dehydration should result in the *Z*-configured $C^{1'}{=}C^{5}$ bond in the butenolide core of **1**.[13,14] Entities like the 3-alkenyl-5-(α-hydroxyalkyl)butenolide exhibiting the required *ul* relationship[15] between their stereocenters can be obtained by appropriate modification of the termini of diethyl tartrate (**6**). We showed this in a model study[16] and chose to exploit it here. Compound **4** was endowed with an oxo function in order to take up allenylsulfone **2** in a (Sylvestre) Julia olefination and with a bromoolefin moiety for a Stille coupling with alkenylstannane **3**. Both the allenylsulfone **2** and the alkenylstannane **3** were to be derived from (−)-actinol (**5**).[17] Compound **5** is a common starting material for the synthesis of 4″-hydroxylated[18] carotenoids like zeaxanthin[19] and peridinin.[10–12]

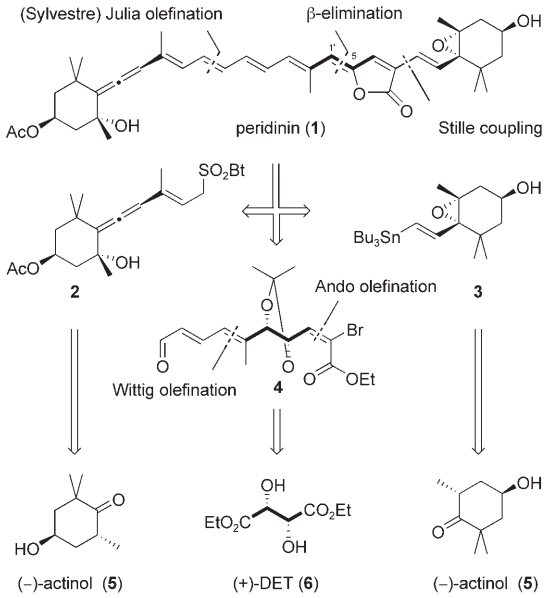

Scheme 1. Retrosynthetic analysis of peridinin (**1**). Bt = benzothiazolyl (formula in bottom line of Scheme 4).

Starting from (+)-diethyl tartrate (**6**), the ester-containing Weinreb amide **7** was prepared in four steps and 58% overall yield as described earlier[16] (Scheme 2). The selective reduction both of the ester (→CH_2OH) and amide (→CHO) moieties succeeded only when a distinct excess of $NaAlH_4$ was used. $LiAlH_4$ and diisobutylaluminum hydride (DIBAL) were either inert or degraded the substrate, while $NaBH_4$ in MeOH reduced the amide moiety selectively, yet differently (→CH_2OH) than desired. The resulting hydroxyaldehyde **8** was not purified because of its instability, and thus crude **8** was subjected to the Ando-type[21] Horner–Wadsworth–Emmons olefination with a mixture of bromophosphonates **9a** and **9b** developed for this purpose.[22] This gave hydroxybromoacrylate **10**[23] with 95% *E* selectivity.[24] Subsequent oxidation with MnO_2 delivered the desired oxobromoacrylate **4**. However, the lability of this compound forced us to treat it without

[*] Dr. T. Olpp,[+] Prof. Dr. R. Brückner
Institut für Organische Chemie und Biochemie
Universität Freiburg
Albertstrasse 21, 79104 Freiburg (Germany)
Fax: (+49) 761-203-6100
E-mail: reinhard.brueckner@organik.chemie.uni-freiburg.de

[+] Current address:
Department of Chemistry, Building 18–344
Massachusetts Institute of Technology
77 Massachusetts Avenue, Cambridge, MA 02139 (USA)

[**] This work was generously supported by the Fonds der Chemischen Industrie (Kekulé fellowship for T.O.) and by the Deutsche Forschungsgemeinschaft. We are grateful to Dr. Thomas Netscher (DSM Nutritional Products, Basel) for a donation of (−)-actinol.

Supporting information for this article (the NMR data of **1** and (6′*cis*)-**1**) is available on the WWW under http://www.angewandte.org or from the author.

 © 2006 Wiley-VCH Verlag GmbH & Co. KGaA, Weinheim

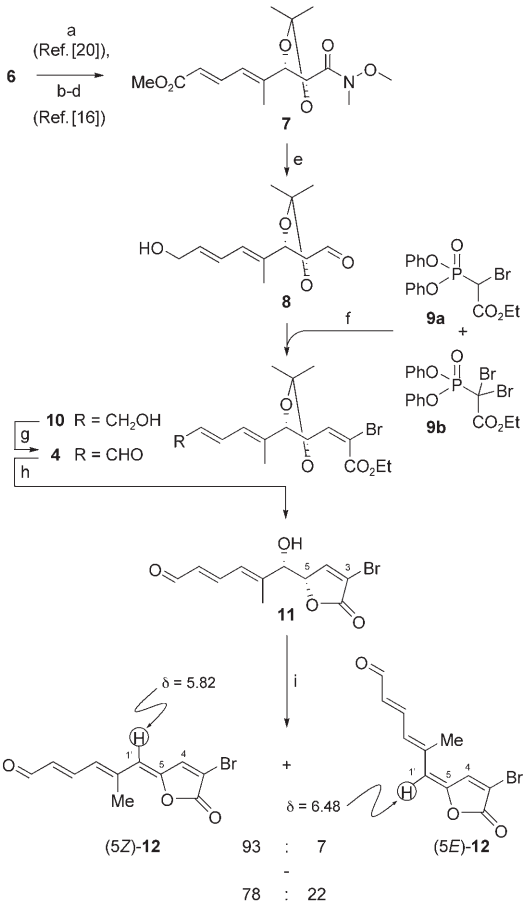

Scheme 2. Synthesis of the butenolide moiety **12** [^{1}H NMR shifts (500 MHz, $CDCl_3$) supporting the configuration assignment are circled] of peridinin (**1**) via oxobromoacrylate **4**. a) 2,2-Dimethoxypropane (1.2 equiv), *p*-TsOH (cat.), toluene, reflux, 2 h, 87% diethyl (*R*,*R*)-2,3-*O*,*O*-isopropylidenetartrate and 11% ethyl methyl (*R*,*R*)-2,3-*O*,*O*-isopropylidenetartrate (in a mixture; $\Sigma = 98\%$; Ref. [20]: $\Sigma = 96\%$); b) Ref. [16]: HNMe(OMe)·HCl (4 equiv), Me_3Al (4 equiv), CH_2Cl_2, −15 °C, 1 h, 99%; c) Ref. [16]: MeMgBr (1.0 equiv), THF, 0 °C, 1 h, 66%; d) Ref. [16]: $MeO_2C{-}CH{=}CH{-}CH{=}PPh_3$ (2.0 equiv), toluene, reflux, 30 h, 90%, $E/Z > 99{:}1$; e) $NaAlH_4$ (3.0 equiv), THF, −40 °C, 15 min; f) **9a**/**9b** mixture[22] (0.83 and 0.46 equiv, respectively, $\Sigma = 1.29$ equiv), NaH (1.0 equiv), THF, 0 °C, 10 min, addition of **8**, 3 h, 47% (over two steps), 95:5 *E*/*Z* mixture; g) MnO_2 (40 equiv), CH_2Cl_2, 25 °C, 2 h, 84% crude product; h) F_3CCO_2H/H_2O (9:1), 25 °C, 5 min, 92%; i) 1,1′-thiocarbonyldiimidazole (5 equiv), CH_2Cl_2 (degassed), di-*tert*-butylcresol (250 ppm), exclusion of light, −78 °C, 10 min, 51%.

purification or delay with 90% trifluoroacetic acid. Within 5 min the acetal was removed and the resulting diol lactonized to provide the 5-(α-hydroxyalkyl)butenolide **11** (77% yield over two steps).

Surprisingly the ensuing *anti* elimination **11**→**12** failed under established[16] Mitsunobu conditions (PPh_3, diethyl azodicarboxylate, THF, −30 °C; Scheme 2). This was also true for related 5-(α-hydroxyalkyl)butenolides, for example, the coupling product obtained from **11** and **3**, and the diol obtained from **10** by deprotection/lactonization. Dehydration of 5-(α-hydroxyalkyl)butenolide **11** to give 5-alkylidenebutenolide **12** was finally effected at −78 °C by reaction with excess 1,1′-thiocarbonyldiimidazole for 10 min. When the previously described precautions were put into effect (absence of light, degassed solvents, radical scavenger)[16] we obtained **12** in 51% yield. To our chagrin, **12** was formed in *Z*/*E* mixtures with ratios ranging from 93:7 to 78:22.

The syntheses of allenylsulfone **2** and alkenylstannane **3** proceeded via epoxyalkyne **14** as a common intermediate; the latter, in turn, was derived from (−)-actinol (**5**)[17] (Scheme 3).

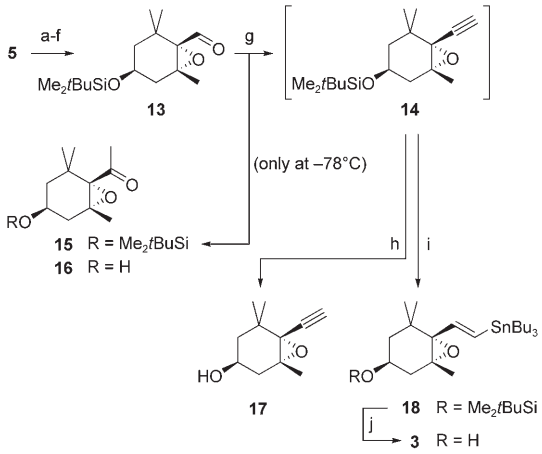

Scheme 3. Synthesis of alkenylstannane **3**. a) Me_2tBuSiCl (1.07 equiv), NEt_3 (1.1 equiv), DMAP (1.05 equiv), CH_2Cl_2, 0 °C, 6 h, 97% (Ref. [10b] 93%); b) LDA (1.12 equiv), addition of product from (a), −78 °C, 1 h, addition of $PhN(SO_2CF_3)_2$ (1.5 equiv), 25 °C, 2 d, 81% (Ref. [10b] 89%); c) stream of CO, MeOH (30 equiv), $[Pd(PPh_3)_4]$ (3 mol%), NEt_3 (3 equiv), DMF, 80 °C, 24 h, 99% (Ref. [11]: 97%); d) DIBAL (2.5 equiv), CH_2Cl_2, −78 °C, 1 h, 81% (Ref. [11] with $LiAlH_4$: 87%); e) *t*BuOOH (2.0 equiv), $Ti(OiPr)_4$ (1.5 equiv), (−)-diisopropyl tartrate (2.3 equiv), 4 Å molecular sieves, CH_2Cl_2, −30 °C, 30 min, 95%, *de* > 98% (Ref.[11] 99%, 92% *de*; Ref. [12] 98%, > 98% *de*); f) Dess–Martin periodinane,[25] CH_2Cl_2, 25 °C, 45 min, 92% (Swern oxidations: Ref. [11] 100%, Ref. [12] 91%); g) $Me_3SiCH{=}N{=}N$ (1.2 equiv), LDA (1.1 equiv), THF, −30 °C, 10 min (Ref. [12]: 92%); h) Bu_4NF (3 equiv), THF, 25 °C, 100 min, 75% over two steps (Ref. [12]: 78%); i) Bu_3SnH (1.1 equiv), $[Pd(PPh_3)_4]$ (2 mol%), THF, 0 °C, 90 min, 53% over two steps; j) Bu_4NF (3 equiv), THF, 25 °C, 19 h, 63%. DMAP = 4-dimethylaminopyridine, DMF = dimethyl formamide, LDA = lithium diisopropylamide.

In the introductory steps we followed the literature procedure through *tert*-butyldimethylsilylation,[10b] enol triflate formation,[10b] methoxycarbonylation to give the unsaturated ester,[11] and DIBAL reduction to give the allyl alcohol.[11] In the subsequent Sharpless epoxidation conducted with substoichiometric amounts of $Ti(OiPr)_4$ (0.2 equiv) and (−)-diisopropyl tartate (DIPT, 0.3 equiv), we obtained a mixture of desired and undesired epoxyalcohol. Our diastereoselectivity (36% *de*) and yield (76%) were distinctly worse than those reported by Katsumura et al. obtained under identical conditions (92% *de*, 99% yield).[11] However, when we employed 1.5 equiv of $Ti(OiPr)_4$ and 2.3 equiv of (−)-DIPT, the epoxidation proceeded with > 98% *de* and 95% yield to provide the epoxyalcohol even on a 14-g scale. Oxidation with the Dess–Martin periodinane[25] delivered epoxyaldehyde **13**. The C_1 extension of this compound at −30 °C with Shioiri's lithiodiazomethane[26] followed by desilylation with Bu_4NF led to the desired alkyne **17** selectively (75% yield over two

 © 2006 Wiley-VCH Verlag GmbH & Co. KGaA, Weinheim

steps).[27] Alkyne **17** was an intermediate en route to allenylsulfone **2** (Scheme 4) but was discarded as a precursor of alkenylstannane **3** (Scheme 3) because its hydrostannylation was ineffective. When $[Pd(PPh_3)_4]$ was used as a catalyst,

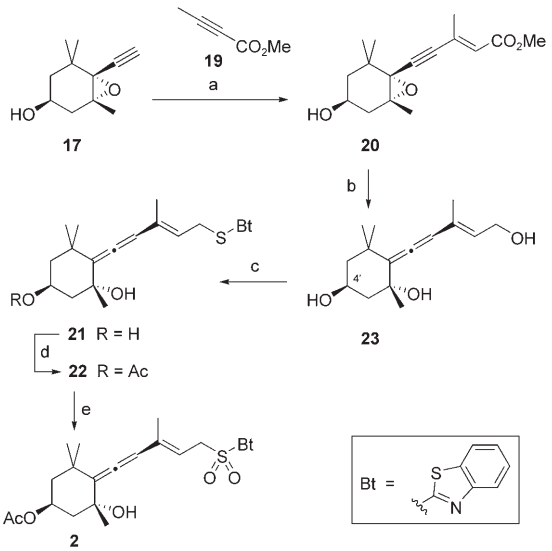

Scheme 4. Synthesis of the allenylsulfone **2**. a) **19** (1.2 equiv), [Pd(OAc)$_2$] (5 mol%), tris(2,6-dimethoxyphenyl)phosphane (5 mol%), THF, 25°C, 44 h, 61%; b) DIBAL (8 equiv), CH_2Cl_2, 0°C, 10 min, 91%; c) PPh_3 (1.0 equiv), 2-mercaptobenzothiazole (1.0 equiv), diethyl azodicarboxylate (1.0 equiv), THF, 25°C, 10 min, 86%; d) Ac_2O (3 equiv), DMAP (10 mol%), pyridine, 25°C, 10 min, 97%, 98:2 *E*/*Z* mixture; e) H_2O_2 (50 equiv), $(NH_4)_6Mo_7O_{24}\cdot 4H_2O$ (0.3 equiv), EtOH, 25°C, 2.5 h, 99%, 74:26 *E*/*Z* mixture.

the yield was 39%, and with $[PdCl_2(PPh_3)_2]$ the yield was 36%; this is in contrast to yields of 69%[12] and >64%[28] obtained under the latter conditions elsewhere. Alkenylstannane **3** was prepared more efficiently by hydrostannylating the silyl-protected alkyne **14**, instead of the silyl-free alkyne **17**, and desilylating thereafter. This sequence furnished **3** in 33% rather than 29% overall yield in three steps from aldehyde **13**.

The transformation of epoxyalkyne **17** into allenylsulfone **2** began with the palladium-catalyzed addition[29] of the former to methyl tetrolate (**19**; Scheme 4). This led to the unsaturated epoxyester **20** with complete *E* selectivity. When **20** was treated with 8 equiv of DIBAL, the unsaturated ester moiety gave an allyl alcohol and the epoxyalkyne moiety an allenol. The latter proceeded with complete 1,3-chirality transfer[30] such that triol **23**[31] resulted as a single stereoisomer (91%). The OH groups of this triol were perfectly differentiable in the following derivatizations: Firstly, 2-mercaptobenzothiazole replaced the allylic OH group in a Mukaiyama redox condensation in the presence of PPh_3 and diethyl azodicarboxylate[32] affording dihydroxysulfide **21** in 86% yield. Secondly, acetylation with Ac_2O/DMAP occurred at the secondary rather than tertiary OH group, which provided acetoxyhydroxysulfide **22** in 97% yield. The product contained 2% of the *Z* isomer, which could not be removed by flash chromatography on silica gel.[33] $(NH_4)_6Mo_7O_{24}$-catalyzed oxidation with H_2O_2[34] carried sulfide **22** on into key sulfone **2**. The yield of **2** and its configurational homogeneity could not be maximized concomitantly: When **22** was oxidized for 2.5 h, **2** was obtained in 99% yield as an inseparable[33] 74:26 *E*/*Z* mixture; when the reaction time was limited to 60 min, **2** was isolated in 88% yield as a 90:10 *E*/*Z* mixture.

The final steps of the synthesis of peridinin (**1**) consisted of combining oxobromobutenolide **12** with alkenylstannane **3** and allenylsulfone **2** (Scheme 5). Because of the configurational lability of polyenes **12**, **24**, and **1** all transformations were conducted in degassed solvents, in the absence of light, and in the presence of a radical scavenger. A Stille coupling[35] of **12** (5*Z*/5*E* 93:7) with **3** (*E*/*Z* 100:0)—catalyzed by [Pd(PPh$_3$)$_4$] and cocatalyzed by CuI[36]—gave the butenolide-containing pentaene **24** in 83% yield as a 75:22:3 mixture of isomers. This mixture and allenylsulfone **2** (*E*/*Z* 74:26) were deprotonated with a large excess of KHMDS in the final (Sylvestre) Julia olefination.[37] Within 5 min this furnished 61% of a mixture of peridinin isomers, the major constituent

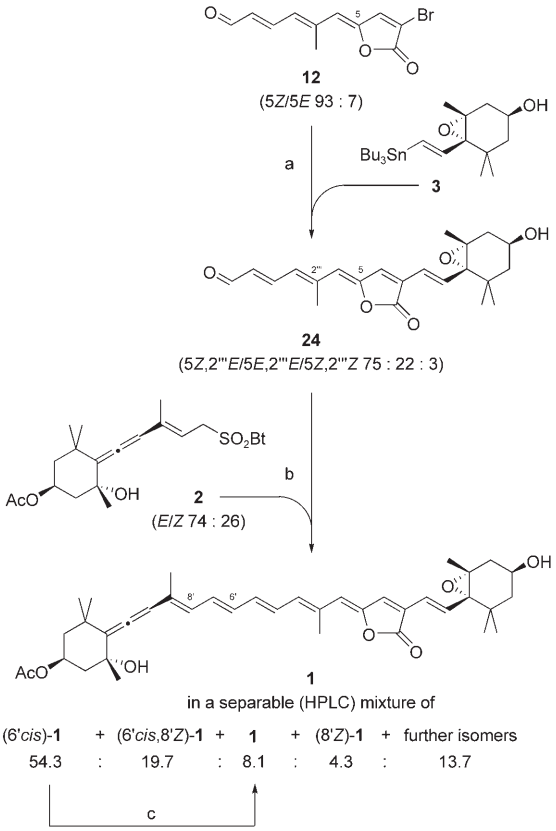

Scheme 5. Total synthesis of peridinin (**1**[18]). a) **3** (1.2 equiv), [Pd(PPh$_3$)$_4$] (10 mol%), CuI (1.65 equiv), di-*tert*-butylcresol (250 ppm), *N*-methylpyrrolidone (degassed), exclusion of light, 25°C, 18 h, 83% yield of the isomeric mixture; b) addition of KHMDS (5.0 equiv) to solution of **24** (1.0 equiv of indicated mixture) and **2** (1.2 equiv of indicated mixture) in THF (degassed), di-*tert*-butylcresol (250 ppm), exclusion of light, −78°C, 5 min, 61%; c) CH_3CN/H_2O (70:30), 25°C, exclusion of light, 37 d, HPLC, 57% pure **1** [or 89% **1** taking into account 37% yield of recovered (6′*cis*)-**1**]. KHMDS = potassium hexamethyldisilazanide.

 © 2006 Wiley-VCH Verlag GmbH & Co. KGaA, Weinheim

being (6′*cis*)-**1** (54%). The ratio of isomers (6′*cis*)-**1**/**1**—originating from precursors (5*Z*,2‴*E*)-**24** and *E*-**2**—was 87:13, and the ratio of isomers (6′*cis*,8′*Z*)-**1**/(8′*Z*)-**1**—originating from precursors (5*Z*,2‴*E*)-**24** and *Z*-**2**—was 82:18. These findings agree well with recent reports on the *cis* selectivity of diene- or polyene-delivering olefinations with other allyl-(benzothiazolyl)sulfones.[38] After isomer separation by preparative reversed-phase HPLC, we obtained our first specimen of correctly configured synthetic peridinin (**1**). More interestingly, the purified isomer (6′*cis*)-**1**, which was our major olefination product, gave synthetic peridinin (**1**) selectively upon prolonged storage of a solution in 70% aq acetonitrile at room temperature in the dark. After 37 days we isolated **1** in 57% yield, and unchanged (6′*cis*)-**1** was recovered in 37% yield; this corresponds to a conversion to **1** in 89% yield.

The ^{1}H NMR shifts and $J_{H,H}$ values determined at 500 MHz in a CD_3OD solution of synthetic peridinin (**1**) and its ^{13}C NMR shifts recorded at 125.7 MHz agree well with the data reported for natural peridinin (**1**) under identical conditions.[39] The same is true with respect to the eight ^{1}H NMR shift values (500 MHz) for the olefinic carbon atoms published for natural peridinin (**1**) in C_6D_6.[40]

We also undertook an intensive NMR study of isomer **1** possessing the natural configuration and of its precursor (6′*cis*)-**1** exhibiting the unnatural configuration of the $C^{6'}$=$C^{7'}$ [18] bond. We used C_6D_6 solutions because in this solvent the signal (^{1}H) dispersion was greater than in the previously used[39] CD_3OD, and we were able to assign *all* ^{1}H and ^{13}C resonances individually. The ROESY spectra of **1** and (6′*cis*)-**1** proved the two stereostructures based on appropriate nOe crosspeaks. Specifically, the configurations of the double bonds were assigned in this manner, the relative configurations of the stereocenters established, and even the 3D structure of the allene moiety elucidated.

In summary, we have accomplished a highly convergent total synthesis of peridinin (**1**). Starting from actinol (**5**) and diethyl tartrate (**6**), **1** was synthesized in 15 steps plus two HPLC separations in the longest linear sequence. A single HPLC separaration may have sufficed if the isomerization (6′*cis*)-**1**→**1** had been effected with the originally obtained (6′*cis*)-**1**/**1**/(6′*cis*,8′*Z*)-**1**/(8′*Z*)-**1** mixture rather than with pure (6′*cis*)-**1**. The overall yield was 7.7% and the total number of steps[41] 29.[42] Key transformations were the differential reduction **7**→**8** of an ester-containing Weinreb amide, the *E*-selective olefination **8**→**10** by the Ando-type bromophosphonates **9a**/**9b**, the *anti*-selective β-elimination **11**→**12** upon treatment with 1,1′-thiocarbonyldiimidazole, which established the $C^{1'}$=C^5 bond *Z*-selectively in an unprecedented manner, and the *cis*→*trans* isomerization (6′*cis*)-**1**→**1** as the ultimate step.

Received: February 7, 2006
Published online: May 9, 2006

Keywords: butenolides · carotenoids · elimination · olefination · total synthesis

[1] E. Hofmann, P. M. Wrench, F. P. Sharples, R. G. Hiller, W. Welte, K. Diederichs, *Science* **1996**, *272*, 1788–1791.
[2] a) D. M. Anderson, *Sci. Am.* **1994**, *271(2)*, 62–68; b) E. Culotta, *Science* **1992**, *257*, 1476–1477; c) http://www.whoi.edu/redtide/.
[3] H. Nishino, *Mutat. Res.* **1998**, *402*, 159–163.
[4] J. A. Haugan, T. Aakermann, S. Liaaen-Jensen, *Methods Enzymol.* **1992**, *213*, 231–245.
[5] *Carotenoids* (Eds.: G. Britton, S. Liaaen-Jensen, H. Pfander), *Carotenoids—Handbook* (compiled by A. Z. Mercadante, E. S. Egeland), Birkhäuser, Basel, **2004**.
[6] γ-Alkylidenebutenolide rings are also present in the following carotenoids: a) peridinol: Ref. [6c]; b) anhydroperidinol: D. J. Repeta, R. B. Gagosien, *Geochim. Cosmochim. Acta* **1984**, *48*, 1265–1277; c) pyrrhoxanthin: two-dimensional structure: J. E. Johansen, W. A. Svec, S. Liaaen-Jensen, F. T. Haxo, *Phytochemistry* **1974**, *13*, 2261–2271; three-dimensional structure: T. Aakermann, S. Liaaen-Jensen, *Phytochemistry* **1992**, *31*, 1779–1782; d) pyrrhoxanthinol: Ref. [6c]; e) hydratopyrrhoxanthinol: S. Hertzberg, V. Partali, S. Liaaen-Jensen, *Acta Chem. Scand. Ser. B* **1988**, *42*, 495–503; f) uriolide: P. Foss, R. R. L. Guillard, S. Liaaen-Jensen, *Phytochemistry* **1986**, *25*, 119–124; g) deepoxyuriolide: E. S. Egeland, S. Liaaen-Jensen, *Phytochemistry* **1995**, *40*, 515–520; h) anhydrouriolide: Ref. [6g]; i) 3′-dehydrouriolide: Ref. [6g]; j) unnamed carotenoid: T. Maoka, K. Hashimoto, N. Akimoto, Y. Fuhiwara, *J. Nat. Prod.* **2001**, *64*, 578–581; k) unnamed carotenoid: M. Suzuki, K. Watanabe, S. Fujiwara, T. Kurasawa, T. Wakabayashi, M. Tsuzuki, K. Iguchi, T. Yamori, *Chem. Pharm. Bull.* **2003**, 724–727.
[7] a) I. E. Swift, B. V. Milborrow, *Biochem. J.* **1981**, *199*, 69–74; b) I. E. Swift, B. V. Milborrow, *Biochem. J.* **2005**, *389*, 919–919 (retraction of prior findings).
[8] F. Schütt, *Ber. Dtsch. Bot. Ges.* **1890**, *8*, 9–32.
[9] Two-dimensional structure: a) H. H. Strain, W. A. Svec, K. Aitzetmüller, M. C. Grandolfo, J. J. Katz, H. Kjøsen, S. Norgård, S. Liaaen-Jensen, F. T. Haxo, P. Wegfahrt, H. Rapoport, *J. Am. Chem. Soc.* **1971**, *93*, 1823–1825; three-dimensional structure: b) H. H. Strain, W. A. Svec, P. Wegfahrt, H. Rapoport, F. T. Haxo, S. Norgård, H. Kjøsen, S. Liaaen-Jensen, *Acta Chem. Scand. Ser. B* **1976**, *30*, 109–120; c) J. E. Johansen, G. Borch, S. Liaaen-Jensen, *Phytochemistry* **1980**, *19*, 441–444.
[10] a) Synthesis of a racemic mixture of diastereomers of **1**: M. Ito, Y. Hirata, Y. Shibata, K. Tsukida, *J. Chem. Soc. Perkin Trans. 1* **1990**, 197–199; b) synthesis of enantiomerically and diastereomerically pure **1**: Y. Yamano, M. Ito, *J. Chem. Soc. Perkin Trans. 1* **1993**, 1599–1610.
[11] a) N. Furuichi, H. Hara, T. Osaki, H. Mori, S. Katsumura, *Angew. Chem.* **2002**, *114*, 1065–1068; *Angew. Chem. Int. Ed.* **2002**, *41*, 1023–1026; b) N. Furuichi, H. Hara, T. Osaki, M. Takano, H. Mori, S. Katsumura, *J. Org. Chem.* **2004**, *69*, 7949–7959.
[12] B. Vaz, R. Alvarez, R. Brückner, A. R. de Lera, *Org. Lett.* **2005**, *7*, 545–548.
[13] a) Review: R. Brückner, *Chem. Commun.* **2001**, 141–152; individual reports: b) J. Schmidt-Leithoff, R. Brückner, *Helv. Chim. Acta* **2005**, *88*, 1943–1958; c) F. von der Ohe, R. Brückner, *New J. Chem.* **2000**, *24*, 659–669; d) I. Hanisch, R. Brückner, *Synlett* **2000**, 374–378; e) K. Siegel, R. Brückner, *Chem. Eur. J.* **1998**, *4*, 1116–1122; f) F. C. Görth, A. Umland, R. Brückner, *Eur. J. Org. Chem.* **1998**, 1055–1062.
[14] Reviews on other approaches to γ-alkylidenebutenolides: a) E.-i. Negishi, M. Kotora, *Tetrahedron* **1997**, *53*, 6707–6738; b) R. Brückner, *Curr. Org. Chem.* **2001**, *5*, 679–718; c) R. Rossi, F. Bellina in *Targets in Heterocyclic Systems: Chemistry and Properties*, *Vol. 5* (Eds.: O. A. Attanasi, D. Spinelli), Società Chimica Italiana, **2002**, pp. 169–198.

 © 2006 Wiley-VCH Verlag GmbH & Co. KGaA, Weinheim

[15] Nomenclature according to D. Seebach, V. Prelog, *Angew. Chem.* **1982**, *94*, 696 – 702; *Angew. Chem. Int. Ed. Engl.* **1982**, *21*, 654 – 660.

[16] T. Olpp, R. Brückner, *Angew. Chem.* **2005**, *117*, 1577 – 1581; *Angew. Chem. Int. Ed.* **2005**, *44*, 1553 – 1557.

[17] Preparation of **5**: a) H. G. W. Leuenberger, W. Boguth, E. Widmer, R. Zell, *Helv. Chim. Acta* **1976**, *59*, 1832 – 1849; b) Y. Crameri, K. Puentener, M. Scalone (F. Hoffmann-La Roche AG, Switzerland), EPXXDW EP 915076A1 19990512, **1999**; c) T. Hoshino, Y. Setoguchi (DSM Ip Assets B. V., Netherlands), PIXXD2 WO 2004029263A2 20040408 PCT Int. Appl., **2004**.

[18] The nomenclature in this communication is in compliance with general IUPAC rules (http://www. chem.qmul.ac.uk/iupac/). The recommended carotenoid-specific IUPAC nomenclature for peridinin (**1**) can be found in Ref. [5] and Ref. [39].

[19] a) E. Widmer, M. Soukup, R. Zell, E. Broger, H. P. Wagner, M. Imfeld, *Helv. Chim. Acta* **1990**, *73*, 861 – 867; b) M. Soukup, E. Widmer, T. Lukáč, *Helv. Chim. Acta* **1990**, *73*, 868 – 873.

[20] M. Carmack, C. J. Kelley, *J. Org. Chem.* **1968**, *33*, 2171 – 2173.

[21] K. Ando, T. Oishi, M. Hirama, H. Ohno, T. Ibuka, *J. Org. Chem.* **2000**, *65*, 4745 – 4749, and references therein.

[22] T. Olpp, R. Brückner, *Synthesis* **2004**, 2135 – 2152.

[23] All new compounds gave satisfactory ^{1}H and ^{13}C NMR spectra and correct combustion analyses—except the unstable hydroxylaldehyde **8**, aldehydes **11** and **12**, thioethers **21** and **22**, and peridinin (**1**); each of these compounds, however, provided a correct high-resolution mass spectrum.

[24] A one-pot reduction/olefination procedure **7**→**10** failed because of the incompatibility of unconsumed reducing agent with the deprotonated phosphonates **9a** and **9b**.

[25] a) D. B. Dess, J. C. Martin, *J. Org. Chem.* **1983**, *48*, 4155 – 4156; b) D. B. Dess, J. C. Martin, *J. Am. Chem. Soc.* **1991**, *113*, 7277 – 7287.

[26] Method: K. Miwa, T. Aoyama, T. Shioiri, *Synlett* **1994**, 107 – 108.

[27] At lower temperatures (e.g., at −78 °C for 5 min) and again after desilylation, we obtained only half the amount of alkyne (in the cited case: 40 % **17**) but also the corresponding methylketone **15** (in the cited case: 14 %). Probably, **15** results from a ≈[1,2] hydrogen shift in the "Tiffeneau/Demjanov-type substructure" $^{-}O-(H-)C-C-N\equiv N^{+}$ of a zwitterion $^{-}O-(H-)C(-R)-C(-SiMe_3)-N\equiv N^{+}$, which must have formed initially at least to some extent. This side reaction was neither observed during the same transformation earlier[12] nor does it appears to be known from any other Shiorii C_1-extension.

[28] *trans*-Selective hydrostannylation of **17** with Bu_3SnH and cat. $[PdCl_2(PPh_3)_2]$: M. Kuba, N. Furuichi, S. Katsumura, *Chem. Lett.* **2002**, 1248 – 1249.

[29] Method: B. M. Trost, M. T. Sorum, C. Chan, A. E. Harms, G. Rühter, *J. Am. Chem. Soc.* **1997**, *119*, 698 – 708.

[30] DIBAL reduction of carotenoid epoxyalkynes giving allenols: a) original report (to the best of our knowledge): E. Widmer, *Pure Appl. Chem.* **1985**, *57*, 741 – 752; b) specific precedence: M. Ito, Y. Hirata, K. Tsukida, N. Tanaka, K. Hamada, R. Hino, T. Fujiwara, *Chem. Pharm. Bull.* **1988**, *36*, 3328 – 3340.

[31] Different preparations of **23**: a) racemic: Ref. [30b]; b) enantiomerically pure: A. Baumeler, C. H. Eugster, *Helv. Chim. Acta* **1991**, *74*, 469 – 487; c) enantiomerically pure: Ref. [10b]; d) nonstereoselective: M. Nakano, N. Furuichi, H. Mori, S. Katsumura, *Tetrahedron Lett.* **2001**, *42*, 7307 – 7310.

[32] Method: a) J. B. Baudin, G. Hareau, S. A. Julia, O. Ruel, *Tetrahedron Lett.* **1991**, *32*, 1175 – 1178; b) P. R. Blakemore, P. J. Kocienski, A. Morley, K. Muir, *J. Chem. Soc. Perkin Trans. 1* **1999**, 955 – 968.

[33] W. C. Still, M. Kahn, A. Mitra, *J. Org. Chem.* **1978**, *43*, 2923 – 2925.

[34] Method: J. B. Baudin, G. Hareau, S. A. Julia, O. Ruel, *Bull. Soc. Chim. Fr.* **1993**, *130*, 336 – 357.

[35] Review: V. Farina, V. Krishnamurthy, W. J. Scott, *Org. React.* **1997**, *50*, 1 – 652.

[36] Method: L. S. Liebeskind, R. W. Fengl, *J. Org. Chem.* **1990**, *55*, 5359 – 5364.

[37] Method: a) Ref. [32a]; b) Ref. [34]; c) J. B. Baudin, G. Hareau, S. A. Julia, R. Lorne, O. Ruel, *Bull. Soc. Chim. Fr.* **1993**, *130*, 856 – 878.

[38] a) A. Sorg, R. Brückner, *Synlett* **2005**, 289 – 293; b) B. Vaz, R. Alvarez, J. A. Souto, A. R. de Lera, *Synlett* **2005**, 294 – 298; c) Ref. [11].

[39] J. Krane, T. Aakermann, S. Liaaen-Jensen, *Magn. Reson. Chem.* **1992**, *30*, 1169 – 1177.

[40] Y. Yamano (née Hirata), S. Sumiya, K. Suzuki, Y. Kurimoto, Y. Koyama, T. Shimamura, M. Ito, *Tetrahedron Lett.* **1992**, *33*, 2991 – 2994.

[41] Counting HPLC separations as steps.

[42] This compares well with previous syntheses: a) Ito's synthesis of **1** from (*R*)-4-levodione, (*E*)-3-methyl-2-penten-4-in-1-ol, and (*E*,*E*)-6-hydroxy-2-methyl-2,4-hexadienal (Ref. [10]) comprised over 35 steps and included 19 steps in the longest linear sequence (Ref. [41]); b) Katsumura's access to **1** from (*R*,*R*)-actinol and 2-butyn-1-ol (Ref. [11]) consists of 33 steps, 18 thereof in the longest linear sequence (Ref. [41]); c) (*R*,*R*)-actinol, crotonic acid, diethyl methylmalonate, 2-butyn-1-ol, and propynol provided 6′-*epi*-**1** according to Ref. [12], requiring 30 steps overall and 14 in the longest linear sequence.

 © 2006 Wiley-VCH Verlag GmbH & Co. KGaA, Weinheim

Water Clusters

DOI: 10.1002/anie.200504135

Proton Transfer in Ionic Water Clusters**

Zheng Sun, Chi-Kit Siu, O. Petru Balaj, Mirko Gruber, Vladimir E. Bondybey, and Martin K. Beyer**

Current works in cluster chemistry focus on extrapolating information on bulk properties from gas-phase cluster experiments.[1–3] Concerted proton transfer by the Grotthuss mech-

[*] Dr. Z. Sun, Dr. C.-K. Siu, Dr. O. P. Balaj, Dipl.-Chem. M. Gruber, Prof. Dr. V. E. Bondybey, Priv.-Doz. Dr. M. K. Beyer
Department Chemie
Physikalische Chemie 2
Technische Universität München
Lichtenbergstrasse 4, 85747 Garching (Germany)
Fax: (+49) 89-289-13416
E-mail: bondybey@gmail.com

Priv.-Doz. Dr. M. K. Beyer
Institut für Chemie, Sekr. C4
Technische Universität Berlin
Strasse des 17. Juni 135, 10623 Berlin (Germany)
Fax: (+49) 30-314-21102
E-mail: martin.beyer@mail.chem.tu-berlin.de

[**] Financial support from the Deutsche Forschungsgemeinschaft, the Fonds der Chemischen Industrie, the Alexander von Humboldt Foundation (Z.S., C.-K.S.), and the Heisenberg program of the Deutsche Forschungsgemeinschaft (M.K.B.) is gratefully acknowledged. We thank Prof. Dr. Wolfgang Domcke and Prof. Dr. Andrzej Sobolewski for helpful discussion and valuable comments.

© 2006 Wiley-VCH Verlag GmbH & Co. KGaA, Weinheim

anism[4,5] is a key step in aqueous reactions, especially in acid–base chemistry. This process has recently been studied in bulk solution by time-resolved spectroscopy[6] as well as ab initio molecular-dynamics simulations.[7–9] Understanding the conditions for the occurrence of proton transfer in finite clusters is of paramount importance for our qualitative picture of the chemistry of water clusters and their relation to bulk aqueous solution.

It may be expected that protons can wander freely between oxygen atoms in protonated water clusters, as infrared spectroscopic studies[10] of $H(H_2O)_n^+$ indicate the presence of both the Eigen ion (H_3O^+) and the Zundel ion ($H_5O_2^+$) in isomeric clusters with similar energies and sizes. Honma and Armentrout have recently shown that thermally activated proton transfer occurs in the reaction of $H(H_2O)_n^+$ ($n=1$–4) with D_2O.[11] However, it is not known whether proton transfer occurs in clusters such as $(H_2O)_n^-$ and $O_2(H_2O)_n^-$ that do not contain an excess proton. In solution, proton transfer leads to the formation of H atoms from solvated electrons,[12] and HO_2 radicals from superoxide ions.[13] Recent works by Kuo et al.[14] on neutral $(H_2O)_{20}$ and by Sobolewski and Domcke[15] on $(H_2O)_n^-$ have shown that zwitterionic structures containing an H_3O^+/OH^- ion pair are local minima on the potential-energy surfaces of water clusters. Population of these zwitterionic isomers in an experiment would imply proton transfer. Herein, we present a mass-spectrometric study of the reactions of D_2O with ionic water clusters of the types $H(H_2O)_n^+$, $(H_2O)_n^-$, and $O_2(H_2O)_n^-$, which reveals that only within $H(H_2O)_n^+$ are the isotopically scrambled HDO molecules formed. This result indicates that no autoprotolysis occurs in small clusters of the types $(H_2O)_n^-$ and $O_2(H_2O)_n^-$, and renders the formation of the zwitterionic structures unlikely.

The presence of proton transfer—or lack of it—may be probed chemically by observing isotopic scrambling in mixed $(H_2O)_m(D_2O)_nX$ clusters (X denotes a charge carrier, in our case a proton, an excess electron, or a superoxide ion). In a mass-spectrometric experiment, the loss of HDO from a mixed cluster leads to a characteristic change of the cluster mass and thus serves as direct proof of isotopic scrambling and HDO formation.

We treated $H(H_2O)_n^+$, $(H_2O)_n^-$, and $O_2(H_2O)_n^-$ with gaseous D_2O in the ion trap of a Fourier transform ion cyclotron resonance (FT-ICR) mass spectrometer, where the cluster temperature is determined by the interplay of radiative heating by room-temperature black-body radiation and evaporative cooling.[16–20] Recently identified chain, net, and cage structures of protonated water clusters[21,22] represent the structural motifs of energetically low-lying isomers. Since the clusters were continuously heated in our experiment to their dissociation limit, their internal energy was sufficient to form a large number of different isomers. The clusters collide with molecules of the reactant gas at a rate of 3 s^{-1}, which leaves ample time between collisions for rearrangement of the hydrogen bonds.

A nearly random distribution of clusters with even and odd nominal mass was obtained after the exchange of only a few water molecules within $H(H_2O)_n^+$ (Figure 1a), which provides clear evidence for isotopic scrambling. In the presence of protons, the conversion of D_2O into HDO [Eq. (1)] can proceed as illustrated in Scheme 1.

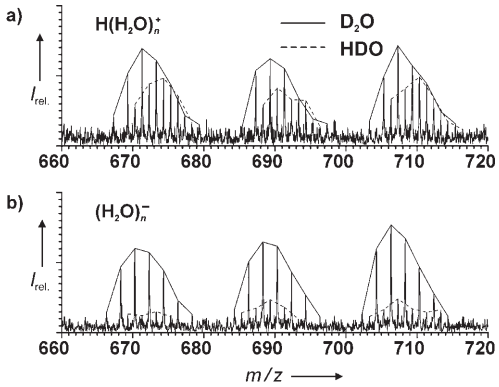

Figure 1. Sections of the mass spectra of the products of the reaction of $H(H_2O)_n^+$ (a) and $(H_2O)_n^-$ (b) with D_2O after 1.4 s (which corresponds to about four collisions with the reactant gas). a) Rapid rearrangement of hydrogen and deuterium in the protonated water cluster leads to formation of HDO, which can be lost by evaporative cooling or exchanged in a collision, thus changing the cluster mass from odd to even. After four D_2O molecules have been exchanged, clusters with odd (solid line) and even (dashed line) nominal mass are already randomly distributed. b) Solvated electrons undergo sequential exchange of H_2O with D_2O without formation of HDO (solid line). The minor amounts of species with odd nominal mass (dashed line) result from the HDO content of the D_2O reactant in the vacuum chamber and the natural deuterium content of the water clusters. The mass window shown covers $n=37$–39.

$$H_3O^+ + D_2O \rightarrow H_2O + HD_2O^+ \rightarrow H_2DO^+ + HDO \quad (1)$$

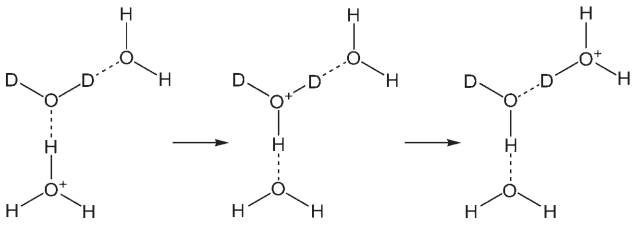

Scheme 1.

Proton transfer by the Grotthuss mechanism will quickly randomize H and D atoms within the cluster, thus forming a significant fraction of HDO molecules. Consequently, HDO species can also be lost by evaporative cooling, which changes the cluster mass from odd to even, or vice versa.

For comparison, we repeated the experiment with water cluster anions ($(H_2O)_n^-$; Figure 1b) as well as with hydrated superoxide ions ($O_2(H_2O)_n^-$). The efficient exchange of D_2O for H_2O and gradual deuteration of the clusters were also observed in this case. Such exchanges [Eq. (2)] result in increases of the cluster mass in increments of two mass units.

$$(H_2O)_{n-m}(D_2O)_m^- + D_2O \rightarrow (H_2O)_{n-m-1}(D_2O)_{m+1}^- + H_2O \quad (2)$$

Clusters with even mass were present almost exclusively after the same reaction time as that in Figure 1a, which

 © 2006 Wiley-VCH Verlag GmbH & Co. KGaA, Weinheim

indicates that isotopic scrambling and proton transfer processes do not occur in water-cluster anions or hydrated superoxide ions in their electronic ground state. The minor contribution of odd-mass clusters in Figure 1 b is attributed to HDO, which was present as a contamination in the reaction gas.

To verify that HDO impurities were indeed responsible for the odd-mass clusters, we treated $(H_2O)_n^-$, $O_2(H_2O)_n^-$, and $H(H_2O)_n^+$ with D_2O for 3.6 s and removed the HDO-containing clusters from the ICR cell by resonant excitation. This selection worked well for $(H_2O)_n^-$ and $O_2(H_2O)_n^-$, whereas for $H(H_2O)_n^+$, the HDO-containing peaks reappeared even during mass selection (Figure 2 a,c,e). After an additional 1.6 s, the $(H_2O)_n^-$ and $O_2(H_2O)_n^-$ mass spectra consist exclusively of even-mass species (Figure 2 b,d), whereas the mass spectrum of the $H(H_2O)_n^+$ reaction products shows an almost statistical distribution of clusters with odd and even mass (Figure 2 f). This mass-selection experiment allows unambiguous discrimination between clusters in which proton transfer occurs and those in which it does not, thus removing the uncertainty introduced by the HDO content of the reaction gas.

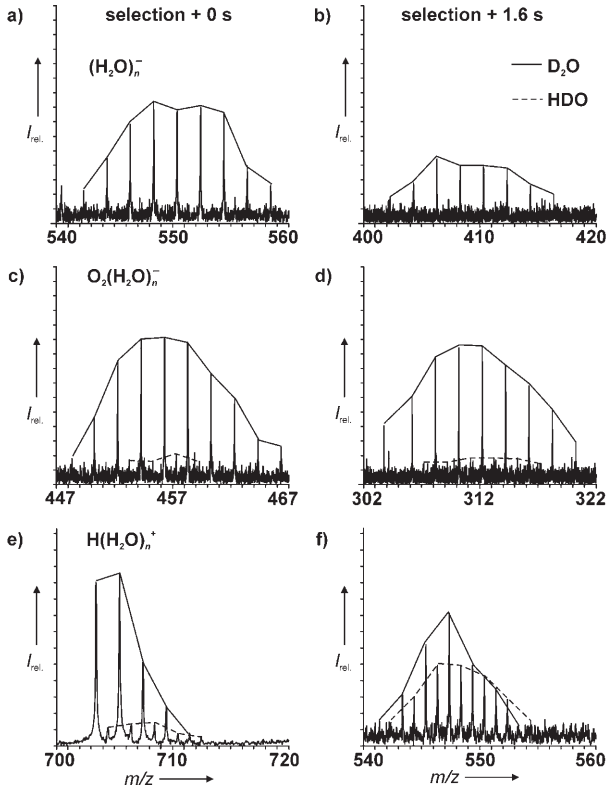

Figure 2. a), c), e) Sections of the mass spectra of the products of the reaction of $(H_2O)_n^-$, $O_2(H_2O)_n^-$, and $H(H_2O)_n^+$ with D_2O at a pressure of 2.5×10^{-9} mbar after 3.6 s; HDO-containing reaction products were removed by resonant excitation. For $(H_2O)_n^-$ (a) and $O_2(H_2O)_n^-$ (c), the selection is almost complete, whereas for $H(H_2O)_n^+$ (e), HDO formation is so efficient that even-numbered mass peaks (dashed line) reappear even during the removal. b), d), f) After an additional reaction delay of 1.6 s, there is still no sign of HDO formation for $(H_2O)_n^-$ (b) and $O_2(H_2O)_n^-$ (d), whereas for $H(H_2O)_n^+$ (f), a statistical distribution of odd- and even-mass species is reached. The intensity loss of $(H_2O)_n^-$ in (b) is due to electron detachment. Cluster sizes shown are a) $n=30$, b) $n=22$, c) $n=23$, d) $n=15$, e) $n=39$, and f) $n=30$.

This absence of proton transfer is in line with the stability of the solvated electron in $(H_2O)_n^-$ on a time scale of many seconds;[23] in contrast, its lifetime in bulk aqueous solution is less than 100 μs.[24] The elimination of atomic hydrogen as a consequence of the recombination of the electron with a proton is not observed in gas-phase water-cluster anions.

Evidently there are significant differences in the long-term dynamics of the two types of clusters in the size range studied: $(H_2O)_n^-$ and $O_2(H_2O)_n^-$ ions are correctly described as a network of hydrogen-bonded water molecules with an excess electron or superoxide ion, in which zwitterionic structures are not formed even transiently. Protonated $H(H_2O)_n^+$ water clusters are acidic nanodroplets in which the O–H bonds are constantly rearranging by the Grotthuss mechanism.

Experimental Section

The experiments were performed on a modified Bruker/Spectrospin CMS47X mass spectrometer equipped with an Apex III data station and an external laser-vaporization source.[25–27] Hydrated electrons ($(H_2O)_n^-$), protonated water clusters ($H(H_2O)_n^+$), and hydrated superoxide ions ($O_2(H_2O)_n^-$) were produced by laser vaporization[28,29] of a solid zinc target with the 5-ns pulse of a frequency-doubled Nd:YAG laser (Continuum Surelite II, 10 Hz, pulse energy 5 mJ), followed by supersonic expansion of the hot plasma entrained in a 50-μs helium pulse which was seeded with traces of water, and, in the case of $O_2(H_2O)_n^-$, O_2. The cluster ions formed were transferred by a series of electrostatic lenses through four stages of differential pumping, decelerated, and stored in the ICR cell. Starting distributions of water clusters typically contained 40 to 60 water molecules. The reactant D_2O (Aldrich, 99.9 % deuterium content) was degassed by three freeze–pump–thaw cycles and was admitted into the ultrahigh-vacuum region of the ICR cell through a leak valve, thus raising the base pressure from 2×10^{-10} to 9.6×10^{-9} mbar. The reaction was monitored by taking mass spectra after varying delays. Because the filling of the cell takes up to 2 s, the reaction had already proceeded to some extent at a nominal time of 0 s.

Although D_2O with a deuterium content of 99.9 % was used, the reaction products as well as an electron-impact spectrum of the reaction gas indicated that 5–10 % HDO was present in the ultrahigh-vacuum region. This HDO is formed by H/D exchange between the D_2O molecules and hydrogen atoms present on the stainless steel, copper, gold, glass, and polymer surfaces of the apparatus. To minimize this effect, the apparatus was conditioned by keeping D_2O present for several days, with repeated heating and cooling cycles. This HDO content is responsible for the peaks with odd nominal mass shown in Figure 1 b. Both spectra shown in Figure 1 were measured within one hour, during which time the D_2O pressure was kept constant, and the HDO content did not change.

Owing to black-body radiation[16–20] and collision-induced dissociation, the clusters lose water molecules one after the other. For clusters with $n \leq 30$,[23] electron detachment competes with water loss for the $(H_2O)_n^-$ species, and their intensity is lost in this size range. Selection of individual cluster sizes is thus not possible because of the gradual shrinking of the clusters. Although there is no evidence for cluster-size effects in the studied mass range, subtle size effects cannot be ruled out.

Received: November 21, 2005
Revised: February 15, 2006
Published online: May 9, 2006

 © 2006 Wiley-VCH Verlag GmbH & Co. KGaA, Weinheim

Keywords: clusters · gas-phase reactions · isotopic labeling · proton transfer · water chemistry

[1] V. E. Bondybey, M. K. Beyer, *Int. Rev. Phys. Chem.* **2002**, *21*, 277 – 306.
[2] A. J. Huneycutt, R. J. Saykally, *Science* **2003**, *299*, 1329 – 1330.
[3] J. R. R. Verlet, A. E. Bragg, A. Kammrath, O. Cheshnovsky, D. M. Neumark, *Science* **2005**, *307*, 93 – 96.
[4] C. J. T. de Grotthuss, *Ann. Chim.* **1806**, *58*, 54 – 74.
[5] N. Agmon, *Chem. Phys. Lett.* **1995**, *244*, 456 – 462.
[6] O. F. Mohammed, D. Pines, J. Dreyer, E. Pines, E. T. J. Nibbering, *Science* **2005**, *310*, 83 – 86.
[7] M. Tuckerman, K. Laasonen, M. Sprik, M. Parrinello, *J. Chem. Phys.* **1995**, *103*, 150 – 161.
[8] D. Asthagiri, L. R. Pratt, J. D. Kress, *Proc. Natl. Acad. Sci. USA* **2005**, *102*, 6704 – 6708.
[9] D. Marx, M. E. Tuckerman, J. Hutter, M. Parrinello, *Nature* **1999**, *397*, 601 – 604.
[10] a) J. C. Jiang, Y. S. Wang, H. C. Chang, S. H. Lin, Y. T. Lee, G. Niedner-Schatteburg, H. C. Chang, *J. Am. Chem. Soc.* **2000**, *122*, 1398 – 1410; b) J. M. Headrick, E. G. Diken, R. S. Walters, N. I. Hammer, R. A. Christie, J. Cui, E. M. Myshakin, M. A. Duncan, M. A. Johnson, K. D. Jordan, *Science* **2005**, *308*, 1765 – 1769.
[11] K. Honma, P. B. Armentrout, *J. Chem. Phys.* **2004**, *121*, 8307 – 8320.
[12] G. V. Buxton, C. L. Greenstock, W. P. Helman, A. B. Ross, *J. Phys. Chem. Ref. Data* **1988**, *17*, 513 – 886.
[13] L. Stryer, *Biochemistry*, 4th ed., W. H. Freeman, New York, **1995**.
[14] J. L. Kuo, C. V. Ciobanu, L. Ojamae, I. Shavitt, S. J. Singer, *J. Chem. Phys.* **2003**, *118*, 3583 – 3588.
[15] A. L. Sobolewski, W. Domcke, *Phys. Chem. Chem. Phys.* **2003**, *5*, 1130 – 1136.
[16] R. C. Dunbar, T. B. McMahon, *Science* **1998**, *279*, 194 – 197.
[17] B. S. Fox, M. K. Beyer, V. E. Bondybey, *J. Phys. Chem. A* **2001**, *105*, 6386 – 6392.
[18] P. D. Schnier, W. D. Price, R. A. Jockusch, E. R. Williams, *J. Am. Chem. Soc.* **1996**, *118*, 7178 – 7189.
[19] D. Thölmann, D. S. Tonner, T. B. McMahon, *J. Phys. Chem.* **1994**, *98*, 2002 – 2004.
[20] M. Sena, J. M. Riveros, *Rapid Commun. Mass Spectrom.* **1994**, *8*, 1031 – 1034.
[21] F. Misaizu, K. Tsukamoto, M. Sanekata, K. Fuke, *Z. Phys. D* **1993**, *26*, S177-S179.
[22] J. W. Shin, N. I. Hammer, E. G. Diken, M. A. Johnson, R. S. Walters, T. D. Jaeger, M. A. Duncan, R. A. Christie, K. D. Jordan, *Science* **2004**, *304*, 1137 – 1140.
[23] M. K. Beyer, B. S. Fox, B. M. Reinhard, V. E. Bondybey, *J. Chem. Phys.* **2001**, *115*, 9288 – 9297.
[24] H. A. Schwarz, *J. Phys. Chem.* **1992**, *96*, 8937 – 8941.
[25] C. Berg, T. Schindler, G. Niedner-Schatteburg, V. E. Bondybey, *J. Chem. Phys.* **1995**, *102*, 4870 – 4884.
[26] O. P. Balaj, I. Balteanu, B. S. Fox-Beyer, M. K. Beyer, V. E. Bondybey, *Angew. Chem.* **2003**, *115*, 5675 – 5677; *Angew. Chem. Int. Ed.* **2003**, *42*, 5516 – 5518.
[27] O. P. Balaj, C. K. Siu, L. Balteanu, M. K. Beyer, V. E. Bondybey, *Int. J. Mass Spectrom.* **2004**, *238*, 65 – 74.
[28] V. E. Bondybey, J. H. English, *J. Chem. Phys.* **1981**, *74*, 6978 – 6979.
[29] T. G. Dietz, M. A. Duncan, D. E. Powers, R. E. Smalley, *J. Chem. Phys.* **1981**, *74*, 6511 – 6512.

 © 2006 Wiley-VCH Verlag GmbH & Co. KGaA, Weinheim